



Water Quality Modelling of the Hawkesbury-Nepean River System - Hawkesbury-Nepean River and South Creek Model

- Final Calibration Report
- 24 February 2014



Water Quality Modelling of the Hawkesbury-Nepean River System - Hawkesbury-Nepean River and South Creek Model

- Final Calibration Report
- 24 February 2014

Sinclair Knight Merz
ABN 37 001 024 095
100 Christie Street
St Leonards NSW 2065 Australia
Postal Address
PO Box 164 St Leonards NSW 2065 Australia
Tel: +61 2 9928 2100
Fax: +61 2 9928 2500
Web: www.skmconsulting.com

COPYRIGHT: The concepts and information contained in this document are the property of Sinclair Knight Merz Pty Ltd. Use or copying of this document in whole or in part without the written permission of Sinclair Knight Merz constitutes an infringement of copyright.

LIMITATION: This report has been prepared on behalf of and for the exclusive use of Sinclair Knight Merz Pty Ltd's Client, and is subject to and issued in connection with the provisions of the agreement between Sinclair Knight Merz and its Client. Sinclair Knight Merz accepts no liability or responsibility whatsoever for or in respect of any use of or reliance upon this report by any third party.

Limitation Statement

This document is given strictly in accordance with and subject to the following limitations and recommendations:

The sole purpose of this report and the associated services performed by Sinclair Knight Merz Pty Ltd (SKM) and their subcontractors is to develop a coupled water quantity and quality model of the Hawkesbury-Nepean river system, in order to examine the water quality benefits (or impacts) resulting from the different scenarios over broad spatial and temporal scales. The model system is developed in accordance with the scope of services set out in the contract between SKM and Sydney Water Corporation (SWC). That scope of services, as described in this report, was developed with Sydney Water Corporation.

In preparing this report, SKM has relied upon, and presumed accurate, any information (or confirmation of the absence thereof) provided by the Sydney Water Corporation and/or from other sources. Except as otherwise stated in the report, SKM has not attempted to verify the accuracy or completeness of any such information, though where possible, data received from external sources was inspected for internal consistency, outliers or values out of range. If the information is subsequently determined to be false, inaccurate or incomplete, then it is possible that any observations and conclusions drawn from the modelling results presented in this report may change.

SKM obtained the data used in this report from a variety of sources. The sources are identified at the time or times outlined in this report. The passage of time, manifestation of latent conditions or impacts of future events may require further examination of the project and subsequent data analysis, and re-evaluation of the data, findings, observations and conclusions expressed in this report. SKM has prepared this report in accordance with the usual care and thoroughness of the consulting profession, for the sole purpose of the project and by reference to applicable standards, procedures and practices at the date of issue of this report. For the reasons outlined above, however, no other warranty or guarantee, whether expressed or implied, is made as to the data, observations and findings expressed in this report, to the extent permitted by law.

This report should be read in full and no excerpts are to be taken as representative of the findings. No responsibility is accepted by SKM for use of any part of this report in any other context.

This Hawkesbury-Nepean River and South Creek Model has been built for the express purpose to provide guidance on changes in water quantity and quality when contrasting different catchment and environmental flow, wastewater and land use scenarios. Overall differences in the statistical properties of flow and constituent concentrations between scenarios can be appropriately inferred by comparing scenarios. This includes differences between mean values, or differences between values that may be exceeded for a given proportion of time. Therefore, the Hawkesbury-Nepean River and South Creek Model may not necessarily produce accurate simulations of flow or constituent concentration at specific locations for specific points in time. Issues that were identified in the pilot model have been addressed to the extent allowed by project scope.



Water Quality Modelling of the Hawkesbury-Nepean River System

This report has been prepared on behalf of, and for the exclusive use of, Sydney Water Corporation, and is subject to, and issued in connection with, the provisions of the agreement between SKM and Sydney Water Corporation. SKM accepts no liability or responsibility whatsoever for, or in respect of, any use of, or reliance upon, this report by any third party.

Contents

1. Introduction	10
1.1. Hawkesbury-Nepean Water Quality Modelling Project	10
1.2. Hawkesbury-Nepean River and South Creek Model Phase	10
1.3. Hawkesbury-Nepean River and South Creek Model Assumptions	14
1.4. Structure of This Report	17
2. Overall Structure of the Source Model	18
2.1. Selection of the Source Modelling Platform	18
2.2. Functional Unit-Subcatchment-Node-Link Structure of the Source model	18
2.3. Run Period for the Hawkesbury-Nepean River and South Creek Catchment Calibration Model	18
3. Spatial Inputs to Catchment Model	20
3.1. Identification of Key Model Locations	20
3.1.1. Upstream Limits of the Hawkesbury-Nepean River and South Creek Model	20
3.1.2. Wastewater Treatment Plant and Recycled Water Plant Discharge Locations	22
3.1.3. Stream-flow Gauges	23
3.1.4. Water Quality Monitoring Sites	23
3.2. Subcatchment Boundaries and Node-Link Network	25
3.3. Functional Units	28
4. Climatic Inputs to Catchment Model	32
4.1. Daily Rainfall	32
4.1.1. Daily Rainfall Stations	32
4.1.2. Development of Daily Rainfall Grids	32
4.1.3. Calculation of Weighting Factors for Monthly Rainfall Totals Using Ordinary Kriging	35
4.1.4. Computation of Daily Rainfall Time Series for Model Subcatchments	37
4.2. Daily Potential Evapotranspiration	37
5. Selection of Component Model Types	41
5.1. Selection of Sacramento Model for Runoff Generation	41
5.2. Selection of Storage Routing Model (Laurenson and Mein) for Flow Routing	41
5.3. Selection of Generation Models for Constituents	42
5.4. Selection of In-Stream Routing and Transformation Models for Constituents	42
6. Point Inputs to the Hawkesbury-Nepean River and South Creek Catchment Model	44
6.1. Warragamba Dam Releases, Mangrove Creek Dam Releases and Flows at Broughton Pass and Pheasants Nest	44

6.2. Wastewater Treatment Plant / Water Recycling Plant Discharges	47
6.3. Irrigation Extractions	48
7. Runoff Generation and Flow Routing Model Calibration	51
7.1. Modelling approach	51
7.2. Parameters	51
7.3. Calibration and Validation of Flow Generation and Routing Models	54
7.3.1. Flow Calibration Objectives and Approach	54
7.3.2. Assignment of Calibration and Validation Periods for Flow	57
7.3.3. Discussion of Flow Calibration and Validation Outcomes	60
7.3.4. Influence of IQQM Modelled Extractions on Flow Calibration and Validation	62
8. Water Quality Constituent Generation Rates	64
8.1. Modelling Approach Used for Each Constituent	64
8.2. Parameter Values Assigned For Constituent Generation	65
8.3. Nutrient Decay Rates in South, Eastern and Cattai Creeks	68
8.4. Event Campaign Monitoring Program (CMP)	71
8.5. Comparison of Constituent Loads at Monitoring Sites	75
8.6. Additional Water Quality Parameters	82
8.6.1. Temperature	83
8.6.2. Dissolved Oxygen	88
8.6.3. pH	93
8.6.4. Total Organic Carbon and Dissolved Organic Carbon	98
8.6.5. Components of Organic Nitrogen	100
8.6.6. Components of Organic Phosphorus	103
9. Model Plug-Ins	106
9.1. Customised Export of Results from Source to TUFLOW/AED	106
10. Introduction to the Hydrodynamic and Water Quality Models	107
11. Data Collation and Review	109
11.1. Preamble	109
11.2. Survey Data	109
11.3. Model Boundaries	113
11.3.1. Diffuse Catchment Inflows	113
11.3.2. Tidal Boundary Conditions	115
11.3.3. Upstream Weir Inflows	115
11.3.4. Wastewater Treatment Plant and Water Recycling Plant Inflows	115
11.4. Meteorological Forcing Data	117
11.5. Tidal Hydrodynamics	119
11.5.1. Tidal Water Levels	119
11.5.2. Tidal Flow	119
11.6. Ambient Water Quality Data	125

12. Model Set-Up	143
12.1. Hydrodynamic Model	143
12.1.1. Model Domain	143
12.1.2. Model Mesh	145
12.1.3. Model Bathymetry	155
12.1.4. Weirs	156
12.1.5. Turbulence Schemes	157
12.1.6. Bed Materials	158
12.1.7. Boundary Conditions	167
12.1.8. Mixing Models	178
12.2. Water Quality Model	178
12.2.1. Simulated Constituents	178
12.2.2. Initial Conditions	179
12.2.3. Boundary Conditions	179
13. Model Calibration and Validation	183
13.1. Preamble	183
13.2. Hydrodynamics	183
13.3. Advection Dispersion/Salinity Recovery	184
13.4. Sediment Transport	185
13.5. Water Quality	186
13.5.1. Temperature	189
13.5.2. Nutrients	189
13.5.3. Primary Productivity	190
13.5.4. Bacteria	190
13.6. Discussion	428
13.6.1. Hydrodynamics	428
13.6.2. Water Quality	429
14. Summary	433
15. References	434
Appendix A WWTP/WRP Discharge Locations	436
Appendix B Rainfall Stations Used For Derivation of Daily Rainfall Grids	439
Appendix C Evaporation Sites Used for Derivation of Daily Evaporation Grids	452
Appendix D Comparison Plots Between Observed and Simulated Flows	453
Appendix E Event Campaign Monitoring Program	465
E.1 Event Campaign Monitoring Program Site Details	466
E.2 Wet Weather Events Captures as per the CMP Events	467

Appendix F Comparison Plots Between Observed and Simulated Concentrations	468
Appendix G Water Quality Sampling Locations	508
Appendix H Comparison of Meteorological Data	518
Appendix I Surface Heat Fluxes	520
Appendix J TUFLOW FV Science Manual	523
Appendix K AED Aquatic Ecodynamics Model Overview	524
Appendix L Final Calibration Parameters	525
Appendix M Diurnal Fluctuations	533
Appendix N Bacterial Model Publication	537
Addendum 1 Flow Duration Curves	538

Document history and status

Revision	Date issued	Reviewed by	Approved by	Date approved	Revision type
1	22/04/2013	T. Church			Draft
2	24/05/2013	T. Church	T. Church	24/05/2013	Draft
3	02/08/2013	T. Church	T. Church	02/08/2013	Final Draft
4	26/08/2013	SKM and BMT WBM	S. Linforth	09/09/2013	Final
5	14/02/2014	S. Linforth	S. Linforth	24/02/2014	Final v2

Distribution of copies

Revision	Copy no	Quantity	Issued to
Draft	1	1xWord	Sydney Water
Final Draft	1	1xWord	Sydney Water
Final	1	1xPDF	Sydney Water
Final v2	1	1xPDF	Sydney Water

Printed:	3 March 2014
Last saved:	24 February 2014 05:01 PM
File name:	I:\ENVR\Projects\EN03013\Deliverables\Reports\3_DetailMdl_Calb\EN03013-NHY-RP-0001-FinalCatchmentModel_Calibration_Finalv2_140224.docx
Author:	Phillip Jordan, Andrew Herron, Agathe Boronkay, Rosemarie Mannik, Donna Hughes, Tony McAlister, Michael Barry, Ian Teakle, Rob Holmes
Project manager:	Tony Church
Name of organisation:	Sydney Water
Name of project:	Water Quality Modelling of the Hawkesbury-Nepean River System
Name of document:	Hawkesbury-Nepean River and South Creek Model Calibration Report
Document version:	Final v2
Project number:	EN03013

Glossary

ADCP	Acoustic Doppler Current Profiler
AED	Aquatic EcoDynamics
BOM	Bureau of Meteorology
CBOD5	Carbonaceous biochemical oxygen demand
CMP	Campaign monitoring program
COE	Coefficient of Efficiency (Nash Sutcliffe Coefficient of Efficiency)
DEM/DTM	Digital elevation/terrain model
DOC	Dissolved Organic Carbon
DWC	Dry weather concentration
EMC	Event mean concentration
FRP	Filterable Reactive Phosphorus
FU	Functional unit
HEPS	Hydroelectric power station
IQQM	Integrated Quantity and Quality Model
Ks	Profile permeability
LiDAR	Light detection and ranging
MHL	Manly Hydraulics Laboratory
MWP	Metropolitan Water Plan
NARCLIM	New South Wales and Australian Capital Territory Regional Climate Model
NCAR	National Center for Atmospheric Research
NCEP	National Center for Environmental Prediction
NH ₄	Ammonium-N
NOAA	National Oceanic and Atmospheric Administration
NO _x	Oxidised nitrogen (sum of nitrate (NO ₂) and nitrite (NO ₃))
NRIC	National Resource Information Centre
OEH	NSW Office of Environment and Heritage
PAWHC	Plant available water holding capacity
PPET	Point potential evapotranspiration
PPFs	Principle profile forms
PWHC	Profile water holding capacity
SCA	Sydney Catchment Authority
SiO ₂	Silicates
SKM	Sinclair Knight Merz
Source IMS	Source Integrated Modelling System
SQL	Structured query language



Water Quality Modelling of the Hawkesbury-Nepean River System

SWC	Sydney Water Corporation
TKN	Total Kjeldahl Nitrogen
TN	Total Nitrogen
TOC	Total Organic Carbon
TP	Total Phosphorus
TSS	Total suspended solids
TUFLOW	Flood and coastal simulation software
TUFLOW-FV	TUFLOW finite volume
WATHNET	Generalised Water Supply Headworks Simulation using Network Linear Programming
WRP	Water recycling plant
WSUD	Water sensitive urban design
WWTP	Wastewater treatment plant

1. Introduction

1.1. Hawkesbury-Nepean Water Quality Modelling Project

The catchment of the Hawkesbury-Nepean River system covers approximately 21,700 km² and includes the Cataract, Cordeaux, Avon, Nepean and Hawkesbury Rivers. The area upstream of the water supply storage dams is approximately 10,000 km², which is just less than half of the total catchment area. Downstream of the dams, major tributaries include Grose River, South Creek, Cattai Creek, Colo River, Mangrove Creek and MacDonald River. Urban growth in the catchment and other parts of Sydney will place increasing demand on the river's resources. Climate change is expected to cause changes in the pattern and distribution of water in the landscape at the same time as the population of greater Sydney is expected to grow by approximately 33% between 2010 and 2036. It is planned that much of this urban growth will occur in the north-west and south-west growth sectors, which are mainly in the catchment of South Creek, although some of this urban growth will extend into other parts of the overall catchment. The increasing urbanisation of the catchment will not only result in a significant increase in demand for potable water, but will also result in changes in land use and commensurate point and diffuse sources of pollution.

The purpose of the Hawkesbury-Nepean Water Quality Modelling Project is to inform Sydney Water of the changes in hydrology, water quality and ecology under different scenarios with a coupled catchment-water quality model system. The model system has the ability to simulate hydrology, hydraulics and biogeochemical processes to examine the water quality benefits (or impacts) resulting from the different scenarios over broad spatial and temporal scales. **Figure 1-1** depicts the project study area and the area to be modelled.

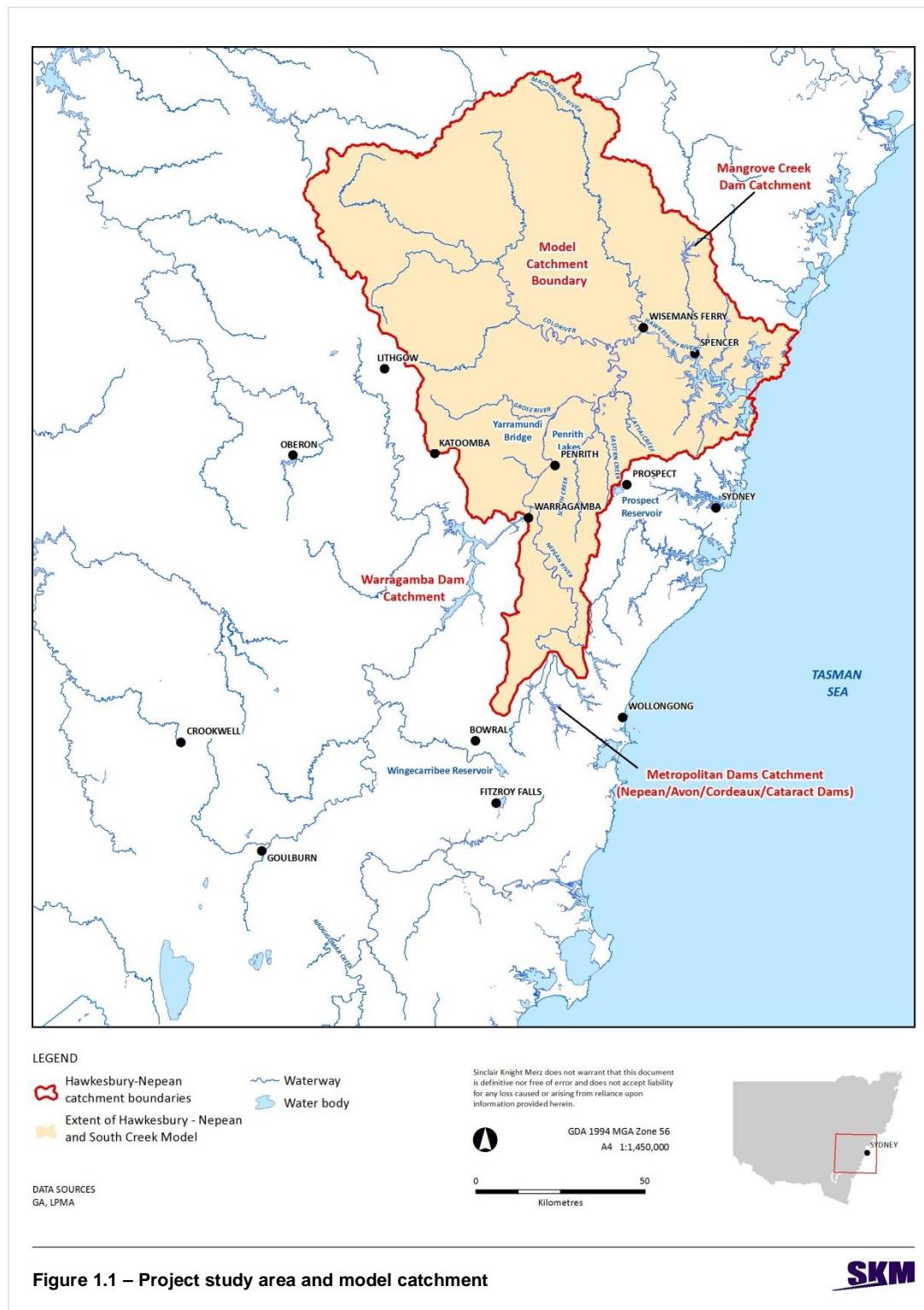
1.2. Hawkesbury-Nepean River and South Creek Model Phase

The model has been developed in two phases: a pilot model phase and a complete model phase. This report documents the complete model phase for the broader Hawkesbury-Nepean River and South Creek Model. The pilot model was limited to the Hawkesbury-Nepean River reach between Warragamba Dam, Wallacia Weir and Spencer. The Hawkesbury-Nepean River and South Creek Model (the complete model) encompasses the entire river and associated catchments downstream of Pheasants Nest and Broughton Pass diversion weirs on the Nepean River, downstream of Warragamba Dam to the Nepean River and then downstream to the sea with the oceanic boundary between Barrenjoey Head to the south and Box Head to the north. Catchment loads and water quality simulations are made over the entire spatial domain.

This Hawkesbury-Nepean River and South Creek model has been built for the express purpose of providing guidance on the likely quantitative differences in water quality and quantity when contrasting different catchment and environmental flow, wastewater and land use scenarios over time. Overall differences in the statistical properties of flow and constituent concentrations between scenarios can be appropriately inferred by comparing scenarios. This includes differences between mean values, or differences between values that may be exceeded for a given proportion of time. Moreover, while the model has been developed to simulate flow and constituent concentrations at specific locations for specific points in time, the real benefit of the model is in the assessment of the

Water Quality Modelling of the Hawkesbury-Nepean River System

overall outcomes of a particular suite of management actions across the spatial and temporal domain encompassed by the model compared to an alternative suite of actions or a “do nothing” scenario.



SINCLAIR KNIGHT MERZ

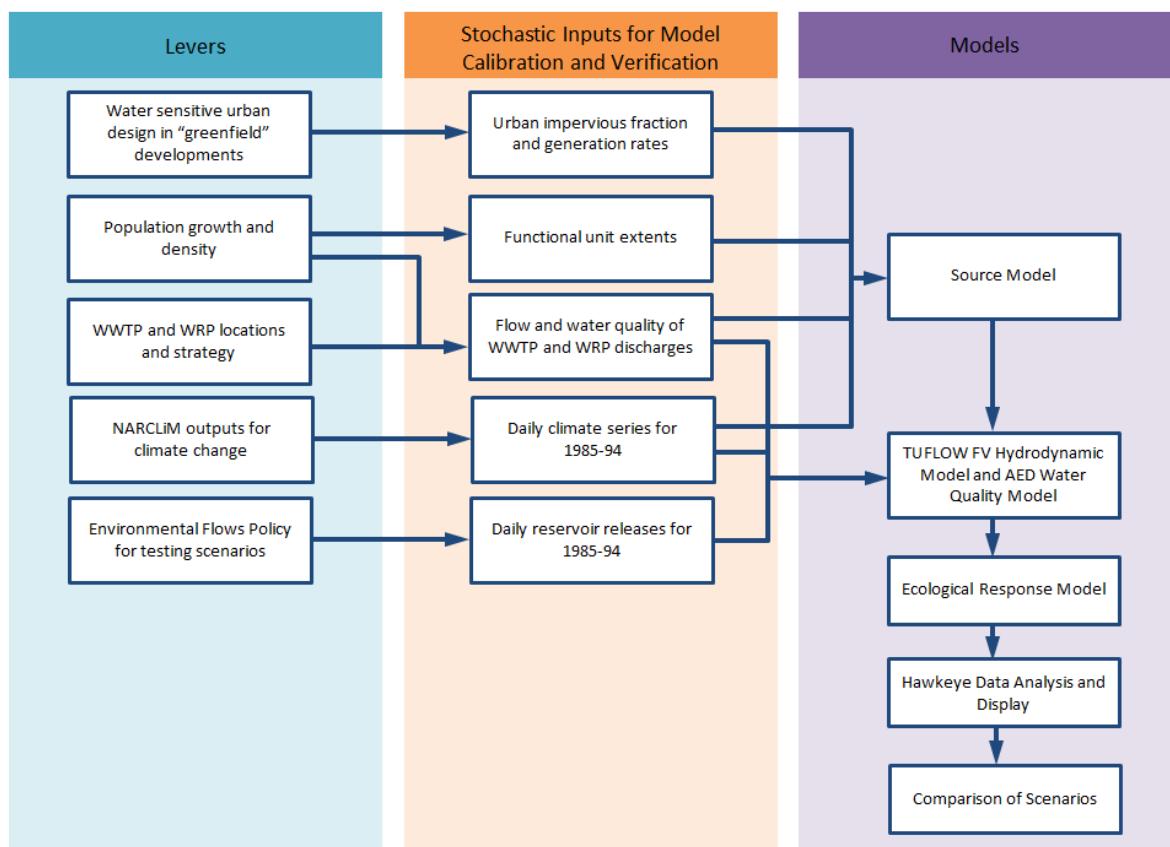
Figure 1-2 shows a conceptual diagram of the inputs to the different models used to simulate the water quality scenarios under investigation. The catchment model (Source) is used to simulate the generation of flows and water quality constituent loads from the catchments that feed into the Hawkesbury-Nepean River system. The catchment model also represents extractions of water by licensed diverters within the system. The daily time series of flows and water quality loads generated at the end of each of the tributary catchments are then input via a plug-in into the TUFLOW/AED hydrodynamic and water quality model for the Hawkesbury-Nepean River system. Results from both models at key reporting locations are exported into the Hawkeye database, so that results and comparisons between scenarios can be generated.

The complete TUFLOW/AED model incorporates daily time series of flow and water quality for releases from Warragamba Dam and releases made from Avon, Cataract, Cordeaux and Nepean Dams, which are input to the model as flows at Pheasants Nest and Broughton Pass weirs. Ten of the seventeen existing wastewater treatment plant discharges are included in the model as point inputs to the Source catchment model, with the remaining seven discharges as direct inputs to the TUFLOW/AED model. Irrigation extractions from the mainstream Hawkesbury-Nepean River occur directly from the TUFLOW/AED model while the remaining tributary extractions occur via the Source model.

Figure 1-2 also shows the changes made to model structure in order to facilitate testing of scenarios including:

- 1) Environmental release policies, which were represented as changes in the input time series for flow and water quality from Warragamba Dam to the TUFLOW/AED model;
- 2) Changes to WWTP and WRP discharges, represented as modified daily time series of loads from WWTPs and WRPs into either the catchment model or the TUFLOW/AED model depending on the actual or envisaged location of the effluent discharge;
- 3) Population growth as represented by changes in land use from non-urban to urban areas in the catchment model;
- 4) Implementation of water sensitive urban design in “green field” or new urban areas to limit the loads of sediment and nutrients generated from these areas. These are represented as changes in generation rates for constituents from the new urban land use in the catchment model.
- 5) Assimilation of nutrients in catchment streams subject to increasing urbanisation facilitated by decay functions within the catchment model; and
- 6) Climate change scenarios facilitated by the NARCLIM downscaling project and changed rainfall-runoff parameterisation of the catchment model.

Water Quality Modelling of the Hawkesbury-Nepean River System



■ **Figure 1-2 Conceptual Flow Chart of how the models work together to simulate scenarios**

The models used in this study have been calibrated and validated against observed data collected in the field via routine sampling programs, flow gauging or via specifically designed Campaign Monitoring Programs (CMPs).

Data was provided by:

- NSW Government agencies including Sydney Water, Sydney Catchment Authority, NSW Office of Water, Office of Environment and Heritage, Manly Hydraulics Laboratory and Land and Property information.
- Local Government agencies including Hornsby Council, Gosford Council, Blacktown City Council, Penrith City Council, The Hills Council, Hawkesbury City Council and Camden Council.
- National agencies including the Bureau of Meteorology and CSIRO.

The CMPs directly associated with the calibration of the Hawkesbury-Nepean River and South Creek Model include:

- 1) Event CMP – auto-samplers were installed at six locations to capture water quality data for multiple storm events, on both the rising and falling limbs of each event.

- 2) Acoustic Doppler Current Profiles (ADCP) CMP – currents were measured in the main channel of the Hawkesbury-Nepean River. Measurements were taken at six sites concurrently on two occasions (one spring tide and one neap tide).
- 3) Total and Dissolved Organic Carbon (TOC and DOC) CMP – TOC and DOC were measured monthly at existing Sydney Water routine water quality monitoring sites.

The field data are variable and potential sources of uncertainty include:

- Uncertainty in recording water levels at gauge sites;
- Uncertainty in converting water level recordings to gauged flows using stage versus flow rating curves, particularly when the rating curve has been extrapolated above the highest rated flow (Tomkins 2012);
- Changes in constituent loads in the sample between the collection point and the laboratory; and
- Uncertainty in estimating loads of constituents over a hydrograph from point measurements using laboratory analysis of samples.

For this project, a particularly important source of uncertainty in attempting to validate model predictions of constituent concentrations are differences in spatial and temporal sampling of the field data and the predictions produced by the models. The Source model produces the daily mean concentration across a cross section in a river system. By contrast water quality sampling programs capture the concentration at one point in the cross section (usually at the surface and usually near to one bank of the stream) at one instant on the day the sample is collected. Due to temporal variations in the concentration during the day and spatial variations in concentration across the cross section considered, the concentration recorded in the sample for a constituent may be considerably different from the true mean daily concentration of the same constituent passing through the cross section. As a result, direct comparison of the daily mean concentration estimated from the model with a field sample value will over represent the scatter between the modelled concentration and the true value of the mean daily concentration that could be achieved by more exhaustive field sampling.

Although the TUFLOW/AED model runs at sub-daily time step, the input time series are flows and constituent loads provided from the Source model that are constant throughout each day of the model run. For similar reasons to those set out above, comparing depth averaged constituent concentrations from TUFLOW/AED at one grid cell with concentrations collected from instantaneous sampling will over-represent the scatter between observed and modelled concentrations and may not necessarily reflect the performance of the model.

1.3. Hawkesbury-Nepean River and South Creek Model Assumptions

Table 1-1 lists the assumptions used in the Hawkesbury-Nepean River and South Creek Model.

■ **Table 1-1 Hawkesbury-Nepean River and South Creek Model Assumptions**

Model	Assumptions
Structure	The complete model is fully three dimensional across the entire domain.
Bathymetry	Riffle data was included in the complete model. Some alterations to the riffle zone bathymetry were required for model stability/runtime optimisation.
LiDAR	LiDAR data was used in the region around Penrith to include some flood storage capability in the complete model.
Warragamba environmental flow	Quality of Warragamba eflow releases was extrapolated from measured water quality at 0-6 m below the surface. This is assumed adequate for this purpose. For calibration, the model used actual recorded releases from Warragamba Dam.
Upper Nepean environmental flow	Calibration of the model used actual recorded releases from Warragamba Dam and actual gauged flows from Broughton Pass and Pheasants Nest (largely driven by actual releases from the Upper Nepean Dams).
Protection of environmental flow	In calibration model runs (2006, 2007 and 2011 period), there was no protection of environmental flow releases and irrigators were assumed to take their full unrestricted demand.
Penrith Weir	All weirs from Pheasants Nest / Broughton Pass to Penrith were included in the complete model and appropriate head/discharge relationships used to define crest overflows.
Upper Nepean Weirs	All Upper Nepean weirs were included as a structure within the model, with an appropriate head to flow relationship to simulate their effect on river flow processes.
St Marys Advanced Water Recycling Plant	Actual recorded releases from St Marys Advanced Water Recycling Plant were used for calibration of the model, with water quality also determined from monitoring data at the outlet of the plant.
Penrith Lakes	No inputs to, or releases from, Penrith Lakes were included in the model.
Overbank Flows	The complete model includes flood storage capability in the Penrith region and LiDAR data was used to set the bathymetry in this region. Elsewhere in the model is contained within the river bank. Note that the model is not a flood model.
Water extraction – agriculture	For the calibration period, the model assumed unconstrained extractions, based on the long term extraction limits in the Water Sharing Plan: Upper Nepean and Warragamba Extraction Management Unit (excluding SCA) is 11 GL; Hawkesbury & Lower Nepean EMU is 71 GL.
Export rates	The model used Event Mean Concentration (EMC) and Dry Weather Concentration (DWC) models for generation of most constituents for most land uses. Parameters for the generation models were obtained from literature, documented in the model calibration report and checked against water quality sampling and campaign monitoring data (where appropriate data was available). Some checks of mean annual generation rates (in tonnes of constituent per unit catchment area per year) were performed against OEH data.



Water Quality Modelling of the Hawkesbury-Nepean River System

Model	Assumptions
Rainfall runoff	Modelled using Sacramento rainfall runoff models, calibrated to observed flow time series at gauges within the model domain. Parameters for each functional unit are as documented in the calibration model report.
Rainfall data	<p>Rainfall data was interpolated onto a 0.01° resolution latitude / longitude grid (approximately 1 km spatial resolution) from the 449 rainfall sites. Spatial averages of daily rainfall data were extracted for each of the 375 model subcatchments from the gridded data. The interpolation technique adopted was to weight the data from rainfall sites for each grid cell according to weightings determined using a Kriging algorithm. The algorithm used the 10 sites with highest weightings that recorded valid data for the whole month. The interpolated monthly totals at each grid cell were disaggregated using the pattern of daily rainfalls from the nearest rainfall gauge that contained valid data for the month.</p> <p>Daily time series of rainfall were determined for each subcatchment of the model by averaging the daily totals from the gridded rainfall fields for all grid cells overlapping the boundary of each subcatchment.</p> <p>Climate change was not considered during model calibration runs.</p>
Evaporation data	<p>Point potential evapotranspiration (PPET) was interpolated onto 0.01° grids on a daily basis from mean monthly PPET grid data provided by the Bureau of Meteorology. The monthly data were disaggregated to a daily pattern by interpolating pan evaporation recordings from 26 sites in the catchment. The interpolation procedure used the inverse distance squared weighting technique to the five nearest rainfall gauges to the centre of each grid cell.</p> <p>Daily time series of PPET were determined for each subcatchment of the model by averaging the daily totals from the gridded rainfall fields for all grid cells overlapping the boundary of each subcatchment.</p> <p>Climate change was not considered during model calibration runs.</p>
Decay/transformation	<p>Exponential decay functions were applied for nutrients (TN, NOx, TKN, NH₄, TP and FRP) in five reaches of the catchments of South, Eastern and Cattai creeks. Decay rates were estimated using long term water quality sampling from sites that were upstream and downstream of each reach where decay models were applied.</p> <p>No decay or transformation functions were allowed for any other parts of the model or constituents. Although it is recognised that some other constituents, particularly the bacterial constituents, would be likely to undergo transformations between where they are generated in the landscape and where they are exported from the catchment model to the TUFLOW/AED model, the generation rates applied for these constituents represent net generation rates at the catchment outlet that implicitly allow for decay and transformation within the catchment.</p>
Sediments	<p>Full sediment dynamics is included in the complete model. This includes sediment settling and resuspension (both controlled by hydrodynamic shear also calculated within TUFLOW) and bed storage simulation.</p> <p>The sediment model was spun up for a full two year period prior to the commencement of the water quality calibration period to ensure that the bedform model was initialised with an appropriate distribution of bed sediment.</p>
IQQM	
Extractions	For the calibration runs, diversions were modelled using unrestricted demands estimated from CropMod2 from IQQM and incorporated into the Source model.

1.4. Structure of This Report

A summary of the information contained within each section of this report is provided below.

Chapter 1 – Introduces the project, its broad strategic context and provides a brief description of the study area.

Chapter 2 – Outlines the structure of the Source model. Chapters 3 to 9 relate to this model.

Chapter 3 – Identifies key spatial inputs to the catchment model, including descriptions of the model network set-up and the development of the functional units.

Chapter 4 – Describes the climate data used in the model.

Chapter 5 – Outlines how the component model types and parameters were selected for the runoff generation, the runoff routing, the constituent generation rates and the in-stream constituent routing and transformations.

Chapter 6 – Describes how key input time series data were developed such as dam releases, water treatment plant discharges and extractions for irrigation.

Chapter 7 – Details how the parameters of the rainfall runoff models were derived for the different functional units through the calibration process.

Chapter 8 – Details how generation rates of the constituents were derived for the different functional units through the calibration process.

Chapter 9 – Describes a customised model plug-in to export results from the Source model to the TUFLOW/AED model.

Chapter 10 – Introduces the TUFLOW hydrodynamic model. Chapters 10 to 13 relate to this model.

Chapter 11 – Describes the data collation and review process.

Chapter 12 – Describes the set-up of the model.

Chapter 13 – Describes the model calibration and validation process.

Chapter 14 – Provides conclusions and recommendations for enhancements to the model to be undertaken during the complete model phase of the project.

2. Overall Structure of the Source Model

2.1. Selection of the Source Modelling Platform

The Source modelling platform was used as the catchment model for this project (Welsh et al., 2012). The version that was used for the calibration model was version 3.1.

2.2. Functional Unit-Subcatchment-Node-Link Structure of the Source model

Source models river systems as a series of nodes interconnected with links. This sequence of nodes and links forms a network in which water and materials are fed at the nodes and routed along the links. The nodes and links model the processes of interest such as runoff generation, constituent generation and filtering.

Typically a node is placed where:

- Flow and/or constituents enters the river network, such as a WWTP or WRP discharge;
- Flow and/or constituents exits the river network, such as extractions for irrigation;
- Model outputs such as flows and/or constituent concentrations, are required, such as at stream gauging stations or water monitoring sites in order to compare simulation and observation; and/or
- A confluence between two streams.

In addition to the places of interest listed above, nodes can be added in order to break a large subcatchment into several subcatchments of desired size.

Each link defines a reach. Links act to store water and to route or process water and constituents passing between nodes.

Functional units (FUs) are areas within a subcatchment that have similar behaviour in terms of runoff and/or constituent generation. These FUs are based on combinations of land use or cover (e.g. forest, crops, urban areas), management activities, position in the landscape (flat, hillslope and ridge) and/or soil type. Each subcatchment is composed of one or more FUs.

2.3. Run Period for the Hawkesbury-Nepean River and South Creek Catchment Calibration Model

There have been considerable changes historically to the location and treatment technologies used for the WWTP and WRPs. Daily flows and regular water quality sampling data on the outflows from the plants were only relevant to current technologies from 1 July 1998 through to 31 December 2011. Therefore two versions of the calibration model were produced. They are:

- 1) Version 1 is a flow only model, which has an overall run period from 11 November 1976 through to 31 December 2011. This version of the model was used for calibration and validation to recorded flow data only.

- a. Of this period, calibration and validation was performed to recorded flows (where available) for sites that are downstream of a WWTP or WRP from 1 July 1998 to 31 December 2011 only (concurrent with the daily plant discharge data) and
 - b. Of this overall period, calibration and validation was performed to recorded flows (where available) for sites that are on tributaries not downstream of a WWTP or WRP from 1 January 1978 to 31 December 2011, allowing for just over 1 year of model “warm up” period.
- 2) Version 2 includes both flow and water quality constituents in the model. It has an overall run period from 1 January 1998 through to 31 December 2011. This version was used for validation plots of constituent water quality data.

It was verified that both models produce identical time series of flows for the overlapping period (1 July 1998 through to 31 December 2011, after allowing for a reasonable warm up period for each model). For flow calibration and validation, the recorded flow data at gauges was randomly separated into calibration years (approximately two-thirds of the data at each site) and validation years (the remaining data, approximately one-third of the data at each site). Only the calibration data set was provided to the Source model and modellers for calibration purposes. The random allocation of calibration and validation years for flow data is discussed in more detail in Section 7.3.2.

Modelled flow and water quality constituent outputs from the Source model for the period 1 January 2006 to 31 December 2007 was provided as input to the calibration and validation of the hydrodynamic and water quality model (TUFLOW/AED). The 2-year modelled period has the largest amount of data available in terms of flows and constituents within the estuary and contains both dry and wet periods.

Modelled flow outputs from the Source model were also provided for the period 1 November 2011 to 31 December 2011, as input to calibration of the hydrodynamic model over the period that was concurrent with the Acoustic Doppler Current Profiling (ADCP) measurements taken during the ADCP CMP.

3. Spatial Inputs to Catchment Model

3.1. Identification of Key Model Locations

The following section describes key model locations, including upstream boundary conditions, wastewater treatment plant (WWWP)/water recycling plant (WRP) inputs, stream-flow gauges and water quality monitoring locations.

Key model locations described in subsequent sections are shown in **Figure 3-1**.

3.1.1. Upstream Limits of the Hawkesbury-Nepean River and South Creek Model

The upstream boundary locations for the model are:

- Immediately downstream of Warragamba Dam on the Warragamba River;
- Immediately downstream of Mangrove Creek Dam on Mangrove Creek;
- Cataract River at Broughton Pass Weir; and
- Nepean River at Pheasants Nest.

Daily time series of flow and water quality are provided at each of these four locations.

Flows at each location represent a combination of controlled releases and spills from the water supply reservoirs that are located upstream of each of these locations. For the calibration period for the hydrodynamic model (2006, 2007 and Nov-Dec 2011), daily recorded flow time series were available at each of these locations. Some infilling was required for short periods of missing data in the time series at each location. This infilling was undertaken using linear regression or correlation with flows Camden or Penrith. This was only required on isolated days to ensure full time series were available. Releases from Mangrove Creek Dam throughout the hydrodynamic model calibration period were generally low and virtually all of these releases were then diverted from the diversion weir located downstream on Mangrove Creek. Mangrove Creek dam did not spill during the hydrodynamic model calibration period.

An analysis of water quality sampling data was performed for the sites immediately downstream of Warragamba Dam, Broughton Pass and Pheasants Nest. The analysis undertaken were correlations between flow and constituent concentrations (i.e. power curve functions). Since the flows at these points almost exclusively represent controlled releases from dams, the constituent concentrations at each location demonstrate no correlation with flow rate and are relatively consistent. Mean concentrations were therefore applied for each water quality constituent, based upon:

- Mean of monitored constituent concentrations for Cataract River at Broughton Pass Weir;
- Mean of monitored constituent concentrations for Nepean River at Pheasants Nest; and
- Mean of monitored constituent concentrations in the upper 6 metres of storage at Warragamba Dam, for releases from Warragamba Dam.

Water Quality Modelling of the Hawkesbury-Nepean River System

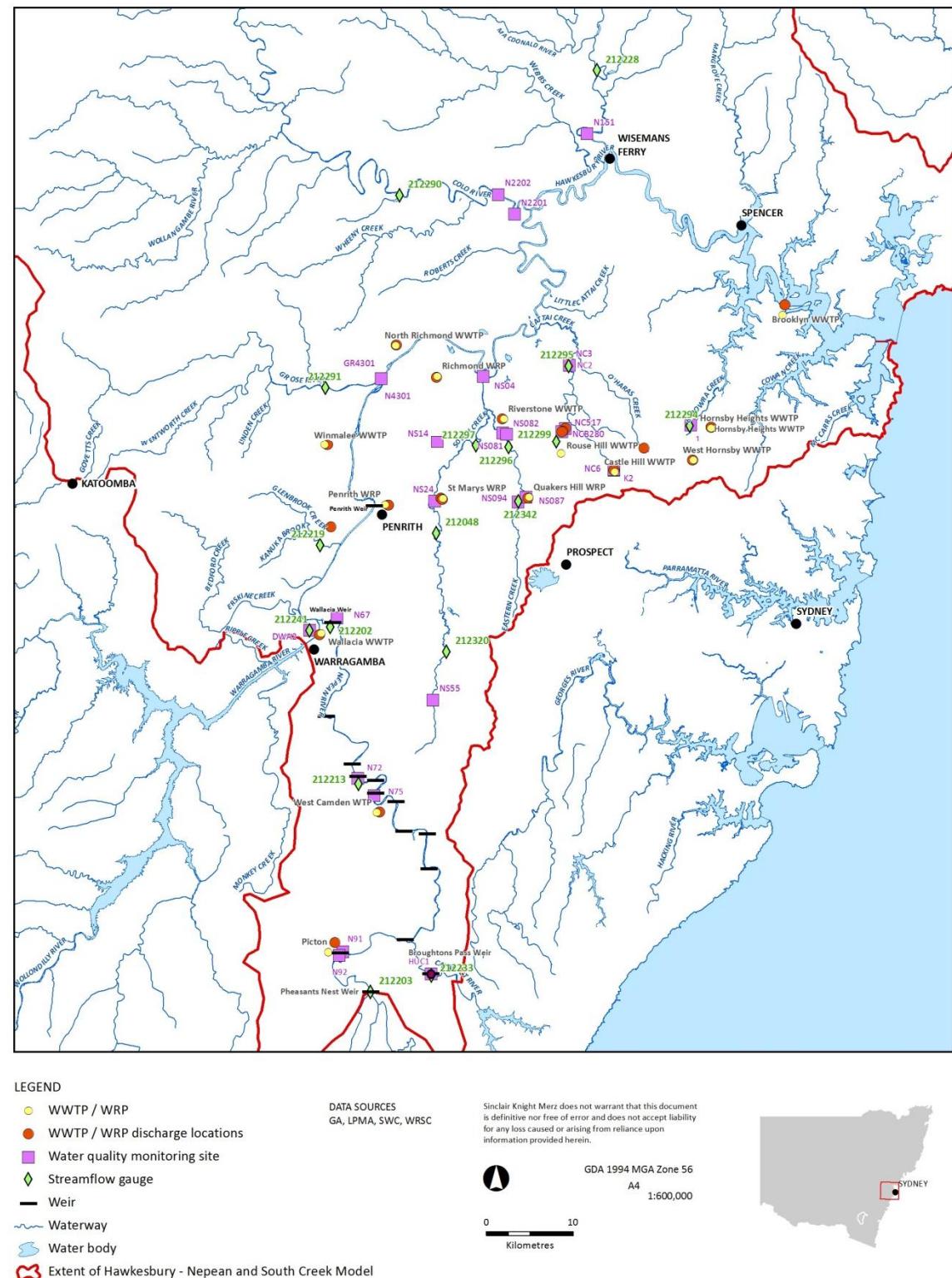


Figure 3.1 – Location of Key Model Locations within the Catchment

SINCLAIR KNIGHT MERZ

3.1.2. Wastewater Treatment Plant and Recycled Water Plant Discharge Locations

The Hawkesbury-Nepean River and South Creek Model incorporates the discharges of WWTPs and WRPs at the locations listed in **Table 3-1**.

The WWTP and WRP site information listed in **Table 3-1** was provided by Sydney Water for all WWTP/WRP locations within the model domain. Locations of WWTP and WRP discharge monitoring points, which in some cases may be distant from the site, were provided by Sydney Water and are listed in **Appendix A**.

■ **Table 3-1 Wastewater Treatment Plant and Water Recycling Plant Discharge Details**

Site	Discharge Details
Penrith WRP ^b	Re-use locally and at Hickey's Park Playing Fields.
	Some excess discharged to Boundary Creek.
Quakers Hill WRP ^a	Re-use locally and at Ashlar/Medalist Golf Course.
	Some excess discharged to Breakfast Creek.
St Marys WRP ^a	Re-use locally and at Dunheved Golf Course with remainder discharged to Nepean River. Some excess discharged to South Creek (via an unnamed creek).
Richmond WRP ^a	Re-used for irrigation at the UWS Richmond Campus. Excess overflows are discharged to Rickabys Creek.
North Richmond WWTP ^b	Discharged to Redbank Creek thence to the Hawkesbury River.
Riverstone WWTP ^a	Discharged to Eastern Creek thence to South Creek.
Wallacia WWTP ^a	Discharged to Warragamba River.
Rouse Hill WRP ^a	Recycled back to households for non-potable use. Excess discharged to Second Ponds Creek to Cattai Creek.
Castle Hill WRP ^a	Discharged to Cattai Creek.
Brooklyn WWTP ^b	Discharged to Hawkesbury River (at the Peats Ferry Bridge).
Winmalee WWTP ^b	Discharged into an unnamed Creek (adjacent to the treatment plant). The unnamed Creek drains into the Winmalee Lagoon (an arm of the Nepean River at Yarramundi).
Hornsby Heights WWTP ^a	Discharged to Calna Creek in the Berowra Creek catchment.
Picton WRP ^b	Re-used on-site for agricultural irrigation. Precautionary discharge to Stonequarry Creek.
West Camden WRP ^a	Re-used at the Agricultural Institute. Remainder discharged via Matahill Creek to the Nepean River.
West Hornsby WWTP ^a	Discharged to Waitara Creek thence to Berowra Creek.
McGraths Hill ^b	Discharged to wetlands adjacent to South Creek.
South Windsor ^b	Discharged to South Creek thence to Hawkesbury River.

^a Locations modelled in the Source model.

^b Locations modelled in TUFLOW.

3.1.3. Stream-flow Gauges

Ten stream-flow gauging stations, shown in **Figure 3-1** were used either for calibration or validation of the runoff generation and routing models to gauged flows. Of these, four are located on the left bank and are therefore representative of mostly forested catchments, four are on the right bank encompassing several land use types while two are on the Upper Nepean River and also represent mixed runoff catchments and releases from the Upper Nepean dams. The flows recorded at these stream-flow gauging stations are representative of the hydrologic response of all the FUs present in the model. Comparisons between observed and simulated flows at these locations enable us to calibrate the parameters of the rainfall-runoff models for all FUs. Information regarding these gauging stations is provided in **Table 3-2**.

- **Table 3-2 Stream gauging stations used for calibration and validation of flows and runoff generation**

Station Number	Station Name	Data Start Year
212320	South Creek at Mulgoa Road	1970
212219	Glenbrook Creek at Jellybean Pool	1990
212228	MacDonald River at St Albans	1990
212290	Colo River at Upper Colo	1975
212291	Grose River at Burrallow	1987
212296	Eastern Creek at Riverstone	1982
212295	Cattai Creek at Maraylya	1980
212294	Berowra Creek at Galston Gorge	1994
212202	Nepean River at Wallacia	1976
212297	South Creek at Richmond Road	1998
212213	Nepean River at Mt Hunter Weir	1987

3.1.4. Water Quality Monitoring Sites

Data from 26 water quality monitoring sites were used either to derive generation rate relationships (refer to **Section 8.2**) or for comparison between observed and simulated constituent concentrations (refer to **Section 8.5**). Data from four water quality monitoring sites were analysed to derive generation rate relationships used in the Source model for forested catchments – these sites were located on the Colo (two sites), Grose and MacDonald rivers. Information regarding these water quality sites is provided in **Table 3-3**.

For the purposes of comparing total constituent loads and separating the record into periods dominated by baseflow and quickflow (which in turn provide guidance on generation rates between dry weather and event runoff conditions), flow gauging data was used from nearby streamflow gauges. The streamflow gauge numbers and names are also shown in **Table 3-3**. In some cases there was no streamflow gauge that would be sufficiently representative of flow at the water quality monitoring site, so for these locations modelled flows from the Source model at the location were used to estimate the daily time series of flows.



Water Quality Modelling of the Hawkesbury-Nepean River System

An analysis was also performed to develop a relationship between flow and water quality constituent loads at Warragamba Dam, Broughton Pass and Pheasants Nest. These relationships were developed to create boundary input time-series of water quality for the TUFLOW/AED model, based on recorded flows. Information regarding these water quality sites is provided in **Table 3-4**.

The water quality measurements of interest for the Source model include: total nitrogen (TN), oxidised nitrogen (NO_x which refers to the sum of NO_2 and NO_3), total Kjeldahl nitrogen (TKN which includes organic nitrogen, ammonia and ammonium), ammonium (NH_4^+), total phosphorus (TP), filtered reactive phosphorus (FRP), silicates (SiO_2), total suspended solids (TSS), Enterococci and salinity.

- **Table 3-3 Water quality sites used for comparison between observed and simulated constituent concentrations and loads**

Waterway	Water quality station ID	Station name	Period of record		Streamflow Gauge Number and Name
Colo River	N2201	Lower Colo River 4 km u/s Hawkesbury River	1984	1988	212290, Upper Colo
	N2202	Colo River at Morans Rock, Putty Road Bridge	2008	2010	212290, Upper Colo
Grose River	GR4301/ N4301	Grose River u/s Nepean River at Yarramundi Reserve, Springwood Rd	1984	2001	212291, Burrallow
MacDonald River	N151	MacDonald River 3 km u/s Hawkesbury	1984	1988	212228, St Albans
South Creek	NS04	Lower South Creek Fitzroy Bridge	2008	2010	*
	NS14	South Creek at Richmond Road	1990	2011	*
	NS24	South Creek u/s St Marys WWTP	1997	2009	*
	NS55	South Creek Bringelly Road	1989	1995	212320, Mulgoa Road
Eastern Creek	NS081	Eastern Creek d/s Riverstone WWTP 300m d/s outlet	1995	2008	212296, Riverstone
	NS082	Eastern Creek u/s Riverstone WWTP	1995	2011	212296, Riverstone
	NS094	Eastern Creek u/s Breakfast Creek	1998	2001	212342, Quakers Hill
Breakfast Creek (tributary of Eastern Creek)	NS087	Breakfast Creek at Station Rd d/s Quakers Hill WWTP	1995	2011	*
Cattai Creek	NC2	Cattai Creek - at Maraylya, Pitt Town Rd	1990	2010	212295, Maraylya
	NC3	Cattai Creek - at Maraylya, Pitt Town Rd	1990	2010	212295, Maraylya

Waterway	Water quality station ID	Station name	Period of record		Streamflow Gauge Number and Name
	NC6	Cattai Creek - d/s Castle Hill WRP u/s confluence w Second Ponds Creek	2007	2010	*
	K2	Cattai Creek - at end of Connelly Way d/s Castle Hill WWTP	2005	2011	*
Second Ponds Creek (tributary of Cattai Creek)	NC517	Second Ponds Creek - Outflow of wetlands Rouse Hill WRP	2007	2010	212299, Windsor Road
	NCB280	Second Ponds Creek at Rouse Hill WRP	1998	2010	212299, Windsor Road
Berowra Creek	1	Galston Gorge	1994	2012	212294, Galston Gorge
Nepean River	N72	Nepean River at Cobbity Road Bridge	1984	2001	212216, Camden Weir
	N75	Nepean River at Sharpes Weir	1984	2011	212216, Camden Weir
	N91	Nepean River at Maldon Bridge	1985	2008	212208, Maldon Weir
	N92	Nepean River at Maldon Weir	1985	2011	212208, Maldon Weir

* No streamflow gauge that would be appropriate for this water quality monitoring site. Baseflow and quickflow periods were identified using the daily flow time series generated from the Source model at this location.

■ **Table 3-4 Water quality sites used as point inputs**

Waterway	Water quality station ID	Station name	Period of Record		Streamflow Gauge Number
Warragamba River	DWA2 at 3 m depth	Warragamba Dam	1996*	2005*	212241
Nepean River	N92	Nepean River d/s Pheasants Nest Weir	1985*	2011*	212203
Cataract River	HUC1	Cataract River at Broughton Pass Weir	2007*	2011*	212233

* Years of data availability varied by constituent, with maximum records from years indicated, with some constituents being available for considerably less years.

3.2. Subcatchment Boundaries and Node-Link Network

The subcatchment boundaries were created using ArcGIS Hydrotools v1.4 (for ArcGIS 9.3.1) and a Digital Elevation Model (DEM), which has a horizontal resolution of 25 m. The DEM was obtained from the Division of Local Government from within the NSW Department of Premier and Cabinet and was hydrologically corrected, to remove spurious pits and dams before use. In addition to the DEM, boundary locations were based on the location of stream-flow gauges and waterway

confluences. The model includes a total of 555 subcatchments. Across the model, the mean area of the subcatchments is 21.2km².

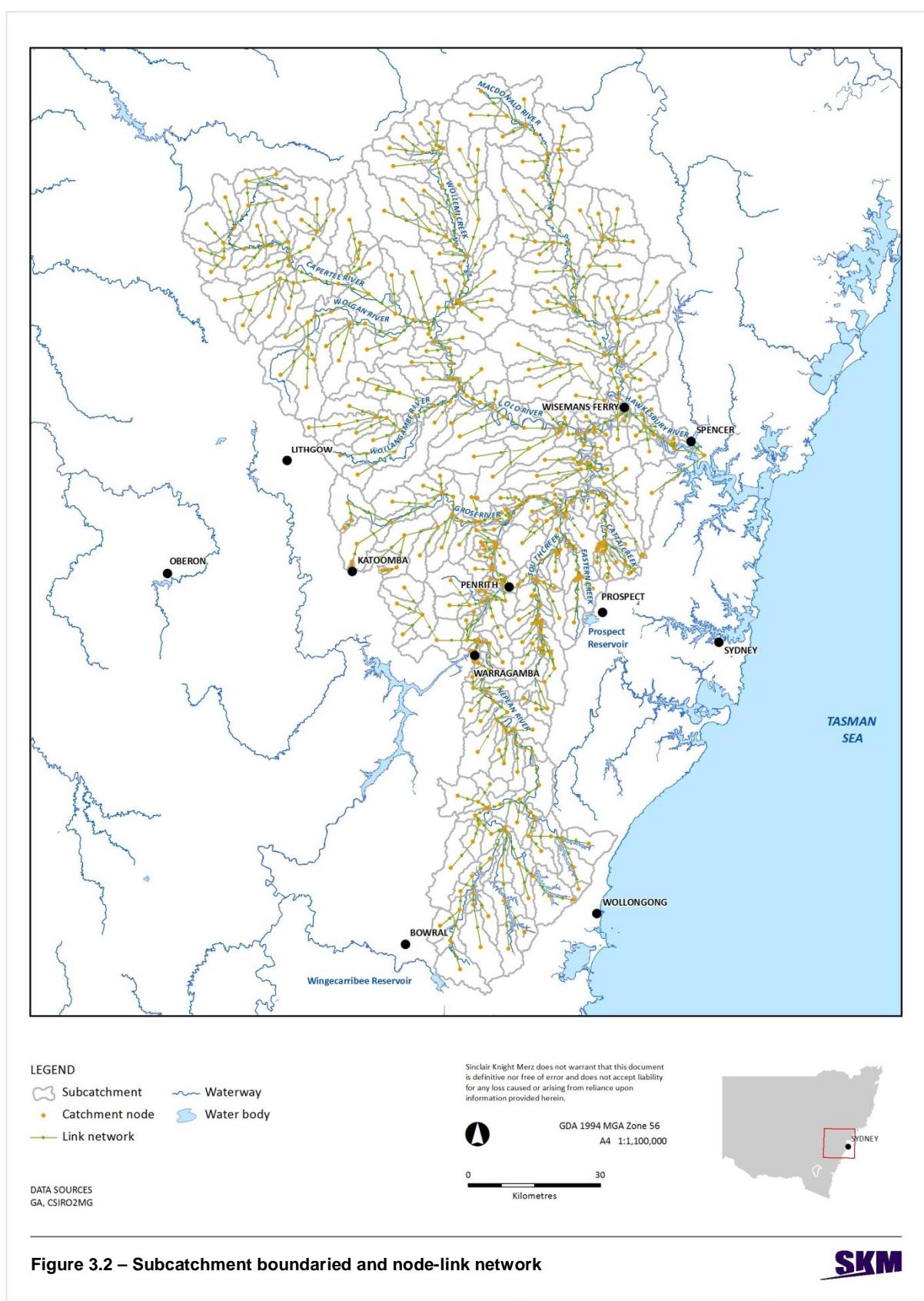
The subcatchment sizes fall within two groups:

- 232 of the subcatchments are less than 10 km² each in area and these are mainly located along the main stem of the Upper Nepean River and along the lower part of the South Creek catchment, where a large number of smaller catchments were required to provide adequate delineation of local contributions to flow and load for integration with the TUFLOW/AED model;
- 323 of the subcatchments are greater than 10 km² in area (varying in area between 10 and 119 km², with a mean value of 33.3 km²) and combined, these produce flows and constituent loads from 91% of the total area modelled.

A Node-Link Network was also created using ArcGIS. A node was created for each catchment, and a link created between each upstream and downstream catchment node. The network was created using the subcatchments and project DEM. A manual review of the network was then performed and corrections made, based on visual examination of the terrain layer. Irrigation extractions were then included by modifying the node-link network adding new nodes at the approximate location of each extraction point and adding new links to reconnect the additional nodes back into the original network.

The catchment boundaries and node link network are shown in **Figure 3-2**.

Water Quality Modelling of the Hawkesbury-Nepean River System



4/07/2013 | I:\ENVR\Projects\EN03013\Technical\GIS\Spatial\Directory\ArcGIS\HN_007\Fig3_4_NodeLink_v4b_r1v1.mxd
Sydney Spatial Team - Prepared by : MS
Checked by : JC

SINCLAIR KNIGHT MERZ

3.3. Functional Units

The Functional Units (FUs) represent areas of similar hydrological response. For the Hawkesbury-Nepean River and South Creek Model, FUs were defined by land use types.

The FUs are based on the NSW Office of Environment and Heritage (OEH) land use dataset (1999-2006). There was a small area of approximately 679 km² near Hornsby not covered by this OEH layer. This area was in-filled with a 50 m land use dataset created by SKM in 1995, supplemented by visual inspection of 2011 AUSIMAGE imagery. The use of this 1995 land use layer is considered acceptable as change to land use in that area is considered negligible between 1995 and current.

The OEH and SKM land use datasets were classified into eight initial FUs: cropping; peri-urban; mining and quarrying; urban; water; forest; grazing; and horticulture. The mapping of OEH and SKM dataset land use categories to FUs is provided in **Table 3-5** and **Table 3-6**, respectively.

■ **Table 3-5 Mapping of OEH land use categories to FUs**

OEH Land Use Category	Functional Unit
Cropping	Cropping
Horticulture	Horticulture
Conservation Area	Forest
Tree & Shrub Cover	Forest
Grazing	Grazing
Intensive Animal Production	Peri-urban
Mining & Quarrying	Mining and quarrying
Special Category	Each polygon was assessed individually and subsequently assigned to the most appropriate FU
Transport & Other Corridors	Urban
Power Generation	Urban
Urban	Urban
River & Drainage System	Water
Wetland	Water

■ **Table 3-6 Mapping of SKM land use categories to FUs**

OEH Land Use Category	Functional Unit
Open land	Grazing
Main roads	Urban
Woody	Forest
Water bodies	Water
Low density urban	Urban
Medium density urban	Urban
High density urban	Urban
Light industrial / commercial	Urban

OEH Land Use Category	Functional Unit
Heavy industrial	Urban
CBD	Urban

Additional information associated with the OEH “Special Category” land use was used to assign such areas to a particular FU. The mapping of OEH dataset “Special Category” land use to FUs is provided in **Table 3-7**.

■ **Table 3-7 Mapping of OEH Special Category land use to FUs**

OEH Land Use Detailed Description (“special category” land use)	Functional Unit
Land vested with an aboriginal land council	Forest
Production from dry land agriculture and plantations	Cropping
Farm infrastructure – house, machinery & storage sheds and garden areas	Peri-urban
Defence facilities	Peri-urban

Some OEH land use types assigned to the Urban FU using the rules in **Table 3-5** had Detailed Description values that subsequently re-assigned the areas as Peri-urban. The Detailed Description field values used in such re-assignments are listed in **Table 3-8**.

Figure 3-3 depicts the distribution of the final land use categories and the total areas assigned within the Source model to each FU are listed in **Table 3-9**.

■ **Table 3-8 The OEH Urban category assigned to the Peri-urban FU**

Land Use Detailed Description
Areas irrigated with effluent from sewage disposal ponds
Cemetery
Glider field for recreational activities
Golf courses, greens and fairways with internal housing allotments
Hobby farm (as distinct from rural residential. Small, single blocks no longer used for rural purposes
Hobby farm (as distinct from rural residential. Small, single blocks no longer used for rural purposes - with a woody vegetation cover
Landfill (garbage)
Rural Quarantine Site (animals, crops, horticulture & pastures)
Rural recreation. Blocks are isolated and not associated with an urban area
Rural residential
Rural residential - with a woody vegetation cover of woodland
Sewage disposal ponds
Urban recreation

■ **Table 3-9 Total area covered in model by each functional unit**

Functional Unit	Total Area (km ²)	Proportion of catchment (%)
Forest	8735.0	74%
Cropping	7.3	<1%
Horticulture	83.8	<1%
Grazing	1574.2	13%
Peri-urban	549.3	5%
Mining & Quarrying	39.3	<1%
Urban	560.5	5%
Water	228.4	2%
Total	11777.8	

Water Quality Modelling of the Hawkesbury-Nepean River System

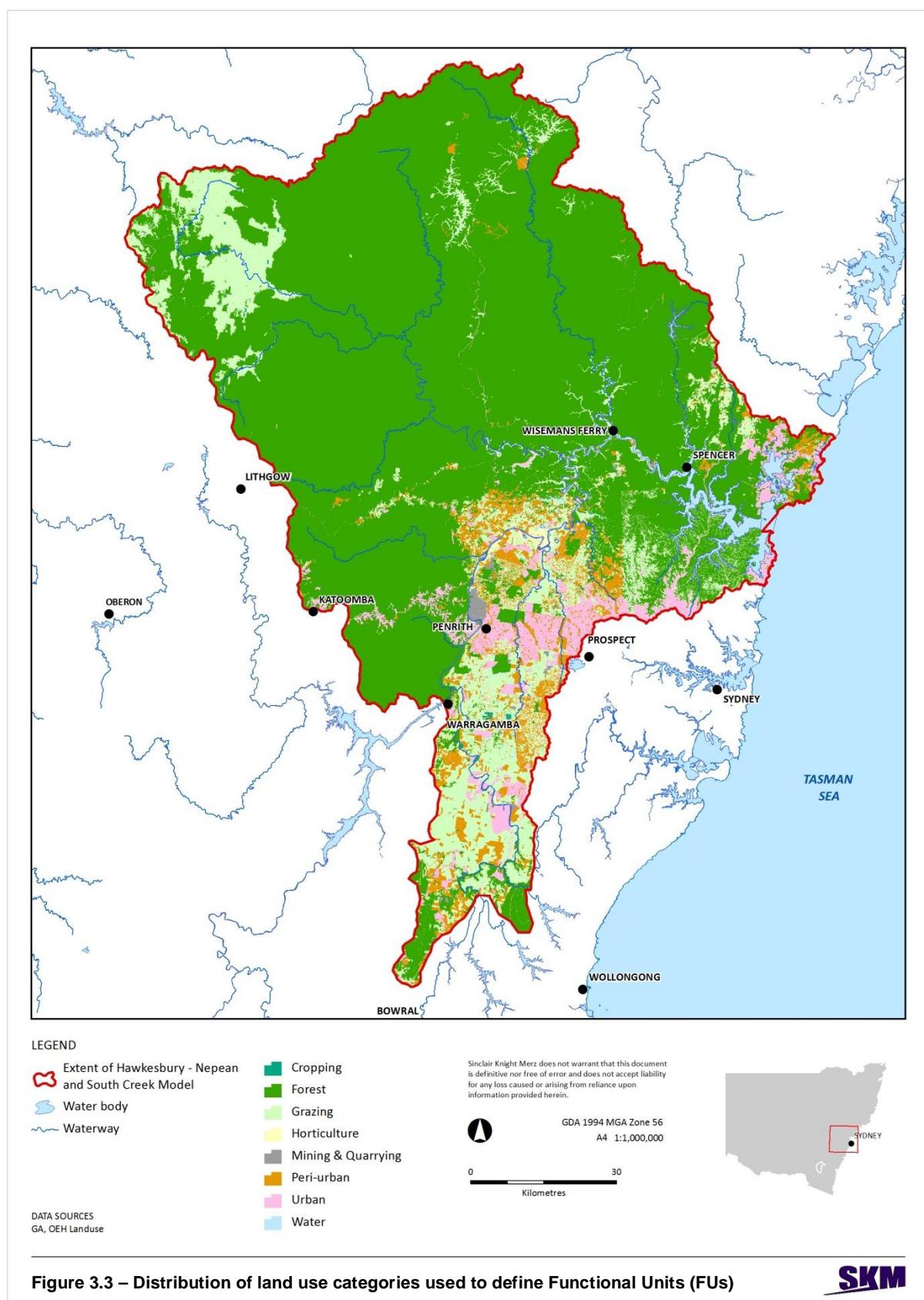


Figure 3.3 – Distribution of land use categories used to define Functional Units (FUs)

4/07/2013 | I:\ENVR\Projects\EN03013\Technical\GIS\Spatial_Directory\ArcGIS\HN_007_Fig3_5_LandUse_FU_v5b.mxd
Sydney Spatial Team - Prepared by : MS
Checked by : JC

SINCLAIR KNIGHT MERZ

4. Climatic Inputs to Catchment Model

4.1. Daily Rainfall

4.1.1. Daily Rainfall Stations

Data from 478 stations were used to grid the rainfall input to the Source model of which 276 are operated by the Bureau of Meteorology, 33 by Sydney Catchment Authority, 167 by Sydney Water and two by New South Wales Office of Water. The list of the stations used for derivation of daily rainfall grids is given in **Appendix B**. **Figure 4-1** shows the location of rainfall stations in the Hawkesbury-Nepean catchment.

Rainfall is recorded at 9am. The data covers the period between 1861 and 2012.

4.1.2. Development of Daily Rainfall Grids

The Source model has the capacity to import gridded rainfall. This capacity enables the model to represent the spatial and temporal variability in rainfall across the study area.

A computer program was developed to form grids of daily rainfall data in the correct format to be imported into the Source model. The grids have a spatial resolution of 0.01° of latitude by 0.01° of longitude, reference to the Geodetic Datum of Australia (1994). This is approximately equivalent to each grid cell being 0.92 km in the east-west direction by 1.11 km in the north south direction. The gridding procedure involves the following steps:

- 1) At each of the 478 daily rainfall stations, the daily totals are accumulated to form monthly totals at each site. Any station that has more than one day of data missing or poor quality data (quality code greater than 150) in a particular month has that monthly total flagged at that site as "missing data".
- 2) For the centroid of every grid cell, a weighting factor for monthly rainfall totals is computed, using an ordinary Kriging algorithm, which is described in more detail in Section 4.1.3.
- 3) For each grid cell in each month, the ten gauges with the highest weighting factor that had a valid (not missing) monthly total for the month are identified.
- 4) For each grid cell in each month, the monthly total is computed by taking the weighted mean of the monthly total at the ten nearest rainfall gauges, with the weighting factor computed using the ordinary Kriging algorithm. Since the weighting factor will typically be highest for gauges that have the lowest adjusted distance to the centroid of each grid cell, gauges that are near to the grid cell and/or at a similar elevation to the grid cell will typically have the highest weighting factor and are therefore more likely to be used in interpolation of the monthly rainfall total.
- 5) For each grid cell in each month, the calculated monthly total from the previous step is disaggregated to daily values. The disaggregation is conducted by identifying the gauge nearest (in ordinary horizontal distance) to the centroid of the grid cell that had a valid monthly total and then using the pattern of the daily rainfall totals within that month to derive the pattern of daily totals at the grid cell.



Water Quality Modelling of the Hawkesbury-Nepean River System

- 6) Steps 1 to 5 are repeated for every cell in the grid and for every month for which daily gridded data are required.

Daily rainfall grids were generated for the entire period between 11 November 1976 and 31 December 2011.

Water Quality Modelling of the Hawkesbury-Nepean River System

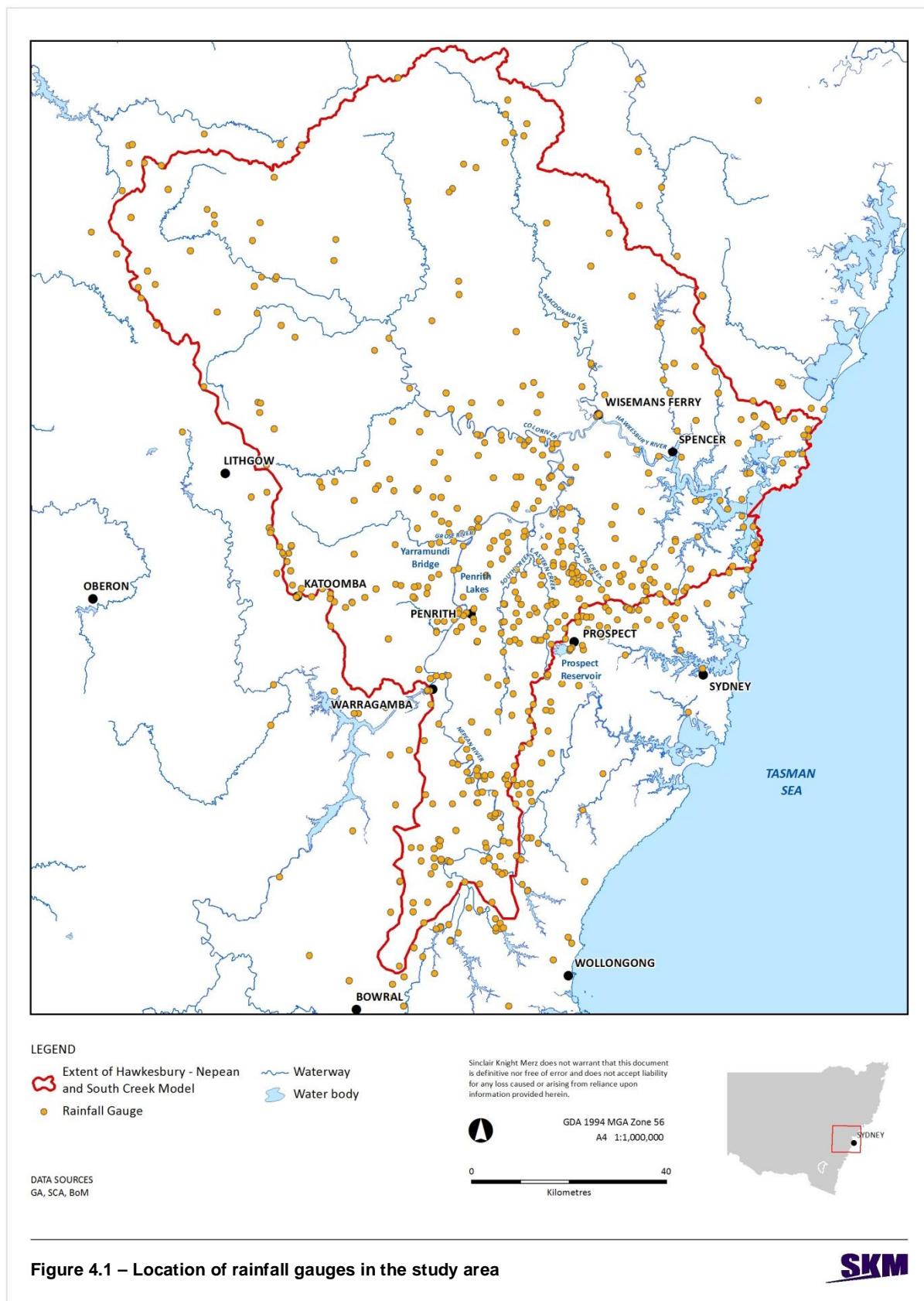


Figure 4.1 – Location of rainfall gauges in the study area

4/07/2013 | I:\ENVR\Projects\EN03013\Deliverables\Reports\3_DetailMdl_Calb\EN03013-NHY-RP-0001-FinalCatchmentModel_Calibration_Finalv2_140224.docx
Sydney Spatial Team - Prepared by : MS
Checked by : JC

SINCLAIR KNIGHT MERZ

4.1.3. Calculation of Weighting Factors for Monthly Rainfall Totals Using Ordinary Kriging

Kriging is an algorithm for interpolating values to a grid from a series of observations (such as a rainfall total) from various points across the grid area. Kriging has been demonstrated to produce an interpolation that minimises the error in the interpolation process.

Ordinary Kriging is the most commonly used type of Kriging, which assumes a constant but unknown mean value of the interpolated grid.

For the centroid of any grid cell, using true Ordinary Kriging the interpolated monthly rainfall totals are given by the equation:

$$\hat{R} = (\lambda_1 \quad \dots \quad \lambda_n) \begin{pmatrix} R_1 \\ \vdots \\ R_n \end{pmatrix} \quad (4.1)$$

where \hat{R} is the interpolated monthly rainfall at the grid cell, λ are the weights at each of the gauges and R are the monthly rainfall totals at each of the gauges. The weights computed under ordinary Kriging satisfy the condition that:

$$\sum_{i=1}^n \lambda_i = 1 \quad (4.2)$$

and they are computed from the equation:

$$\begin{pmatrix} \lambda_1 \\ \vdots \\ \lambda_n \\ \mu \end{pmatrix} = \left[\begin{pmatrix} \gamma(x_1, x_1) & \dots & \gamma(x_1, x_n) & 1 \\ \vdots & \ddots & \vdots & \\ \gamma(x_1, x_n) & \dots & \gamma(x_n, x_n) & 1 \\ 1 & \dots & 1 & 0 \end{pmatrix} \right]^{-1} \begin{pmatrix} \gamma(x_1, x_*) \\ \vdots \\ \gamma(x_n, x_*) \\ 1 \end{pmatrix} \quad (4.3)$$

where γ is the estimated value of the semivariogram between two locations, with the locations designated by x_1 to x_n being the locations of the monthly rainfall gauges and x_* being the location of the centroid of the grid cell at which the interpolation is being carried out. The estimated semivariogram is computed according to Equation 4.4, which is described below. The additional parameter μ is a Lagrange multiplier, which could be used to estimate the error involved in the interpolation process but which is not used any further in our interpolation process.

The set of rainfall gauges with valid monthly rainfall totals changes for every month and therefore a full implementation of Ordinary Kriging would require computation of a new set of weighting factors for every grid cell for every individual month. This would be a very computationally intensive process. For this project, an alternative procedure was adopted where the weighting factors for every grid cell were computed at the start of the interpolation process assuming that a valid monthly rainfall total was available for every gauge. For each grid cell, the monthly gauges were then ranked from the highest to lowest weighting factor. Rainfall totals were then computed using only the ten gauges with the highest weighting. The weighting factors were then re-scaled so that the sum of the weights equalled unity.

Values of semivariance were computed for the monthly rainfall totals between every pair of rainfall gauges using the equation:

$$\hat{\gamma}(x_i, x_j) = \frac{1}{2N} \sum_{t=1}^N (R_i - R_j)^2 \quad (4.4)$$

where N is the number of months with concurrent valid monthly rainfall totals at both gauges i and j and t is the month number. To reduce the influence of data points that would have otherwise been computed using small sample sizes, only pairs where N was greater than 100 months were used in fitting the semivariogram. Even with this constraint, there were 25,097 pairs of gauges with sufficient concurrent valid data to compute a semivariance from more than 100 months data.

Due to the strong influence of the terrain on observed rainfall totals, there are typically much stronger correlations between totals recorded at two locations that are at the same elevation but further away from each other, than two locations that are closer but at different elevations. Similarly, the influence of the terrain in this region is such that there are stronger correlations in a North-South direction than in an East-West direction. To accommodate for the influence of the terrain, an adjusted distance was calculated between each of the rainfall gauges according to:

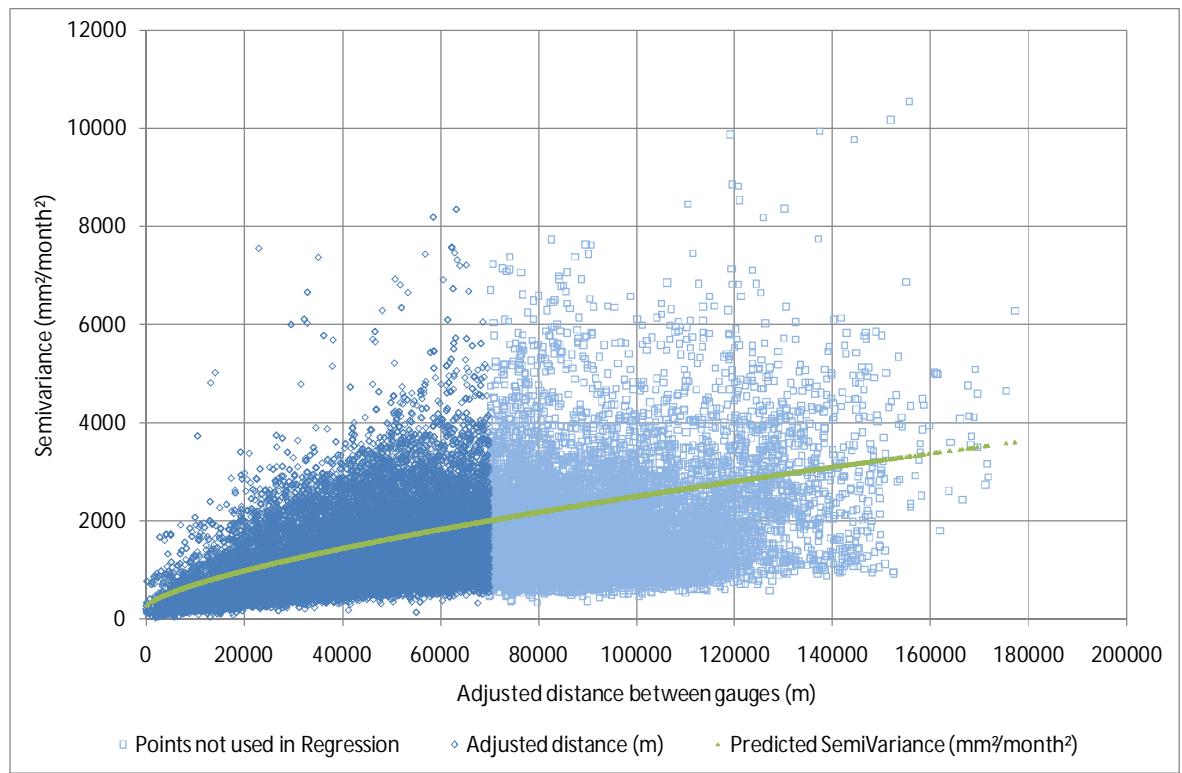
$$h = \sqrt{(E_i - E_j)^2 + [k_{NS}(N_i - N_j)]^2 + [k_z(z_i - z_j)]^2} \quad (4.5)$$

where h is the adjusted distance, E is the Easting coordinate (in metres to Map Grid of Australia 1994 Zone 56), N is the Northing coordinate (in metres to Map Grid of Australia 1994 Zone 56) and z is the ground elevation to Australian Height Datum. k_{NS} is a scale factor on distances in the North-South direction and k_z is a scale factor on differences in elevation.

A least squares regression approach was used to fit the semivariogram curve to the empirical data on semivariance for all of the pairs of gauges that had an adjusted distance of less than 70 km. The fitted semivariogram curve was given by the equation:

$$\gamma = 266 + e^{(0.7\log_e h - 0.348)} \quad (4.6)$$

where h is the adjusted distance computed with $k_{NS} = 0.65$ and $k_z = 90$. The values of the k constants in the adjusted distance equation were fitted to maximise the correlation between the fitted semivariogram and the empirical computed semivariance values. The high value of k_z reflects the very strong influence of elevation on monthly rainfall totals. The fitted semivariogram is shown in **Figure 4-2**. The correlation (R) between the logarithm of the semivariance and the logarithm of the adjusted distance described by Equation 4.5 was 0.64.



- **Figure 4-2 Empirical semivariance in monthly rainfall totals observed between pairs of rainfall stations in the Hawkesbury-Nepean River model area and fitted semivariogram**

4.1.4. Computation of Daily Rainfall Time Series for Model Subcatchments

The daily rainfall grids and the climate data were imported into the Source model to calculate the average daily rainfall accumulation for each catchment. The climate data import tool identifies overlapping grid cells in each catchment. It then computes the average of the daily totals from those grid cells to provide the daily value for the catchment average rainfall for use in the model. The same daily rainfall totals are applied to all functional units within each catchment.

4.2. Daily Potential Evapotranspiration

The Source model has the capacity to import evaporation data. This enables the model to represent the spatial and temporal variability in point potential evapotranspiration (PPET) across the study area.

There were two sources of data that were combined to create the grids:

- Mean monthly grids of PPET for the period 1961-1990, for each month of the year at 0.05° resolution, supplied by the Bureau of Meteorology (BOM).
- Daily recorded pan evaporation data from 26 pan evaporation gauges located around the study area. These gauges run for various periods of record, with some starting as early as 1956 up to the end of 2011. Details of these sites are provided in **Appendix C. Figure 4-3** shows the location of evaporation stations in the Hawkesbury-Nepean catchment.

A decreasing trend in potential evapotranspiration has been observed across Australia and for virtually every other continent across the world. Several studies have found that for South Eastern Australia, the reduction in PPET is 3 mm/year (McVicar et al., 2012).

A computer program was developed to form grids of daily PPET data in the correct format to be imported into the Source model. The grids have a spatial resolution of 0.01° of latitude by 0.01° of longitude, referenced to the Geodetic Datum of Australia (1994). This is approximately equivalent to each grid cell being 0.92 km in the East-West direction by 1.11 km in the North South direction. The gridding procedure involves the following steps:

- 1) At each of the 26 daily pan evaporation stations, the daily totals are accumulated to form monthly totals at each site. Any station that has more than one day of data missing or poor quality data (quality code greater than 150) in a particular month has that monthly total flagged at that site as "missing data". Data from these station-months are omitted in the subsequent analysis. The remaining data are termed "valid data".
- 2) For the location of each of the pan evaporation stations, the mean monthly PPET value for the corresponding grid cell (calculated at step 8) is extracted and added to a running total for every month where valid pan evaporation data was available.
- 3) For the location of each of the pan evaporation stations, a pan factor is calculated, as:

$$PF_i = \frac{\sum_{y,m} E_{Pan,i,y,m}}{\sum_{y,m} PPET_{i,y,m}} \quad (4.7)$$

where PF_i is the pan factor for evaporation station i , E_{Pan} is the recorded pan evaporation for the particular month and year at evaporation station i and $PPET_{i,y,m}$ is the estimated PPET from the mean monthly grid at the same location as the evaporation station.

- 4) For each 0.01° cell in the grid, the corresponding cell in the mean monthly PPET grid from the BOM for the 1961-1990 climate reference period was identified.
- 5) The twelve mean monthly values were accumulated to form an annual total at the corresponding grid cell.
- 6) The monthly pattern (mean PPET value for the month divided by the mean annual PPET value) was derived for the 1961-1990 climate reference period, using the formula:

$$MF_m = \frac{PPET_{1961-1990Ref,m}}{PPET_{1961-1990Ref}} \quad (4.8)$$

- 7) For the year to be generated, the climate trend adjusted mean annual PPET total was calculated as:

$$PPET_y = PPET_{1961-1990Ref} - 3(y - 1976) \quad (4.9)$$

- 8) For the month to be generated, the climate trend adjusted mean monthly PPET total was calculated as:

$$PPET_{y,m} = PPET_y \times MF_m \quad (4.10)$$

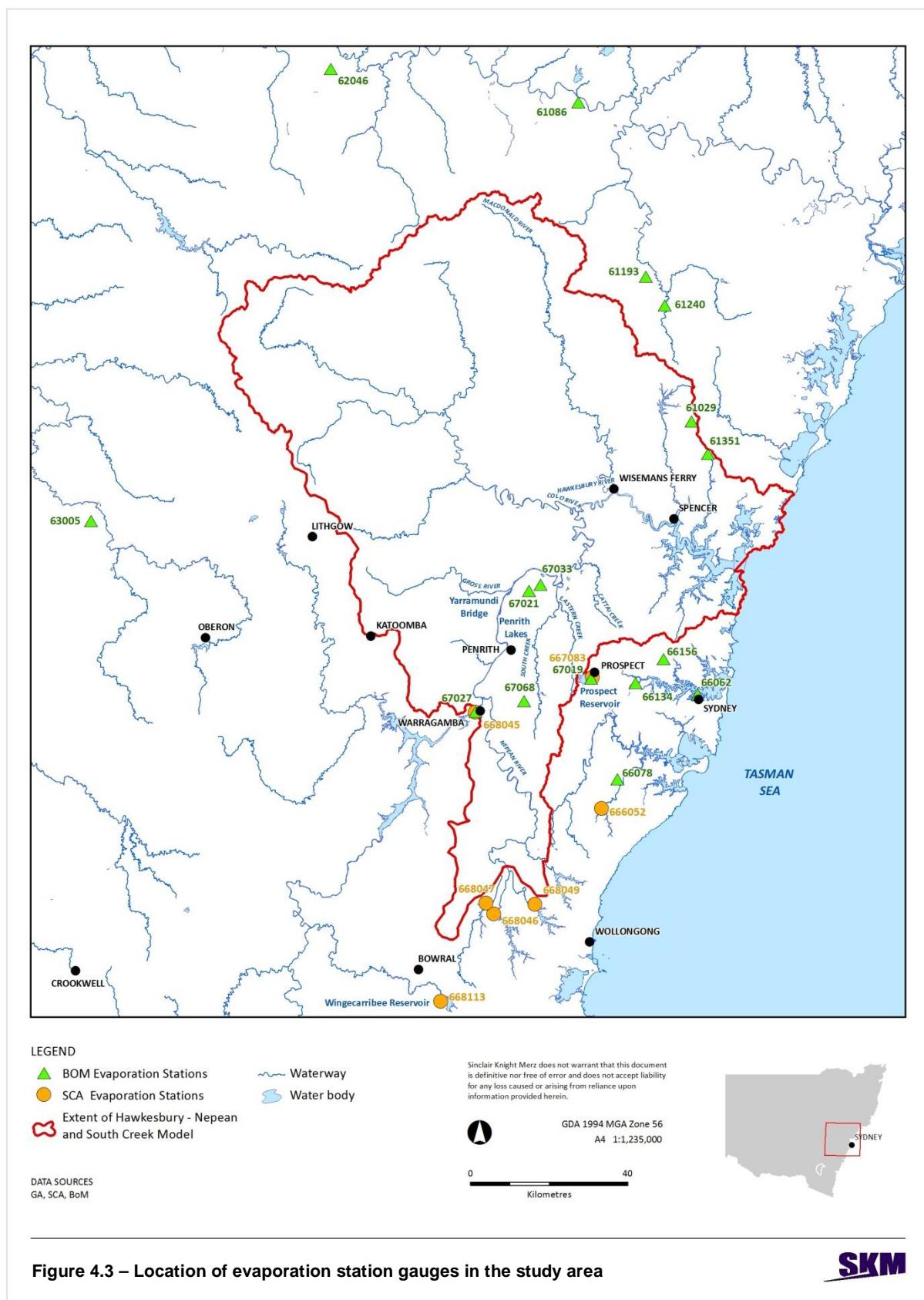
- 9) For each of the pan evaporation stations, a pan factor corrected ratio of the total mean monthly pan evaporation to the climate trend corrected PPET for the month is computed as

$$ER_{i,y,m} = \frac{1}{PF_i} \times \frac{E_{Pan,i,y,m}}{PPET_{i,y,m}} \quad (4.11)$$

- 10) The distance from each pan evaporation station to the centroid of each grid cell is calculated. For the five pan evaporation stations that have a valid monthly pan evaporation total and are nearest to the grid cell, a weighting factor is calculated on the basis of the inverse of the square of the horizontal distance to the evaporation gauge.
- 11) A weighted value of the evaporation ratio is computed for each grid cell using the weighting factors (from step 10) and the evaporation ratios computed at the gauges (from step 9).
- 12) The PPET value for the month is computed by multiplying the interpolated value of the evaporation ratio (from step 11) and the climate trend adjusted mean monthly PPET (from step 8).
- 13) For each grid cell in each month, the calculated monthly total from the previous step is disaggregated to daily values. The disaggregation is conducted by identifying the gauge nearest (in horizontal distance) to the centroid of the grid cell that had a valid monthly total and then using the pattern of the daily pan evaporation totals within that month to derive the pattern of daily totals at the grid cell.
- 14) Steps 7 to 13 are repeated for every cell in the grid and for every month for which daily gridded data are required.

Daily PPET grids were generated for the entire period between 11 November 1976 and 31 December 2011.

Water Quality Modelling of the Hawkesbury-Nepean River System



SINCLAIR KNIGHT MERZ

5. Selection of Component Model Types

5.1. Selection of Sacramento Model for Runoff Generation

The Source model provides several pre-defined rainfall runoff models that can be used to compute runoff from functional units and catchments within the model (Welsh et al., 2012).

The Sacramento conceptual rainfall runoff model (Burnash and Ferial, 1972) was adopted for runoff generation within the Hawkesbury-Nepean River and South Creek Model. The choice of the Sacramento rainfall runoff model was motivated by its:

- Demonstrated capacity to accurately simulate hydrographs of surface runoff from Australian catchments (Simons et al., 1996; Chiew et al., 2008; Chiew et al., 2009);
- Ability to accurately simulate the surface runoff and baseflow contributions to flow, which become important when generation of constituent loads using an Event Mean Concentration Dry Weather Concentration model are used; and
- Familiarity amongst hydrological modellers in New South Wales, particularly with the Office of Water, as Sacramento has been used for many years with the IQQM modelling framework.

5.2. Selection of Storage Routing Model (Laurenson and Mein) for Flow Routing

The Laurenson and Mein (Laurenson and Mein, 1997; Mein et al., 1974) storage routing model was chosen to represent routing of flows. The Laurenson and Mein formulation is given by the equation:

$$S = kQ^m \quad (5.1)$$

where S is the storage in the link (in m^3), Q is the flow out of the reach (in m^3/s) and k and m are parameters of the equation that control the shape of the conceptual storage relationship.

Observations of hydraulic behaviour in many catchments in Australia and throughout the world has found that the m value typically varies in a range between 0.7 and 1, with a value of m commonly adopted in Australian hydrology (I.E.Aust., 1987). The k parameter is strongly correlated with the length of the reach or reaches in the model, as the volume of storage is observed to increase with reach length. The Laurenson and Mein method has been demonstrated to work well on a large number of Australian catchments and is widely applied across a number of models for hydrology and flood forecasting in Australia (I.E. Aust., 1987). Regional estimates of appropriate model parameters, at least for flood situations, are therefore widely available from the literature. In most applications of the Laurenson and Mein flow routing method, the constant k for each reach is scaled in direct proportion to the length of the stream reach that is being modelled.

The subcatchment-node-link network for the Hawkesbury-Nepean River and South Creek Model has been formed in such a way that most of the subcatchments are of similar area and the links are of similar size (refer to **Figure 3-2**). An m value of 0.8 was adopted for all links in the model, which is consistent with accepted practice in modelling of flows (IEAust, 1987). The value of the routing delay parameter, k , was optimised for each of the gauged catchments as part of the calibration between observed and modelled daily flows.

5.3. Selection of Generation Models for Constituents

An Event Mean Concentration Dry Weather Concentration (EMCDWC) approach was used for constituent generation for all functional units for: TN, NO_x, TKN, NH₄, TP, FRP, SiO₂, TSS, salinity, faecal coliforms and enterococci. The EMCDWC model was used because it has been widely applied in water quality modelling in Australia, within the eWater Source and the MUSIC modelling frameworks. It is considered suitable for this modelling application. There is a complimentarily large volume of literature (i.e. Bartley et al, 2012, Duncan, 1999, SCA, 2003 and EPA, 1997) and previous knowledge on EMC and DWC parameter values for catchments with these land uses.

There were a number of constituents in the model, for which there is very limited local monitoring data available to provide a robust relationship between generation and land use. The components of organic nitrogen and the components of organic phosphorus were subdivided from the total values produced by the Source model, using representative ratios of each of the relevant components. Total and dissolved organic carbon constituent concentrations were applied as constant values for consistent regions of the catchment model domain, on the basis that there was little systematic variation in these constituent concentrations (see Section 8.6).

Temperature, dissolved oxygen and pH typically vary according to a seasonal pattern. These constituents were therefore represented by a sinusoidal curve, fitted to monitoring data applied across consistent regions of the catchment model domain.

5.4. Selection of In-Stream Routing and Transformation Models for Constituents

The Source model routes constituents in stream links at the same rate as the passage of the flow hydrograph along the link. There is evidence, as documented in Jones et al. (1994) that there is significant assimilation of nutrients as flows pass along South, Eastern and Cattai creeks. Explicit decay functions were therefore applied for several of the nutrient species across five reaches in the catchments of South, Eastern and Cattai creeks. The decay functions adopted within Source in each of these links represent the reduction in concentration of each selected constituent according to an exponential decay function, of the form:

$$L(t) = L(t - 1) 2^{-T/K} \quad (5.2)$$

Where $L(t)$ is the load of nutrient in the reach on day t , T is the travel time for water and constituents through the reach and K is the decay half-life of the particular constituent.

The decay half-life parameter values for each water quality constituent in each link were calculated by analysing observed water quality data taken on the same day at corresponding upstream and downstream locations on each stream. Although in some cases there are several links in the Source model between the sampling locations used to estimate the decay parameters, decay models were only applied on one of the links located between the coupled sampling locations. Although decay functions could have been applied across two or more links between each of the sampling locations, the outcome of applying the decay functions at one link in terms of reducing constituent concentrations that flow to the TUFLOW/AED model from those generated from the catchment are the same and the simpler approach was adopted. **Table 5-1** outlines the location of



Water Quality Modelling of the Hawkesbury-Nepean River System

the decay models in Source along with their applicable constituents. Section 8.3 details further the decay rates applied.

■ **Table 5-1 Decay transformation models applied to nutrients in the Source model**

Creek Name	Constituents Decay Model was Applied To	Upstream Monitoring Site	Downstream Monitoring Site	Link Name in Source Model where Decay Models Applied
South	TN, NOx, TKN, NH ₄ , TP, FRP	NS23	NS14	South_Creek_Left01
South	TN, NOx, TKN	NS14	NS04	IS_SthCreek_003
Eastern	NH ₃ , FRP	NS085	NS082	IQQM_EasternCk_Residuals_Link2
Cattai	TN, NOx, TKN, NH ₄ , TP, FRP	NC5	NC3	CattaiResidual_Link7
Cattai	TN, NOx, TKN, NH ₄ , TP, FRP	NC75	NC5	CattaiResidual_Link4

No other transformation functions were applied to constituents in any other parts of the catchment model.

6. Point Inputs to the Hawkesbury-Nepean River and South Creek Catchment Model

6.1. Warragamba Dam Releases, Mangrove Creek Dam Releases and Flows at Broughton Pass and Pheasants Nest

There are four locations where releases from dams are incorporated into the model:

- 1) Releases into the Warragamba River from Warragamba Dam;
- 2) Nepean River at Pheasants Nest Weir, which is downstream of Nepean, Avon and Cordeaux dams;
- 3) Cataract River at Broughton Pass Weir, which is downstream of Cataract Dam; and
- 4) Releases into Mangrove Creek from Mangrove Creek Dam.

The Nepean tunnel, which connects Pheasants Nest to Broughton Pass Weir allows for flows to be directed between the two weirs.

Time series of flow and water quality constituents from point sources were included into the TUFLOW/AED model for the first three locations listed above, for the periods covering calibration and validation of the TUFLOW/AED model (1 January 2006 to 31 December 2007 and 1 November to 31 December 2011). Mangrove Creek Dam discharges into Mangrove Creek, which is represented as a link in the Source model of the catchment. No gauging data was available on Mangrove Creek for the TUFLOW/AED model calibration and validation period. However, it is known that Mangrove Creek Dam did not spill over this period. Any releases from the dam during the calibration and validation period would have been relatively minor. These would have been matched by diversions at the weir downstream to supply Gosford Wyong Water and hence not entered the Hawkesbury-Nepean River. Therefore, for the period since 2006, the Source model represents only runoff generated by the subcatchments of Mangrove Creek downstream of the dam and ignores both dam releases and the diversion to the Central Coast.

Point inputs at Broughton Pass and Pheasants Nest were used for two purposes in the model calibration process:

- 1) Direct inputs at the upstream end of the TUFLOW/AED model; and
- 2) Calibration of the flows generated from the rainfall runoff models for the intermediate catchment. The flow time series from flow gauges at Broughtons Pass and Pheasants Nest were entered into the Source model for the Source model calibration period that runs from 11 November 1976 to 31 December 2011.

Warragamba Dam releases were direct inputs to the TUFLOW/AED model.

Warragamba Dam releases were not input to the Source model for this longer period (ie 1976 to 2011) because there were no gauges on the main stem of the Nepean River downstream of Wallacia.

Daily flow gauging data was available for Broughton Pass from 17 March 1983 and for Pheasants Nest from 17 November 1983. There were relatively minor periods of missing data over the 2005-2011 period at each gauge. Missing data were infilled by regression using data from other gauges in the area. This provided a continuous time series for the period from 2005-2011, required for the hydrodynamic model. For the period prior to 2005, the flows at Broughton Pass and Pheasants Nest were used to calibrate the rainfall runoff models at gauges downstream on the Nepean River. A complete series was not required because calibration and validation at the downstream gauges was restricted to periods when a complete month of daily flow data was available at both Broughton Pass and Pheasants Nest. The following **Table 6-1** describes the missing periods and the regressions used to infill any missing data.

Outflows from Warragamba Dam flow are through the Warragamba Rivulet into the Nepean River. This flow results from:

- Releases from the dam (or “environmental drinking water and riparian releases”);
- Spills from the dam;
- HEPS releases, or hydropower plant releases. These releases occur when reservoir levels are within 1 m of full supply; and
- Inflows from the small local catchment downstream of the dam wall.

Releases are supplied via the Warragamba Pipeline that enters Warragamba Rivulet downstream of Warragamba Weir. A gauge station (212240) exists on the Warragamba Rivulet, however it provides water level data only, as no rating curve is available. HEPS and Spill flows pass through Warragamba Weir (gauge 212241).

Time series flow data for the Warragamba Rivulet into the Nepean River from 1 January 1990 to 31 December 2011 was constructed and in-filled as needed using Daily Return System data and hourly Warragamba Weir data supplied by SCA. Details on how the time series was constructed and assumptions used are provided below (**Table 6-2**).



Water Quality Modelling of the Hawkesbury-Nepean River System

- **Table 6-1 Summary of infilling requirements for Broughton Pass and Pheasants Nest**

Location	Number of days with recorded daily data*	Number of Missing Days	Percentage of Missing Data Days	Infilling Relationship	R ² of Infilling relationship	Number of Days Applied
Broughton Pass (BP)	2528	28	1.1%	BP Flow = 7.4 Local runoff from Source model to BP	0.31	28
Pheasants Nest (PN)	1822	734	28.7%	If flow at Camden available: PN Flow = 63 + 0.43 Camden Flow+ 0.14 BP Flow	0.88	254
				If flow at Camden not available: PN Flow = 120 + 1.04 BP Flow	0.61	480

* Period 2005-2011

■ **Table 6-2 Data sources of constructed Warragamba Dam flow time-series**

Flow Component	Input Dataset	Details
HEPS and Spill flows	Warragamba Weir (212241) hourly dataset Daily Return System data	HEPS and Spill flows were identified through Warragamba Weir (gauge 212241) hourly flow dataset, which was provided by SCA for the period 1 January 1990 to 1 April 2005. Hourly data was accumulated to daily totals. Missing data during high flow events was in-filled using daily HEPS and Spill data. Daily Return System data was provided by SCA from January 1990 through June 2011. The last event for both types of releases occurred in 1998. Only three HEPS release events occurred in the daily data for which no hourly weir values were recorded (in 1990, 1994 and 1998). The Return System daily data was disaggregated to an hourly time-step following a pattern of other events of similar magnitude in the Warragamba Weir hourly record. Timing of the hourly patterns was matched to the downstream gauge on Warragamba Rivulet (212240). Missing hourly data during low flow times were in-filled using hourly low flow values near the missing times. Hourly data was accumulated to daily totals.
Catchment inflows	Warragamba Weir (212241) hourly dataset	As hourly weir gauge data from Warragamba Weir (212241) beyond 2005 was not available, inflows from the small local catchment downstream of the dam wall beyond that date were assumed to be negligible. For the period where hourly data was available, it was accumulated to daily totals.
Release flows	Daily Return System data	Release data was provided on a daily time-step from January 1990 through June 2011 as part of the Daily Return System data. Release flows are constant throughout the day and adjusted by dam operators once a day at approximately 8-9am. As Warragamba Weir hourly data was only provided up to 1 April 2005, the constructed dam outflow time-series from 2005 onwards only reflected release data.

6.2. Wastewater Treatment Plant / Water Recycling Plant Discharges

Records of flow and selected constituent discharges at the Wastewater Treatment Plant (WWTP) and Water Recycling Plant (WRP) outlets were available at the ten sites included in the Source model:

- Castle Hill WWTP
- Hornsby Heights WWTP
- Quakers Hill WRP
- Richmond WRP
- Riverstone WWTP
- Rouse Hill WRP
- St Marys WRP
- Wallacia WWTP

SINCLAIR KNIGHT MERZ

- West Camden WRP
- West Hornsby WWTP

Daily flows from 1 July 1998 were available at all sites. TN, NO_x; TKN; NH₄ and TP values were normally measured every six days at each WWTP. Measurements for SiO₂ and FRP were much more infrequent or in some instances absent.

The following constituents were included as part of the WWTP discharges modelled in Source: TN, NO_x; TKN; NH₄; TP; FRP; SiO₂; TSS, salinity, faecal coliforms and Enterococci. To form continuous daily time series, missing values in the time series were patched using linear interpolation. When only one or no data exist, an average concentration from another WWTP was substituted.

6.3. Irrigation Extractions

Irrigation extractions occur from the main river and from contributing tributaries. Metered extractions in the catchment are only available since 2011, therefore estimated irrigation extractions have been sourced from the Hawkesbury-Nepean IQQM model (version 7.68.3) developed by the NSW Office of Water (NOW). The IQQM model simulates a period from 1909 to 2011. The modelled time series supplied from the IQQM model by NOW were unrestricted irrigation demands. The proportional impact of demands is greatest on flow and water quality during periods of low flow in the river. There is uncertainty in the estimated daily extraction time series because they come from a crop model which is not informed by extraction data. The largest uncertainties in estimated extractions would be during dry periods, when flows are low.. During periods of high flow, the uncertainties in estimation of demands (from the use of the IQQM crop model approach) are unlikely to significantly affect the model outcomes in the estuary, since extractions and uncertainties in extractions are typically low during those periods. The focus of the flow calibration was on the upper proportion of the flow duration curve, as it was recognised that during periods of low modelled flows, there may be large divergences between recorded and modelled flows. The large divergences are due to overestimation of the impact of diversions.

The locations of irrigation extractions from the main river that were included in the TUFLOW model are listed in **Table 6-3**.

Upper tributary extractions (included in the Source model) are smaller than those typically extracted from the Hawkesbury-Nepean River (included in the TUFLOW-FV model). Extractions to irrigators that were included in the Source model are shown in **Table 6-4**. Modelled IQQM extraction points have not been validated against irrigation licences as it is assumed that this was undertaken by the Office of Water.

■ **Table 6-3 Summary of IQQM irrigation extraction locations included in the TUFLOW modelling - mainstream**

Node number in IQQM model	Location
14	Nepean River from Douglas Park Weir Pool
24	Nepean River at Appin

SINCLAIR KNIGHT MERZ



Water Quality Modelling of the Hawkesbury-Nepean River System

Node number in IQQM model	Location
31	Nepean River from Bergins Weir Pool
33	Nepean River from Menangle Weir Pool
35	Nepean River from Thurns Weir Pool
38	Nepean River from Navigation Creek
42	Nepean River from Sharpes Weir Pool
44	Nepean River from Camden Weir Pool
46	Nepean River from Cobbity Weir Pool
49	Nepean River from Matahill
51	Nepean River from Mt Hunter Weir Pool
59	Nepean River from Mt Hunter River
61	Nepean River from Theresa Weir Pool
63	Nepean River from Brownlow Hill Weir Pool
65	Nepean River from Wallacia Weir Pool
70	Nepean River at Scotchey Creek
110	South Creek to Richmond Rd
112	South Creek Richmond Road to Eastern Creek
119	South Creek Downstream of Eastern Creek
205	Nepean River at Narellan Creek
211	Nepean River at Cobbity Irrigators
214	Nepean River at Eagle Creek
215	Nepean River at Bringelly
217	Nepean River at Bushrangers
220	Nepean River at Duncan Creek
293	Nepean River at Mackenzie Creek
150	Hawkesbury River near Webbs Creek
303	Hawkesbury River near Calna Creek
183	Hawkesbury River near Cowan Creek
78	Nepean River from Penrith Weir Pool
291	Nepean River at Yarramundi Lagoon
295	Nepean River at 428 Irrigator
81	Nepean River from Penrith Weir to Yarramundi
277	Nepean River from Yarramundi to Grose River
107	Hawkesbury River from Grose River to South Creek
123	Hawkesbury River from South Creek to Cattai Creek
136	Hawkesbury River from Cattai Creek to Colo River
145	Hawkesbury River from Colo River to Macdonald River
161	Hawkesbury River from Macdonald River to Mangrove Creek
181	Hawkesbury River from Moony Mooney Creek to Cowan Creek

- **Table 6-4 Summary of IQQM irrigation extraction locations included in the Source modelling - tributaries**

Catchment/Waterway	IQQM irrigation node	Comment
MacDonald River	147 517, 520	Shown in IQQM layout to be upstream of gauge 212228
Colo River	139	Shown in IQQM layout to be upstream of gauge 212290
Currency Creek	296	
Unnamed (South Creek confluence to Currency Creek)	295	
Redbank Creek	291	
Grose River	101	Shown in IQQM layout to be upstream of gauge 212291
Shaw's Creek	274	
Mulgoa Creek	224	
South Creek	304 112 + 110 119 + 293 413	
Eastern Creek	317 116 114	Upstream of WWTP inflow Upstream of gauge 212296
Cattai Creek	320 + 318 128 + 130 435, 436, 437, 438	Upstream of gauge site 212295
Mangrove Creek	534 535	
Berowra Creek	551 555 561 562 566	
Cowan Creek	590	
Upper Nepean	305 306, 309 310	

Note: Some nodes in IQQM on South, Eastern and Cattai creeks are combined in the Source model to reduce complexity and maintain the level of detail appropriate for the model.

7. Runoff Generation and Flow Routing Model Calibration

7.1. Modelling approach

The Sacramento model was used for runoff generation within the Source framework. Model parameters were fitted using a combination of automated calibration via the calibration tool within the Source and manual manipulation to achieve a fit between gauged flows and model outputs.

7.2. Parameters

The Sacramento rainfall runoff model was fitted to runoff generation for all Functional Units (FUs), except for the "Water" FU which was assigned to "Nil runoff" which indicates that no flow is generated from all the water bodies in the catchment. A total of 22 parameters per FU were assigned for the Sacramento model (a description is outlined in **Table 7-1**). The parameters resulting from the flow calibration are provided in **Table 7-2**.

■ **Table 7-1 Sacramento model parameter descriptions**

Parameter	Description	Units	Min	Max
ADIMP	The additional fraction of pervious area, which develops impervious characteristics under soil saturation, conditions. <i>ADIMP</i> spill only occurs when both tension stores are full.	-	0	1
LZFPM	Lower Zone Free Water Primary Maximum, the maximum capacity from which primary base flow can be drawn.	mm	0	60
LZFSM	Lower Zone Free Water Supplemental Maximum, the maximum volume from which supplemental base flow can be drawn.	mm	0	50
LZPK	The ratio of water in <i>LZFPM</i> , which drains as base flow each day.	-	0	1
LZSK	The ratio of water in <i>LZFSM</i> which drains as base flow each day.	-	0	1
LZTWM	Lower Zone Tension Water Maximum, the maximum capacity of lower zone tension water. Water from this store can only be removed through evapotranspiration.	mm	0	500
PCTIM	The impervious fraction of the basin, and contributes to direct runoff.	-	0	1
PFREE	The minimum proportion of percolation from the upper zone to the lower zone directly available for recharging the lower zone free water stores.	-	0	1
REXP	An exponent determining the rate of change of the percolation rate with changing lower zone water storage.	-	0	3
RSERV	Fraction of lower zone free water unavailable for transpiration	-	0	1



Water Quality Modelling of the Hawkesbury-Nepean River System

Parameter	Description	Units	Min	Max
SARVA	A decimal fraction representing that portion of the basin normally covered by streams, lakes and vegetation that can deplete stream flow by evapotranspiration.	-	0	1
SIDE	The decimal fraction of observed base flow, which leaves the basin, as groundwater flow.	-	0	1
SSOUT	The volume of the flow which can be conveyed by porous material in the bed of stream.	-	0	1
UH1	The first component of the unit hydrograph, ie the proportion of runoff not lagged	-	0	1
UH2	The second component of the unit hydrograph, ie the proportion of runoff lagged by one time-step	-	0	1
UH3	The third component of the unit hydrograph, ie the proportion of runoff lagged by two timesteps	-	0	1
UH4	The fourth component of the unit hydrograph, ie the proportion of runoff lagged by three time-steps	-	0	1
UH5	The fifth component of the unit hydrograph, ie the proportion of runoff lagged by four timesteps	-	0	1
UZFWM	Upper Zone Free Water Maximum, this storage is the source of water for interflow and the driving force for transferring water to deeper depths.	mm	0	80
UZK	The ratio of water in UZFWM, which drains as interflow each day.	-	0	1
UZTWM	Upper Zone Tension Water Maximum. The maximum volume of water held by the upper zone between field capacity and the wilting point which can be lost by direct evaporation and evapotranspiration from soil surface. This storage is filled before any water in the upper zone is transferred to other storages.	mm	0	100
ZPERC	The factor applied to Pbase to define maximum percolation rate.	-	0	80

■ **Table 7-2 Sacramento model parameters**

Parameter	Eastern Creek	Colo River	Grose River	Upper Nepean River	South Creek	Berowra Creek	Right Bank	Left Bank
ADIMP	0.078	0.133	0.048	0.3	0.157	0.128	0.26	0.1
LZFPM	54.907	29.856	6.774	0	36.414	6.329	5.214	30
LZFSM	10.62	30.719	32.88	15.373	6.57	15.451	9.751	34.878
LZPK	0.9	0.274	0.265	0.151	0.395	0.225	0.83	1
LZSK	0.097	0.021	0.01	0.015	0.08	0.047	0.02	0.018
LZTWM	50	495.051	400	234.768	424.733	302.766	222.506	463.472
PCTIM	0.004	0.001	0.001	0.015	0.007	0.004	0.012	0.001
PCTIM Urban	0.498	0.332	0.42	0.35	0.242	0.468	0.39	0.4
PCTIM Peri Urban	0.022	0.108	0.15	0.073	0.024	0.064	0.04	0.15
PFREE	0.292	0.236	0.236	0.386	0.195	0.219	0.298	0.26

SINCLAIR KNIGHT MERZ

Parameter	Eastern Creek	Colo River	Grose River	Upper Nepean River	South Creek	Berowra Creek	Right Bank	Left Bank
REXP	1.077	0.909	0.953	0.985	0.84	0.963	0.942	1
RSERV	0.3	0.3	0.3	0.3	0.3	0.3	0.3	0.3
SARVA	0.01	0.01	0	0.01	0.01	0.01	0.01	0.01
SIDE	0	0.04	0.035	0	0	0	0	0
SSOUT	0	0	0	0	0	0	0	0
UH1	0.9	0.9	1	0.9	0.9	0.9	0.9	0.9
UH2	0.1	0.1	0	0.1	0.1	0.1	0.1	0.1
UH3	0	0	0	0	0	0	0	0
UH4	0	0	0	0	0	0	0	0
UH5	0	0	0	0	0	0	0	0
UZFWM	42.712	29.682	73.09	35	54.426	37.126	36.067	71.426
UZK	0.02	0.463	0.201	0.02	0.178	0.203	0.09	0.149
UZTWM	73.162	21.717	50	53.725	81.564	61.505	72.077	72.644
ZPERC	1.308	36.411	37.71	9.468	1.587	2.547	23.676	31.189

As part of the calibration process it was determined that, while the overall flows being represented by the Sacramento rainfall-runoff model were appropriate, the split between baseflow and quickflow (the sum of which is total flow) was not representative. A representative split is required to ensure correct loads of the water quality variables are allocated in the model. To facilitate a more reasonable split between baseflow and quickflow, a one parameter baseflow separation model was implemented within the existing Sacramento model.

The model implemented is the Chapman and Maxwell (1996) baseflow filter and is:

$$q_{b(i)} = \frac{k}{2-k} q_{b(i-1)} + \frac{1-k}{2-k} q_{(i)} \quad (7.1)$$

Where:

$q_{b(i)}$ is the baseflow at the current timestep (mm)

$q_{b(i-1)}$ is the baseflow from the previous timestep (mm)

$q_{(i)}$ is the total runoff at the current timestep (mm)

k is the baseflow filter parameter

A threshold parameter was added to the baseflow separation model, to avoid the generation of small volumes of surface runoff from small rainfall events, particularly when those events occur across urban areas (with a high proportion of impervious area) and during otherwise relatively dry periods. The threshold and baseflow filter parameter values are outlined in **Table 7-3** below.

■ **Table 7-3 Additional parameter values for enhanced Sacramento rainfall-runoff model**

Land Use	K	Threshold (mm)
Urban	0.95	10
Remainder	0.95	1

7.3. Calibration and Validation of Flow Generation and Routing Models

7.3.1. Flow Calibration Objectives and Approach

Comparison plots between observed and simulated flows at the gauging stations listed in **Table 7-5** are provided in **Appendix D**. For each station three graphs are presented: the full simulation time series, the time series between 1 January 2006 and 31 December 2007 and the scatter plot of the values. An example is provided in **Figure 7-1**, which displays the results at stream gauging station 212290 on the upper Colo River.

The overall objective of the model calibration was to accurately reproduce the daily hydrograph of flow observed at the gauge. When coupled with the model of the estuary, the overall performance of the system model is more sensitive and responsive to runoff during high flow events than during low flow periods. While it was important therefore to capture reasonable performance across all of the flow hydrograph, including baseflow, the most important feature of the performance of the flow generation model is its ability to capture the overall volume of runoff and the shape of the hydrograph from each catchment during runoff events.

A combination of manual and automated model calibration techniques were adopted within the Source model. The approach taken during calibration of the model was to:

- Set the impervious fraction for each functional unit to proportions that were consistent with observations from aerial photography and satellite imagery;
- Set initial upper and lower bounds for the other parameters of the Sacramento model to a relatively wide plausible range but informed by calibration of the model on other catchments;
- Perform automated calibration to observed flow data to obtain initial values of the upper zone capacities and coefficients;
- Manually adjust the parameters of the lower zone stores to match the lower half of the flow duration curve with the flow duration curve for the calibration period;
- Re-run automated calibration to re-define the parameters of the upper zone stores and the impervious fractions, this time concentrating on the fit to the volume and shape of runoff events, via optimisation using the Nash-Sutcliffe Coefficient of Efficiency (COE) Nash and Sutcliffe 1970; and
- Adjust the routing delay parameter (K) in the storage routing models within the links upstream of each gauge to better match the shape of runoff hydrographs at each gauge.



Water Quality Modelling of the Hawkesbury-Nepean River System

The Nash Sutcliffe COE is ubiquitously used in hydrology for demonstrating the performance of rainfall runoff models. It is similar to a coefficient of determination used in regression analysis. The Nash Sutcliffe COE penalises models that produced biased predictions of flow. It is defined as:

$$COE = 1 - \frac{\sum_{t=1}^T (Q_{obs,t} - Q_{mod,t})^2}{\sum_{t=1}^T (Q_{obs,t} - \bar{Q}_{obs})^2} \quad (7.2)$$

Where:

t is the day of the model run

T is the number of days to be compared between the observed and modelled data

$Q_{obs,t}$ is the observed flow day t of the model run

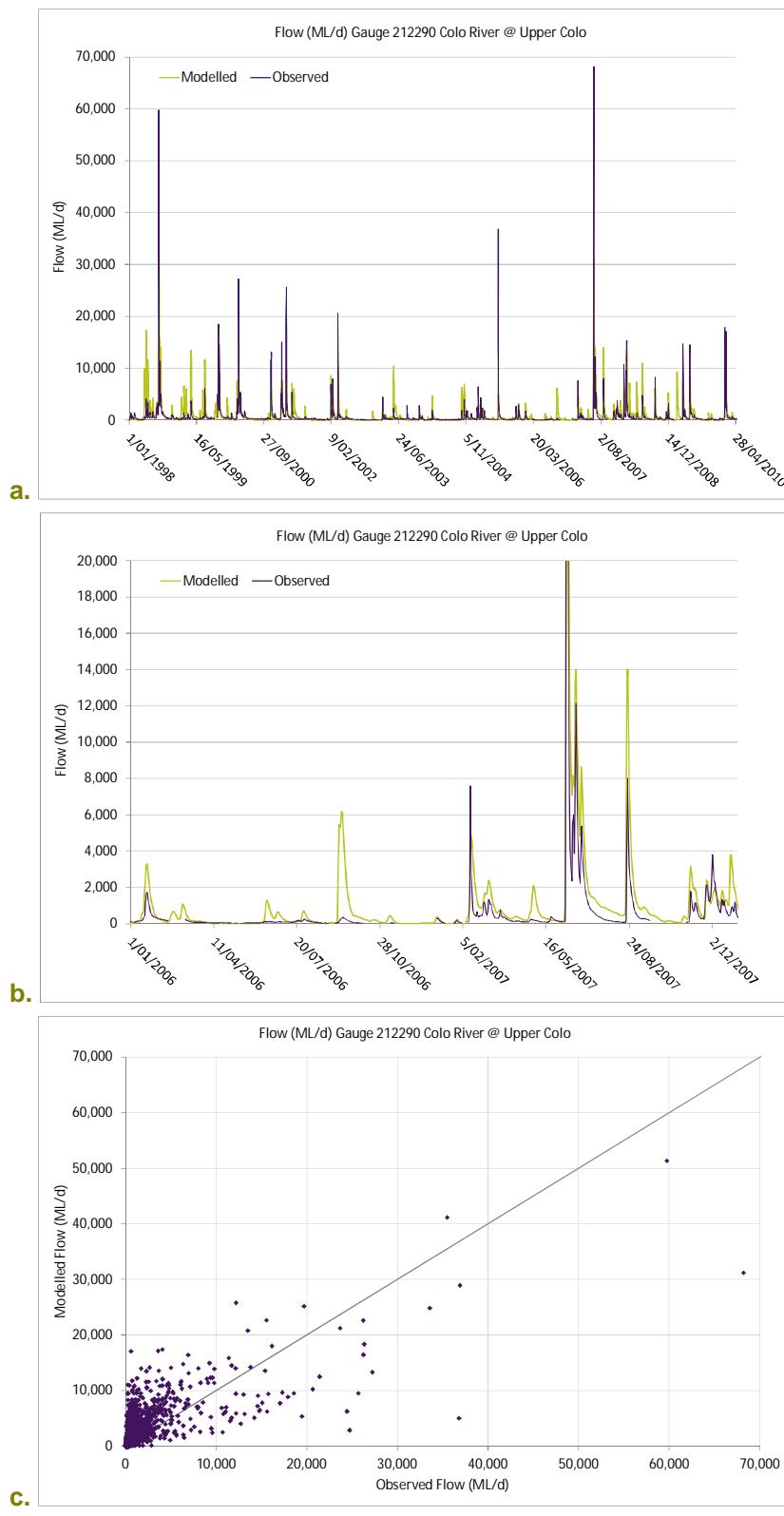
$Q_{mod,t}$ is the modelled flow day t of the model run

\bar{Q}_{obs} is the mean of the observed flows over the period.

The overall outcome of calibration was a balance between:

- Matching the shape of the flow duration curve at lower flows;
- Matching the slope of baseflow recessions after events;
- Visually matching the shape and volume of flow generated during runoff events, and;
- Achieving reasonable values of the COE, as an indicator of the performance of the model during those higher flow periods.

Water Quality Modelling of the Hawkesbury-Nepean River System



■ **Figure 7-1 Comparison between observed and simulated flow – Upper Colo River (212290)**

7.3.2. Assignment of Calibration and Validation Periods for Flow

For the purposes of calibration and validation of the flow generation models in the Source model, flow data was separated into independent calibration and validation periods. This was achieved by randomly selecting approximately two-thirds of the total number of years as calibration years and using the remaining one-third of years as validation years. Statistics are therefore presented at each gauge for three periods:

- 1) All of the years that were randomly selected as calibration years for the flow generation models in Source;
- 2) All of the years that were randomly selected as validation years for the flow generation models in Source;
- 3) The period 2006-2007, adopted for calibration and validation of the TUFLOW hydrodynamic model of the estuary. Note that both 2006 and 2007 were designated as validation years for the flow generation models in the Source model. Hence statistics from this period represent a sub-set of all of the validation years (from dot point 2).

The first two periods provide an overall indication of the performance of the model over the entire period when data was available. The performance over the 2006-2007 period could be argued as a more relevant measure, as this indicates the performance of the rainfall runoff generation models over the period when they are coupled to the hydrodynamic model.

The process for selection of calibration and validation years was as follows:

- The calendar years of 2006 and 2007 were selected as validation years for flow time series produced by the catchment model. This was because these two years represent the years that were adopted for calibration and validation of the TUFLOW/AED model for the Hawkesbury estuary.
- Daily rainfall data was obtained for two rainfall sites that had (nearly) continuous long term records: Site 63043 at Kurrajong, which is between North Richmond and Lithgow in the Colo River catchment; and Site 67015 at Bringelly, which is in the South Creek catchment. Annual rainfall totals were calculated at each of these two sites for each calendar year between 1900 and 2009 (except for 1994 at Bringelly, as there was no data collected during that year).
- On the basis of the annual rainfall totals at each site, calendar years were categorised as “wet” if they fell within the top 25 percent of all years recorded at that site, “dry” if they fell within the bottom 25 percent of all years recorded at that site and “medium” if they fell in the middle 50 percent of all years.
- For most years, the designation as wet, dry or medium was the same at both the Kurrajong and Bringelly sites. Where a particular year was categorised as wet at one site and medium at the other; or dry at one site and medium at the other, the categorisation was performed by summing the annual rainfall total for both sites and testing whether the year would sit within the wet, medium or dry categories on the basis of the sum of annual totals at both sites.

- Over the period between 1980 and 2009 (inclusive), this resulted in seven years categorised as wet, eight years categorised as dry and fifteen years categorised as medium.
- Two years were randomly selected from among the seven wet years (1988 and 1990) for use as validation years, in addition to 2007 which was pre-selected for validation and was also a wet year. The remaining four wet years (1981, 1984, 1987 and 1992) became calibration years.
- The same process of randomly selecting two additional dry years for validation (1993 and 1994) in addition to 2006 which was pre-selected for validation as a dry year. The remaining five dry years became calibration years.
- The same approach was adopted to randomly select five of the medium years for validation and ten of the medium years for validation.

Table 7-4 lists the years adopted for calibration and validation of the flow generation and routing models. These were applied consistently across all sites, as long as there was valid daily flow data available at the particular site. The ranks are based on the annual rainfall – a rank of one indicates the wettest year and the largest rank represents the driest year.

■ **Table 7-4 Assignment of calibration and validation years for flow modelling in catchment model**

Comments	Year	Year Category	Assignment	Rank of Annual Rainfall at Kurrajong*	Rank of Annual Rainfall at Bringelly*
	Pre-1980	Varies	Calibration		
	1980	Dry	Calibration	105	102
	1981	Wet	Calibration	8	43
	1982	Dry	Calibration	77	106
	1983	Average	Validation	38	33
	1984	Wet	Calibration	28	15
Scenario	1985	Average	Calibration	54	39
Scenario	1986	Average	Calibration	19	53
Scenario	1987	Wet	Calibration	23	41
Scenario	1988	Wet	Validation	10	3
Scenario	1989	Average	Calibration	29	36
Scenario	1990	Wet	Validation	7	7
Scenario	1991	Average	Calibration	70	40
Scenario	1992	Wet	Calibration	24	14
Scenario	1993	Dry	Validation	107	88
Scenario	1994	Dry	Validation	111	Missing data
	1995	Average	Calibration	59	28
	1996	Average	Calibration	74	69
	1997	Dry	Calibration	83	91
	1998	Average	Calibration	49	18
	1999	Average	Calibration	37	65
	2000	Average	Calibration	61	85
	2001	Average	Calibration	76	89
	2002	Dry	Calibration	88	94
	2003	Dry	Calibration	95	70
	2004	Average	Validation	85	60
	2005	Average	Validation	68	62
TUFLOW/AED Model Calibration	2006	Dry	Validation	110	104
TUFLOW/AED Model Validation	2007	Wet	Validation	17	24
	2008	Average	Calibration	50	35
	2009	Average	Validation	75	77

SINCLAIR KNIGHT MERZ

Comments	Year	Year Category	Assignment	Rank of Annual Rainfall at Kurrajong*	Rank of Annual Rainfall at Bringelly*
	2010	Average	Calibration	39	37
TUFLOW/AED Model Validation	2011	Average	Calibration	56	29

* Rank 1 is wettest year on record at the site, Rank 111 is the driest year on record.

7.3.3. Discussion of Flow Calibration and Validation Outcomes

Table 7-5 summarises calibration performance statistics for each gauge by providing daily Nash Sutcliffe COE at each gauge for the three periods discussed above. The COE is just one indicator of model performance that was used to calibrate the model, along with matching to the shape and timing of generated runoff, rate of recession of baseflows and the shape of the flow duration curve. A COE at a daily time step of 0.5 represents a reasonable level of skill in performance of the rainfall runoff model, which provides a reasonable representation of the shape and magnitude of flow hydrographs for most of the events in the record. The performance of the calibrated rainfall runoff models is generally good over both periods considered, with COE values greater than 0.5 for the independent validation period at all gauges except for two (Grose River and Cattai Creek). The COE values improve further for all gauges (except South Creek at Mulgoa Road) when the comparison is restricted only to the 2006-2007 period, which was the period used for calibration and validation of the TUFLOW/AED model.

- **Table 7-5 Nash Sutcliffe Coefficient of Efficiencies to daily flows achieved at each gauge over calibration, validation period and 2006-2007**

Gauge Name and Number	Calibration Years	Validation Years	2006-2007
Colo River at Upper Colo 212290	0.51	0.50	0.76
MacDonald River at St Albans 212228	0.52	0.77	0.73
Glenbrook Creek at Jellybean Pool 212219	0.37	0.52	0.75
Grose River Downstream Burrallow Creek 212291	0.23	0.41	0.47
South Creek at Mulgoa Road 212320	0.66	0.59	0.20
South Creek at Richmond Road 212297	0.33	0.54	0.58
Cattai Creek at Maraylya 212295	0.76	0.28	1
Eastern Creek at Riverstone 212296	0.63	0.67	0.69
Nepean River at Wallacia 212202	0.50	0.54	2
Nepean River at Mount Hunter Weir 212213	0.72	0.51	2

¹ Recorded flow data not available for this period.

² Recorded levels available at weirs but rated flows not available for this period.

For the four gauges on the left bank, representing the largely forested catchments (Colo, MacDonald, Glenbrook and Grose) the Source model achieved a COE above 0.7 at three of the four gauges for the 2006-2007 period and 0.47 at the remaining gauge (Grose River). Considerable effort was expended during the model calibration process to improve the representation of daily

SINCLAIR KNIGHT MERZ

runoff from the forested catchments. Further improvement was limited by the relative sparseness of the daily rain gauge network across these large catchments on the left bank and the limited capacity of this network to detect the true spatial extent of storm events that can occur across parts of this catchment. Further improvement in the calibration of rainfall runoff models for the left bank forested catchments may be achieved by increasing the density of coverage of rainfall gauges in the area, or by using an alternative means of capturing the spatial and temporal pattern of rainfall such as weather radar.

The four gauges on the right bank represent the runoff from the largely urban, peri-urban and agricultural catchments of South, Eastern and Cattai creeks. They had mixed results in calibration of the rainfall runoff models. The calibration performance for Eastern Creek is generally good across the entire period (COE greater than 0.6 for all three periods considered). The calibration for Cattai Creek is very good during the calibration period (COE of 0.76) but much poorer over the validation period (COE of 0.28). The performance over the whole calibration and validation period at the most downstream gauge considered on South Creek (Richmond Road gauge) is reasonable (COE of 0.33 and 0.54 for calibration and validation periods respectively), and slightly better in the 2006-2007 period (0.58). A much poorer performance was achieved from the site further upstream on South Creek (Mulgoa Road in 2006-07 (0.20). The variation in performance of the rainfall runoff model calibration over these periods is probably a combination of the use of modelled irrigation extractions (since no metered data was available), which would particularly affect:

- The performance during low flow periods;
- The inability of the rain gauge network to detect the true spatial and temporal variability of rainfall events and;
- The use of a daily rainfall runoff model in these creeks, which due to their higher impervious fractions and smaller catchment areas may be responding to shorter duration rainfall events than can be captured by a rainfall runoff model running on a daily time step.

Overcoming these problems would require metering of irrigation extractions and possibly consideration of an alternative rainfall runoff model structure that operates on a shorter time step (say hourly).

Comparisons between modelled and gauged flow were performed at two gauges on the Upper Nepean River: Wallacia Weir and Mount Hunter Weir. COE achieved at both gauges were above 0.5 for both the calibration and validation periods. However, these COE values should not be taken as robust performance. Flows in the Upper Nepean River are influenced significantly by releases from the Upper Nepean Dams, extractions from the weir pools by irrigators and the historical operation of the weirs to convey flows (or not convey flows) through the system. In calibrating the rainfall runoff model parameters for the catchments in the Upper Nepean, focus was given to fitting the shape, volume and magnitude of the peak flow for runoff events. The reason for this is because the influences of releases from the dams, weir operations and extractions would normally be less significant during events (typically flows above 1000 ML/d, representing approximately the top 10% of recorded flows). For gauges along the Upper Nepean River, when recorded flows were less than 1000 ML/d, the recorded flows were strongly affected by operations of the weirs and extractions,

SINCLAIR KNIGHT MERZ

which are both not well recorded historically. This makes it difficult to isolate the runoff generated from intermediate catchments for the purpose of calibrating rainfall runoff model parameters.

7.3.4. Influence of IQQM Modelled Extractions on Flow Calibration and Validation

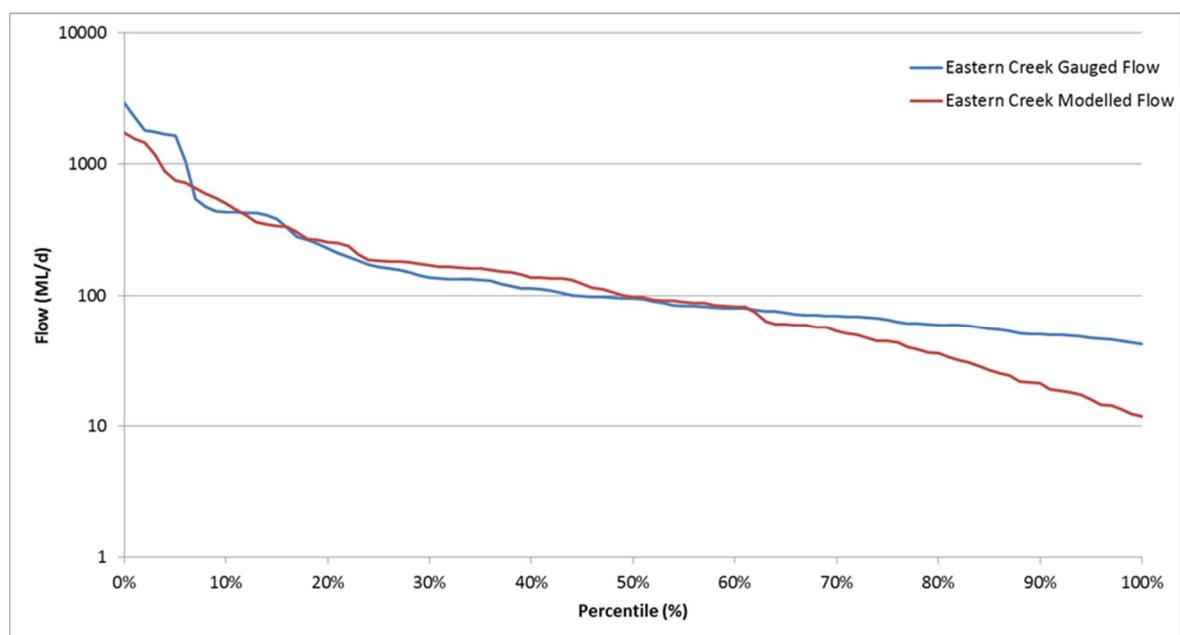
Extractions were included in the model runs and in most cases they occurred upstream of the gauge locations. There was virtually no metering of irrigator extractions prior to 2010. As a result, there was no metered data available over a timeframe sufficiently long to represent the actual extractions that have occurred in the system.

In the absence of actual data on extractions, all extractions were represented using the unrestricted demand time series, provided by Office of Water from the IQQM model of the system. The IQQM model estimates extractions using a soil water balance model for the estimated areas of crops irrigated in the system. The soil water moisture balance represents the soil moisture state according to the climatic variables prevailing in the area at the time, such as rainfall, potential evapotranspiration and daily maximum and minimum air temperature. The crop model assumes that irrigation water is applied to make up for any deficit in the water that would naturally be supplied by net rainfall in the area.

It is understood that restrictions have only been applied to irrigation diversions in very recent years. Prior to this, restrictions on extractions were relatively rare and/or they were lightly enforced. However physical constraints, such as very low water levels, may have stopped irrigators taking water at times when unrestricted demands from a crop model would have indicated that extractions would be occurring. This becomes particularly evident when examining the modelled flow duration curves for the calibration years for South, Eastern, Cattai and Berowra creeks. The curves (see **Figure 7-2** as an example) show an obvious downward kink at the lower end of the curve indicating that during modelled low flow periods the modelled unrestricted demands, estimated using IQQM, draw more water from the creeks than would have otherwise been estimated to remain in the creeks. The absence of corresponding downward kinks in the lower part of the observed flow duration curves indicate that the unrestricted demands estimated during these periods are very likely to be much higher than the actual demands.

The inability of the flow generation and routing models in the Source model to accurately predict flows during periods of low flow and high irrigation demand is not considered a significant problem for the overall model. Flow and water quality in the estuary are mostly driven by the predicted flows and loads from moderate to high flows, rather than during periods of low flows, when the major contributors to fluxes in the estuary would be releases from the dams, WWTP and WRP discharges and tidal fluctuations. Importantly, in scenario runs the modelled extractions will be modified to represent the rules that are stated in the Metropolitan Water Sharing Plan. This specifies minimum threshold flows in the stream at which diversions to irrigators can commence. Representation of these rules within the Source model should largely avoid the problem identified above, with modelled diversions being curtailed or restricted during periods when flows were modelled to be low. Once measured extraction data become available it is recommended that this issue be re-examined to better predict extractions during periods of low flow.

Water Quality Modelling of the Hawkesbury-Nepean River System



■ **Figure 7-2 Flow duration curve for Eastern Creek**

8. Water Quality Constituent Generation Rates

8.1. Modelling Approach Used for Each Constituent

Constituent generation rates were derived for each FU. The model incorporates the following constituents: TN, NO_x, TKN, NH₄, TP, FRP, TSS, SiO₂, faecal coliform bacteria, Enterococci and salinity.

The development of the generation rate values was initially based on literature values (i.e. Bartley et al, 2012, Duncan, 1999, SCA, 2003 and EPA, 1997) that were then modified based on observed versus modelled results. Generation rates were also informed by the additional water quality sampling that was undertaken as part of the campaign monitoring program (CMP) for the project.

Event Mean Concentration (EMC) Dry Weather Concentration (DWC) models were applied to all functional units. Advice provided by OEH on annual export rates for TN and TP were used in some cases to adjust the EMC and DWC values adopted for Cropping, all Grazing and all Horticulture FUs. The EMC and DWC coefficients for the Mining & Quarrying FU are derived from SKM (1997).

Water quality sites were associated with stream gauging stations when possible to compute loads based on observed and simulated flows and concentrations. **Table 8-1** lists the water quality sites for which observed and simulated constituent concentrations were compared.

■ **Table 8-1 Water quality sites used in the calibration**

Waterway	Water quality station ID	Station name	Streamflow Gauge ID
Colo River	N2201	Lower Colo River 4 km u/s Hawkesbury River	212290
	N2202	Colo River at Morans Rock, Putty Road Bridge	212290
Grose River	GR4301/ N4301	Grose River u/s Nepean River at Yarramundi Reserve, Springwood Rd	212291
MacDonald River	N151	MacDonald River 3 km u/s Hawkesbury	212228
South Creek	NS04	Lower South Creek Fitzroy Bridge	--
	NS14	South Creek at Richmond Road	--
	NS24	South Creek u/s St Marys WRP	--
	NS55	South Creek Bringelly Road	212320
Eastern Creek	NS081	Eastern Creek d/s Riverstone WWTP 300m d/s outlet	212296
	NS082	Eastern Creek u/s Riverstone WWTP	212296
	NS094	Eastern Creek u/s Breakfast Creek	212342
Breakfast Creek (tributary of Eastern Creek)	NS087	Breakfast Creek at Station Rd d/s Quakers Hill WRP	--



Water Quality Modelling of the Hawkesbury-Nepean River System

Waterway	Water quality station ID	Station name	Streamflow Gauge ID
Cattai Creek	NC2	Cattai Creek - at Maraylya, Pitt Town Rd	212295
	NC3	Cattai Creek - at Maraylya, Pitt Town Rd	212295
	NC6	Cattai Creek - d/s Castle Hill WRP u/s confluence w Second Ponds Creek	--
	K2	Cattai Creek - at end of Connelly Way d/s Castle Hill WWTP	--
Second Ponds Creek (tributary of Cattai Creek)	NC517	Second Ponds Creek - Outflow of wetlands Rouse Hill WRP	212299
	NCB280	Second Ponds Creek at Rouse Hill WRP	212299
Berowra Creek	1	Galston Gorge	212294
Nepean River	N72	Nepean River at Cobbity Road Bridge	212216
	N75	Nepean River at Sharpes Weir	212216
	N91	Nepean River at Maldon Bridge	212208
	N92	Nepean River at Maldon Weir	212208

8.2. Parameter Values Assigned For Constituent Generation

The parameter values assigned to the generation rate model for the catchments are provided in **Table 8-2** to **Table 8-5**.

The equation for the EMC/DWC generation model is outlined below.

$$\text{Load} = \text{SlowFlow} \times \text{DWC} + \text{QuickFlow} \times \text{EMC} \quad (8.1)$$

Where:

Load - total calculated load (kg/d)

SlowFlow - portion of flow representing base flow from the catchment (ML/d)

DWC - dry weather concentration (mg/L)

QuickFlow - portion of flow representing direct runoff from the catchment (ML/d)

EMC - event mean concentration (mg/L)



Water Quality Modelling of the Hawkesbury-Nepean River System

- **Table 8-2 Event Mean Concentration for all catchments except Colo, Grose and the Left Bank in the Source model**

Constituent	Urban	Peri-urban	Mining & Quarrying	Cropping	Grazing	Horticulture	Forest
TN (mg/L)	1.9	2	2.2	3	1.7	3	0.7
NO _x (mg/L)	0.88	0.76	0.84	1.14	0.65	1.14	0.175
TKN (mg/L)	1.02	1.24	1.36	1.86	1.05	1.86	0.525
NH ₄ (mg/L)	0.114	0.082	0.091	0.123	0.07	0.123	0.0136
TP (mg/L)	0.2	0.22	0.45	0.3	0.2	0.4	0.05
FRP (mg/L)	0.093	0.085	0.174	0.116	0.077	0.154	0.015
TSS (mg/L)	120	45	100	40	40	70	40
SiO ₂ (mg/L)				6.2			4.5
Salinity (mg/L)				100			
Faecal coliforms (cfu/100ml)	20,000	1,000	4,000	1,000	20,000	1,000	600
Enterococci (cfu/100ml)	11,600	580	2,320	580	11,600	580	348

- **Table 8-3 Dry Weather Concentration for all catchments except Colo, Grose and the Left Bank in the Source model**

Constituent	Urban	Peri-urban	Mining & Quarrying	Cropping	Grazing	Horticulture	Forest
TN (mg/L)	0.9	0.9		0.8			0.2
NO _x (mg/L)	0.21	0.2		0.18			0.05
TKN (mg/L)	0.69	0.7		0.62			0.15
NH ₄ (mg/L)	0.058	0.048		0.043			0.0136
TP (mg/L)	0.09	0.09		0.05			0.01
FRP (mg/L)	0.037	0.025		0.014			0.005
TSS (mg/L)	16	15		20			6
SiO ₂ (mg/L)				3.9			1.1
Salinity (mg/L)				200			
Faecal coliforms (cfu/100ml)	20,000	1,000	4,000	1,000	20,000	1,000	600
Enterococci (cfu/100ml)	11,600	580	2,320	580	11,600	580	348

- **Table 8-4 Event Mean Concentration for Colo, Grose and the Left Bank in the Source model**

Constituent	Urban	Peri-urban	Mining & Quarrying	Cropping	Grazing	Horticulture	Forest
TN (mg/L)				0.7			
NO _x (mg/L)				0.175			
TKN (mg/L)				0.525			
NH ₄ (mg/L)				0.0136			
TP (mg/L)				0.05			
FRP (mg/L)				0.015			
TSS (mg/L)				40			
SiO ₂ (mg/L)				6.2			4.5
Salinity (mg/L)				100			
Faecal coliforms (cfu/100ml)	20,000	1,000	4,000	1,000	20,000	1,000	600
Enterococci (cfu/100ml)	11,600	580	2,320	580	11,600	580	348

- **Table 8-5 Dry Weather Concentration for Colo, Grose and the Left Bank in the Source model**

Constituent	Urban	Peri-urban	Mining & Quarrying	Cropping	Grazing	Horticulture	Forest
TN (mg/L)				0.2			
NO _x (mg/L)				0.05			
TKN (mg/L)				0.15			
NH ₄ (mg/L)				0.0136			
TP (mg/L)				0.01			
FRP (mg/L)				0.005			
TSS (mg/L)				6			
SiO ₂ (mg/L)				3.9			1.1
Salinity (mg/L)				200			
Faecal coliforms (cfu/100ml)	20,000	1,000	4,000	1,000	20,000	1,000	600
Enterococci (cfu/100ml)	11,600	580	2,320	580	11,600	580	348

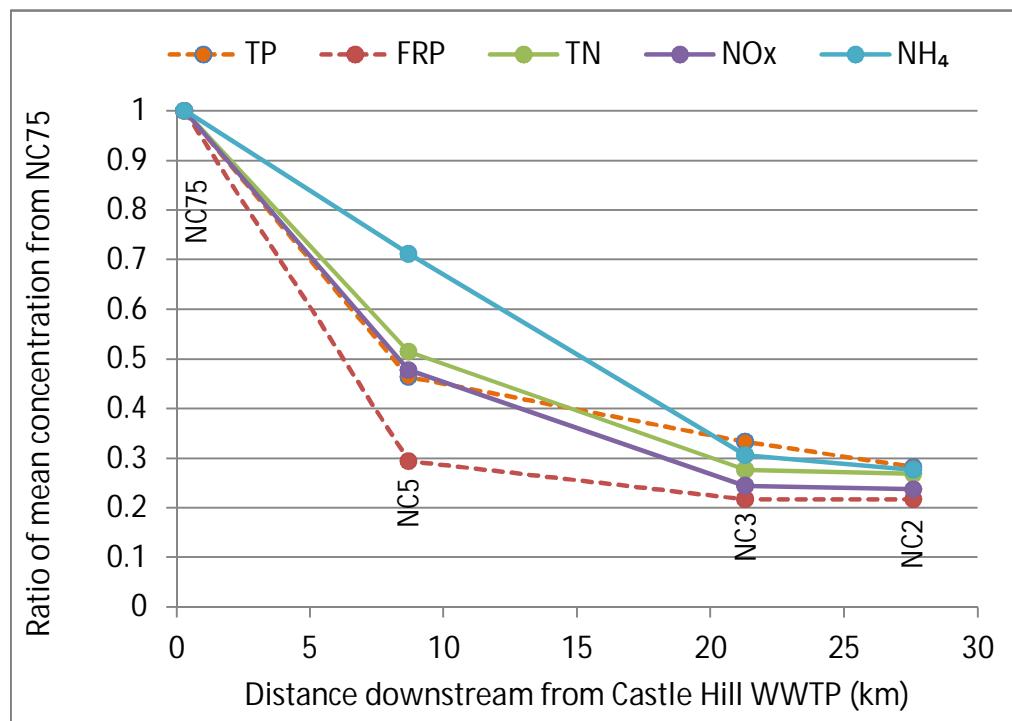
8.3. Nutrient Decay Rates in South, Eastern and Cattai Creeks

Decay models were applied for some of the nutrient species along five links of the catchment model within South, Eastern and Cattai creeks.

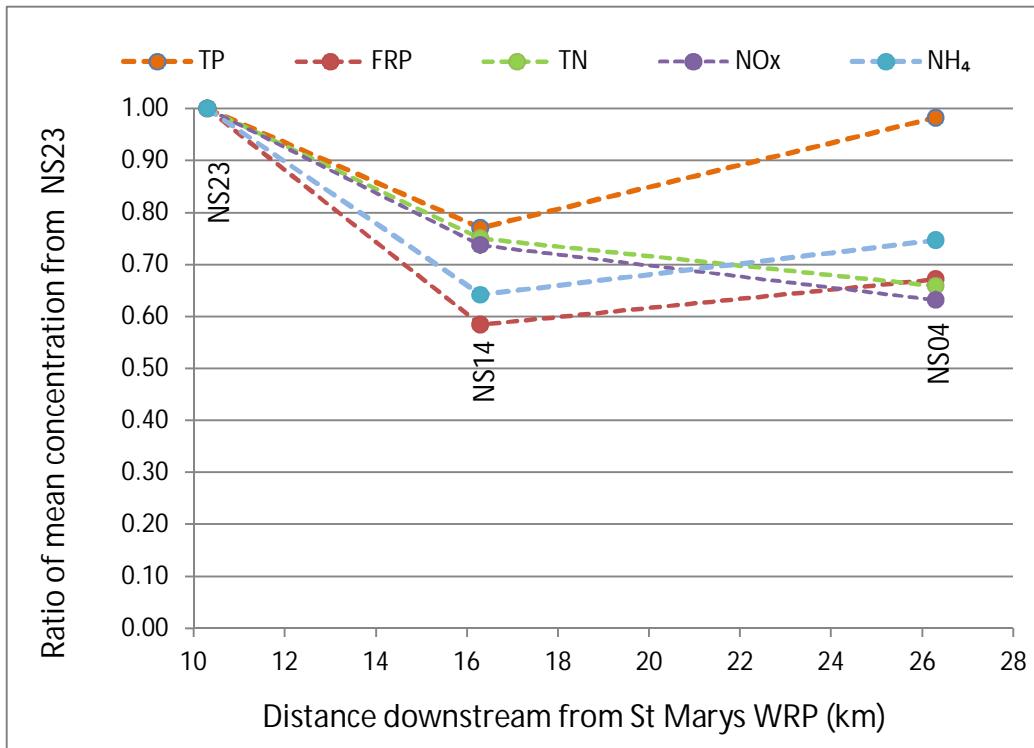
The factors causing nutrient assimilation in Cattai, South and Eastern creeks are well documented in Jones et al. (1994). This analysis draws on the Jones et al. (1994) study as a basis for analysing the available water quality data to determine decay rates for modelling in the Source model. This will simulate the behaviour of nutrient assimilation in specific reaches of the Cattai, South and Eastern creeks. Analysis of corresponding physicochemical data (eg, water temperature, pH, turbidity) shows similar trends as found by Jones et al. (1994), therefore, similar conclusions can be drawn for the factors influencing nutrient assimilation.

The attenuation of constituents was mapped by analysing dry weather water quality data from upstream and downstream sites. The nutrient attenuation plots use the sites immediately downstream of a WWTP/WRP discharge as the reference location from which to determine the loss of nutrients due to assimilation. In order to account for dilution effects from catchment inflows, the streamflow record was restricted to flows occurring on days with no or low rainfall (<5mm), thus representing a near hydrodynamic steady state. The corresponding nutrient concentrations from those days of low flows were then used to calculate nutrient attenuation.

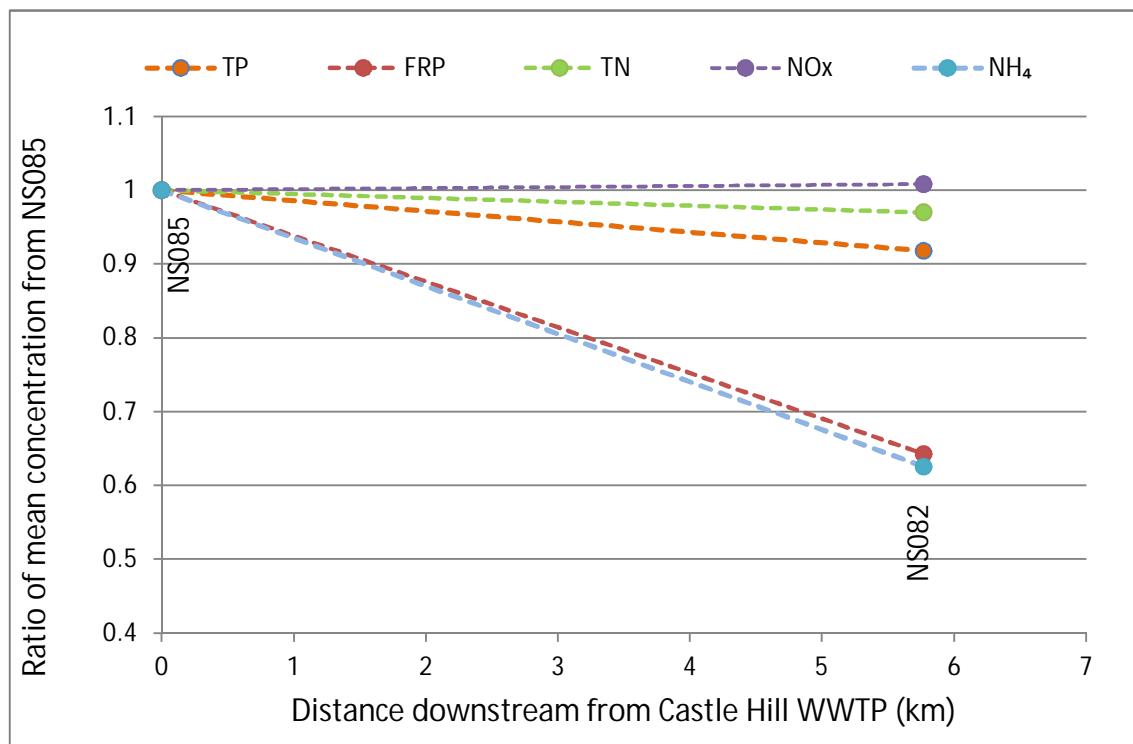
Figure 8-1, Figure 8-2 and Figure 8-3 show the reduction in the mean constituent concentrations between sampling sites along Cattai, South and Eastern creeks. The negative slope in the graphs with distance downstream of each WWTP indicates nutrient assimilation between sites. The slope indicates the “rate” of nutrient assimilation.



- Figure 8-1 Reduction in mean constituent concentrations due to nutrient assimilation in Cattai Creek**



- Figure 8-2 Reduction in mean constituent concentrations due to nutrient assimilation in South Creek**



- **Figure 8-3 Reduction in mean constituent concentrations due to nutrient assimilation in Eastern Creek**

Decay half-lives were applied to each of the nutrient constituents that demonstrated decay in South, Eastern and Cattai creeks. The decay half-life parameters were determined by iterative adjustment, with the intention of minimising the sum of square differences between the monitored and modelled concentrations at the downstream site. The adopted decay half-lives for each constituent, in each of the links applied in the Source model are as shown in **Table 8-6** below.

- **Table 8-6 Decay half-lives (k in seconds) applied for nutrient constituents in the Source model**

Creek Name	South_Creek_Left01	IS_SthCreek_003	IQQM_EasternCk_Residuals_Lin2	CattaiResidual_Link7	CattaiResidual_Link4
TN	440000	330000	-	220000	220000
NOx	440000	330000	-	220000	220000
TKN	440000	330000	-	220000	220000
NH ₄	118530	-	177860	200930	133700
TP	162690	-		317260	116330
FRP	134170	-	304560	396580	52880

8.4. Event Campaign Monitoring Program (CMP)

The event CMP collected event water quality monitoring data for Forested, Peri-Urban and Agricultural catchments.

Event monitoring sites were chosen from existing stream gauging stations. A list of event CMP sites is shown in **Appendix E.1**.

The events captured by each CMP are listed in **Appendix E.2**. Due to the limited volume of each autosampler bottle, analyte prioritisation was as follows:

- Nutrients – TN, TP, NO_x, FRP, NH₄, TKN, SiO₂;
- Bacteria – Faecal coliforms, *Clostridium perfringens*, Enterococci;
- TOC and DOC;
- TSS;
- CBOD₅;
- pH;
- Conductivity; and
- Turbidity.

The constituents used in the Source model were validated using the CMP data (**Table 8-7** to **Table 8-9**). For catchments with agricultural and peri-urban land uses (**Table 8-7**) the generation rates used in the Source model for faecal coliforms, Enterococci, total nitrogen (TN), total phosphorus (TP), silicates (SiO₂) and total Kjedahl nitrogen (TKN) were all close to the mean or median of the observed event data. Ammonium (NH₄), oxidised nitrogen (NO_x) and filterable reactive phosphorus (FRP) had modelled concentrations which were higher than those observed in the events. As this is based on only a few events and the modelled values are generally within the range of the observed values, no changes were made to the generation rates adopted in the Source model. This is also applicable for total suspended solids (TSS) where the modelled concentration is lower than the mean and median of observed values.

For the catchments which have predominantly urban land uses (**Table 8-8**) the generation rates used for faecal coliforms, Enterococci, ammonium and total suspended solids in the Source model were similar to the mean or median values of the observed events. The other variables were generally within the range of the observed events. As with the agricultural land use type described above, the modelled values were within acceptable ranges and did not require adjustment.

The third land use type examined was the forested land use (**Table 8-9**). As there were only two events, the results were compared directly between the recorded and calculated values for each event. It was observed that there was some difference between the modelled and the observed event mean concentrations. Some of the observed results were unexpected for a particular land use. For example, observed event concentrations for TN, TKN and TSS, were considerably higher than expected from a forested catchment. No adjustment was made to the EMC or DWC within the Source model for TN, TKN or TSS based on the CMP data. Increasing the EMC's in the Source model for forested catchments would have made them higher than the EMC's in the model for SINCLAIR KNIGHT MERZ



Water Quality Modelling of the Hawkesbury-Nepean River System

urban, peri urban and agriculture. The TN, TKN and TSS concentrations recorded during the two forested land use CMP events were considered not to be typical for events measured over longer time scales (compared with concentrations recorded from forested landuse in other catchments by SCA, 2003 and Bartley *et al.*, 2012). If these high concentrations/outliers were adopted for all forest regions or just the forest regions in the Colo catchment, this would have been inconsistent with the large volume of sampling results from further downstream..



Water Quality Modelling of the Hawkesbury-Nepean River System

- **Table 8-7 Comparison between observed EMC calculated for seven events on Ropes and Stonequarry creeks to EMC values used in the Source model for Peri-Urban and Agricultural (Horticulture and Grazing) land use types**

Parameter	Faecal coliforms (CFU/100ml)	Enterococci (CFU/100ml)	NH ₄ (mg/L)	NO _x (mg/L)	TN (mg/L)	TKN (mg/L)	TP (mg/L)	FRP (mg/L)	SiO ₂ (mg/L)	TSS (mg/L)
Number of Events	7	7	7	7	7	7	7	7	7	7
Mean Event	16918	11486	0.024	0.301	1.644	1.343	0.248	0.034	5.825	188
Median Event	11044	9091	0.026	0.287	1.550	1.182	0.208	0.035	5.228	149
Minimum of Event	5659	3605	0.010	0.163	1.025	0.738	0.147	0.008	2.401	38
Maximum of Event	52992	30226	0.045	0.387	2.537	2.262	0.509	0.063	10.584	600
Modelled Grazing	20000	11600	0.070	0.650	1.700	1.050	0.200	0.077	6.200	40
Modelled Peri-Urban	1000	580	0.082	0.760	2.000	1.240	0.220	0.085	6.200	45
Modelled Horticulture	1000	580	0.123	1.140	3.000	1.860	0.400	0.154	6.200	70

- **Table 8-8 Comparison between observed EMC calculated for four events on South and Eastern creeks to EMC values used in the Source model for Urban and Peri-Urban land use types**

Parameter	Faecal coliforms (CFU/100ml)	Enterococci (CFU/100ml)	NH ₄ (mg/L)	NO _x (mg/L)	TN (mg/L)	TKN (mg/L)	TP (mg/L)	FRP (mg/L)	SiO ₂ (mg/L)	TSS (mg/L)
Number of Events	4	4	4	4	4	4	4	4	4	4
Mean Event	12596	7310	0.115	0.56	2.40	1.83	0.38	0.142	8.82	101
Median Event	4597	2609	0.036	0.54	2.39	1.95	0.31	0.107	9.63	83
Minimum of Event	641	24	0.012	0.29	1.72	1.22	0.30	0.058	5.16	28
Maximum of Event	40551	23997	0.377	0.89	3.11	2.22	0.58	0.293	10.85	212
Modelled Urban	20000	11600	0.114	0.88	1.90	1.02	0.20	0.093	6.20	120
Modelled Peri-Urban	1000	580	0.082	0.76	2.00	1.24	0.22	0.085	6.20	45

SINCLAIR KNIGHT MERZ



Water Quality Modelling of the Hawkesbury-Nepean River System

- Table 8-9 Comparison between observed EMC calculated for two events on the Colo and Grose rivers to an EMC computed in the Source model by applying the relevant power curve adopted for forested catchments to the flow data collected during each event at each site

Parameter	Faecal coliforms (CFU/100ml)	Enterococci (CFU/100ml)	NH ₄ (mg/L)	NO _x (mg/L)	TN (mg/L)	TKN (mg/L)	TP (mg/L)	FRP (mg/L)	SiO ₂ (mg/L)	TSS (mg/L)
Colo Event	371	1026	0.0100	0.04	7.02	6.99	0.09	0.003	5.45	197
Colo Modelled Event	600	348	0.0136	0.10	0.48	0.380	0.03	0.012	4.50	13
Grose Event	428	496	0.0100	0.02	2.92	2.900	0.04	0.002	3.33	41
Grose Modelled Event	600	348	0.0136	0.10	0.49	0.391	0.03	0.013	4.50	14

8.5. Comparison of Constituent Loads at Monitoring Sites

Comparison between observed and simulated concentrations at the 23 water quality sites listed in **Table 8-1** are provided in **Appendix F** as Box & Whisker plots and exceedance plots.

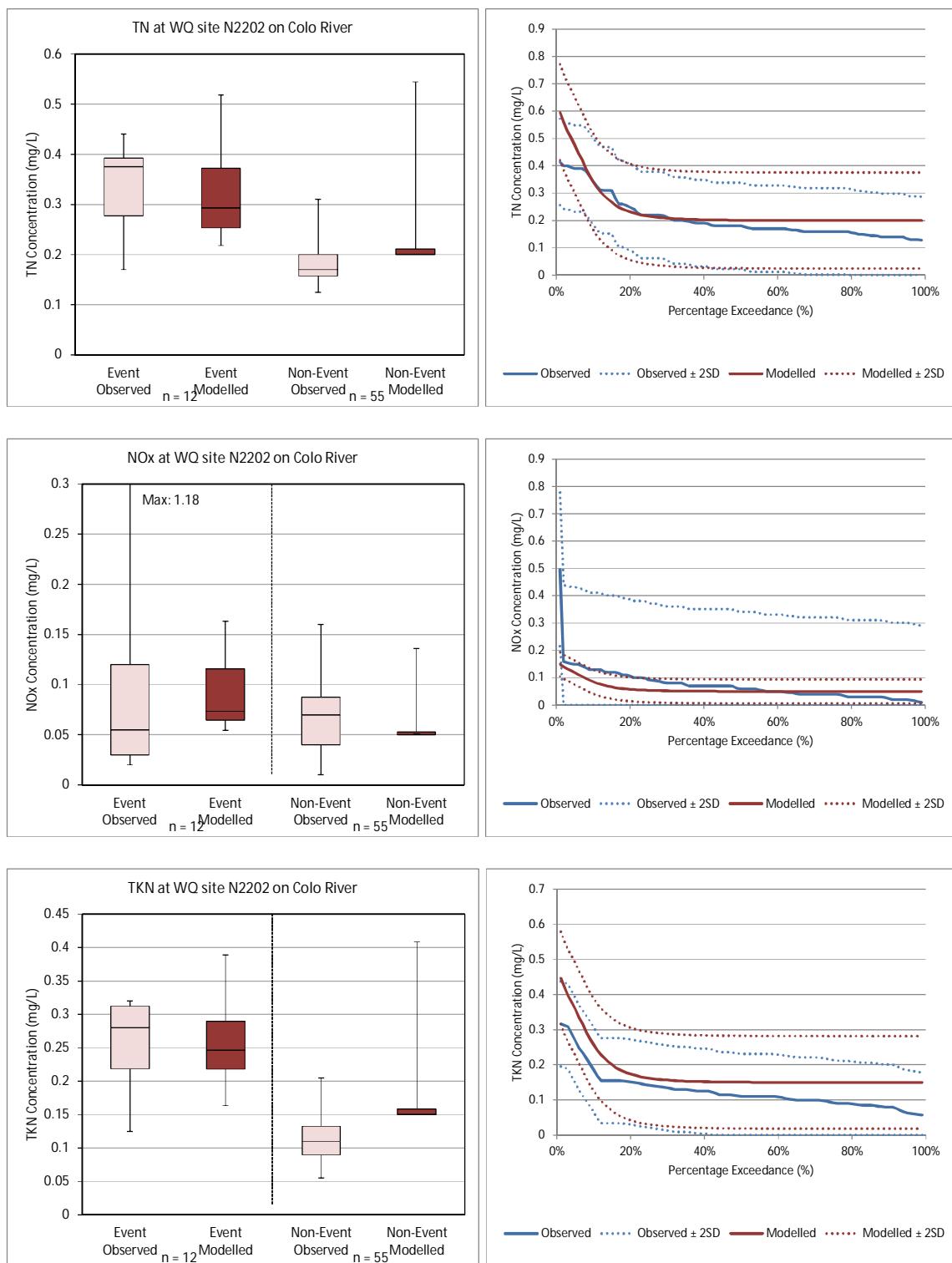
The box and whisker plots show the 25th and 75th percentiles, with the median concentration shown by the line across the box. The whiskers show the minimum and maximum values. The “event” concentrations were separated from the “non-event” concentrations in the comparison process. An “event” concentration is defined by flows with a probability of exceedance of <20%. The numbers of observations used to produce the plots are indicated at the bottom of the graphs.

The exceedance plots show the observed and modelled concentrations (solid lines) with the range of uncertainty represented by two standard deviations either side of the measured or modelled values. Two standard deviations is a statistical measure which represents 95% of the variance in the results. It is assumed that this range will capture the representative variance of both the modelled and observed constituent loads.

The number of constituents included in the comparison varies among sites, depending on the constituents monitored. However all comparisons have results for TN, NO_x, NH₄, TKN, TP and FRP. **Figure 8-4**, **Figure 8-5** and **Figure 8-6** are box and whisker plots of observed and modelled concentrations at the water quality sites N2202 on the Colo River, N4301/GR4301 on the Grose River and NS14 on South Creek. These plots, which are representative of the three largest tributaries in the model in terms of flows and loads delivered to the estuary, show reasonably good agreement between observed and modelled values for the six constituents above for the purposes of the Hawkesbury-Nepean River and South Creek Model.

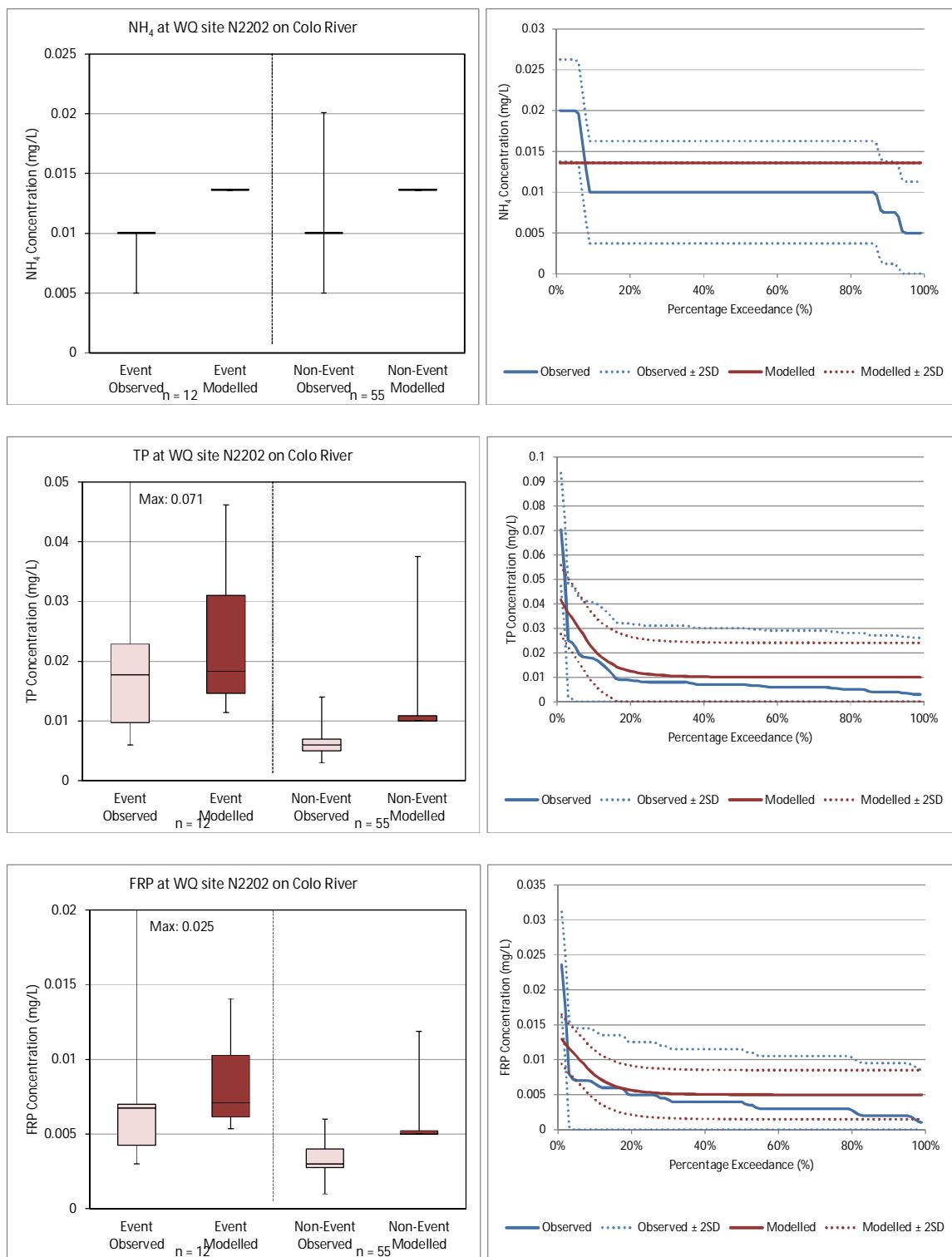
The exceedance plots show how representative the modelled constituents are compared to the observed values. **Appendix F** shows that for all constituents except salinity (in some instances) the modelled and the observed results show good correlation. Salinity concentrations observed at sampling locations in the catchment model were generally lower than those observed at sites within the estuary. The generation rates for salinity were selected to calibrate the model to the estuary sites, in preference to matching the salinity concentrations recorded at the sampling locations in the catchments.

Water Quality Modelling of the Hawkesbury-Nepean River System



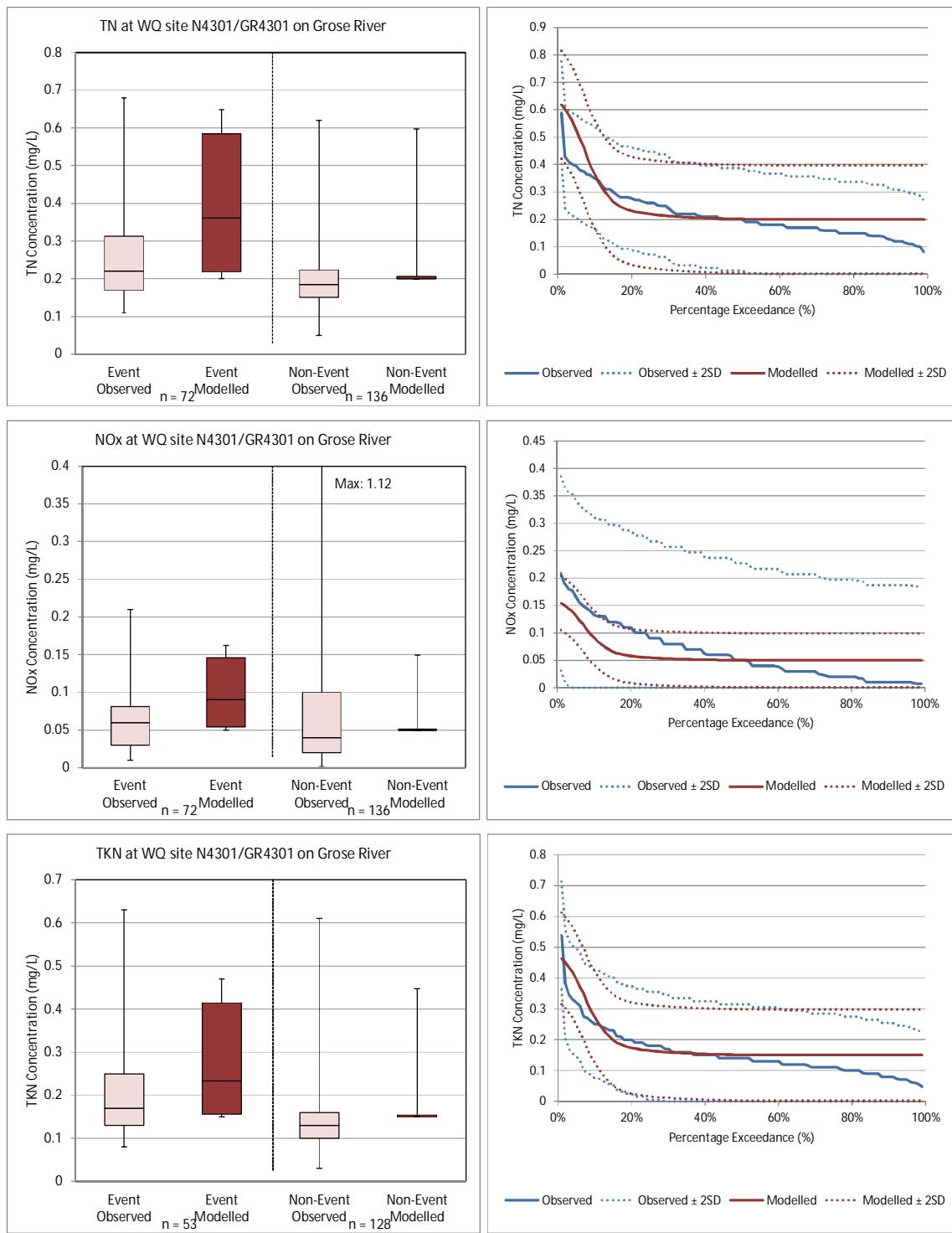
■ **Figure 8-4 Modelled and observed constituent concentrations at the water quality monitoring site N2202 on the Colo River**

Water Quality Modelling of the Hawkesbury-Nepean River System



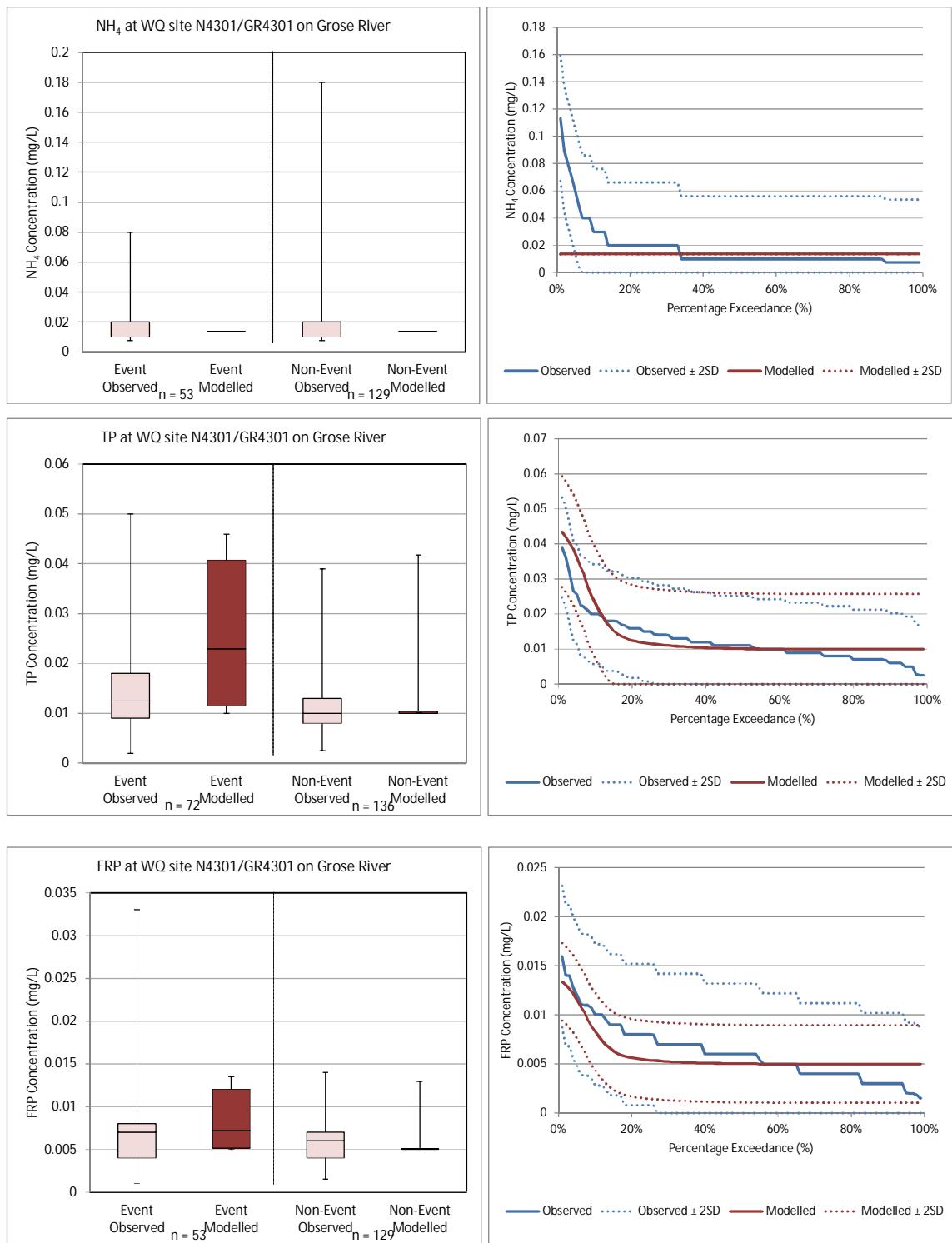
■ **Figure 8-4 (cont.) Modelled and observed constituent concentrations at the water quality monitoring site N2202 on the Colo River**

Water Quality Modelling of the Hawkesbury-Nepean River System



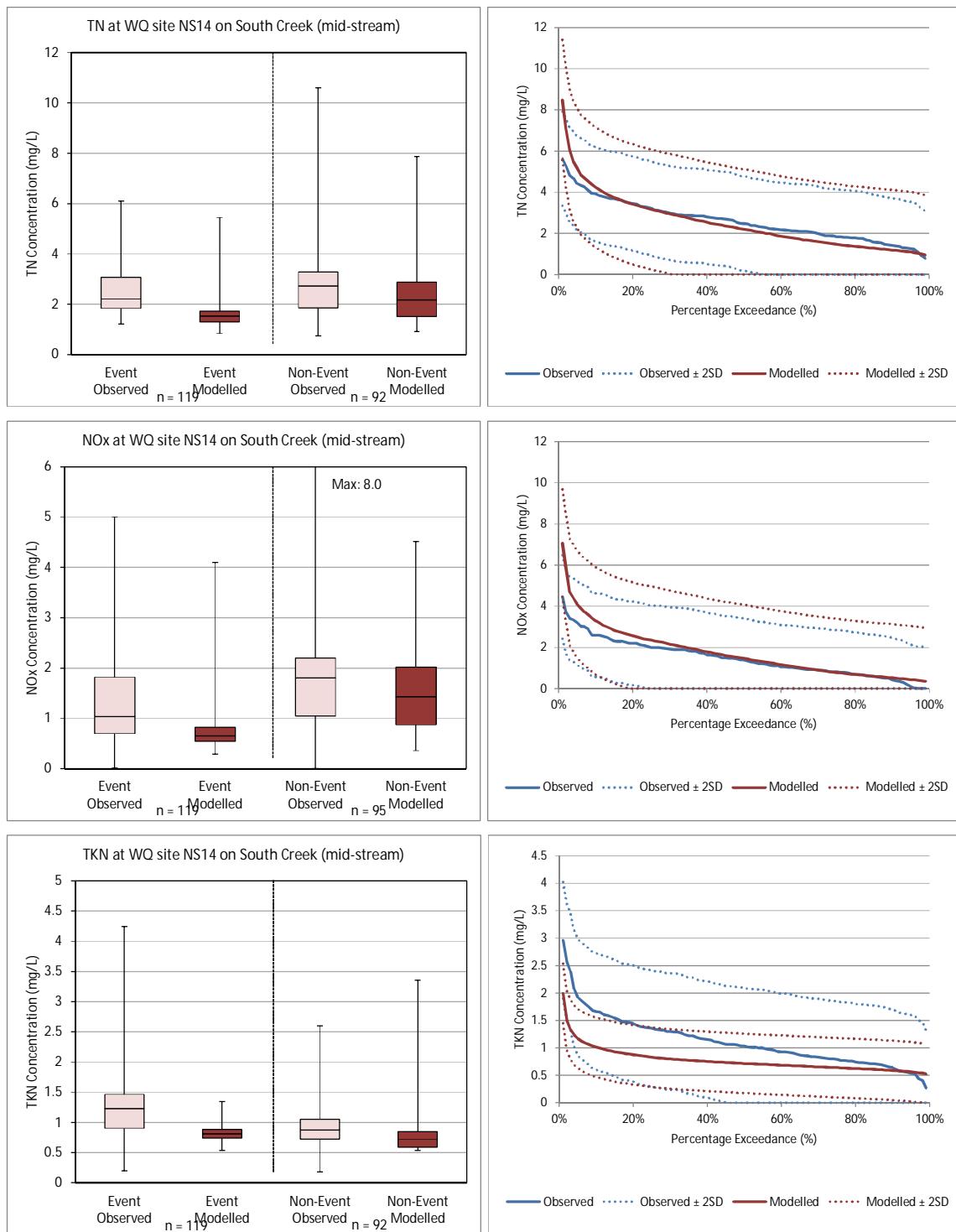
■ **Figure 8-5 Modelled and observed constituent concentrations at the water quality monitoring site N4301/GR4301 on the Grose River**

Water Quality Modelling of the Hawkesbury-Nepean River System



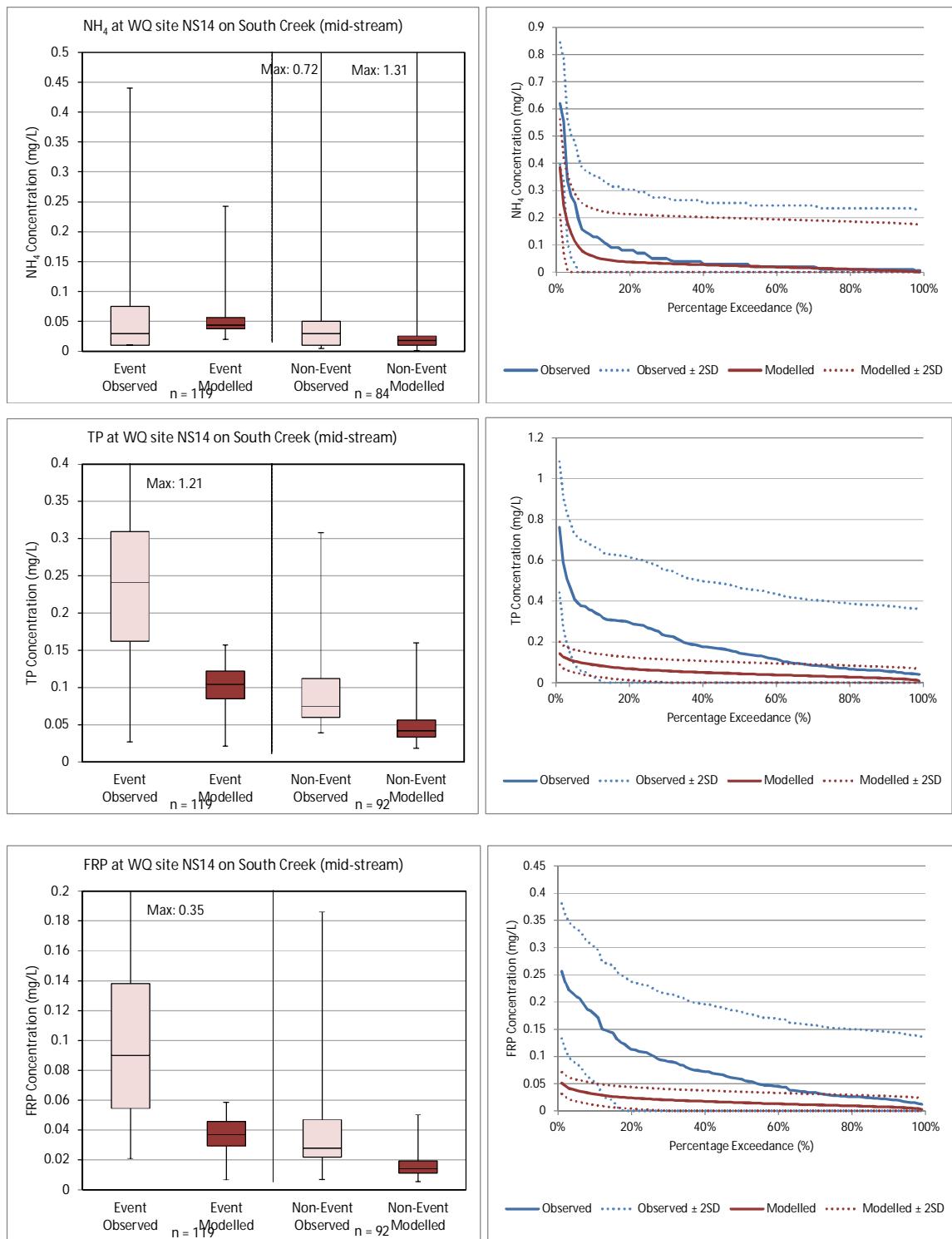
■ **Figure 8-5 (cont.) Modelled and observed constituent concentrations at the water quality monitoring site N4301/GR4301 on the Grose River**

Water Quality Modelling of the Hawkesbury-Nepean River System



■ **Figure 8-6 Modelled and observed constituent concentrations at the water quality monitoring site NS14 on South Creek**

Water Quality Modelling of the Hawkesbury-Nepean River System



■ **Figure 8-6 (cont.) Modelled and observed constituent concentrations at the water quality monitoring site NS14 on South Creek**

8.6. Additional Water Quality Parameters

Water quality parameters including total and dissolved organic carbon, dissolved oxygen, pH and temperature were required by the TUFLOW/AED model in addition to those already modelled within the Source model. These parameters were examined and calibrated against observed data, as discussed below.

The data used to determine these relationships was taken from data provided by various stakeholders operating within the Hawkesbury-Nepean catchment, including OEH, Sydney Water, SCA and MHL. The number of sample data points used for each representative region is summarised in **Table 8-10** below. The full list of sites and data used is provided in **Appendix G**.

- **Table 8-10 Number of samples available and used to create relationships for water quality parameters**

Location	Dissolved Oxygen	pH	Temperature	Dissolved Organic Carbon	Total Organic Carbon
Broughton Pass (Cataract River)	136	136	136	139	139
Cattai Creek	845	1610	1274	9	9
Colo River			56291	9	9
Eastern Creek	875	1163	1033	18	18
Hawkesbury River	38244	100662	87059	265	65
Nepean River	310	307	310	334	148
Pheasants Nest	804	509	813	118	61
South Creek	1584	2075	1771	24	24
Warragamba River	50609	50589	51154	2794	2573

In using the data, certain assumptions were made. These assumptions were:

- Warragamba – data was collected within the dam and therefore measured at various depths. The readings were averaged across the sample depths to provide one measurement to represent the dam at each time step. In general there was only a small amount of variability across the different sampling depths within Warragamba. As such taking the average was an appropriate method for ensuring a single value per timestep.
- Representative catchment data – for each of the representative catchments there were sometimes multiple gauging locations. To provide a larger data set these measurements were combined to create one representative data set for the catchment.
- Fitted sinusoidal equations – a number of the water quality parameters were able to be represented by sine equations as the parameters varied in response to the time of the year. These equations were fitted using the statistical properties of the data sets to represent the best overall fit.

8.6.1. Temperature

This section outlines the temperature relationships developed across the Hawkesbury-Nepean Catchment. The relationships have been developed using a sine relationship with time of year being the key driver. The equation is of the form:

$$T = a \sin(2\pi t + b) + c \quad (8.2)$$

Where:

T = water temperature in degrees Celsius

t = the current day as a fraction of the year

a = amplitude of the temperature signal

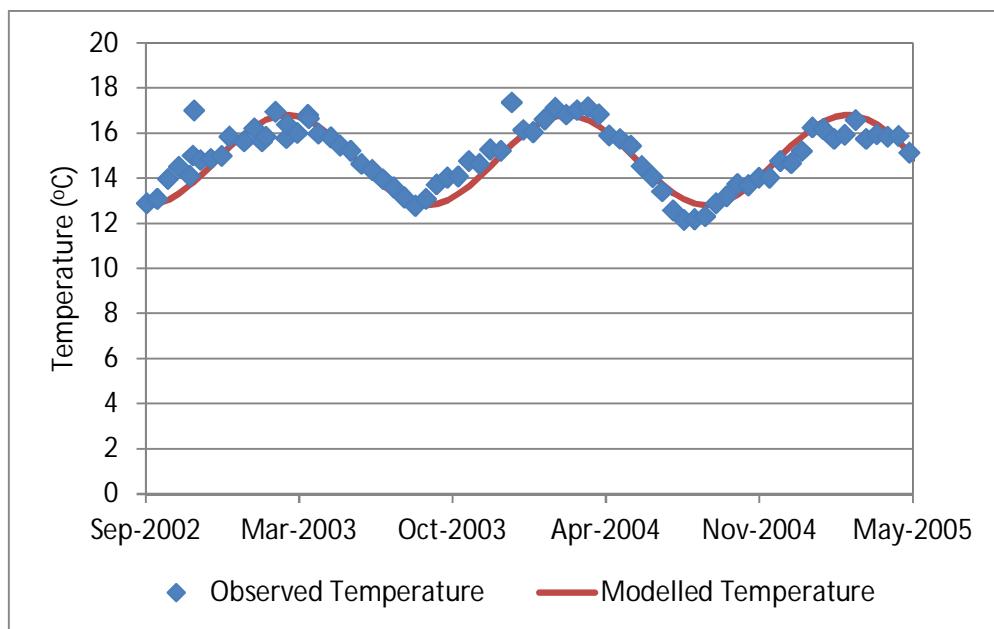
b = phase of the temperature signal

c = average temperature

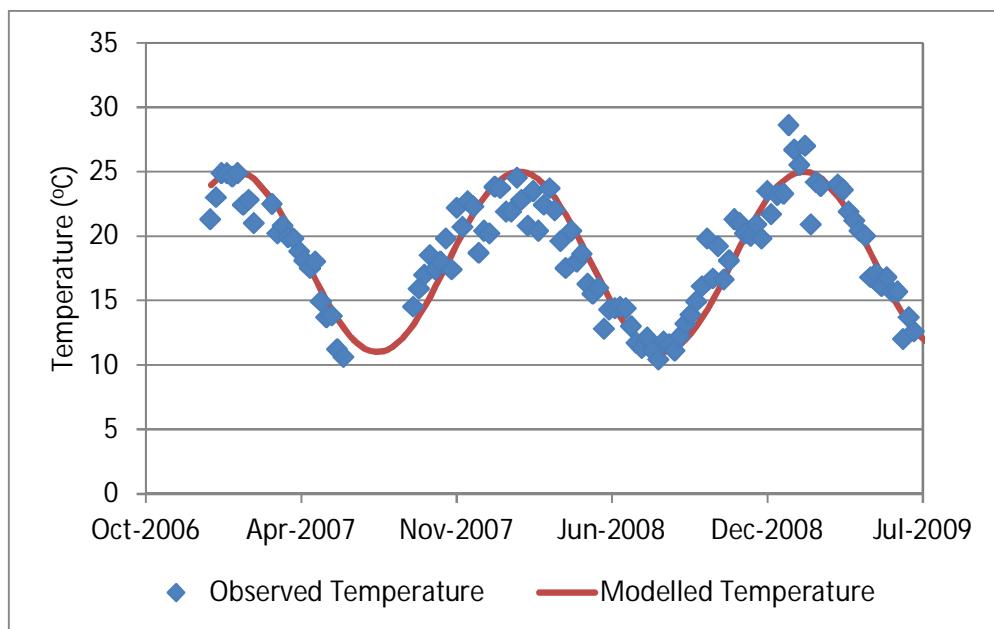
The coefficients for each of the locations are outlined in **Table 8-11**. Plots of selected periods at each location are outlined from **Figure 8-7** to **Figure 8-15** with the full available series outlined in **Appendix G**.

- **Table 8-11 Equation coefficients for water temperature in the Hawkesbury-Nepean catchment**

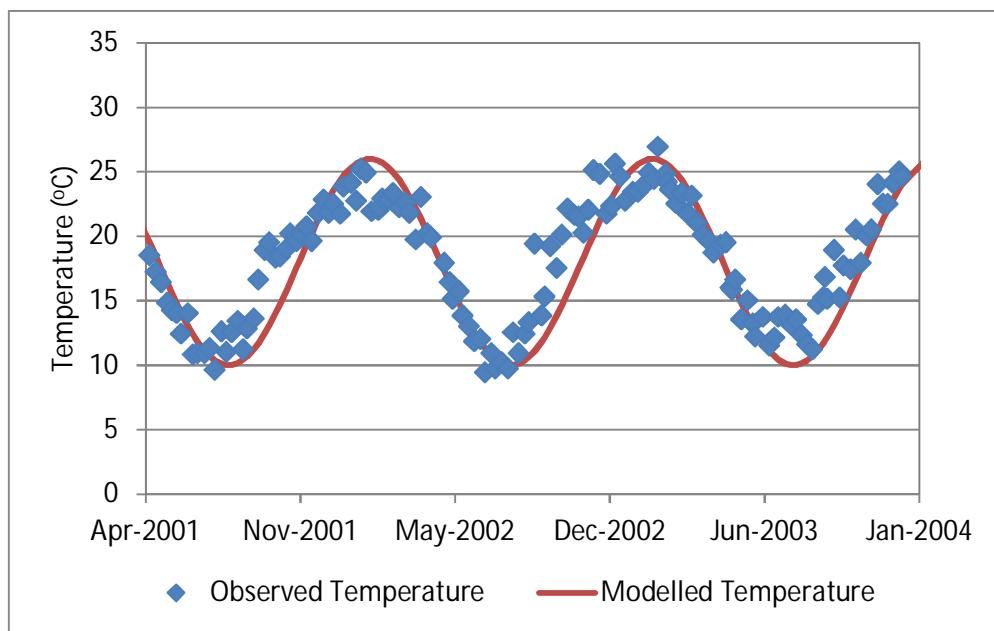
Location	Amplitude (a) (°C)	Phase (b) (time)	Date of maximum temperature	Date of minimum temperature	Mean (°C)
Warragamba River	2	0.5	4 th March	4 th September	14.8
Cataract River at Broughton Pass	7	1	6 th February	6 th October	18
Nepean River at Pheasants Nest	8	1	6 th February	6 th October	18
South Creek	8	1	6 th February	6 th October	18
Eastern Creek	7	1	6 th February	6 th October	18.5
Cattai Creek	6	1	6 th February	6 th October	17
Colo River	7	1	6 th February	6 th October	19
Nepean River	8	1	6 th February	6 th October	18
Hawkesbury River	8	1	6 th February	6 th October	19.5



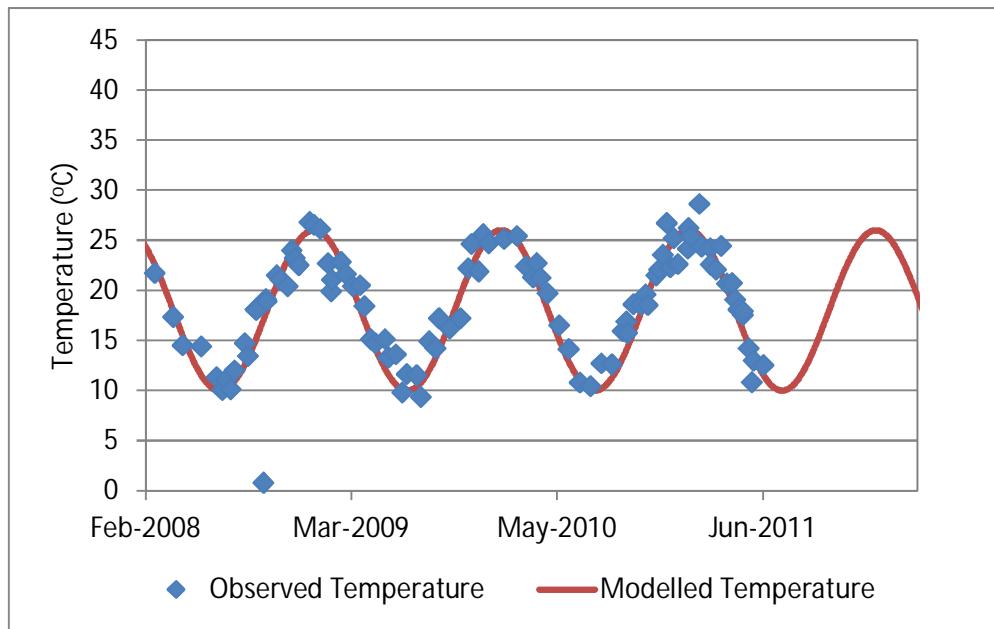
■ **Figure 8-7 Example of Warragamba River water temperature with fitted relationship**



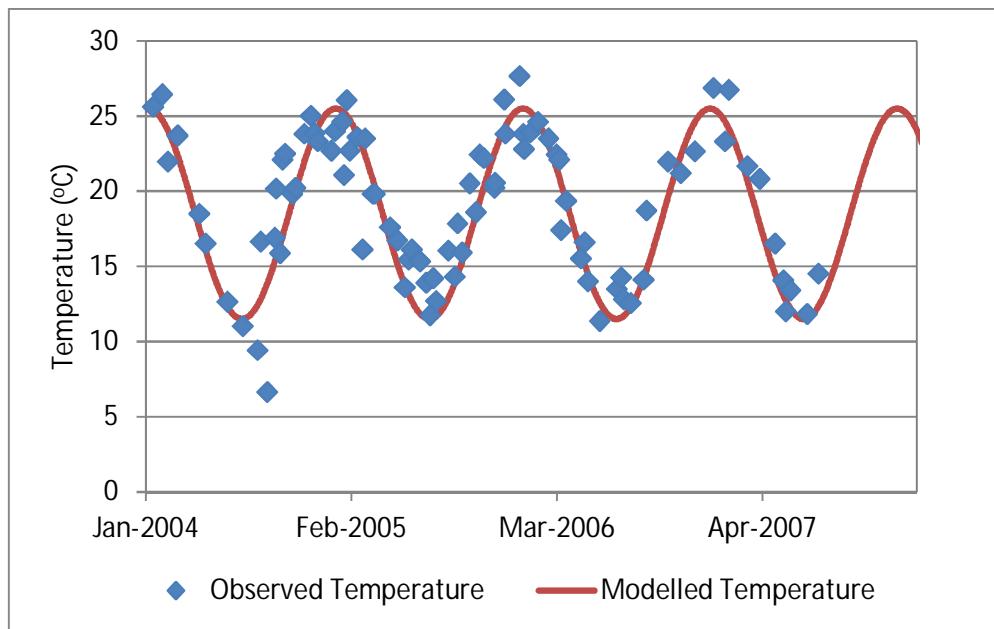
■ **Figure 8-8 Example of Broughton Pass (Cataract River) water temperature with fitted relationship**



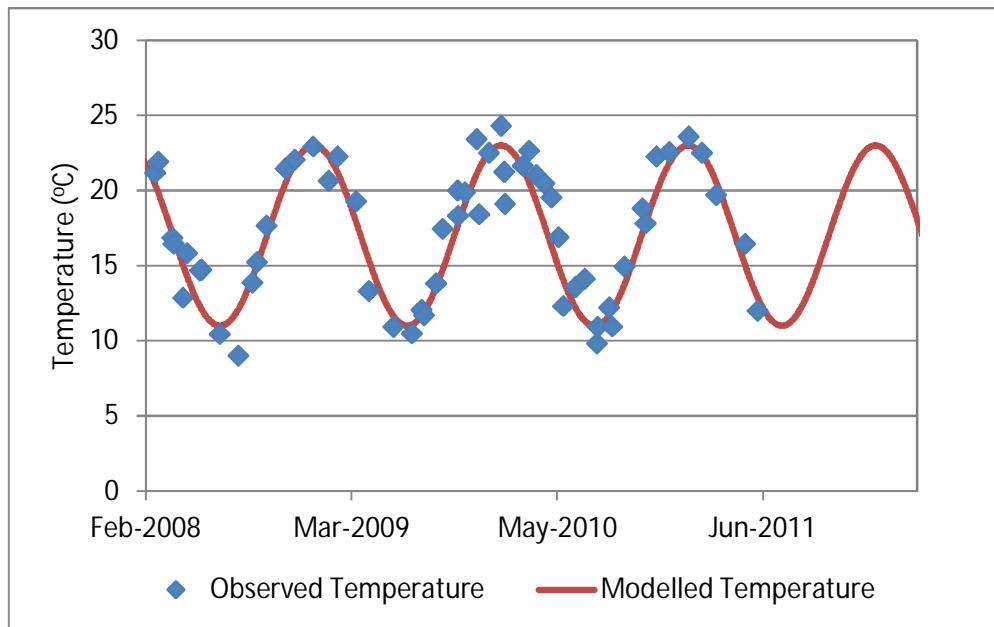
- **Figure 8-9 Example of Pheasants Nest (Nepean River) water temperature with fitted relationship**



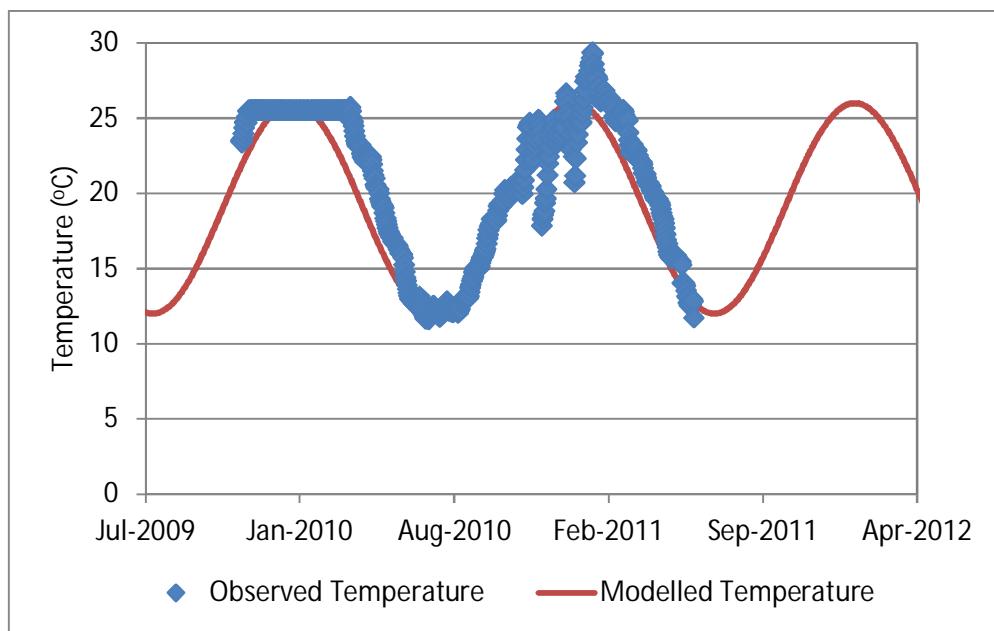
- **Figure 8-10 Example of South Creek water temperature with fitted relationship**



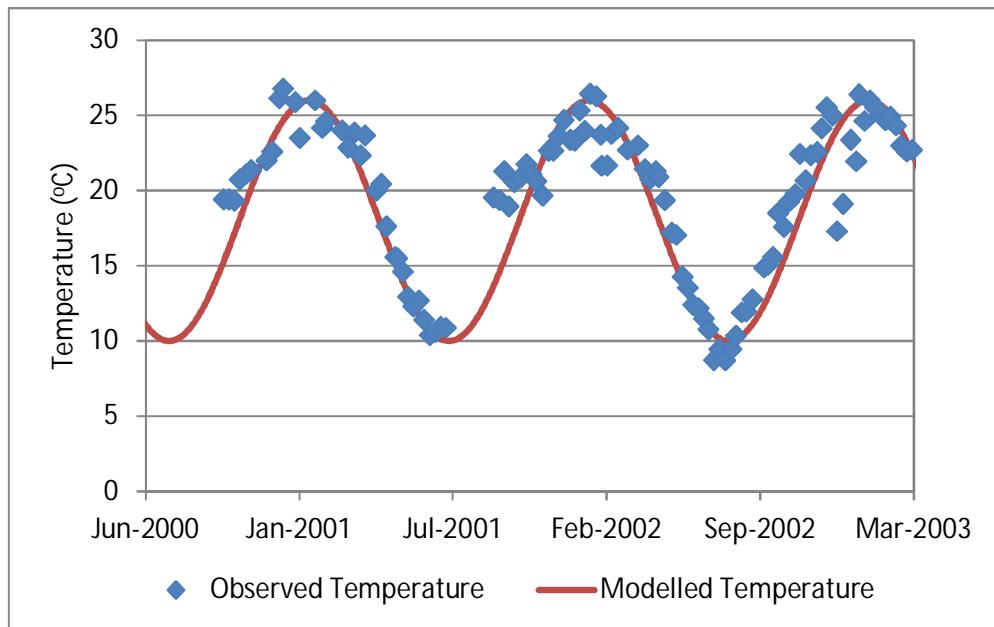
■ **Figure 8-11 Example of Eastern Creek water temperature with fitted relationship**



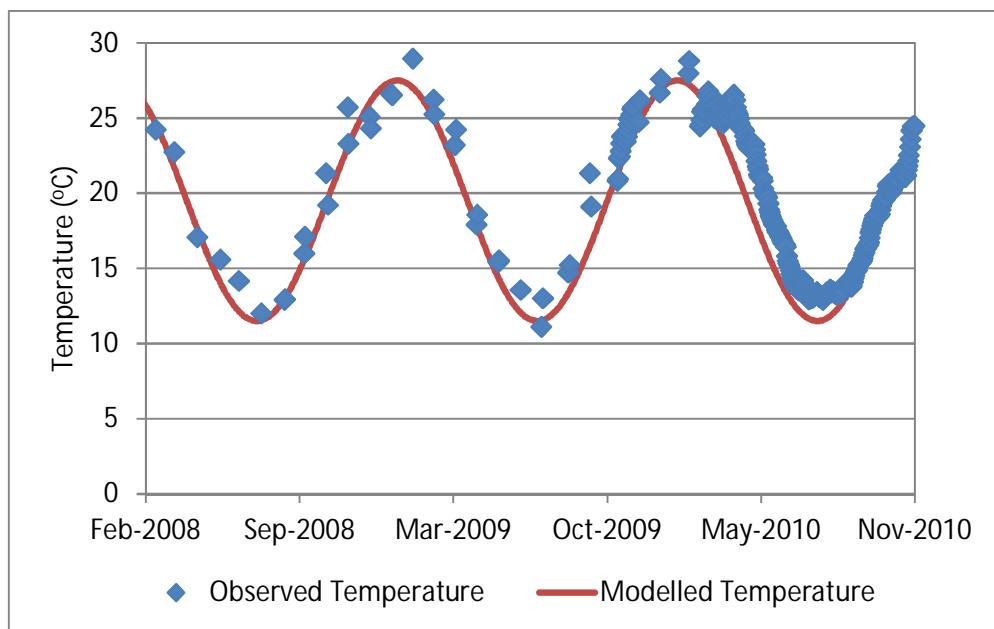
■ **Figure 8-12 Example of Cattai Creek water temperature with fitted relationship**



■ **Figure 8-13 Example of Colo River water temperature with fitted relationship**



■ **Figure 8-14 Example of representative Nepean River water temperature with fitted relationship**



- **Figure 8-15 Example of representative Hawkesbury River water temperature with fitted relationship**

8.6.2. Dissolved Oxygen

This section outlines the dissolved oxygen relationships developed across the Hawkesbury-Nepean Catchment. The relationship is a sine relationship with time of year being the key driver. The sine equation is of the form:

$$DO = a \sin(2\pi t + b) + c \quad (8.3)$$

Where:

DO = dissolved oxygen concentration in mg/L

t = the current day as a fraction of the year

a = amplitude of dissolved oxygen range

b = phase of dissolved oxygen

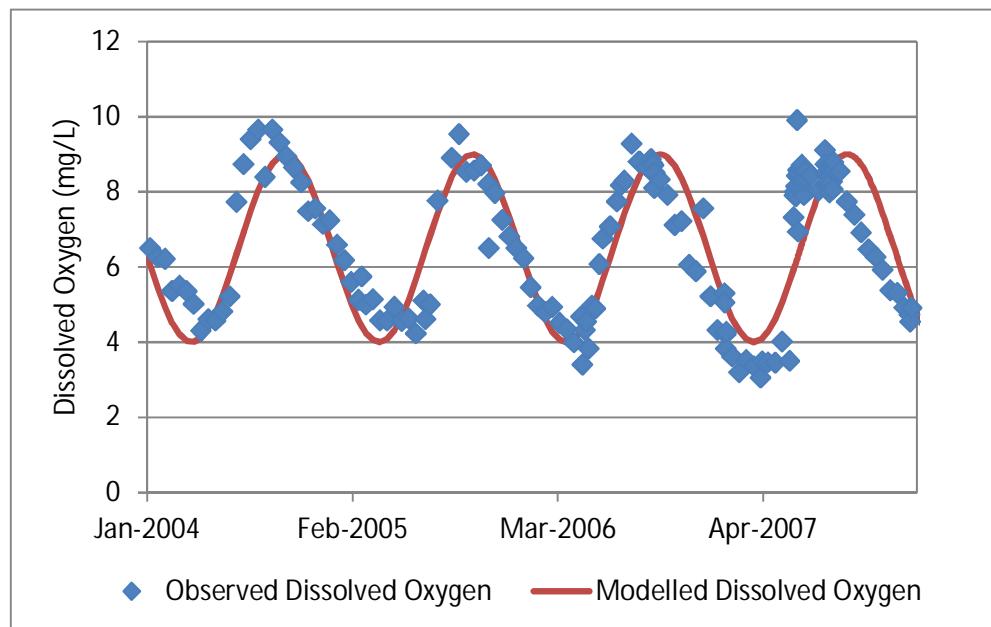
c = average dissolved oxygen

The coefficients for each of the locations are outlined in **Table 8-12** for the sine relationships. Plots of selected periods of the sine relationships at each location are outlined from **Figure 8-16** to **Figure 8-23** with the full available series outlined in **Appendix G**.

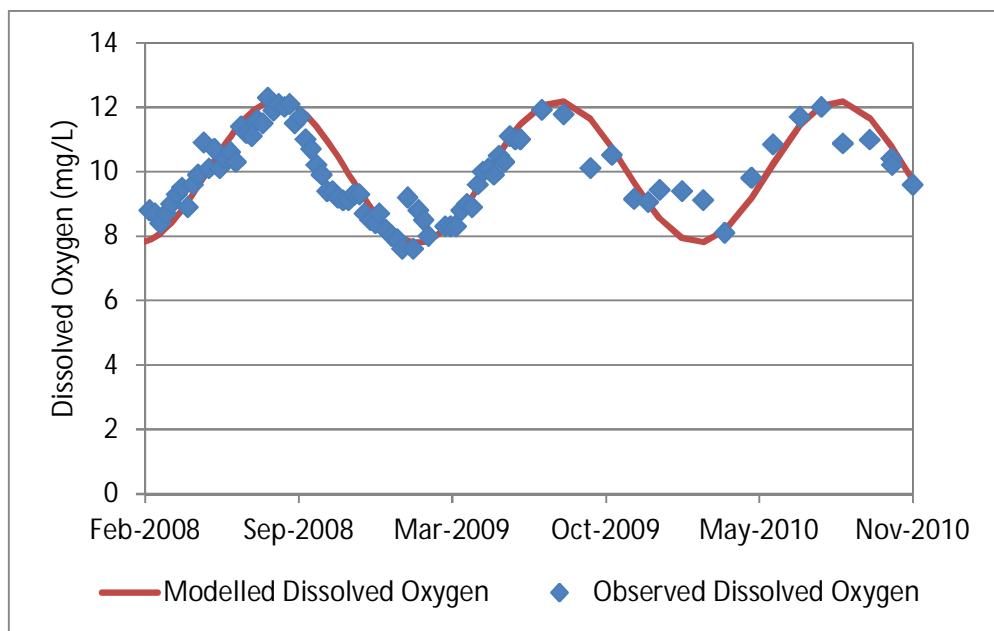
Water Quality Modelling of the Hawkesbury-Nepean River System

- **Table 8-12 Sine equation coefficients for dissolved oxygen in the Hawkesbury-Nepean catchment**

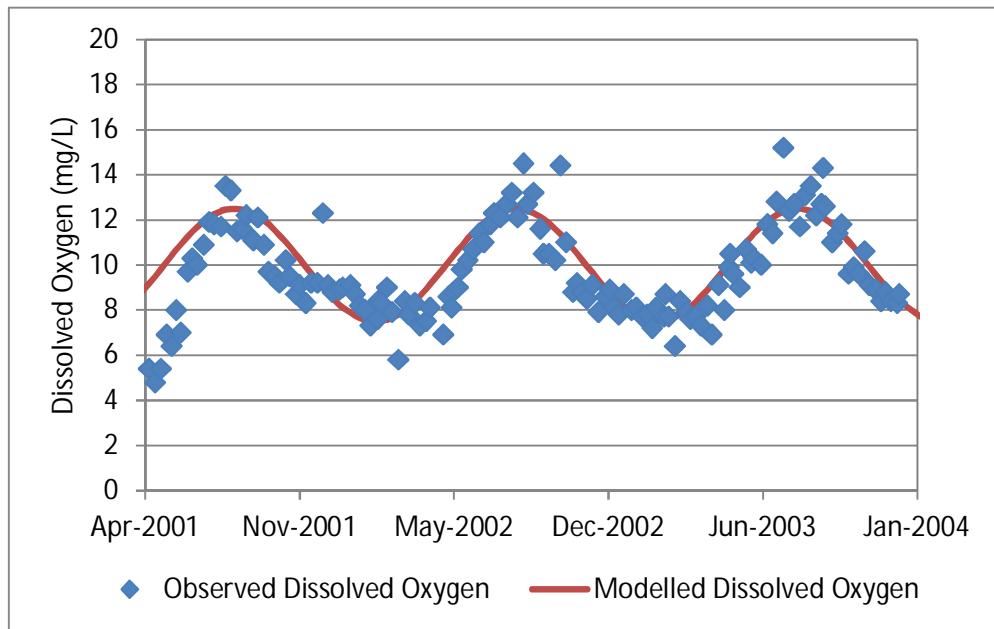
Location	Amplitude (a) (mg/l)	Timing (b) (time)	Date of maximum dissolved oxygen	Date of minimum dissolved oxygen	Mean (mg/L)
Warragamba River	2.5	3	16 th April	16 th October	6.5
Cataract River at Broughton Pass	2.2	4	13 th June	13 th December	10
Nepean River Pheasants Nest	2.5	4	13 th June	13 th December	10
South Creek	2.5	4	13 th June	13 th December	6.5
Eastern Creek	2	4	13 th June	13 th December	6.2
Cattai Creek	2.25	4	13 th June	13 th December	8.5
Colo River	No Data – use Cattai Creek numbers				
Nepean River	2.5	3.5	15 th May	15 th September	9
Hawkesbury River	2.5	3.5	15 th May	15 th September	8.5



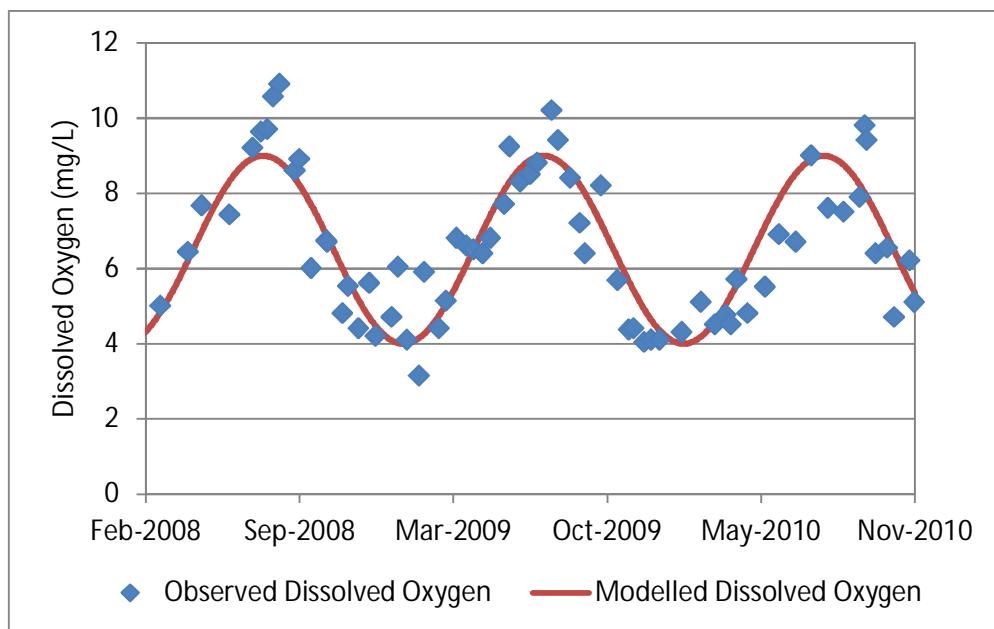
- **Figure 8-16 Example of Warragamba River dissolved oxygen with fitted sine relationship**



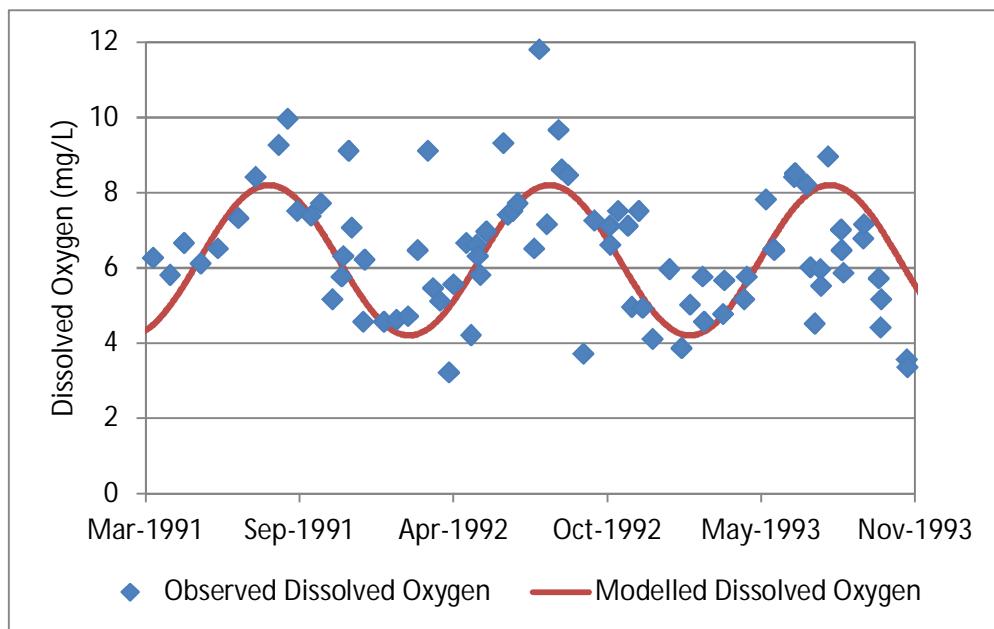
- **Figure 8-17 Example of Broughton Pass(Cataract River) dissolved oxygen with fitted sine relationship**



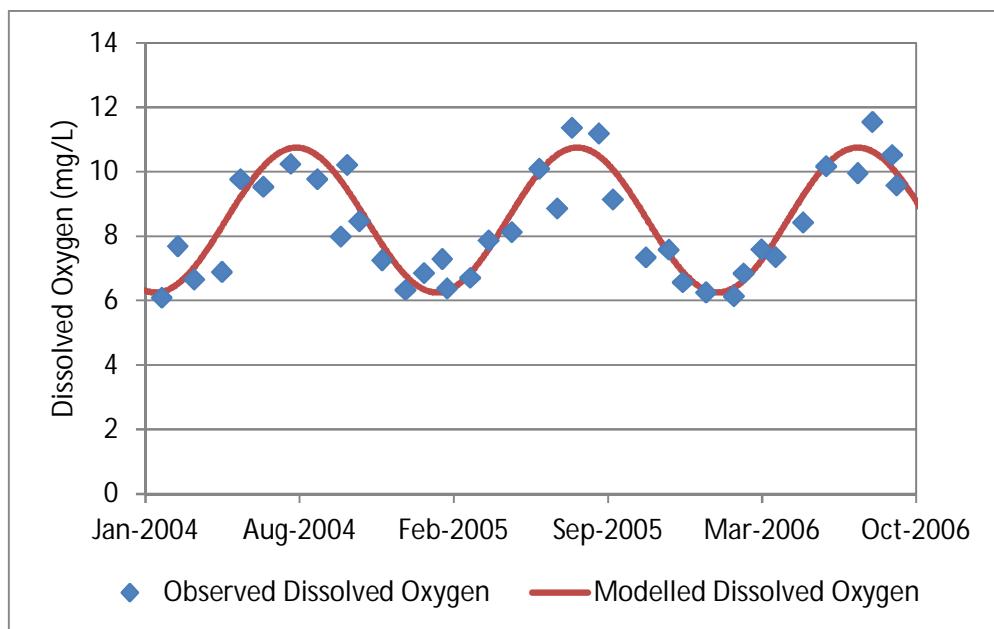
- **Figure 8-18 Example of Pheasants Nest (Nepean River) dissolved oxygen with fitted sine relationship**



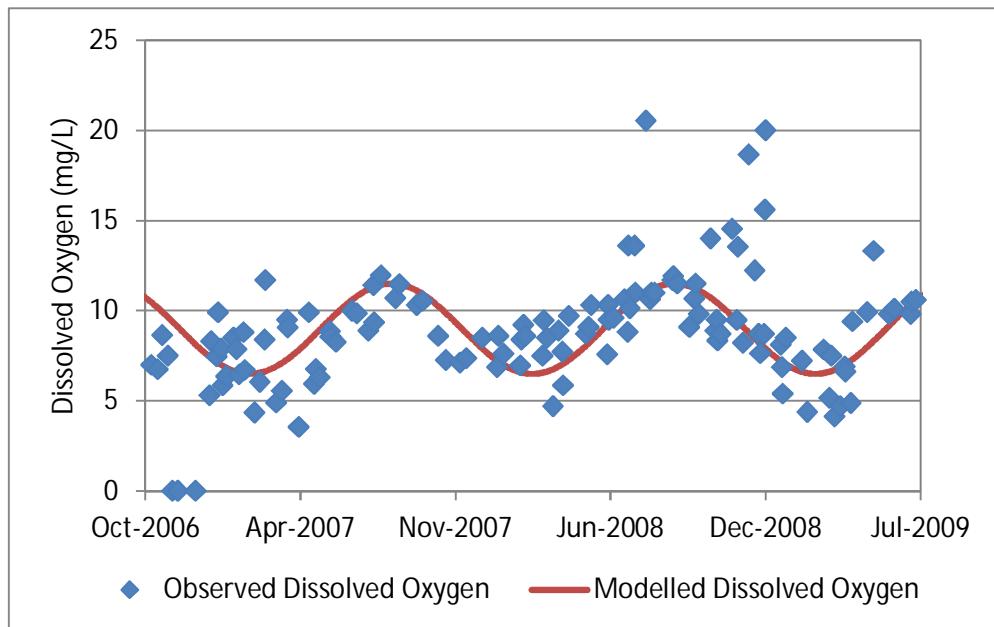
■ **Figure 8-19 Example of South Creek dissolved oxygen with fitted sine relationship**



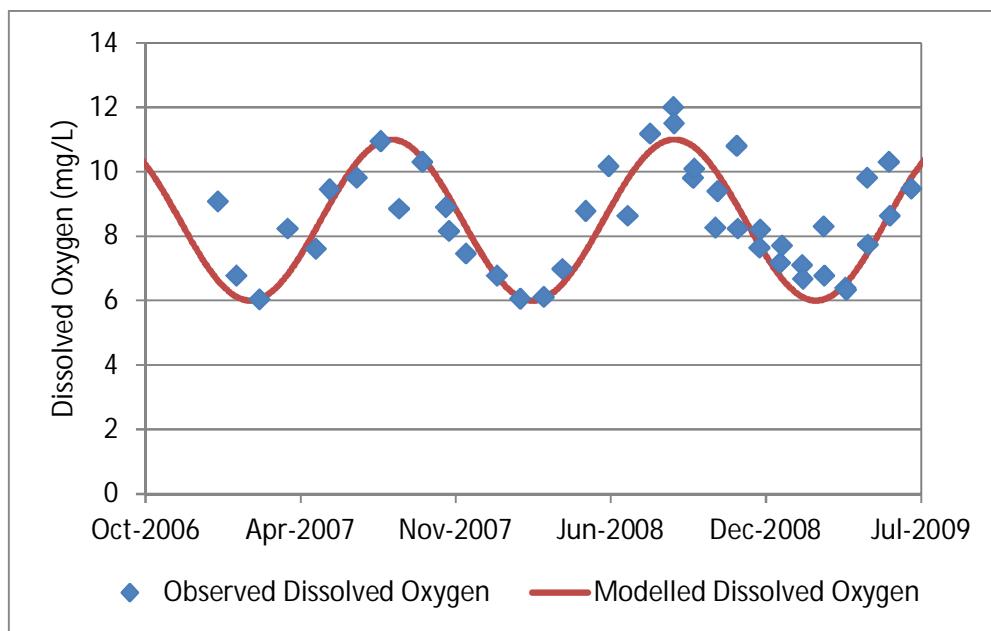
■ **Figure 8-20 Example of Eastern Creek dissolved oxygen with fitted sine relationship**



■ **Figure 8-21 Example of Cattai Creek dissolved oxygen with fitted sine relationship**



■ **Figure 8-22 Example of representative Nepean River dissolved oxygen with fitted sine relationship**



- **Figure 8-23 Example of representative Hawkesbury River dissolved oxygen with fitted sine relationship**

8.6.3. pH

This section outlines the pH relationships developed across the Hawkesbury-Nepean Catchment. The relationships have been developed using a sine relationship with time of year being the key driver. The equation is of the form:

$$pH = a \sin(2\pi t + b) + c \quad (8.4)$$

Where:

pH = pH of the water courses

t = the current day as a fraction of the year

a = amplitude of pH

b = phase of pH

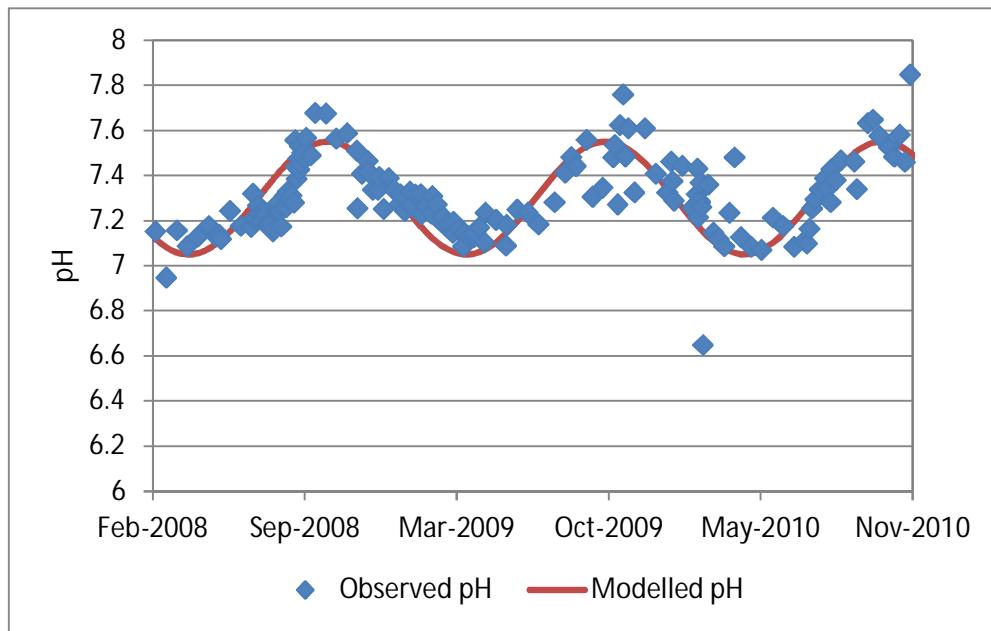
c = average pH

The coefficients for each of the locations are outlined in **Table 8-13**. Plots of selected periods at each location are outlined from **Figure 8-24** to **Figure 8-31** with the full available series outlined in **Appendix G**. There was insufficient evidence of a seasonal trend in pH for Eastern Creek, Nepean River or the Hawkesbury River and therefore a constant value was applied (equivalent to the mean of the observed data points) in these parts of the catchment.

Water Quality Modelling of the Hawkesbury-Nepean River System

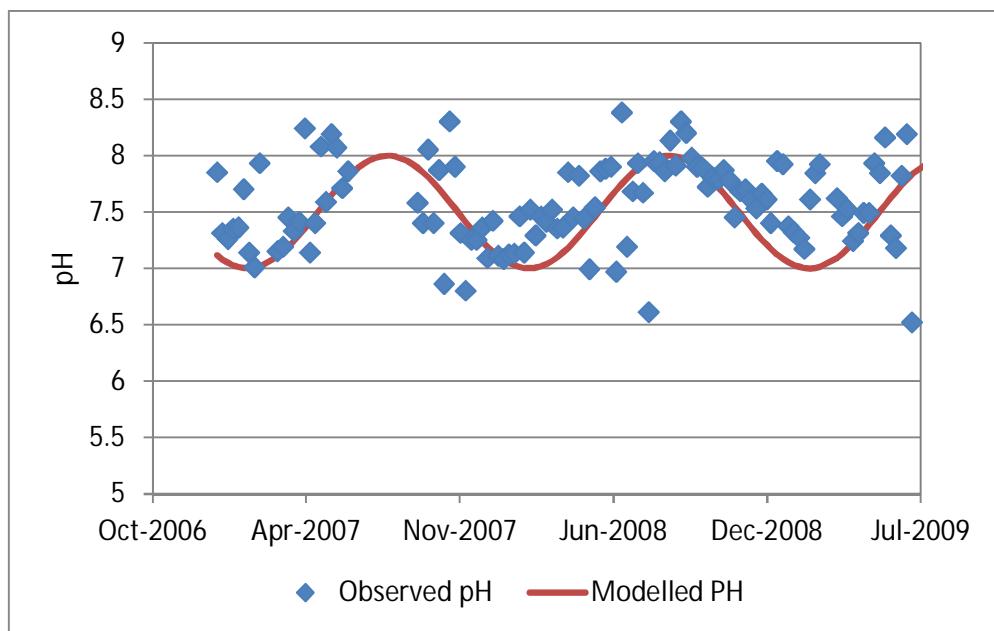
- **Table 8-13 Sine equation coefficients for pH in the Hawkesbury-Nepean catchment**

Location	Amplitude (a)	Timing (b) (time)	Date of maximum pH	Date of minimum pH	Mean
Warragamba River	0.25	3	16 th April	16 th October	7.3
Cataract River at Broughton Pass	0.5	4	13 th June	13 th December	7.5
Nepean River at Pheasants Nest	0.5	3	16 th April	16 th October	8.5
South Creek	0.3	4	13 th June	13 th December	7.5
Eastern Creek			Constant = 7.5		
Cattai Creek	0.4	4	13 th June	13 th December	7.5
Colo River			Use Cattai Creek numbers		
Nepean River			Constant = 7.5		
Hawkesbury River			Constant = 8		

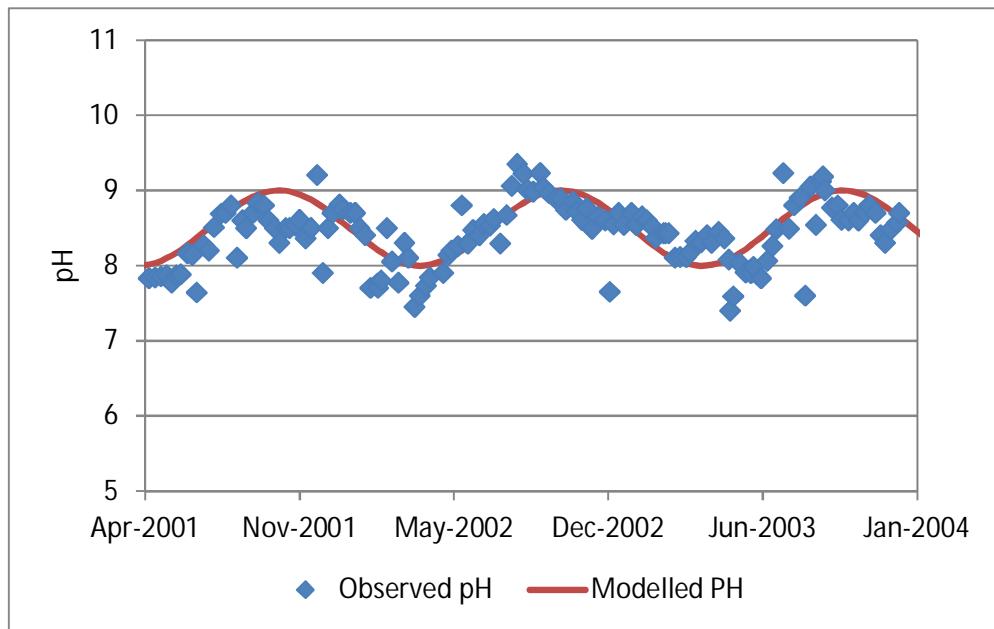


- **Figure 8-24 Example of Warragamba River pH with fitted relationship**

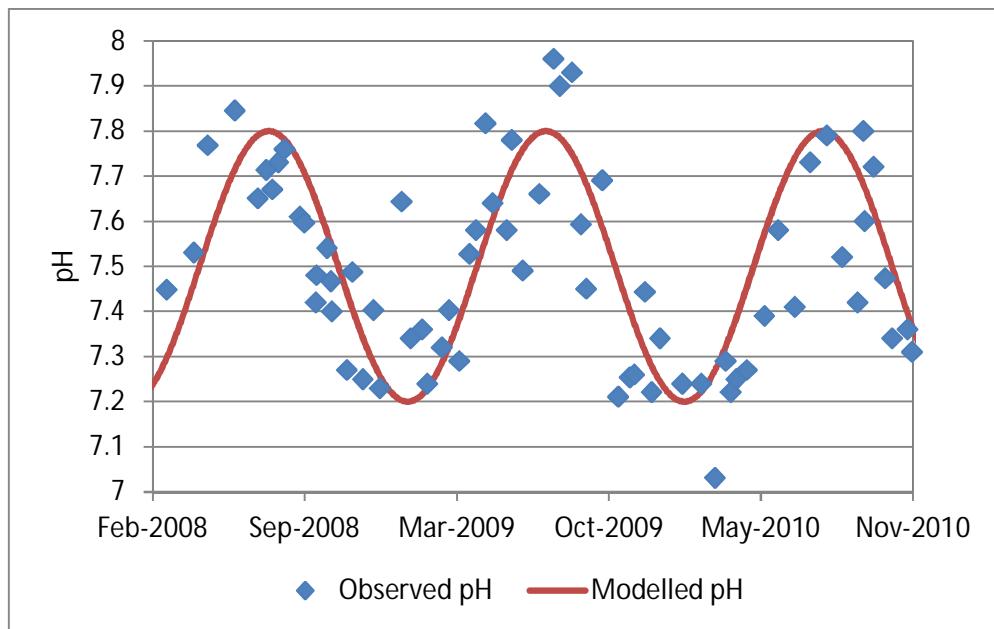
Water Quality Modelling of the Hawkesbury-Nepean River System



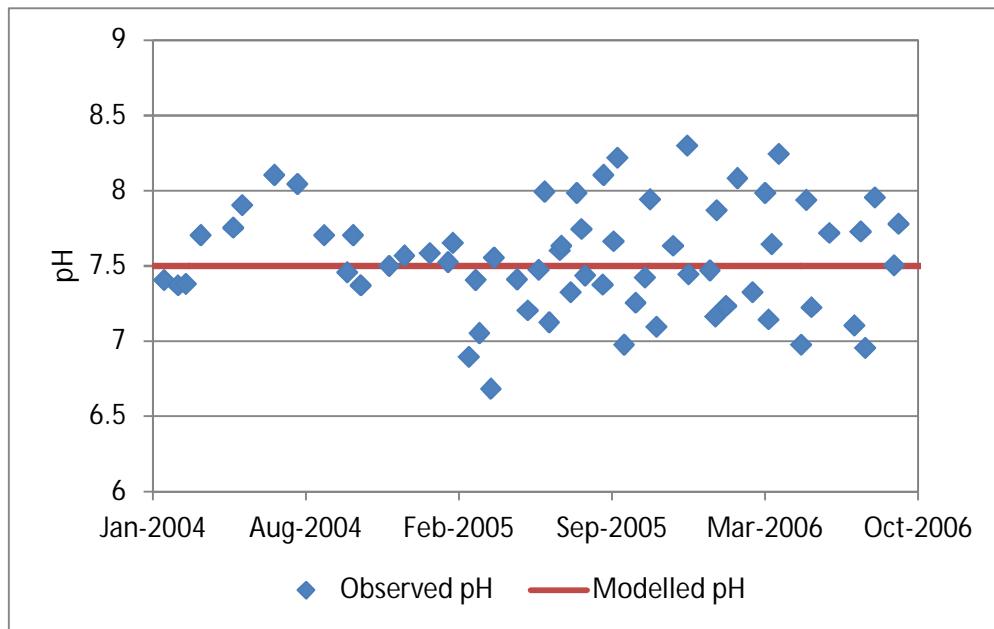
■ **Figure 8-25 Example of Broughton Pass (Cataract River) pH with fitted relationship**



■ **Figure 8-26 Example of Pheasants Nest (Nepean River) pH with fitted relationship**

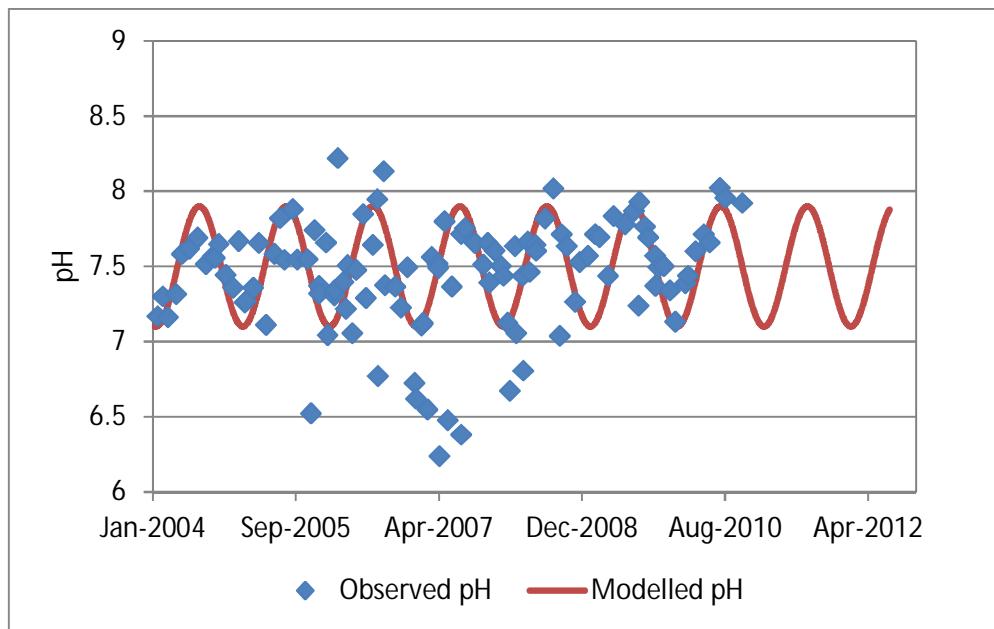


■ **Figure 8-27 Example of South Creek pH with fitted relationship**

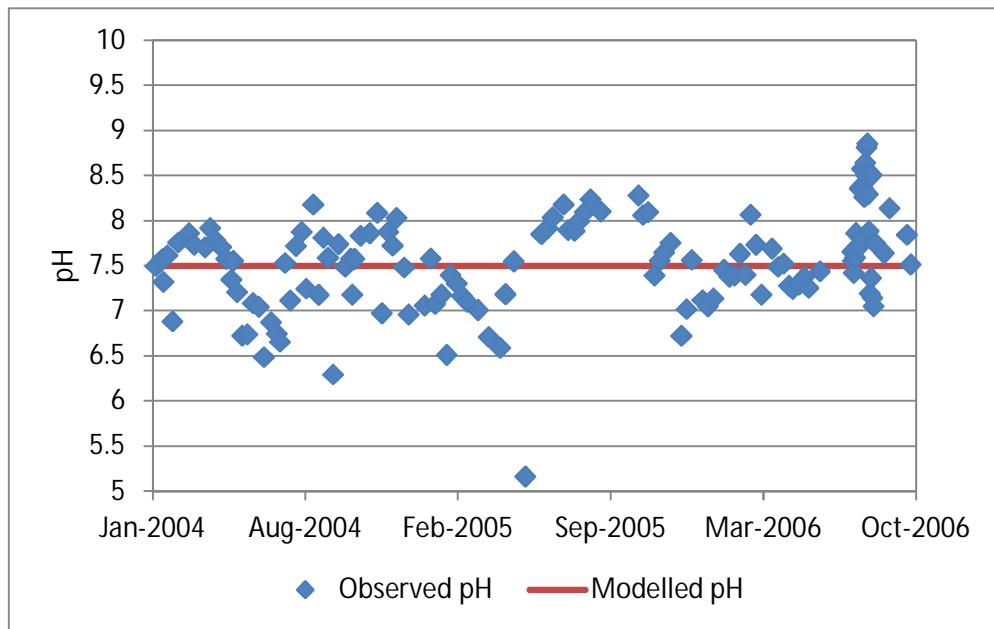


■ **Figure 8-28 Example of Eastern Creek pH with fitted relationship**

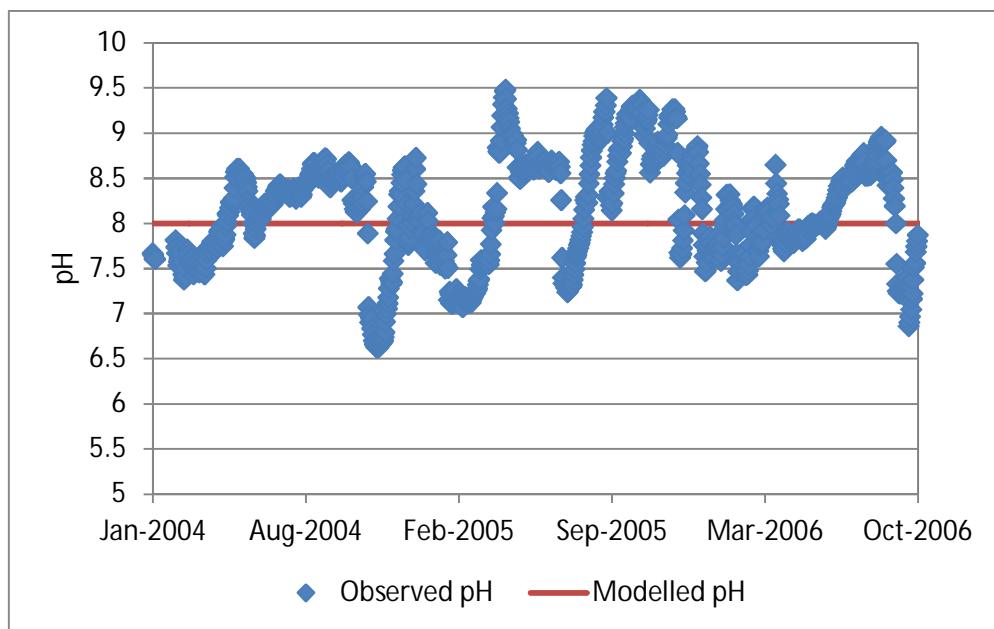
Water Quality Modelling of the Hawkesbury-Nepean River System



■ **Figure 8-29 Example of Cattai Creek pH with fitted relationship**



■ **Figure 8-30 Example of representative Nepean River pH with fitted relationship**



■ **Figure 8-31 Example of representative Hawkesbury River pH with fitted relationship**

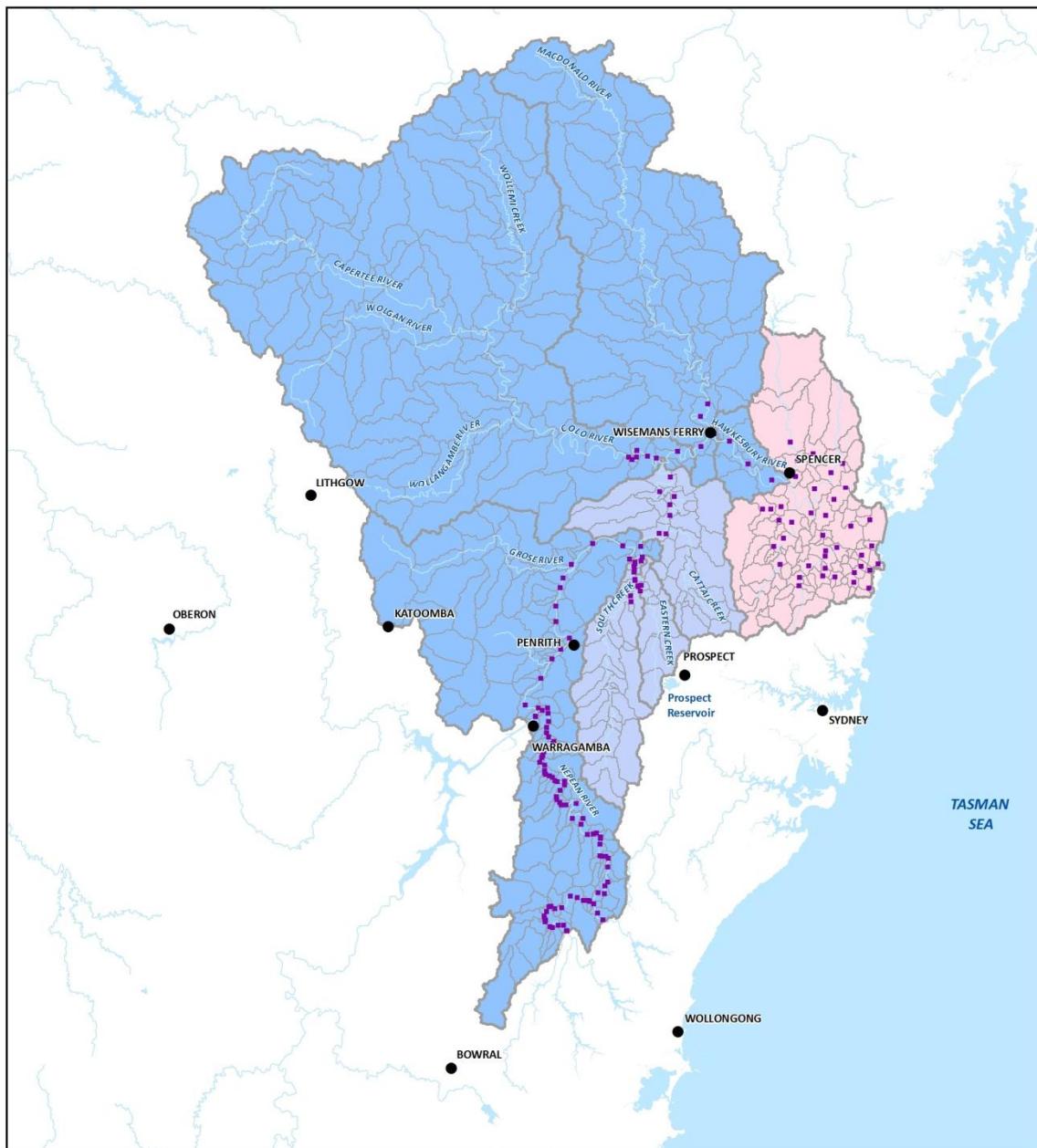
8.6.4. Total Organic Carbon and Dissolved Organic Carbon

This section outlines how total and dissolved organic carbon (TOC/DOC) have been used in the model. As the TOC and DOC show relatively constant concentrations over time the average of the TOC and DOC values was used to represent these constituents. **Table 8-14** outlines the constants for the TOC and DOC. The spatial distribution is outlined in **Figure 8-32**. Higher TOC and DOC values were observed in South, Eastern and Cattai creeks than in the other catchments, which was most likely caused by the relatively large proportion of flows in these creeks that were derived from WWTP / WRP discharges.

■ **Table 8-14 Constants for Total Organic Carbon and Dissolved Organic Carbon in the Hawkesbury-Nepean catchment**

Location	Dissolved Organic Carbon (mg/L)	No. samples of Dissolved Organic Carbon	Total Organic Carbon (mg/L)	No. samples of Total Organic Carbon
Warragamba River	4.0	358	4.5	335
Cataract River at Broughton Pass	4.2	139	4.2	139
Nepean River at Pheasants Nest	4.3	118	4.4	61
South Creek	12.8	15	14.7	15
Eastern Creek	9.9	6	11.2	6
Cattai Creek	10.8	9	12.0	9
Colo River	6.1	9	6.7	9
Nepean River	4.8	192	5.1	88
Hawkesbury River	6.1	108	7.7	21

Water Quality Modelling of the Hawkesbury-Nepean River System



LEGEND

- Subcatchment
- Waterway
- TUFLOW Inflow Points

% of DOC/TOC

75 - 80%
80 - 85%
85 - 90%
90 - 95%

Sinclair Knight Merz does not warrant that this document is definitive nor free of error and does not accept liability for any loss caused or arising from reliance upon information provided herein.



GDA 1994 MGA Zone 56
A4 1:1,100,000

DATA SOURCES
GA, CSIRO2MG

0 Kilometres



Figure 8.32 – Dissolved organic carbon as a percentage of total organic carbon



4/07/2013 | I:\ENVR\Projects\EN03013\Technical\GIS\Spatial\Directory\ArcGIS\HN_007_DOC_3.mxd
Sydney Spatial Team | Prepared by: MG
Checked by: JC

SINCLAIR KNIGHT MERZ

8.6.5. Components of Organic Nitrogen

TUFLOW/AED also requires input loads of dissolved and particulate organic and inorganic nitrogen and phosphorus. This section outlines how the components of organic nitrogen were determined. The Source model contains the following components – total nitrogen, ammonium, total Kjedahl nitrogen and oxidised nitrogen. As further speciation of nitrogen was required in the outputs, data from OEH was used to determine the values of each of the components of total nitrogen. The components of organic nitrogen (particulate and dissolved) were then examined to determine if a simple percentage split could be used. The results are outlined in **Table 8-15** to **Table 8-17** below. It is important to note that there was insufficient information available to undertake this for the Warragamba River, Nepean River at Pheasants Nest and Cataract River at Broughtons Pass. For these locations, the regional results of the corresponding catchments were used. For example, the Warragamba River used the results from the Nepean Catchment.

In the data provided by OEH, the following parameters were available – ammonia, oxidised nitrogen, total dissolved nitrogen and total nitrogen. These were used to calculate the individual components of total nitrogen based on the following equations:

$$\text{Dissolved Inorganic N} = \text{Ammonia} + \text{Oxidised Nitrogen}$$

$$\text{Dissolved Organic N} = \text{Total Dissolved N} - \text{Dissolved Inorganic N}$$

$$\text{Particulate Organic N} = \text{Total N} - \text{Total Dissolved N}$$

For use in the Hawkesbury-Nepean River modelling the following equations were used to provide a method for outputting concentrations at required locations for particulate and dissolved organic nitrogen.

$$\text{Total N} = \text{Total Organic N} + \text{Total Inorganic N}$$

$$\text{Total Organic N} = \text{Particulate Organic N} + \text{Dissolved Organic N}$$

$$\text{Total Inorganic N} = \text{Ammonia} + \text{Oxidised Nitrogen}$$

- **Table 8-15 Particulate Organic Nitrogen (PON) summary concentration**

Particulate Organic Nitrogen	Cattai Creek	Lower Cattai Creek	Colo River	Eastern Creek	Grose River	Nepean River	South Creek
No. samples	7	7	11	2	10	13	12
Median (mg/L)	0.095	0.163	0.096	0.050	0.071	0.085	0.111
Mean (mg/L)	0.111	0.213	0.138	0.050	0.119	0.122	0.125
Minimum (mg/L)	0.031	0.025	0.001	0.034	0.000	0.026	0.051
Maximum (mg/L)	0.251	0.449	0.376	0.066	0.393	0.394	0.222



Water Quality Modelling of the Hawkesbury-Nepean River System

- **Table 8-16 Dissolved Organic Nitrogen (DON) summary concentration**

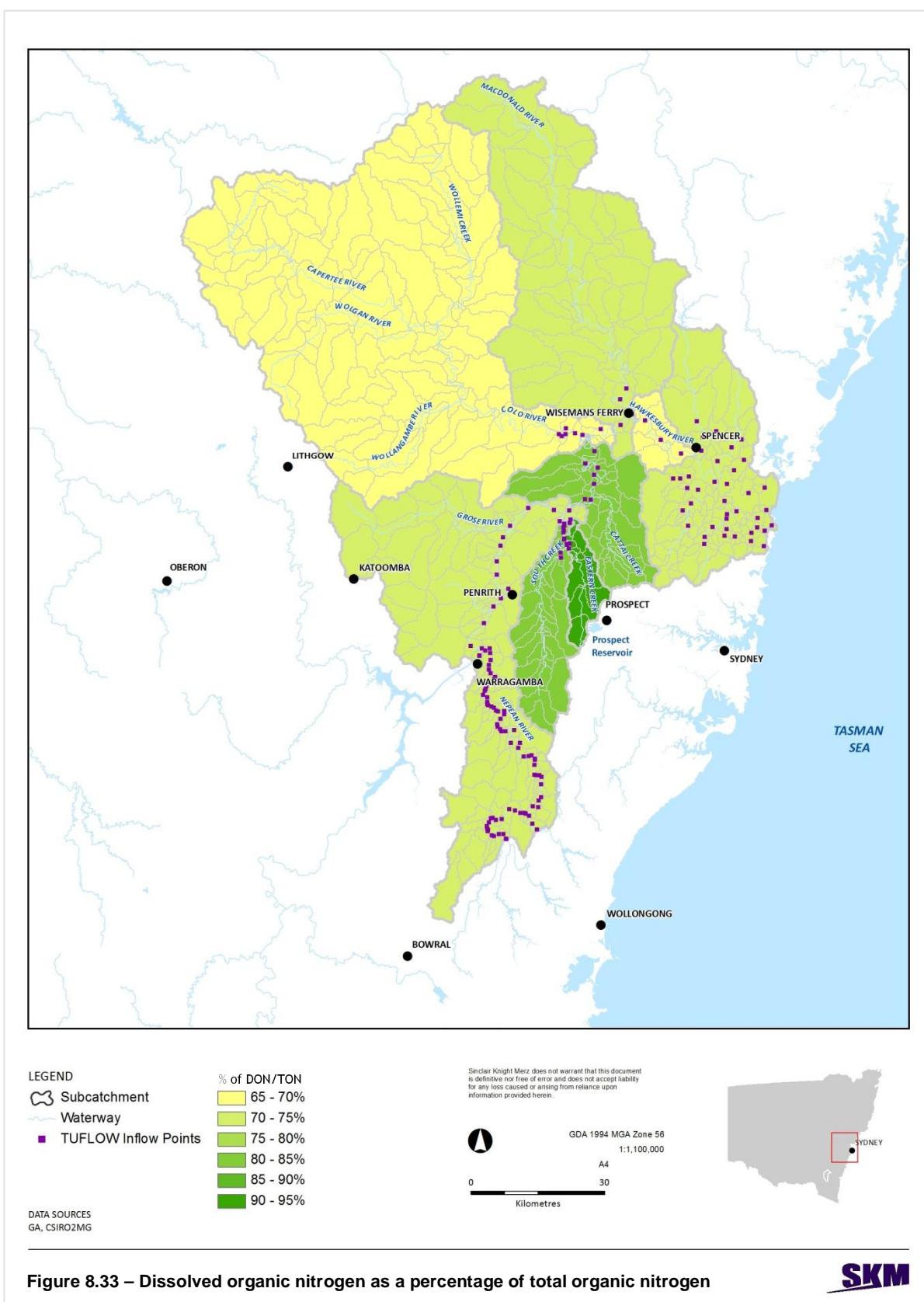
Dissolved Organic Nitrogen	Cattai Creek	Lower Cattai Creek	Colo River	Eastern Creek	Grose River	Nepean River	South Creek
No. samples	8	7	11	2	11	13	12
Median (mg/L)	0.459	0.451	0.223	0.691	0.225	0.384	0.566
Mean (mg/L)	0.457	0.440	0.211	0.691	0.203	0.355	0.584
Minimum (mg/L)	0.295	0.346	0.062	0.677	0.060	0.002	0.254
Maximum (mg/L)	0.640	0.517	0.509	0.705	0.376	0.531	0.825

- **Table 8-17 Dissolved Organic Nitrogen as a percentage of Total Organic Nitrogen (bold indicates the values to be used)**

DON/TON %	Cattai Creek	Lower Cattai Creek	Colo River	Eastern Creek	Grose River	Nepean River	South Creek
No. samples	7	7	11	2	11	13	12
Median	80%	71%	68%	93%	80%	80%	83%
Mean	81%	71%	66%	93%	73%	75%	82%
Minimum	68%	53%	39%	91%	41%	1%	71%
Maximum	94%	93%	99%	95%	100%	92%	92%

The spatial distribution is outlined in **Figure 8-33**.

Water Quality Modelling of the Hawkesbury-Nepean River System



SINCLAIR KNIGHT MERZ

8.6.6. Components of Organic Phosphorus

This section outlines how the components of organic phosphorus were derived. Data available from the Source model was total phosphorus and filterable reactive phosphorus (FRP). As further speciation of phosphorus was required, data from OEH was used to determine the values of each of the components of total phosphorus. The components of organic phosphorus (particulate and dissolved) were then examined to determine if a simple percentage split could be used. The results are outlined in **Table 8-18** to **Table 8-20** below. It is important to note that there was insufficient information available to undertake this for the Warragamba River, Nepean River at Pheasants Nest and Cataract River at Broughton Pass. For these locations, the regional results of the corresponding catchments were used. For example, Warragamba used the results from the Nepean Catchment.

In the data provided by OEH, the following parameters were available – phosphate (FRP), total dissolved phosphorus and total phosphorus. These were used to calculate the individual components of total phosphorus based on the following equations:

$$\text{Dissolved Organic P} = \text{Total Dissolved P} - \text{FRP}$$

$$\text{Particulate Organic P} = \text{Total P} - \text{Total Dissolved P}$$

For the Hawkesbury-Nepean River modelling the following equations were used to provide a method to estimate output concentrations at required locations for particulate and dissolved organic phosphorus.

$$\text{Total P} = \text{Total Organic P} + \text{Total Inorganic P}$$

$$\text{Total Organic P} = \text{Particulate Organic P} + \text{Dissolved Organic P}$$

$$\text{Total Inorganic P} = \text{FRP}$$

■ **Table 8-18 Particulate Organic Phosphorus (POP) summary concentration**

Particulate Organic Phosphorus	Cattai Creek	Lower Cattai Creek	Colo River	Eastern Creek	Grose River	Nepean River	South Creek
No. samples	8	7	11	2	11	40	12
Median (mg/L)	0.028	0.039	0.008	0.032	0.008	0.013	0.044
Mean (mg/L)	0.033	0.052	0.011	0.032	0.013	0.023	0.045
Minimum (mg/L)	0.013	0.021	0.001	0.017	0.001	0.000	0.017
Maximum (mg/L)	0.089	0.131	0.026	0.047	0.043	0.080	0.089

- **Table 8-19 Dissolved Organic Phosphorus (DOP) summary concentration**

Dissolved Organic Phosphorus	Cattai Creek	Lower Cattai Creek	Colo River	Eastern Creek	Grose River	Nepean River	South Creek
No. samples	8	7	10	2	11	13	12
Median (mg/L)	0.011	0.008	0.003	0.011	0.003	0.008	0.011
Mean (mg/L)	0.011	0.008	0.003	0.011	0.003	0.008	0.012
Minimum (mg/L)	0.007	0.004	0.001	0.007	0.001	0.000	0.004
Maximum (mg/L)	0.017	0.015	0.006	0.014	0.005	0.019	0.023

- **Table 8-20 Dissolved Organic Phosphorus as a percentage of Total Organic Phosphorus (bold indicates values to be used)**

DOP/TOP %	Cattai Creek	Lower Cattai Creek	Colo River	Eastern Creek	Grose River	Nepean River	South Creek
No. samples	8	7	10	2	11	13	12
Median	26%	15%	27%	29%	25%	26%	21%
Mean	28%	16%	30%	29%	27%	28%	22%
Minimum	16%	10%	8%	13%	11%	2%	16%
Maximum	43%	29%	79%	45%	70%	52%	34%

The spatial distribution is outlined in **Figure 8-34**.

Water Quality Modelling of the Hawkesbury-Nepean River System

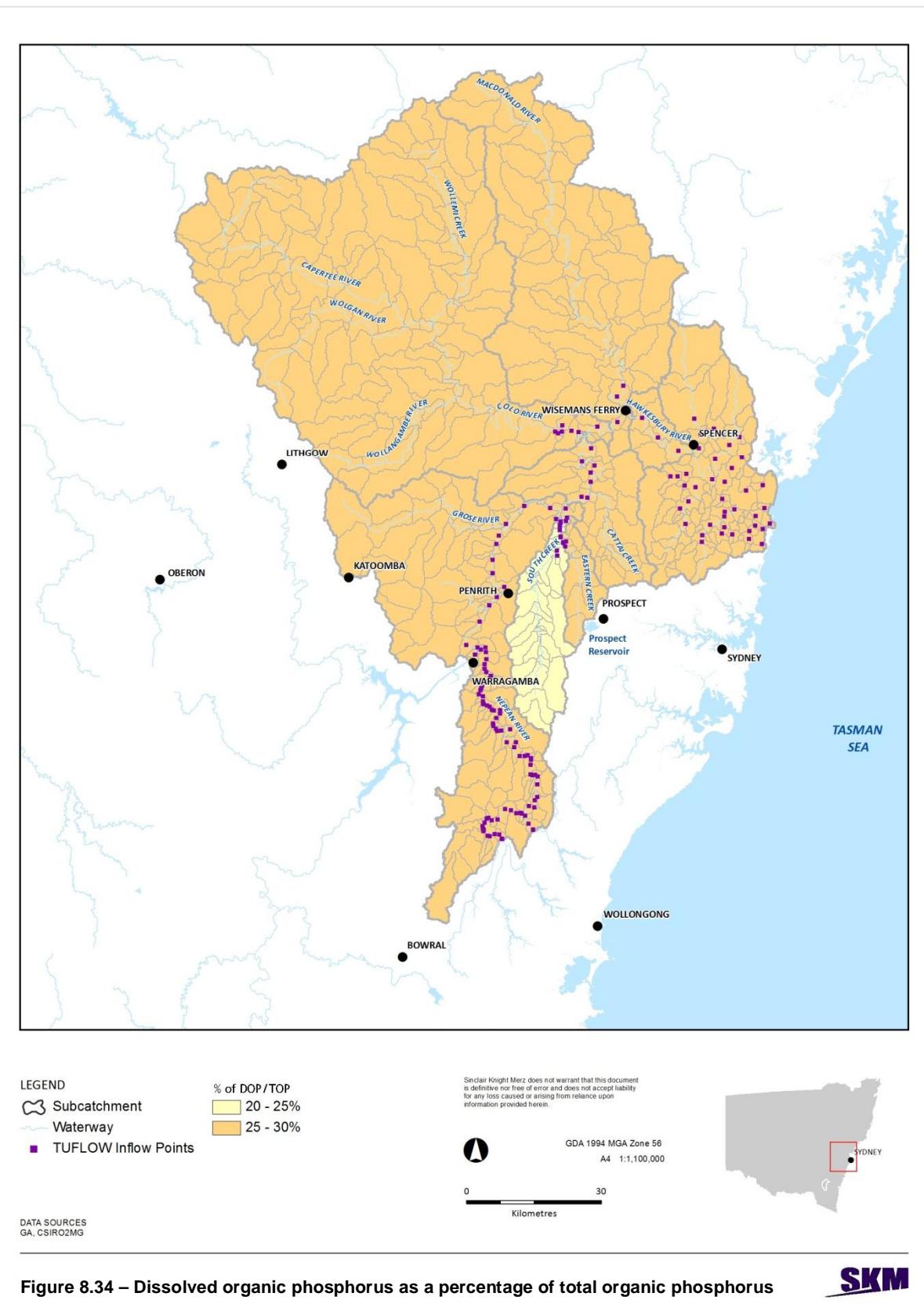


Figure 8.34 – Dissolved organic phosphorus as a percentage of total organic phosphorus

4/07/2013 | I:\ENVR\Projects\EN03013\Technical\GIS\Spatial_Direct\ArcGIS\HawN_007_DOP_v3.mxd
Sydney Spatial Team - Prepared by: MS
Checked by: JC

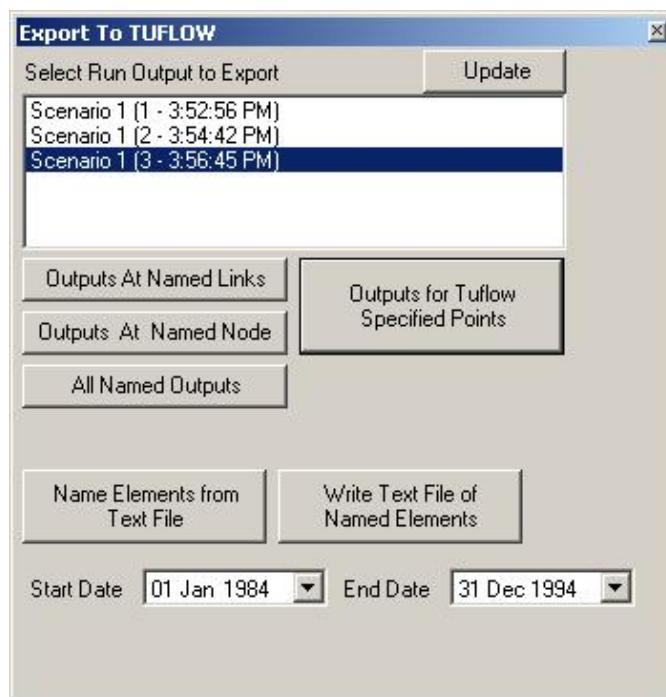
SINCLAIR KNIGHT MERZ

9. Model Plug-Ins

9.1. Customised Export of Results from Source to TUFLOW/AED

There are 163 locations in the model where outputs from the Source model become inputs to the TUFLOW/AED model. At each of these locations, daily time series for the entire period of the model run are provided for flow and also for the concentrations of each of the constituents in the catchment model. Using the standard Source interface, it would be very inefficient and potentially prone to error to manually export the daily time series from a Source model run for each of these individual locations one-by-one. A custom “plug-in” model was therefore developed in Visual Studio .NET, using the C# programming language, to quickly export a large quantity of selected model outputs.

A screen shot of the interface for the plug-in, which is available after a Source model run has been completed is shown in **Figure 9-1**. The plug-in creates a comma separated variable (CSV) file for each of the input locations to the TUFLOW/AED model using a pre-defined linear combination of the daily flow and concentration time series calculated at nominated nodes or links within the Source model. Since the CSV files have a consistent format and naming convention, the TUFLOW/AED model can be configured to easily and consistently import the time series created by the Source model run.

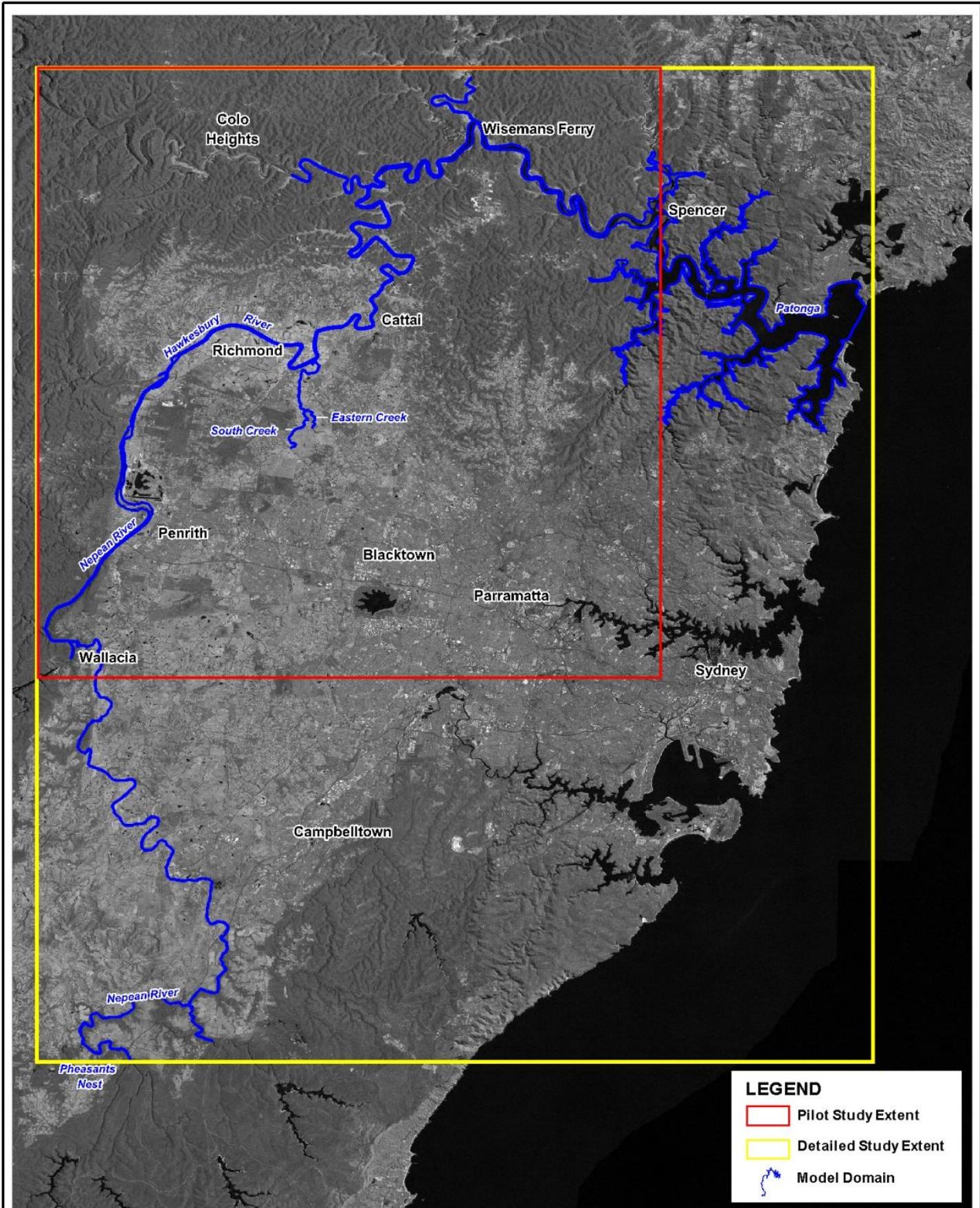


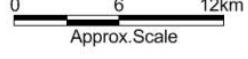
- **Figure 9-1 Screen shot the user interface for the plug-in that exports Source results to TUFLOW/AED**

10. Introduction to the Hydrodynamic and Water Quality Models

This section presents an outline of the work conducted and analyses undertaken to support and inform the development of an in-stream hydrodynamic and water quality model of the Hawkesbury-Nepean River system. This model was developed using the TUFLOW-FV hydraulic modelling suite, coupled to the AED water quality and ecosystem process model. Separate Source modelling to provide catchment flows and diffuse load boundary conditions for the TUFLOW/AED model was conducted separately and the results reported in Sections 2-9.

This work follows on from the pilot scale model, previously developed in an earlier stage of this project. The pilot model extended from Spencer at the downstream end, to Wallacia Weir and Warragamba Dam at the upstream end. The complete model described in this report expands the pilot domain so that it spans the Hawkesbury and Nepean rivers from Barrenjoey at the ocean mouth to Pheasants Nest on the Nepean River and Broughtons Pass on Cataract River (near the head of the Nepean River). The domains of both the pilot and complete models are illustrated in **Figure 10-1**.



Title:	Figure:	Rev:
Pilot and Complete Receiving Water Quality Model Extents	10-1	A
BMT WBM endeavours to ensure that the information provided in this map is correct at the time of publication. BMT WBM does not warrant, guarantee or make representations regarding the currency and accuracy of information contained in this map.		 www.bmtwbm.com.au
  Approx. Scale		

11. Data Collation and Review

11.1. Preamble

Several data sets were required to develop the model. Specifically, data was required to:

- Specify bathymetric river form throughout (survey data);
- Define open ocean and catchment inflow boundaries (Source inflows and ocean boundaries);
- Specify wastewater treatment plant (WWTP) and water recycling plant (WRP) flows and loads;
- Set water quality initial conditions (in-stream monitoring data); and
- Provide calibration and validation information.

The key data sets used for the above purposes are described below.

11.2. Survey Data

A wide range of bathymetric data sets was used to assign bathymetry to the model. These are provided in **Table 11-1** below.

■ **Table 11-1 Bathymetric Data and Sources**

Description	Source ¹
Upstream of Wallacia up to Pheasants Nest and Broughton Pass	SCA
Sackville to Wallacia (including South and Eastern Creeks)	Sydney Water
Broken Bay to up to Pheasants Nest and Broughton Pass	Sydney Water
Broken Bay to Bar Point during 1952	OEH
Broken Bay, Pittwater, Cowen Creek, and Broken Bay to Bar Point	OEH
Broken Bay and Pittwater	OEH
Bedrock Shelf (next to Penrith Lakes)	OHN Contractor ²
Riffle at Yarramundi	Sydney Water
Riffle at Castlereagh	Sydney Water
Riffles Jacksons Lane to Penrith Weir	Sydney Water
Spencer to Wallacia	Sydney Water
Wisemans Ferry to Windsor	Sydney Water
Berowra during 1995	OEH
Broken Bay during 1977 to 1978	OEH
Brooklyn during 2006	OEH
Wisemans Ferry to Cattai during 1978 to 1980	OEH
Broken Bay to Wisemans Ferry during 1978 to 1980	OEH
Cattai to Freemans Reach during 1987 to 1988	OEH



Water Quality Modelling of the Hawkesbury-Nepean River System

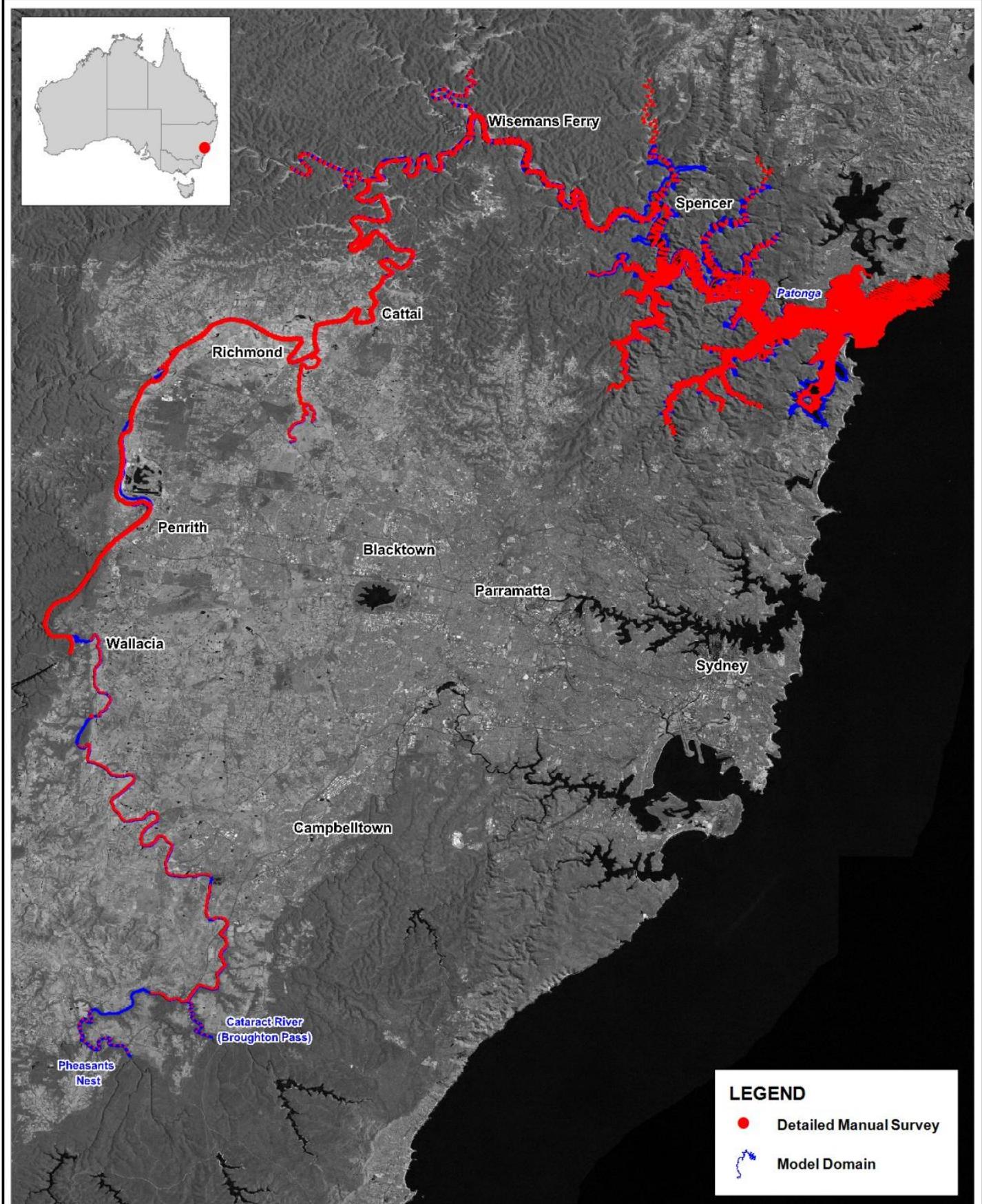
Description	Source ¹
Freemans Reach to Yarramundi during 1983 to 1985	OEH
Broken Bay to Spencer	OEH
Penrith	OEH
Spencer to Wallacia	OEH

¹ OEH – Office of Environment and Heritage

² OHN – Office of Hawkesbury-Nepean (now NSW Office of Water)

The locations and sources of all survey data used in this study are presented in **Figure 11-1**.

Study cartographers reviewed and post processed this data set to construct a consistent and robust digital elevation model (DEM) of the study area, illustrated in **Figure 11-2**. This DEM was subsequently used to set bathymetric values at each computational cell of the TUFLOW model. For those areas outside the spatial extent of the data coverage shown in **Figure 11-2** (e.g. in the deep gullies downstream of Pheasants Nest and Broughton Pass), relevant information was either extracted from a coarser, whole of catchment, DEM previously developed by BMT WBM, or interpolated from the raw data supplied.



Title:
Survey Data Coverage

Figure:
11-1

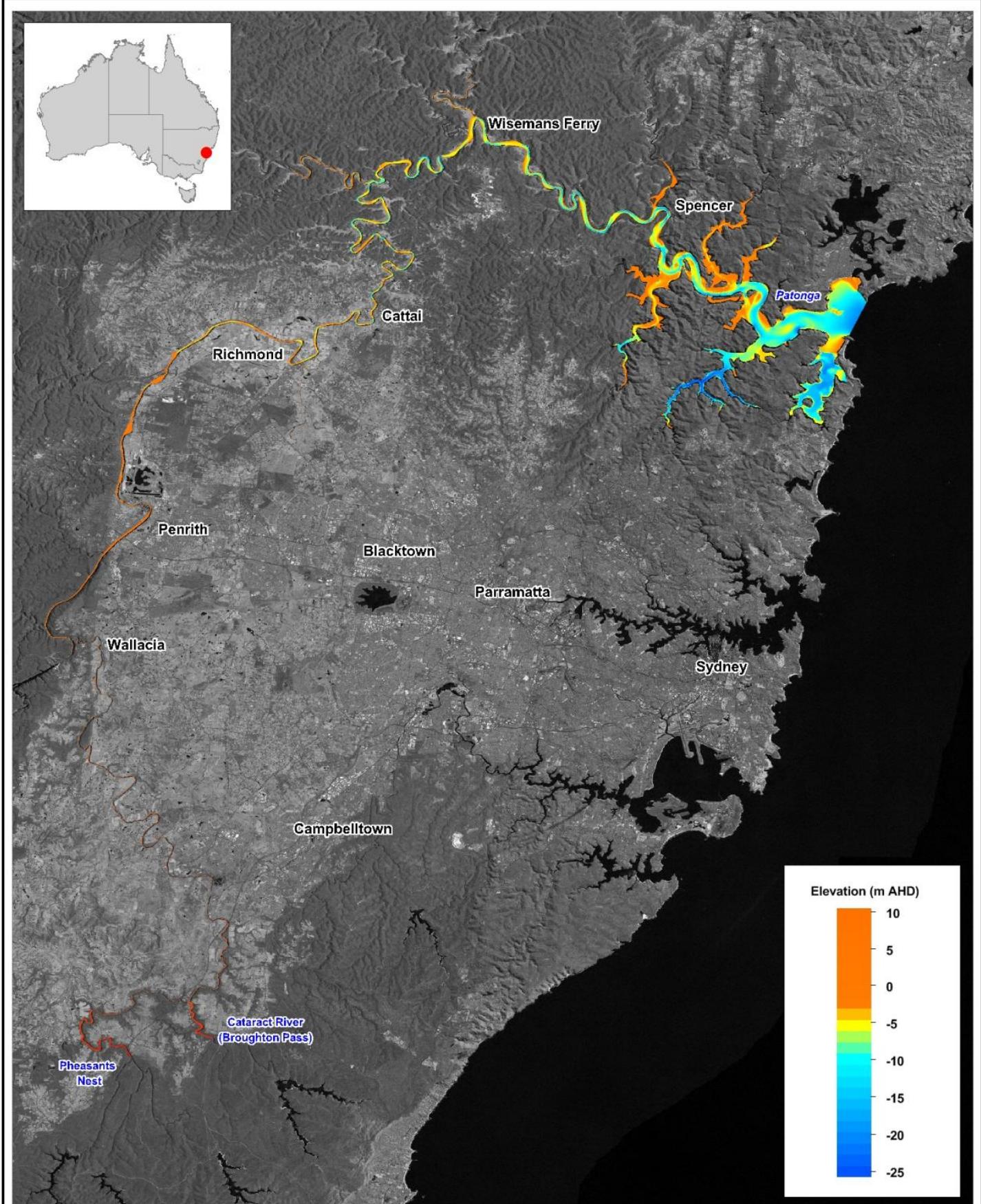
Rev:
A

BMT WBM endeavours to ensure that the information provided in this map is correct at the time of publication. BMT WBM does not warrant, guarantee or make representations regarding the currency and accuracy of information contained in this map.



0 6 12km
Approx. Scale

 **BMT WBM**
www.bmtwbm.com.au



Title:
Digital Elevation Model

Figure:
11-2

Rev:
A

BMT WBM endeavours to ensure that the information provided in this map is correct at the time of publication. BMT WBM does not warrant, guarantee or make representations regarding the currency and accuracy of information contained in this map.



0 6 12km
Approx. Scale

 **BMT WBM**
www.bmtwbm.com.au

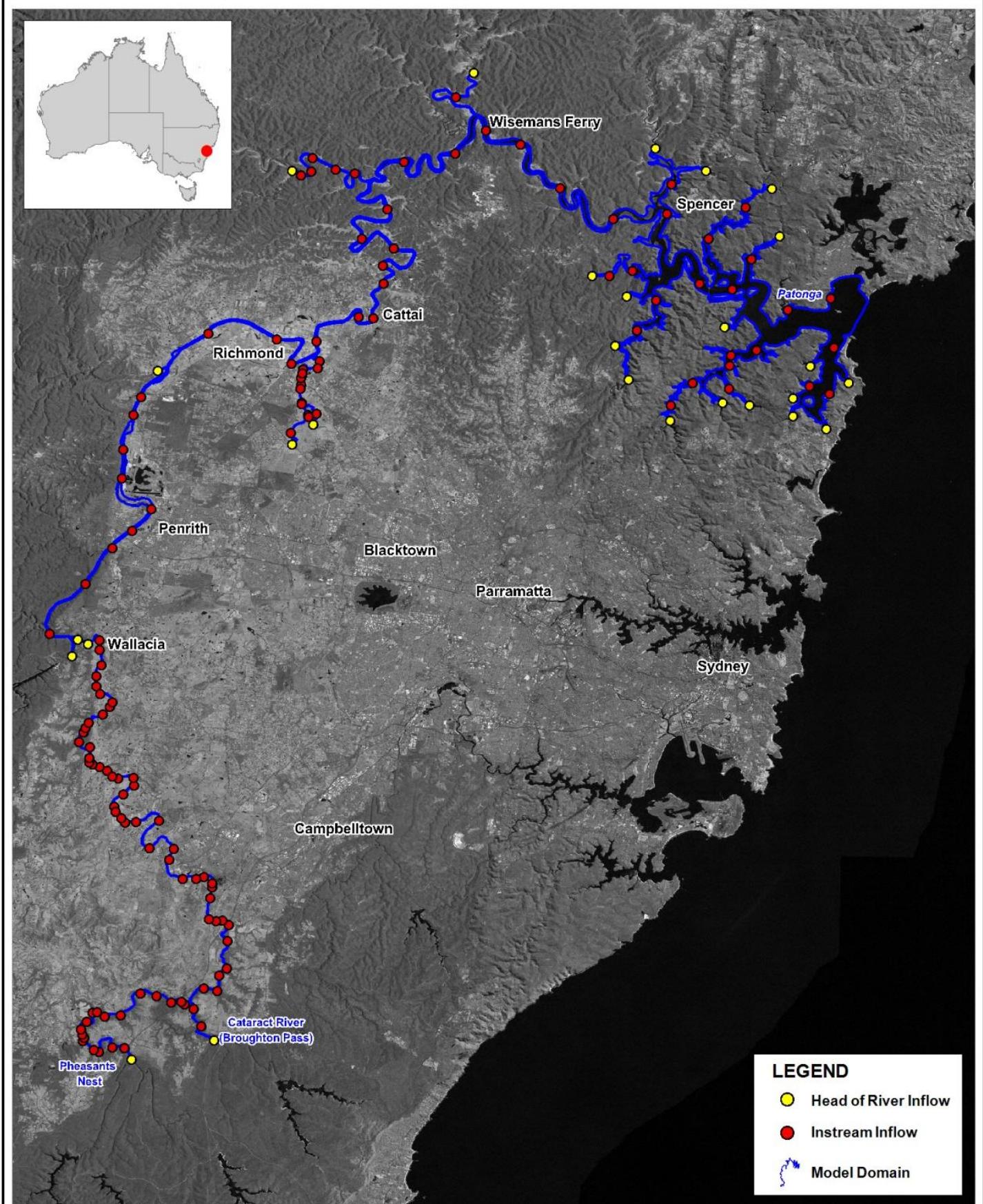
11.3. Model Boundaries

Data were required to force the model at various inflow and tidal boundaries. These are described below.

11.3.1. Diffuse Catchment Inflows

Diffuse catchment inflows were provided solely from the Source model of the surrounding areas. Given the complexity of the river network, considerable effort was expended in making sure that the Source and TUFLOW/AED models were linked consistently with no missing or multiply counted inflows. The linkages between the Source model and TUFLOW/AED are shown in **Figure 11-3**.

At each of these linkage points, the Source model provided the TUFLOW/AED model with daily hydrologic flows and all required constituents for in-stream water quality modelling purposes.



Title:
Source Catchments and TUFLOW AED Linkages

Figure:
11-3

Rev:
A

BMT WBM endeavours to ensure that the information provided in this map is correct at the time of publication. BMT WBM does not warrant, guarantee or make representations regarding the currency and accuracy of information contained in this map.



N

0

10

20km

Approx. Scale

11.3.2. Tidal Boundary Conditions

The downstream model water level boundaries were defined using tidal gauging data at Patonga. Water quality conditions were defined using ambient monitoring data collected by various organisations including Hornsby Shire Council and CSIRO databases.

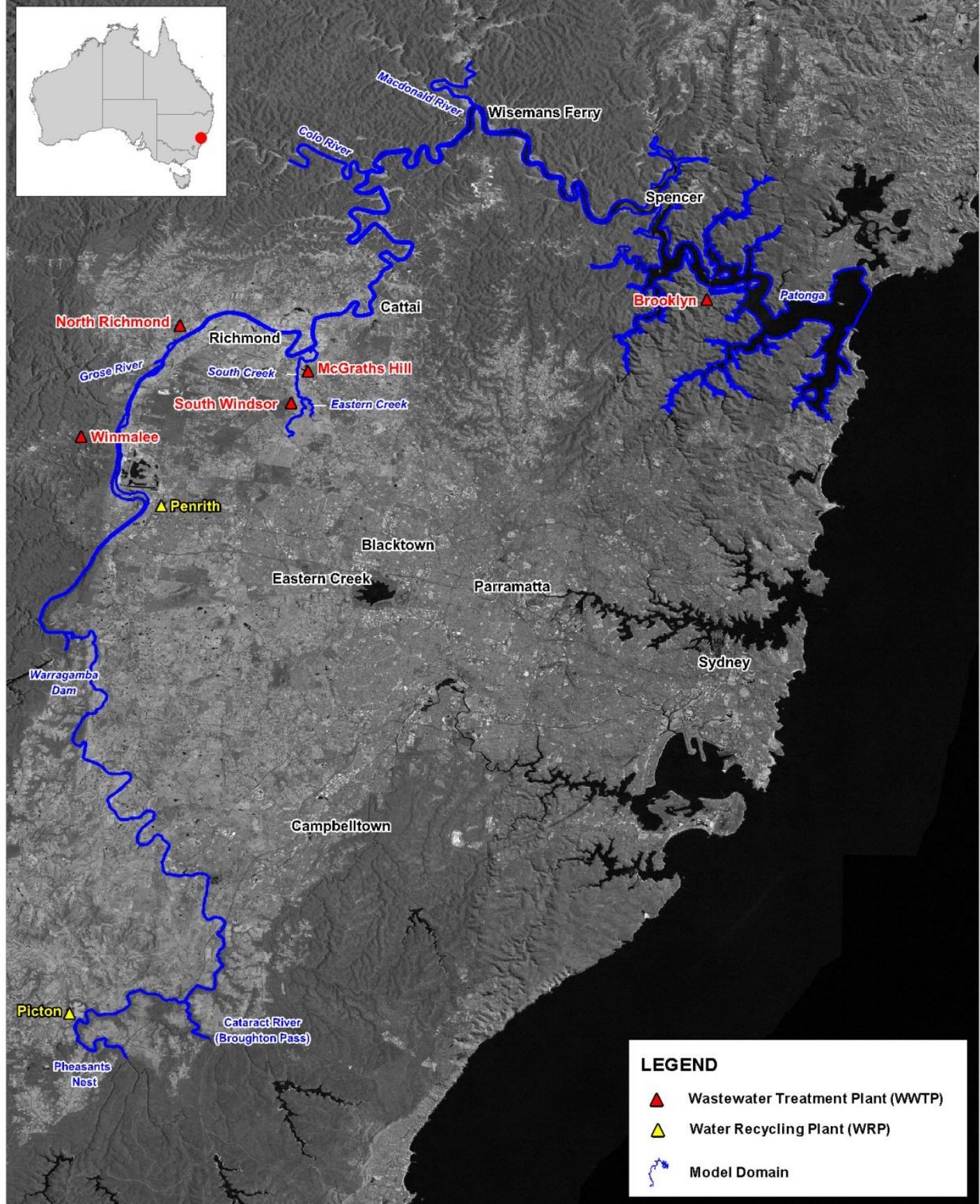
11.3.3. Upstream Weir Inflows

The upstream model boundaries at Pheasants Nest and Broughton Pass were historical measurements.

11.3.4. Wastewater Treatment Plant and Water Recycling Plant Inflows

The study area contains numerous wastewater treatment plants (WWTPs) and water recycling plants (WRPs) which discharge various quantities and qualities of treated effluent, either directly to the main river or a tributary. WWTPs/WRPs that discharge directly (or almost directly) to the river were included in the TUFLOW modelling, while those that discharge to the tributaries were included within the Source model. **Figure 11-4** illustrates the location of those WWTPs which were included within the TUFLOW modelling. McGrath Hill and South Windsor plants are not operated by Sydney Water.

Winmalee WWTP is located approximately 3km from the main river stem and its wastewater discharge undergoes biogeochemical transformations and removal of nutrients as it flows from the outfall point to the confluence with the main river. Monitoring data was used to quantify these processes and develop a relationship between the water quality concentrations at the discharge and water quality at the point source boundary for the model. The wastewater discharge applied to the TUFLOW-AED model was based on monitoring data collected at the confluence of the Winmalee stream discharge and the main river stem, so took into account instream processing between the discharge pipe and the Nepean River.



Title:

Wastewater Treatment Plants (WWTPs) and Water Recycling Plants (WRPs) Included in the TUFLOW/AED Model

BMT WBM endeavours to ensure that the information provided in this map is correct at the time of publication. BMT WBM does not warrant, guarantee or make representations regarding the currency and accuracy of information contained in this map.



0 6 12km
Approx. Scale



Figure:

11-4

Rev:

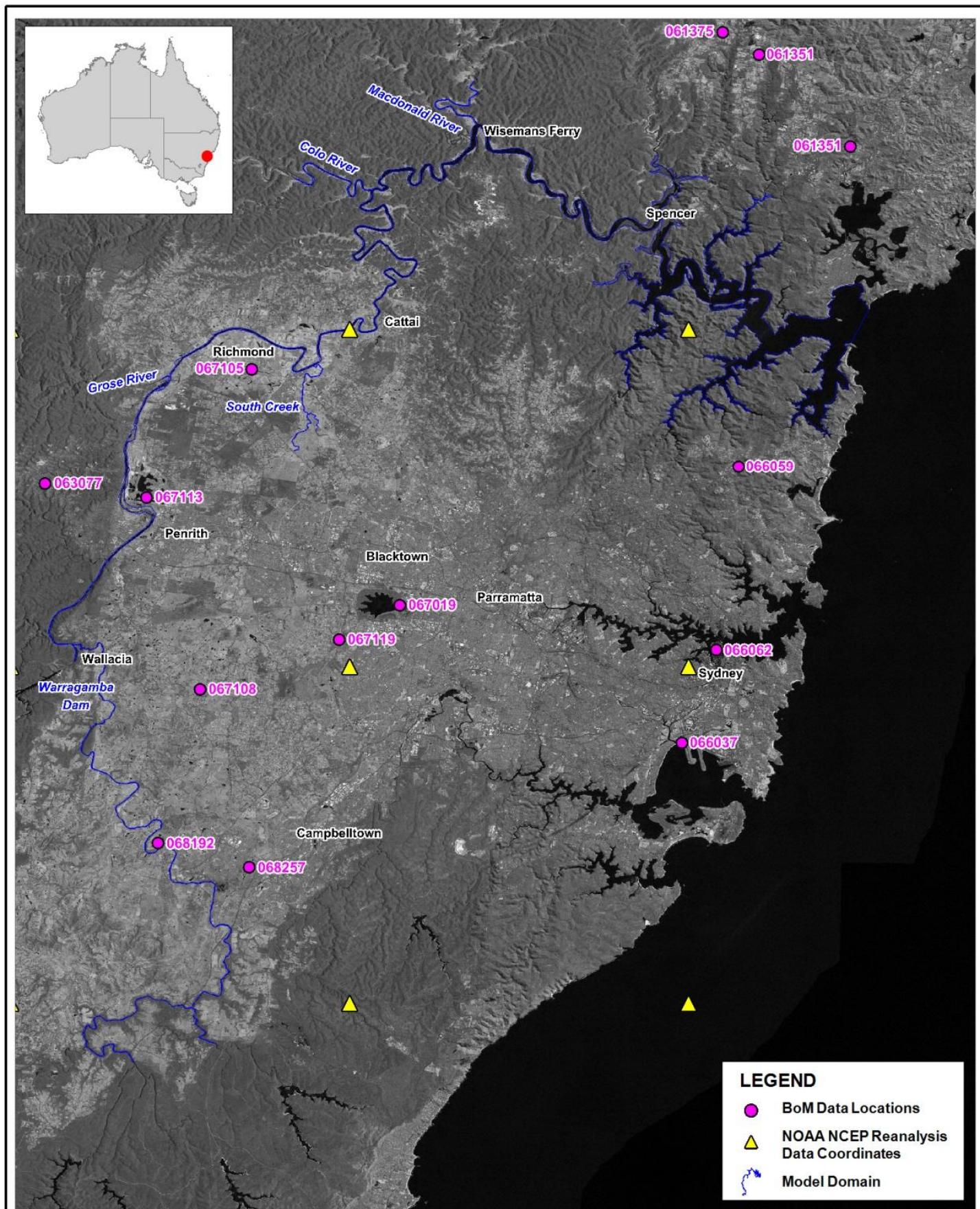
A

11.4. Meteorological Forcing Data

Relevant meteorological data were required to force the in-stream hydraulic and water quality modelling suite. In particular, meteorological data were used to simulate atmospheric exchange processes that influence water temperatures, hydrodynamics and surface re-aeration. In this regard, two sources of data were accessed and utilised in developing relevant information sets with which to inform the model. These sources were as follows:

- Bureau of Meteorology – recorded data from the Bureau of Meteorology (BOM) were obtained for relevant sites within close proximity of the study area. These sites are illustrated in **Figure 11-5**; and
- Global Climate Models – modelled results were also obtained from BMT ARGOSS to support the study. These results were obtained from relevant global climate models (NOAA - NCEP/ NCAR (National Oceanic and Atmospheric Administration - National Center for Environmental Prediction/National Center for Atmospheric Research Re-Analysis Data (<http://www.esrl.noaa.gov/psd/data/gridded/reanalysis/>))). It was found that the results of this modelling did not require any gap-filling in recorded data, were in reasonable agreement with the BOM data, provided added insights into local and regional spatial variability in meteorological forcing, and ultimately provided good results for simulations of ambient water temperature (**Appendix H**). Some example figures of the correlation between the data sets at site 067105 (Richmond) are presented in the Appendices. These results were therefore adopted in the complete model. Locations at which model results were obtained from these Global Climate Models are also illustrated in **Figure 11-5**.

Appendix I presents the equations adopted in TUFLOW FV to calculate the surface heat exchange.



Title:
Meteorological Data Site Locations

Figure:

11-5

Rev:

A

BMT WBM endeavours to ensure that the information provided in this map is correct at the time of publication. BMT WBM does not warrant, guarantee or make representations regarding the currency and accuracy of information contained in this map.



0

10

20km

Approx. Scale

11.5. Tidal Hydrodynamics

Data describing tidal hydrodynamics were required to both force the downstream TUFLOW model boundary and provide data within the model domain against which to assess model performance. These data sets were tidal water levels and tidal flows.

11.5.1. Tidal Water Levels

Tidal water level data used in this study is presented in **Figure 11-6**. The following general comments can be made in regard to the behaviour of tides in the estuarine reaches of the river system:

- Between the ocean (Patonga) and Spencer there is a phase lag in tides of the order of one hour, a slight increase in low tide levels and appreciable amplification in high tide levels;
- Between Spencer to Colo Junction, the tide continues to accumulate a phase lag, low water tidal levels continue to increase slightly and substantial high tide water level amplification occurs;
- Between Colo Junction and Freemans Reach, there is a major increase in low tide levels and high tide levels reduce. At Freemans Reach, high and low tides lag some 6.5 and 8.5 hours behind those at Patonga, respectively;
- Despite being separated by only 7 kilometres, the tidal stations at Windsor and Freemans Reach show that a typical tidal range of 0.7 m at Windsor is almost entirely suppressed by the time it reaches Freemans Reach, where the corresponding tidal ranges are 0.08 m. This is most likely due to the very large hydrodynamic attenuation applied to the tidal flows by macrophyte growth. This is discussed further in the model validation Section 13; and
- Between Freemans Reach and Castlereagh, the tidal signal disappears almost completely with evidence of a ‘flatline’ tidal record at Castlereagh that varies abruptly in time. This is consistent with the presence of some kind of transient hydraulic control between the two sites (possibly at Yarramundi), such as a transient blockage or similar. This is not confirmed.

Example data that illustrate the above features are shown in **Figure 11-7**.

11.5.2. Tidal Flow

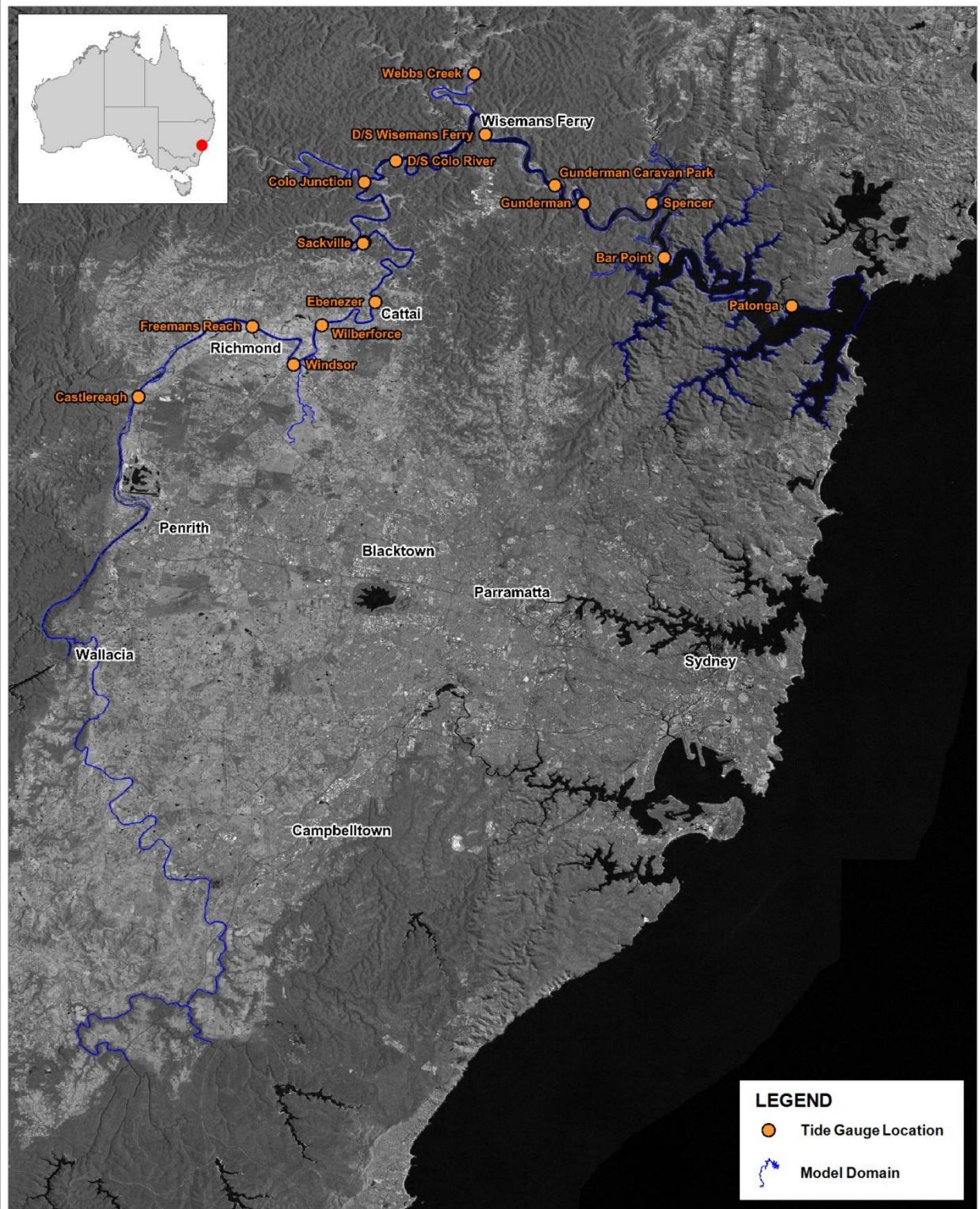
Tidal flow data were collected over a complete ebb-flood cycle on two occasions during the Acoustic Doppler Current Profile (ADCP) Campaign Monitoring Program (CMP). These data were crucial to the study in that they enabled detailed calibration of the flow characteristics of the TUFLOW model. The locations in which flow data were collected are shown in **Figure 11-8**, and representative flow data are presented in **Figure 11-9**. Full flow data are presented in the model calibration sections.



Water Quality Modelling of the Hawkesbury-Nepean River System

The following general comments can be made with regard to these data:

- Flow rates (both in ebb and flood) progressively decrease by factors of 10 to 20 between Bar Point and Wilberforce, depending on river flow and tidal conditions. The largest relative decrease occurs during spring tides; and
- Peak flow rates at Gunderman, Colo and Wilberforce lag behind Bar Point by approximately 20-30 minutes, 2.5 hours and 5.5 hours, respectively.



Title:
Tidal Hydrodynamic Data Site Locations

Figure:

11-6

Rev:

A

BMT WBM endeavours to ensure that the information provided in this map is correct at the time of publication. BMT WBM does not warrant, guarantee or make representations regarding the currency and accuracy of information contained in this map.

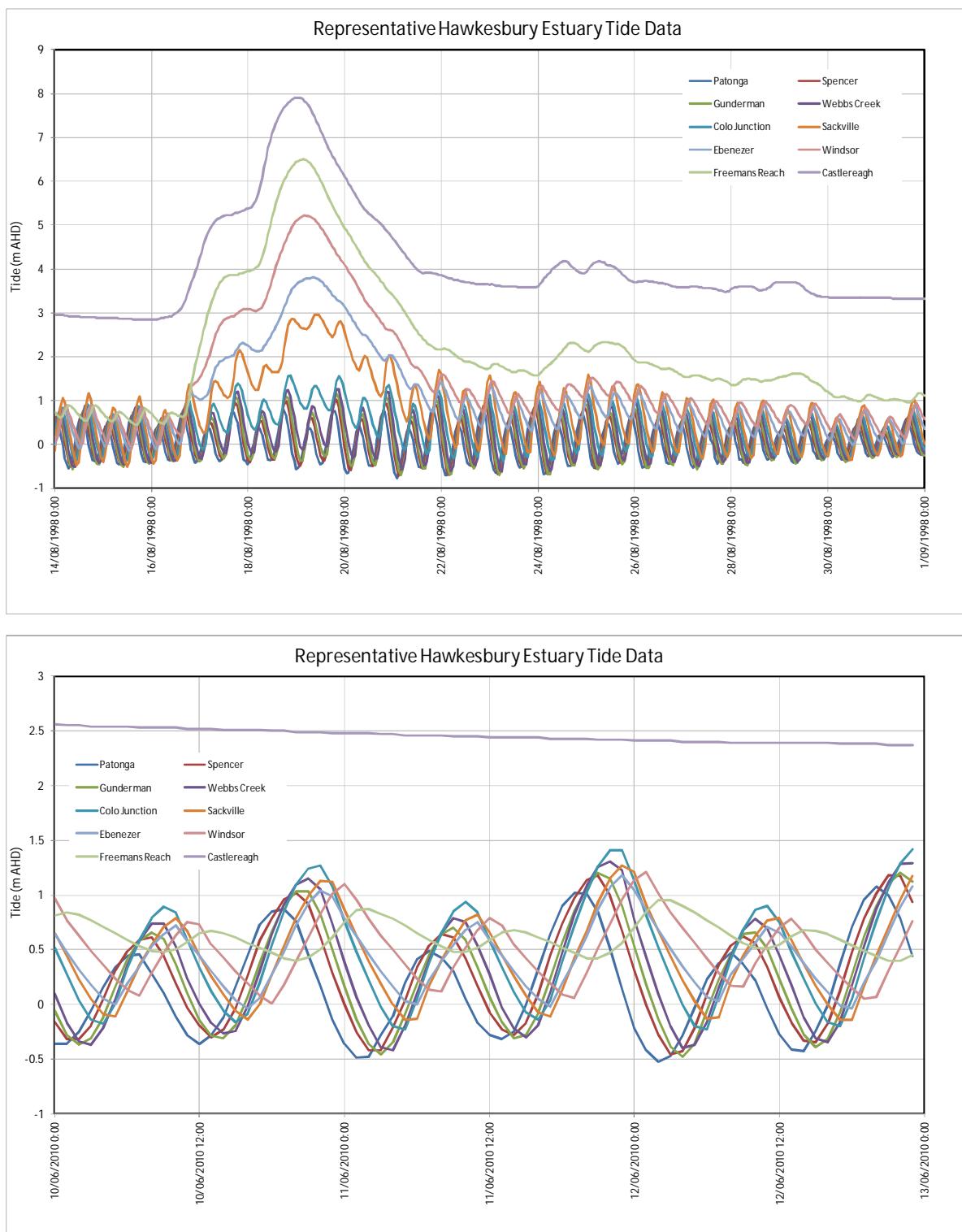


0 10 20km
Approx. Scale

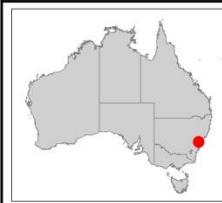
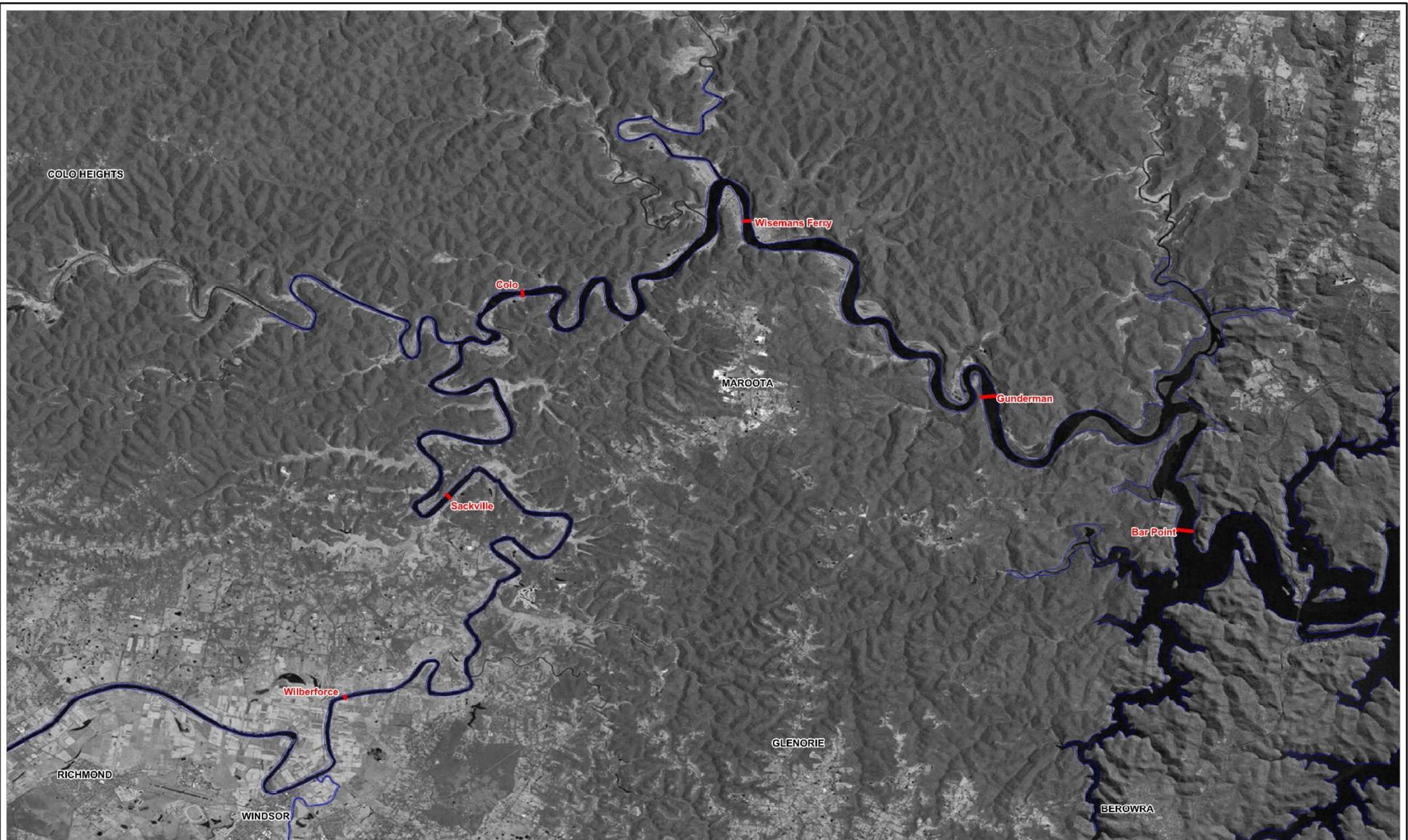
BMT WBM
www.bmtwbm.com.au



Water Quality Modelling of the Hawkesbury-Nepean River System



■ **Figure 11-7 Example Tidal Hydrodynamic Data**



LEGEND

— CMP Flow Data Locations

Model Domain

Title:
CMP Flow Data Locations

BMT WBM endeavours to ensure that the information provided in this map is correct at the time of publication. BMT WBM does not warrant, guarantee or make representations regarding the currency and accuracy of information contained in this map.

Filepath : I:\B18388_I_BRH_HawkesburyNepean\DRG130509\WQU_008_130509.CMP Flow Data Location.wor

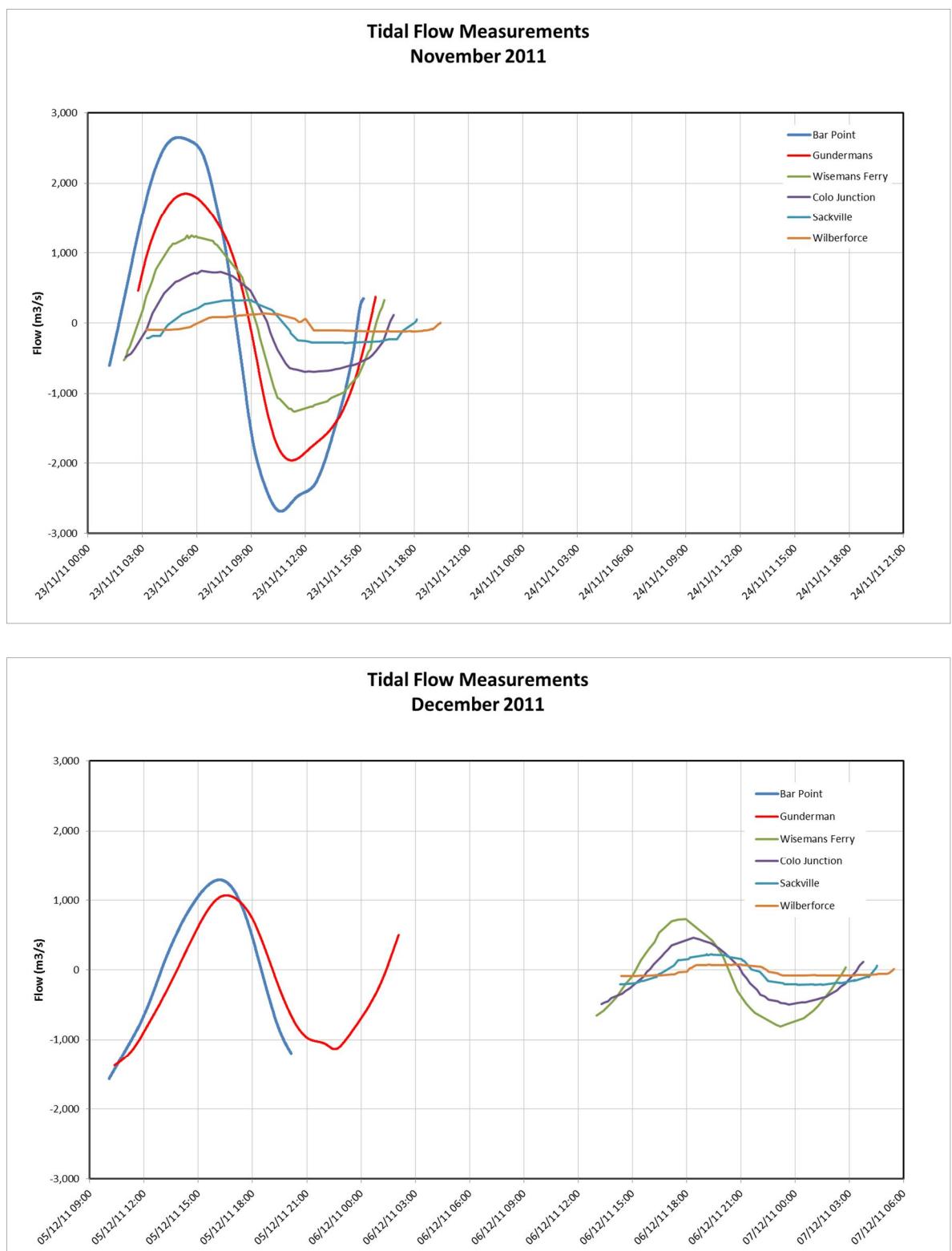
Figure:
11-8

Rev:
A

N 0 3 6km
Approx. Scale



Water Quality Modelling of the Hawkesbury-Nepean River System



- **Figure 11-9 Tidal Flow Measurements during ADCP CMP Period. Upper Panel: Spring Tides. Lower Panel: Neap Tides**

11.6. Ambient Water Quality Data

Water quality data were required to define the downstream TUFLOW model boundary conditions and to provide data ‘within’ the model domain against which the model can be initialised and assessed. Ambient water quality and bacteria data were provided for a wide range of locations within the study domain. The sites used for calibration, validation and boundary conditions are presented in **Figure 11-10**. Example data for these sites (selected within Upstream, Middle Reach, and Estuary) are also shown in **Figure 11-11** (total nitrogen) and **Figure 11-12** (total phosphorus). Due to the influence of wastewater treatment plants and water recycling plants, the scales adopted for the upper and particularly middle reaches are different to the scale adopted for the lower reach.

As well as showing all data as per the time series presented in **Figure 11-11** and **Figure 11-12**, it is often informative to show these data as ‘box and whiskers’ statistical representations, which can greatly aid the understanding of those key water quality processes which are taking place within a study area. **Figure 11-13** to **Figure 11-24** show selected water quality data for relevant parameters using all data that are available post-2004. Note that 2004 was chosen as a cut-off date for analysis as prior to the year 2000 there were major upgrades in effluent management within the catchment (as evidenced in **Figure 11-11** and **Figure 11-12**). A period of four years was arbitrarily allowed to enable water quality levels within the system to stabilise following these changes in treatment. The period of analysis and number of samples for each of the variables used for the computation of statistics in these ‘box and whiskers’ plots are presented in **Table 11-2**.

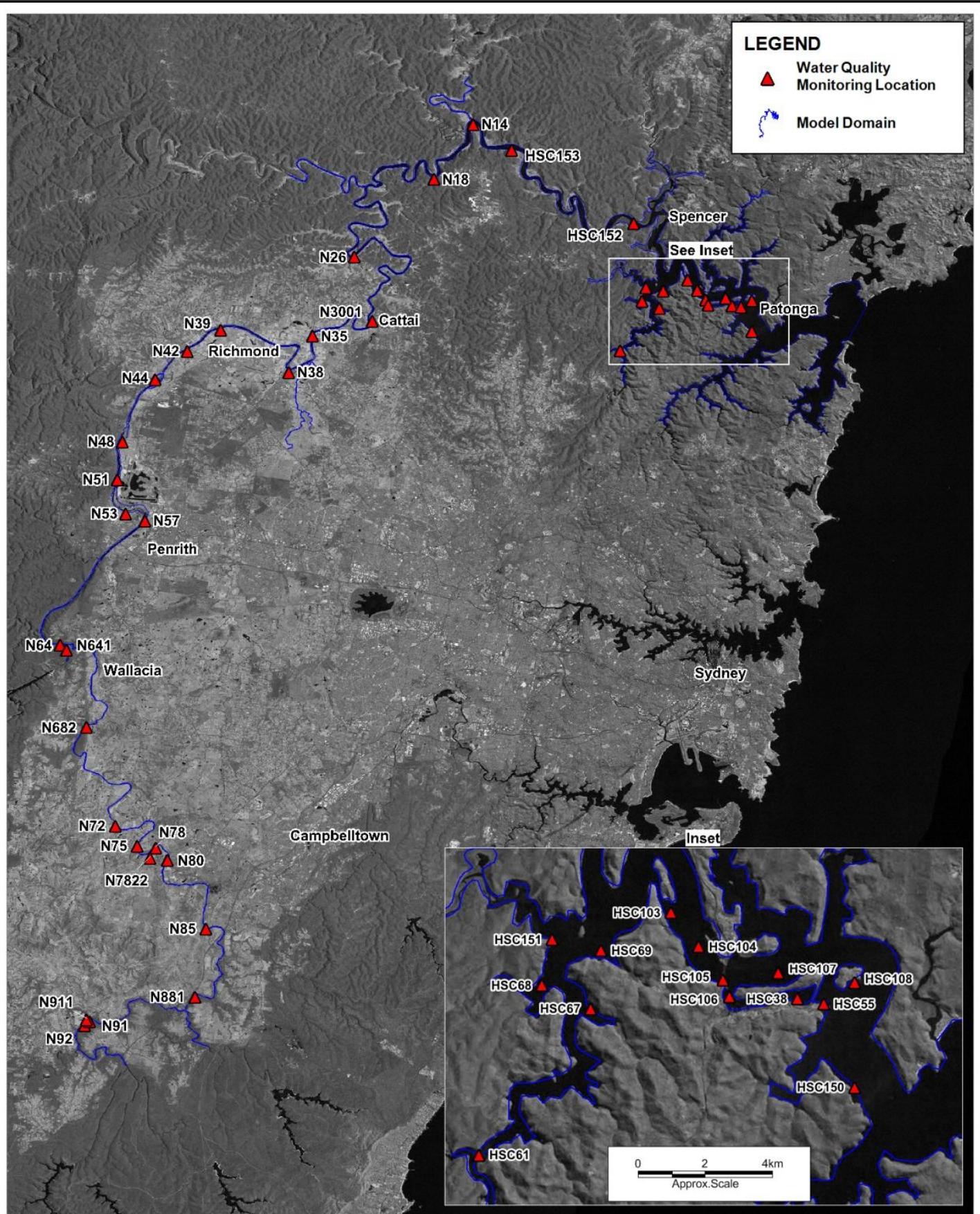
From these data, the following observations can be made:

- Salinity/conductivity data illustrates that any oceanic exchange or tidal flushing influence on water quality will be largely limited to those reaches downstream of Wiseman’s Ferry (site N14);
- Temperature data shows consistent behaviour, with:
 - Slightly greater temperature ranges in the sections of the river with numerous shallower pool and riffle sequences (e.g. sites N39, N42 and N44); and
 - Markedly lower temperatures at the site immediately downstream of the Warragamba Dam (site N641), presumably reflecting environmental flow releases from cooler water layers in the dam.
- Dissolved oxygen data indicates typically near saturation oxygen levels, again with the greatest natural variability apparent in the shallower pool and riffle locations (e.g. sites N39, N42 and N57);
- Turbidity data shows low levels and typically quite ‘clear’ waters upstream of the South Creek confluence (site N38), however downstream of South Creek there is a marked increase in turbidity levels, most likely due to the impact of run-off from South Creek and its associated extensive areas of peri-urban horticulture and urban land use;
- Nitrogen data shows that:
 - Ammonium concentrations throughout this system are quite low, with some indication of elevated levels downstream of South Creek (site N35 in particular); and



Water Quality Modelling of the Hawkesbury-Nepean River System

- Nitrate levels indicate the influence of the point source WWTP/WRP loads from the Winmalee Sewage Treatment Plant (evident at site N461) and South Creek (evident at site NS04) where they are both measured.
- Phosphorus data shows that:
 - Filterable reactive phosphorus (FRP) concentrations in the Nepean River upstream of South Creek are very low, with some evidence of elevated FRP levels below the South Creek confluence; and
 - Total phosphorus levels exhibit similar behaviour to FRP, with possibly even greater evidence of nutrient enrichment of the Hawkesbury-Nepean by discharges from South Creek.
- From the chlorophyll a data, it is evident that algal levels in the Nepean River upstream of South Creek are typically quite low, whereas there is significant growth of phytoplankton downstream of the confluence of South Creek.



Title:

Ambient Water Quality Monitoring Locations

Figure:

11-10

Rev:

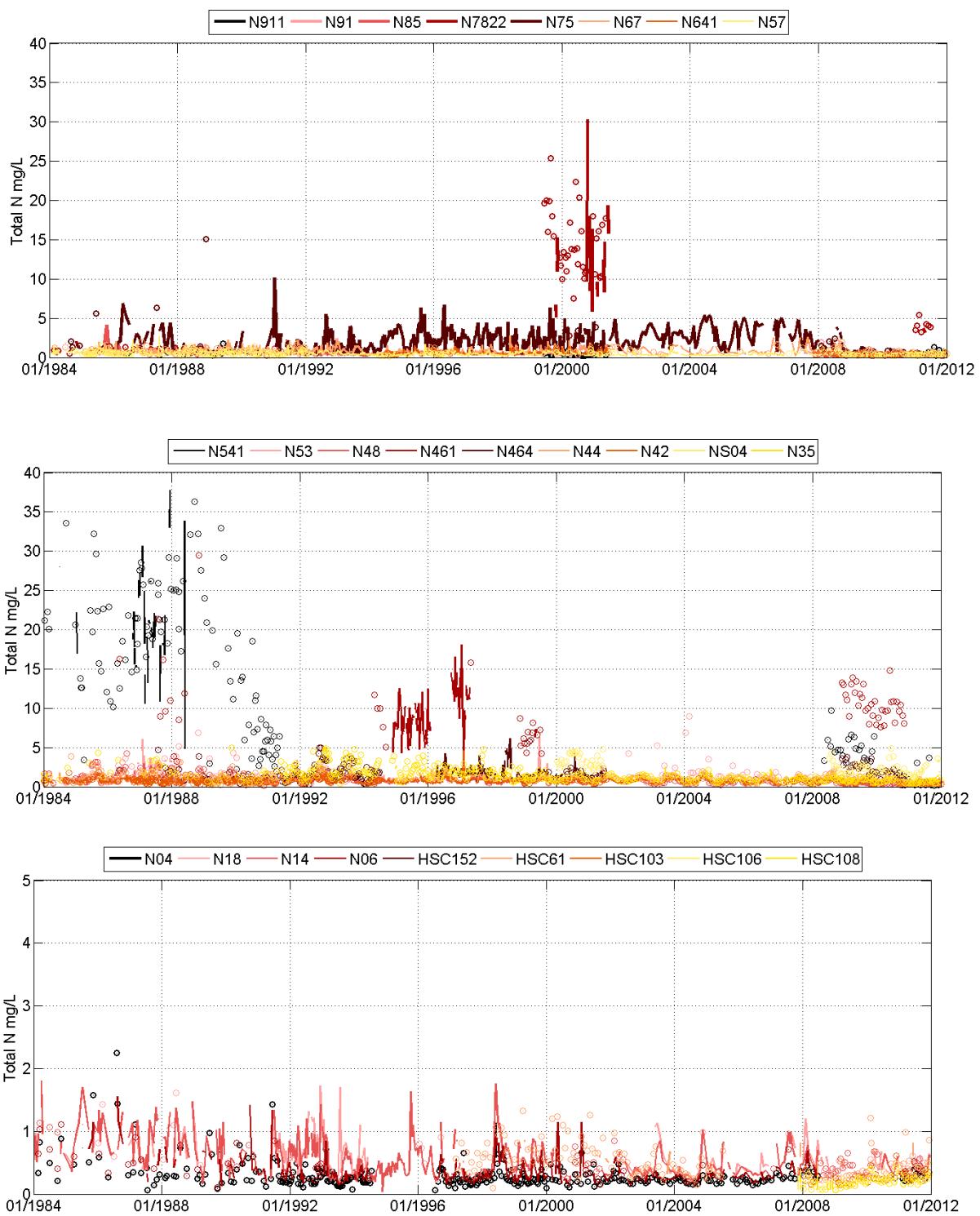
A

BMT WBM endeavours to ensure that the information provided in this map is correct at the time of publication. BMT WBM does not warrant, guarantee or make representations regarding the currency and accuracy of information contained in this map.



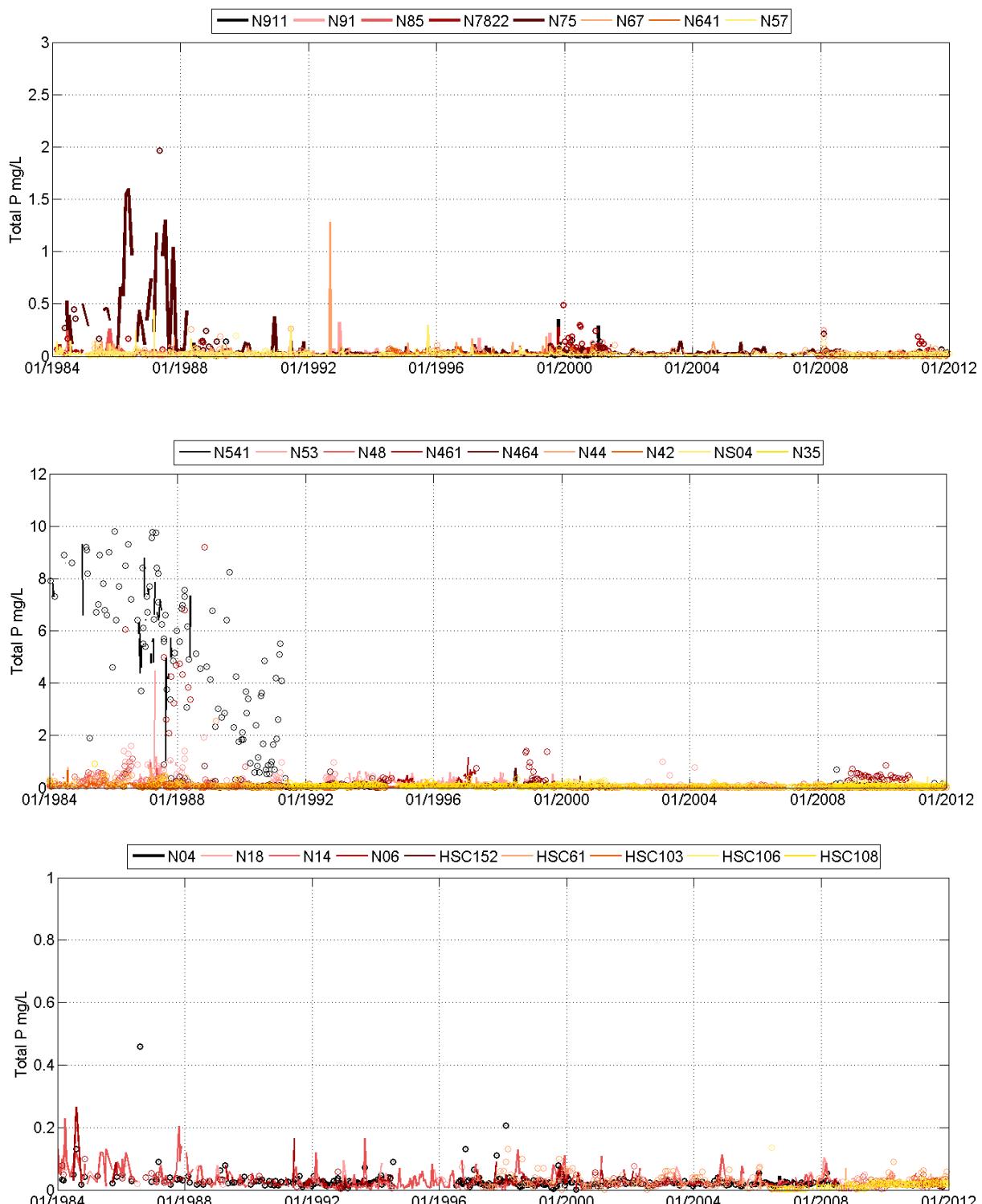
0 10 20km
Approx. Scale

Water Quality Modelling of the Hawkesbury-Nepean River System



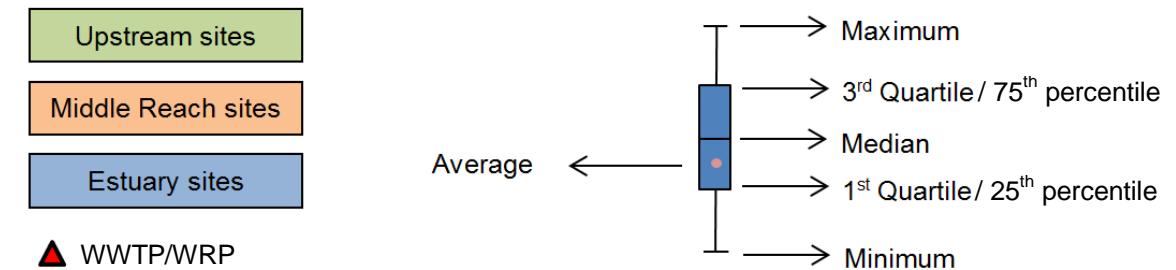
- **Figure 11-11 Example Water Quality Data – Total Nitrogen. Upper Panel: Upstream Reach Stations. Middle Panel: Middle Reach Stations; Lower Panel: Downstream Reach Stations. Contiguous data shown as lines and non-contiguous as dots.**

Water Quality Modelling of the Hawkesbury-Nepean River System



- **Figure 11-12 Example Water Quality Data – Total Phosphorus. Upper Panel: Upstream Reach Stations. Middle Panel: Middle Reach Stations; Lower Panel: Downstream Reach Stations. Contiguous data shown as lines and non-contiguous as dots.**

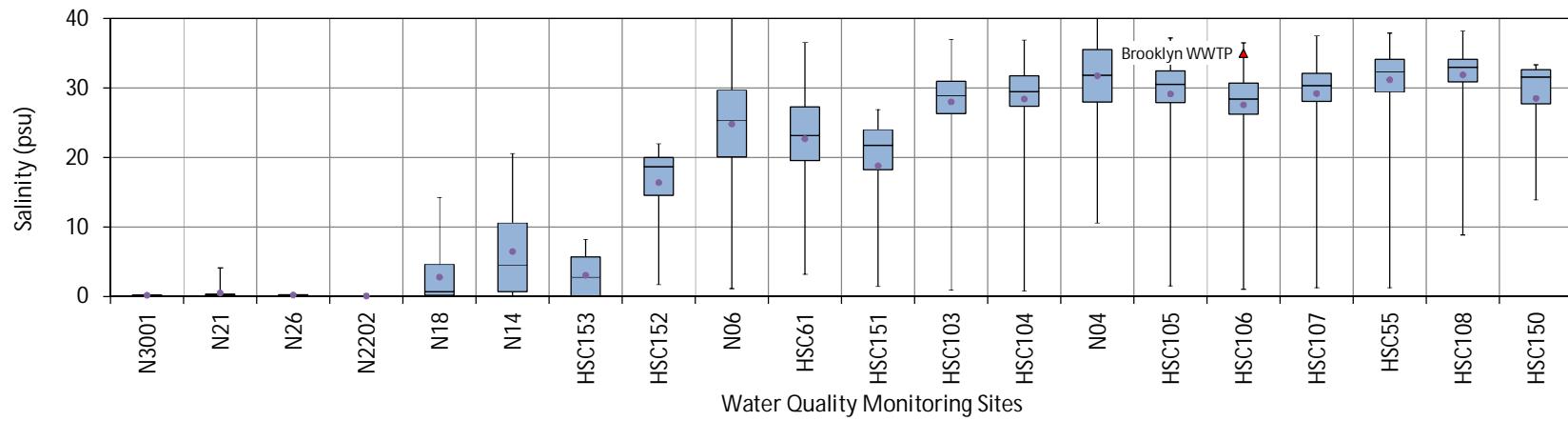
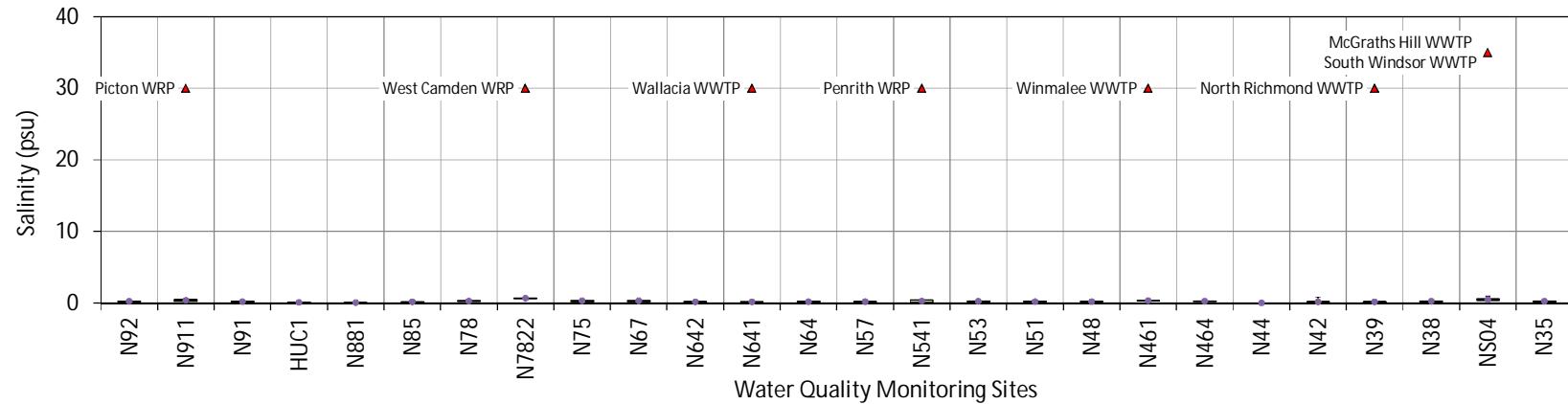
Water Quality Modelling of the Hawkesbury-Nepean River System



- **Figure 11-13 Colour code and symbols adopted in Figure 11-14 to Figure 11-24**



Water Quality Modelling of the Hawkesbury-Nepean River System

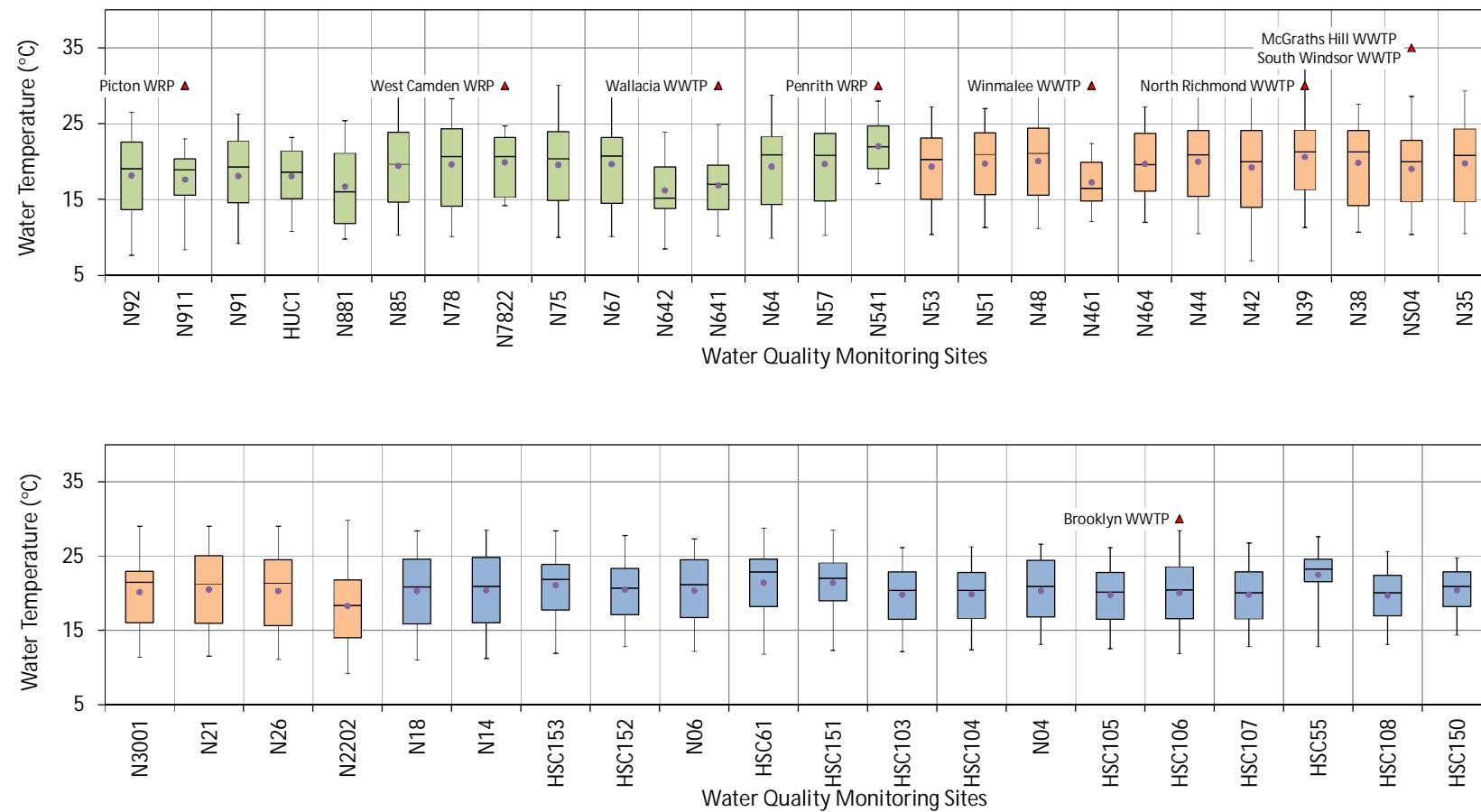


■ **Figure 11-14 Analysed Ambient Water Quality Data – Salinity**

SINCLAIR KNIGHT MERZ



Water Quality Modelling of the Hawkesbury-Nepean River System

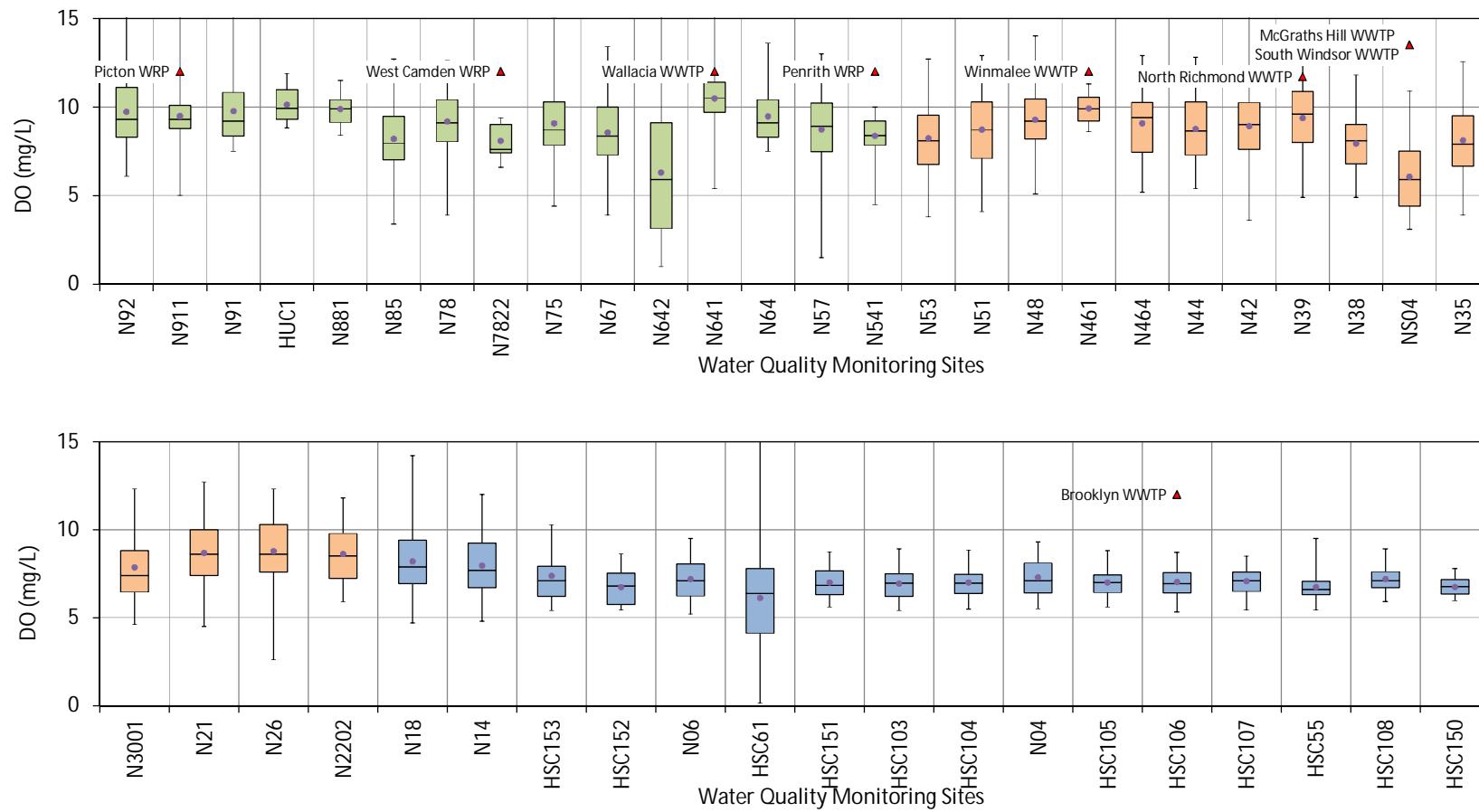


■ **Figure 11-15 Analysed Ambient Water Quality Data – Temperature**

SINCLAIR KNIGHT MERZ



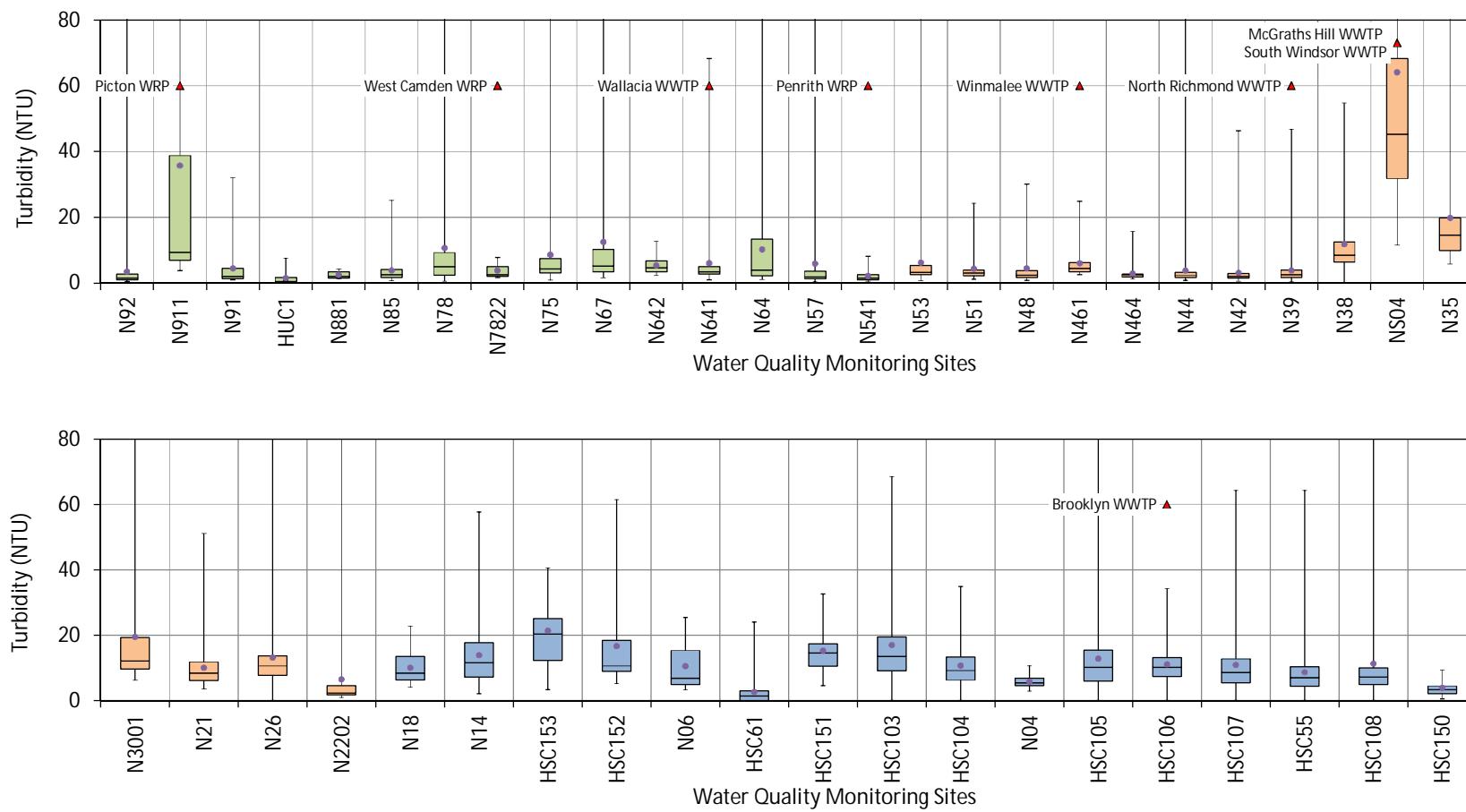
Water Quality Modelling of the Hawkesbury-Nepean River System



■ **Figure 11-16 Analysed Ambient Water Quality Data – Dissolved Oxygen**



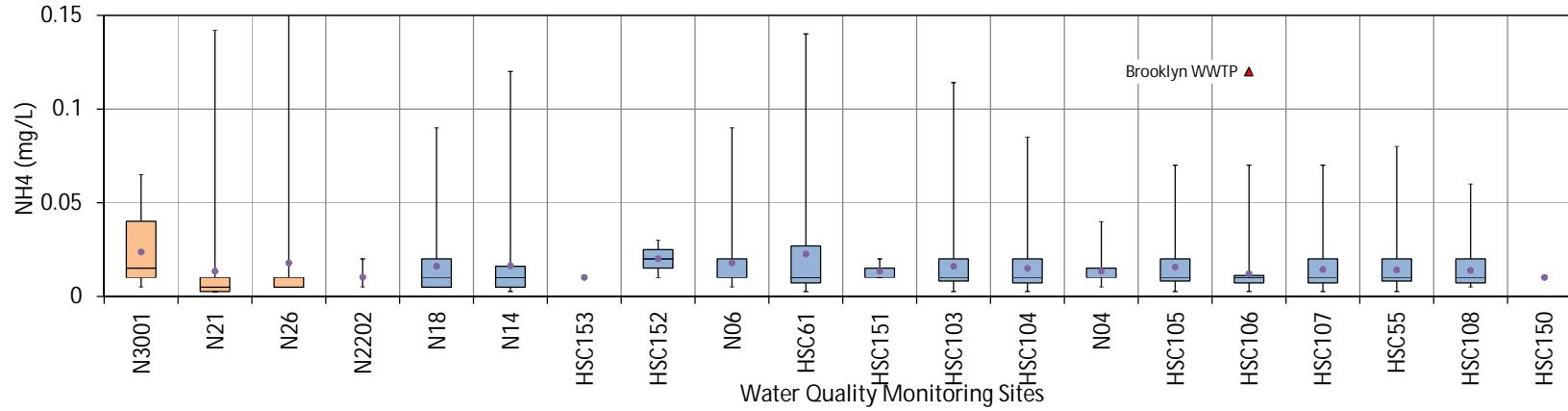
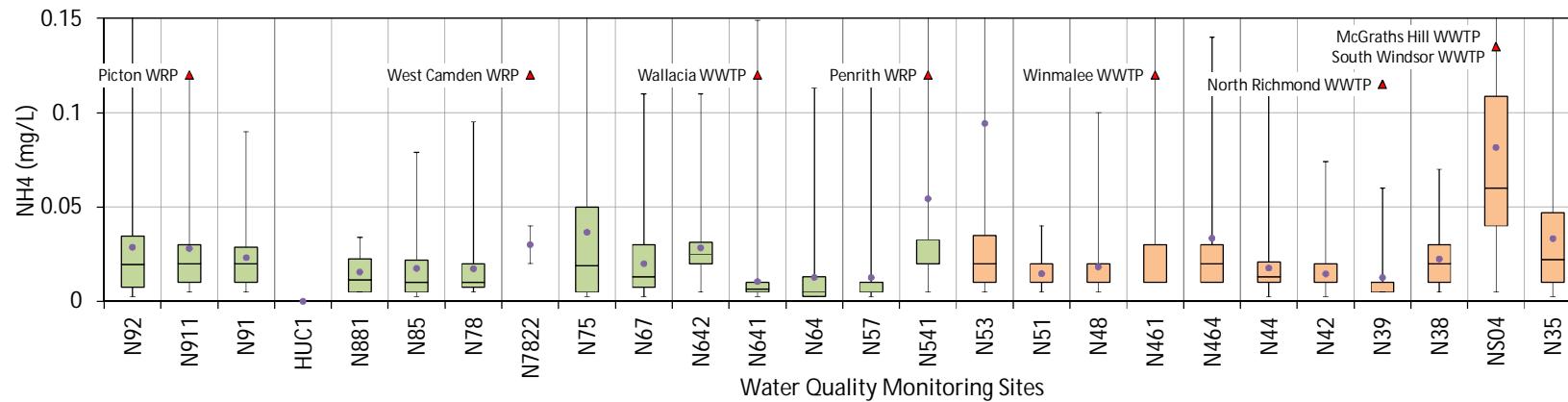
Water Quality Modelling of the Hawkesbury-Nepean River System



■ **Figure 11-17 Analysed Ambient Water Quality Data –Turbidity**



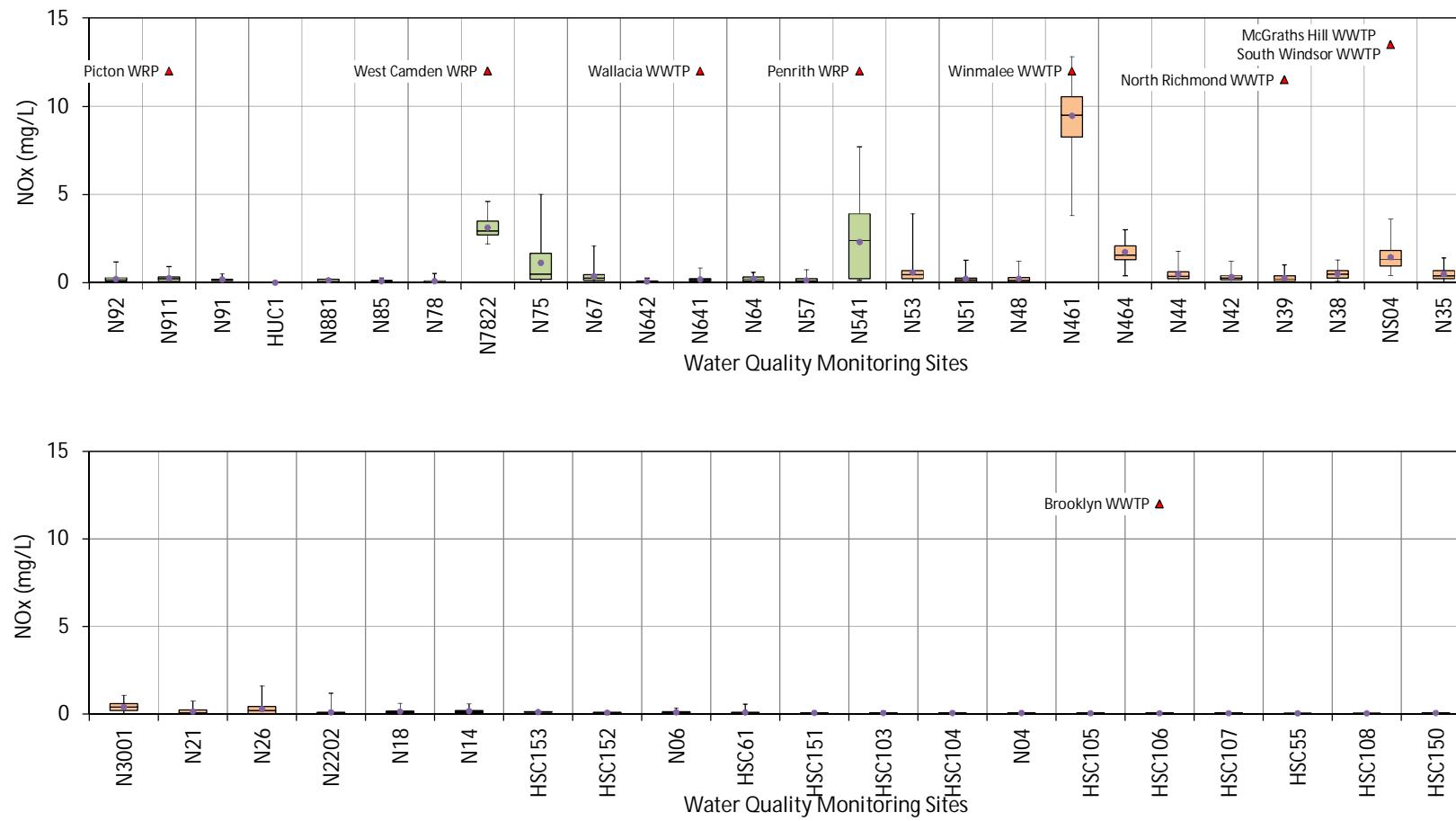
Water Quality Modelling of the Hawkesbury-Nepean River System



■ Figure 11-18 Ambient Water Quality Data – Ammonium



Water Quality Modelling of the Hawkesbury-Nepean River System

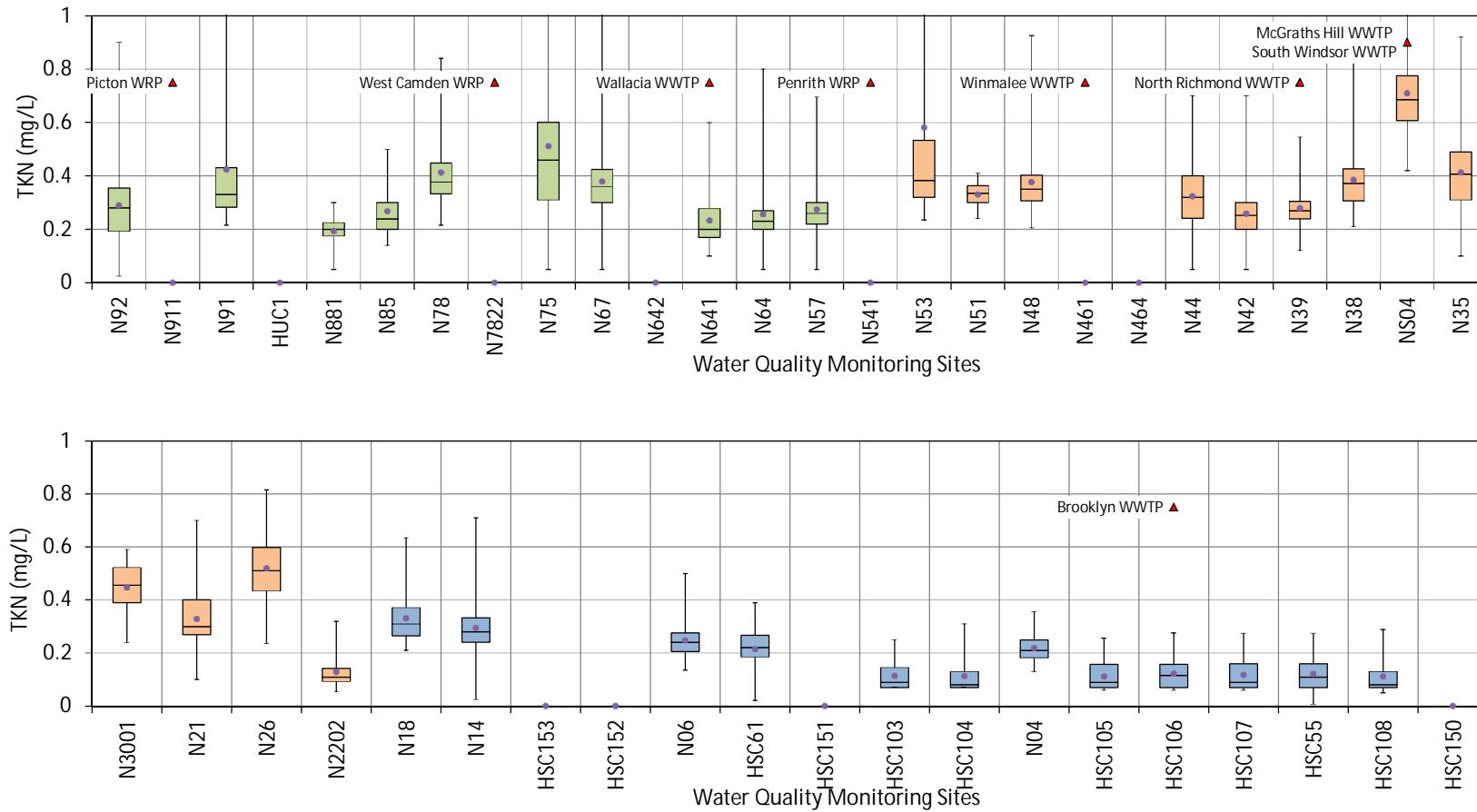


■ Figure 11-19 Ambient Water Quality Data – Oxidised Nitrogen

SINCLAIR KNIGHT MERZ



Water Quality Modelling of the Hawkesbury-Nepean River System

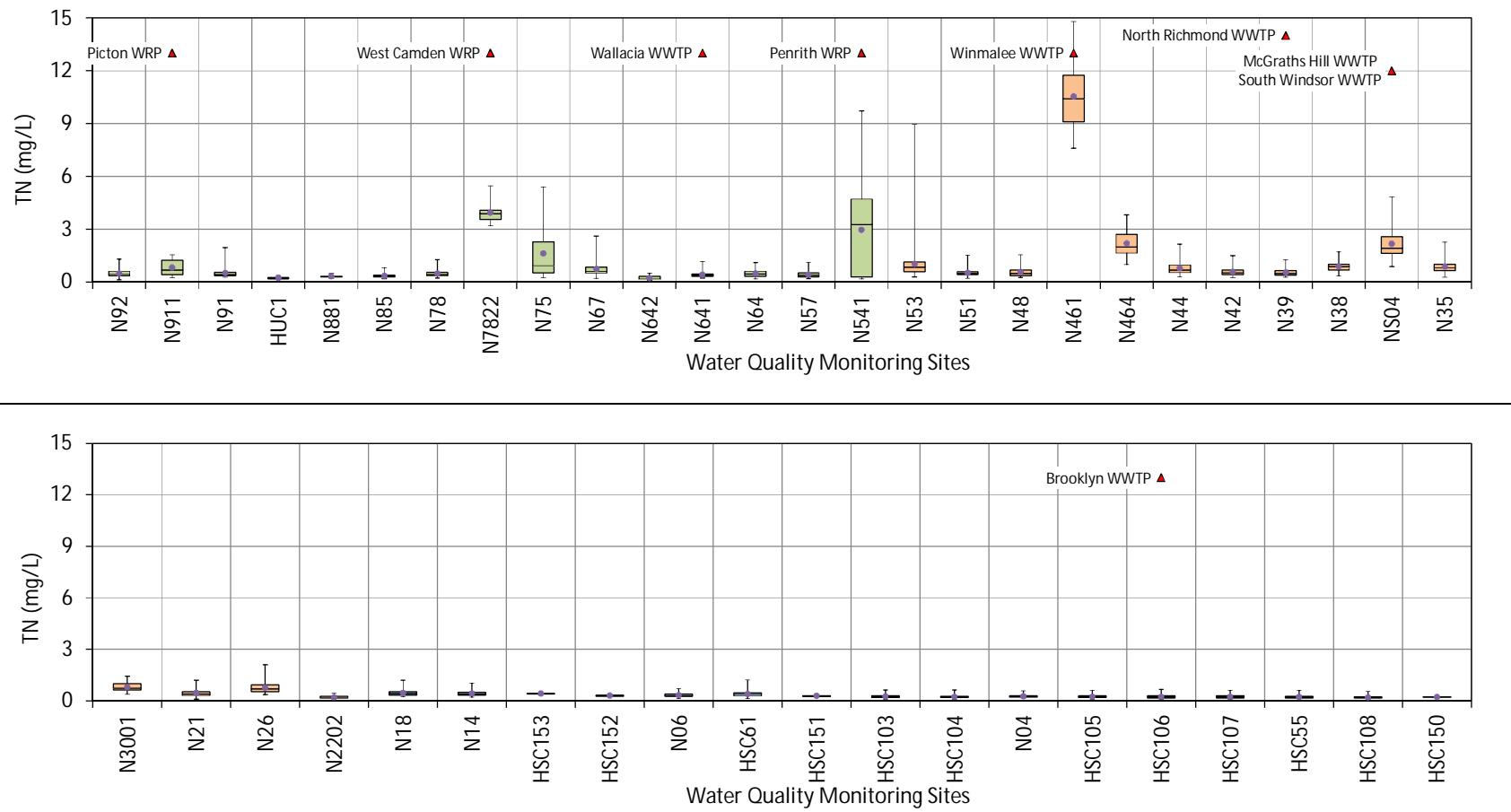


■ **Figure 11-20 Ambient Water Quality Data – Total Kjeldahl Nitrogen**

SINCLAIR KNIGHT MERZ



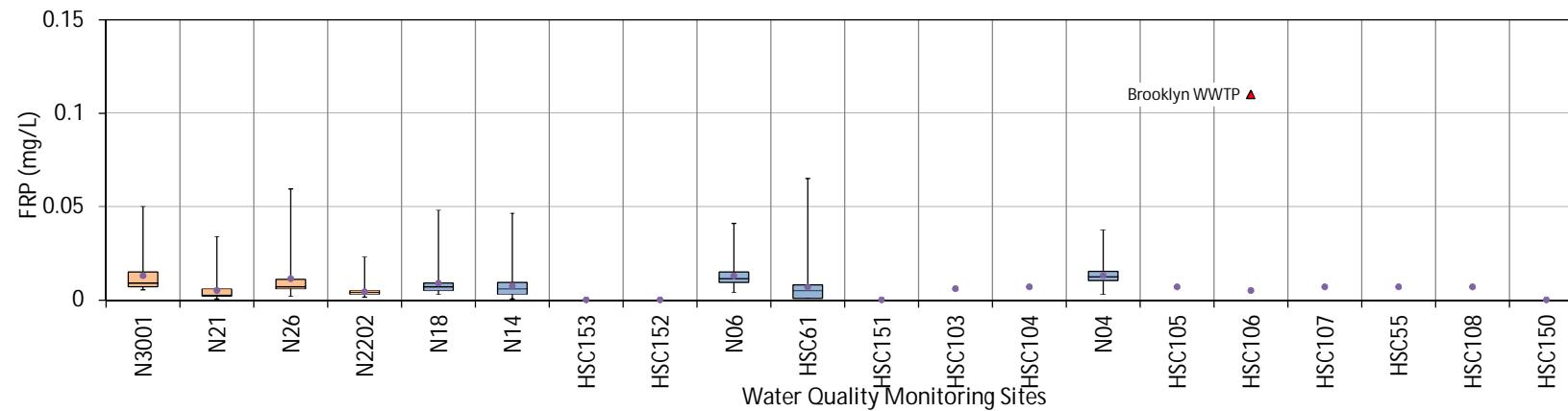
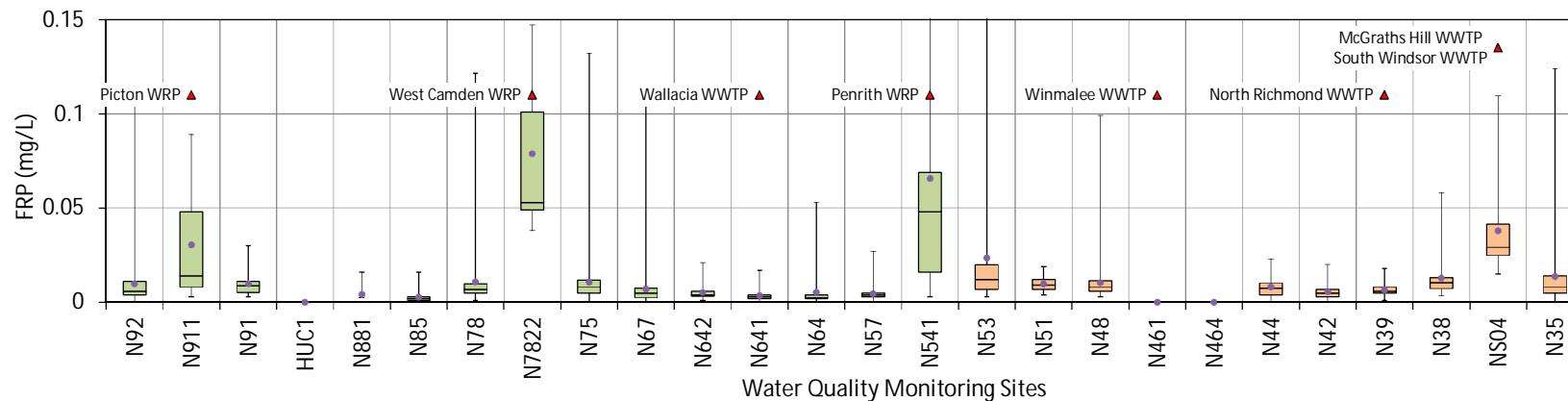
Water Quality Modelling of the Hawkesbury-Nepean River System



■ **Figure 11-21 Ambient Water Quality Data – Total Nitrogen**



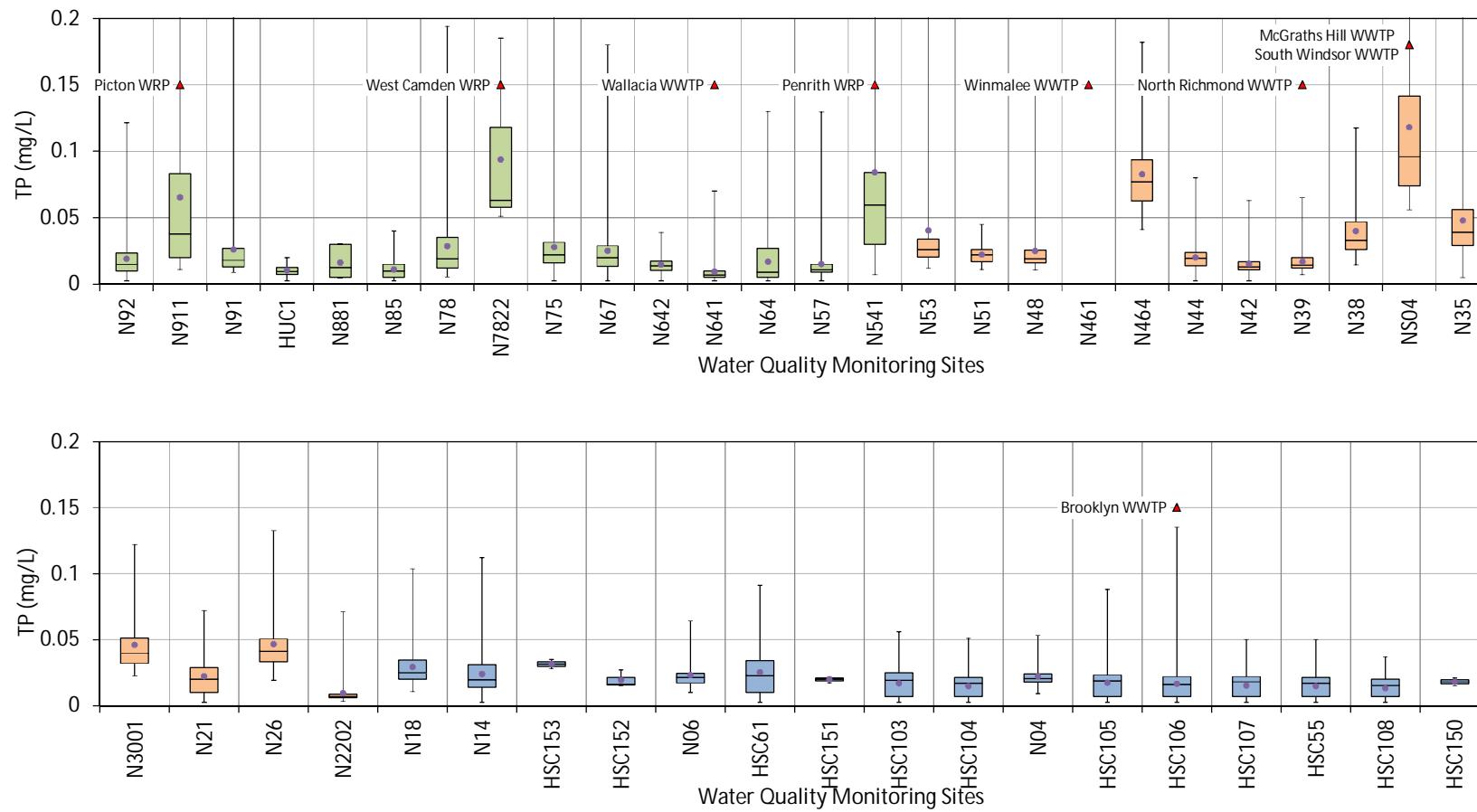
Water Quality Modelling of the Hawkesbury-Nepean River System



■ Figure 11-22 Ambient and Water Quality Data – Filterable Reactive Phosphorus



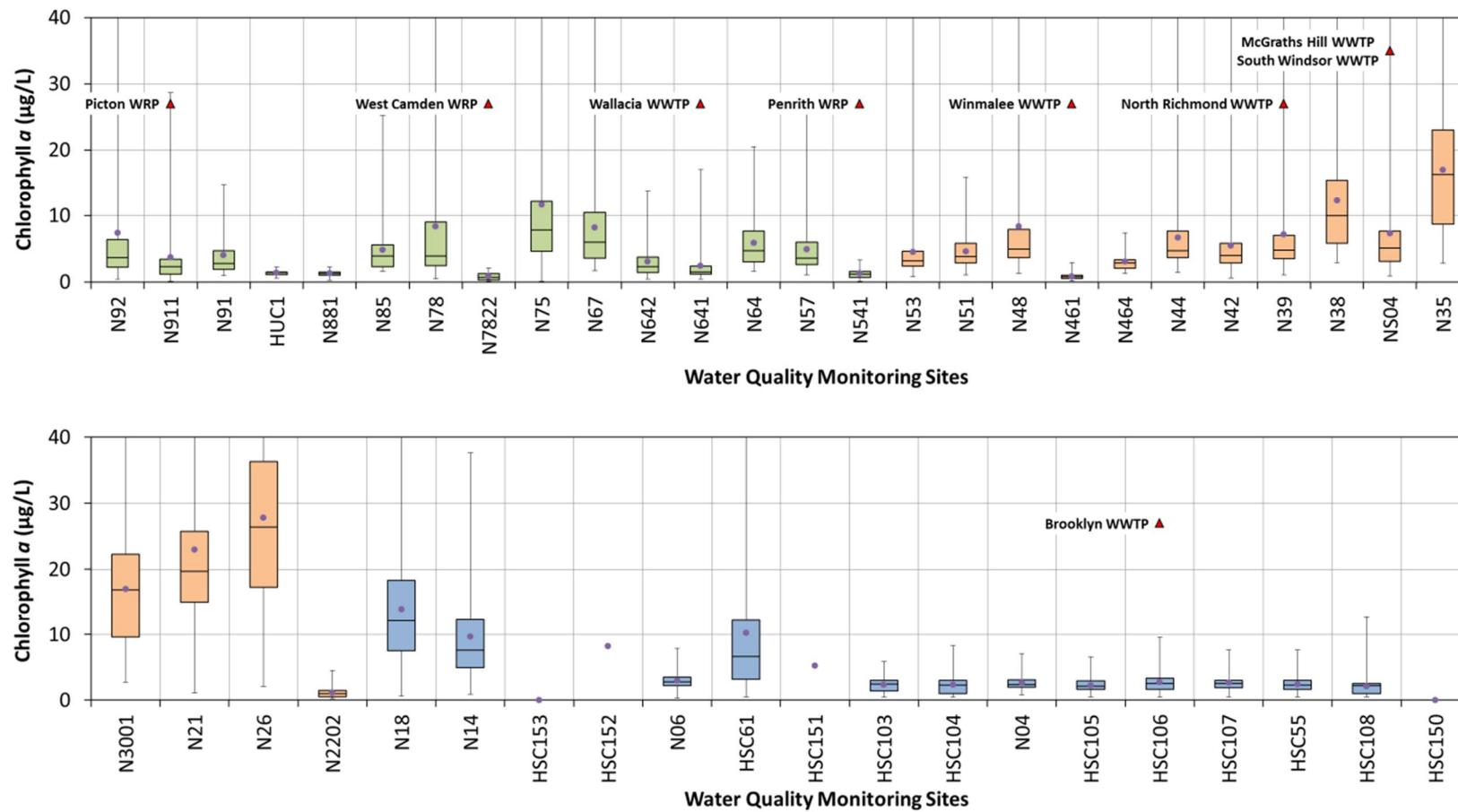
Water Quality Modelling of the Hawkesbury-Nepean River System



■ **Figure 11-23 Ambient and Water Quality Data – Total Phosphorus**



Water Quality Modelling of the Hawkesbury-Nepean River System



■ Figure 11-24 Ambient and Water Quality Data – Chlorophyll a

Water Quality Modelling of the Hawkesbury-Nepean River System

■ **Table 11-2 Period and Number of Samples Used in the Calculations of the Statistics Presented in the Box and Whisker Plots**

Monitoring Sites	Reach	Time Period of Analyses	n.samples for each water quality constituent											
			Salinity	Temp	DO	Turb	NH4	NOx	TKN	TN	FRP	TP	Chl-a	
N92	Upstream	Jan/2004 - Apr/2012	171	161	160	160	158	158	135	158	158	158	158	164
N911	Upstream	Jan/2011 - Apr/2012	35	34	34	34	35	35	0	35	35	35	35	35
N91	Upstream	Jul/2007 - Apr/2012	37	37	38	37	38	38	15	38	38	38	38	36
HUC1	Upstream	Jan/2011 - May/2012	21	21	21	21	0	0	0	4	0	4	4	17
N881	Upstream	Jan/2007 - Apr/2012	23	8	8	8	8	8	8	8	8	8	8	23
N85	Upstream	Nov/2007 - Apr/2012	33	54	54	54	53	53	53	53	53	53	53	53
N78	Upstream	Jan/2004 - Jun/2011	63	63	63	63	63	63	54	63	63	63	63	56
N7822	Upstream	Jan/2011 - Jun/2011	9	9	9	9	9	9	0	9	9	9	9	Jan-00
N75	Upstream	Jan/2004 - Apr/2012	160	159	159	159	150	154	131	151	151	151	151	150
N67	Upstream	Jan/2004 - Feb/2011	172	172	172	172	153	167	126	167	153	167	171	
N642	Upstream	May/2008 - Mar/2012	47	47	47	47	36	47	0	47	36	47	47	47
N641	Upstream	Sep/2006 - May/2012	105	105	105	105	90	103	54	103	90	103	103	104
N64	Upstream	Nov/2007 - Apr/2012	67	67	67	66	53	65	53	65	53	65	65	66
N57	Upstream	Jan/2004 - Apr/2012	184	184	184	184	165	178	140	178	165	178	178	
N541	Upstream	May/2008 - Apr/2012	39	39	39	39	39	39	0	39	39	38	39	
N53	Middle	Jan/2004 - Apr/2012	111	111	111	111	111	111	54	111	111	111	111	104
N51	Middle	Jul/2008 - Apr/2012	58	58	58	57	57	58	35	58	58	58	58	58
N48	Middle	Jan/2004 - Apr/2012	115	115	115	115	114	115	83	115	115	115	115	109
N461	Middle	Nov/2008 - Nov/2010	35	35	35	35	35	35	0	35	0	35	35	35
N464	Middle	Nov/2008 - Nov/2010	35	35	35	35	35	35	0	35	0	35	35	
N44	Middle	Jan/2004 - Apr/2012	0	173	173	173	150	167	126	164	151	164	168	
N42	Middle	Jan/2004 - Apr/2012	501	501	494	468	163	164	138	491	164	491	488	
N39	Middle	Jan/2004 - Apr/2012	118	118	118	118	104	117	81	117	104	117	112	
N38	Middle	Jan/2004 - Jun/2008	53	53	53	51	52	52	52	52	52	52	52	45
NS04	Middle	Sep/2008 - Dec/2011	69	69	69	69	54	69	35	69	54	69	69	
N35	Middle	Jan/2004 - Apr/2012	155	157	157	157	156	156	142	156	156	156	156	151
N3001	Middle	Sep/2008 - Apr/2012	69	71	71	71	57	71	35	71	57	71	71	
N21	Middle	Jan/2004 - Apr/2012	102	103	103	102	102	102	102	102	102	102	102	
N26	Middle	Jan/2004 - Apr/2012	108	110	110	109	110	110	88	110	110	110	110	103
N2202	Middle	Sep/2008 - Apr/2012	58	58	58	58	57	58	35	57	58	58	58	
N18	Lower	Jan/2004 - Apr/2012	108	110	110	57	110	110	88	110	110	110	110	103
N14	Lower	Jan/2004 - Apr/2012	116	117	117	103	116	116	116	116	116	116	116	111
HSC153	Lower	Dec/2010 - Apr/2012	18	18	17	2	2	0	2	0	2	0	2	0
HSC152	Lower	Nov/2010 - Apr/2012	14	14	13	13	3	3	0	3	0	3	1	
N06	Lower	Jan/2004 - Feb/2012	70	70	70	12	70	70	57	70	57	70	57	64
HSC61	Lower	Jan/2004 - Apr/2012	342	344	334	342	93	122	20	93	109	122	114	
HSC151	Lower	Nov/2010 - Apr/2012	20	20	19	18	3	3	0	3	0	3	1	
HSC103	Lower	Jun/2006 - Apr/2012	73	74	72	74	61	76	18	61	1	76	69	
HSC104	Lower	Jun/2006 - Apr/2012	73	74	72	74	61	76	18	61	1	76	Mar-00	
N04	Lower	Jan/2004 - Feb/2012	72	72	72	12	73	73	59	71	59	71	63	
HSC105	Lower	Jun/2006 - Apr/2012	74	75	73	75	61	76	18	61	1	76	70	
HSC106	Lower	Jun/2006 - Apr/2012	74	75	73	75	62	77	18	62	1	77	71	
HSC107	Lower	Jun/2006 - Apr/2012	72	73	71	73	62	77	17	62	1	77	71	
HSC55	Lower	Dec/2004 - Apr/2012	193	194	192	194	150	180	45	149	1	179	174	
HSC108	Lower	Jun/2006 - Apr/2012	70	72	71	72	62	77	17	62	1	77	71	
HSC150	Lower	Dec/2010 - Apr/2012	19	19	18	18	2	2	0	2	0	2	0	

12. Model Set-Up

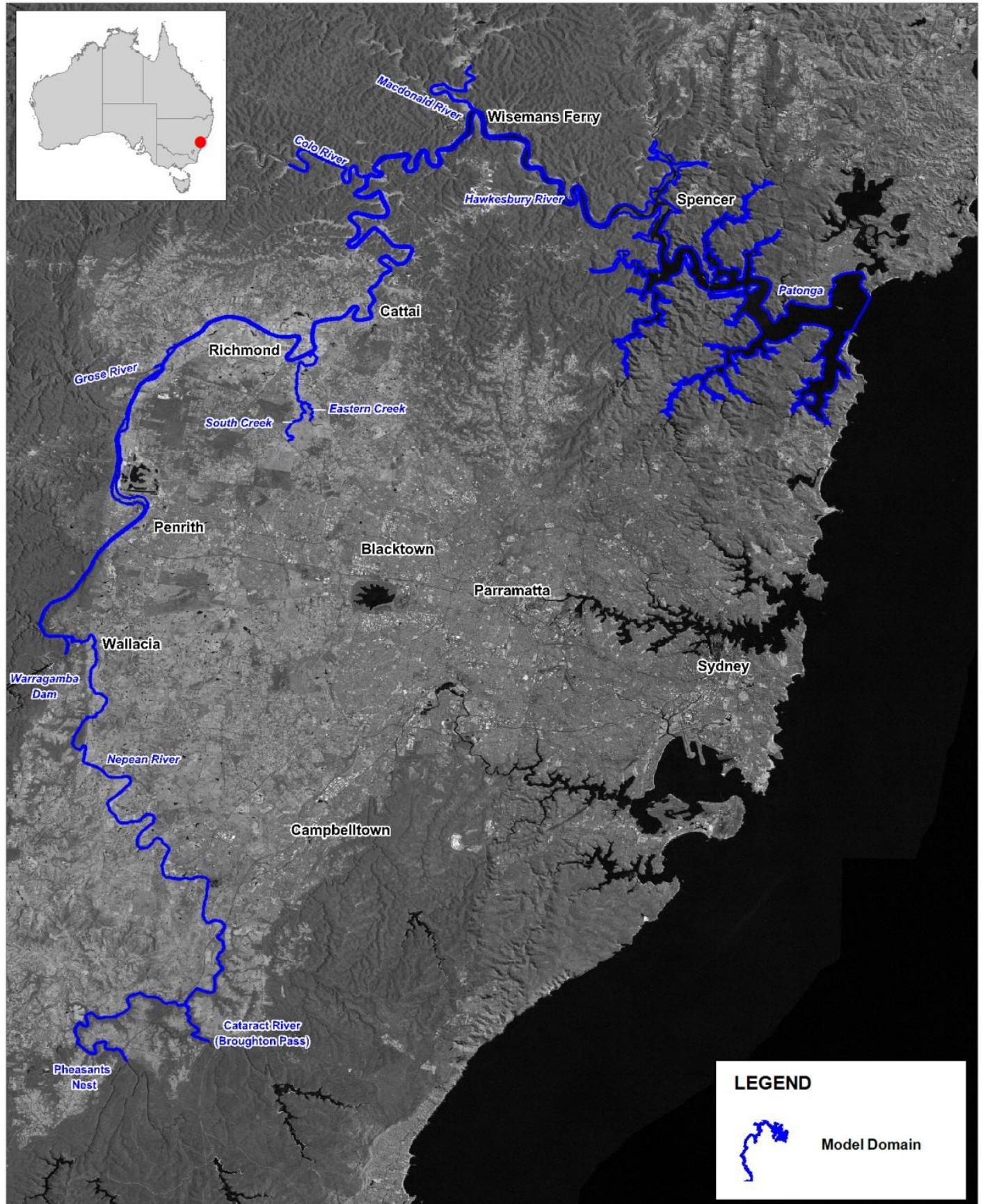
12.1. Hydrodynamic Model

Each component of the model build process is described below. In addition, a science manual describing in detail the formulations used in TUFLOW is presented in **Appendix J**, with a further manual on the water quality module provided in **Appendix K**.

12.1.1. Model Domain

The model domain consists of the Hawkesbury-Nepean River system from Barrenjoey (ocean) to Pheasants Nest (on the Nepean River) and Broughton Pass (on the Cataract River). The model domain is presented in **Figure 12-1**. The tributaries included are:

- Downstream of the Warragamba Dam to the Nepean River confluence;
- South Creek from approximately 550 m downstream of Richmond Road to the confluence with Eastern Creek;
- Eastern Creek from Bandon Road to the confluence with South Creek;
- South Creek from the confluence with Eastern Creek to the confluence with the Hawkesbury River;
- Colo River from the confluence with Wheeny Creek to the confluence with the Hawkesbury River;
- MacDonald River from Central McDonald to the confluence with the Hawkesbury River near Wisemans Ferry; and
- Several smaller creeks in the lower part of the estuary, including:
 - Mangrove Creek (northern margin);
 - Mooney Mooney Creek (northern margin);
 - Mullet Creek(northern margin);
 - Big Boy Creek (southern margin);
 - Colbar Creek (southern margin);
 - Calabash Creek (southern margin);
 - Berowra Creek (southern margin);
 - Cowan Creek (southern margin);
 - Coal and Candle Creek (southern margin); and
 - McCarr's Creek (southern margin).



Title:
Model Domain

Figure:
12-1

Rev:
A

BMT WBM endeavours to ensure that the information provided in this map is correct at the time of publication. BMT WBM does not warrant, guarantee or make representations regarding the currency and accuracy of information contained in this map.



0

10

20km

Approx. Scale

12.1.2. Model Mesh

The model mesh extends downstream to Barrenjoey (ocean) and upstream to the diversion weirs on Pheasants Nest (Nepean River) and Broughton Pass (Cataract River). Fine tuning of model element positioning was undertaken in some places to ensure that inspected bed levels better reproduced the river alignments and bathymetry. Significant effort was also expended to include some flood storage in the TUFLOW model in wetlands just south of Penrith Lakes.

Considerable effort was expended to design an appropriate mesh which would capture a number of the areas of the river where the channel passes through a wide – narrow – wide sequence. Poorly defined meshes in such sequences can cause excessive numerical flow constriction and commensurate energy losses. Considerable effort was also expended iterating between the raw survey data, the constructed DEM and the model mesh to ensure that key bathymetric attributes of the river were adequately captured but that they did not artificially cause numerical drag or interference within the simulation.

In particular, ‘smoothing’ the model bathymetry around tight and narrow constrictions (such as Wiseman’s Ferry) was investigated, where the simple interrogation of underlying bathymetry onto the much coarser model mesh lead to generation of artificial numerical features. These features caused (incorrect) enhanced dissipation of tidal energy and as such resulted in significant attenuation of the modelled tidal wave through the system. This smoothing was only applied in these tight bend areas as it offered a means by which to allow the model to reproduce tidal dynamics without needing to unreasonably increase model spatial resolution and generate unacceptable computational overhead.

In the vertical, a hybrid mesh was developed to make feasible computations over such a large model domain. In this hybrid mesh approach, a sigma-coordinate mesh with two vertical elements overlayed a fixed z-coordinate mesh consisting of variable grid sizes. A sigma coordinate, or ‘terrain-following’, mesh is one where the same number of levels is used to discretise cells with different depths (e.g. 5 levels of 1m each are used to discretise a cell of depth 5m, while 5 levels of 2m each are used to discretise a cell of depth 10m). This is distinct from a z-coordinate system where the levels are at fixed depths and differing numbers of levels are used to discretise a cell at a particular depth (e.g. 5 levels of 1m each are used to discretise a depth of 5m, but 10 levels of 1m each are needed for a depth of 10m). Using a sigma coordinate system for depths above -2.0 m AHD allows the model to accurately simulate the complex surface dynamics with a minimum of resolution, while using z-coordinates at depth allows the model to avoid using higher resolution where it is not necessary. In this way, model runtimes were kept at a minimum while retaining the ability to accurately simulate the hydrodynamics of the system.

The z-coordinate mesh covered the tidal extent of the system with grid cells between -30.0 and -2.0 m AHD. The vertical resolution was 5.0 m between -30.0 m AHD and -15.0 m AHD, 3.0 m between -15.0 m AHD and -12.0 m AHD, and 2.0 m thereon to -2.0 m AHD.

The sigma-coordinate cells covered the entire domain between the free-surface (at whatever height was required to match ambient water levels) and -2.0 m AHD. For locations where the bathymetry was above -2.0 m AHD, the two sigma coordinate cells formed the vertical model discretisation.

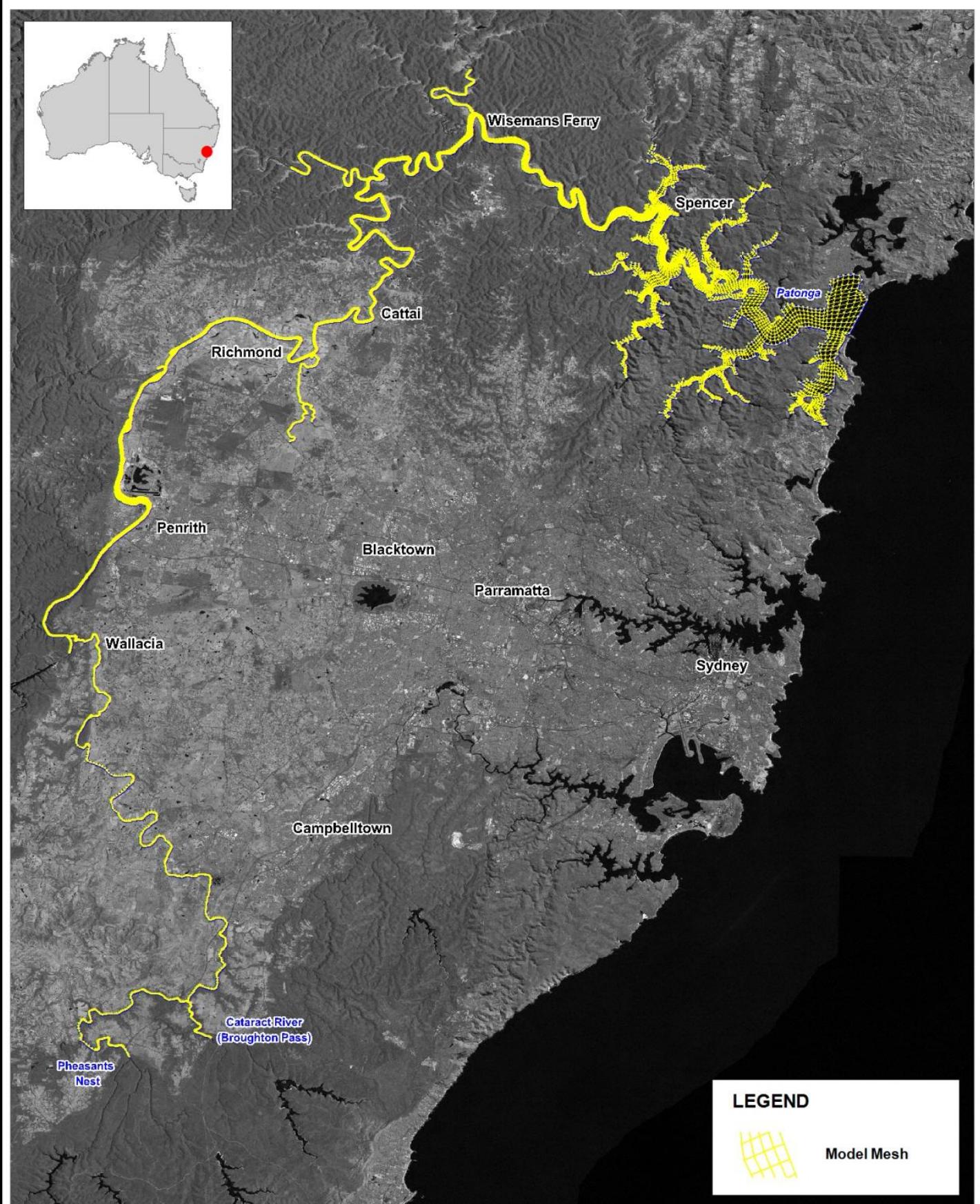
SINCLAIR KNIGHT MERZ



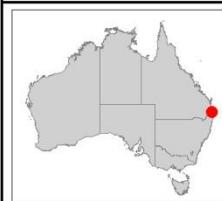
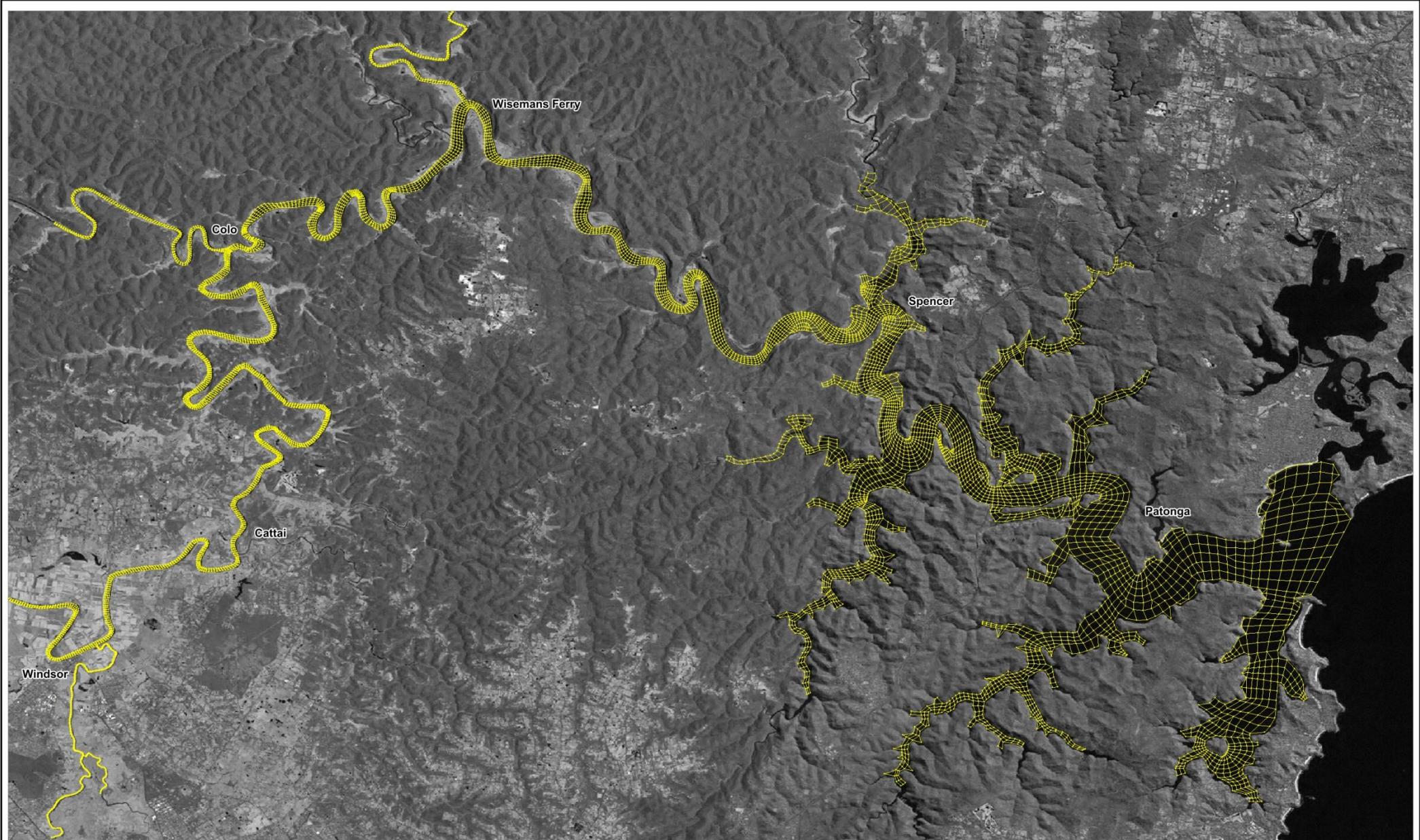
Water Quality Modelling of the Hawkesbury-Nepean River System

This means that the entire model domain is three-dimensional, with the smallest number of vertical layers anywhere being 2 (i.e. the two sigma layers).

The overall mesh is presented in **Figure 12-2**. **Figure 12-3** to **Figure 12-9** present a series of figures that zoom in on each section of mesh. The mesh of the Bents Basin region is presented as part of this series as it is of interest to some stakeholders.



Title: Overall Model Mesh	Figure: 12-2	Rev: A
BMT WBM endeavours to ensure that the information provided in this map is correct at the time of publication. BMT WBM does not warrant, guarantee or make representations regarding the currency and accuracy of information contained in this map.	 0 10 20km Approx. Scale	 BMT WBM www.bmtwbm.com.au



LEGEND



Model Mesh

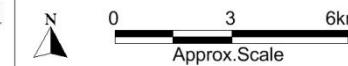
Title:

Mesh – Barrenjoey to Windsor

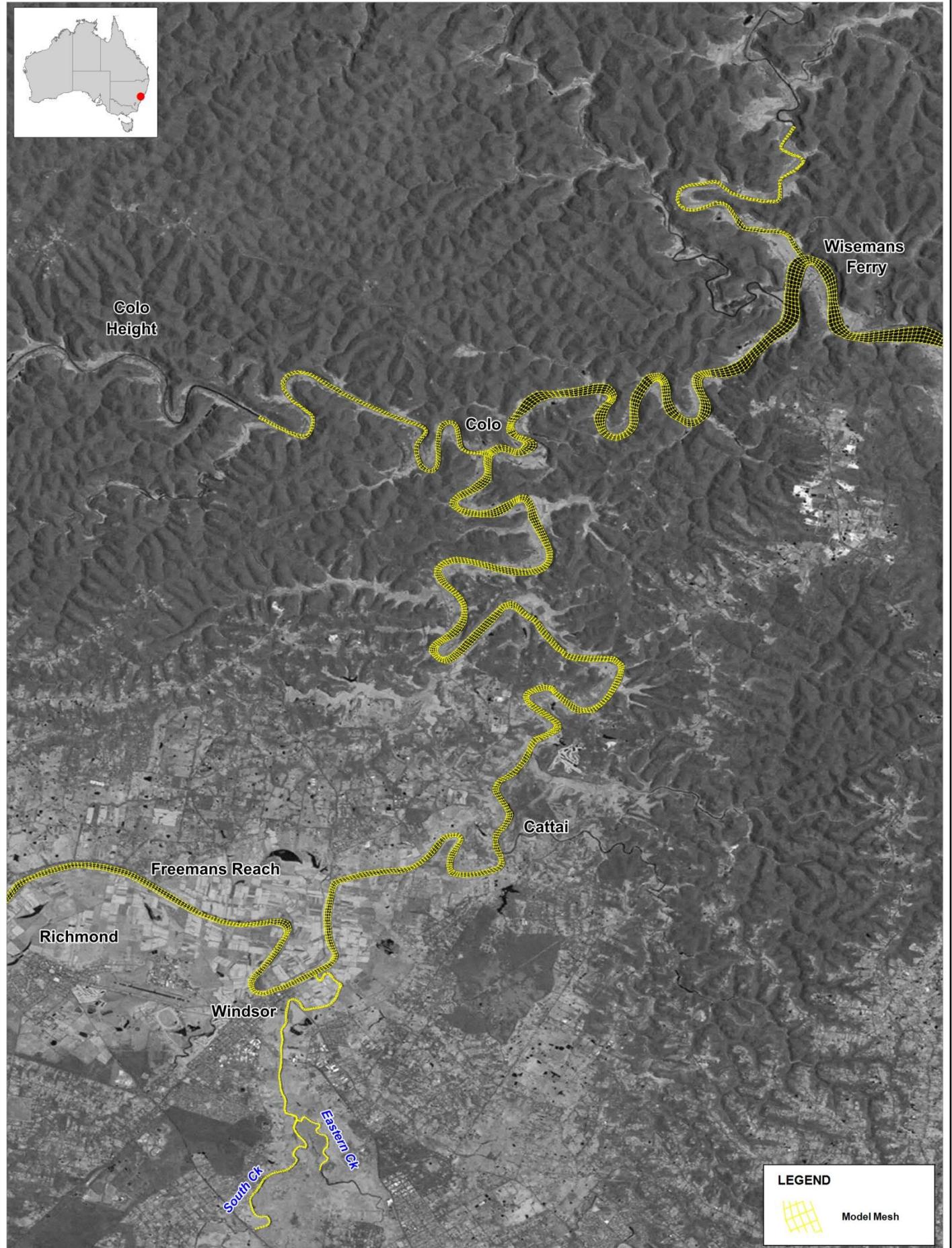
BMT WBM endeavours to ensure that the information provided in this map is correct at the time of publication. BMT WBM does not warrant, guarantee or make representations regarding the currency and accuracy of information contained in this map.

Figure:
12-3

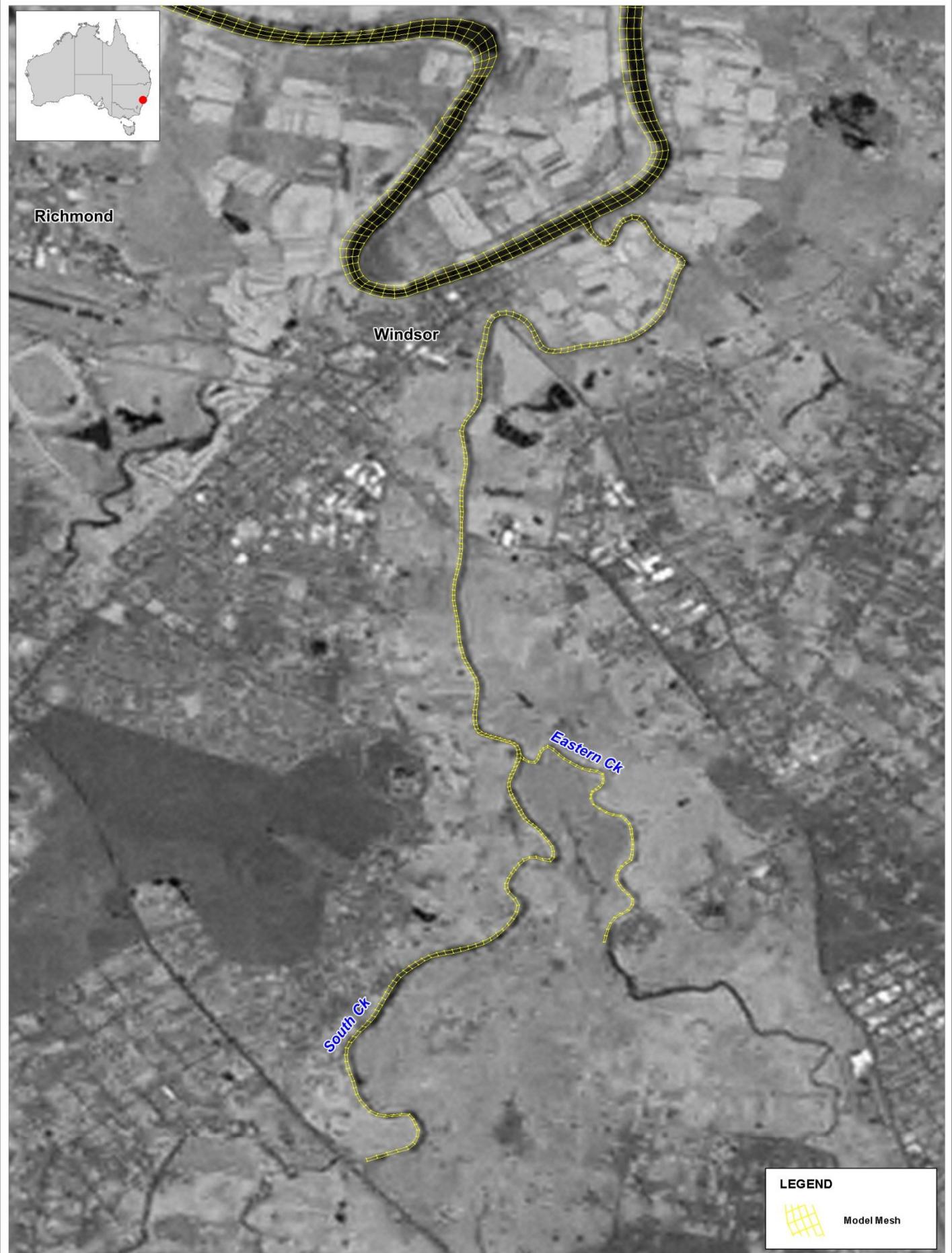
Rev:
A



Approx. Scale



Title:	Figure:	Rev:
Mesh – Wisemans Ferry to South Creek	12-4	A
BMT WBM endeavours to ensure that the information provided in this map is correct at the time of publication. BMT WBM does not warrant, guarantee or make representations regarding the currency and accuracy of information contained in this map.	  0 2 4km Approx. Scale	
Filepath: \\B18388_1_BRH_HawkesburyNepean\DRG\130509\WQU_013_130510 Mesh_Colo to South Creek.wor		



Title:
Mesh - South and Eastern Creeks

Figure:

12-5

Rev:

A

BMT WBM endeavours to ensure that the information provided in this map is correct at the time of publication. BMT WBM does not warrant, guarantee or make representations regarding the currency and accuracy of information contained in this map.



0 2 4km
Approx. Scale

BMT WBM
www.bmtwm.com.au



Title:
Mesh - South Creek to Wallacia

Figure:
12-6

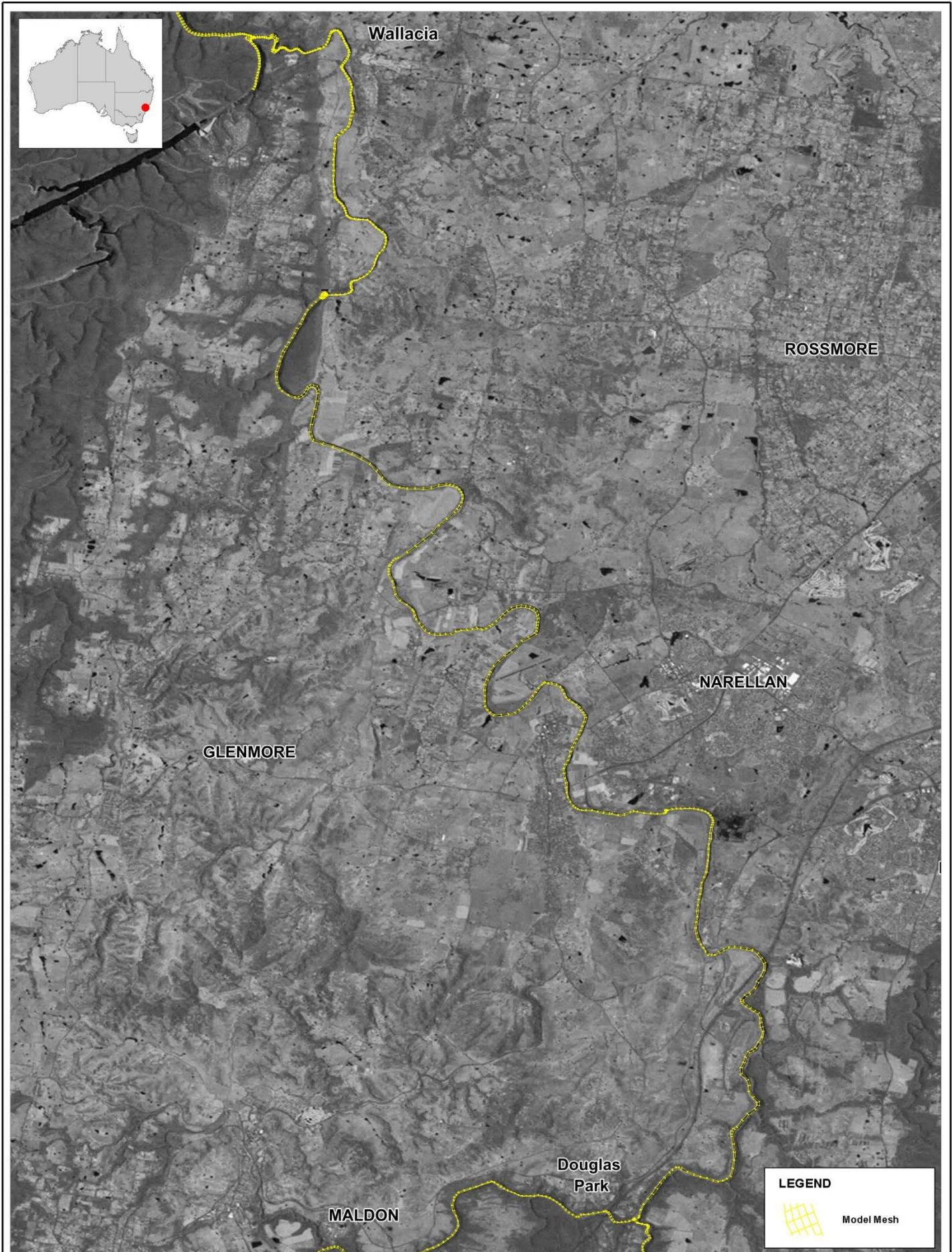
Rev:
A

BMT WBM endeavours to ensure that the information provided in this map is correct at the time of publication. BMT WBM does not warrant, guarantee or make representations regarding the currency and accuracy of information contained in this map.



0 2 4km
Approx. Scale

BMT WBM
www.bmtwbm.com.au



Title:
Mesh -Wallacia to Douglas Park

Figure:
12-7

Rev:
A

BMT WBM endeavours to ensure that the information provided in this map is correct at the time of publication. BMT WBM does not warrant, guarantee or make representations regarding the currency and accuracy of information contained in this map.



0 3 6km
Approx. Scale

BMT WBM
www.bmtwbm.com.au



Title:
Mesh -Bents Basin

Figure:
12-8

Rev:
A

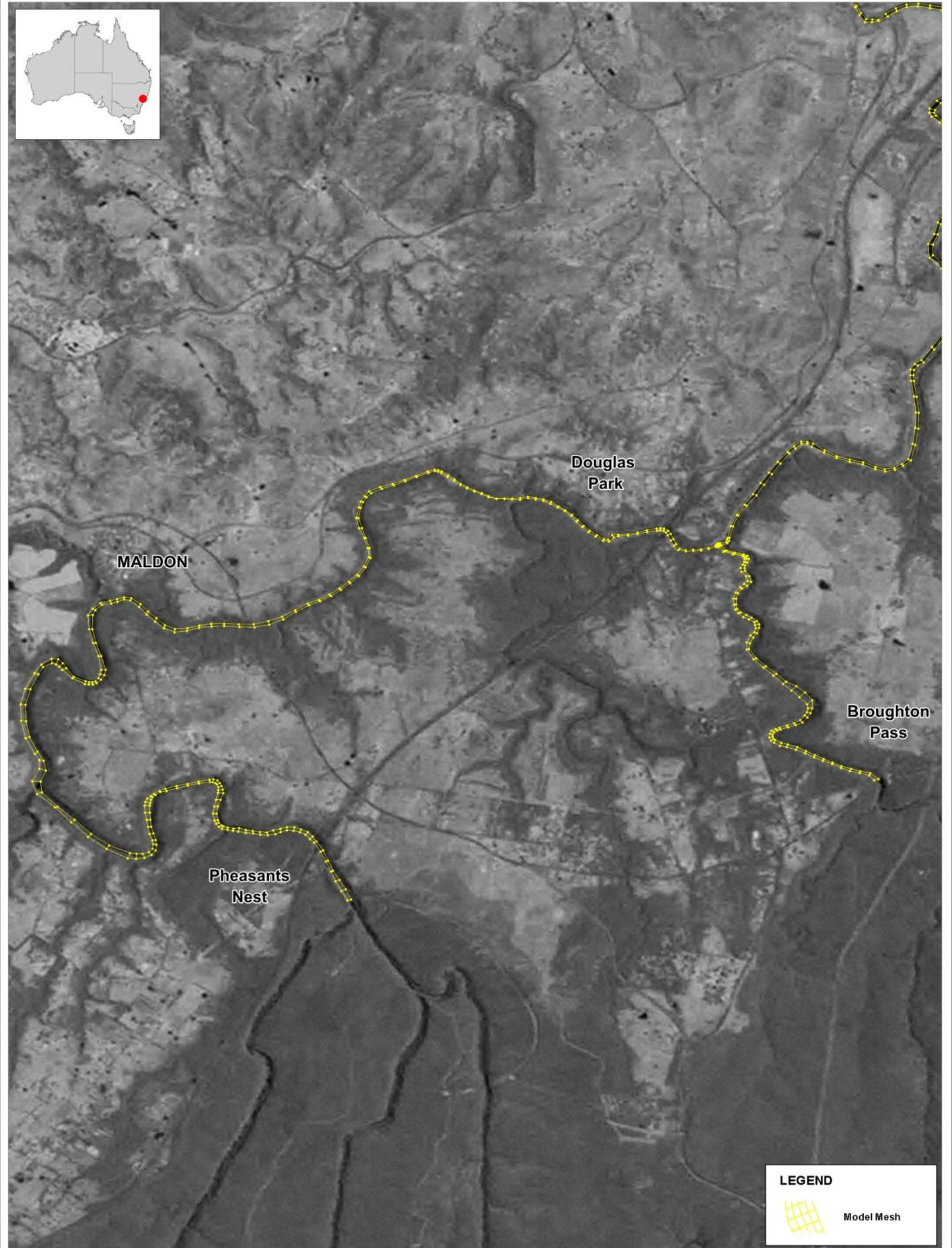
BMT WBM endeavours to ensure that the information provided in this map is correct at the time of publication. BMT WBM does not warrant, guarantee or make representations regarding the currency and accuracy of information contained in this map.



0 200 400m

Approx. Scale

 **BMT WBM**
www.bmtwbm.com.au

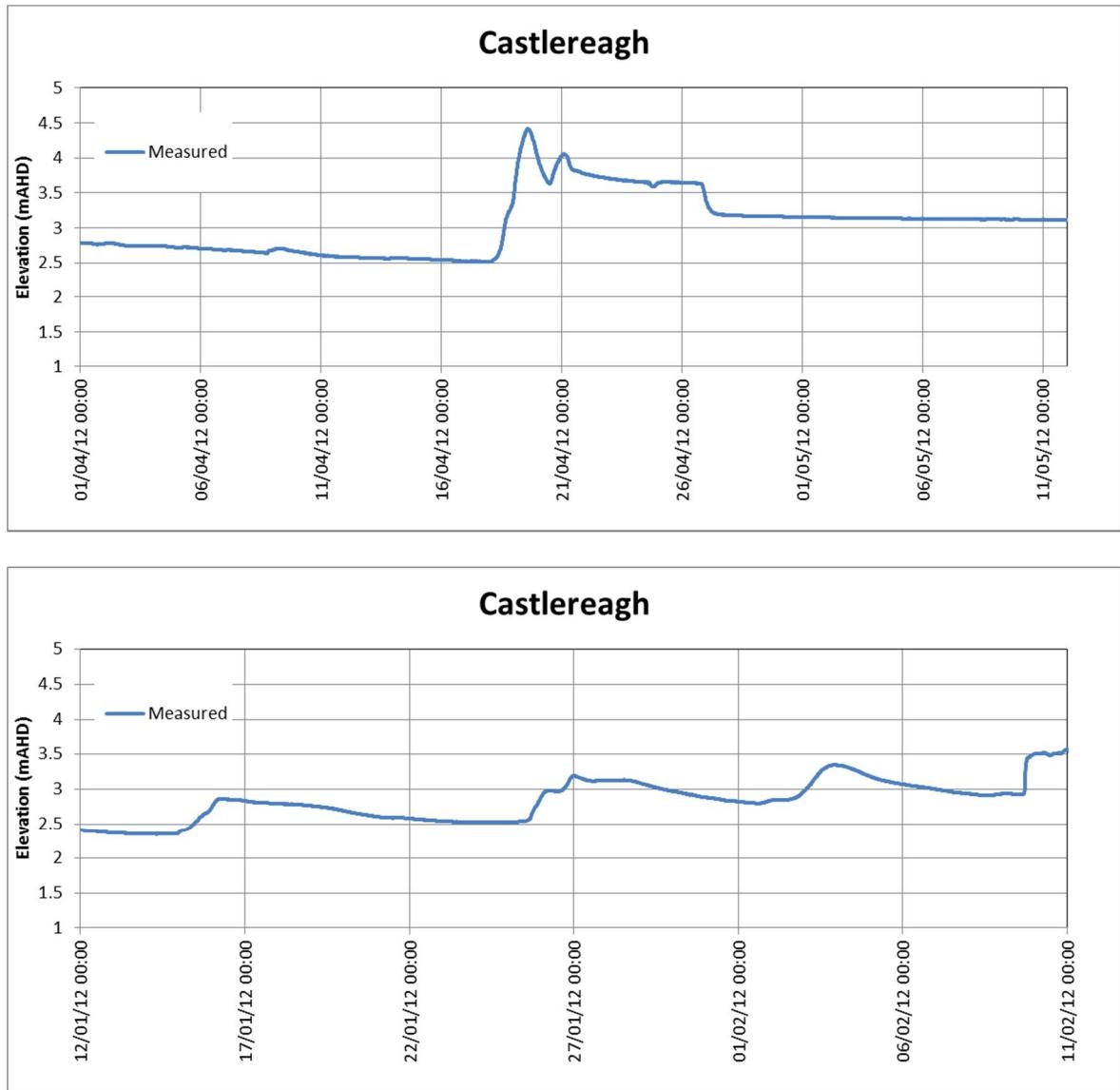


Title:	Figure:	
Mesh – Douglas Park to Pheasants Nest and Broughton Pass	12-9	Rev: A
BMT WBM endeavours to ensure that the information provided in this map is correct at the time of publication. BMT WBM does not warrant, guarantee or make representations regarding the currency and accuracy of information contained in this map.	 0 1 2km Approx. Scale	 www.bmtwbm.com.au
Filepath :I:\B18388_I_BRH_HawkesburyNepean\DRG\130509\WQU_018_130510\Mesh_Douglas Park to Pheasants Nest and Broughtons Pass.wor		

12.1.3. Model Bathymetry

Model bathymetry was set via an interrogation of the previously described DEM of the river network. This provided the most detailed representation of the actual bathymetry within the model solution. Notwithstanding this, some manual alterations of the interrogated DEM were necessary to address the following:

- The inspection of the DEM revealed that it did not necessarily capture the correct hydraulic properties of the river channels. For example, the different spatial resolution of the DEM and model mesh meant that in some locations artificial cross-channel benches (i.e. cells spanning the channel and with a shallower depth than those immediately upstream and downstream) were introduced into the TUFLOW model that were not present in the higher resolution DEM. These benches were removed manually;
- In some cases, the model bathymetry (whilst accurately interrogating the DEM at set locations) resulted in ‘blocky’ artificial bedforms, especially in regions of high tortuosity and rapidly changing bed depth. This blockiness resulted in the development of artificial (numerical) drag at these locations, and this drag acted as a sink for tidal energy and consequently slowed tidal flows and interfered with river thalweg phase shifts. These areas were manually smoothed to remove this numerical drag issue. One such location where this was applied was the river bend at Wisemans Ferry;
- For similar reasons as the above, model interrogation of the DEM was not always satisfactory through known riffle zones – the individual interrogation points in the model did not combine to properly capture riffle zone bed forms. In such cases, the highly detailed sounding data supplied by Sydney Water was used to manually reassign model bed heights in some riffle zones such that they were accurately reflected in the model bathymetry; and
- On examination of the water level records at Castlereagh, it was evident that a downstream hydraulic control was setting the gauged water level during low flow levels, and that this control height changes in time. Two snapshots of the Castlereagh gauge data are presented in **Figure 12-10** to illustrate this. In the upper panel, the hydraulic control clearly sets the water level at approximately 2.5m, and after a major flow event, the height changes to more than 3 metres. Similarly, the lower panel shows the control height changing from less than 2.5 m to almost 3 m, again in response to high flow events. The control height in the model over the calibration period was set to match the observed data.



■ **Figure 12-10 Example Gauge Data at Castlereagh**

12.1.4. Weirs

All weirs were included in the model:

- Penrith;
- Wallacia;
- Theresa Park;
- Brownlow Hill;
- Mt Hunter;

- Cobbity;
- Sharpes;
- Camden;
- Menangle;
- Douglas Park; and
- Maldon.

These weirs were included in the model post-upgrade state as part of the hydrodynamic calibration process. The weirs were upgraded in 2009/10 to allow environmental flow releases from the Upper Nepean Dams to pass. Weir heights and ratings data were provided by the Sydney Catchment Authority. It is noted that this approach to weir parameterisation is different to that adopted in the water quality model setup (see subsequent sections) which was over the corresponding 2006-2007 calibration period. Pre-upgrade weirs were used in the water quality model calibration, as this is consistent with the state of the weirs over the 2006-2007 model calibration period.

An attempt was made to include environmental flows in the weir models for those weirs fitted with this flow capability over the 2011 hydrodynamic model calibration period. However data was found to be unsuitable for inclusion in the model over the 2011 CMP period and was excluded from the modelling. This has no impact on the tidal calibration (which is the sole focus of this hydrodynamic calibration task over the CMP period) as these environmental flows are far removed from the tidal section and the environmental flow magnitudes are orders of magnitude smaller than typical tidal flows. Environmental flows were also excluded from the 2006 2007 water quality calibration as these flows were not in operation at that time. All environmental flows associated with weirs and dams will be included (and be alterable) in the pending execution of scenarios as the modelling framework has been specifically designed to account for this inclusion.

12.1.5. Turbulence Schemes

The horizontal mixing model used was a Smagorinsky formulation with a Smagorinsky coefficient of 0.2 and a length scale related to the local mesh size. Details on this scheme can be found in **Appendix J**.

The vertical mixing model used was a $k-\omega$ formulation provided as part of the General Ocean Turbulence Model (GOTM; <http://www.gotm.net/index.php>) package, which is a package used by several 3D hydrodynamic modelling systems to provide a variety of vertical mixing schemes. The $k-\omega$ scheme is a second-order formulation which utilises the Boussinesq approximation to reduce computational overhead, and therefore provides an accurate simulation while keeping runtimes to a minimum. The default parameter values provided by GOTM were applied and full details of the scheme are provided in Umlauf & Burchard (2003).

12.1.6. Bed Materials

The TUFLOW model used a quadratic drag law at the bed interface, which assumed a logarithmic drag profile over the bottom cell (**Appendix J**). This algorithm uses a bottom roughness length scale to vary the drag applied for a given bed morphology, which is derived from Manning's n values supplied by the user. As there are a large range of sediment types or bed morphologies throughout the model domain, a spatially varying bottom roughness was applied, which involved assigning areas of similar morphology a single roughness value. These regions are presented in **Figure 12-12**, with a series of zoomed figures showing these areas in more detail (**Figure 12-13** to **Figure 12-18**). Manning's n values are presented in model material number / Manning's n values pairs in **Table 12-1**. Shaded entries correspond to material numbers as specified in the model, and the adjacent entry to each is the specified Manning's roughness.

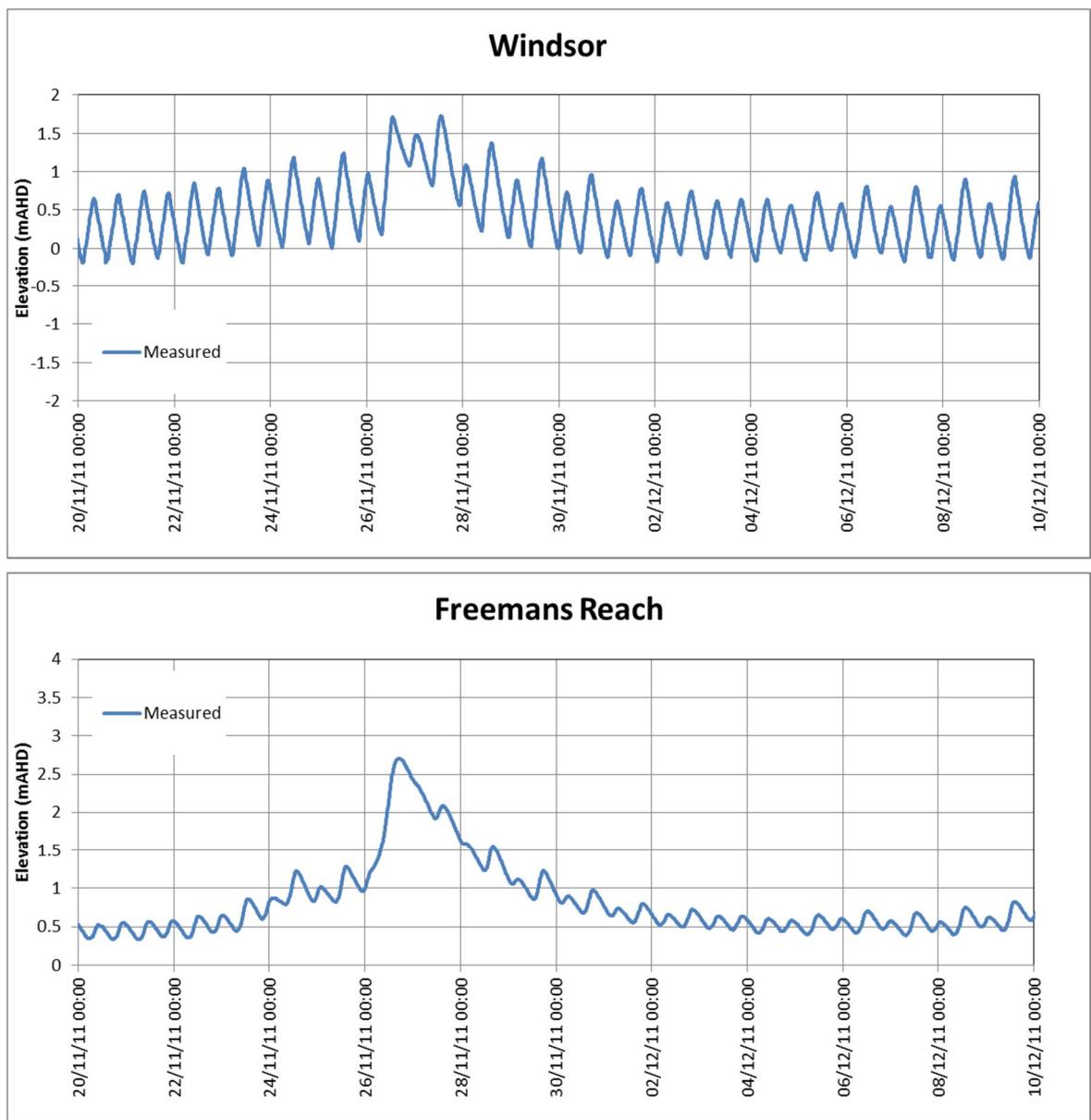
▪ **Table 12-1 Bottom Roughness Assignments**

1	0.016	7	0.028	13	0.016	19	0.016	25	0.030	31	0.035	37	0.035
2	0.017	8	0.028	14	0.016	20	0.016	26	0.035	32	0.035	38	0.035
3	0.020	9	0.03	15	0.016	21	0.025	27	0.035	33	0.035	39	0.035
4	0.020	10	0.07	16	0.016	22	0.025	28	0.035	34	0.035	40	0.030
5	0.021	11	0.07	17	0.016	23	0.025	29	0.035	35	0.035	101	0.025
6	0.030	12	0.024	18	0.016	24	0.035	30	0.035	36	0.035	102	0.025

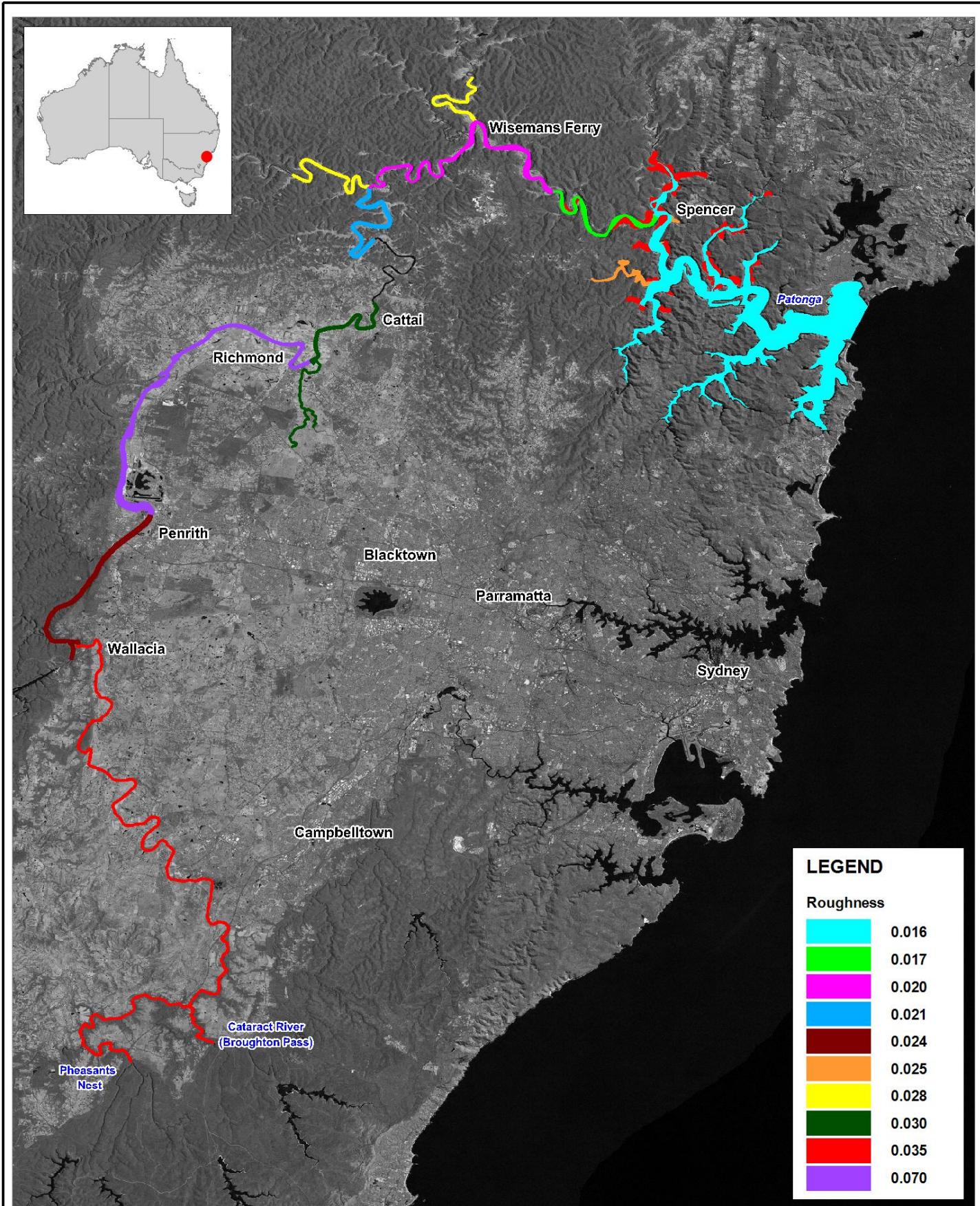
It was necessary to set roughness to relatively high values in the reaches where significant macrophyte growth is known to occur. One example is the region along the Hawkesbury-Nepean River from the South Creek confluence to Penrith Weir. In this region, significant tidal damping was evident from examination of the measured water levels, as presented in **Figure 12-11**. The ordinate has been set to the same range on both plots to facilitate visual comparison.

The tidal stations are separated by a river reach distance of only 7 kilometres, however a typical tidal range of 0.7 m at Windsor is almost entirely suppressed by the time it reaches Freemans Reach, where the corresponding tidal ranges are 0.08 m. This is equivalent to a rate of tidal dampening between the two sites of approximately 8.5 cm/km. To provide context for this dramatic attenuation in tidal signal, the corresponding rate of tidal dampening between Colo and Windsor is 1.2 cm/km, some 7 to 8 times less than the rate of dampening between Windsor and Freemans Reach.

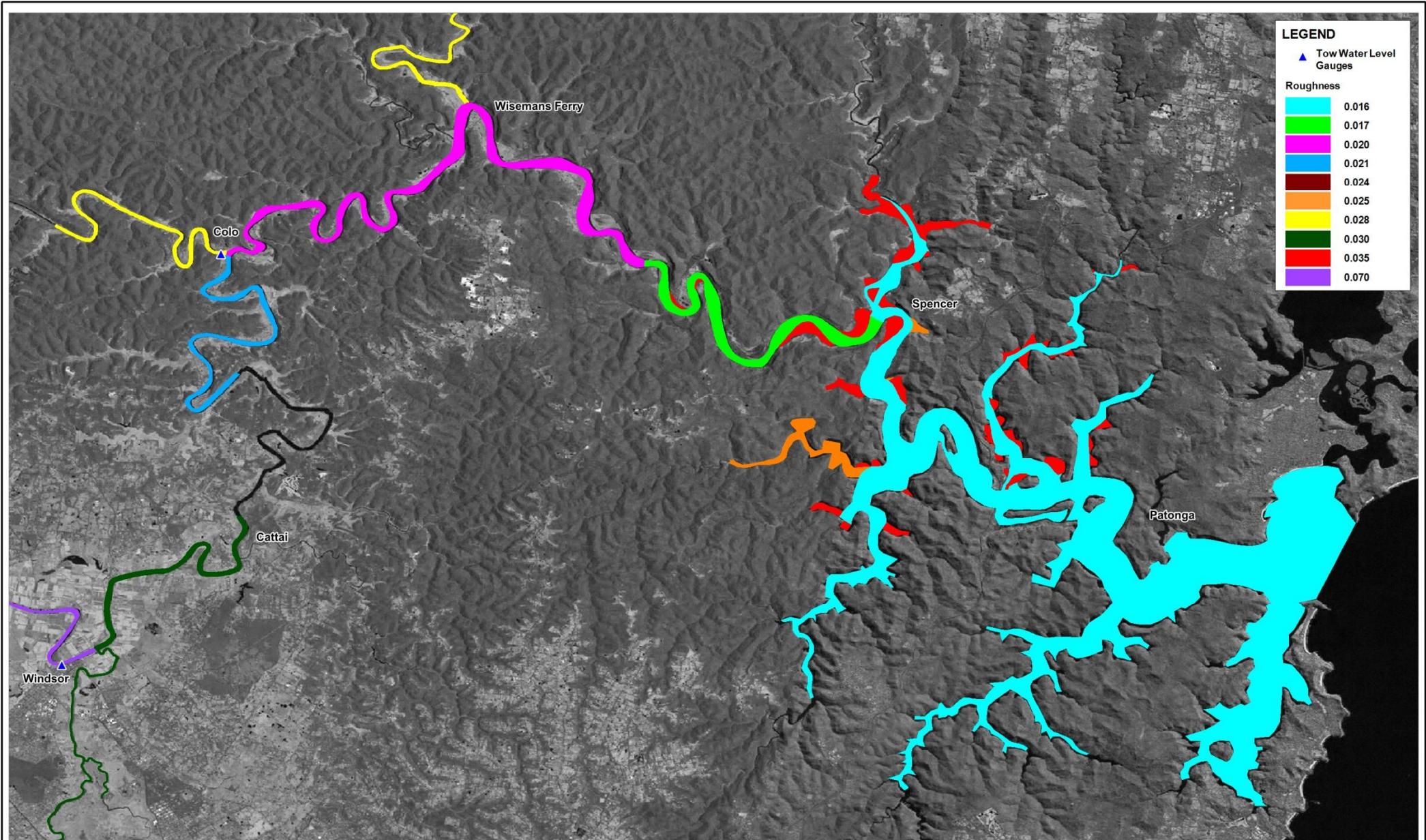
Given that the bathymetry was of a high standard and did not warrant alteration, it was determined that the most appropriate way in which to capture this pronounced tidal dampening was through inclusion of large roughness coefficients in the region. The unusual nature of this particular river reach required this approach to be taken – it is acknowledged that these roughness values would not be appropriate in typical river reach sections where macrophyte growth is absent.



■ **Figure 12-11 Tidal Dampening Between Windsor and Freemans Reach**



BMT WBM endeavours to ensure that the information provided in this map is correct at the time of publication. BMT WBM does not warrant, guarantee or make representations regarding the currency and accuracy of information contained in this map.	 BMT WBM www.bmtwbm.com.au
Filepath : I:\B18388_I_BRH_HawkesburyNepean\DRG\130509\WQU_019_130510_Bottom Roughness Regions.wor	



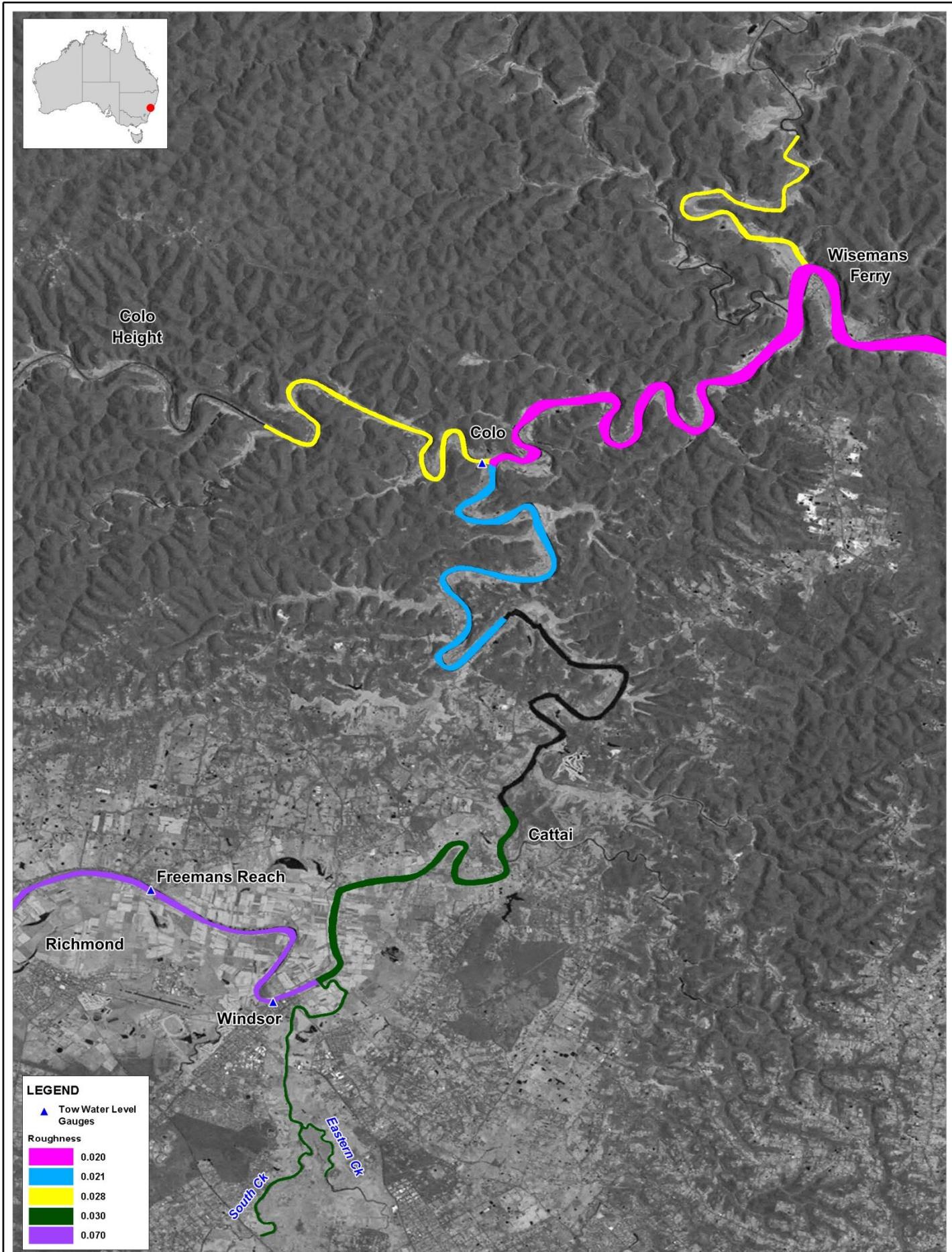
Title:
Bottom Roughness – Barrenjoey to Windsor

BMT WBM endeavours to ensure that the information provided in this map is correct at the time of publication. BMT WBM does not warrant, guarantee or make representations regarding the currency and accuracy of information contained in this map.

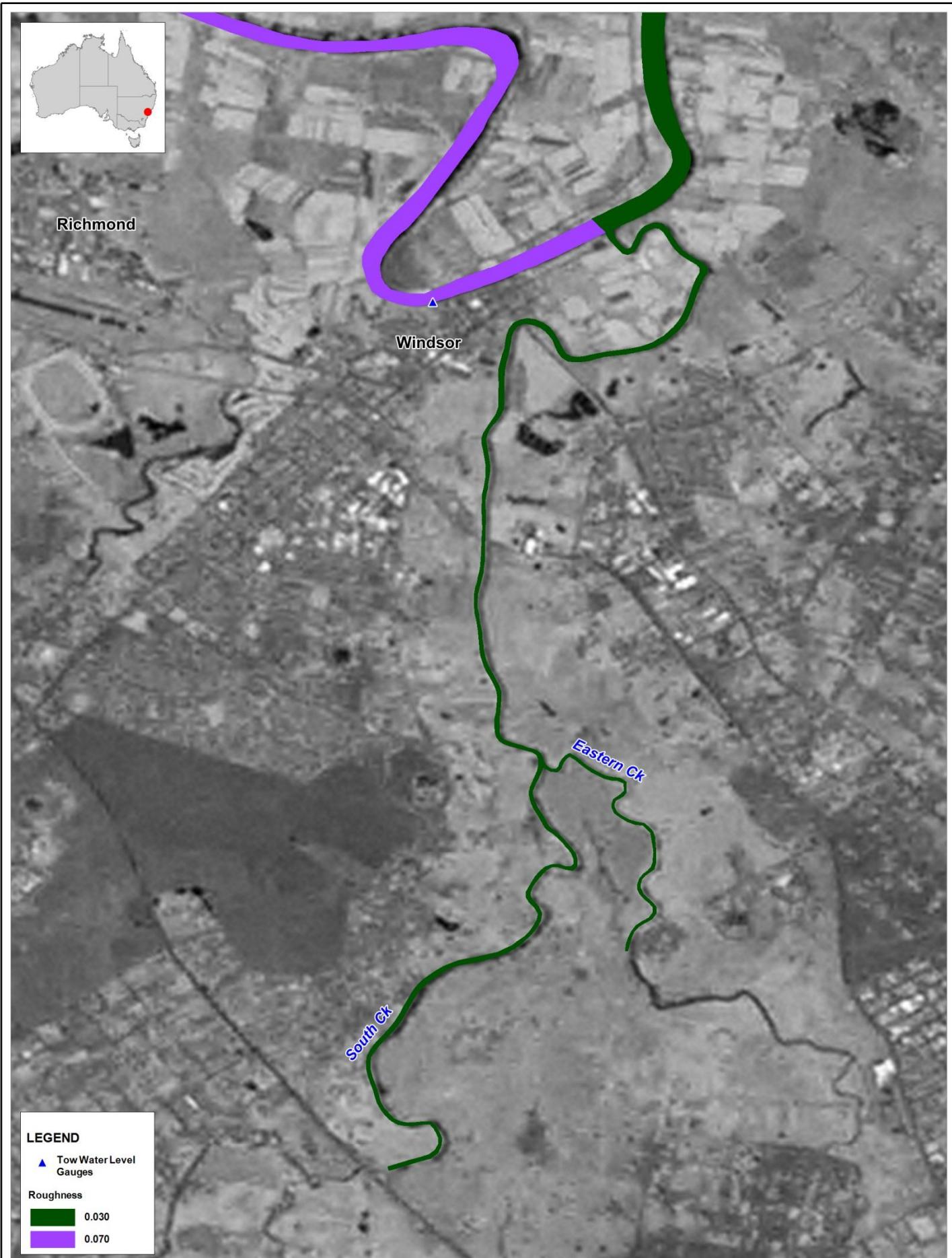
Filepath : I:\B18388_I_BRH_HawkesburyNepean\DRG\130509\WQU_020_130510_Roughness_Barrenjoey to Colo.wor



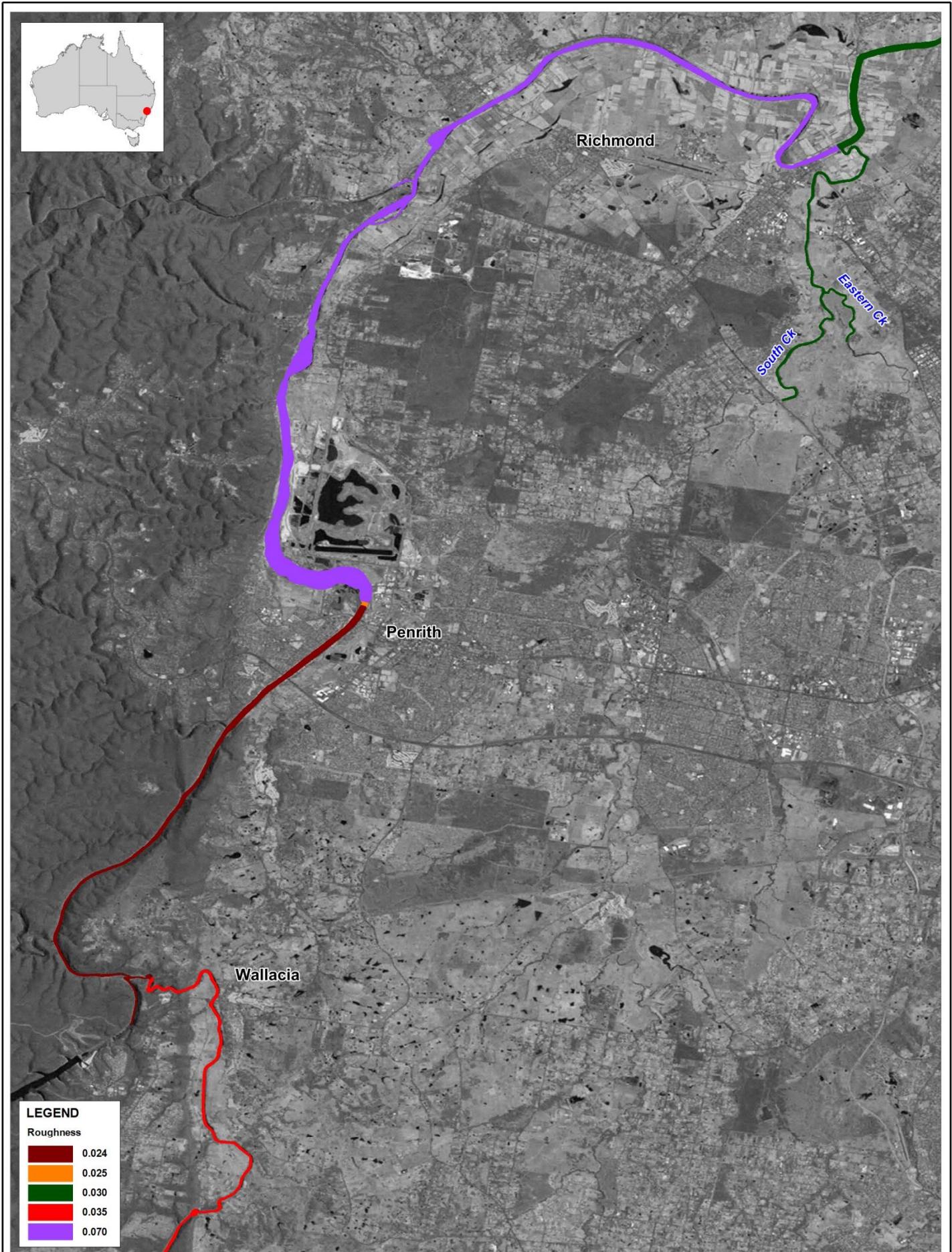
Figure: **12-13** Rev: **A**



Title: Bottom Roughness – Wisemans Ferry to South Creek	Figure: 12-14	Rev: A
BMT WBM endeavours to ensure that the information provided in this map is correct at the time of publication. BMT WBM does not warrant, guarantee or make representations regarding the currency and accuracy of information contained in this map.	N	0 2 4km Approx. Scale
<small>Filepath :I:\B18388_I_BRH_HawkesburyNepean\DRG130509\WQU_021_130510 Roughness_Colo to South Creek.wor</small>		



Title: Bottom Roughness- South and Eastern Creeks		Figure: 12-15	Rev: A
BMT WBM endeavours to ensure that the information provided in this map is correct at the time of publication. BMT WBM does not warrant, guarantee or make representations regarding the currency and accuracy of information contained in this map.	N 	0 2 4km Approx. Scale	 BMT WBM www.bmtwbm.com.au



Title:

Bottom Roughness - South Creek to Wallacia

Figure:

12-16

Rev:

A

BMT WBM endeavours to ensure that the information provided in this map is correct at the time of publication. BMT WBM does not warrant, guarantee or make representations regarding the currency and accuracy of information contained in this map.



0 2 4km
Approx. Scale



Title:
Bottom Roughness - Wallacia to Douglas Park

Figure:
12-17

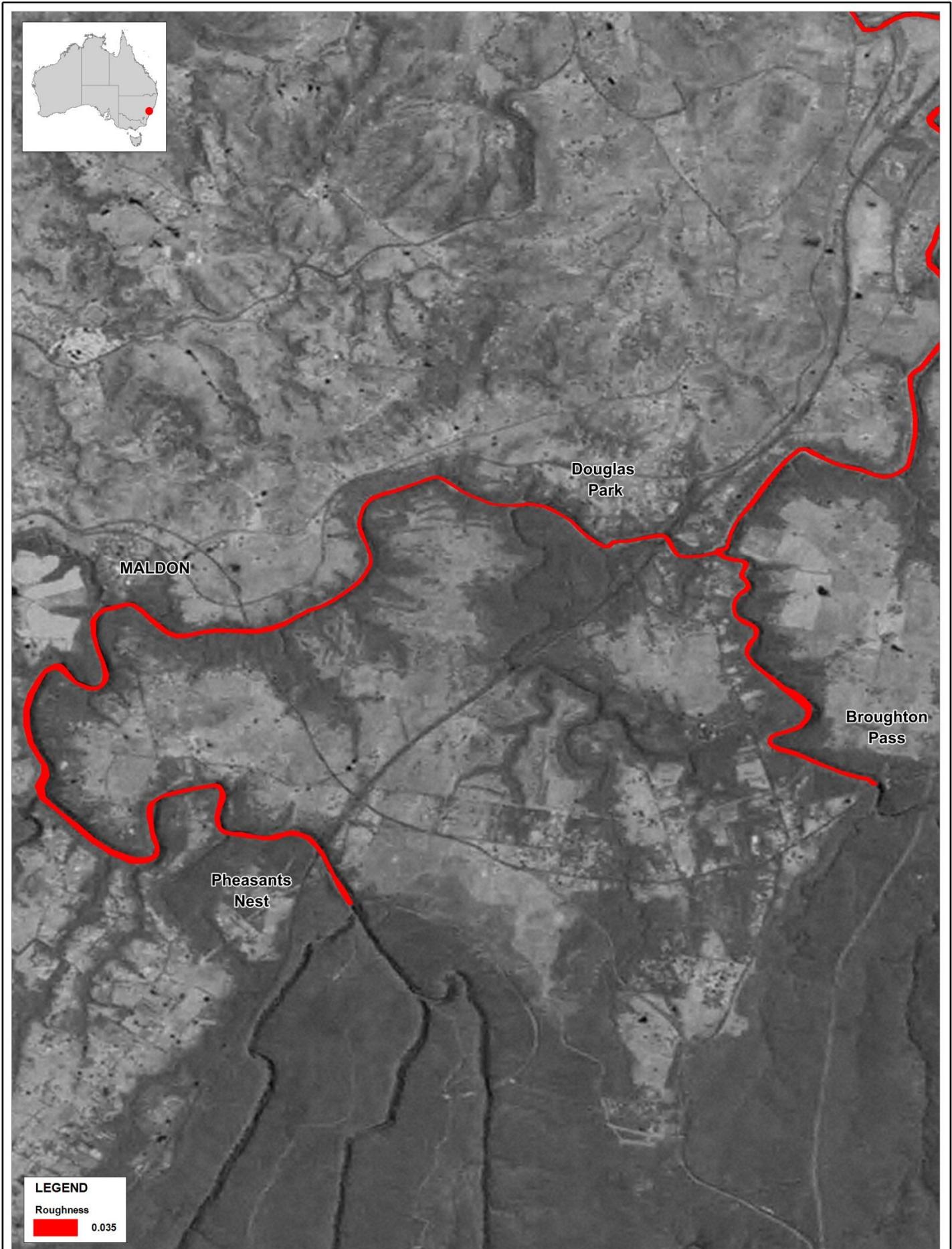
Rev:
A

BMT WBM endeavours to ensure that the information provided in this map is correct at the time of publication. BMT WBM does not warrant, guarantee or make representations regarding the currency and accuracy of information contained in this map.



0 3 6km
Approx. Scale

 **BMT WBM**
www.bmtwbm.com.au



Title:	Bottom Roughness – Douglas Park to Pheasants Next and Broughton Pass	Figure:	12-18	Rev:
			A	
BMT WBM endeavours to ensure that the information provided in this map is correct at the time of publication. BMT WBM does not warrant, guarantee or make representations regarding the currency and accuracy of information contained in this map.		N	0 1 2km	Approx. Scale
Filepath: \\B18388_J_BRH_HawkesburyNepean\\DRG\\130509\\WQU_025_130510 Roughness_Douglas Park to Pheasants Nest and Broughtons Pass.wor				BMT WBM www.bmtwbm.com.au

12.1.7. Boundary Conditions

12.1.7.1. Open Boundaries

The open ocean boundary was set as follows:

- Tidal elevation: Synthesised tides from constituents at Patonga.
- Temperature: Synoptic variation synthesised from the CARS2009 database (<http://www.marine.csiro.au/~dunn/cars2009/>) at the point nearest the boundary CSIRO (2011).
- Salinity: Assumed constant equals to 37.5, based on observations at sampling site HSC108.
- Suspended solids: Assumed constant equals to 8.0 mg/L.

The salinity on the open ocean boundary was set to 37.5 throughout 2006 and 2007. This is slightly higher than would normally be expected. This decision was based around analysis of salinity observations made in the Hornsby Shire Council area of the estuary, which is the data set closest to the open boundary. Those data show that ambient salinities were quite high throughout.

Because this salinity is slightly higher than would be expected, a series of model run sensitivity tests were executed to examine the impact that altering the open ocean boundary salinity has on estuarine salt transport. Three runs were selected that had salinities set to 35, 37.5 and 40 (it is noted that the latter is too high, it was selected just for testing purposes). The results are presented in **Figure 12-19** and **Figure 12-20** for a salinity of 35, **Figure 12-21** and **Figure 12-22** for a salinity of 37.5, and **Figure 12-23** (2007 only) for a salinity of 40.

The results show that there is a roughly linear response in the estuary (at HSC sites) with the boundary condition changes. When the boundary is set to 35, the internal model predictions in the HSC area are too low. When the boundary is set to 40, the same predictions are too high. The upper estuarine sites are less influenced, although the boundary condition signal is still observable, with the salt limit being slightly further downstream in the case of the 35 salinity boundary.

Given the above, following this sensitivity analysis and considering the HSC data, 37.5 was selected for the boundary. Without this, the model would appear spurious throughout the lower estuary (i.e. Pittwater/Berowra area). It is noteworthy that this analysis shows that it is not possible to reproduce the (high) HSC salinity measurements with a boundary set at lower salinities: the HSC measurements and boundary condition assignments are closely linked (as expected). Importantly, there is no (significant) mechanism in the model to generate (increase) salinity other than advection in through the boundary. Whilst the model does include evaporative salinity increases, this will contribute negligible salinity increases in the deepwater and well flushed HSC regions.

Finally, if the salinity is set to 35 at the open boundary for the scenario simulations, it is expected that the slightly altered position of the salt limit will have little effect on the transport and/or transformation of other simulated water quality constituents in this region – the details of the salt wedge propagation will have only a small influence on local mixing processes, especially in comparison to the influence of tidal advection. It is also expected that the slight change in salt limit SINCLAIR KNIGHT MERZ

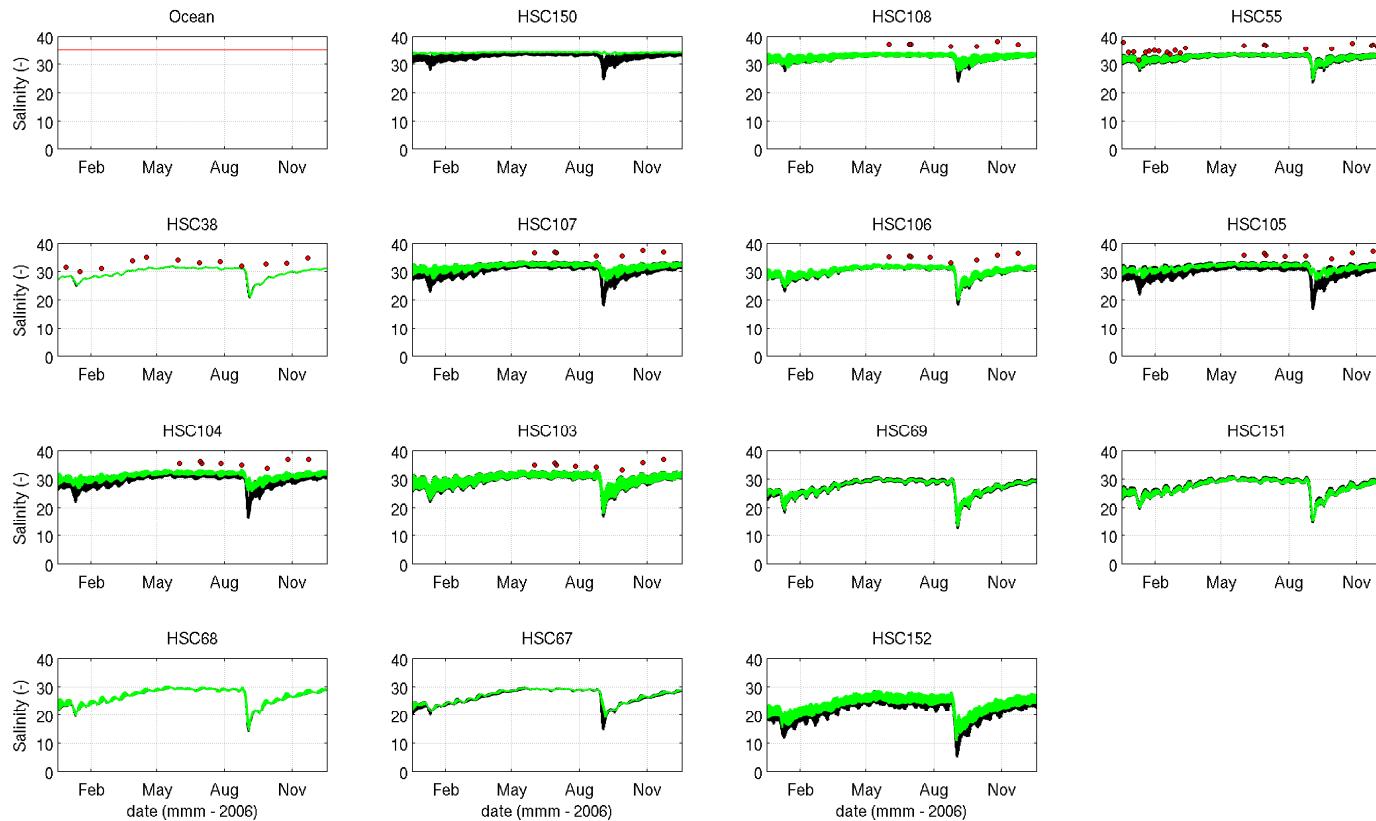


Water Quality Modelling of the Hawkesbury-Nepean River System

position shown above will have negligible influence over scenario outcomes at the temporal (10 year) scale of the scenarios, for these reasons. Further, the key water quality processes examined in this study occur in fresh waters (i.e. from Wisemans Ferry upstream) and as such are not at all influenced by salinity dynamics.



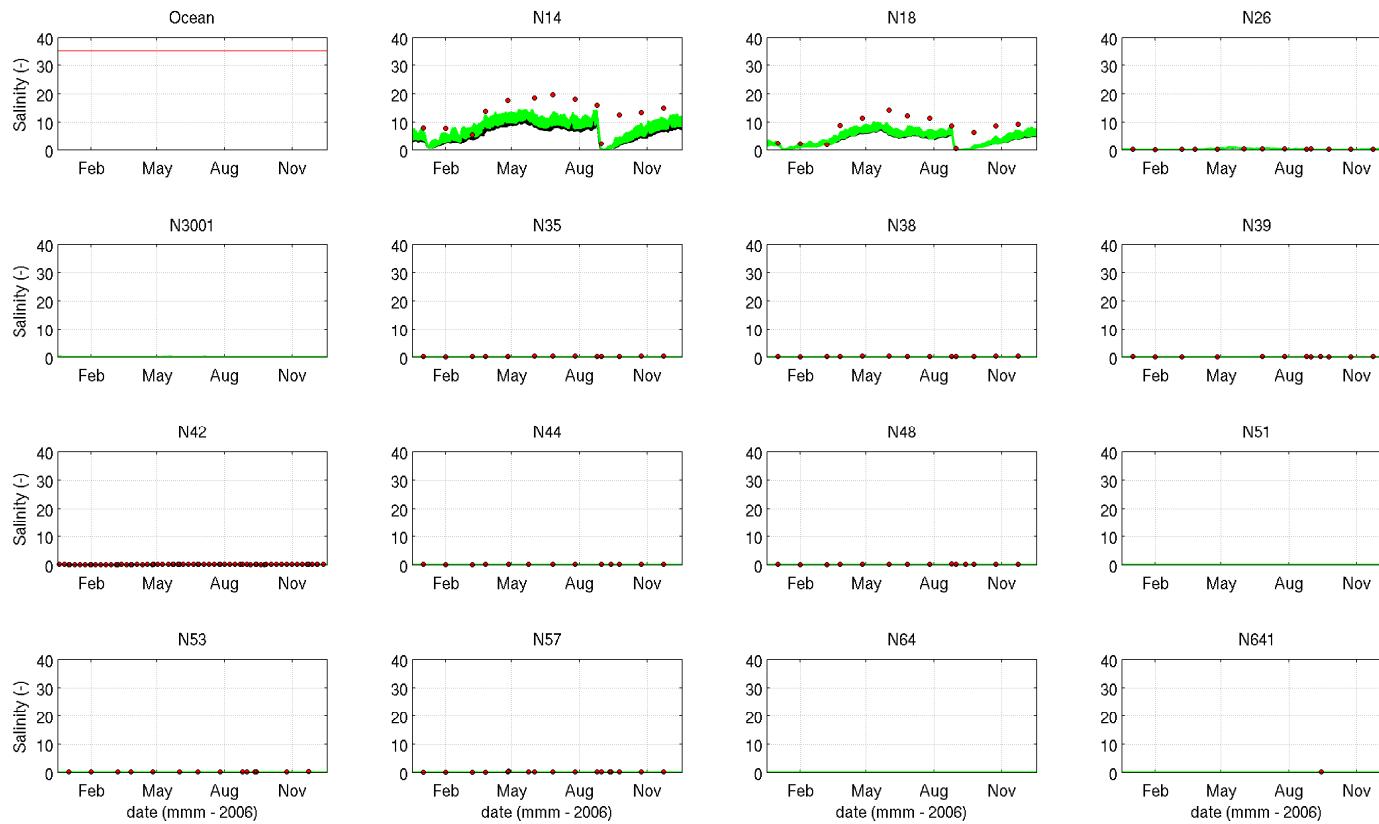
Water Quality Modelling of the Hawkesbury-Nepean River System



- **Figure 12-19 Salinity Boundary Condition set at 35 (2006) (measured data (red), modelled surface (black) and modelled bottom (green))**



Water Quality Modelling of the Hawkesbury-Nepean River System

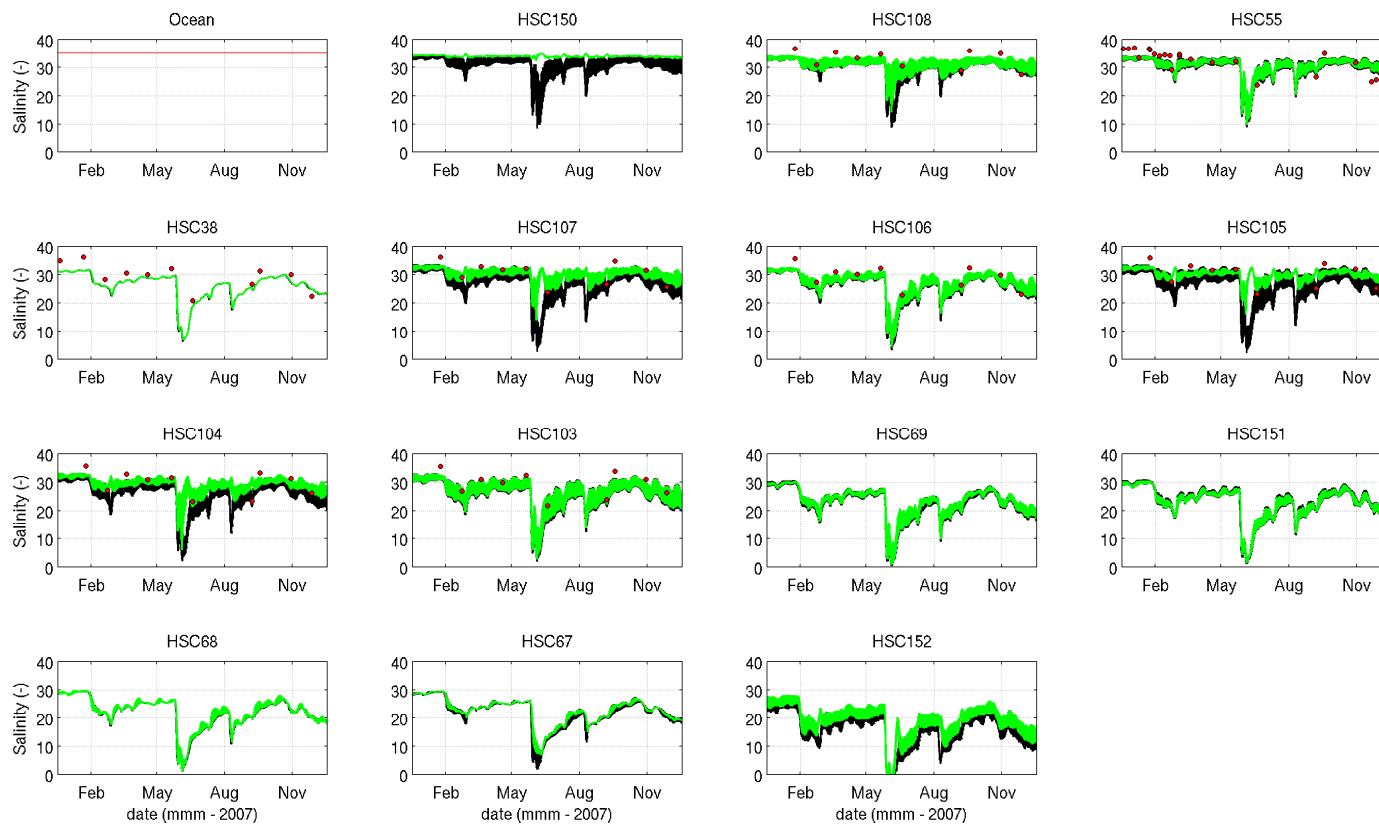


- **Figure 12-19 (Cont.) Salinity Boundary Condition set at 35 (2006) (measured data (red), modelled surface (black) and modelled bottom (green))**

SINCLAIR KNIGHT MERZ



Water Quality Modelling of the Hawkesbury-Nepean River System

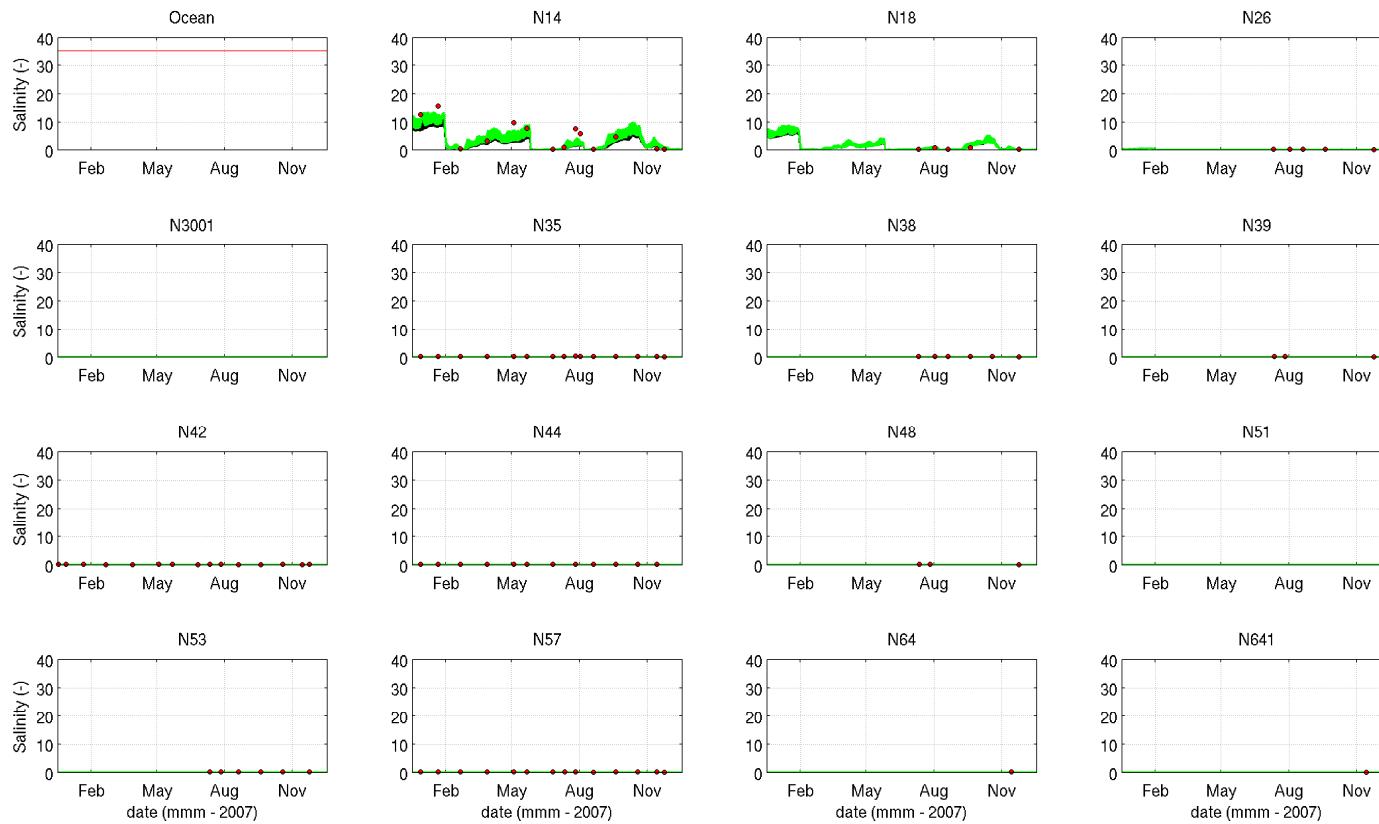


- **Figure 12-20 Salinity Boundary Condition set at 35 (2007) (measured data (red), modelled surface (black) and modelled bottom (green))**

SINCLAIR KNIGHT MERZ

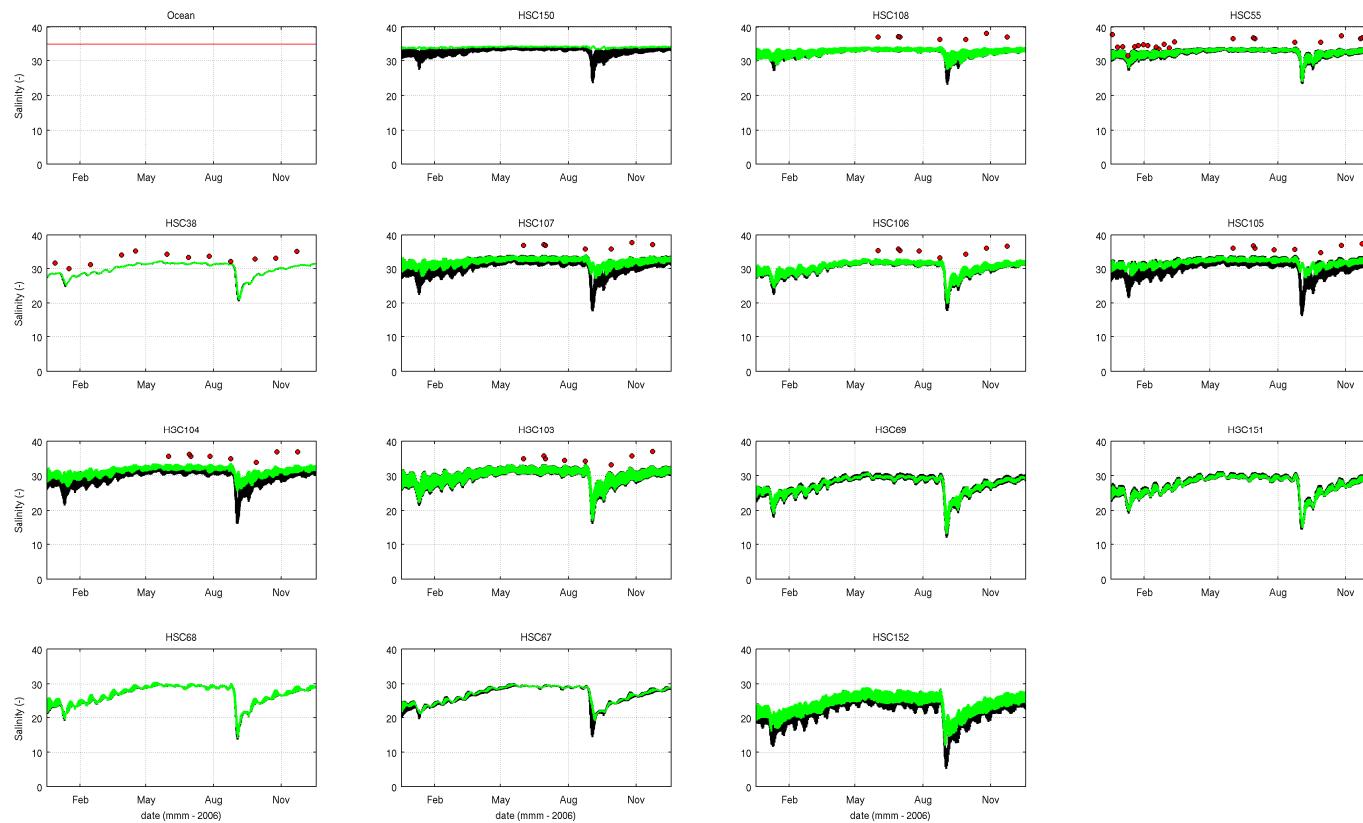


Water Quality Modelling of the Hawkesbury-Nepean River System



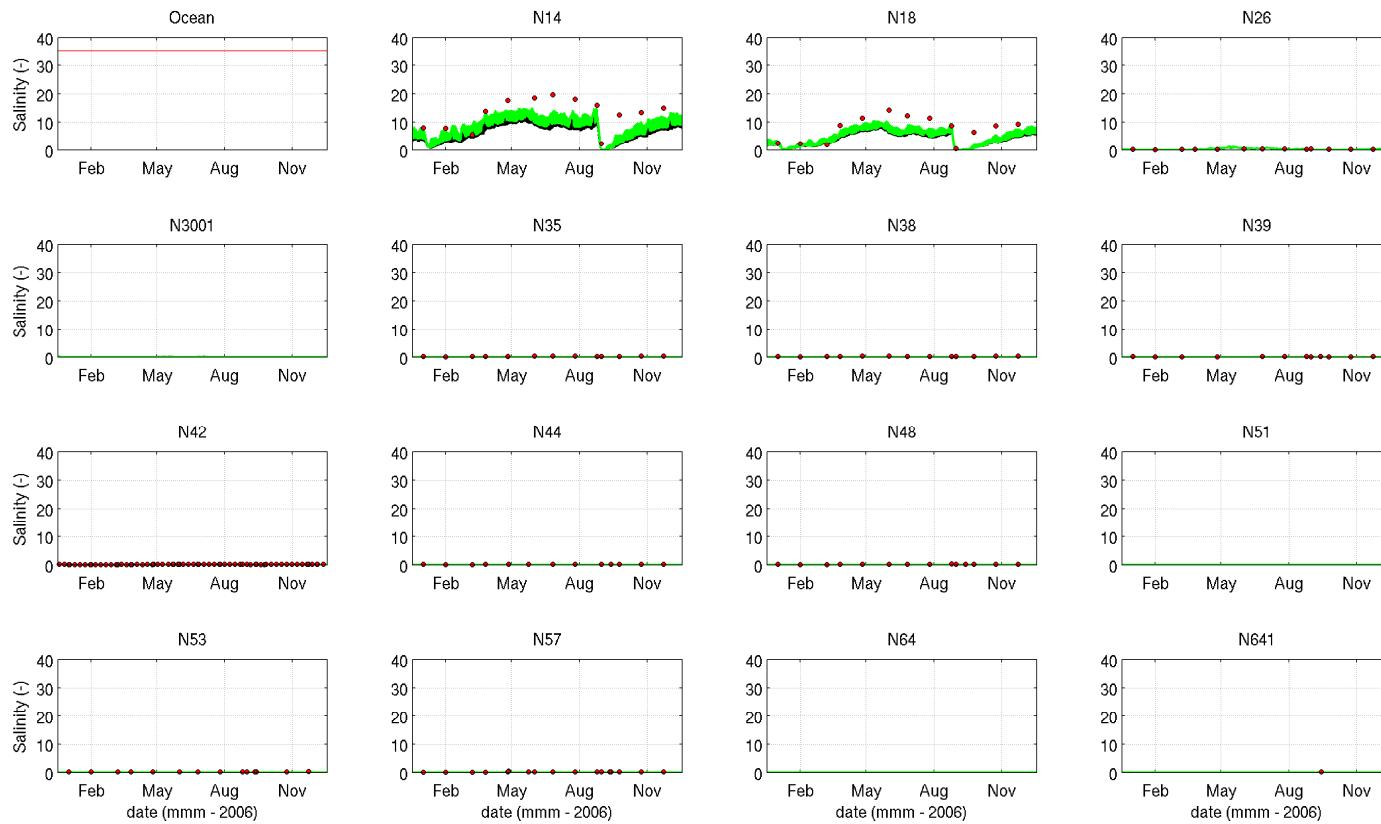
- **Figure 12-20 (Cont.) Salinity Boundary Condition set at 35 (2007) (measured data (red), modelled surface (black) and modelled bottom (green))**

SINCLAIR KNIGHT MERZ



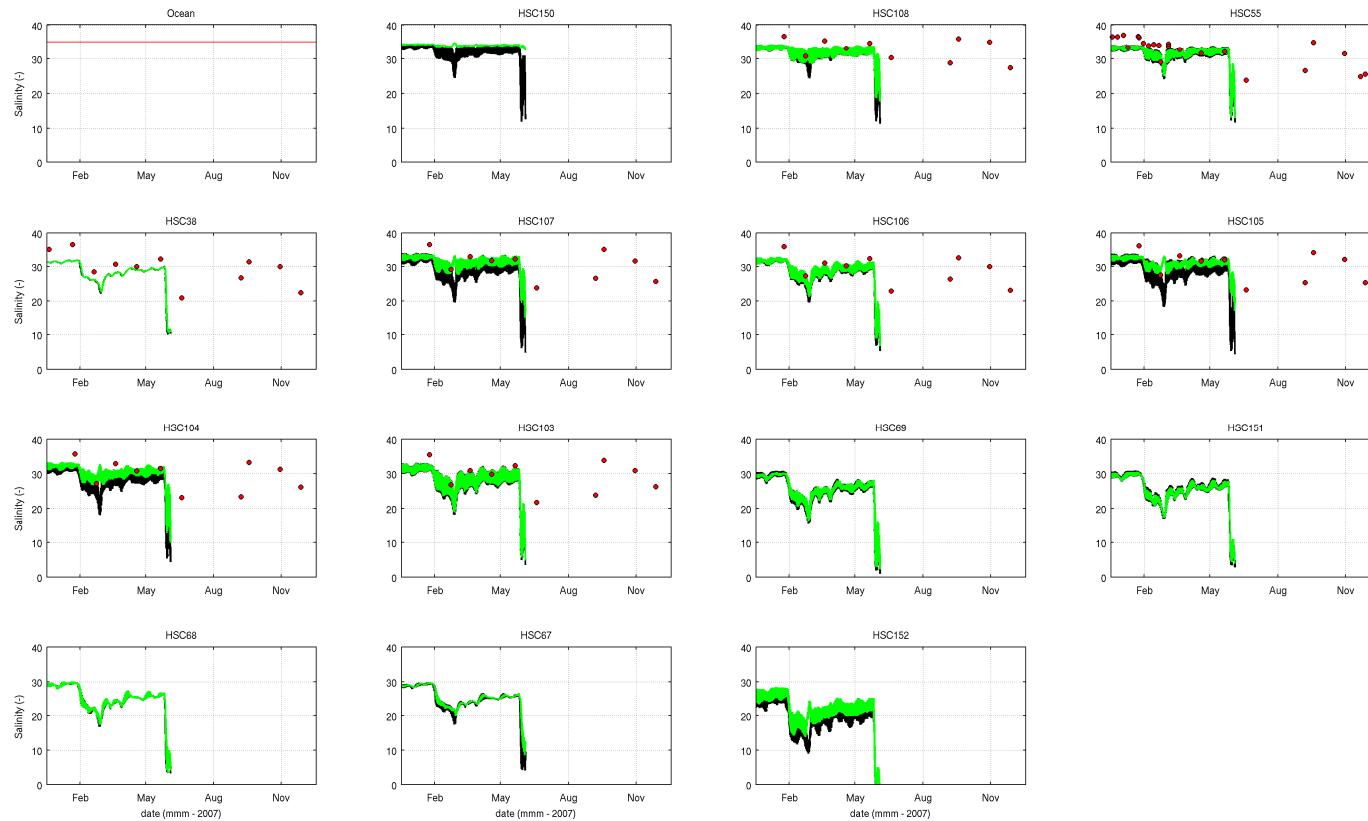
- **Figure 12-21 Salinity Boundary Condition set at 37.5 (2006) (measured data (red), modelled surface (black) and modelled bottom (green))**

SINCLAIR KNIGHT MERZ



- **Figure 12-21 (Cont.) Salinity Boundary Condition set at 37.5 (2006) (measured data (red), modelled surface (black) and modelled bottom (green))**

SINCLAIR KNIGHT MERZ

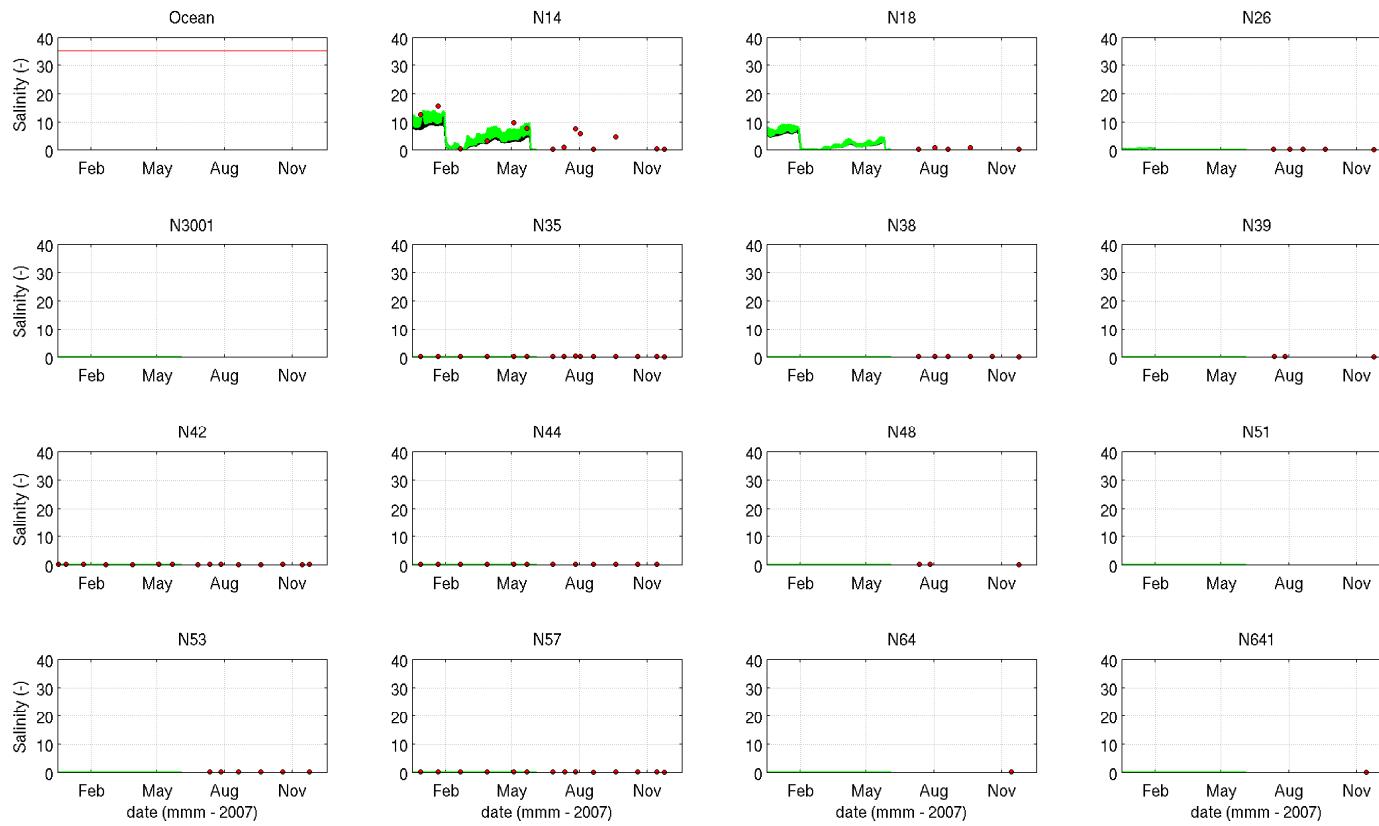


- **Figure 12-22 Salinity Boundary Condition set at 37.5 (2007) (measured data (red), modelled surface (black) and modelled bottom (green))**

SINCLAIR KNIGHT MERZ

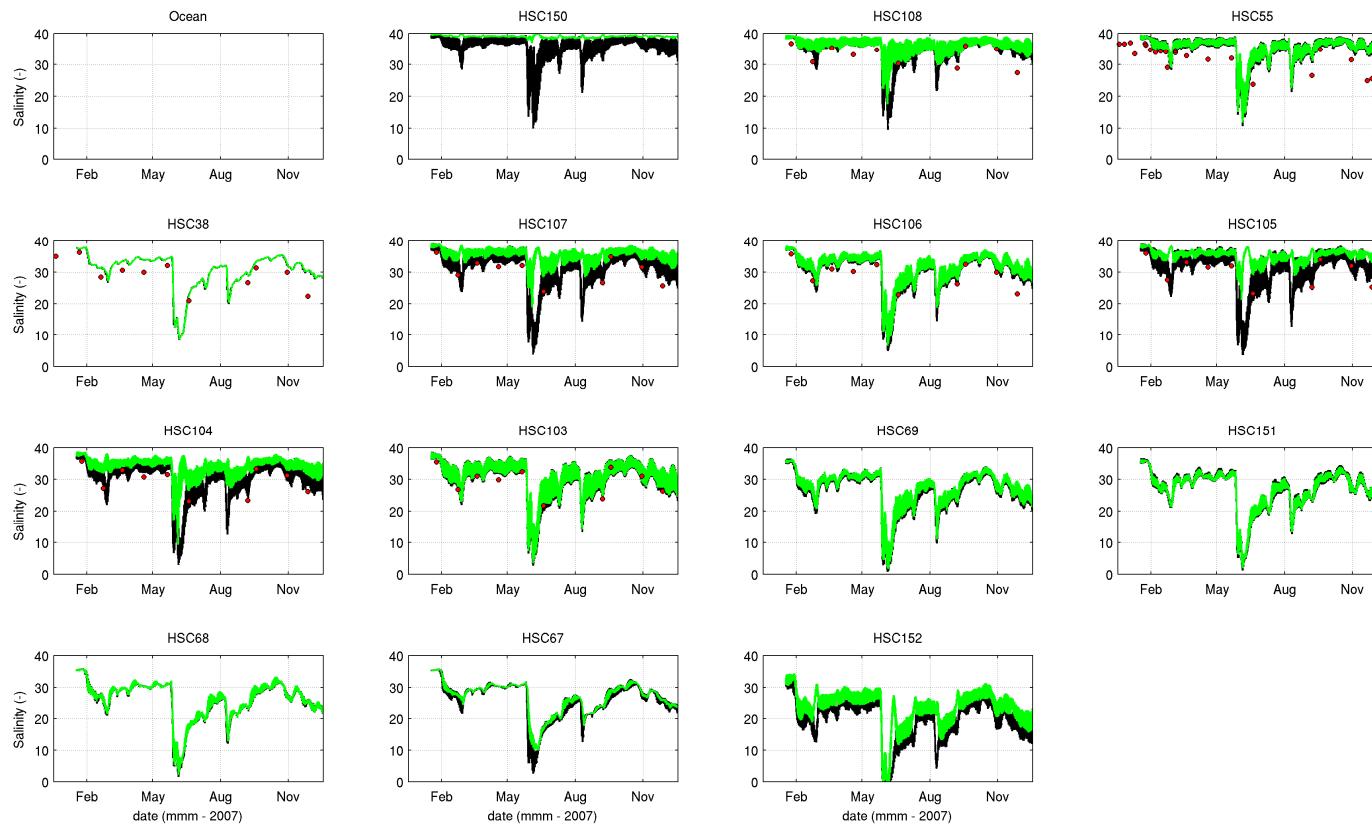


Water Quality Modelling of the Hawkesbury-Nepean River System



- **Figure 12-22 (Cont.) Salinity Boundary Condition set at 37.5 (2007) (measured data (red), modelled surface (black) and modelled bottom (green))**

SINCLAIR KNIGHT MERZ



- **Figure 12-23 Salinity Boundary Condition set at 40 (2007) (measured data (red), modelled surface (black) and modelled bottom (green))**

SINCLAIR KNIGHT MERZ

12.1.7.2. Inflows

All inflows were provided from the Source model, both in terms of flows and water quality concentrations (see Sections 7 and 8).

12.1.7.3. Irrigation Extractions

All irrigation extractions were provided from the Source model and are discussed in Section 6.3.

12.1.7.4. Wastewater Treatment Plants

All WWTP inflows and concentrations were provided by Sydney Water.

12.1.8. Mixing Models

The mixing models deployed in this study were:

- Momentum mixing: Smagorinsky.
- Scalar mixing: Smagorinsky.
- Vertical mixing: Turbulent closure scheme from the well known GOTM library. A second order k- ϵ model was adopted using the generic length scale approach with constant stability functions (see above).

12.2. Water Quality Model

12.2.1. Simulated Constituents

The following constituents were simulated in the water quality model:

- Physicals:
 - Dissolved oxygen;
- Silicate;
- Nutrients:
 - Ammonium;
 - Nitrate;
 - Filterable reactive phosphorus;
 - Adsorbed filterable reactive phosphorus;
 - Dissolved organic nitrogen;
 - Particulate organic nitrogen;
 - Dissolved organic phosphorus;
 - Particulate organic phosphorus;
 - Organic Carbon;
 - Dissolved organic carbon;
 - Particulate organic carbon;

- Algae:
 - Green algae;
 - Blue-green algae;
 - Freshwater diatoms;
 - Marine diatoms;
- Bacteria:
 - Faecal coliforms
 - E. coli; and
 - Enterococci.

Appendix K includes the AED water quality model manual, and details of the bacterial model schematisation.

12.2.2. Initial Conditions

Initial conditions were sourced from available data and interpolated across the model domain as required.

12.2.3. Boundary Conditions

12.2.3.1. Open Ocean

The following boundary conditions at the open ocean were applied:

- Dissolved oxygen: assumed constant and equal to 6.9 mg/L;
- Filterable reactive phosphorus: assumed constant and equal to 0.0015 mg/L;
- Particulate and dissolved organic phosphorus: assumed constant and equal to 0.0005 mg/L;
- Nitrate: assumed constant and equal to 0.010 mg/L;
- Ammonium: assumed constant and equal to 0.013 mg/L;
- Particulate and dissolved organic nitrogen: assumed constant and equal to 0.10 mg/L;
- Silica: assumed constant and equal to 0.68 mg/L; and
- Particulate and dissolved organic carbon: assumed constant and equal to 1.80 mg/L;
- Algae: assumed a constant and equals to 0.10 mg/L of carbon or 2.00 µg/L of chlorophyll a, subdivided as:
 - Green algae: assumed constant and equal to 14.2 µg/L of carbon or 0.28 µg/L of chlorophyll a;
 - Blue-green algae: assumed constant and equal to 2.62 µg/L of carbon or 0.066 µg/L of chlorophyll a;
 - Freshwater diatoms: assumed constant and equal to 1.05 µg/L of carbon or 0.021 µg/L of chlorophyll a; and

- Marine diatoms: assumed constant and equal to 81.5 µg/L of carbon or 1.63 µg/L of chlorophyll a.
- Bacteria:
 - Constant and equal to zero.

12.2.3.2. Catchment inflows

All inflows were provided from the Source model (see Section 7).

12.2.3.3. Wastewater Treatment Plants

Some inflows were provided from the Source model (see Section 7) while others were separate direct inputs into the model.

12.2.3.4. Extractions

No boundary specifications required as flows are leaving the model.

12.2.3.5. Sediment Dynamics

Model inputs in this regard have been based on information from a NSW department of Environment Climate Change & Water report (Gruber et al. 2010 - *Final Report - Nutrient Transformation and Attenuation within Tidal Rivers*). This report summarises a study that undertook ex-situ nutrient benthic flux measurements along a significant reach of the Hawkesbury River.

By way of summary, Gruber et al. (2010) subdivided the Hawkesbury River in the zones as specified in the Figure below (reproduced from that publication).

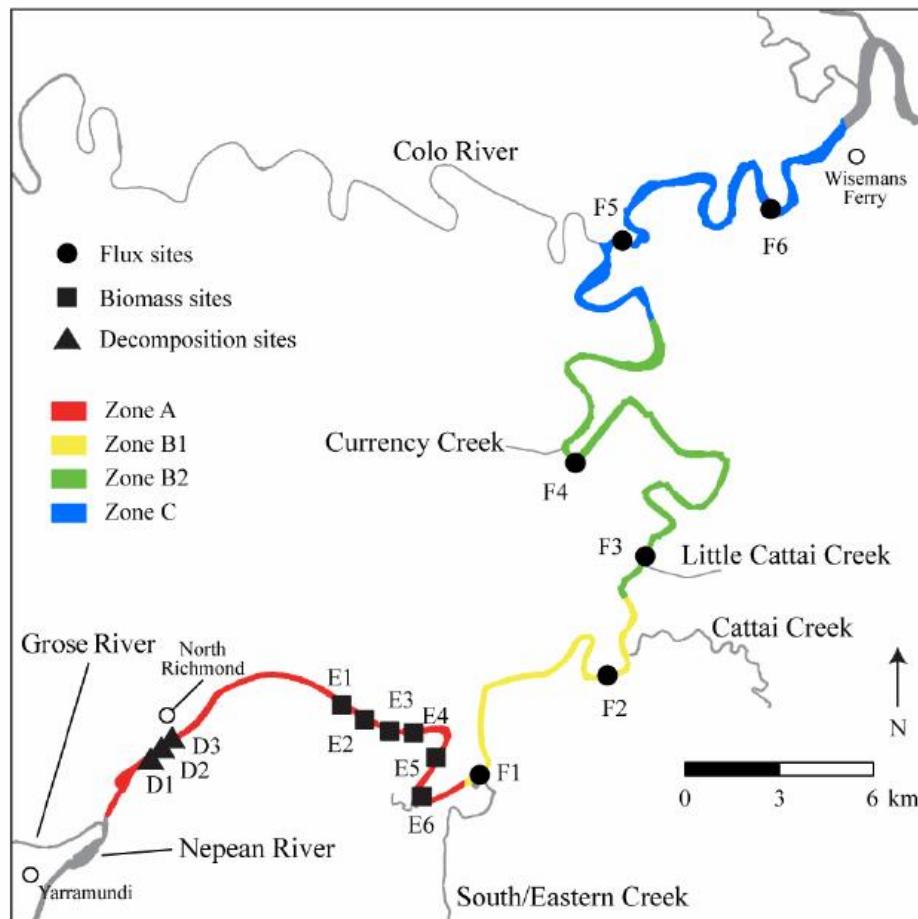


Figure 5-2. Study area showing major inflows and sampling sites within functional zones

Gruber et al (2010) identified that the river operates differently in terms of its dominant loci of ecological processes (e.g. benthic vs pelagic). The following excerpts help to identify the main findings of the report that were of relevance to the approach adopted in the modelling (italics are ours):

"While Shallow and Deep experimental treatments sometimes yielded significant differences in nutrient fluxes, the hypsometry of the study region...led to a dominance of Deep (net heterotrophic) over Shallow processes. As a result, *the benthos was a major source of TDN and TDP that typically equalled or exceeded loads entering from the catchment...* Given that portions of the channel (especially in Zones B2 and C) were often much deeper than the Deep treatment (2 m), and that nutrient release from these deep regions was fairly large... it is likely that benthic fluxes measured in this study underestimated true fluxes. (...)"

"In the case of phosphorus, the largest fractions of DIP in inflows occurred during summer and autumn, which also displayed the greatest degree of transformation. DIP and DOP were transformed to PP (the largest exported fraction) regardless of season. *A large increase in PP tended to occur in*

Zone B2; however, corresponding decreases in DOP and DIP were not observed..., which suggests an internal source of P fuelling phytoplankton production."

*"The major source of nutrients to the tidal fresh region was the inflow of South and Eastern Creeks, which contained treated effluent from multiple STPs. Additionally, the benthos served as a source of dissolved N and P, especially DON and DOP in the lower reaches of the fluvio-tidal region. The important primary producers in this system were phytoplankton and the submersed macrophyte species *Egeria densa*. Highly depressed phosphorus concentrations in the *Egeria*-dominated portion of the river coupled with elevated phosphorus content in leaf tissue suggested that this species was an extremely efficient competitor for nutrients and substantially reduced the effects of large upstream nutrient loading on downstream portions of the Hawkesbury River. Further downstream, nutrient uptake was dominated by phytoplankton (*chlorophyll a maximum*, Zone B2)."*

*"This preliminary finding suggests that *Egeria densa* is extremely efficient in the uptake and incorporation of phosphorus into its tissues, likely resulting in the depressed phosphorus concentrations of water leaving Zone A. Based on light levels in Zone A, depths between 0-1.8m received sufficient light for growth of *Egeria*".*

The report also provides values of nutrient uptake by *Egeria densa*. – “Benthic and macrophyte production represented key sources and sinks of nutrients, while pelagic fluxes represented an important nutrient transformation. Net daily pelagic and benthic fluxes were separated into shallow (Ps, Bs) and deep (Pd, Bd) compartments, respectively. Macrophyte uptake occurred in Zone A over SE and depended on a rate (e) that was calculated on a per-biomass (B) basis. Uptake rates were assumed to be constant with season and were set as $0.078 \text{ mg P g DW}^{-1} \text{ day}^{-1}$ and $0.36 \text{ mg N g DW}^{-1} \text{ day}^{-1}$ (Feijoo et al. 2002)”.

Given the above, model parameterisation of sediment flux was adapted to account for nutrient uptake by macrophytes. It is noted that this zone of competitive *Egeria densa* uptake is consistent with the zone in which a large Manning's n was applied to capture the strong hydraulic resistance provided by these macrophytes. A full list of all sediment fluxes applied to the water quality model is provided in **Appendix L (Table L-7)**.

13. Model Calibration and Validation

13.1. Preamble

The model was iteratively calibrated to tidal hydrodynamics, salinity, suspended solids and finally water quality. The calibration process is described below.

13.2. Hydrodynamics

The model's hydrodynamics were calibrated using the data collected during the Acoustic Doppler Current Profile (ADCP) CMP in late 2011, together with independent water level data collected by MHL. The location of the ADCP CMP transects and MHL tide gauges are presented above (**Figure 11-6** and **Figure 11-8**)

Two periods were selected for assessing the model's hydrodynamic performance, and these corresponded to the spring and neap tides of the ADCP CMP period:

- Spring: 22 November to 24 November 2011
- Neap: 5 December to 7 December 2011

A significant rainfall event occurred during the ADCP CMP period between transect events. This provided an opportunity to examine water levels and flows during inflow events (albeit only via water levels) as well as typical riverine conditions.

Hydrodynamic calibration data is presented in **Figure 13-1** to **Figure 13-8**. Water levels are presented for the entire period of 22 November to 7 December 2011 (**Figure 13-1**), and in more detail over each of CMP ADCP event periods listed above (**Figure 13-2** and **Figure 13-3**). Flows are presented in a similar fashion, over the entire period in **Figure 13-4** and over the CMP event periods in **Figure 13-5** and **Figure 13-6**. In addition to flows and water levels comparisons of depth-averaged velocities at different tidal stages are presented in **Figure 13-7** and **Figure 13-8**.

The predictive capability of the model both in terms of water levels and flows is presented below for both for the entire period of 22 November to 7 December 2011, and in more detail over each of ADCP CMP event periods. Water level comparisons are presented first, followed by flow comparisons. Blue and red coloured series are measured and modelled data, respectively (**Figure 13-1** to **Figure 13-6**).

Comments that can be made in regard to these model results are as follows:

- The model is reproducing tidal water level phase lag, amplification and dampening well throughout. There are some minor discrepancies between measured and modelled series, with the most notable being at Castlereagh. The difficulties in establishing the hydraulic control at that site, and capturing the very significant tidal signal attenuation process in the region have been discussed in Section 12.1.3.
- Throughout the model, the rate the water level increases, peaks and returns to normal levels following the rainfall event in late November, are well reproduced by the model. This provides confidence that, at least in terms of water levels, the model configuration is able

to adequately capture hydrodynamic processes in response to a reasonable range of catchment hydrologic conditions.

- The model is reproducing the flows measured during the ADCP CMP well. The progressive phasing and magnitude variations in flow between Bar Point and Wilberforce were well captured. Additionally, despite the relatively low resolution in the transversal direction (required to balance computational effort over this very large domain), the variation of velocity magnitude and direction across the channel were shown to follow the field measurements at different stages of the tide. This is a critical result as it shows that the model is correctly transporting water mass throughout – this is essential for subsequent water quality calibration and scenario tasks.

Hydrodynamic calibration data is presented in **Figure 13-1** to **Figure 13-6**.

13.3. Advection Dispersion/Salinity Recovery

In a similar manner to the above, the advection dispersion algorithms within the model were tested against the range of available data sets. In this instance, the following were selected:

- Salinity data collected at ADCP CMP sites; and
- All MHL data available over the full water quality model calibration period (2006 and 2007, see subsequent sections).

This approach was adopted to make use of the ADCP CMP data (albeit over a relatively short period) and also to look at broader advection-dispersion performance across a longer (2 year) period.

Advection dispersion calibration data is presented in **Figure 13-9** to **Figure 13-15**. It is noted that in **Figure 13-9** different scales were used in the plotting of salinity across different sites. The application of the different scales was done in such a way as to better define the details revealed in the data and model results.

The model comparisons with the field data for the calibration and validation periods (**Figure 13-10** to **Figure 13-15**) are presented in the following formats:

- Timeseries plots of salinity at key locations along the model domain;
- Exceedance plots; and
- Statistical ('box and whiskers') plots of both observed and modelled results presented as longitudinal profiles along the model domain for each of the two model years.

For the timeseries plots (**Figure 13-10** and **Figure 13-13**) red dots refer to field data, the green line refers to model results at the bottom, and the black line refers to model data at the surface.

Similarly, for the exceedance plots (**Figure 13-11** and **Figure 13-14**), red dots refer to field data, the green line refers to model results at the bottom, and the black line refers to model data at the surface.

Dotted lines refer to percentiles plus and minus two standard deviations. Exceedance plots are presented only for populations with more than six samples.

For the 'box and whisker' plots (**Figure 13-12** and **Figure 13-15**), red boxes refer to field data, green boxes refer to model results at the bottom, and the blue boxes refer to model data at the surface. The red triangles show the locations directly downstream of indicated WRPs and WWTPs. When maximum values are larger than the top range of the scale they are indicated on the top left side (field) or the top right side (model surface) of the boxes. Also, the number of samples used to produce each group of boxes is annotated in each sampling station.

As before, different scales were used in the timeseries and exceedance plots of salinity across the Middle and Lower Reaches of the river system (**Figure 13-10**, **Figure 13-11**, **Figure 13-13** and **Figure 13-14**). No figures were produced for the Upper Reach as it was fresh throughout. Again, in the Middle and Lower Reaches cases, the application of the different scales was done in such a way as to better define the details revealed in the data and model results. For consistency, the same ranges were maintained across 2006 and 2007, as well as between timeseries and exceedance plots.

13.4. Sediment Transport

The 2006 - 2007 period was used to examine sediment transport model skill, using the cohesive sediment module of TUFLOW FV. This uses a Mehta formulation to simulate the exchange of sediments between the bed and the water column. The effective clear water sediment settling velocity of sediment, w_s , is directly specified and is assumed to have no dependence on suspended sediment concentration (e.g. flocculation or hindered settling). The modelled rate of sediment deposition (in $\text{g/m}^2/\text{s}$) is a function of the near-bed sediment concentration (TSS), the still-water fall velocity (w_s) and the bed shear stress (τ_b), according to the relationship:

$$Q_d = w_s \cdot TSS \cdot \max\left(0, 1 - \frac{\tau_b}{\tau_{cd}}\right) \quad \text{units } [\text{g/m}^2/\text{s}]$$

Where τ_{cd} is a model parameter defining the critical shear stress for deposition. As such, sediment settling is reduced below still water value by the action of bed shear stress and associated vertical mixing in the water column.

The rate of erosion is calculated according to:

$$Q_e = E \cdot \max\left(0, \frac{\tau_b}{\tau_{ce}} - 1\right) \quad \text{units } [\text{g/m}^2/\text{s}]$$

Where Q_e is the erosion rate constant and τ_{ce} is the critical bed shear stress for erosion.

The calibration process led to the adoption of the following model parameters:

- Critical shear stress for erosion $\tau_{ce} = 0.2 \text{ Pa}$;
- Critical shear stress for deposition $\tau_{cd} = 0.1 \text{ Pa}$; and
- Erosion rate constant $E = 0.01 \text{ g/m}^2/\text{s}$.

In addition, the model was run for an initial “warm up” period to allow the sediment to redistribute within the model. This process allowed the bed composition in each area to evolve towards an initial condition which was likely to reflect the actual local natural bed composition.

Sediment calibration data is presented in **Figure 13-16** to **Figure 13-21**. Similarly to results of salinity, timeseries plots (**Figure 13-16** and **Figure 13-19**), exceedance plots (**Figure 13-17** and **Figure 13-20**), and ‘box-and-whiskers’ plots (**Figure 13-18** and **Figure 13-21**) are presented. The formats adopted in these plots follow the same pattern specified for salinity.

13.5. Water Quality

There are a number of well established steps in calibrating and validating a water quality model, which encompass the following:

- Temperature calibration – temperature controls the rates at which many key water quality processes occur. As such the ability of a model to reproduce observed temperature behaviour is crucial. This is therefore the first step in such a modelling process;
- Nutrients and organic matter –second to temperature in importance are the levels of nutrients, organic matter and oxygen being predicted by a model. If these constituents are not adequately reproduced, the model will not be able to reliably simulate algal growth and primary productivity processes;
- Primary productivity – the final step in the calibration process is to reproduce key primary productivity processes. These essentially comprise phytoplankton growth, die off and interaction with other water quality parameters (e.g. organic carbon, dissolved oxygen, etc.); and
- Bacteria simulation – this simulation is relatively independent of the above, other than bacteria being sensitive to light and temperature. As such, these were considered separately from the above during the model calibration process. It is noted that other models that explicitly simulate microbial activity take a slightly different approach to that adopted here.

One ‘dry’ year (2006) for calibration and a ‘wet’ year (2007) for validation were selected for calibration and validation purposes. It is noted of course, that this stepwise process was obviously not solely sequential and that iteration back and forth through these steps was often required to examine the model response as a whole. Doing so ensured a systematic approach and calibrated the complex non-linear feedback loops that exist between the above general calibration stages.

In terms of the detailed parameterisation of the model, this commenced with a parameter set based on both previous experience and literature values. Following comparison of model predictions against measurement, the steps outlined above were followed (but not necessarily in isolation or the order presented) to progress model calibration.

Within these steps, typically a range of ad hoc sensitivity tests were undertaken to investigate which parameters provided the clearest model response, and when appropriate, these were then the focus of model calibration. Sensitivity testing revealed, for example, that sensitive parameters sometimes varied in their influence on model response as the iterative calibration process progressed, and so this ad hoc approach worked well in identifying such trends and continually focussing calibration efforts.

Based on this iterative approach, the following parameters were given the most focus as part of this calibration study:

- Sediment flux of DOP & FRP around South & Eastern Creek and downstream to Cattai Creek.
- Sediment flux parameters for inorganic nutrients around the stretch from Penrith Weir to the confluence with South Creek, specifically as these incorporated estimates of nutrient uptake through benthic production by macrophytes.
- Remineralisation of organic matter to inorganic nutrients.
- Nitrification & denitrification rates.
- Phytoplankton parameters (addressed in the algal report) including:
 - Temperature response;
 - Salinity response;
 - Phosphorus uptake behaviour;
 - Growth rates; and
 - Internal phosphorus simulation.

A complete list of final calibration parameters is included in [Appendix L](#).

Given that the key contribution of AED to the modelling effort was via provision of in-stream cycling and processing capability, the calibration effort was initially focussed on the dry period of September 2006 to early January 2007. During this period the inflows were small, and as such attention was directed to internal cycling and processing pathways without the complication of catchment inflows. Once the model performance over this period was satisfactory, the entire 2006 year was executed and model performance checked. Some minor parameter adjustments were made and the model was then executed over 2007 (wet period) with its parameterisation unchanged. If shortcomings were identified, then alterations to the model parameterisation were applied over the dry period again, and iterated through time as described above.

Focussing on these different climatic conditions enabled rigorous testing of the model's ability to reproduce the extremes of a system being dominated firstly by point source discharges and internal SINCLAIR KNIGHT MERZ

cycling (2006), and secondly to one being dominated by catchment or diffuse sources (2007). This process also operates as an ‘independent’ test of the Source modelling.

The 2006-2007 period from a water quality perspective is quite different to conditions currently being experienced in the model domain; due to recent (early 2011) major changes in how wastewater discharges interact with the system. These changes will be included in the receiving water quality modelling for the various scenario assessments.

Model robustness is demonstrated by comparing simulated water quality levels with observed water quality behaviour in the form of:

- Timeseries representations at key locations along the model domain;
- Exceedance plots;
- Statistical ('box and whiskers') plots of both observed and modelled results presented as longitudinal profiles along the model domain for each of the two model years; and
- Selected constituent algal limitation functions. These functions show which algal species are limited by the various water quality parameters. Phosphorous, nitrogen, silicate and temperature functions were selected as these are the key constituents in the river system that limit algal growth. All limitation functions have a value between 0 and 1 (with the exception of temperature). A value of 1 indicates that the constituent being considered is not limiting algal growth at all. A value of 0 indicates that the constituent being considered is entirely limiting and is preventing any algal growth. Intermediate values between 0 and 1 indicate partial limitation. The temperature limitation factor is a multiplier applied to maximum growth rates and can vary from 0 to approximately 1.5. If algal species A has a higher temperature limitation value than algal species B at a given time, but they both have the same maximum growth rate specified, algal species A will grow preferentially to algal species B.

In all figures, red, black and green represent measured data, and surface and bottom model predictions, respectively. In some cases, vertical gradients in simulated constituents were small, so green and black lines are coincident. In these instances, the green line will overlay the black line, giving the appearance that only green (bottom) is plotted, however this is not the case – the black line is simply obscured by the green line due to the similarity of top and bottom constituent concentrations. In addition, any exceedance curves for annual data sets that have less than six points have not been plotted. Where this is the case, axes have been removed from figures (rather than plotting blanks axes) however the relative positions of axes within a figure has been maintained so as to allow easy visual comparisons and assessments.

Finally, due to large variations in measured data, it was difficult to determine a consistent vertical axis for a given constituent across all sites and time periods. It was also difficult to present key features that occur at different timescales in a single figure (e.g. seasonal and diurnal temperature fluctuations). As a result, not all axes for a given constituent use the same vertical scale. However, a balance has attempted to be found between showing all data and using a large scale range that makes variations in small numbers difficult to read. This applies to both timeseries and exceedance

SINCLAIR KNIGHT MERZ

plots for water quality variables. Diurnal fluctuations predicted by the model are presented in **Appendix M**.

13.5.1. Temperature

Temperature calibration was relatively straightforward, and required no real calibration effort. Calibration data is presented in **Figure 13-22** to **Figure 13-27**. Timeseries plots are presented in **Figure 13-22** and **Figure 13-25**, exceedance plots are presented in **Figure 13-23** and **Figure 13-26**, whilst ‘box-and-whisker’ plots are presented in **Figure 13-24** and **Figure 13-27**.

13.5.2. Nutrients

The calibration and validation results of the model to relevant nutrient, organic and physical (dissolved oxygen) parameters are presented in **Figure 13-28** to **Figure 13-78**.

Dissolved oxygen (DO) timeseries plots are presented in **Figure 13-28** and **Figure 13-31**, exceedance plots are presented in **Figure 13-29** and **Figure 13-32**, and ‘box-and-whisker’ plots in **Figure 13-30** and **Figure 13-33**.

Filterable reactive phosphorus (FRP) timeseries plots are presented in **Figure 13-34** and **Figure 13-37**, exceedance plots are presented in **Figure 13-35** and **Figure 13-38**, and ‘box-and-whisker’ plots in **Figure 13-36** and **Figure 13-39**.

Total Phosphorus (TP) timeseries plots are presented in **Figure 13-40** and **Figure 13-43**, exceedance plots are presented in **Figure 13-41** and **Figure 13-44**, and ‘box-and-whisker’ plots in **Figure 13-42** and **Figure 13-45**.

Oxidised nitrogen (NO_x) timeseries plots are presented in **Figure 13-46** and **Figure 13-49**, exceedance plots are presented in **Figure 13-47** and **Figure 13-50**, and ‘box-and-whisker’ plots in **Figure 13-48** and **Figure 13-51**.

Ammonia (NH₄) timeseries plots are presented in **Figure 13-52** and **Figure 13-55**, exceedance plots are presented in **Figure 13-53** and **Figure 13-56**, and ‘box-and-whisker’ plots in **Figure 13-54** and **Figure 13-57**.

Total Nitrogen (TN) timeseries plots are presented in **Figure 13-58** and **Figure 13-61**, exceedance plots are presented in **Figure 13-59** and **Figure 13-62**, and ‘box-and-whisker’ plots in **Figure 13-60** and **Figure 13-63**.

Silica (Si) timeseries plots are presented in **Figure 13-64** and **Figure 13-67**, exceedance plots are presented in **Figure 13-65** and **Figure 13-68**, and ‘box-and-whisker’ plots in **Figure 13-66** and **Figure 13-69**.

Dissolved Organic Carbon (DOC) timeseries plots are presented in **Figure 13-70** and **Figure 13-73**, exceedance plots are presented in **Figure 13-71** and **Figure 13-74**, and ‘box-and-whisker’ plots in **Figure 13-72** and **Figure 13-75**.

Total Organic Carbon (TOC) timeseries plots are presented in **Figure 13-76** and **Figure 13-78**, and 'box-and-whisker' plots in Figure 13-77. TOC had less than six measurements from each monitoring site in 2006 and no measurements in 2007. Therefore, TOC exceedance plots are not shown, whilst 'box-and-whisker' plots are only presented in 2006.

13.5.3. Primary Productivity

The primary productivity (chlorophyll a) model calibration and validation results are presented in **Figure 13-79** to **Figure 13-84**. Timeseries plots are presented in **Figure 13-79** and **Figure 13-82**, exceedance plots are presented in **Figure 13-80** and **Figure 13-83**, whilst 'box-and-whisker' plots are presented in **Figure 13-81** and **Figure 13-84**.

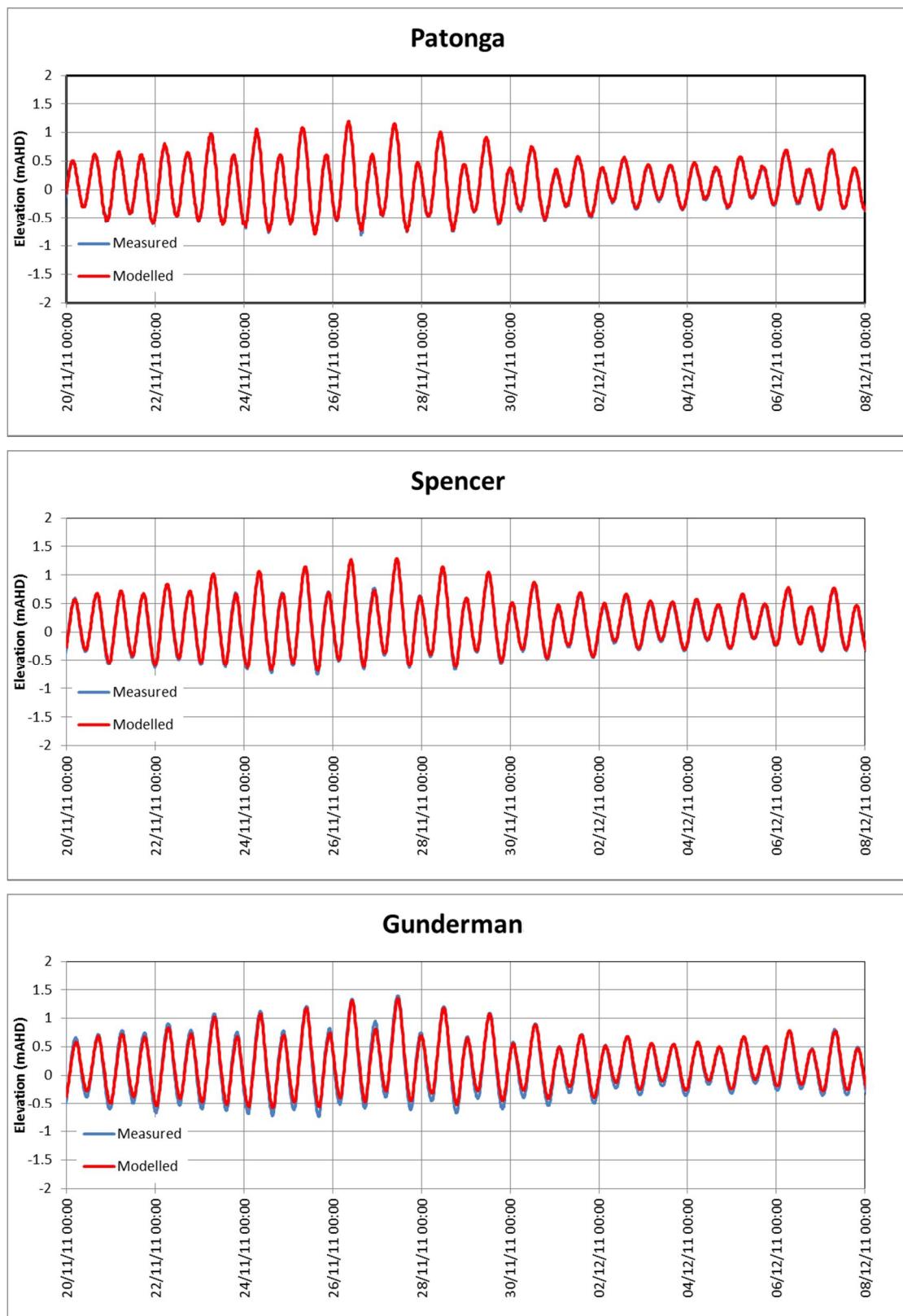
13.5.4. Bacteria

Three bacteria groups were simulated representing faecal coliforms, *Escherichia coli* (E. coli), and Enterococci. The bacterial model calibration and validation results are presented in **Figure 13-95** to **Figure 13-100**.

Faecal coliforms timeseries plots are presented in **Figure 13-95** and **Figure 13-98**, exceedance plots are presented in **Figure 13-96** and **Figure 13-99**, and 'box-and-whisker' plots in **Figure 13-97** and **Figure 13-100**.

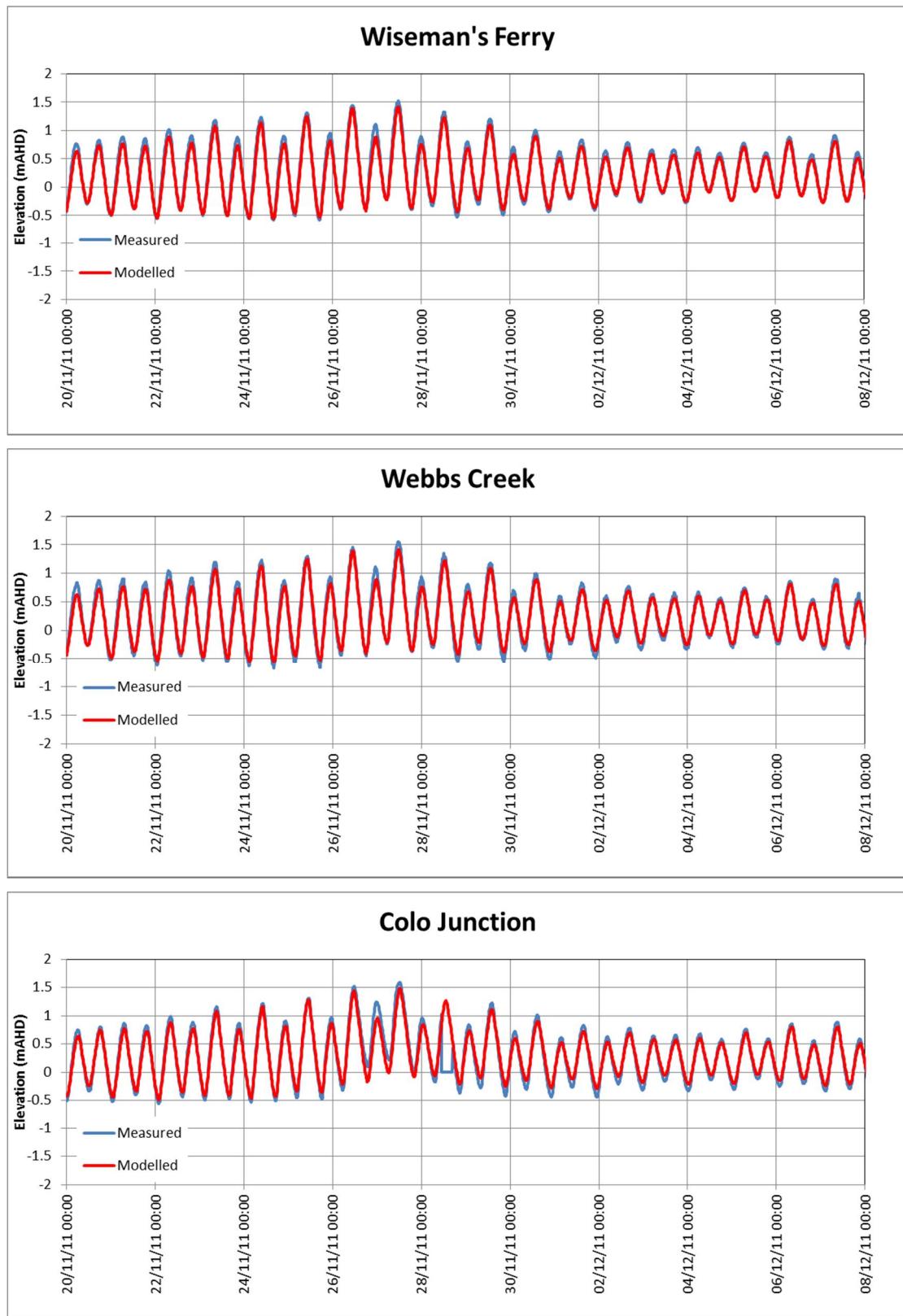
E. Coli timeseries plots are presented in **Figure 13-101** and **Figure 13-104**, exceedance plots are presented in **Figure 13-102** and **Figure 13-105**, and 'box-and-whisker' plots in **Figure 13-103** and **Figure 13-106**.

Enterococci timeseries plots are presented in **Figure 13-107** and **Figure 13-110**, exceedance plots are presented in **Figure 13-108** and **Figure 13-111**, and 'box-and-whisker' plots in **Figure 13-109** and **Figure 13-112**.



■ **Figure 13-1 Water Level Calibration (Patonga, Spencer and Gunderman) – 22 November to 7 December 2011**

SINCLAIR KNIGHT MERZ

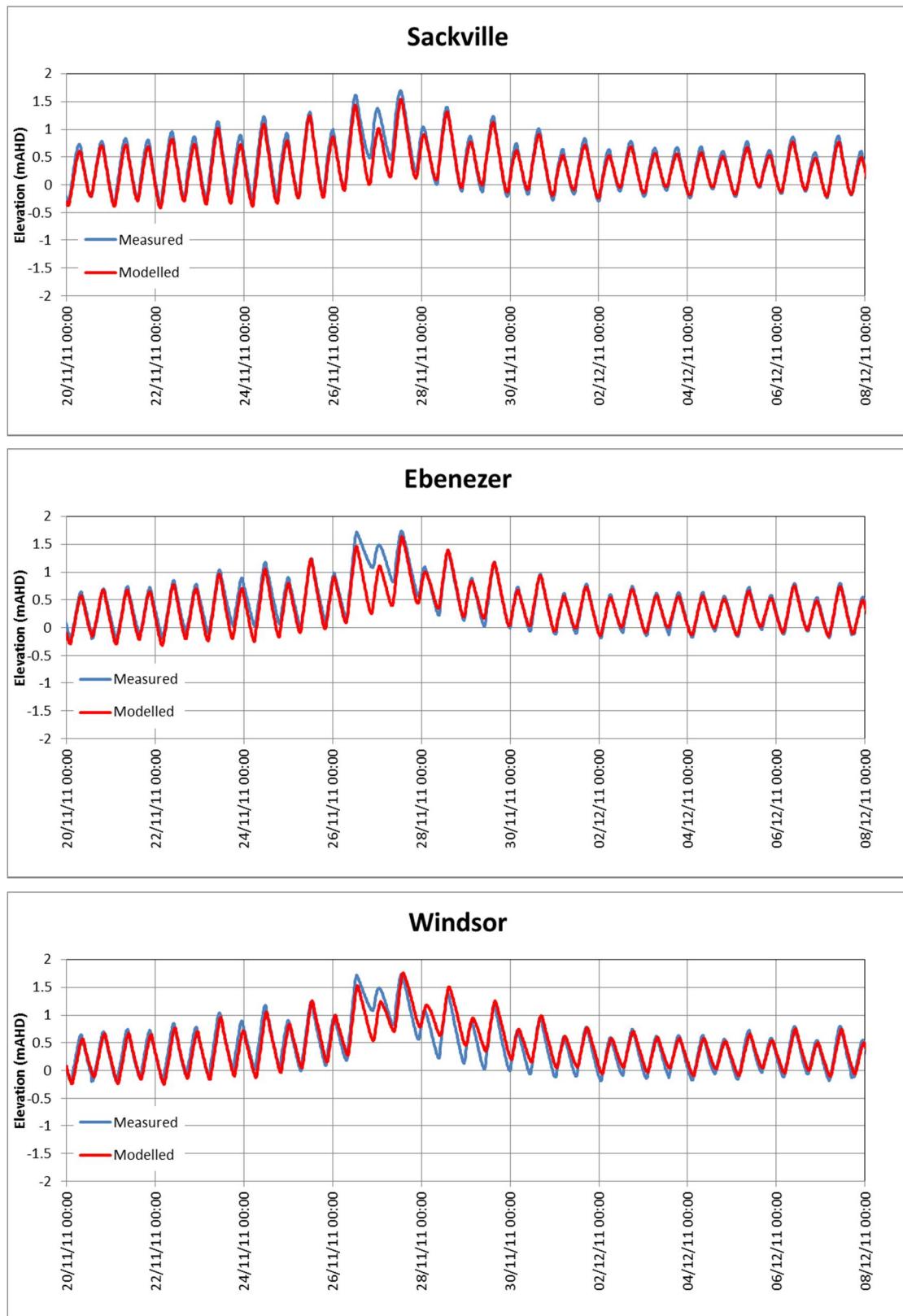


■ **Figure 13-1 (Cont.) Water Level Calibration (Wiseman's Ferry, Webb's Creek and Colo Junction) – 22 November to 7 December 2011**

SINCLAIR KNIGHT MERZ

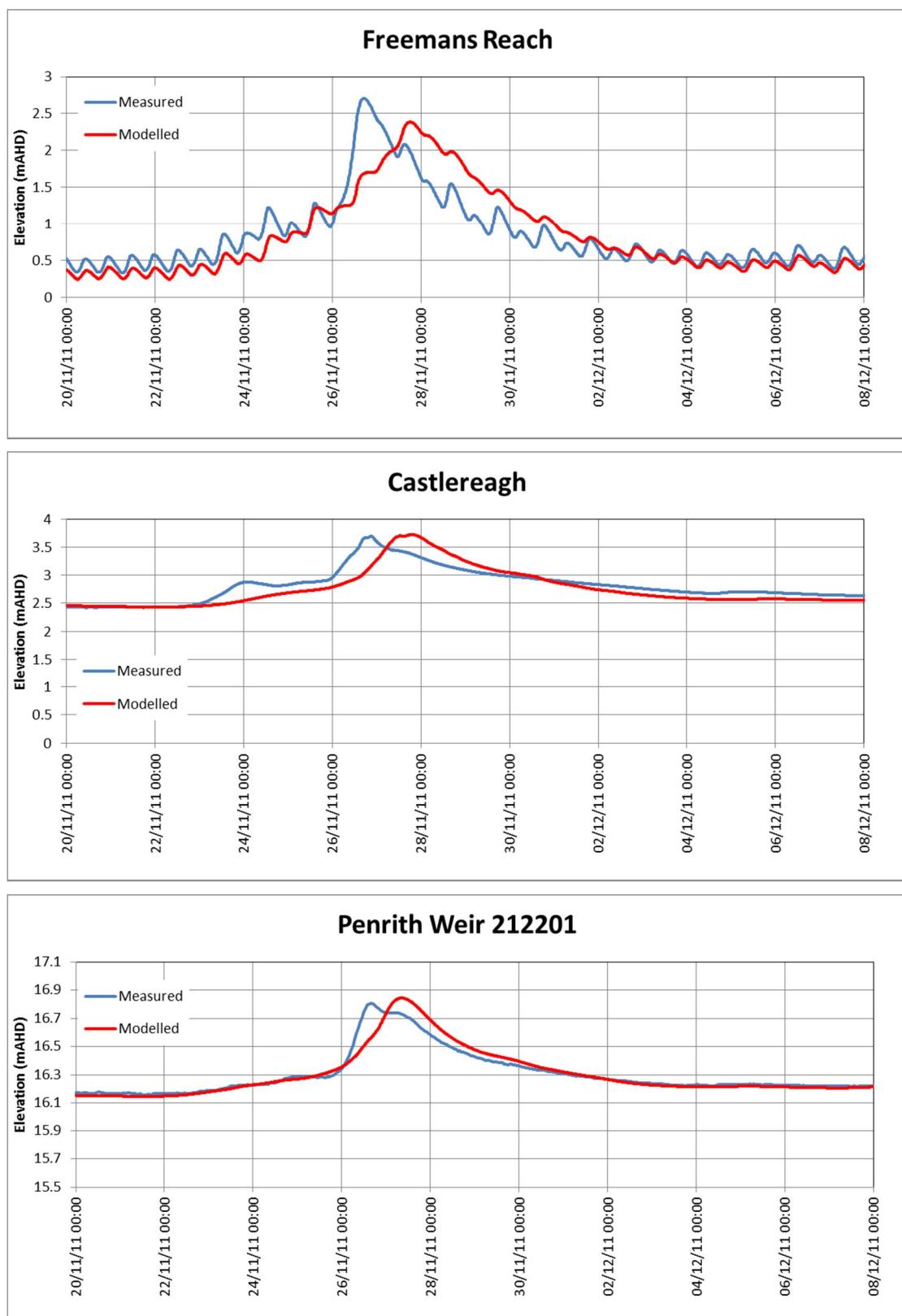


Water Quality Modelling of the Hawkesbury-Nepean River System



■ **Figure 13-1 (Cont.) Water Level Calibration (Sackville, Ebenezer and Windsor) – 22 November to 7 December 2011**

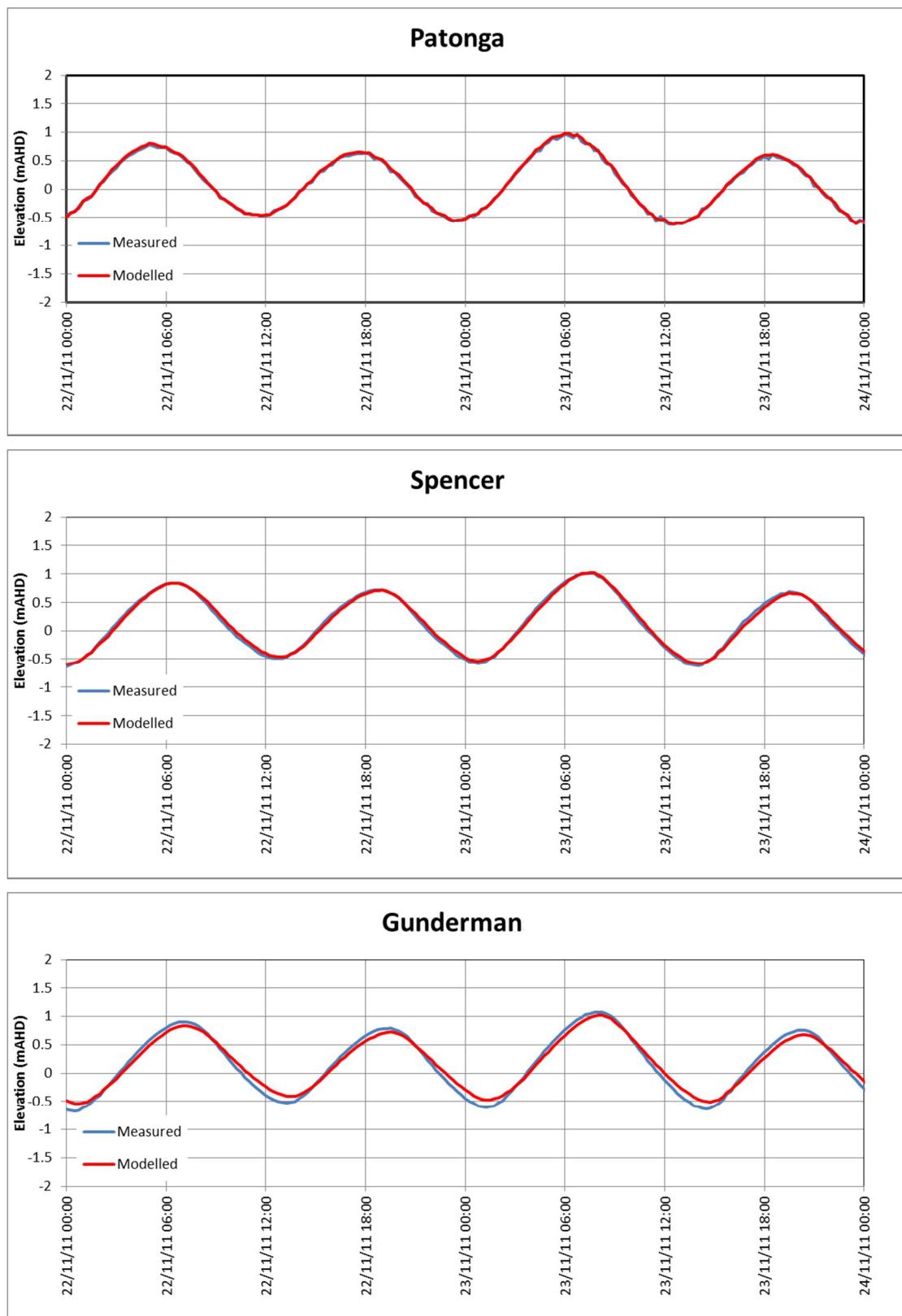
SINCLAIR KNIGHT MERZ



■ **Figure 13-1 (Cont.) Water Level Calibration (Freeman's Reach, Castlereagh and Penrith Weir) – 22 November to 7 December 2011**

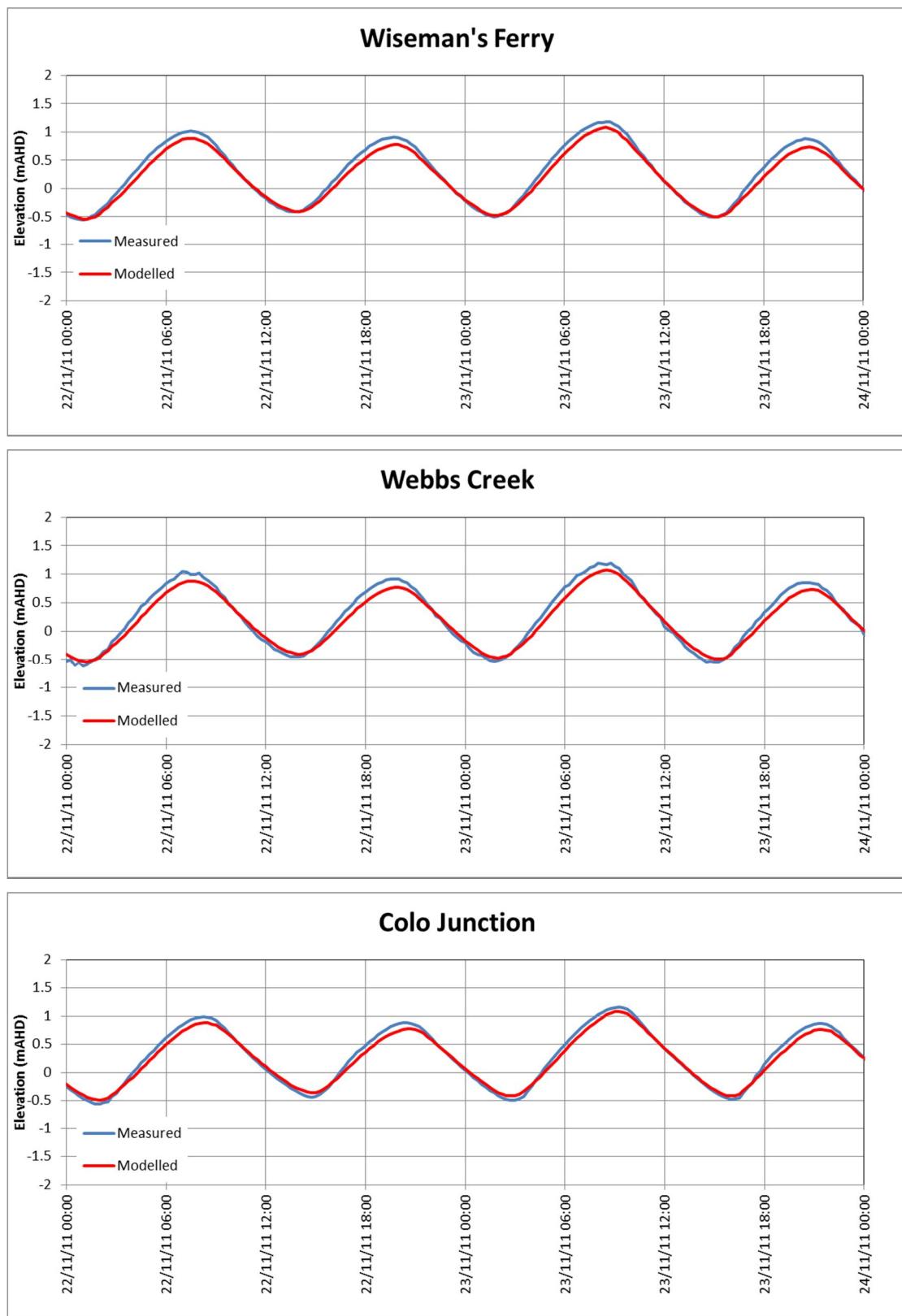
SINCLAIR KNIGHT MERZ

Water Quality Modelling of the Hawkesbury-Nepean River System



■ **Figure 13-2 Water Level Calibration 2011 (Patonga, Ebenezer, Gunderman) – Spring Tide**

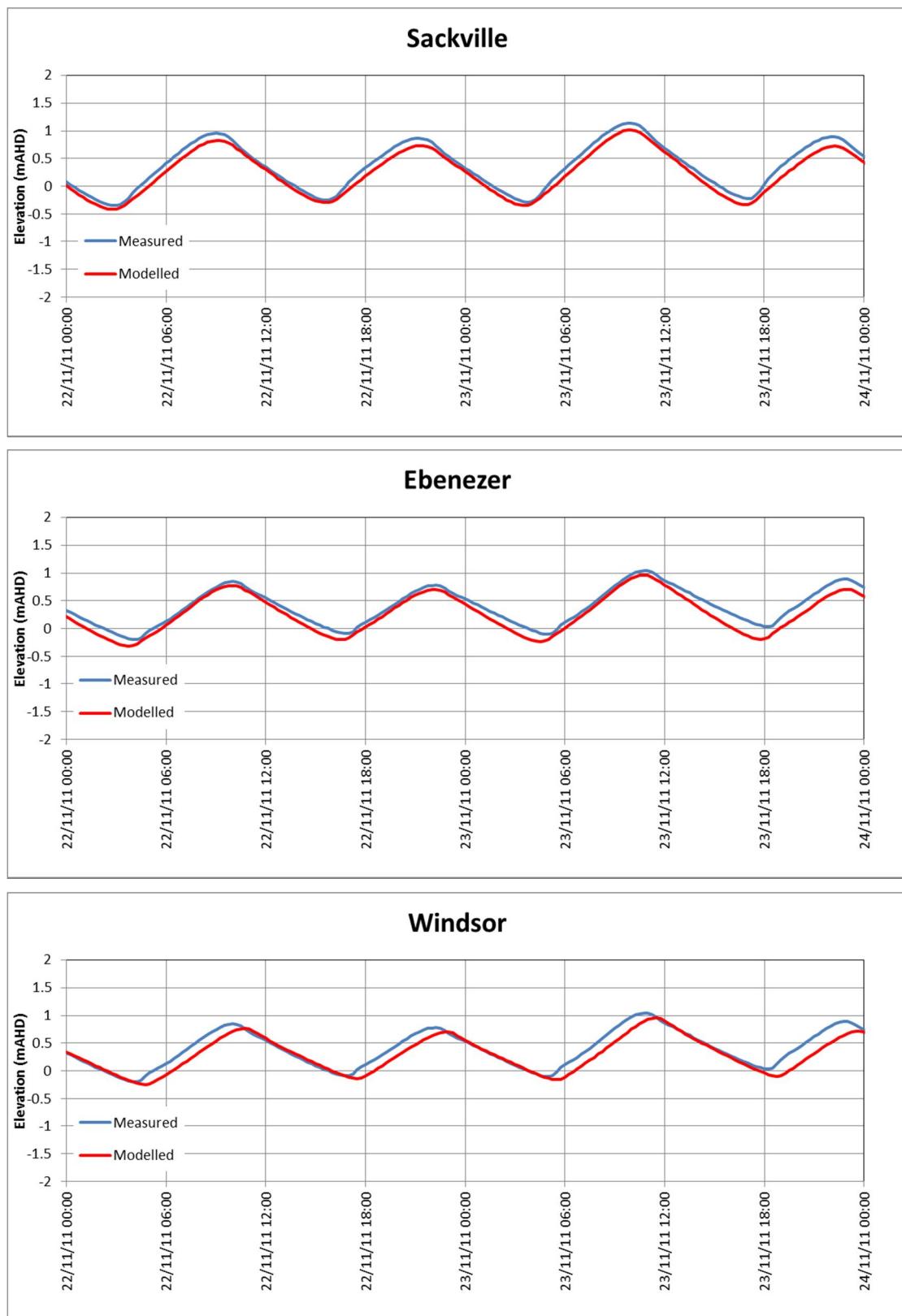
SINCLAIR KNIGHT MERZ



■ **Figure 13-2 (Cont.) Water Level Calibration 2011 (Wiseman's Ferry, Webbs Creek, Colo Junction) – Spring Tide**

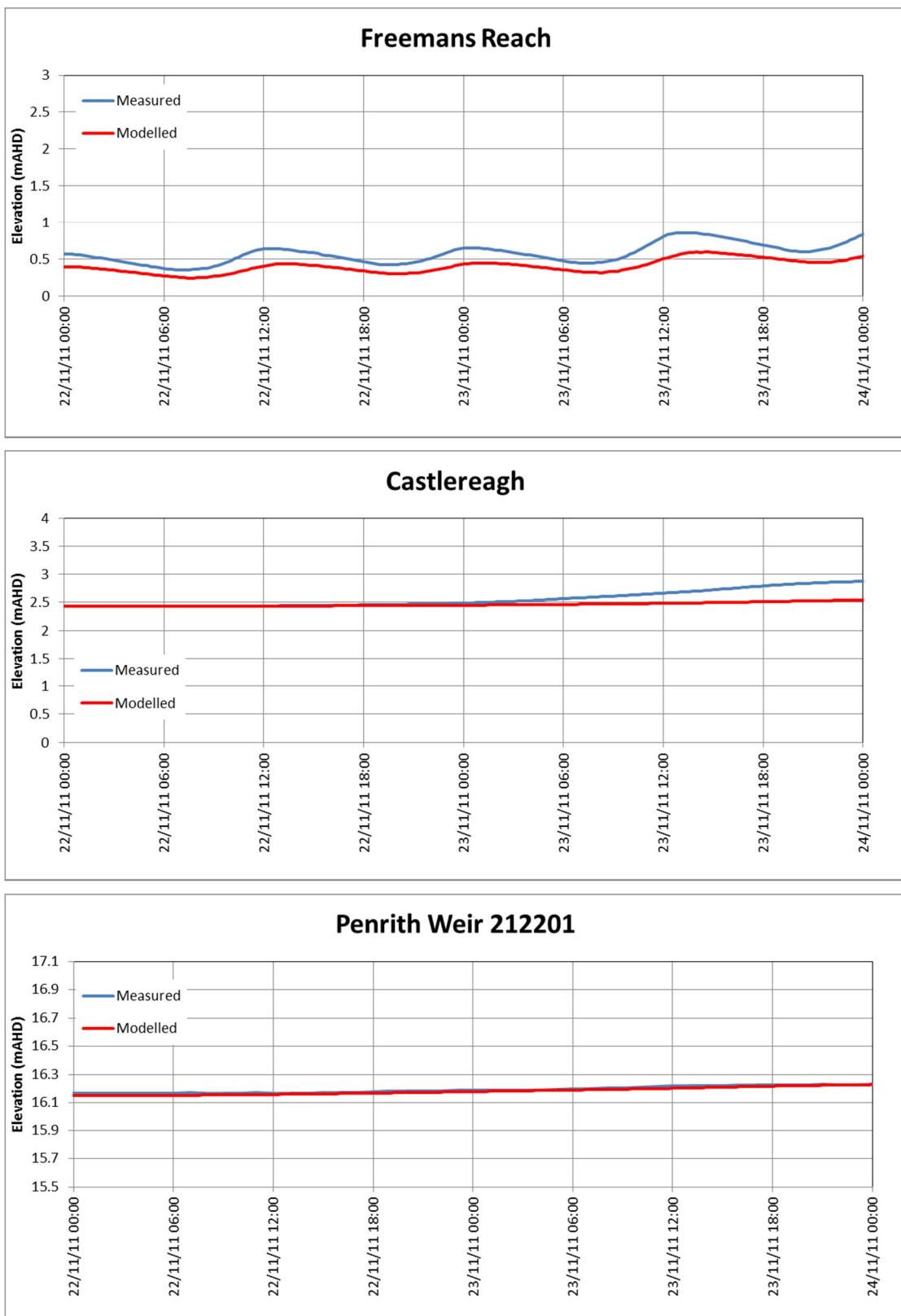
SINCLAIR KNIGHT MERZ

Water Quality Modelling of the Hawkesbury-Nepean River System



■ **Figure 13-2 (Cont.) Water Level Calibration 2011 (Sackville, Ebenezer, Windsor) – Spring Tide**

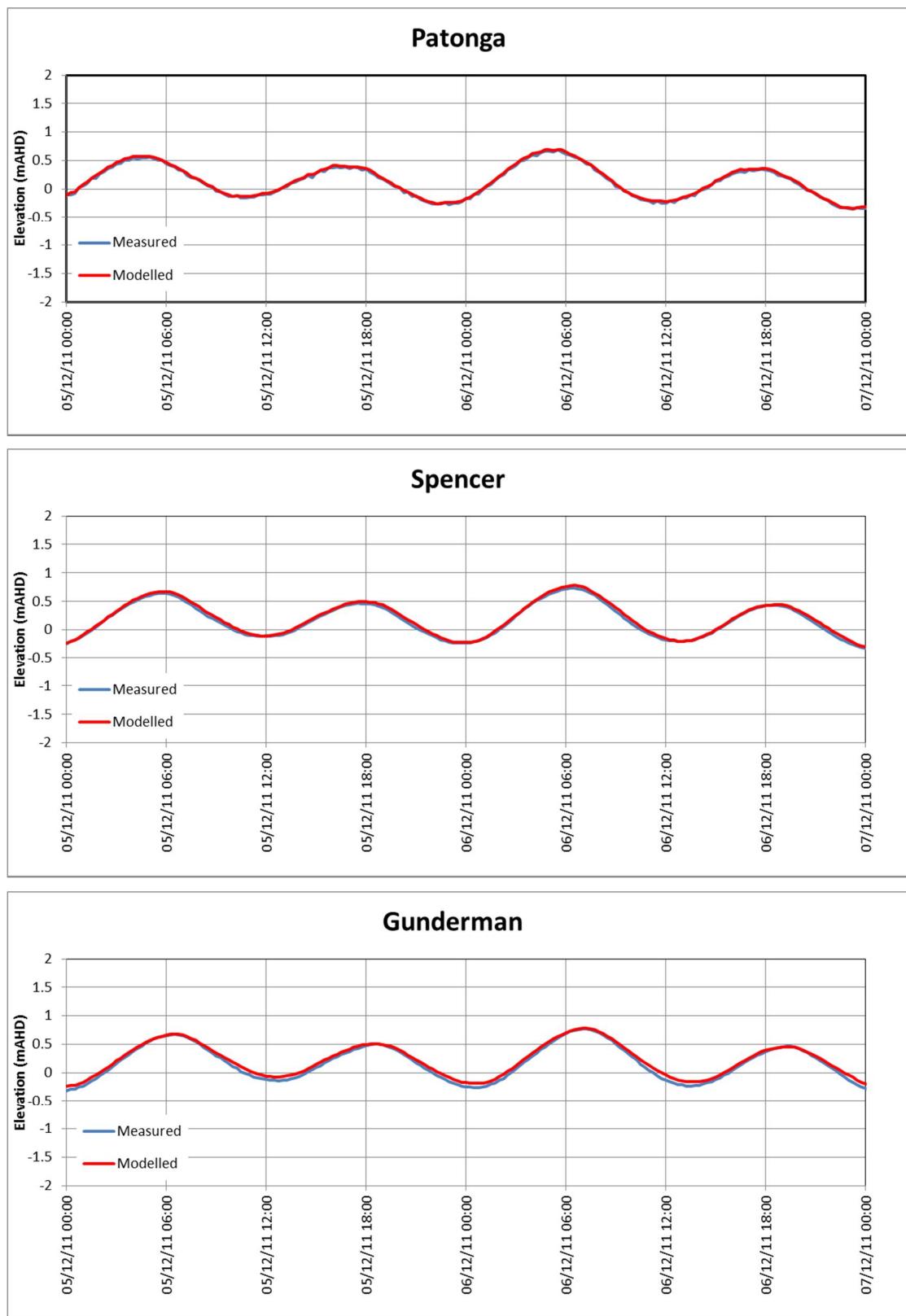
SINCLAIR KNIGHT MERZ



■ **Figure 13-2 (Cont.) Water Level Calibration 2011 (Freemans Reach, Castlereagh, Penrith Weir) – Spring Tide**

SINCLAIR KNIGHT MERZ

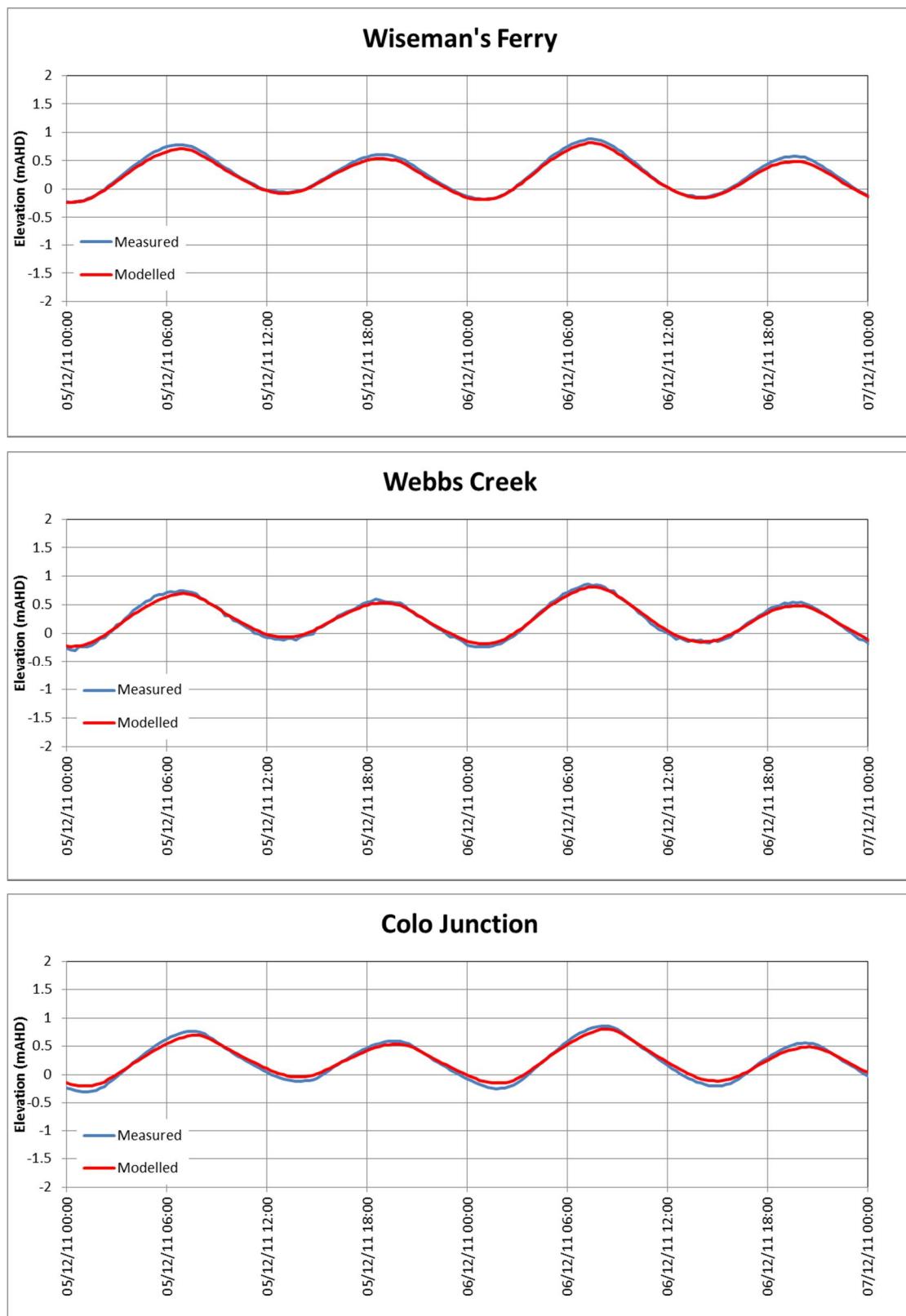
Water Quality Modelling of the Hawkesbury-Nepean River System



■ **Figure 13-3 Water Level Calibration 2011 (Patonga, Spencer, Gunderman) – Neap Tide**

SINCLAIR KNIGHT MERZ

Water Quality Modelling of the Hawkesbury-Nepean River System

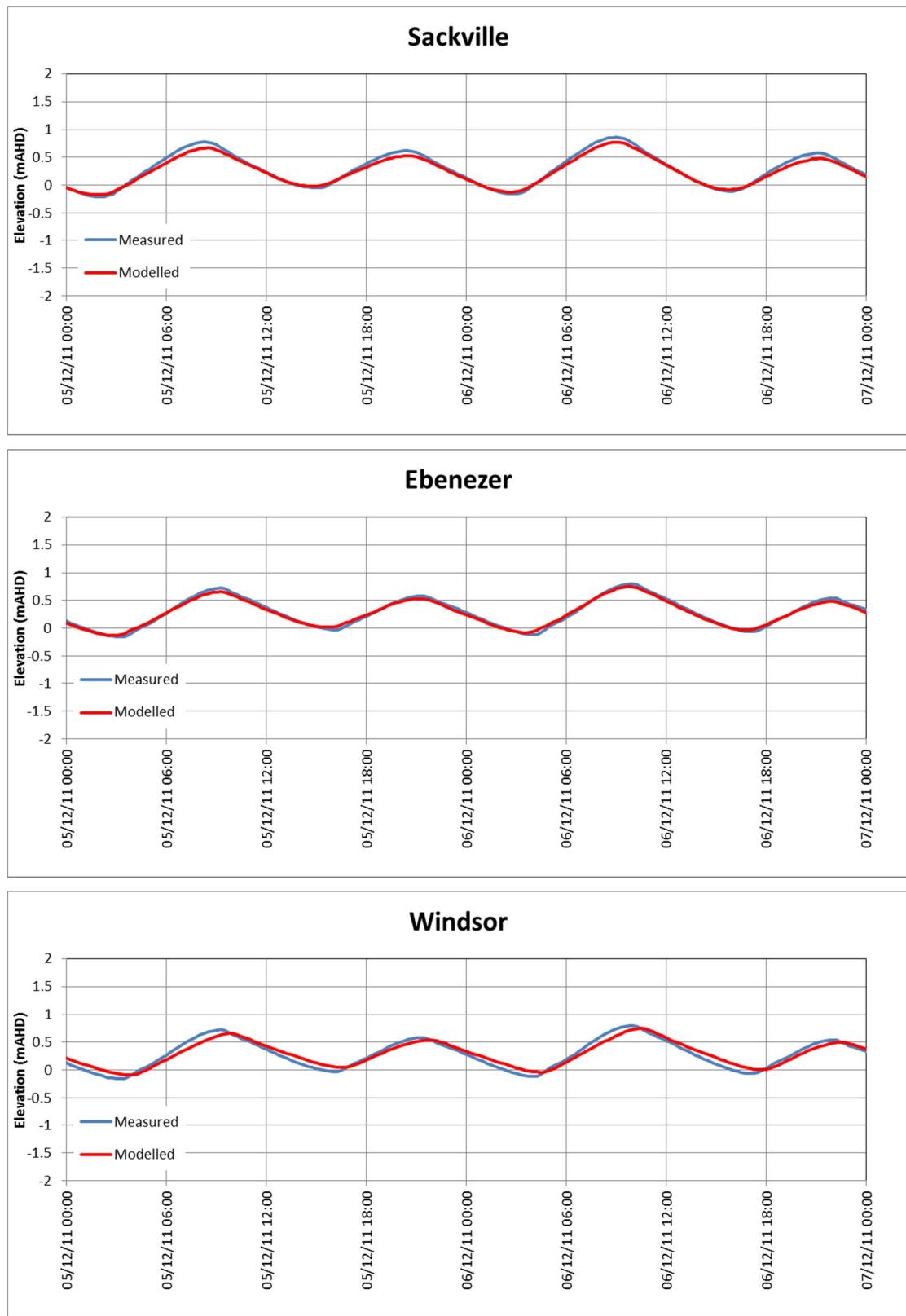


■ **Figure 13-3 (Cont.) Water Level Calibration 2011 (Wiseman's Ferry, Webbs Creek, Colo Junction) – Neap Tide**

SINCLAIR KNIGHT MERZ

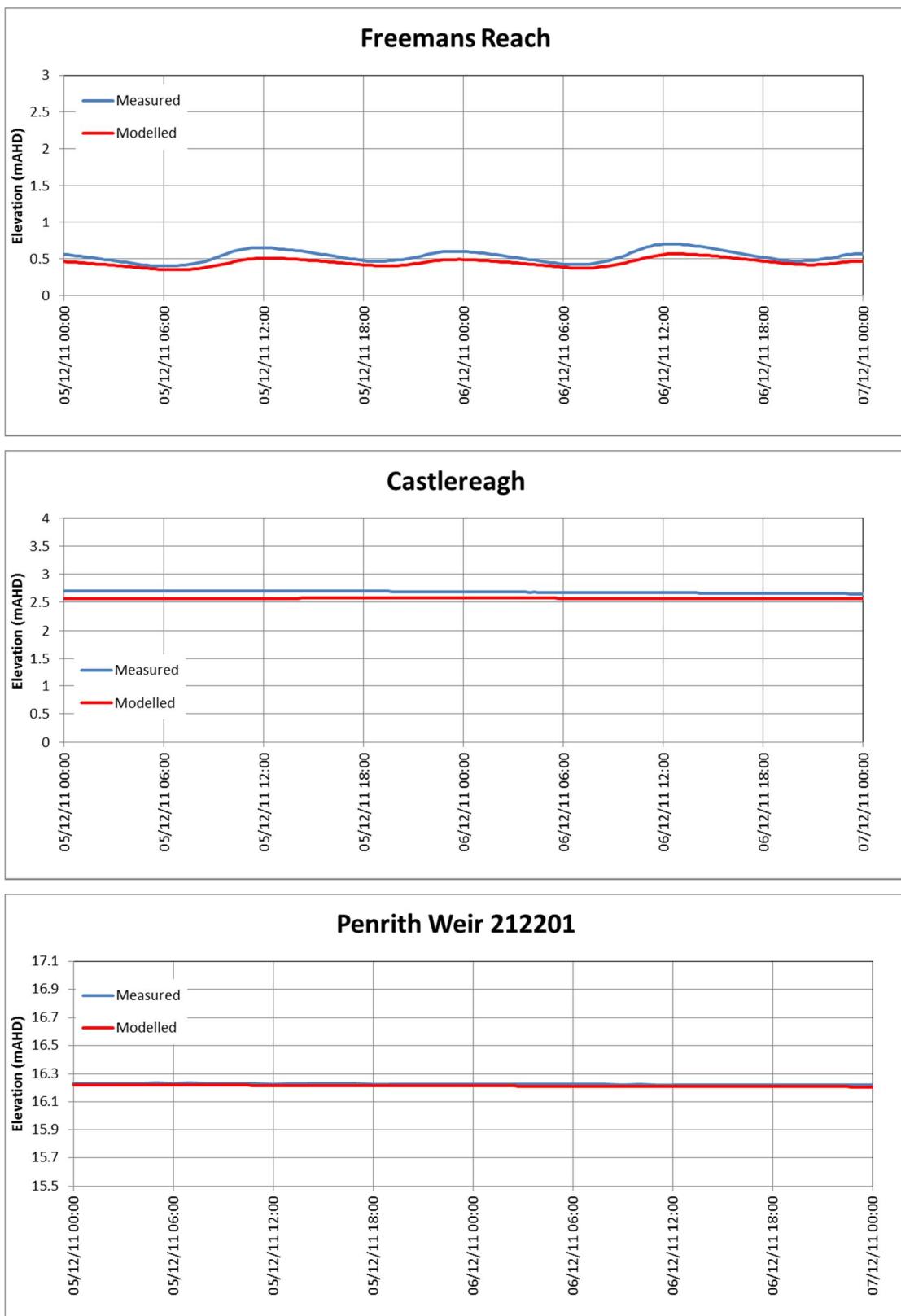


Water Quality Modelling of the Hawkesbury-Nepean River System



■ **Figure 13-3 (Cont.) Water Level Calibration 2011 (Sackville, Ebenezer, Windsor) – Neap Tide**

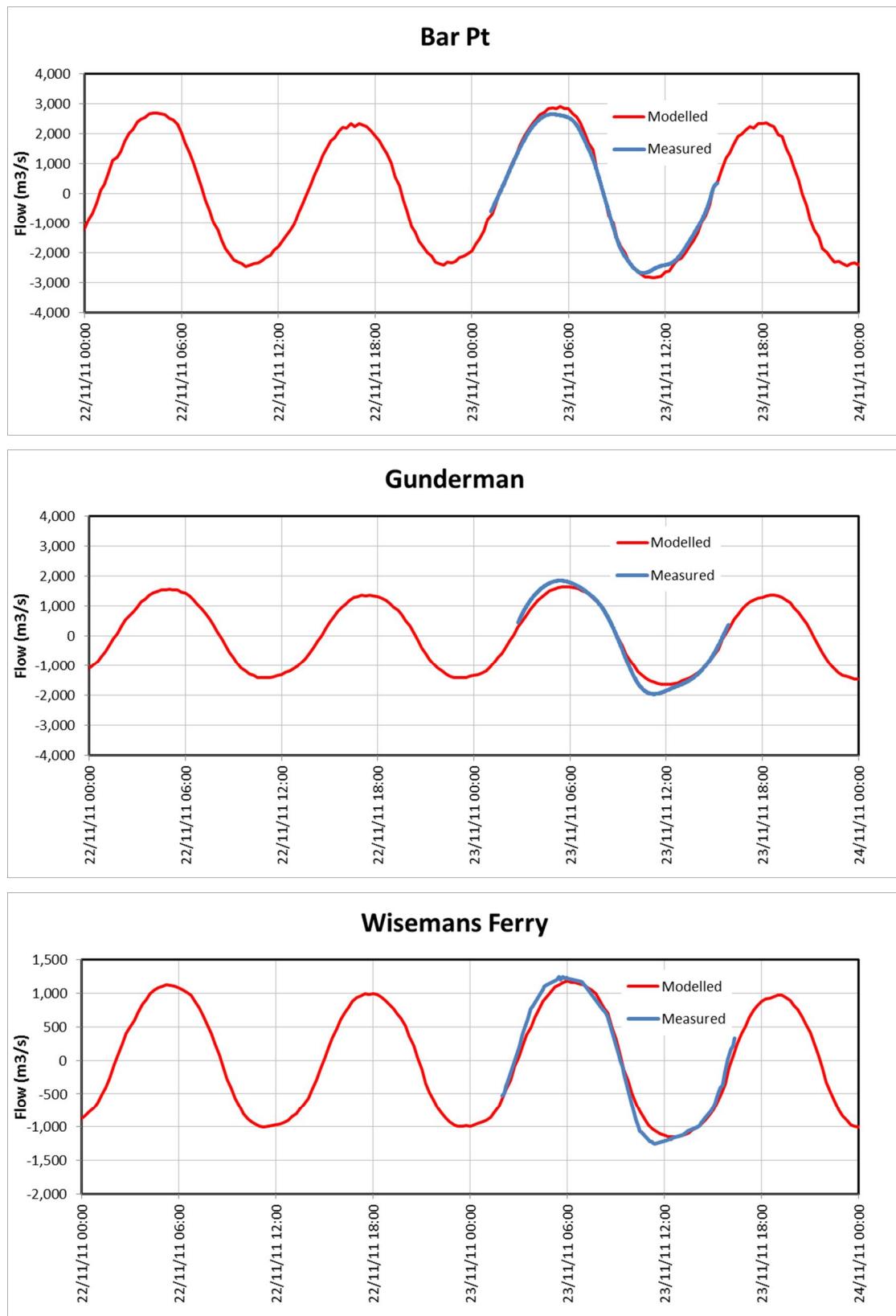
SINCLAIR KNIGHT MERZ



■ **Figure 13-3 (Cont.) Water Level Calibration 2011 (Freemans Reach, Castlereagh, Penrith Weir) – Neap Tide**

SINCLAIR KNIGHT MERZ

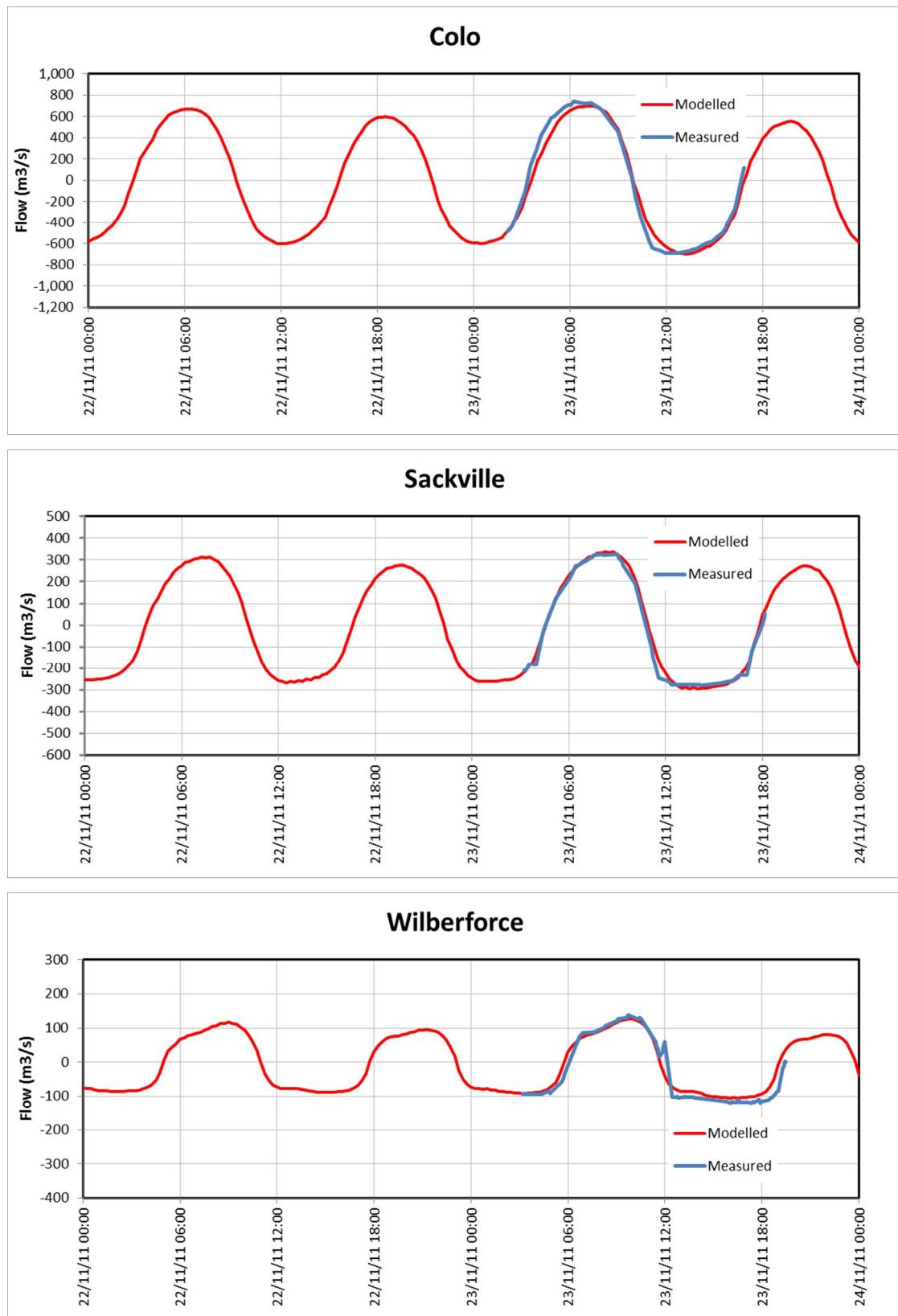
Water Quality Modelling of the Hawkesbury-Nepean River System



■ **Figure 13-4 ADCP CMP Flow Calibration (Bar Point, Gunderman, Wiseman's Ferry) – 22 November to 7 December 2011**

SINCLAIR KNIGHT MERZ

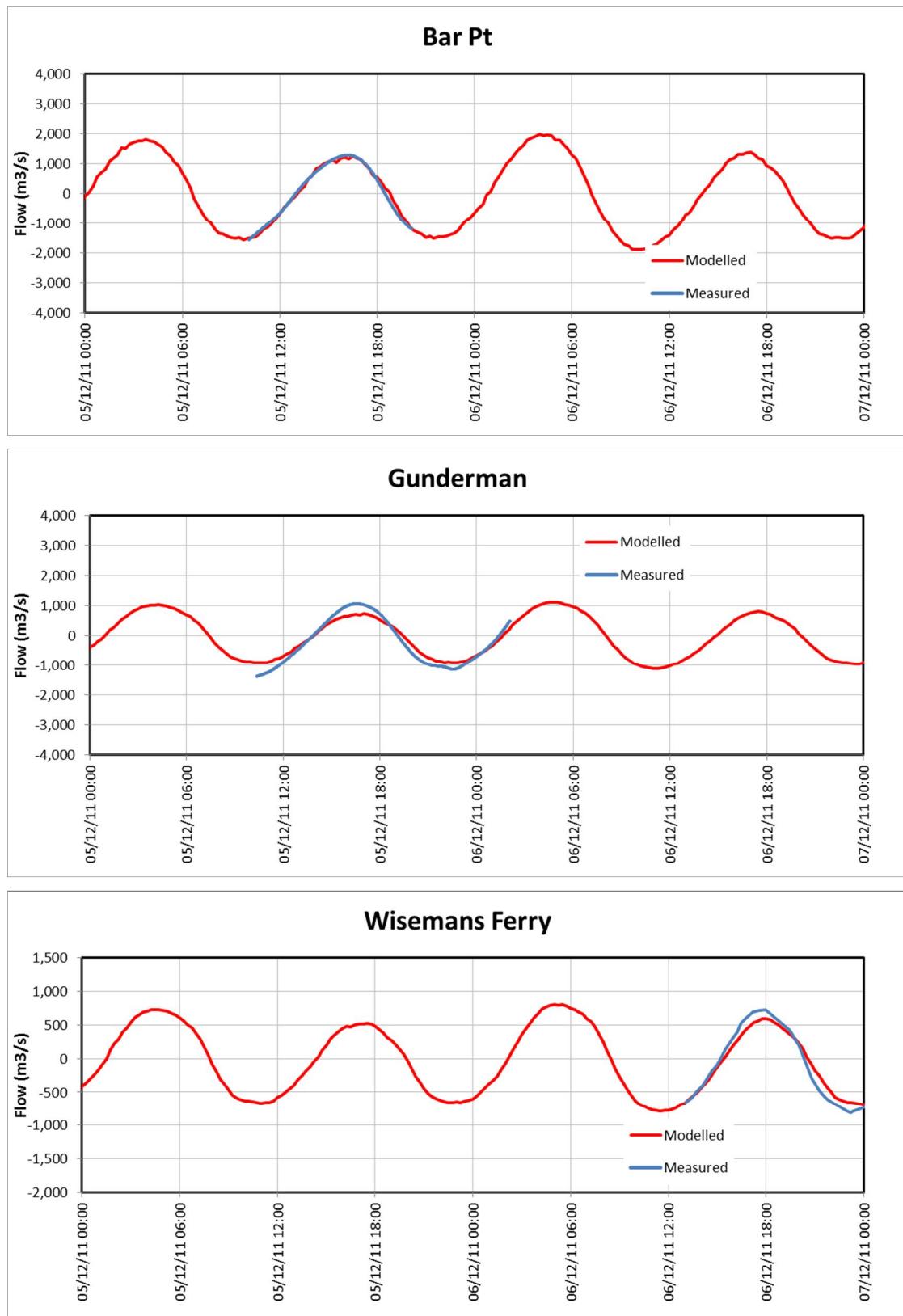
Water Quality Modelling of the Hawkesbury-Nepean River System



■ **Figure 13-4 (Cont.) ADCP CMP Flow Calibration 2011 (Colo, Sackville, Wilberforce) – 22 November to 7 December 2011**

SINCLAIR KNIGHT MERZ

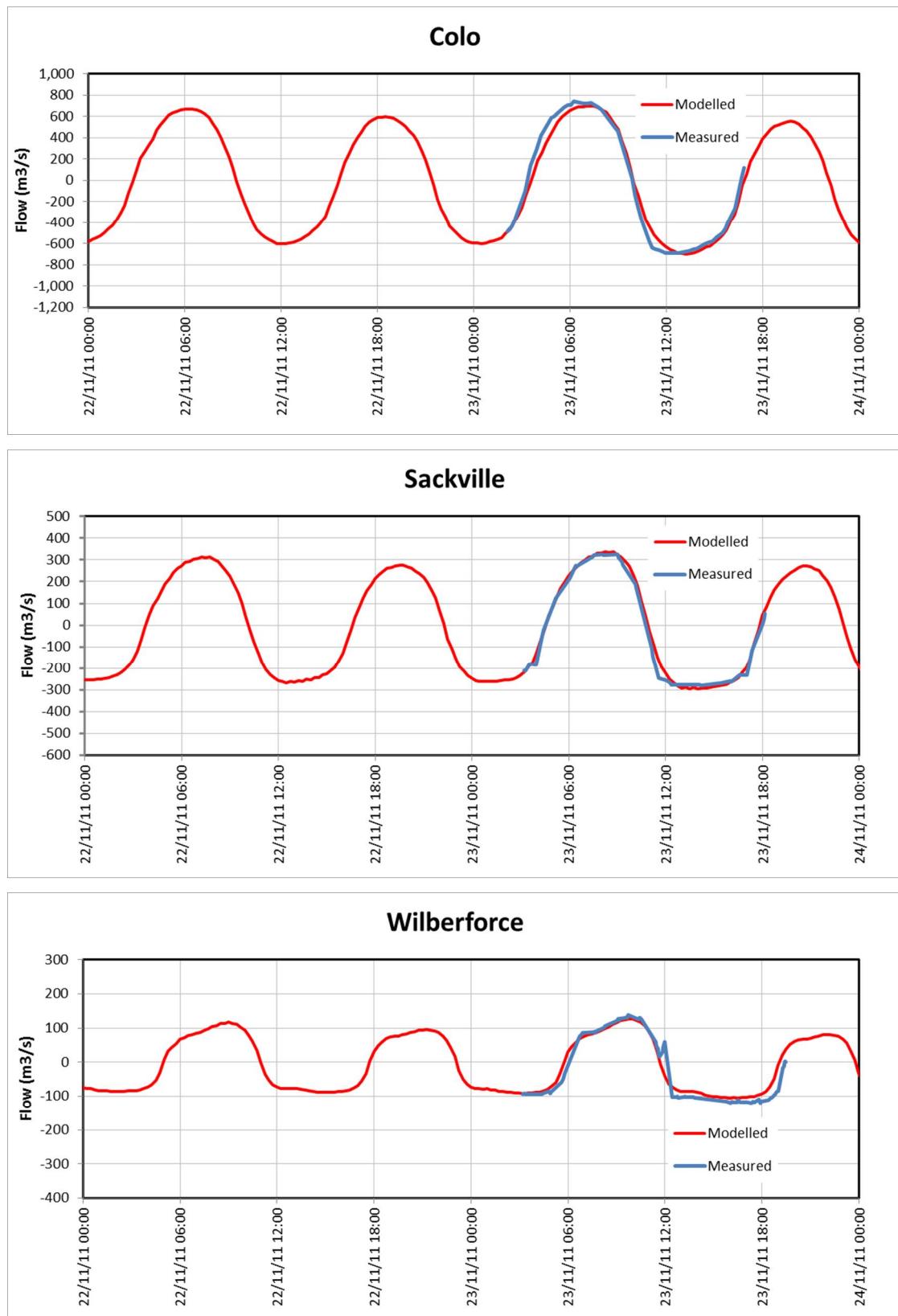
Water Quality Modelling of the Hawkesbury-Nepean River System



■ **Figure 13-5 ADCP CMP Flow Calibration 2011 (Bar Point, Gunderman, Wiseman's Ferry) – Spring Tide**

SINCLAIR KNIGHT MERZ

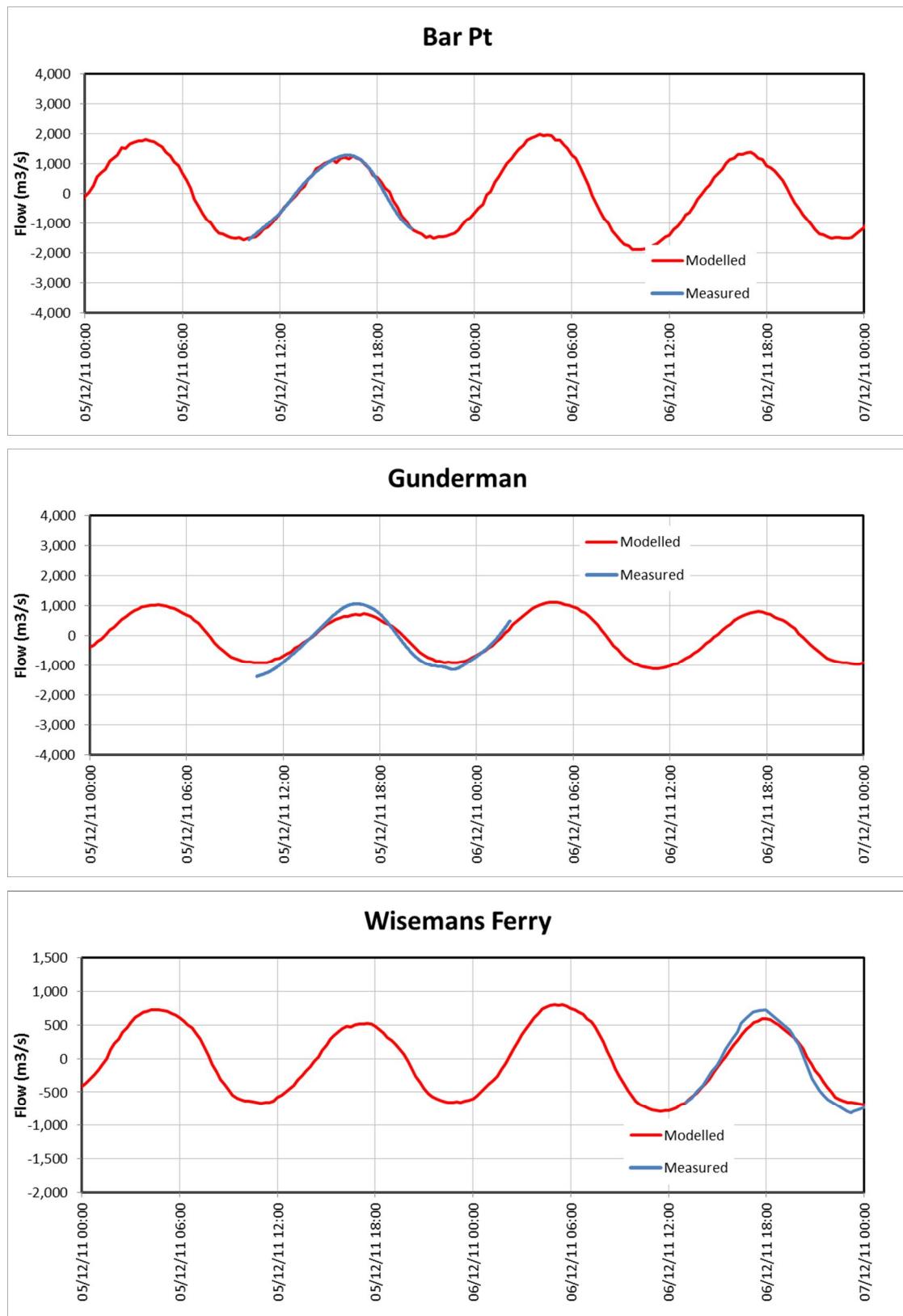
Water Quality Modelling of the Hawkesbury-Nepean River System



■ **Figure 13-5 (Cont.) ADCP CMP Flow Calibration 2011 (Colo, Sackville, Wilberforce) – Spring Tide**

SINCLAIR KNIGHT MERZ

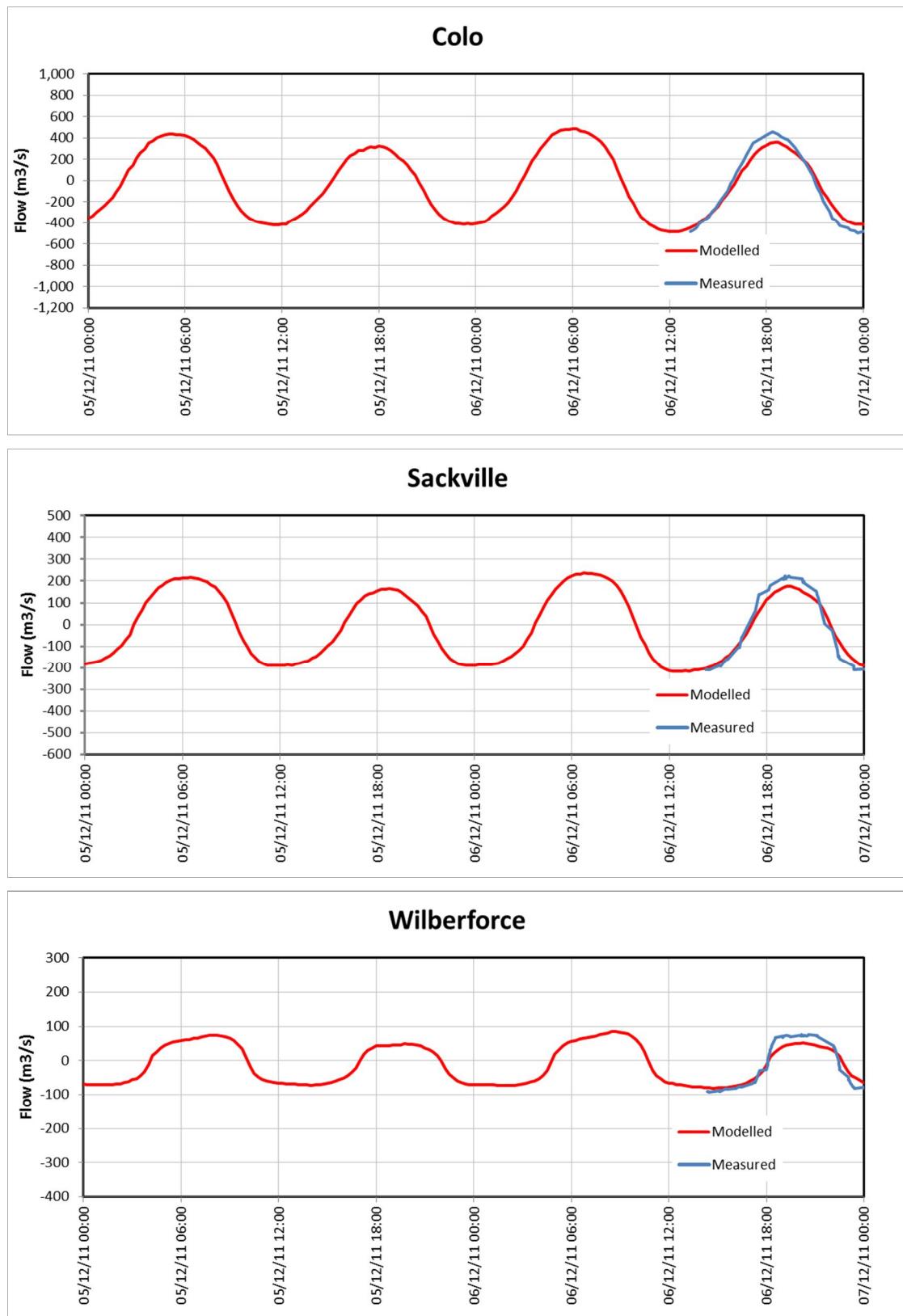
Water Quality Modelling of the Hawkesbury-Nepean River System



■ **Figure 13-6 CMP Flow Calibration 2011 (Bar Point, Gunderman, Wiseman's Ferry) – Neap Tide**

SINCLAIR KNIGHT MERZ

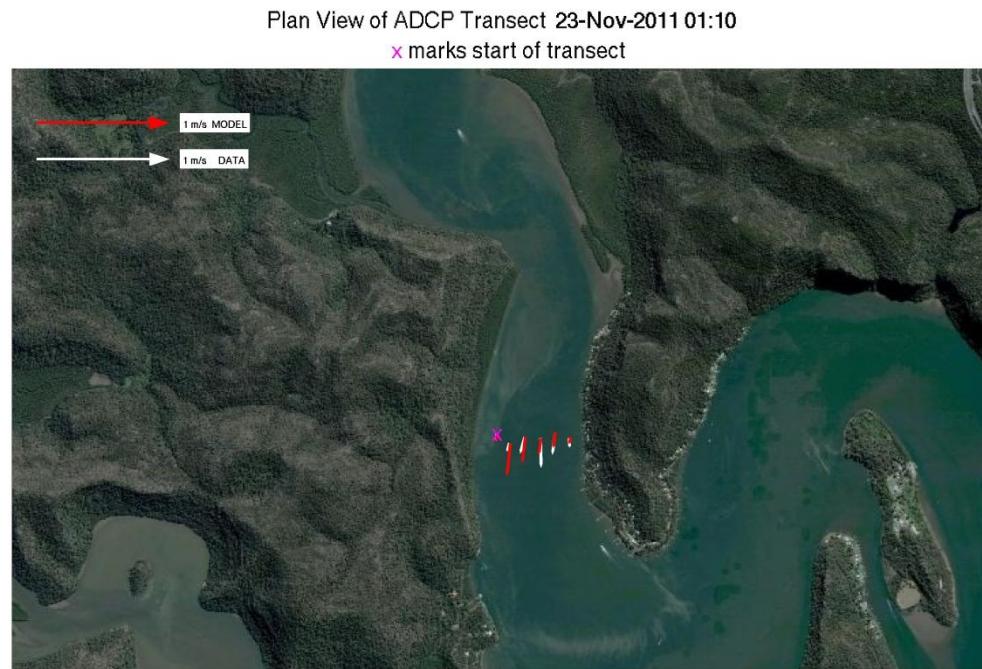
Water Quality Modelling of the Hawkesbury-Nepean River System



■ **Figure 13-6 (Cont.) ADCP CMP Flow Calibration 2011 (Colo, Sackville, Wilberforce) – Neap Tide**

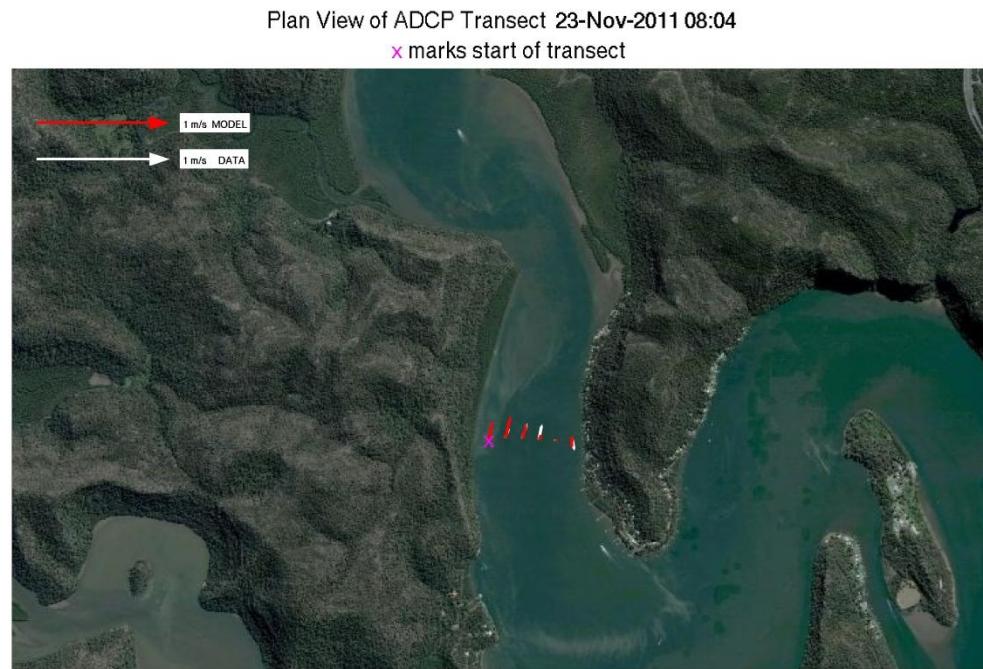
SINCLAIR KNIGHT MERZ

Water Quality Modelling of the Hawkesbury-Nepean River System



- **Figure 13-7 Comparisons of Depth-Averaged Velocities Transects across the Hawkesbury River at Bar Point. Upper Panel: Transect Collected on 23/11/11 01:10 (Slack Water). Lower Panel: Transect Collected on 23/11/11 04:31 (Flood Peak).**

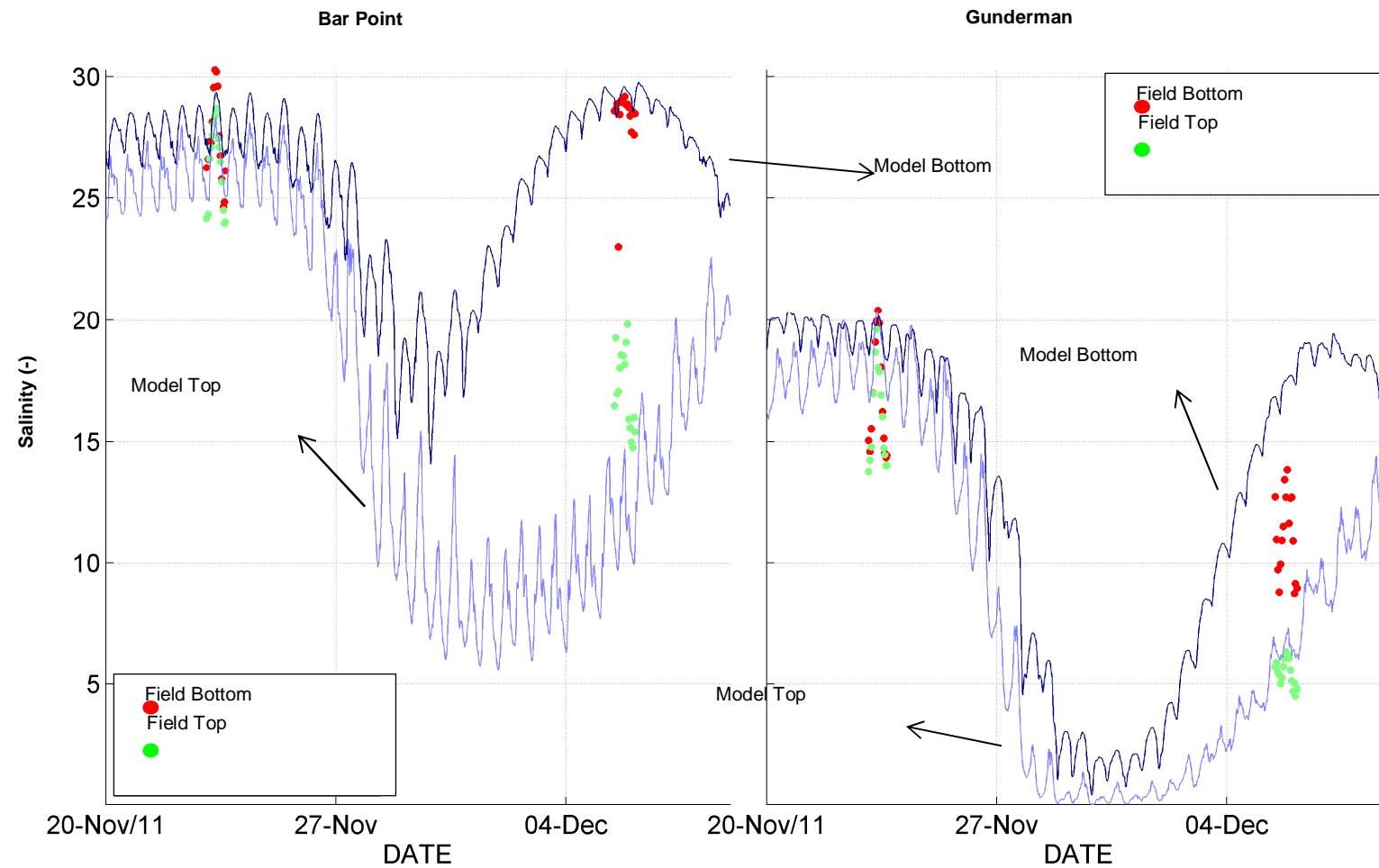
Water Quality Modelling of the Hawkesbury-Nepean River System



- **Figure 13-8 Comparisons of Depth-Averaged Velocities Transects across the Hawkesbury River at Bar Point. Upper Panel: Transect Collected on 23/11/11 08:04 (Slack Water). Lower Panel: Transect Collected on 23/11/11 11:33 (Peak Ebb Tide).**



Water Quality Modelling of the Hawkesbury-Nepean River System

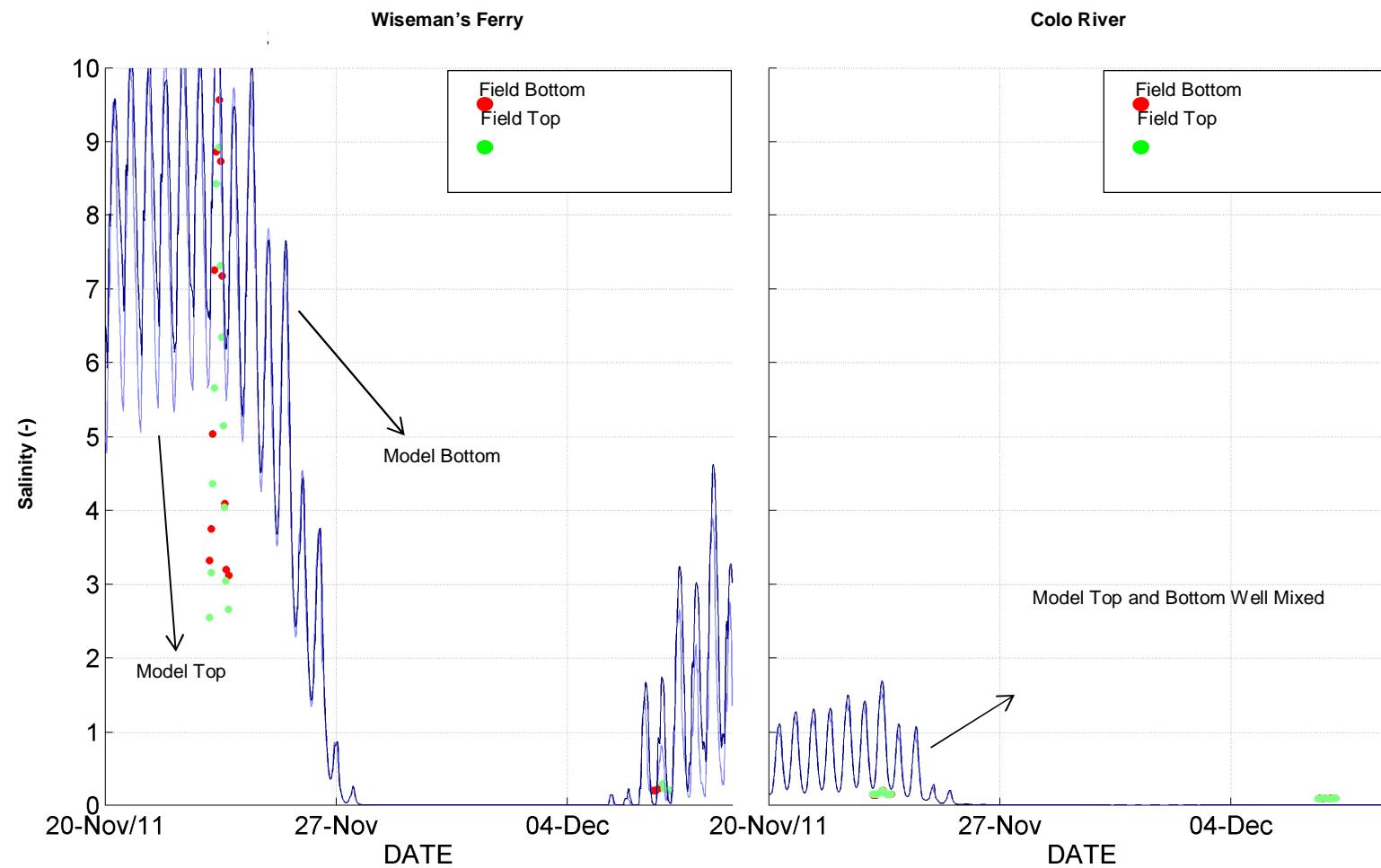


■ **Figure 13-9 ADCP CMP Salinity Calibration 2011**

SINCLAIR KNIGHT MERZ



Water Quality Modelling of the Hawkesbury-Nepean River System

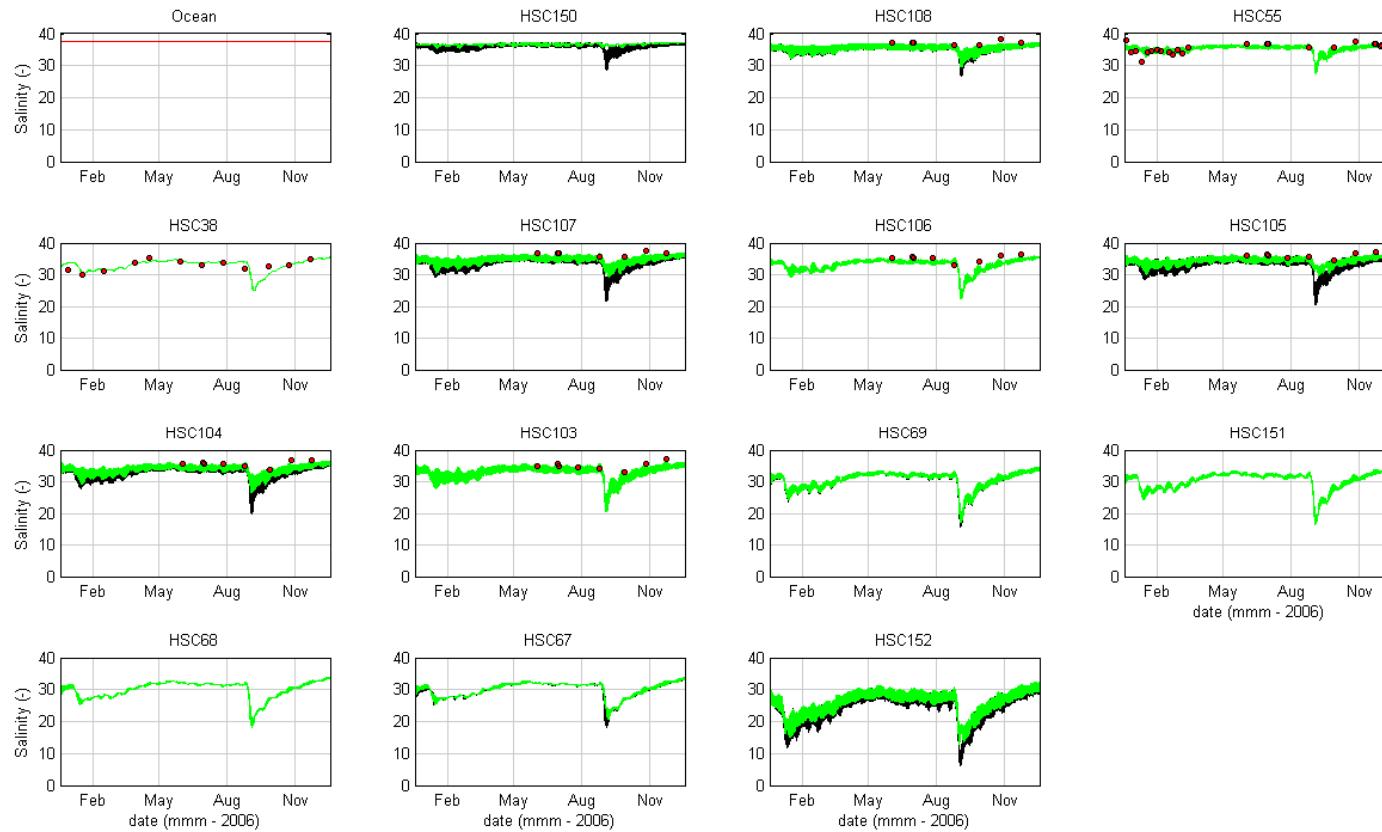


■ **Figure 13-9 (Cont.) ADCP CMP Salinity Calibration 2011**

SINCLAIR KNIGHT MERZ



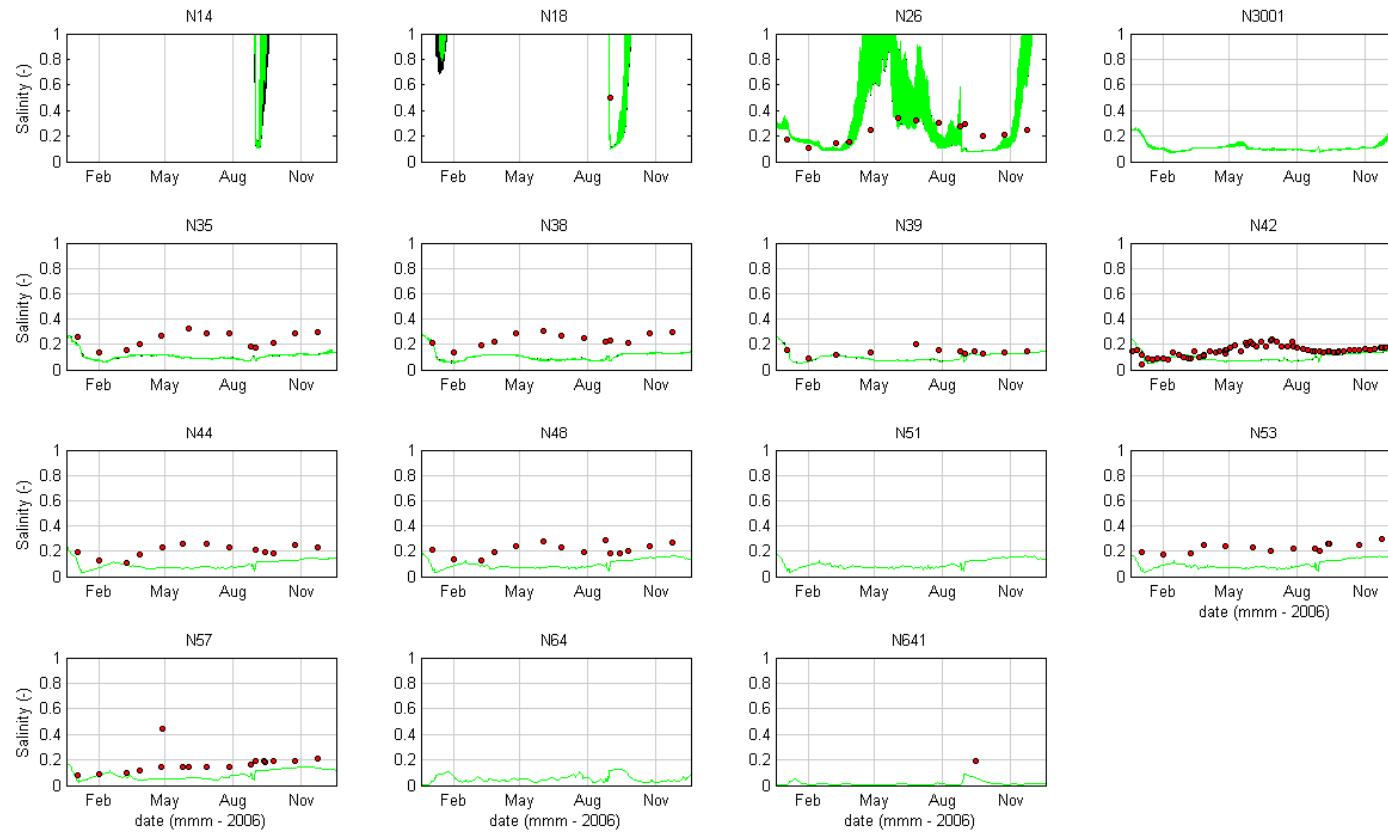
Water Quality Modelling of the Hawkesbury-Nepean River System



■ **Figure 13-10 Salinity Calibration 2006 (measured data (red), modelled surface (black) and modelled bottom (green))**



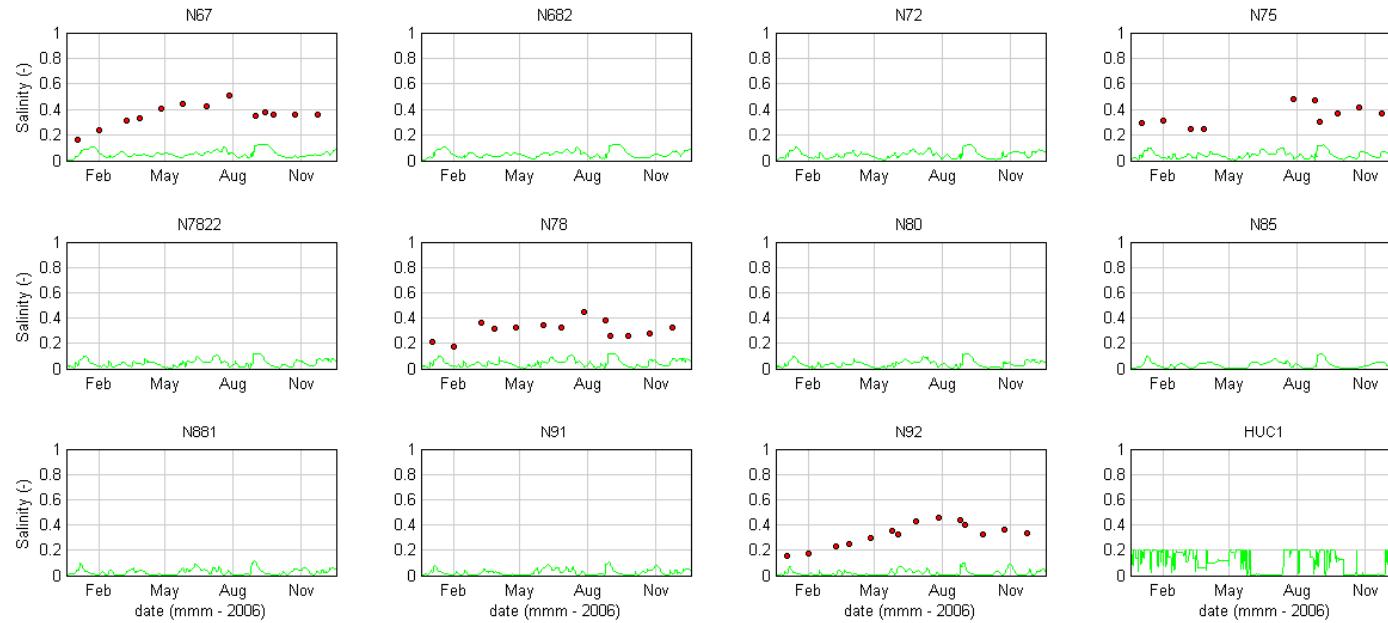
Water Quality Modelling of the Hawkesbury-Nepean River System



■ **Figure 13-10 (Cont.) Salinity Calibration 2006 (measured data (red), modelled surface (black) and modelled bottom (green))**



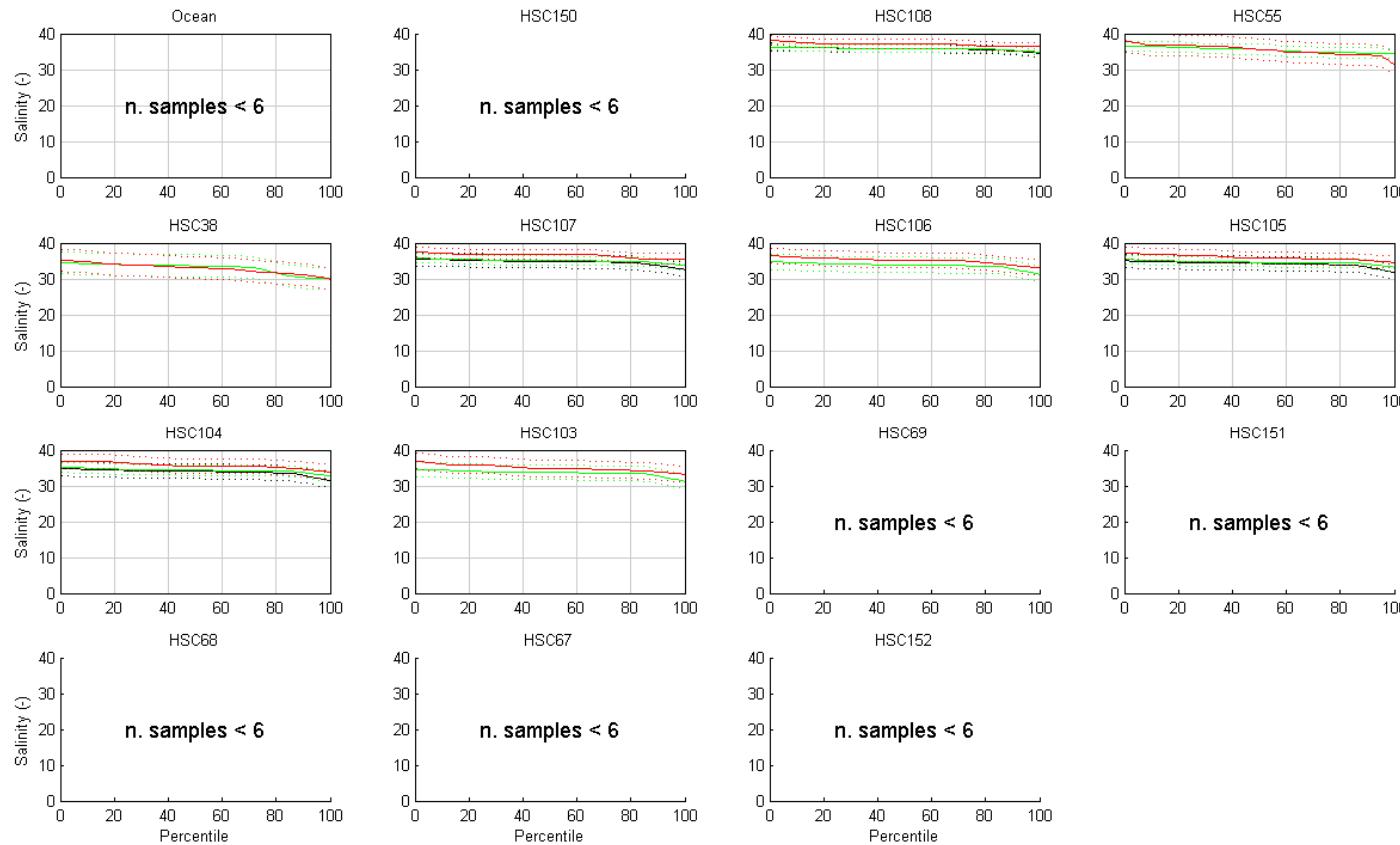
Water Quality Modelling of the Hawkesbury-Nepean River System



- **Figure 13-10 (Cont.) Salinity Calibration 2006 (measured data (red), modelled surface (black) and modelled bottom (green))**



Water Quality Modelling of the Hawkesbury-Nepean River System

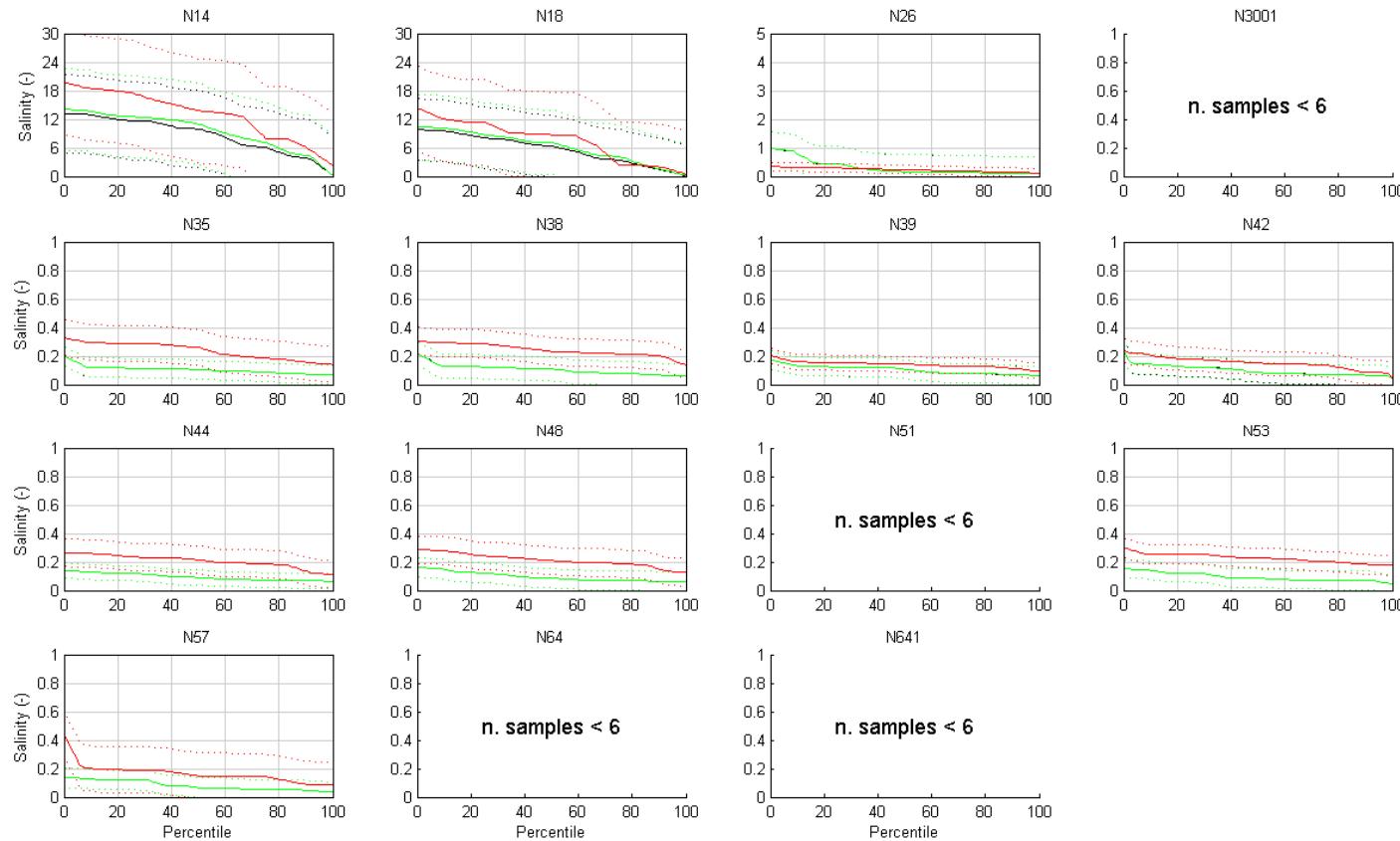


- **Figure 13-11 Exceedance Plots – Salinity Calibration 2006 (+/- 2SD) (measured data (red), modelled surface (black) and modelled bottom (green))**

SINCLAIR KNIGHT MERZ



Water Quality Modelling of the Hawkesbury-Nepean River System

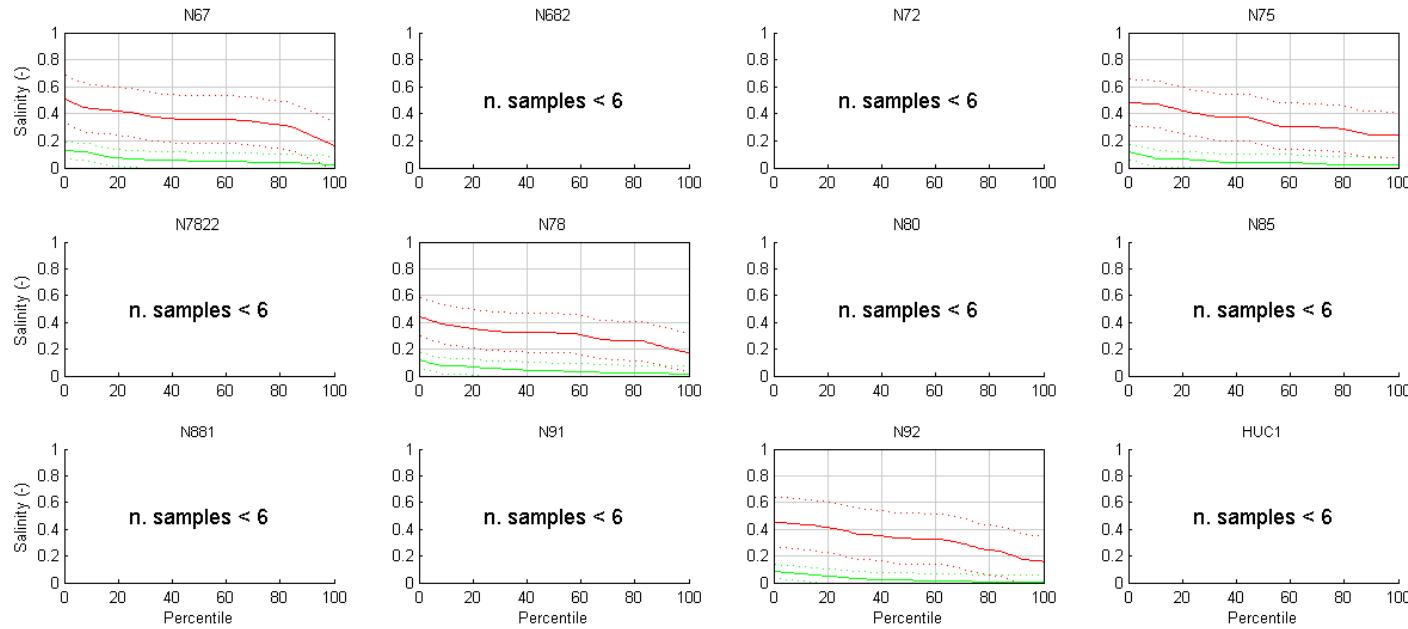


- **Figure 13-11 (Cont.) Exceedance Plots – Salinity Calibration 2006 (+/- 2SD) (measured data (red), modelled surface (black) and modelled bottom (green))**

SINCLAIR KNIGHT MERZ



Water Quality Modelling of the Hawkesbury-Nepean River System

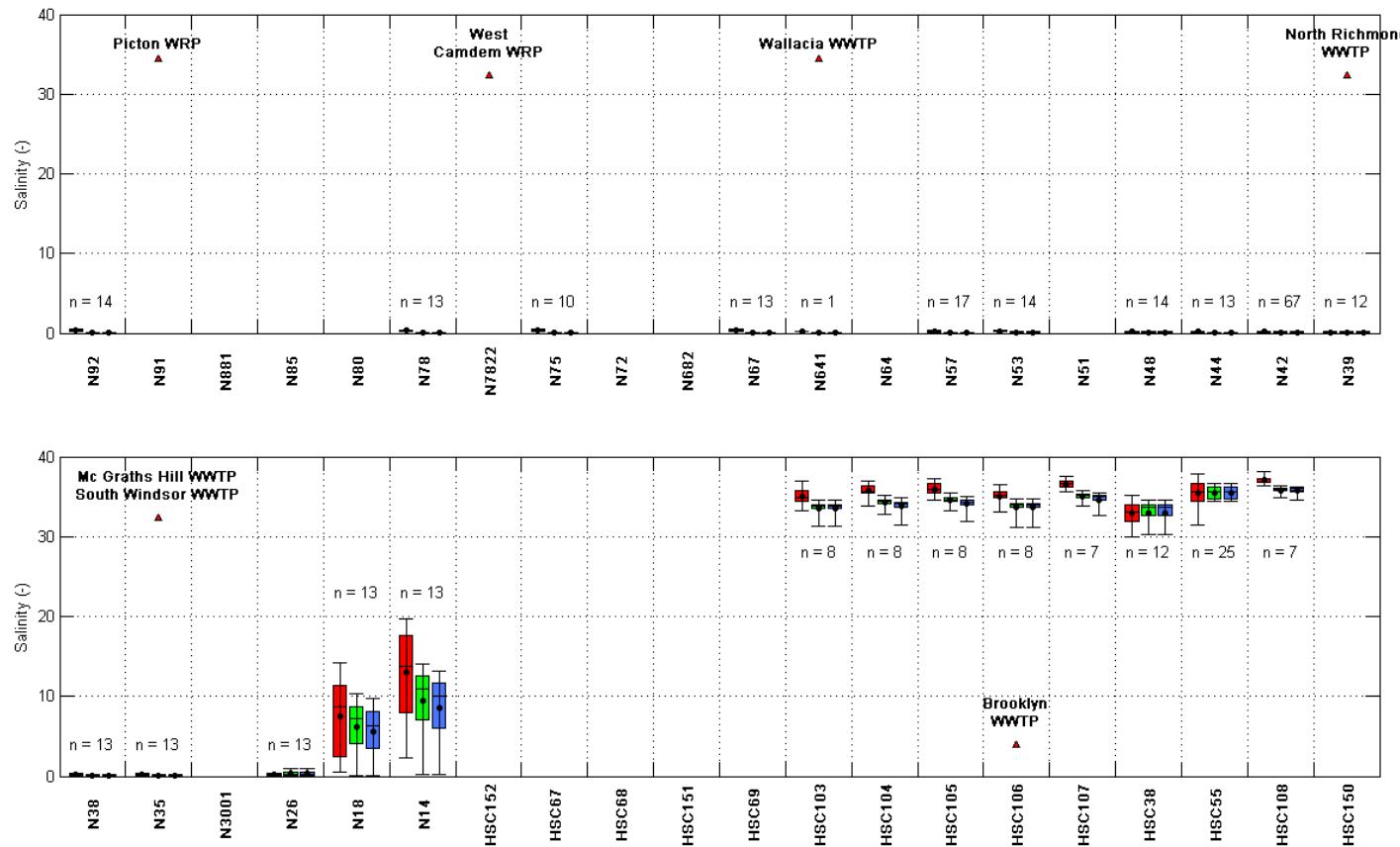


- Figure 13-11 (Cont.) Exceedance Plots – Salinity Calibration 2006 (+/- 2SD) (measured data (red), modelled surface (black) and modelled bottom (green))

SINCLAIR KNIGHT MERZ



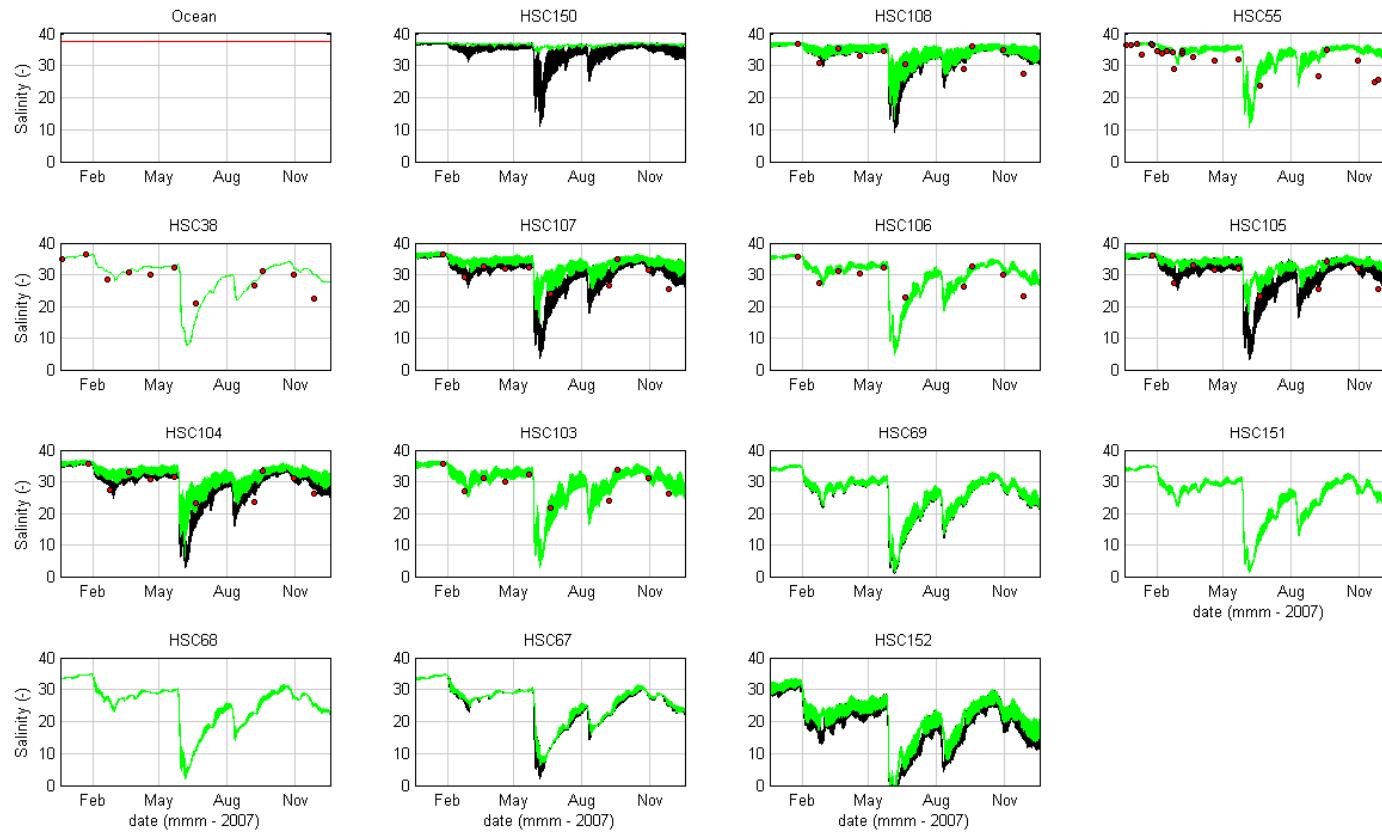
Water Quality Modelling of the Hawkesbury-Nepean River System



- **Figure 13-12 Box and Whisker Plots – Salinity Calibration 2006 (measured data (red), modelled surface (blue) and modelled bottom (green))**



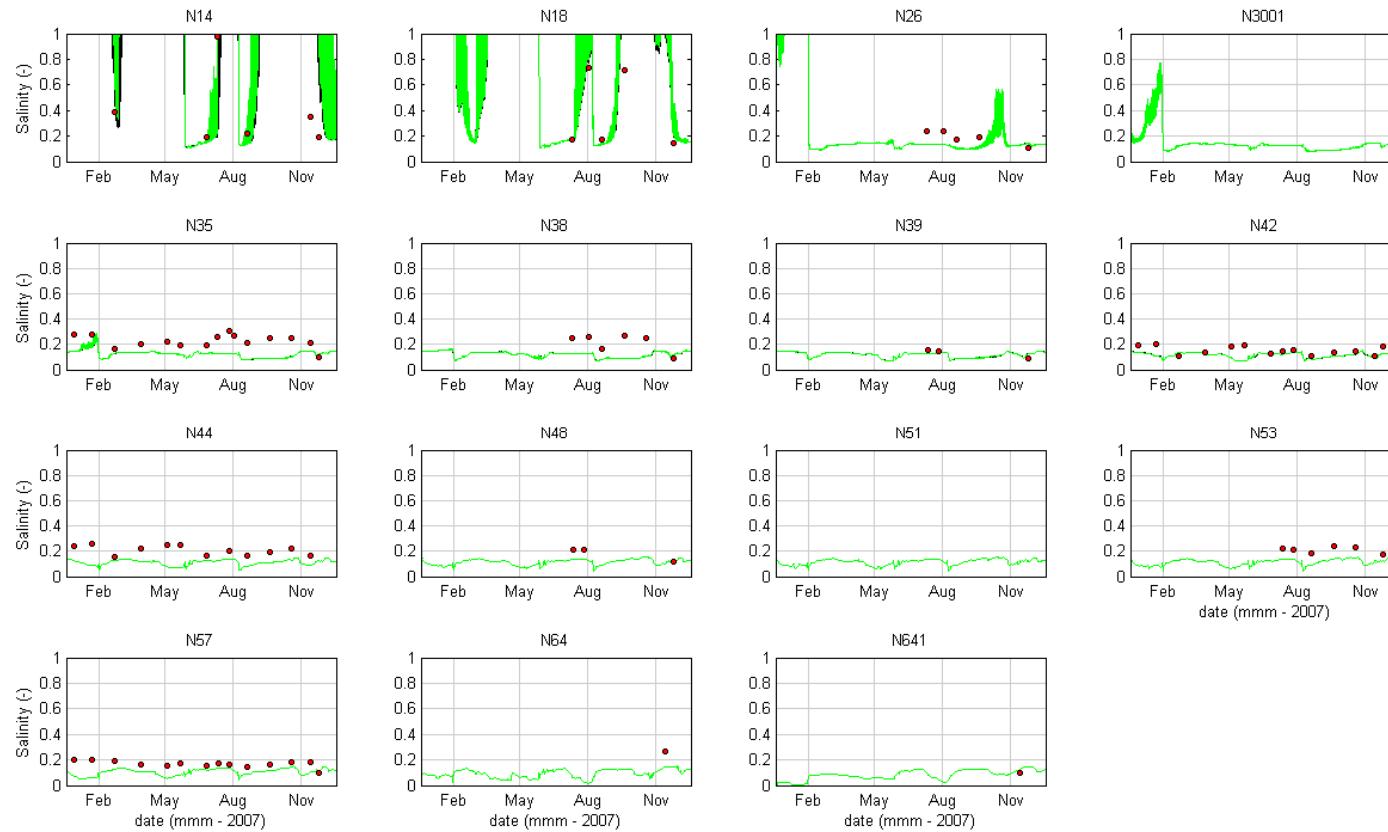
Water Quality Modelling of the Hawkesbury-Nepean River System



■ **Figure 13-13 Salinity Validation 2007 (measured data (red), modelled surface (black) and modelled bottom (green))**



Water Quality Modelling of the Hawkesbury-Nepean River System

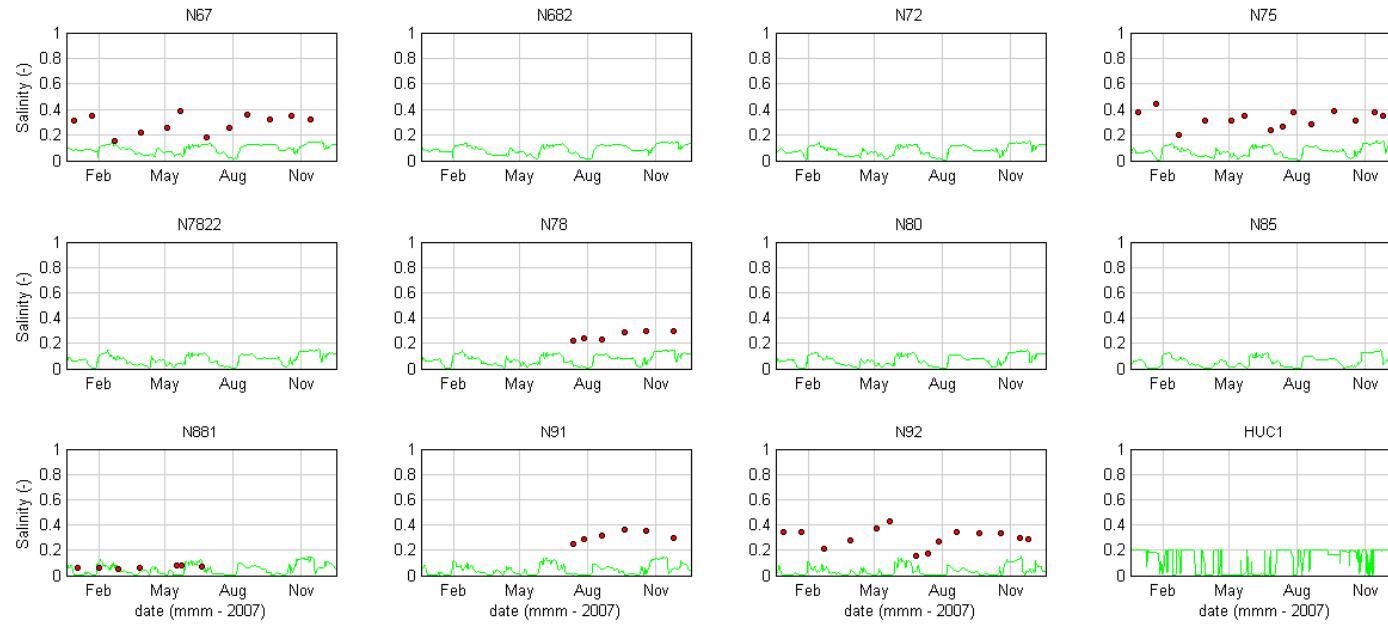


■ **Figure 13-13 (Cont.) Salinity Validation 2007 (measured data (red), modelled surface (black) and modelled bottom (green))**

SINCLAIR KNIGHT MERZ



Water Quality Modelling of the Hawkesbury-Nepean River System

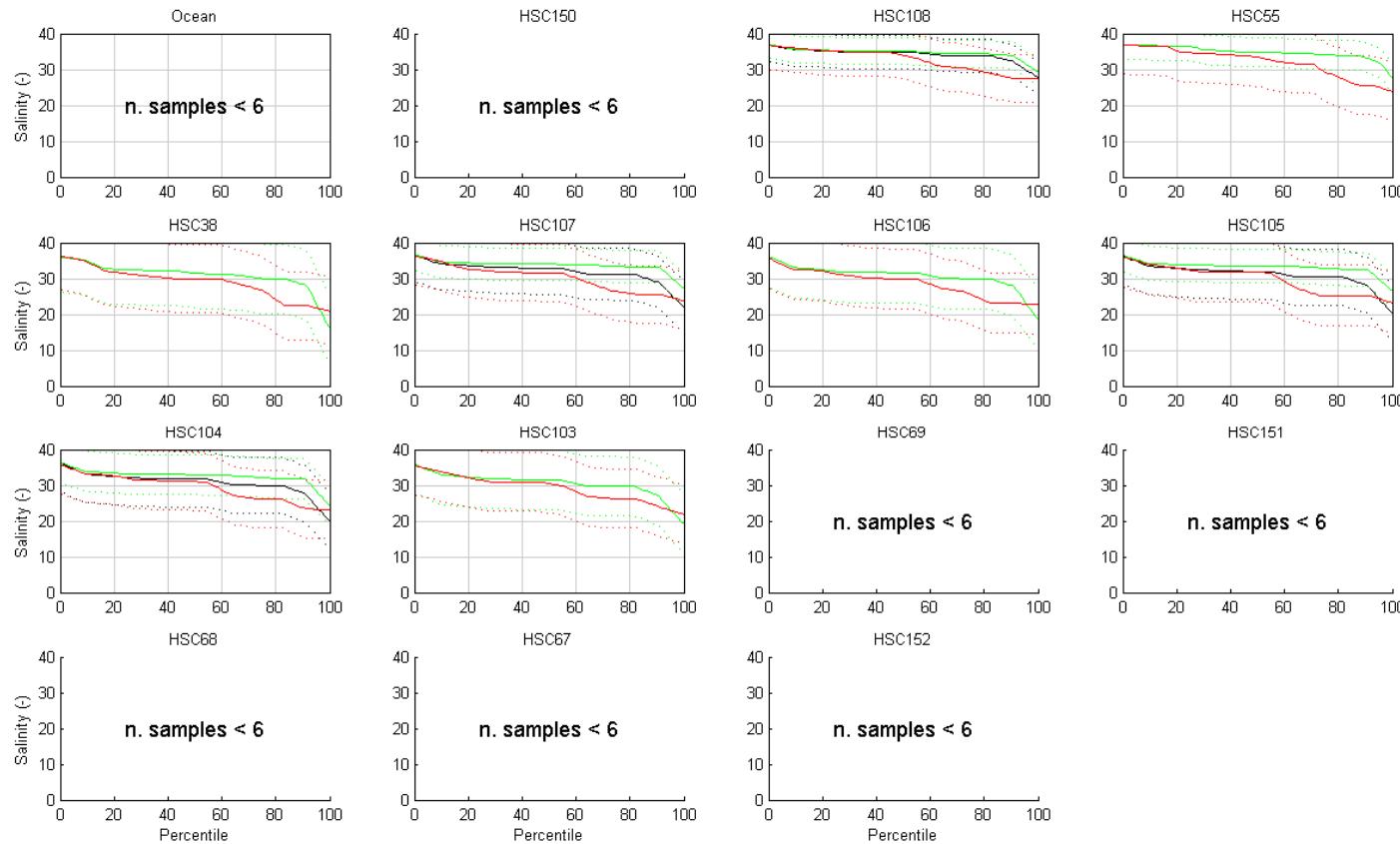


■ **Figure 13-13 (Cont.) Salinity Validation 2007 (measured data (red), modelled surface (black) and modelled bottom (green))**

SINCLAIR KNIGHT MERZ



Water Quality Modelling of the Hawkesbury-Nepean River System

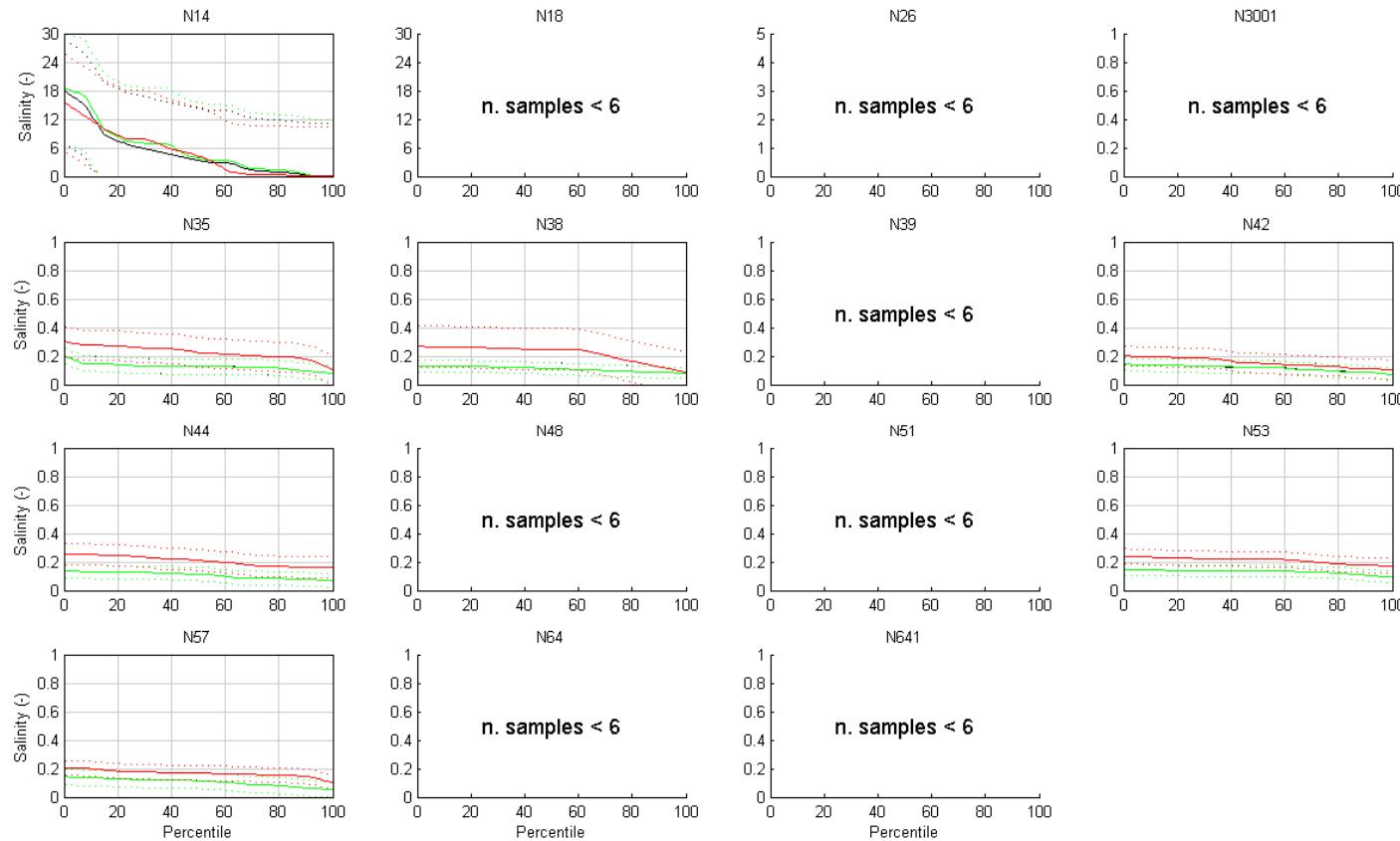


- **Figure 13-14 Exceedance Plots – Salinity Validation 2007(+/- 2SD) (measured data (red), modelled surface (black) and modelled bottom (green))**

SINCLAIR KNIGHT MERZ



Water Quality Modelling of the Hawkesbury-Nepean River System

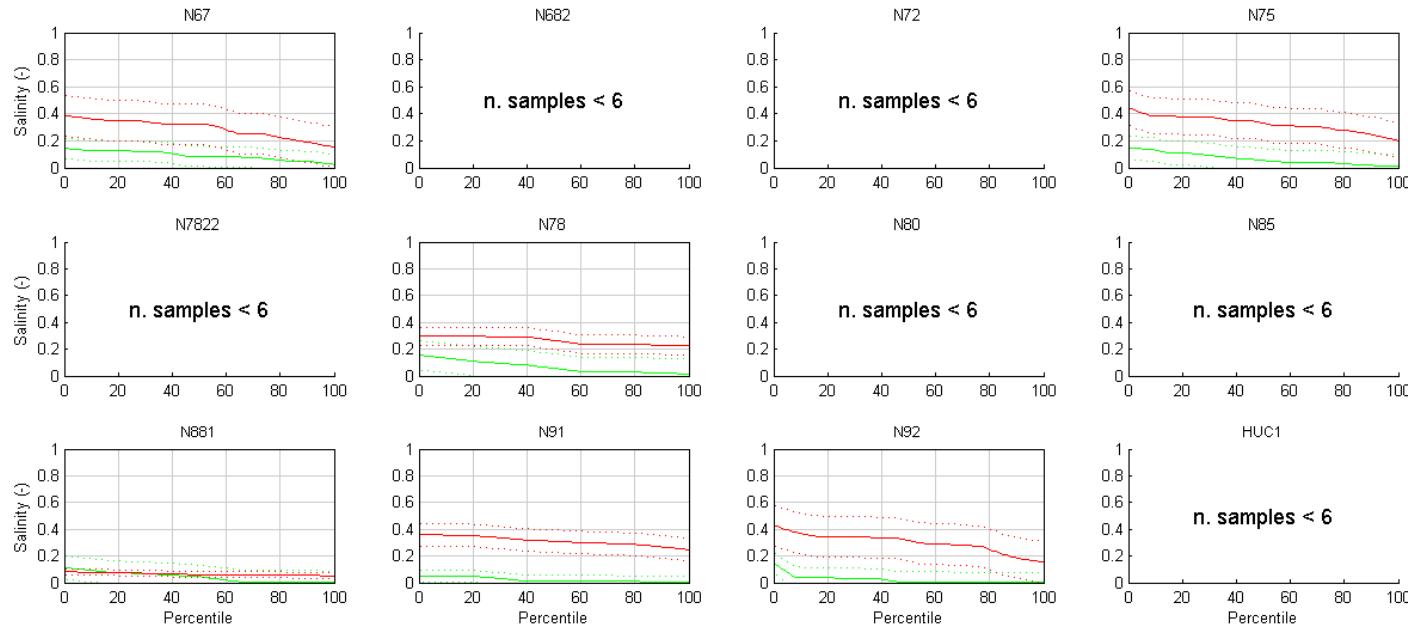


- **Figure 13-14 (Cont.) Exceedance Plots – Salinity Validation 2007(+/- 2SD) (measured data (red), modelled surface (black) and modelled bottom (green))**

SINCLAIR KNIGHT MERZ



Water Quality Modelling of the Hawkesbury-Nepean River System

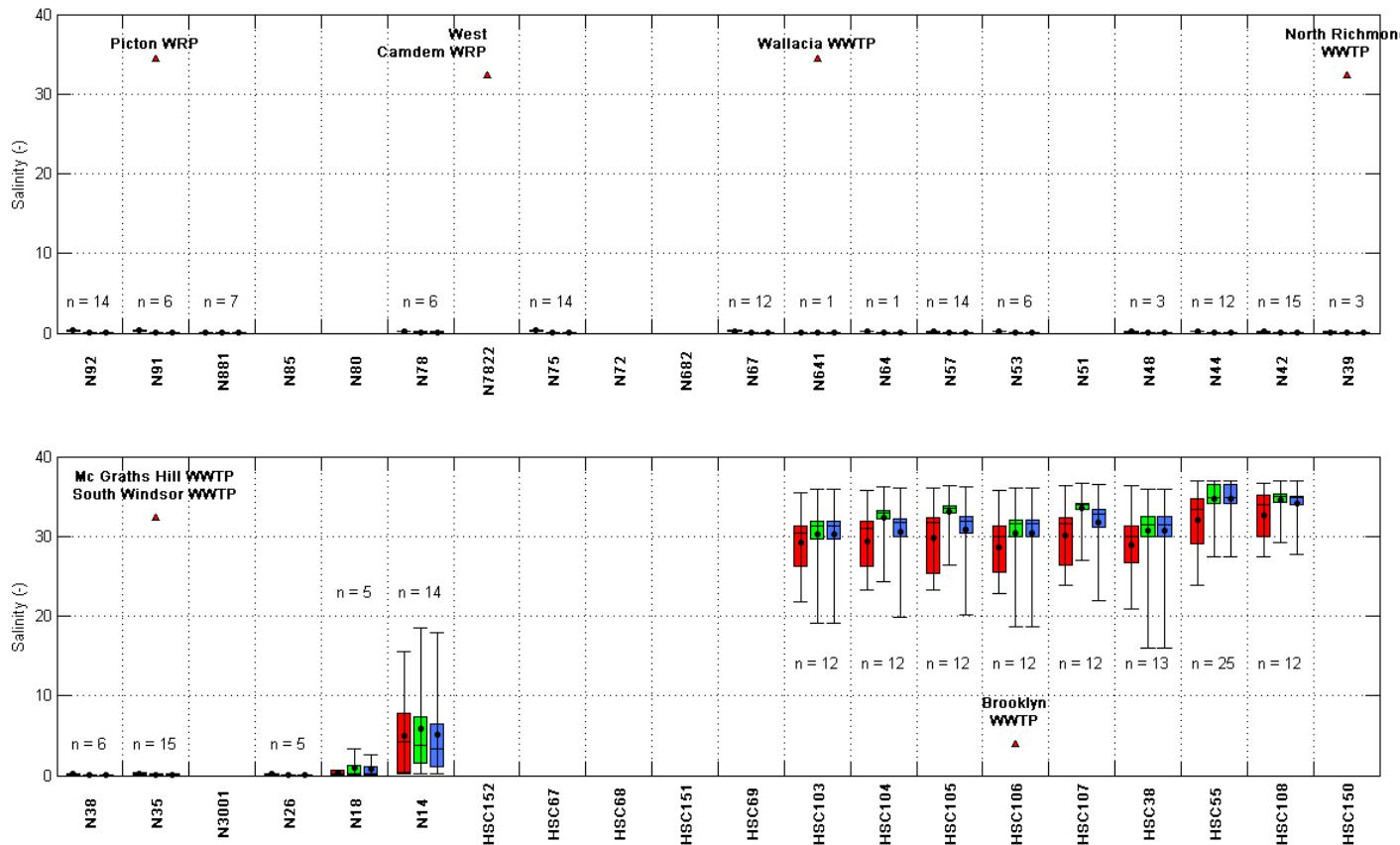


- Figure 13-14 (Cont.) Exceedance Plots – Salinity Validation 2007(+/- 2SD) (measured data (red), modelled surface (black) and modelled bottom (green))

SINCLAIR KNIGHT MERZ



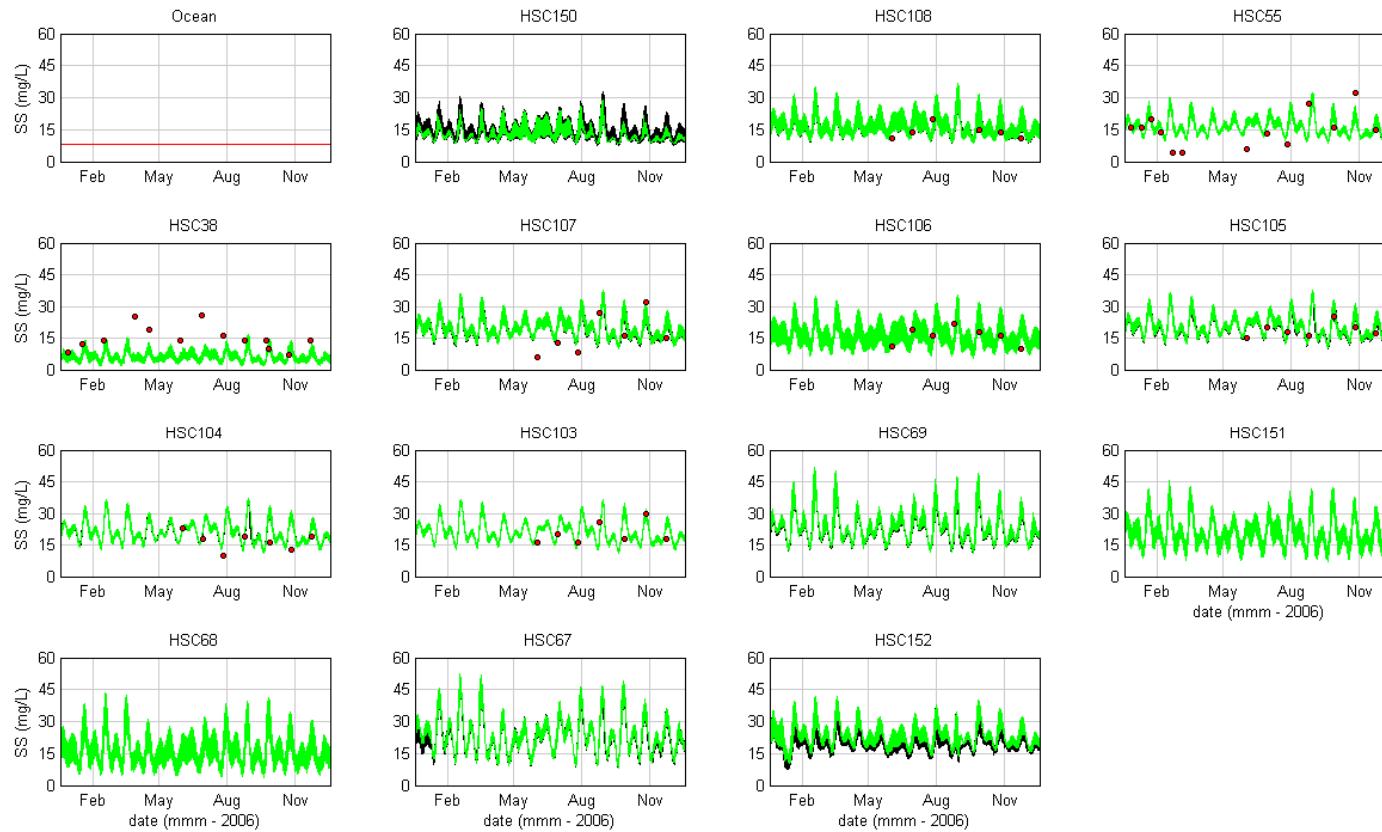
Water Quality Modelling of the Hawkesbury-Nepean River System



- **Figure 13-15 Box and Whisker Plots – Salinity Validation 2007 (measured data (red), modelled surface (blue) and modelled bottom (green))**



Water Quality Modelling of the Hawkesbury-Nepean River System

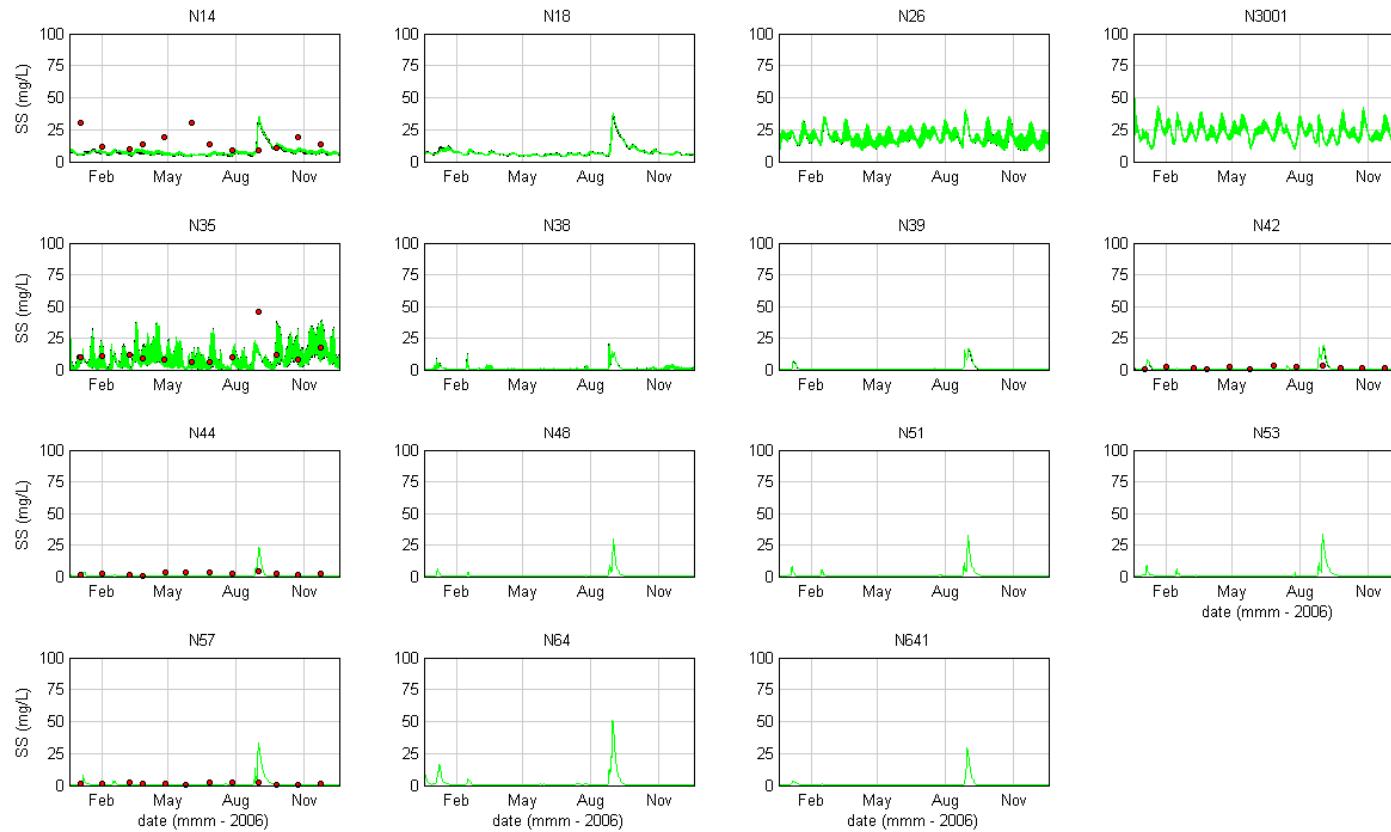


■ **Figure 13-16 Sediment Calibration 2006 (measured data (red), modelled surface (black) and modelled bottom (green))**

SINCLAIR KNIGHT MERZ



Water Quality Modelling of the Hawkesbury-Nepean River System

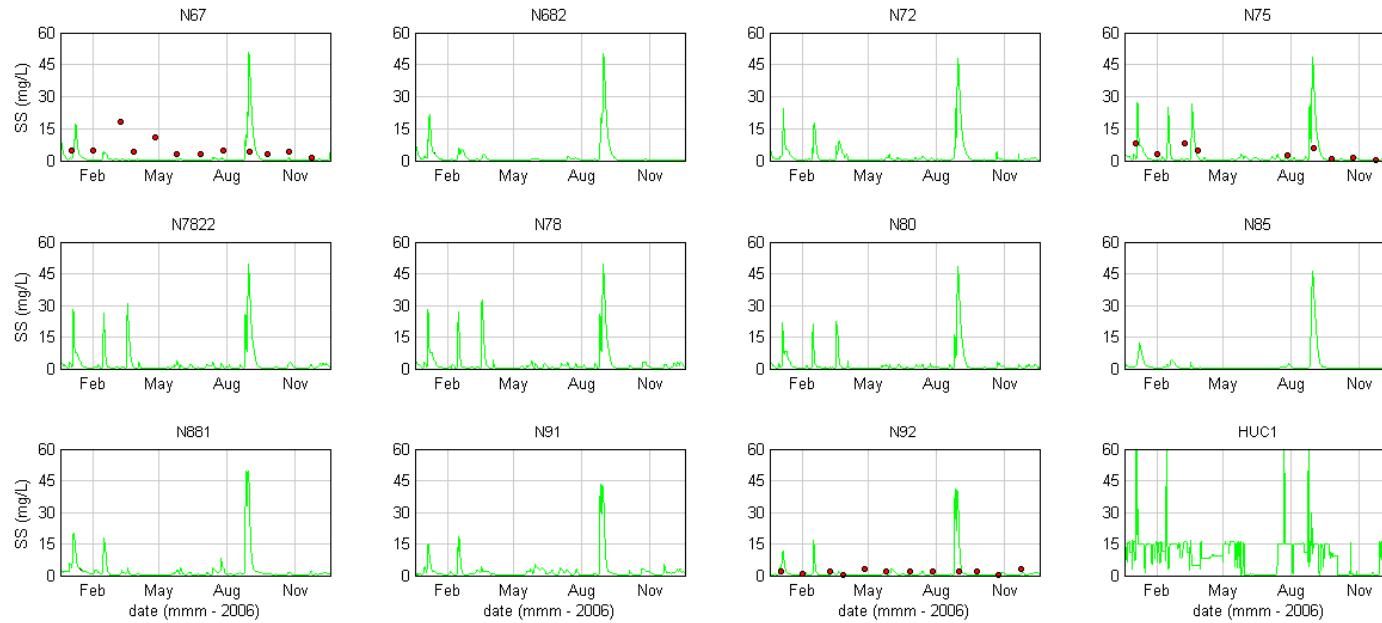


■ **Figure 13-16 (Cont.) Sediment Calibration 2006 (measured data (red), modelled surface (black) and modelled bottom (green))**

SINCLAIR KNIGHT MERZ



Water Quality Modelling of the Hawkesbury-Nepean River System

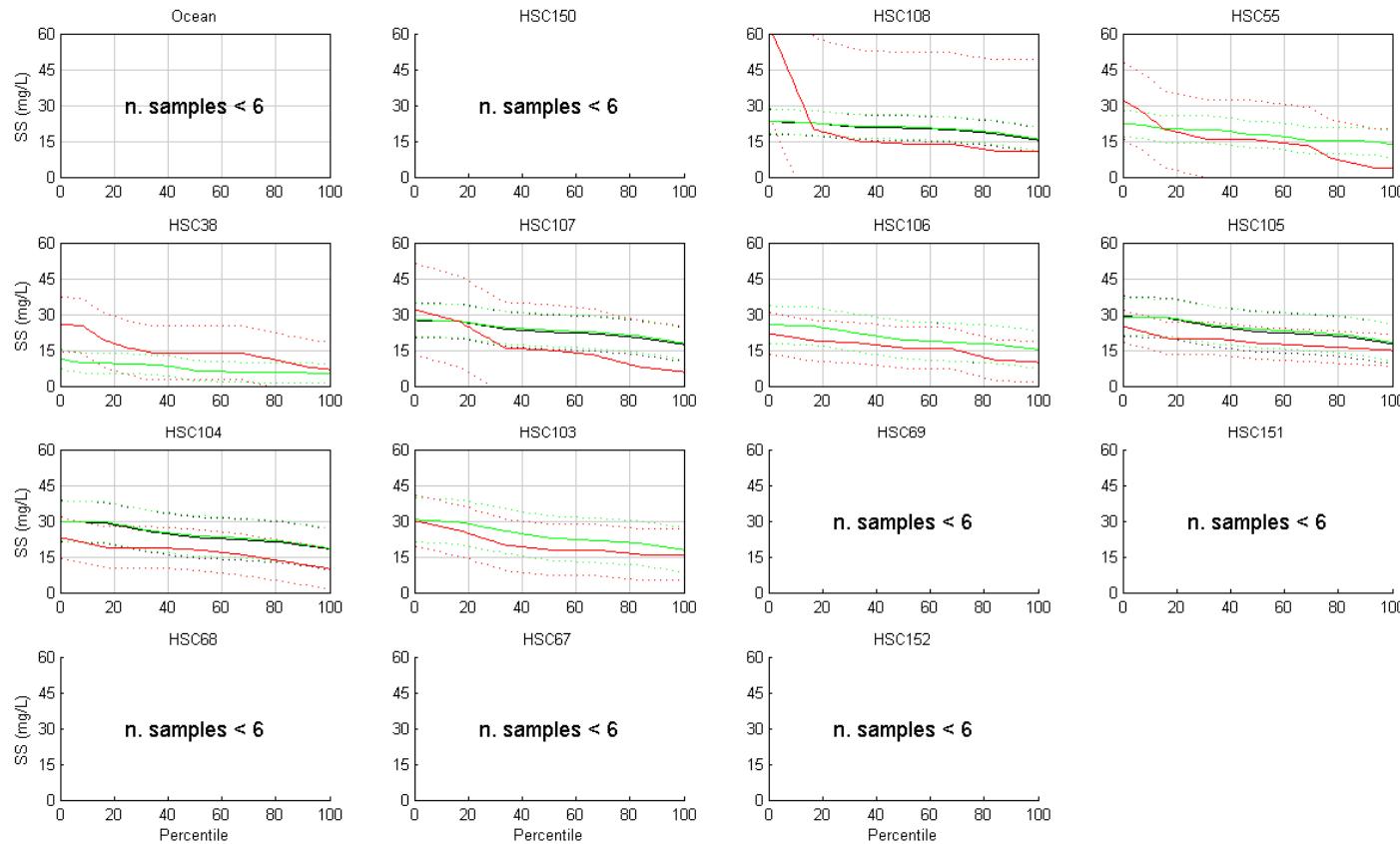


- **Figure 13-16 (Cont.) Sediment Calibration 2006 (measured data (red), modelled surface (black) and modelled bottom (green))**

SINCLAIR KNIGHT MERZ



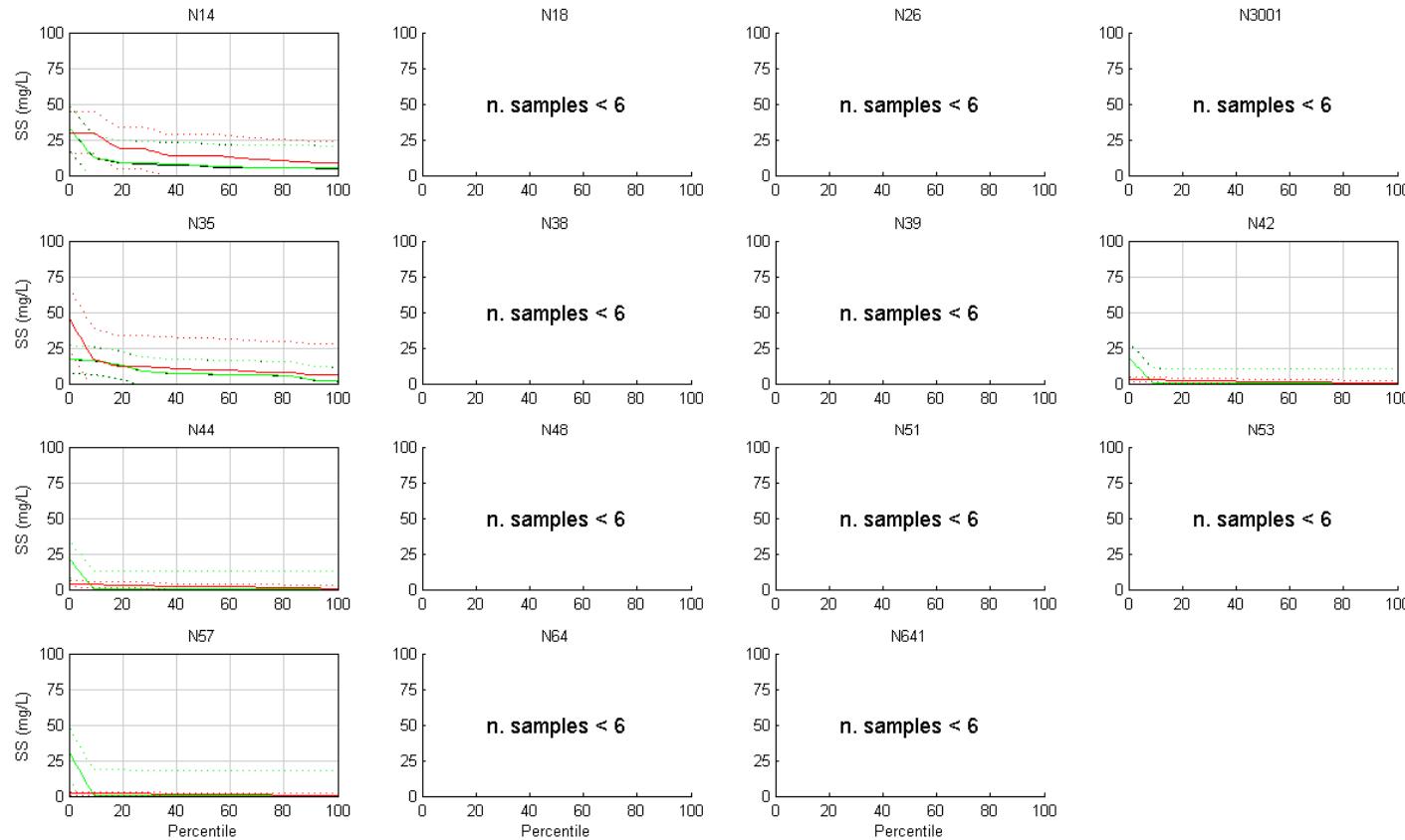
Water Quality Modelling of the Hawkesbury-Nepean River System



- **Figure 13-17 Exceedance Plots – Sediment Calibration 2006 (+/- 2SD) (measured data (red), modelled surface (black) and modelled bottom (green))**

SINCLAIR KNIGHT MERZ

Water Quality Modelling of the Hawkesbury-Nepean River System

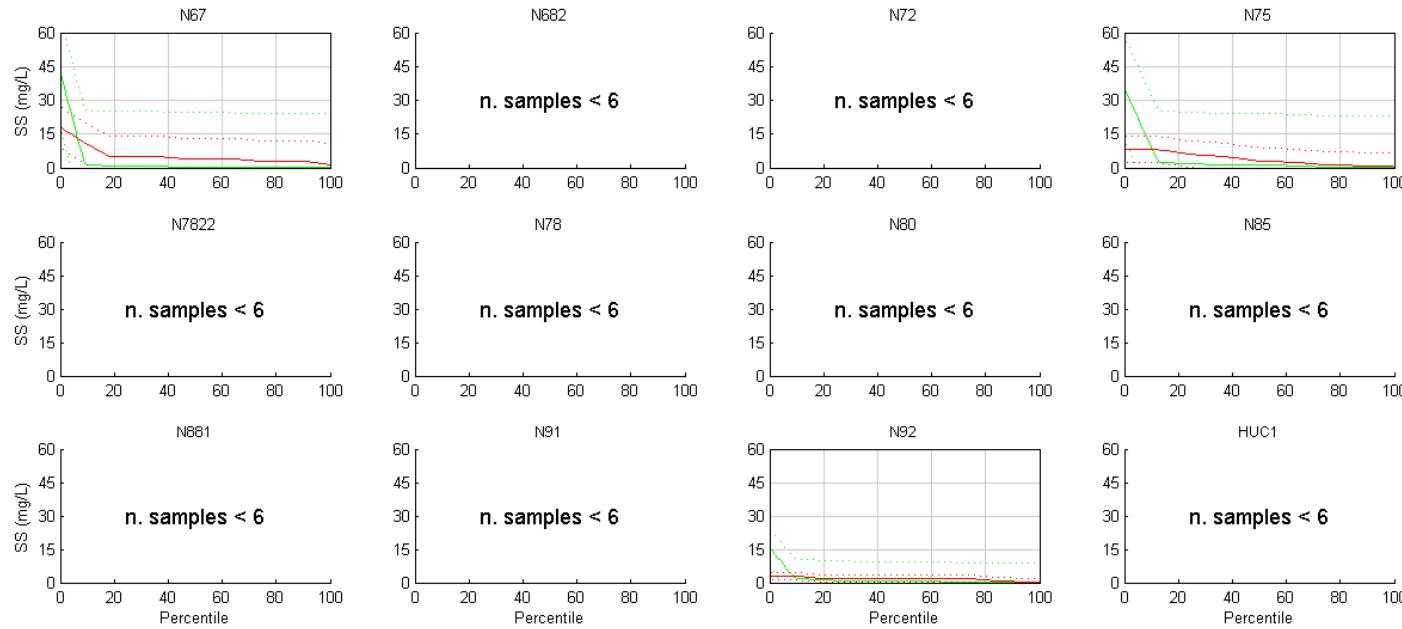


- Figure 13-17 (Cont.) Exceedance Plots – Sediment Calibration 2006 (+/- 2SD) (measured data (red), modelled surface (black) and modelled bottom (green))

SINCLAIR KNIGHT MERZ



Water Quality Modelling of the Hawkesbury-Nepean River System

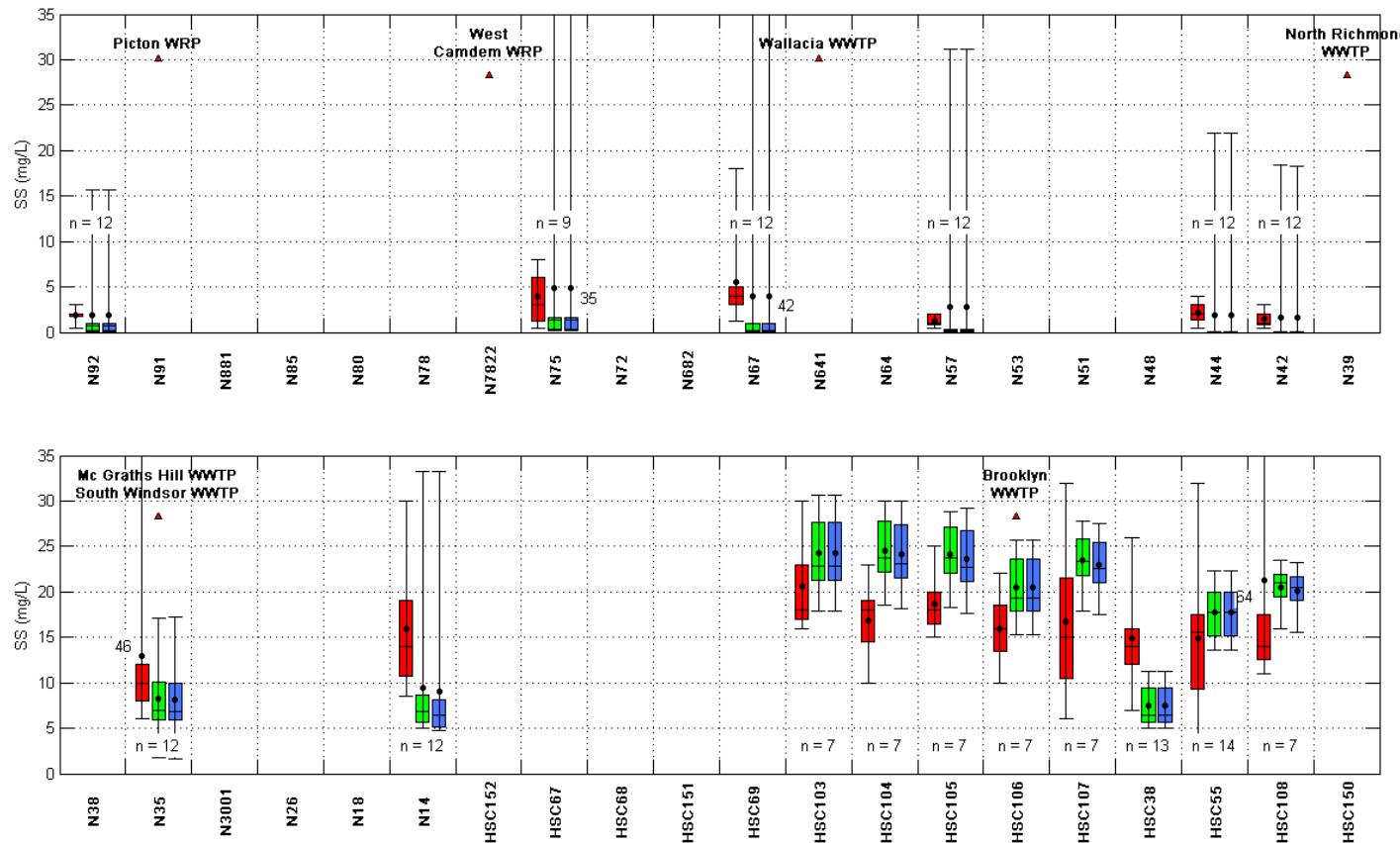


- Figure 13-17 (Cont.) Exceedance Plots – Sediment Calibration 2006 (+/- 2SD) (measured data (red), modelled surface (black) and modelled bottom (green))

SINCLAIR KNIGHT MERZ



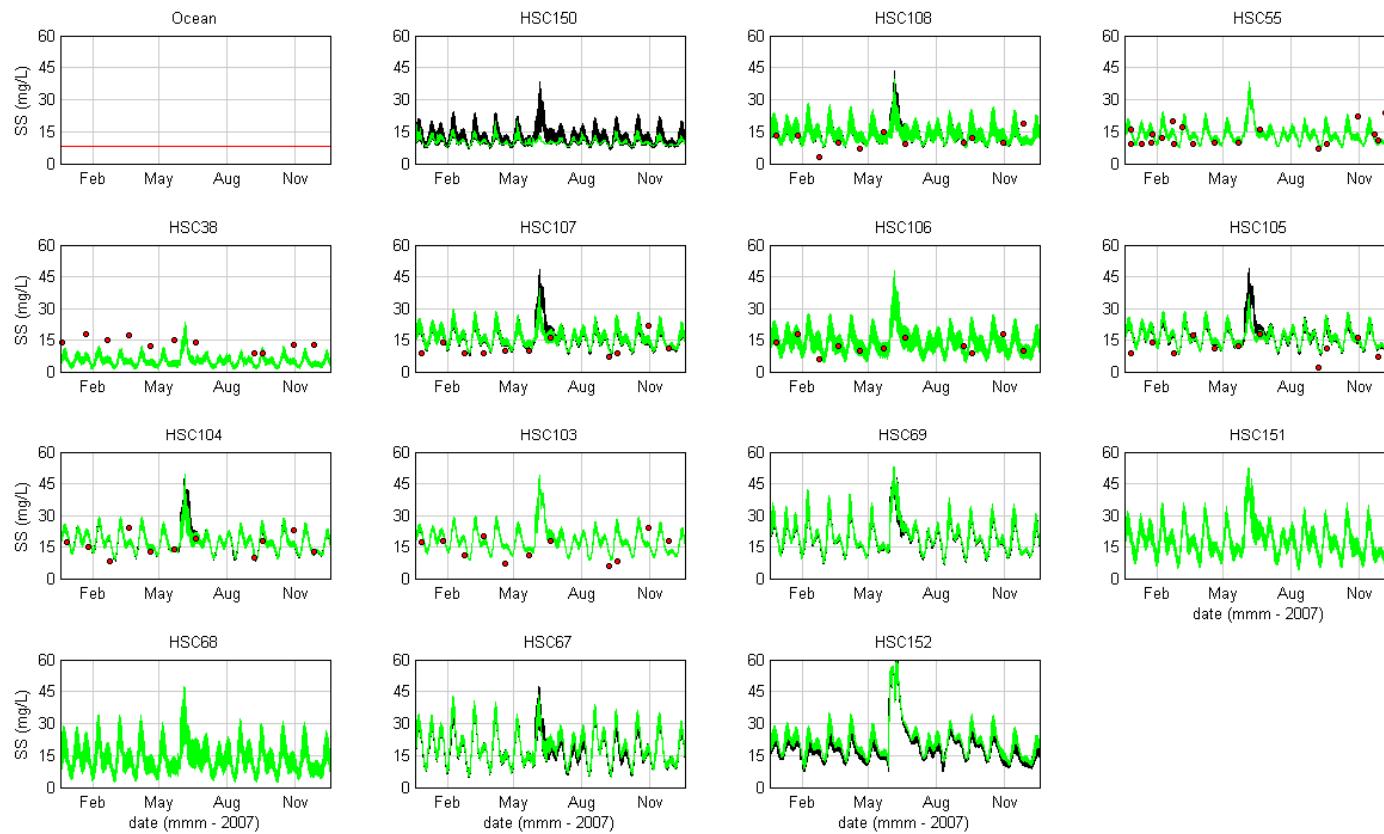
Water Quality Modelling of the Hawkesbury-Nepean River System



- **Figure 13-18 Box and Whisker Plots – Sediment Calibration 2006 (measured data (red), modelled surface (blue) and modelled bottom (green))**



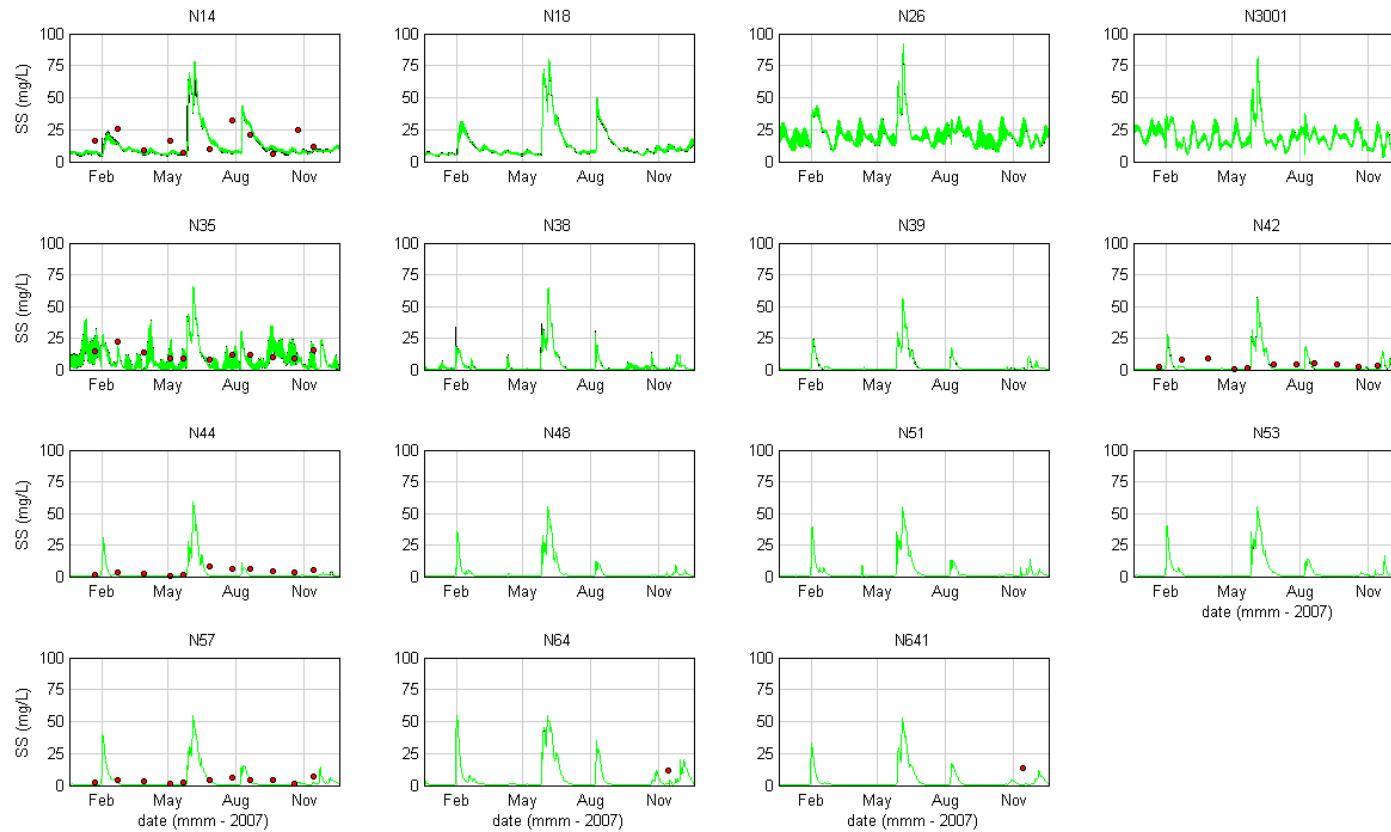
Water Quality Modelling of the Hawkesbury-Nepean River System



■ **Figure 13-19 Sediment Validation 2007 (measured data (red), modelled surface (black) and modelled bottom (green))**



Water Quality Modelling of the Hawkesbury-Nepean River System

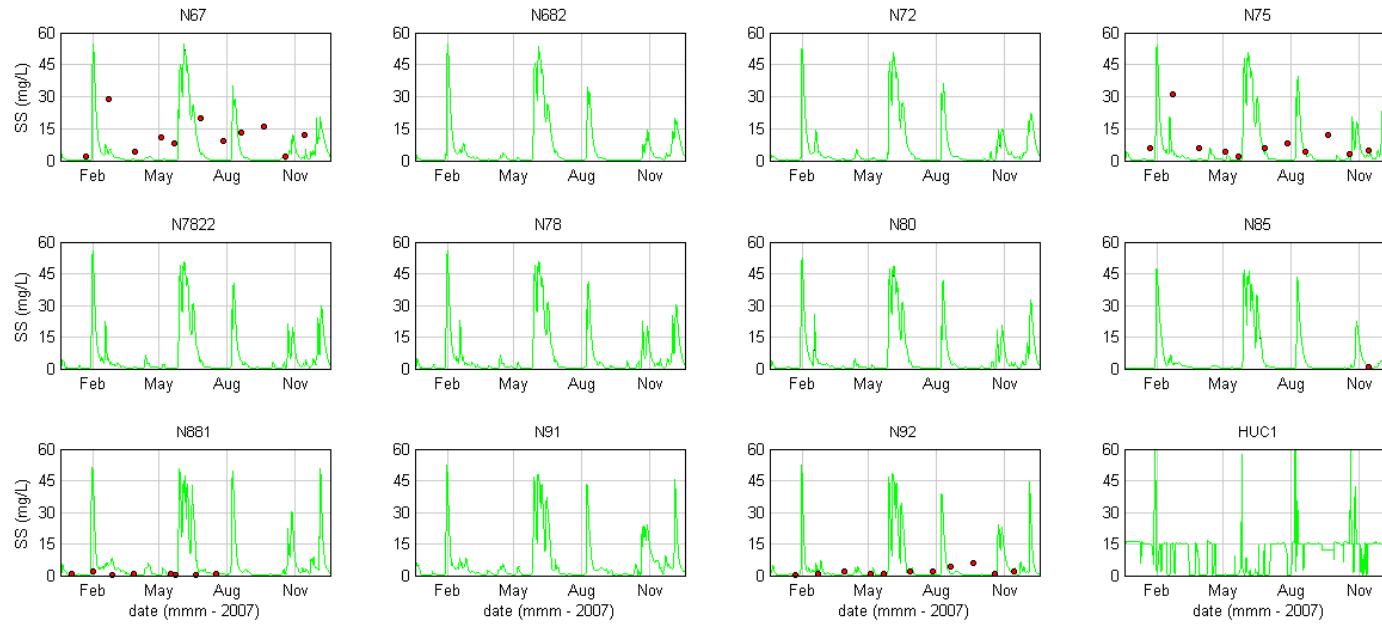


■ Figure 13-19 (Cont.) Sediment Validation 2007 (measured data (red), modelled surface (black) and modelled bottom (green))

SINCLAIR KNIGHT MERZ



Water Quality Modelling of the Hawkesbury-Nepean River System

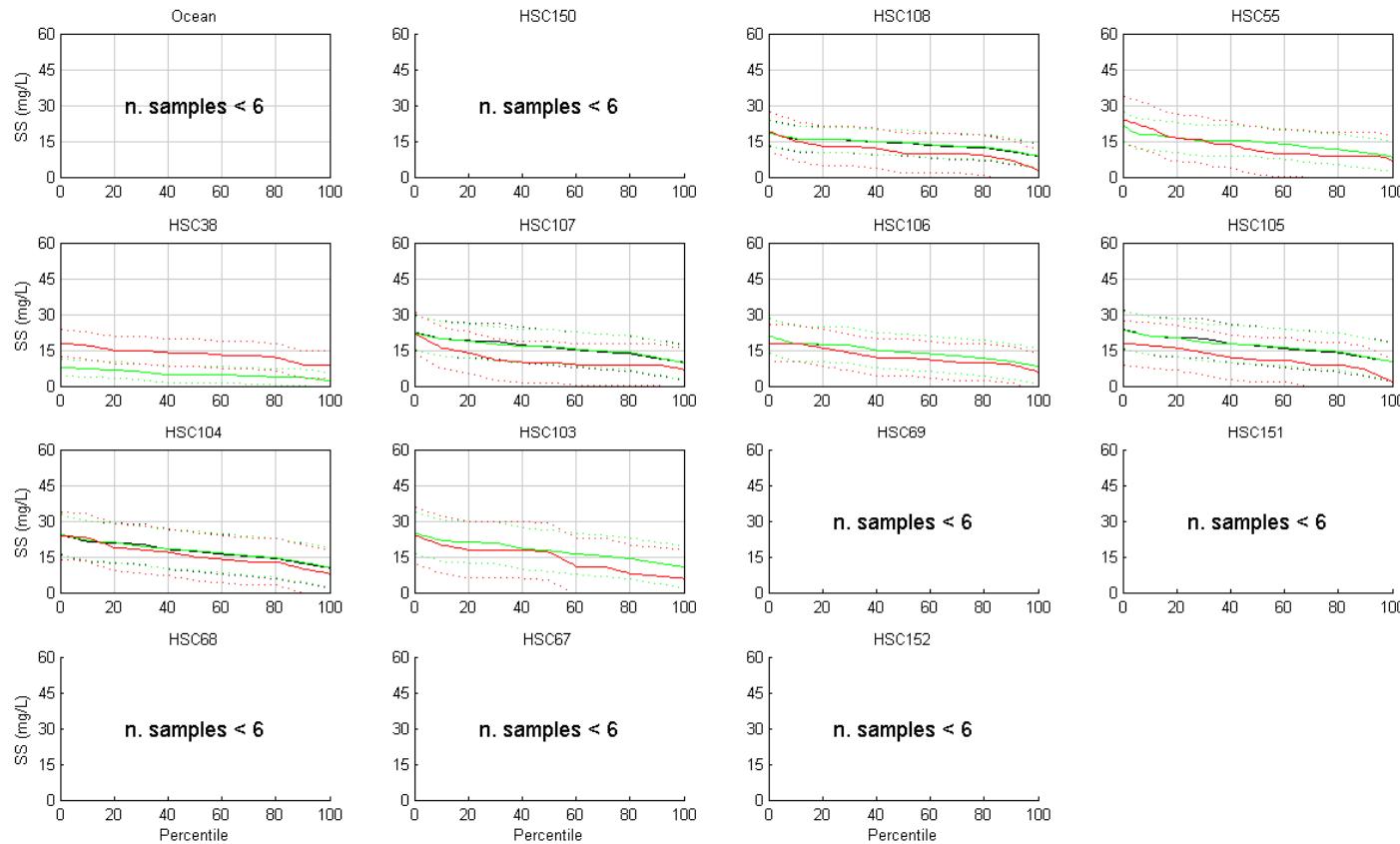


- **Figure 13-19 (Cont.) Sediment Validation 2007 (measured data (red), modelled surface (black) and modelled bottom (green))**

SINCLAIR KNIGHT MERZ



Water Quality Modelling of the Hawkesbury-Nepean River System

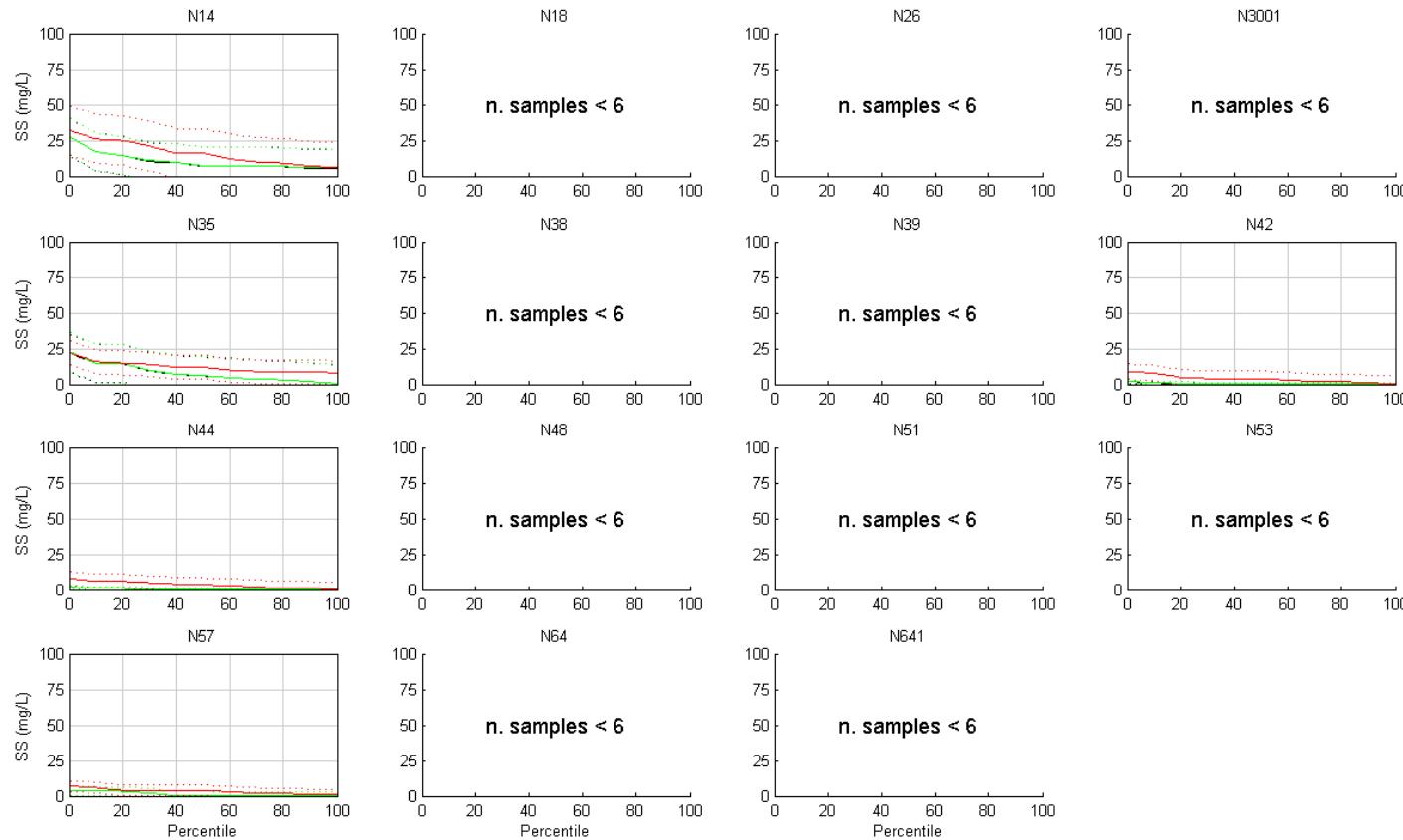


- **Figure 13-20 Exceedance Plots – Sediment Validation 2007 (+/- 2SD) (measured data (red), modelled surface (black) and modelled bottom (green))**

SINCLAIR KNIGHT MERZ

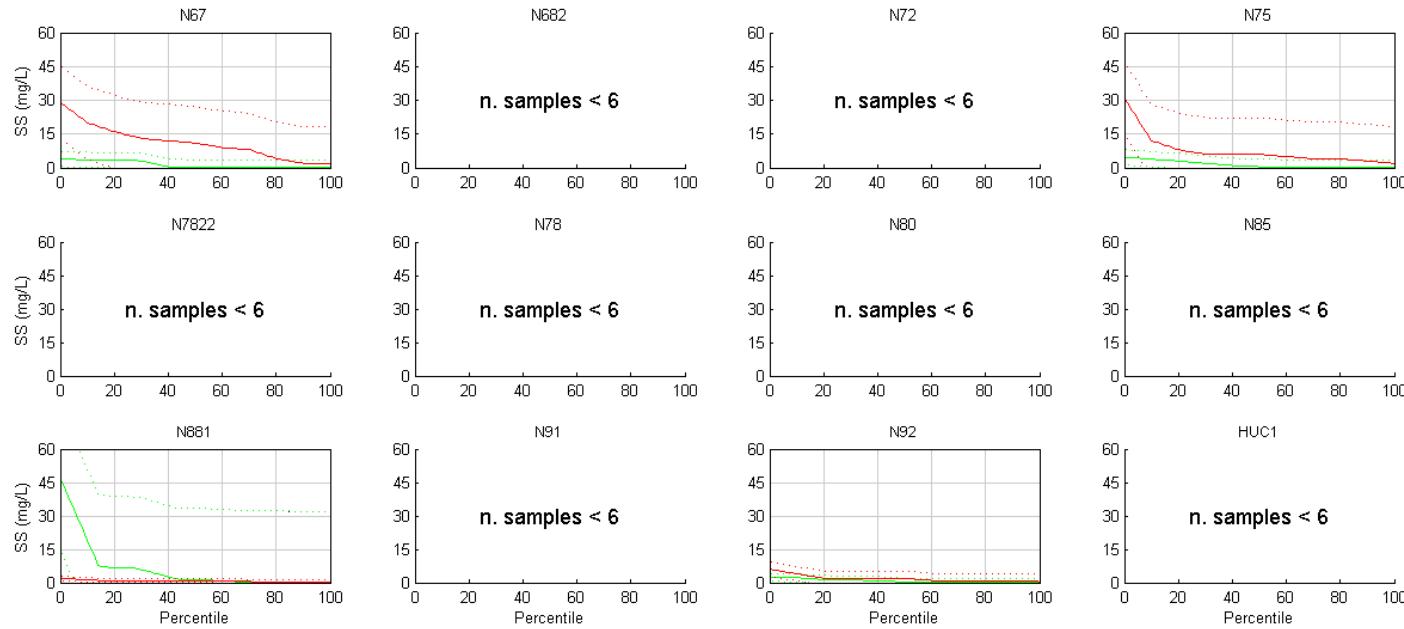


Water Quality Modelling of the Hawkesbury-Nepean River System



- **Figure 13-20 (Cont.) Exceedance Plots – Sediment Validation 2007 (+/- 2SD) (measured data (red), modelled surface (black) and modelled bottom (green))**

SINCLAIR KNIGHT MERZ

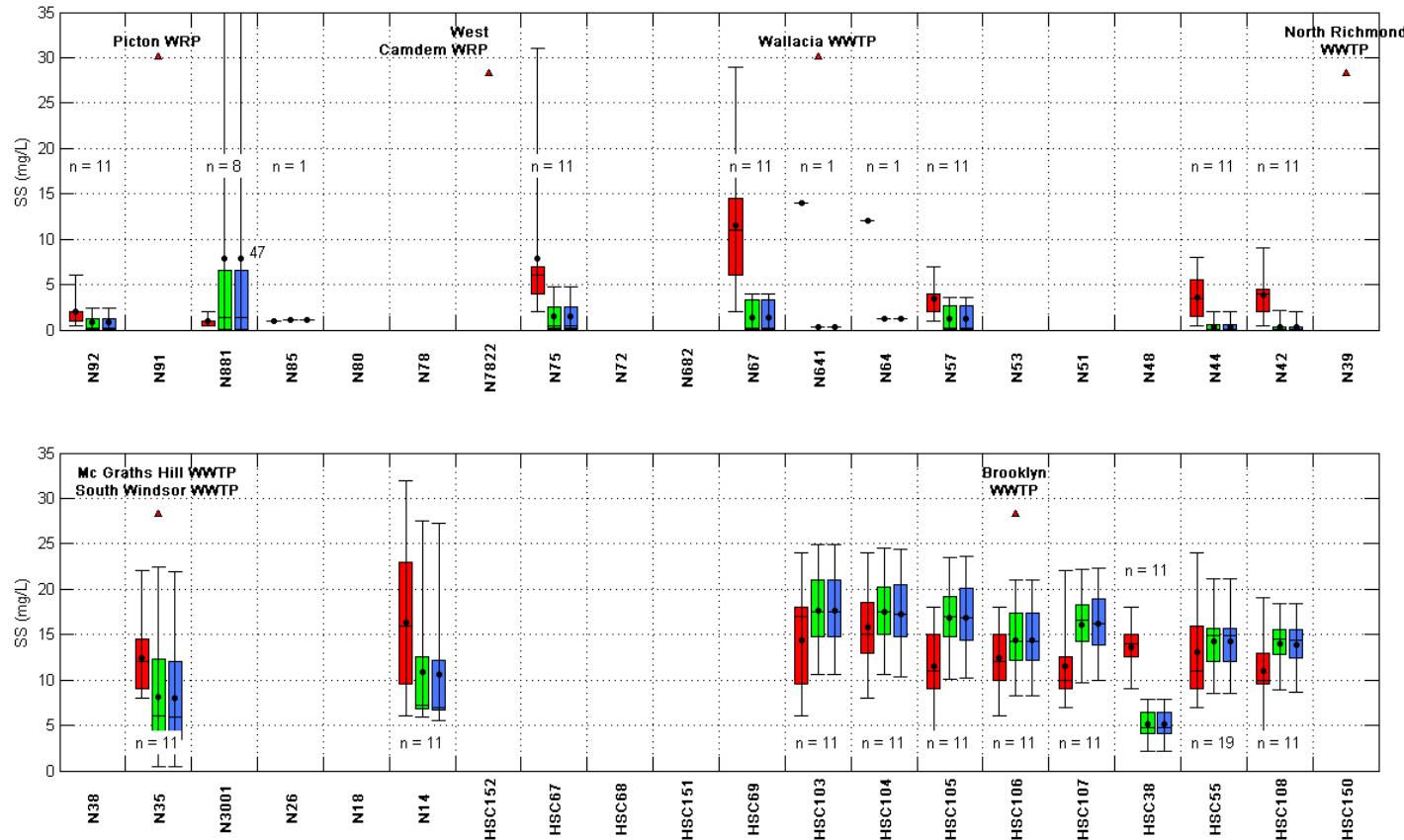


- Figure 13-20 (Cont.) Exceedance Plots – Sediment Validation 2007 (+/- 2SD) (measured data (red), modelled surface (black) and modelled bottom (green))

SINCLAIR KNIGHT MERZ



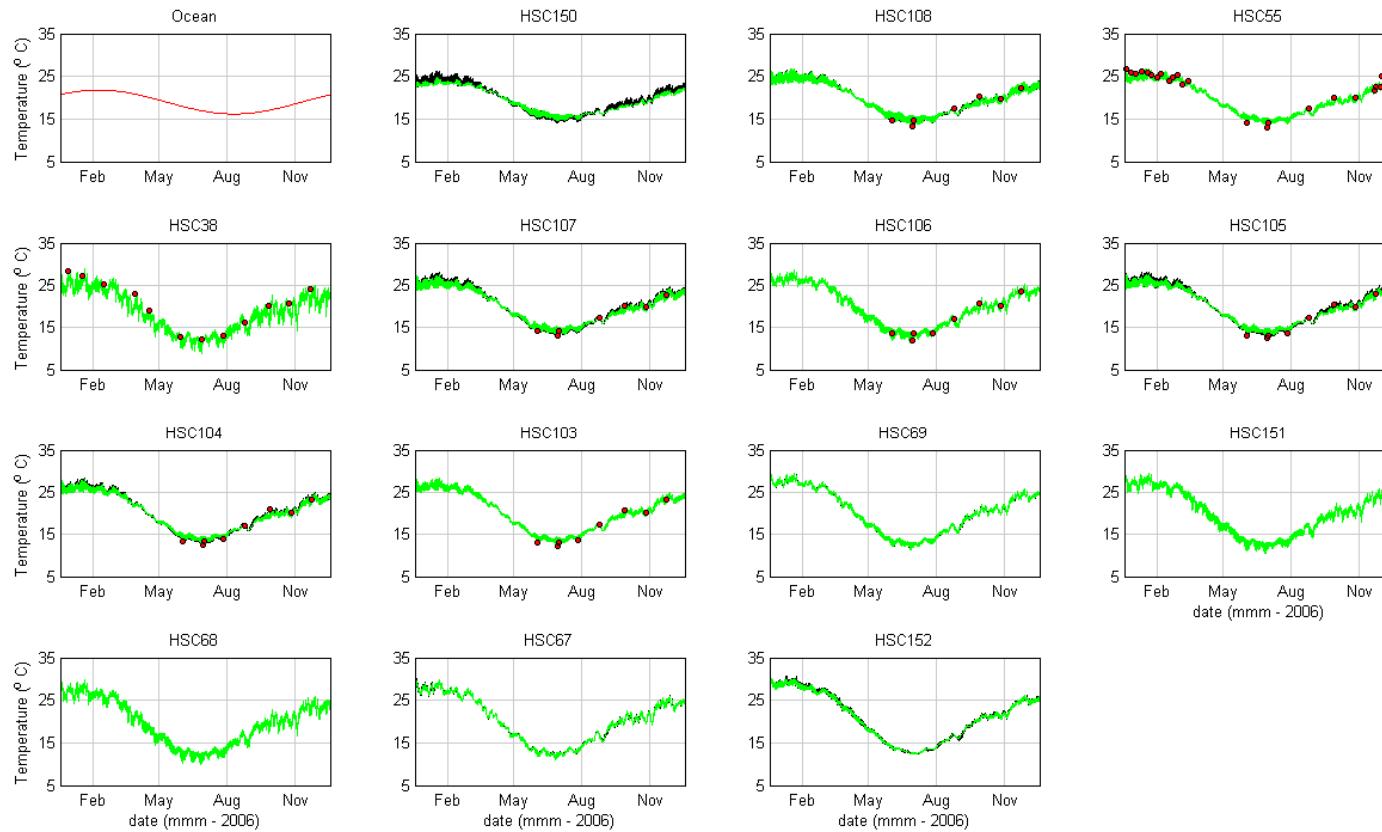
Water Quality Modelling of the Hawkesbury-Nepean River System



- **Figure 13-21 Box and Whisker Plots – Sediment Validation 2007 (measured data (red), modelled surface (blue) and modelled bottom (green))**



Water Quality Modelling of the Hawkesbury-Nepean River System

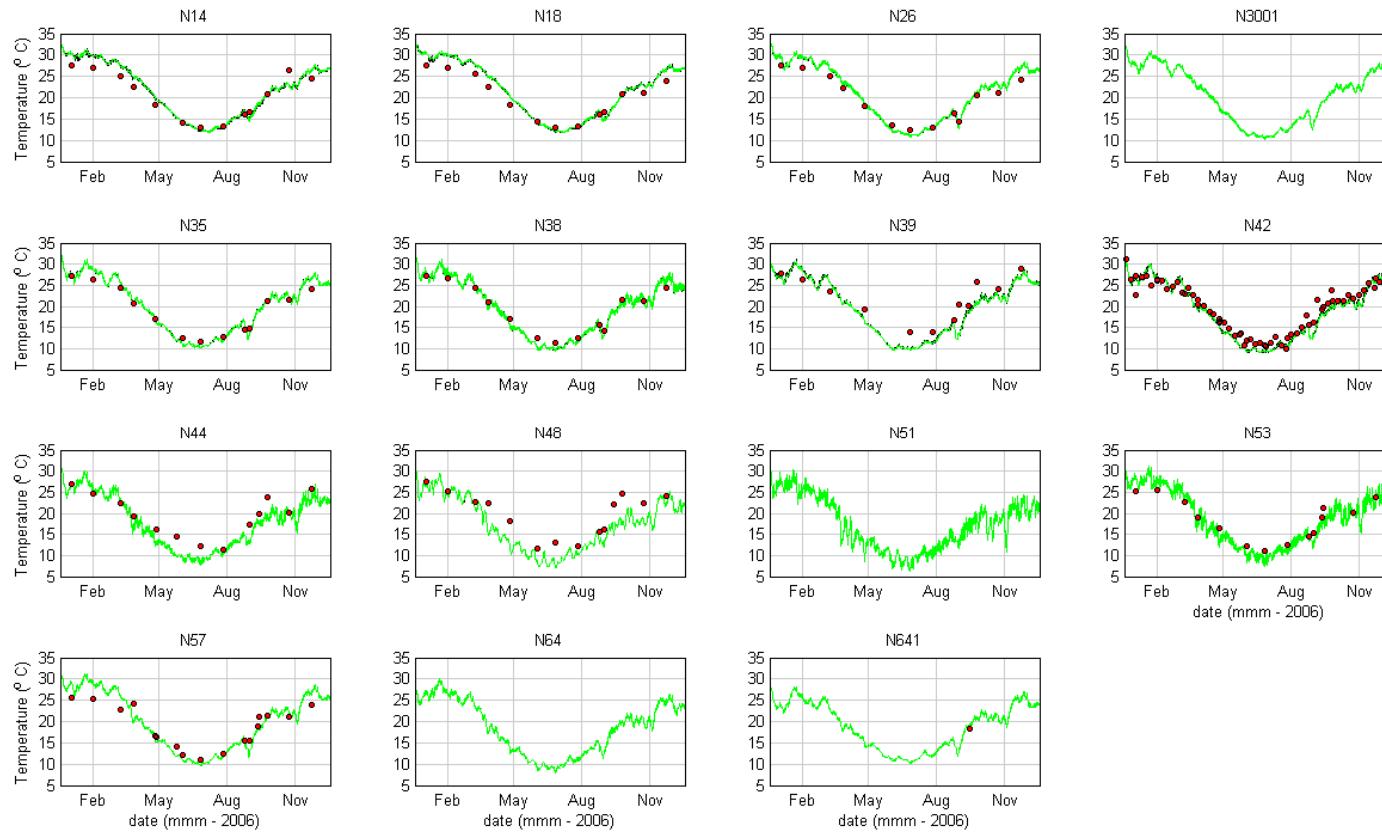


■ **Figure 13-22 Temperature Calibration 2006 (measured data (red), modelled surface (black) and modelled bottom (green))**

SINCLAIR KNIGHT MERZ



Water Quality Modelling of the Hawkesbury-Nepean River System

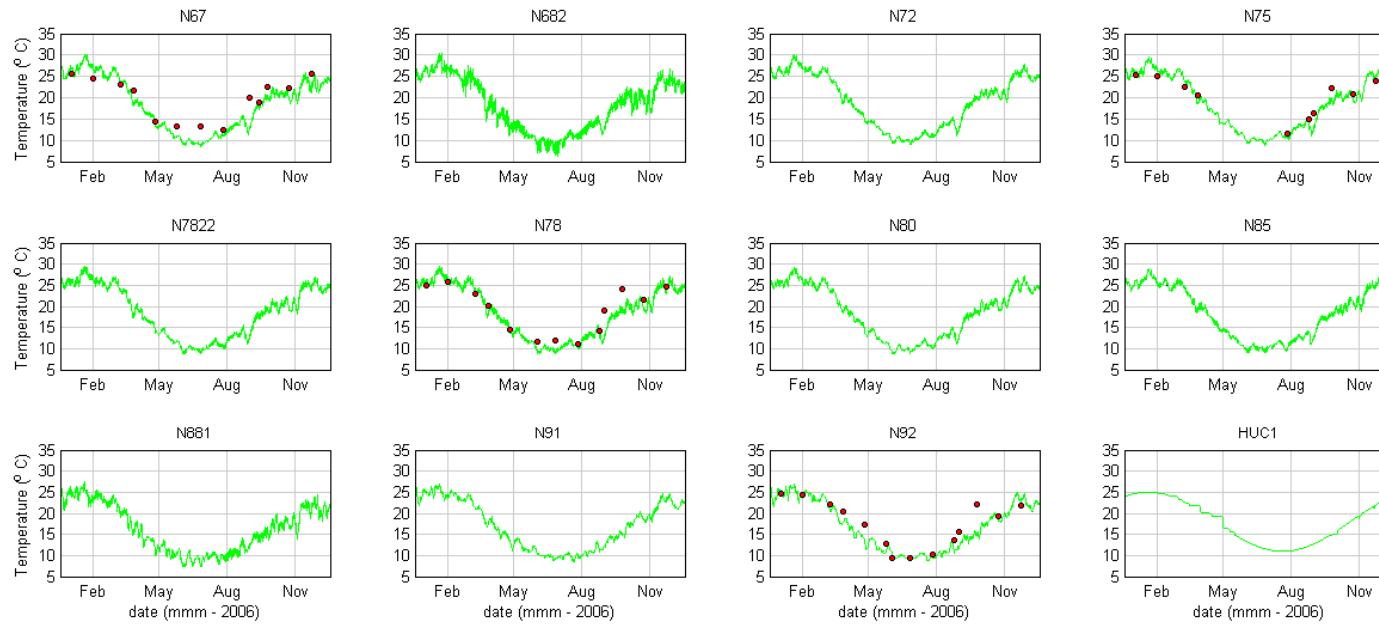


■ **Figure 13-22 (Cont.) Temperature Calibration 2006 (measured data (red), modelled surface (black) and modelled bottom (green))**

SINCLAIR KNIGHT MERZ



Water Quality Modelling of the Hawkesbury-Nepean River System

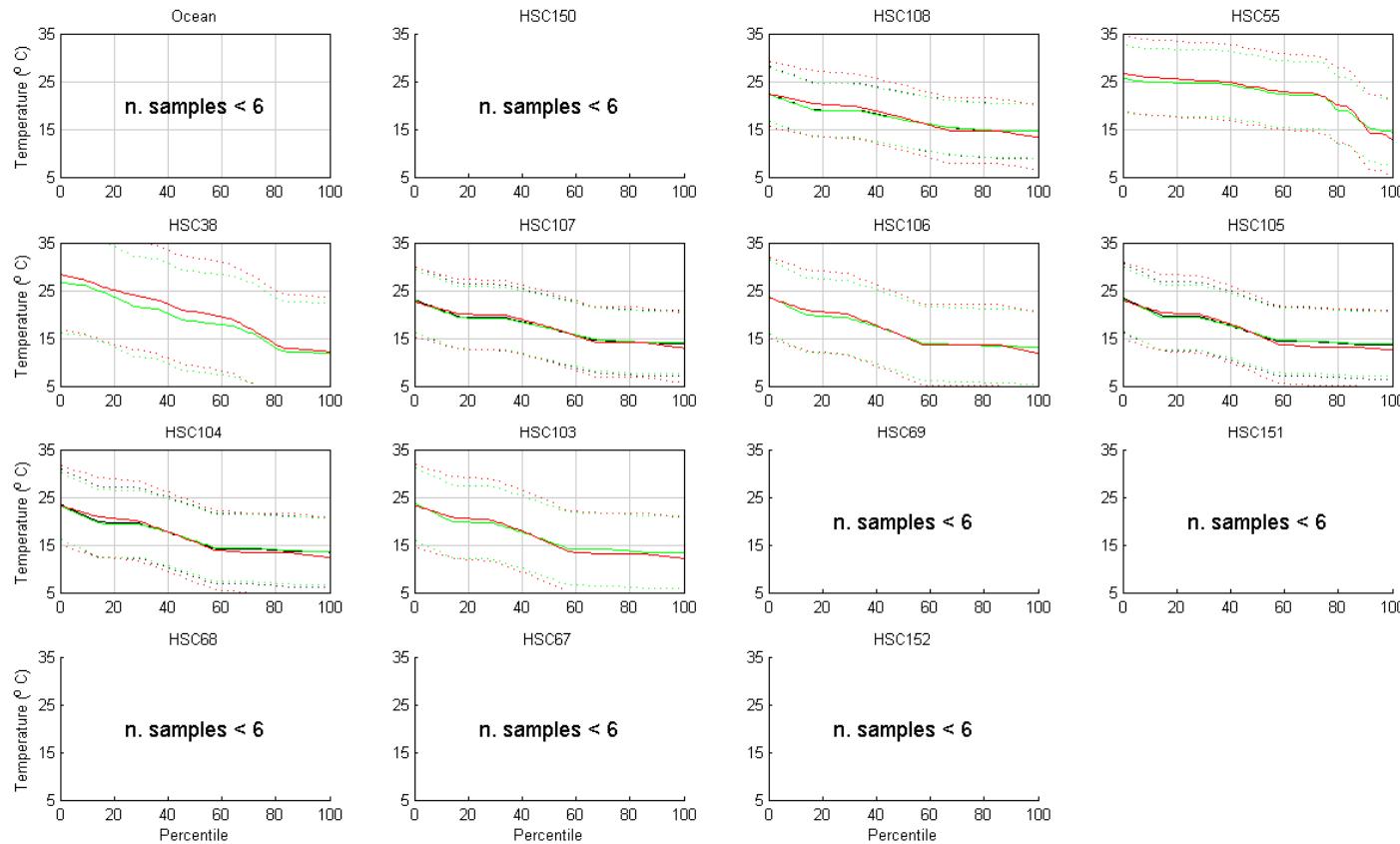


■ **Figure 13-22 (Cont.) Temperature Calibration 2006 (measured data (red), modelled surface (black) and modelled bottom (green))**

SINCLAIR KNIGHT MERZ



Water Quality Modelling of the Hawkesbury-Nepean River System

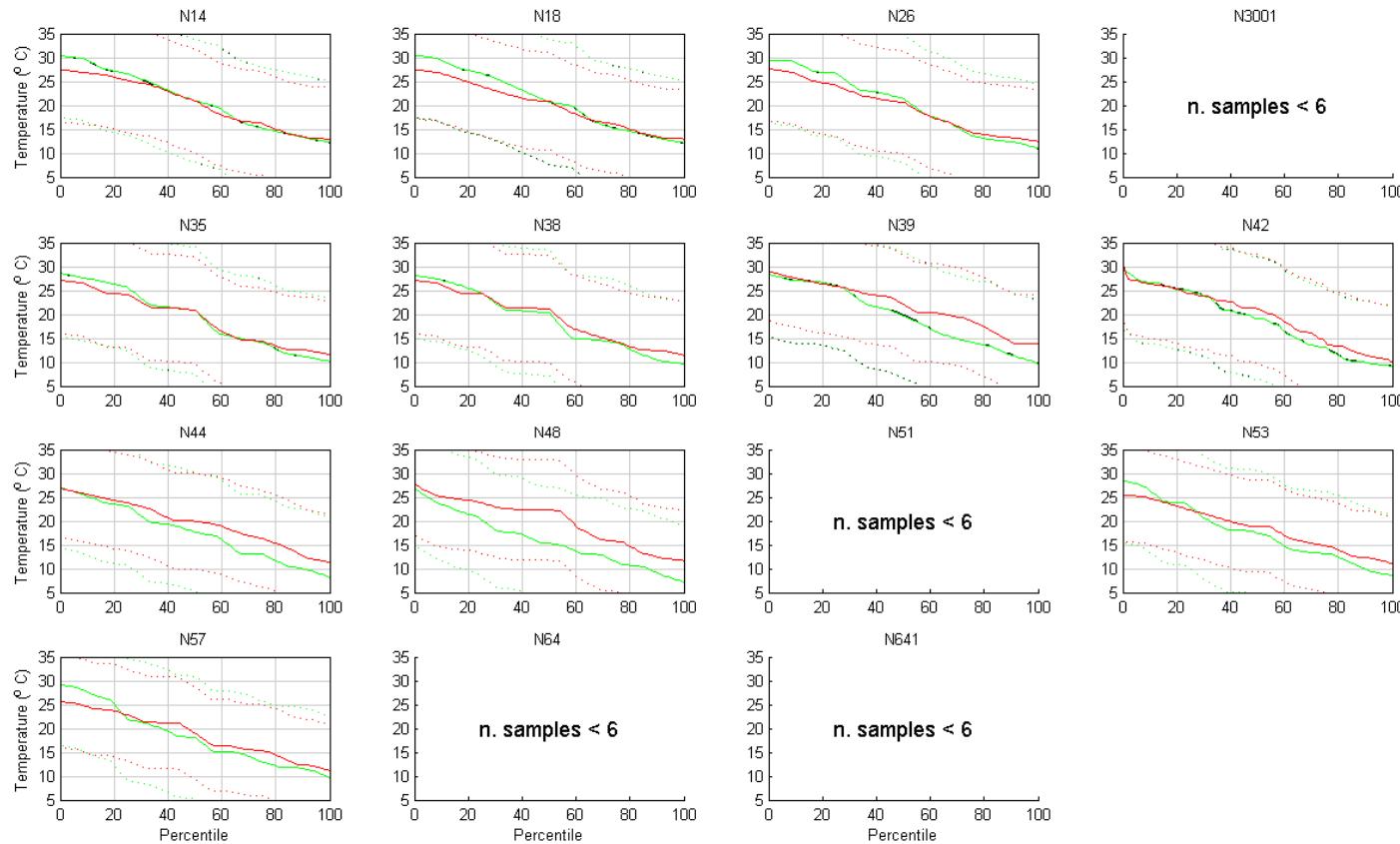


- **Figure 13-23 Exceedance Plots – Temperature Calibration 2006 (+/- 2SD) (measured data (red), modelled surface (black) and modelled bottom (green))**

SINCLAIR KNIGHT MERZ



Water Quality Modelling of the Hawkesbury-Nepean River System

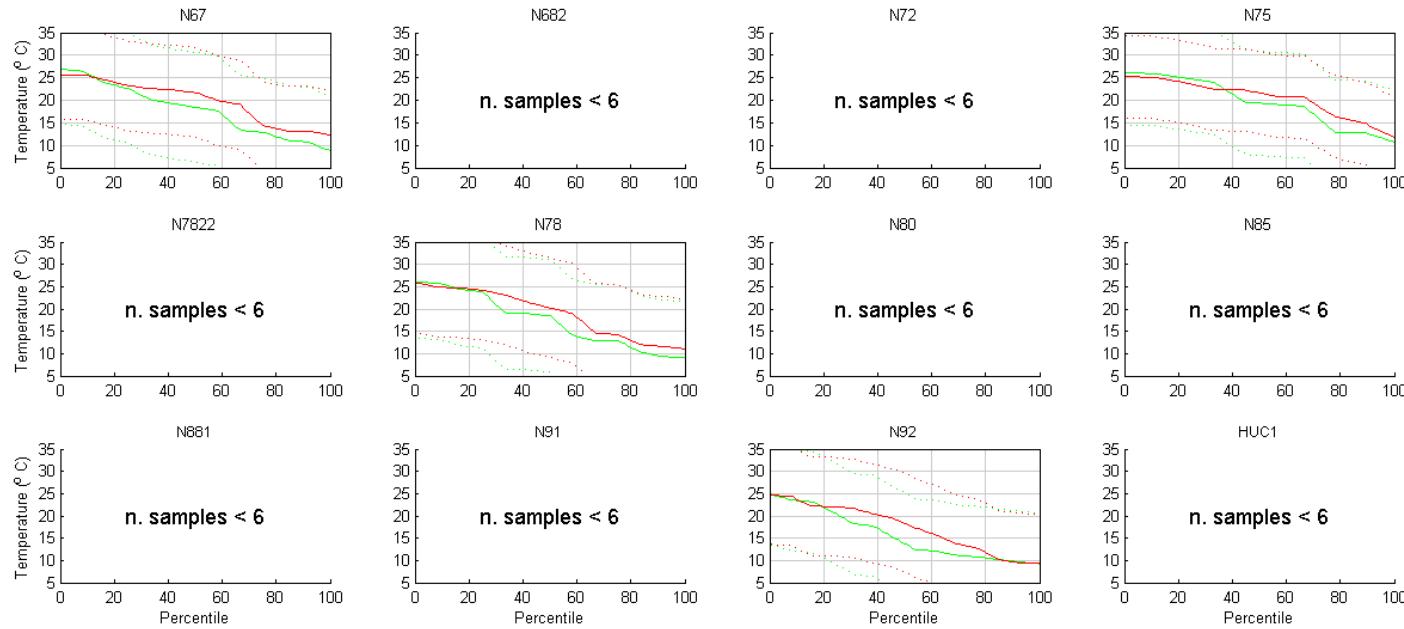


- Figure 13-23 (Cont.) Exceedance Plots – Temperature Calibration 2006 (+/- 2SD) (measured data (red), modelled surface (black) and modelled bottom (green))

SINCLAIR KNIGHT MERZ



Water Quality Modelling of the Hawkesbury-Nepean River System

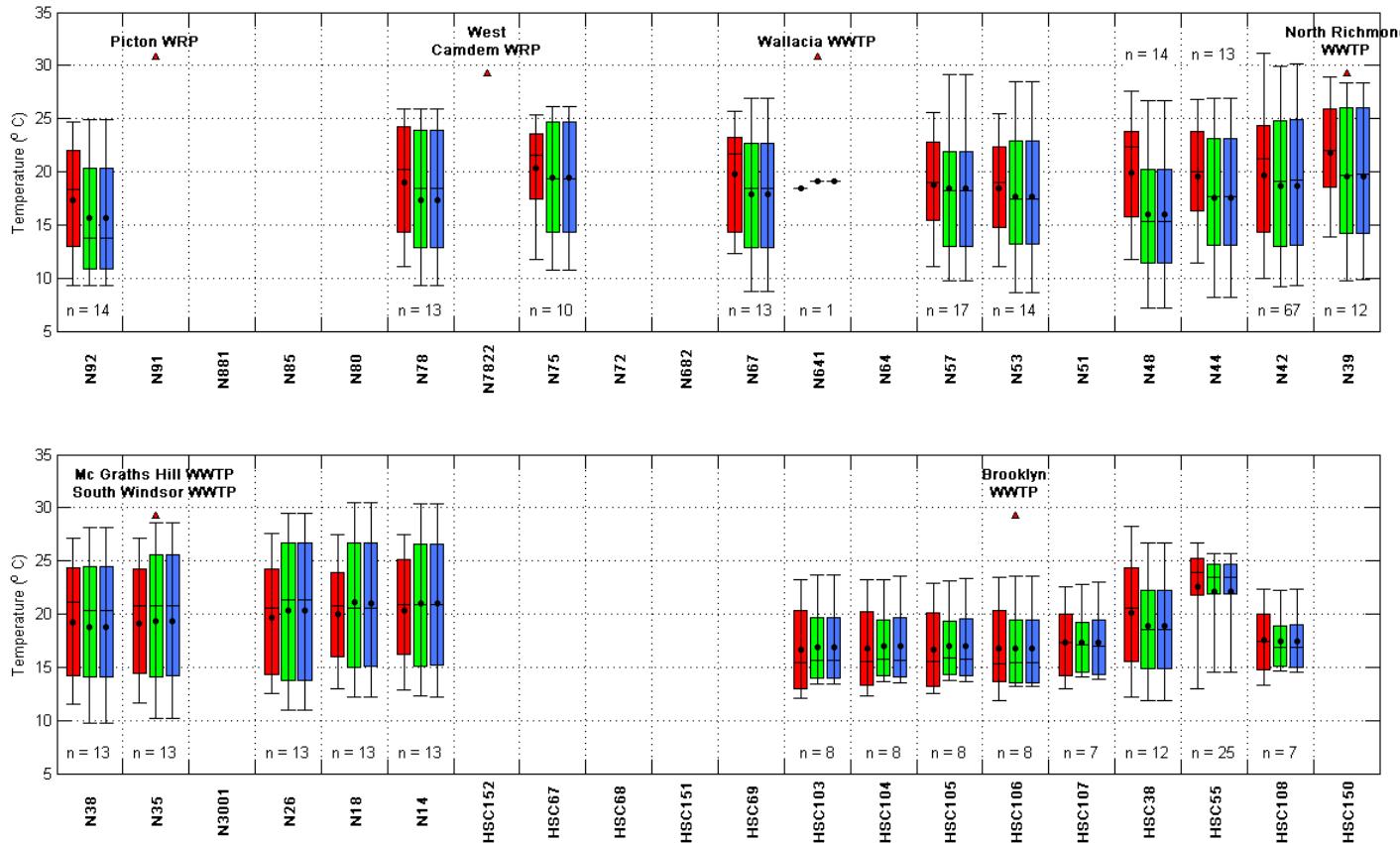


- Figure 13-23 (Cont.) Exceedance Plots – Temperature Calibration 2006 (+/- 2SD) (measured data (red), modelled surface (black) and modelled bottom (green))

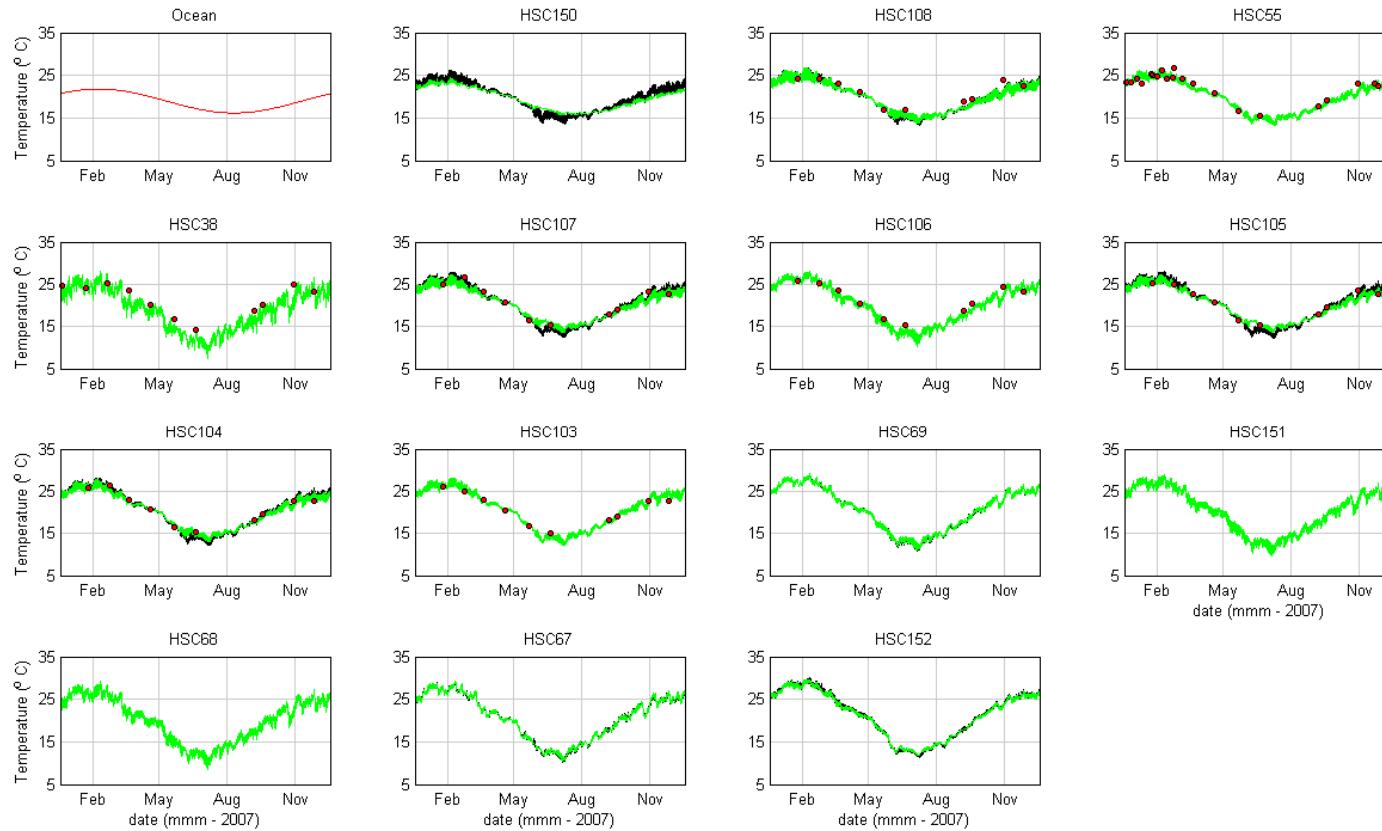
SINCLAIR KNIGHT MERZ



Water Quality Modelling of the Hawkesbury-Nepean River System



- Figure 13-24 Box and Whisker Plots – Temperature Calibration 2006 (measured data (red), modelled surface (blue) and modelled bottom (green))

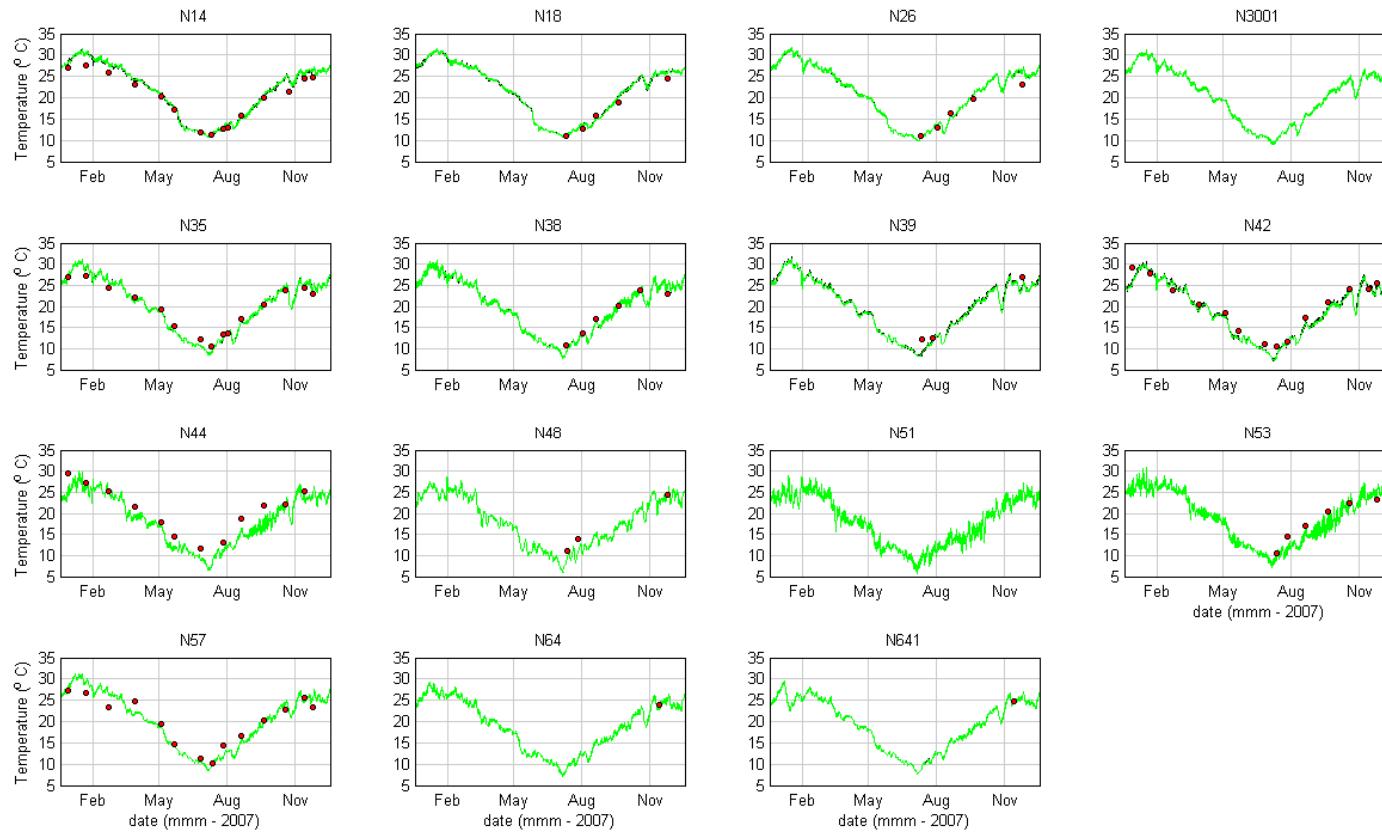


■ **Figure 13-25 Temperature Validation 2007 (measured data (red), modelled surface (black) and modelled bottom (green))**

SINCLAIR KNIGHT MERZ



Water Quality Modelling of the Hawkesbury-Nepean River System

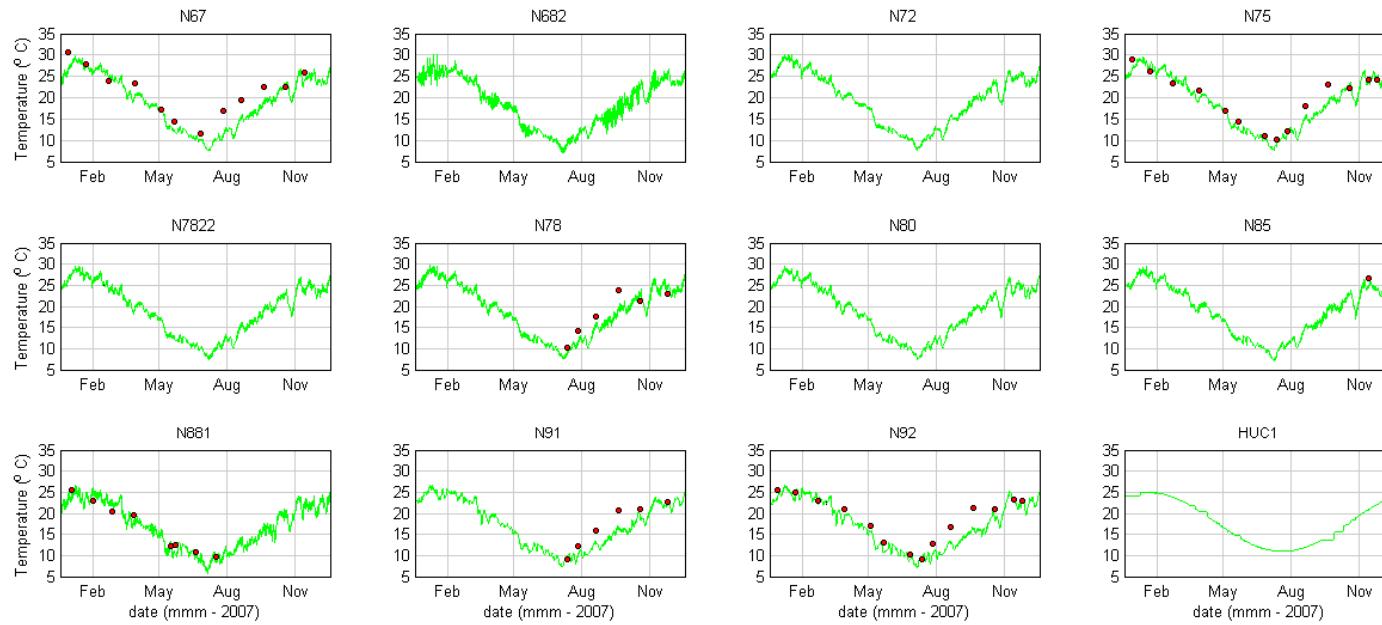


■ **Figure 13-25 (Cont.) Temperature Validation 2007 (measured data (red), modelled surface (black) and modelled bottom (green))**

SINCLAIR KNIGHT MERZ



Water Quality Modelling of the Hawkesbury-Nepean River System

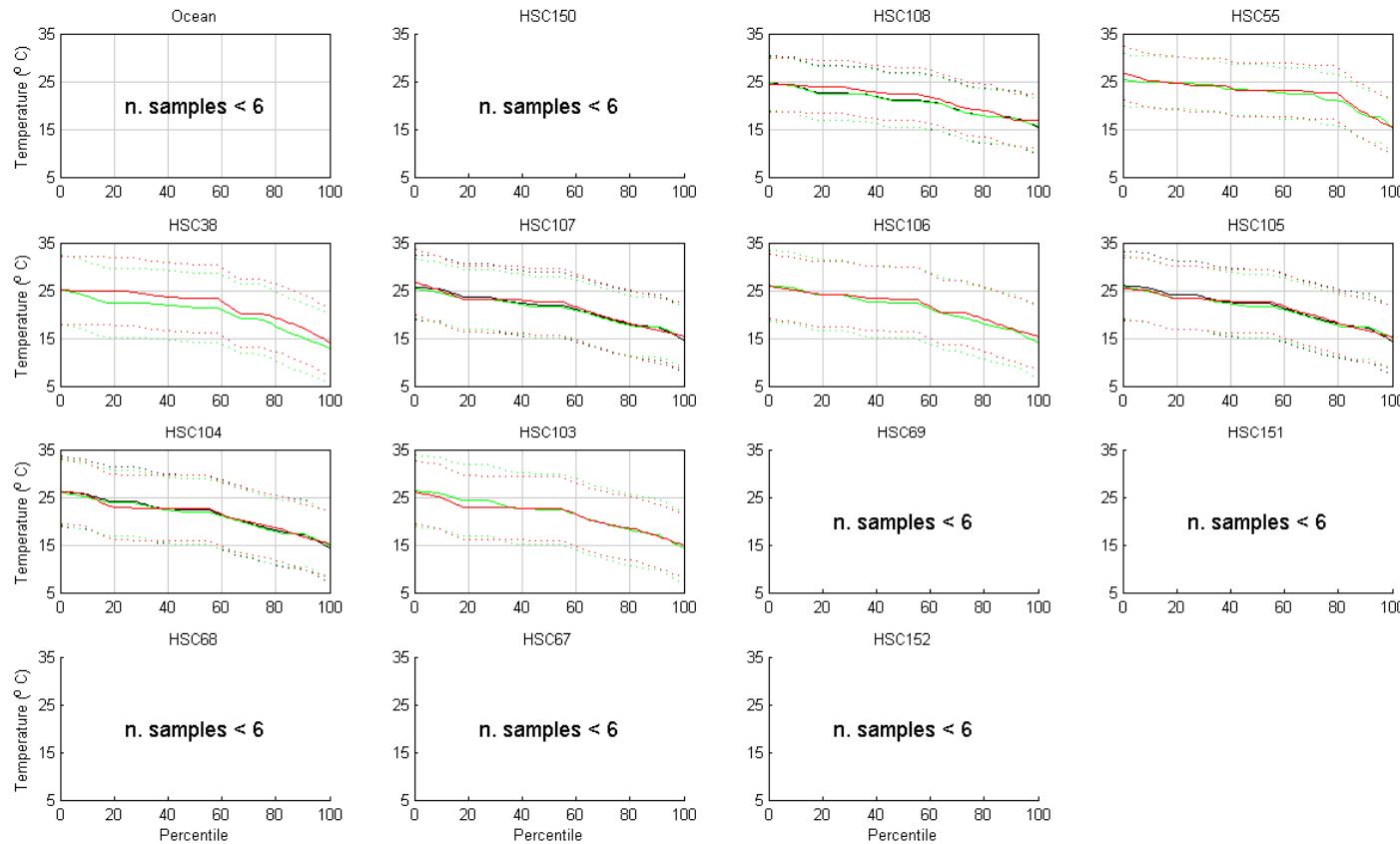


■ Figure 13-25 (Cont.) Temperature Validation 2007 (measured data (red), modelled surface (black) and modelled bottom (green))

SINCLAIR KNIGHT MERZ



Water Quality Modelling of the Hawkesbury-Nepean River System

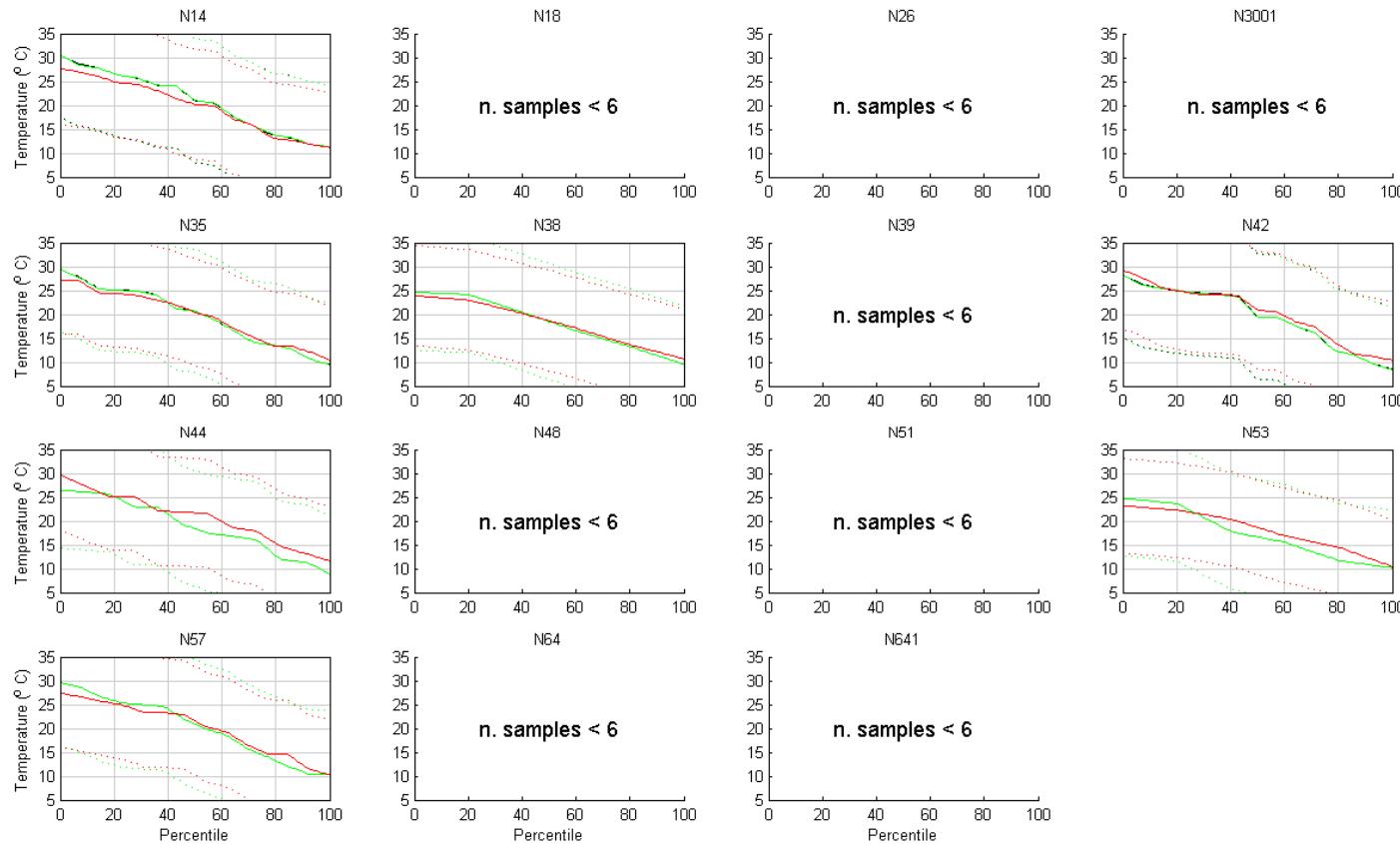


- **Figure 13-26 Exceedance Plots – Temperature Validation 2007 (+/- 2SD) (measured data (red), modelled surface (black) and modelled bottom (green))**

SINCLAIR KNIGHT MERZ



Water Quality Modelling of the Hawkesbury-Nepean River System

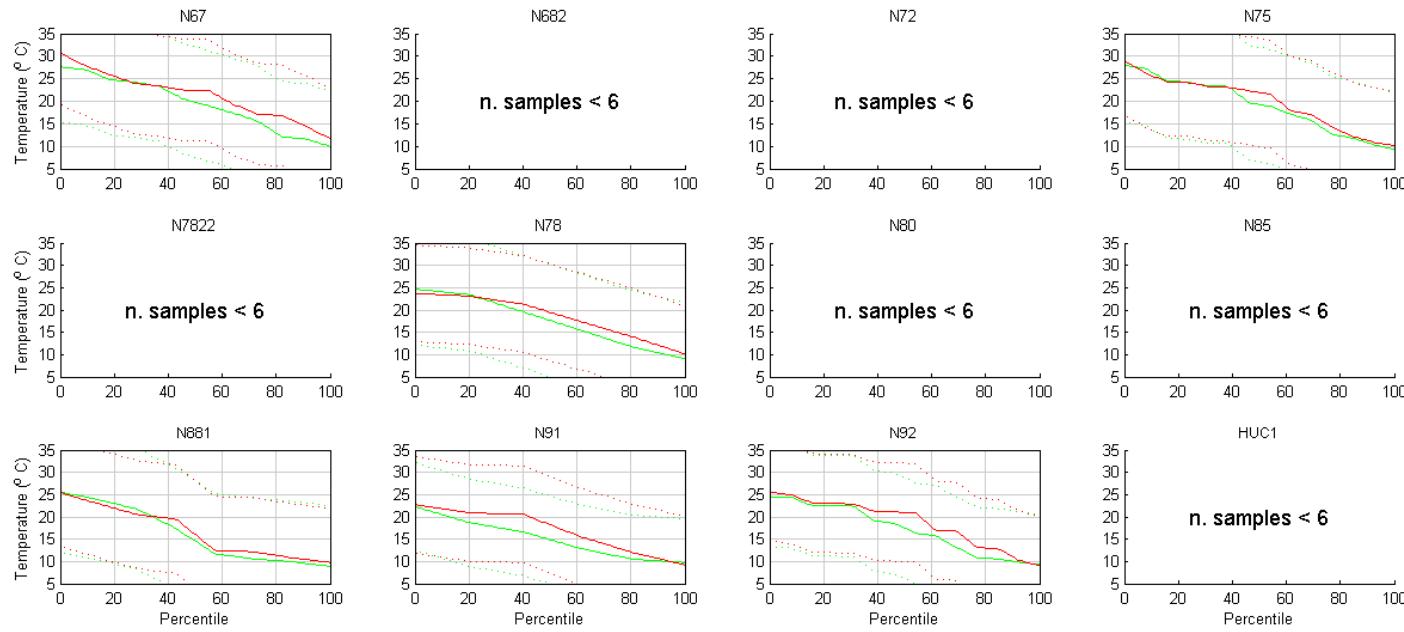


- **Figure 13-26 (Cont.) Exceedance Plots – Temperature Validation 2007 (+/- 2SD) (measured data (red), modelled surface (black) and modelled bottom (green))**

SINCLAIR KNIGHT MERZ



Water Quality Modelling of the Hawkesbury-Nepean River System

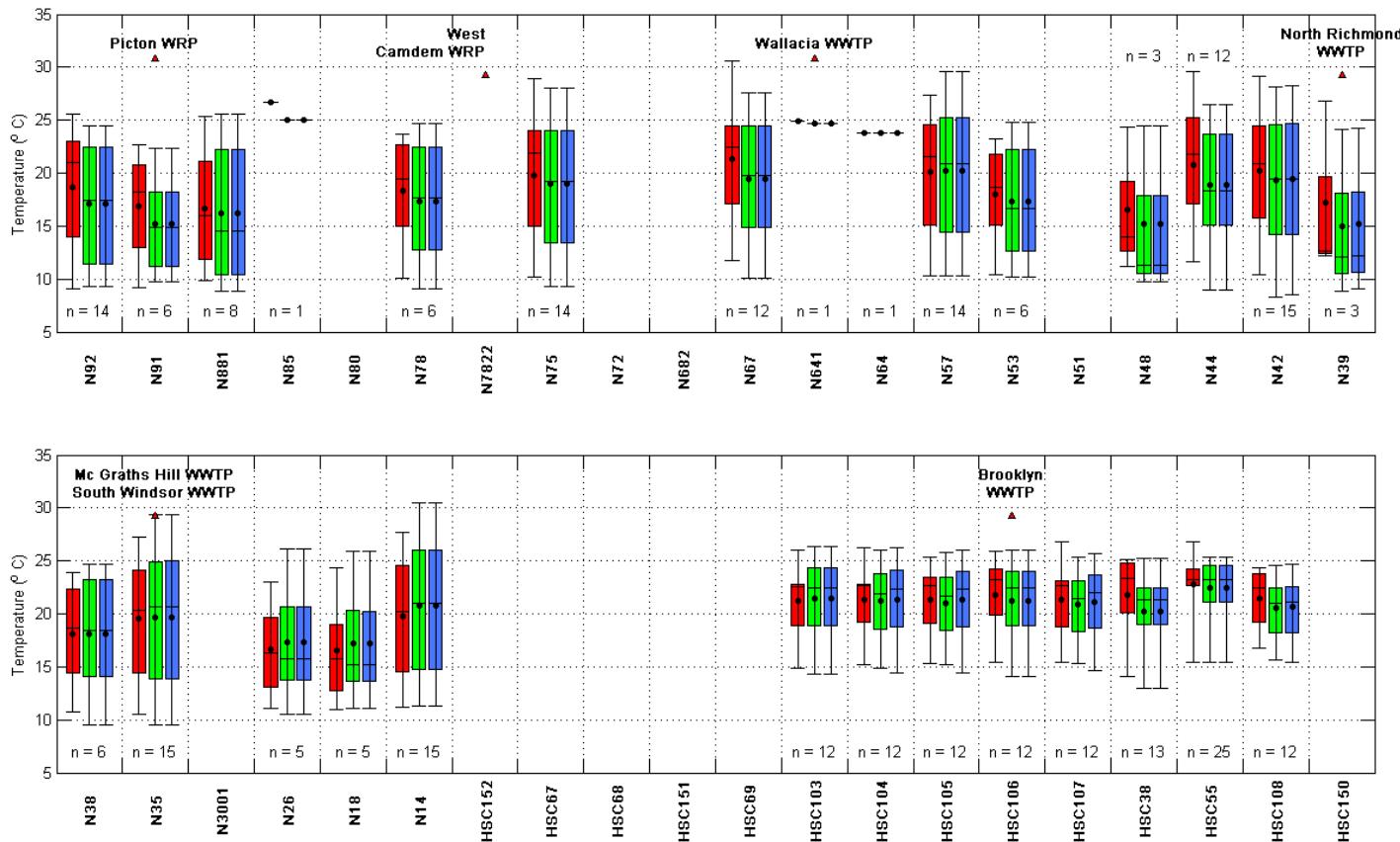


- Figure 13-26 (Cont.) Exceedance Plots – Temperature Validation 2007 (+/- 2SD) (measured data (red), modelled surface (black) and modelled bottom (green))

SINCLAIR KNIGHT MERZ



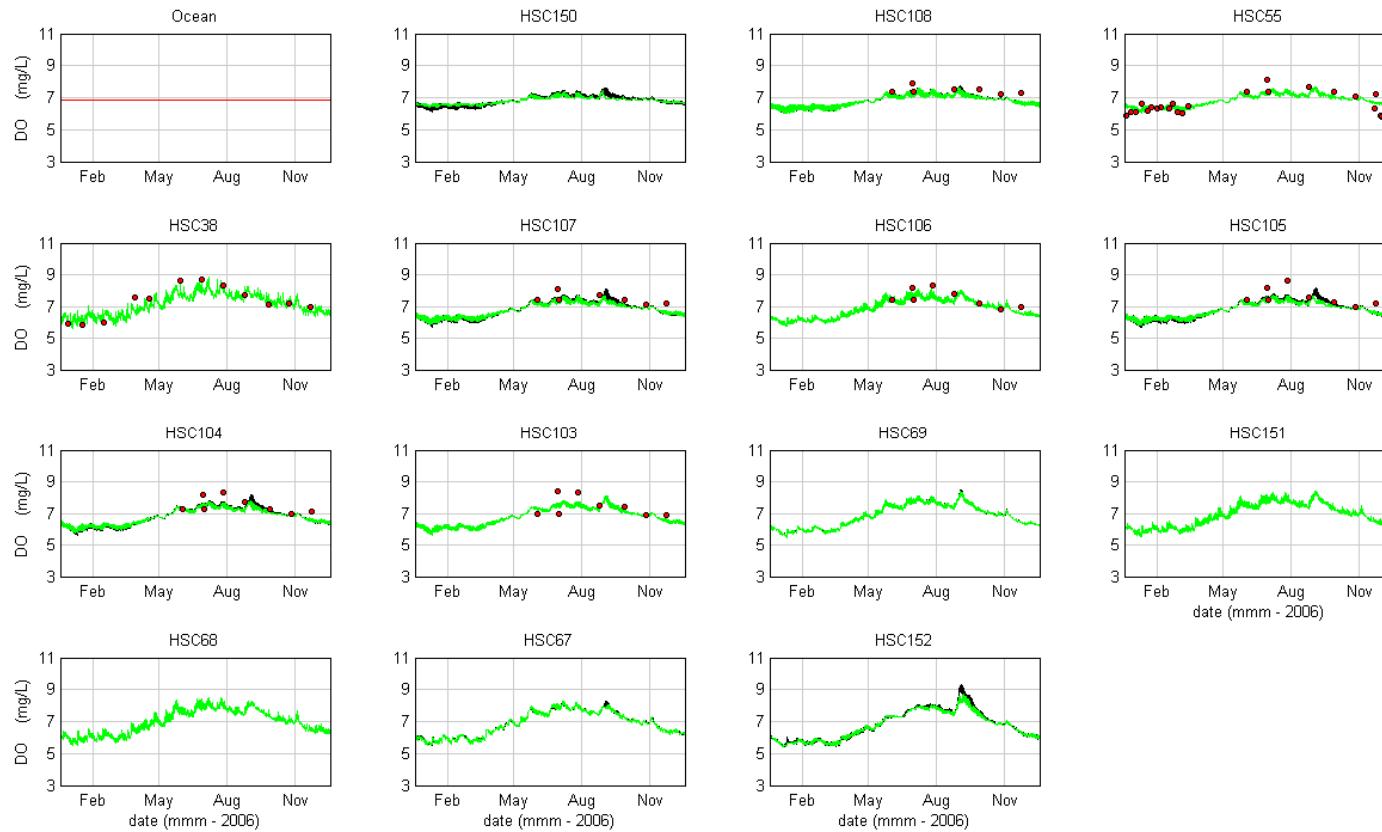
Water Quality Modelling of the Hawkesbury-Nepean River System



■ **Figure 13-27 Box and Whisker Plots – Temperature Validation 2007 (measured data (red), modelled surface (blue) and modelled bottom (green))**



Water Quality Modelling of the Hawkesbury-Nepean River System

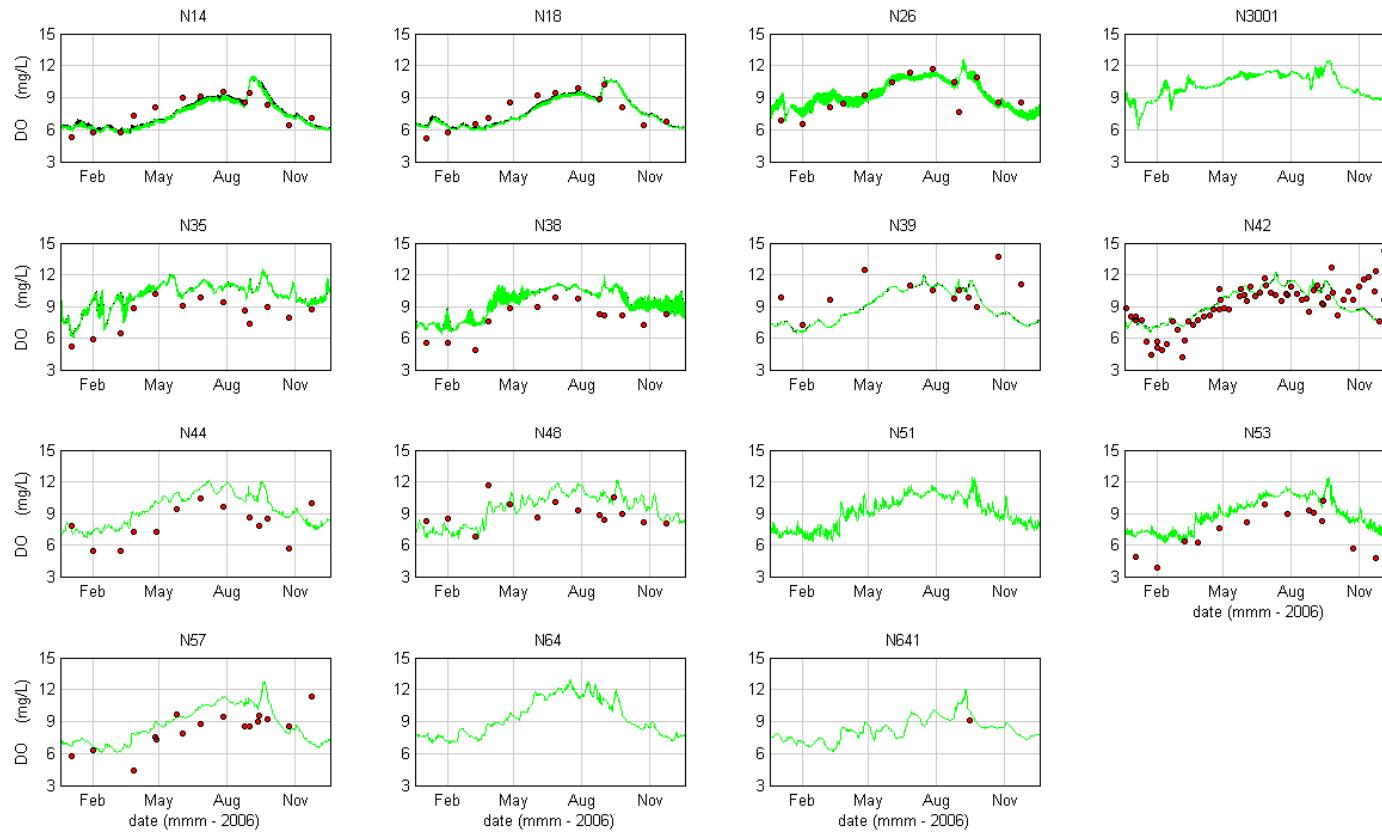


■ **Figure 13-28 Dissolved Oxygen Calibration 2006 (measured data (red), modelled surface (black) and modelled bottom (green))**

SINCLAIR KNIGHT MERZ



Water Quality Modelling of the Hawkesbury-Nepean River System

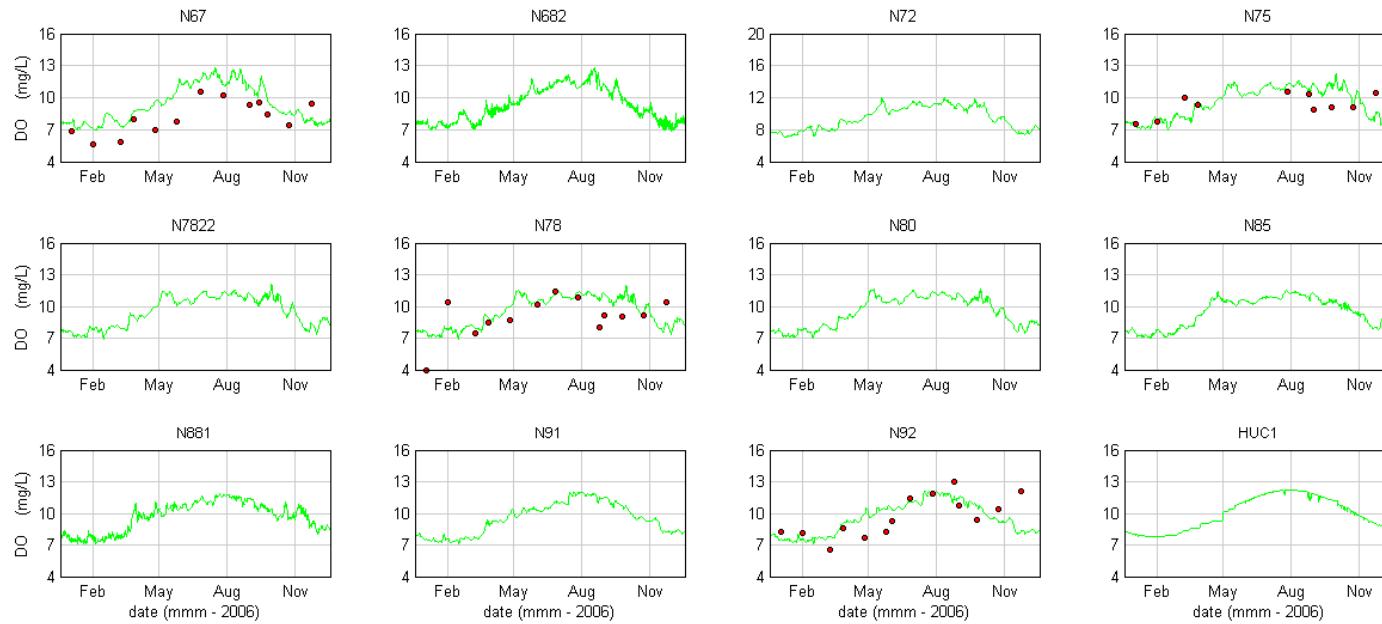


- **Figure 13-28 (Cont.) Dissolved Oxygen Calibration 2006 (measured data (red), modelled surface (black) and modelled bottom (green))**

SINCLAIR KNIGHT MERZ



Water Quality Modelling of the Hawkesbury-Nepean River System

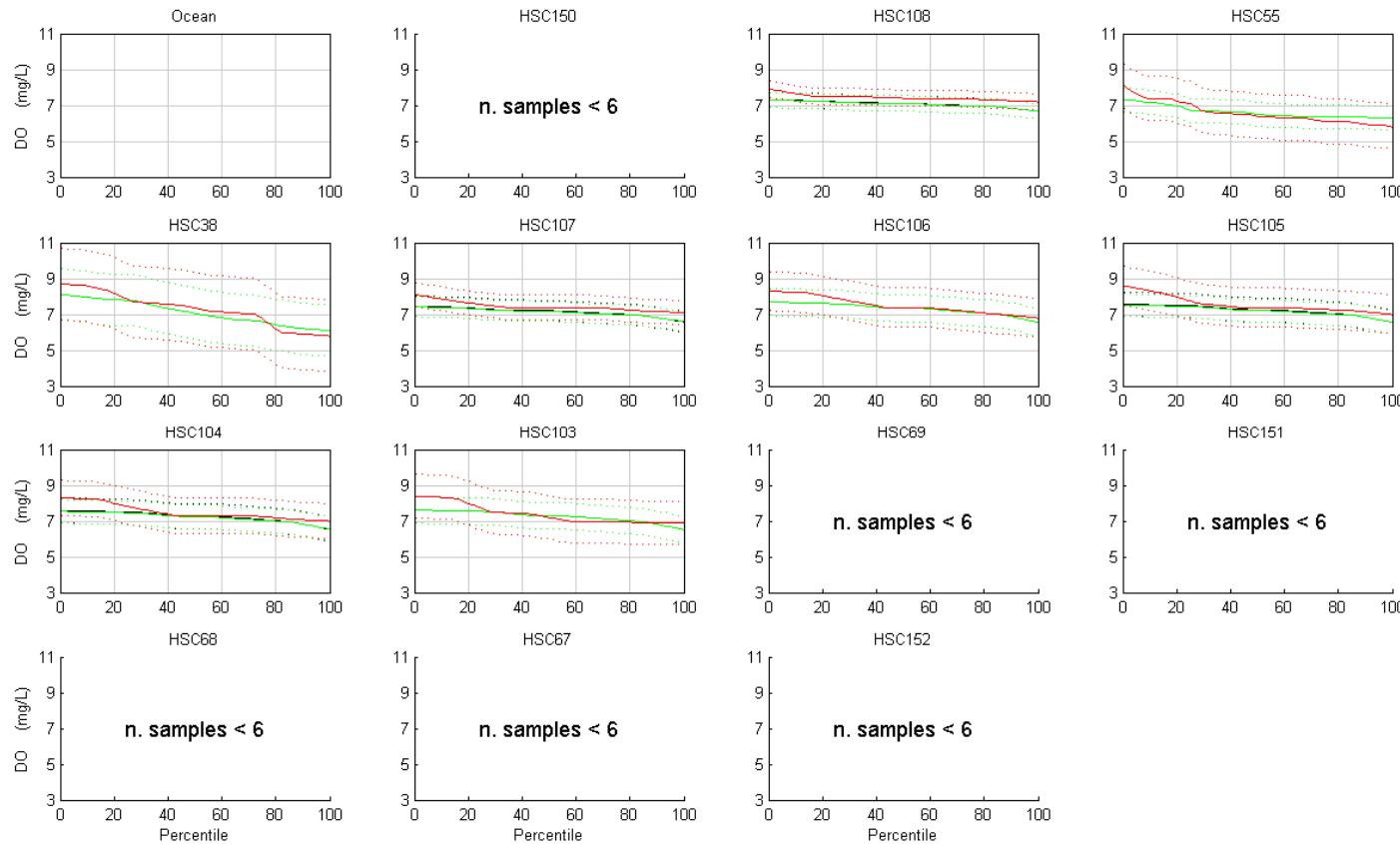


- **Figure 13-28 (Cont.) Dissolved Oxygen Calibration 2006 (measured data (red), modelled surface (black) and modelled bottom (green))**

SINCLAIR KNIGHT MERZ



Water Quality Modelling of the Hawkesbury-Nepean River System

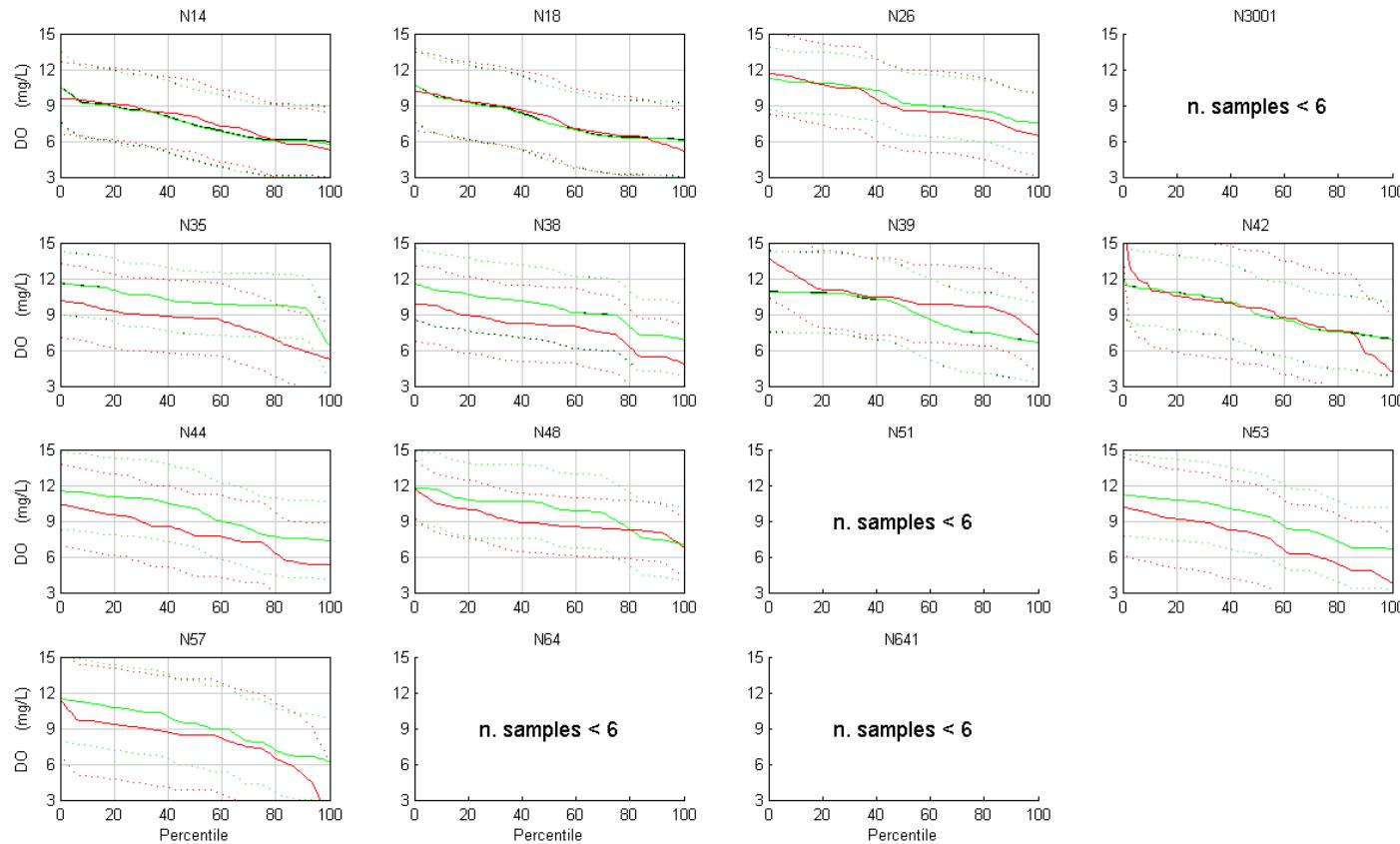


- **Figure 13-29 Exceedance Plots – Dissolved Oxygen Calibration 2006 (+/- 2SD) (measured data (red), modelled surface (black) and modelled bottom (green))**

SINCLAIR KNIGHT MERZ



Water Quality Modelling of the Hawkesbury-Nepean River System

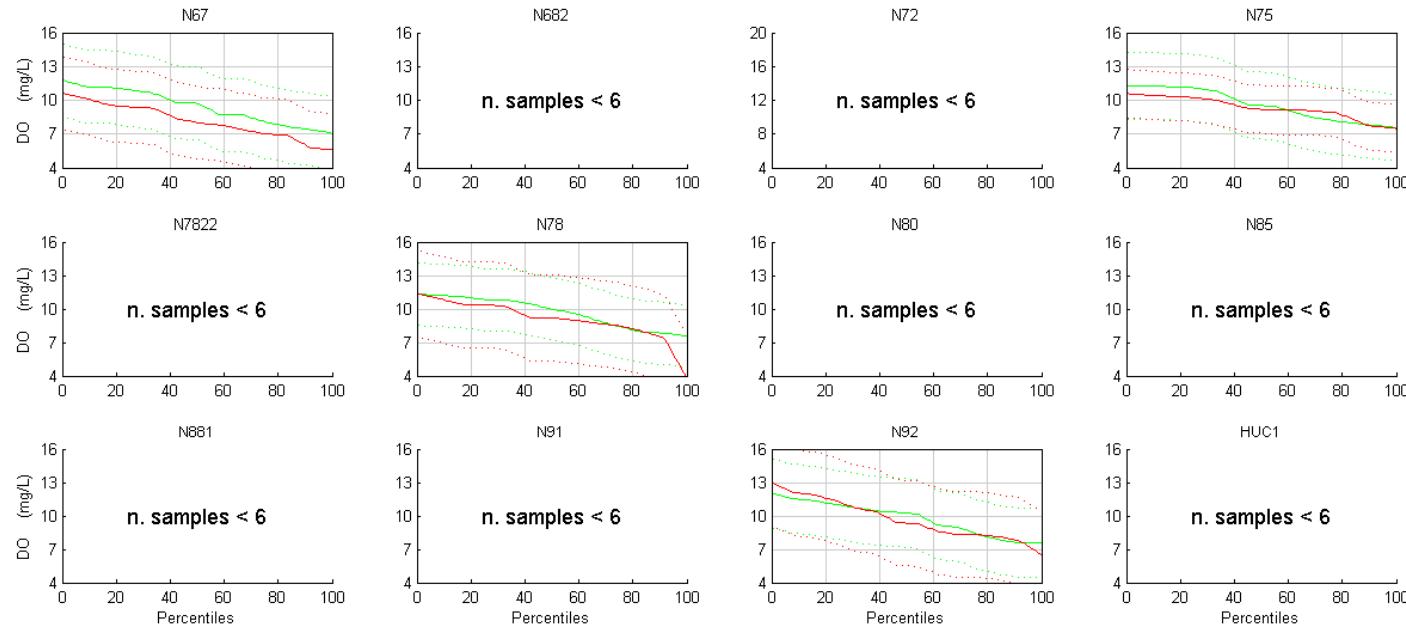


- Figure 13-29 (Cont.) Exceedance Plots – Dissolved Oxygen Calibration 2006 (+/- 2SD) (measured data (red), modelled surface (black) and modelled bottom (green))

SINCLAIR KNIGHT MERZ



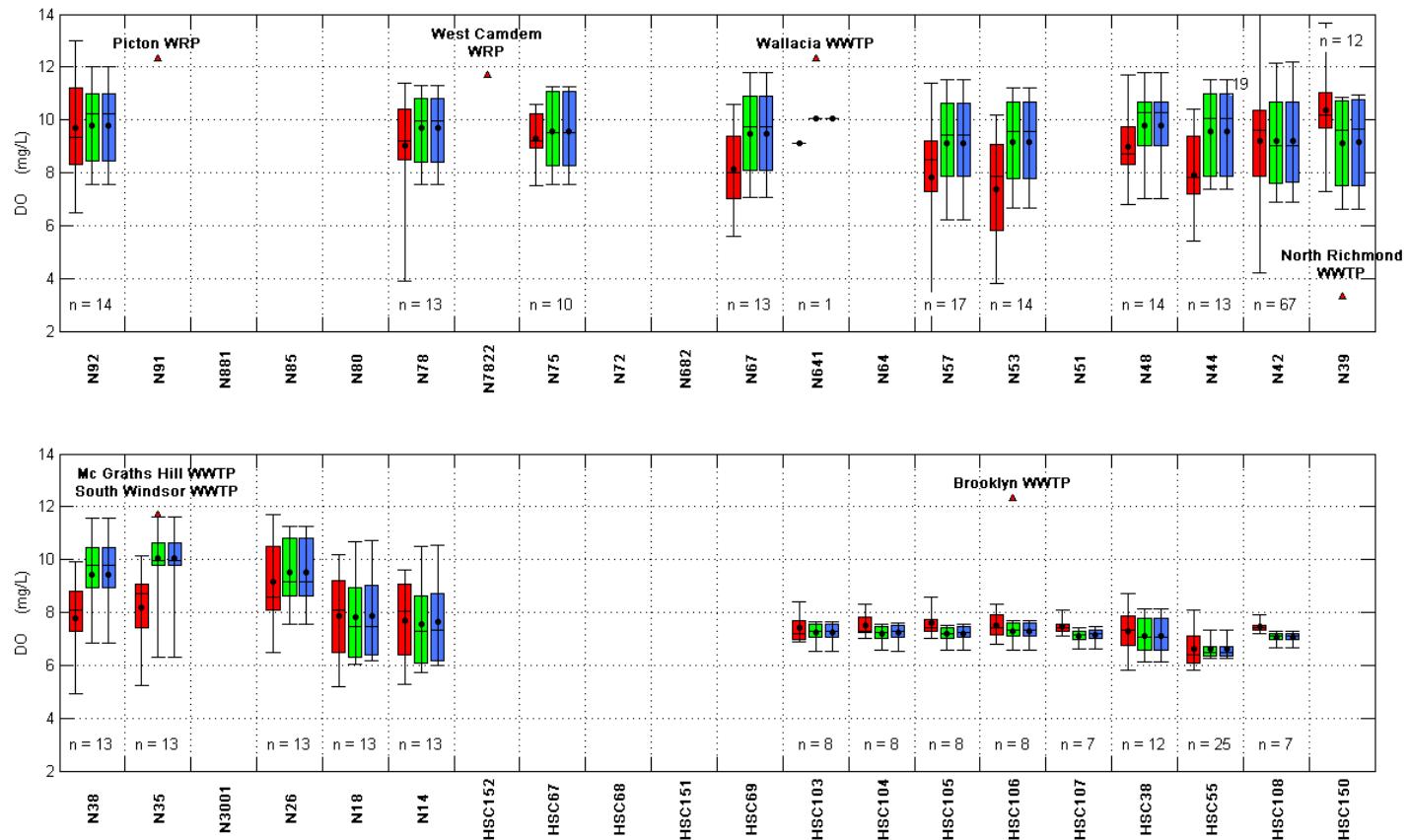
Water Quality Modelling of the Hawkesbury-Nepean River System



- Figure 13-29 (Cont.) Exceedance Plots – Dissolved Oxygen Calibration 2006 (+/- 2SD) (measured data (red), modelled surface (black) and modelled bottom (green))

SINCLAIR KNIGHT MERZ

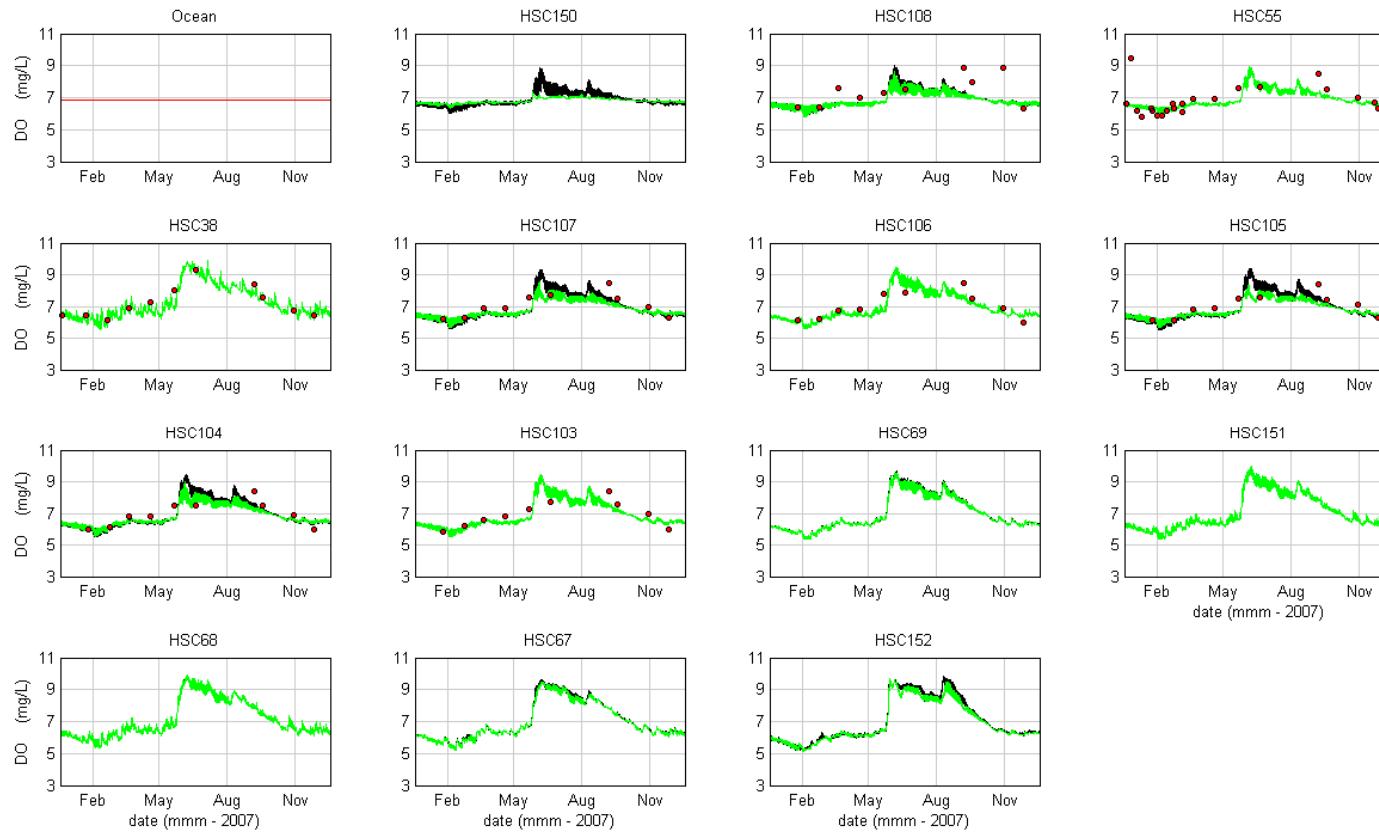
Water Quality Modelling of the Hawkesbury-Nepean River System



■ Figure 13-30 Box and Whisker Plots – Dissolved Oxygen Calibration 2006 (measured data (red), modelled surface (blue) and modelled bottom (green))



Water Quality Modelling of the Hawkesbury-Nepean River System

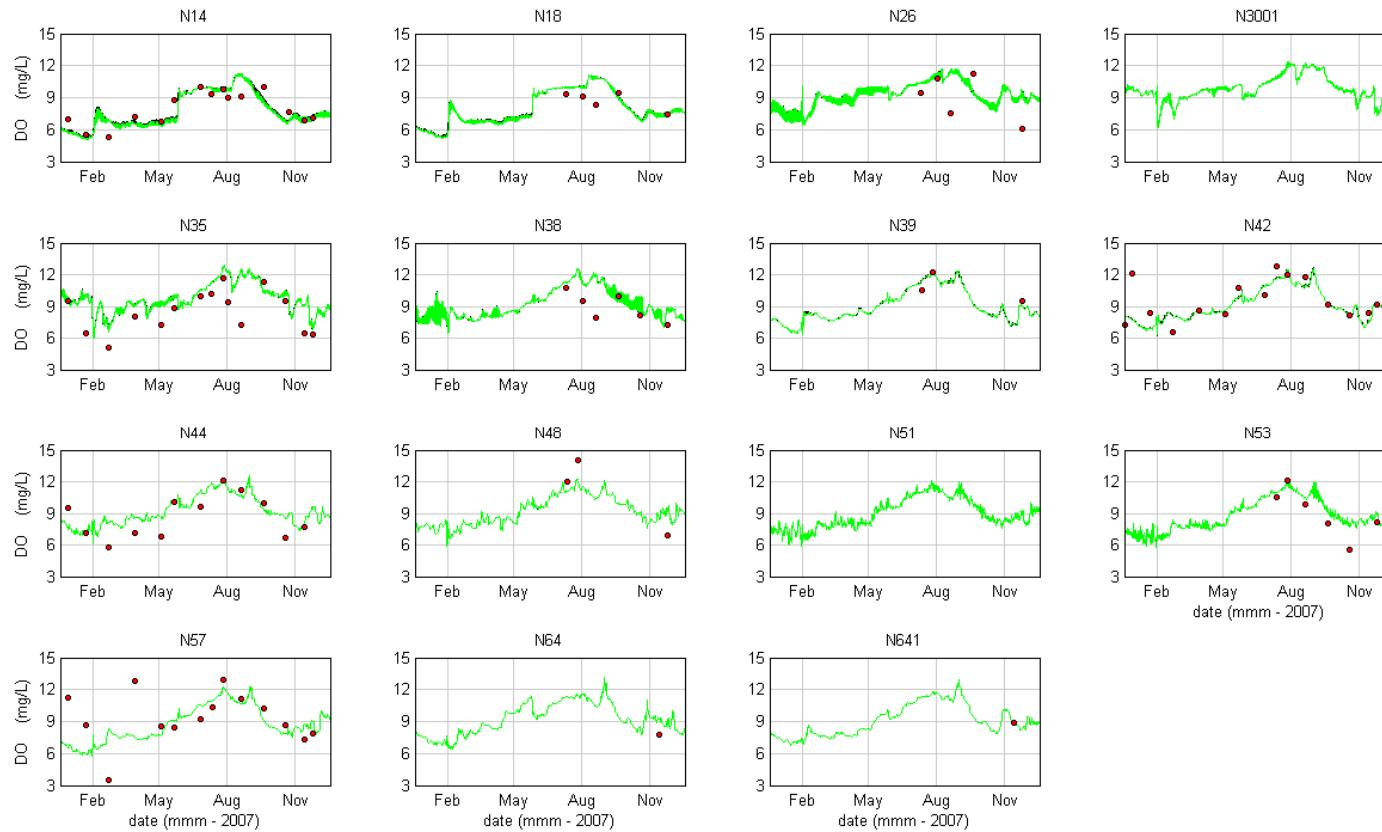


■ **Figure 13-31 Dissolved Oxygen Validation 2007 (measured data (red), modelled surface (black) and modelled bottom (green))**

SINCLAIR KNIGHT MERZ



Water Quality Modelling of the Hawkesbury-Nepean River System

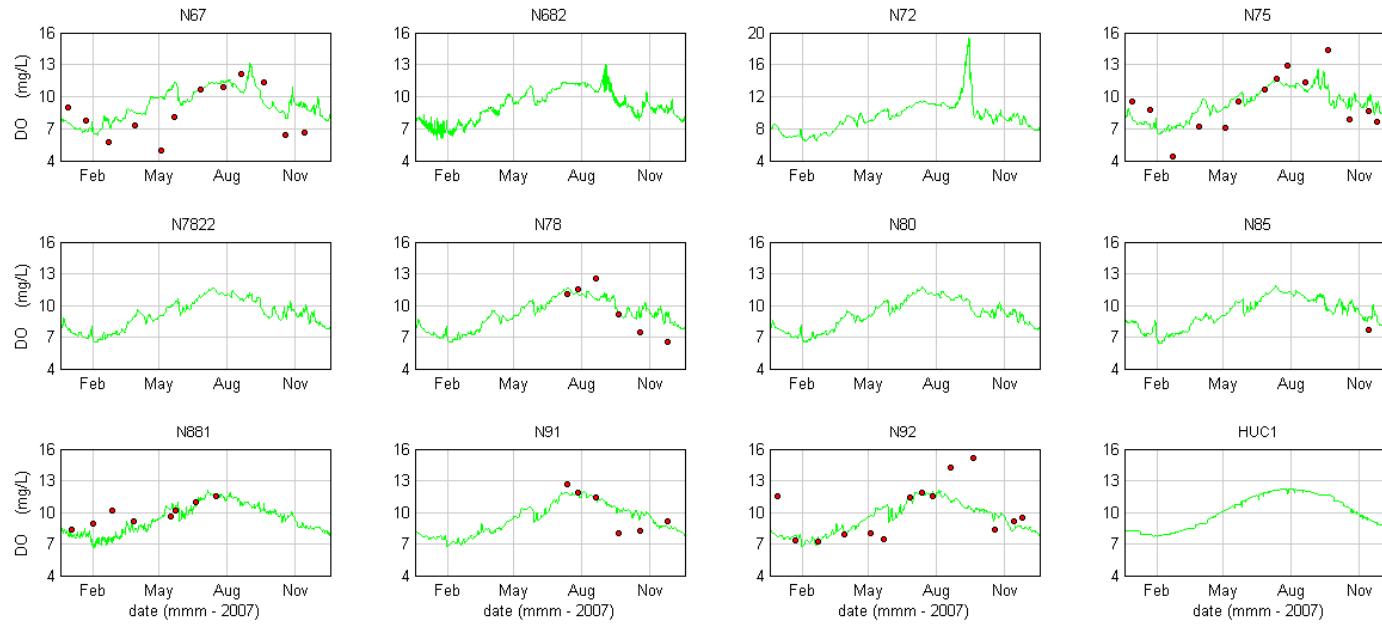


- **Figure 13-31 (Cont.) Dissolved Oxygen Validation 2007 (measured data (red), modelled surface (black) and modelled bottom (green))**

SINCLAIR KNIGHT MERZ



Water Quality Modelling of the Hawkesbury-Nepean River System

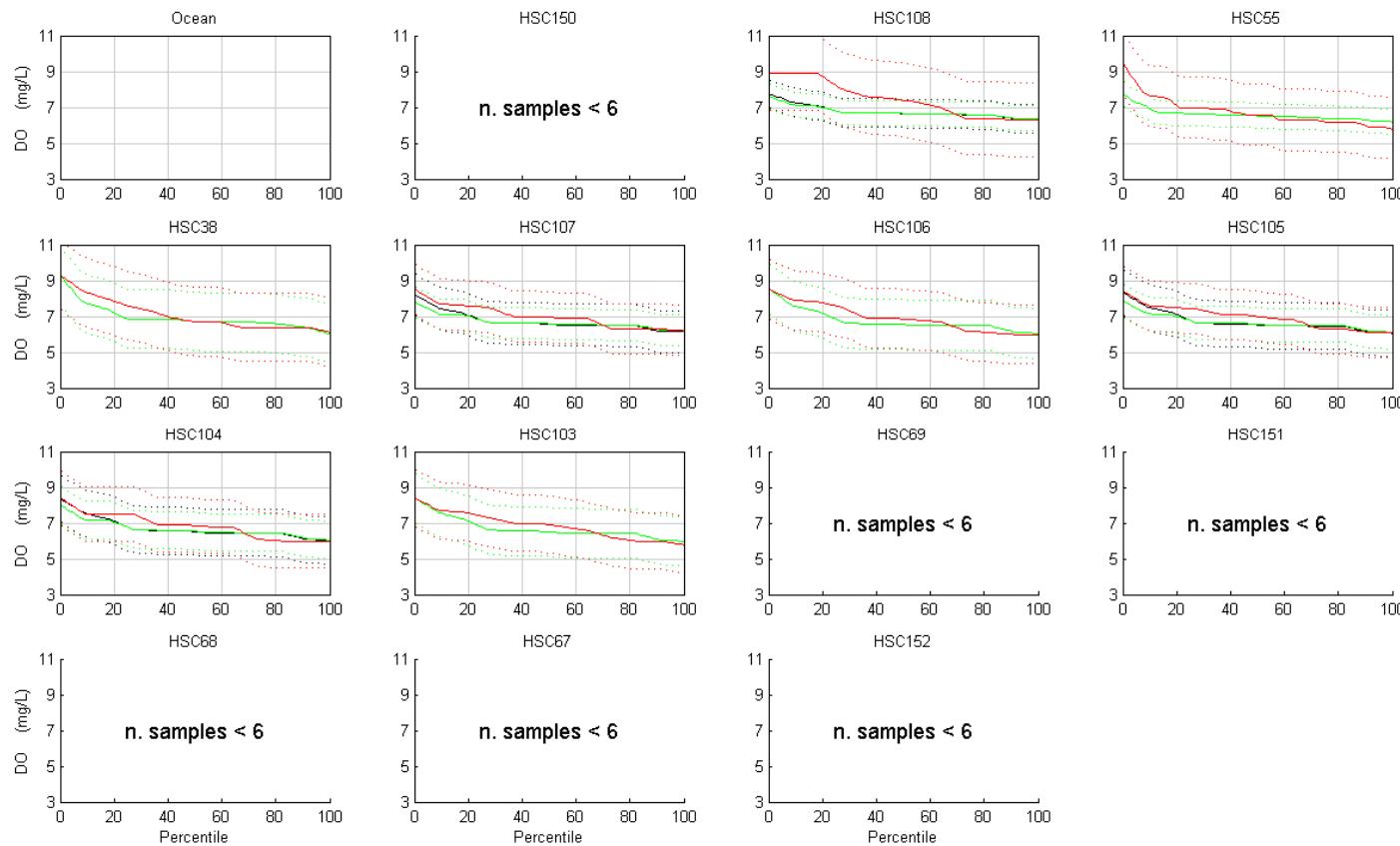


- **Figure 13-31 (Cont.) Dissolved Oxygen Validation 2007 (measured data (red), modelled surface (black) and modelled bottom (green))**

SINCLAIR KNIGHT MERZ



Water Quality Modelling of the Hawkesbury-Nepean River System

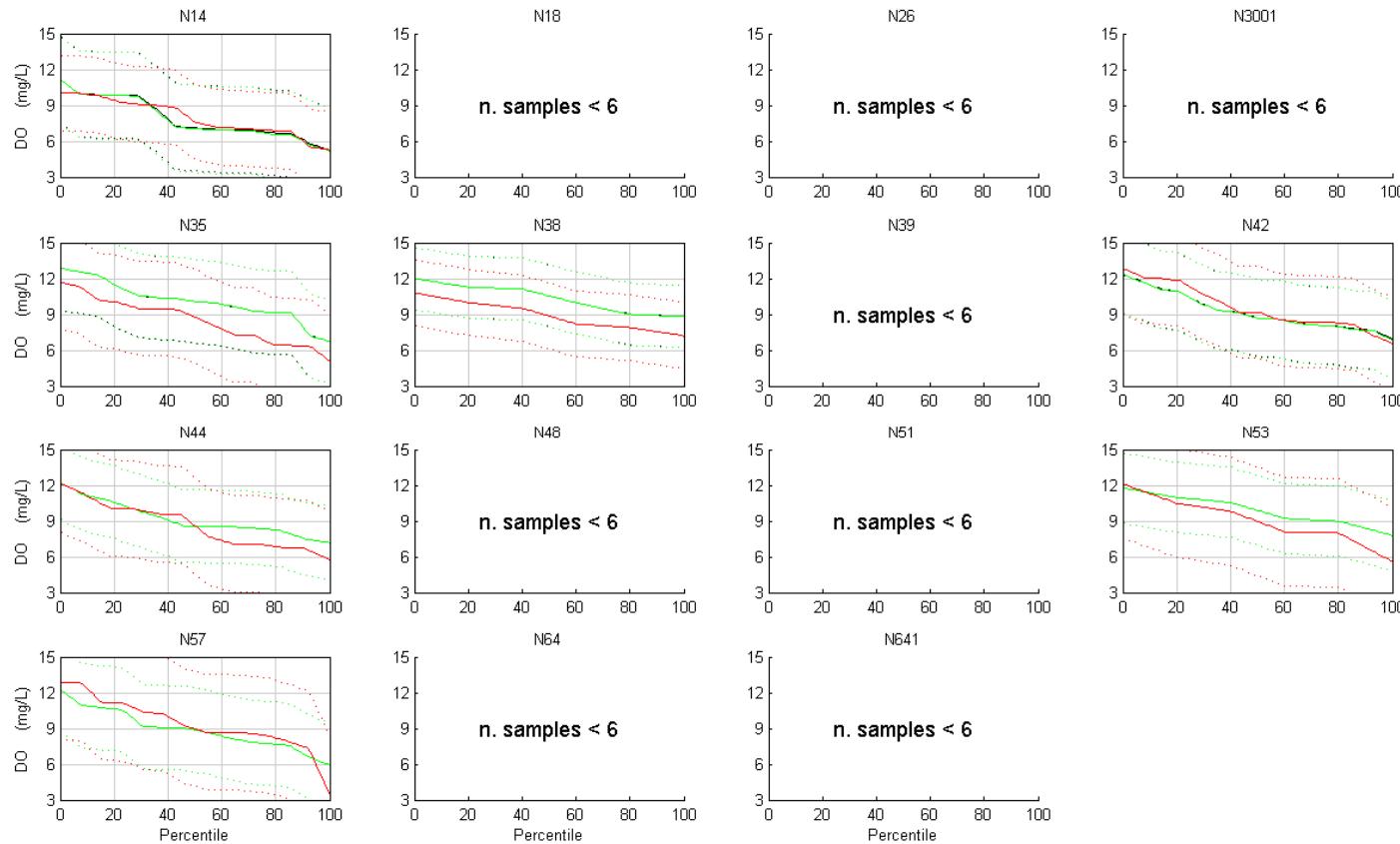


- **Figure 13-32 Exceedance Plots – Dissolved Oxygen Validation 2007 (+/- 2SD) (measured data (red), modelled surface (black) and modelled bottom (green))**

SINCLAIR KNIGHT MERZ



Water Quality Modelling of the Hawkesbury-Nepean River System

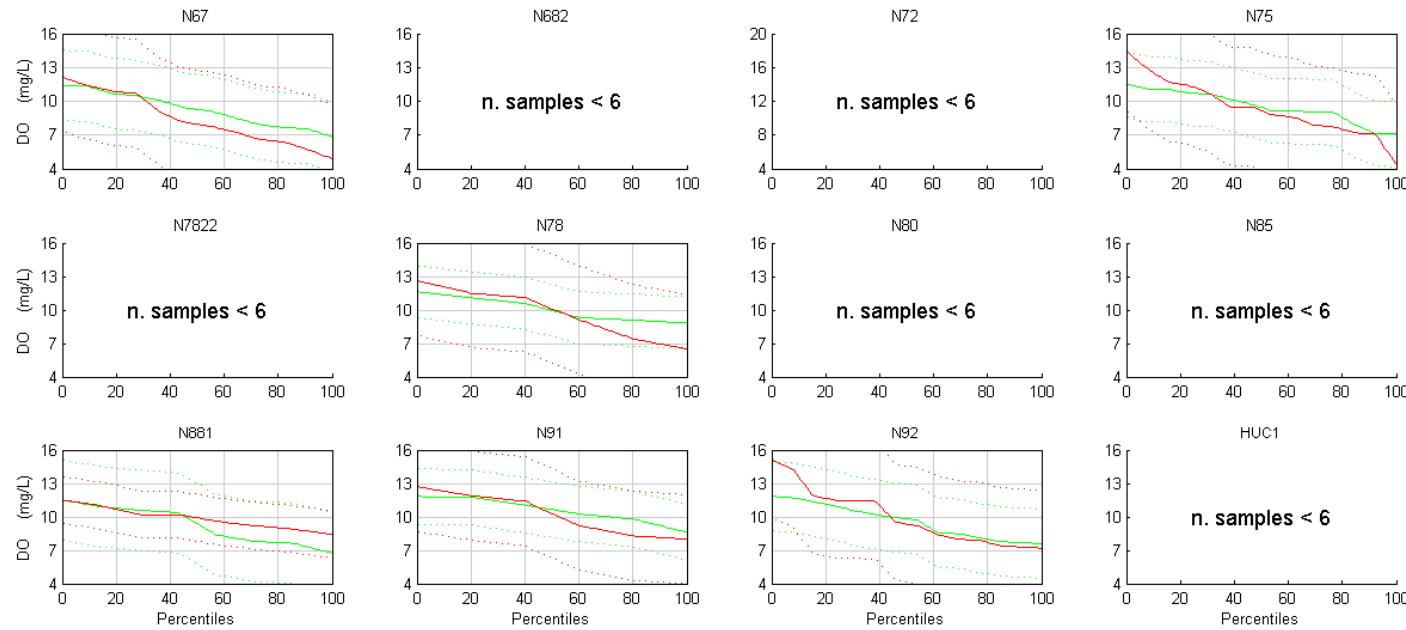


- **Figure 13-32 (Cont.) Exceedance Plots – Dissolved Oxygen Validation 2007 (+/- 2SD) (measured data (red), modelled surface (black) and modelled bottom (green))**

SINCLAIR KNIGHT MERZ



Water Quality Modelling of the Hawkesbury-Nepean River System

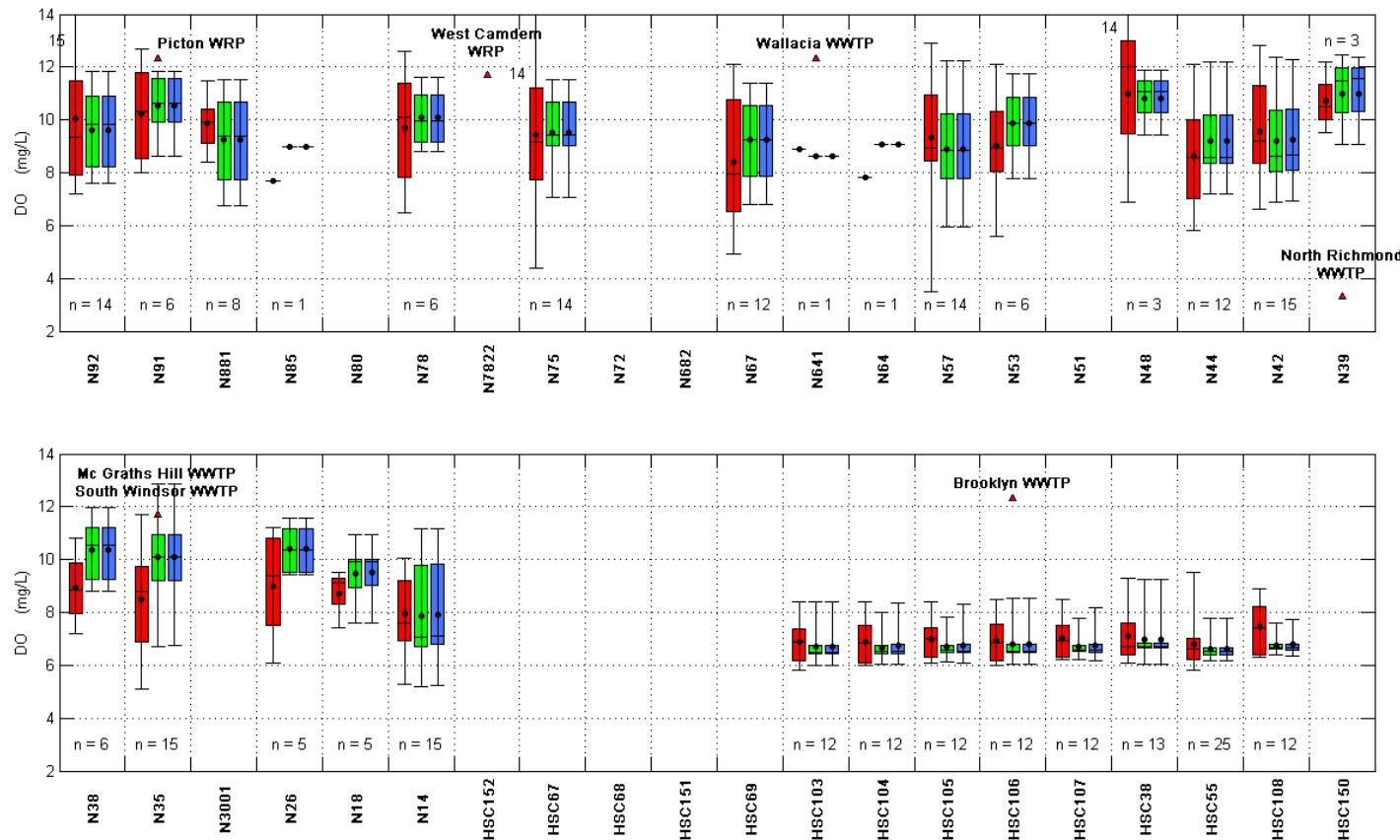


- Figure 13-32 (Cont.) Exceedance Plots – Dissolved Oxygen Validation 2007 (+/- 2SD) (measured data (red), modelled surface (black) and modelled bottom (green))

SINCLAIR KNIGHT MERZ



Water Quality Modelling of the Hawkesbury-Nepean River System



■ **Figure 13-33 Box and Whisker Plots – Dissolved Oxygen Validation 2007 (measured data (red), modelled surface (blue) and modelled bottom (green))**



Water Quality Modelling of the Hawkesbury-Nepean River System

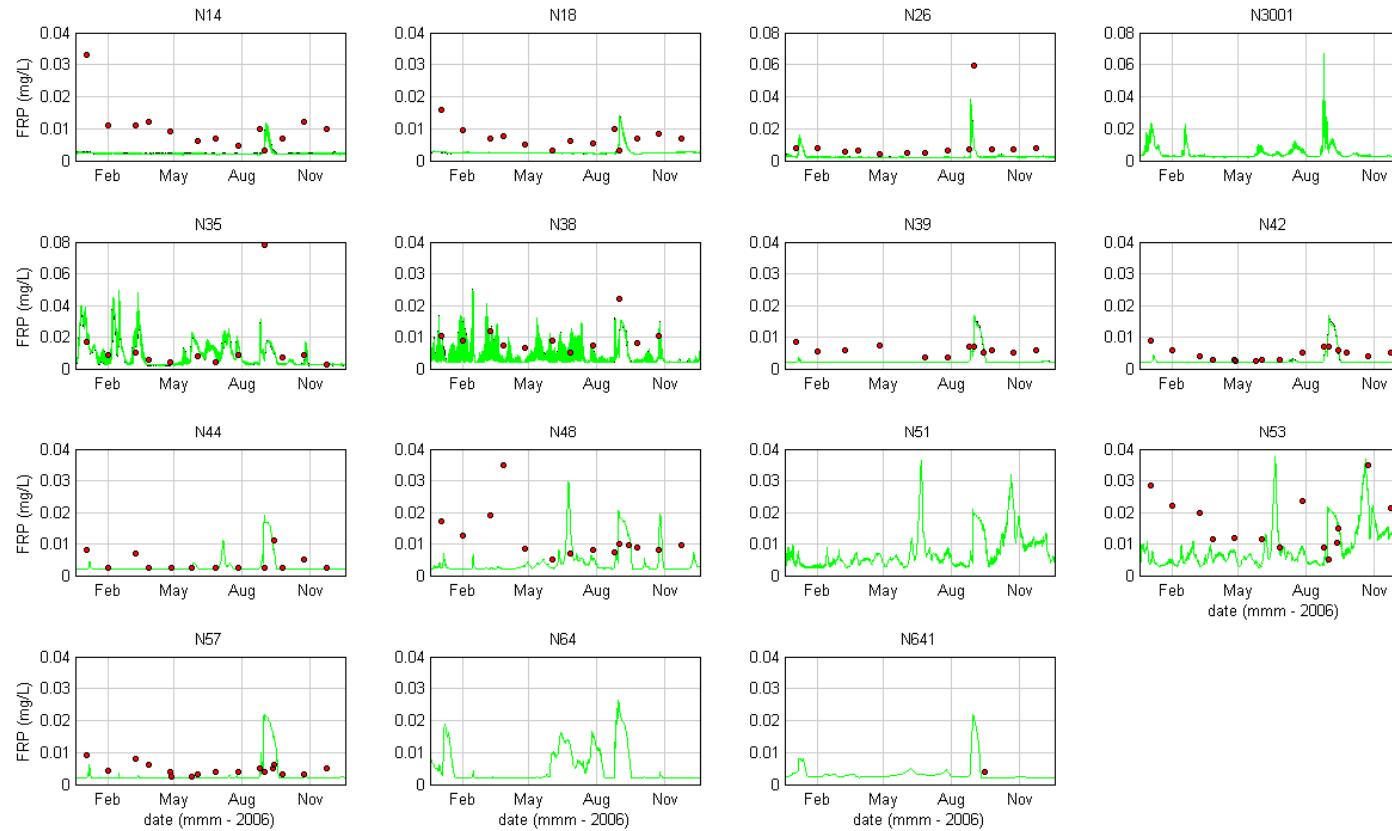


- **Figure 13-34 Filterable Reactive Phosphorus Calibration 2006 (measured data (red), modelled surface (black) and modelled bottom (green))**

SINCLAIR KNIGHT MERZ



Water Quality Modelling of the Hawkesbury-Nepean River System

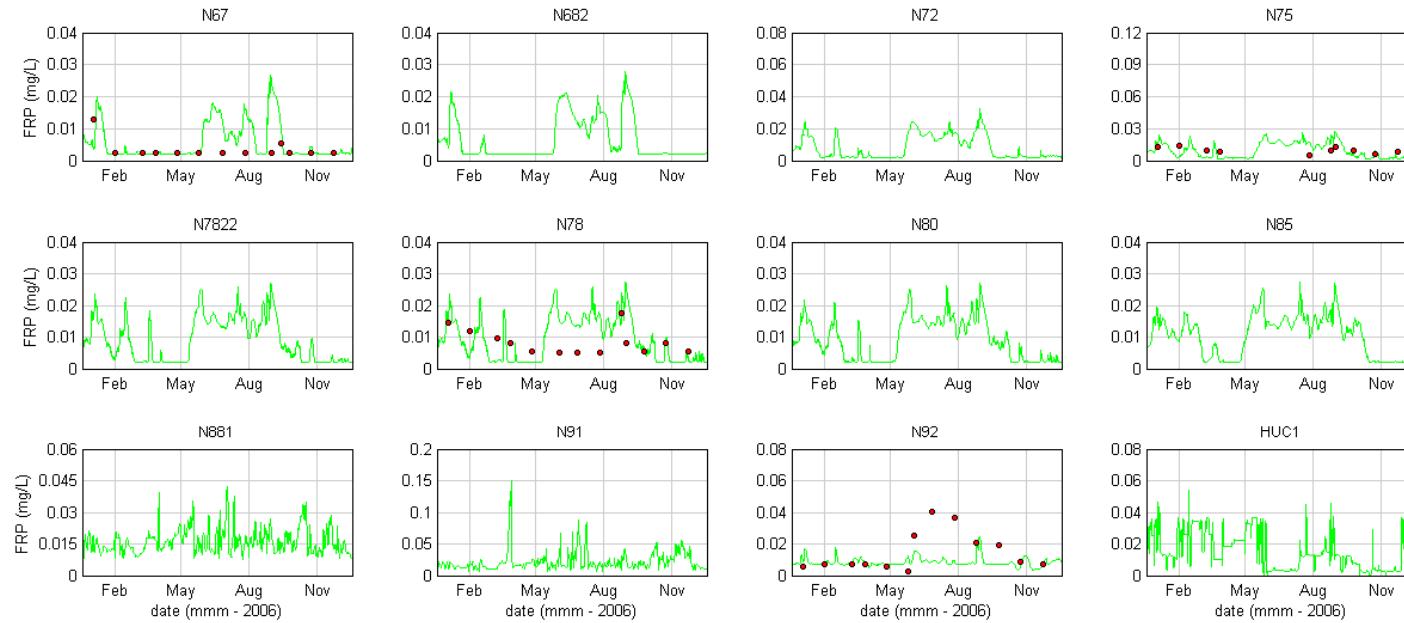


- **Figure 13-34 (Cont.) Filterable Reactive Phosphorus Calibration 2006 (measured data (red), modelled surface (black) and modelled bottom (green))**

SINCLAIR KNIGHT MERZ



Water Quality Modelling of the Hawkesbury-Nepean River System

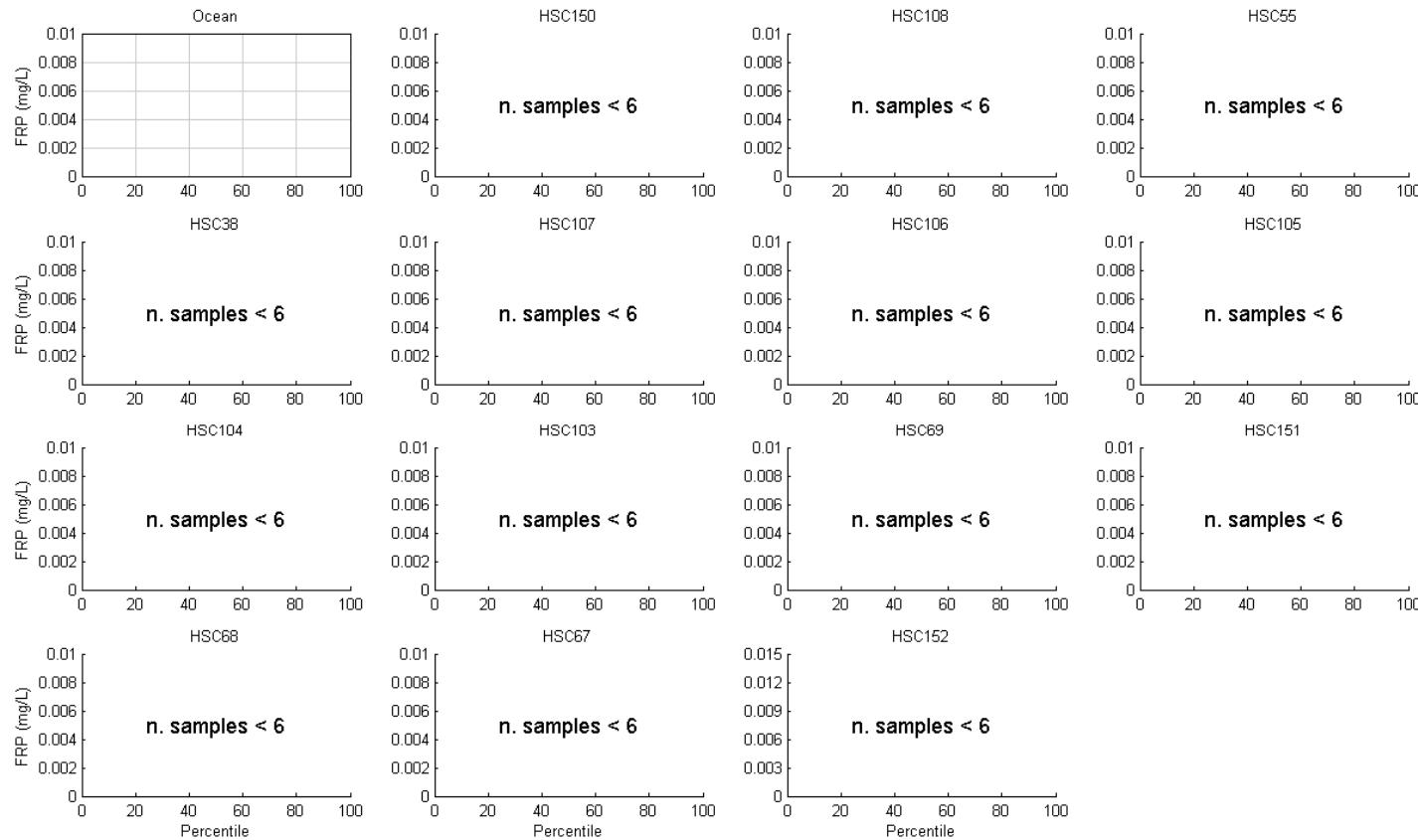


- **Figure 13-34 (Cont.) Filterable Reactive Phosphorus Calibration 2006 (measured data (red), modelled surface (black) and modelled bottom (green))**

SINCLAIR KNIGHT MERZ



Water Quality Modelling of the Hawkesbury-Nepean River System

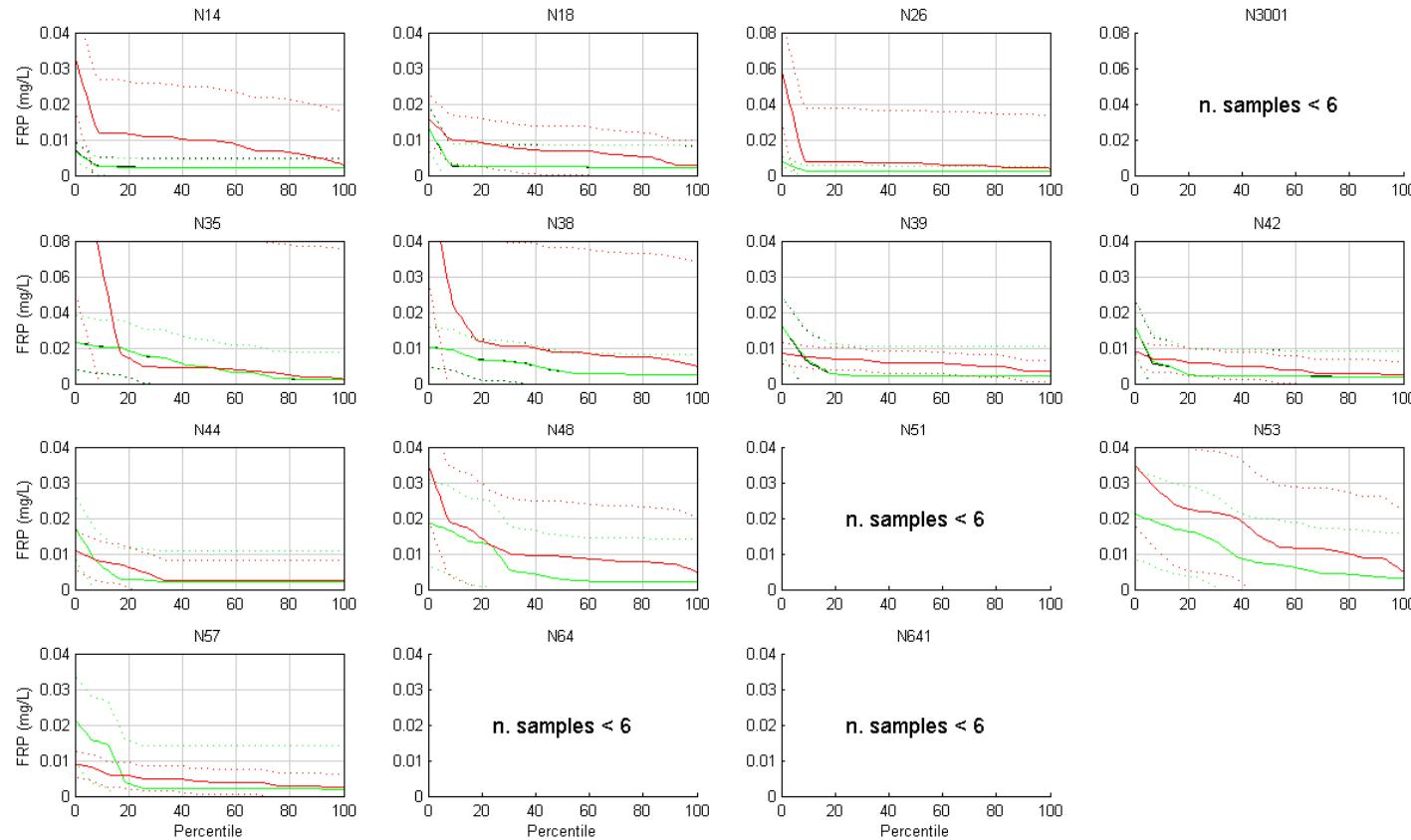


- Figure 13-35 Exceedance Plots – Filterable Reactive Phosphorus Calibration 2006 (+/- 2SD) (measured data (red), modelled surface (black) and modelled bottom (green))

SINCLAIR KNIGHT MERZ



Water Quality Modelling of the Hawkesbury-Nepean River System

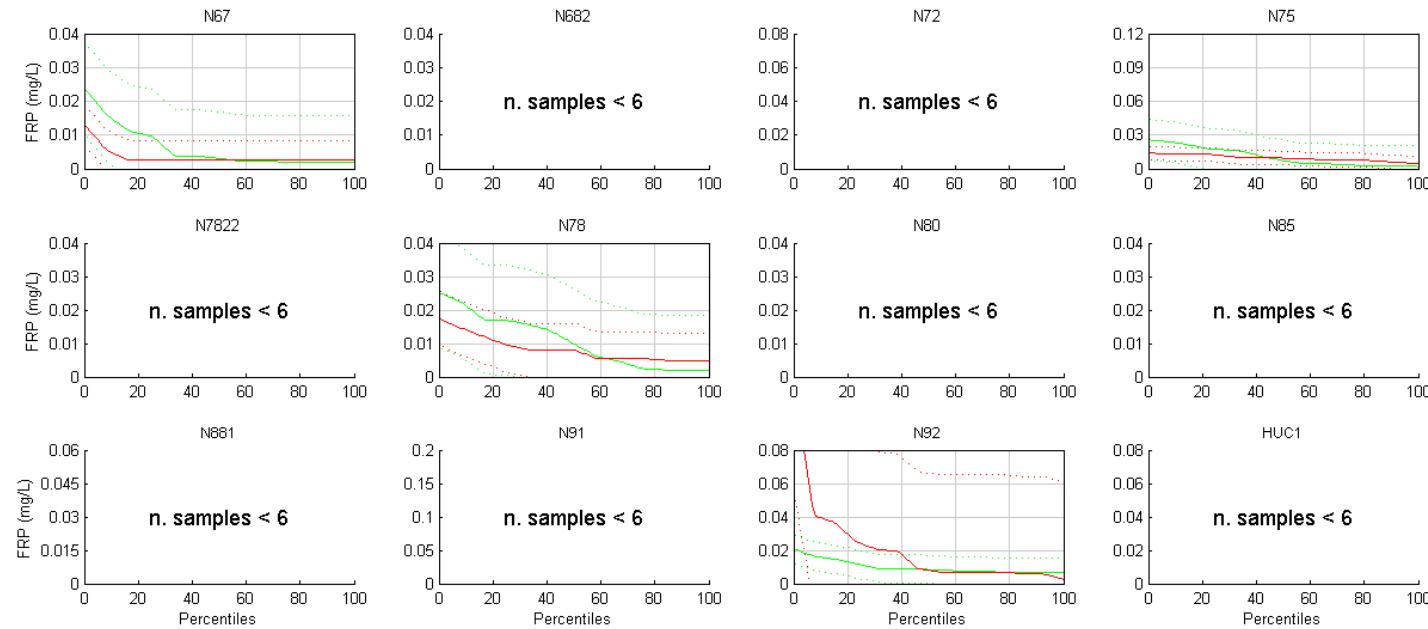


- Figure 13-35 (Cont.) Exceedance Plots – Filterable Reactive Phosphorus Calibration 2006 (+/- 2SD) (measured data (red), modelled surface (black) and modelled bottom (green))

SINCLAIR KNIGHT MERZ



Water Quality Modelling of the Hawkesbury-Nepean River System

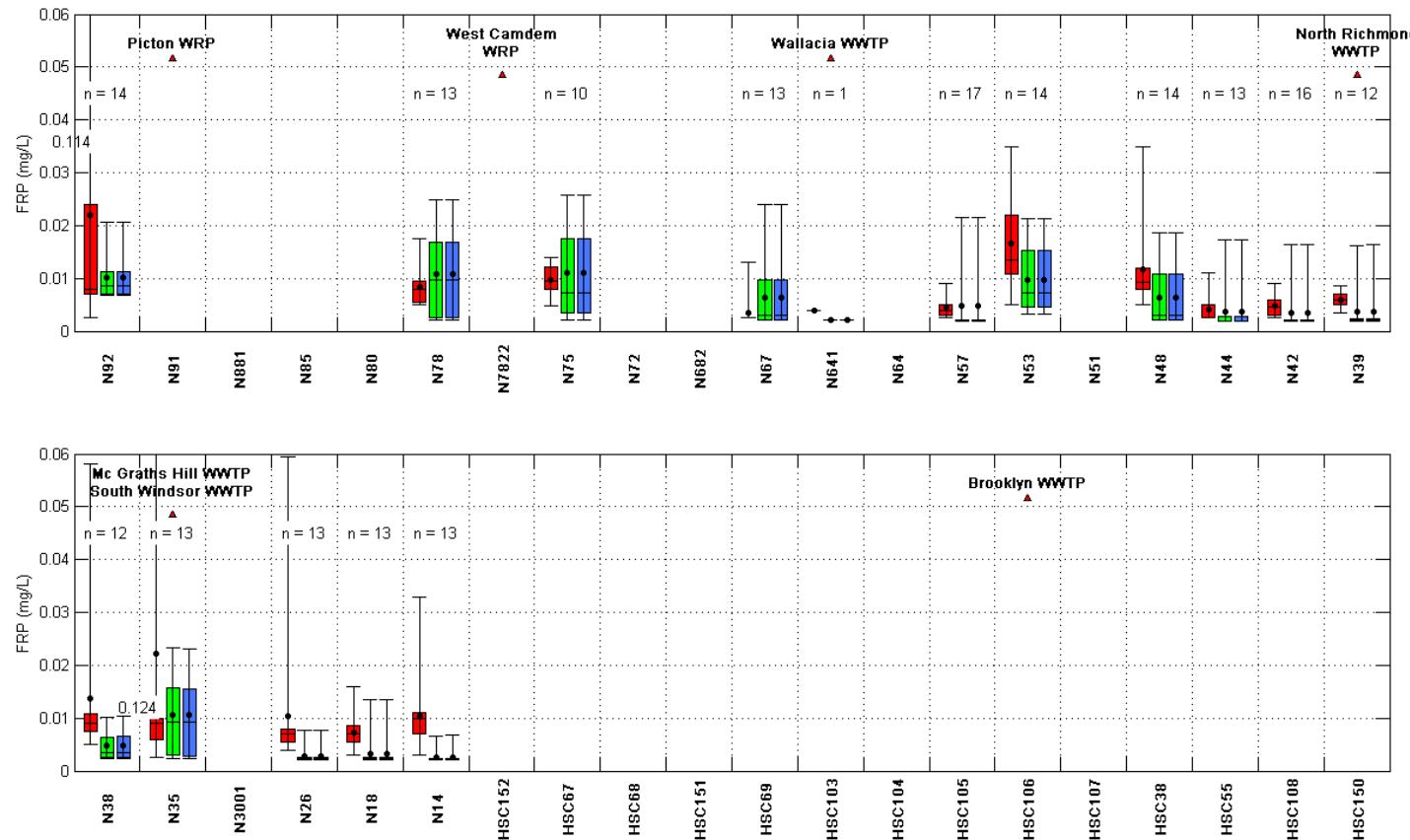


- Figure 13-35 (Cont.) Exceedance Plots – Filterable Reactive Phosphorus Calibration 2006 (+/- 2SD) (measured data (red), modelled surface (black) and modelled bottom (green))

SINCLAIR KNIGHT MERZ



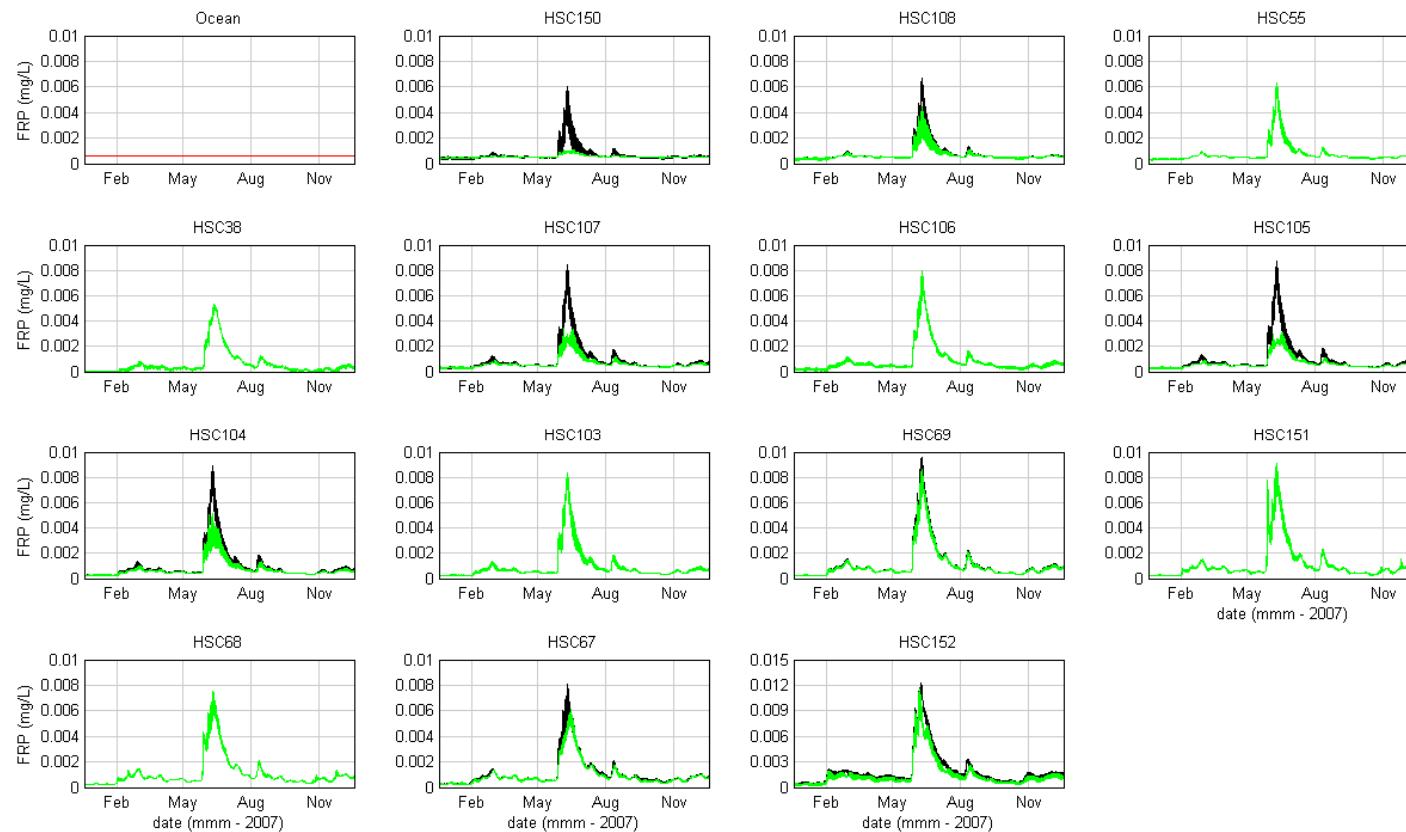
Water Quality Modelling of the Hawkesbury-Nepean River System



- **Figure 13-36 Box and Whisker Plots – Filterable Reactive Phosphorus Calibration 2006 (measured data (red), modelled surface (blue) and modelled bottom (green))**



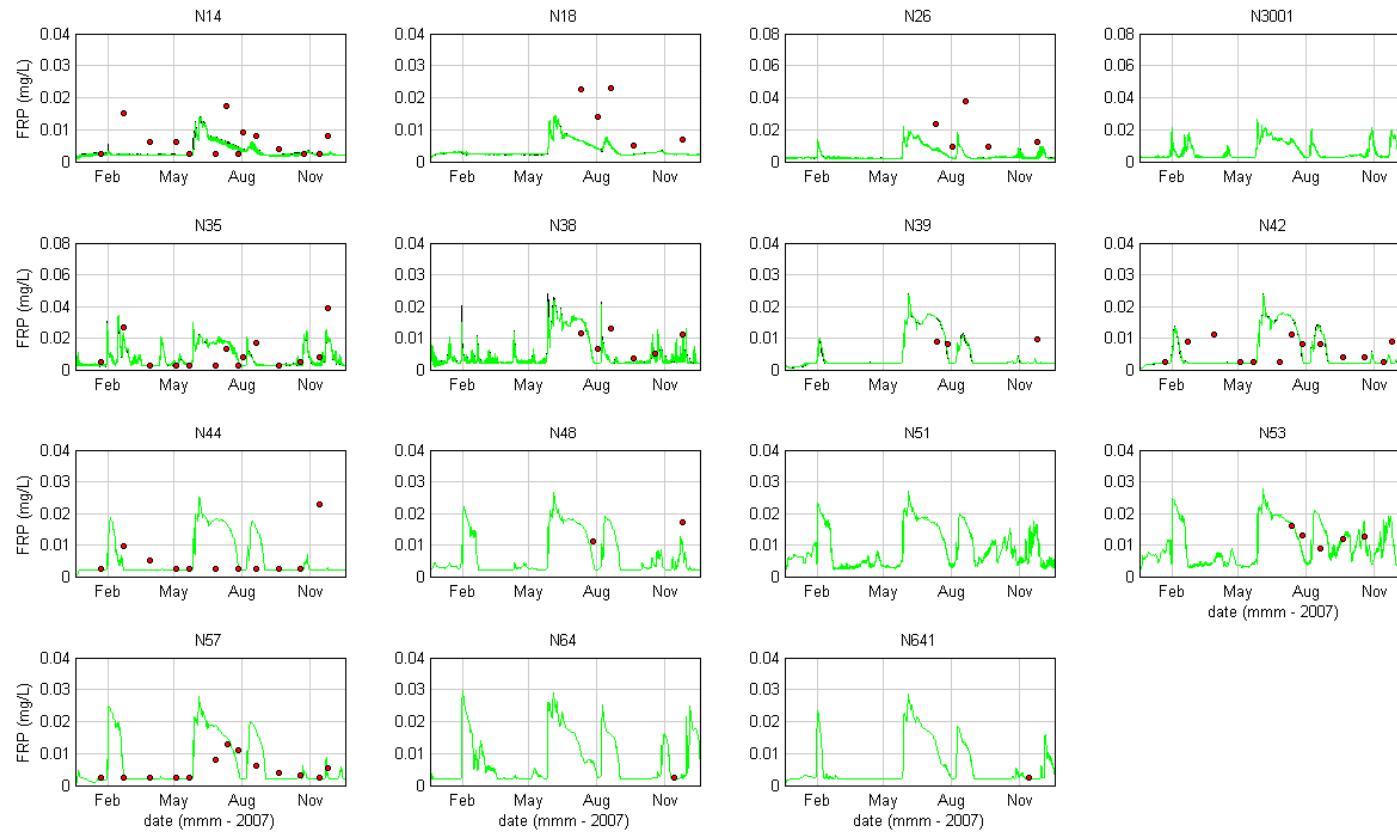
Water Quality Modelling of the Hawkesbury-Nepean River System



- **Figure 13-37 Filterable Reactive Phosphorus Validation 2007 (measured data (red), modelled surface (black) and modelled bottom (green))**



Water Quality Modelling of the Hawkesbury-Nepean River System

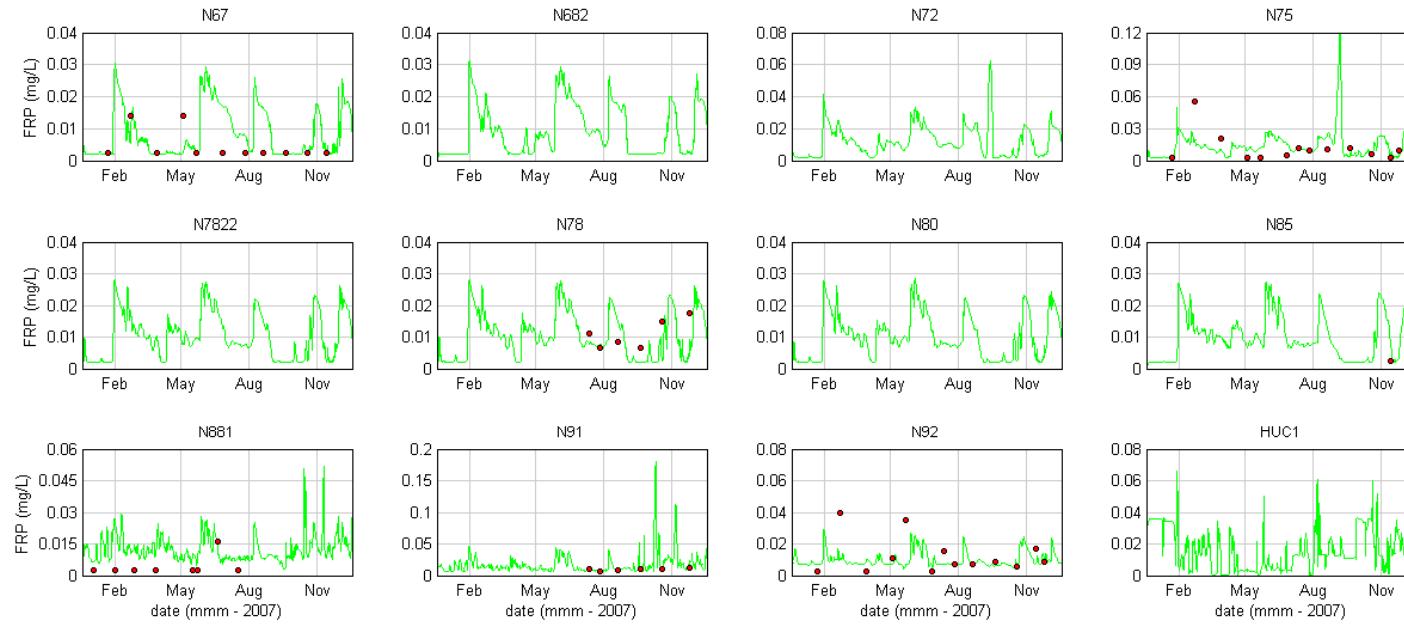


- **Figure 13-37 (Cont.) Filterable Reactive Phosphorus Validation 2007 (measured data (red), modelled surface (black) and modelled bottom (green))**

SINCLAIR KNIGHT MERZ



Water Quality Modelling of the Hawkesbury-Nepean River System

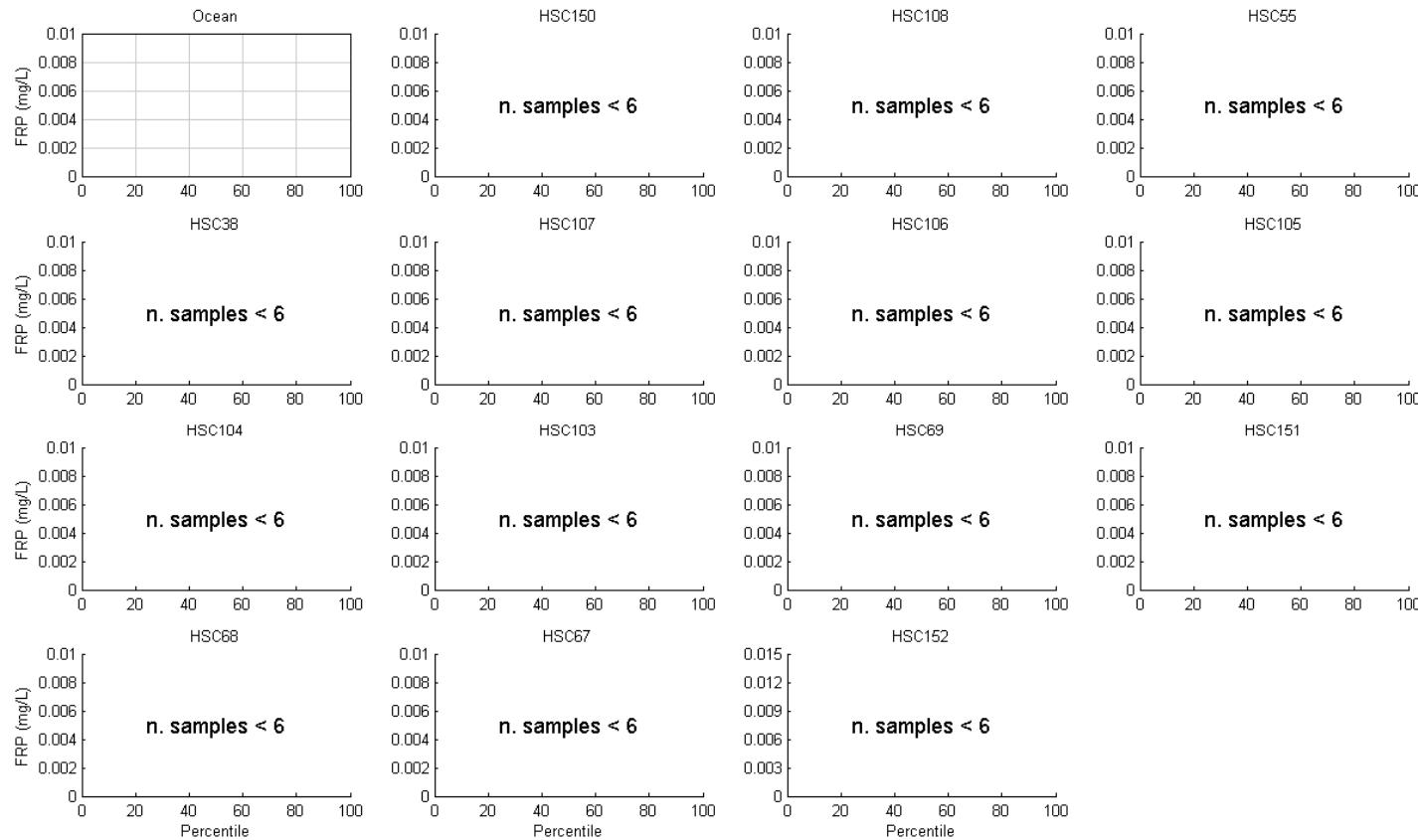


- Figure 13-37 (Cont.) Filterable Reactive Phosphorus Validation 2007 (measured data (red), modelled surface (black) and modelled bottom (green))

SINCLAIR KNIGHT MERZ



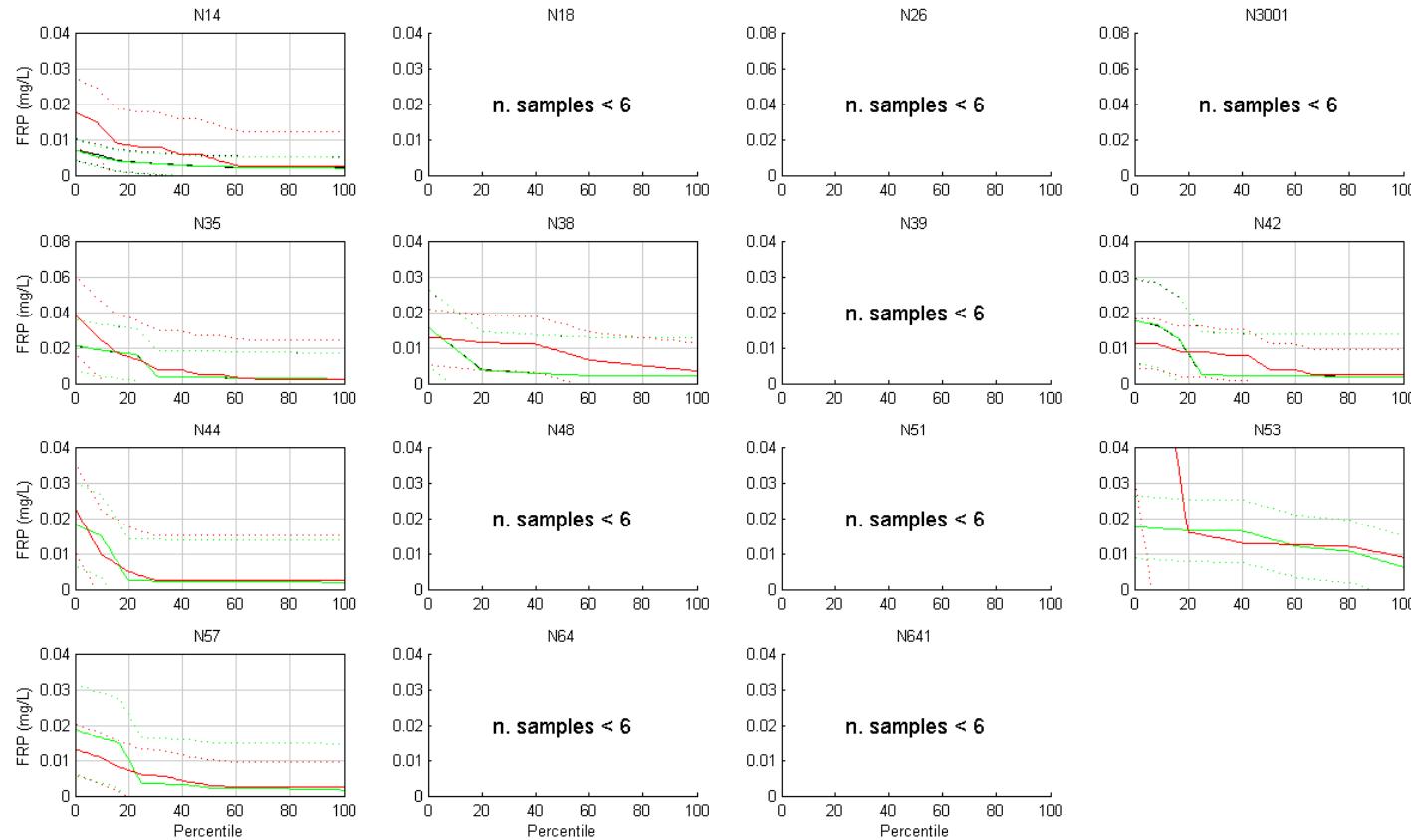
Water Quality Modelling of the Hawkesbury-Nepean River System



- **Figure 13-38 Exceedance Plots – Filterable Reactive Phosphorus Validation 2007 (+/- 2SD) (measured data (red), modelled surface (black) and modelled bottom (green))**

SINCLAIR KNIGHT MERZ

Water Quality Modelling of the Hawkesbury-Nepean River System

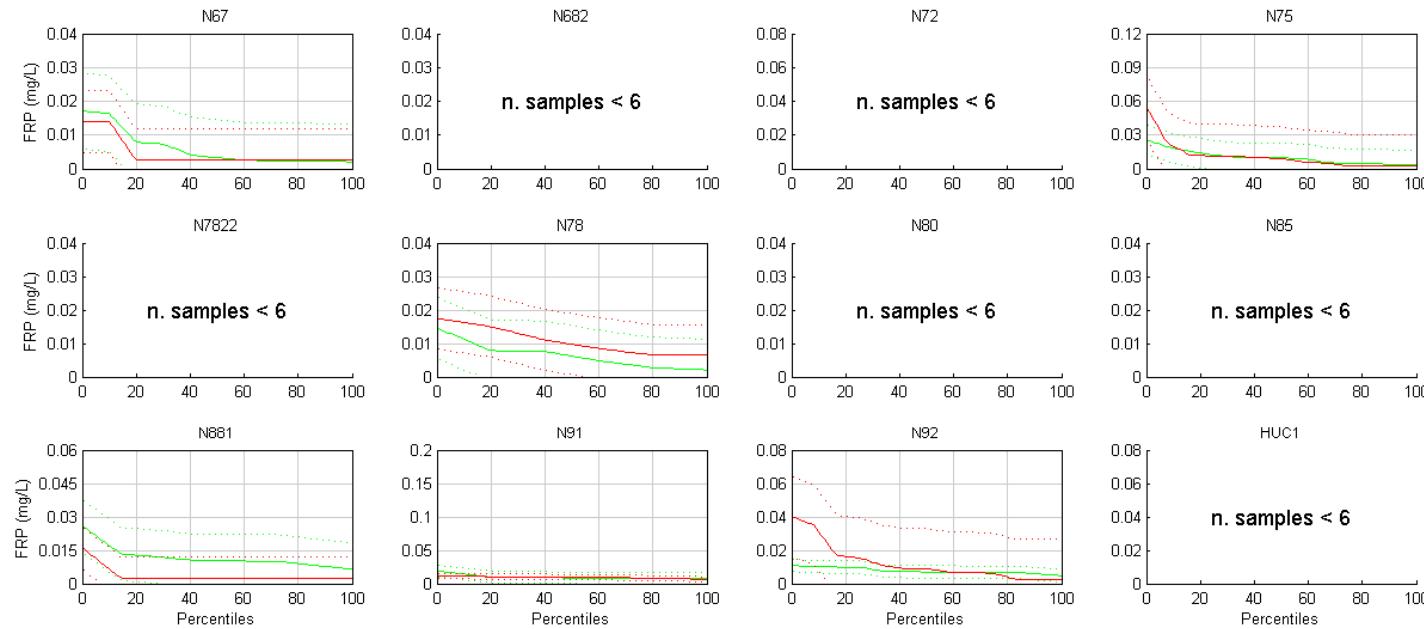


- Figure 13-38 (Cont.) Exceedance Plots – Filterable Reactive Phosphorus Validation 2007 (+/- 2SD) (measured data (red), modelled surface (black) and modelled bottom (green))

SINCLAIR KNIGHT MERZ



Water Quality Modelling of the Hawkesbury-Nepean River System

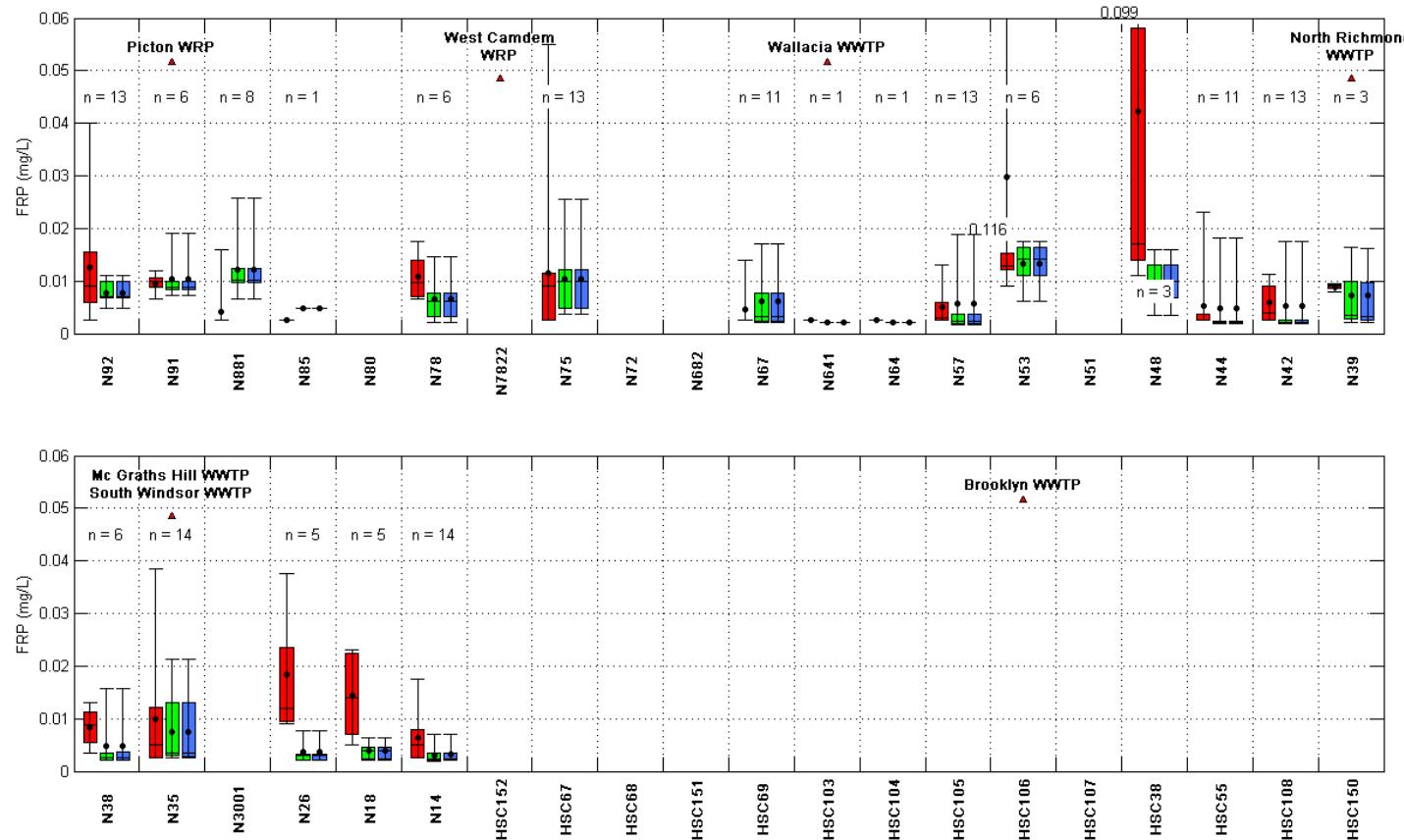


- Figure 13-38 (Cont.) Exceedance Plots – Filterable Reactive Phosphorus Validation 2007 (+/- 2SD) (measured data (red), modelled surface (black) and modelled bottom (green))

SINCLAIR KNIGHT MERZ



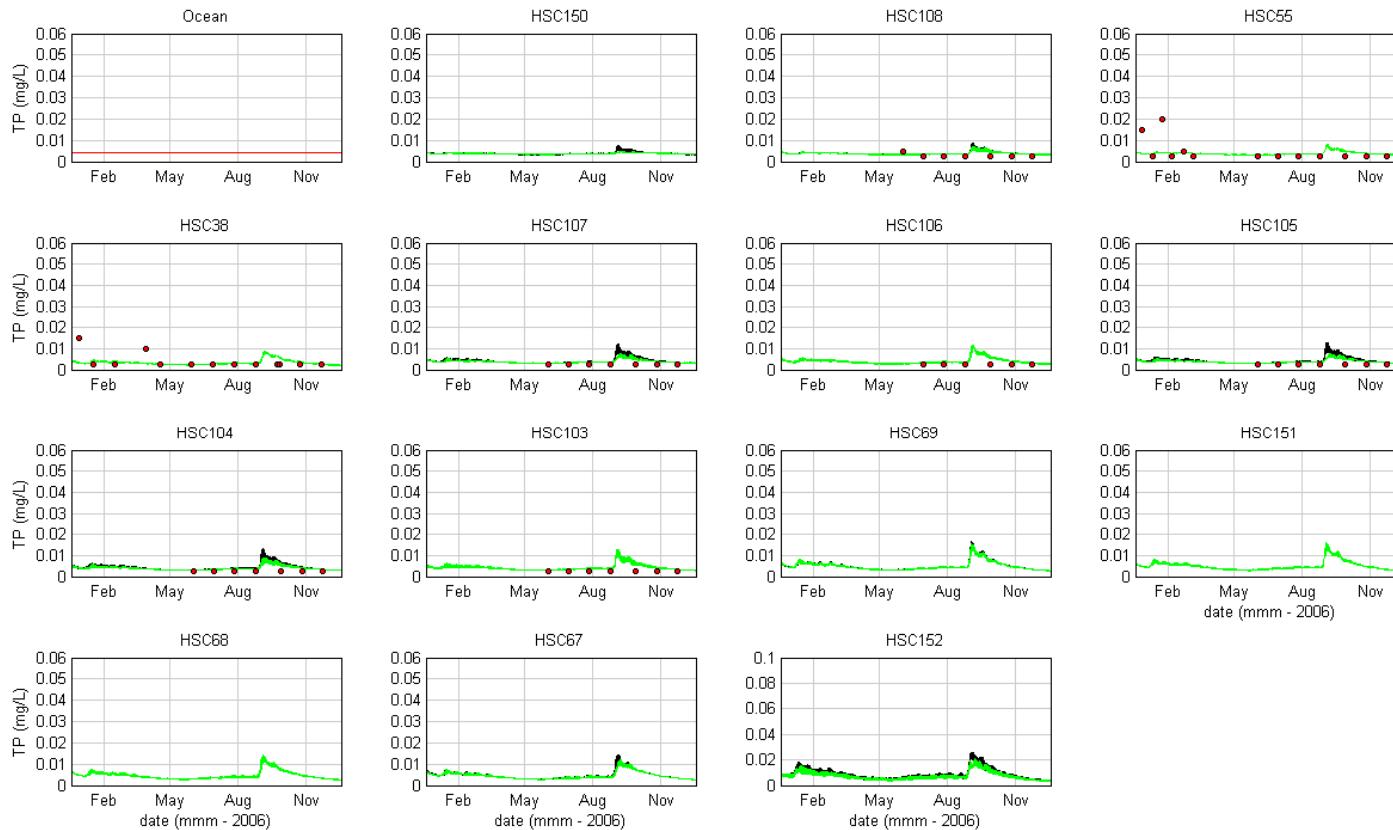
Water Quality Modelling of the Hawkesbury-Nepean River System



- **Figure 13-39 Box and Whisker Plots – Filterable Reactive Phosphorus Validation 2007 (measured data (red), modelled surface (blue) and modelled bottom (green))**



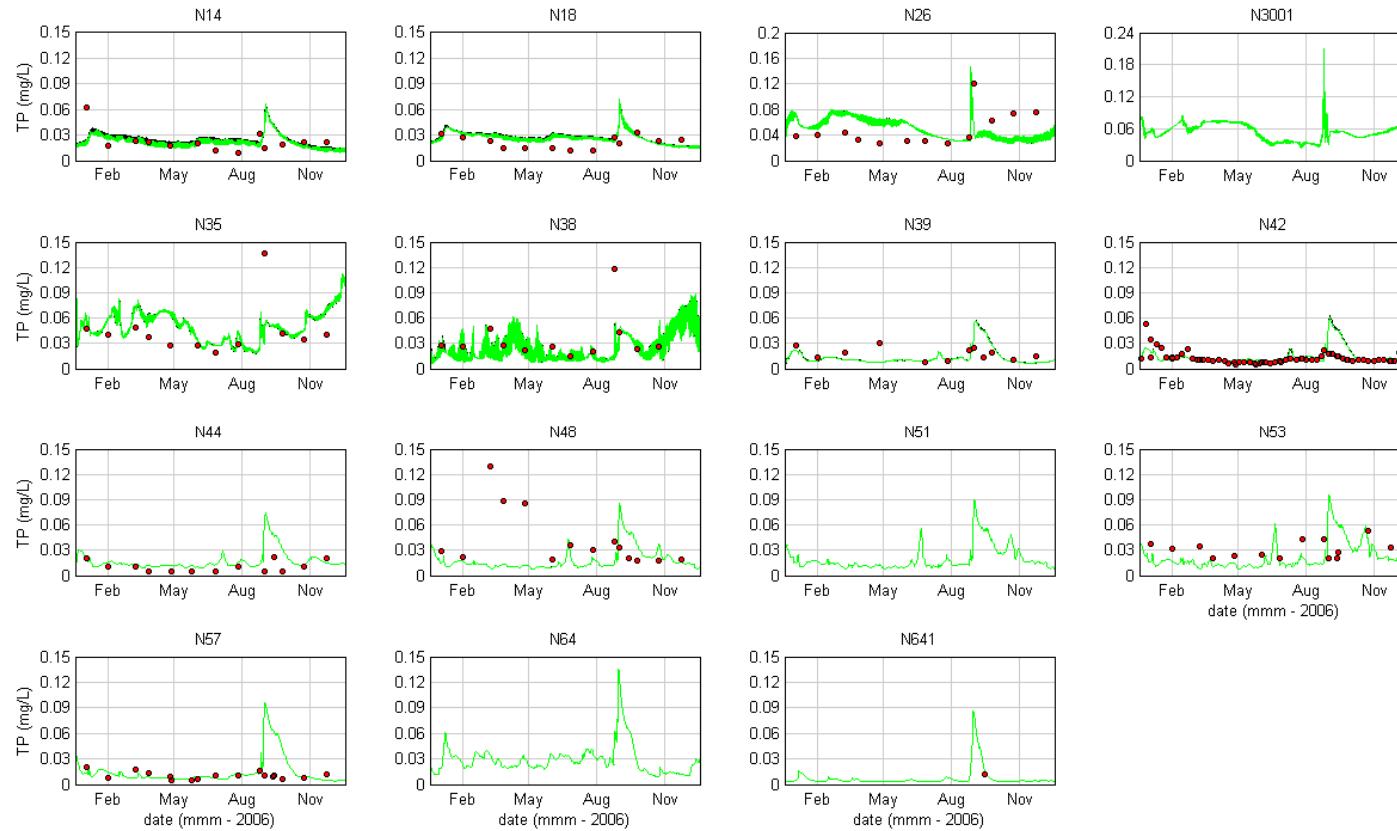
Water Quality Modelling of the Hawkesbury-Nepean River System



■ **Figure 13-40 Total Phosphorus Calibration 2006 (measured data (red), modelled surface (black) and modelled bottom (green))**



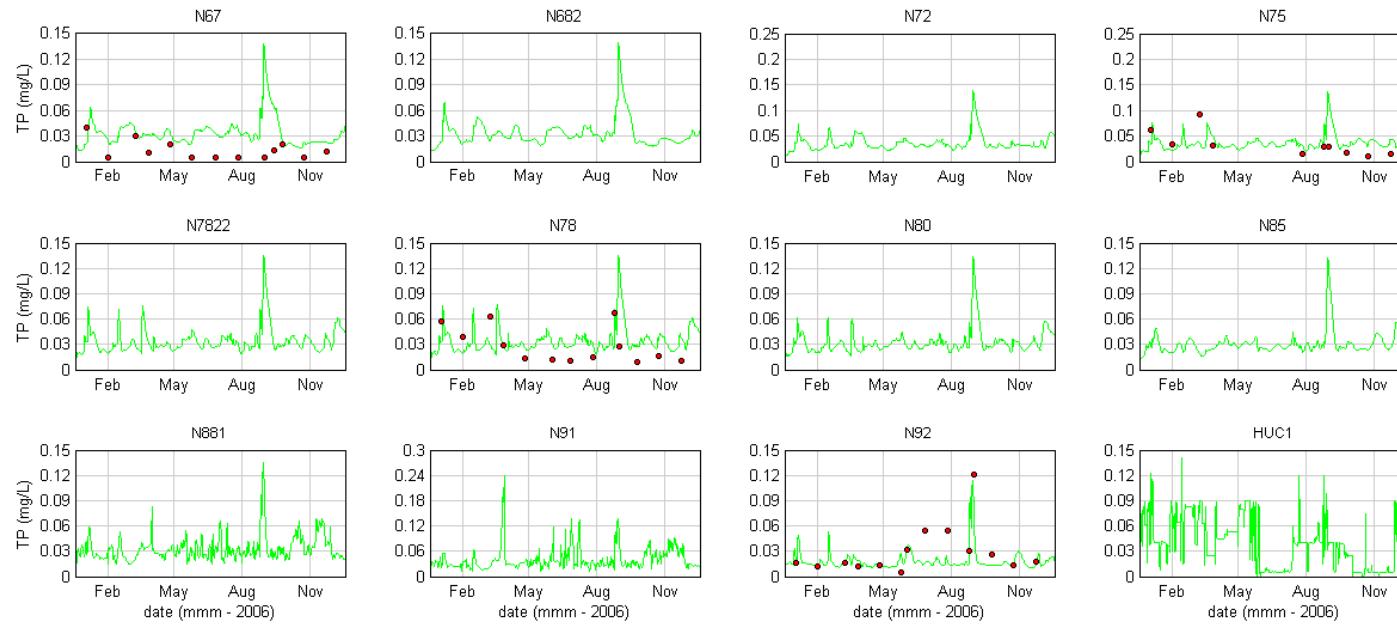
Water Quality Modelling of the Hawkesbury-Nepean River System



- Figure 13-40 (Cont.) Total Phosphorus Calibration 2006 (measured data (red), modelled surface (black) and modelled bottom (green))



Water Quality Modelling of the Hawkesbury-Nepean River System

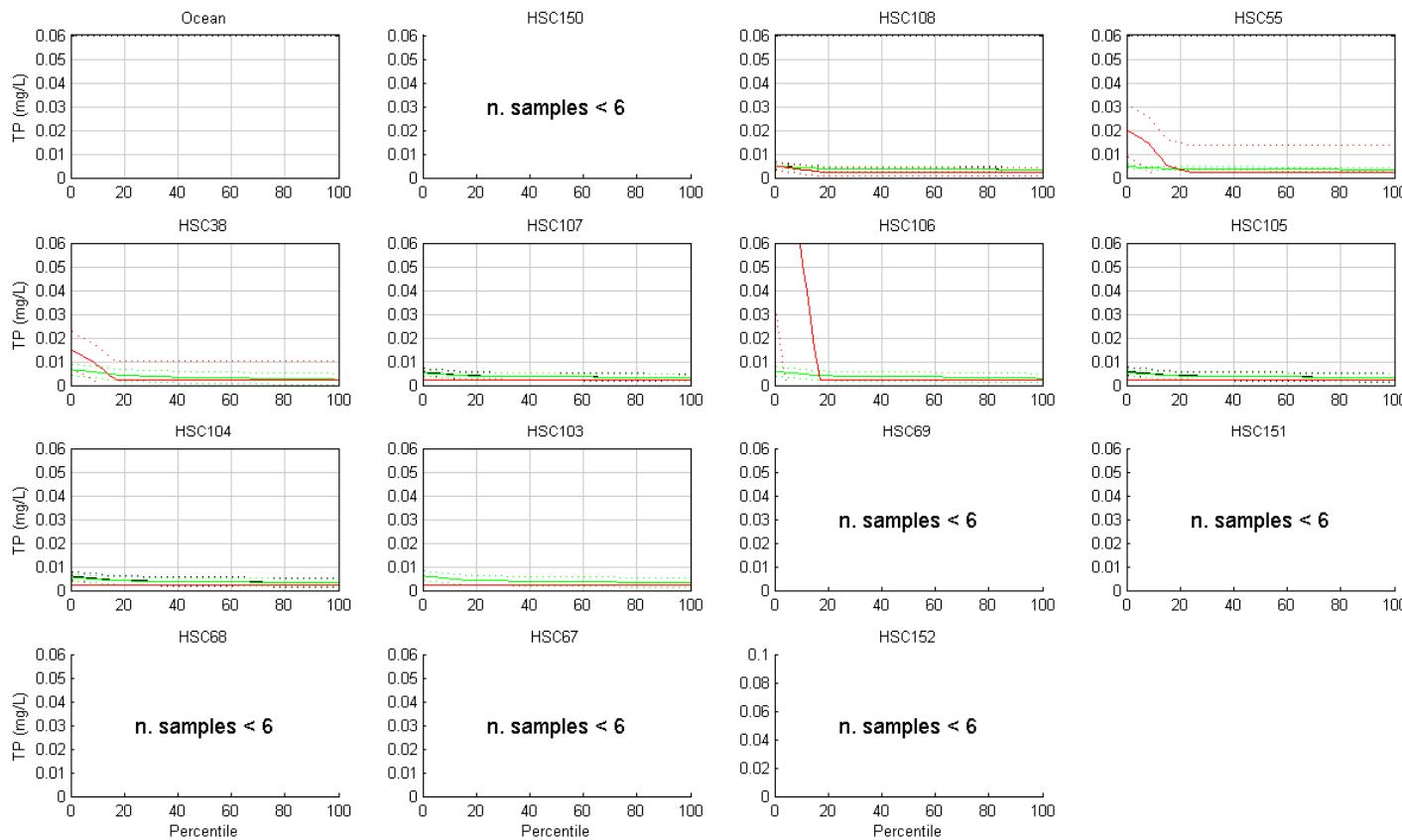


- **Figure 13-40 (Cont.) Total Phosphorus Calibration 2006 (measured data (red), modelled surface (black) and modelled bottom (green))**

SINCLAIR KNIGHT MERZ



Water Quality Modelling of the Hawkesbury-Nepean River System

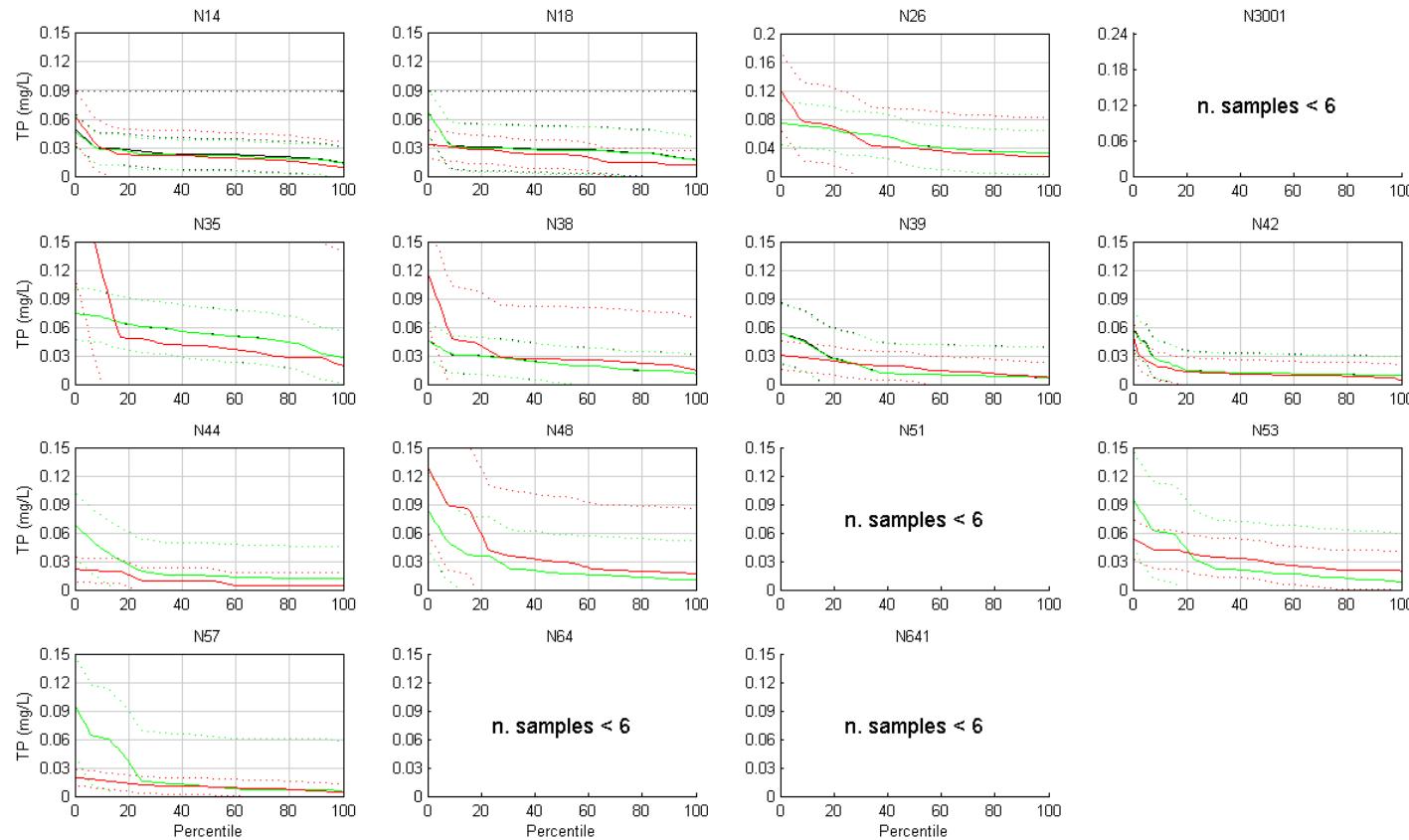


- Figure 13-41 Exceedance Plots – Total Phosphorus Calibration 2006 (+/- 2SD) (measured data (red), modelled surface (black) and modelled bottom (green))

SINCLAIR KNIGHT MERZ



Water Quality Modelling of the Hawkesbury-Nepean River System

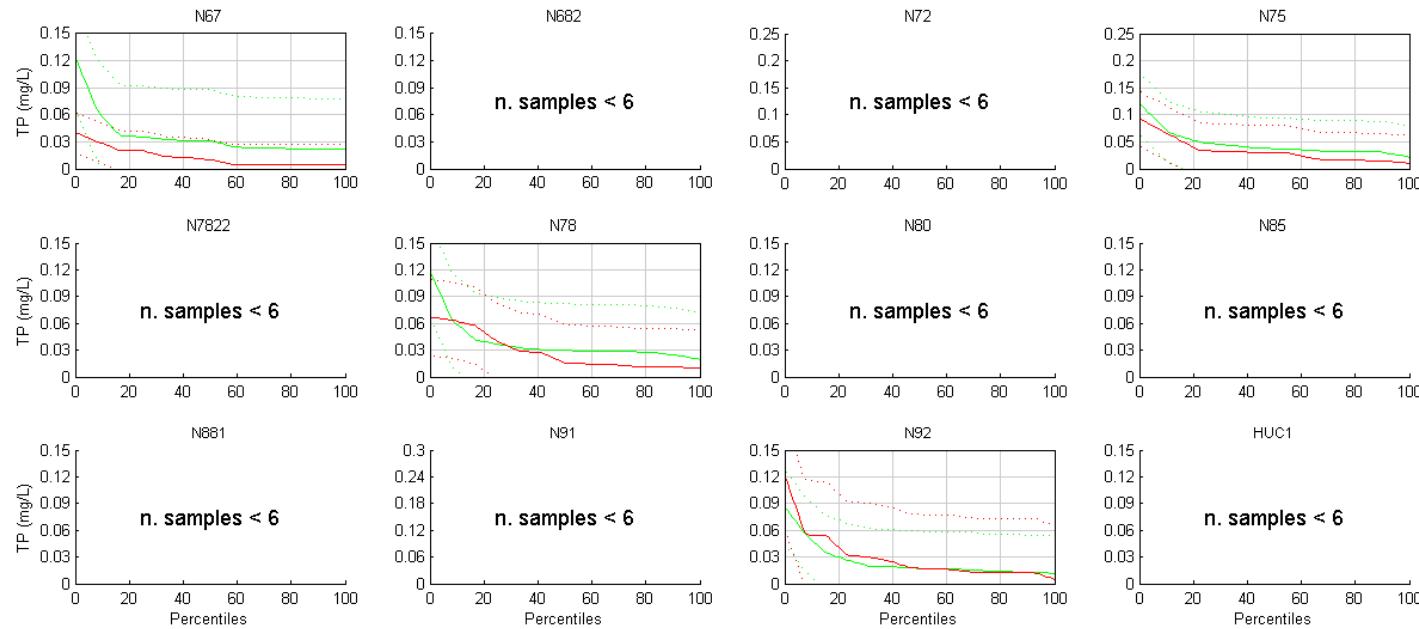


- Figure 13-41 (Cont.) Exceedance Plots – Total Phosphorus Calibration 2006 (+/- 2SD) (measured data (red), modelled surface (black) and modelled bottom (green))

SINCLAIR KNIGHT MERZ



Water Quality Modelling of the Hawkesbury-Nepean River System

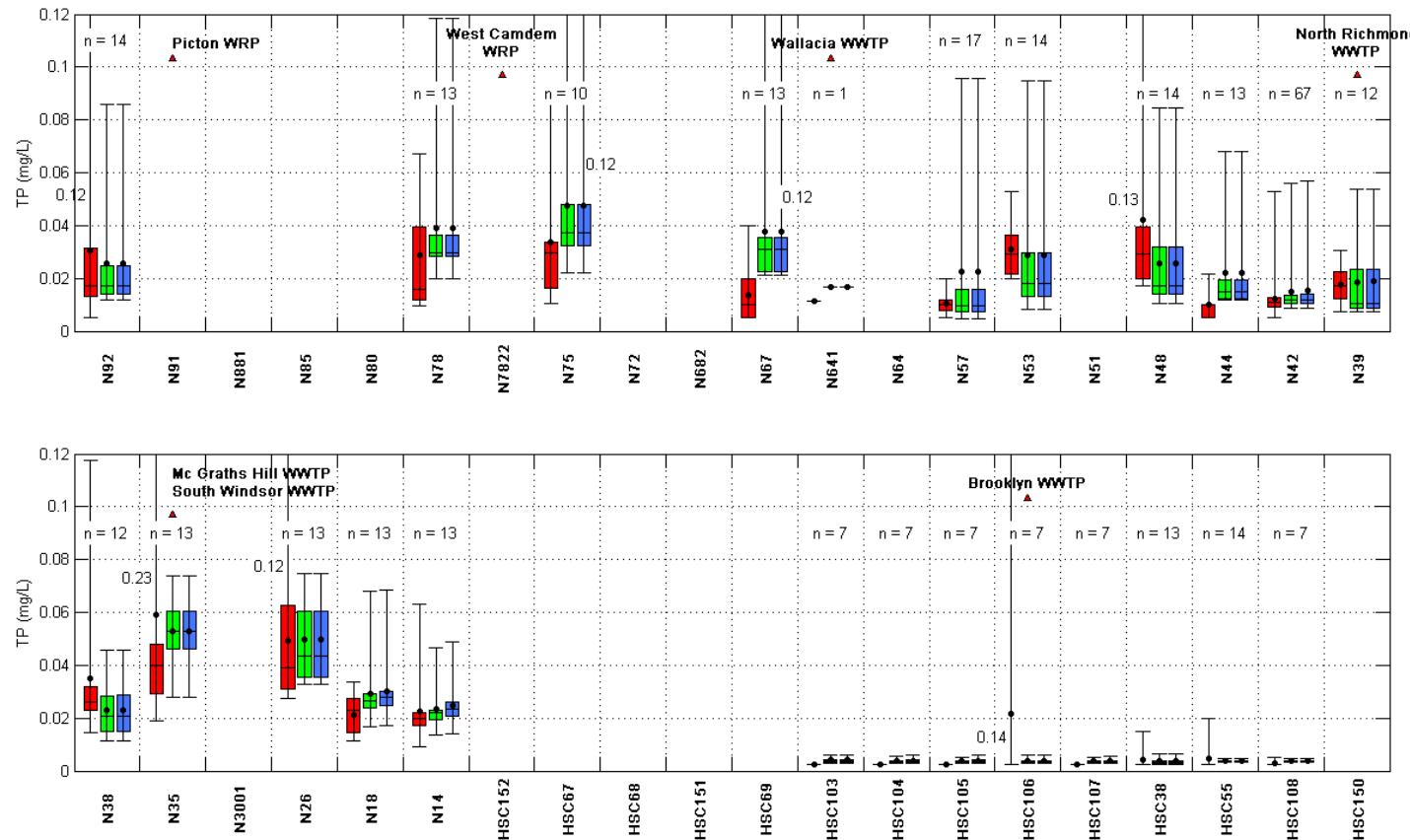


- Figure 13-41 (Cont.) Exceedance Plots – Total Phosphorus Calibration 2006 (+/- 2SD) (measured data (red), modelled surface (black) and modelled bottom (green))

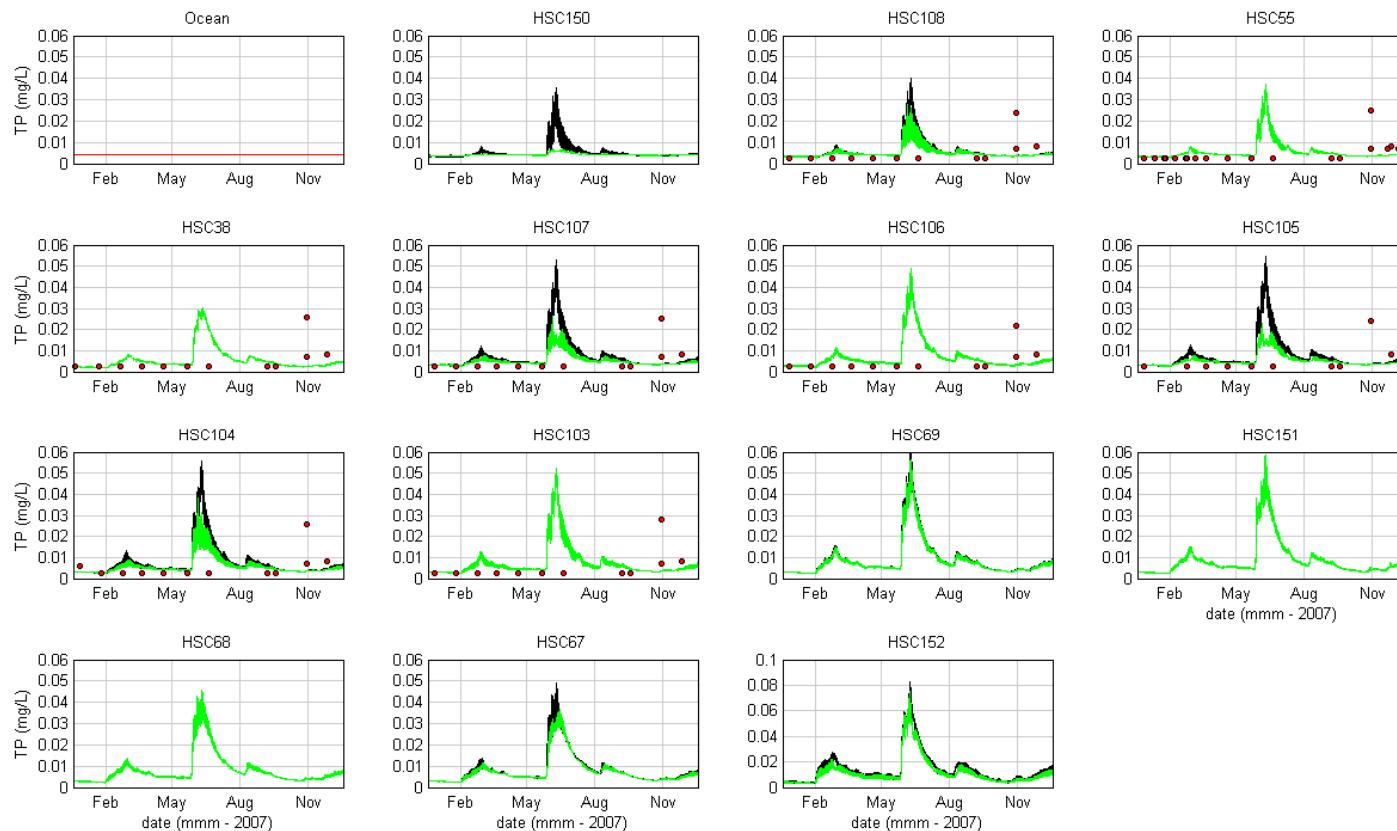
SINCLAIR KNIGHT MERZ



Water Quality Modelling of the Hawkesbury-Nepean River System



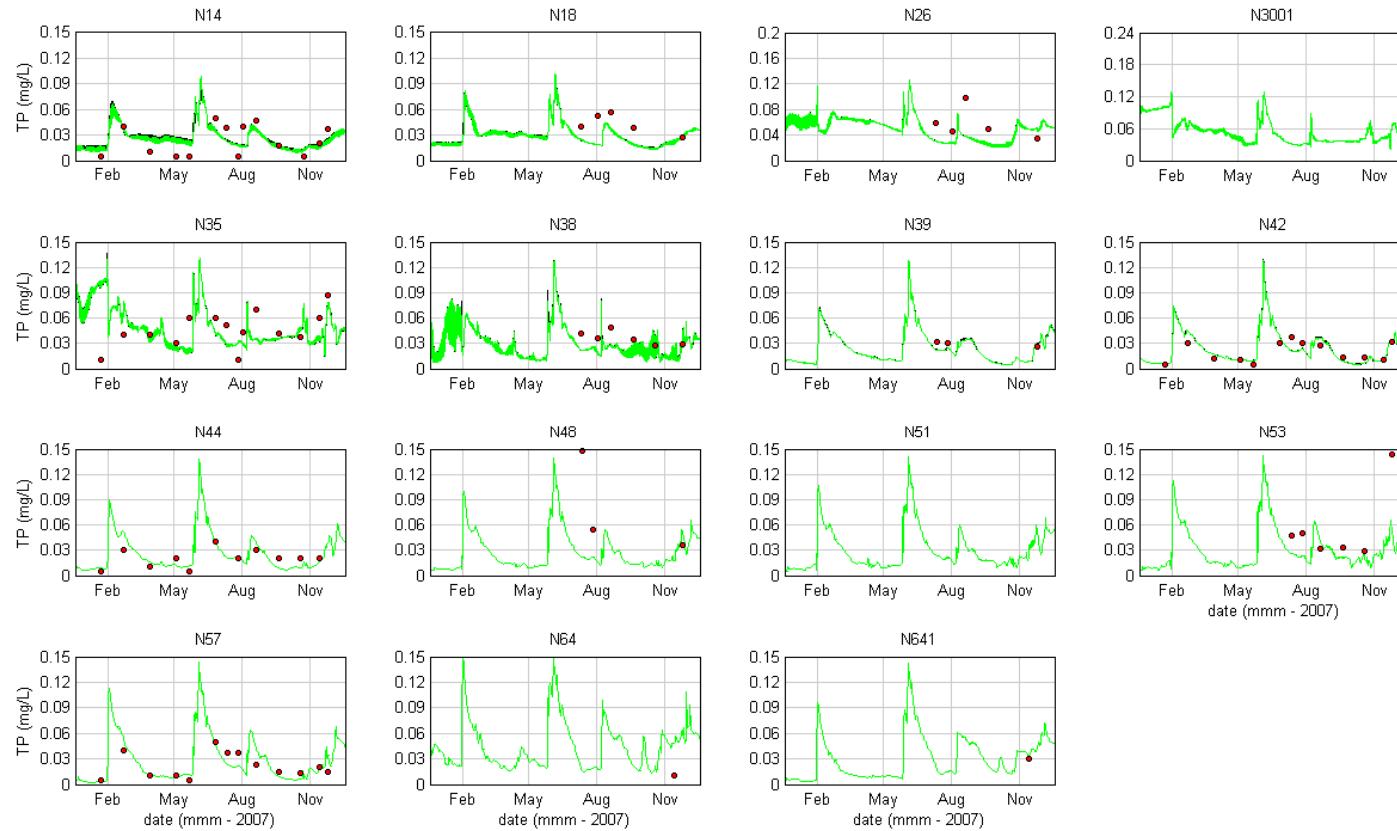
■ **Figure 13-42 Box and Whisker Plots – Total Phosphorus Calibration 2006 (measured data (red), modelled surface (blue) and modelled bottom (green))**



■ **Figure 13-43 Total Phosphorus Validation 2007 (measured data (red), modelled surface (black) and modelled bottom (green))**



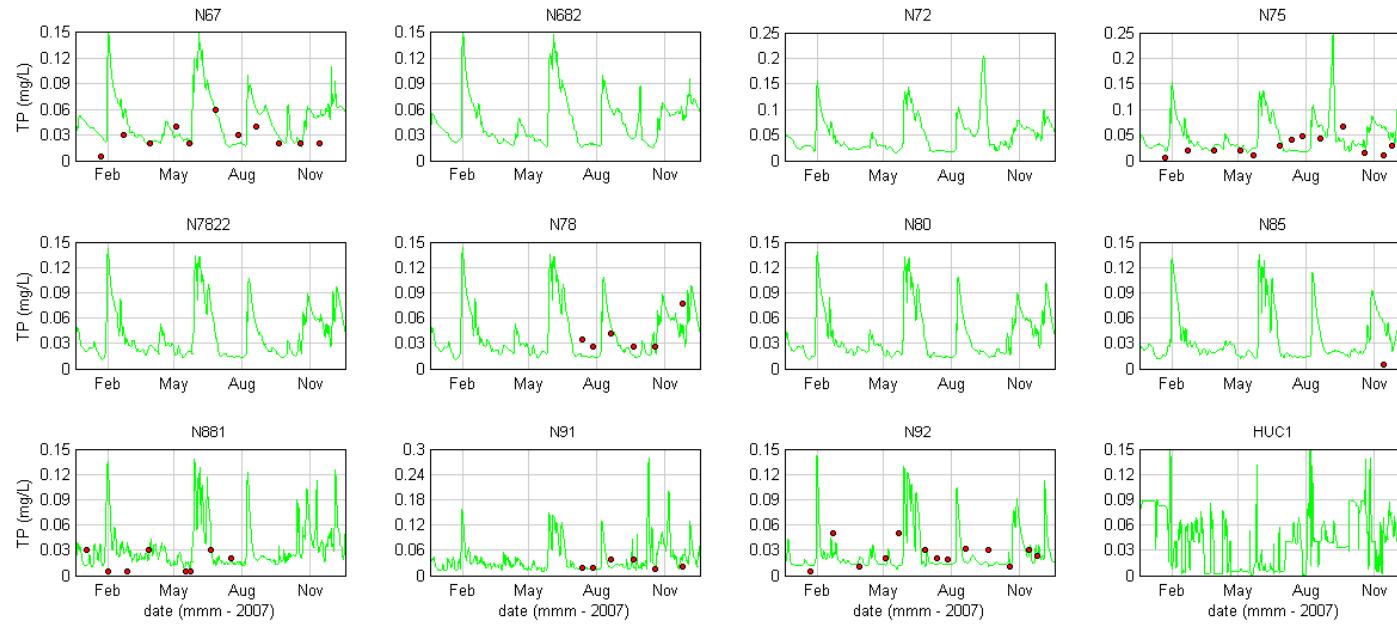
Water Quality Modelling of the Hawkesbury-Nepean River System



- **Figure 13-43 (Cont.) Total Phosphorus Validation 2007 (measured data (red), modelled surface (black) and modelled bottom (green))**



Water Quality Modelling of the Hawkesbury-Nepean River System

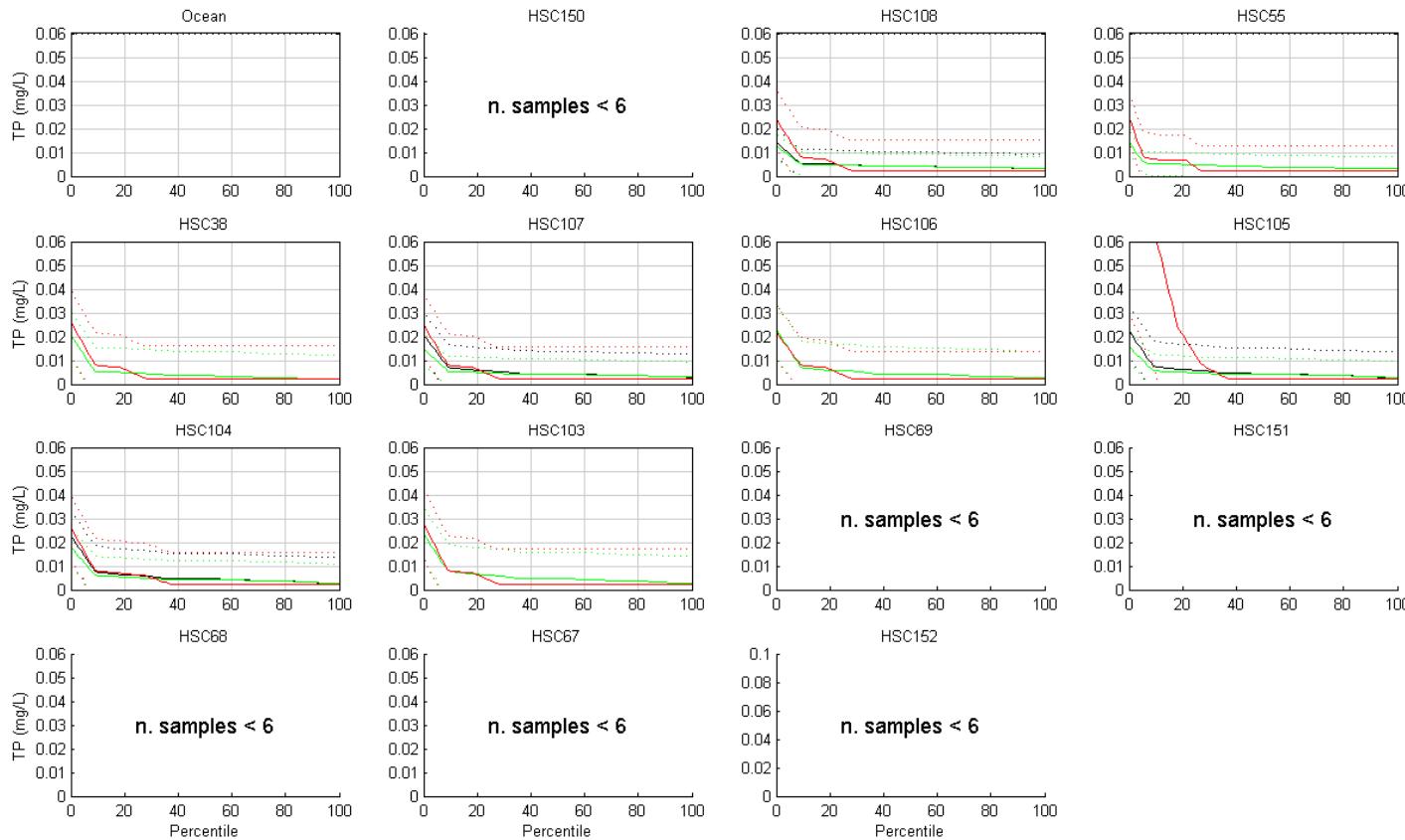


- Figure 13-43 (Cont.) Total Phosphorus Validation 2007 (measured data (red), modelled surface (black) and modelled bottom (green))

SINCLAIR KNIGHT MERZ



Water Quality Modelling of the Hawkesbury-Nepean River System

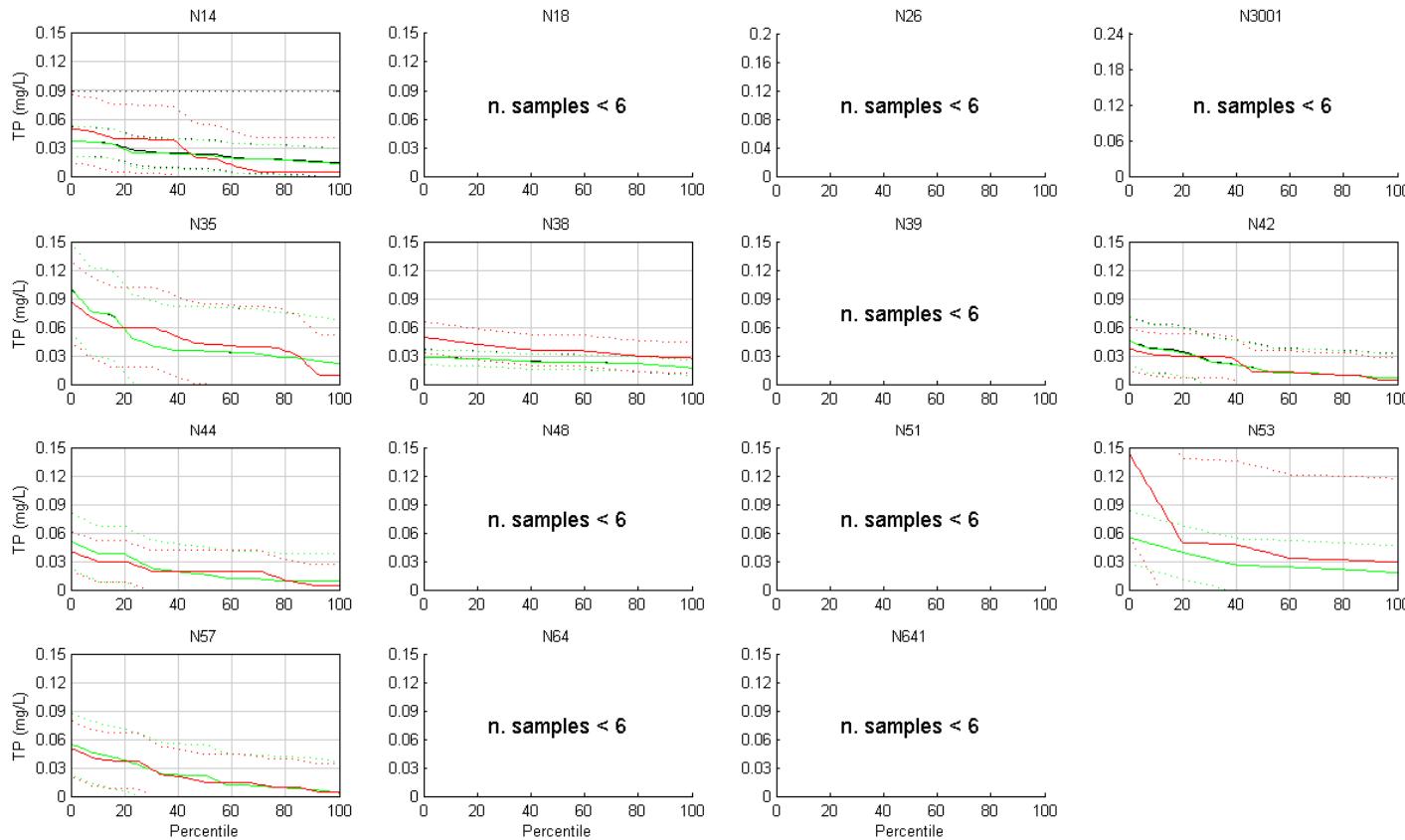


- **Figure 13-44 Exceedance Plots – Total Phosphorus Validation 2007 (+/-2SD) (measured data (red), modelled surface (black) and modelled bottom (green))**

SINCLAIR KNIGHT MERZ



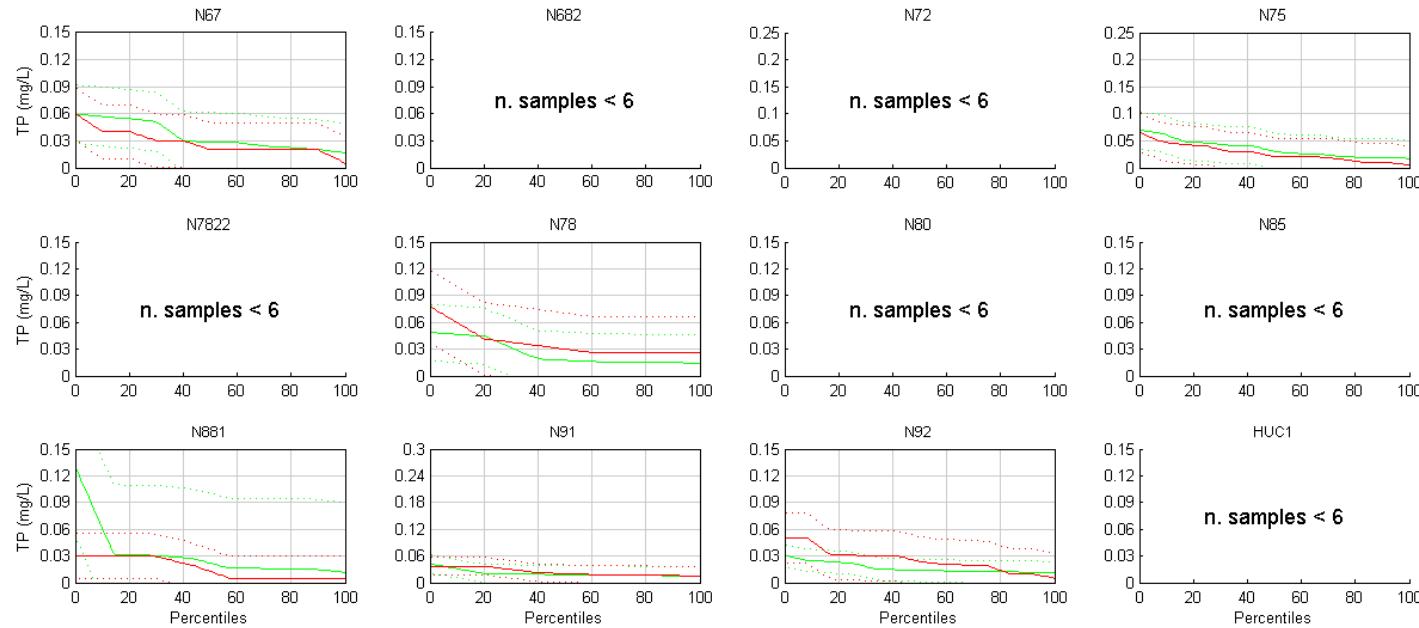
Water Quality Modelling of the Hawkesbury-Nepean River System



- Figure 13-44 (Cont.) Exceedance Plots – Total Phosphorus 2007 (+/-2SD) (measured data (red), modelled surface (black) and modelled bottom (green))



Water Quality Modelling of the Hawkesbury-Nepean River System

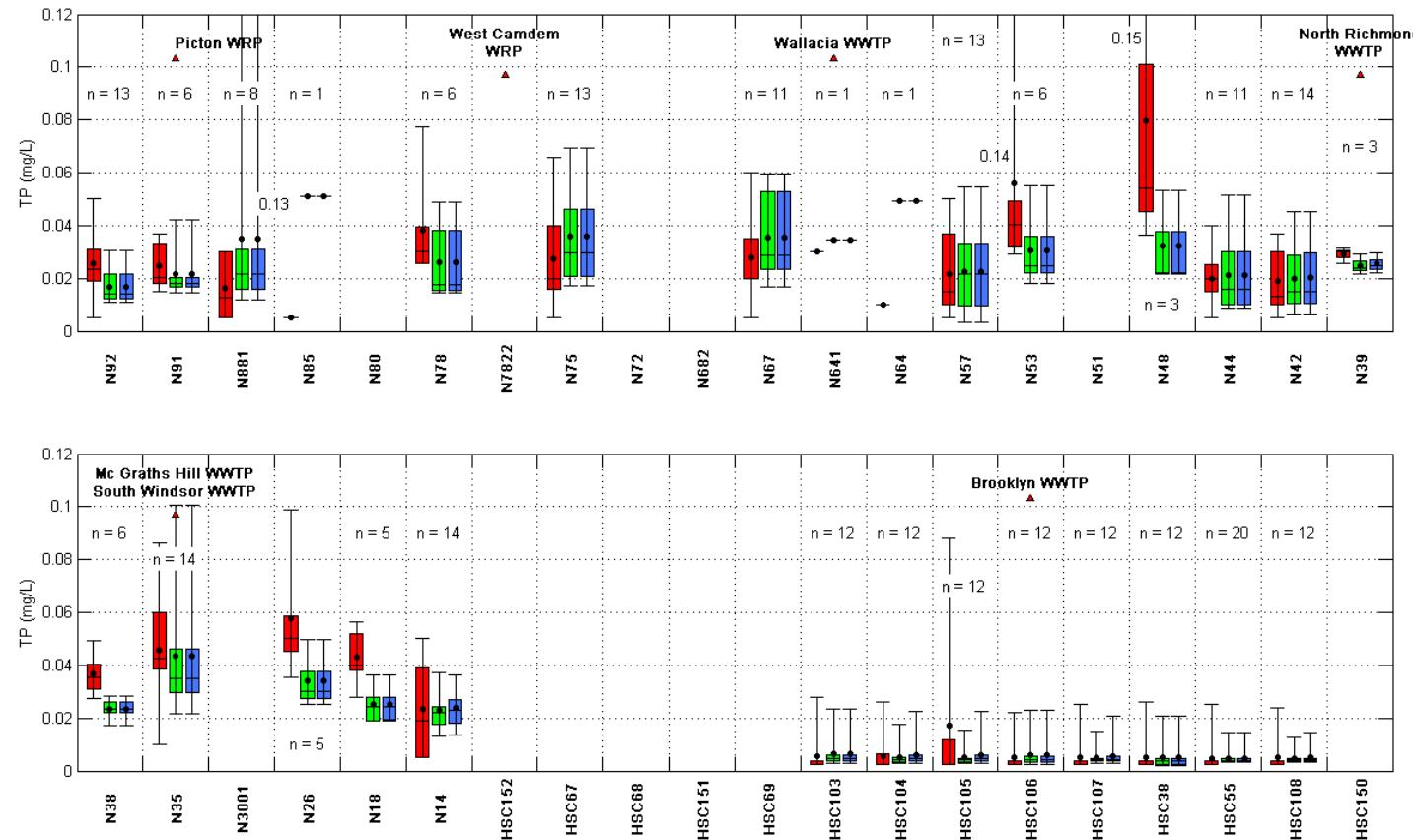


- Figure 13-44 (Cont.) Exceedance Plots – Total Phosphorus Validation 2007(+/-2SD) (measured data (red), modelled surface (black) and modelled bottom (green))

SINCLAIR KNIGHT MERZ



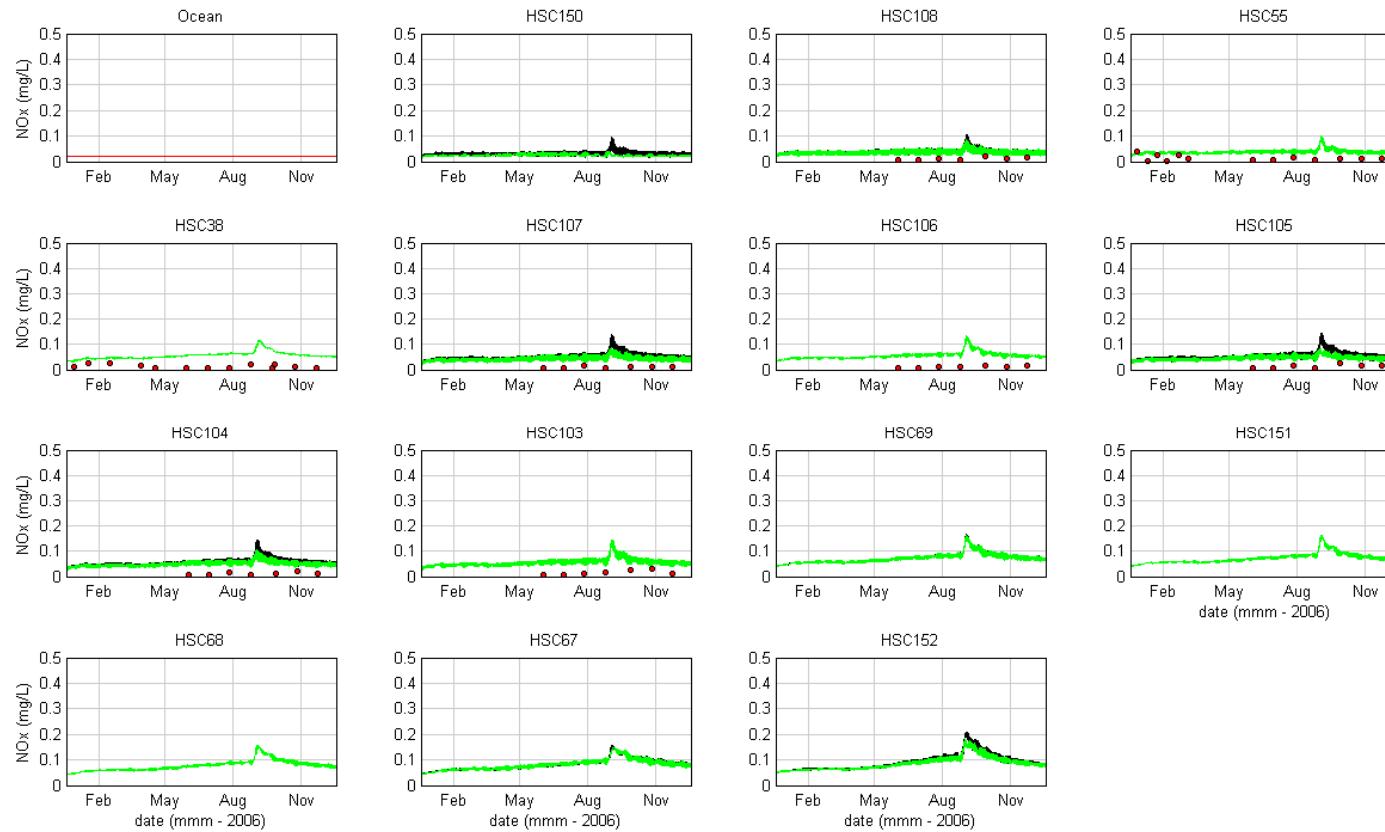
Water Quality Modelling of the Hawkesbury-Nepean River System



■ Figure 13-45 Box and Whisker Plots – Total Phosphorus Validation 2007 (measured data (red), modelled surface (blue) and modelled bottom (green))



Water Quality Modelling of the Hawkesbury-Nepean River System

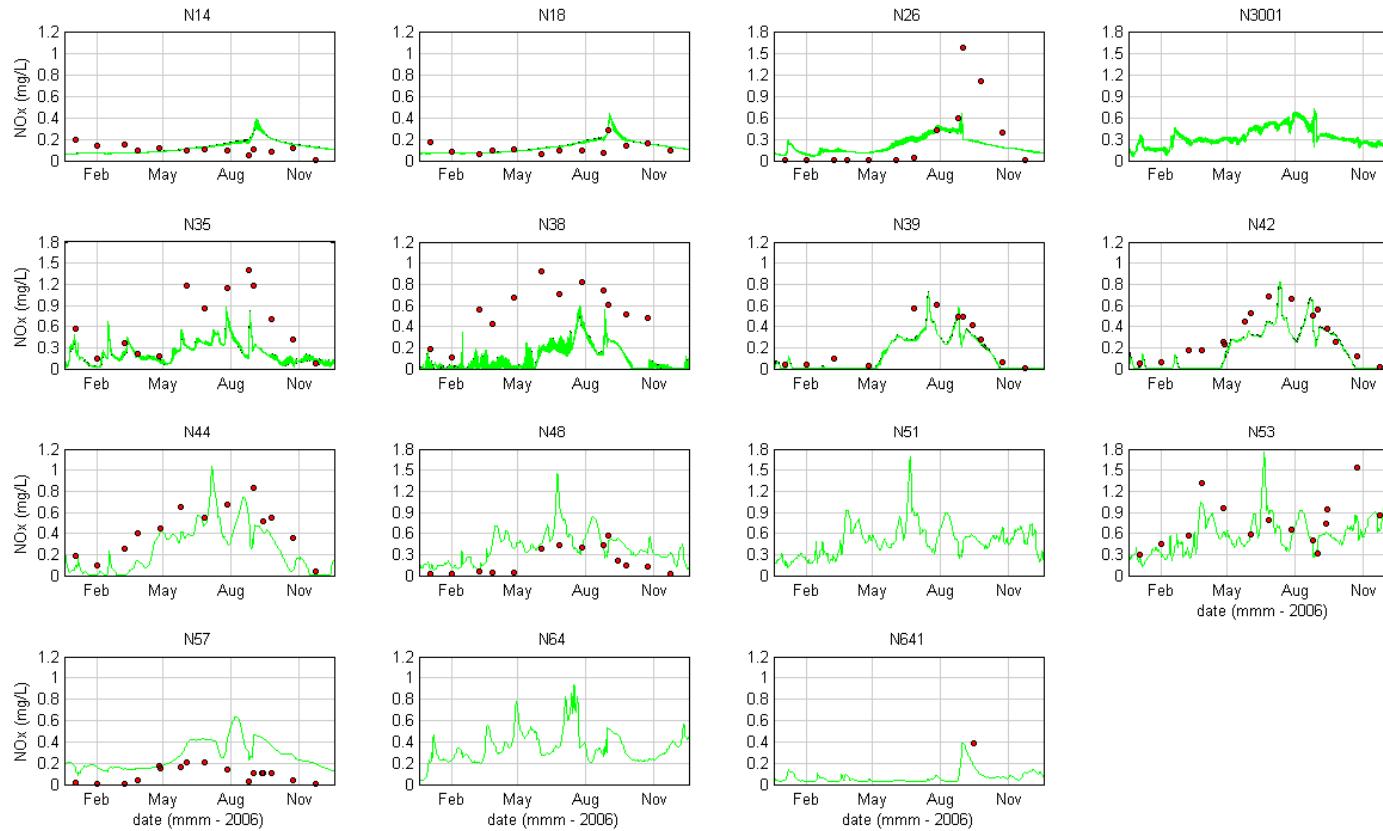


■ **Figure 13-46 Oxidised Nitrogen Calibration 2006 (measured data (red), modelled surface (black) and modelled bottom (green))**

SINCLAIR KNIGHT MERZ



Water Quality Modelling of the Hawkesbury-Nepean River System

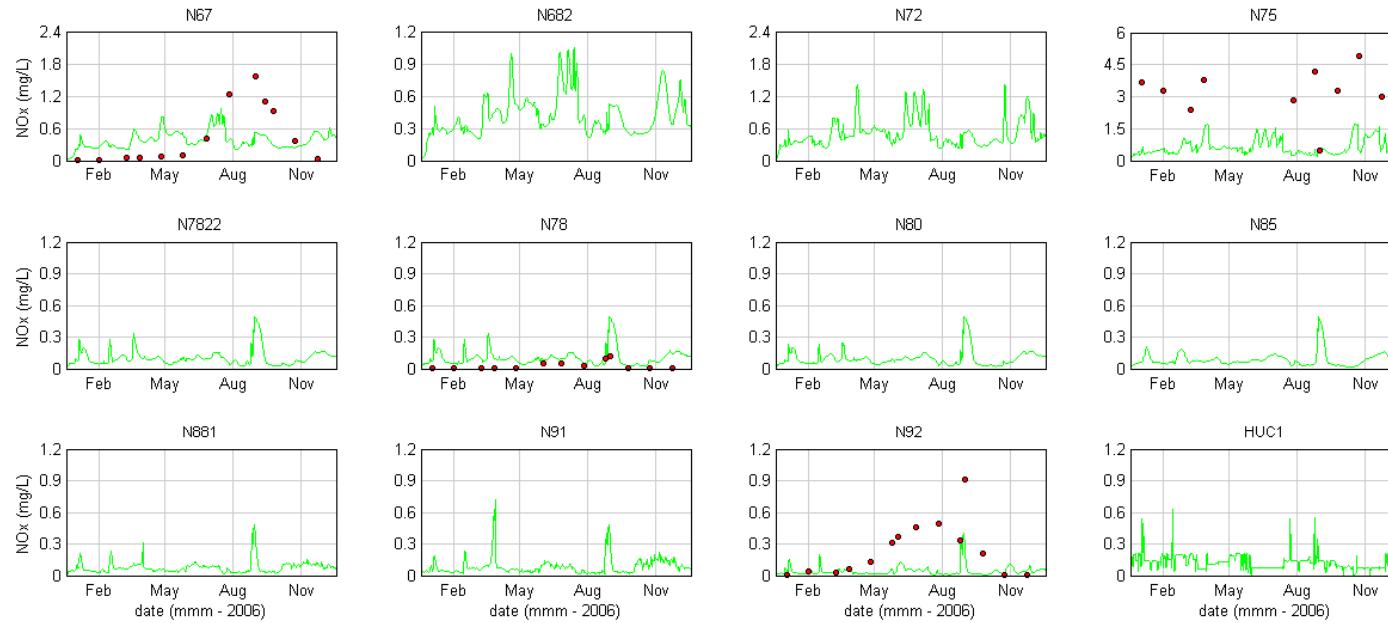


- Figure 13-46 (Cont.) Oxidised Nitrogen Calibration 2006 (measured data (red), modelled surface (black) and modelled bottom (green))

SINCLAIR KNIGHT MERZ



Water Quality Modelling of the Hawkesbury-Nepean River System

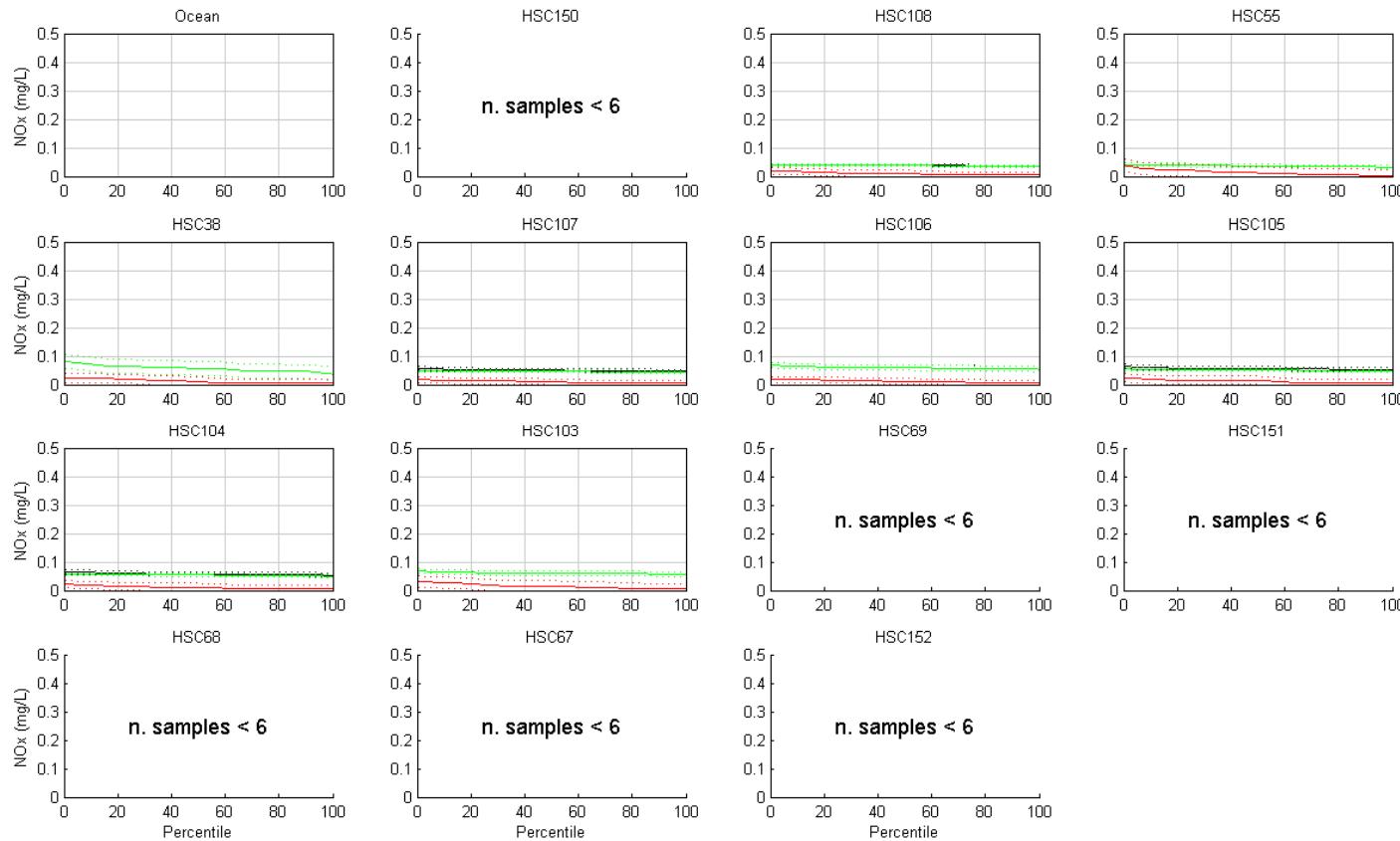


- Figure 13-46 (Cont.) Oxidised Nitrogen Calibration 2006 (measured data (red), modelled surface (black) and modelled bottom (green))

SINCLAIR KNIGHT MERZ



Water Quality Modelling of the Hawkesbury-Nepean River System

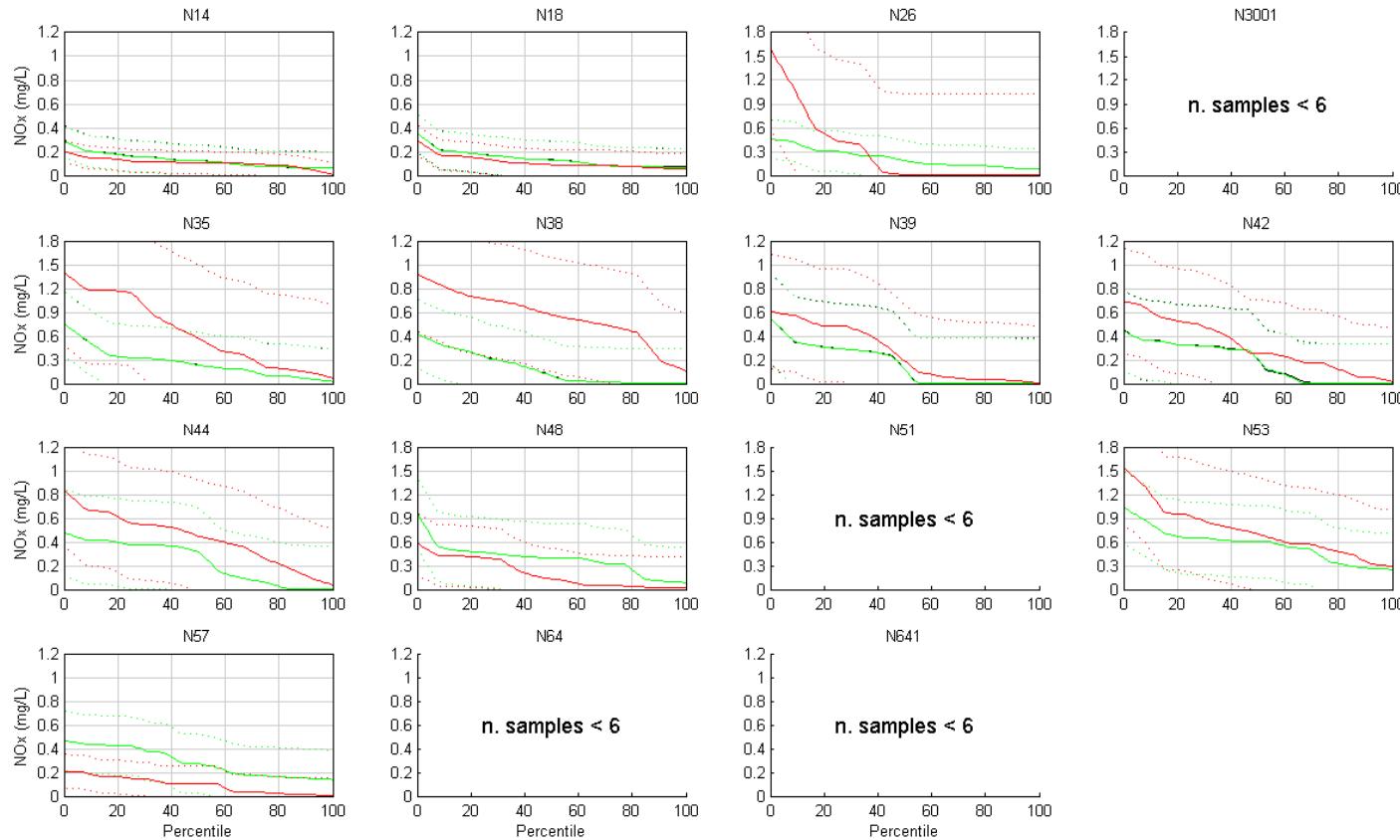


- **Figure 13-47 Exceedance Plots – Oxidised Nitrogen Calibration 2006 (+/- 2SD) (measured data (red), modelled surface (black) and modelled bottom (green))**

SINCLAIR KNIGHT MERZ



Water Quality Modelling of the Hawkesbury-Nepean River System

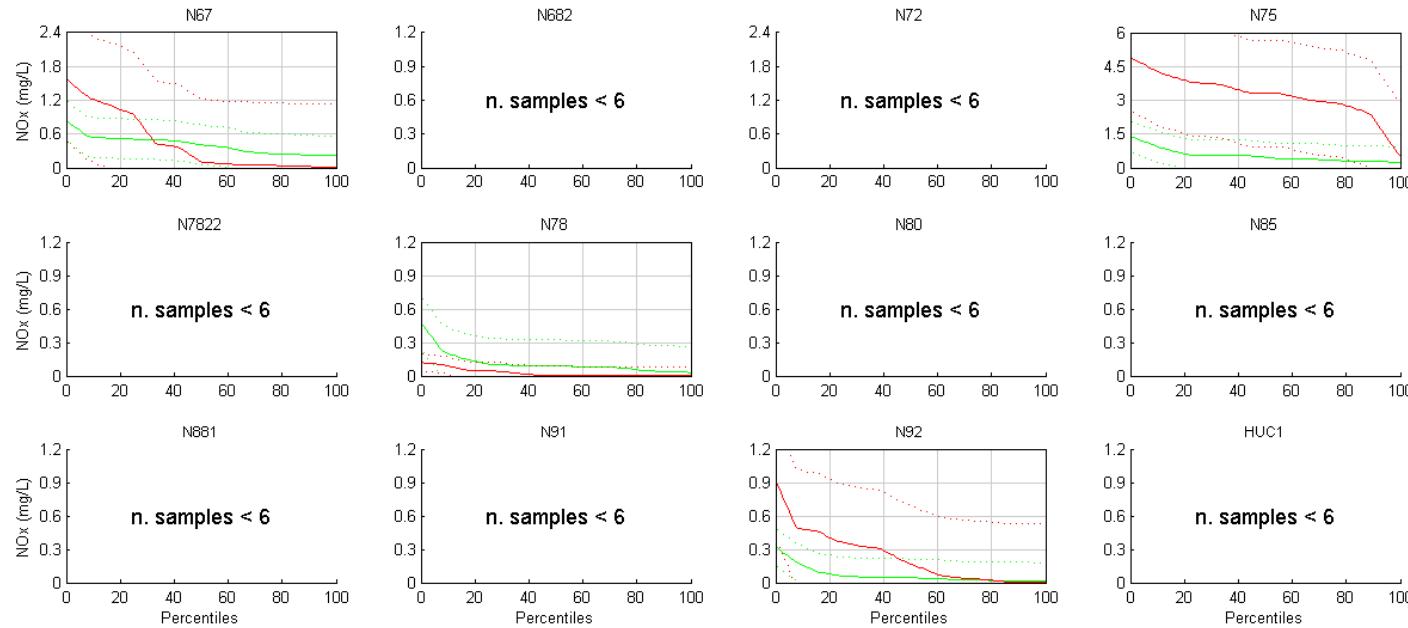


- Figure 13-47 (Cont.) Exceedance Plots – Oxidised Nitrogen Calibration 2006 (+/- 2SD) (measured data (red), modelled surface (black) and modelled bottom (green))

SINCLAIR KNIGHT MERZ



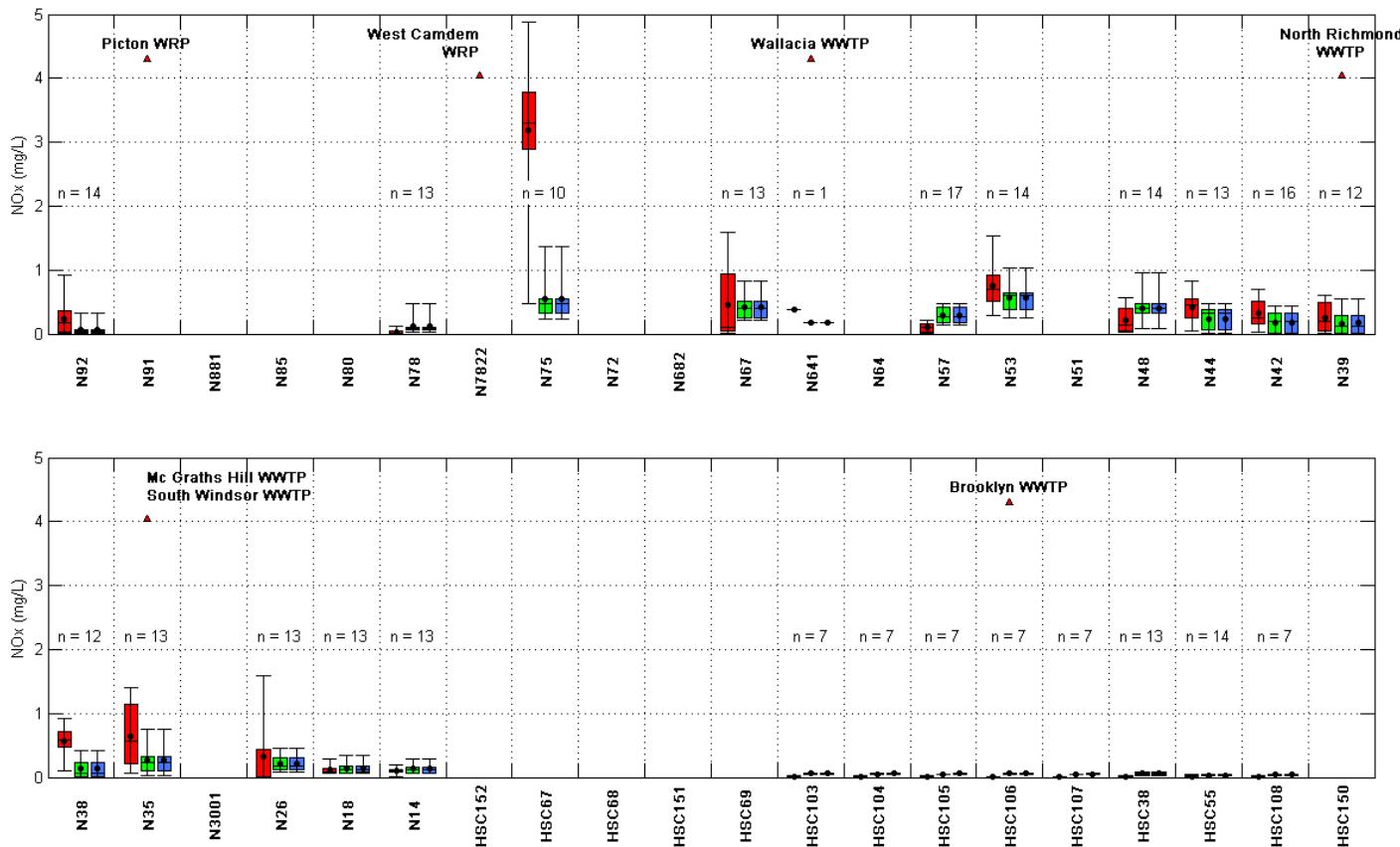
Water Quality Modelling of the Hawkesbury-Nepean River System



- Figure 13-47 (Cont.) Exceedance Plots – Oxidised Nitrogen Calibration 2006 (+/- 2SD) (measured data (red), modelled surface (black) and modelled bottom (green))

SINCLAIR KNIGHT MERZ

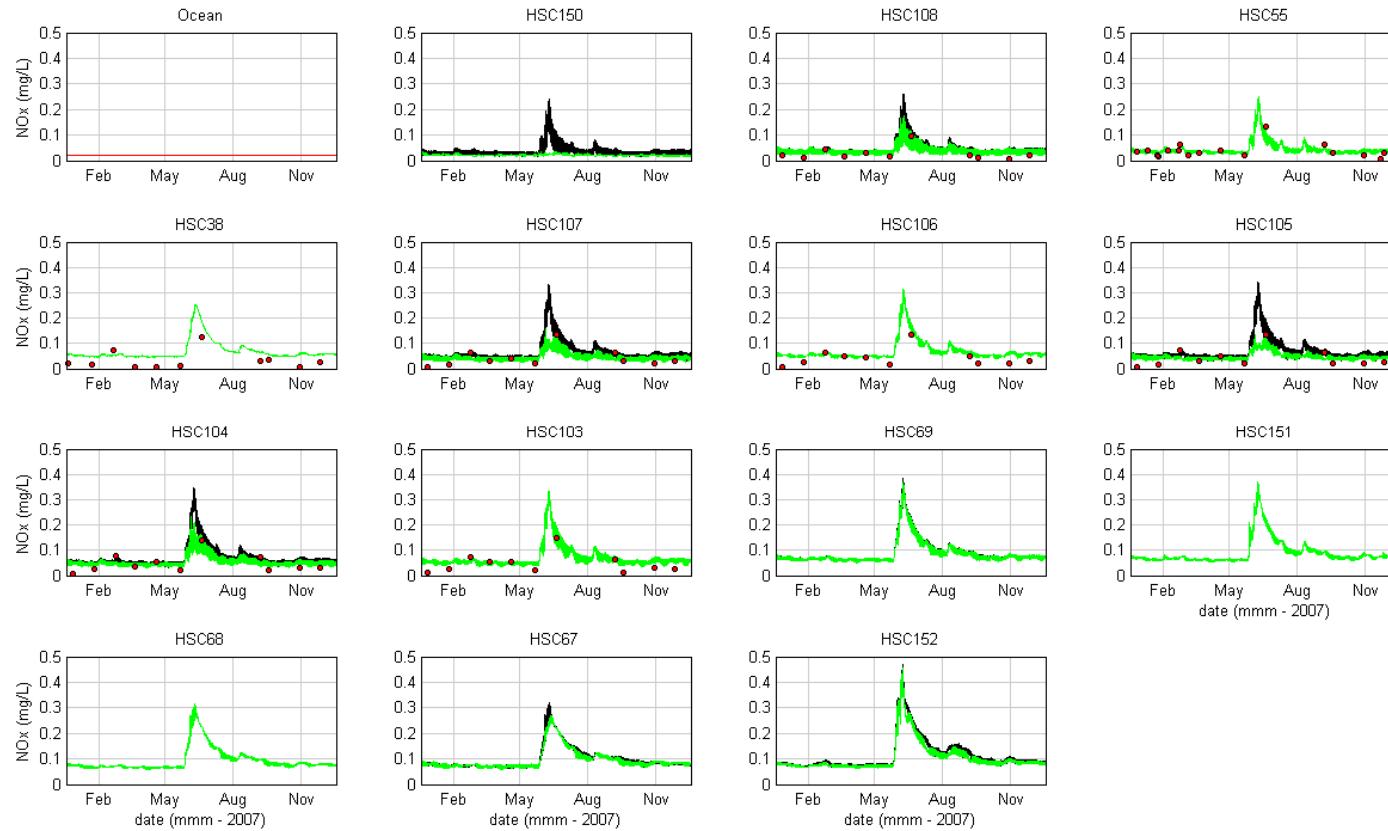
Water Quality Modelling of the Hawkesbury-Nepean River System



■ **Figure 13-48 Box and Whisker Plots – Oxidised Nitrogen Calibration 2006 (measured data (red), modelled surface (blue) and modelled bottom (green))**



Water Quality Modelling of the Hawkesbury-Nepean River System

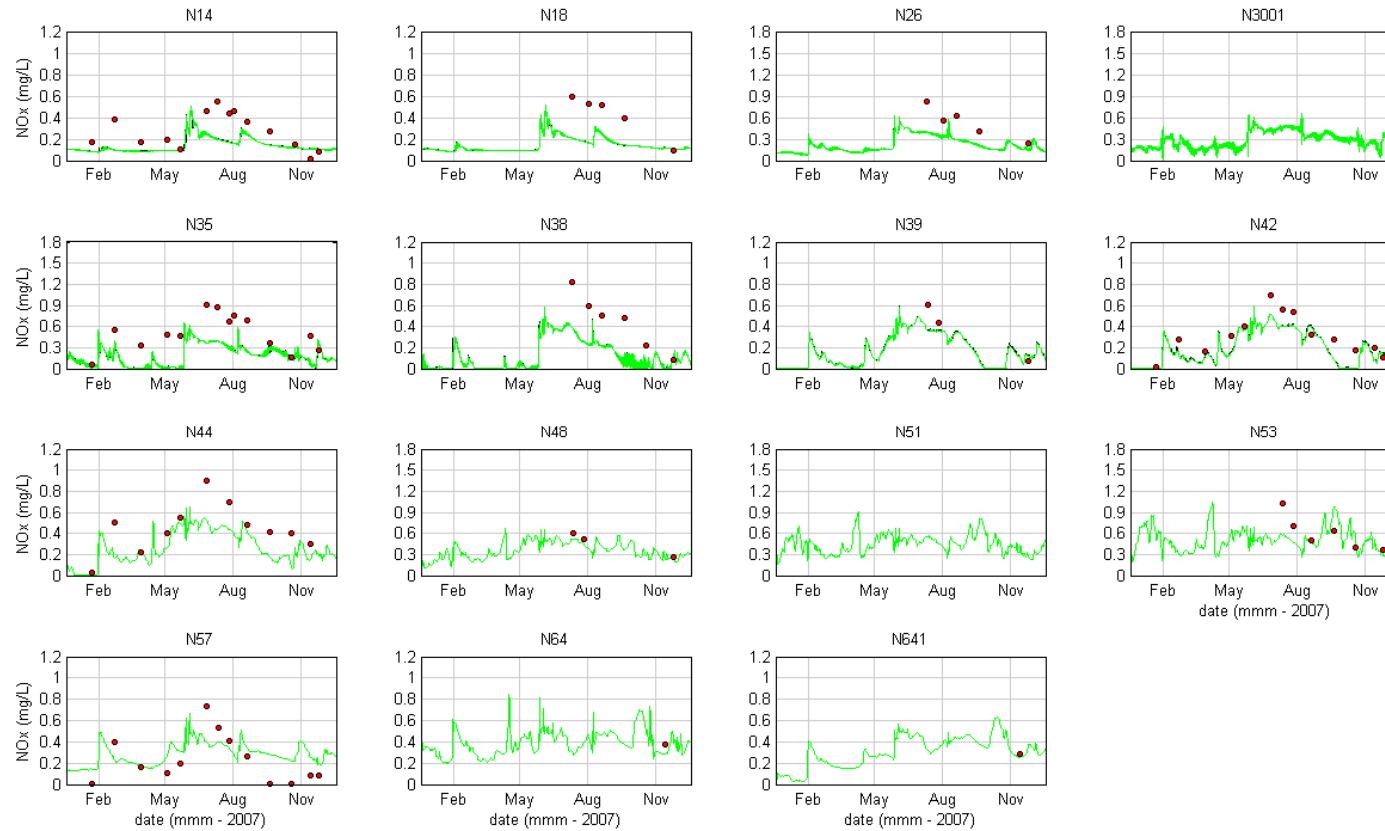


■ **Figure 13-49 Oxidised Nitrogen Validation 2007 (measured data (red), modelled surface (black) and modelled bottom (green))**

SINCLAIR KNIGHT MERZ



Water Quality Modelling of the Hawkesbury-Nepean River System

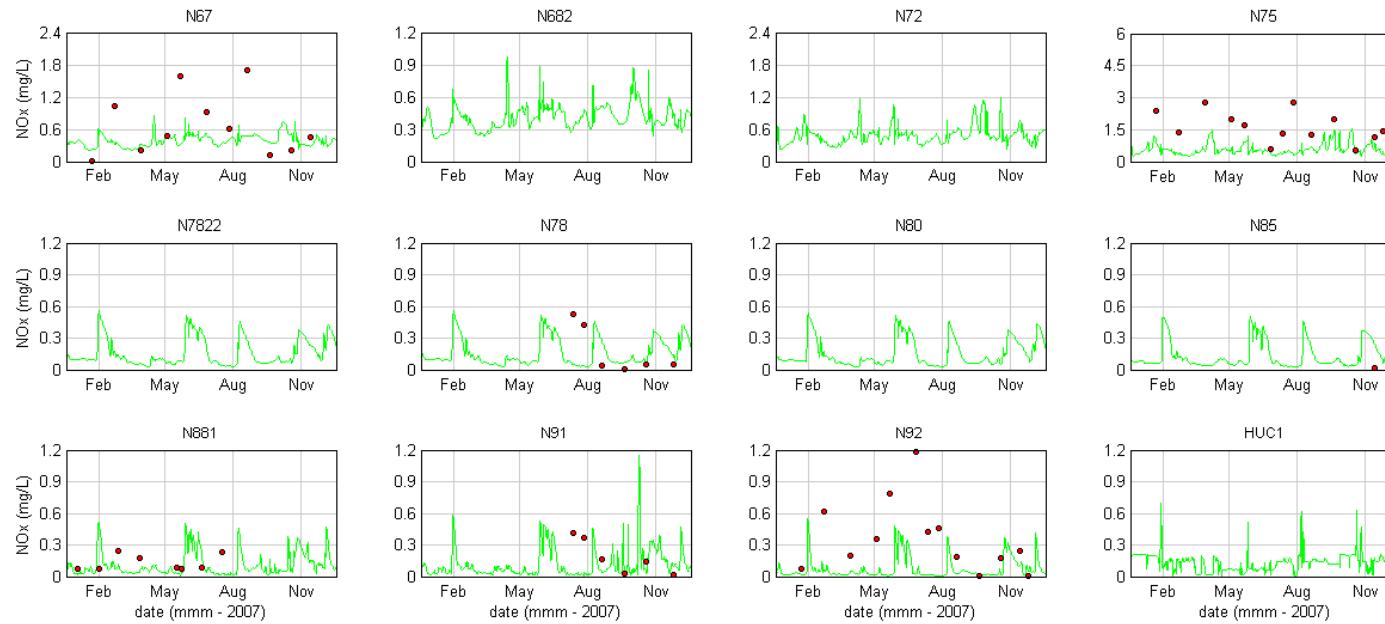


- **Figure 13-49 (Cont.) Oxidised Nitrogen Validation 2007 (measured data (red), modelled surface (black) and modelled bottom (green))**

SINCLAIR KNIGHT MERZ



Water Quality Modelling of the Hawkesbury-Nepean River System

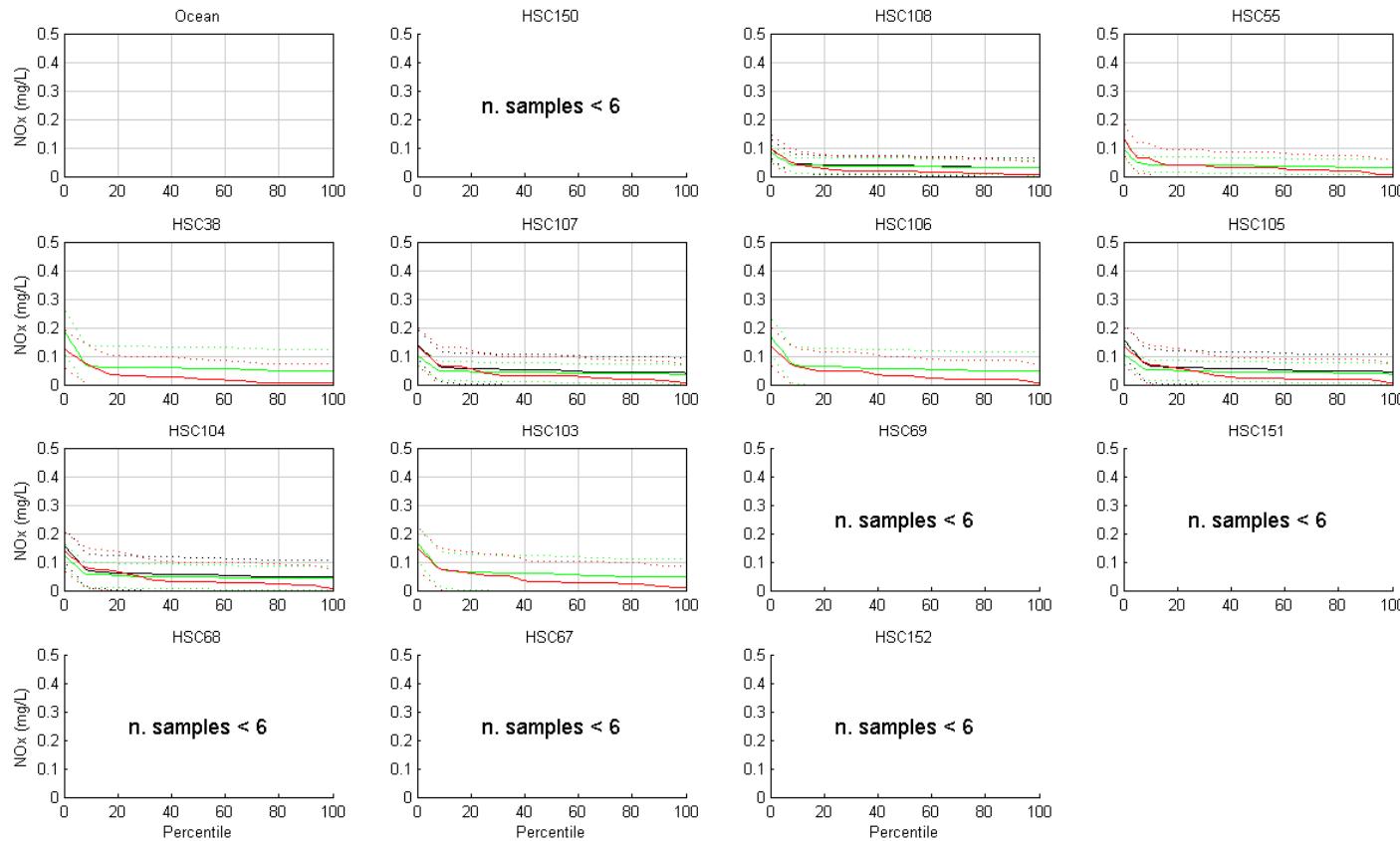


- **Figure 13-49 (Cont.) Oxidised Nitrogen Validation 2007 (measured data (red), modelled surface (black) and modelled bottom (green))**

SINCLAIR KNIGHT MERZ



Water Quality Modelling of the Hawkesbury-Nepean River System

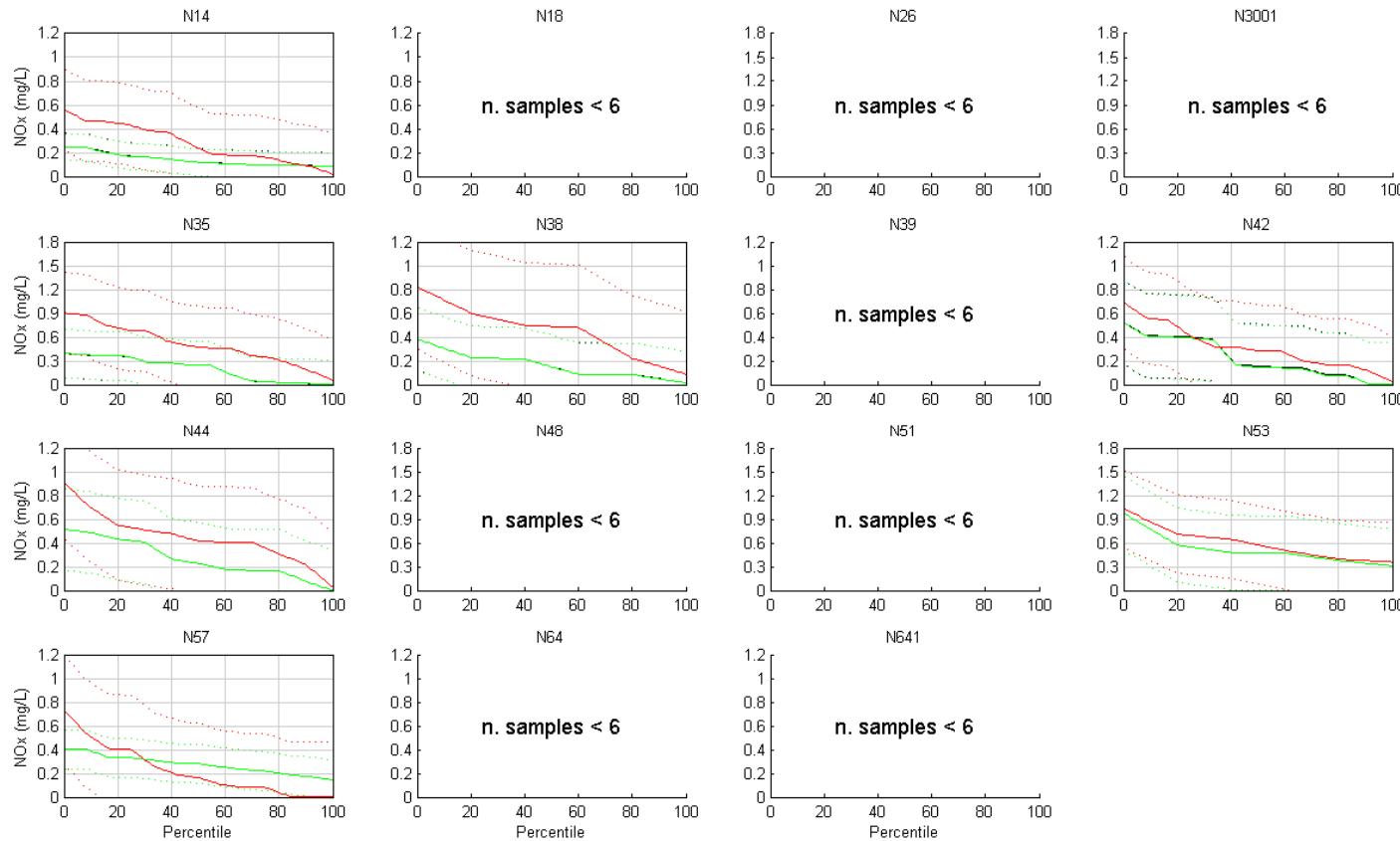


- Figure 13-50 Exceedance Plots – Oxidised Nitrogen Validation 2007 (+/- 2SD) (measured data (red), modelled surface (black) and modelled bottom (green))

SINCLAIR KNIGHT MERZ



Water Quality Modelling of the Hawkesbury-Nepean River System

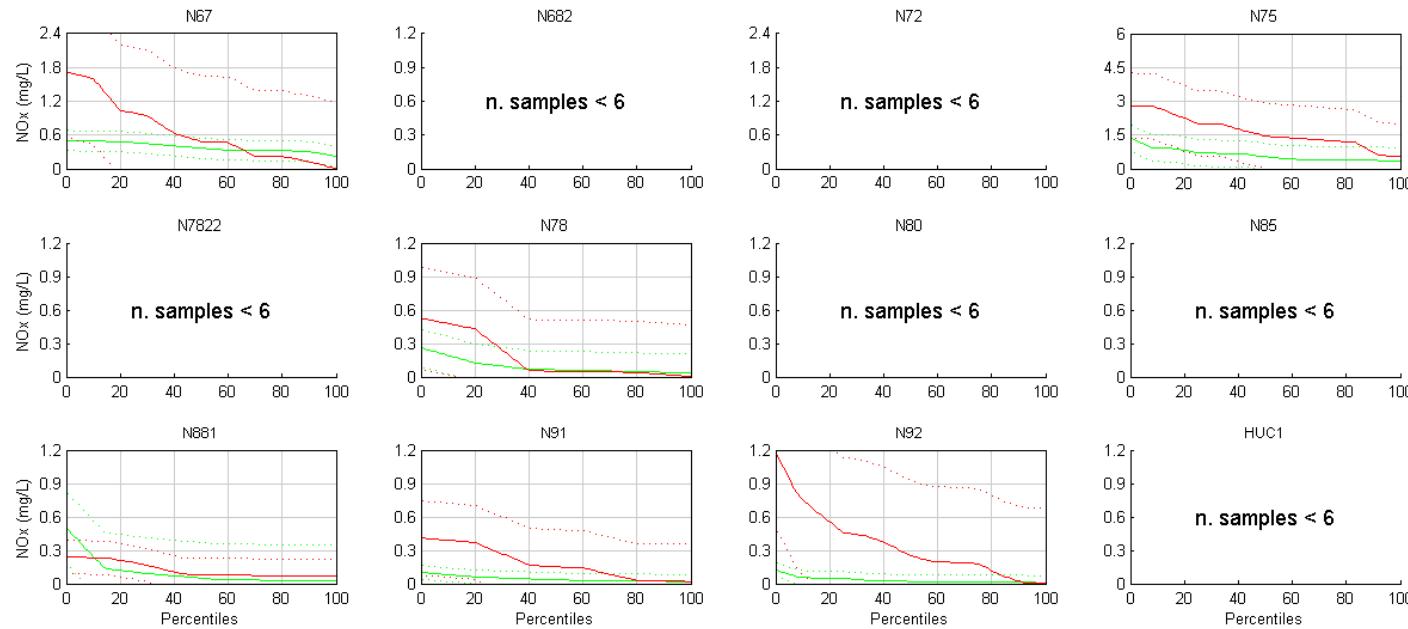


- Figure 13-50 (Cont.) Exceedance Plots – Oxidised Nitrogen Validation 2007 (+/- 2SD) (measured data (red), modelled surface (black) and modelled bottom (green))

SINCLAIR KNIGHT MERZ



Water Quality Modelling of the Hawkesbury-Nepean River System

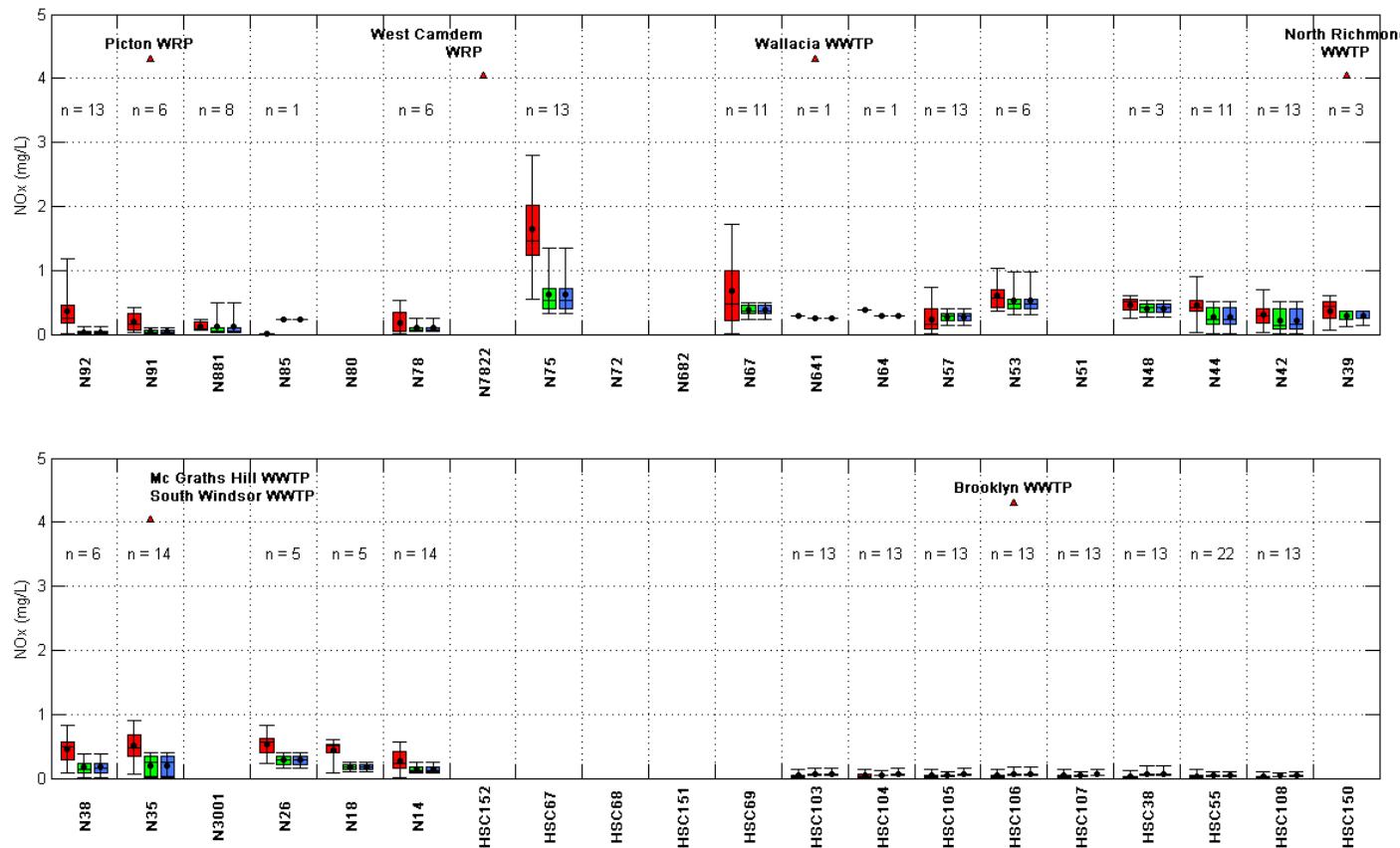


- Figure 13-50 (Cont.) Exceedance Plots – Oxidised Nitrogen Validation 2007 (+/- 2SD) (measured data (red), modelled surface (black) and modelled bottom (green))

SINCLAIR KNIGHT MERZ



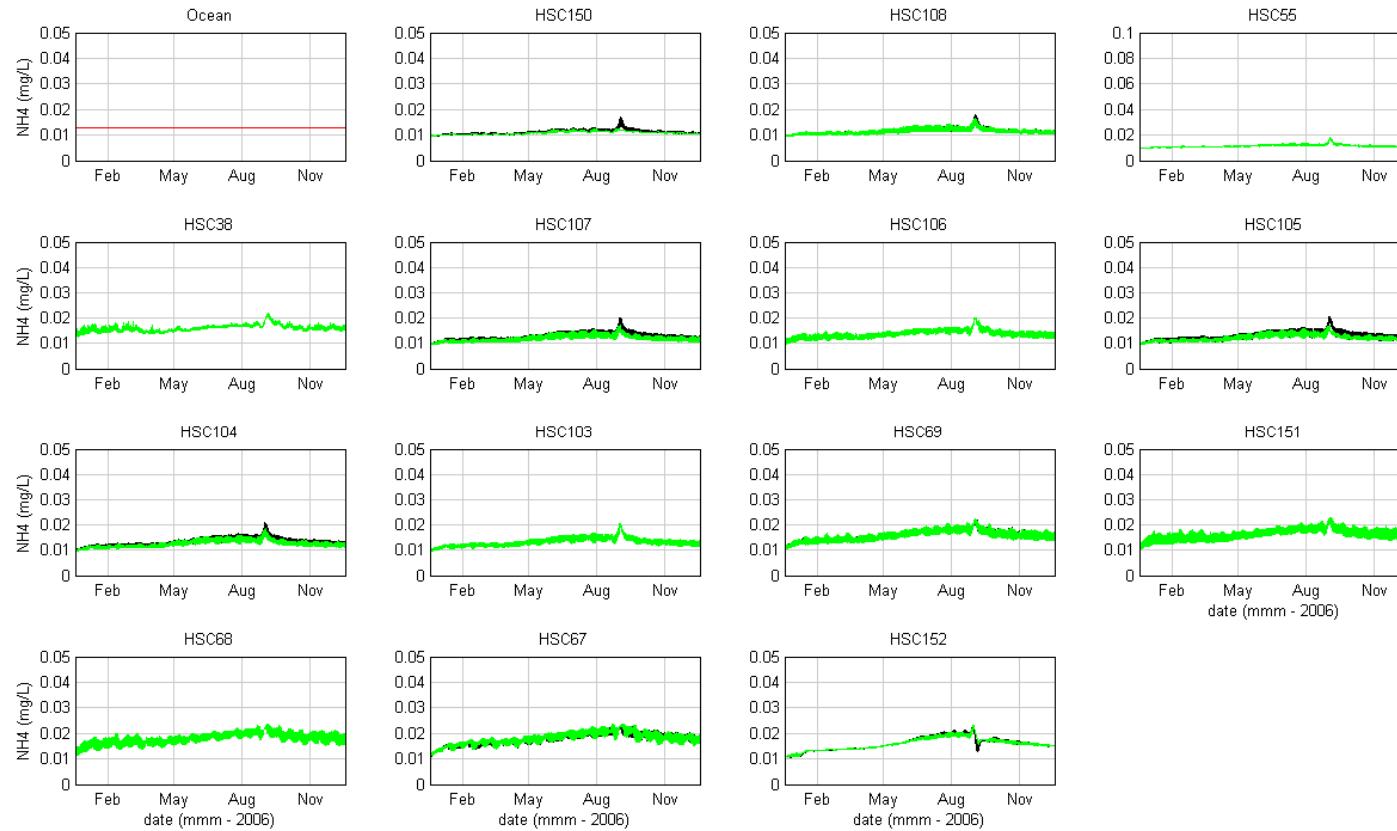
Water Quality Modelling of the Hawkesbury-Nepean River System



■ **Figure 13-51 Box and Whisker Plots – Oxidised Nitrogen Validation 2007 (measured data (red), modelled surface (blue) and modelled bottom (green))**



Water Quality Modelling of the Hawkesbury-Nepean River System

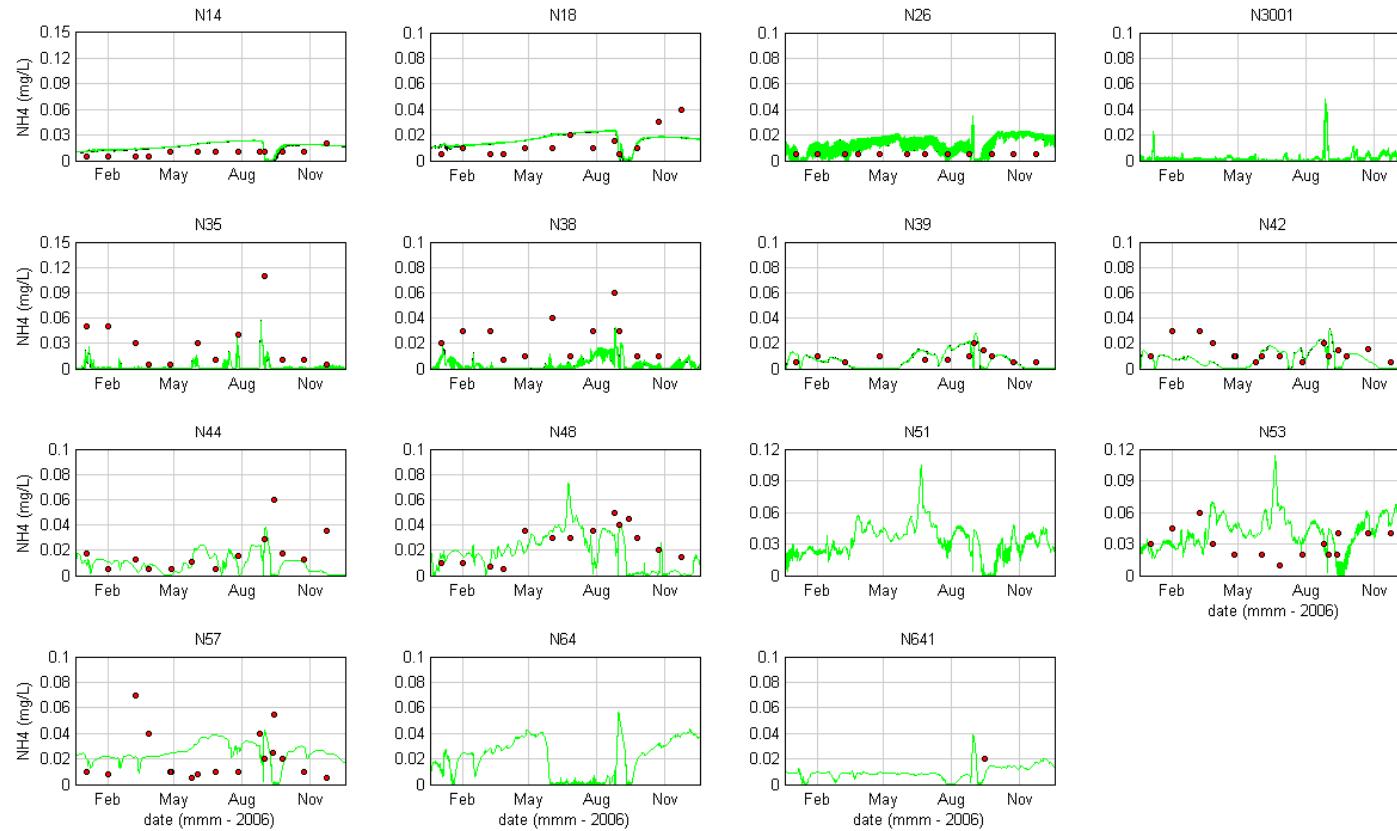


■ **Figure 13-52 Ammonium Calibration 2006 (measured data (red), modelled surface (black) and modelled bottom (green))**

SINCLAIR KNIGHT MERZ



Water Quality Modelling of the Hawkesbury-Nepean River System

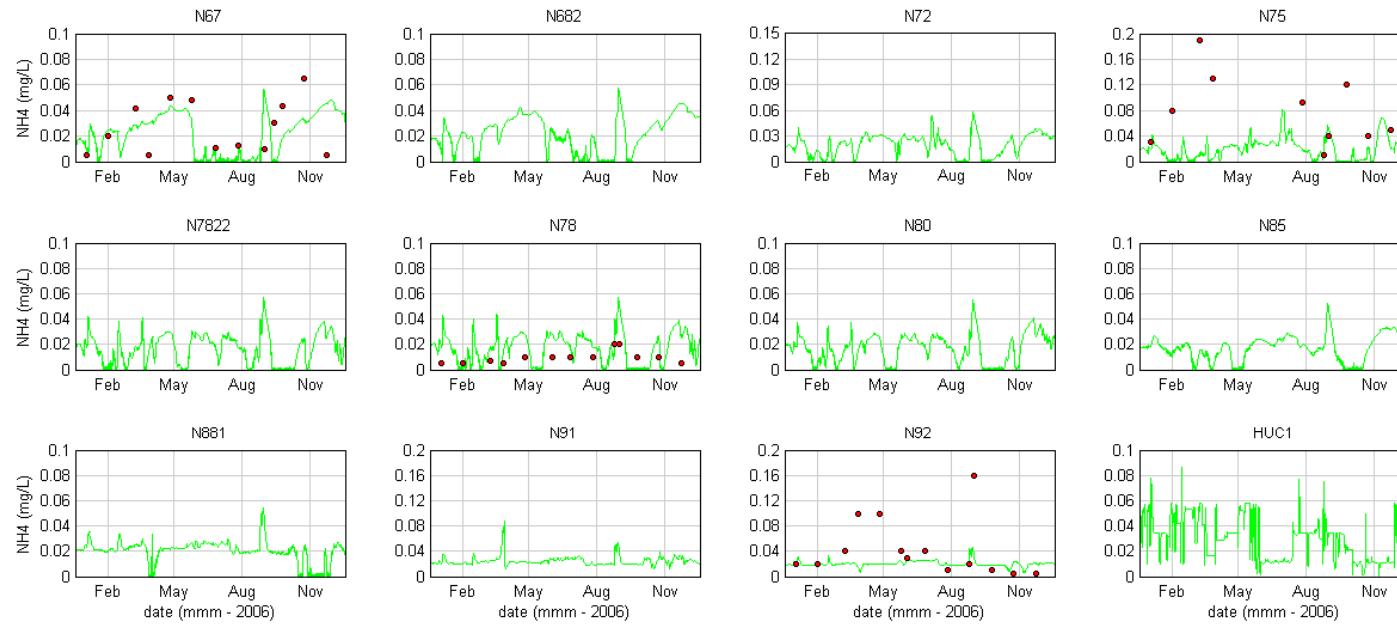


■ **Figure 13-52 (Cont.) Ammonium Calibration 2006 (measured data (red), modelled surface (black) and modelled bottom (green))**

SINCLAIR KNIGHT MERZ



Water Quality Modelling of the Hawkesbury-Nepean River System

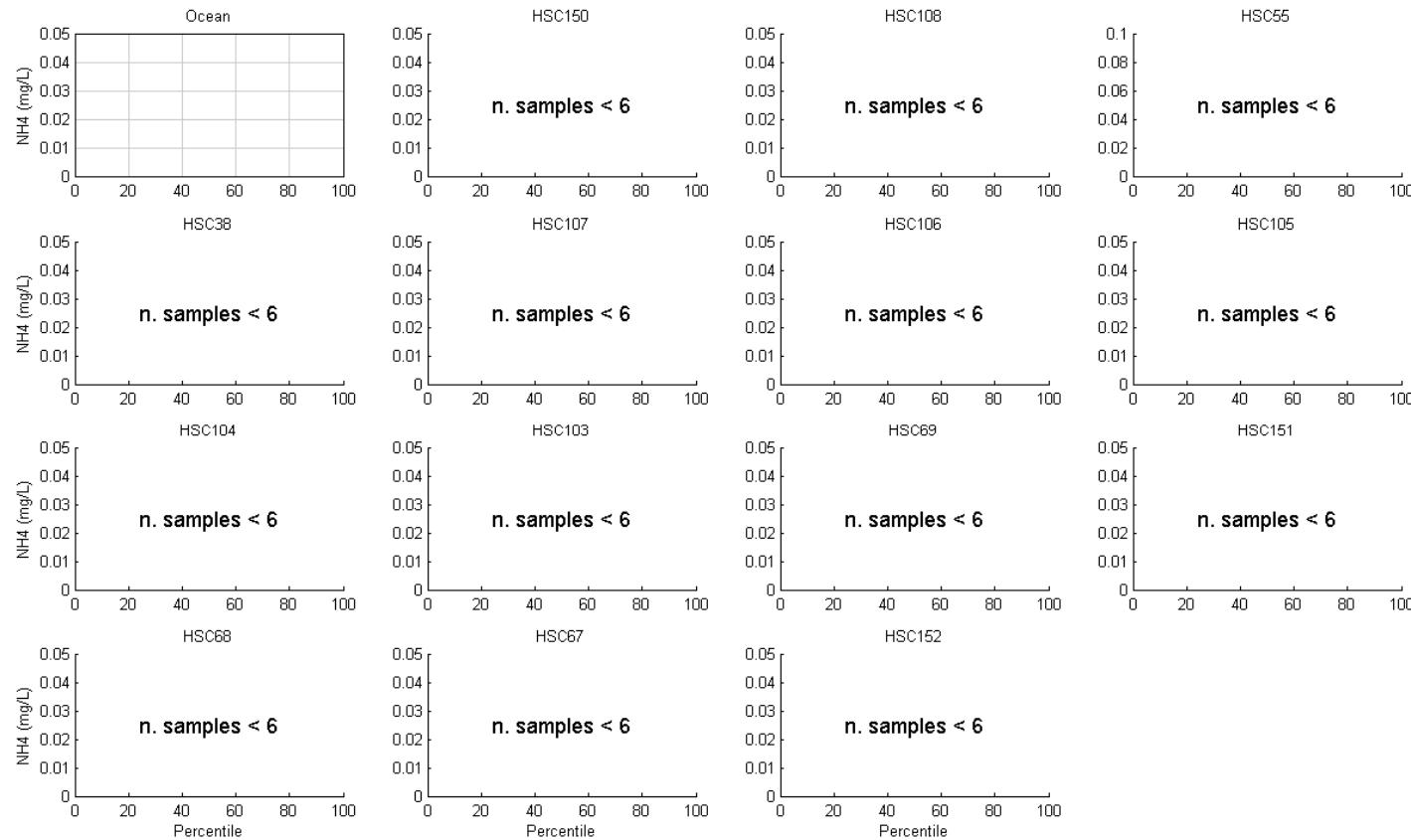


- Figure 13-52 (Cont.) Ammonium Calibration 2006 (measured data (red), modelled surface (black) and modelled bottom (green))

SINCLAIR KNIGHT MERZ



Water Quality Modelling of the Hawkesbury-Nepean River System

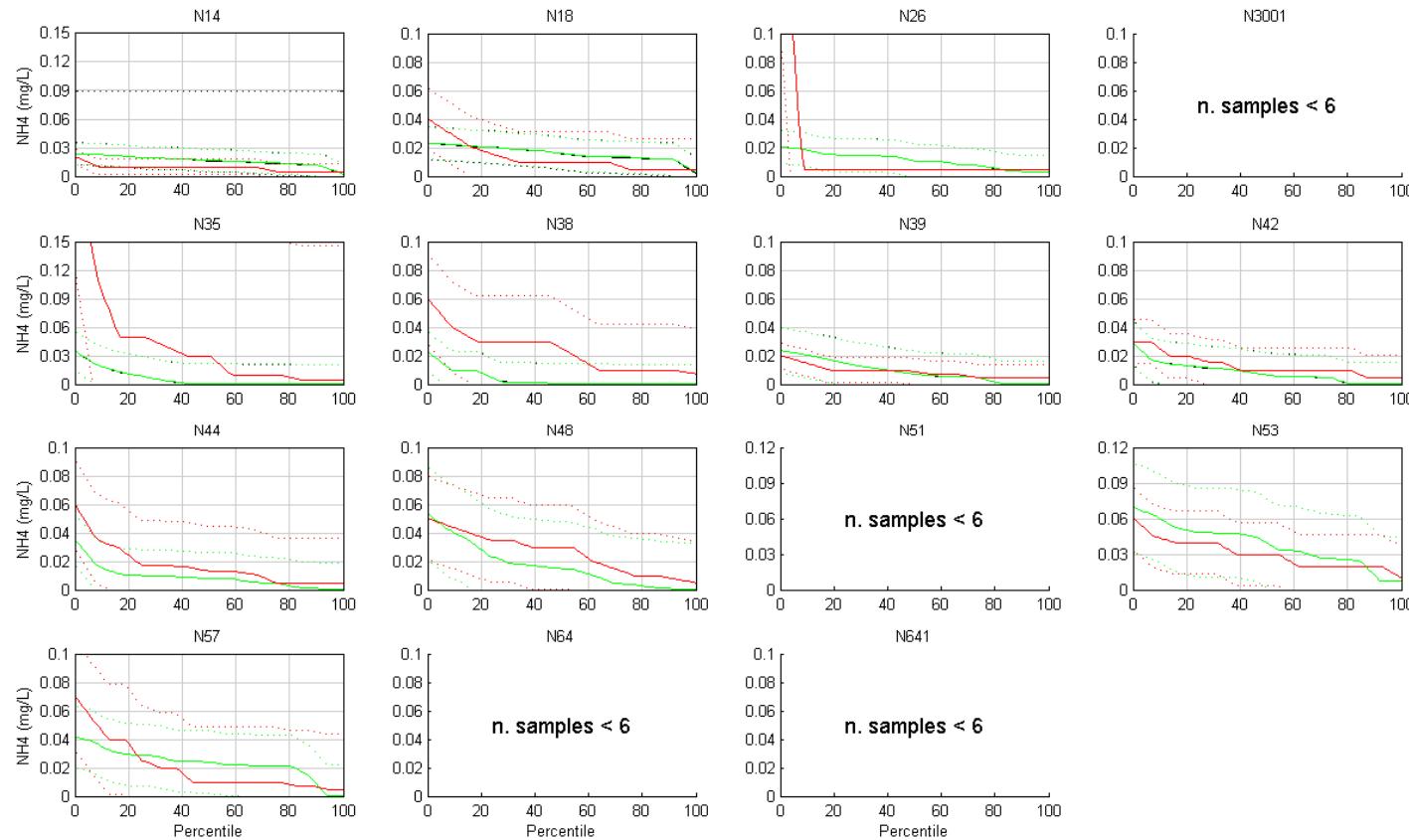


- Figure 13-53 Exceedance Plots – Ammonium Calibration 2006 (+/- 2SD) (measured data (red), modelled surface (black) and modelled bottom (green))

SINCLAIR KNIGHT MERZ



Water Quality Modelling of the Hawkesbury-Nepean River System

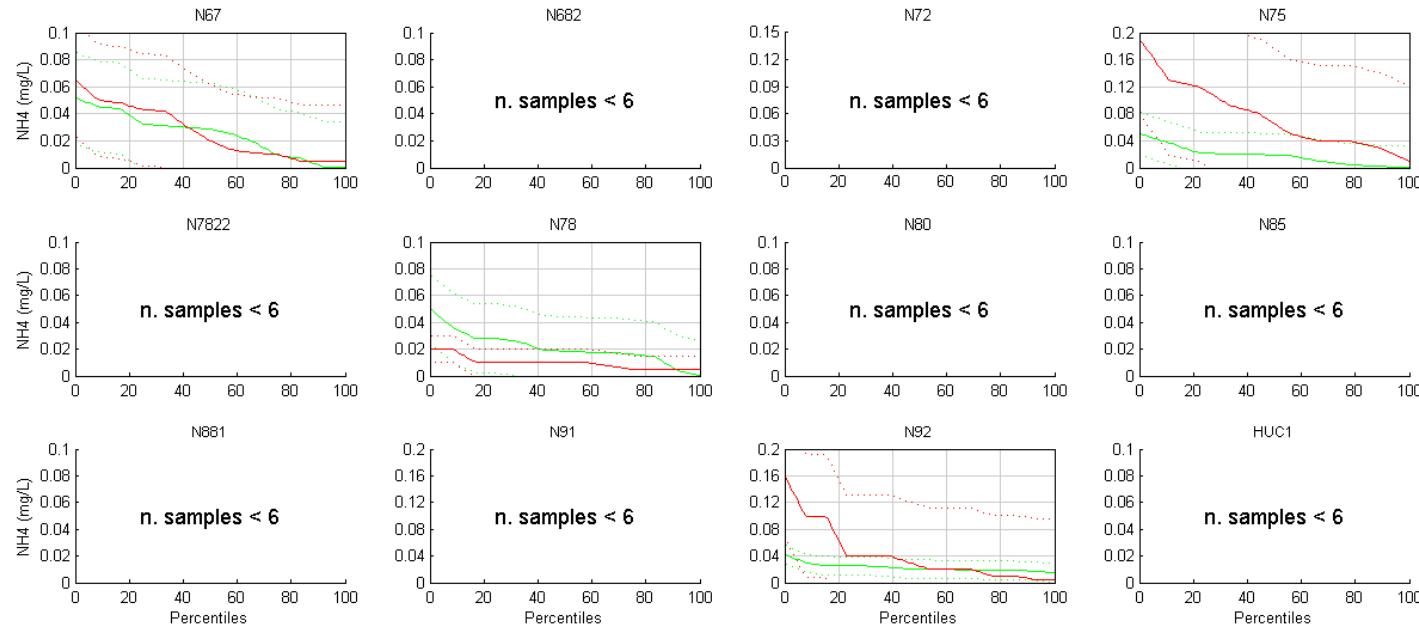


- Figure 13-53 (Cont.) Exceedance Plots – Ammonium Calibration 2006 (+/- 2SD) (measured data (red), modelled surface (black) and modelled bottom (green))

SINCLAIR KNIGHT MERZ



Water Quality Modelling of the Hawkesbury-Nepean River System

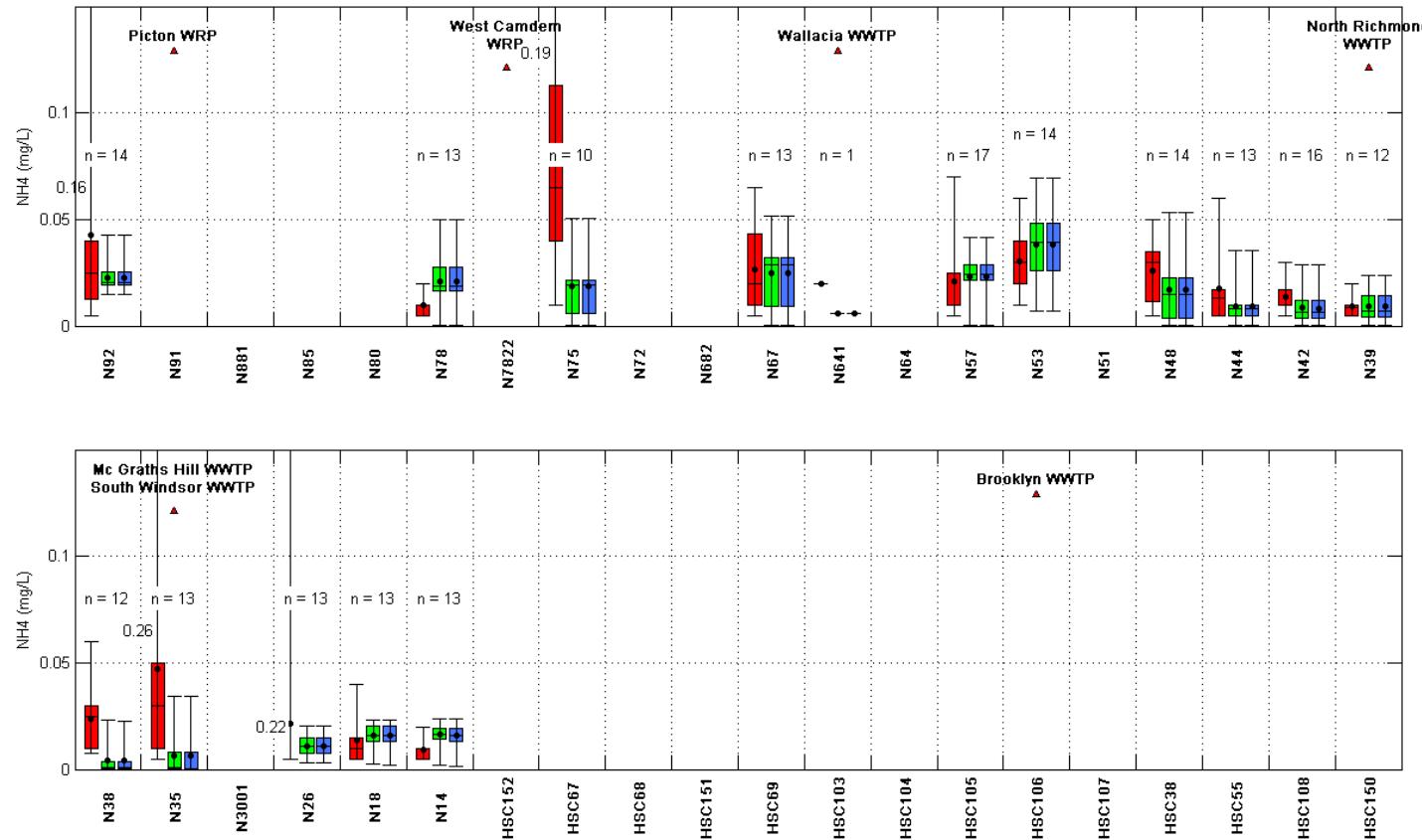


- Figure 13-53 (Cont.) Exceedance Plots – Ammonium Calibration 2006 (+/- 2SD) (measured data (red), modelled surface (black) and modelled bottom (green))

SINCLAIR KNIGHT MERZ



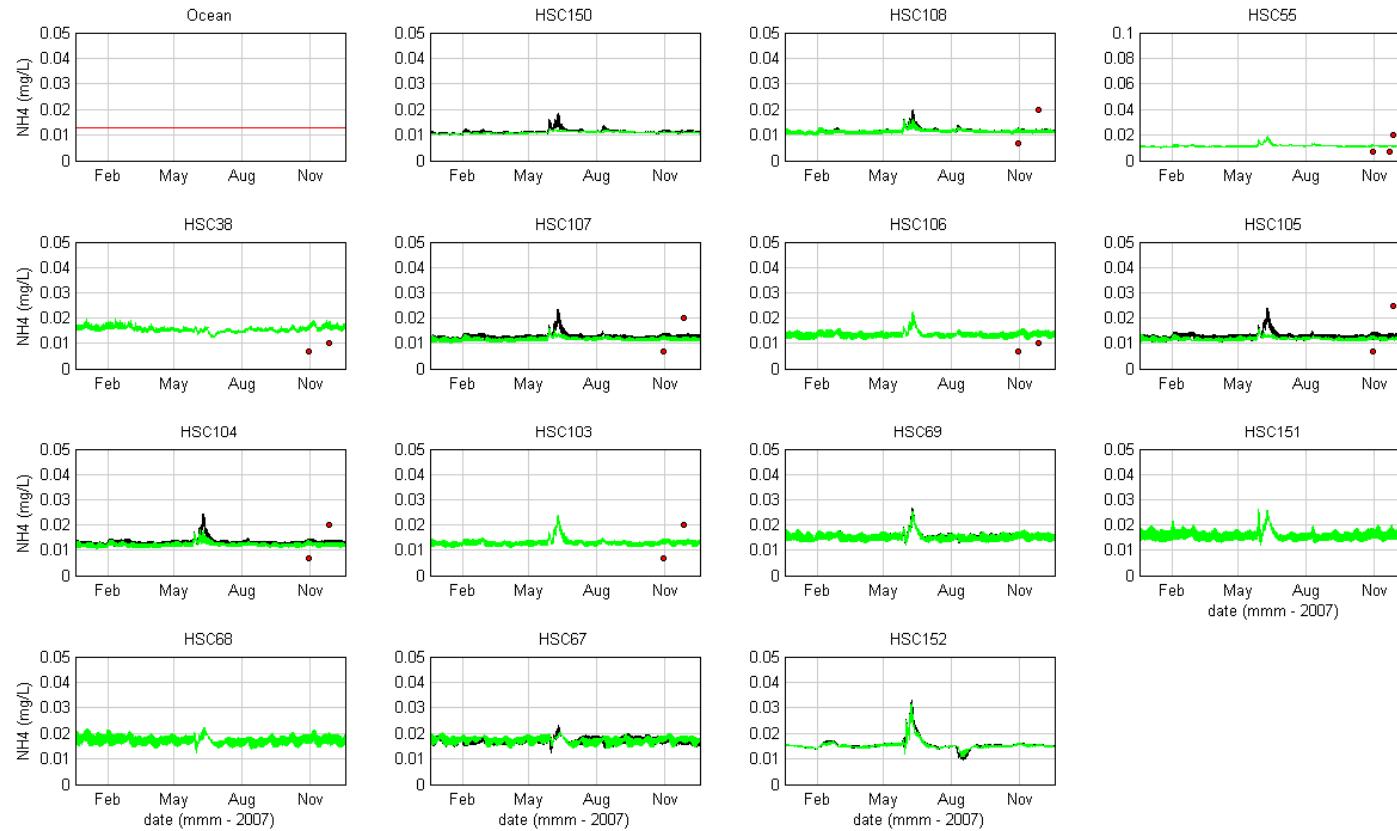
Water Quality Modelling of the Hawkesbury-Nepean River System



- **Figure 13-54 Box and Whisker Plots – Ammonium Calibration 2006 (measured data (red), modelled surface (blue) and modelled bottom (green))**



Water Quality Modelling of the Hawkesbury-Nepean River System

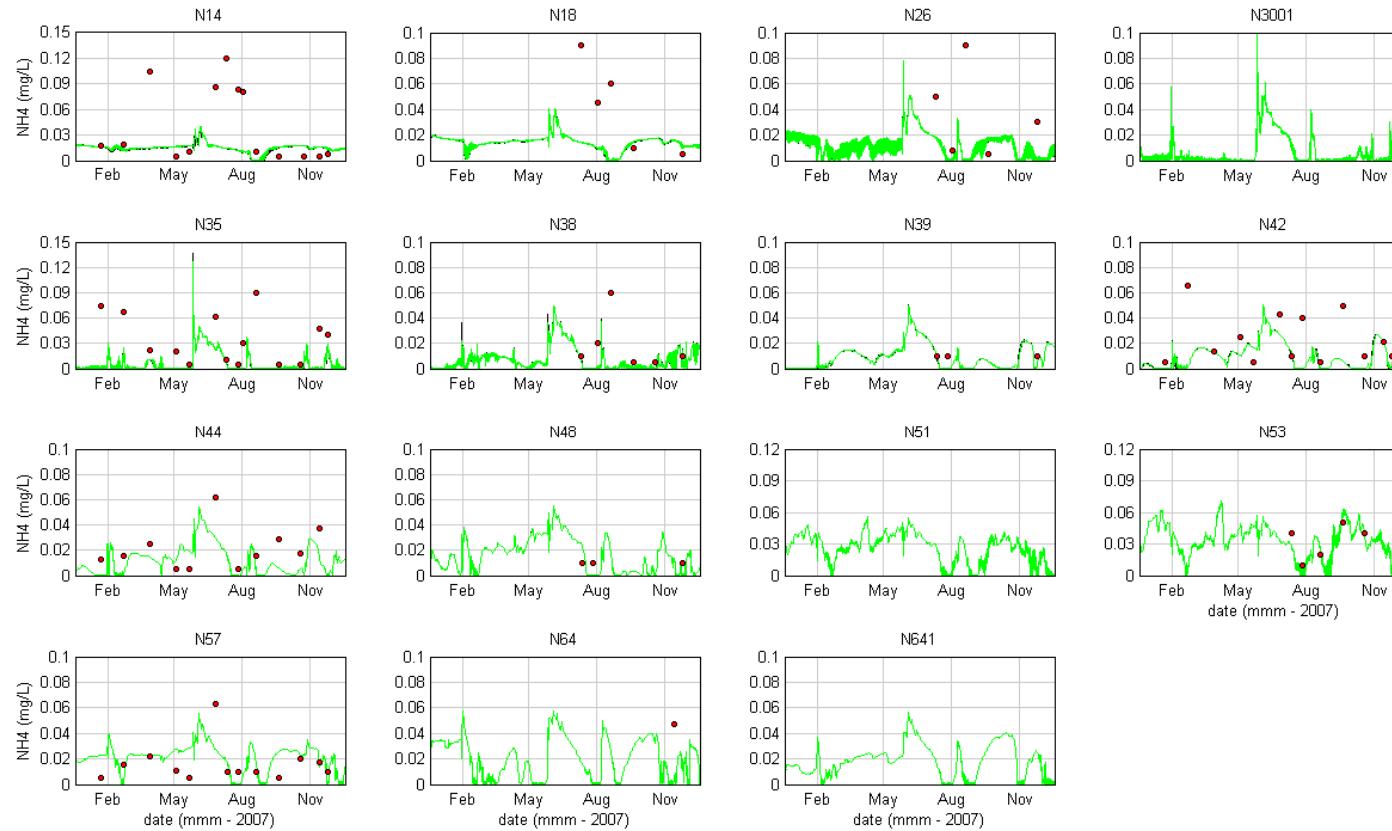


■ **Figure 13-55 Ammonium Validation 2007 (measured data (red), modelled surface (black) and modelled bottom (green))**

SINCLAIR KNIGHT MERZ



Water Quality Modelling of the Hawkesbury-Nepean River System

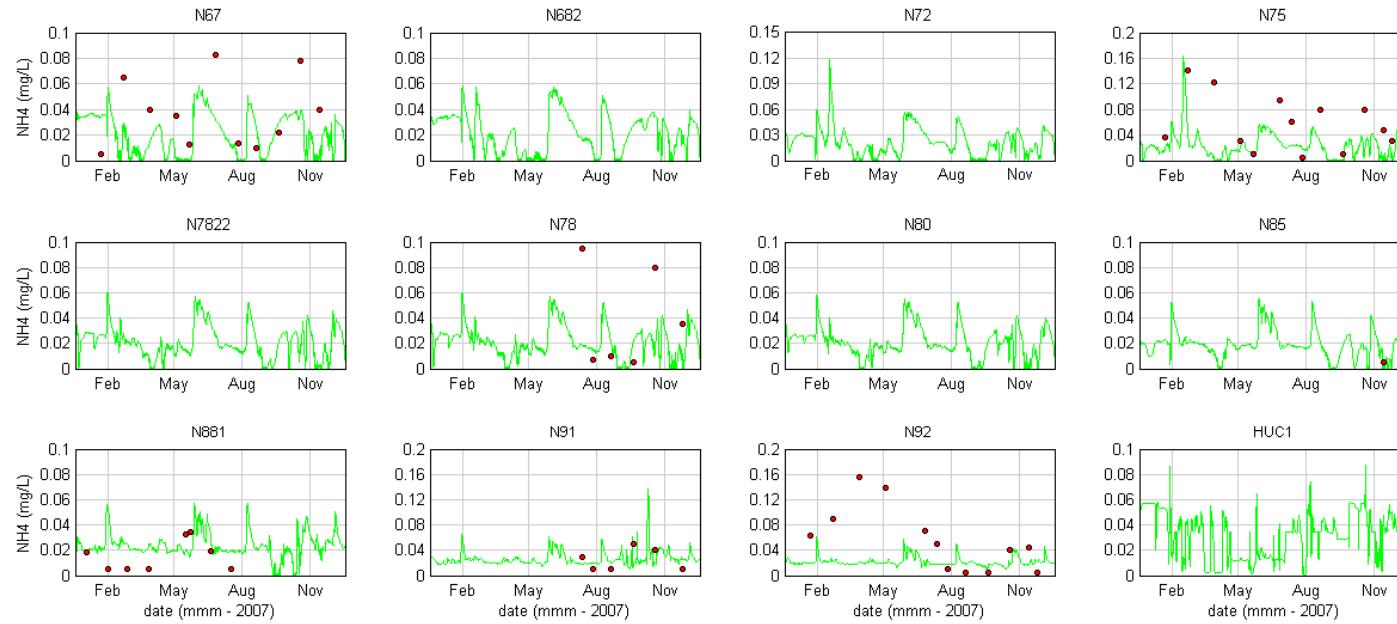


■ Figure 13-55 (Cont.) Ammonium Validation 2007 (measured data (red), modelled surface (black) and modelled bottom (green))

SINCLAIR KNIGHT MERZ



Water Quality Modelling of the Hawkesbury-Nepean River System

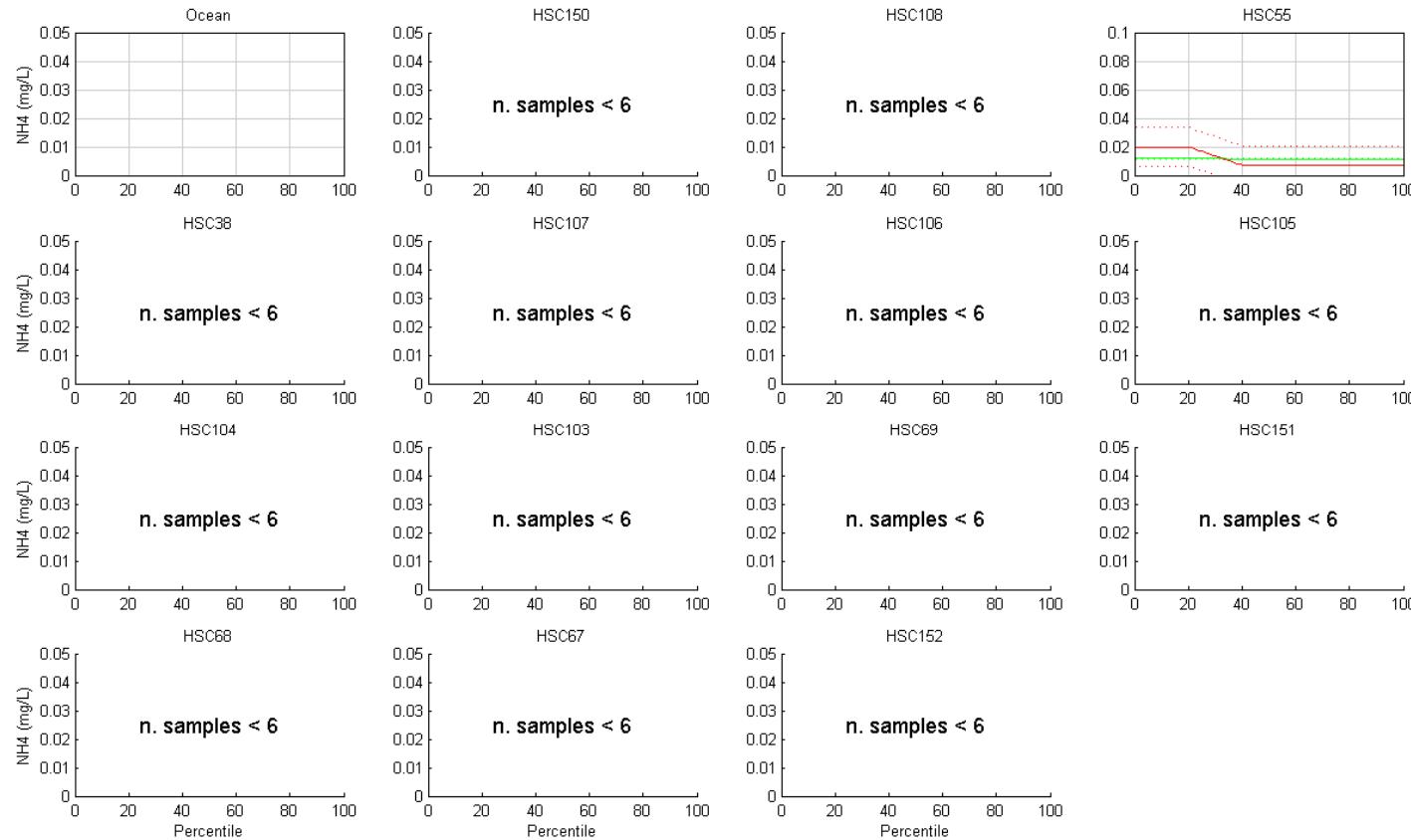


■ Figure 13-55 (Cont.) Ammonium Validation 2007 (measured data (red), modelled surface (black) and modelled bottom (green))

SINCLAIR KNIGHT MERZ



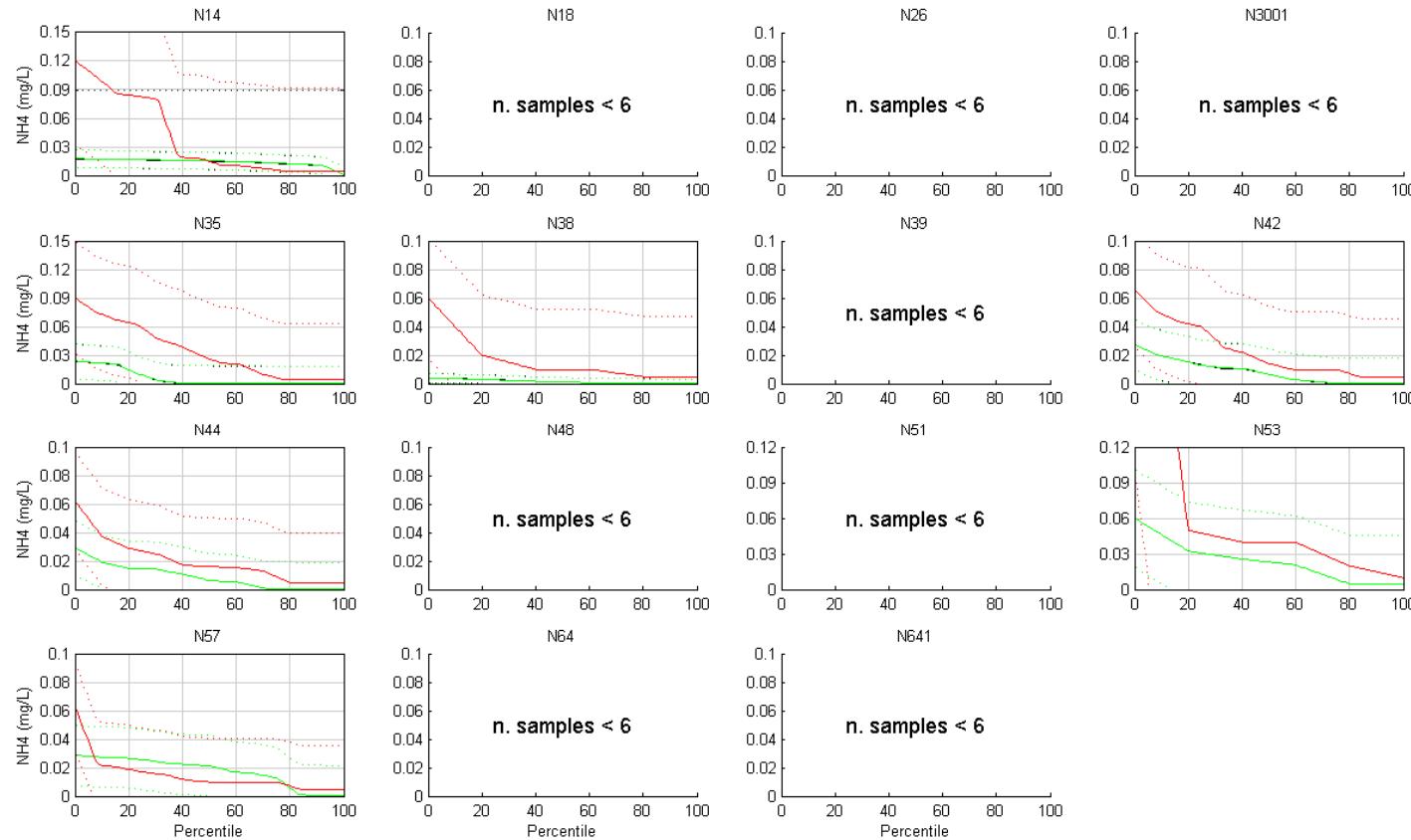
Water Quality Modelling of the Hawkesbury-Nepean River System



- **Figure 13-56 Exceedance Plots – Ammonium Validation 2007 (+/- 2SD) (measured data (red), modelled surface (black) and modelled bottom (green))**

SINCLAIR KNIGHT MERZ

Water Quality Modelling of the Hawkesbury-Nepean River System

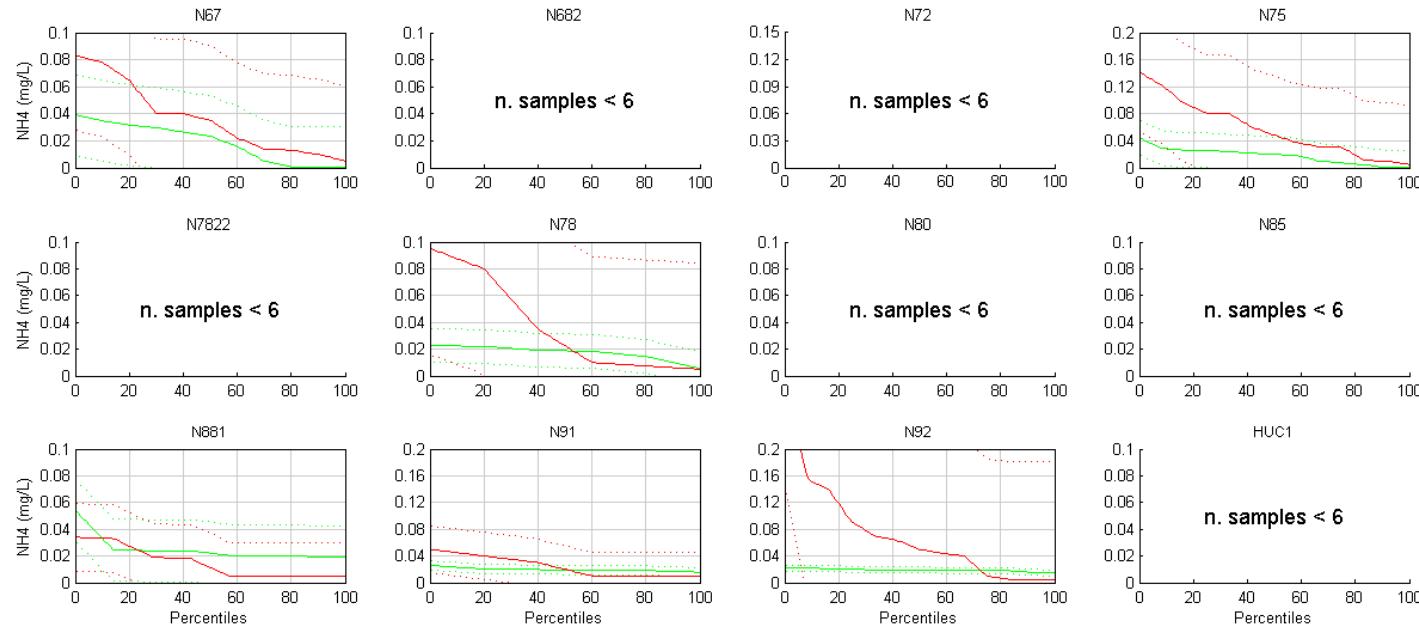


- Figure 13-56 (Cont.) Exceedance Plots – Ammonium Validation 2007 (+/- 2SD) (measured data (red), modelled surface (black) and modelled bottom (green))

SINCLAIR KNIGHT MERZ



Water Quality Modelling of the Hawkesbury-Nepean River System

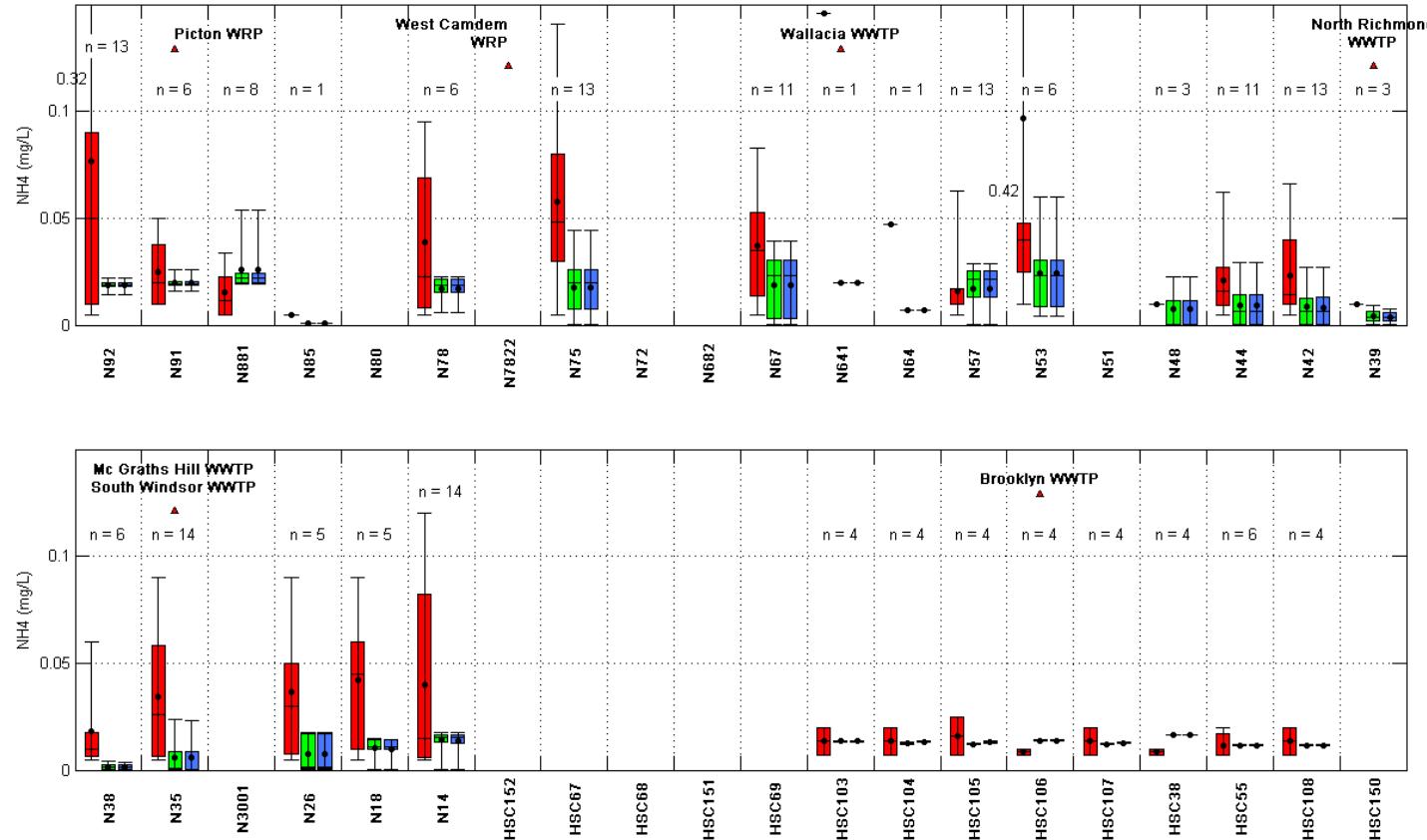


- Figure 13-56 (Cont.) Exceedance Plots – Ammonium Validation 2007 (+/- 2SD) (measured data (red), modelled surface (black) and modelled bottom (green))

SINCLAIR KNIGHT MERZ



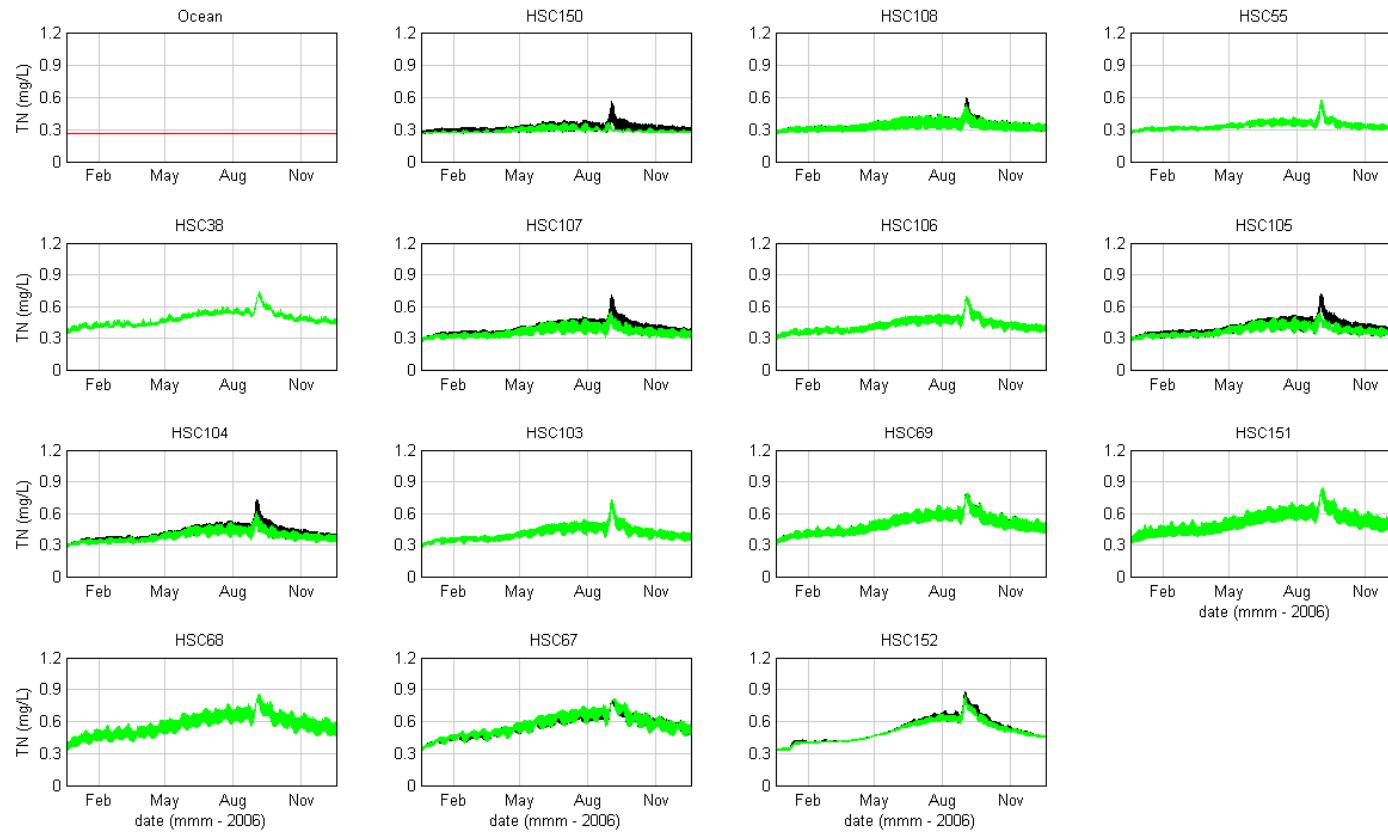
Water Quality Modelling of the Hawkesbury-Nepean River System



- Figure 13-57 Box and Whisker Plots – Ammonium Validation 2007 (measured data (red), modelled surface (blue) and modelled bottom (green))



Water Quality Modelling of the Hawkesbury-Nepean River System

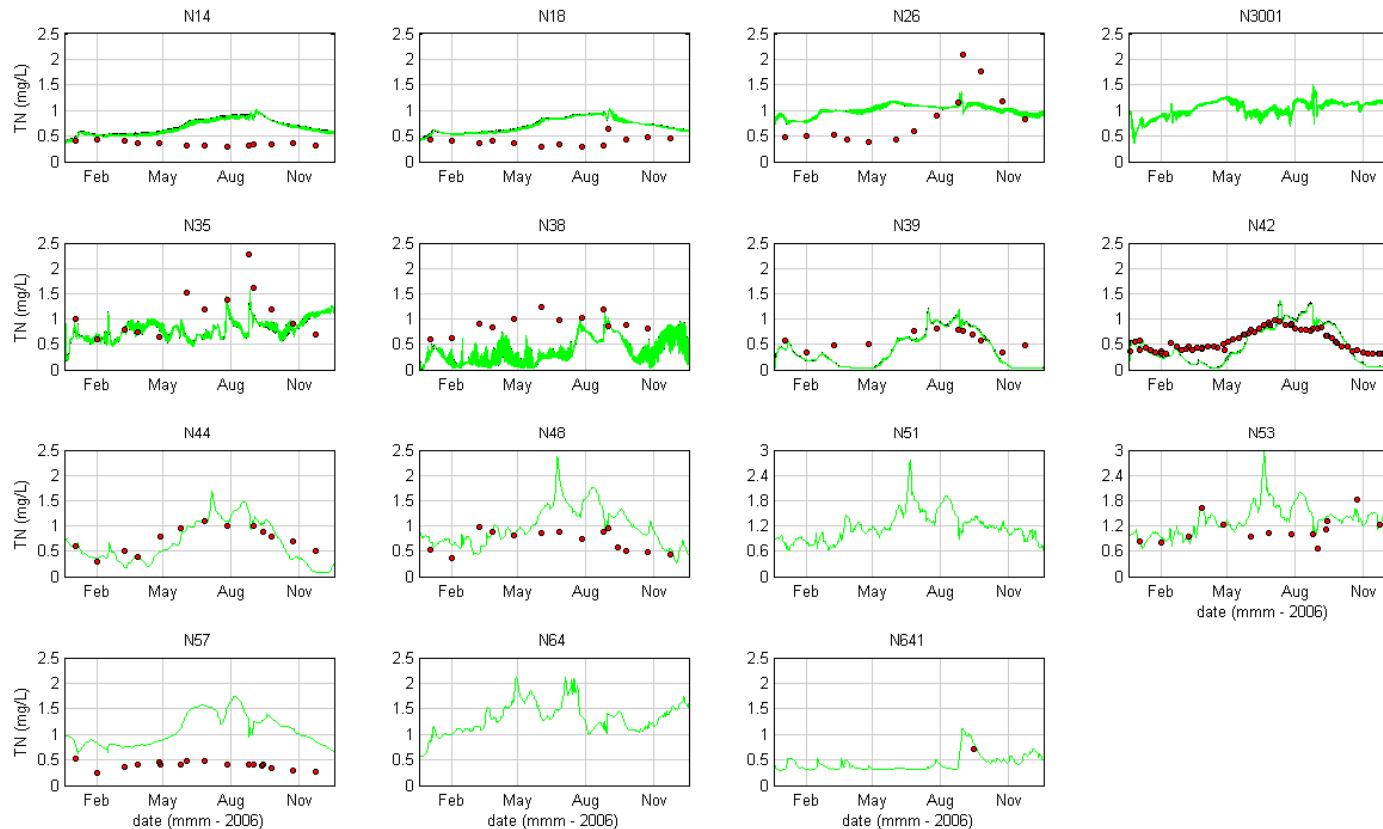


■ **Figure 13-58 Total Nitrogen Calibration2006 (measured data (red), modelled surface (black) and modelled bottom (green))**

SINCLAIR KNIGHT MERZ



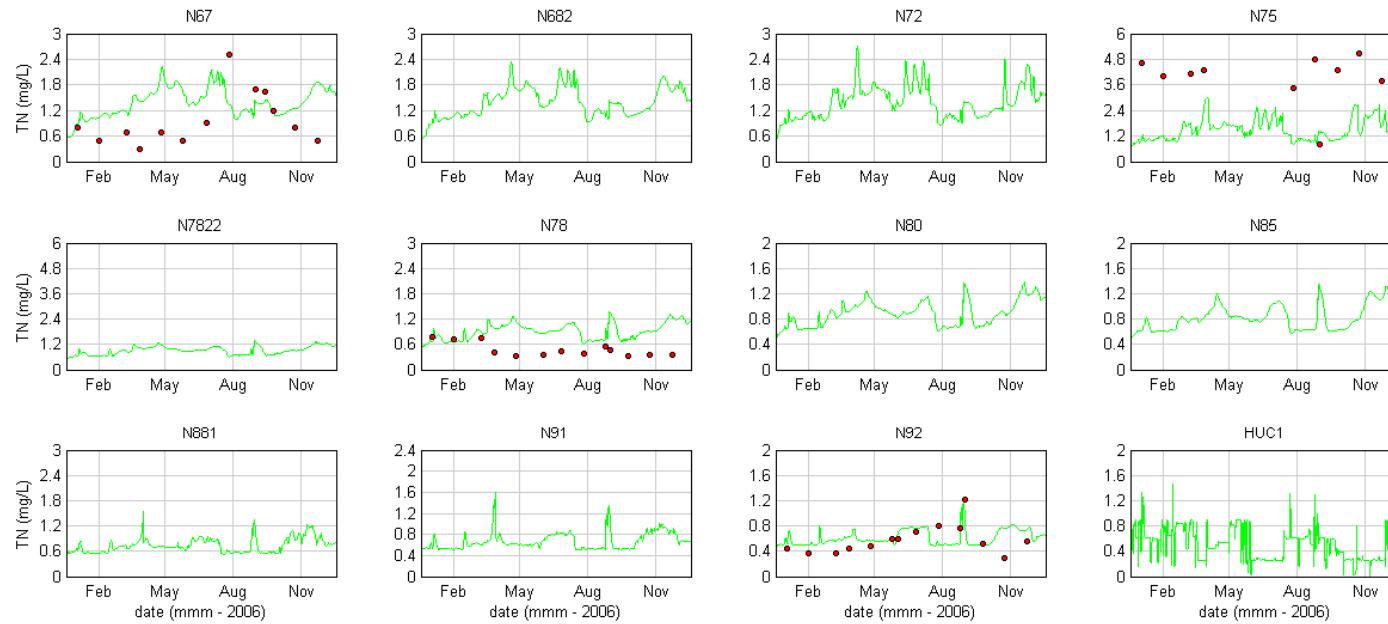
Water Quality Modelling of the Hawkesbury-Nepean River System



■ **Figure 13-58 (Cont.) Total Nitrogen Calibration 2006 (measured data (red), modelled surface (black) and modelled bottom (green))**



Water Quality Modelling of the Hawkesbury-Nepean River System

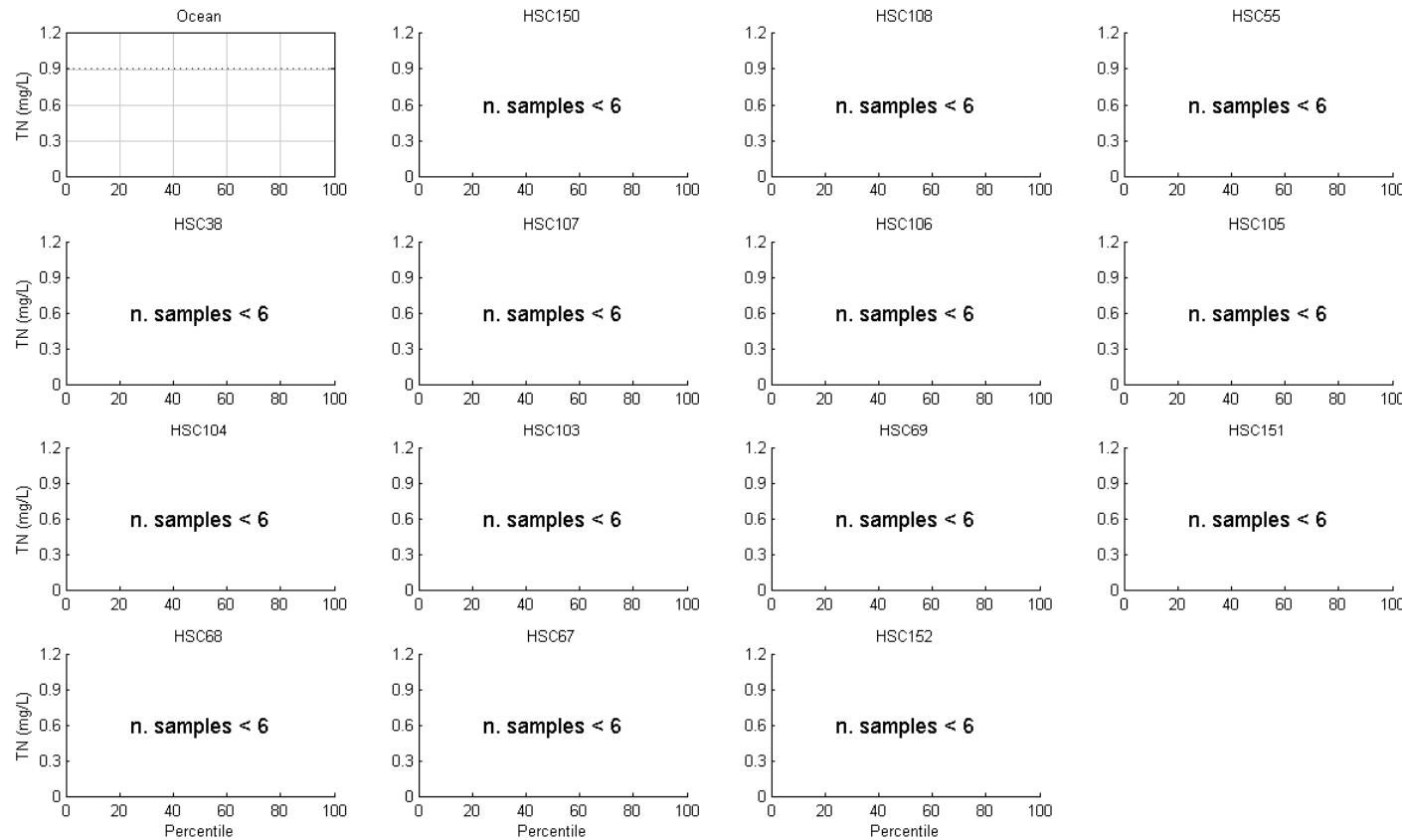


■ **Figure 13-58 (Cont.) Total Nitrogen Calibration 2006 (measured data (red), modelled surface (black) and modelled bottom (green))**

SINCLAIR KNIGHT MERZ



Water Quality Modelling of the Hawkesbury-Nepean River System

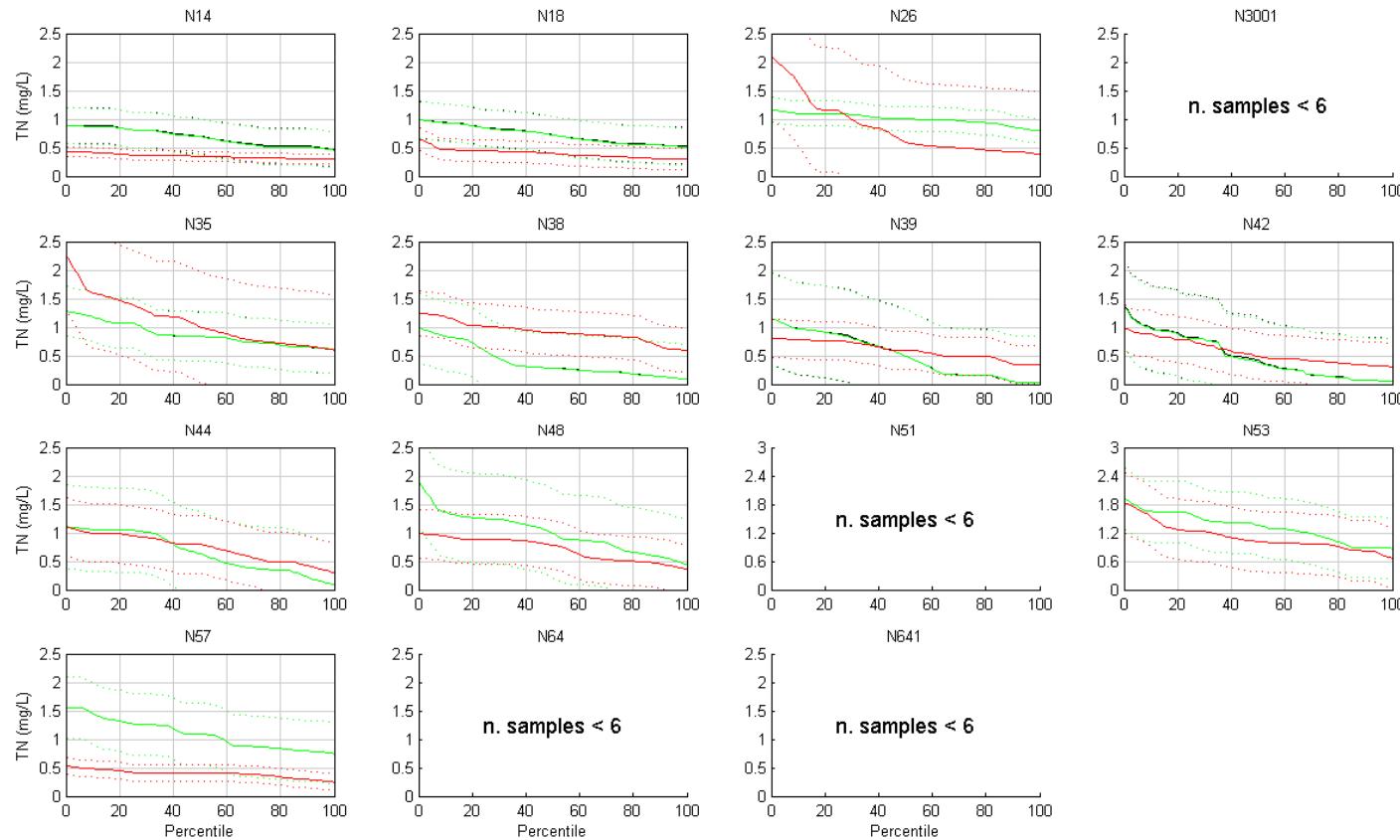


- **Figure 13-59 Exceedance Plots – Total Nitrogen Calibration 2006 (+/- 2SD) (measured data (red), modelled surface (black) and modelled bottom (green))**

SINCLAIR KNIGHT MERZ



Water Quality Modelling of the Hawkesbury-Nepean River System

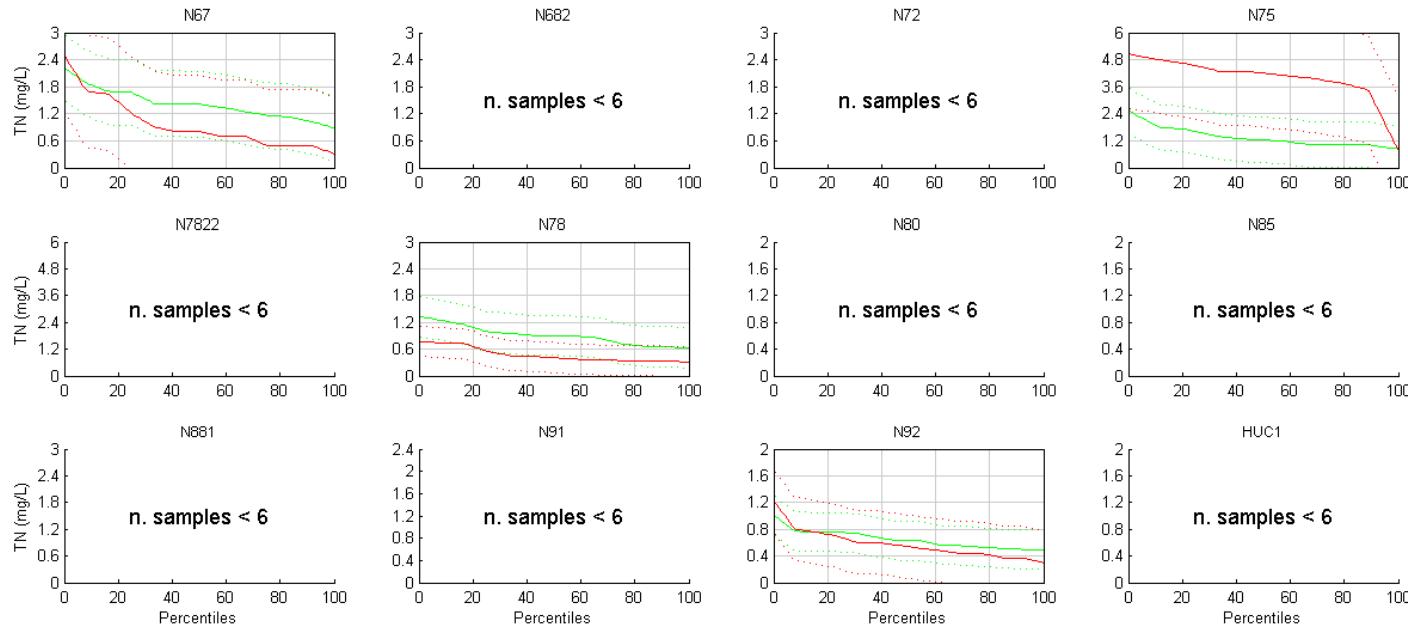


- **Figure 13-59 (Cont.) Exceedance Plots – Total Nitrogen Calibration 2006 (+/- 2SD) (measured data (red), modelled surface (black) and modelled bottom (green))**

SINCLAIR KNIGHT MERZ



Water Quality Modelling of the Hawkesbury-Nepean River System

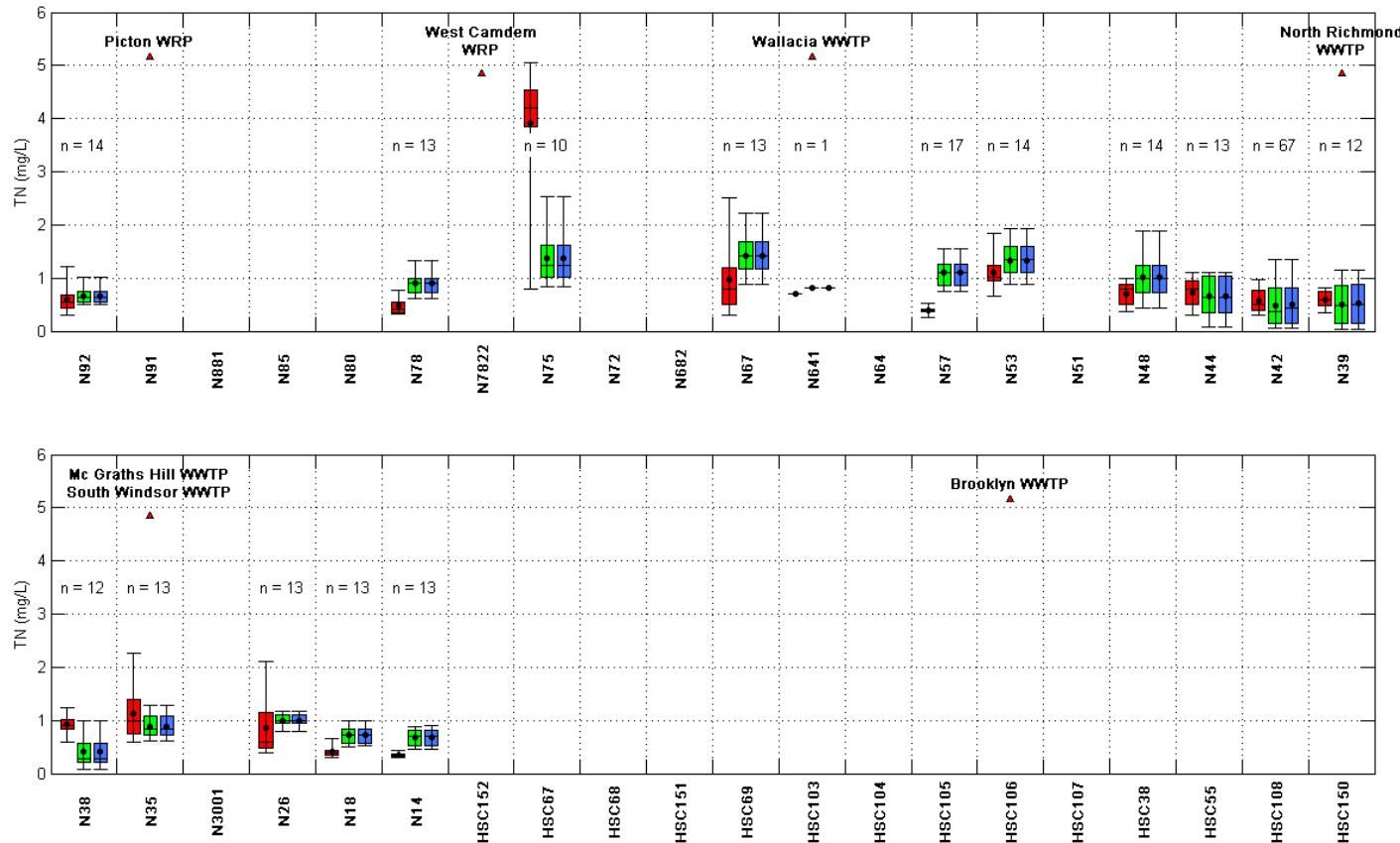


- Figure 13-59 (Cont.) Exceedance Plots – Total Nitrogen Calibration 2006 (+/- 2SD) (measured data (red), modelled surface (black) and modelled bottom (green))

SINCLAIR KNIGHT MERZ



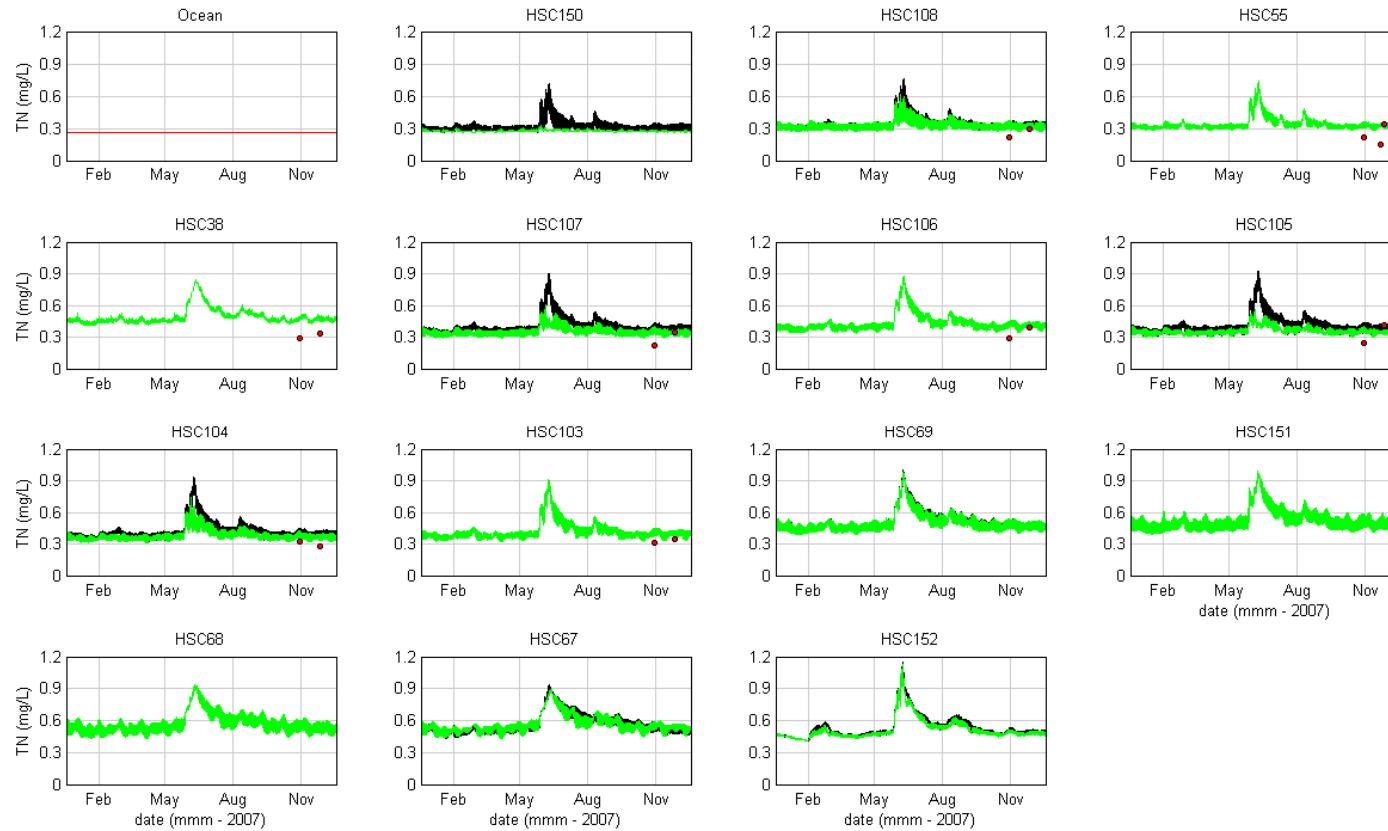
Water Quality Modelling of the Hawkesbury-Nepean River System



■ Figure 13-60 Box and Whisker Plots – Total Nitrogen Calibration 2006 (measured data (red), modelled surface (blue) and modelled bottom (green))



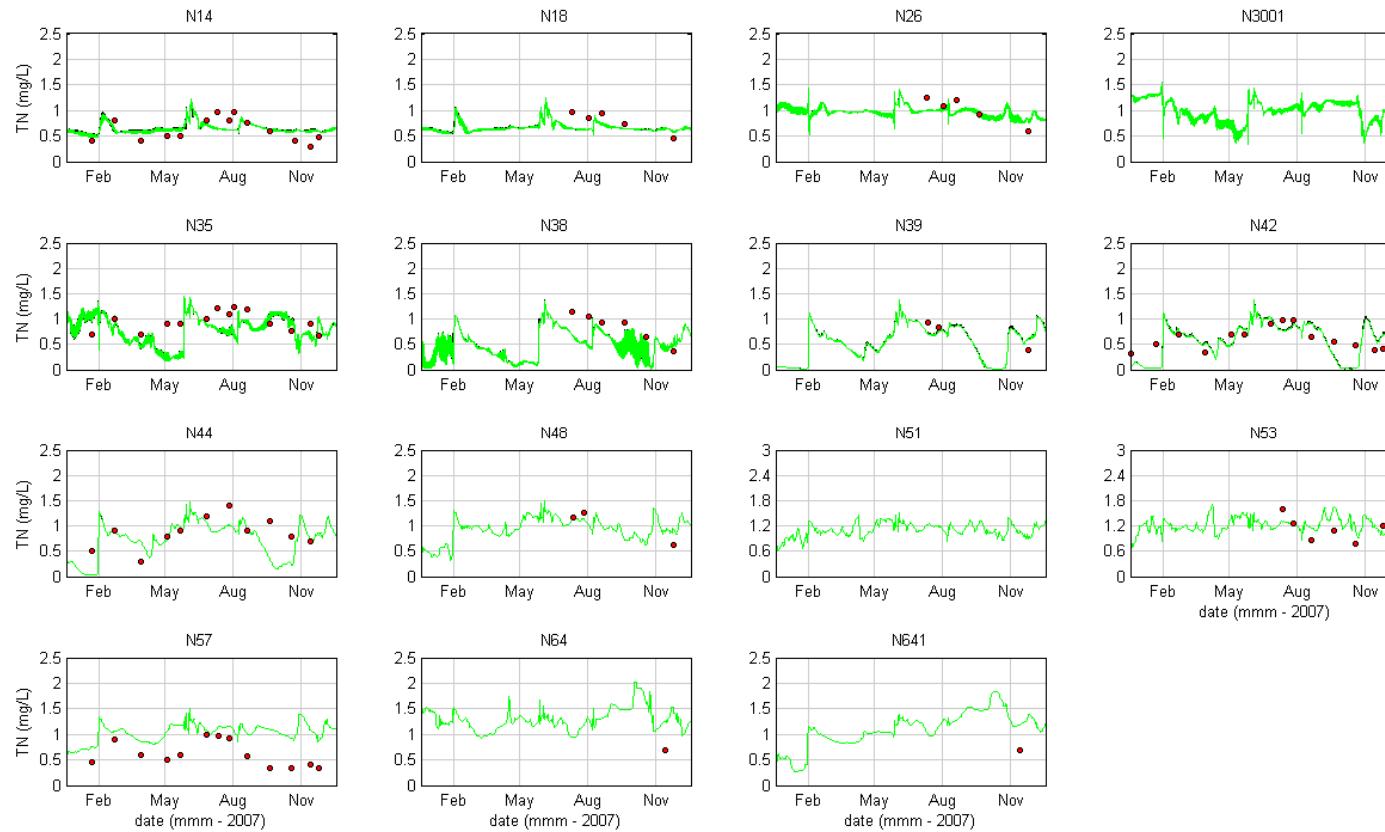
Water Quality Modelling of the Hawkesbury-Nepean River System



■ **Figure 13-61 Total Nitrogen Validation 2007 (measured data (red), modelled surface (black) and modelled bottom (green))**



Water Quality Modelling of the Hawkesbury-Nepean River System

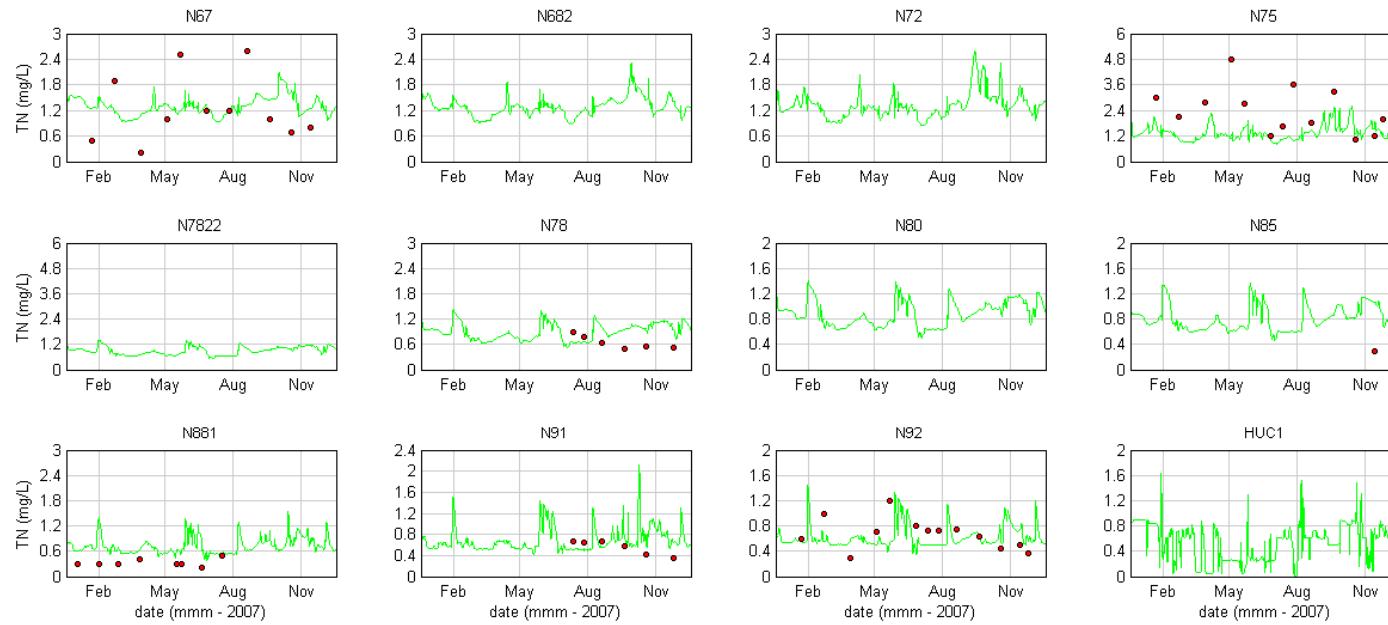


■ **Figure 13-61 (Cont.) Total Nitrogen Validation 2007 (measured data (red), modelled surface (black) and modelled bottom (green))**

SINCLAIR KNIGHT MERZ



Water Quality Modelling of the Hawkesbury-Nepean River System

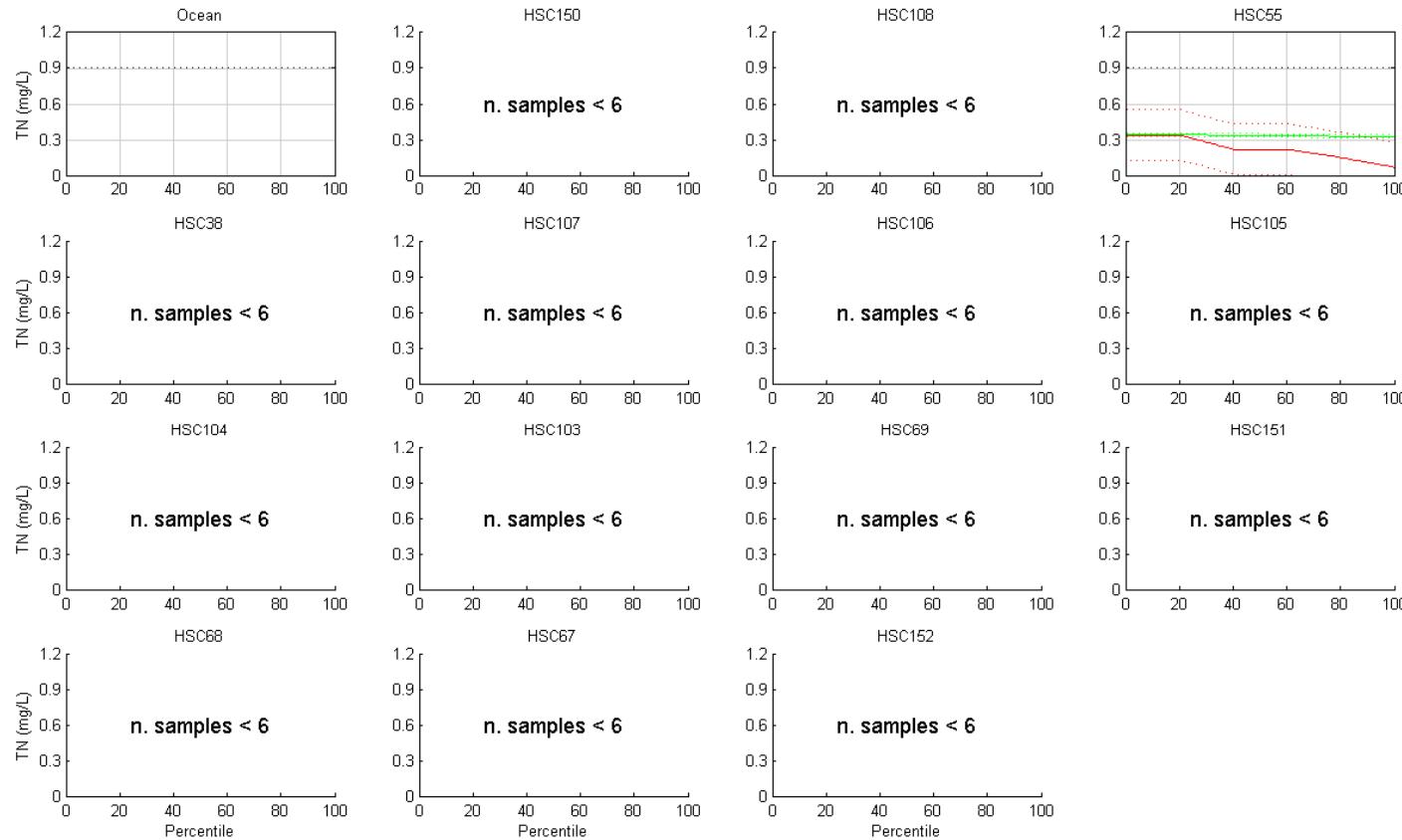


- **Figure 13-61 (Cont.) Total Nitrogen Validation 2007 (measured data (red), modelled surface (black) and modelled bottom (green))**

SINCLAIR KNIGHT MERZ



Water Quality Modelling of the Hawkesbury-Nepean River System

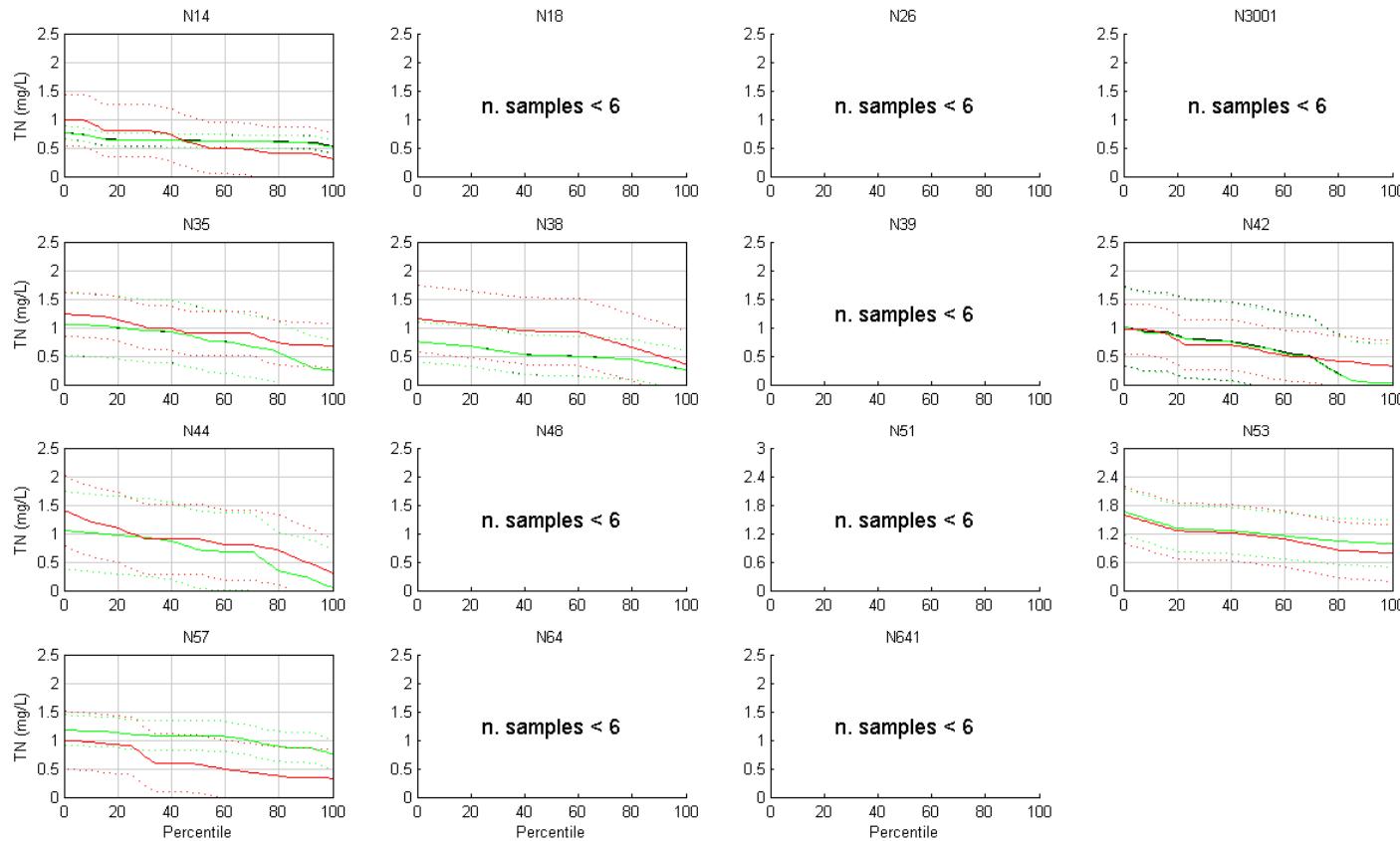


- **Figure 13-62 Exceedance Plots – Total Nitrogen Validation 2007 (+/- 2SD) (measured data (red), modelled surface (black) and modelled bottom (green))**

SINCLAIR KNIGHT MERZ



Water Quality Modelling of the Hawkesbury-Nepean River System

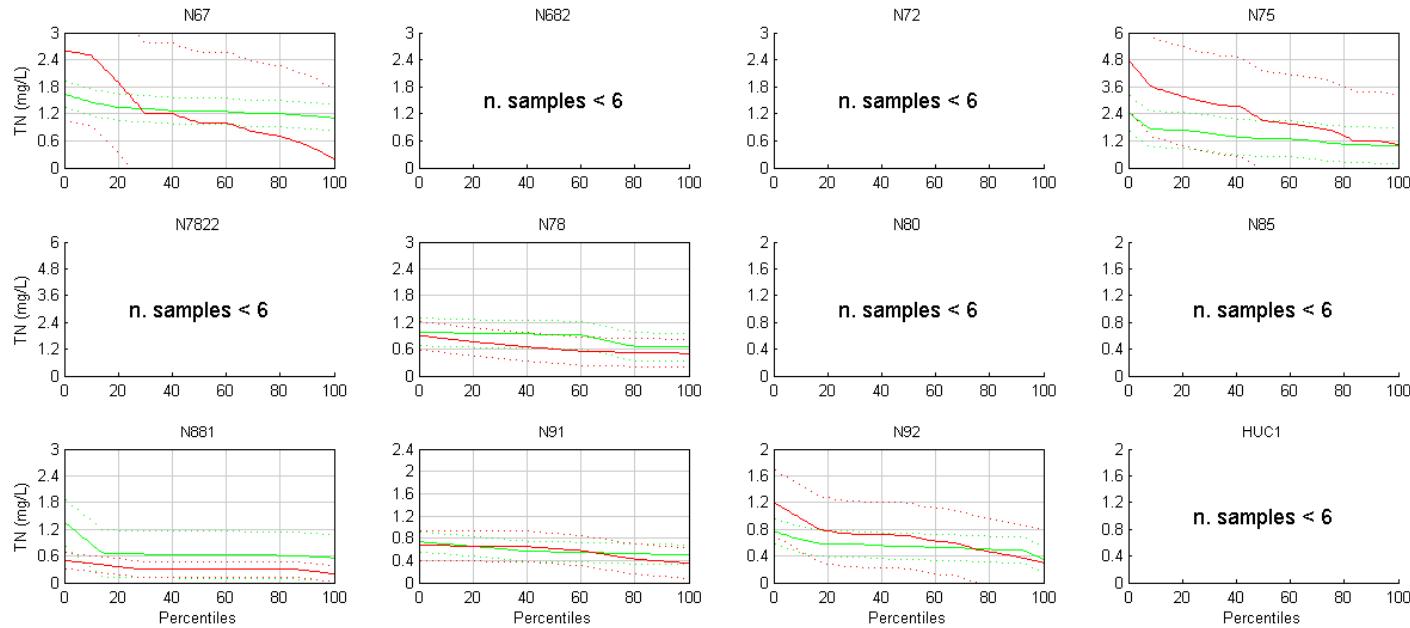


- Figure 13-62 (Cont.) Exceedance Plots – Total Nitrogen Validation 2007 (+/- 2SD) (measured data (red), modelled surface (black) and modelled bottom (green))

SINCLAIR KNIGHT MERZ

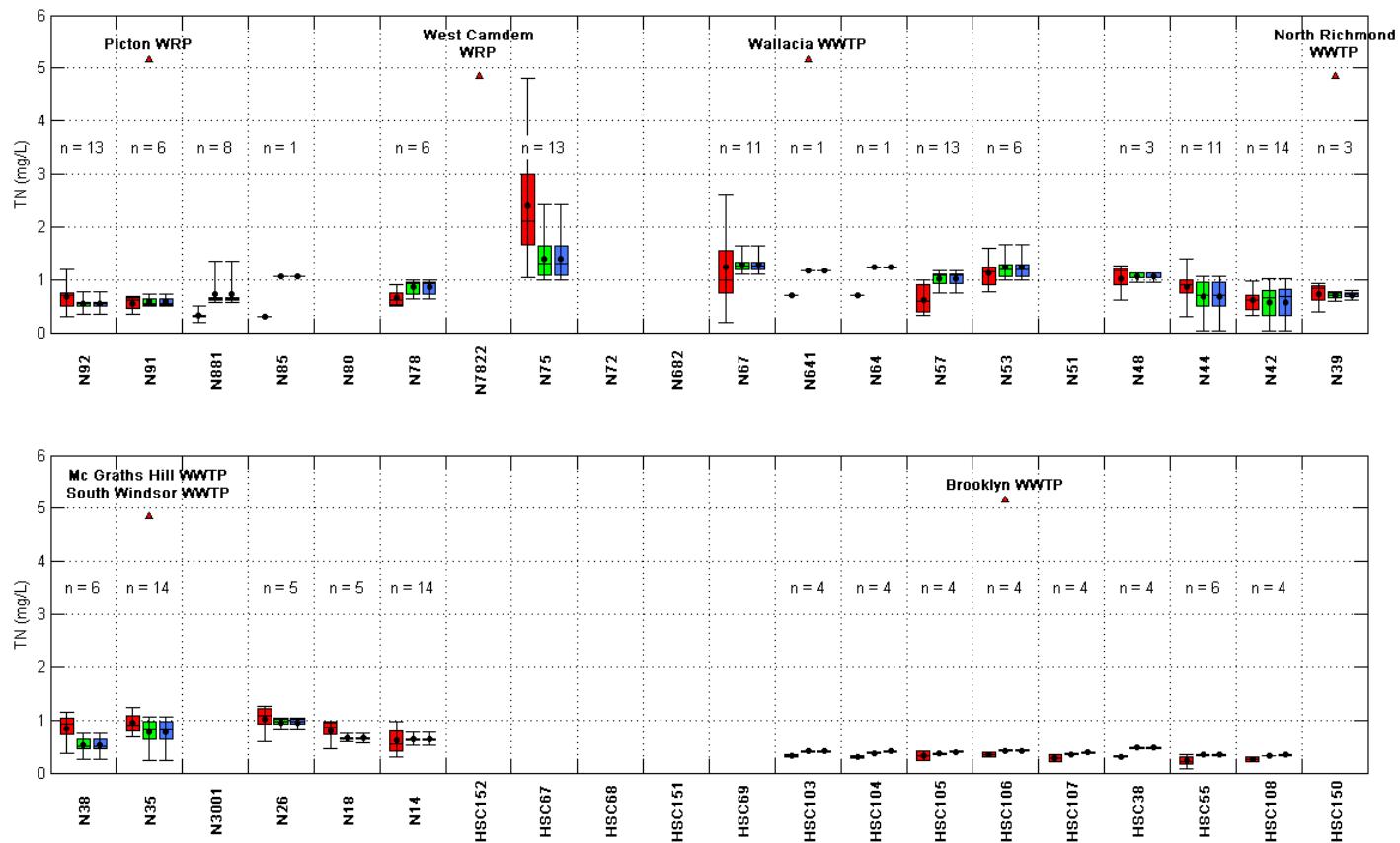


Water Quality Modelling of the Hawkesbury-Nepean River System



- Figure 13-62 (Cont.) Exceedance Plots – Total Nitrogen Validation 2007 (+/- 2SD) (measured data (red), modelled surface (black) and modelled bottom (green))

SINCLAIR KNIGHT MERZ

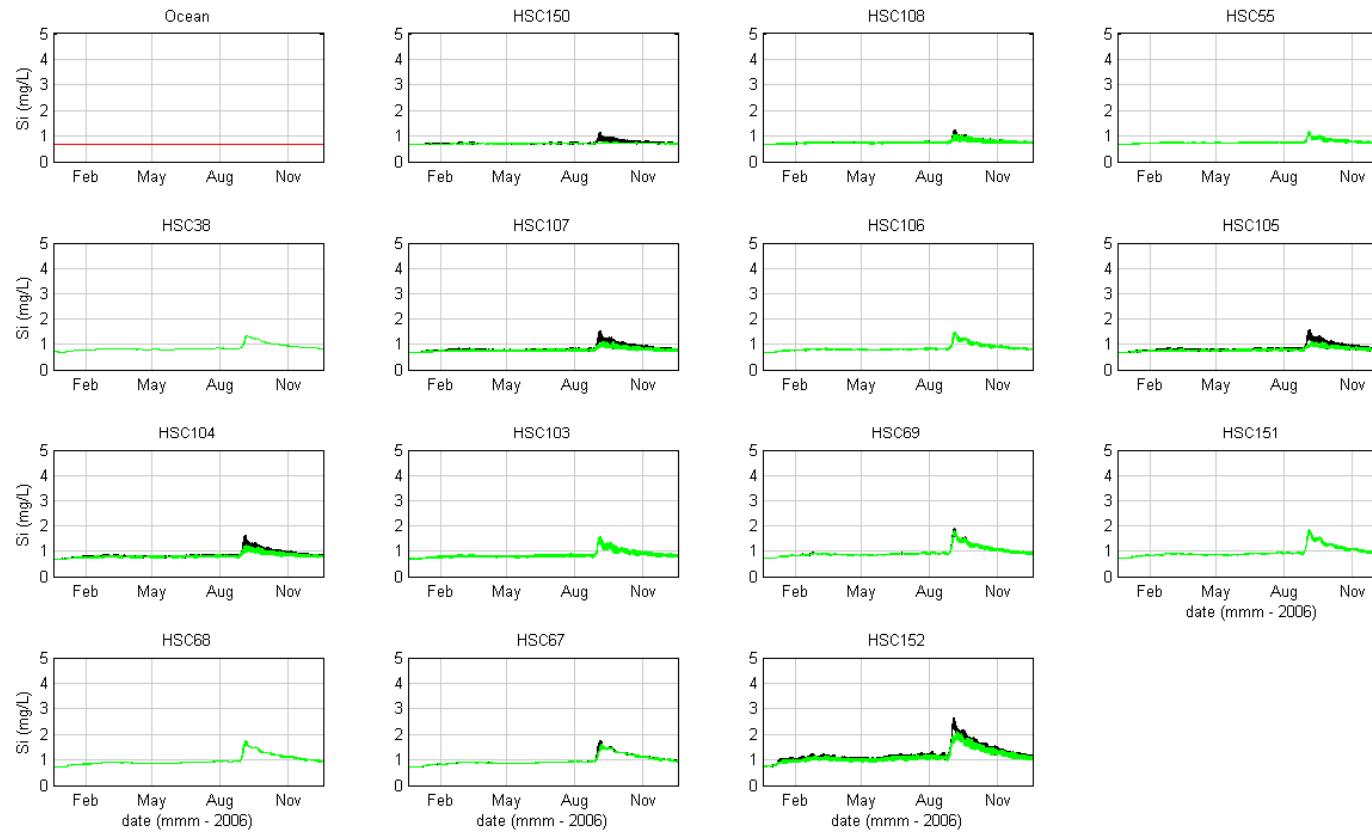


- Figure 13-63 Box and Whisker Plots – Total Nitrogen Validation 2007 (measured data (red), modelled surface (blue) and modelled bottom (green))

SINCLAIR KNIGHT MERZ



Water Quality Modelling of the Hawkesbury-Nepean River System

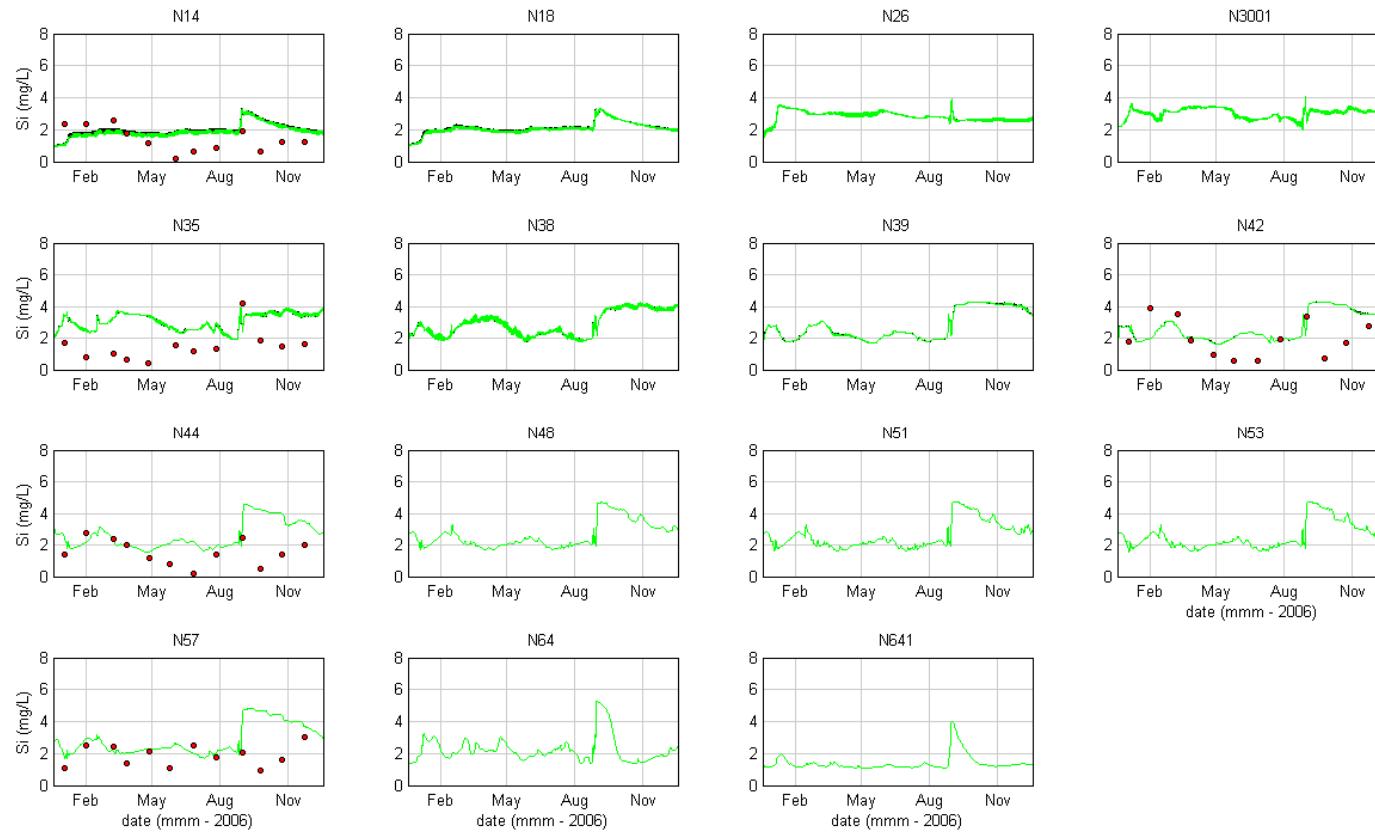


■ **Figure 13-64 Silica Calibration 2006 (measured data (red), modelled surface (black) and modelled bottom (green))**

SINCLAIR KNIGHT MERZ

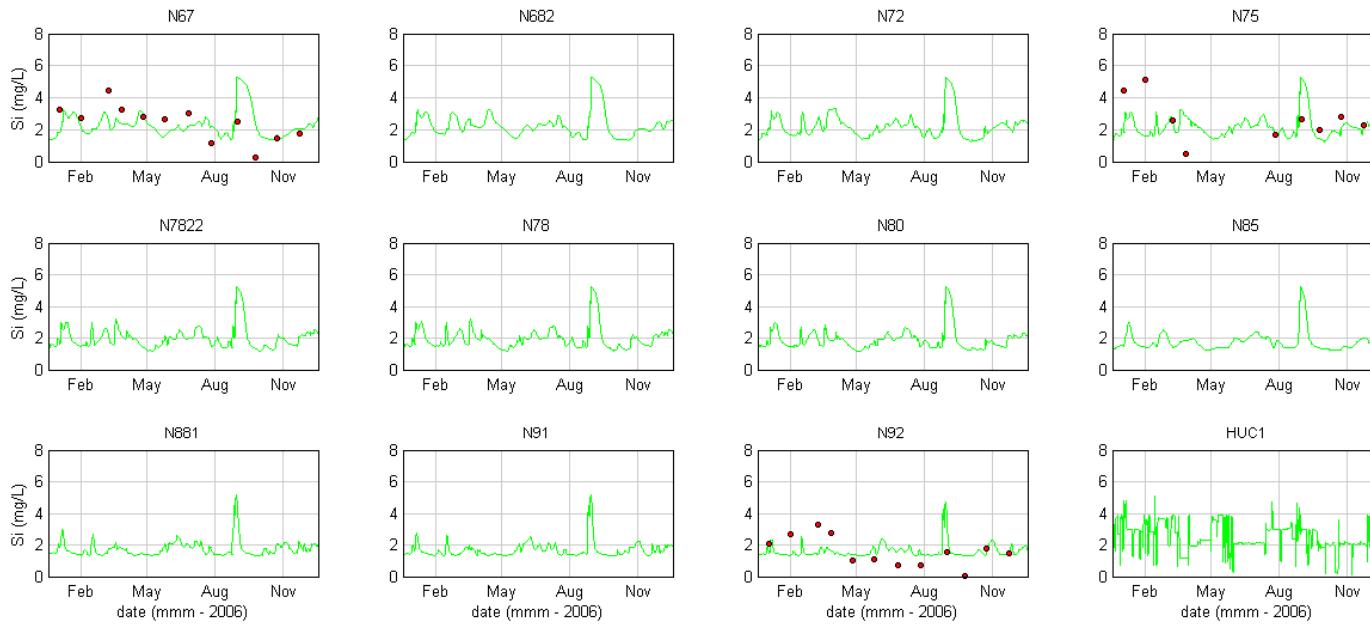


Water Quality Modelling of the Hawkesbury-Nepean River System



■ **Figure 13-64 (Cont.) Silica Calibration 2006 (measured data (red), modelled surface (black) and modelled bottom (green))**

SINCLAIR KNIGHT MERZ

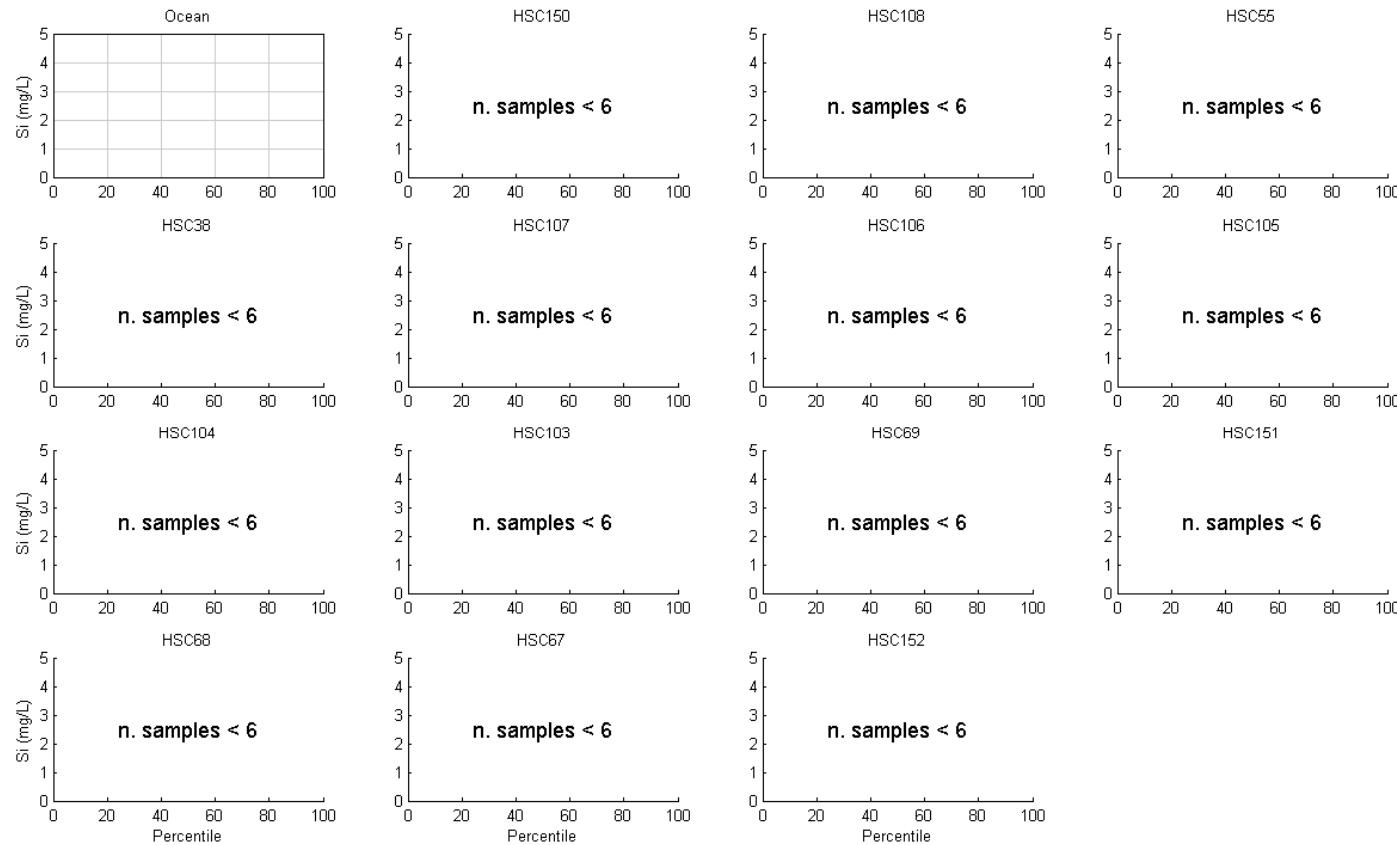


■ Figure 13-64 (Cont.) Silica Calibration 2006 (measured data (red), modelled surface (black) and modelled bottom (green))

SINCLAIR KNIGHT MERZ



Water Quality Modelling of the Hawkesbury-Nepean River System

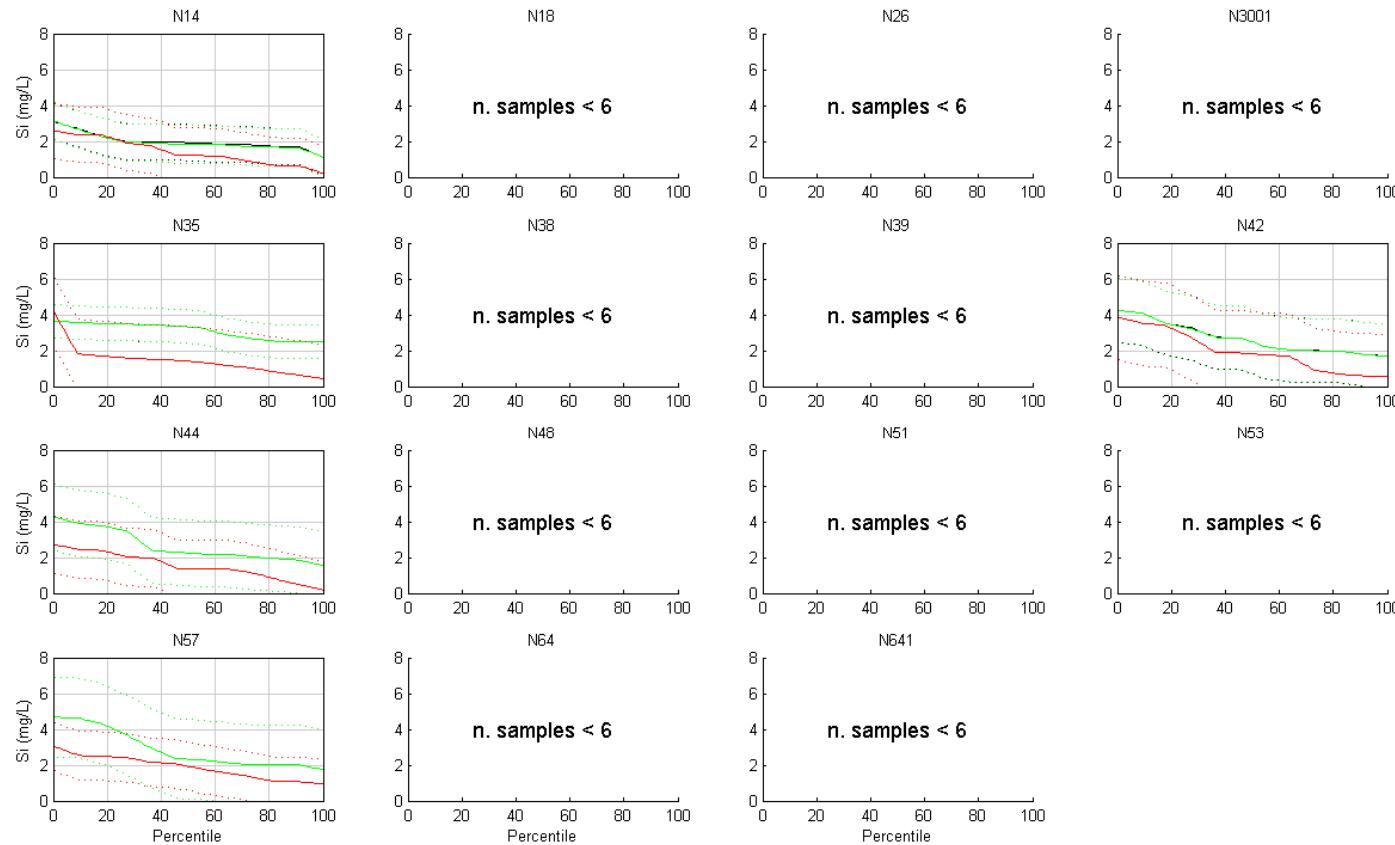


- Figure 13-65 Exceedance Plots – Silica Calibration 2006 (+/- 2SD) (measured data (red), modelled surface (black) and modelled bottom (green))

SINCLAIR KNIGHT MERZ



Water Quality Modelling of the Hawkesbury-Nepean River System

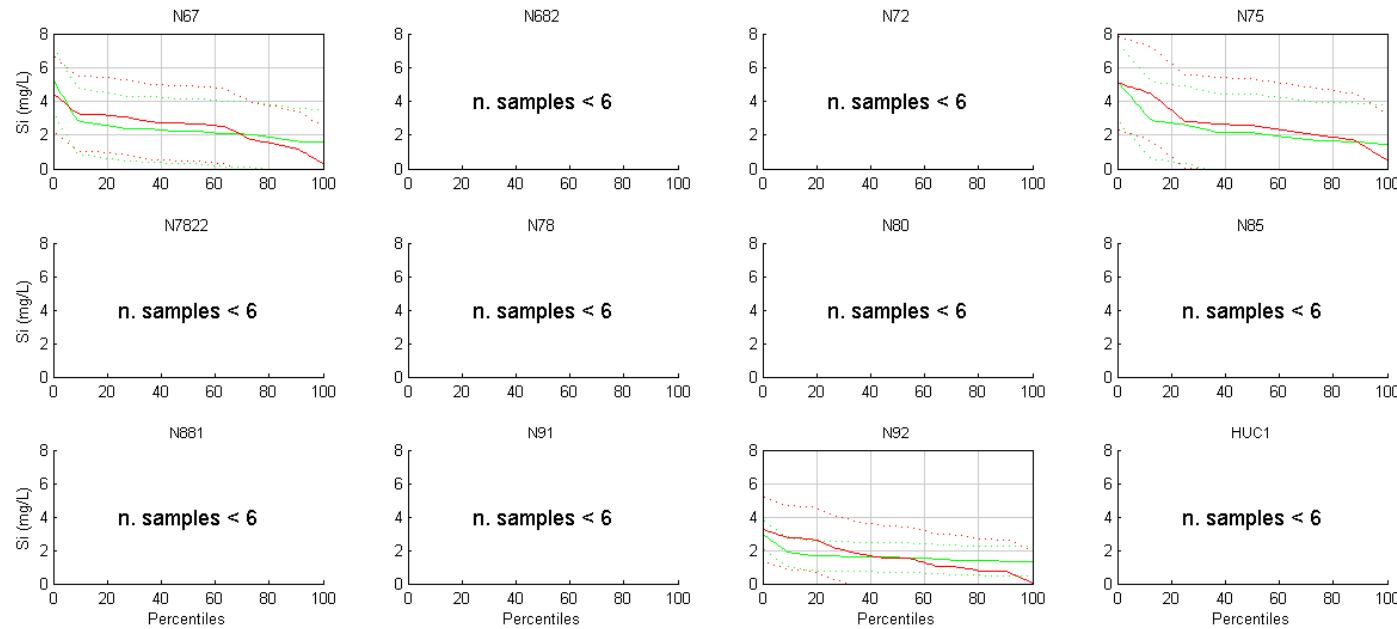


- **Figure 13-65 (Cont.) Exceedance Plots – Silica Calibration 2006 (+/- 2SD) (measured data (red), modelled surface (black) and modelled bottom (green))**

SINCLAIR KNIGHT MERZ



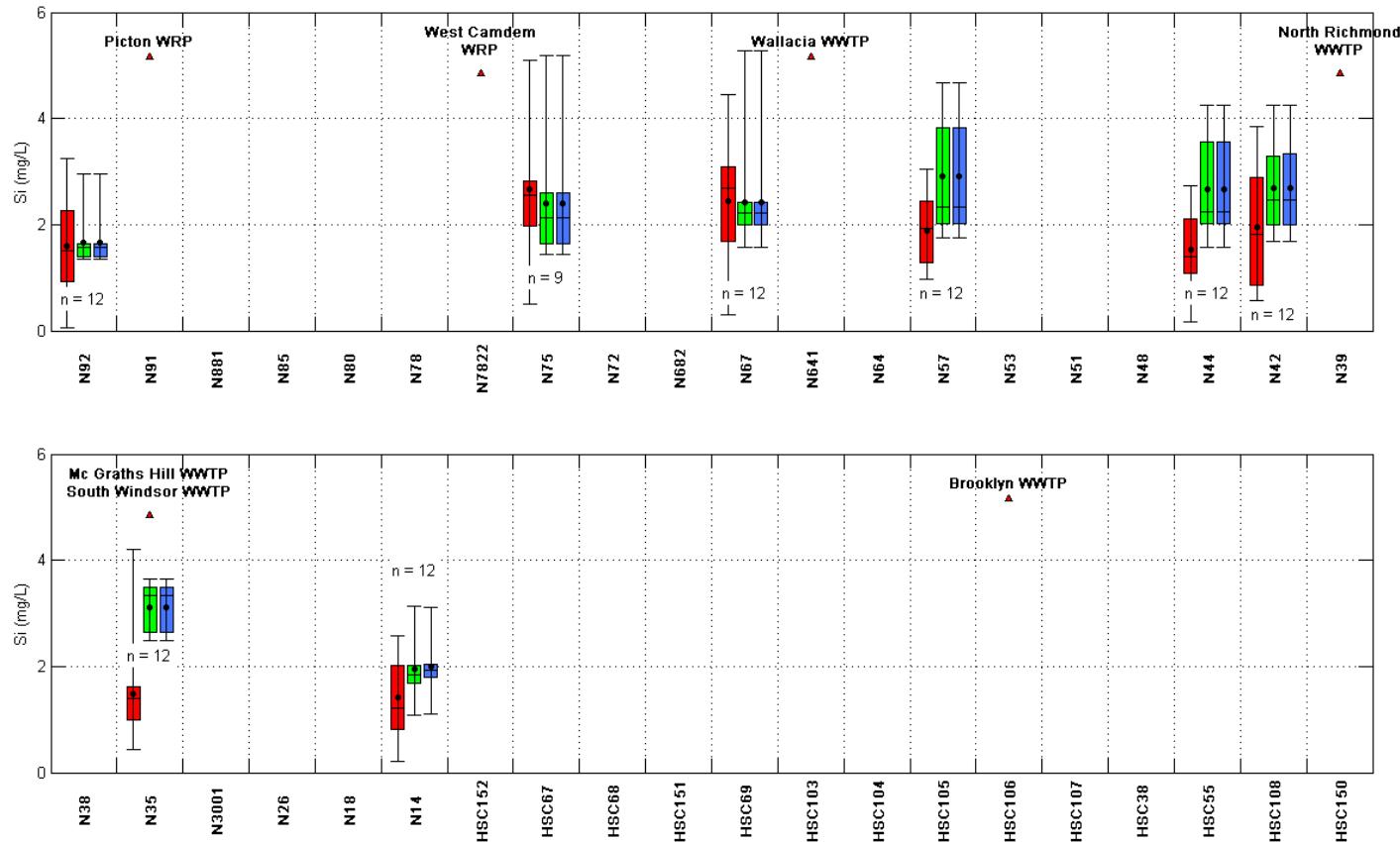
Water Quality Modelling of the Hawkesbury-Nepean River System



- Figure 13-65 (Cont.) Exceedance Plots – Silica Calibration 2006 (+/- 2SD) (measured data (red), modelled surface (black) and modelled bottom (green))

SINCLAIR KNIGHT MERZ

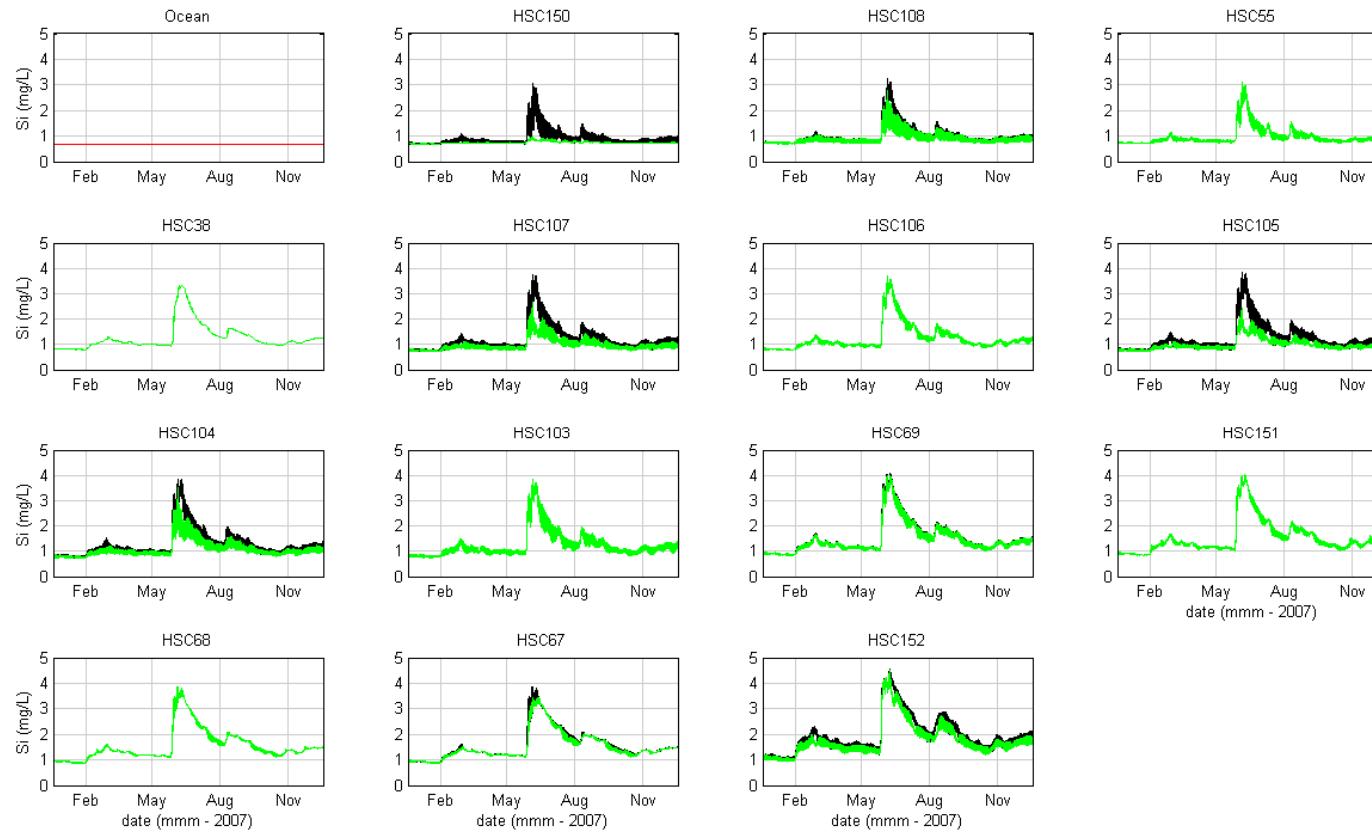
Water Quality Modelling of the Hawkesbury-Nepean River System



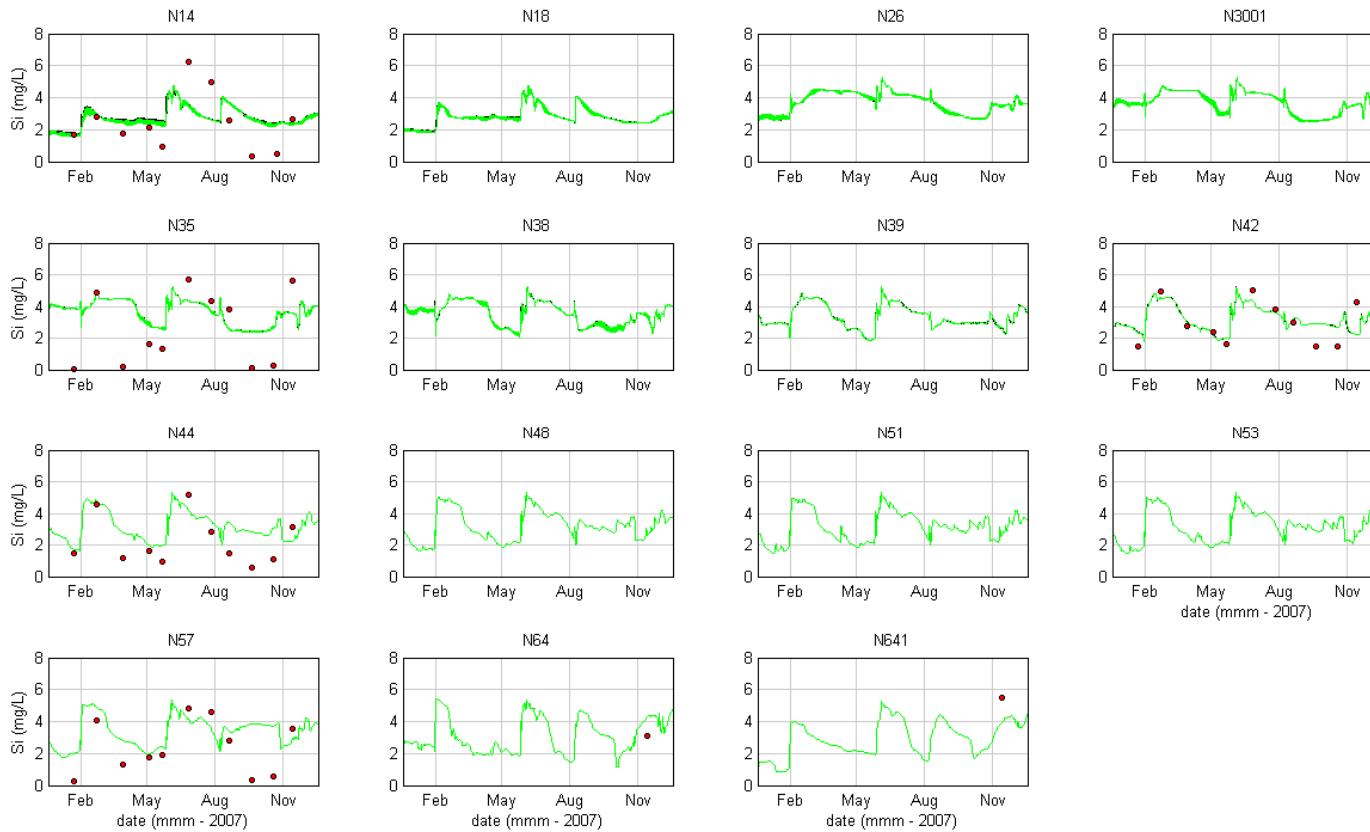
■ Figure 13-66 Box and Whisker Plots – Silica Calibration 2006 (measured data (red), modelled surface (blue) and modelled bottom (green))



Water Quality Modelling of the Hawkesbury-Nepean River System

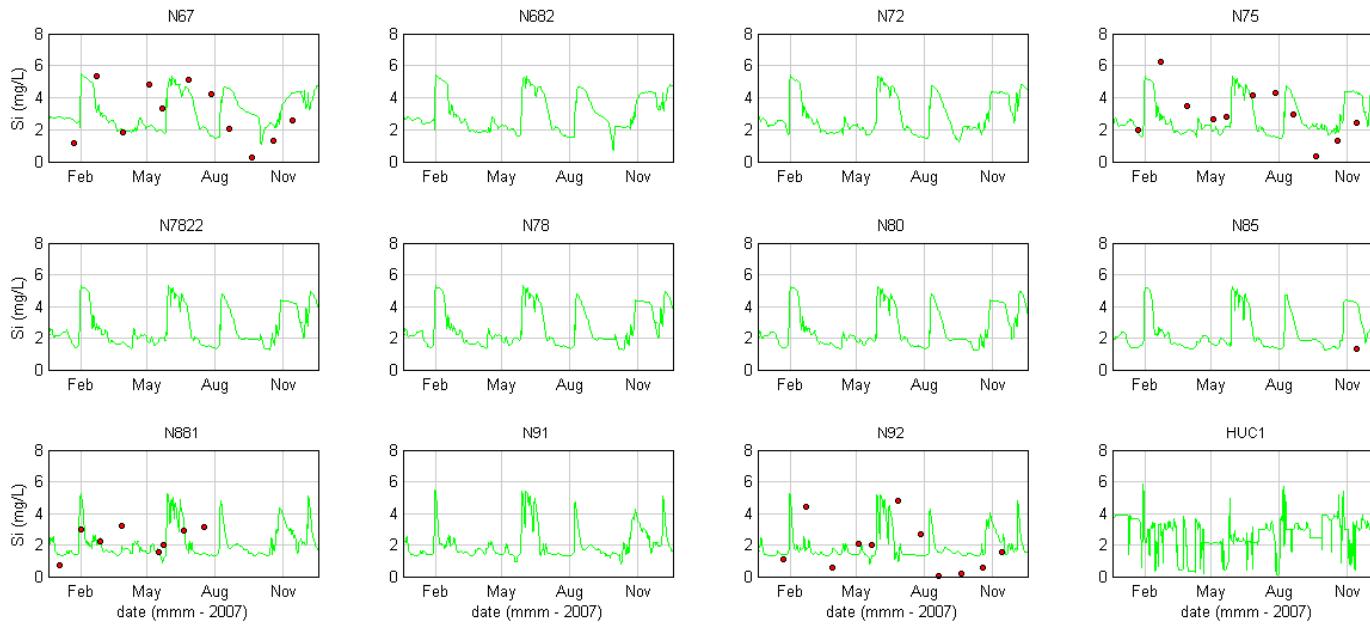


■ **Figure 13-67 Silica Validation 2007 (measured data (red), modelled surface (black) and modelled bottom (green))**



■ **Figure 13-67 (Cont.) Silica Validation 2007 (measured data (red), modelled surface (black) and modelled bottom (green))**

SINCLAIR KNIGHT MERZ

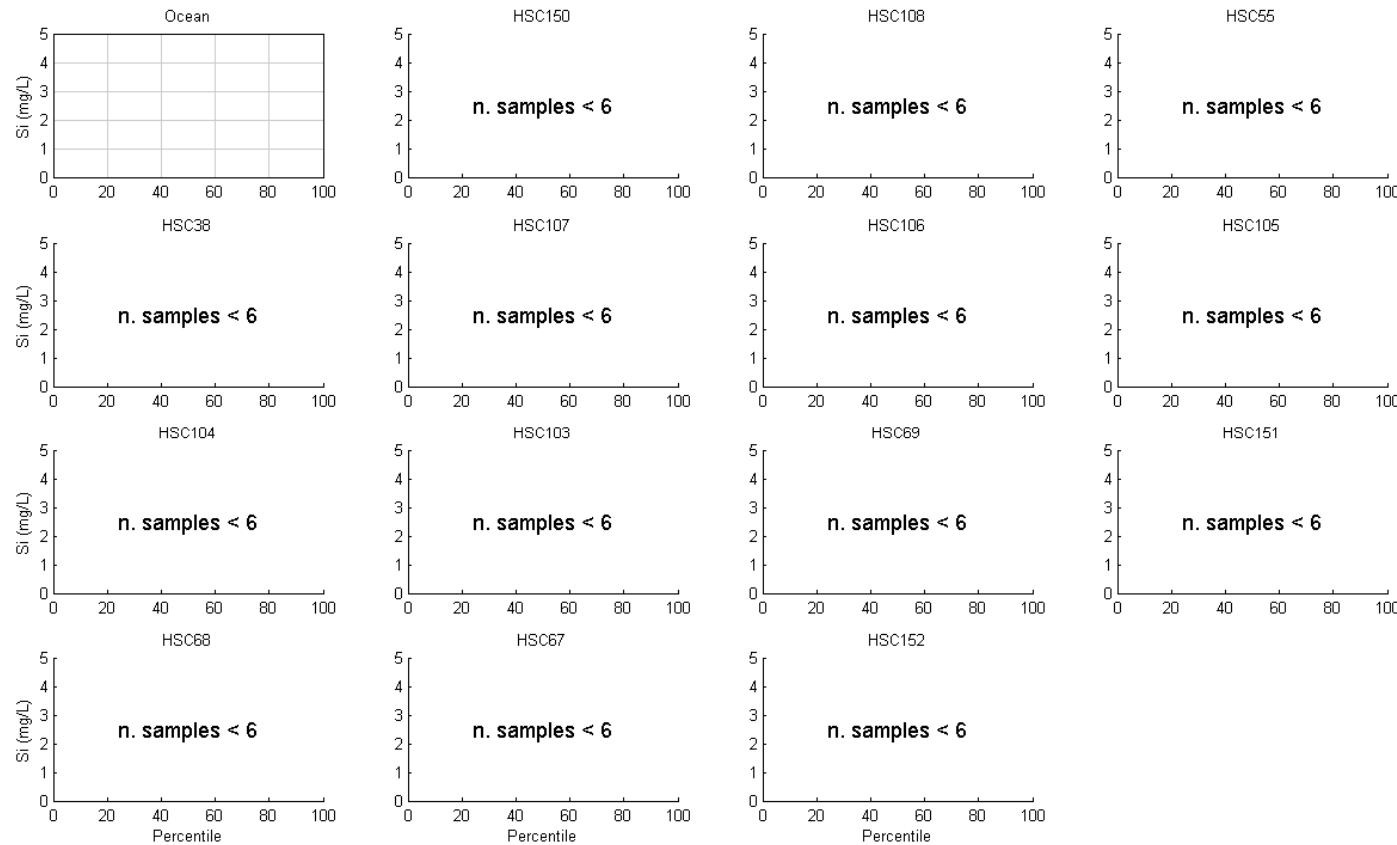


■ **Figure 13-67 (Cont.) Silica Validation 2007 (measured data (red), modelled surface (black) and modelled bottom (green))**

SINCLAIR KNIGHT MERZ



Water Quality Modelling of the Hawkesbury-Nepean River System

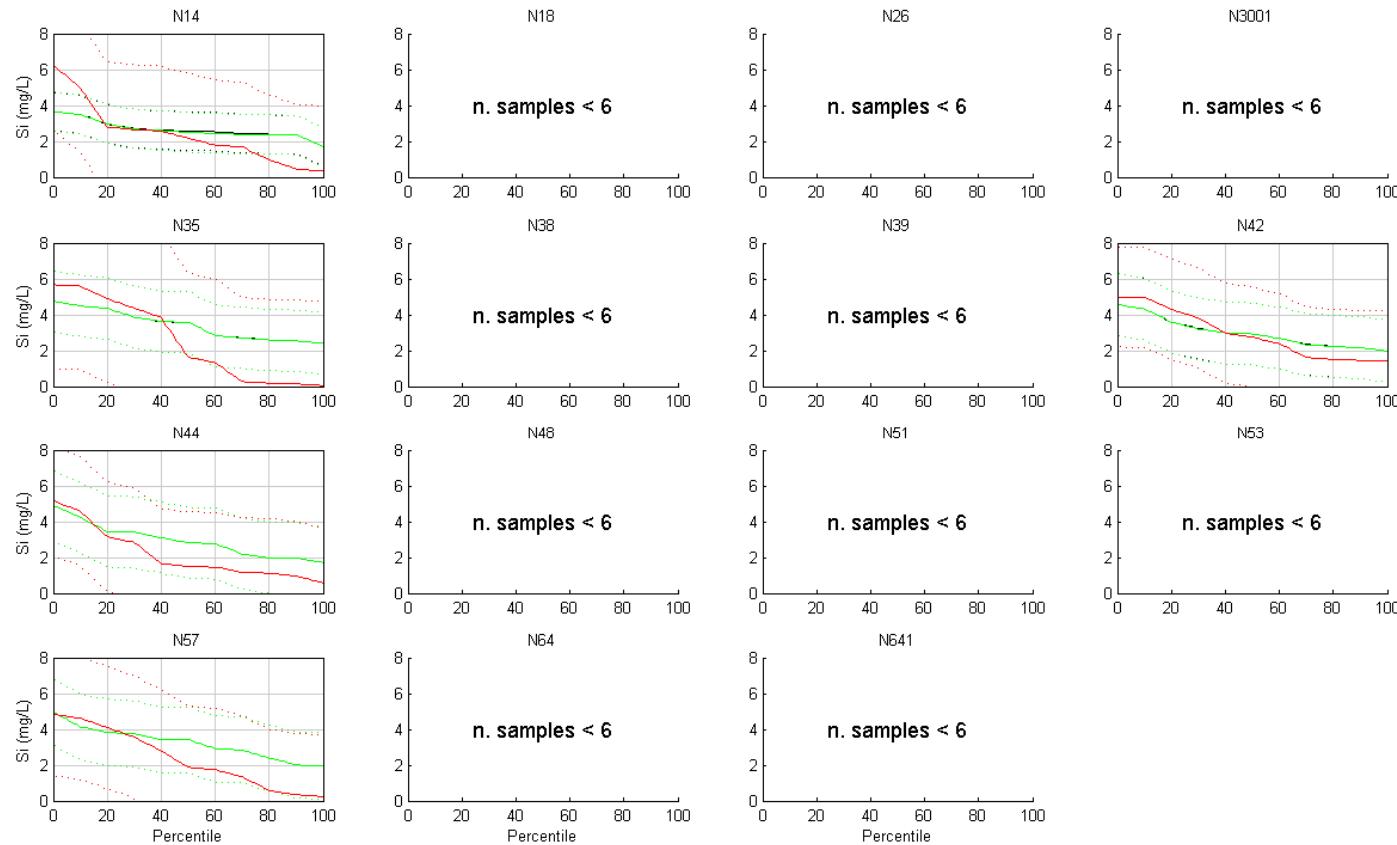


- **Figure 13-68 Exceedance Plots – Silica Validation 2007 (+/- 2SD) (measured data (red), modelled surface (black) and modelled bottom (green))**

SINCLAIR KNIGHT MERZ



Water Quality Modelling of the Hawkesbury-Nepean River System

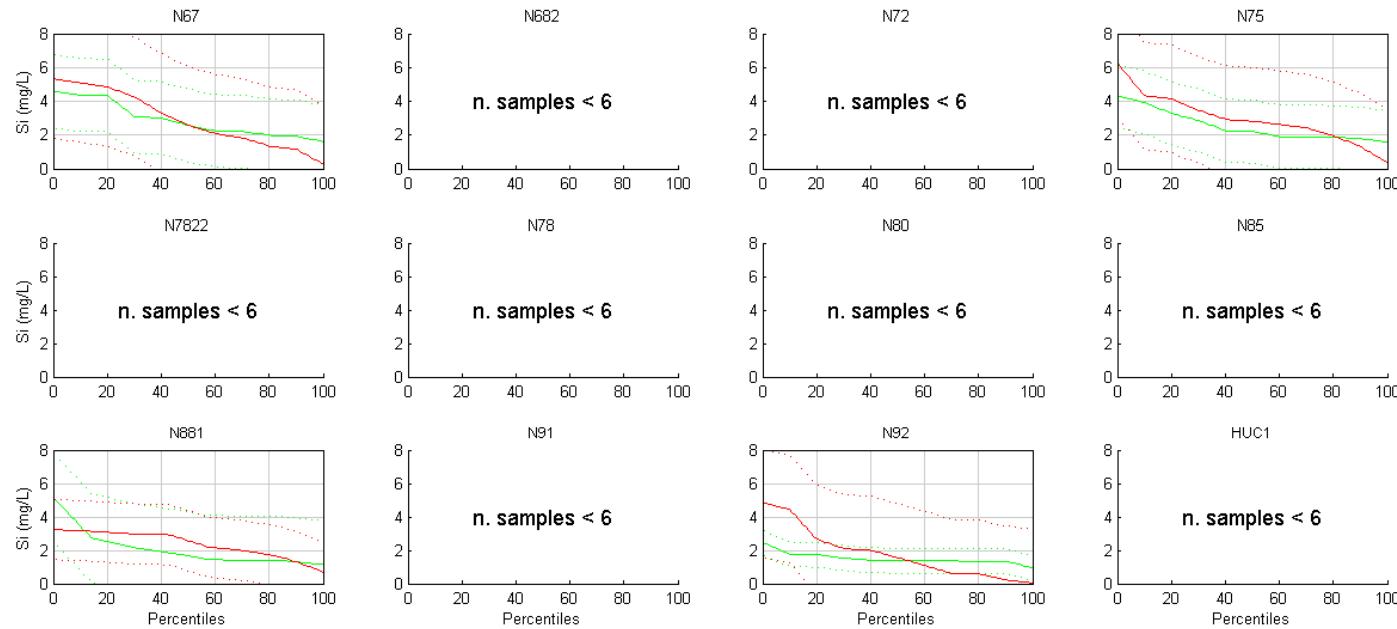


- **Figure 13-68 (Cont.) Exceedance Plots – Silica Validation 2007(+/- 2SD) (measured data (red), modelled surface (black) and modelled bottom (green))**

SINCLAIR KNIGHT MERZ



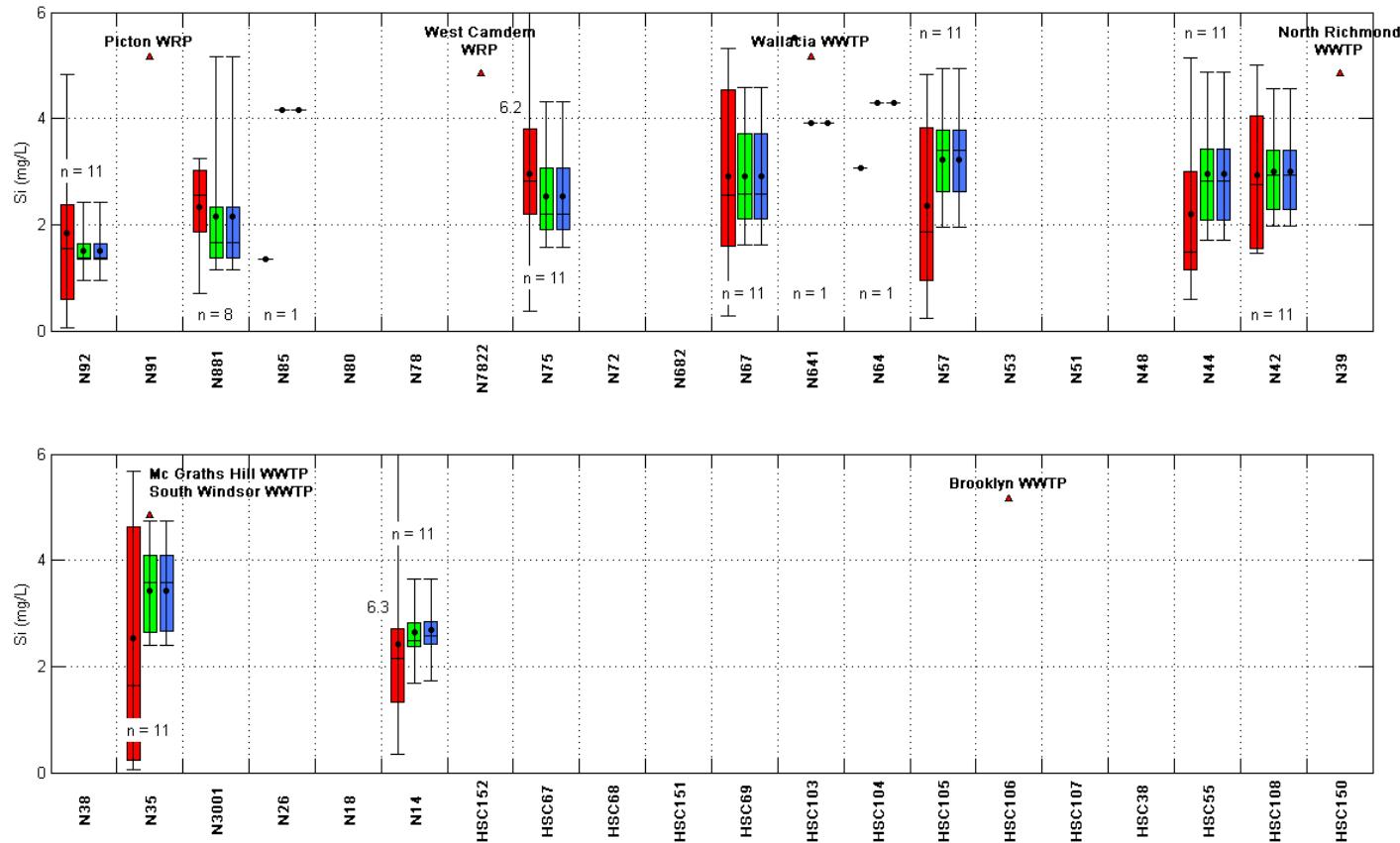
Water Quality Modelling of the Hawkesbury-Nepean River System



- Figure 13-68 (Cont.) Exceedance Plots – Silica Validation 2007 (+/- 2SD) (measured data (red), modelled surface (black) and modelled bottom (green))

SINCLAIR KNIGHT MERZ

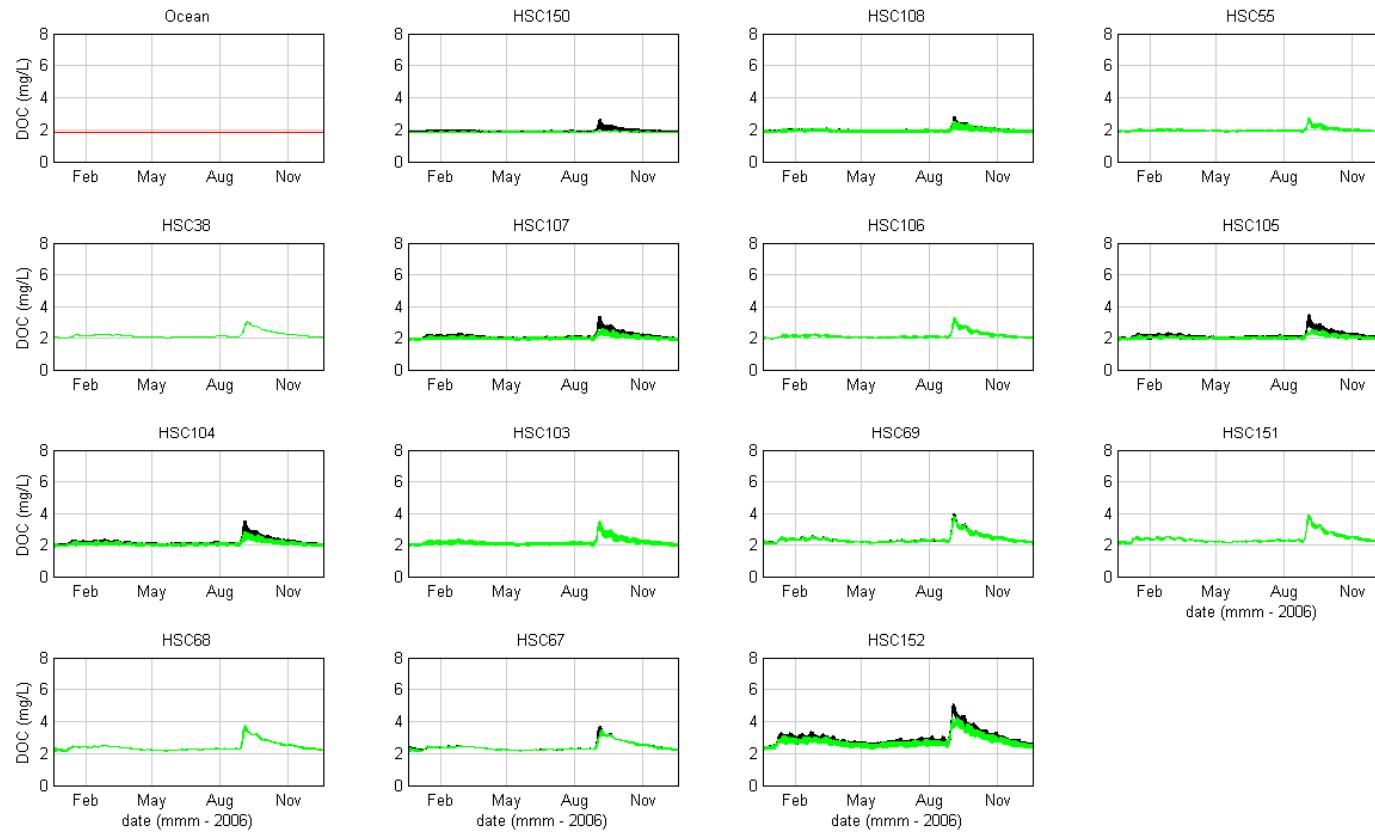
Water Quality Modelling of the Hawkesbury-Nepean River System



■ **Figure 13-69 Box and Whisker Plots – Silica Validation 2007 (measured data (red), modelled surface (blue) and modelled bottom (green))**



Water Quality Modelling of the Hawkesbury-Nepean River System

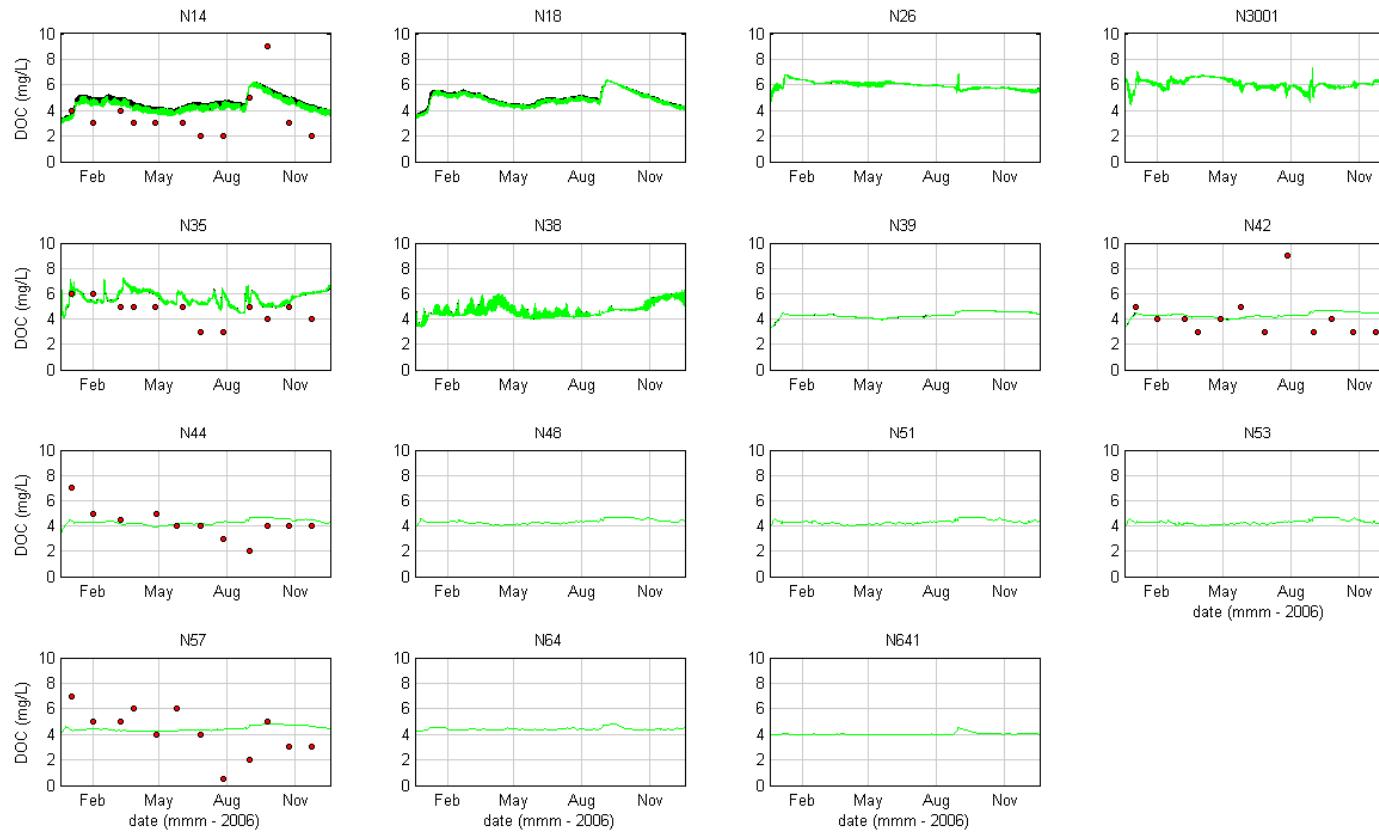


- **Figure 13-70 Dissolved Organic Carbon Calibration 2006 (measured data (red), modelled surface (black) and modelled bottom (green))**

SINCLAIR KNIGHT MERZ



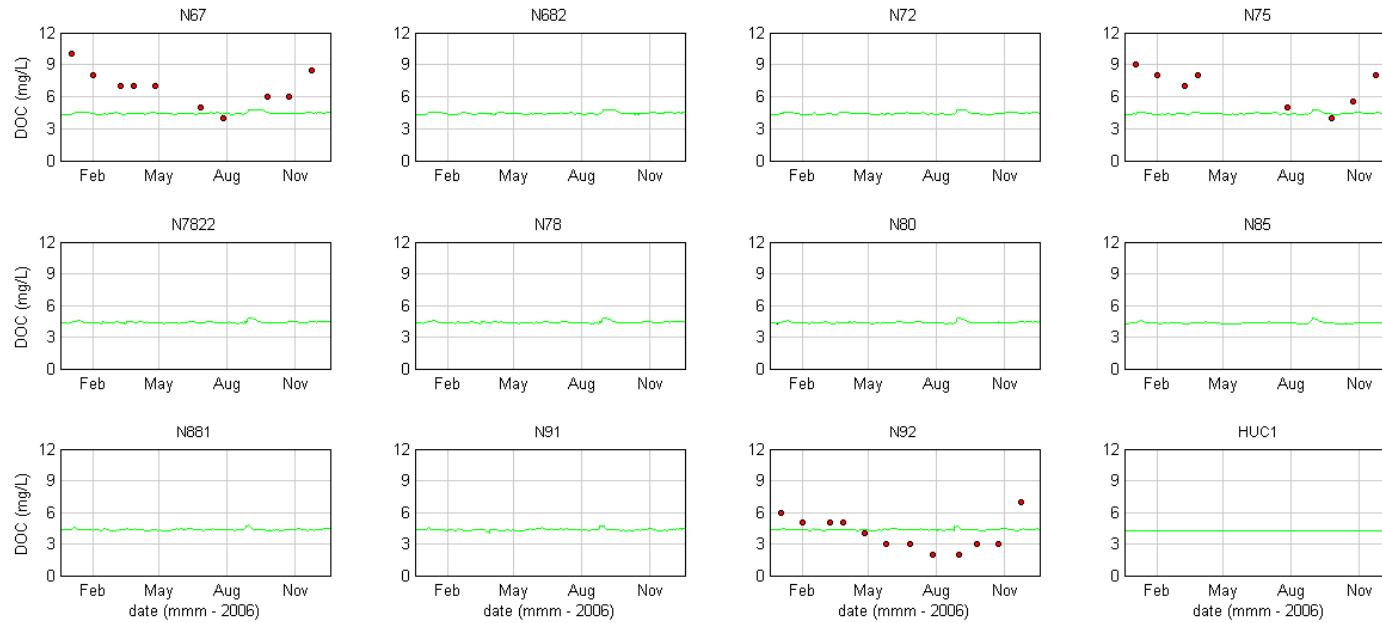
Water Quality Modelling of the Hawkesbury-Nepean River System



- **Figure 13-70 (Cont.) Dissolved Organic Calibration Carbon 2006 (measured data (red), modelled surface (black) and modelled bottom (green))**



Water Quality Modelling of the Hawkesbury-Nepean River System

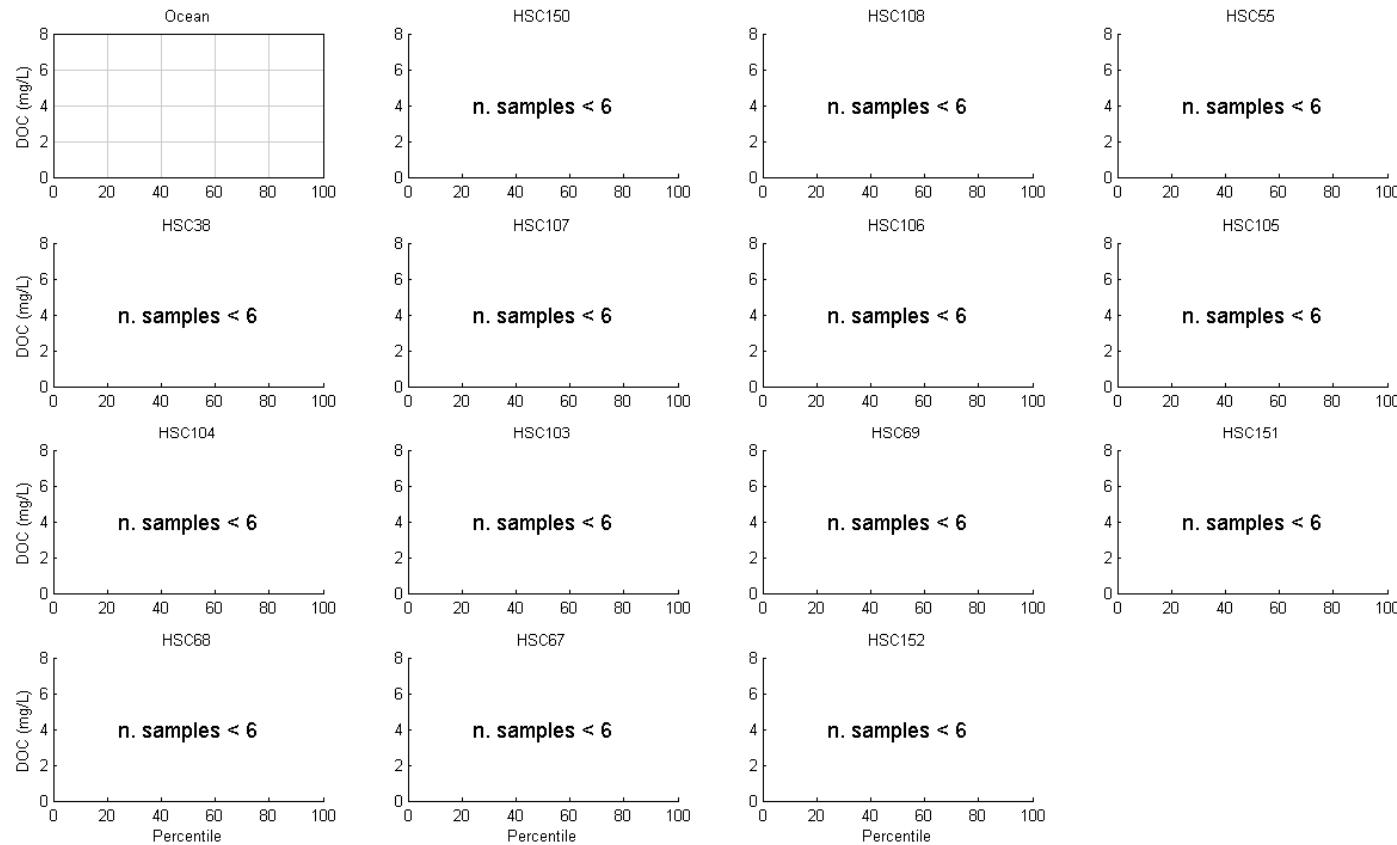


- **Figure 13-70 (Cont.) Dissolved Organic Carbon Calibration 2006 (measured data (red), modelled surface (black) and modelled bottom (green))**

SINCLAIR KNIGHT MERZ



Water Quality Modelling of the Hawkesbury-Nepean River System

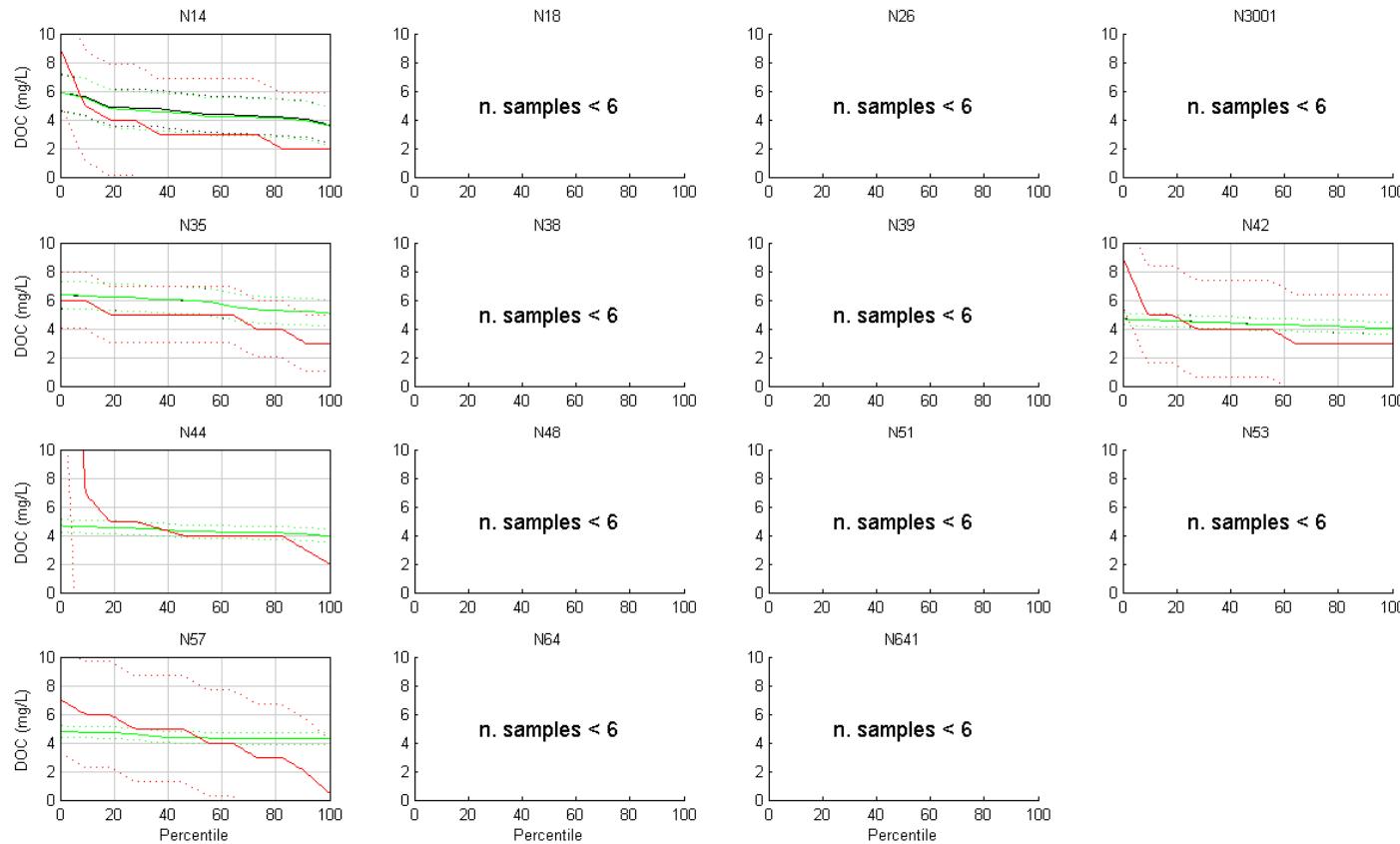


- **Figure 13-71 Exceedance Plots – Dissolved Organic Carbon Calibration 2006 (+/- 2SD) (measured data (red), modelled surface (black) and modelled bottom (green))**

SINCLAIR KNIGHT MERZ



Water Quality Modelling of the Hawkesbury-Nepean River System

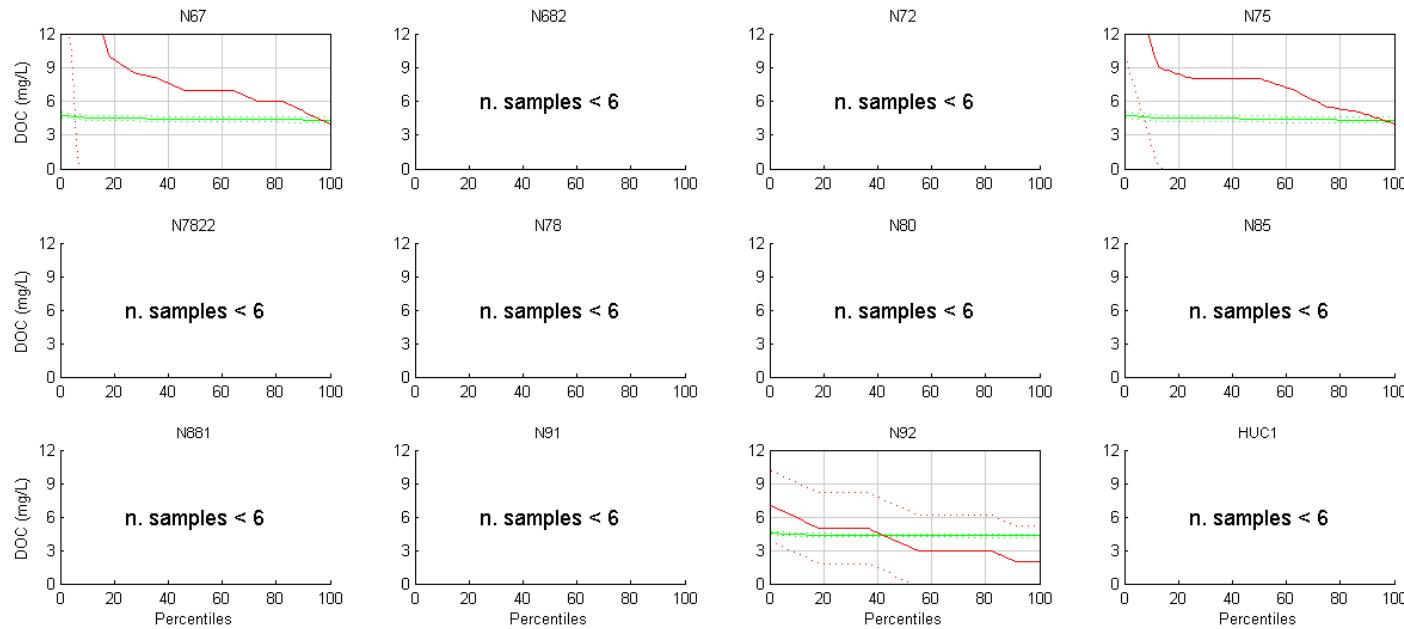


- **Figure 13-71 (Cont.) Exceedance Plots – Dissolved Organic Carbon Calibration 2006 (+/- 2SD) (measured data (red), modelled surface (black) and modelled bottom (green))**

SINCLAIR KNIGHT MERZ



Water Quality Modelling of the Hawkesbury-Nepean River System

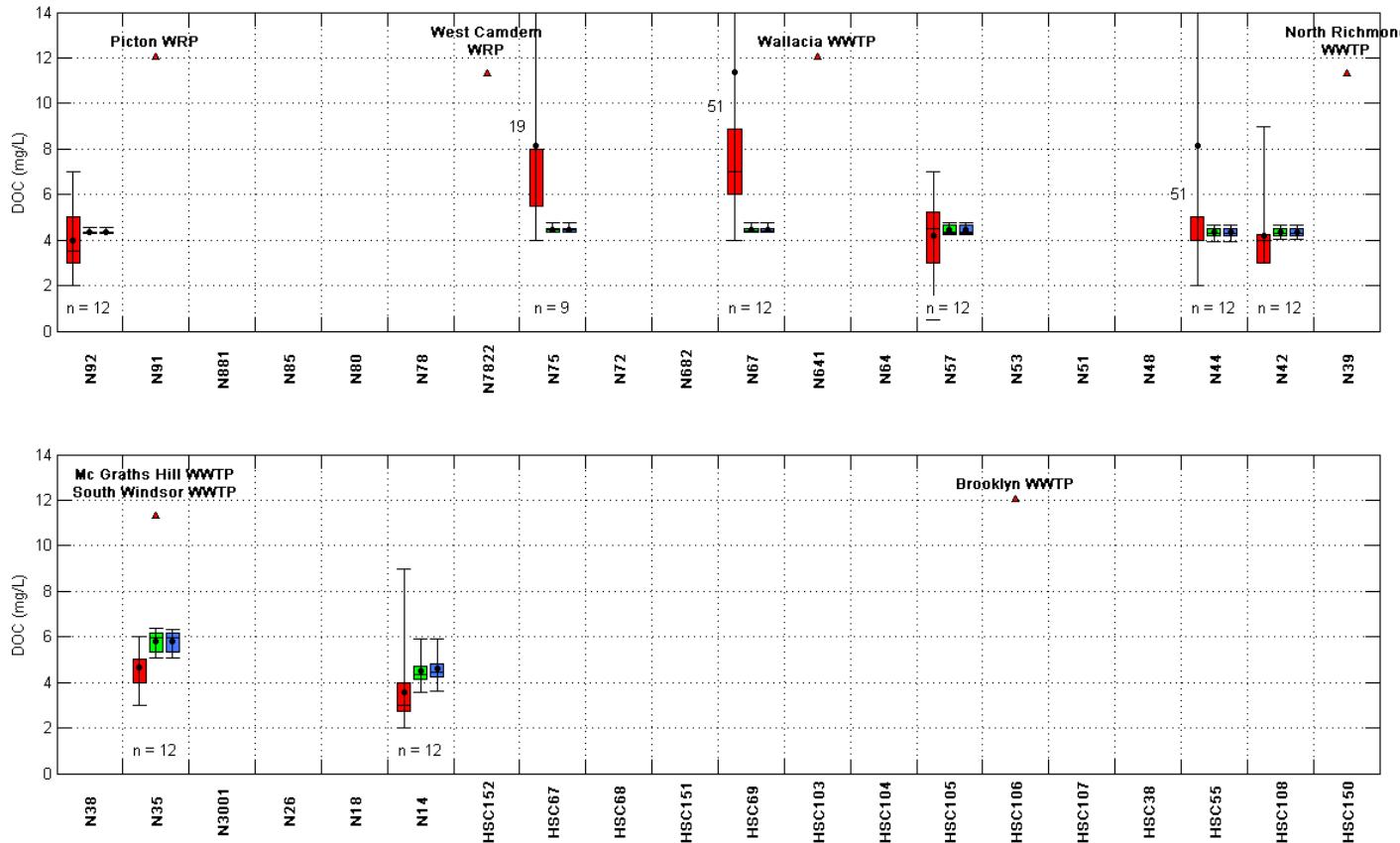


- Figure 13-71 (Cont.) Exceedance Plots – Dissolved Organic Carbon Calibration 2006 (+/- 2SD) (measured data (red), modelled surface (black) and modelled bottom (green))

SINCLAIR KNIGHT MERZ



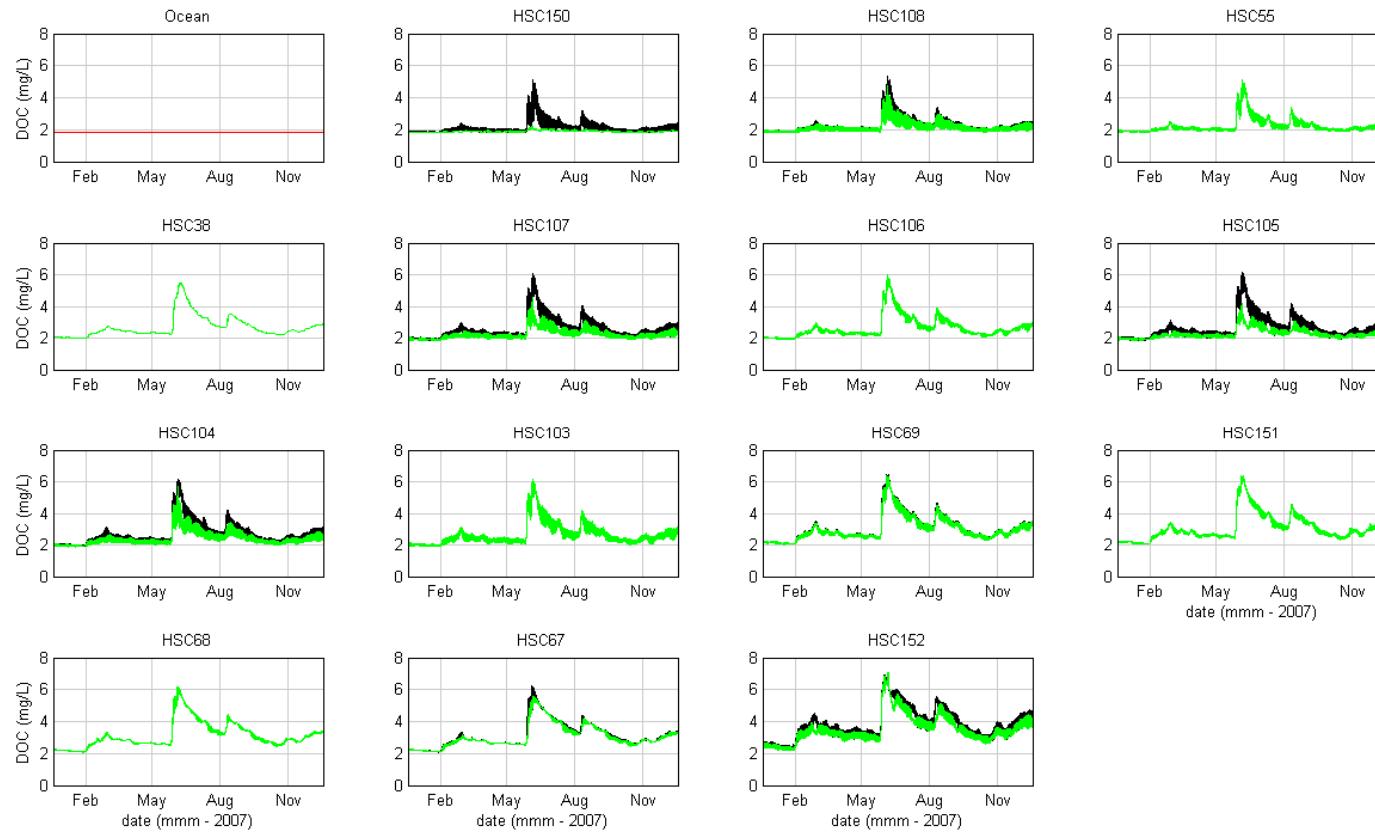
Water Quality Modelling of the Hawkesbury-Nepean River System



■ Figure 13-72 Box and Whisker Plots – Dissolved Organic Carbon Calibration 2006 (measured data (red), modelled surface (blue) and modelled bottom (green))



Water Quality Modelling of the Hawkesbury-Nepean River System

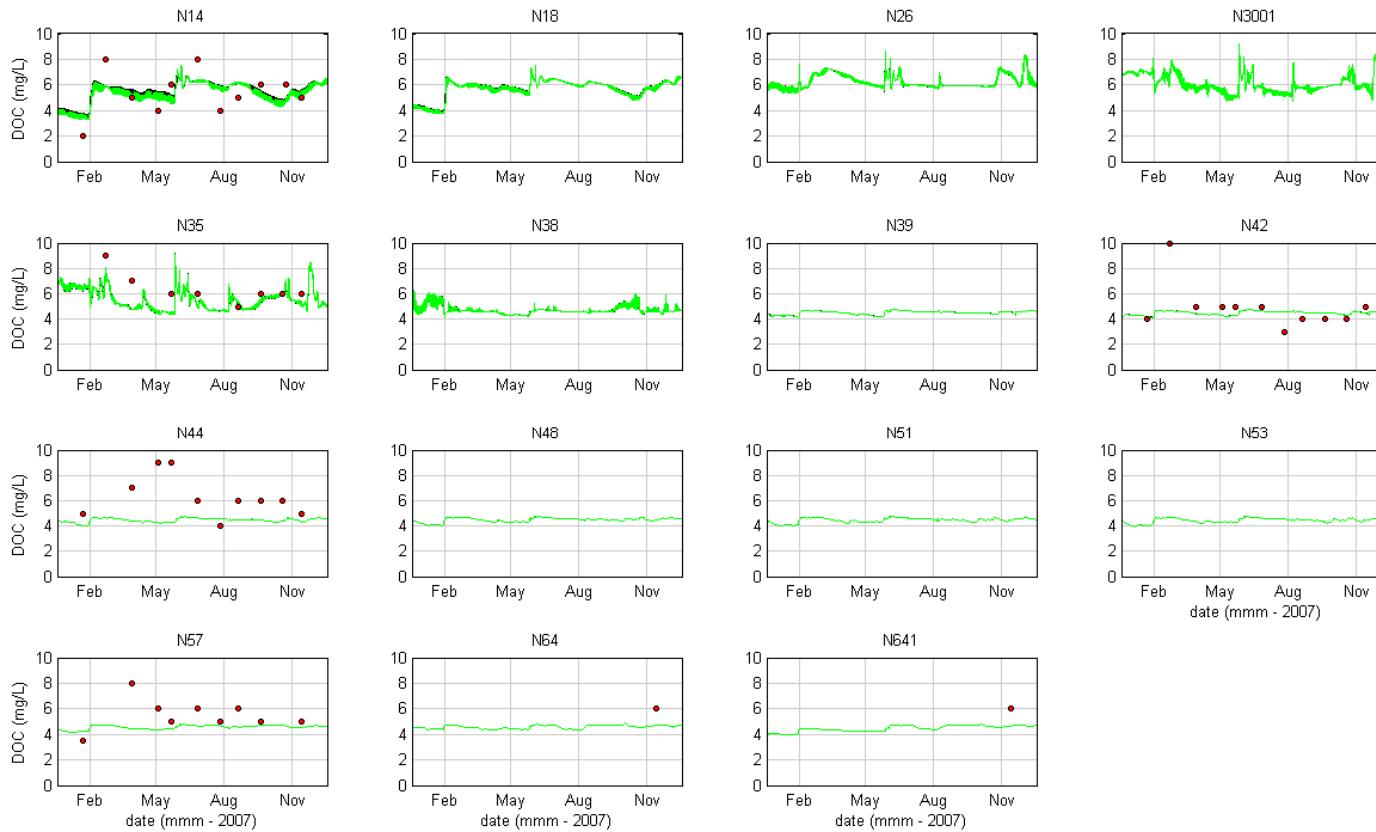


- **Figure 13-73 Dissolved Organic Carbon Validation 2007 (measured data (red), modelled surface (black) and modelled bottom (green))**

SINCLAIR KNIGHT MERZ



Water Quality Modelling of the Hawkesbury-Nepean River System

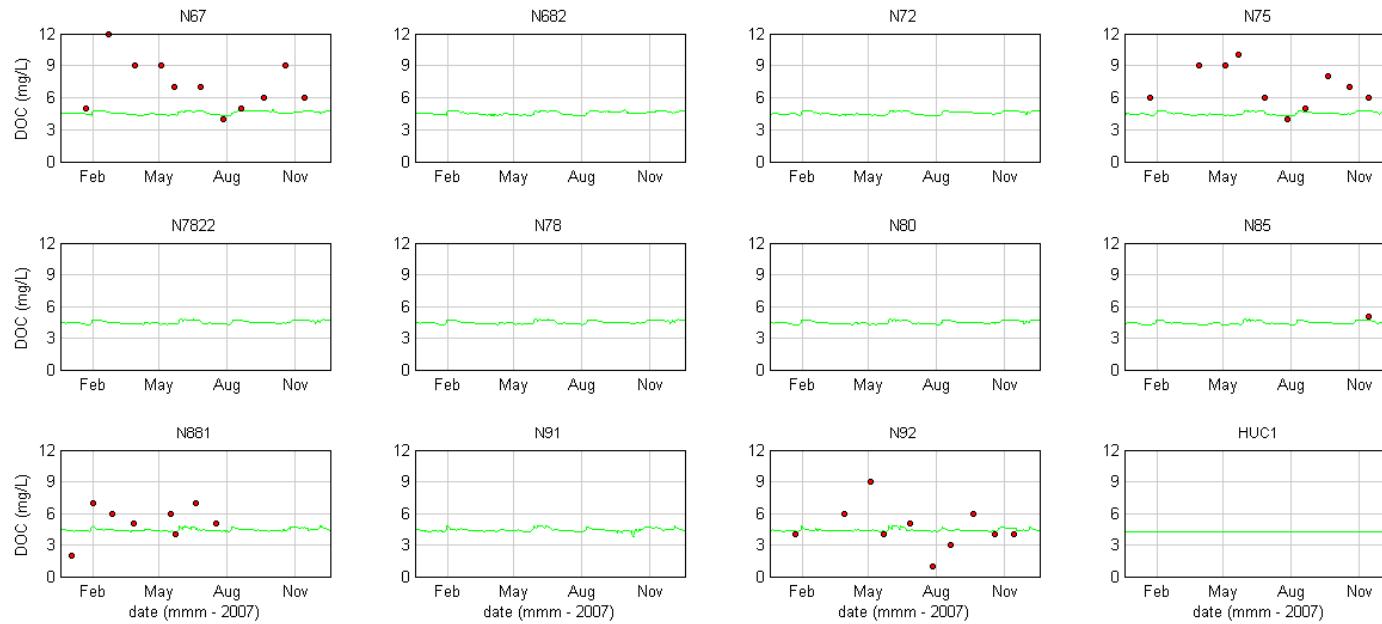


- **Figure 13-73 (Cont.) Dissolved Organic Carbon Validation 2007 (measured data (red), modelled surface (black) and modelled bottom (green))**

SINCLAIR KNIGHT MERZ



Water Quality Modelling of the Hawkesbury-Nepean River System

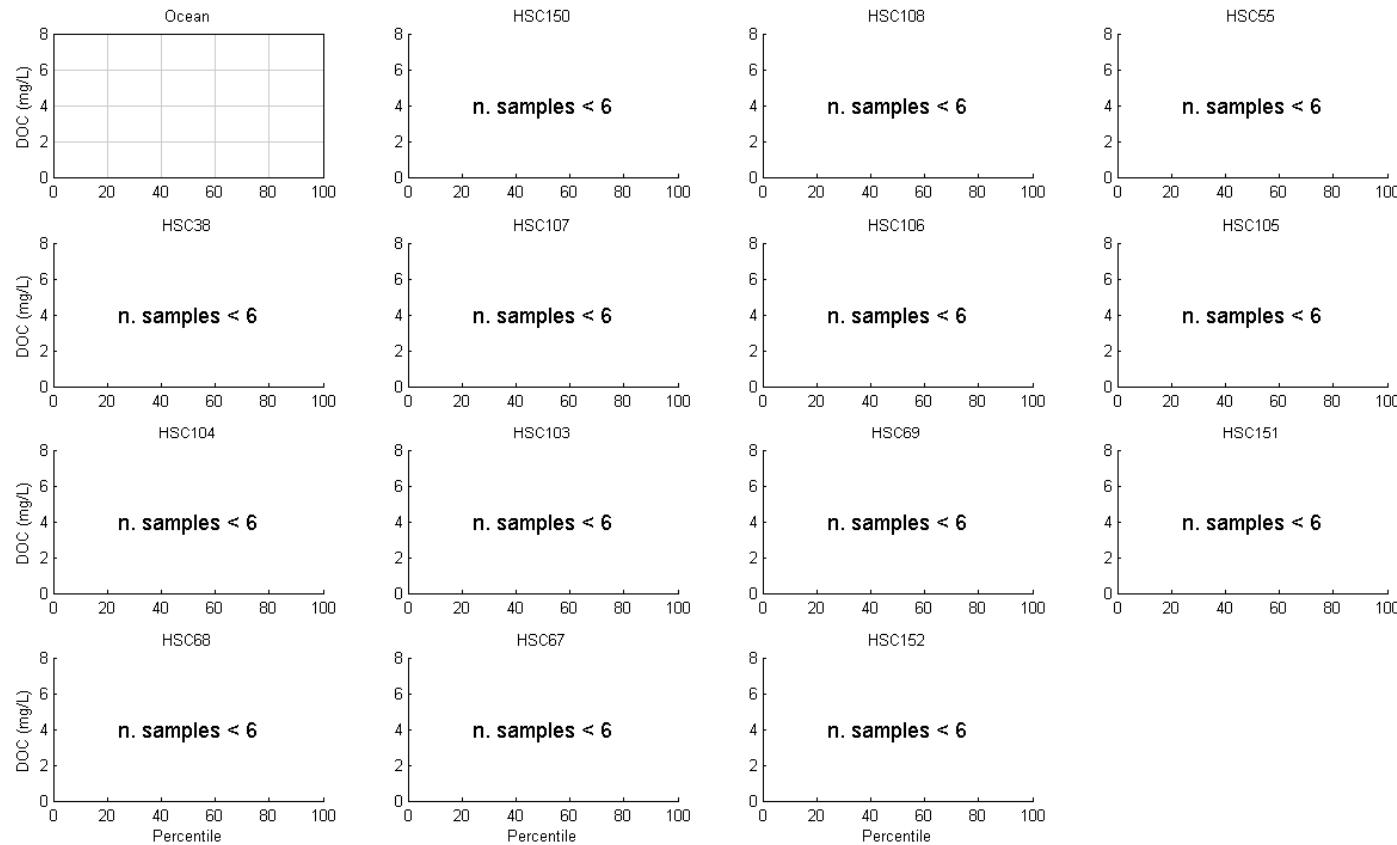


- **Figure 13-73 (Cont.) Dissolved Organic Carbon Validation 2007 (measured data (red), modelled surface (black) and modelled bottom (green))**

SINCLAIR KNIGHT MERZ



Water Quality Modelling of the Hawkesbury-Nepean River System

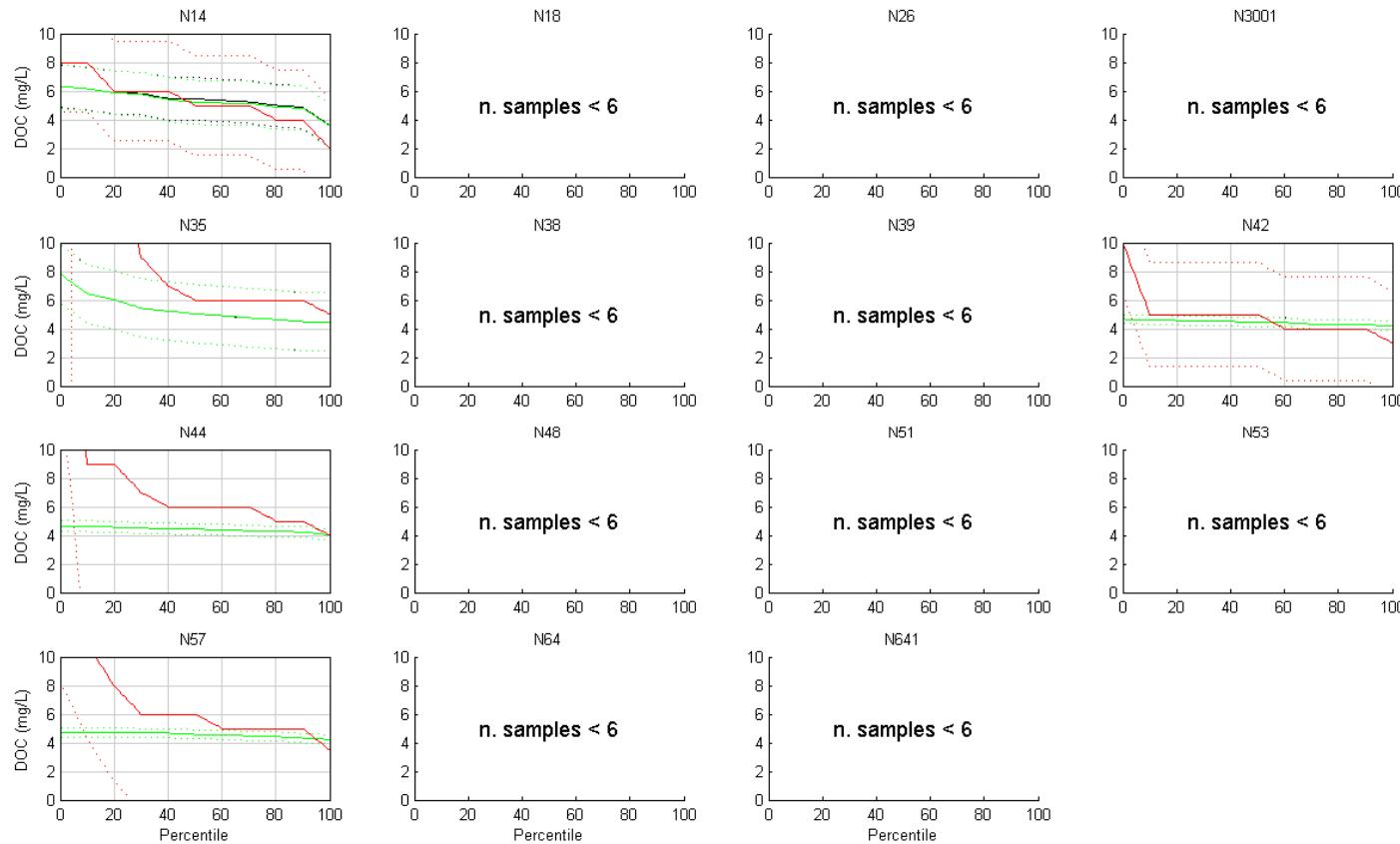


- **Figure 13-74 Exceedance Plots – Dissolved Organic Carbon Validation 2007 (+/- 2SD) (measured data (red), modelled surface (black) and modelled bottom (green))**

SINCLAIR KNIGHT MERZ



Water Quality Modelling of the Hawkesbury-Nepean River System

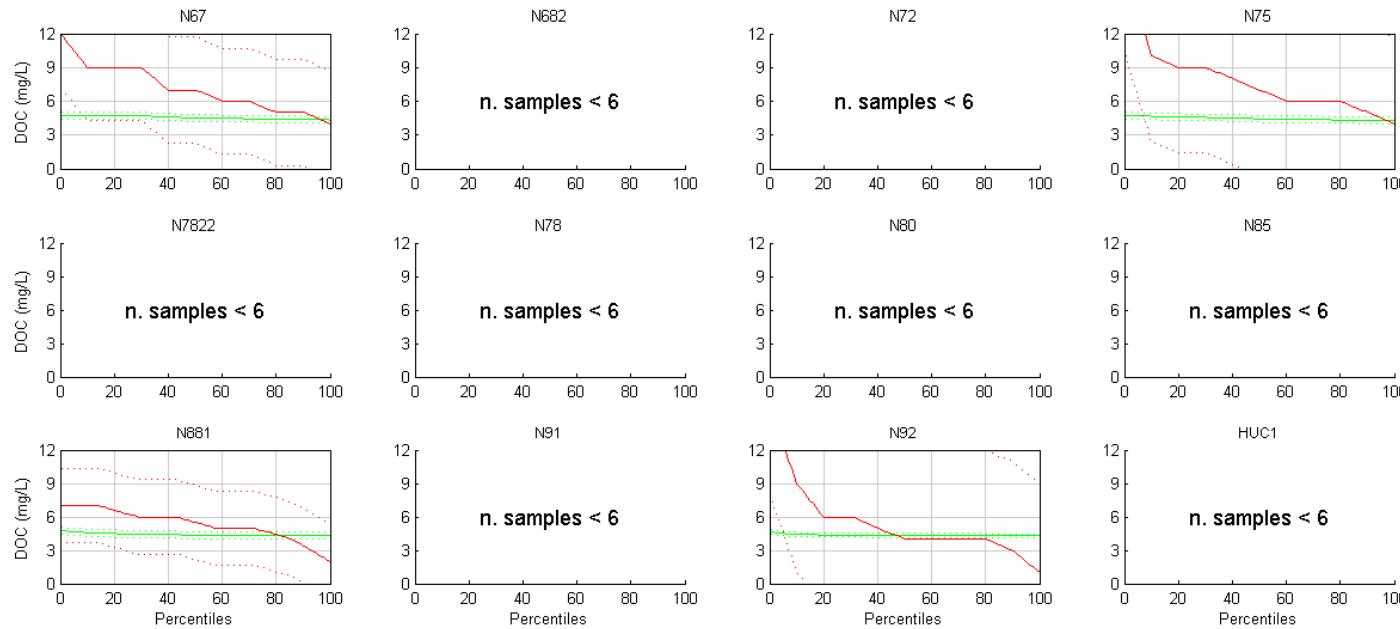


- **Figure 13-74 (Cont.) Exceedance Plots – Dissolved Organic Carbon Validation 2007 (+/- 2SD) (measured data (red), modelled surface (black) and modelled bottom (green))**

SINCLAIR KNIGHT MERZ



Water Quality Modelling of the Hawkesbury-Nepean River System

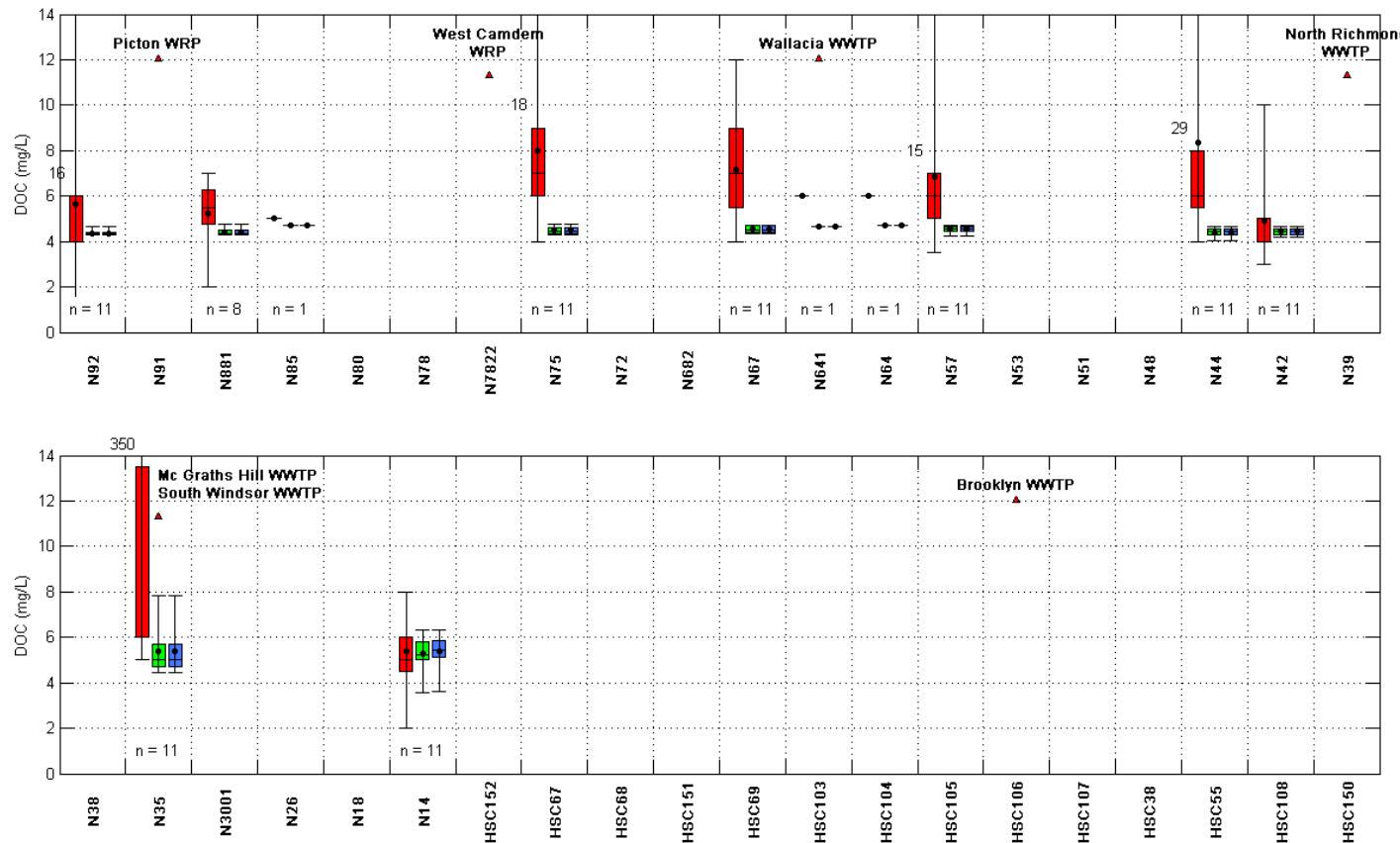


- Figure 13-74 (Cont.) Exceedance Plots – Dissolved Organic Carbon Validation 2007 (+/- 2SD) (measured data (red), modelled surface (black) and modelled bottom (green))

SINCLAIR KNIGHT MERZ



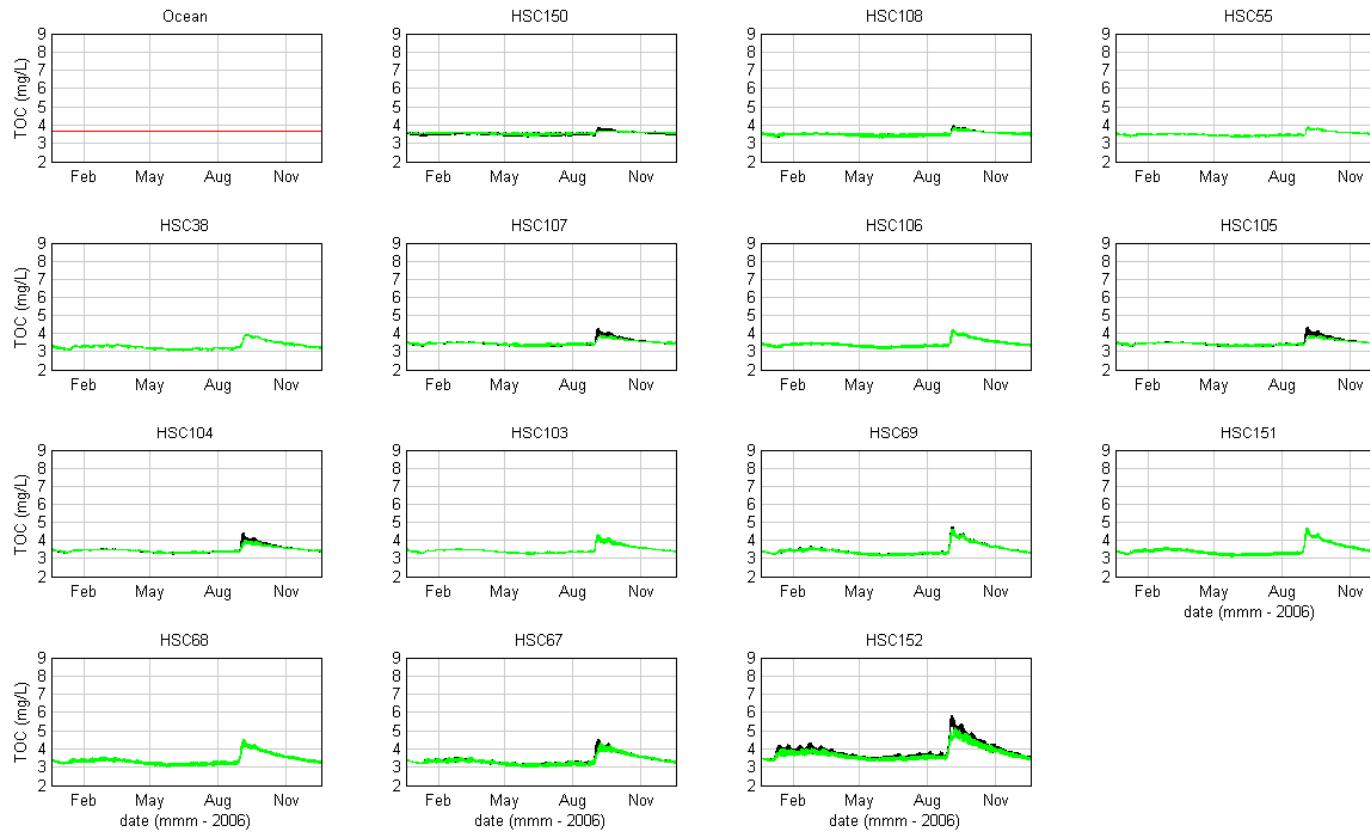
Water Quality Modelling of the Hawkesbury-Nepean River System



- Figure 13-75 Box and Whisker Plots – Dissolved Organic Carbon Validation 2007 (measured data (red), modelled surface (blue) and modelled bottom (green))

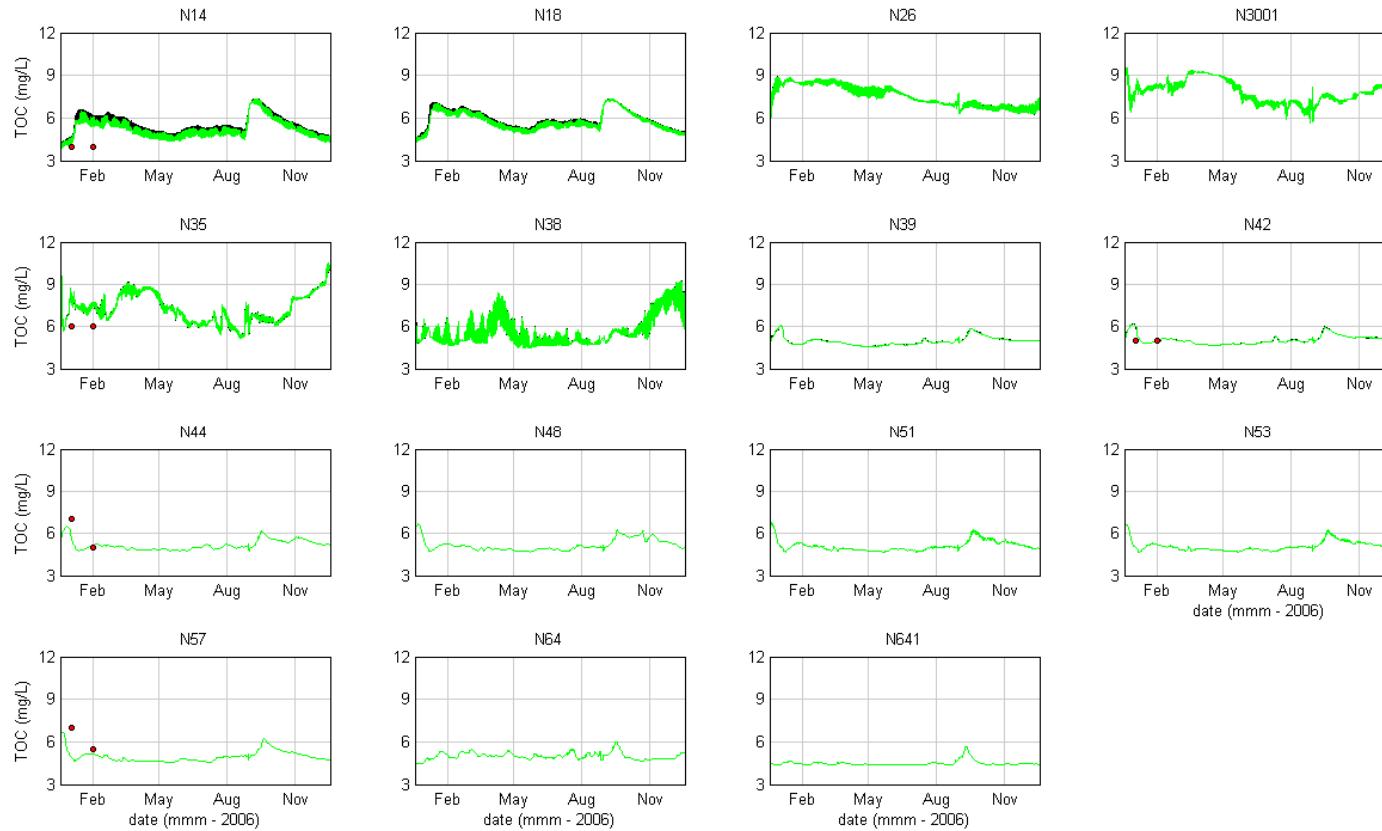


Water Quality Modelling of the Hawkesbury-Nepean River System



■ Figure 13-76 Total Organic Carbon Calibration 2006 (measured data (red), modelled surface (black) and modelled bottom (green))

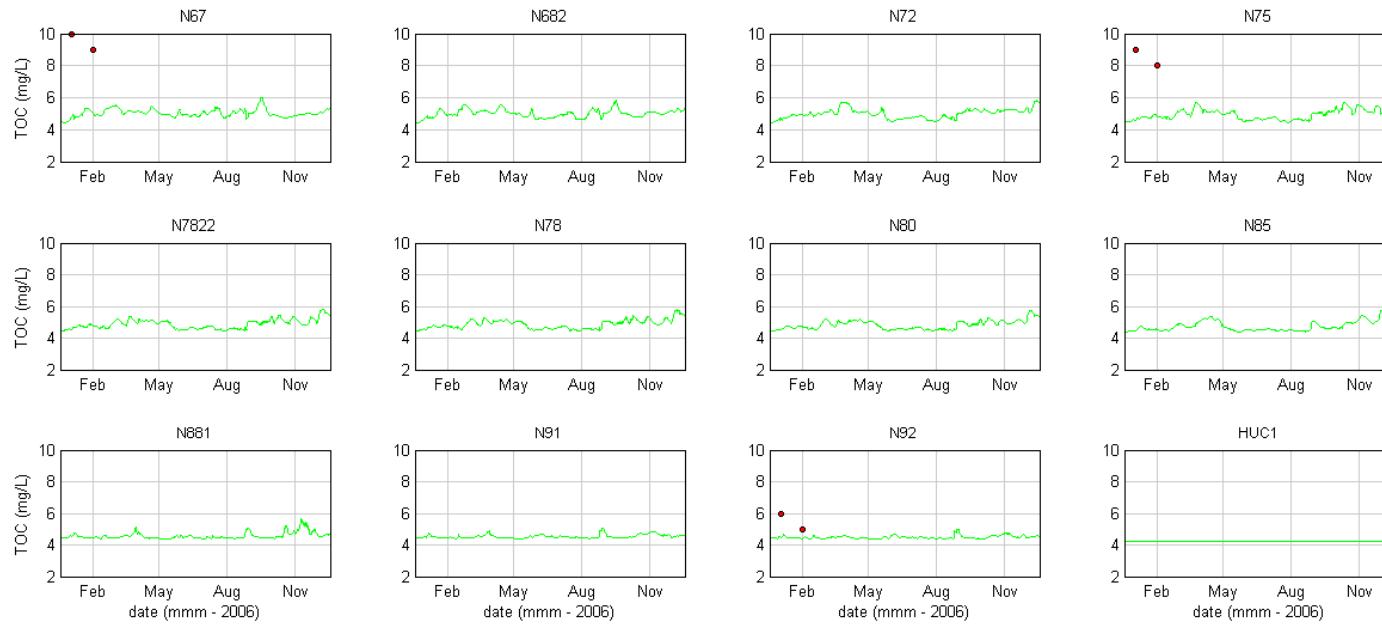
SINCLAIR KNIGHT MERZ



- **Figure 13-76 (Cont.) Total Organic Carbon Calibration 2006 (measured data (red), modelled surface (black) and modelled bottom (green))**



Water Quality Modelling of the Hawkesbury-Nepean River System

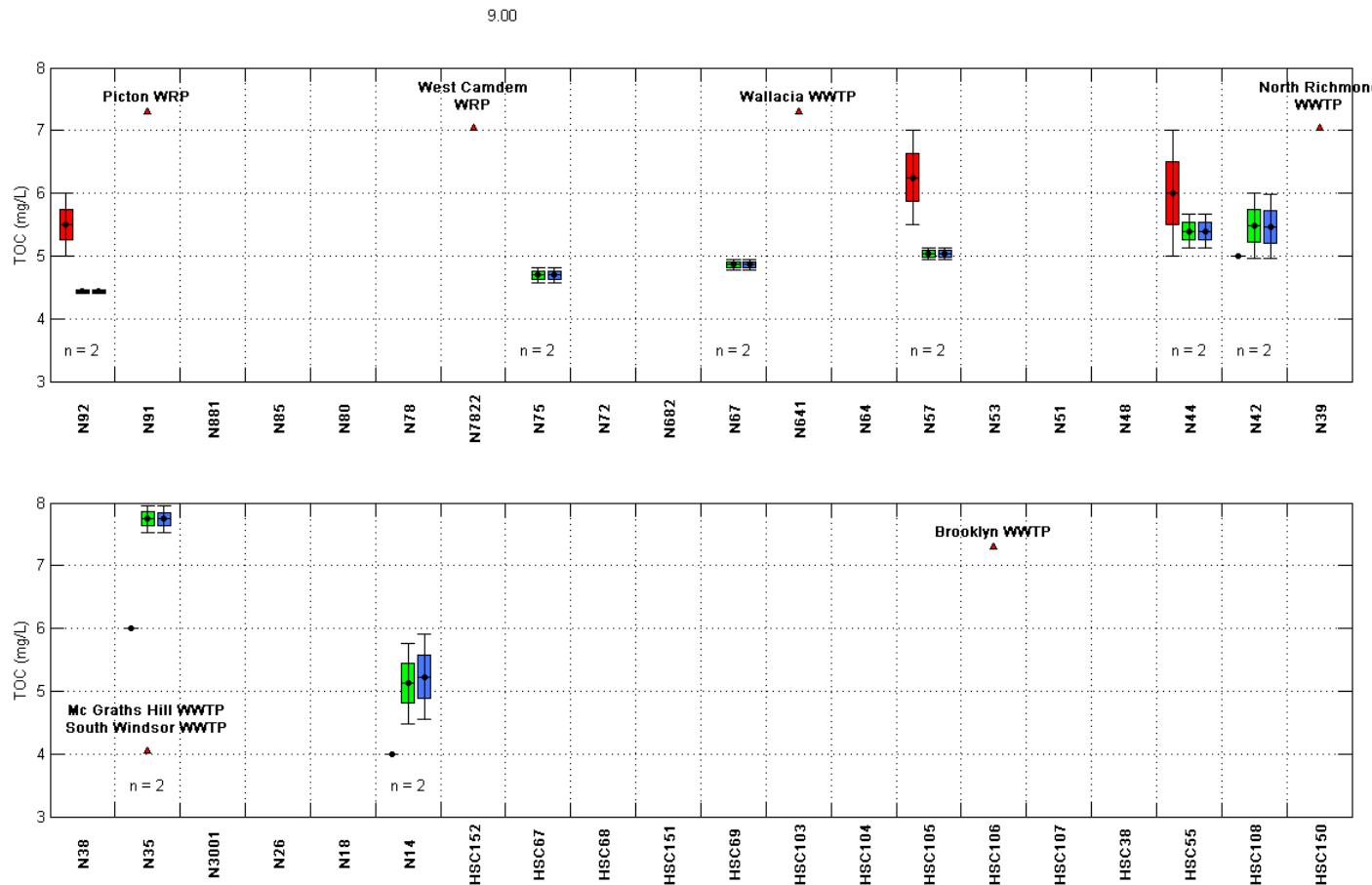


- **Figure 13-76 (Cont.) Total Organic Carbon Calibration 2006 (measured data (red), modelled surface (black) and modelled bottom (green))**

SINCLAIR KNIGHT MERZ



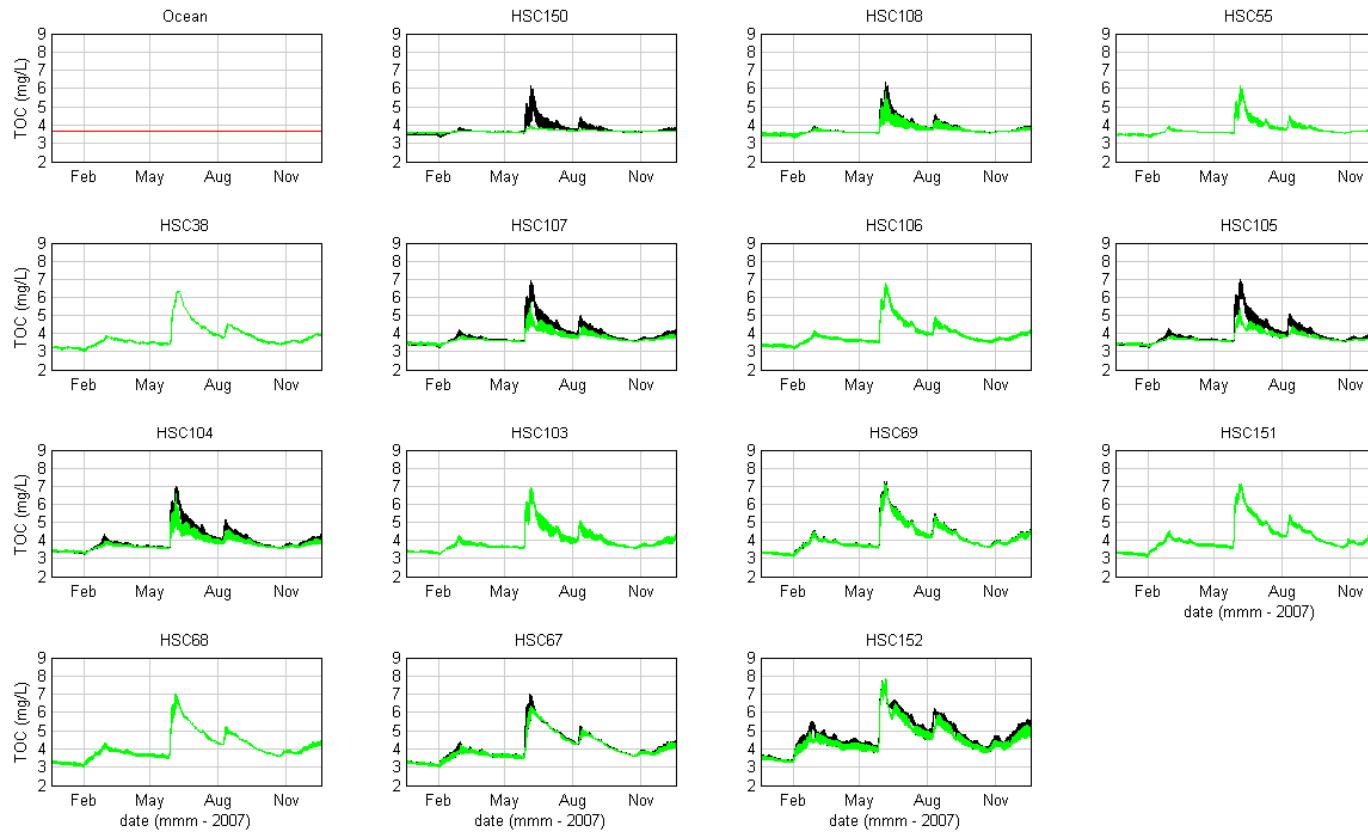
Water Quality Modelling of the Hawkesbury-Nepean River System



- **Figure 13-77 Box and Whisker Plots – Total Organic Carbon Calibration 2006 (measured data (red), modelled surface (blue) and modelled bottom (green))**



Water Quality Modelling of the Hawkesbury-Nepean River System

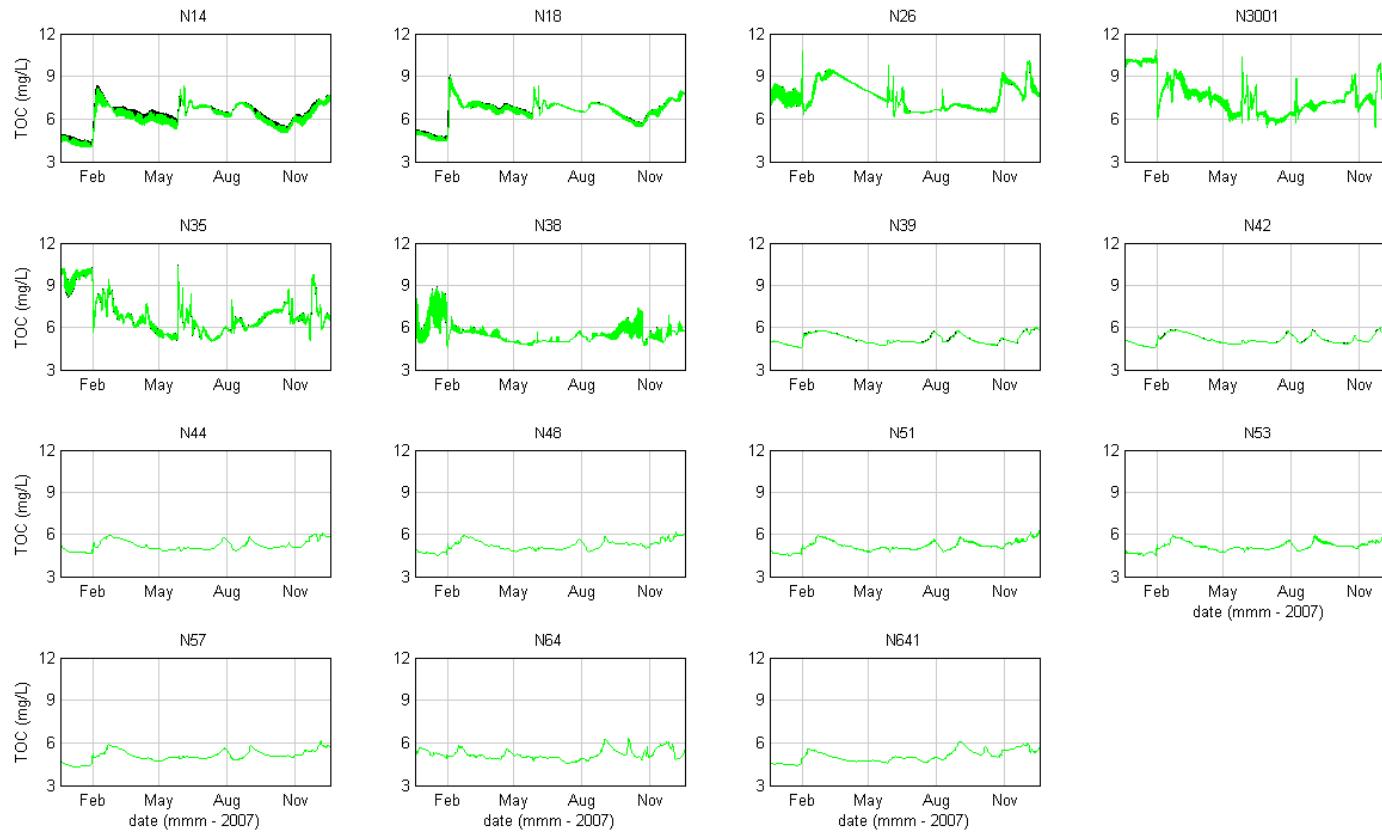


■ **Figure 13-78 Total Organic Carbon Validation 2007 (measured data (red), modelled surface (black) and modelled bottom (green))**

SINCLAIR KNIGHT MERZ



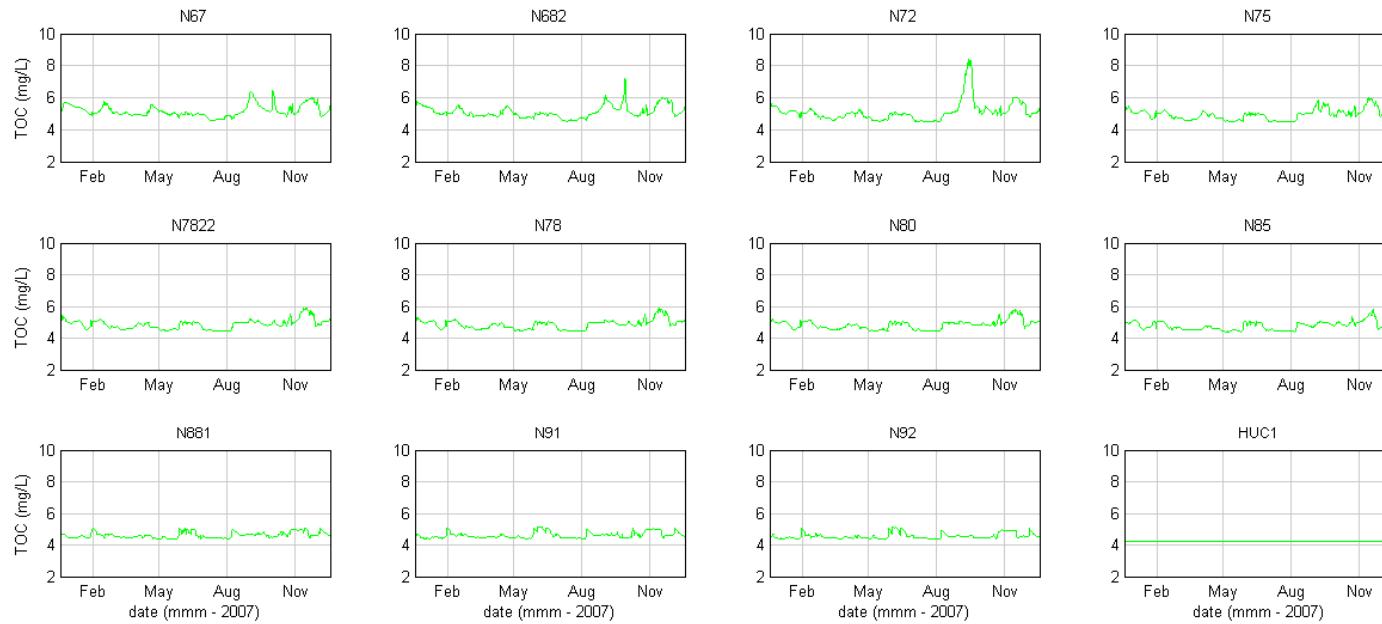
Water Quality Modelling of the Hawkesbury-Nepean River System



- Figure 13-78 (Cont.) Total Organic Carbon Validation 2007 (measured data (red), modelled surface (black) and modelled bottom (green))



Water Quality Modelling of the Hawkesbury-Nepean River System

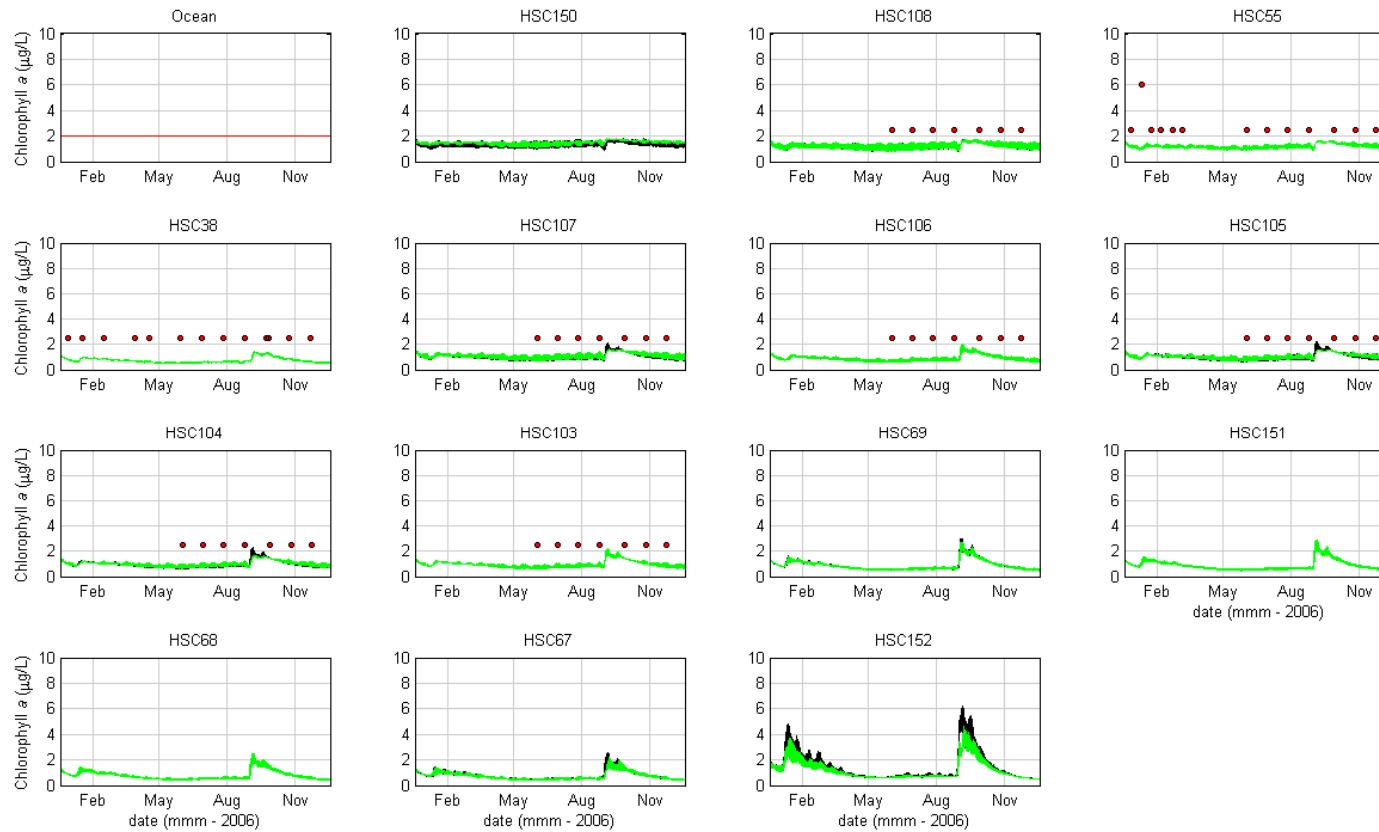


- **Figure 13-78 (Cont.) Total Organic Carbon Validation 2007 (measured data (red), modelled surface (black) and modelled bottom (green))**

SINCLAIR KNIGHT MERZ



Water Quality Modelling of the Hawkesbury-Nepean River System

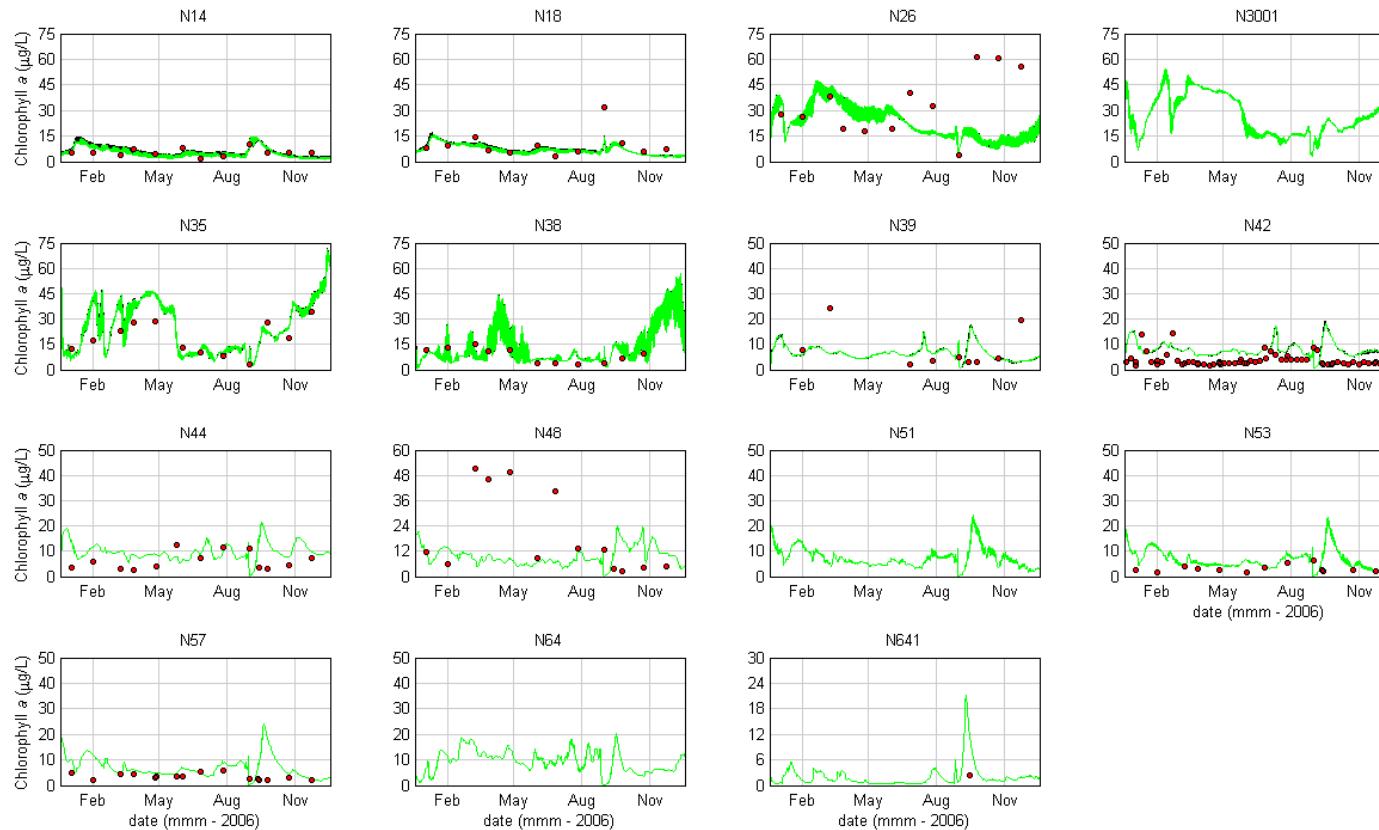


■ **Figure 13-79 Chlorophyll a Calibration 2006 (measured data (red), modelled surface (black) and modelled bottom (green))**

SINCLAIR KNIGHT MERZ



Water Quality Modelling of the Hawkesbury-Nepean River System

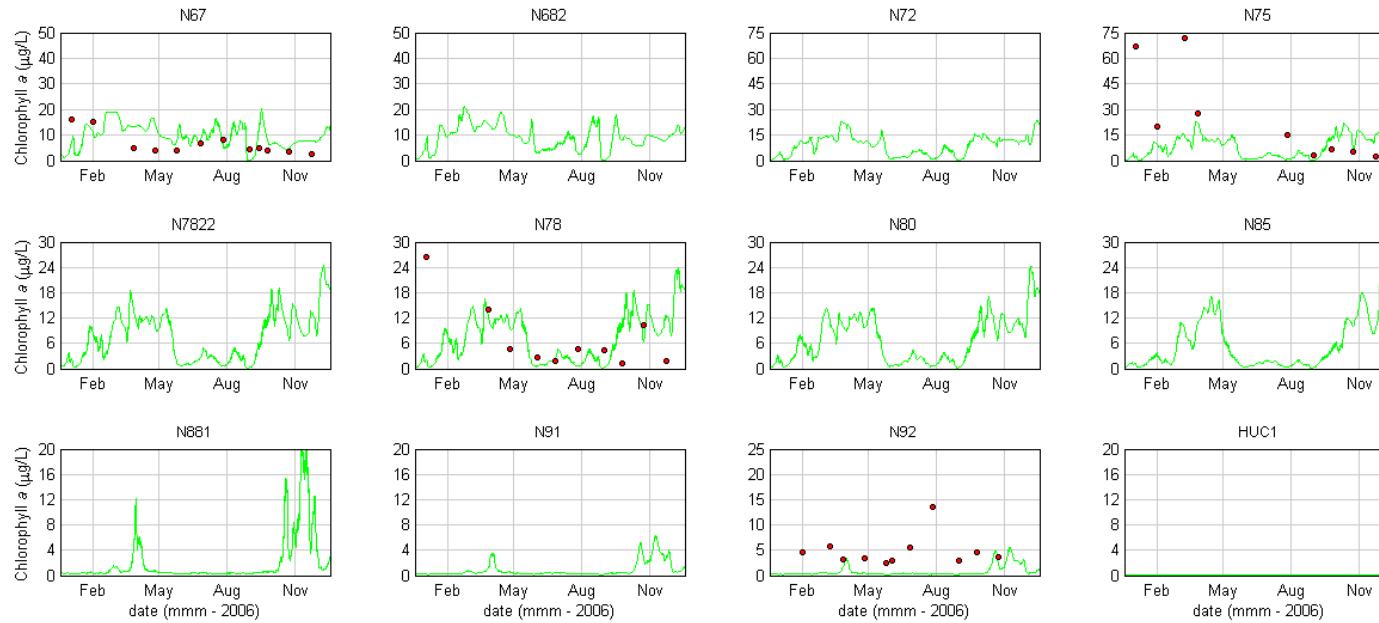


■ Figure 13-79 (Cont.) \ Chlorophyll a Calibration 2006 (measured data (red), modelled surface (black) and modelled bottom (green))

SINCLAIR KNIGHT MERZ



Water Quality Modelling of the Hawkesbury-Nepean River System

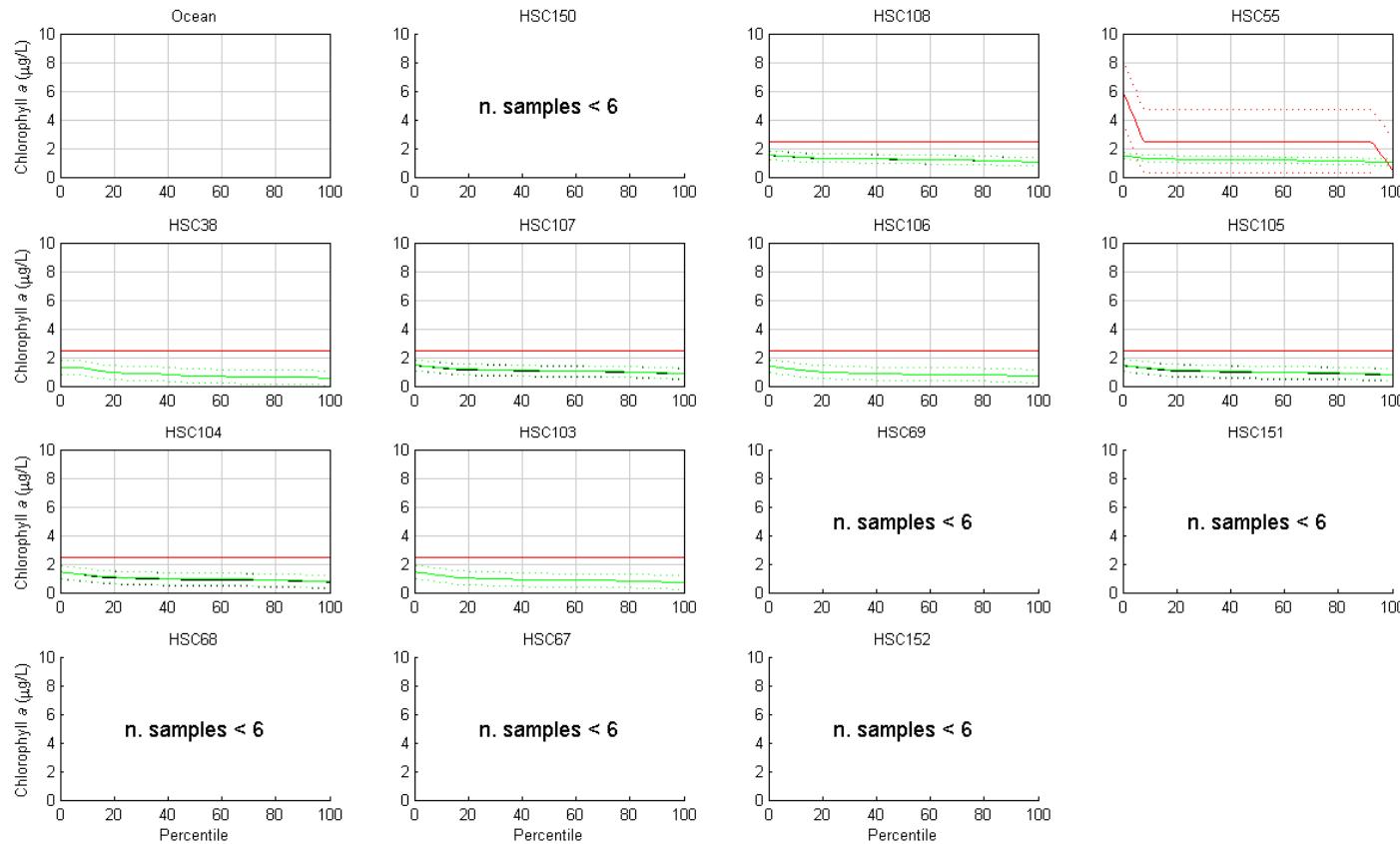


- Figure 13-79 (Cont.) Chlorophyll a Calibration 2006 (measured data (red), modelled surface (black) and modelled bottom (green))

SINCLAIR KNIGHT MERZ



Water Quality Modelling of the Hawkesbury-Nepean River System

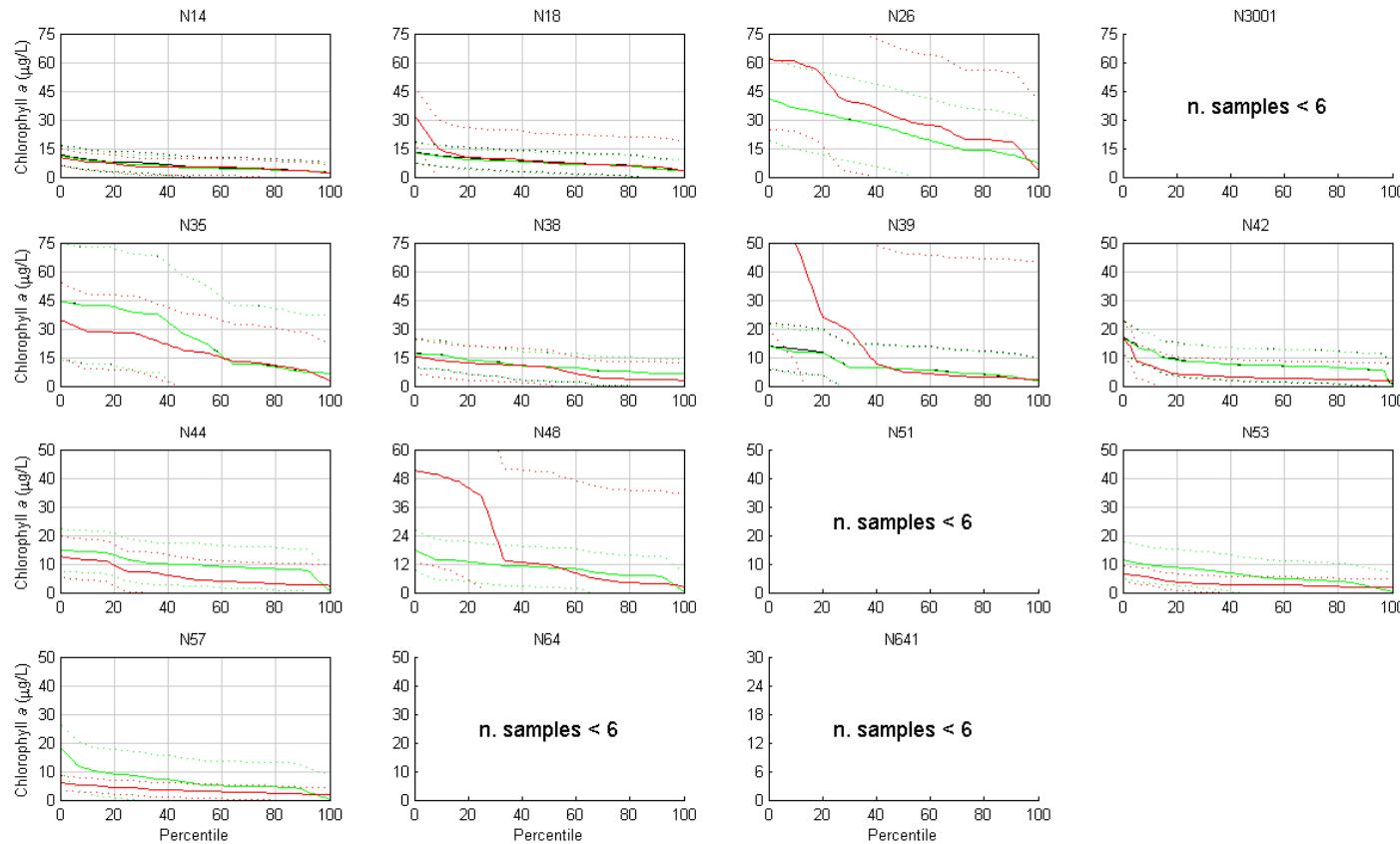


- **Figure 13-80 Exceedance Plots – Chlorophyll a Calibration 2006 (+/- 2SD) (measured data (red), modelled surface (black) and modelled bottom (green))**

SINCLAIR KNIGHT MERZ



Water Quality Modelling of the Hawkesbury-Nepean River System

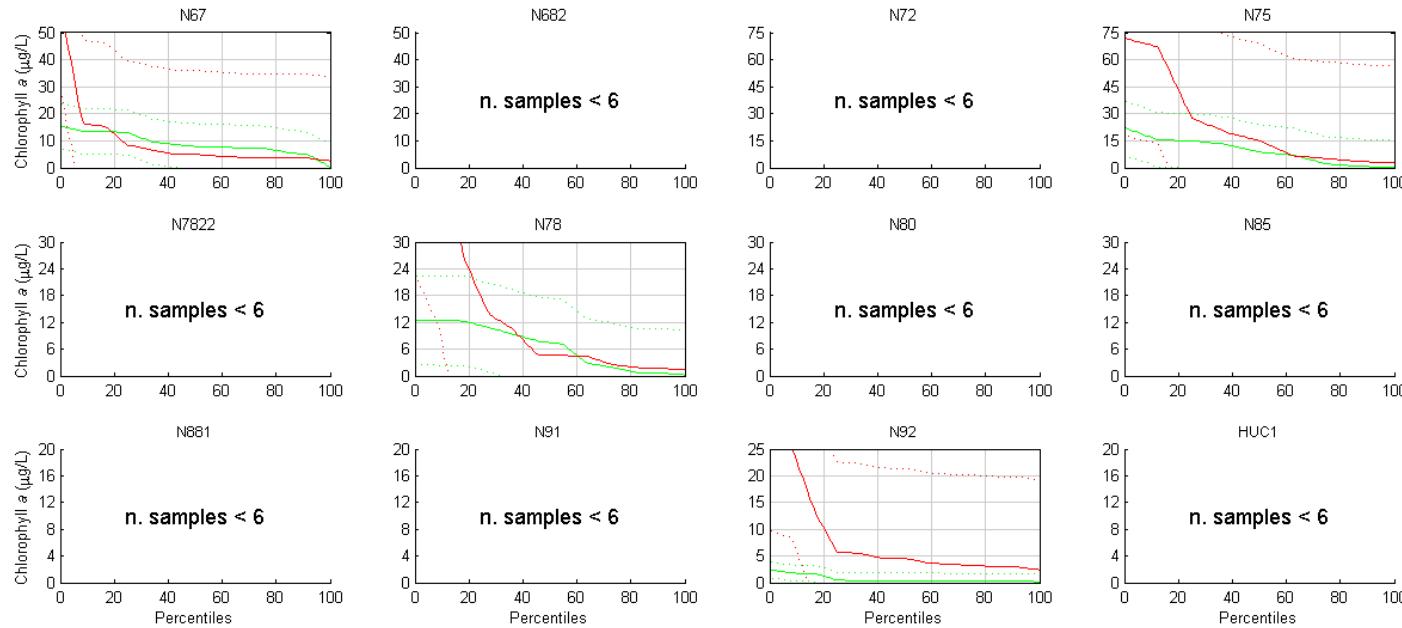


- Figure 13-80 (Cont.) Exceedance Plots – Chlorophyll a Calibration 2006 (+/- 2SD) (measured data (red), modelled surface (black) and modelled bottom (green))

SINCLAIR KNIGHT MERZ



Water Quality Modelling of the Hawkesbury-Nepean River System

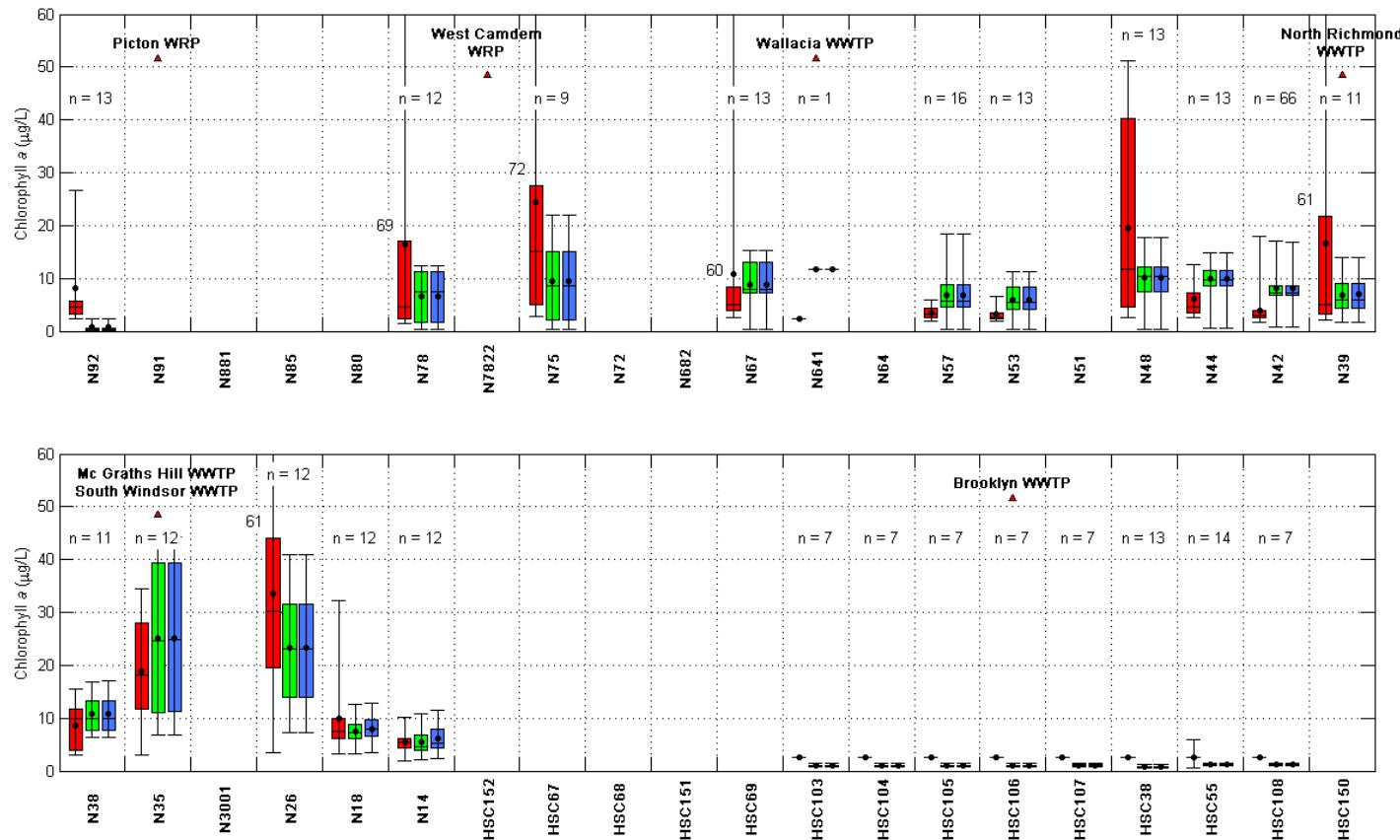


- Figure 13-80 (Cont.) Exceedance Plots – Chlorophyll a Calibration 2006 (+/- 2SD) (measured data (red), modelled surface (black) and modelled bottom (green))

SINCLAIR KNIGHT MERZ



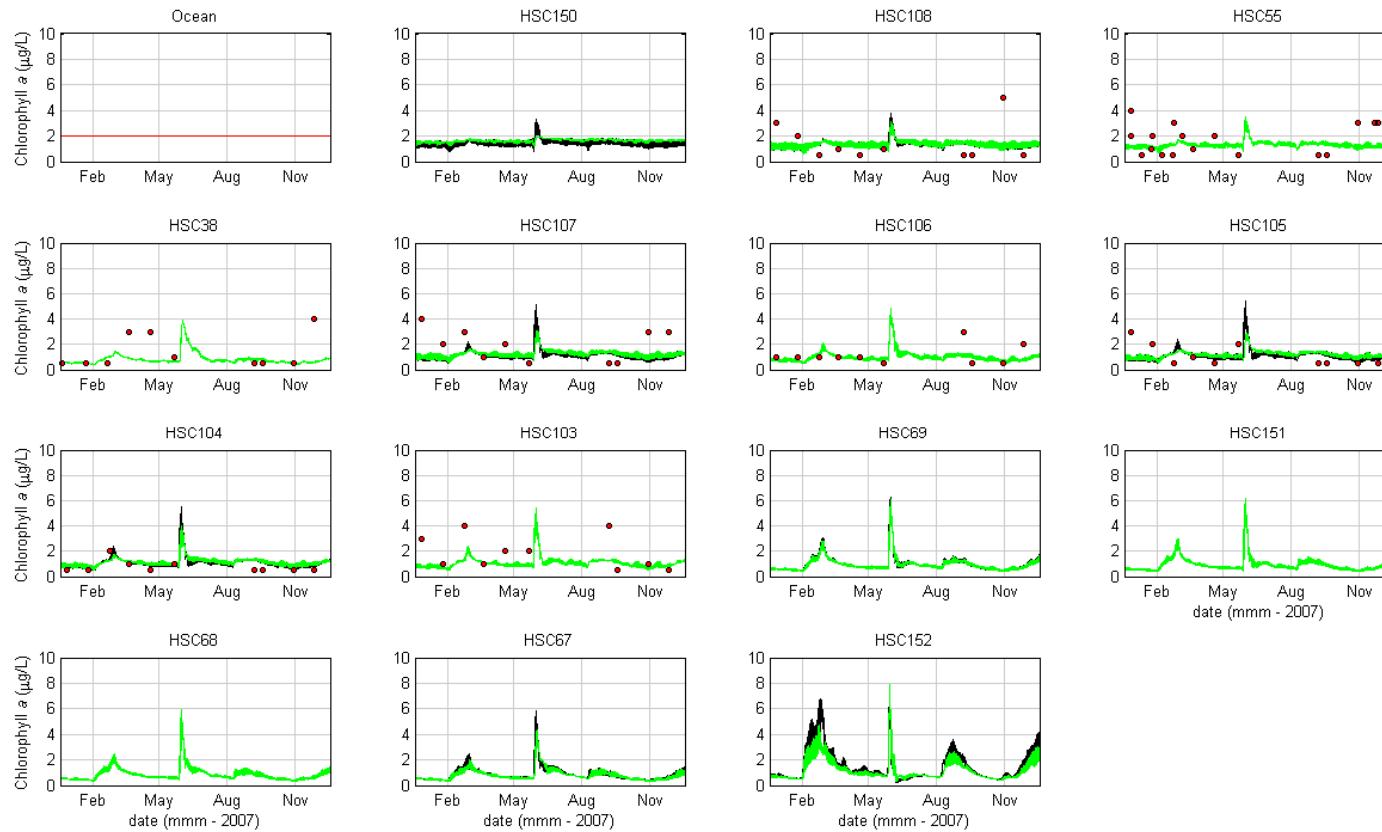
Water Quality Modelling of the Hawkesbury-Nepean River System



- **Figure 13-81 Box and Whisker Plots – Chlorophyll a Calibration 2006 (measured data (red), modelled surface (blue) and modelled bottom (green))**



Water Quality Modelling of the Hawkesbury-Nepean River System

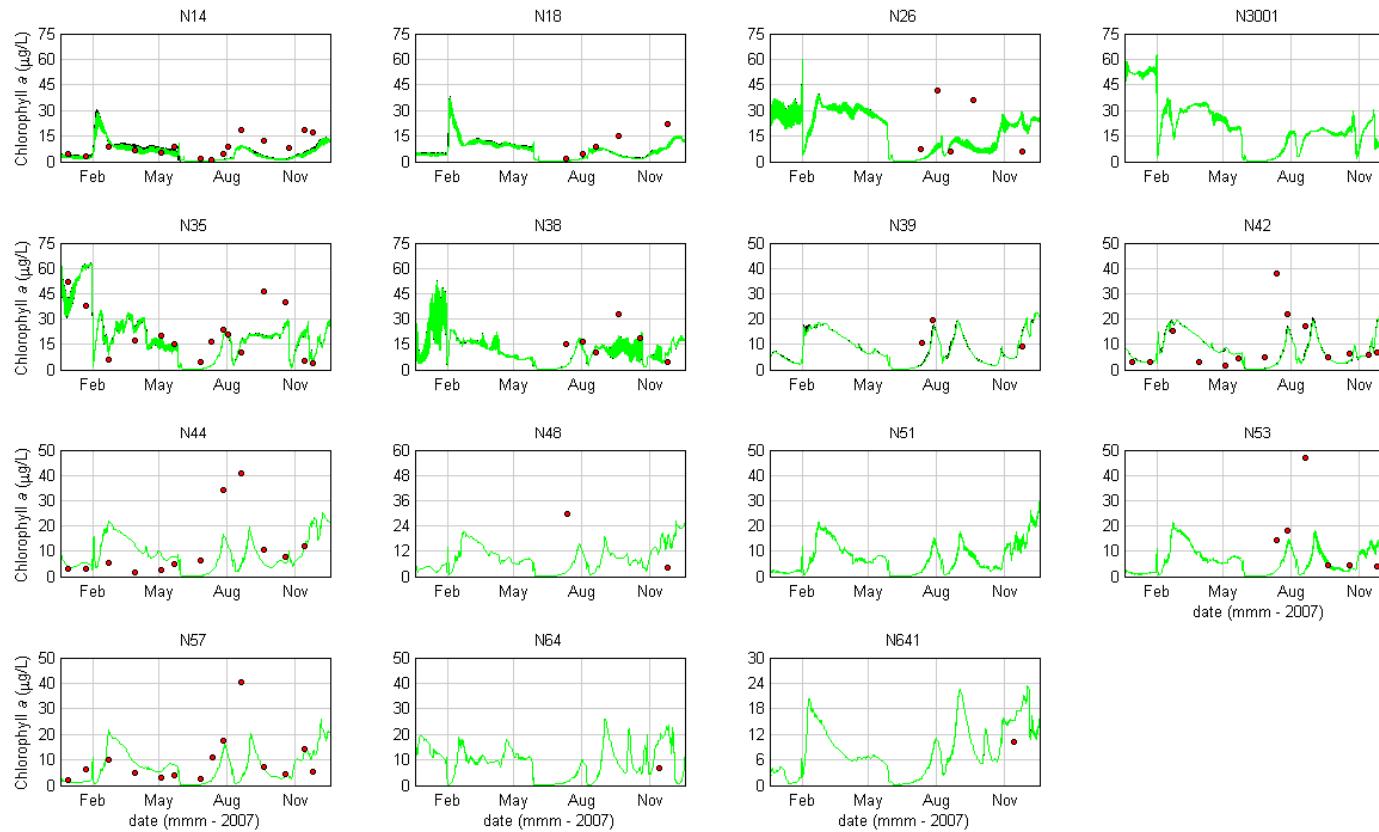


■ **Figure 13-82 Chlorophyll a Validation 2007 (measured data (red), modelled surface (black) and modelled bottom (green))**

SINCLAIR KNIGHT MERZ



Water Quality Modelling of the Hawkesbury-Nepean River System

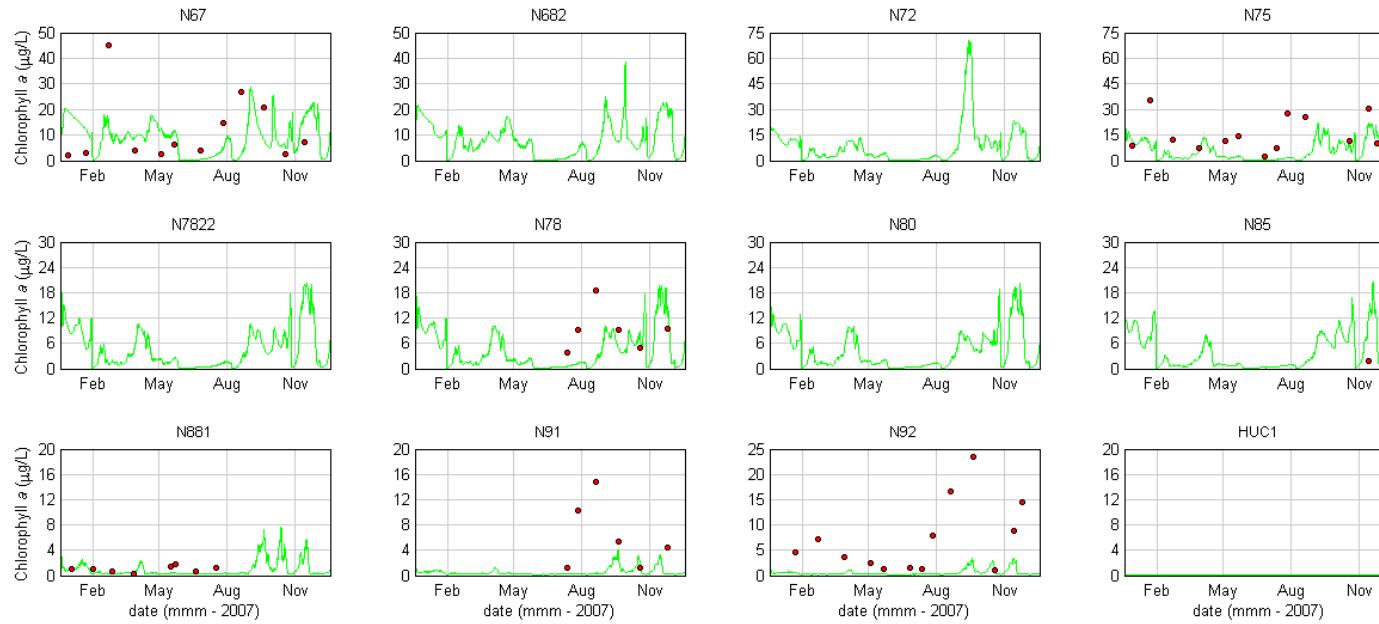


■ **Figure 13-82 (Cont.) Chlorophyll a Validation 2007 (measured data (red), modelled surface (black) and modelled bottom (green))**

SINCLAIR KNIGHT MERZ



Water Quality Modelling of the Hawkesbury-Nepean River System

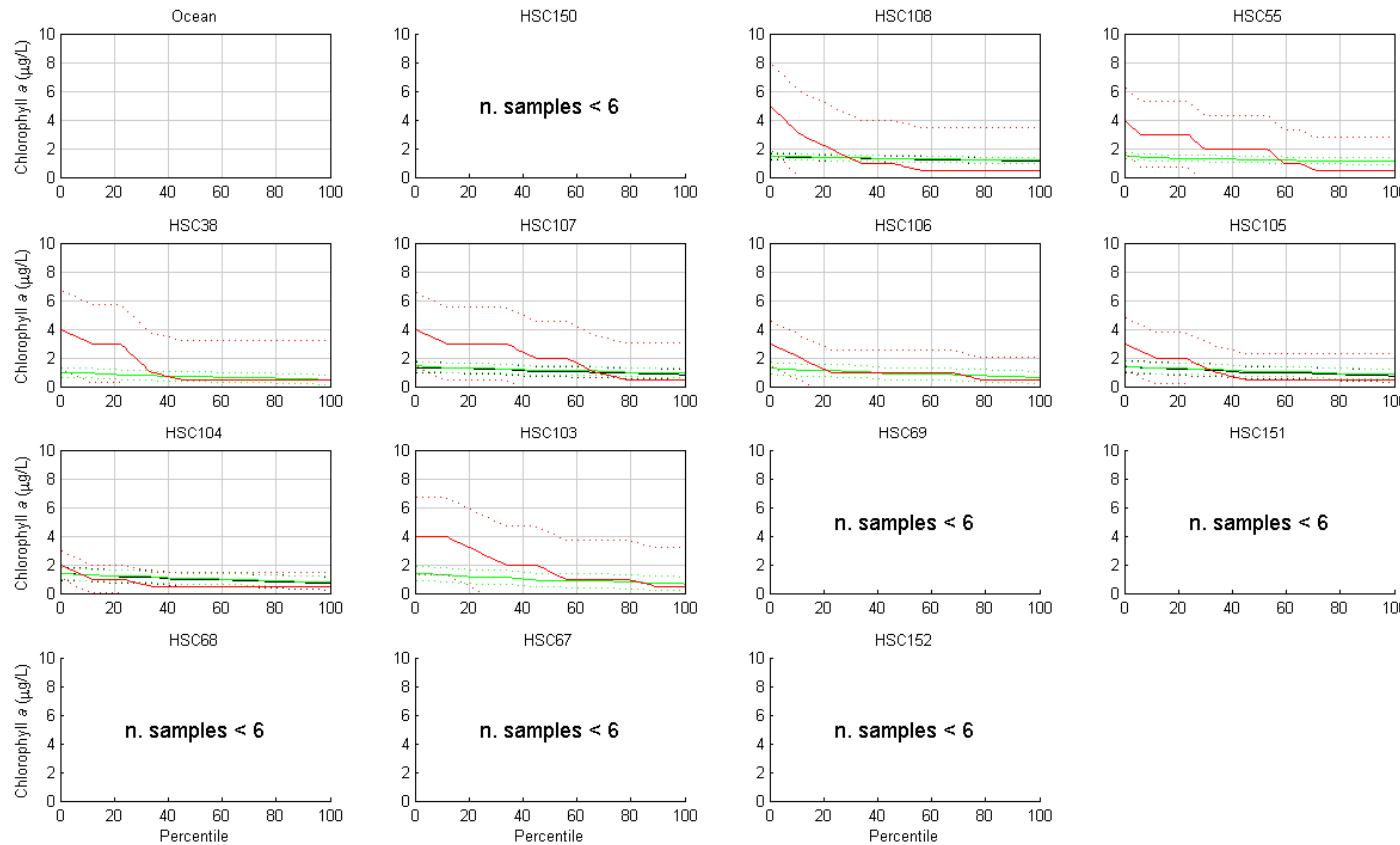


- **Figure 13-82 (Cont.) Chlorophyll a Validation 2007 (measured data (red), modelled surface (black) and modelled bottom (green))**

SINCLAIR KNIGHT MERZ



Water Quality Modelling of the Hawkesbury-Nepean River System

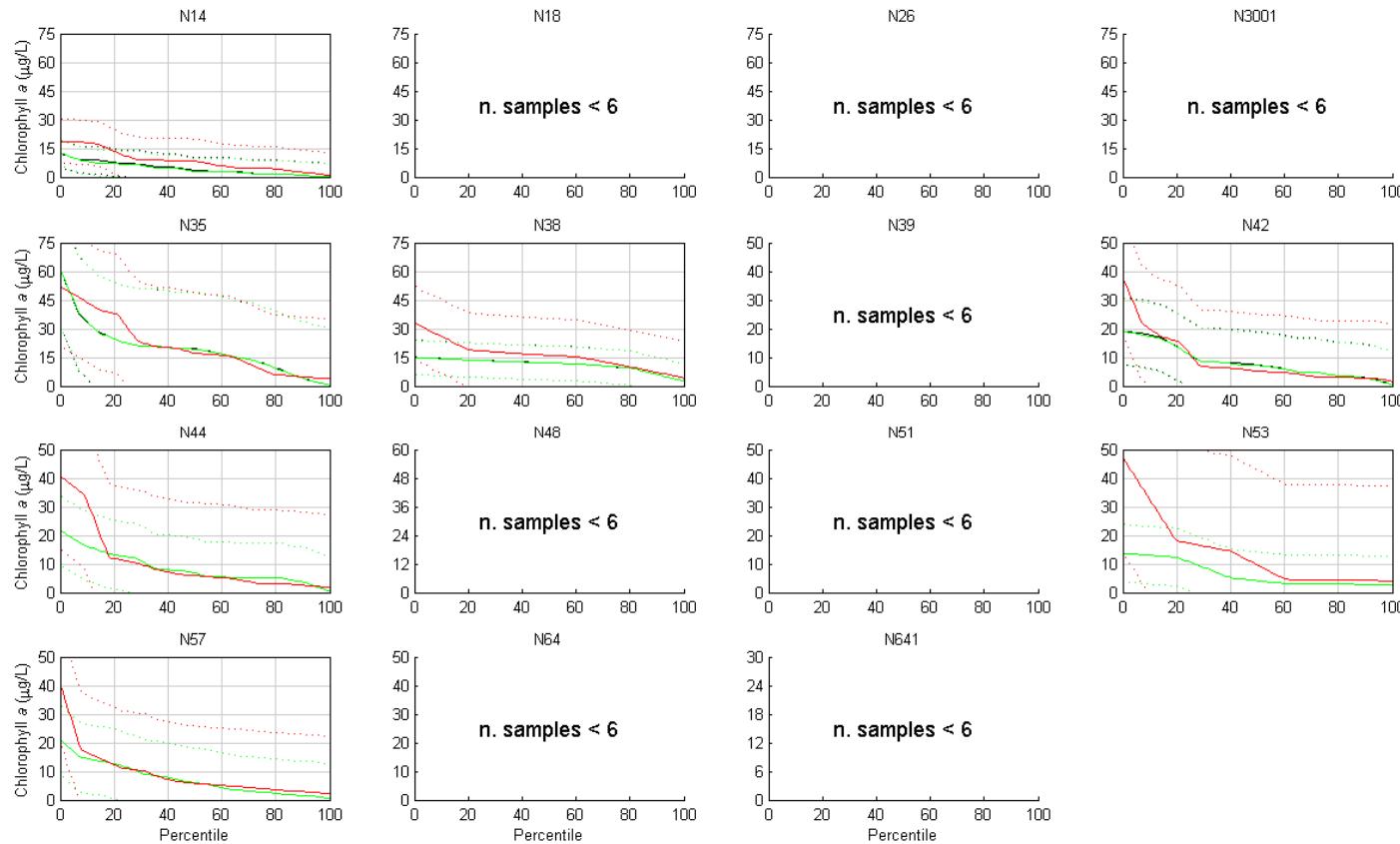


- **Figure 13-83 Exceedance Plots – Chlorophyll a Validation 2007 (+/- 2SD) (measured data (red), modelled surface (black) and modelled bottom (green))**

SINCLAIR KNIGHT MERZ



Water Quality Modelling of the Hawkesbury-Nepean River System

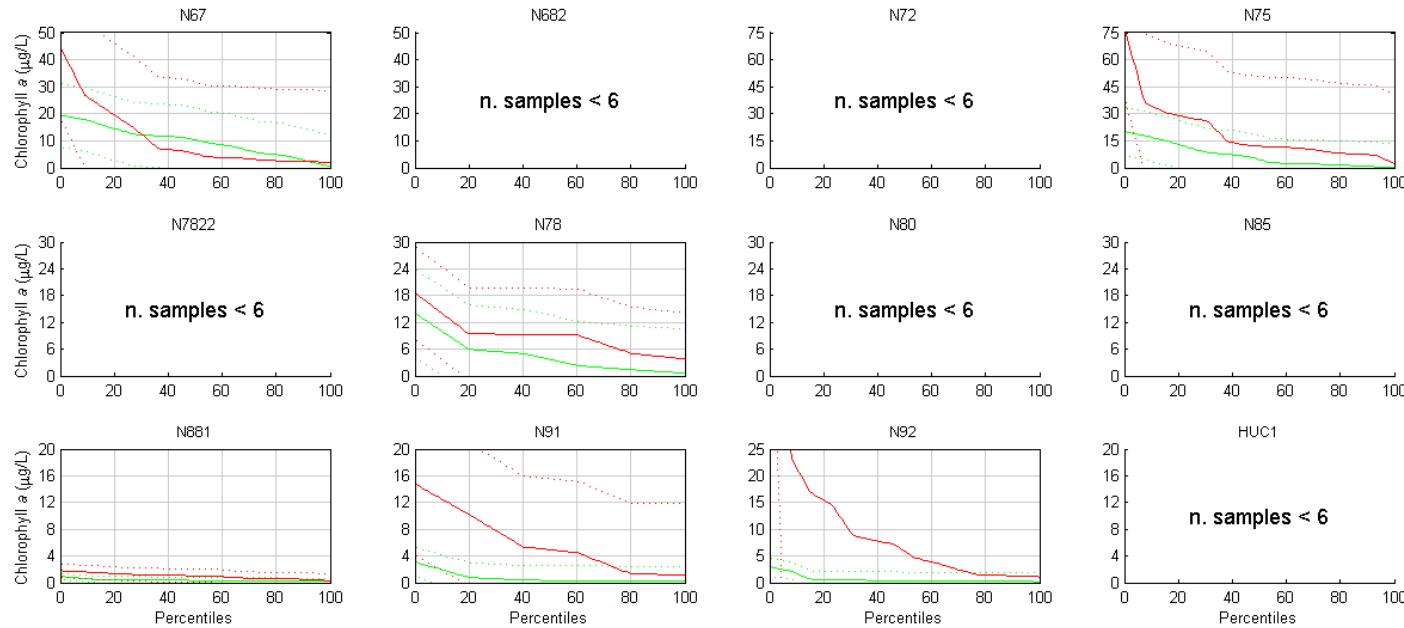


- Figure 13-83 (Cont.) Exceedance Plots – Chlorophyll a Validation 2007 (+/- 2SD) (measured data (red), modelled surface (black) and modelled bottom (green))

SINCLAIR KNIGHT MERZ



Water Quality Modelling of the Hawkesbury-Nepean River System

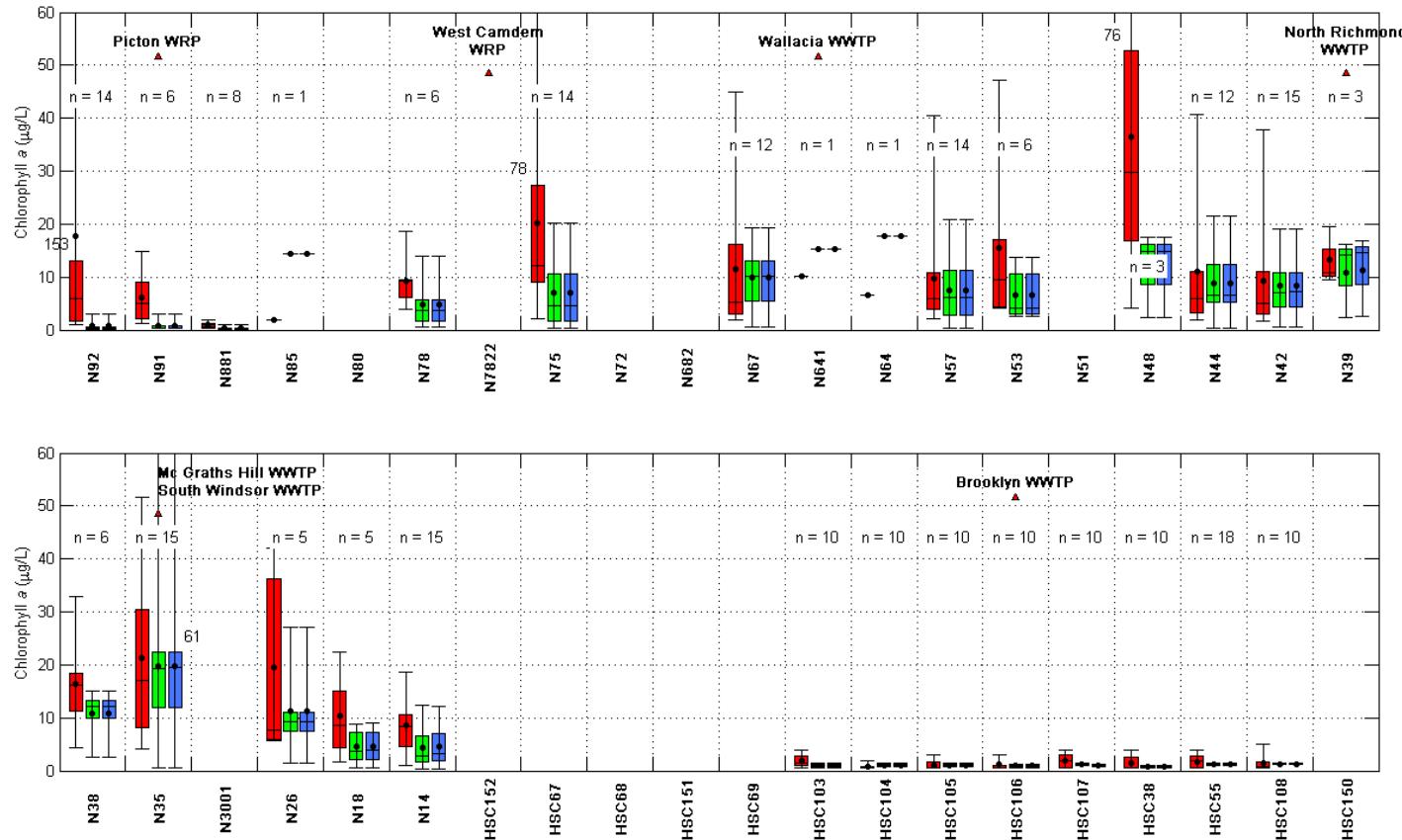


- Figure 13-83 (Cont.) Exceedance Plots – Chlorophyll a Validation 2007 (+/- 2SD) (measured data (red), modelled surface (black) and modelled bottom (green))

SINCLAIR KNIGHT MERZ



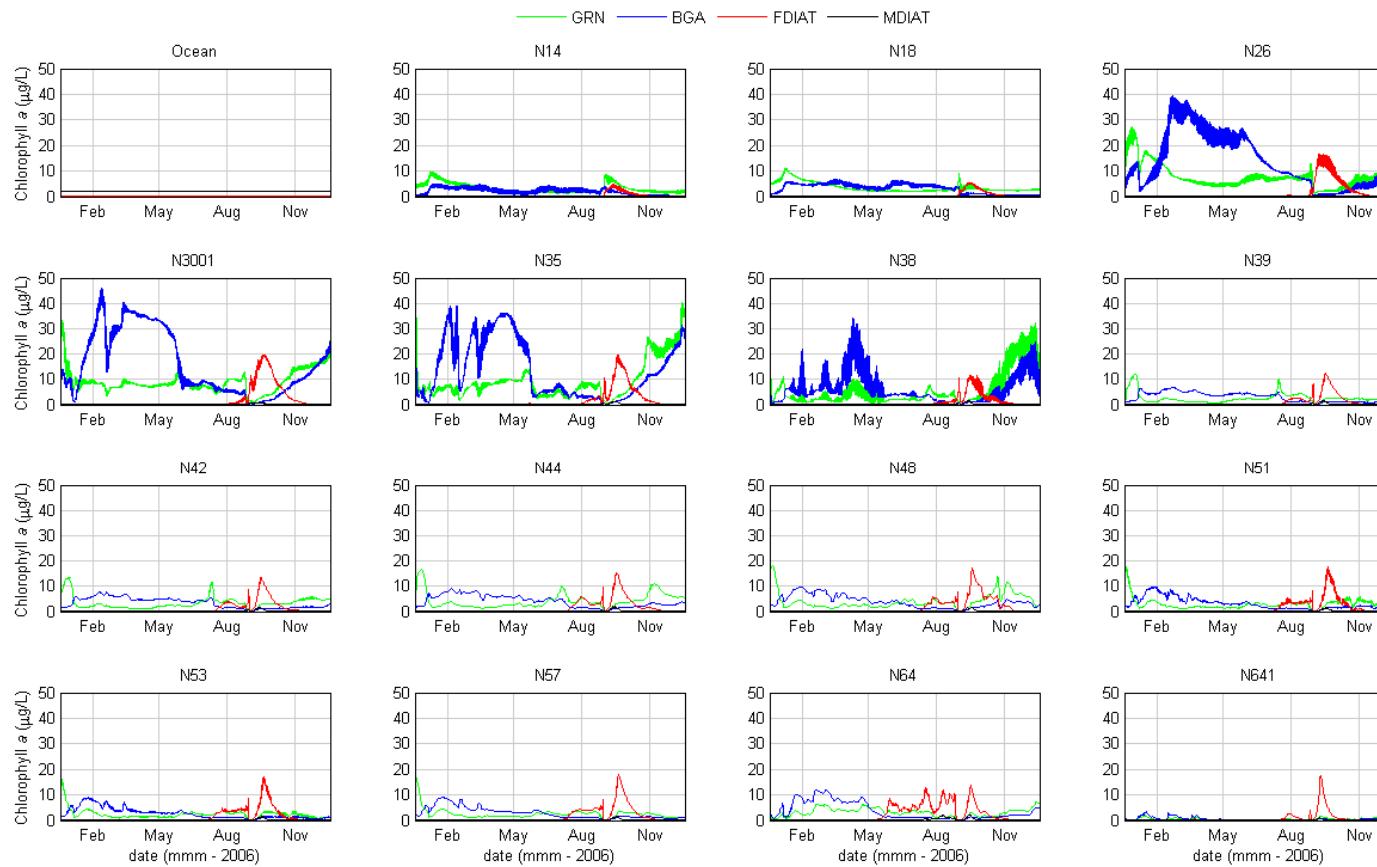
Water Quality Modelling of the Hawkesbury-Nepean River System



- **Figure 13-84 Box and Whisker Plots – Chlorophyll a Validation 2007 (measured data (red), modelled surface (blue) and modelled bottom (green))**



Water Quality Modelling of the Hawkesbury-Nepean River System

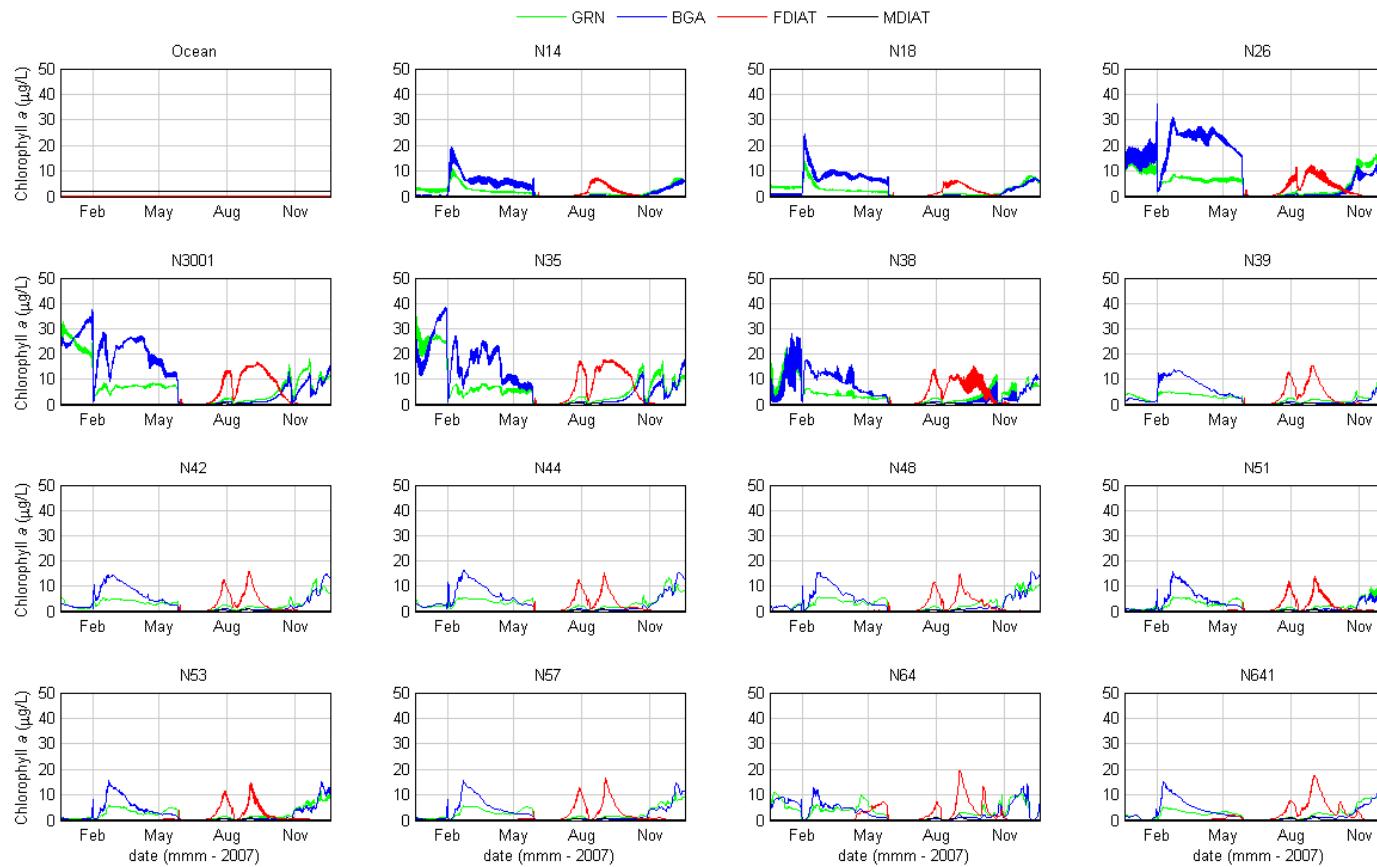


- **Figure 13-85 Modelled Algae Groups Chlorophyll a Calibration 2006 (Middle Reach only) (green algae (green), blue-green algae (blue), freshwater diatoms (red) and marine diatoms (black))**

SINCLAIR KNIGHT MERZ



Water Quality Modelling of the Hawkesbury-Nepean River System

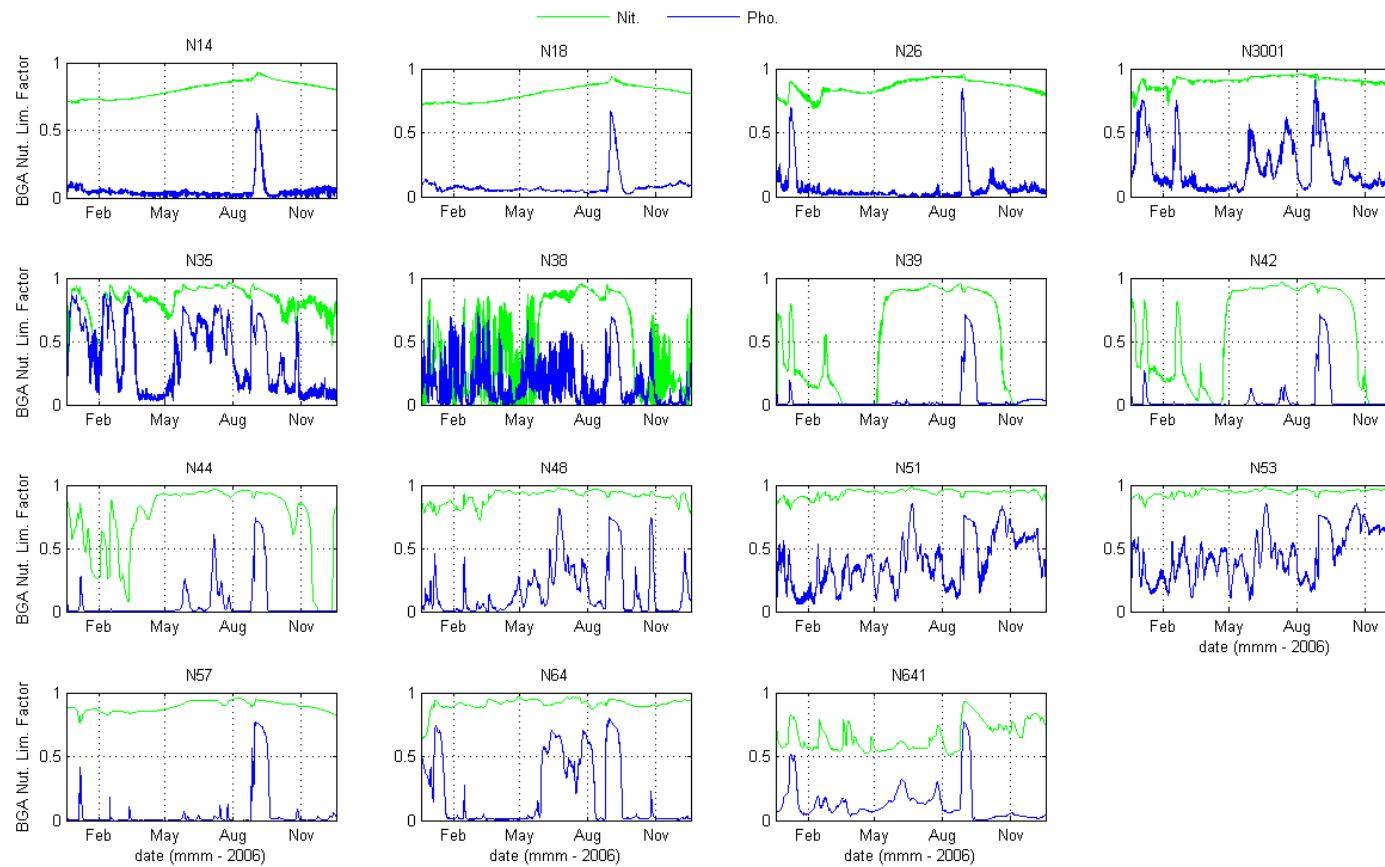


- **Figure 13-86 Modelled Algae Groups Chlorophyll a Validation 2007 (Middle Reach only) (green algae (green), blue-green algae (blue), freshwater diatoms (red) and marine diatoms (black))**

SINCLAIR KNIGHT MERZ



Water Quality Modelling of the Hawkesbury-Nepean River System

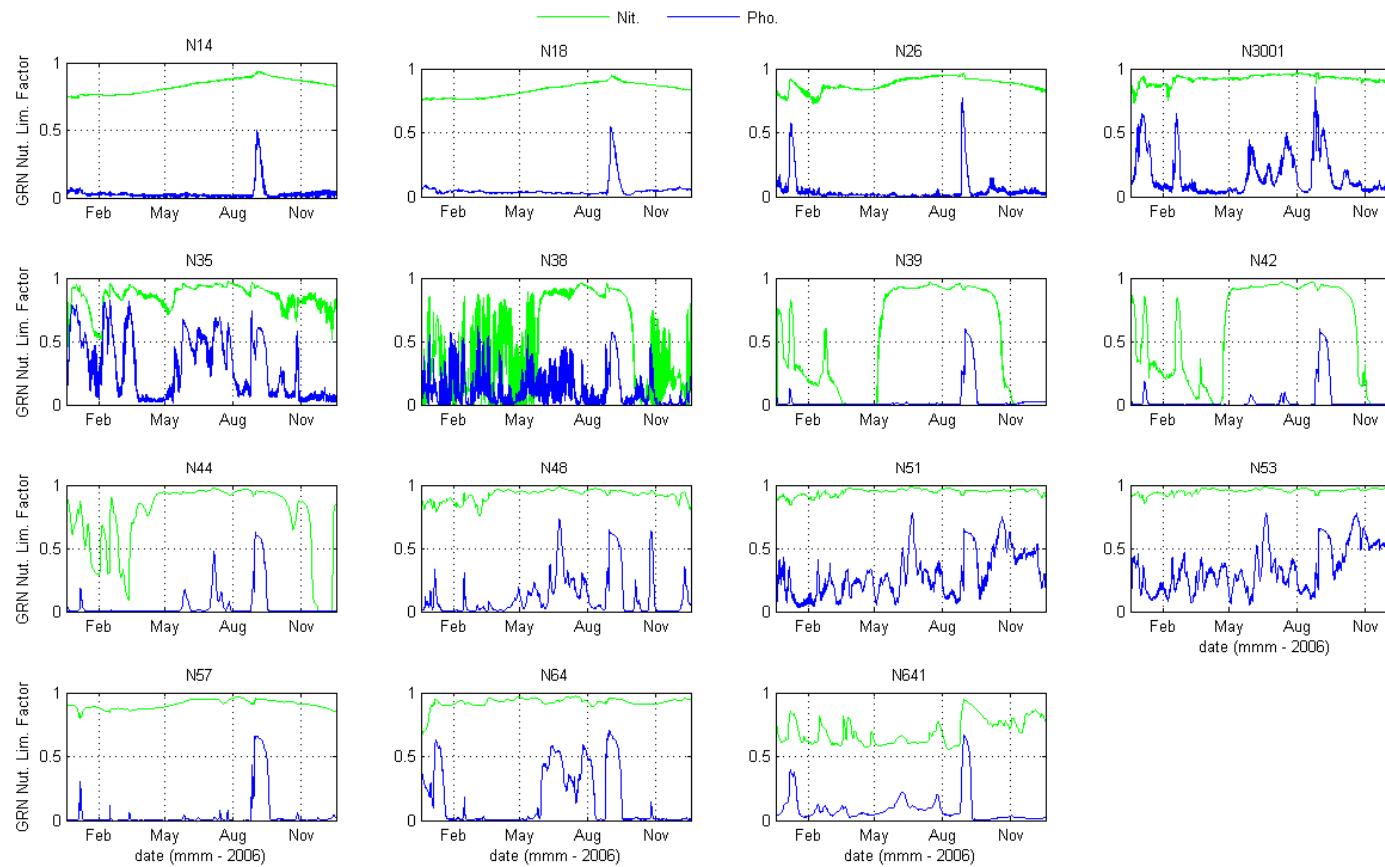


- Figure 13-87 Modelled Nutrient Limitation Functions for the Blue Green Algae Group Calibration 2006 (Middle Reach only) (nitrogen (green) and phosphorus (blue))

SINCLAIR KNIGHT MERZ



Water Quality Modelling of the Hawkesbury-Nepean River System

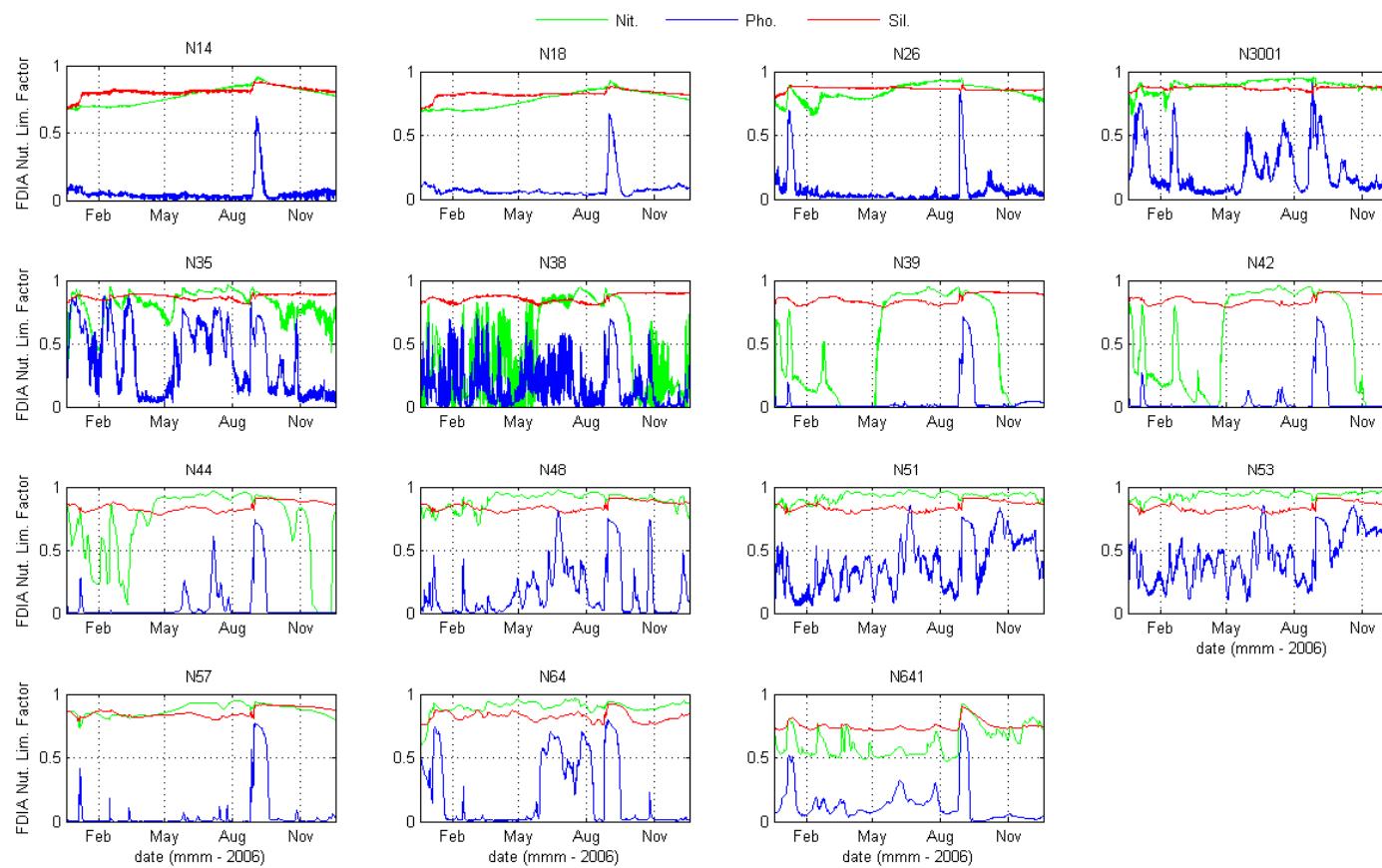


- **Figure 13-88 Nutrient Limitation Functions for the Green Algae Group Calibration 2006 (Middle Reach only) (nitrogen (green) and phosphorus (blue))**

SINCLAIR KNIGHT MERZ



Water Quality Modelling of the Hawkesbury-Nepean River System

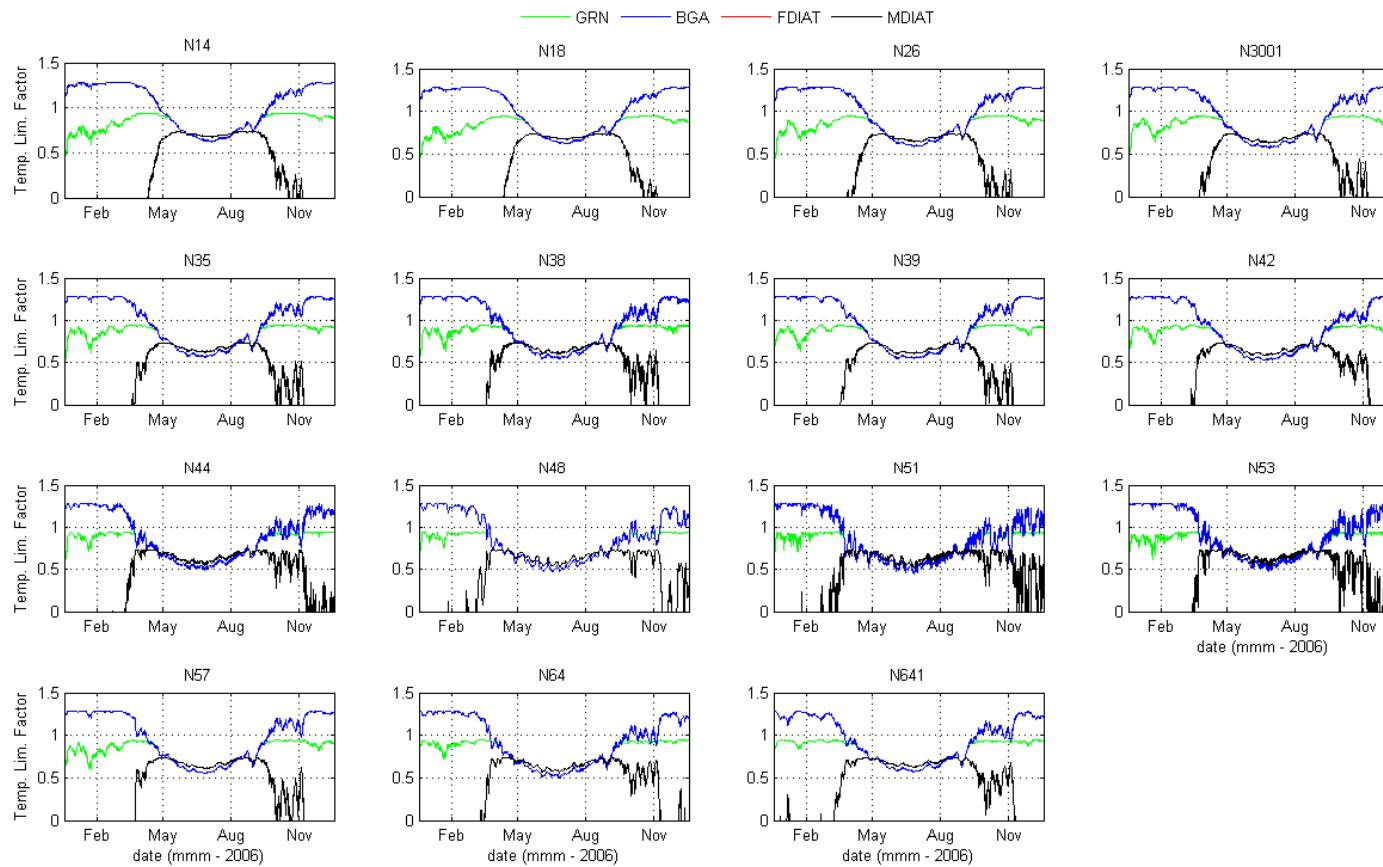


- **Figure 13-89 Nutrient Limitation Functions for the Freshwater Diatoms Algae Group Calibration 2006 (Middle Reach only) (nitrogen (green), phosphorus (blue) and silicate (red))**

SINCLAIR KNIGHT MERZ



Water Quality Modelling of the Hawkesbury-Nepean River System

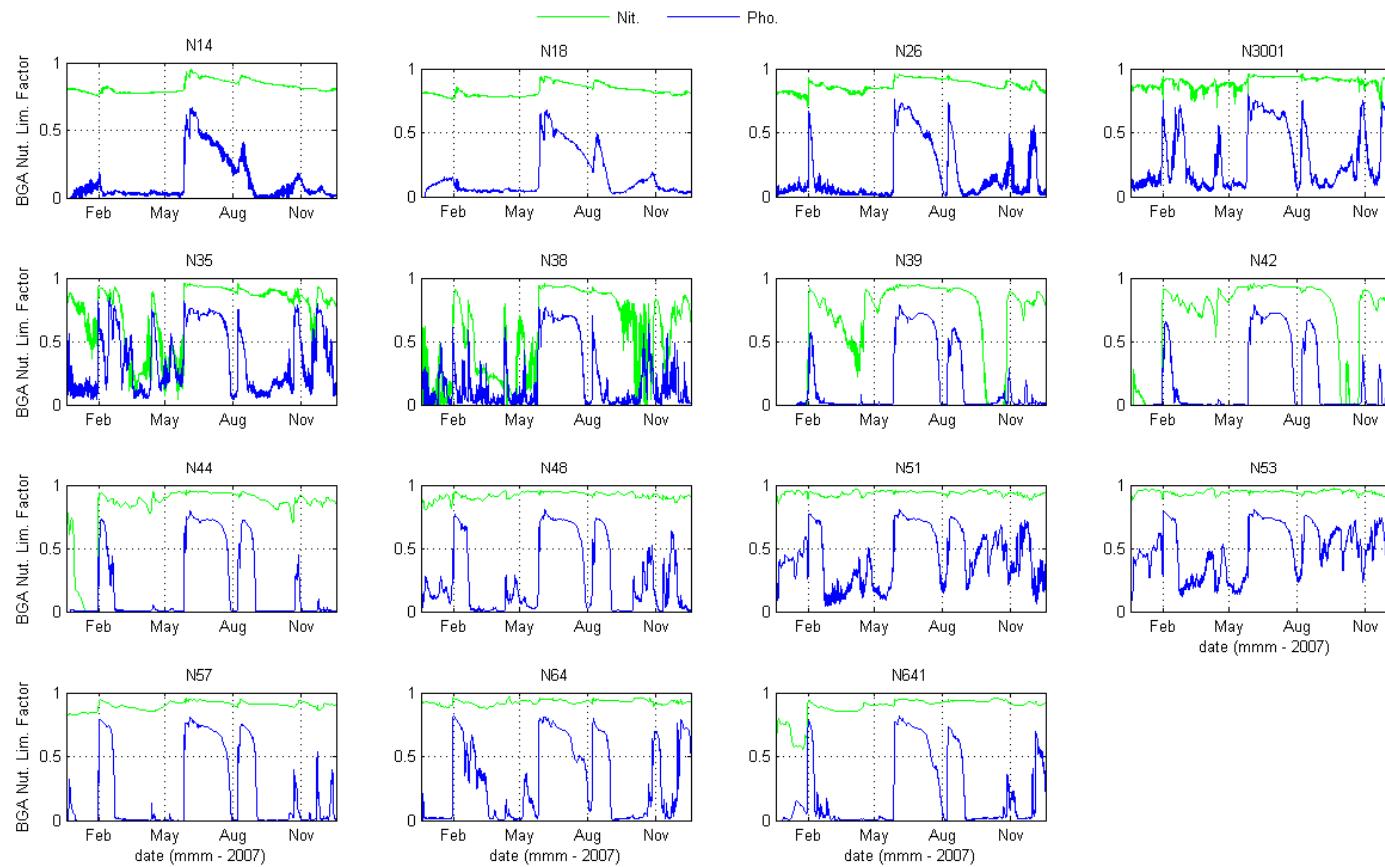


- **Figure 13-90 Temperature Limitation Functions for All Algae Groups Calibration 2006 (Middle Reach only) (green algae (green), blue-green algae (blue), freshwater diatoms (red) and marine diatoms (black))**

SINCLAIR KNIGHT MERZ



Water Quality Modelling of the Hawkesbury-Nepean River System

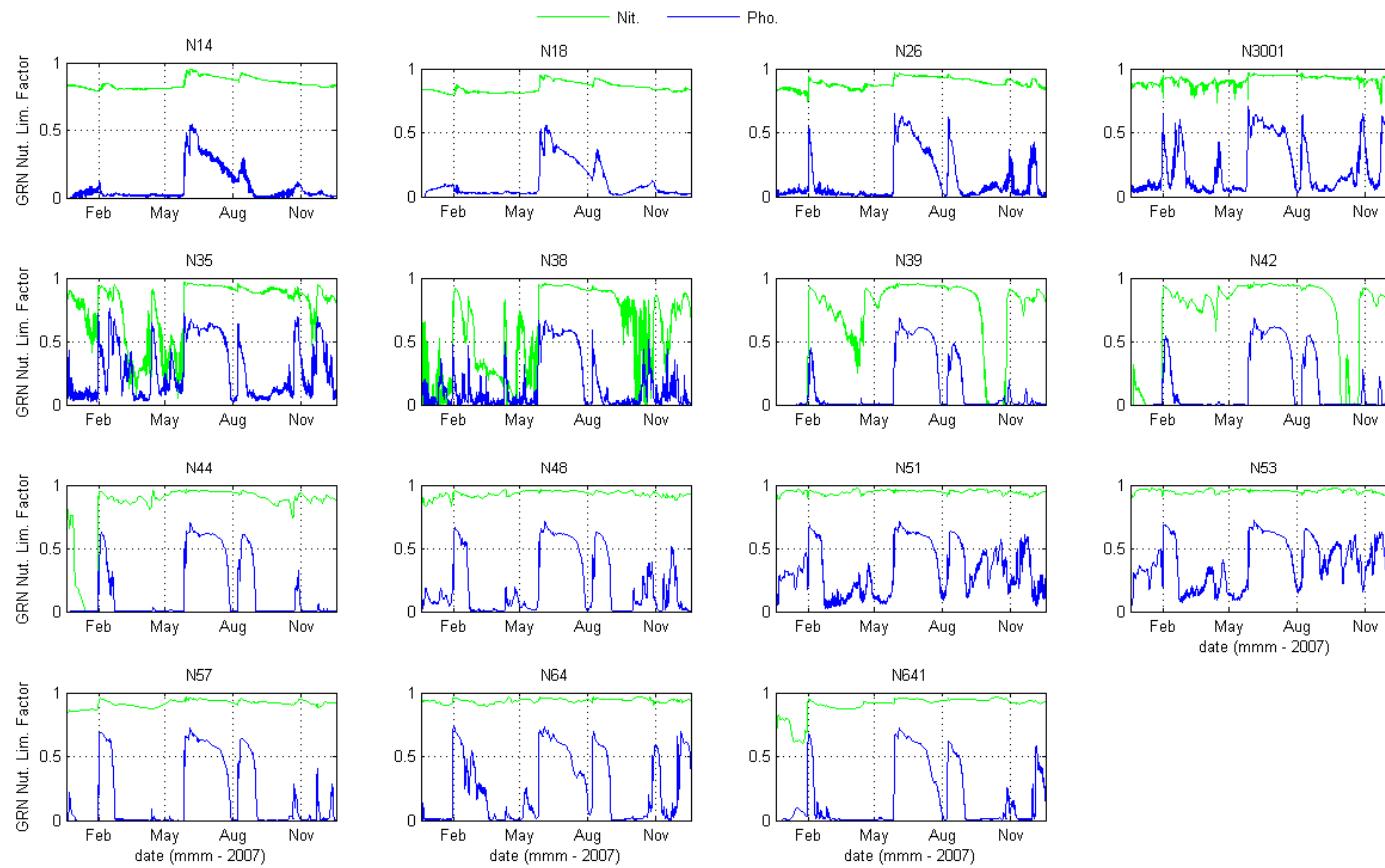


- **Figure 13-91 Nutrient Limitation Functions for the Blue Green Algae Group Validation 2007 (Middle Reach only) (nitrogen (green) and phosphorus (blue))**

SINCLAIR KNIGHT MERZ



Water Quality Modelling of the Hawkesbury-Nepean River System

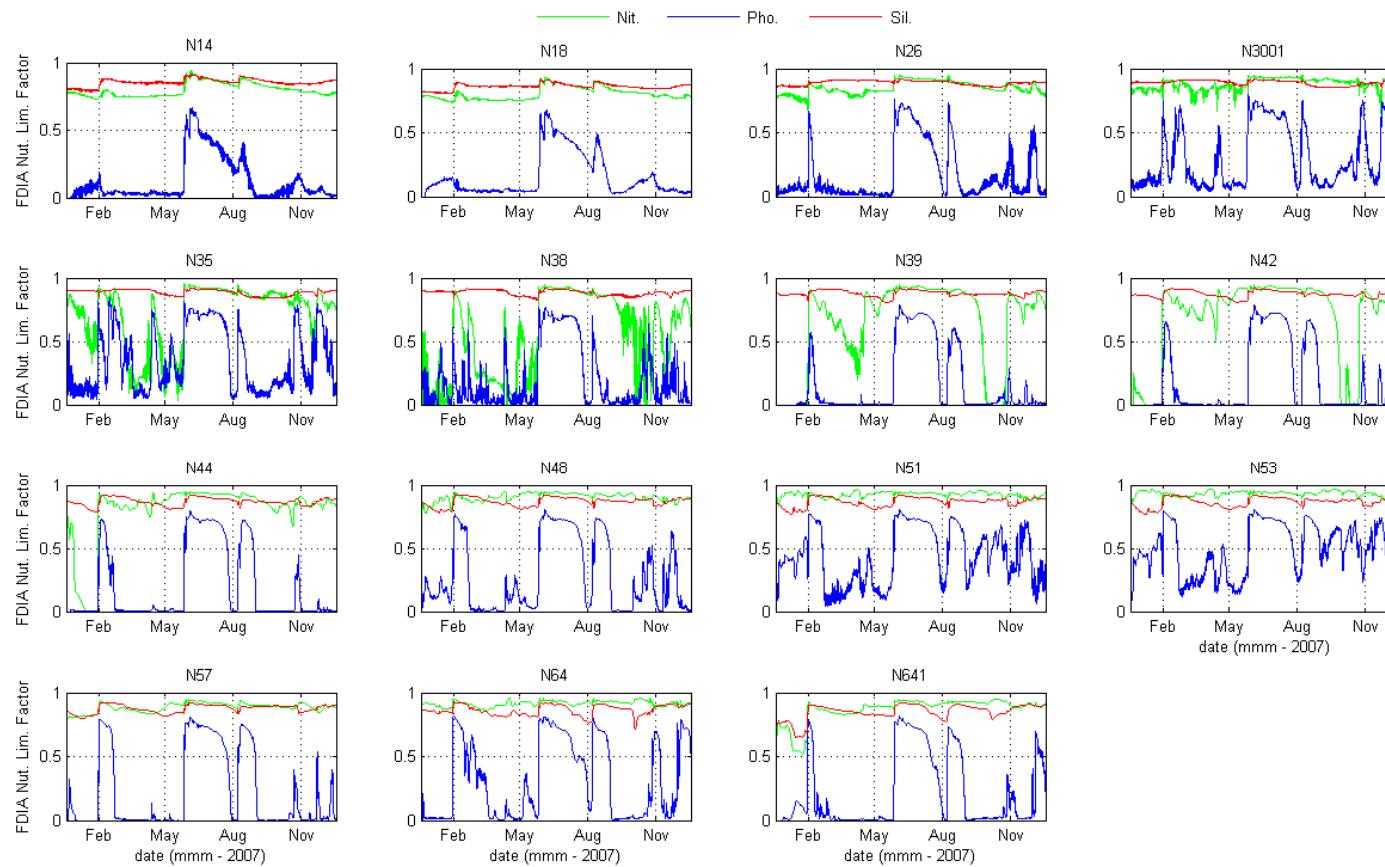


- **Figure 13-92 Nutrient Limitation Functions for the Green Algae Group Validation 2007 (Middle Reach only) (nitrogen (green) and phosphorus (blue))**

SINCLAIR KNIGHT MERZ



Water Quality Modelling of the Hawkesbury-Nepean River System

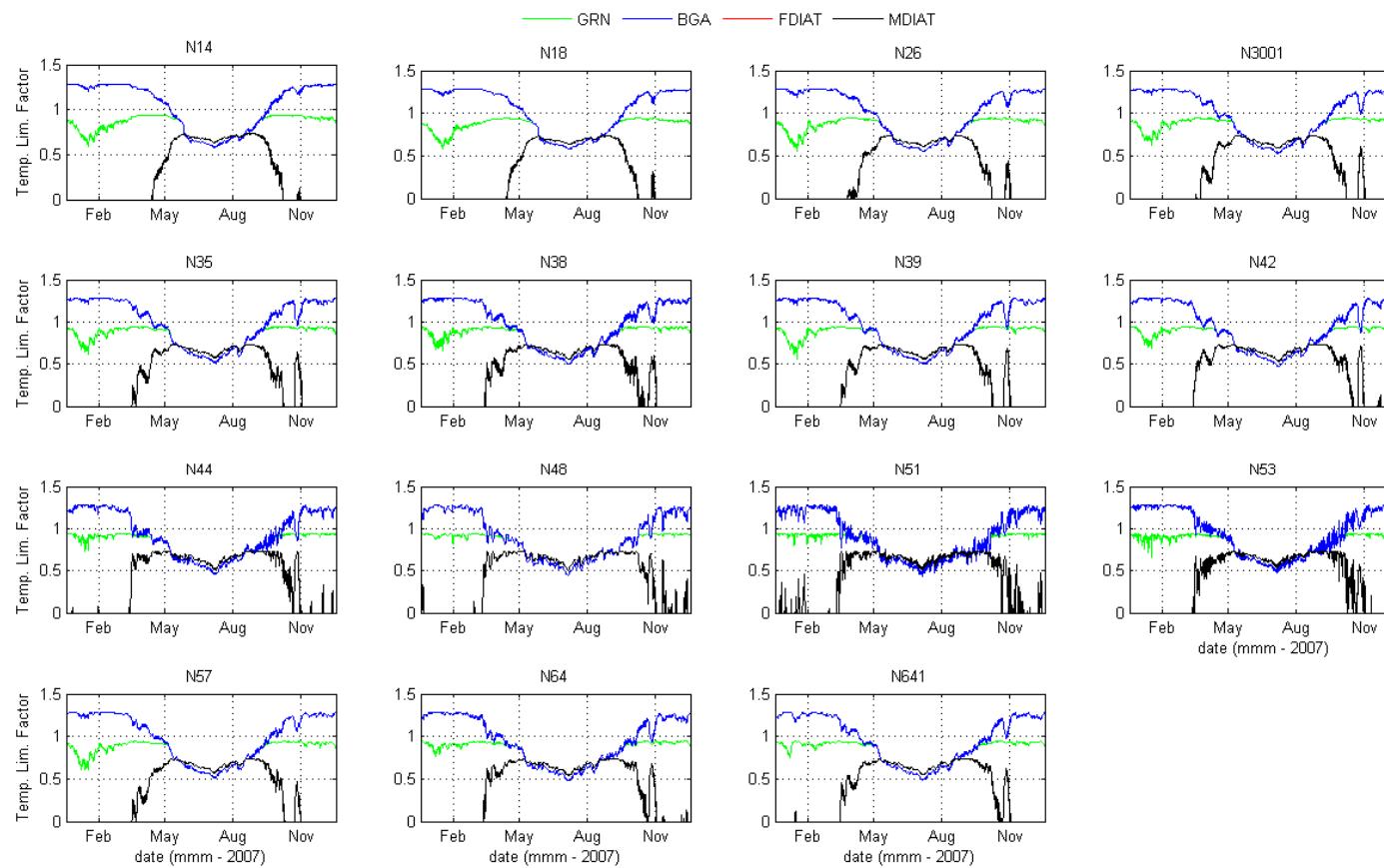


- **Figure 13-93 Nutrient Limitation Functions for the Diatoms Algae Group Validation 2007 (Middle Reach only) (nitrogen (green), phosphorus (blue) and silicate (red))**

SINCLAIR KNIGHT MERZ



Water Quality Modelling of the Hawkesbury-Nepean River System

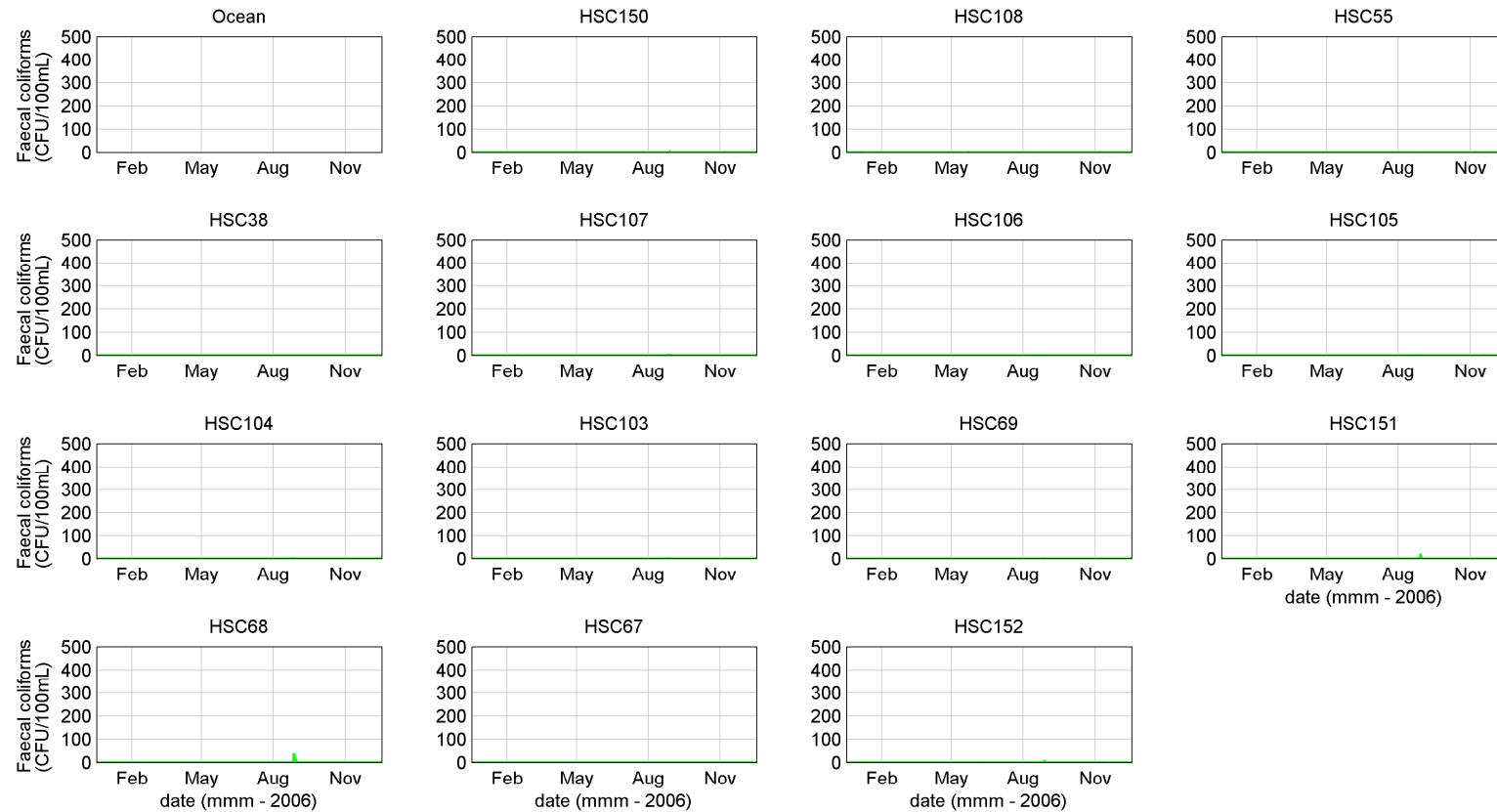


- **Figure 13-94 Temperature Limitation Functions for All Algae Groups Validation 2007 (Middle Reach only) (green algae (green), clue-green algae (blue), freshwater diatoms (red) and marine diatoms (black))**

SINCLAIR KNIGHT MERZ



Water Quality Modelling of the Hawkesbury-Nepean River System

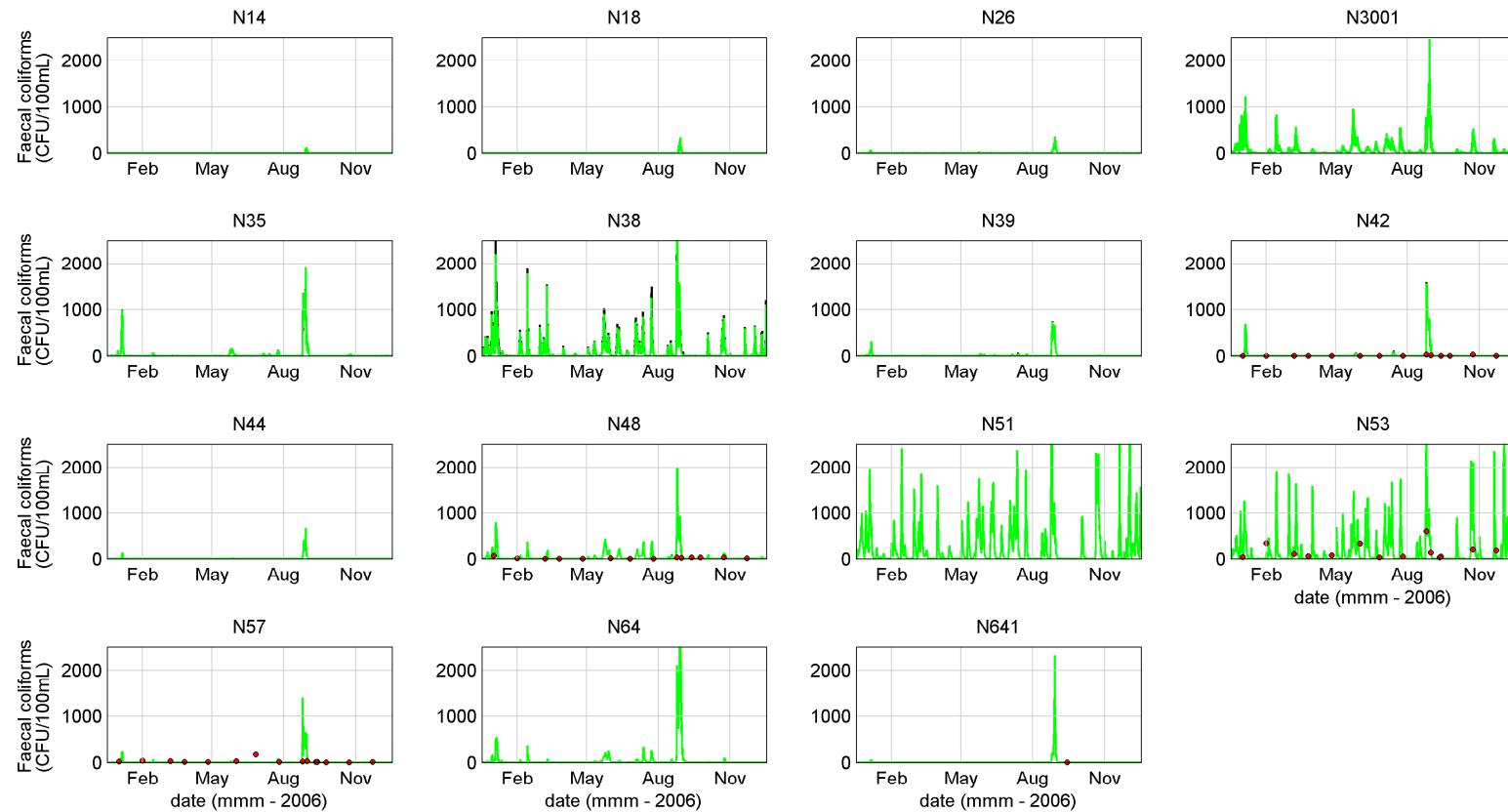


■ **Figure 13-95 Faecal coliforms Calibration 2006 (measured data (red), modelled surface (black) and modelled bottom (green))**

SINCLAIR KNIGHT MERZ



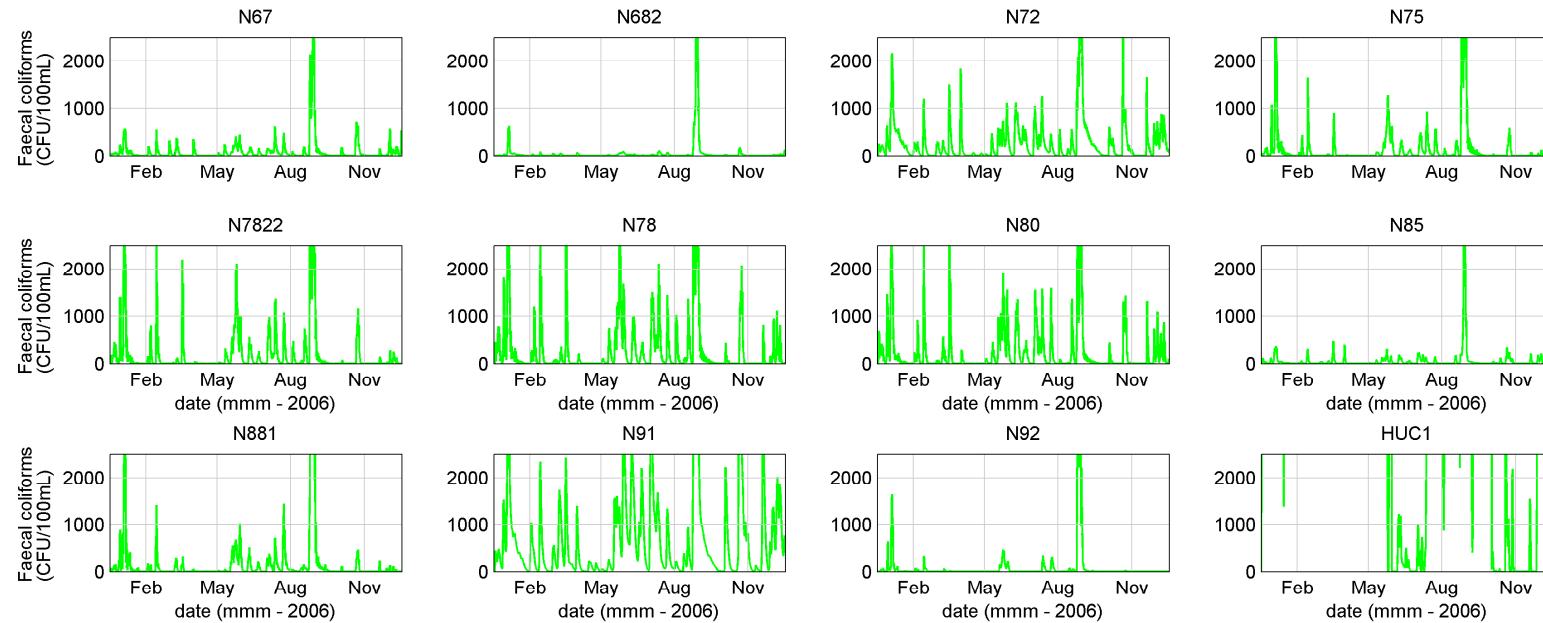
Water Quality Modelling of the Hawkesbury-Nepean River System



■ Figure 13-95 (Cont.) Faecal coliforms Calibration 2006 (measured data (red), modelled surface (black) and modelled bottom (green))



Water Quality Modelling of the Hawkesbury-Nepean River System

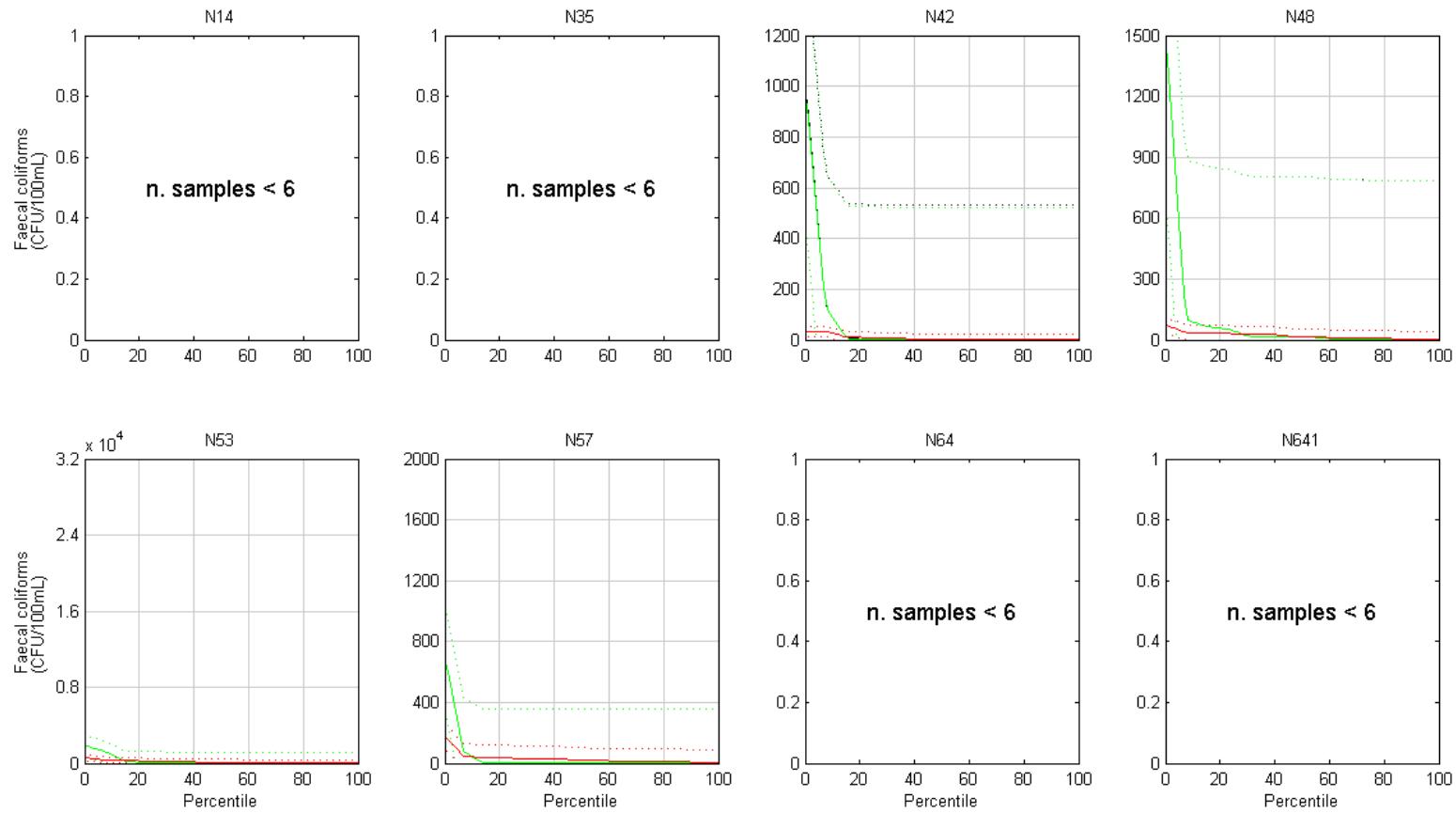


- **Figure 13-95 (Cont.) Faecal coliforms Calibration 2006 (measured data (red), modelled surface (black) and modelled bottom (green))**

SINCLAIR KNIGHT MERZ

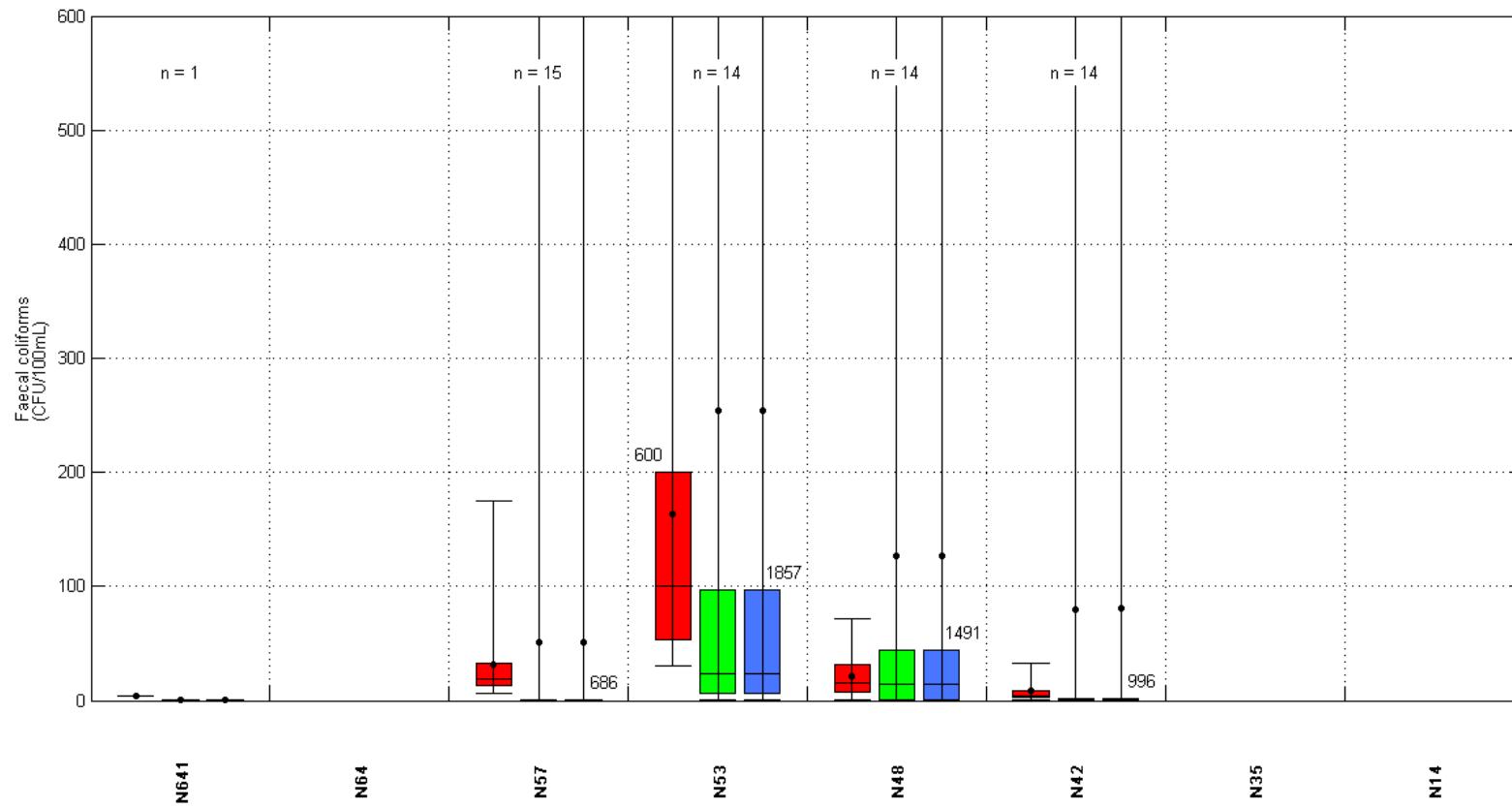


Water Quality Modelling of the Hawkesbury-Nepean River System



- **Figure 13-96 Exceedance Plots – Faecal coliforms Calibration 2006 (+/- 2SD) (measured data (red), modelled surface (black) and modelled bottom (green))**

Water Quality Modelling of the Hawkesbury-Nepean River System

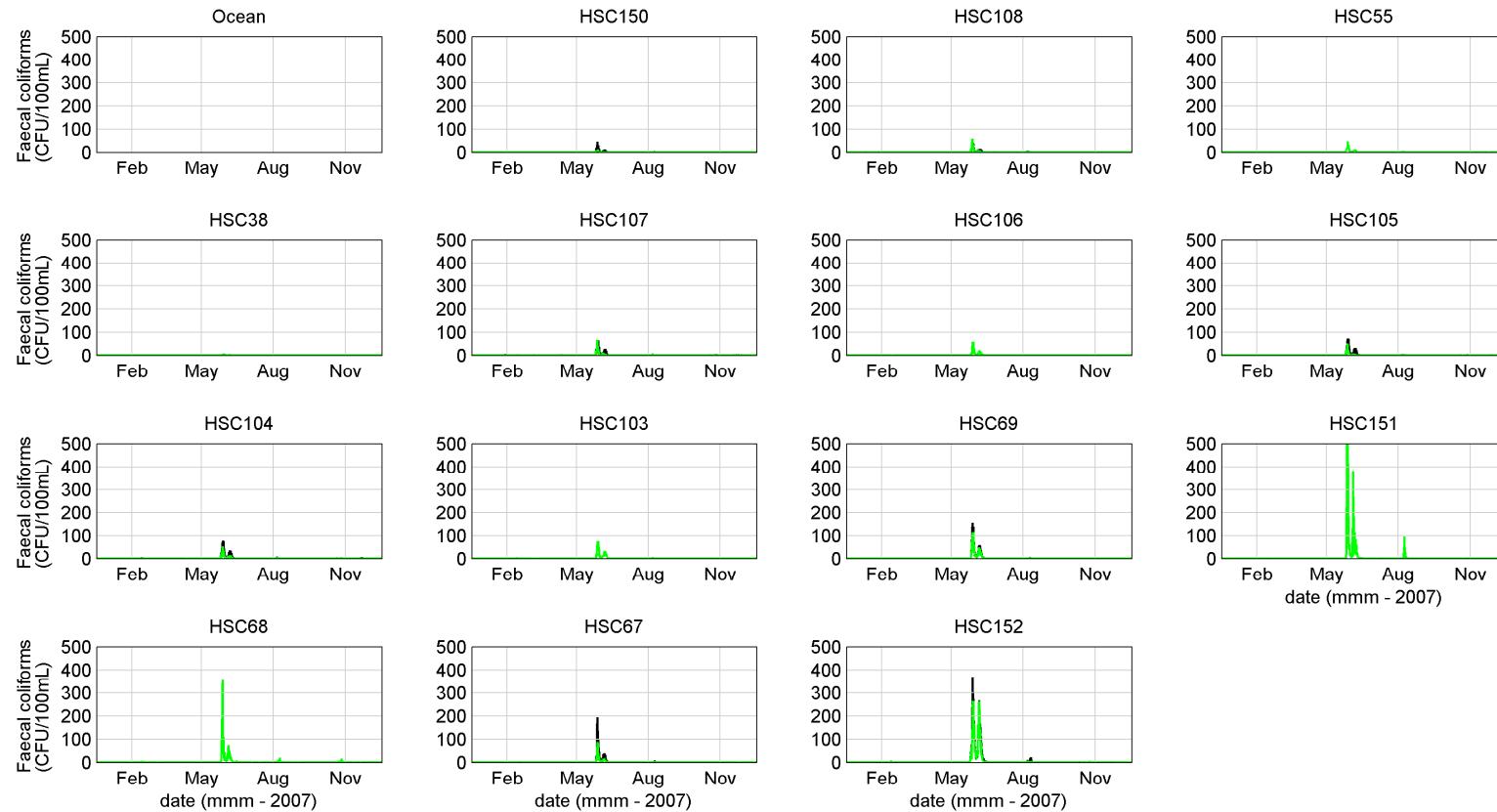


- **Figure 13-97 Box and Whisker Plots – Faecal coliforms Calibration 2006 (measured data (red), modelled surface (blue) and modelled bottom (green))**

SINCLAIR KNIGHT MERZ



Water Quality Modelling of the Hawkesbury-Nepean River System

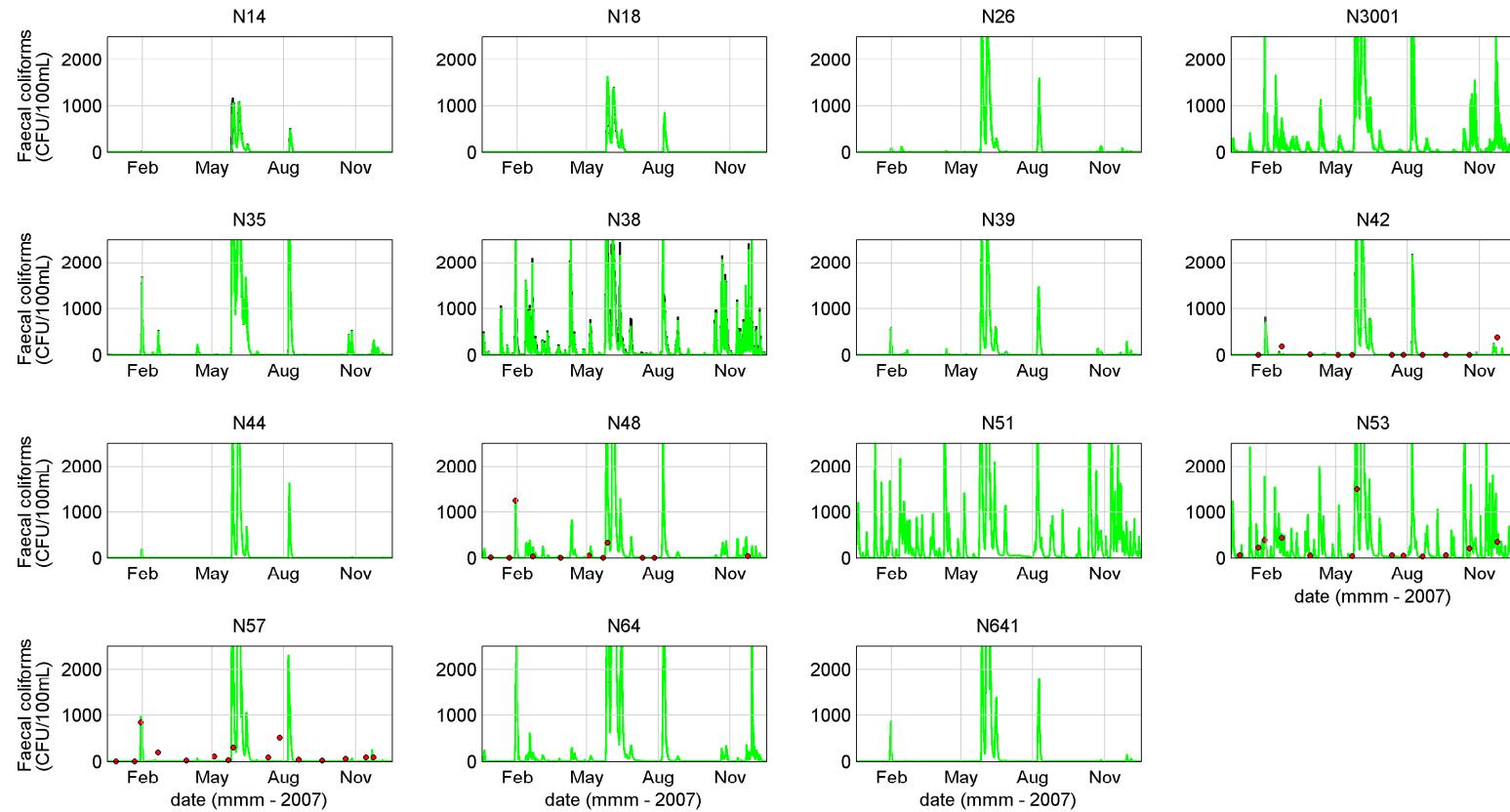


■ **Figure 13-98 Faecal coliforms Validation 2007 (measured data (red), modelled surface (black) and modelled bottom (green))**

SINCLAIR KNIGHT MERZ



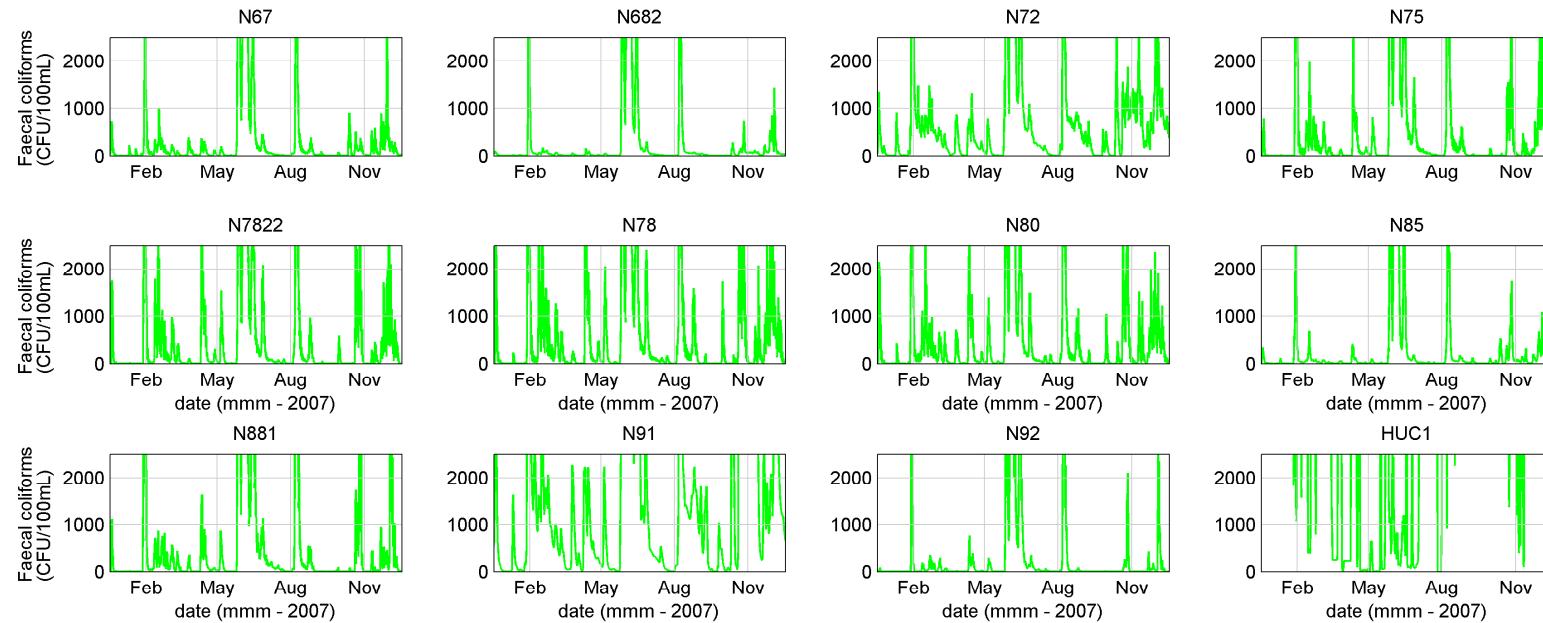
Water Quality Modelling of the Hawkesbury-Nepean River System



■ **Figure 13-98 (Cont.) Faecal coliforms Validation 2007 (measured data (red), modelled surface (black) and modelled bottom (green))**



Water Quality Modelling of the Hawkesbury-Nepean River System

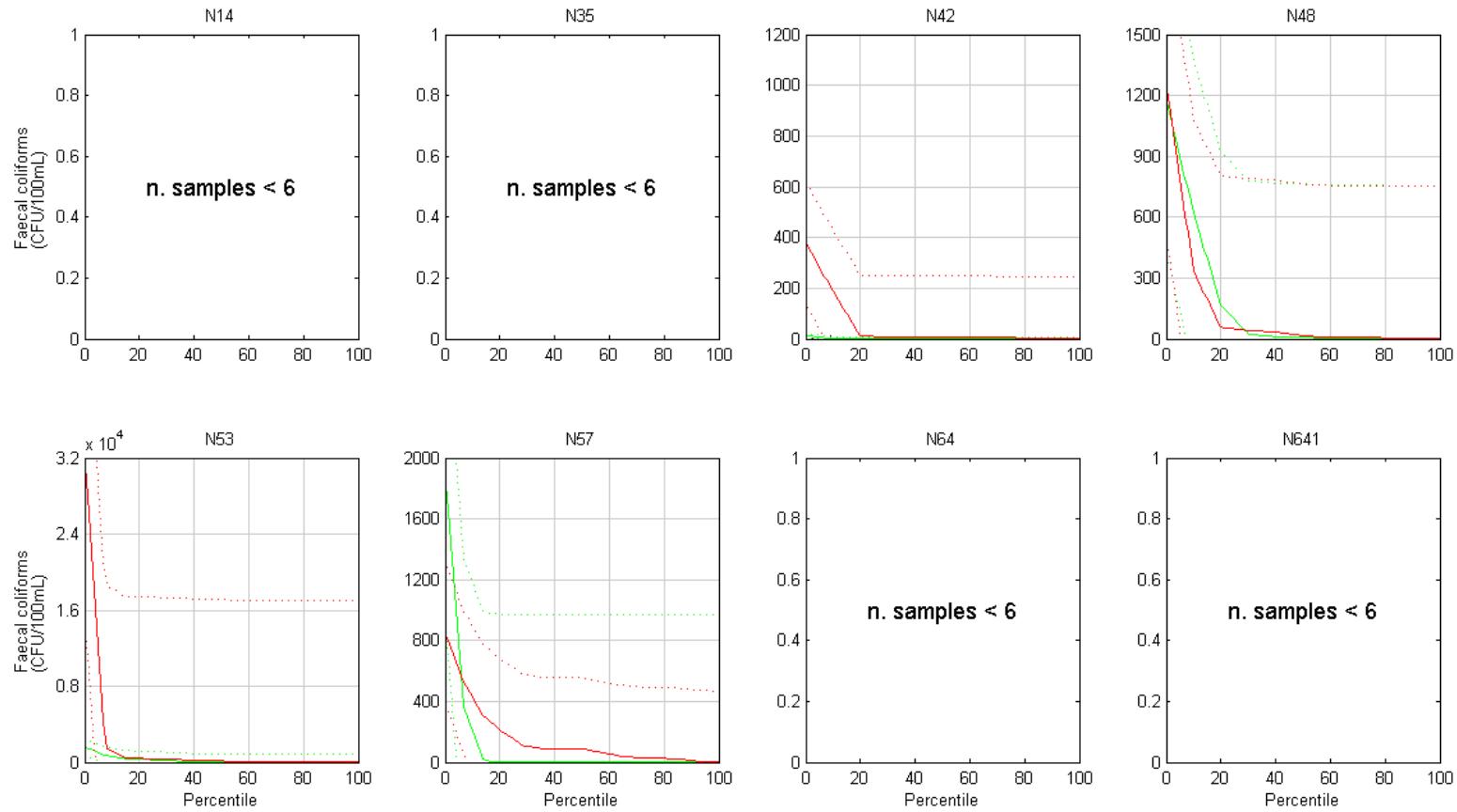


■ Figure 13-98 (Cont.) Faecal coliforms Validation 2007 (measured data (red), modelled surface (black) and modelled bottom (green))

SINCLAIR KNIGHT MERZ

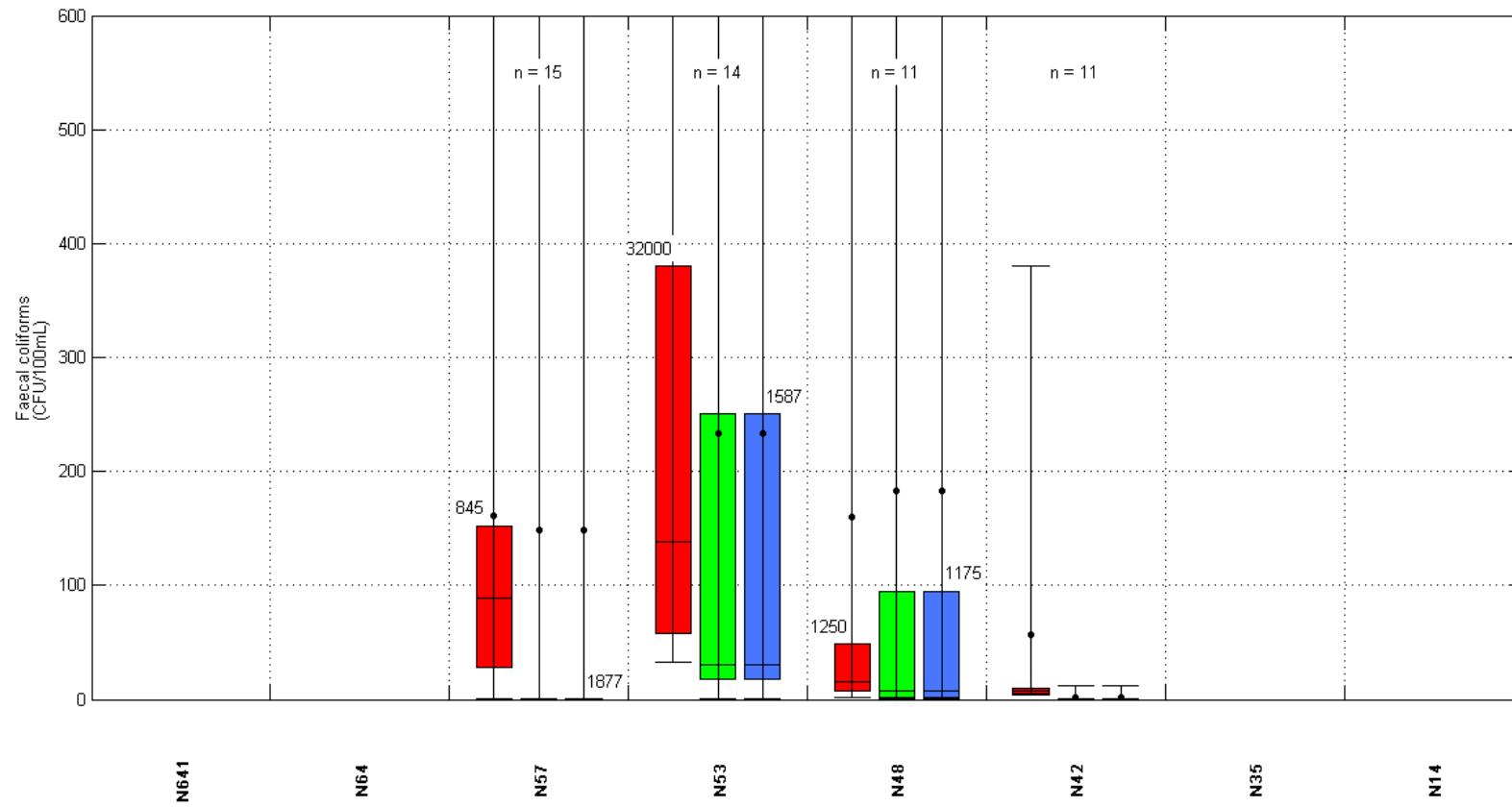


Water Quality Modelling of the Hawkesbury-Nepean River System



- **Figure 13-99 Exceedance Plots – Faecal coliforms Validation 2007 (+/- 2SD) (measured data (red), modelled surface (black) and modelled bottom (green))**

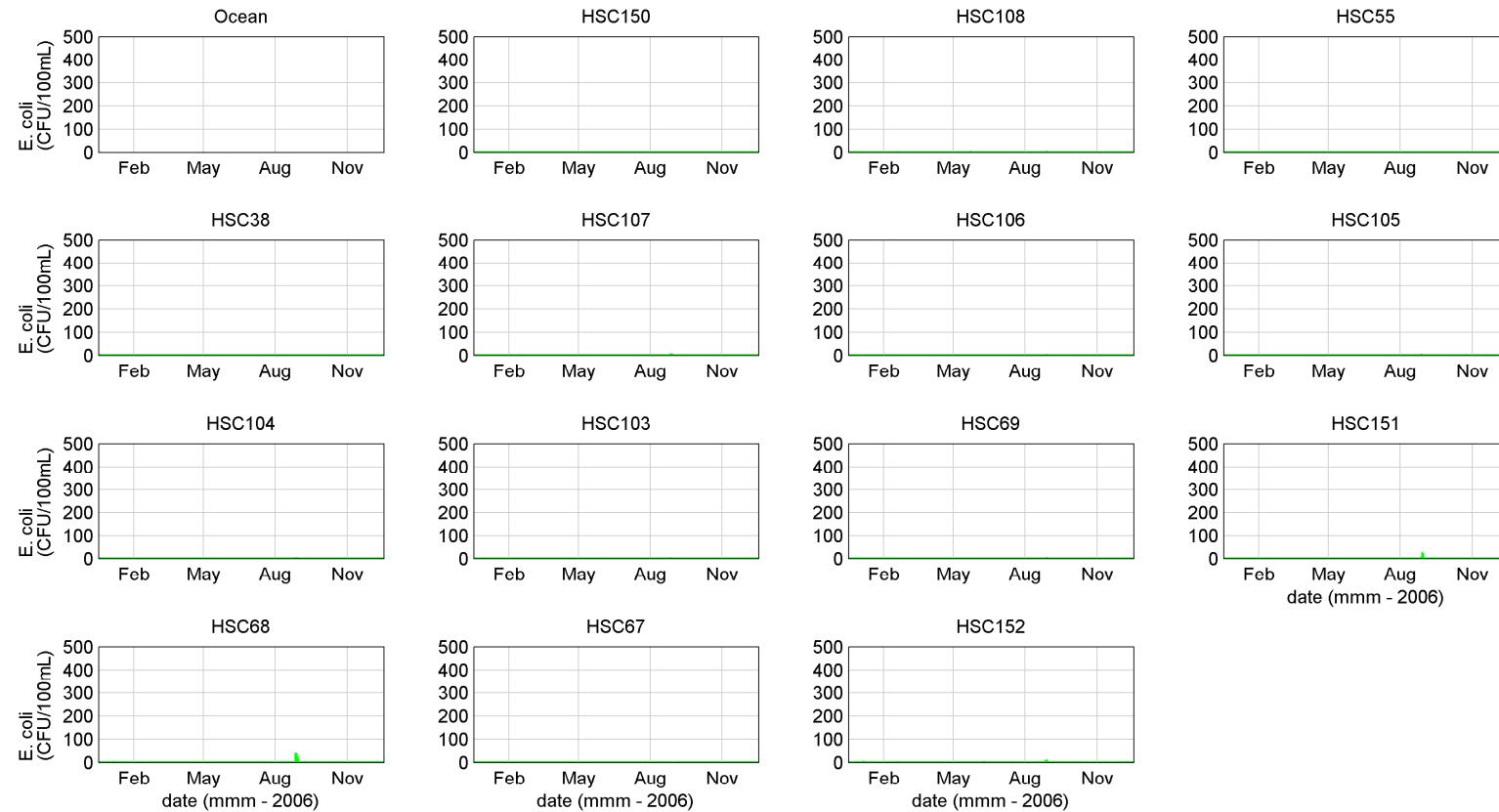
Water Quality Modelling of the Hawkesbury-Nepean River System



- Figure 13-100 Box and Whisker Plots – Faecal coliforms Validation 2007 (measured data (red), modelled surface (black) and modelled bottom (green))



Water Quality Modelling of the Hawkesbury-Nepean River System

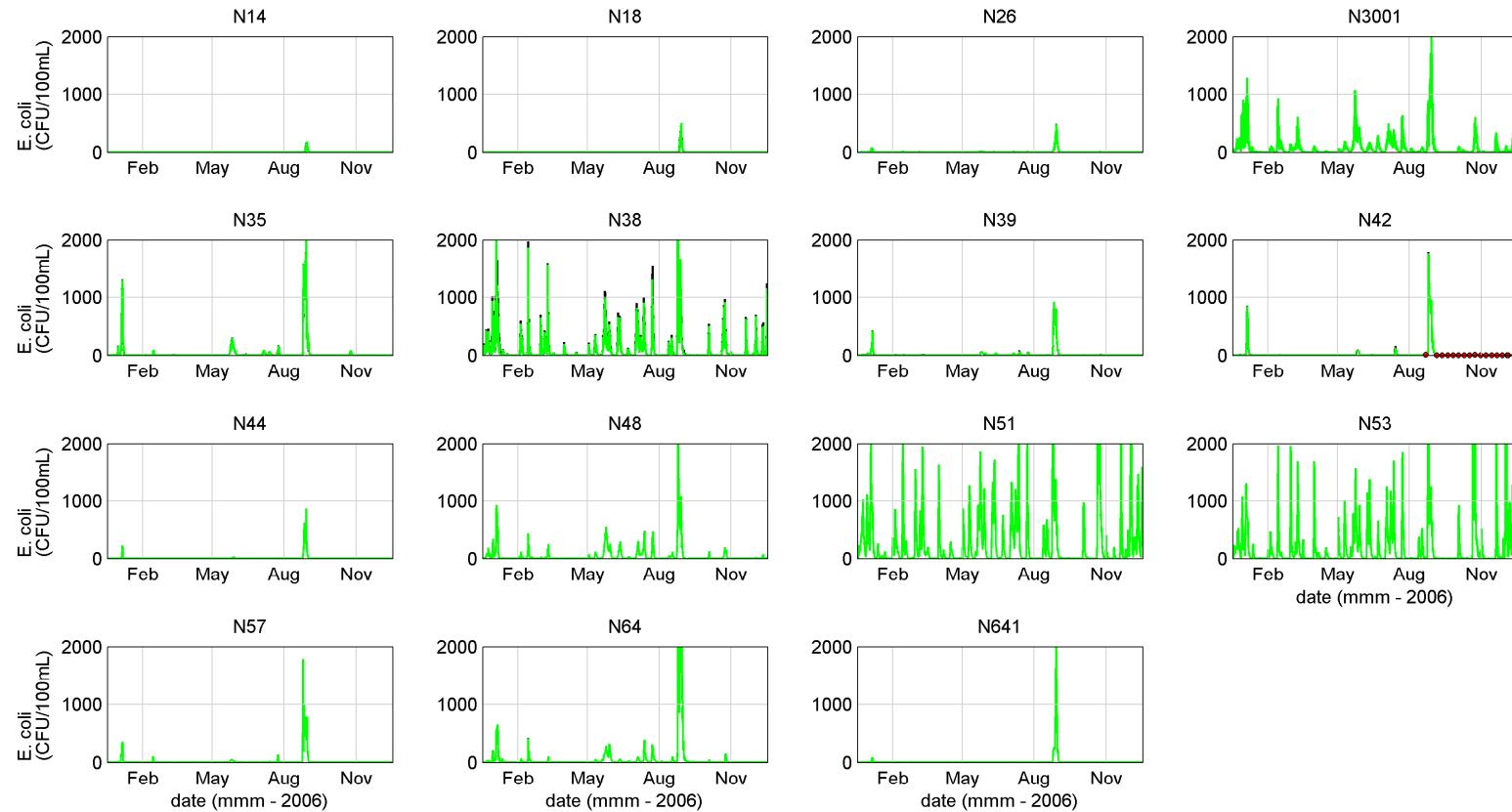


■ **Figure 13-101 *E. coli* Calibration 2006 (measured data (red), modelled surface (black) and modelled bottom (green))**

SINCLAIR KNIGHT MERZ



Water Quality Modelling of the Hawkesbury-Nepean River System

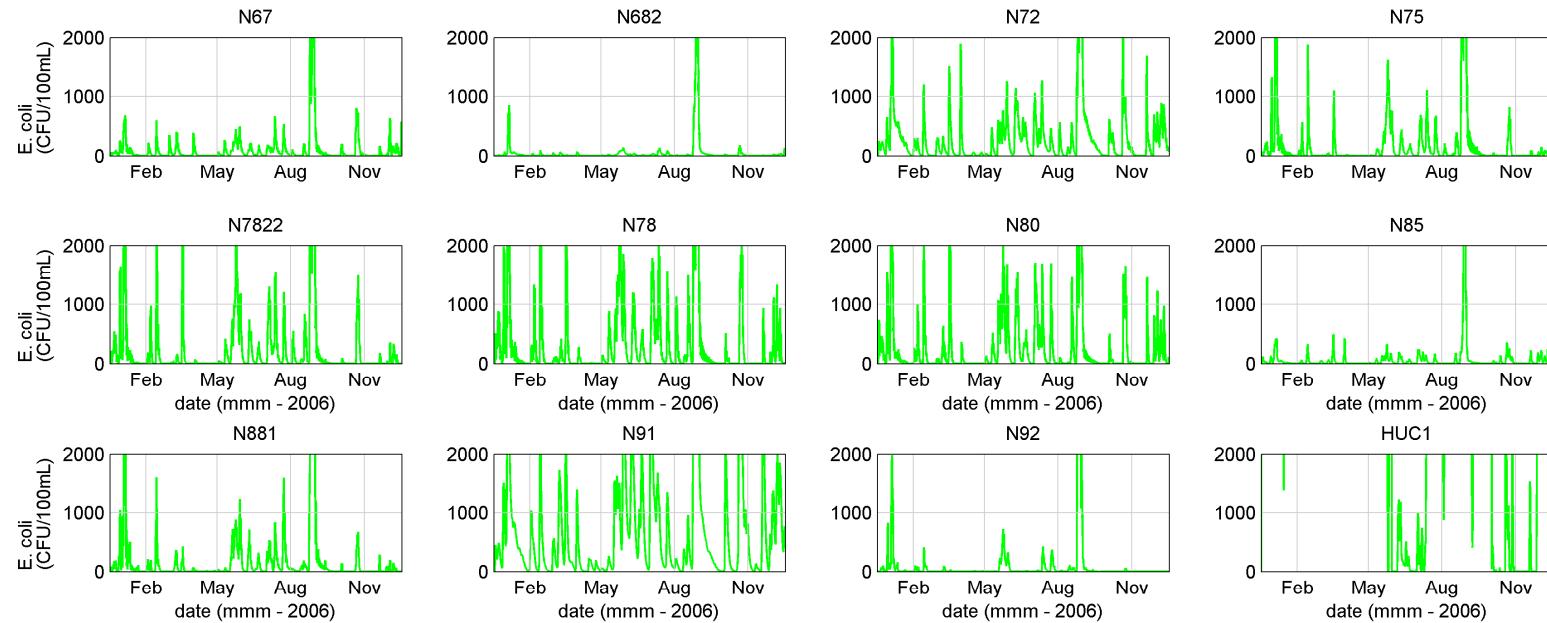


■ Figure 13-101 (Cont.) *E. coli* Calibration 2006 (measured data (red), modelled surface (black) and modelled bottom (green))

SINCLAIR KNIGHT MERZ



Water Quality Modelling of the Hawkesbury-Nepean River System

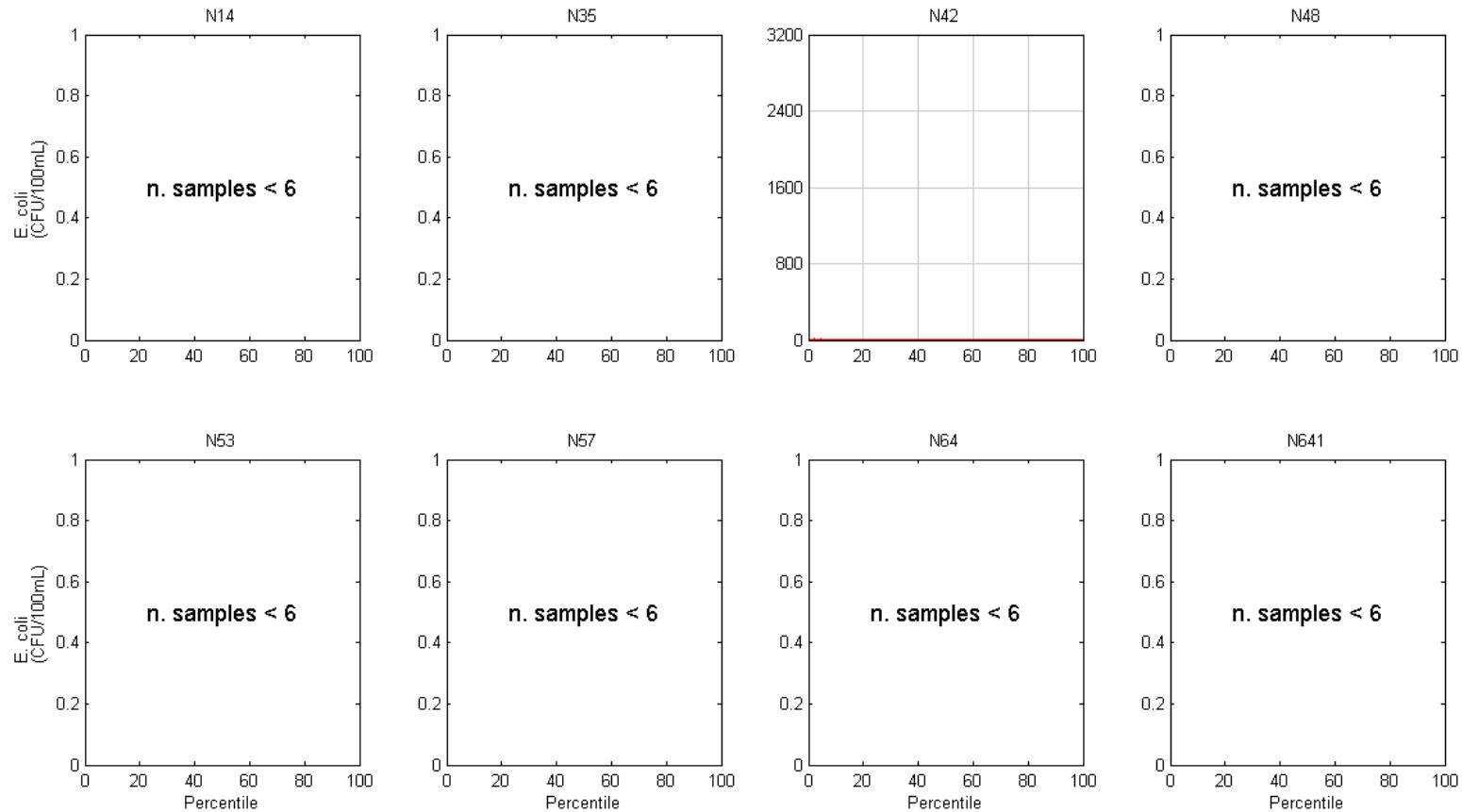


- **Figure 13-101 (Cont.) *E. coli* Calibration 2006 (measured data (red), modelled surface (black) and modelled bottom (green))**

SINCLAIR KNIGHT MERZ



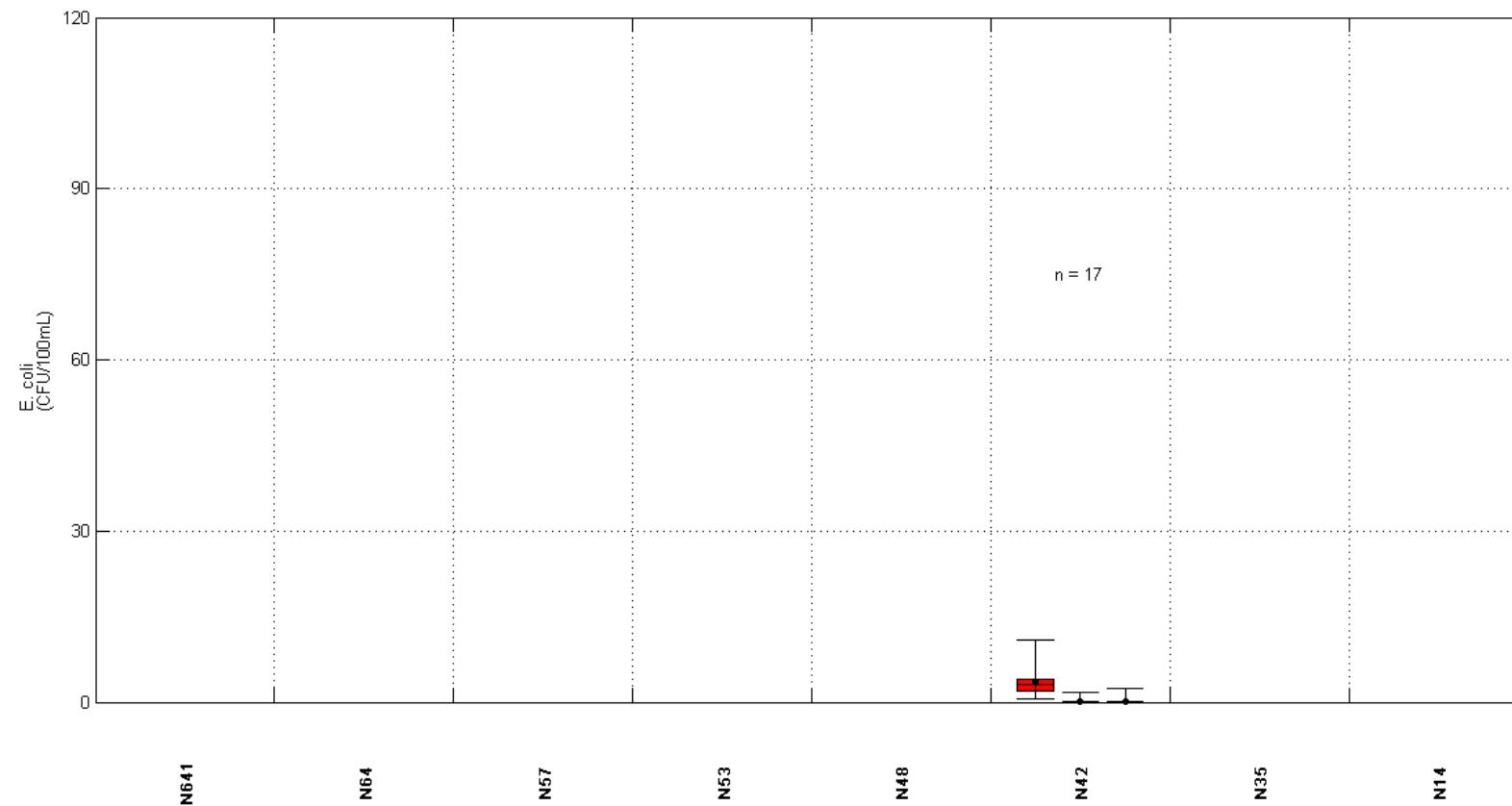
Water Quality Modelling of the Hawkesbury-Nepean River System



- **Figure 13-102 Exceedance Plots – *E. coli* Calibration 2006(+/- 2SD) (measured data (red), modelled surface (black) and modelled bottom (green))**



Water Quality Modelling of the Hawkesbury-Nepean River System

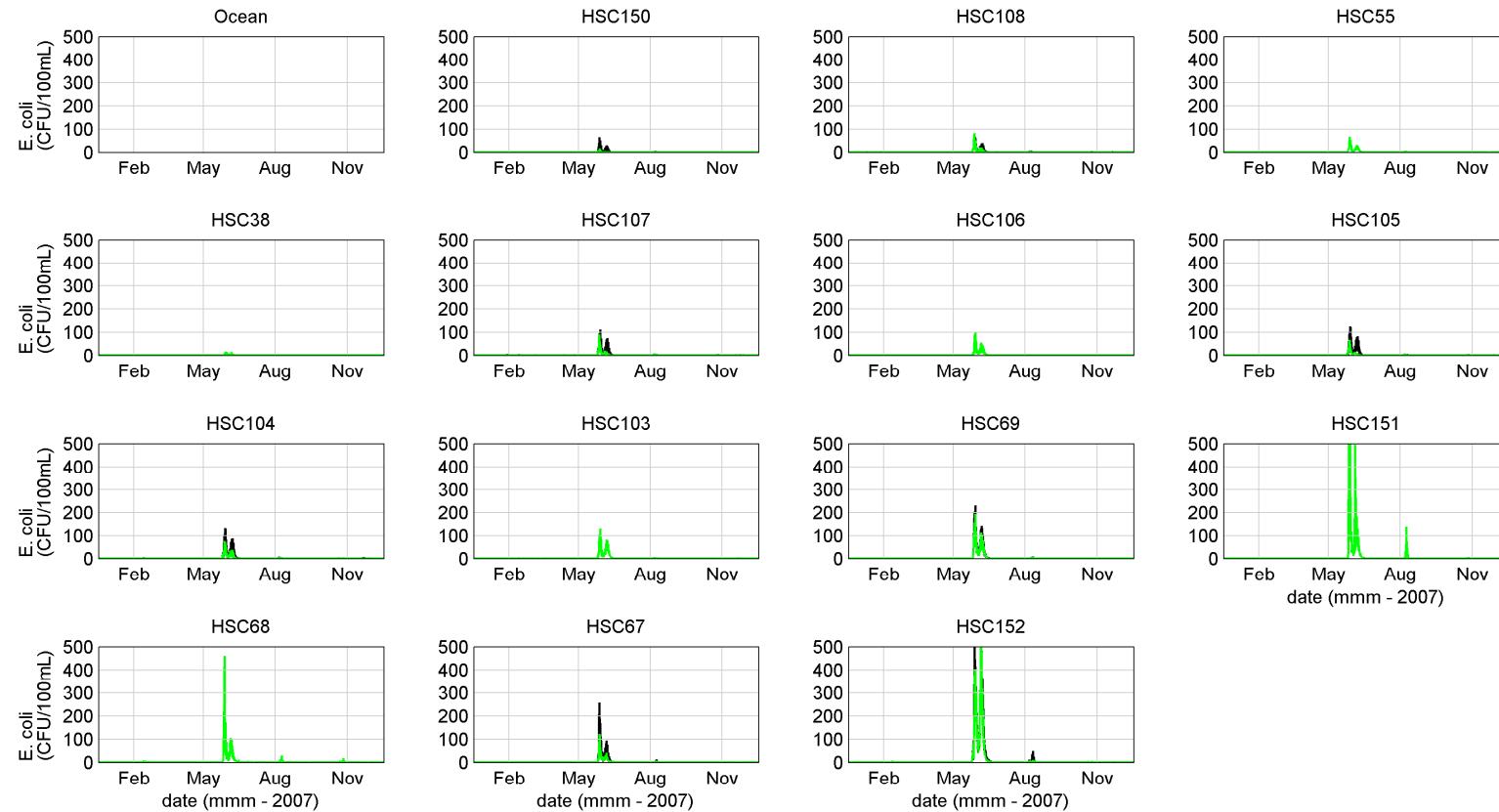


- **Figure 13-103 Box and Whisker Plots – E. coli Calibration 2006 (measured data (red), modelled surface (blue) and modelled bottom (green))**

SINCLAIR KNIGHT MERZ



Water Quality Modelling of the Hawkesbury-Nepean River System

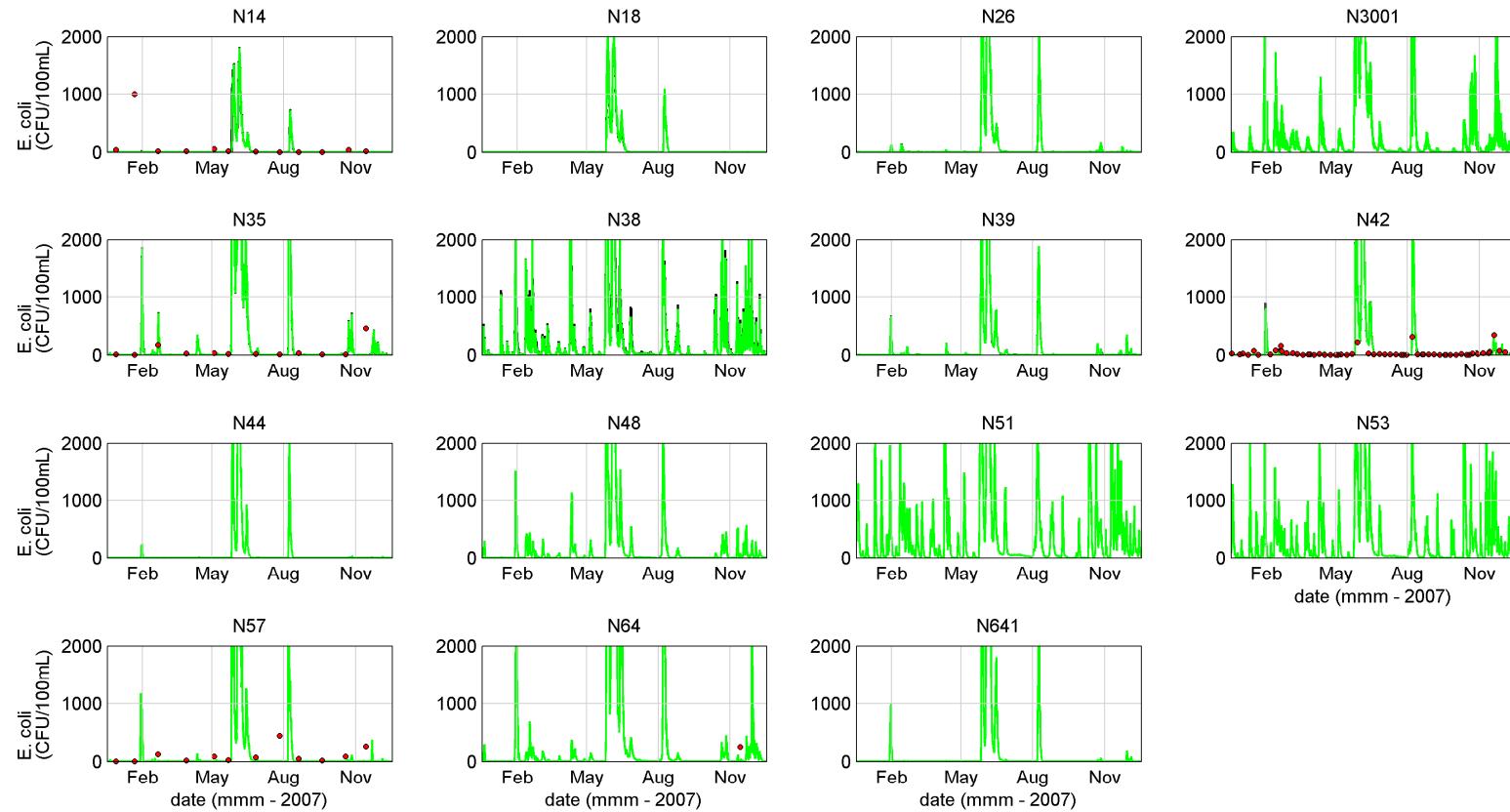


■ Figure 13-104 *E. coli* Validation 2007 (measured data (red), modelled surface (black) and modelled bottom (green))

SINCLAIR KNIGHT MERZ



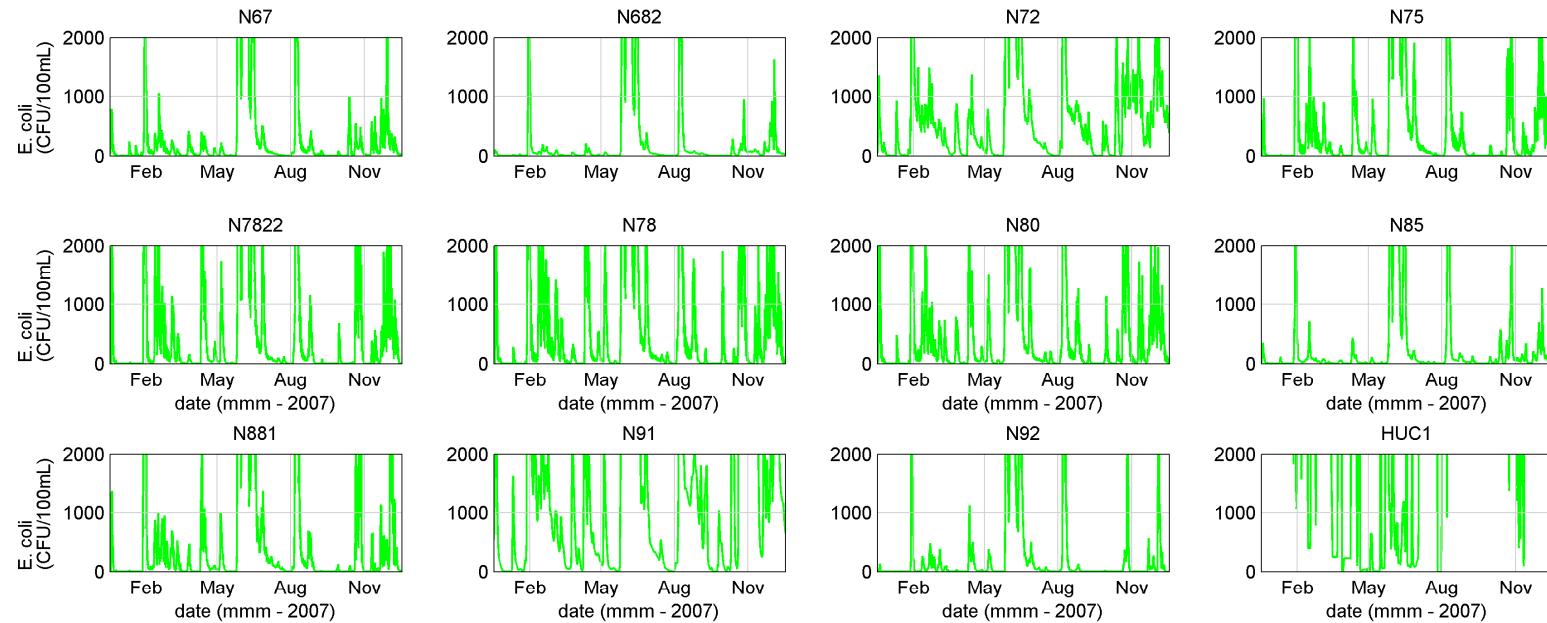
Water Quality Modelling of the Hawkesbury-Nepean River System



■ **Figure 13-104 (Cont.) *E. coli* Validation 2007 (measured data (red), modelled surface (black) and modelled bottom (green))**



Water Quality Modelling of the Hawkesbury-Nepean River System

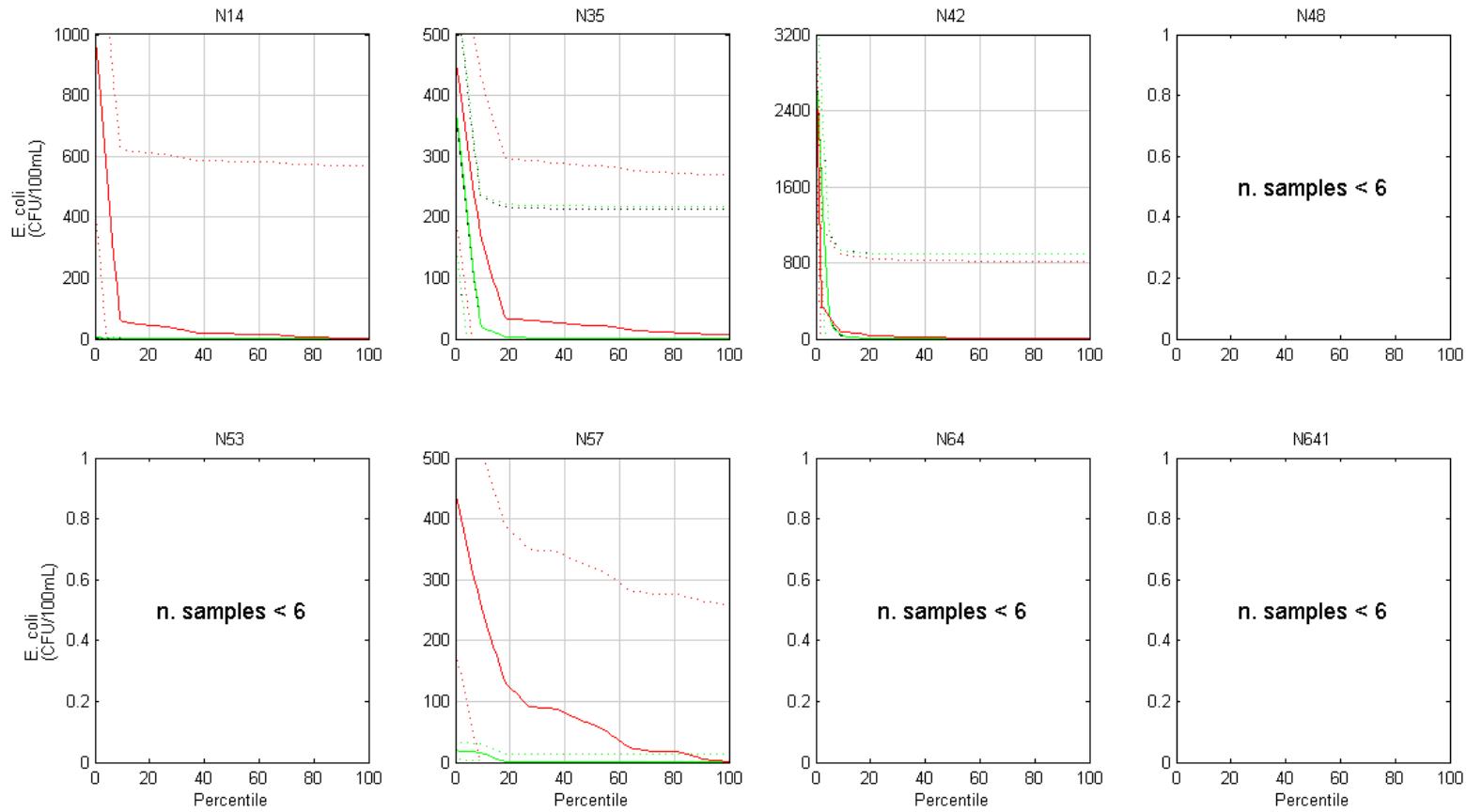


- **Figure 13-104 (Cont.) *E. coli* Validation 2007 (measured data (red), modelled surface (black) and modelled bottom (green))**

SINCLAIR KNIGHT MERZ

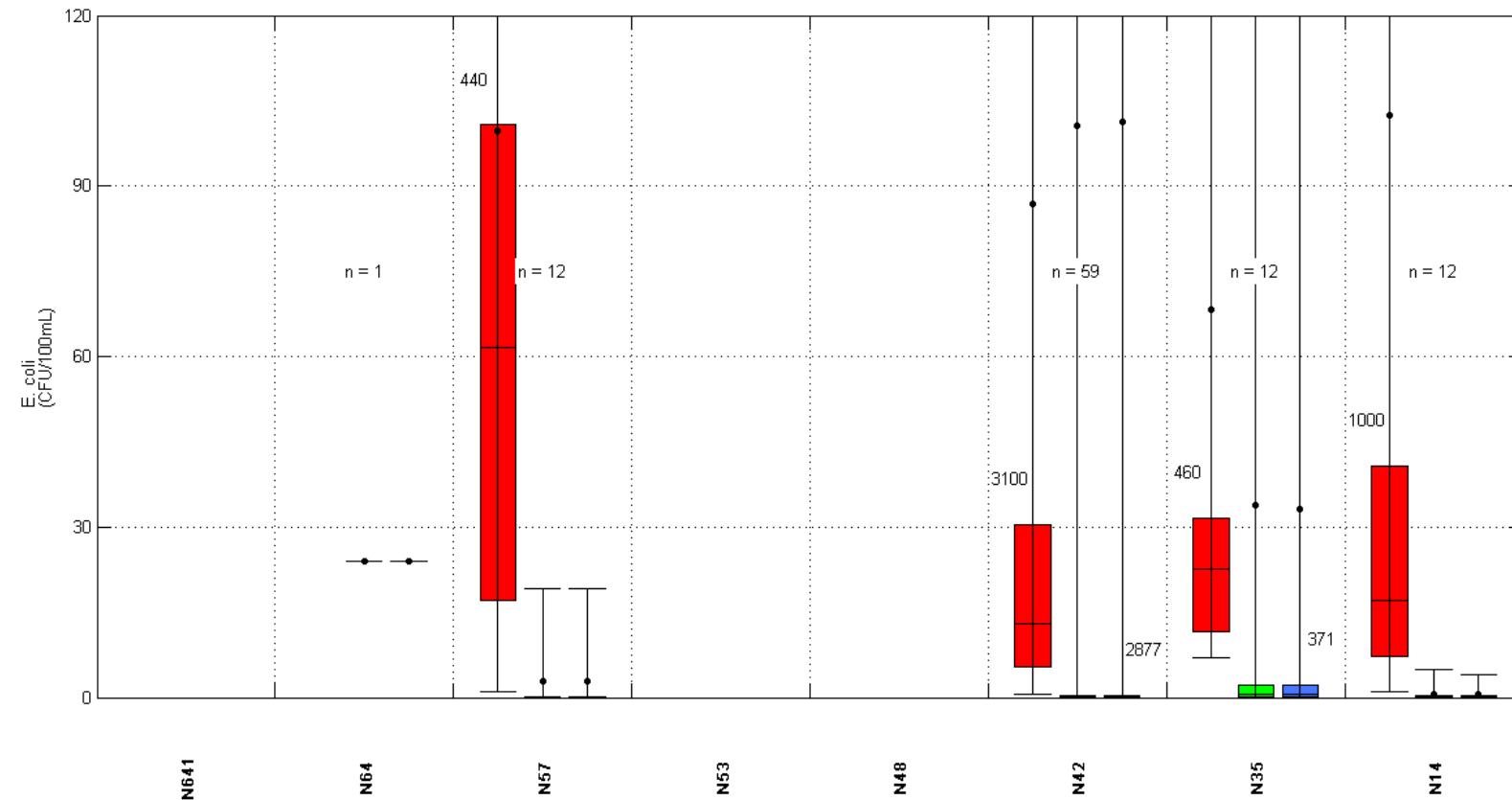


Water Quality Modelling of the Hawkesbury-Nepean River System



- **Figure 13-105 Exceedance Plots – *E. coli* Validation 2007 (+/- 2SD) (measured data (red), modelled surface (black) and modelled bottom (green))**

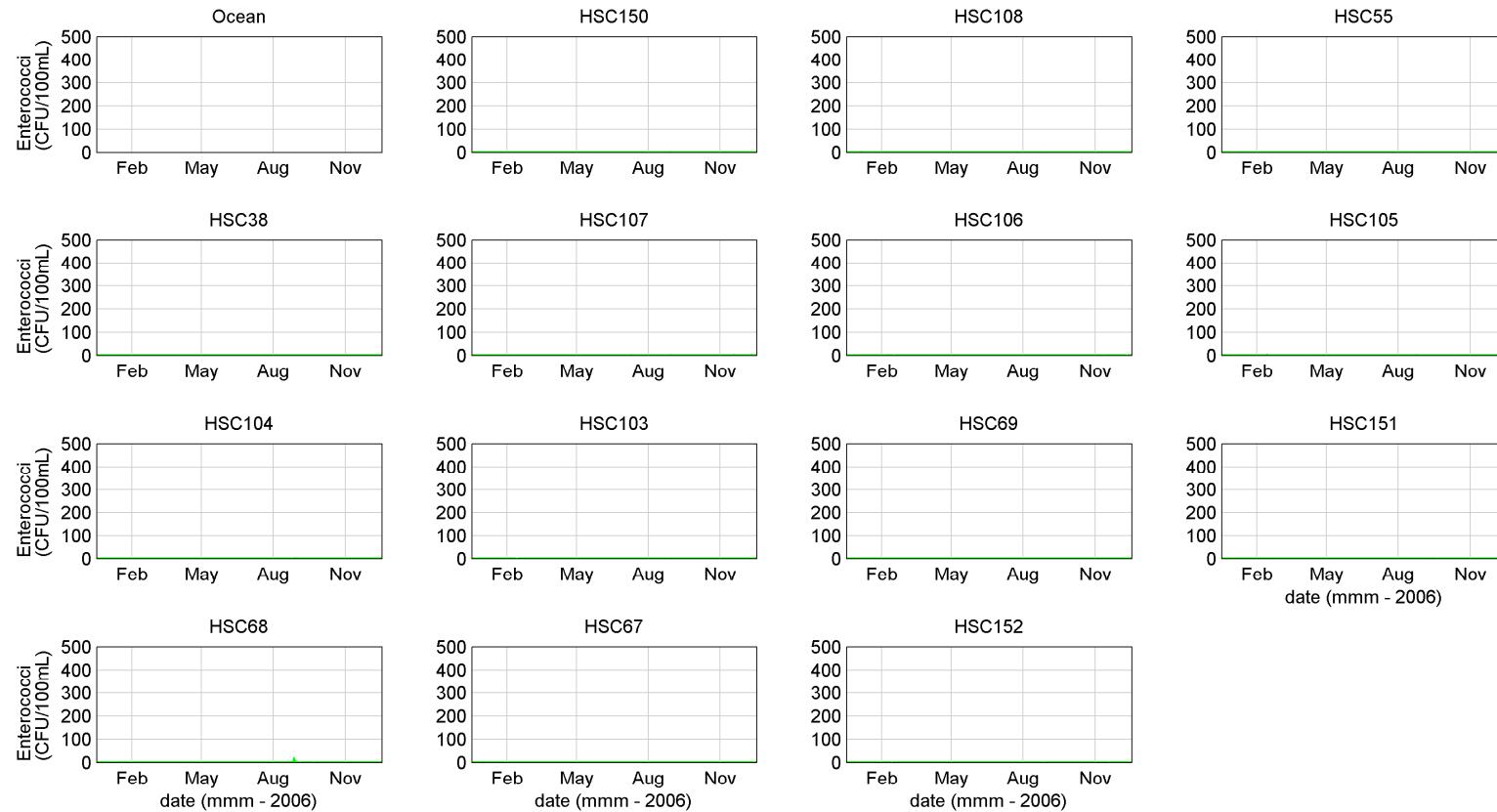
Water Quality Modelling of the Hawkesbury-Nepean River System



- Figure 13-106 Box and Whisker Plots – *E. coli* Validation 2007 (measured data (red), modelled surface (black) and modelled bottom (green))



Water Quality Modelling of the Hawkesbury-Nepean River System

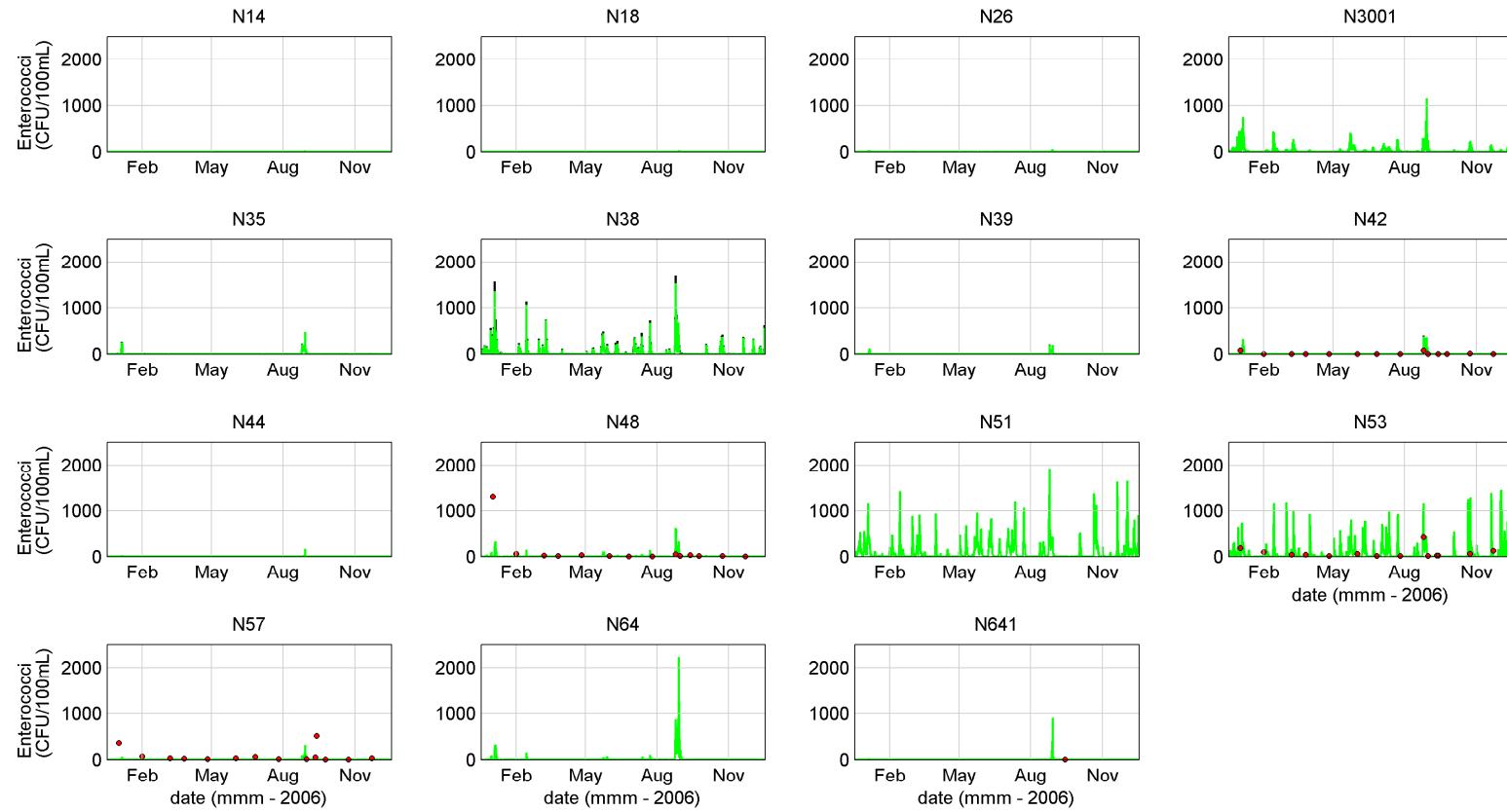


■ **Figure 13-107 Enterococci Calibration 2006 (measured data (red), modelled surface (black) and modelled bottom (green))**

SINCLAIR KNIGHT MERZ



Water Quality Modelling of the Hawkesbury-Nepean River System

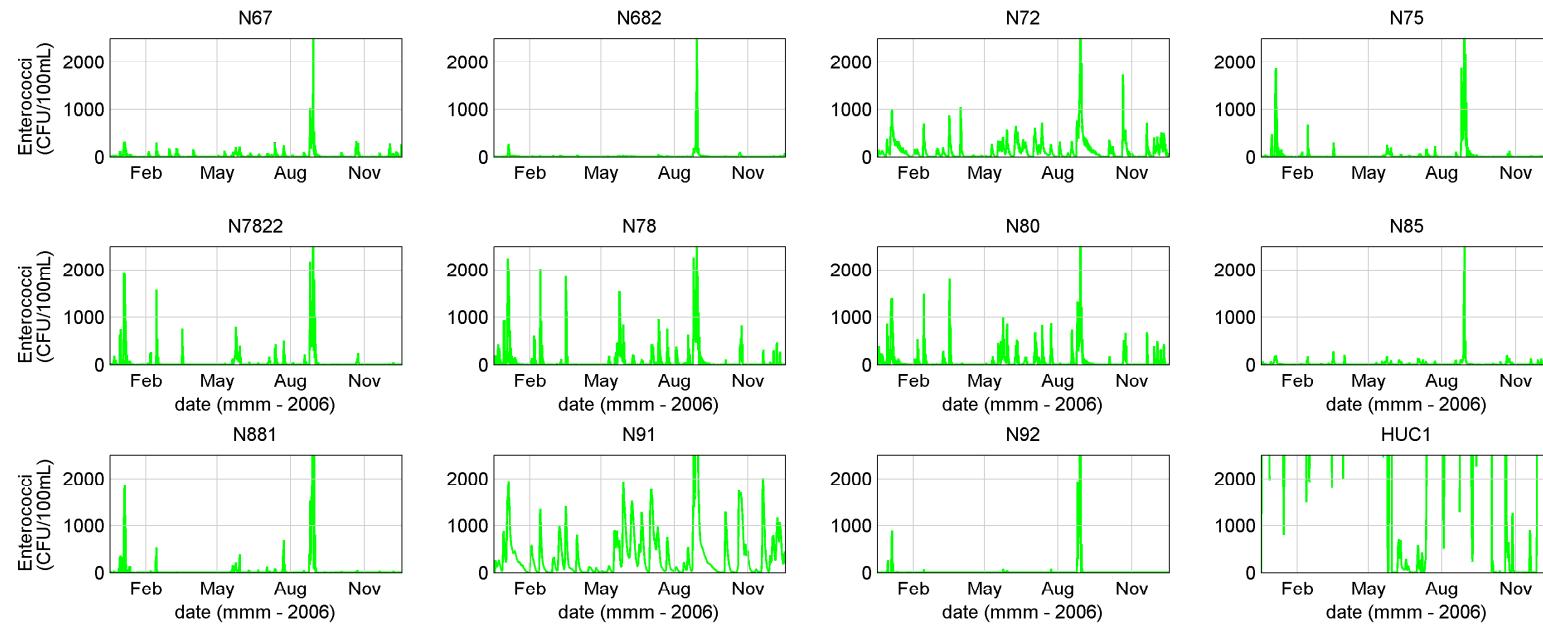


■ **Figure 13-107 (Cont.) Enterococci Calibration 2006 (measured data (red), modelled surface (black) and modelled bottom (green))**

SINCLAIR KNIGHT MERZ



Water Quality Modelling of the Hawkesbury-Nepean River System

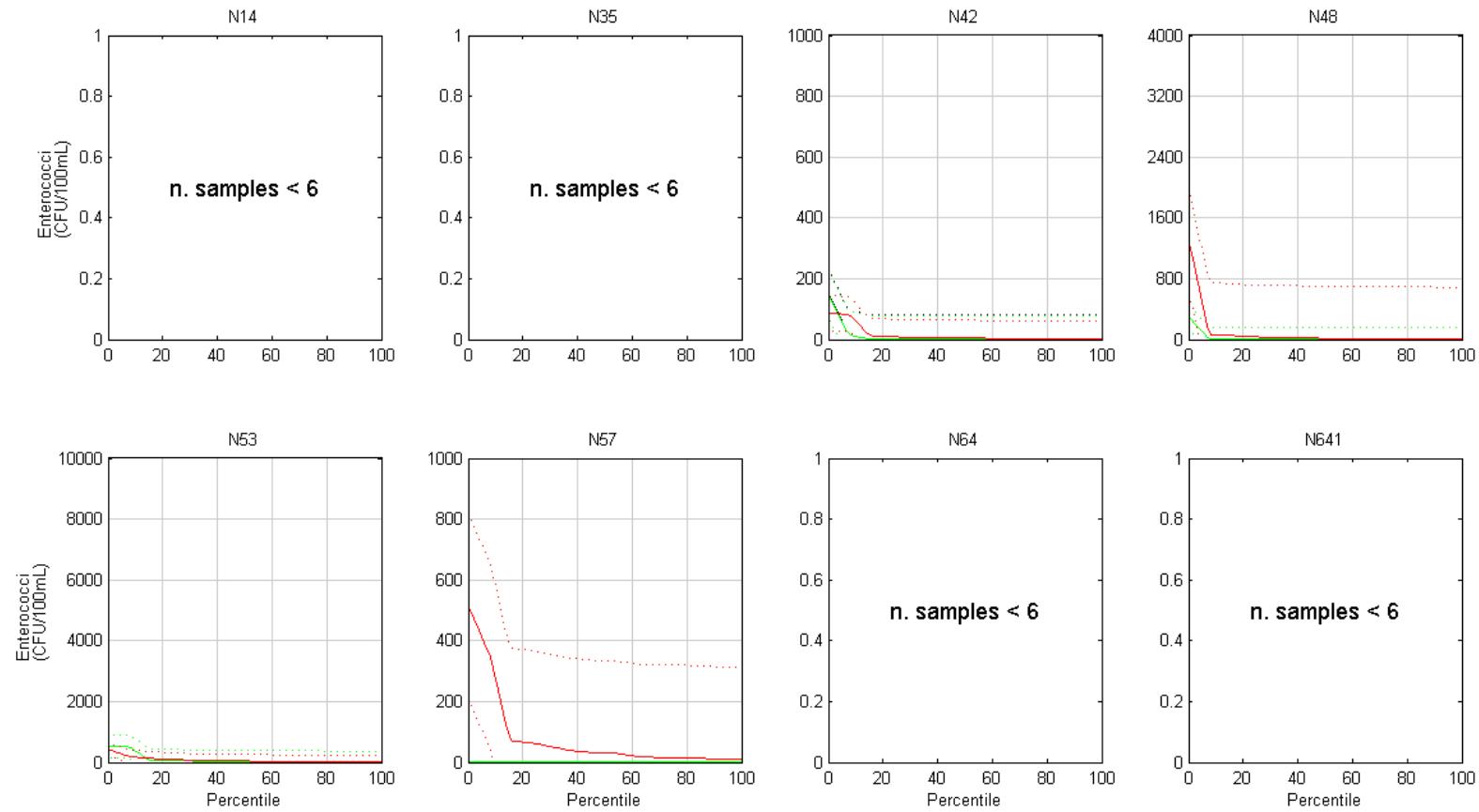


- **Figure 13-107 (Cont.) Enterococci Calibration 2006 (measured data (red), modelled surface (black) and modelled bottom (green))**

SINCLAIR KNIGHT MERZ



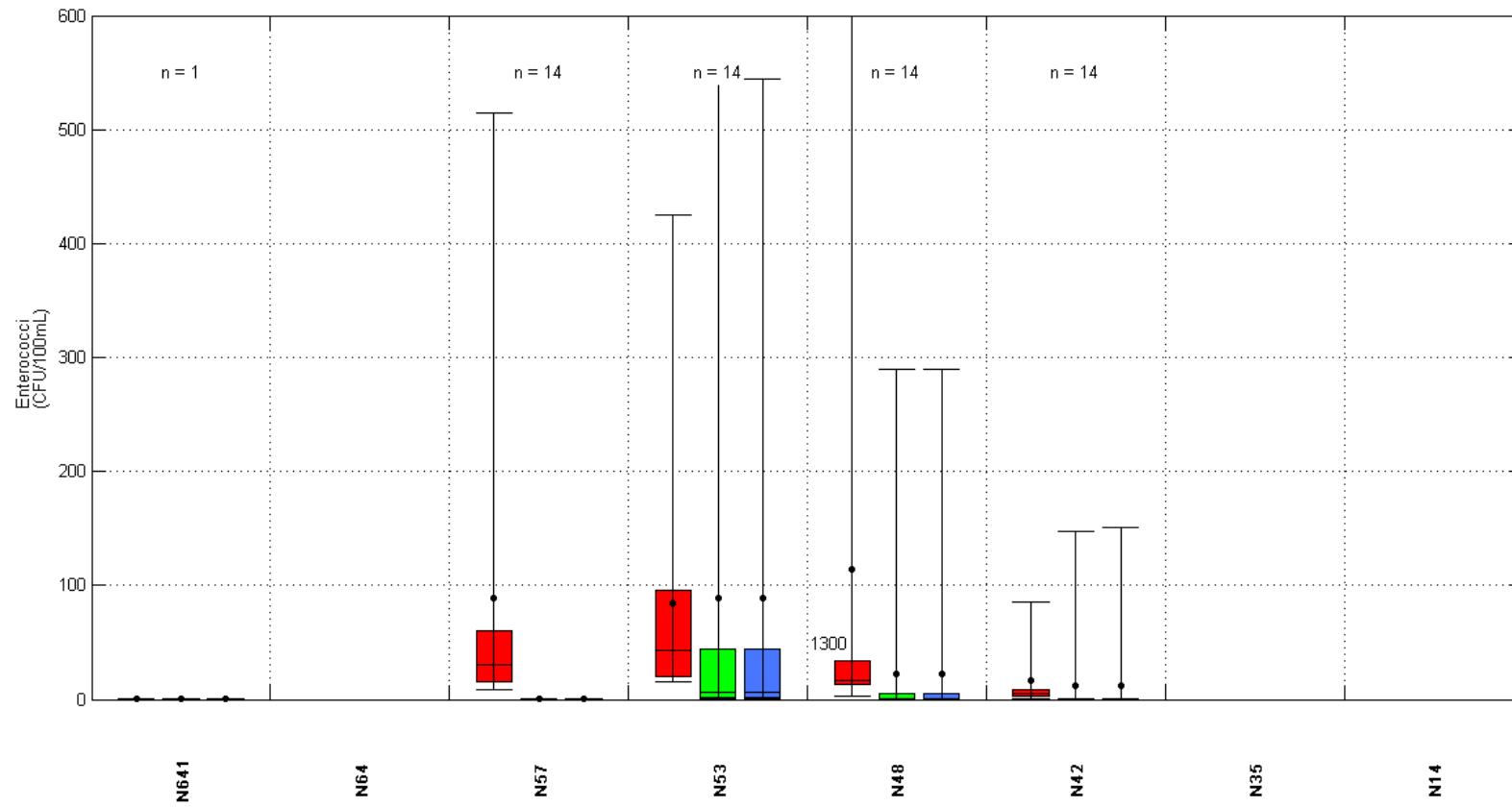
Water Quality Modelling of the Hawkesbury-Nepean River System



- Figure 13-108 Exceedance Plots – *Enterococci Calibration 2006 (+/- 2SD)* (measured data (red), modelled surface (black) and modelled bottom (green))

SINCLAIR KNIGHT MERZ

Water Quality Modelling of the Hawkesbury-Nepean River System

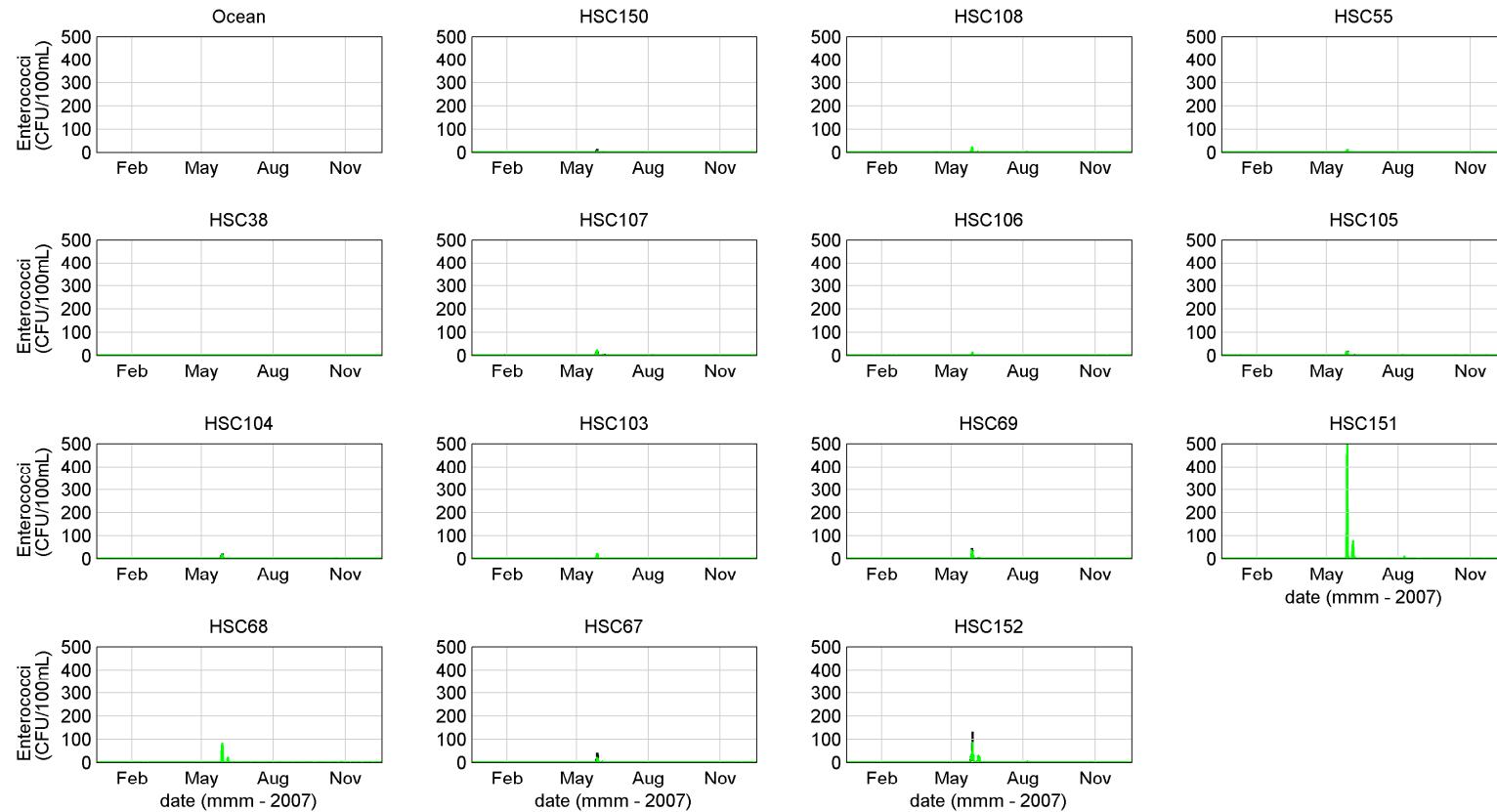


- Figure 13-109 Box and Whisker Plots – *Enterococci* Calibration 2006 (measured data (red), modelled surface (blue) and modelled bottom (green))

SINCLAIR KNIGHT MERZ



Water Quality Modelling of the Hawkesbury-Nepean River System

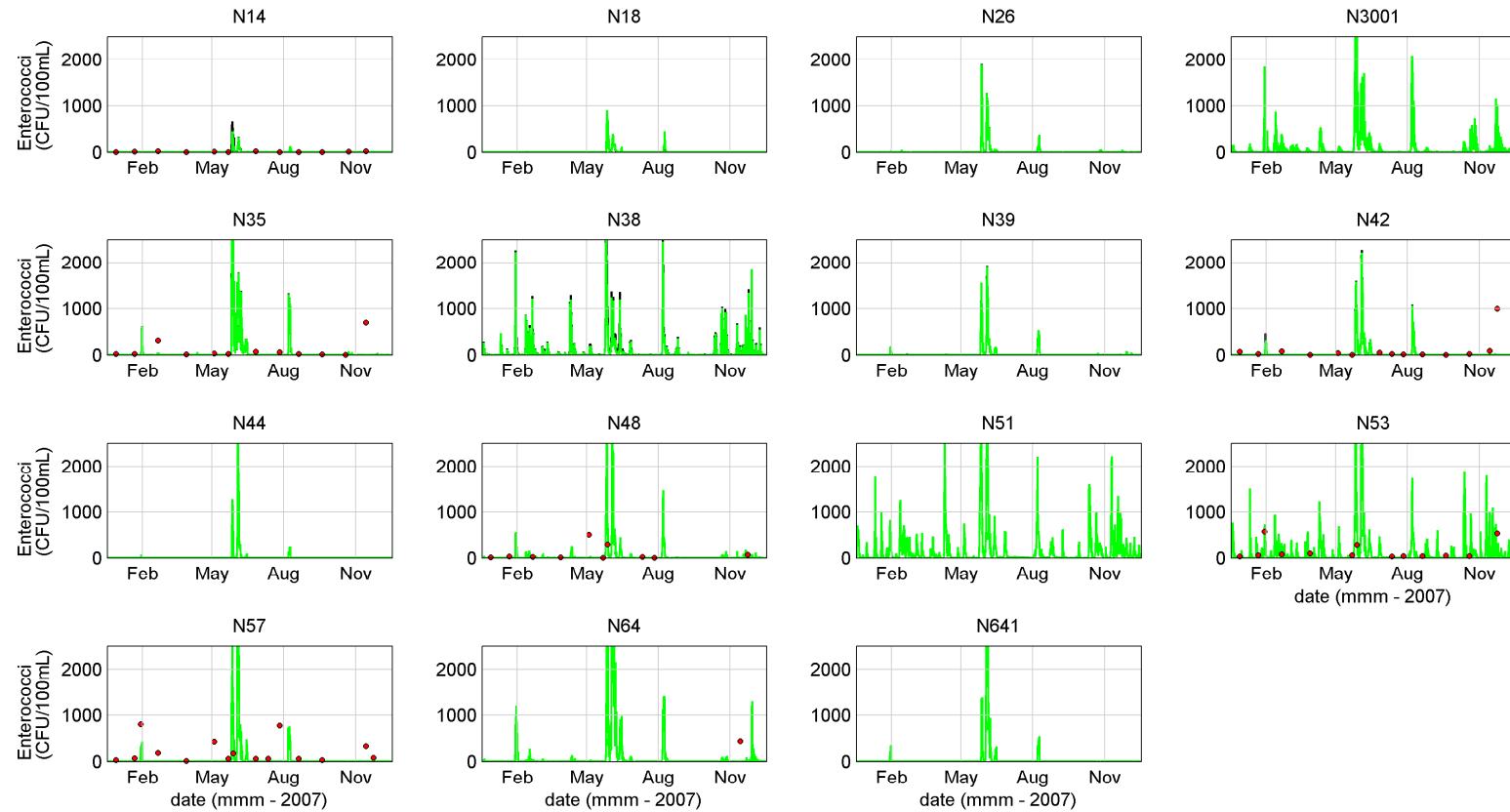


■ **Figure 13-110 Enterococci Validation 2007 (measured data (red), modelled surface (black) and modelled bottom (green))**

SINCLAIR KNIGHT MERZ



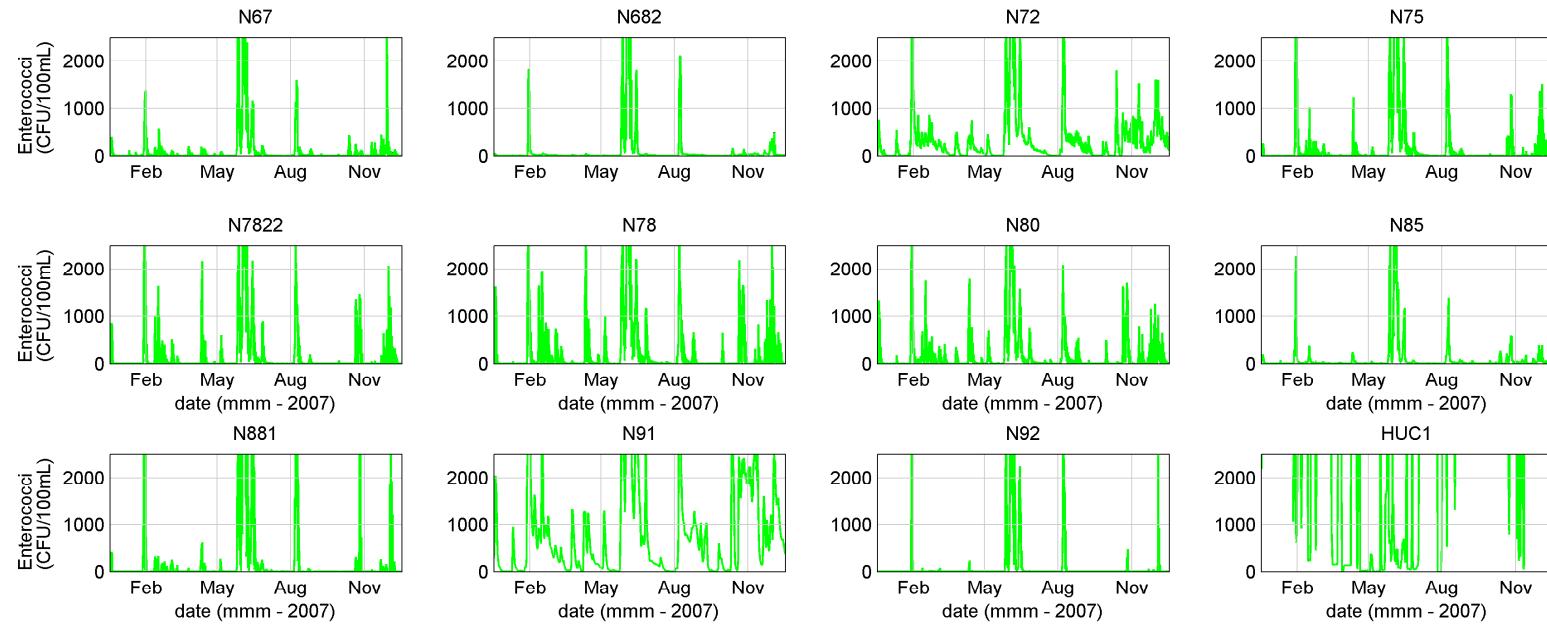
Water Quality Modelling of the Hawkesbury-Nepean River System



■ **Figure 13-110 (Cont.) Enterococci Validation 2007 (measured data (red), modelled surface (black) and modelled bottom (green))**



Water Quality Modelling of the Hawkesbury-Nepean River System

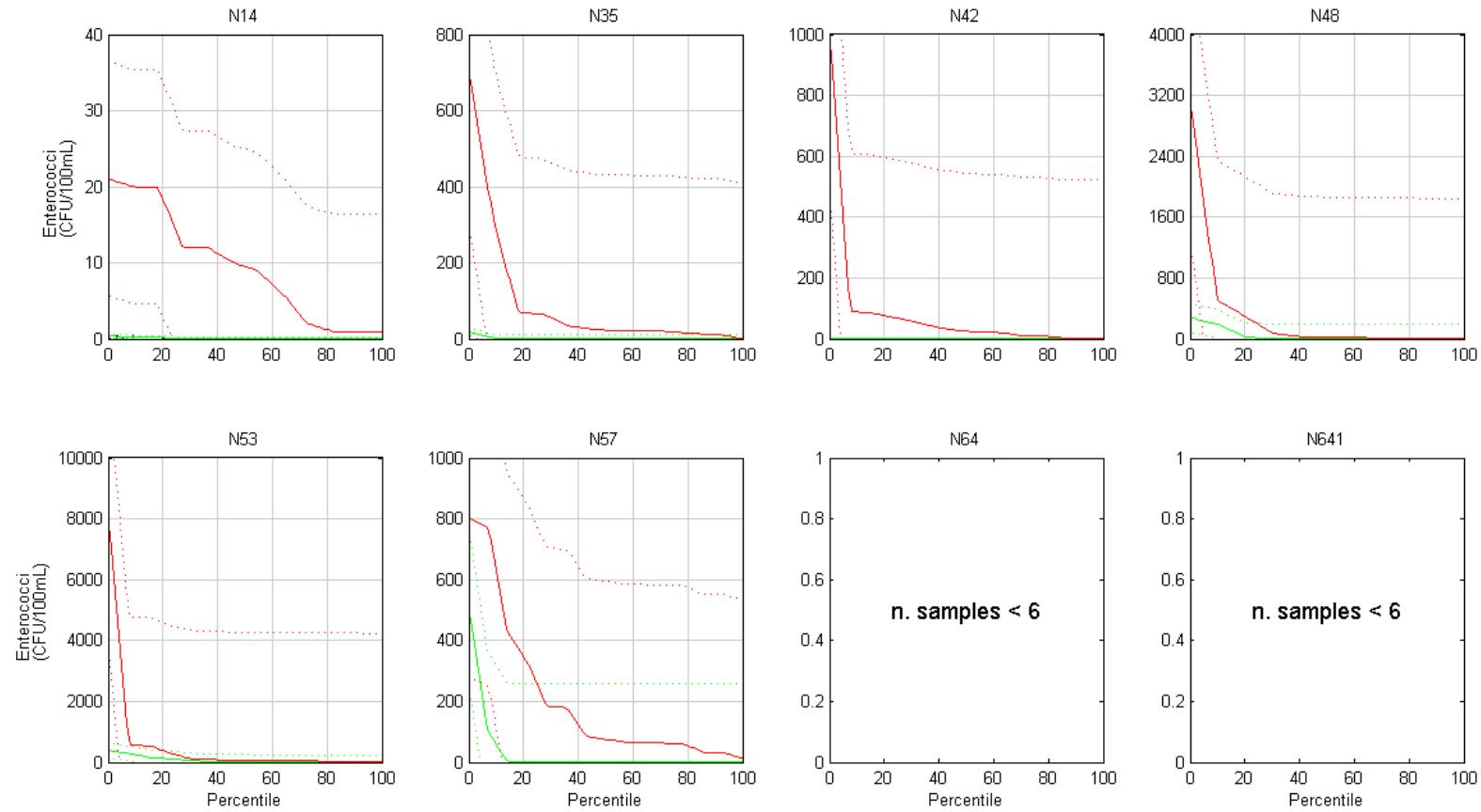


■ **Figure 13-110 (Cont.) Enterococci Validation 2007 (measured data (red), modelled surface (black) and modelled bottom (green))**

SINCLAIR KNIGHT MERZ



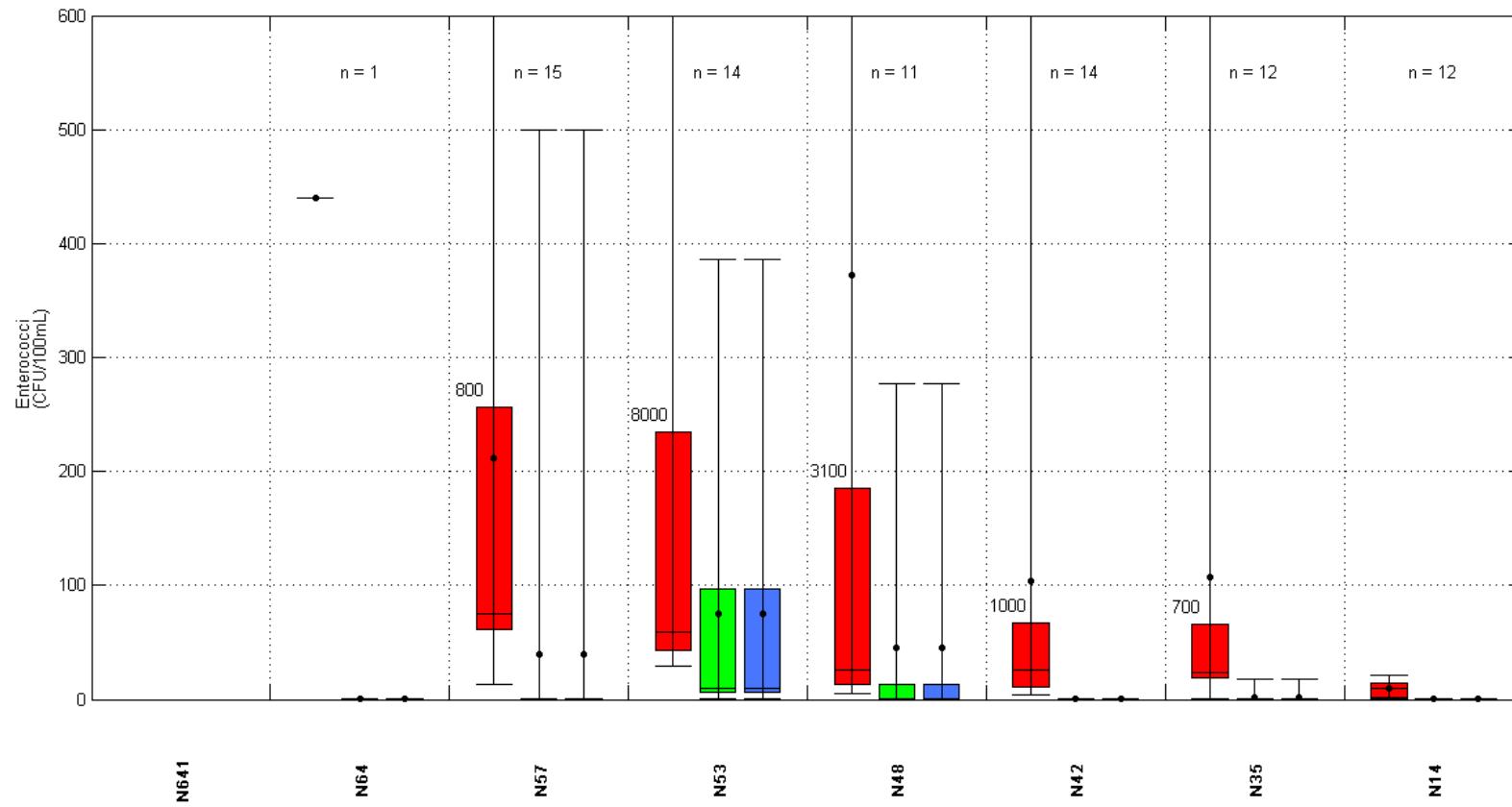
Water Quality Modelling of the Hawkesbury-Nepean River System



- **Figure 13-111 Exceedance Plots – *Enterococci Validation 2007 (+/- 2SD)* (measured data (red), modelled surface (black) and modelled bottom (green))**

SINCLAIR KNIGHT MERZ

Water Quality Modelling of the Hawkesbury-Nepean River System



- Figure 13-112 Box and Whisker Plots – *Enterococci Validation 2007* (measured data (red), modelled surface (black) and modelled bottom (green))

13.6. Discussion

The previously presented data is complex and exhaustive, and as such it is felt that providing comment on each and every model/measurement comparison is not useful. Rather, this discussion is structured to reflect the manner in which model calibration and validation data was presented. Specifically, comment is provided on each of the broad groups of simulated constituents, and within each, focus on the model's ability to capture key environmental processes.

13.6.1. Hydrodynamics

13.6.1.1. Tidal Wave and Flows

The model predicted well all key hydrodynamic features. Of particular note is the model's ability to predict both the tidal wave propagation and attenuation, and the integrated tidal flow characteristics of the system. Satisfactory prediction of these quantities is essential in underpinning the subsequent water quality calibration.

The model generally predicts well the details of the magnitude, direction and distribution of velocity profiles across the ADCP sections of the 2011 CMP. In many cases, the model correctly predicts cross channel shear, for example. There are instances where the model and measured velocity vectors diverge somewhat, but as described previously, this is most likely due to the coarseness of the model mesh in these areas, where this coarseness has been arrived at through a process of balancing the relative importance of model resolution and computational overhead. If future investigations require detailed resolution of these velocity profiles, then the current hydrodynamic model could be easily reduced in spatial extent and its mesh resolution increased in any particular area of interest. Doing so would support detailed three dimensional analysis of any velocity features of interest with relatively little effort, particularly since appropriate hydrodynamic boundary conditions to force such a 'nested' high resolution model could be sourced directly from the current TUFLOW model.

13.6.1.2. Salinity

The model generally predicts well the recovery of salt observed during the CMP period. In some instances model predictions diverge slightly from the CMP measurements, however, these are most likely due to the influence on salt wedge recovery of fine scale bathymetric features not able to be resolved within TUFLOW at a reasonable computational expense. As above, the current model could be easily adapted to better represent these recoveries, but doing so is not the focus of the current study, which seeks to investigate long term, large scale system dynamics.

In this regard, the model reproduces well the salinities measured at all MHL gauging stations throughout the domain. This points to the model correctly predicting system wide and longer term transport dynamics of the estuary. Doing so is critical to the success of this study.

13.6.1.3. Temperature

The model predicts well temperature throughout the domain, including an excellent representation of both seasonal and diurnal water temperature dynamics (the latter are presented in the appendices). The model also predicts well top to bottom thermal stratification processes. In this regard, the model also captures nicely the influence of the spring-neap tidal cycle on thermal stratification processes. The figures in the appendices clearly show the development of top to bottom temperature gradients developing at a return period of approximately two weeks. This development coincides with the occurrence of neap tides, where vertical mixing driven by tidal action is attenuated and thus less energy is available to mix the estuarine waters vertically.

13.6.1.4. Sediment

The model predicts well the sediment characteristics of the estuary. The influence of catchment derived suspended sediment is clear in the non-tidal reaches, where the TUFLOW predictions for suspended sediment match closely catchment inflow events.

Importantly, the model performs well in the tidal reaches, with the neap-spring tidal cycles of deposition and resuspension clearly evident in the model predictions. These generally match well with long term campaign measurements. It is interesting to note that the measurements are clearly aliased in time at their monthly frequency: the model reveals that sediment movement is far more dynamic than what might be suggested from interpolation of monthly field measurements.

13.6.2. Water Quality

13.6.2.1. Dissolved Oxygen

The model reproduces well the seasonal trends in dissolved oxygen, and shows the increase in DO (in mg/L) from summer to winter evident in field measurements.

The diurnal variations in dissolved oxygen concentrations are also well captured by the model (as presented in the appendices) both in terms of hour to hour variations, and vertical stratification. With regard to the latter, the model (as with temperature) also captures nicely the influence of the spring-neap tidal cycle on dissolved oxygen vertical profiles.

13.6.2.2. Nitrogen

Total nitrogen is generally predicted well through the model domain. In the lower estuarine section displays relatively constant TN concentrations, a trend which is consistent with monitoring data. The exception to this is during 2007 when a large inflow event occurs and a spike in TN is predicted in the lower Hawkesbury. No monitoring data was available over the time of this spike.

Seasonality in TN is also generally reproduced in sites where this is evident in the monitoring data (e.g. N42, N44). This trend is dominated by the contributions of oxidised nitrogen and ammonium, whose concentrations are responsive to sediment release processes, which are in turn temperature (and hence seasonally) dependent.

SINCLAIR KNIGHT MERZ

The two sites where the model diverges noticeably from measurements are N75 and N57. The water quality at N75 is dominated by discharges from West Camden WRP (supplied by others), and the model underpredicts TN at this site. Anecdotal evidence suggests that it is possible that data collected at this site are not representative of the channel wide conditions that are simulated in AED. Specifically, the model is only two cells wide at this location so will generate some numerical dilution across the channel width that means model concentrations will be lower than measurements, which is the case.

Significant nutrient uptake by macrophyte is known to occur in Penrith weir pool (N57), and considerable effort was spent in adjusting nutrient fluxes (see model calibration section) to account for this uptake within the model at this location. It was found that both nitrogen and phosphorus concentration predictions were indeed sensitive to this parameter at N57, and that adjustment downwards saw reductions in ambient concentrations predictions. In doing so however, it was felt that it was necessary to maintain a relatively constant proportionality between these nitrogen and phosphorus sediment flux reductions, given that the nutrients are most likely consumed by macrophyte growth in constant ratios. This assumption produced a good fit for TP/FRP (see below) but then limited the extent to which nitrogen predictions could be further reduced at N57 using this parameterisation. This suggests that some other process might be at play in this weir pool (such as large denitrification) to account for this overprediction. This could be investigated further, however given the relatively isolated nature of this overprediction, this was not pursued as part of the current work.

Other than a slight underprediction of oxidised nitrogen at N35 and N38, the model captures well these dynamics throughout the model domain, including the seasonality signature in the measured data.

Ammonium is generally well reproduced throughout the model. The exception is N92 (which is within the Picton weir pool) in both 2006 and 2007, where the model underpredicts ammonium. This issue has been investigated and it is believed that the high measured concentrations are most likely due to localised delivery of fertiliser derived nutrients to the weir pool from a nearby agricultural property. The property is directly adjacent to the Picton weir pool and because it is an intensive agricultural operation (aerial photos suggest it is a market garden) it is almost certain to apply fertilisers as part of its operation. It is believed that direct runoff of excess fertiliser (which is not specifically captured in Source) is the most likely cause of this discrepancy and the high measured concentrations.

13.6.2.3. Phosphorus

The model generally predicts total phosphorus very well, with all key trends and processes captured. The only exception is N48 in 2007, however it is noted that only three measured data points are available at this site over 2007, so the comparison with model predictions is problematic.

Filterable reactive phosphorus (FRP) is also generally predicted very well throughout the model domain. In particular, the model is able to maintain the observed ‘minimum’ background FRP concentrations at all times, without predicting zero concentration. The model also replicates the

measurements that show elevated FRP concentrations during some mid-winter periods, where temperatures are too low for substantial algal growth. When water temperatures begin to increase, FRP concentrations drop (consistent with observations) in response to algal (diatom) uptake.

13.6.2.4. Silicate

Silicate is generally well produced throughout the model, and shows a response to diatom growth at some locations and times, although silicate is never completely limiting. Some silicate limitation is shown during the winter months of 2007 (when diatoms grow) however the divergence of the limitation factors downwards from 1 is rarely less than 0.75. At these times, phosphorus is the limiting constituent.

13.6.2.5. Algae

The model represents chlorophyll a concentrations and algal succession very well throughout the domain. Key features that it captures (primarily as related to the middle model reach) are:

- Summer/winter blooms. The model clearly resolves both summer and winter (primarily 2007) time algal blooms. These blooms are evident in the monitoring data and are dominated by greens/blue-greens and diatoms in summer and winter, respectively. Capturing this algal succession is critical to the execution of this study in that most scenarios seek to investigate (at least in part) the influence of catchment load and environmental release changes on in-stream algal dynamics.
- Chlorophyll a near South Creek. The model captures the drastic increases in chlorophyll a concentrations in the reach that includes the confluence of South Creek with the main river stem. The box and whisker plots presented earlier demonstrate this well.
- Estuarine reach dynamics. The model is broadly consistent with algal measurements in the lower Hawkesbury reaches in that predictions are for continually low chlorophyll a concentrations. Having said that however, the measured data in this reach is suspect in that all values are identical, with the exception of one data point. This does point to some detection limit issues in the measured data, however the absolute values of the data are significantly greater than typically accepted detection limits.

The exceptions to the above are at some times at sites N48, N75 and N92. Site N48 is directly downstream of the confluence of the Winmalee plant and the main river stem. Given that the monitoring data demonstrated uptake of bioavailable nutrients between Winmalee discharge and the river confluence, it is likely that at least some of this uptake is by algae. If these algae were to be advected into the main river stem then this would bias upwards chlorophyll a measurements. This algal discharge is not captured by the model.

As discussed previously, N75 is located directly downstream of the West Camden plant. The potential for non-process related differences between measured data and modelled output at this site has been discussed above with regard to nutrients. It is believed that the same applies here with respect to chlorophyll a.

SINCLAIR KNIGHT MERZ

Also discussed previously is the likely direct influence, of local market garden runoff into the Picton weir pool, on measurements at N92. It is believed that the runoff of excess nutrients from this adjacent site may be the cause of in-pool algal growth and subsequent elevated chlorophyll a measurements in the Picton weir pool. This direct (and specific) input of this agricultural site has not been included in the Source modelling

13.6.2.6. Bacteria

It is noted that very little data exist against which to perform calibration of bacteria. As such, the decay and die off behaviour of the bacteria were the focus of the calibration effort – without reasonable spatial coverage of measurements detailed calibration is not possible. The publication used to build the bacterial model (which is co-authored by project collaborator A/Prof M Hipsey) has been provided with this report in **Appendix N**. The science in this publication was used in full, other than the simulation of growth, which is not applicable to this receiving system.

Given the temporal sparseness of the measured bacterial data, ANOVA and t-test analyses were considered in at least trying to assess whether the means of the measured data and modelled output sets are statistically similar. Despite several efforts however, this analysis approach yielded no meaningful outcomes, and, more importantly, could not take into account the temporal variation dynamics of each data set in assessing similarity. In particular, this test would only compare the overall variation of the bacterial data from model output and measured data, or a subset thereof, without taking into account their chronology or relative timing. Given that chronology is important in determining the correlation between the two data sets, and no replicate data was available to add time as a dimension to any statistical analysis anyway, this approach was not pursued.

14. Summary

A water quantity and quality model for the Hawkesbury-Nepean River and South Creek has been developed. The catchment model was developed in the Source model and covers the entire area of the catchment from downstream of Warragamba Dam, downstream of Pheasants Nest and downstream of Broughton Pass to the ocean. The catchment model is used to generate daily flows and loads of the water quality constituents. Point sources to the model include flows and loads from the wastewater treatment and water recycling plants.

Daily flows and loads are fed into the TUFLOW model that extends along the entire length of the main stem of the Hawkesbury-Nepean River from Pheasants Nest and Broughtons Pass to the sea, and it also extends up South Creek. The biogeochemical interactions are modelled across the same domain as the TUFLOW model using AED.

The combined flow and water quality modelling system was calibrated and validated against a large set of data collected around the catchment over the last several decades, including daily flow data at gauging stations, routine water quality sampling, water quality sampling undertaken for events during the campaign monitoring program, tide gauges and estuarine data.

Development of the Assimilation and Integration Framework (known as "Hawkeye") will allow the easy display of data generated by the composite model. In addition, model scenarios can be logically stored in the model run library.

It is important to note that the model is appropriate for the system as it was simulated during this time period. In the future, as the catchment and climate changes, it will be necessary to review the status of the model and update it with current data.

15. References

- Bartley, R., Speirs, W.J., Ellis, T.W. and Waters, D.K. (2012) A review of sediment and nutrient concentration data from Australia for use in catchment water quality models, *Marine Pollution Bulletin*, 64 (4-9) 101-116, doi:1.1016/j.marpolbul.2011.08.009
- Burnash, R.J.C. and Fernal, R.L. (1972) Generalized hydrologic modelling, a key to drought analysis. 2nd Int. Symposium in Hydrology, Fort Collins, Colorado.
- Chapman, T. and Maxwell, A. 1996, Baseflow separation - comparison of numerical methods with tracer experiments 23rd Hydrology and Water Symposium: Water and the Environment. Preprints of Papers. 21-24 May 1996, Hobart, Tasmania, v.1, pp.539-545
- Chiew, F.H.S., J. Teng, J. Vaze, D. A. Post, J. M. Perraud, D. G. C. Kirono, N. R. Viney (2009) Estimating climate change impact on runoff across southeast Australia: Method, results, and implications of the modeling method, *Water Resources Research*, 45 (10), doi: 10.1029/2008WR007338
- Chiew F.H.S., Vaze J., Viney N.R., Jordan P.W., Perraud J.-M., Zhang L., Teng J., Young W.J., Penaarancibia J., Morden R.A., Freebairn A., Austin J., Hill P.I., Wiesenfeld C.R. and Murphy R. (2008) *Rainfall-runoff modelling across the Murray-Darling Basin*. A report to the Australian Government from the CSIRO Murray-Darling Basin Sustainable Yields Project. CSIRO, Australia. 62pp.
- Duncan, H.P. (1999), Urban Stormwater Quality: A Statistical Overview, Report 99/3, Cooperative Research Centre for Catchment Hydrology, February 1999.
- EPA (1997) Managing Urban Stormwater: Council Handbook.
- Feijoó, C., García, M.E., Momo, F. and Toja, J. (2002) Nutrient Absorption by the Submerged Macrophyte *Egeria densa* Planch.: Effect of Ammonium and Phosphorus Availability in the Water Column on Growth and Nutrient Uptake. *Lirnnetica* 21(1-2): 93-104.
- Gruber R, Ferguson A and Haine B 2010, 'Nutrient attenuation and transformation within tidal rivers', Department of Environment, Climate Change and Water NSW (ed), *Final report 2007/RD/0018* for NSW Environmental Trust, 44 pp.
- Institution of Engineers Australia (1987) Australian Rainfall and Runoff: A Guide to Flood Estimation, Pilgrim, D. and Cordery, I. (Eds), Canberra.
- Jones, D.R., Jung, R.F., Hall, B.J., Arakel, A., Mora, S., Hanna, R., 1994, Assimilative Capacity of Creeks in Sydney's North West Sector, Investigation Report CET/IR 336, Final Report, Prepared by CSIRO Coastal Zones Program Division of Coal and Engery Technology and Australian Water Technologies EnSight for NSW Environment Trust Research Contract No. 83.
- Laurenson E.M. & Mein R.G., 1997. *RORB - Version 4, Runoff routing program - User Manual*. 2nd Edition, Department of Civil Engineering, Monash University/Montech Pty Ltd, Melbourne.
- McVicar, T., Roderick, M., Donohue, R., Li, L., Van Niel, T., Thomas, A., Grieser, J., Jhajharia, D., Himri, Y., Mahowald, N., Mescherskaya, A., Kruger, A., Rehman, S., and Dinpashoh, Y. (2012). Global review and synthesis of trends in observed terrestrial near-surface wind speeds: Implications for evaporation. *Journal of Hydrology*, 416-417: 182-205. doi: 10.1016/j.jhydrol.2011.10.024



Water Quality Modelling of the Hawkesbury-Nepean River System

Mein R.G., Laurenson E.M. & McMahon T.A., 1974. *Simple nonlinear model for flood estimation*. ASCE, Journal of the Hydraulics Division, vol. 100, pp. 1507-1518.

Nash, J.E. and Sutcliffe, J.V., 1970 River flow forecasting through conceptual models, Part 1: A discussion of principles, *Journal of Hydrology*, Vol. 10, No. 3, pp. 282-290. font

Simons,M., Podger,G. and Cooke,R (1996) IQQM—A hydrologic modelling tool for water resource and salinity management, *Environmental Software*, **11** (1-3), 185-192, doi:10.1016/S0266-9838(96)00019-6.

SCA (2003) Observed rates of contaminant exports from the Lake Burragorang and Nepean Catchments. December 2003.

SKM, 1997. *Preliminary Assessment of Nutrient Discharges from Estuaries*. Document prepared for the Environment Protection Authority.

SKM, 2011. Development of WQ modelling framework for the MDB Phase 1 - scoping study. Final Report to the Murray-Darling Basin Authority. 7 June 2011.

Tomkins, K. M. (2012), Uncertainty in streamflow rating curves: methods, controls and consequences. *Hydrol. Process.*. doi: 10.1002/hyp.9567

Umlauf L.; Burchard H (2003), A generic length-scale equation for geophysical turbulence models. *Journal of Marine Research*, **61**(2) pp. 235-265(31).

Welsh W.D., Vaze J., Dutta D., Rassam D., Rahman J.M., Jolly I.D., Wallbrink P., Podger G.M., Bethune M., Hardy M., Teng J., Lerat J. (2012). An integrated modelling framework for regulated river systems. *Environmental Modelling and Software*. doi: 10.1016/j.envsoft.2012.02.022



Water Quality Modelling of the Hawkesbury-Nepean River System

Appendix A WWTP/WRP Discharge Locations

Site	Name	Abbreviation	Zone	Easting	Northing	Datum	Active	Commence	Cease	Type	Note
911021	ST MARYS WRP PLANT EFFLUENT TO CREEK & AWTP	ST MARYS PLANT EFF	56	293208	6264989	MGA94	T	18/12/1984		WRP	Discharge to waterway
911030	ST MARYS WRP SPS204 O/FLOW	ST MARYS SPS204 O/F	56	293351	6264868	MGA94	F	25/01/1973	19/04/1994	OF	
911031	ST MARYS SPS204 No 4 OVERFLOW	ST MARYS SPS204 O/F	56	293351	6264868	MGA94	F	10/11/1983	1/01/2005	OF	
911040	ST MARYS WRP EFFLUENT OVERFLOW ADP002 (LPt)	ST MARYS EFF O/F	56	293351	6264868	MGA94	T	18/11/1989		OF	
912031	RICHMOND WRP (NEW WORKS) O/F TO CREEK	RICHMOND WRP O/F	56	292671	6278967	MGA94	T	22/02/2005		OF	Discharge to waterway
918020	QUAKERS HILL WRP EFFLUENT ADP001 (LPt)	QUAKERS HILL EF (LP)	56	303177	6265002	MGA94	T	20/06/1980		WRP	Discharge to waterway
921020	WEST HORNSBY WWTP EFFLUENT (LPT)	W. HORNSBY EFFLUENT	56	322143	6269362	MGA94	T	1/07/2002		WWTP	Discharge to waterway
921023	WEST HORNSBY WWTP DISINFECTED STORMWATER EFFLUENT	DISINFECTED EFFLUENT	56	322143	6269362	MGA94	T	8/06/2004		WWTP	
924021	CASTLE HILL WRP TOTAL EFFLUENT (LPt)	CASTLE HILL EFF (LP)	56	313087	6268210	MGA94	T	9/09/1996		WRP	Discharge to waterway
924022	CASTLE HILL WRP BIOLOGICAL BYPASS	CASTLE HILL BYPASS	56	313087	6268210	MGA94	T	1/07/2002		WRP	
924023	CASTLE HILL WRP FILTER BYPASS	CASTLE HILL F BYPASS	56	313087	6268210	MGA94	T	1/06/2007		WRP	
928021	WEST CAMDEN WRP EFFLUENT ADP001 (LPt)	W CAMDEN PH2 EFF LP	56	286148	6228955	MGA94	T	3/04/1985		WRP	Discharge to waterway
928030	WEST CAMDEN WRP SECONDARY BYPASS	WEST CAMDEN BYPASS	56	286148	6228955	MGA94	T	10/09/1992		WRP	

SINCLAIR KNIGHT MERZ



Water Quality Modelling of the Hawkesbury-Nepean River System

Site	Name	Abbreviation	Zone	Easting	Northing	Datum	Active	Commence	Cease	Type	Note
929030	PICTON WRP OVERFLOW	PICTON WRP OVERFLOW	56	281032	6213847	MGA94	T	1/07/2002		OF	
931020	ROUSE HILL WRP EFFLUENT	ROUSE HILL WRP EFF	56	307126	6272735	MGA94	T	19/07/2001		WRP	Discharge to waterway
931030	ROUSE HILL WRP WETLAND BYPASS	RH022 WETLAND BYPASS	56	307527	6273096	MGA94	T	31/10/2006		WRP	
931031	ROUSE HILL WRP TOTAL BIOLOGICAL BYPASS	ROUSE HILL WRP BYPAS	56	307199	6272782	MGA94	T	1/07/2002		WRP	
931040	ROUSE HILL WRP OUTLET FLOW TO WETLAND BASIN	RH021 TO WETLANDS	56	307126	6272735	MGA94	T	21/12/2006		WRP	
933020	NORTH RICHMOND WWTP EFFLUENT	NORTH RICHMOND EFF	56	288077	6282654	MGA94	T	5/07/1979		WWTP	Discharge to waterway
933021	NORTH RICHMOND WWTP STORM EFFLUENT	NORTH RICHMOND EFF	56	288077	6282654	MGA94	T	5/07/1979		WWTP	
934020	ROUND CORNER WWTP EFFLUENT ADP001 (Lpt)	ROUND CNR EFF (LP)	56	316540	6270732	MGA94	F	11/07/1985	1/07/2001	WWTP	Discharge to waterway
940020	HORNSBY HEIGHTS WWTP EFFLUENT	HORNSBY HTS WWTP EFF	56	324280	6273208	MGA94	T	1/05/2002		WWTP	Discharge to waterway
940030	HORNSBY HEIGHTS WWTP SECONDARY BYPASS	HH WWTP SEC BYPASS	56	324280	6273208	MGA94	T	28/06/1995		WWTP	
940031	HORNSBY HEIGHTS WWTP TERTIARY BYPASS	HH WWTP TERT BYPASS	56	324280	6273208	MGA94	T	28/06/1995		WWTP	
940032	HORNSBY HEIGHTS WWTP OVERFLOW	HORNSBY HEIGHTS O/F	0	324280	6273208	MGA94	F	1/07/2002	1/07/2003	OF	
942020	RIVERSTONE WWTP EFFLUENT	RIVERSTONE WWTP EFF	56	300271	6274199	MGA94	T	10/10/2002		WWTP	Discharge to waterway
945020	WALLACIA WWTP EFFLUENT	WALLACIA EFFLUENT	56	279217	6249318	MGA94	T	14/08/2006		WWTP	Discharge to waterway
945031	WALLACIA WWTP BYPASS FLOW	WALLACIA BYPASS	56	279217	6249318	MGA94	T	14/08/2006		WWTP	

SINCLAIR KNIGHT MERZ



Water Quality Modelling of the Hawkesbury-Nepean River System

Site	Name	Abbreviation	Zone	Easting	Northing	Datum	Active	Commence	Cease	Type	Note
946020	PENRITH WRP PLANT EFFLUENT ADP001 (LPt)	PENRITH WRP PLANT EF	56	287157	6264186	MGA94	T	6/12/1990		WRP	Discharge to waterway
946022	REPLACEMENT FLOW TO BOUNDARY CREEK FROM AWTP	REPLACEMENT FLOW	56	287157	6264186	MGA94	T	1/08/2011		WRP	Discharge to waterway
946023	RFP FINAL EFFLUENT TO CREEK	FINAL EFF TO CREEK	56	287157	6264186	MGA94	T	1/08/2011		WRP	Discharge to waterway
960030	GLENBROOK WWTP SPS OVERFLOW (ADP002)	GLENBROOK WWTP O/F	56	280558	6261687	MGA94	F	28/03/1992	22/08/2005	OF	
964020	WINMALEE WWTP EFFLUENT ADP001 (LPt)	WINMALEE WWTP EFF LP	56	280145	6271140	MGA94	T	1/01/1985		WWTP	Discharge to waterway
964030	WINMALEE WWTP SECONDARY BYPASS	WINMALEE WWTP BYPASS	56	280145	6271140	MGA94	F	1/01/1985	22/10/1995	WWTP	
964040	WINMALEE WWTP STORM EFFLUENT ADP002 (LPt)	WINMALEE BYPASS NEW	56	280145	6271140	MGA94	T	31/12/1984		WWTP	
974020	BROOKLYN WWTP FINAL EFFLUENT FLOW TRANSMITTER	BROOKLYN WWTP F/E	56	332763	6287263	MGA94	T	22/12/2007		WWTP	Discharge to waterway
974021	BROOKLYN WWTP UV EFFLUENT FLOW TRANSMITTER	BROOKLYN WWTP UV EFF	56	332763	6287263	MGA94	T	22/12/2007		WWTP	

SINCLAIR KNIGHT MERZ

Appendix B Rainfall Stations Used For Derivation of Daily Rainfall Grids

Site Number	Site Name	Source	Start	End
63182	Bilpin (Mountain Lagoon)	Bureau of Meteorology	1/01/1962	1/12/1973
63168	Capertee (Lochaber)	Bureau of Meteorology	1/01/1962	1/12/1981
63171	Blackheath (Cliffview)	Bureau of Meteorology	1/01/1962	1/12/1967
63173	Rothesay (Wentworth Falls)	Bureau of Meteorology	1/01/1962	1/12/1970
63177	Glen Davis Post Office	Bureau of Meteorology	1/01/1962	1/12/1986
63178	Crown View	Bureau of Meteorology	1/01/1962	1/12/1968
63179	Capertee (The Meadows)	Bureau of Meteorology	1/01/1962	1/09/2001
63202	Blackheath 1	Bureau of Meteorology	1/01/1895	1/12/1906
63181	Colo Upper 1	Bureau of Meteorology	1/01/1928	1/12/1971
63139	Newnes Junction Village	Bureau of Meteorology	1/01/1959	1/12/1986
63183	Valley Heights (Sun Valley Rd)	Bureau of Meteorology	1/09/2002	Current
63184	Blaxland Ridge	Bureau of Meteorology	1/01/1962	1/12/1979
63185	Glenbrook Bowling Club	Bureau of Meteorology	1/01/1963	Current
63191	Capertee Post Office	Bureau of Meteorology	1/01/1895	1/12/1923
63192	Excelsior	Bureau of Meteorology	1/01/1923	1/12/1932
63042	Kurrajong Post Office	Bureau of Meteorology	1/01/1932	1/04/1991
63180	Glen Alice (Watervale)	Bureau of Meteorology	1/01/1931	1/04/2000
63081	Faulconbridge (Erts)	Bureau of Meteorology	1/11/1999	Current
66063	Wahroonga Reservoir	Bureau of Meteorology	1/01/1906	1/12/1991
63044	Lawson (Wilson Street)	Bureau of Meteorology	1/01/1895	1/03/2006
63045	Leura Post Office	Bureau of Meteorology	1/01/1908	1/07/1996
63056	Mount Victoria (Mt Victoria (Selsdon Str))	Bureau of Meteorology	1/01/1872	1/12/1990
63057	Mount Wilson (Nooroo)	Bureau of Meteorology	1/01/1876	1/12/1978
63062	Lithgow (Newnes Forest Centre)	Bureau of Meteorology	1/04/1938	1/07/2002
63141	Hartley Vale (Vellacott Park)	Bureau of Meteorology	1/01/1959	1/11/1992
63078	Springwood (Journeys End)	Bureau of Meteorology	1/01/1946	1/12/1956
63140	Hillmeads	Bureau of Meteorology	1/01/1959	1/12/1969
63092	Wentworth Falls Post Office	Bureau of Meteorology	1/01/1898	1/12/1973
63105	Grose Vale	Bureau of Meteorology	1/01/1954	1/12/1971
63110	Tyar	Bureau of Meteorology	1/01/1935	1/12/1964
63118	Bilpin (Fern Grove)	Bureau of Meteorology	1/01/1892	Current
63120	Freemans Reach (Dorothy St)	Bureau of Meteorology	1/01/1960	1/11/2000
63131	Angus Place (Wolgan Gap)	Bureau of Meteorology	1/01/1959	1/12/1982
63205	Warrangee	Bureau of Meteorology	1/01/1902	1/12/1914
63077	Springwood Bowling Club	Bureau of Meteorology	1/01/1883	Current
66028	Hornsby (Pretoria Parade)	Bureau of Meteorology	1/01/1923	1/07/1995

SINCLAIR KNIGHT MERZ



Water Quality Modelling of the Hawkesbury-Nepean River System

Site Number	Site Name	Source	Start	End
63286	Winmalee (Pentlands Drive)	Bureau of Meteorology	1/01/1985	Current
63290	Bilpin Post Office	Bureau of Meteorology	1/01/1988	Current
63292	Mount Boyce Aws	Bureau of Meteorology	1/01/1989	Current
63295	Blackheath (Wombat Street)	Bureau of Meteorology	1/01/1991	Current
63301	Bowen Mountain (Grandview Lane)	Bureau of Meteorology	1/04/1959	Current
66008	Brooklyn (Sandbrook Inlet)	Bureau of Meteorology	1/01/1913	Current
63195	Round Swamp	Bureau of Meteorology	1/01/1930	1/12/1939
66027	Hornsby Mwsdb	Bureau of Meteorology	1/01/1946	1/12/1973
63280	Sackville Ferry (Hawkesbury River)	Bureau of Meteorology	1/01/1980	Current
66032	Lindfield West	Bureau of Meteorology	1/01/1950	1/06/1992
66037	Sydney Airport Amo	Bureau of Meteorology	1/01/1974	Current
66044	Cromer Golf Club	Bureau of Meteorology	1/01/1898	Current
66045	Newport Bowling Club	Bureau of Meteorology	1/07/1931	Current
66047	Pennant Hills (Yarrara Road)	Bureau of Meteorology	1/01/1900	Current
66053	Avalon (Wollstonecraft Ave)	Bureau of Meteorology	1/01/2001	Current
66020	Epping Chester Street	Bureau of Meteorology	1/01/1886	1/09/2002
63248	Grose Wold Road	Bureau of Meteorology	1/01/1969	1/06/1994
63206	Wascoe	Bureau of Meteorology	1/01/1903	1/12/1911
63220	Kurrajong Settlement	Bureau of Meteorology	1/01/1920	1/12/1927
63227	Wentworth Falls Country Club	Bureau of Meteorology	1/05/1967	Current
63230	Blaxland Western Highway	Bureau of Meteorology	1/01/1968	1/12/1980
63235	Glen Alice (Wongara)	Bureau of Meteorology	1/01/1968	1/12/1972
63241	Capertee (Bernina)	Bureau of Meteorology	1/01/1968	1/06/1997
63285	Mt Irvine (Booralee)	Bureau of Meteorology	1/01/1986	Current
63247	Glenara	Bureau of Meteorology	1/01/1899	1/12/1969
63281	Blackheath M.C.A.	Bureau of Meteorology	1/01/1981	1/12/1983
63251	Kurrajong Heights (Cudgee)	Bureau of Meteorology	1/01/1986	1/12/1988
63252	Mulgoa	Bureau of Meteorology	1/01/1885	1/12/1919
63256	Bullaburra (Fairview)	Bureau of Meteorology	1/01/1970	1/12/1978
63266	Colo Upper Ward Bros	Bureau of Meteorology	1/01/1972	1/12/1973
63272	Springwood (Euchora)	Bureau of Meteorology	1/01/1885	1/12/1905
63275	Upper Colo (Mount Ward)	Bureau of Meteorology	1/01/1978	Current
63040	Kings Tablelands	Bureau of Meteorology	1/01/1903	1/12/1971
63246	Mount Wilson (Clarine)	Bureau of Meteorology	1/01/1969	Current
61217	St Albans (Espie St)	Bureau of Meteorology	1/01/1963	Current
61191	Bulga (South Wambo)	Bureau of Meteorology	1/08/1959	Current
61198	Wollombi (Wallabadah)	Bureau of Meteorology	1/01/1959	1/12/1968
61209	Putty Tea Rooms	Bureau of Meteorology	1/01/1962	Current
61210	Howes Swamp	Bureau of Meteorology	1/01/1962	1/12/1963

SINCLAIR KNIGHT MERZ



Water Quality Modelling of the Hawkesbury-Nepean River System

Site Number	Site Name	Source	Start	End
61211	Colo Heights (Mountain Pines)	Bureau of Meteorology	1/11/1962	Current
61214	Higher Macdonald	Bureau of Meteorology	1/01/1963	1/12/1975
61255	Wamberal (Dillon Road)	Bureau of Meteorology	1/01/1968	1/11/1988
61216	Lower Mangrove (Popran Rd)	Bureau of Meteorology	1/01/1963	Current
61162	Howes Valley (Putty Road)	Bureau of Meteorology	1/01/1959	Current
61221	Mangrove Upper	Bureau of Meteorology	1/01/1962	1/12/1974
61222	St Albans (Mogo Creek)	Bureau of Meteorology	1/01/1963	1/04/1998
61231	St Albans	Bureau of Meteorology	1/01/1898	1/12/1924
61242	Cessnock (Nulkaba)	Bureau of Meteorology	30/05/1973	Current
61248	Kincumber	Bureau of Meteorology	1/01/1967	1/12/1975
63043	Kurrajong Heights (Bells Line Of Road)	Bureau of Meteorology	1/01/1866	Current
61215	Rylstone (Kelgoola)	Bureau of Meteorology	1/01/1962	Current
61093	Ourimbah (Dog Trap Road)	Bureau of Meteorology	1/08/1953	Current
61003	Avoca Beach	Bureau of Meteorology	1/01/1934	1/12/1970
61023	Gosford (Gertrude Place)	Bureau of Meteorology	1/01/1877	1/08/1993
61029	Kulnura (William Rd)	Bureau of Meteorology	22/02/1969	9/09/1981
61030	Howes Valley (Kindarun)	Bureau of Meteorology	1/01/1914	1/12/1975
61033	Lower Mc Donald	Bureau of Meteorology	1/01/1945	1/12/1951
61036	Mangrove Mountain Post Office	Bureau of Meteorology	1/01/1942	1/12/1979
61165	Kulnura North (Wilcher)	Bureau of Meteorology	1/01/1959	Current
61087	Gosford (Narara Research Station) AWS	Bureau of Meteorology	1/01/1916	Current
61164	Laguna (Murrays Run)	Bureau of Meteorology	1/01/1959	1/12/2009
61100	Broke (Harrowby)	Bureau of Meteorology	1/01/1887	Current
61110	Howes Valley	Bureau of Meteorology	1/04/2001	Current
61119	Wisemans Ferry (Old PO)	Bureau of Meteorology	1/01/1903	Current
61130	Doyles Creek (Wood Park)	Bureau of Meteorology	1/01/1920	Current
61139	Mount Yengo (Marena Stud)	Bureau of Meteorology	1/01/1959	1/12/1972
61149	Glen Alice (Eurella)	Bureau of Meteorology	1/01/1914	1/12/1969
61279	Courangra	Bureau of Meteorology	1/01/1914	1/12/1920
61042	Milbrodale	Bureau of Meteorology	1/01/1934	1/12/1953
63005	Bathurst Agricultural Station	Bureau of Meteorology	1/07/1908	Current
61403	Colo (Riverside Park)	Bureau of Meteorology	1/10/2003	Current
62001	Brogans Creek Cement Quarry	Bureau of Meteorology	1/01/1950	1/12/1978
62006	Charbon Standard Portland Ceme	Bureau of Meteorology	1/01/1929	1/12/1978
62017	Kandos Cement Works	Bureau of Meteorology	1/01/1951	Current
62019	Marloo	Bureau of Meteorology	1/01/1903	1/12/1950
62023	Olinda (Springdale)	Bureau of Meteorology	1/01/1898	1/12/1967
61253	Holgate (Wattle Tree Road)	Bureau of Meteorology	1/01/1968	1/12/1971

SINCLAIR KNIGHT MERZ



Water Quality Modelling of the Hawkesbury-Nepean River System

Site Number	Site Name	Source	Start	End
62090	Clandulla (Edenvale)	Bureau of Meteorology	1/01/1973	1/12/1977
61382	Wyong (Kulnura (Jeavons))	Bureau of Meteorology	1/09/1993	Current
63009	Blackheath (Lawrence St)	Bureau of Meteorology	1/01/1898	Current
63012	Running Stream (Brooklyn)	Bureau of Meteorology	1/01/1899	Current
63013	Berambing	Bureau of Meteorology	1/01/1943	Current
63028	Faulconbridge (St Georges Crescent)	Bureau of Meteorology	1/01/1937	Current
63031	Glen Davis (The Gullies)	Bureau of Meteorology	1/01/1940	1/12/1969
63039	Katoomba (Murri St)	Bureau of Meteorology	1/01/1885	Current
62055	Rylstone (Marsden Forest)	Bureau of Meteorology	1/01/1948	1/12/1984
61341	Woy Woy South (Woy Woy Rd)	Bureau of Meteorology	1/01/1977	1/12/1979
61284	Lambton	Bureau of Meteorology	1/01/1870	1/12/1920
61294	Avoca Beach Bowling Club	Bureau of Meteorology	1/01/1970	Current
61296	Howes Valley (Owensdale)	Bureau of Meteorology	1/01/1970	1/04/1995
61301	Tayar Creek (The Nile)	Bureau of Meteorology	1/01/1930	1/12/1954
61310	Pearl Beach (Crommelin Research Station)	Bureau of Meteorology	1/01/1953	1/04/2003
61319	Gosford North (Glennie St)	Bureau of Meteorology	1/01/1971	Current
61394	Kulnura (Mangrove Creek Dam)	Bureau of Meteorology	1/01/1982	Current
61336	Putty (The Gibba)	Bureau of Meteorology	1/01/1975	Current
61384	Wyong (Kangy Angy (Ourimbah Creek))	Bureau of Meteorology	1/06/1993	Current
61352	Putty (Putty Valley Road)	Bureau of Meteorology	1/01/1984	Current
61354	Marlows Creek (Spencer)	Bureau of Meteorology	1/01/1986	1/07/2004
61355	Kariong (Greenway Close)	Bureau of Meteorology	1/01/1986	1/12/1997
61369	Wamberal (Terrigal Memorial Country Club)	Bureau of Meteorology	1/01/1990	Current
61378	Bateau Bay (Rotherham St)	Bureau of Meteorology	1/10/1993	1/10/1997
61381	Wyong (Mount Elliot)	Bureau of Meteorology	1/06/1994	Current
61334	Glen Alice	Bureau of Meteorology	1/01/1970	Current
68254	Mount Annan Botanic Garden	Bureau of Meteorology	1/01/2002	Current
67104	Box Hill (Hynds Road)	Bureau of Meteorology	1/01/1990	Current
67064	Cecil Park Andersons Res.Farm	Bureau of Meteorology	1/01/1964	1/12/1970
67096	Penrith (Glenroy)	Bureau of Meteorology	1/01/1917	1/12/1923
67097	Prestons Bernera Road	Bureau of Meteorology	1/01/1983	1/12/1985
67098	West Pennant Hills (Oratava Ave)	Bureau of Meteorology	1/01/1941	1/05/2006
67100	Castle Hill (Kathleen Ave)	Bureau of Meteorology	1/01/1985	Current
67101	Box Hill Junction Road	Bureau of Meteorology	1/01/1985	1/12/1995
67092	Quakers Hill Douglas Rd.	Bureau of Meteorology	1/01/1963	1/12/1971
67103	Cattai Mitchell Park Road	Bureau of Meteorology	1/01/1988	1/08/1996
67090	Fiddletown (Bloodwood Road)	Bureau of Meteorology	1/01/1964	Current

SINCLAIR KNIGHT MERZ



Water Quality Modelling of the Hawkesbury-Nepean River System

Site Number	Site Name	Source	Start	End
67106	Berkshire Park First Rd	Bureau of Meteorology	1/01/1992	1/04/1995
67107	Varroville (St James Road)	Bureau of Meteorology	1/12/1992	1/11/1998
67112	North Rocks (Muirfield Golf Club)	Bureau of Meteorology	1/06/1992	Current
67113	Penrith Lakes Aws	Bureau of Meteorology	1/08/1995	Current
67114	Abbotsbury (Fairfield City Farm)	Bureau of Meteorology	1/06/1995	Current
67115	Glenmore Park (Cartwright Cl)	Bureau of Meteorology	1/01/1995	Current
67102	St Clair (Juba Close)	Bureau of Meteorology	1/01/1985	Current
67080	Winston Hills Lanhams Road	Bureau of Meteorology	1/01/1968	1/08/2006
67067	Emu Plains	Bureau of Meteorology	1/01/1911	1/12/1996
67068	Badgerys Ck McMasters F.Stn	Bureau of Meteorology	18/03/1967	29/12/1984
67069	Greenvalley (Miller)	Bureau of Meteorology	1/01/1967	1/12/1971
67071	Thornleigh Bridgeview Crescent	Bureau of Meteorology	1/01/1968	1/12/1972
67073	Maralya Boundary Road	Bureau of Meteorology	1/01/1963	1/05/1995
67076	Quakers Hill Treatment Works	Bureau of Meteorology	1/01/1948	Current
67094	Lower Portland (Hawkesbury River)	Bureau of Meteorology	1/01/1962	Current
67079	Halecote Late Kemps Creek	Bureau of Meteorology	1/01/1892	1/12/1918
67120	Hoxton Park (Ranieri Place)	Bureau of Meteorology	1/02/1998	1/11/2001
67082	Sackville Reach	Bureau of Meteorology	1/01/1891	1/12/1921
67083	Mount Druitt Francis Street	Bureau of Meteorology	1/01/1970	1/12/1976
67084	Orchard Hills Treatment Works	Bureau of Meteorology	1/01/1970	Current
67086	Dural (Old Northern Road)	Bureau of Meteorology	1/01/1973	Current
67087	Glenorie (Gateleigh Park)	Bureau of Meteorology	1/01/1972	1/12/1973
67089	West Pennant Hills (Cumberland State For	Bureau of Meteorology	1/01/1949	Current
67078	Kenthurst	Bureau of Meteorology	1/01/1889	1/12/1920
68208	Weronbi Post Office	Bureau of Meteorology	1/01/1954	1/12/1975
68150	Narellan	Bureau of Meteorology	1/01/1895	1/12/1933
68158	Picton Rumpker Street	Bureau of Meteorology	1/01/1964	1/12/1987
68159	Wedderburn (Booalbyn)	Bureau of Meteorology	1/01/1964	Current
68166	Buxton (Amaroo)	Bureau of Meteorology	1/01/1967	Current
68176	Tahmoor (Ranfurly)	Bureau of Meteorology	1/01/1968	1/12/1972
68193	Bargo Post Office	Bureau of Meteorology	1/01/1902	1/12/1970
67116	Willmot (Resolution Ave)	Bureau of Meteorology	1/10/1995	Current
68207	Cobbity (Roseneath)	Bureau of Meteorology	1/01/1888	1/12/1974
68127	Douglas Park Post Office	Bureau of Meteorology	1/01/1962	1/12/1977
68216	Menangle Bridge (Nepean River)	Bureau of Meteorology	1/01/1963	Current
68225	Camden (Camtrac)	Bureau of Meteorology	1/08/1986	1/07/2000
68227	Ambarvale Clennam Ave	Bureau of Meteorology	1/01/1988	1/10/2001

SINCLAIR KNIGHT MERZ

Water Quality Modelling of the Hawkesbury-Nepean River System

Site Number	Site Name	Source	Start	End
68230	Campbelltown U.W.S.	Bureau of Meteorology	1/01/1992	1/06/1994
66079	Avalon Beach (Avalon (Palmgrove Rd))	Bureau of Meteorology	1/01/1958	Current
61318	Woy Woy (Everglades Country Club)	Bureau of Meteorology	1/12/1964	Current
68200	Douglas Park (St. Marys Towers)	Bureau of Meteorology	1/01/1974	Current
68042	Minto 2	Bureau of Meteorology	1/01/1928	1/12/1949
68059	The Oaks John Street	Bureau of Meteorology	1/01/1912	1/12/1975
68001	Appin (Wilton Road)	Bureau of Meteorology	1/01/1917	Current
68007	Camden (Brownlow Hill)	Bureau of Meteorology	1/01/1882	Current
68011	Camden Bowling Club	Bureau of Meteorology	1/01/1883	1/12/1977
68012	Camden Mwsdb	Bureau of Meteorology	1/01/1946	1/12/1970
68015	Campbelltown 2 Mwsdb	Bureau of Meteorology	1/01/1946	1/12/1970
68133	Tahmoor Post Office	Bureau of Meteorology	1/01/1962	1/12/1974
68037	Kenny Hill	Bureau of Meteorology	1/01/1925	1/12/1970
68128	Alpine	Bureau of Meteorology	1/01/1962	1/12/1970
68047	Nepean Dam	Bureau of Meteorology	1/01/1926	1/12/1970
68052	Picton Council Depot	Bureau of Meteorology	1/01/1880	Current
68065	Wedderburn	Bureau of Meteorology	1/01/1930	1/12/1971
68081	Campbelltown Swimming Centre	Bureau of Meteorology	1/01/1959	1/12/1984
68120	Wilton Post Office	Bureau of Meteorology	1/01/1962	1/12/1980
68122	Cawdor (Woodburn)	Bureau of Meteorology	1/01/1962	Current
67118	Oakhurst (Lawton Place)	Bureau of Meteorology	1/03/1997	1/06/1999
68016	Cataract Dam	Bureau of Meteorology	1/01/1904	Current
67001	Castle Hill 2	Bureau of Meteorology	1/01/1926	1/12/1956
66183	Ingleside (Walter Avenue)	Bureau of Meteorology	1/01/1984	Current
66185	Carlingford (Barellan Av)	Bureau of Meteorology	1/01/1986	Current
66188	Belrose (Evelyn Place)	Bureau of Meteorology	1/01/1991	Current
66189	West Pymble (Wyuna Road)	Bureau of Meteorology	1/04/1992	Current
66190	Ingleburn (Sackville Street)	Bureau of Meteorology	1/12/1992	Current
66205	Wahroonga (Boundary Road)	Bureau of Meteorology	1/03/1998	1/01/2006
67016	Minchinbury	Bureau of Meteorology	1/01/1901	1/12/1970
67000	Eastern Creek (Wonderland)	Bureau of Meteorology	1/02/2000	1/02/2004
66157	Pymble (Canisius College)	Bureau of Meteorology	1/01/1947	Current
67002	Castlereagh (Castlereagh Road)	Bureau of Meteorology	1/01/1939	Current
67003	Colyton (Carpenter St)	Bureau of Meteorology	1/10/2000	Current
67004	Emu Plains	Bureau of Meteorology	1/01/1880	1/12/1973
67012	Kellyville	Bureau of Meteorology	1/01/1930	1/12/1951
67014	Maroota (Old Telegraph Road)	Bureau of Meteorology	1/01/1925	Current
67015	Bringelly (Maryland)	Bureau of Meteorology	1/01/1867	Current

SINCLAIR KNIGHT MERZ



Water Quality Modelling of the Hawkesbury-Nepean River System

Site Number	Site Name	Source	Start	End
66206	St Ives (Richmond Avenue)	Bureau of Meteorology	1/01/1998	Current
66128	Palm Beach (Sunrise Road)	Bureau of Meteorology	1/01/1965	Current
67063	Cobbitty (Cuthill)	Bureau of Meteorology	1/01/1965	1/12/1973
68071	Yerrinbool	Bureau of Meteorology	1/01/1916	1/12/1970
66092	Dural	Bureau of Meteorology	1/01/1963	1/12/1972
66083	Palm Beach Coasters Retreat	Bureau of Meteorology	1/01/1960	1/12/1983
66114	North Turramurra (Dryden Rd)	Bureau of Meteorology	1/05/2005	Current
66119	Mount Kuring-Gai (Ledora Farm)	Bureau of Meteorology	1/01/1964	Current
66159	Hornsby (Mount Wilga)	Bureau of Meteorology	1/01/1969	1/12/1987
66123	Ingleside	Bureau of Meteorology	1/01/1964	1/12/1977
66158	Turramurra (Kissing Point Road)	Bureau of Meteorology	1/01/1912	Current
66131	Riverview Observatory	Bureau of Meteorology	1/01/1993	Current
66141	Mona Vale Golf Club	Bureau of Meteorology	1/01/1969	Current
66142	Duffys Forest (Namba Rd)	Bureau of Meteorology	1/01/1969	Current
66143	Kuring-Gai Chase (West Head)	Bureau of Meteorology	1/01/1969	1/12/1991
66146	Broken Bay Natl Fitness Camp	Bureau of Meteorology	1/01/1969	1/12/1975
66155	Brooklyn (Wobby Beach)	Bureau of Meteorology	1/01/1970	1/12/1975
67010	Glenorie (Old Northern Rd)	Bureau of Meteorology	1/01/1902	Current
66120	Gordon Golf Club	Bureau of Meteorology	1/01/1906	Current
67050	Badgerys Creek School	Bureau of Meteorology	1/01/1919	1/12/1929
67036	Austral Eighth Ave	Bureau of Meteorology	1/01/1964	1/09/1989
67017	Greystanes (Bathurst Street)	Bureau of Meteorology	1/05/2001	Current
67039	Ajana	Bureau of Meteorology	1/01/1963	1/12/1964
67042	Kings Langley (Solander Rd)	Bureau of Meteorology	1/01/1978	Current
67044	Lower Portland (Orange Grove)	Bureau of Meteorology	1/01/1963	1/12/1988
67045	Silverdale	Bureau of Meteorology	1/01/1963	1/12/1965
67046	Richmond North	Bureau of Meteorology	1/01/1905	1/12/1928
67033	Richmond Raaf	Bureau of Meteorology	1/01/1970	29/10/1994
67048	Vineyard (Alrean Glen)	Bureau of Meteorology	1/01/1902	1/12/1921
67037	Schofields Boundary Rd	Bureau of Meteorology	1/01/1963	Current
67051	Beecroft 1	Bureau of Meteorology	1/01/1888	1/12/1920
67052	Berowra (Goodwyn Road)	Bureau of Meteorology	1/01/1903	Current
67053	Castle Hill 1	Bureau of Meteorology	1/01/1916	1/12/1936
67054	Windsor The Peninsula	Bureau of Meteorology	1/01/1861	1/12/1916
67055	Pitt Town Lab.Farm (Scheyville)	Bureau of Meteorology	1/01/1895	1/12/1940
67056	Pitt Town (The Manse)	Bureau of Meteorology	1/01/1885	1/12/1929
67057	Portland Lower	Bureau of Meteorology	1/01/1902	1/12/1920
67059	Blacktown	Bureau of Meteorology	1/01/1963	1/09/1993
67047	Rossmore	Bureau of Meteorology	1/01/1895	1/12/1920
67024	St Marys Bowling Club	Bureau of Meteorology	1/01/1897	1/12/1984

SINCLAIR KNIGHT MERZ



Water Quality Modelling of the Hawkesbury-Nepean River System

Site Number	Site Name	Source	Start	End
67018	Penrith Ladbury Avenue	Bureau of Meteorology	1/01/1890	1/12/1994
67021	Richmond - Uws Hawkesbury	Bureau of Meteorology	29/09/1971	Current
67022	Galston (Rowland Village)	Bureau of Meteorology	1/01/1992	Current
67040	Gunderman (Wisemans Ferry Rd)	Bureau of Meteorology	1/12/1962	Current
67023	Canoelands (Canoelands)	Bureau of Meteorology	1/01/2003	Current
67031	Windsor Bowling Club	Bureau of Meteorology	1/01/1897	Current
67025	St Marys Mwsdb	Bureau of Meteorology	1/01/1947	1/12/1973
67030	Wilberforce (Glen Rock)	Bureau of Meteorology	1/01/1938	1/12/1966
67027	Warragamba	Bureau of Meteorology	19/12/2004	Current
67029	Wallacia Post Office	Bureau of Meteorology	1/01/1943	Current
67026	Seven Hills (Collins St)	Bureau of Meteorology	1/01/1950	Current
561109	Coricudgy (The Ovens)	Sydney Catchment Authority	31/10/1990	Current
562101	Rylstone (Marloo)	Sydney Catchment Authority	22/06/1990	Current
563085	Old Newnes Prison Farm	Sydney Catchment Authority	14/08/1998	Current
563061	Wentworth Falls (Bodington)	Sydney Catchment Authority	15/08/1990	Current
568167	Appin (Inghams Farm)	Sydney Catchment Authority	11/07/1990	Current
563079	Woodford Range	Sydney Catchment Authority	28/06/1990	Current
567108	Wisemans Ferry Bowling Club	Sydney Catchment Authority	27/06/1990	Current
561108	Womerah	Sydney Catchment Authority	26/06/1990	Current
563076	Gospers Mountain	Sydney Catchment Authority	21/06/1990	Current
563082	Wollangambe Junction (Blacksmiths Creek)	Sydney Catchment Authority	29/11/1990	Current
563077	Newnes (Deanes Creek)	Sydney Catchment Authority	30/06/1990	Current
563080	Grose Wold	Sydney Catchment Authority	19/06/1990	Current
563081	Wilberforce	Sydney Catchment Authority	20/06/1990	Current
567110	Forest Glen	Sydney Catchment Authority	27/06/1990	Current
563075	Capertee	Sydney Catchment Authority	19/06/1990	Current
562102	Glen Alice(Yandarra)	Sydney Catchment Authority	22/06/1990	Current
561106	Bala	Sydney Catchment Authority	26/06/1990	Current
561105	Culoul Range (Tari Creek)	Sydney Catchment Authority	26/06/1990	Current
561104	Putty (Tollagong Park)	Sydney Catchment Authority	28/06/1990	Current
561103	Howes Valley (Noisy Point)	Sydney Catchment Authority	9/05/1990	Current
561107	Mount Calore	Sydney Catchment Authority	26/06/1990	Current
561102	Putty Forest (Three Ways)	Sydney Catchment Authority	17/05/1990	Current
561101	Mangrove Mountain (Dubbo Gully)	Sydney Catchment Authority	28/02/1990	Current
568060	Ironbark	Sydney Catchment Authority	24/02/1964	Current
568051	Oakdale (The Bridge)	Sydney Catchment Authority	25/05/1966	Current
563072	Bilpin (Hillside)	Sydney Catchment Authority	15/12/1987	Current
563070	Linden (Woodford Creek Dam)	Sydney Catchment Authority	12/06/1983	Current
568004	Cordeaux Air Strip	Sydney Catchment Authority	2/08/1964	Current

SINCLAIR KNIGHT MERZ



Water Quality Modelling of the Hawkesbury-Nepean River System

Site Number	Site Name	Source	Start	End
568045	Warragamba Met Station	Sydney Catchment Authority	1/01/1981	Current
563046	Mcmahons Lookout	Sydney Catchment Authority	10/06/1960	Current
563059	Katoomba (Cascade Creek Dam No.1)	Sydney Catchment Authority	11/07/1980	Current
568048	Cataract Dam	Sydney Catchment Authority	16/12/1981	Current
563071	Medlow Bath (Lake Medlow Dam)	Sydney Catchment Authority	12/07/1983	Current
212438	Sackville Downstream	Sydney Water	1/07/1991	Current
567150	Blacktown (Dog Pound)	Sydney Water	11/09/1990	Current
567149	Cumberland State Forest (IBM)	Sydney Water	4/12/1990	Current
567148	Kings Langley (NSW Soccer Federation)	Sydney Water	5/09/1990	Current
567147	Baulkham Hills Swimming Pool	Sydney Water	4/09/1990	Current
567146	Greystanes (Cumberland Golf Club)	Sydney Water	11/09/1990	Current
567120	Brooklyn WWTP	Sydney Water	18/12/2007	Current
567113	Blacktown (Ashlar Golf Club)	Sydney Water	5/11/1990	Current
567109	Berowra Reservoir (Formerly Berowra BC)	Sydney Water	30/06/1990	Current
567105	Annangrove	Sydney Water	18/09/2008	Current
567106	Rouse Hill - Kellyville Country Club	Sydney Water	23/10/1990	18/09/2008
567151	Toongabbie Bowling Club	Sydney Water	11/09/1990	Current
567107	Penrith WRP	Sydney Water	6/05/1990	Current
561072	Chittaway	Sydney Water	1/12/1989	1/08/2010
567114	Canley Heights	Sydney Water	12/05/1992	1/07/2009
567162	Lalor Park (Vardys Road)	Sydney Water	12/06/1992	29/08/2005
567171	WS201 Seven Hills	Sydney Water	5/05/2001	Current
567169	Abbotsbury	Sydney Water	27/05/1994	Current
567168	Lethbridge Park	Sydney Water	27/09/1993	17/07/1995
567167	Kellyville (Castlebrook Cemetery)	Sydney Water	23/06/1993	Current
567166	Kenthurst (Jones Road)	Sydney Water	16/03/1993	Current
567165	Rouse Hill WRP	Sydney Water	11/09/1993	Current
567160	Hebersham Reservoir	Sydney Water	19/10/1991	Current
567163	Regentville Rural Fire Service	Sydney Water	14/01/2005	Current
567153	Minchinbury (Pinegrovve Memorial Park)	Sydney Water	6/08/1991	Current
567084	Quakers Hill WRP	Sydney Water	31/12/1960	Current
567161	Erskine Park Reservoir	Sydney Water	19/10/1991	Current
567104	Northmead Bowling Club	Sydney Water	20/03/1990	Current
567159	Mount Pleasant (Cranebrook Reservoir)	Sydney Water	13/08/1991	Current

SINCLAIR KNIGHT MERZ

Water Quality Modelling of the Hawkesbury-Nepean River System

Site Number	Site Name	Source	Start	End
567158	Orchard Hills (Kingswood Road Reservoir)	Sydney Water	23/08/1991	Current
567156	Orchard Hills (Flinders Avenue)	Sydney Water	13/08/1991	Current
567155	Shanes Park (International Transmitter Station)	Sydney Water	23/08/1991	Current
567164	Raby Reservoir	Sydney Water	3/12/1992	Current
561085	Narara	Sydney Water	1/04/1989	Current
567087	St Marys WRP	Sydney Water	31/12/1961	Current
561077	Kincumber	Sydney Water	19/05/1987	Current
561078	Kulnura	Sydney Water	21/06/1989	Current
568161	Berkeley (SPS296)	Sydney Water	28/10/1989	31/10/1990
563078	Leura (Hurley Heights/Mt Hay)	Sydney Water	4/07/1990	25/01/1995
212408	Webbs Creek	Sydney Water	1/06/1981	Current
561079	Lisarow	Sydney Water	6/04/1989	Current
563084	Wilberforce SPS1168	Sydney Water	2/02/2011	Current
563074	Newnes State Forest (East Boundary Road)	Sydney Water	19/06/1990	10/12/1997
212408	Hawkesbury River at Webbs Creek	Sydney Water	26/05/1988	Current
561098	Wyoming	Sydney Water	5/10/1988	Current
563069	North Richmond WWTP	Sydney Water	22/07/1982	Current
563065	Hazelbrook WWTP	Sydney Water	2/12/1981	Current
563064	Glenbrook RAAF (Formerly Glenbrook WWTP)	Sydney Water	1/01/1977	Current
563063	Springwood WWTP	Sydney Water	1/12/1981	19/05/1994
563062	Blackheath WWTP	Sydney Water	4/12/1981	22/08/2008
563060	Katoomba Bowling Club	Sydney Water	17/02/1987	23/07/2009
561084	Mount Elliot	Sydney Water	1/12/1987	Current
567075	Blacktown Survey Depot	Sydney Water	31/01/1970	30/06/1999
567100	Riverstone WWTP	Sydney Water	29/07/1983	Current
567097	Kellyville WWTP	Sydney Water	1/08/1975	12/05/1995
567096	West Hoxton	Sydney Water	26/11/1975	Current
567093	St Johns Park Bowling Club	Sydney Water	31/12/1983	4/11/1993
567092	South Prospect	Sydney Water	1/12/1976	14/12/1992
567085	Richmond WWTP	Sydney Water	25/10/1963	Current
567083	Prospect Reservoir	Sydney Water	1/01/1887	Current
563083	Blackheath Golf Course	Sydney Water	29/09/2008	Current
567076	Castle Hill WRP	Sydney Water	1/09/1973	Current
567102	Dural (WPS14)	Sydney Water	5/04/1990	Current
566146	Mona Vale	Sydney Water	28/06/1984	Current
566145	Avalon	Sydney Water	1/06/1994	Current
563150	Emu Plains Correctional Centre	Sydney Water	2/04/1998	10/08/1998

SINCLAIR KNIGHT MERZ

Water Quality Modelling of the Hawkesbury-Nepean River System

Site Number	Site Name	Source	Start	End
563149	Mount Victoria	Sydney Water	21/11/2008	Current
563148	Mount Victoria WWTP	Sydney Water	25/03/1993	21/08/2008
563146	Winmalee WWTP	Sydney Water	19/04/1990	Current
563090	Katoomba North\092044 2 South Street Katoomba	Sydney Water	4/11/2009	Current
567082	Orchard Hills (Orchard Hills WTW)	Sydney Water	10/04/1970	Current
568152	Corrimal (Turner Esplanade)	Sydney Water	29/08/1987	10/05/1988
568023	Mount Keira(Braziers)	Sydney Water	2/08/1964	Current
568170	Bombo WWTP	Sydney Water	10/02/1990	Current
568169	Port Kembla (SPS176)	Sydney Water	15/09/1990	Current
568168	Menangle Meteorological Station.	Sydney Water	17/07/1990	Current
568166	Picton (Cedar Creek)	Sydney Water	30/06/1990	3/09/2002
568162	Balgownie Reservoir	Sydney Water	1/03/1990	Current
568160	Wollongong (Mangerton Reservoir)	Sydney Water	20/10/1989	25/05/2005
568157	Minnamurra (Kiama Golf Club)	Sydney Water	01/08/1986	3/11/1995
568156	Camden Golf Course	Sydney Water	27/03/1987	Current
568172	Thirroul Bowling Club	Sydney Water	02/11/1990	Current
568153	Corrimal (Collins St)	Sydney Water	15/10/1987	Current
568173	Berkeley (Berkeley Sports and Social Club)	Sydney Water	02/11/1990	Current
568151	Cordeaux	Sydney Water	01/1/1900	1/01/1909
568149	Camden (Brownlow Hill)	Sydney Water	1/08/1985	Current
568147	Camden (Camden Park Reservoir)	Sydney Water	1/08/1985	Current
568145	Goondarin Ck	Sydney Water	7/01/1907	6/01/1922
568139	Buxton	Sydney Water	3/09/1965	Current
568138	Oakdale Wtw	Sydney Water	9/01/1976	Current
568137	Bellambi WWTP	Sydney Water	27/02/1976	06/02/1999
568136	Wollongong WRP	Sydney Water	01/1/1975	Current
568159	Kanahooka (Sps 308)	Sydney Water	11/09/1988	Current
568125	Kenny Hill	Sydney Water	7/01/1925	Current
568155	Menangle (Woodbridge Road)	Sydney Water	25/03/1987	17/07/1990
568313	Rhododendrum Park Parrish Rd Mt Pleasant	Sydney Water	3/06/1997	1/07/2009
66156	Marsfield (Willandra Village)	Sydney Water	30/10/1970	29/12/1982
67019	Prospect Dam	Sydney Water	5/03/1974	Current
61351	Peats Ridge (Waratah Rd)	Sydney Water	30/09/1981	Current
212407	Colo Junction	Sydney Water	1/05/1998	Current
68013	Menangle Jmai	Sydney Water	30/08/1986	14/01/1998
68039	Maddens Ck	Sydney Water	1/01/1907	1/01/1970

SINCLAIR KNIGHT MERZ



Water Quality Modelling of the Hawkesbury-Nepean River System

Site Number	Site Name	Source	Start	End
568352	Thirlmere (Rail Museum)	Sydney Water	28/11/2003	Current
568351	Tahmoor (Inghams Processing Plant)	Sydney Water	18/11/2003	Current
568350	Picton Bowling Club	Sydney Water	7/11/2003	Current
568171	Albion Park Bowling Club	Sydney Water	01/11/1990	Current
568317	Rixon Pass Rd Russel Vale	Sydney Water	5/06/1985	1/07/2009
568122	Burrawang Pumping Stn	Sydney Water	1/01/1973	6/09/1976
568310	CLOVER HILL RD MACQUARIE PASS NATIONAL PARK	Sydney Water	7/08/1985	1/07/2009
568188	Kiama (Water Tank)	Sydney Water	29/10/1992	Current
568187	Jamberoo (Woodstock)	Sydney Water	07/11/1992	Current
568186	Tongarra [Glenhaven]	Sydney Water	7/09/1992	Current
568185	Wongawilli (BHP Dust Monitoring Site)	Sydney Water	9/09/1992	Current
568180	Dapto Citizens Bowling Club	Sydney Water	23/09/1991	Current
568179	Campbelltown Bowling Club	Sydney Water	23/10/1991	Current
568178	Rosemeadow Reservoir At Greco Place	Sydney Water	2/08/1991	Current
568175	Kenny Hill (Trunk Receiving Station)	Sydney Water	2/08/1991	Current
568174	Eagleview Rd Reservoir at Minto	Sydney Water	4/09/1987	Current
568318	Broker Street Russel Vale	Sydney Water	1/04/1985	1/07/2009
568062	Sandy Ck Rd	Sydney Water	2/04/1964	Current
568088	Bargo West	Sydney Water	01/10/1962	31/03/1979
568130	West Camden WRP (Composite)	Sydney Water	30/08/1977	Current
568085	Toorooro Plateau	Sydney Water	31/05/1975	11/04/1980
568081	Wildes Meadow	Sydney Water	14/08/1973	18/10/2002
568079	Gerringong Ck Falls	Sydney Water	9/02/1968	Current
568077	Yarrawa Trig.	Sydney Water	6/03/1969	Current
568075	Tenaitch	Sydney Water	22/05/1974	16/03/1977
568074	Tenbee	Sydney Water	02/02/1974	12/10/1988
568073	Upper Stokes	Sydney Water	27/02/1974	18/03/1977
568121	Camden WWTP	Sydney Water	01/01/1947	28/02/1983
568066	Orange Grove	Sydney Water	2/06/1964	Current
568089	Broughton Pass	Sydney Water	1/01/1884	31/01/1996
568059	Broken Cup Rock	Sydney Water	2/04/1964	Current
568056	Mittagong (Lindsey Fire Tower)	Sydney Water	02/03/1964	14/12/1981
568055	Mittagong (Izzards Knob)	Sydney Water	2/06/1964	Current
568054	Mittagong Maguires Crossing	Sydney Water	1/08/1928	25/10/2002
568053	Picton WRP	Sydney Water	9/04/1998	Current

SINCLAIR KNIGHT MERZ



Water Quality Modelling of the Hawkesbury-Nepean River System

Site Number	Site Name	Source	Start	End
568052	Yerrinbool	Sydney Water	1/01/1916	1/01/1969
568049	Cordeaux Quarters	Sydney Water	25/05/1964	7/11/2002
568047	Nepean Dam	Sydney Water	31/12/1926	13/11/2002
568046	Avon Dam	Sydney Water	8/09/1964	12/11/2002
568044	Warragamba Water Filtration Plant	Sydney Water	29/02/2008	Current
568072	Cobbong	Sydney Water	8/03/1972	30/10/2002
568106	Oakdale (Silver Hills)	Sydney Water	3/01/1956	2/01/1976
568120	Port Kembla WWTP	Sydney Water	1/01/1970	Current
568119	Shellharbour WWTP	Sydney Water	1/01/1974	Current
568118	Wollongong (SPS144)	Sydney Water	9/11/1981	10/08/1998
568117	Corrimal	Sydney Water	1/01/1906	1/01/1961
568116	Cordeaux Dam No.1	Sydney Water	1/01/1908	1/01/1973
568115	Campbelltown WWTP	Sydney Water	01/01/1947	14/03/1986
568113	Wingecarribee Dam	Sydney Water	5/04/1972	15/10/2002
568112	Tallowa Dam	Sydney Water	9/01/1972	Current
568110	Yanderra	Sydney Water	17/10/1962	31/08/1997
568109	Wilton	Sydney Water	1/01/1902	1/01/1965
568087	Appin	Sydney Water	1/01/1907	1/01/1980
568107	Maddens Plains (Sublime Point)	Sydney Water	1/01/1919	1/01/1974
568094	Mittagong (High Range)	Sydney Water	31/12/1944	24/09/2002
568105	Sherbrooke	Sydney Water	01/01/1909	31/12/1970
568104	Robertson (Po)	Sydney Water	01/01/1900	1/01/1982
568102	Mount Murray	Sydney Water	1/10/1962	28/05/1996
568101	Mittagong (Maguires Crossing)	Sydney Water	01/08/1928	30/04/1991
568100	Maddens Ck (Darkes Forest)	Sydney Water	1/01/1907	1/01/1987
568099	Mittagong (Leicester Park)	Sydney Water	31/12/1945	19/11/2002
568098	Mittagong (Kia-Ora)	Sydney Water	1/01/2002	30/11/2002
568096	Jumping Rock	Sydney Water	1/01/1945	Current
568095	Mittagong (Inglewood)	Sydney Water	17/10/1962	31/10/1997
568108	Wedderburn	Sydney Water	6/01/1930	Current
568296	Thurns Road Tbrg	NSW Office of Water	24/01/1991	Current
568295	Lakesland Road Tbrg	NSW Office of Water	5/12/1990	Current

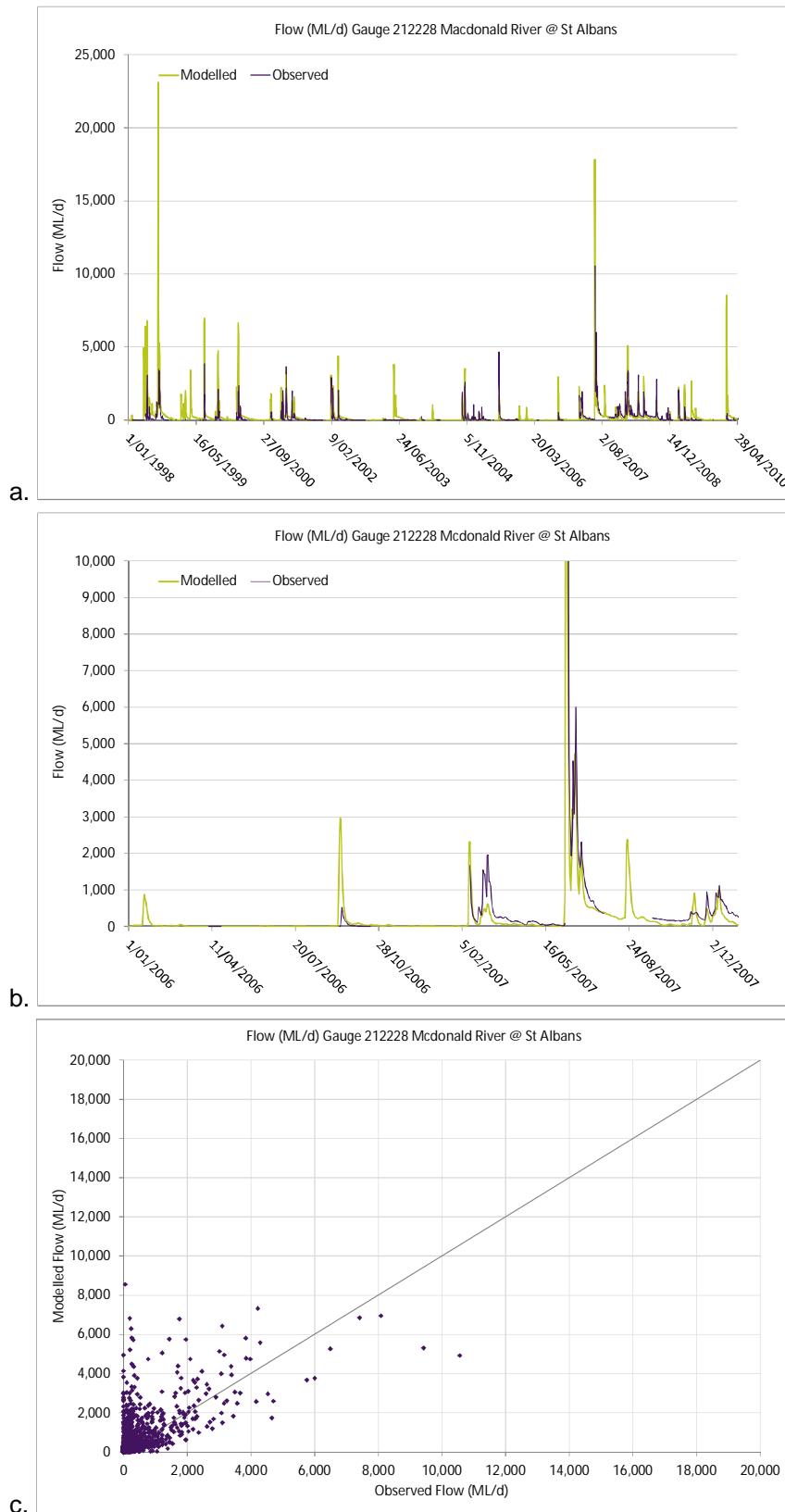
Appendix C Evaporation Sites Used for Derivation of Daily Evaporation Grids

Site Number	Source	Start	End
61029	Bureau of Meteorology	01-Jan-69	31-Dec-81
61086	Bureau of Meteorology	01-Jan-57	30-Apr-72
61193	Bureau of Meteorology	16-Mar-67	30-Nov-69
61240	Bureau of Meteorology	01-Sep-70	30-Apr-71
61242	Bureau of Meteorology	01-Jan-73	25-Apr-12
61351	Bureau of Meteorology	01-Jan-81	04-May-12
62046	Bureau of Meteorology	01-Jan-68	31-Dec-78
63005	Bureau of Meteorology	01-Jan-66	04-May-12
66037	Bureau of Meteorology	01-Jan-74	04-May-12
66062	Bureau of Meteorology	01-Jan-55	31-Dec-66
66078	Bureau of Meteorology	01-Jan-79	31-Dec-82
66131	Bureau of Meteorology	01-Jan-93	04-May-12
66134	Bureau of Meteorology	01-Jan-65	31-Dec-66
66156	Bureau of Meteorology	01-Jan-82	31-Dec-95
666052	Office of Water	01-Jan-76	30-Apr-02
667083	Office of Water	02-Jan-71	31-Jan-02
668045	Office of Water	01-Jan-75	31-May-02
668046	Office of Water	15-Feb-74	28-Feb-02
668047	Office of Water	01-Jan-75	28-Feb-02
668049	Office of Water	19-Feb-74	28-Feb-02
668113	Office of Water	01-Nov-78	28-Feb-02
67019	Bureau of Meteorology	01-Jan-65	04-May-12
67021	Bureau of Meteorology	01-Jan-72	31-Mar-12
67027	Bureau of Meteorology	01-Feb-05	31-Jan-08
67033	Bureau of Meteorology	01-Jan-70	31-Dec-94
67068	Bureau of Meteorology	01-May-67	31-Dec-84

Appendix D Comparison Plots Between Observed and Simulated Flows

Water Quality Modelling of the Hawkesbury-Nepean River System

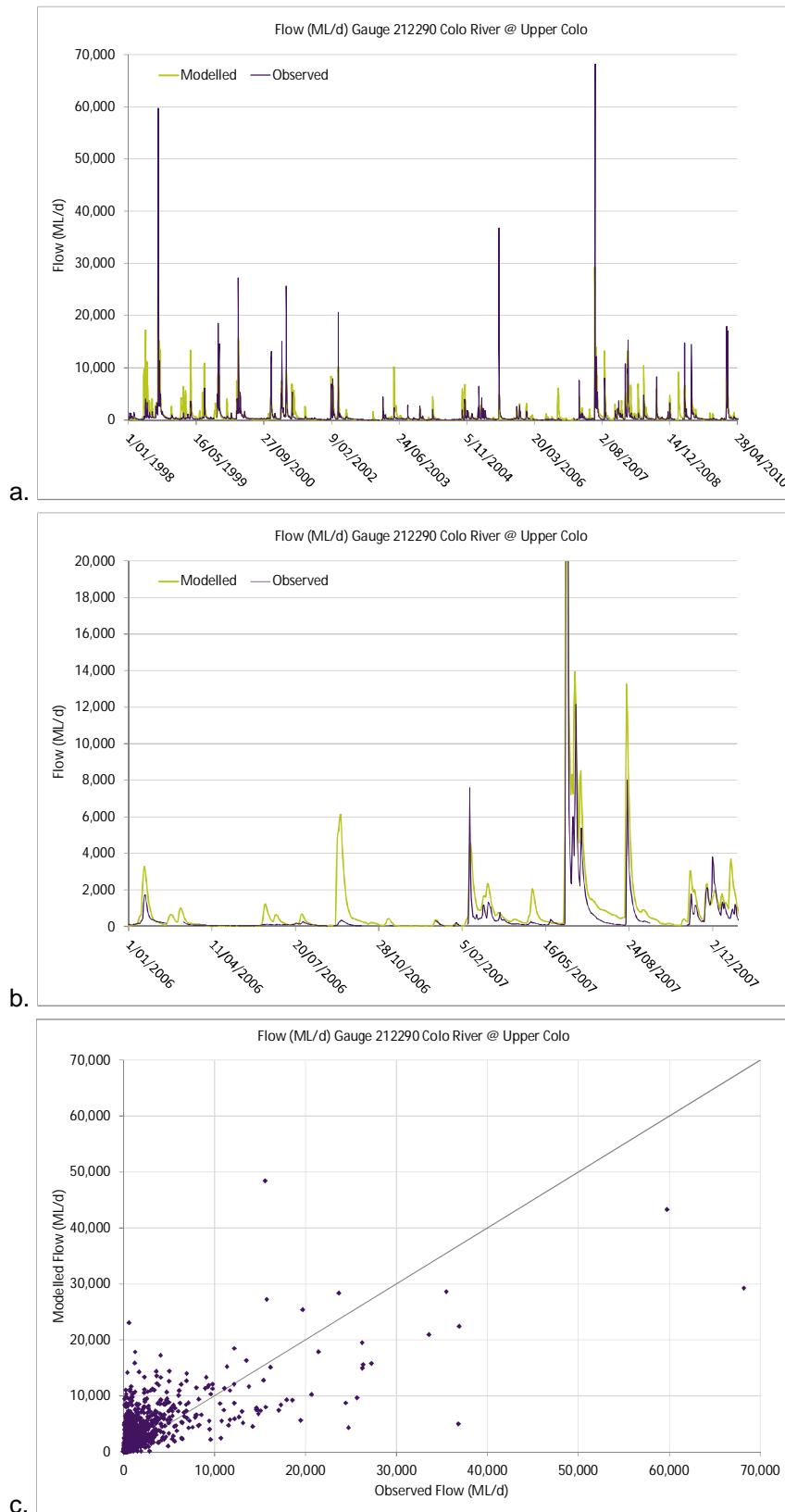
D.1. Macdonald River gauging station 212228



SINCLAIR KNIGHT MERZ

Water Quality Modelling of the Hawkesbury-Nepean River System

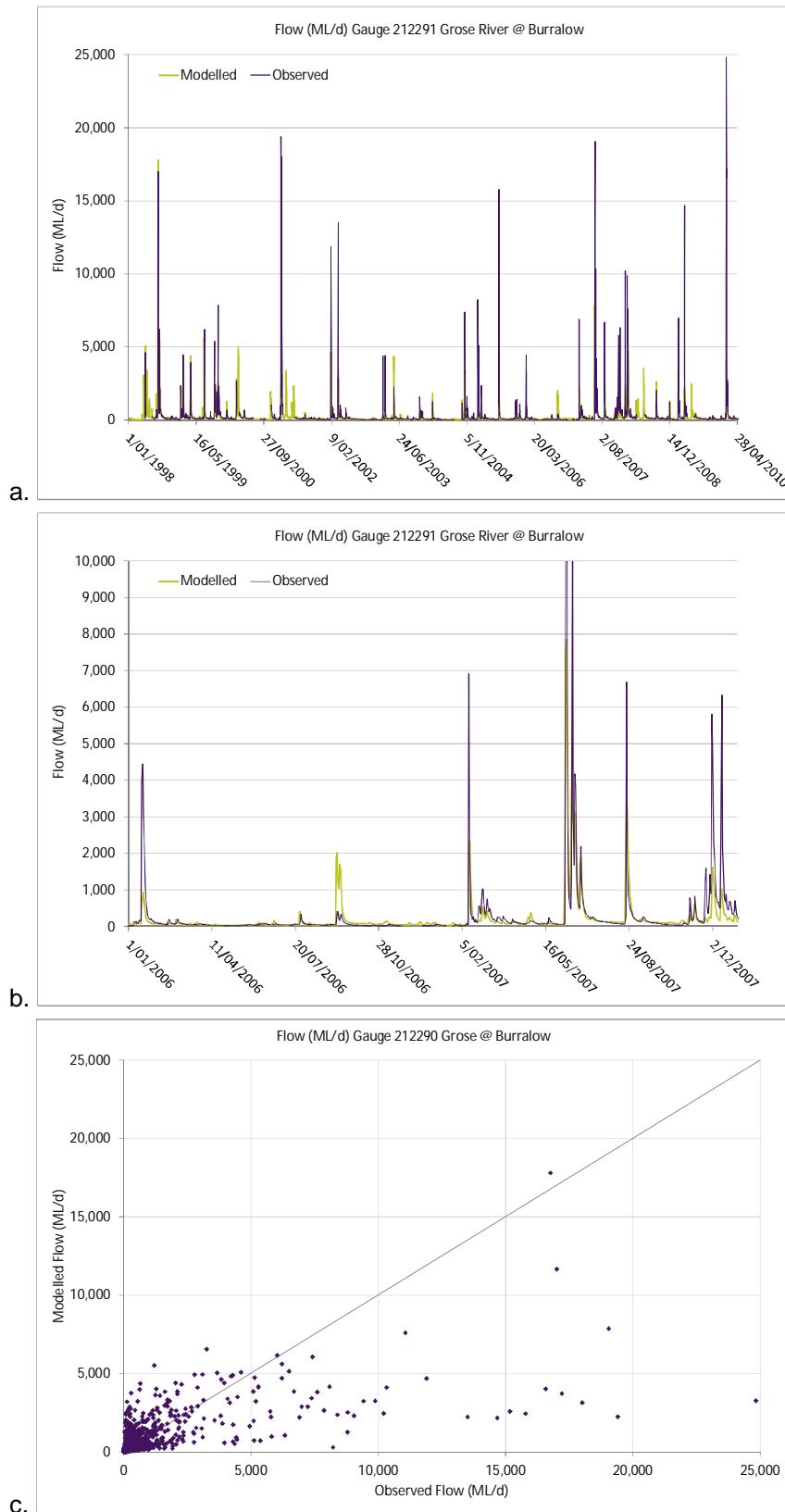
D.2. Upper Colo River gauging station 212290



SINCLAIR KNIGHT MERZ

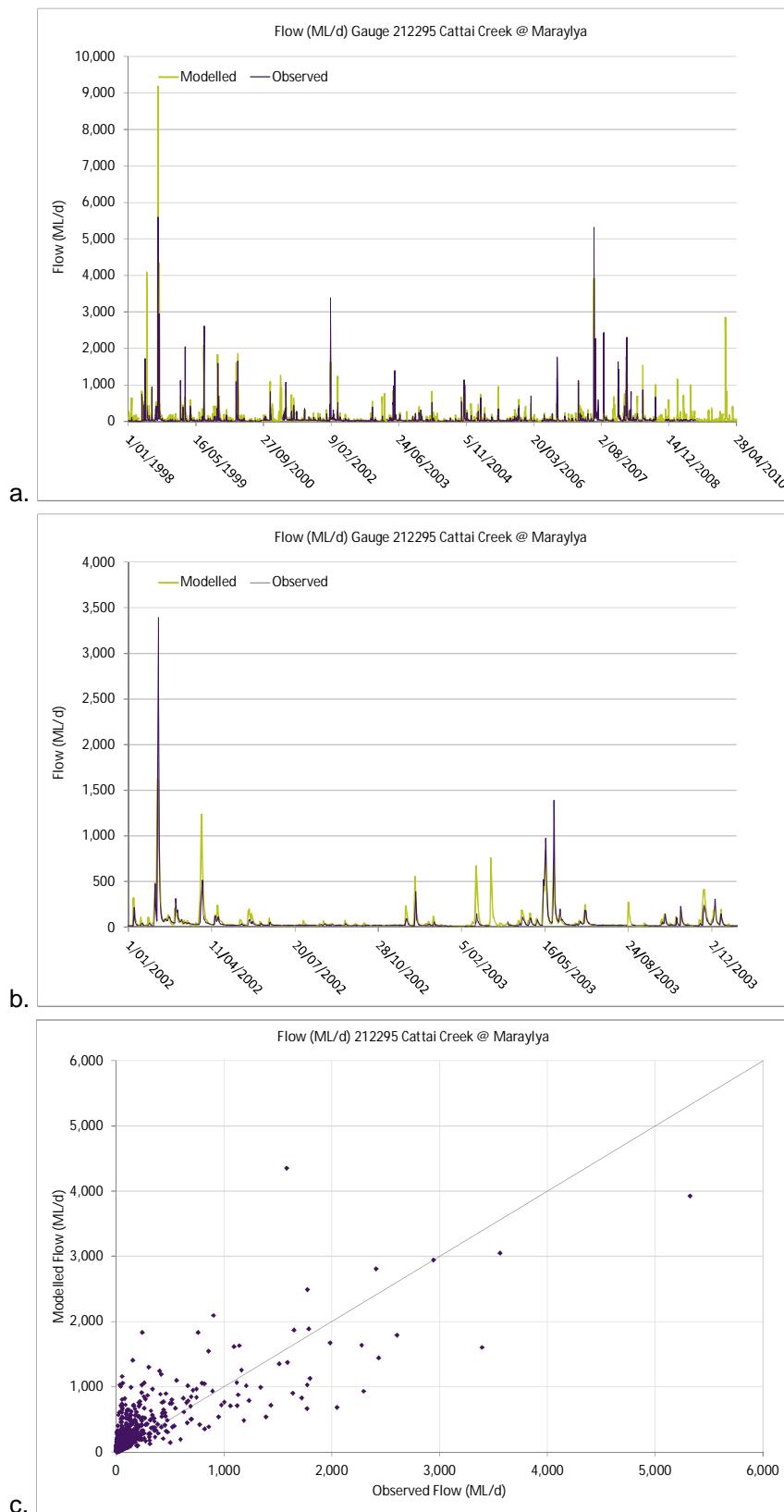
Water Quality Modelling of the Hawkesbury-Nepean River System

D.3. Grose River gauging station 212291



Water Quality Modelling of the Hawkesbury-Nepean River System

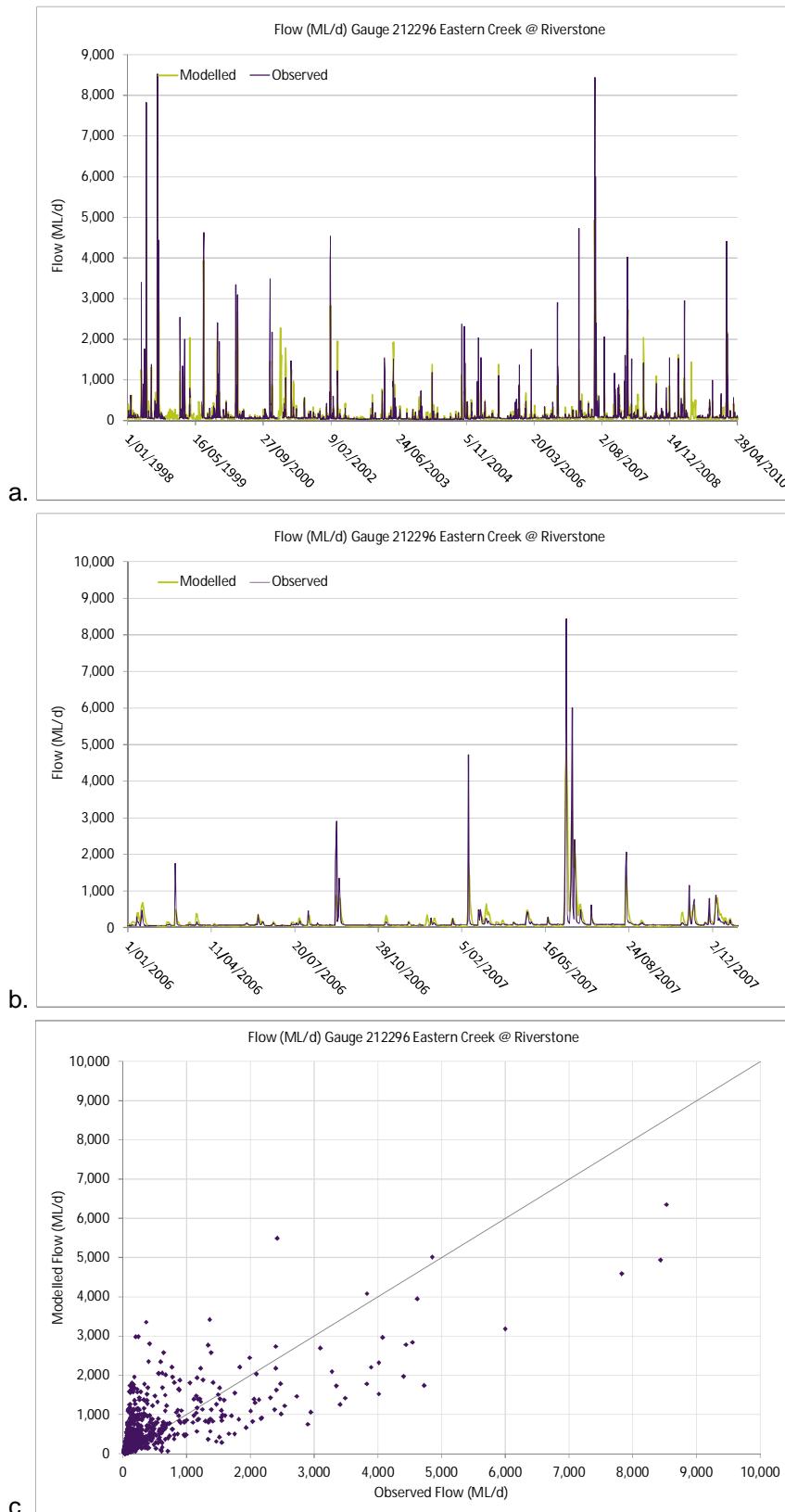
D.4. Cattai Creek at Maraylya gauging station 212295



SINCLAIR KNIGHT MERZ

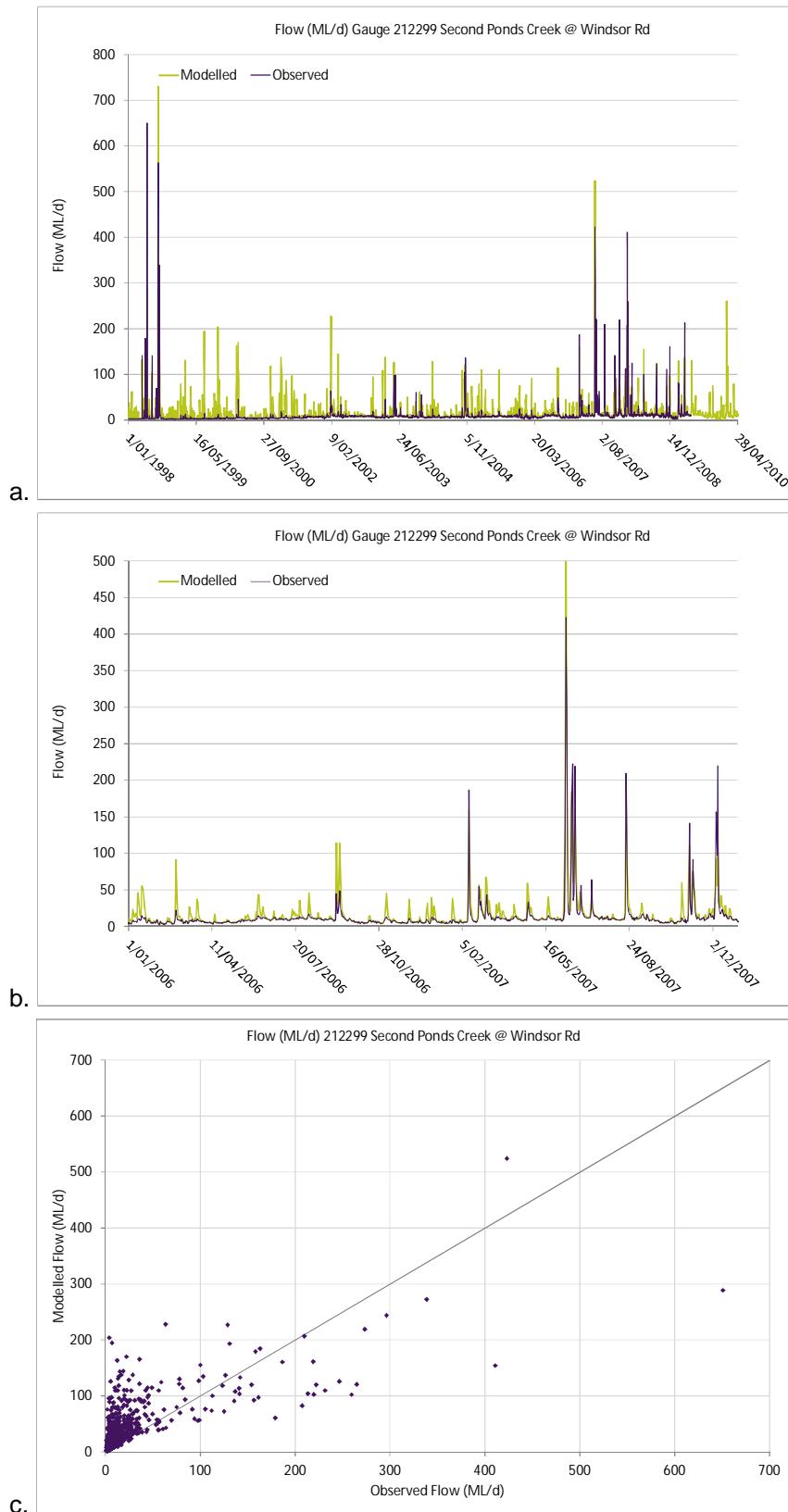
Water Quality Modelling of the Hawkesbury-Nepean River System

D.5. Eastern Creek at Riverstone gauging station 212296



Water Quality Modelling of the Hawkesbury-Nepean River System

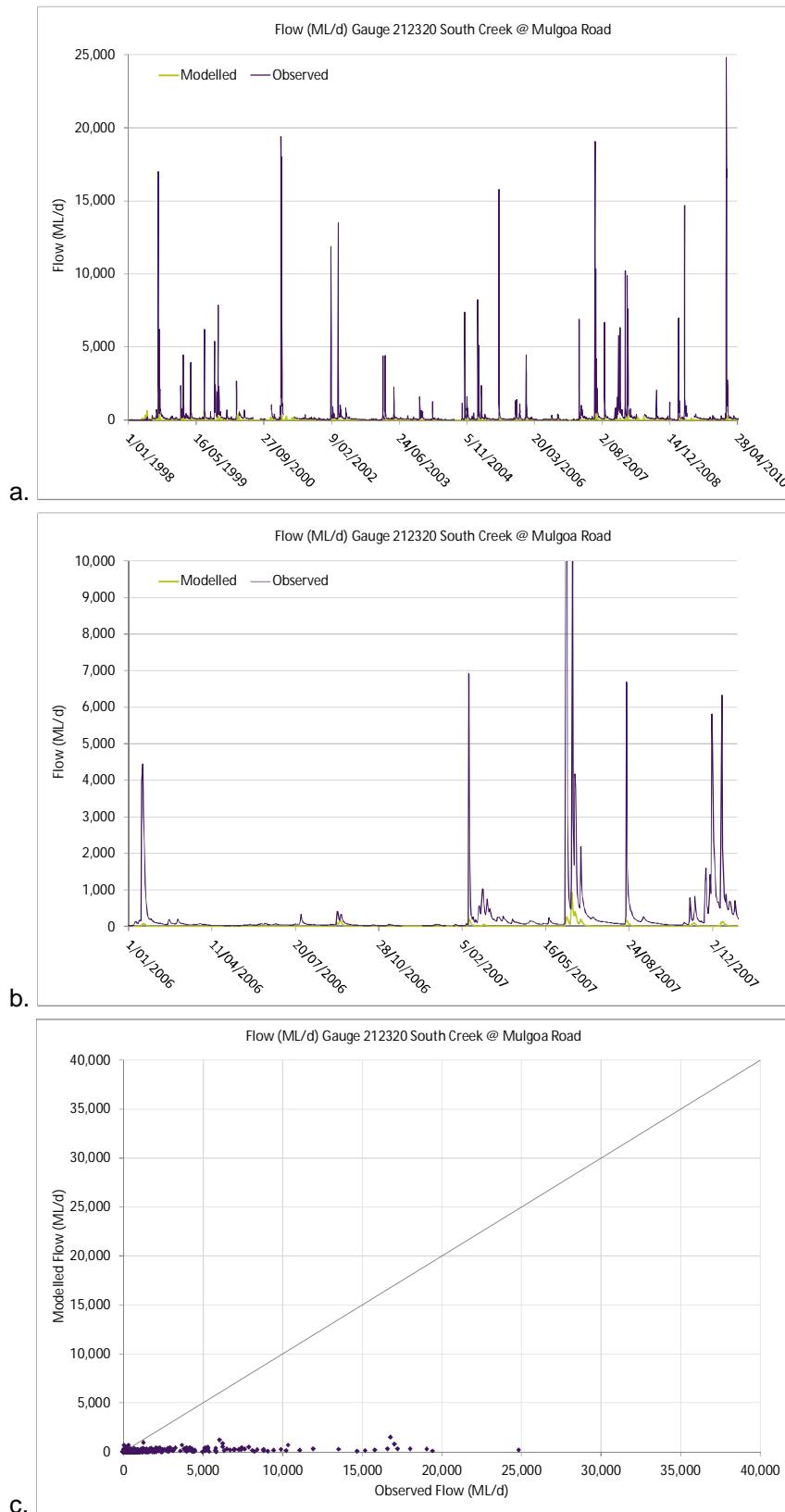
D.6. Second Ponds Creek at Windsor Road gauging station 212299



SINCLAIR KNIGHT MERZ

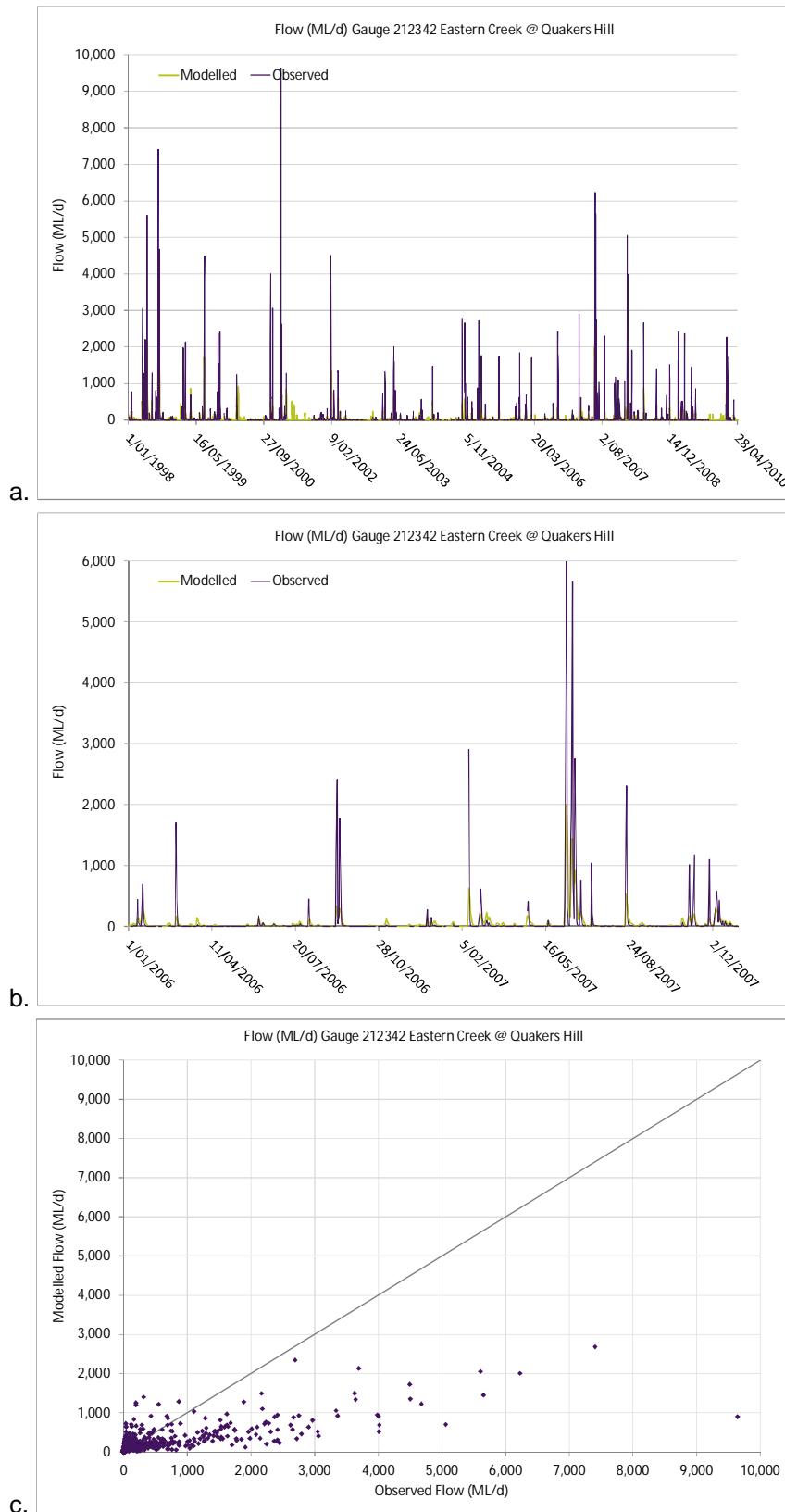
Water Quality Modelling of the Hawkesbury-Nepean River System

D.7. South Creek at Mulgoa Road gauging station 212320



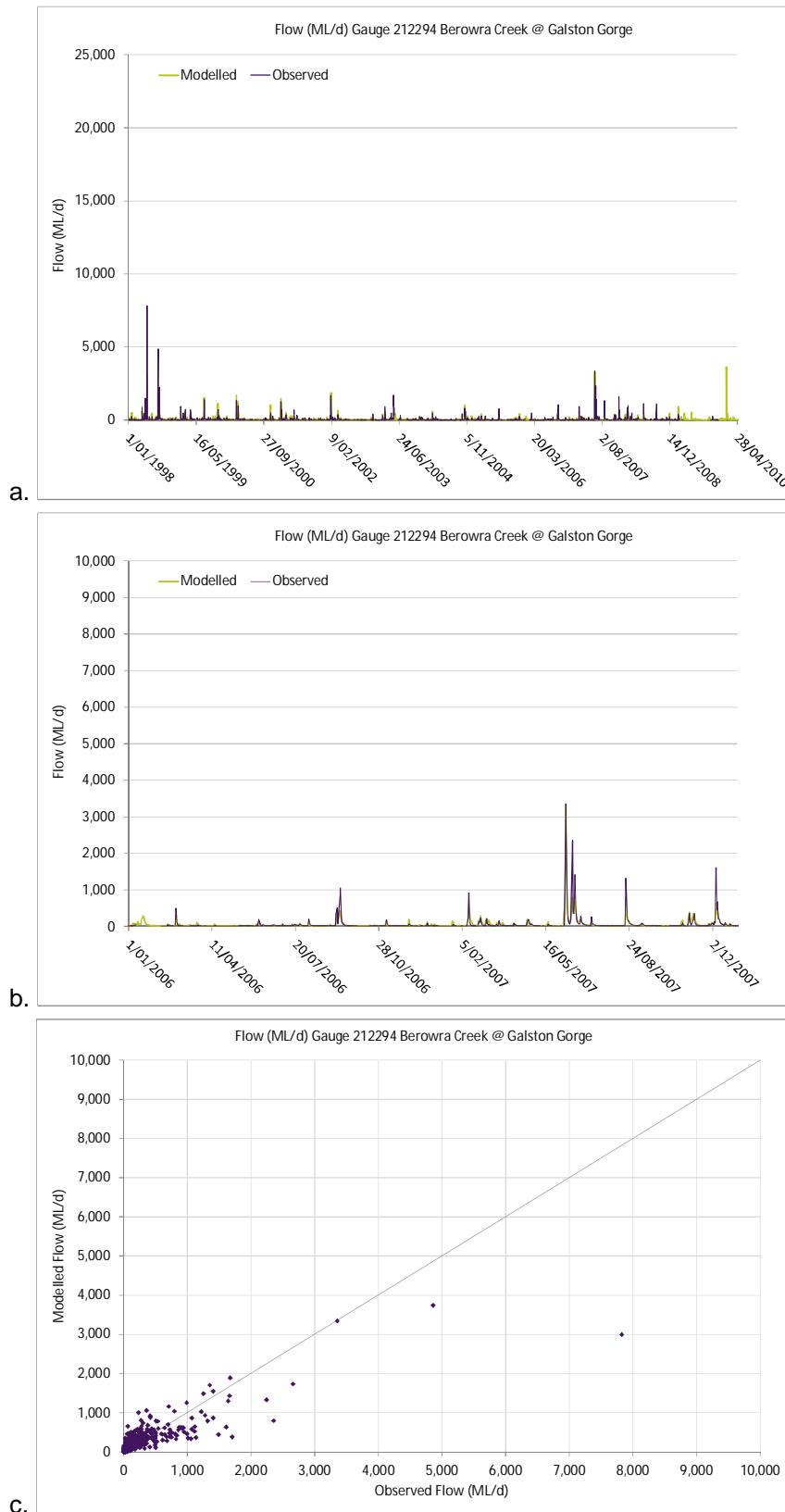
Water Quality Modelling of the Hawkesbury-Nepean River System

D.8. Eastern Creek at Quakers Hill gauging station 212342



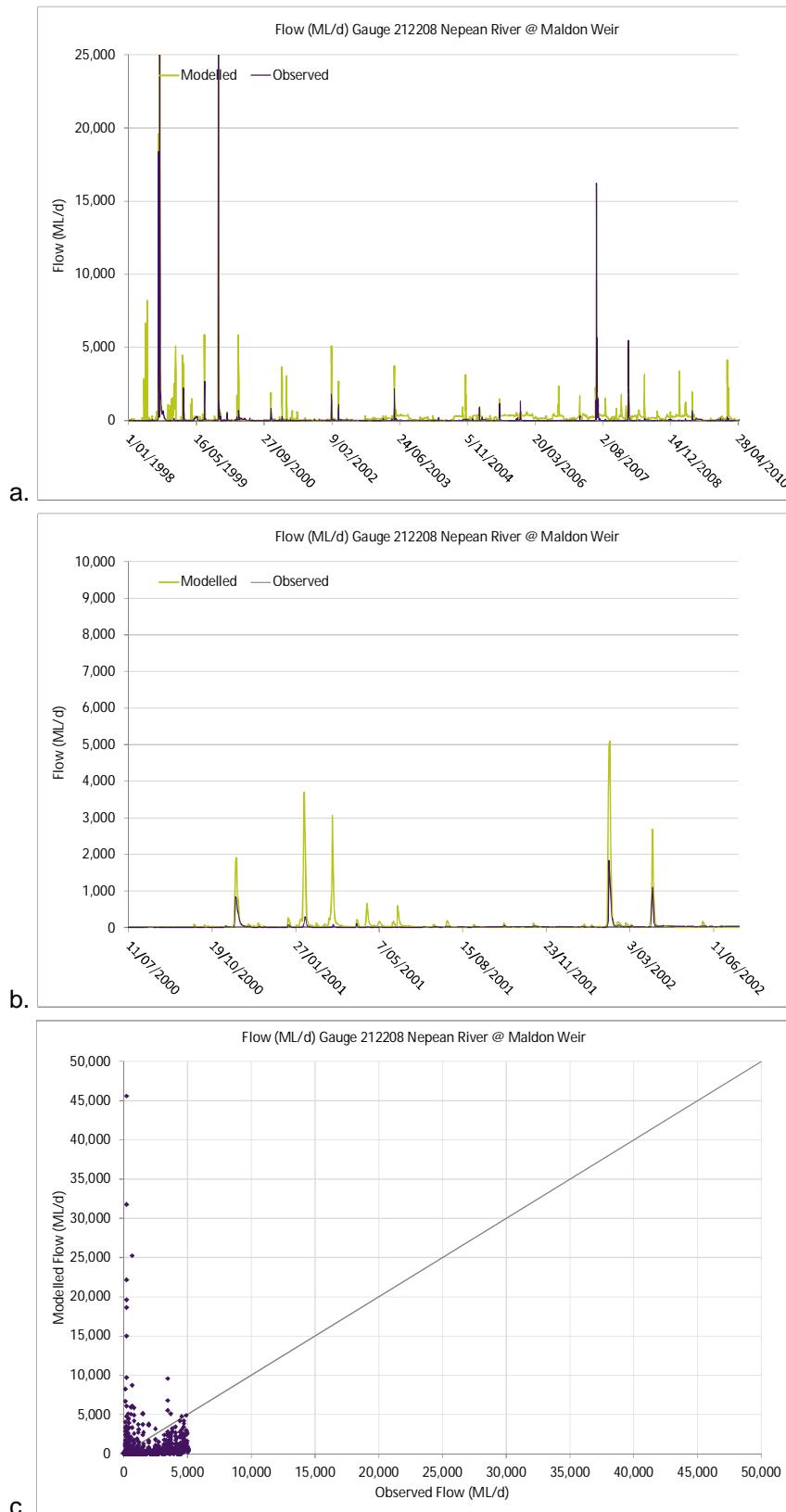
Water Quality Modelling of the Hawkesbury-Nepean River System

D.9. Berowra Creek at Galston Gorge gauging station 212294



Water Quality Modelling of the Hawkesbury-Nepean River System

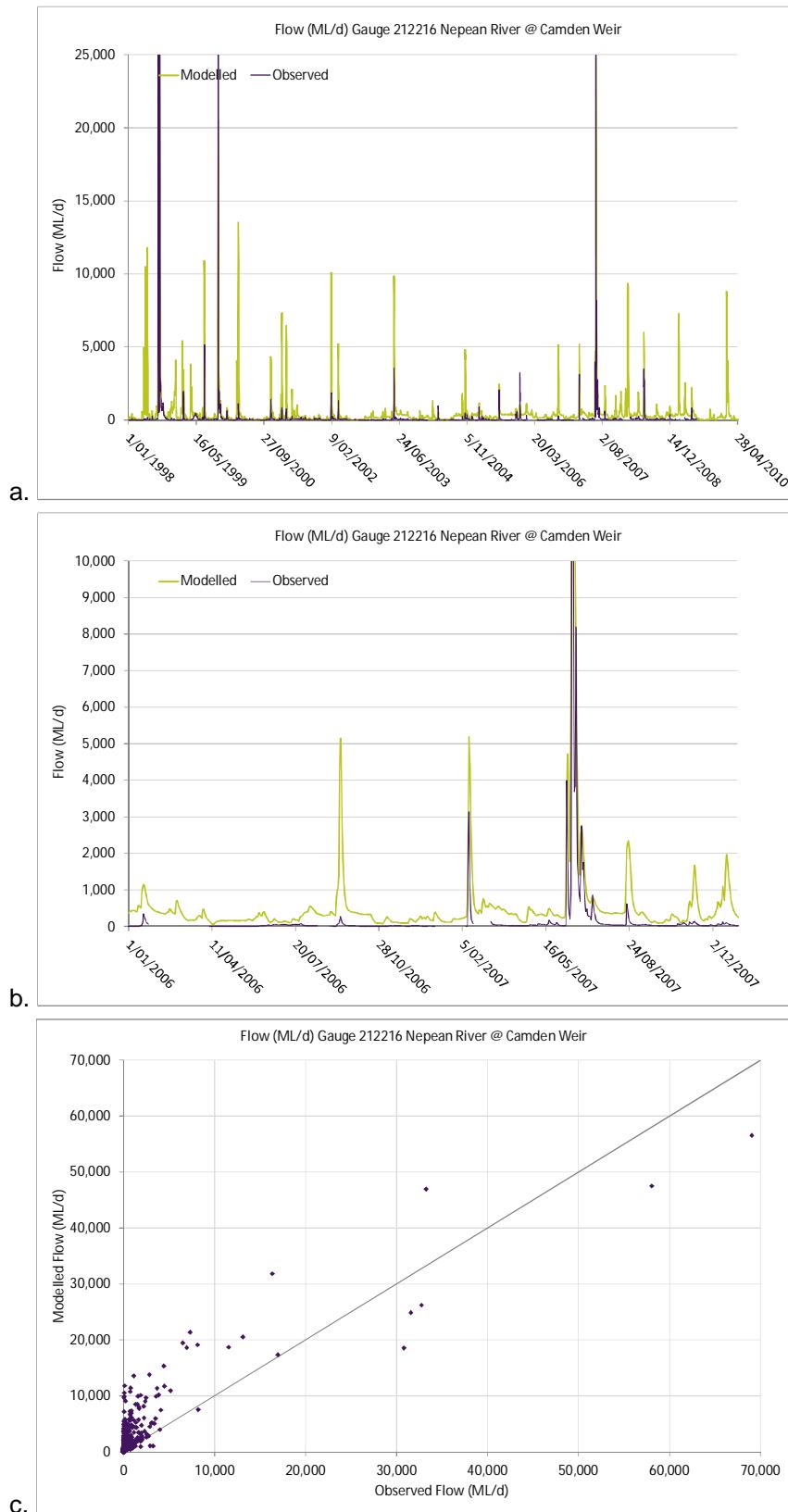
D.10. Nepean River at Maldon Weir gauging station 212208



SINCLAIR KNIGHT MERZ

Water Quality Modelling of the Hawkesbury-Nepean River System

D.11. Nepean River at Camden Weir gauging station 212216



SINCLAIR KNIGHT MERZ

Appendix E Event Campaign Monitoring Program

This section outlines the water quality sampling which was undertaken as part of the Event Campaign Monitoring Program.

The water quality parameters sampled as part of the Event Campaign Monitoring Program were:

- Temperature
- Dissolved oxygen
- pH
- Total organic carbon
- Components of total nitrogen
- Components of total phosphorus



Water Quality Modelling of the Hawkesbury-Nepean River System

E.1 Event Campaign Monitoring Program Site Details

Site name	Station number	Water quality code	Autosampler	Bottle configuration	Site responsibility	Latitude Longitude	Deployed	Decommissioned	Total number of events
South Creek at Mulgoa Road	212320	NS45	Isco 3700 refrigerated	24 bottles 900mL samples	NOW	-33.89360000 150.77080000	March 2012	November 2012	3
Eastern Creek at Quakers Hill	212342	NS0861	Isco Avalanche refrigerated	14 bottles 850 mL samples	SCA	-33.73990000 150.86400000	March 2012	November 2012	6
Ropes Creek at Debrincat Ave	212049	NS212	Isco Avalanche refrigerated	14 bottles 850 mL samples	NOW	-33.75500000 150.79100000	March 2012	November 2012	6
Stonequarry Creek at Picton	212053	N912	Isco Avalanche refrigerated	14 bottles 850 mL samples	NOW	-34.18330000 150.11670000	March 2012	November 2012	2
Colo River at Upper Colo	212290	N2203	Isco Avalanche refrigerated	14 bottles 850 mL samples	SCA	-33.41940000 150.72500000	March 2012	March 2013	1
Grose River at Burrallow	212291	NG4302	Isco non-refrigerated	24 bottles 900mL samples	SCA	-33.61670000 150.62780000	April 2012	March 2013	1



Water Quality Modelling of the Hawkesbury-Nepean River System

E.2 Wet Weather Events Captures as per the CMP Events

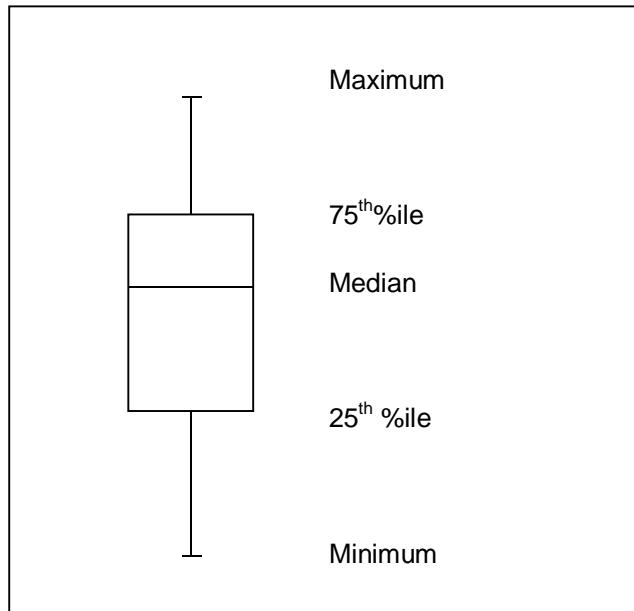
Site name	Station number	Water quality code	Event start date/time	Event finish date/time	No. samples	Grab sample
South Creek at Mulgoa Road	212320	NS45	29/02/12 14:25	5/03/12 9:00	46	23/04/12 10:05
			18/04/12 15:39	21/04/12 13:39	37	
			12/06/12 13:11	13/06/12 7:11	7	
Eastern Creek at Quakers Hill	212342	NS0861	2/03/12 11:25	6/03/12 14:25	34	23/04/12 10:00
			17/03/12 2:05	19/3/12 14:25	15	
			17/4/12 21:14	22/4/12 16:56	24	
			24/5/12 19:40	26/5/12 7:39	15	
			5/6/12 16:12	7/6/12 16:12	13	
			12/10/12 14:45	14/10/12 18:45	14	
Ropes Creek at Debrincat Ave	212049	NS212	29/02/12 12:11	4/03/12 9:11	36	19/3/12 13:40 23/04/12 10:35
			16/03/12 19:56	17/03/12 21:56	15	
			18/04/02 4:19	22/04/12 19:07	23	
			5/06/12 17:15	6/06/12 11:15	10	
			12/06/12 12:09	13/06/12 10:09	12	
			11/10/12 18:46	15/10/12 20:46	24	
Stonequarry Creek at Picton	212053	N912	28/02/12 19:48	4/03/12 11:48	46	
			18/04/12 5:18	19/04/12 1:18	11	
Colo River at Upper Colo	212290	N2203	2/03/12 12:57	4/03/12 12:57	9	
Grose River at Burrallow	212291	NG4302	18/04/12 11:49	20/04/12 12:02	11	23/04/12 10:40

SINCLAIR KNIGHT MERZ

Appendix F Comparison Plots Between Observed and Simulated Concentrations

A comparison between observed and simulated concentrations is presented as box and whisker plots. Box and whisker plots represent the minimum, 25th percentile, median, 75th percentile and maximum concentrations.

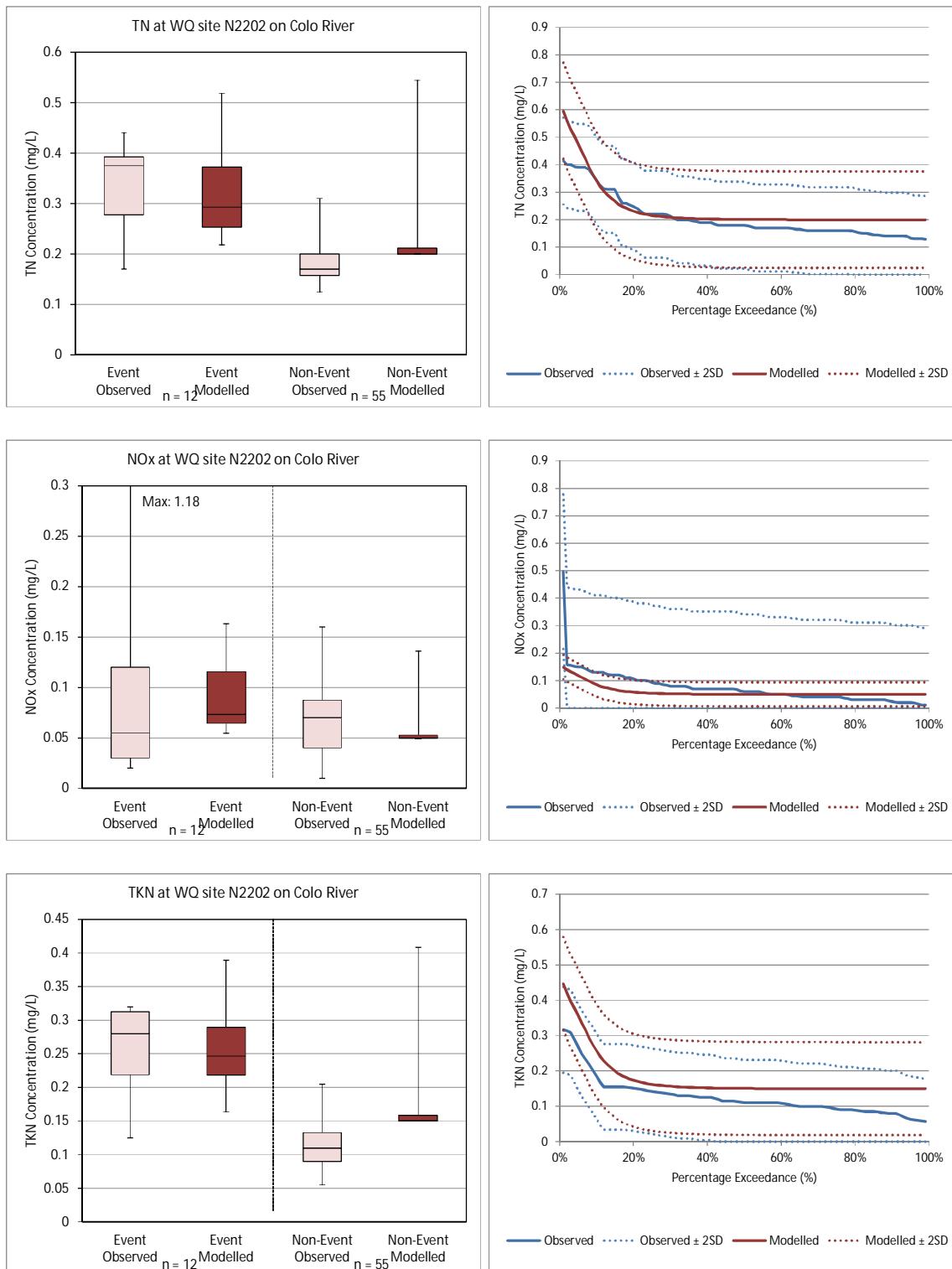
The exceedance plots show the percentile curve as a solid line with plus and minus two standard deviations of the percentile curve as dashed lines.

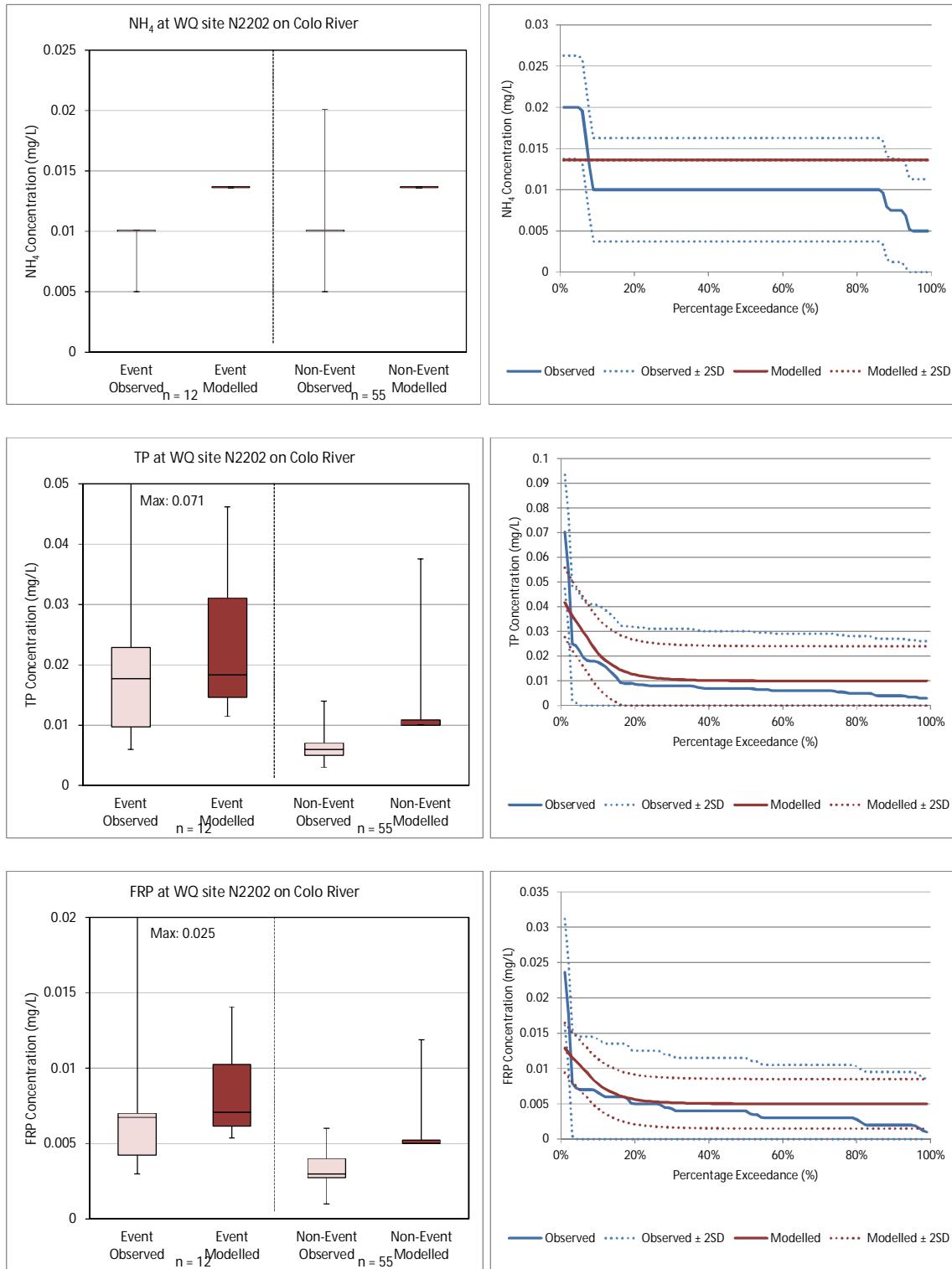
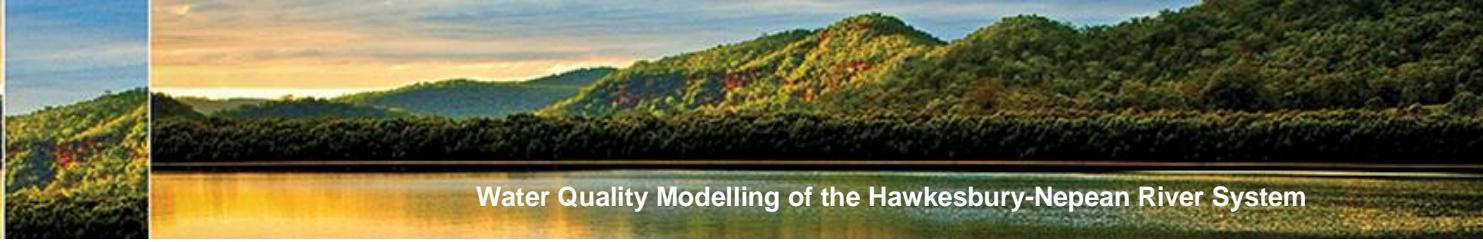




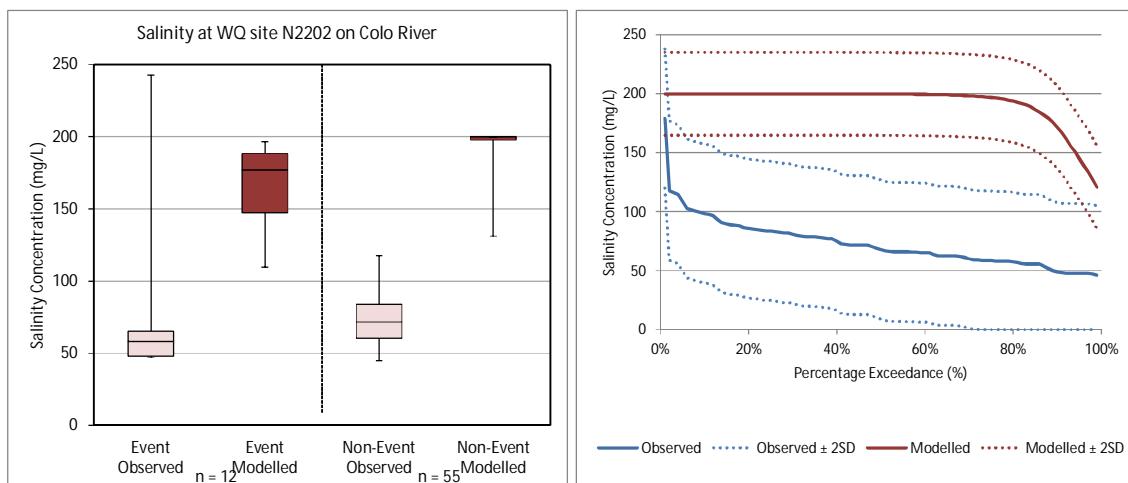
Water Quality Modelling of the Hawkesbury-Nepean River System

F.1. Water quality site N2202 – Colo River



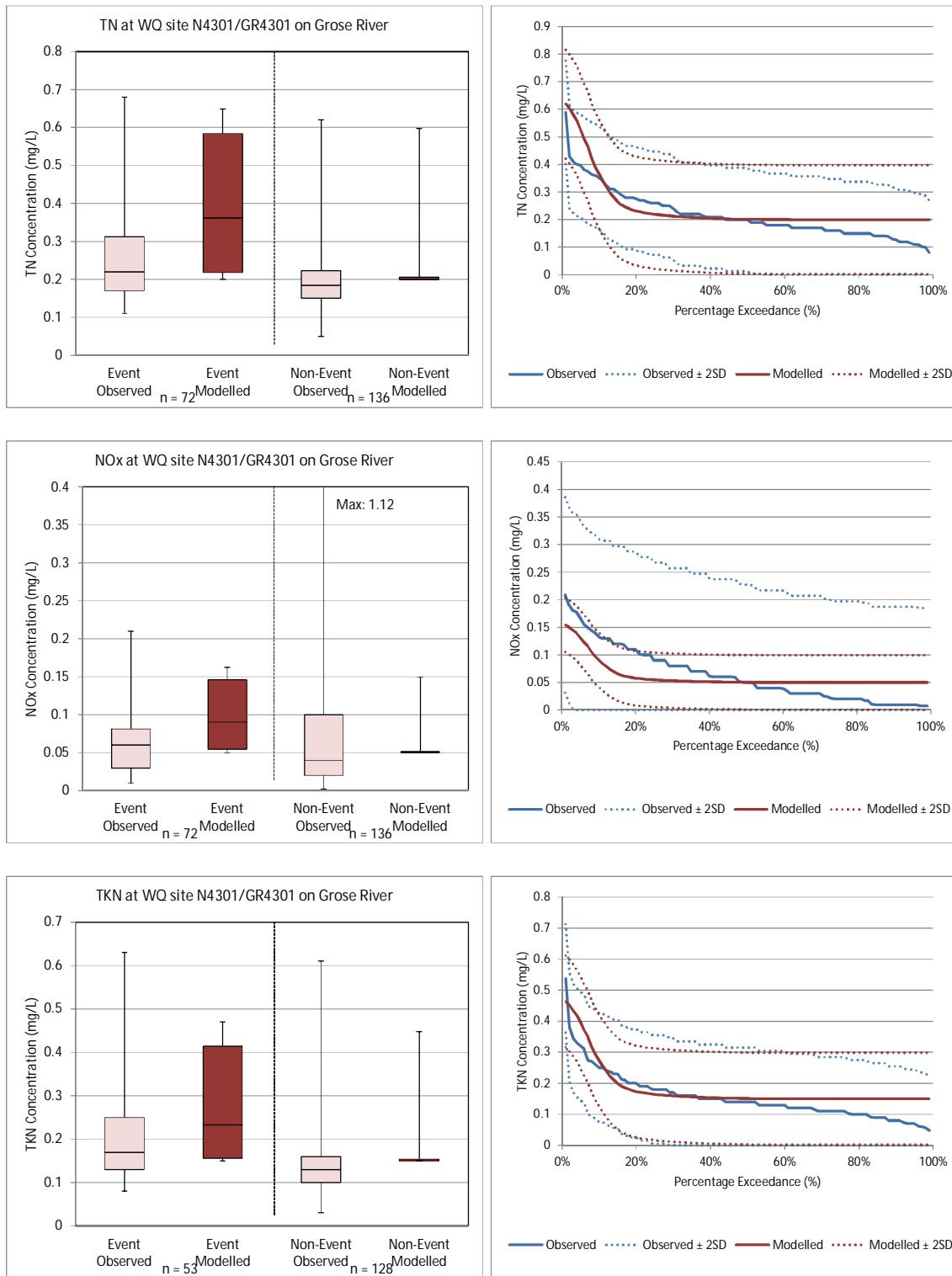


Water Quality Modelling of the Hawkesbury-Nepean River System

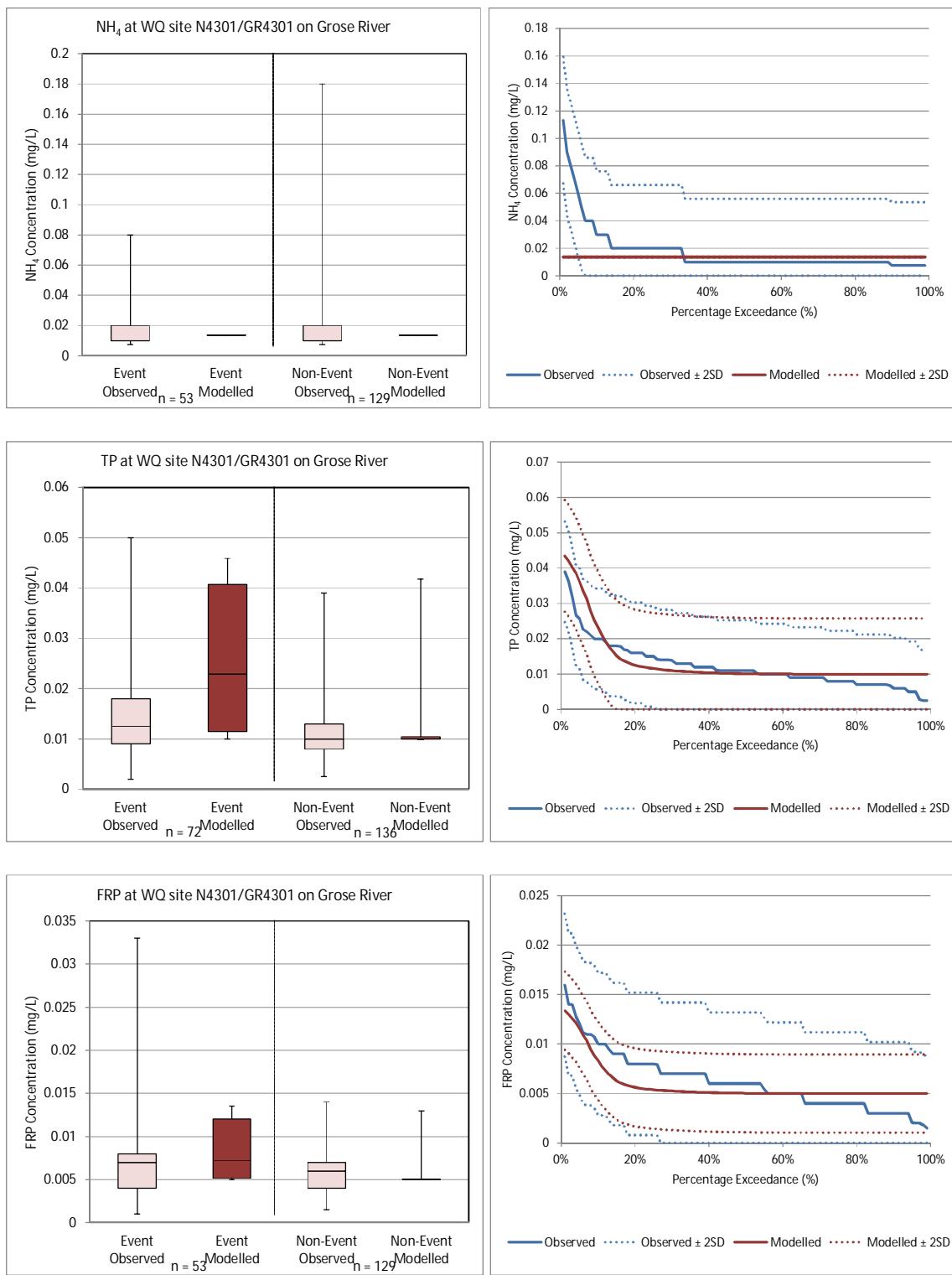




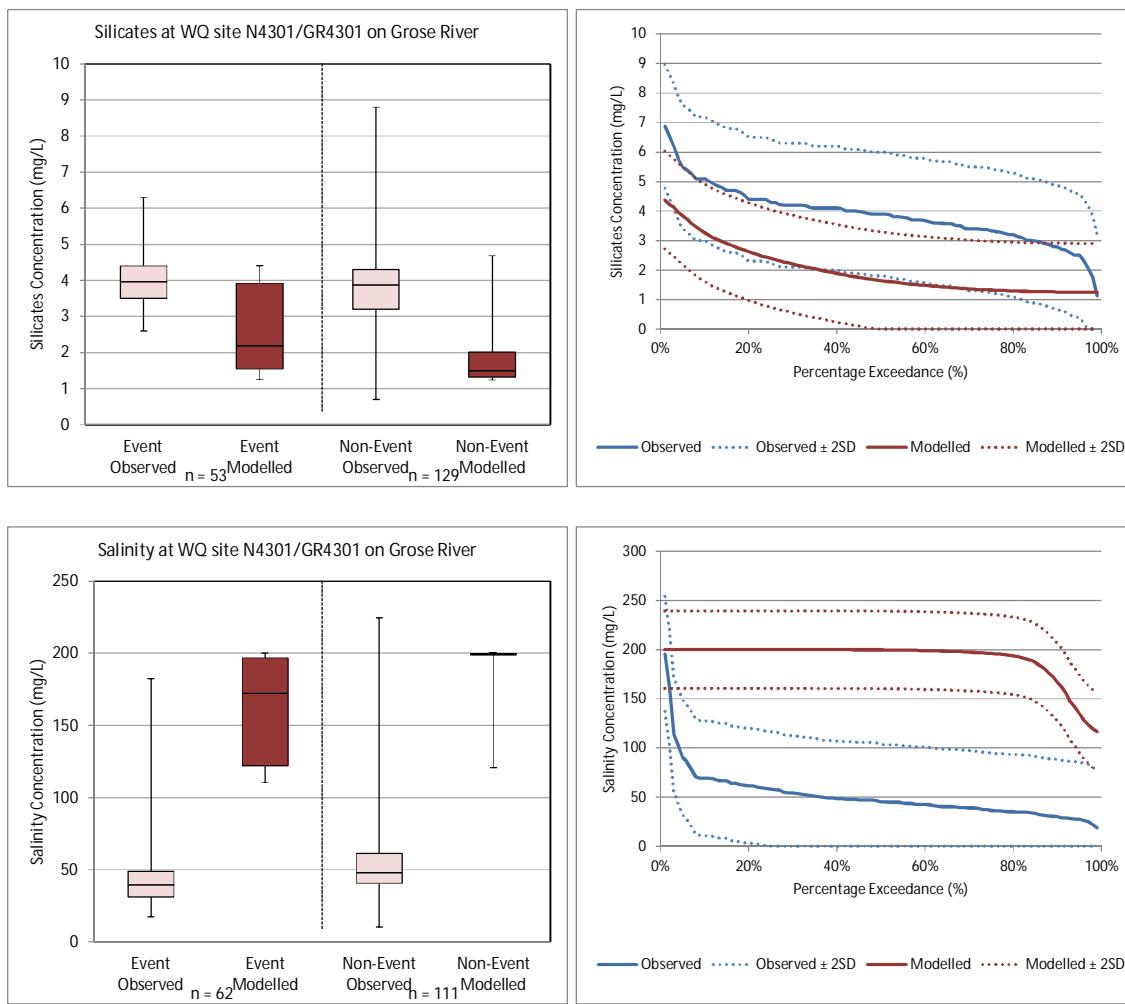
F.2. Water quality site N4301 – Grose River



Water Quality Modelling of the Hawkesbury-Nepean River System

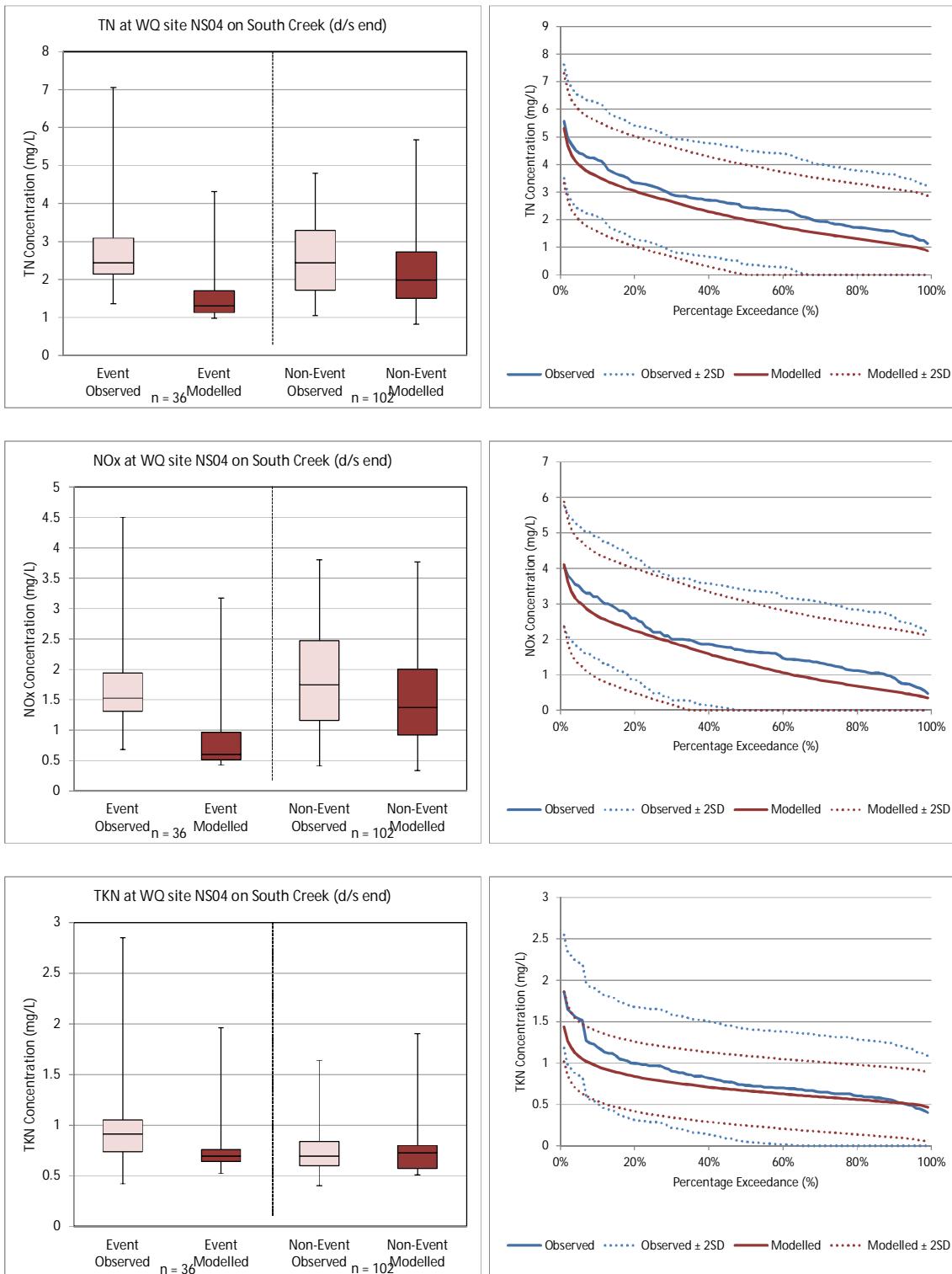


Water Quality Modelling of the Hawkesbury-Nepean River System

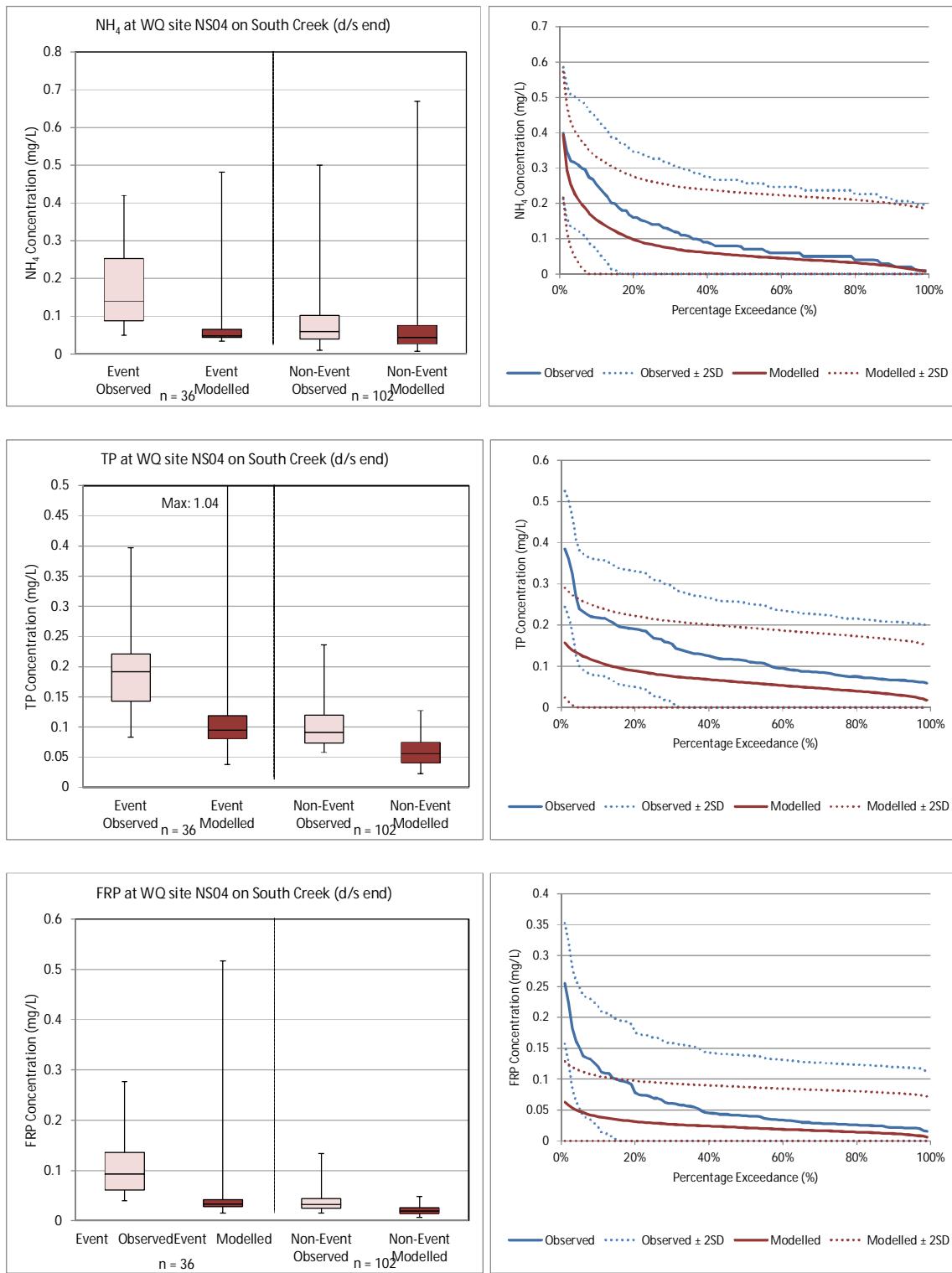




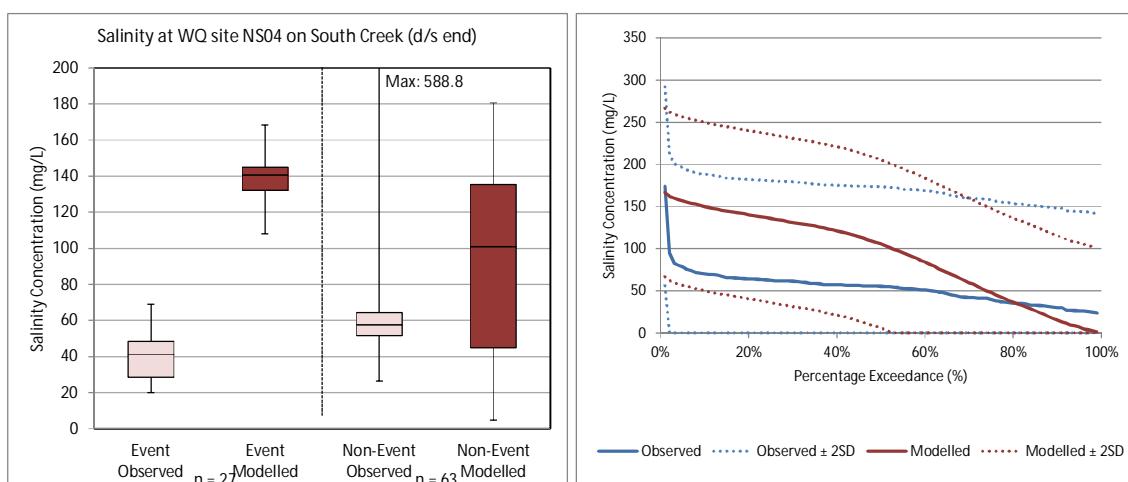
F.3. Water quality site NS04 – South Creek



Water Quality Modelling of the Hawkesbury-Nepean River System

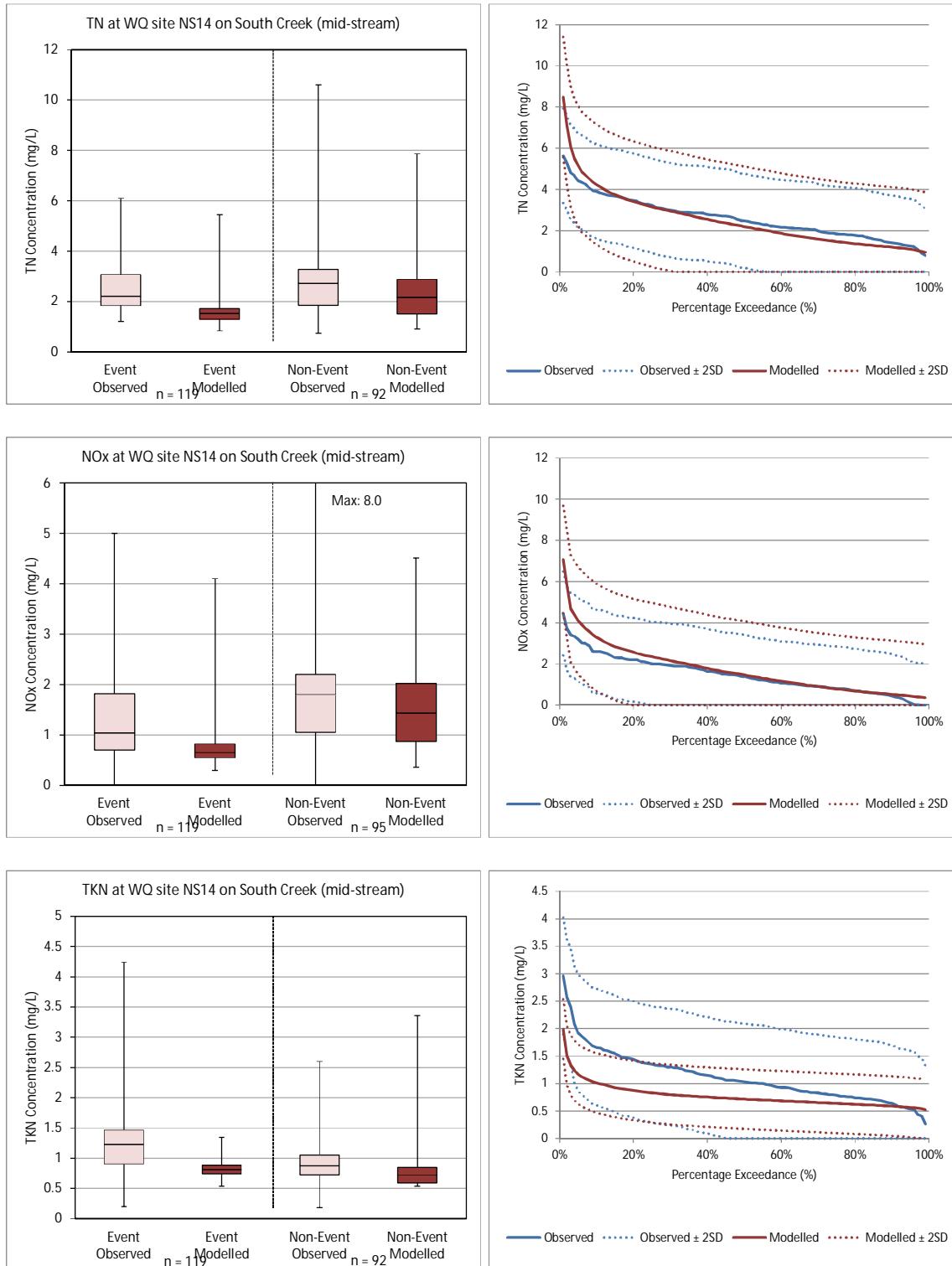


Water Quality Modelling of the Hawkesbury-Nepean River System

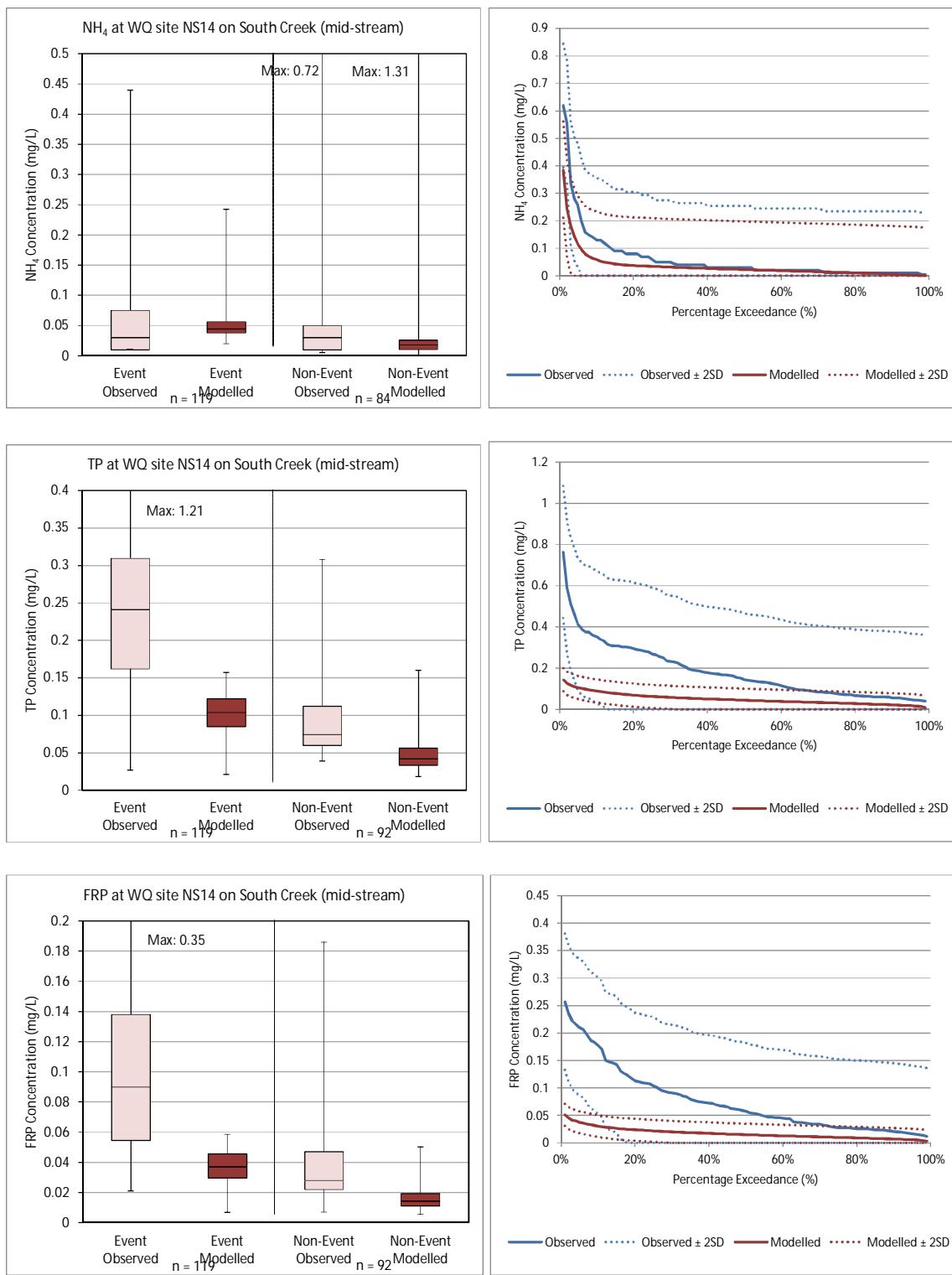


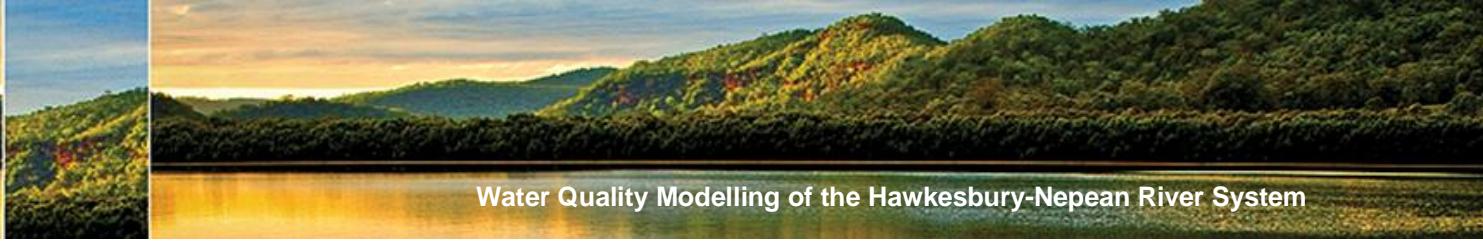


F.4. Water quality site NS14 – South Creek

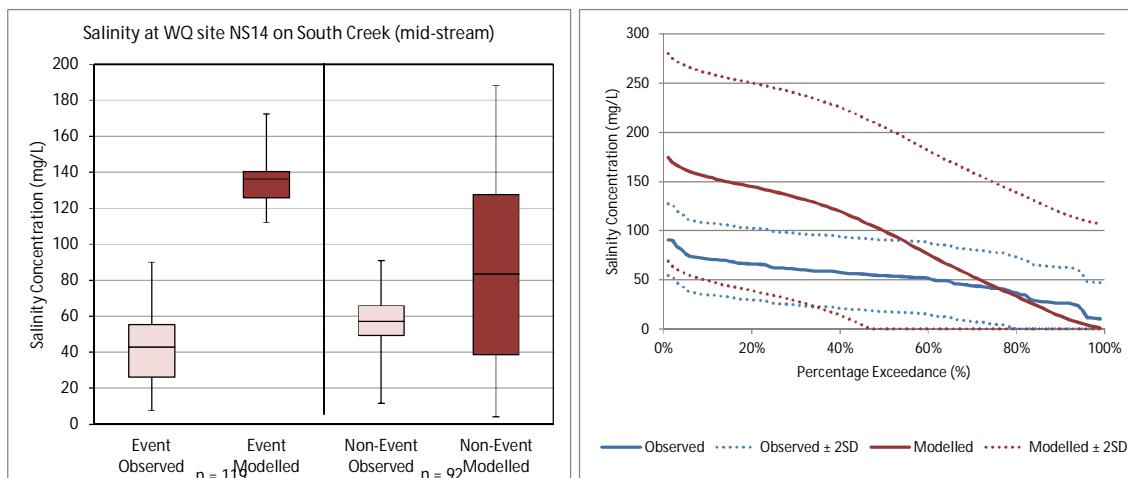


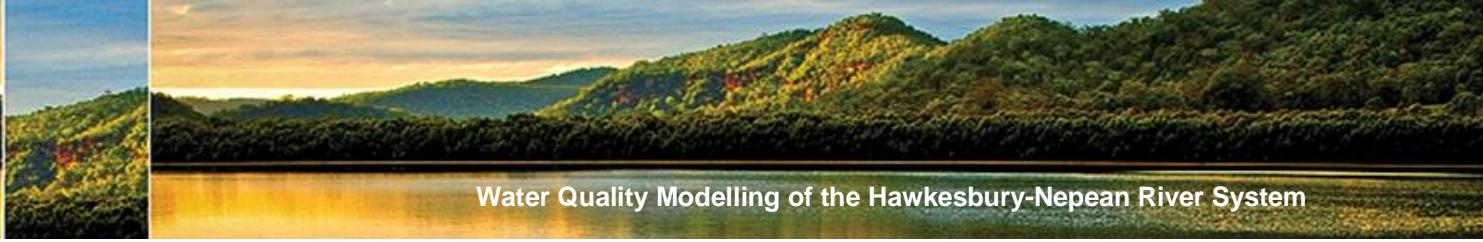
Water Quality Modelling of the Hawkesbury-Nepean River System



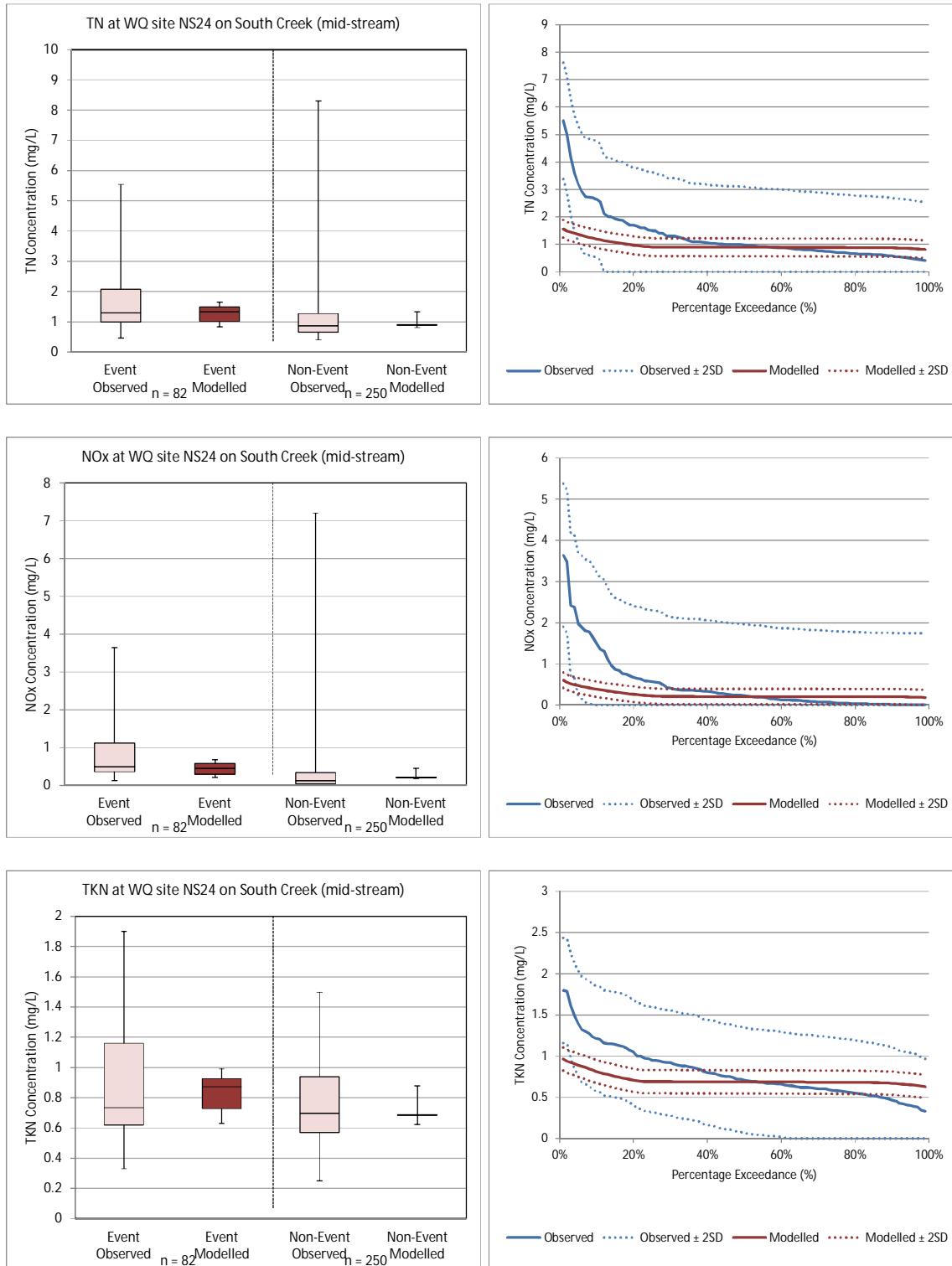


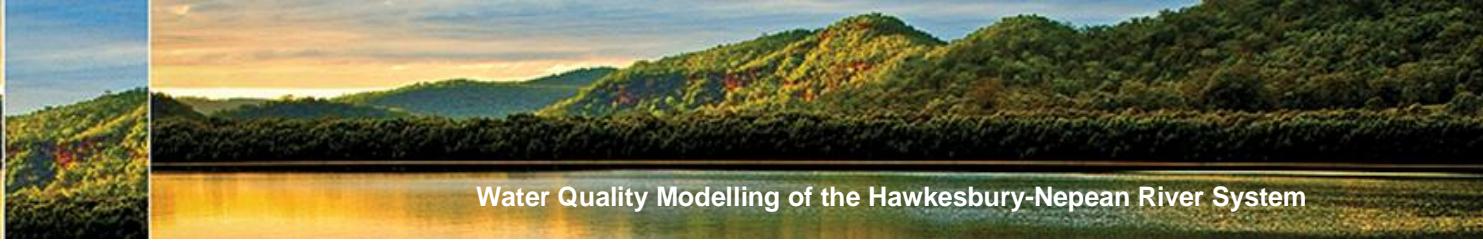
Water Quality Modelling of the Hawkesbury-Nepean River System



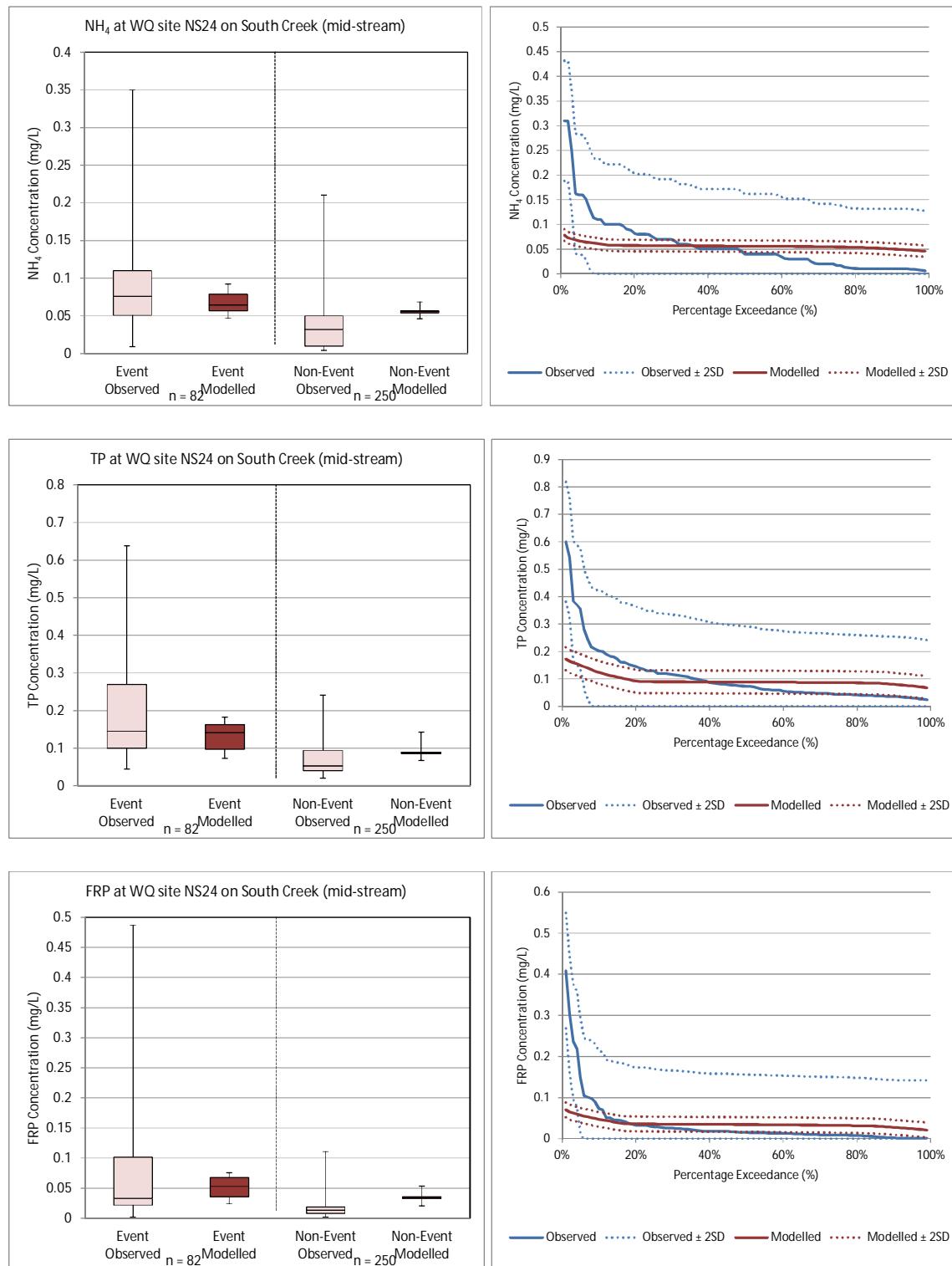


F.5. Water quality site NS24 – South Creek

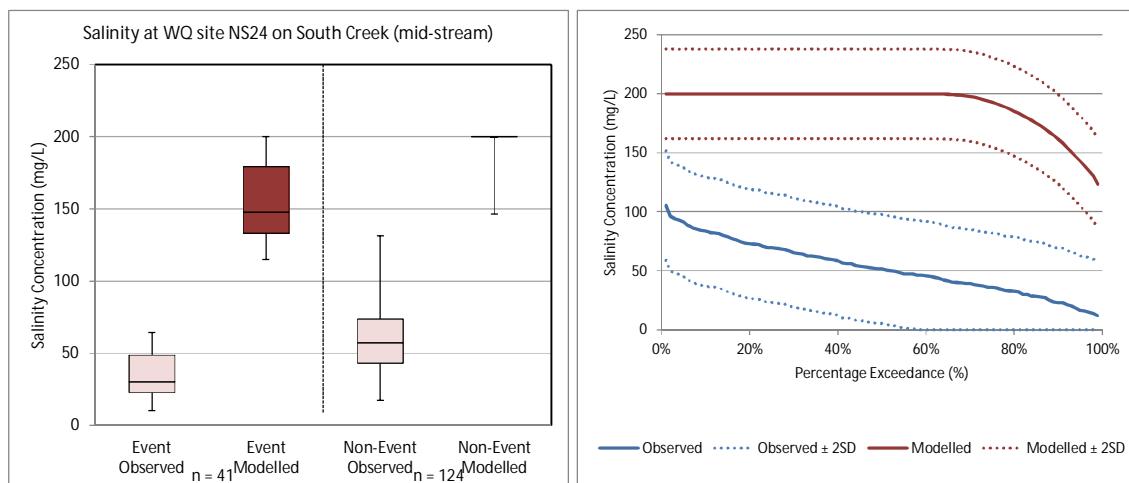




Water Quality Modelling of the Hawkesbury-Nepean River System

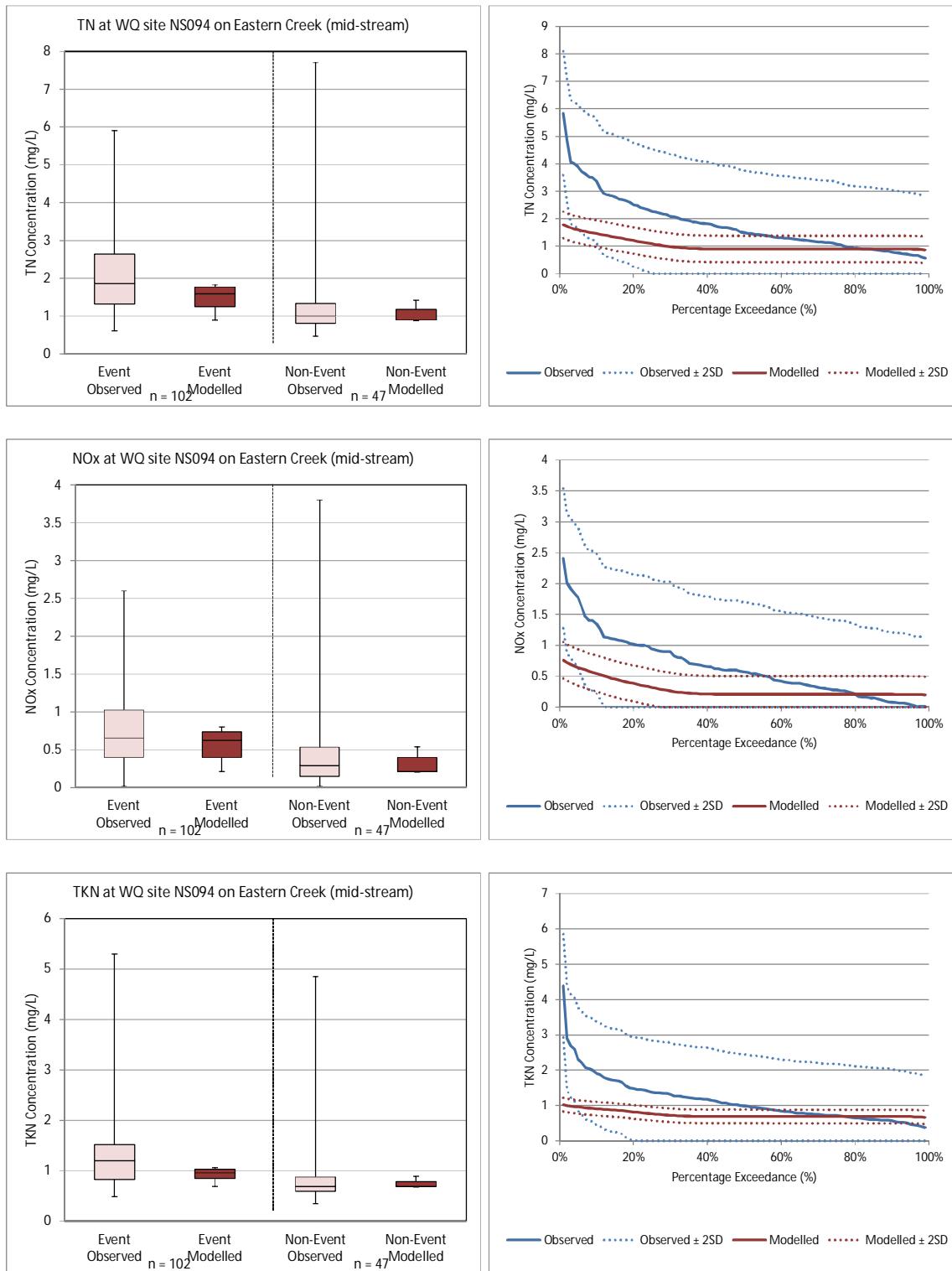


Water Quality Modelling of the Hawkesbury-Nepean River System

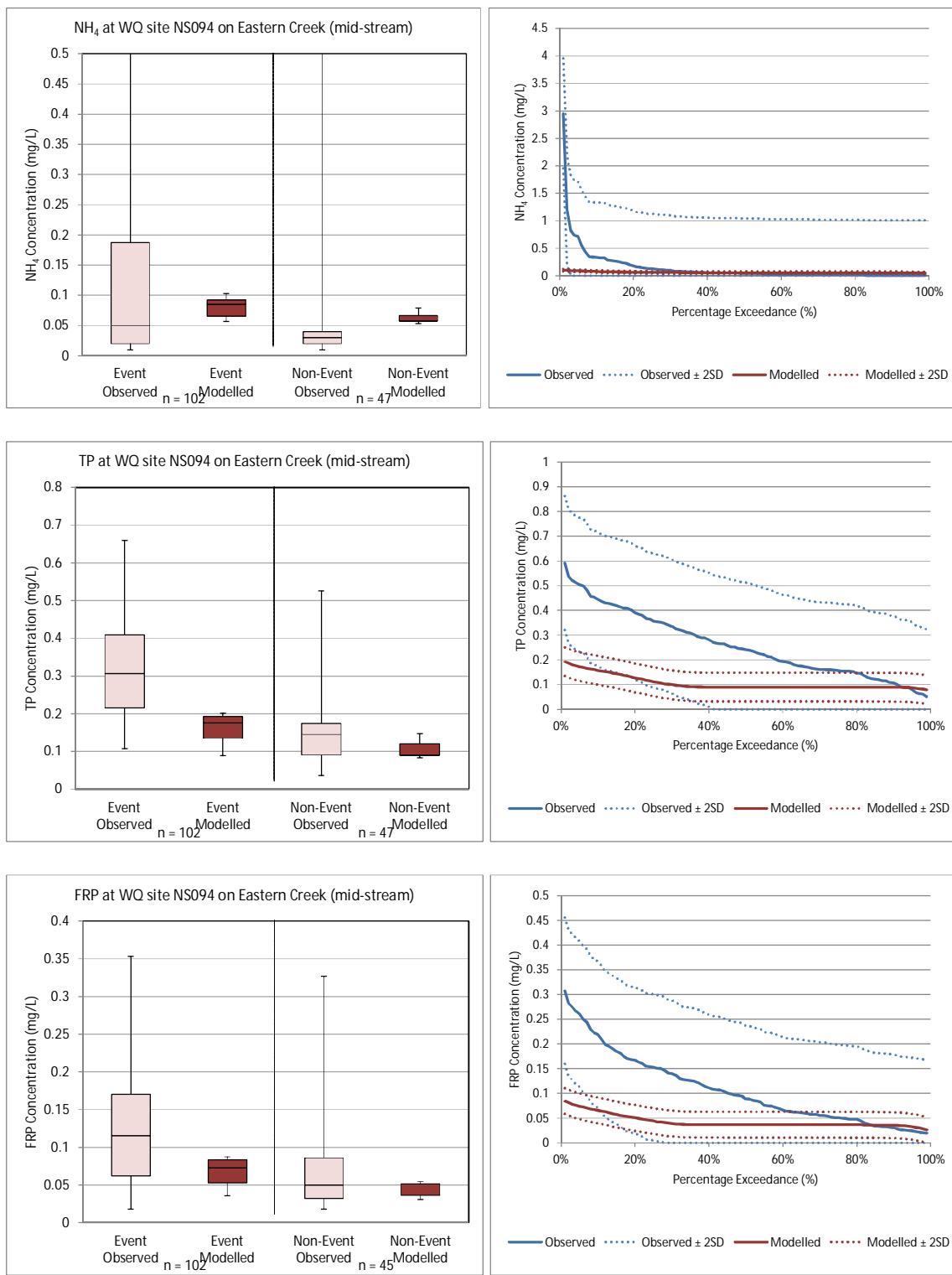


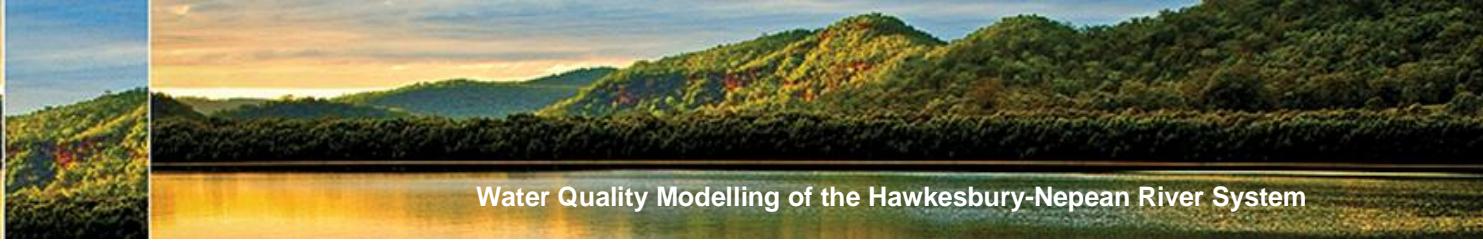


F.6. Water quality site NS094 – Eastern Creek

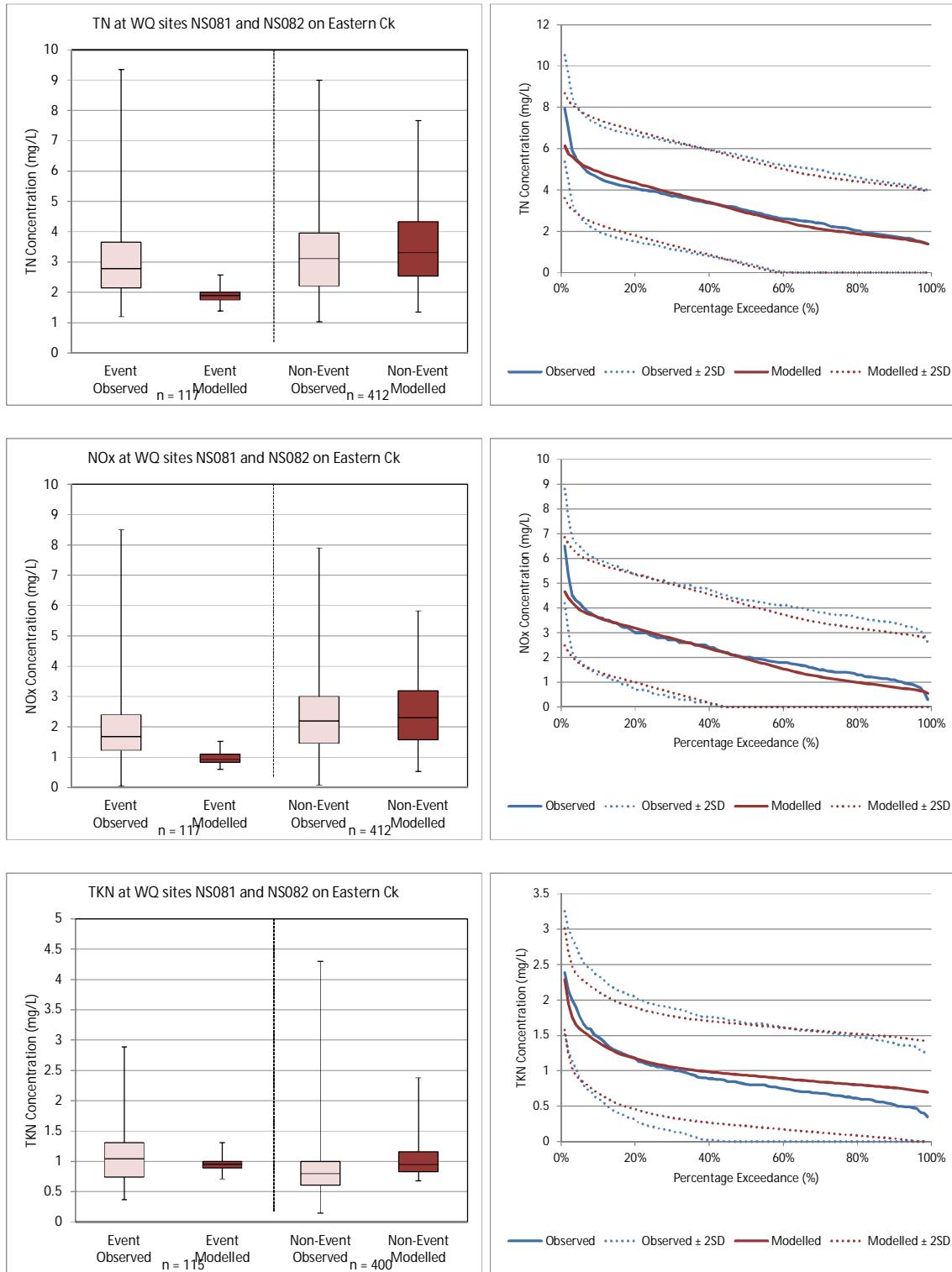


Water Quality Modelling of the Hawkesbury-Nepean River System

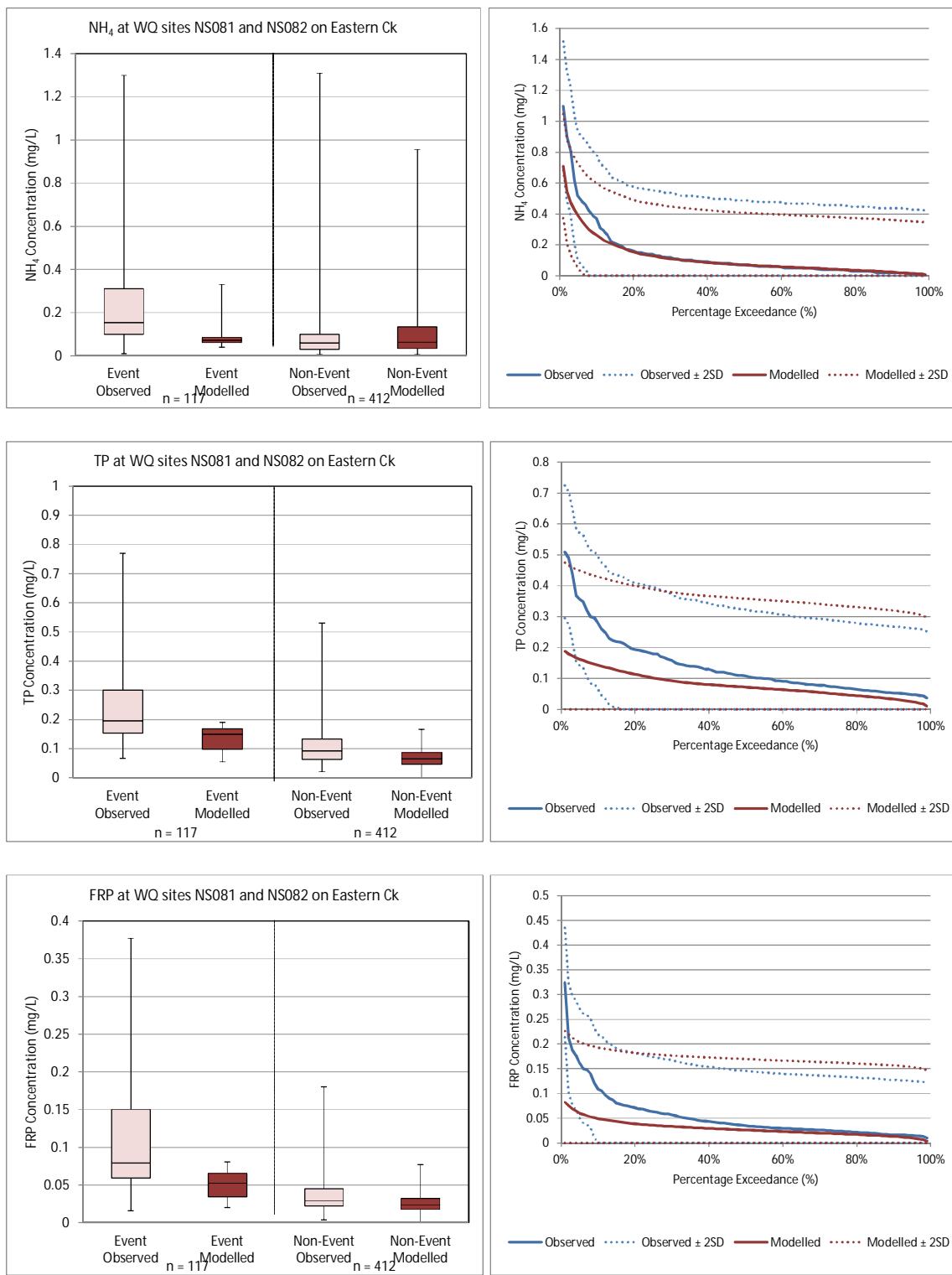




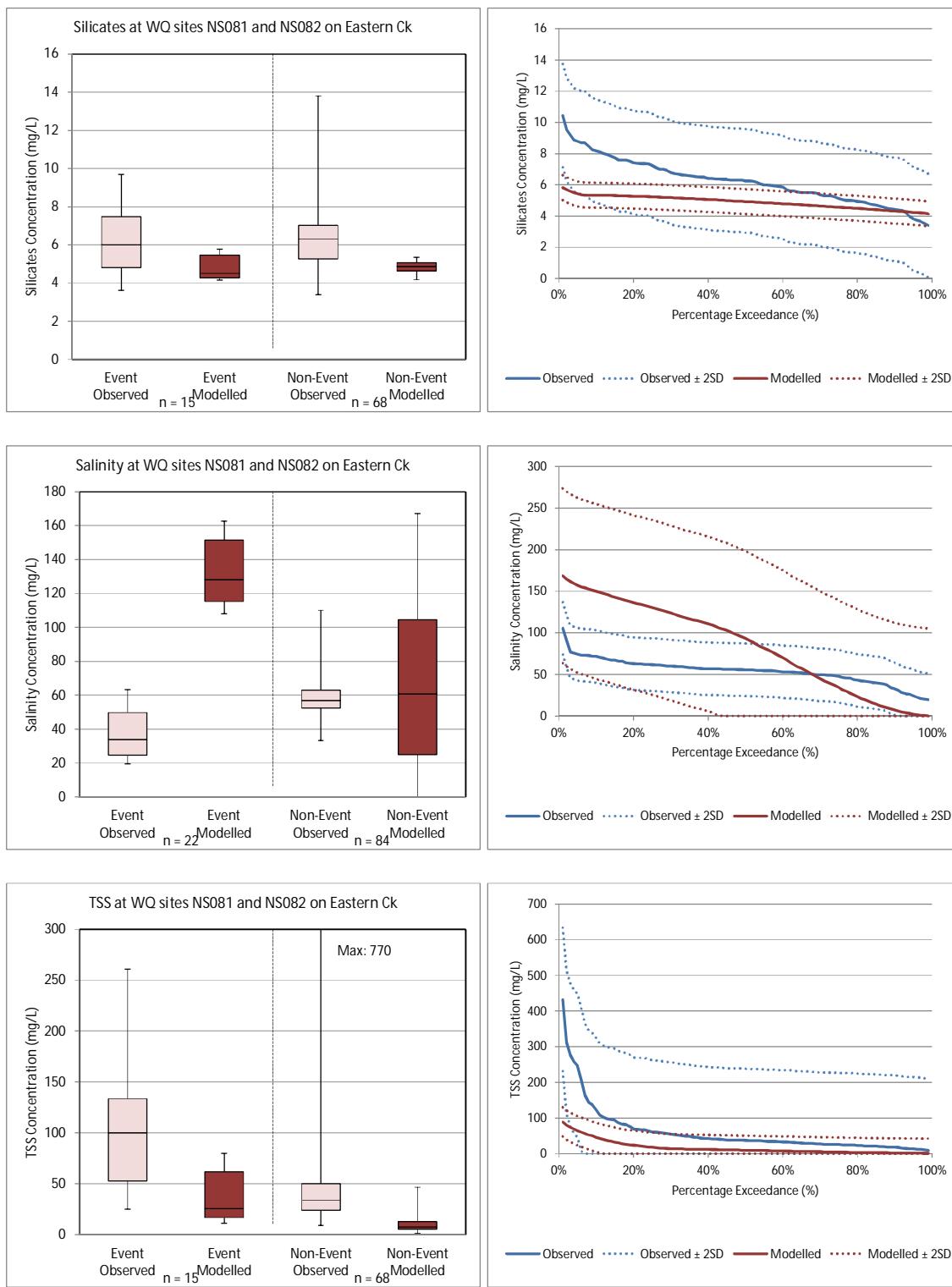
F.7. Water quality sites NS081 and NS082 – Eastern Creek



Water Quality Modelling of the Hawkesbury-Nepean River System

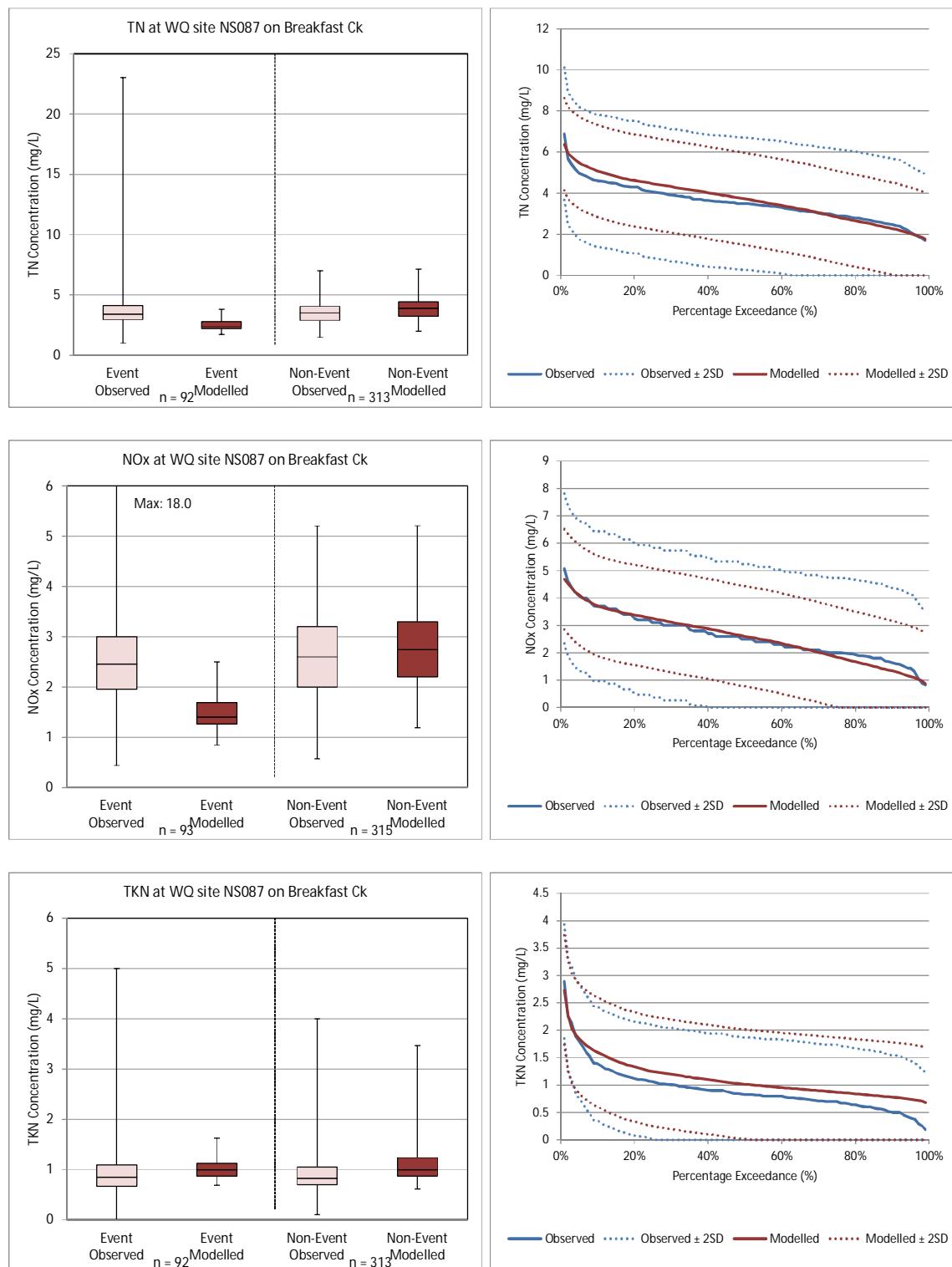


Water Quality Modelling of the Hawkesbury-Nepean River System

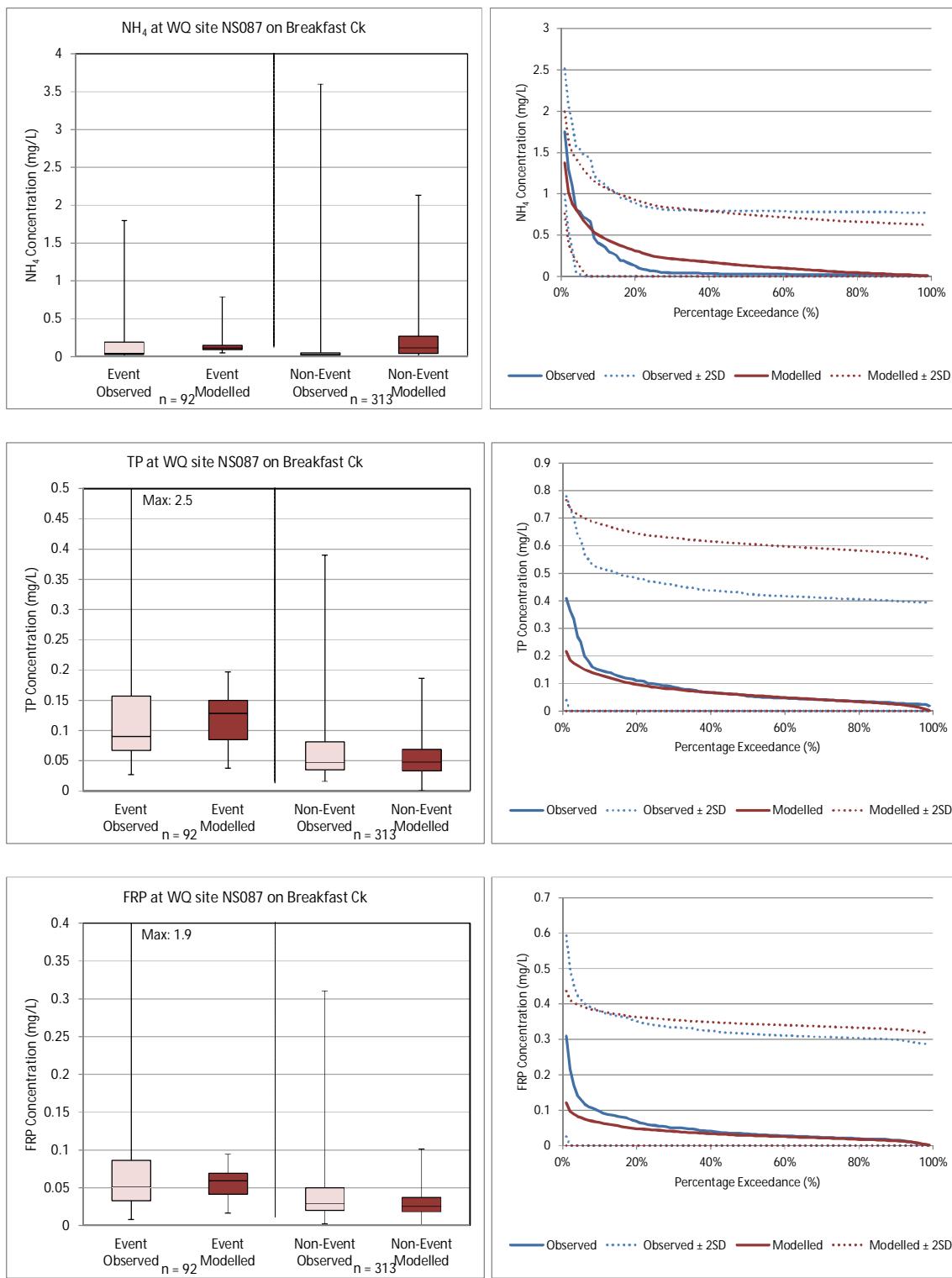




F.9. Water quality site NS087 – Breakfast Creek (tributary of Eastern Creek)

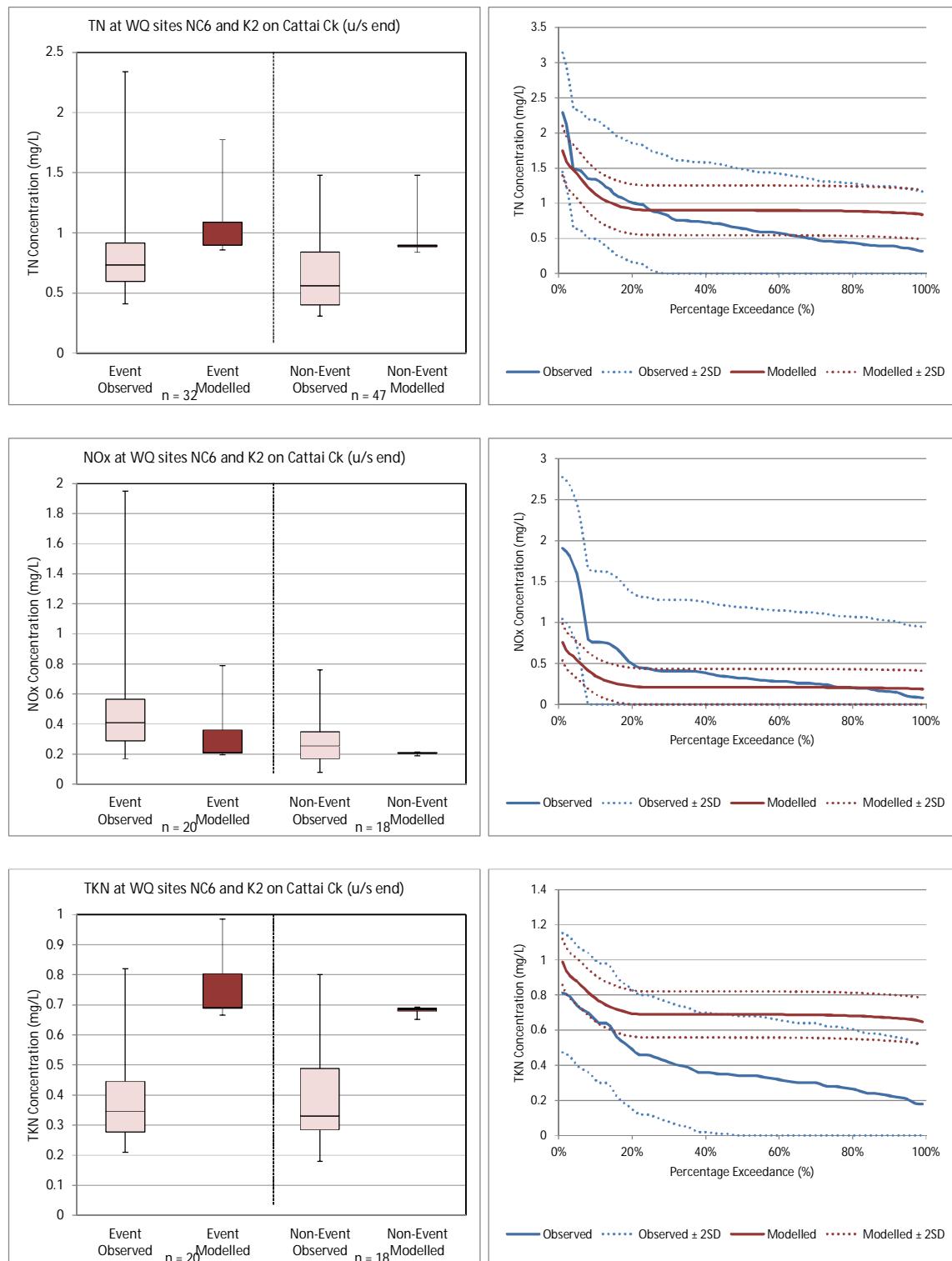


Water Quality Modelling of the Hawkesbury-Nepean River System

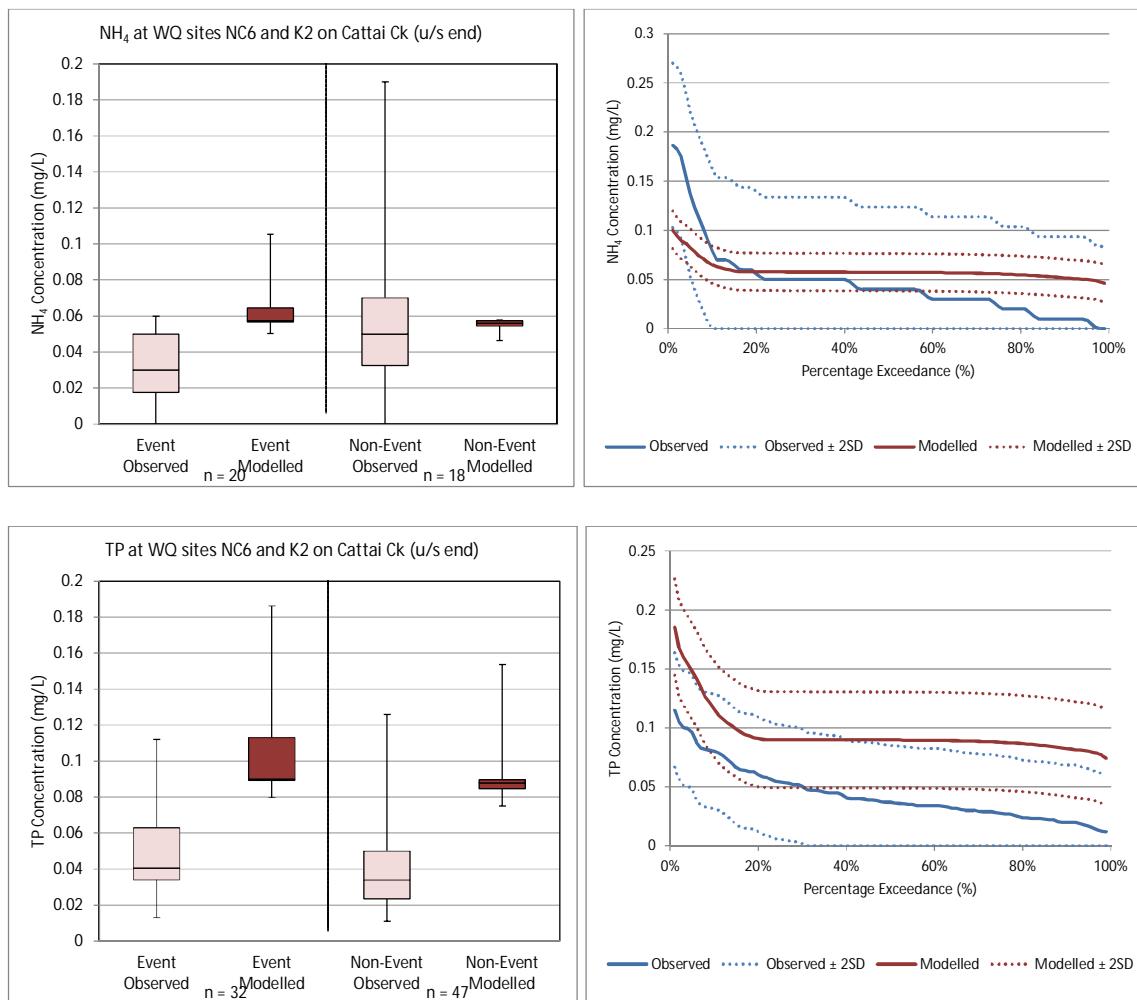


Water Quality Modelling of the Hawkesbury-Nepean River System

F.10. Water quality sites NC6 and K2 – Cattai Creek

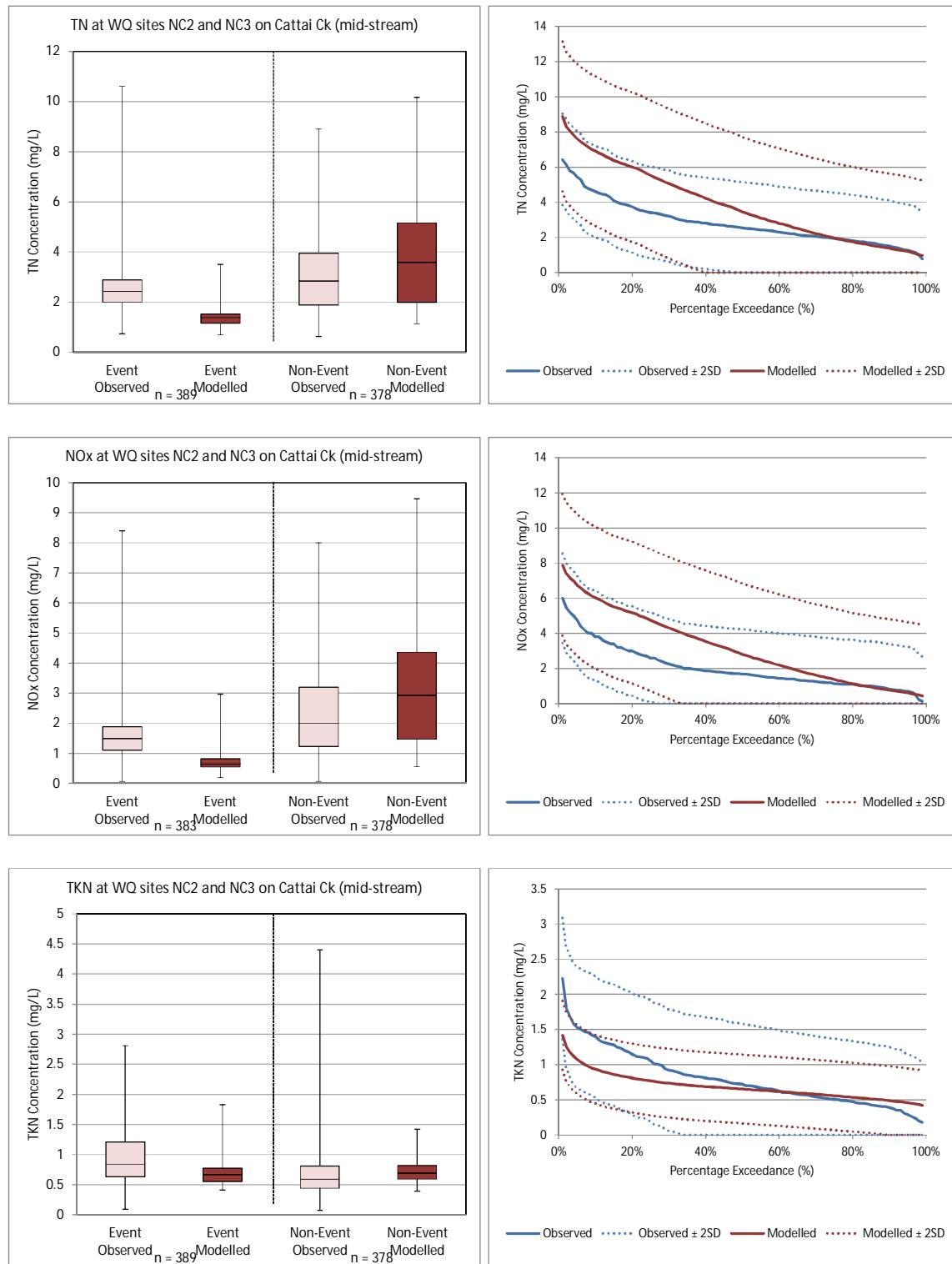


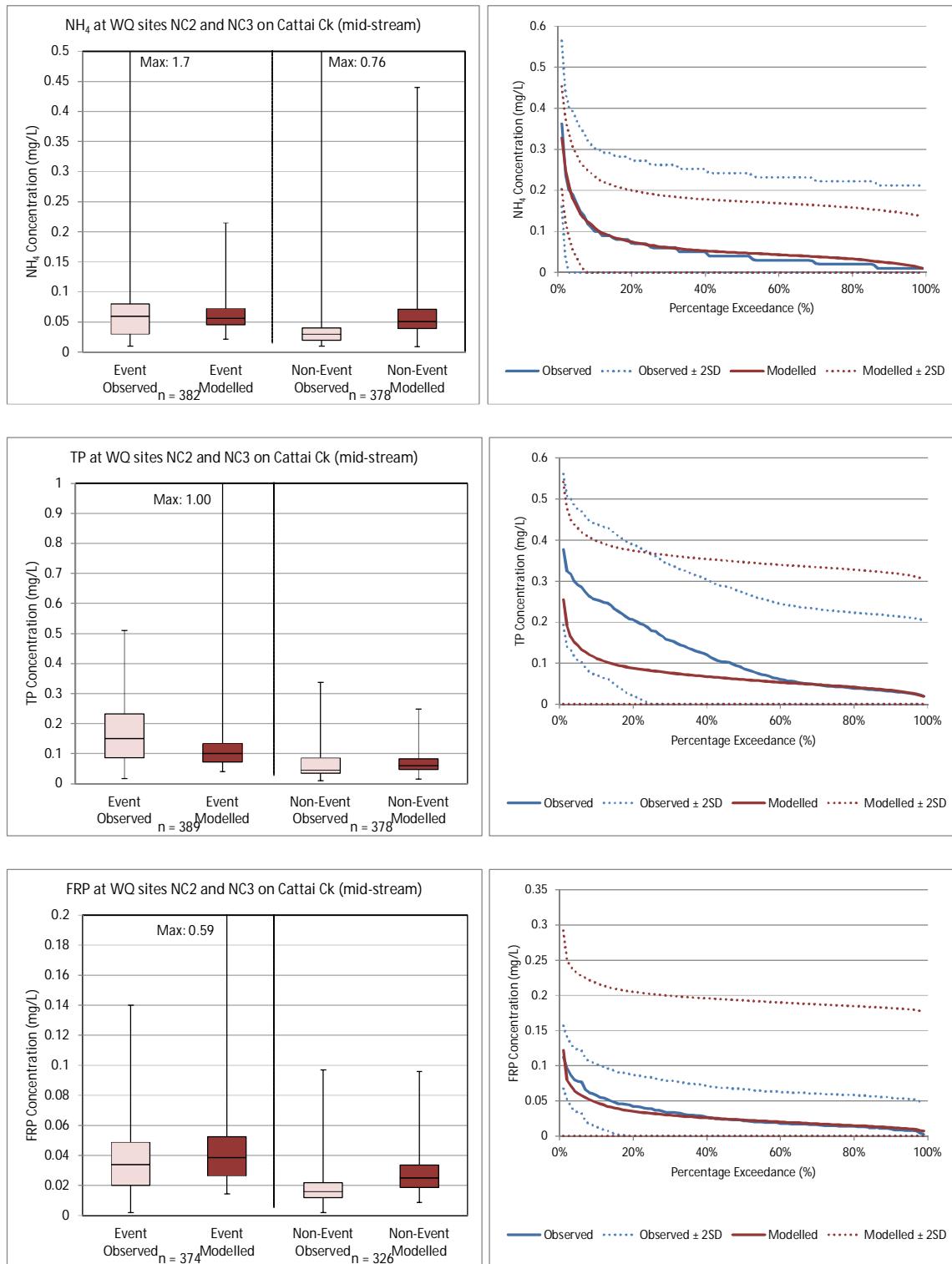
Water Quality Modelling of the Hawkesbury-Nepean River System





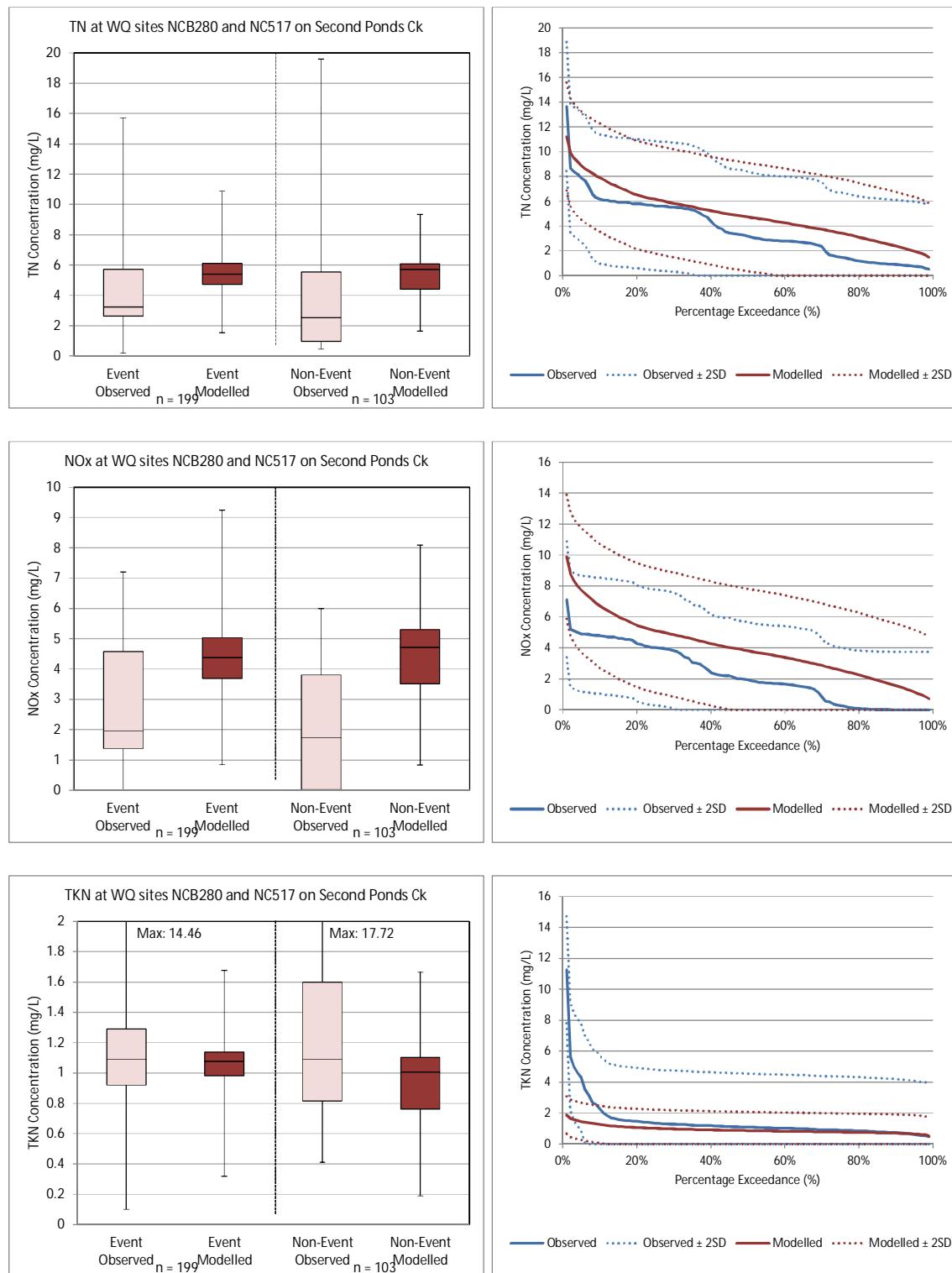
F.11. Water quality sites NC2 and NC3 – Cattai Creek



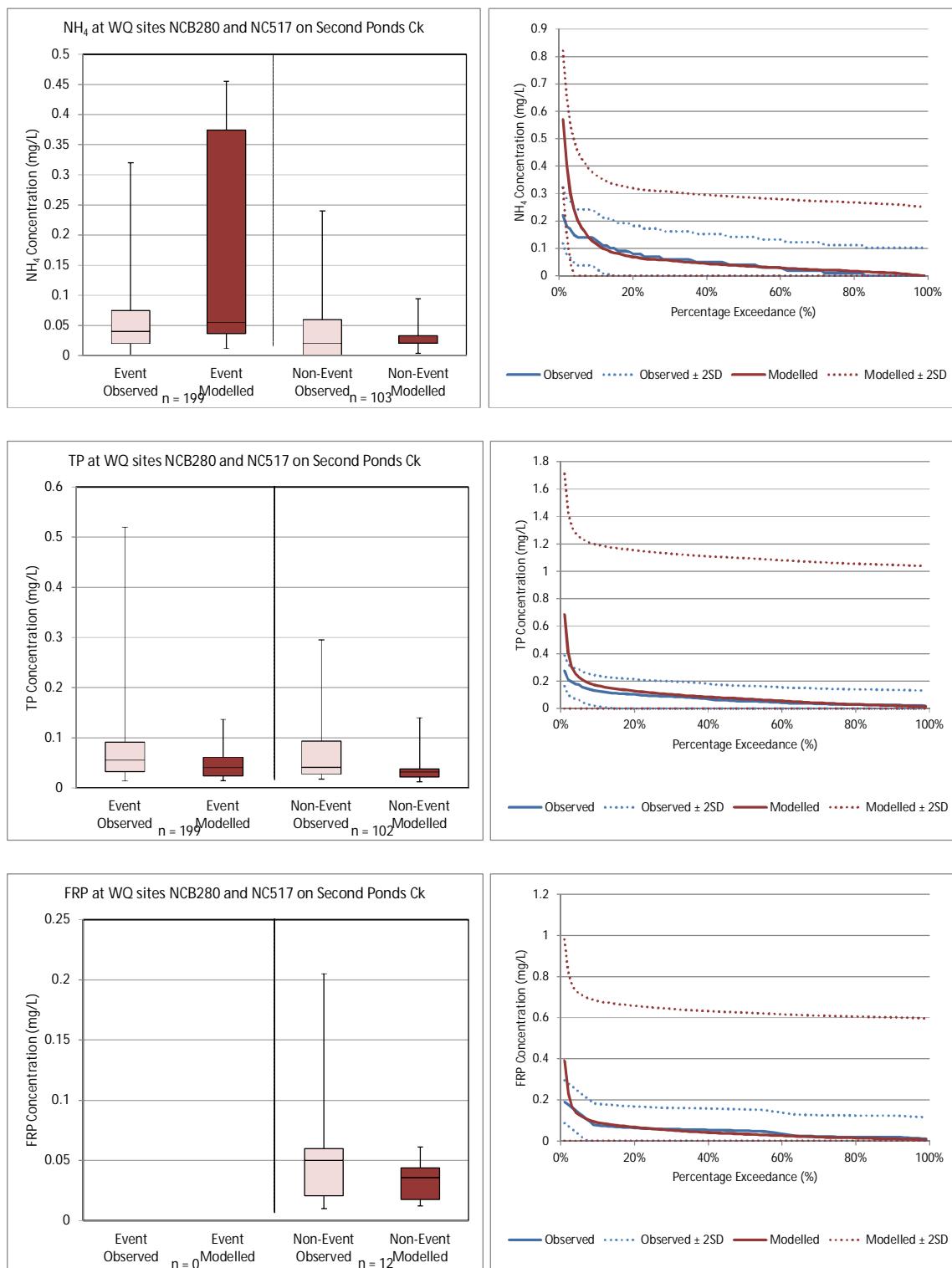




F.12. Water quality sites NCB280 and NC517 – Second Ponds Creek (tributary of Cattai Creek)



Water Quality Modelling of the Hawkesbury-Nepean River System

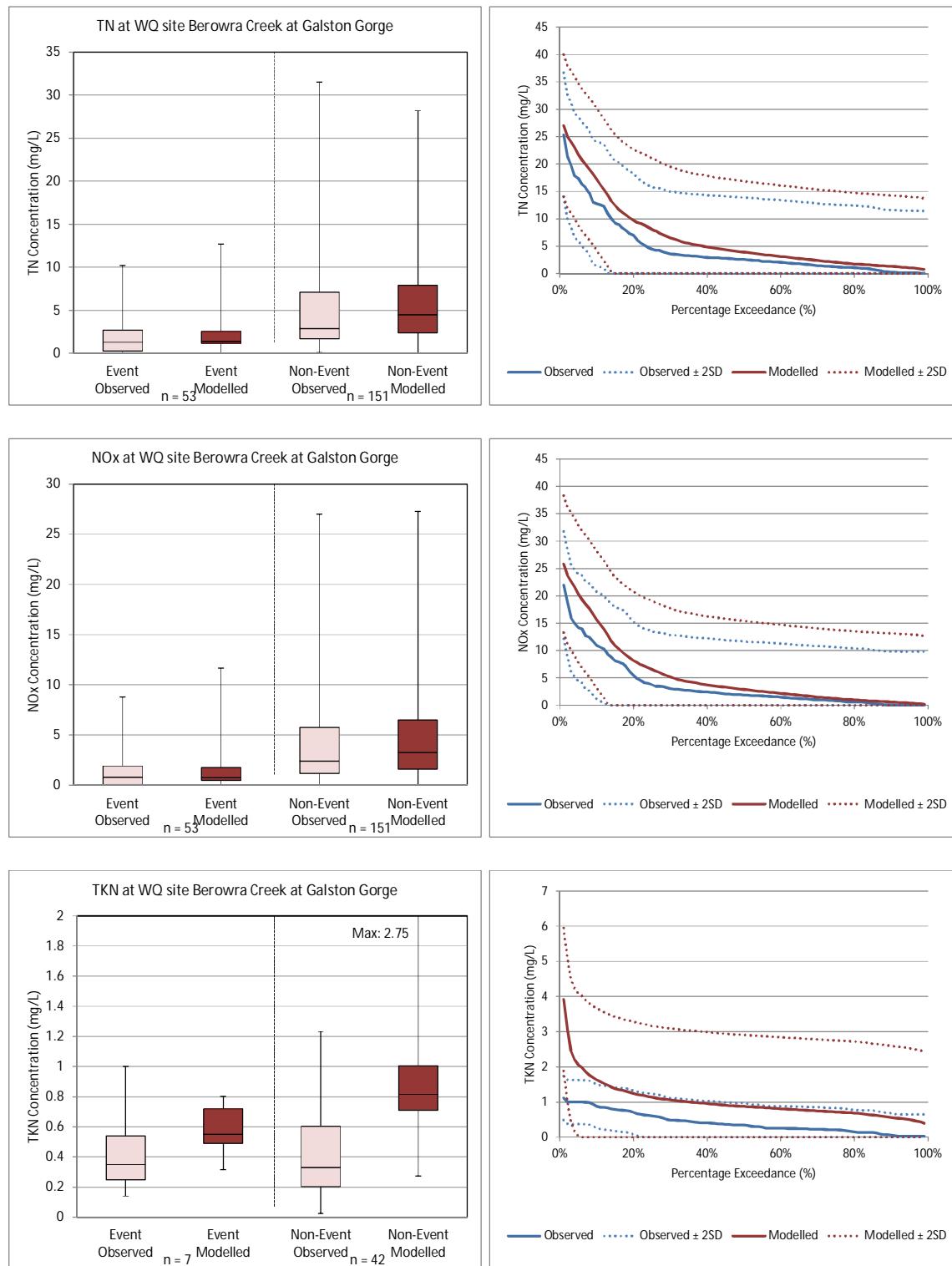


SINCLAIR KNIGHT MERZ



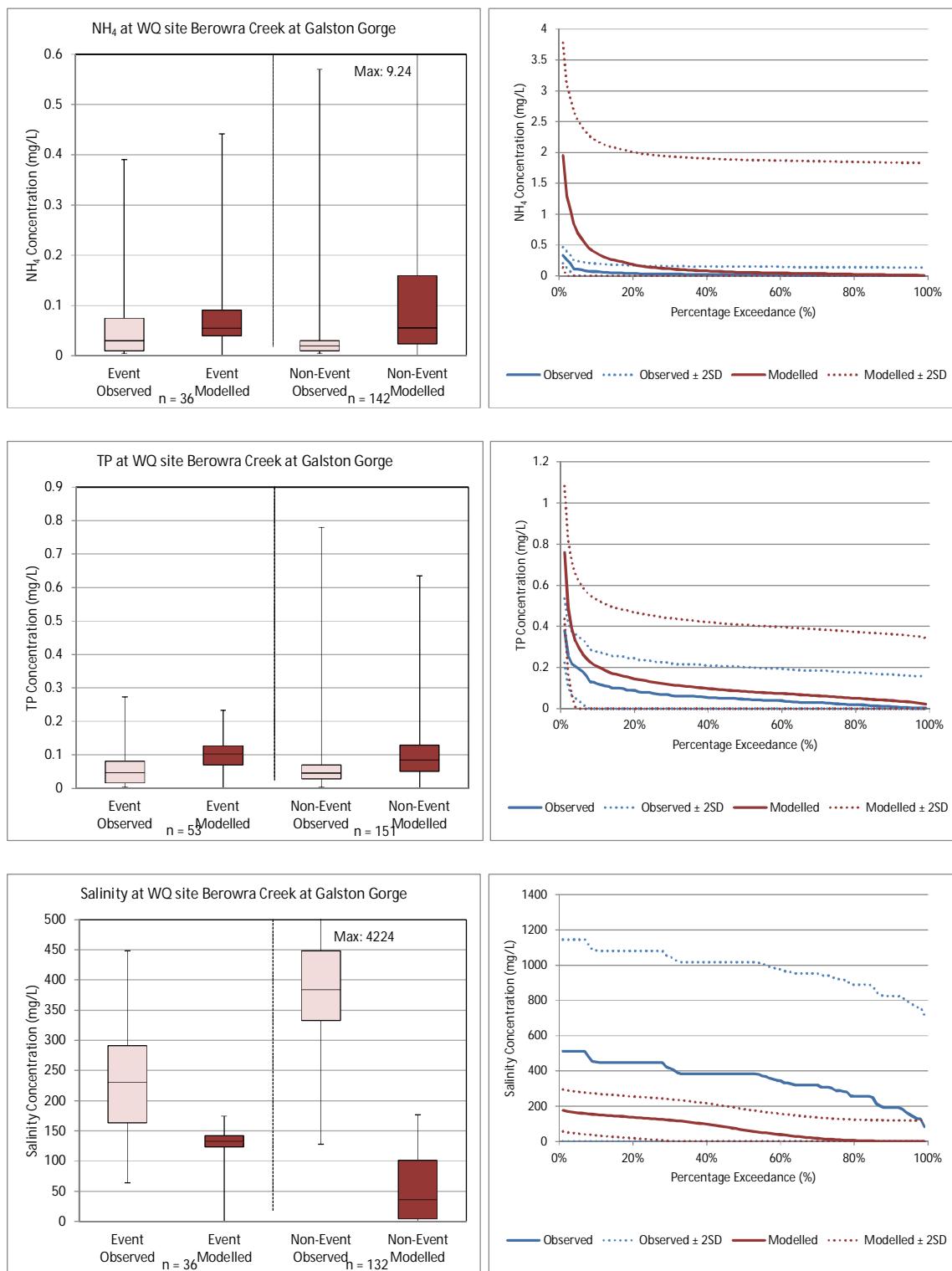
Water Quality Modelling of the Hawkesbury-Nepean River System

F.13. Water quality site – Berowra Creek at Galston Gorge





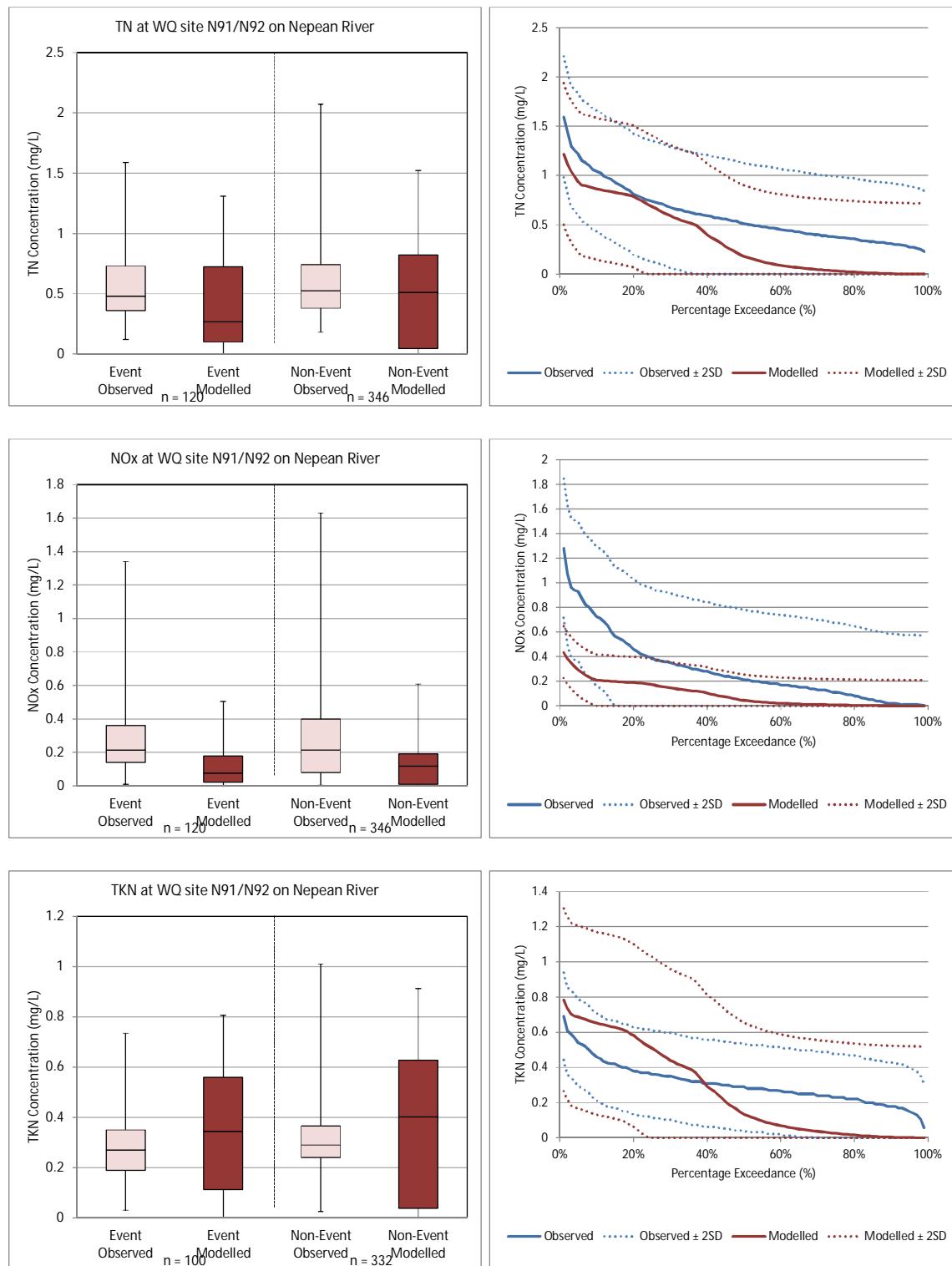
Water Quality Modelling of the Hawkesbury-Nepean River System



SINCLAIR KNIGHT MERZ

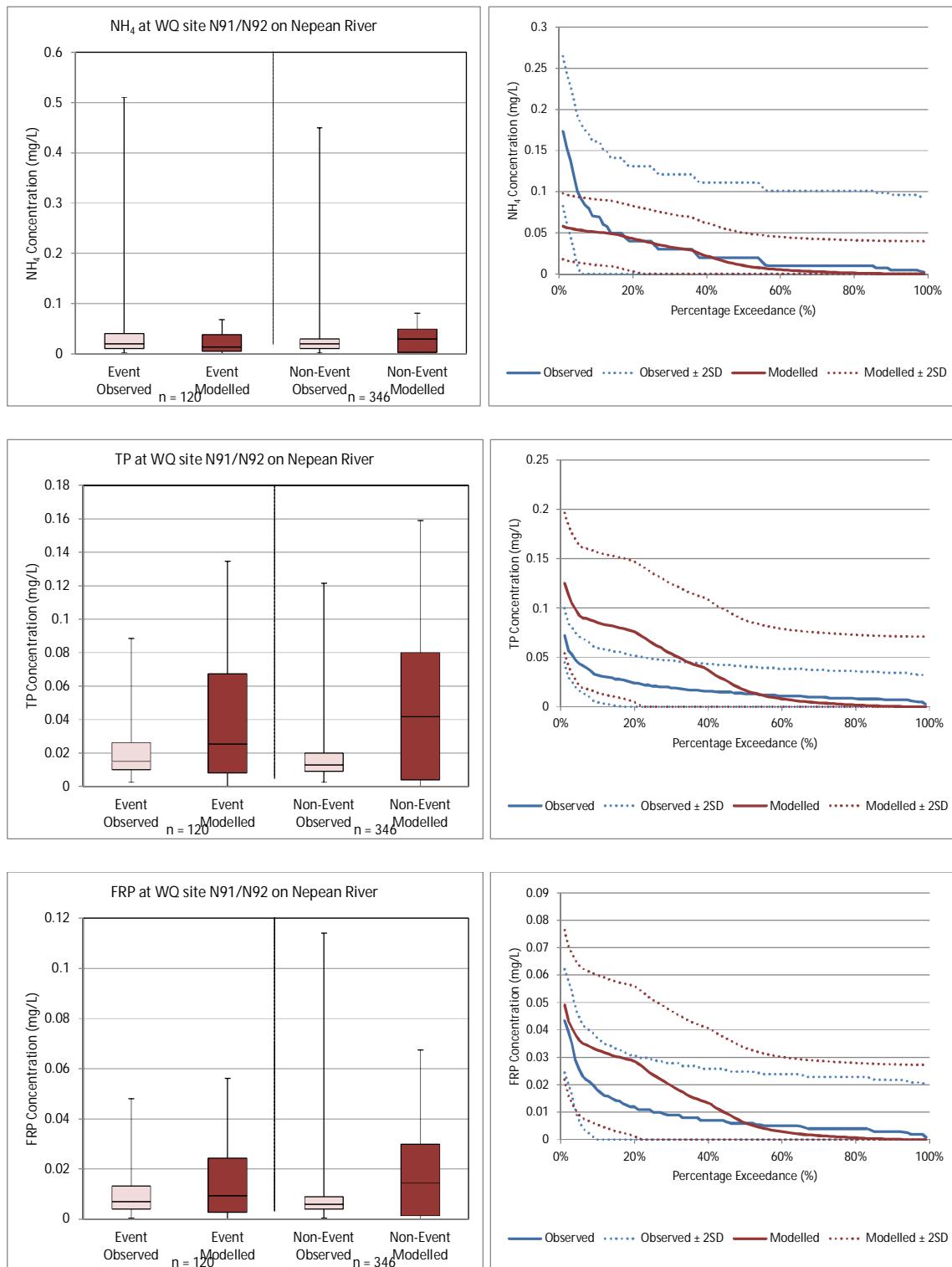


F.14. Water quality site N91 and N92 – Nepean River at Maldon Weir





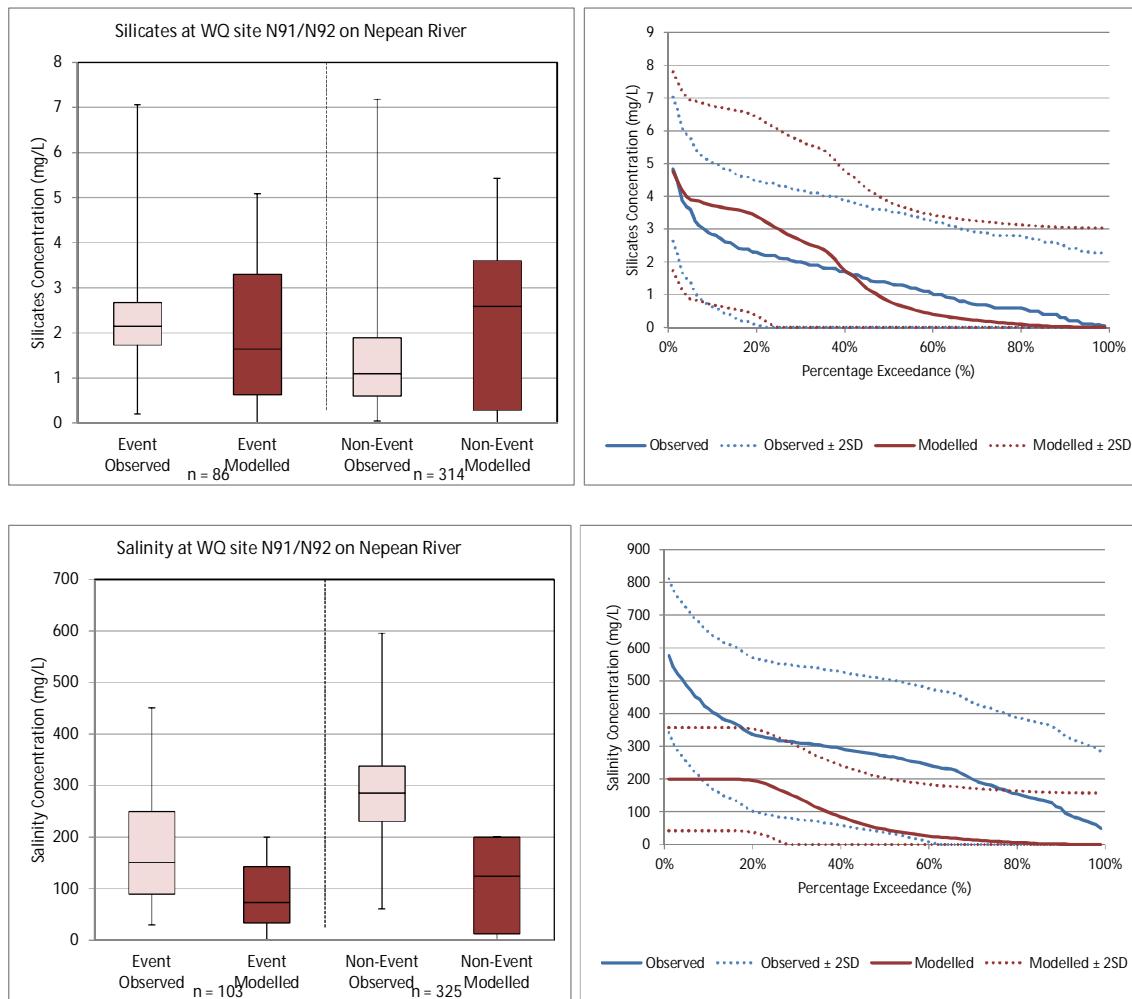
Water Quality Modelling of the Hawkesbury-Nepean River System



SINCLAIR KNIGHT MERZ



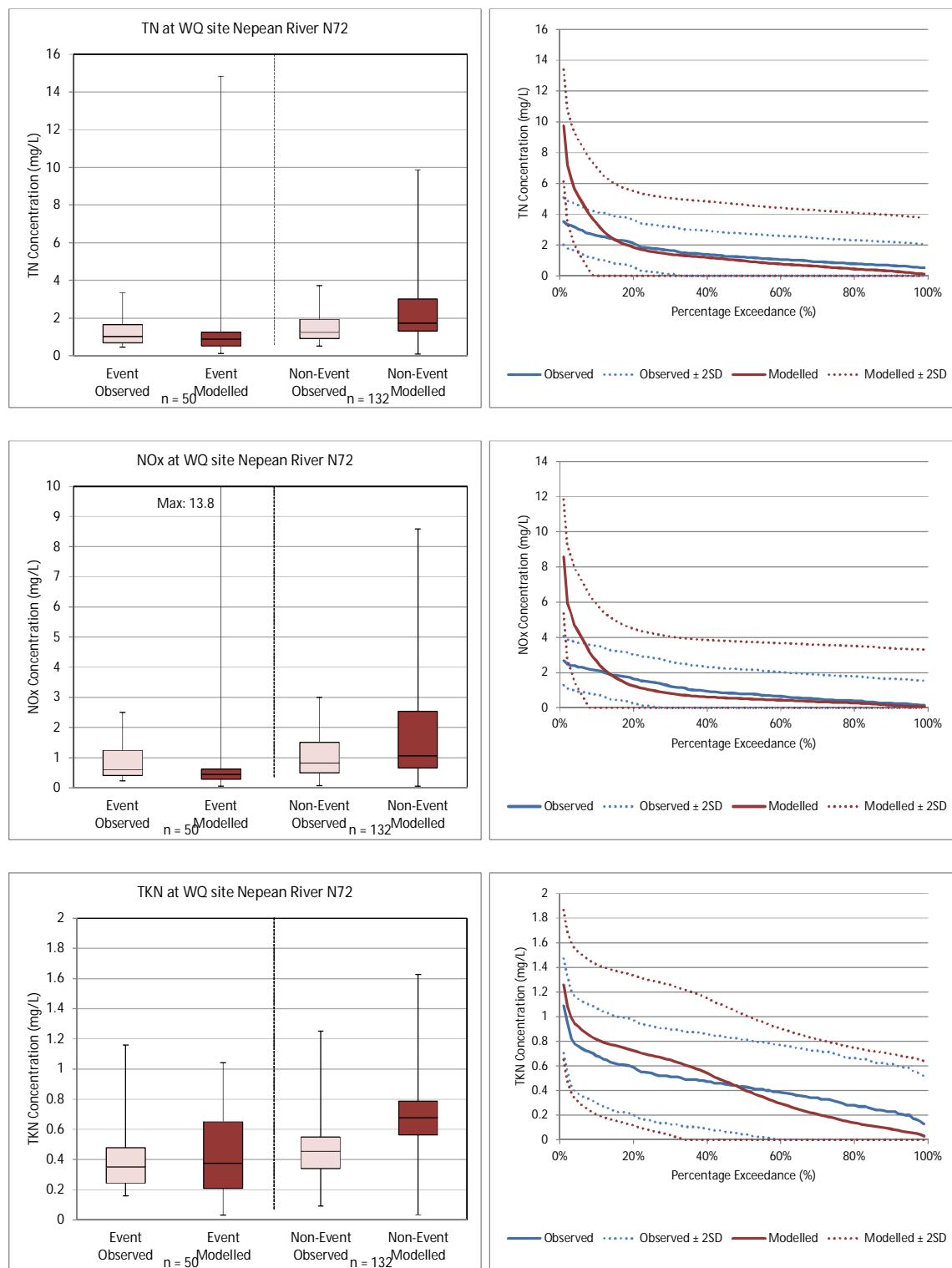
Water Quality Modelling of the Hawkesbury-Nepean River System





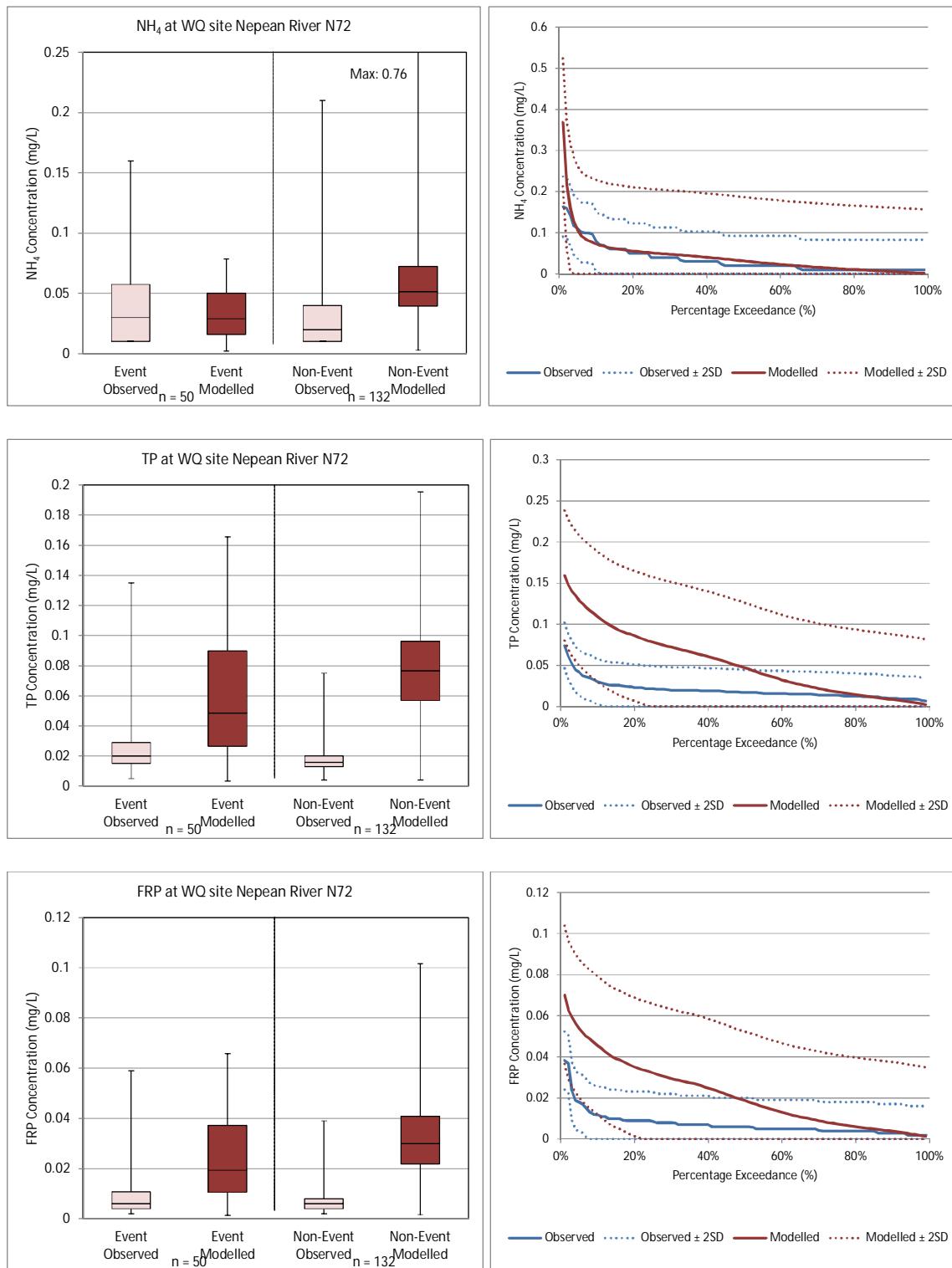
Water Quality Modelling of the Hawkesbury-Nepean River System

F.15. Water quality site N72 – Nepean River at Cobbity Road Bridge





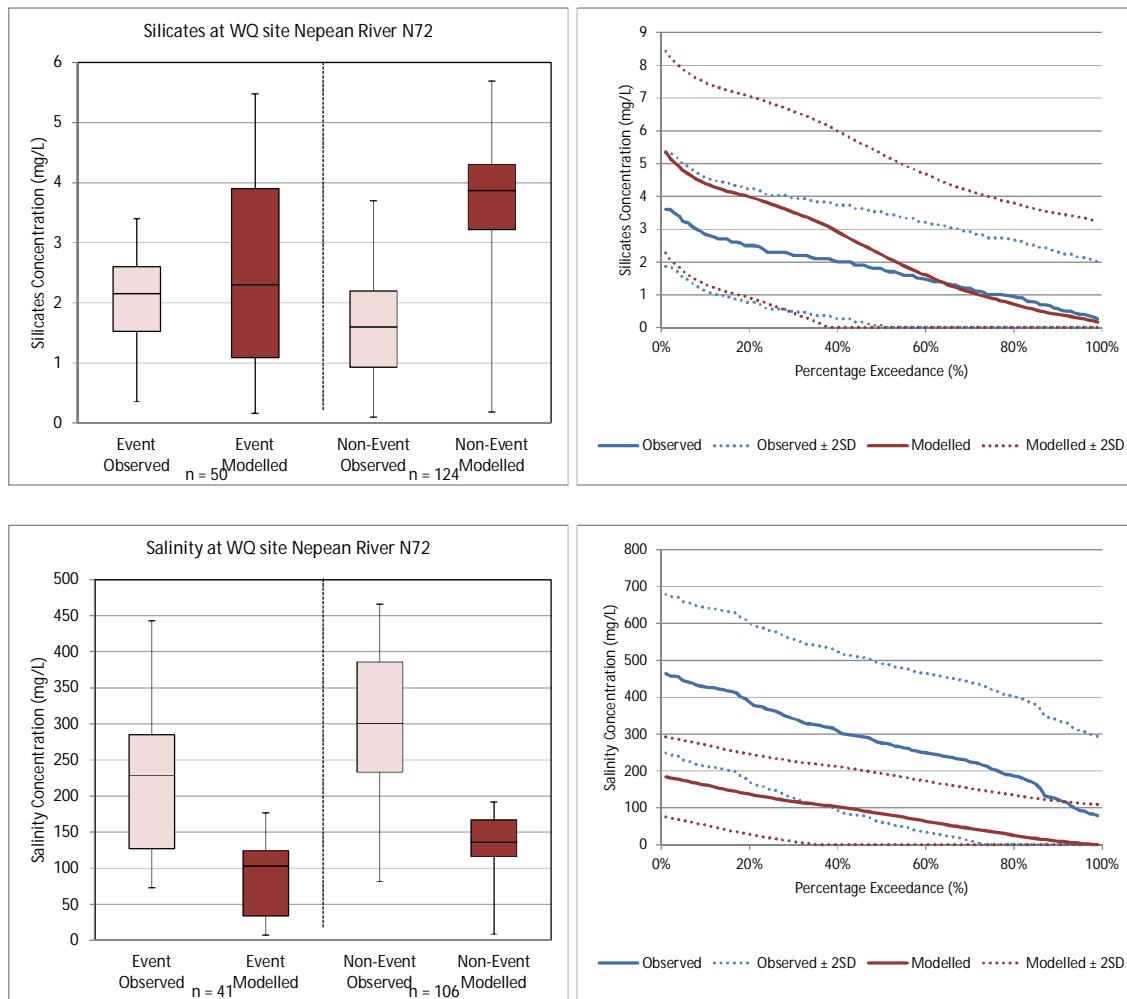
Water Quality Modelling of the Hawkesbury-Nepean River System



SINCLAIR KNIGHT MERZ

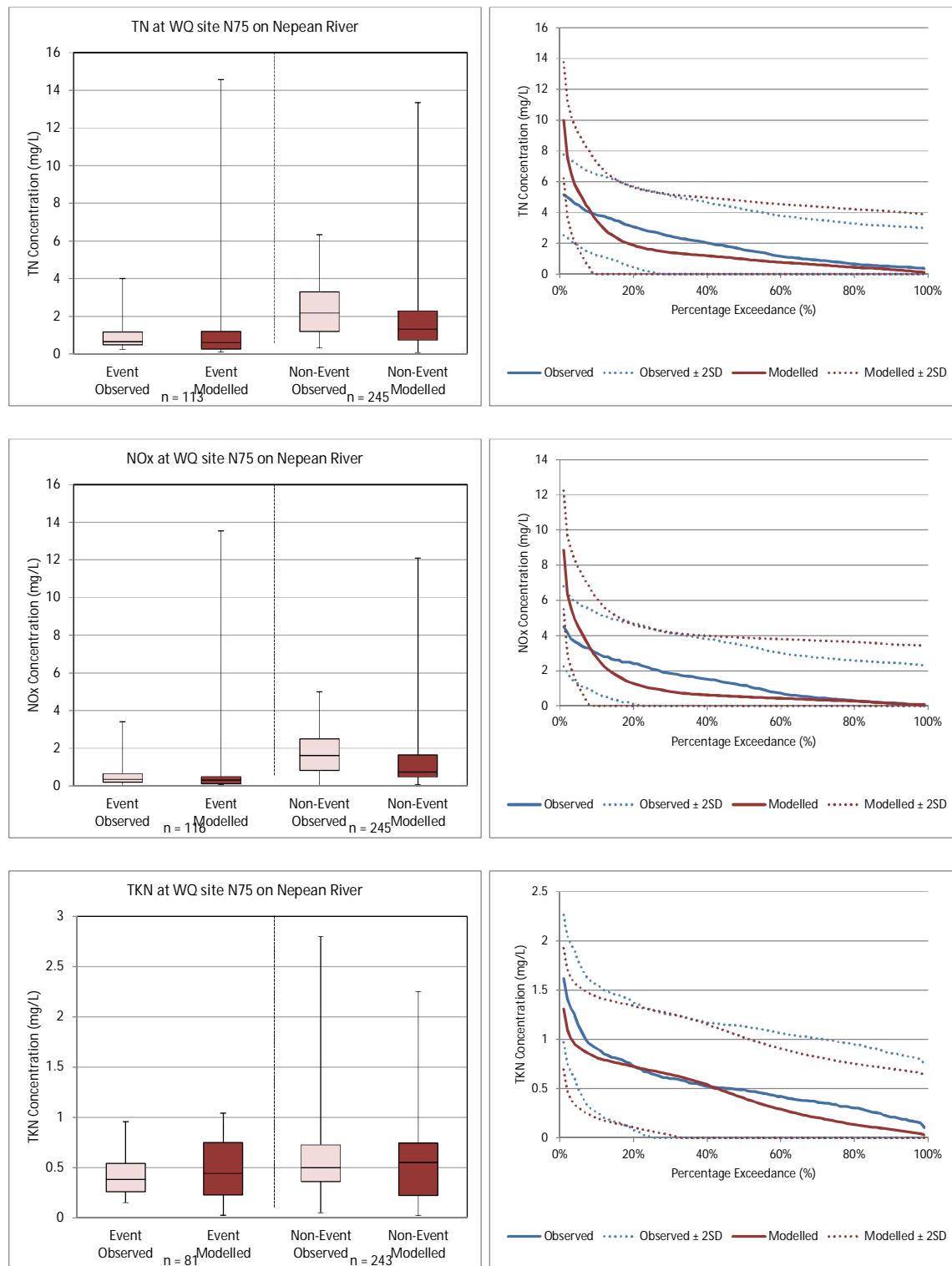


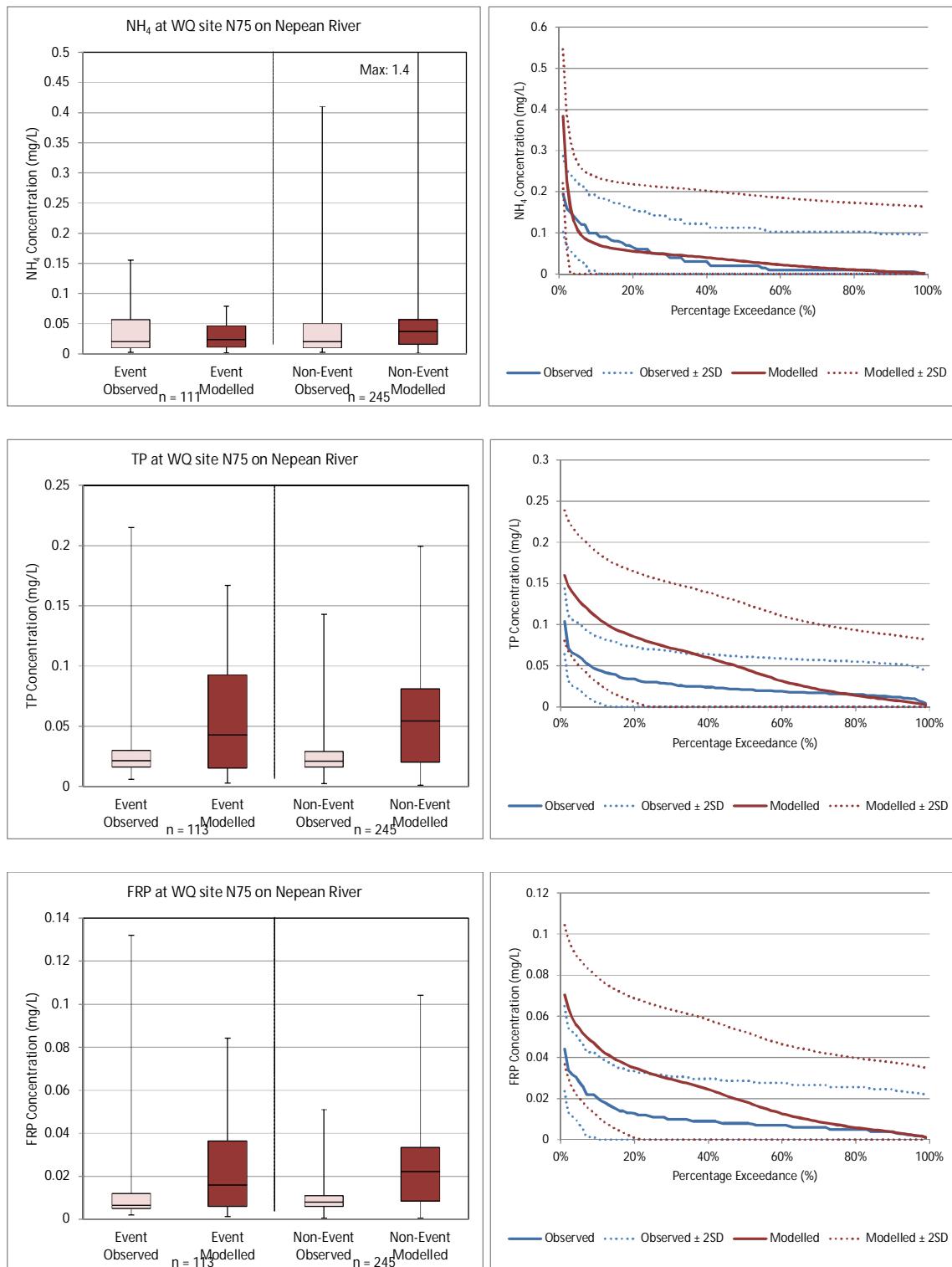
Water Quality Modelling of the Hawkesbury-Nepean River System





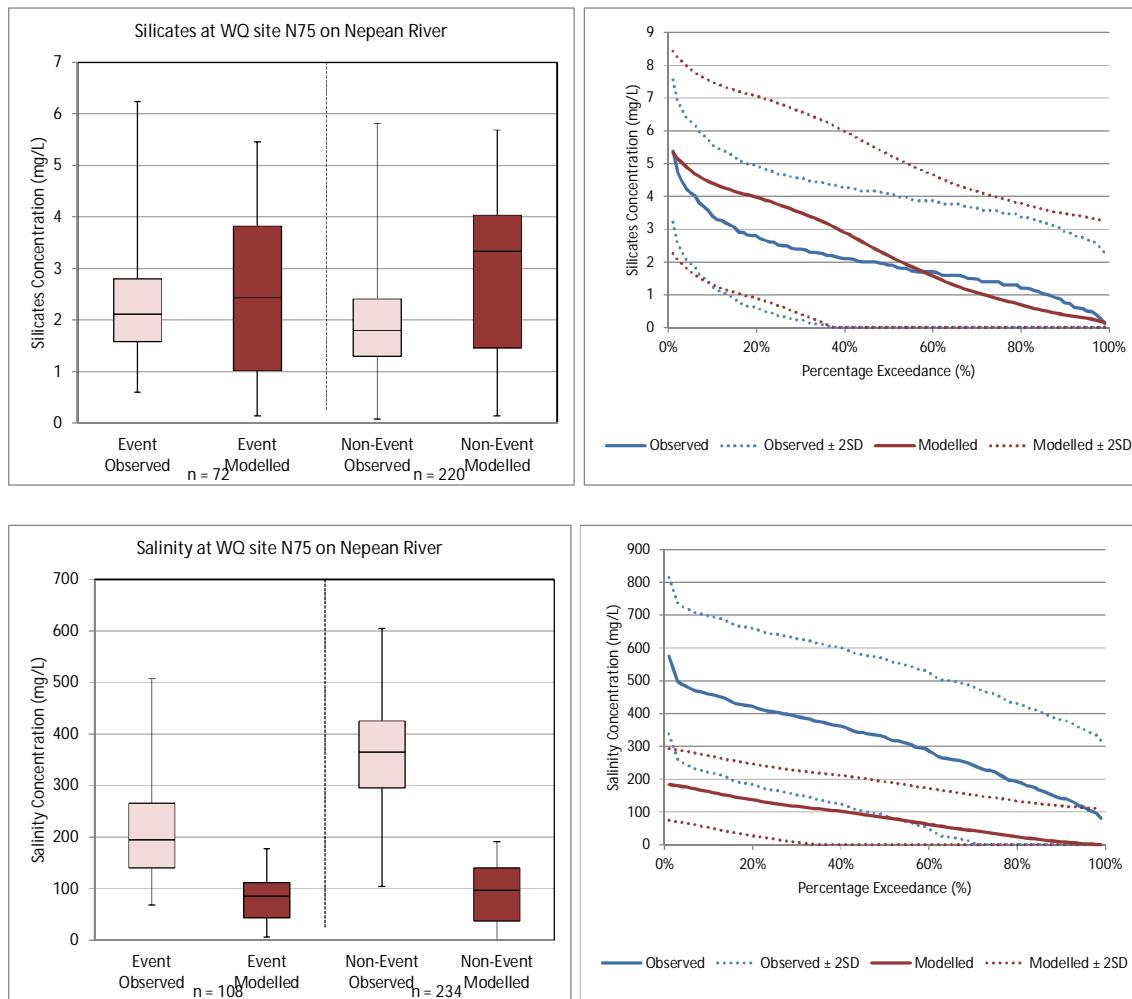
F.16. Water quality site N75 – Nepean River at Sharpes Weir







Water Quality Modelling of the Hawkesbury-Nepean River System





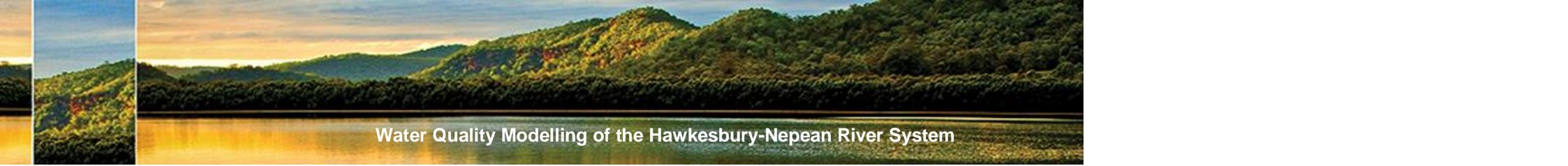
Water Quality Modelling of the Hawkesbury-Nepean River System

Appendix G Water Quality Sampling Locations

Water Quality Sampling Locations and available data for temperature, dissolved oxygen, pH, total organic carbon and dissolved organic carbon

Region	Gauging location	Data Source	Data	Data period	Number of records
South Creek	South Creek @ Stoney Creek Road	Blacktown City Council	Temperature	30/1/1991 – 5/12/1995	15
	South Creek @ Stoney Creek Road	Blacktown City Council	pH	30/1/1991 – 5/12/1995	15
	South Creek @ Stoney Creek Road	Blacktown City Council	Dissolved Oxygen	30/1/1991 – 5/12/1995	14
	South Creek @ Richmond Road	Blacktown City Council	Temperature	1/3/1996 – 1/6/1999	13
	South Creek @ Richmond Road	Blacktown City Council	pH	1/3/1996 – 1/6/1999	13
	South Creek @ Richmond Road	Blacktown City Council	Dissolved Oxygen	1/3/1996 – 1/6/1999	12
	South Creek @ unknown	Blacktown City Council	Temperature	19/8/2004 – 13/6/2007	39
	South Creek @ unknown	Blacktown City Council	pH	7/9/2004 – 2/8/2006	29
	South Creek @ unknown	Blacktown City Council	Dissolved Oxygen	7/9/2005 – 2/5/2007	19
	SO1 – South Creek @ unknown	Blacktown City Council	Temperature	25/9/2008 – 19/2/2009	5
	SO1 – South Creek @ unknown	Blacktown City Council	pH	25/9/2008 – 19/2/2009	5
	SC1 – South Creek @ unknown	Blacktown City Council	Temperature	26/10/2010 – 16/5/2011	8
	SC1 – South Creek @ unknown	Blacktown City Council	pH	26/10/2010 – 16/5/2011	8
	NS26 – South Creek @ Dunheved Golf Club	Sydney Water CMP	Dissolved Organic Carbon	15/11/2011 – 23/4/2012	6
	NS26 – South Creek @ Dunheved Golf Club	Sydney Water CMP	Total Organic Carbon	15/11/2011 – 23/4/2012	6
	NS26 – South Creek @ Dunheved Golf Club	Sydney Water	Temperature	25/1/1994 – 10/5/2011	348
	NS26 – South Creek @ Dunheved Golf Club	Sydney Water	pH	25/1/1994 – 10/5/2011	308
	NS26 – South Creek @ Dunheved Golf Club	Sydney Water	Dissolved Oxygen	25/1/1994 – 10/5/2011	282
	NS23 – South Creek @ Adi Shanes Park	Sydney Water CMP	Dissolved Organic Carbon	15/11/2011 – 23/4/2012	6
	NS23 – South Creek @ Adi Shanes Park	Sydney Water CMP	Total Organic Carbon	15/11/2011 – 23/4/2012	6
	NS23 – South Creek @ Adi Shanes Park	Sydney Water	Temperature	13/12/1993 – 10/5/2011	292
	NS23 – South Creek @ Adi Shanes Park	Sydney Water	pH	13/12/1993 – 10/5/2011	288

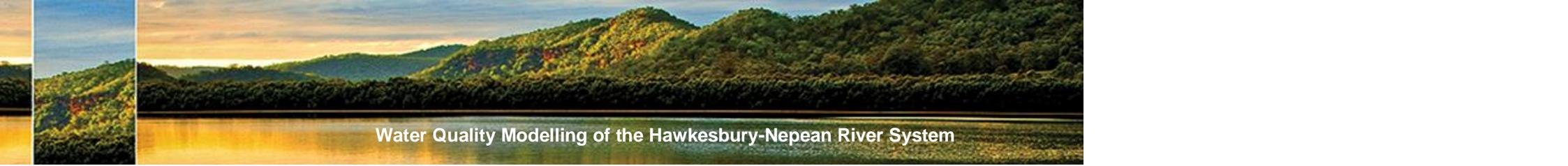
SINCLAIR KNIGHT MERZ



Water Quality Modelling of the Hawkesbury-Nepean River System

Region	Gauging location	Data Source	Data	Data period	Number of records
	NS23 – South Creek @ Adi Shanes Park	Sydney Water	Dissolved Oxygen	13/12/1993 – 10/5/2011	227
	NS14 – South Creek @ Richmond Road Bridge	Sydney Water CMP	Dissolved Organic Carbon	15/11/2011 – 23/4/2012	6
	NS14 – South Creek @ Richmond Road Bridge	Sydney Water CMP	Total Organic Carbon	15/11/2011 – 23/4/2012	6
	NS14 – South Creek @ Richmond Road Bridge	Sydney Water	Temperature	10/1/1990 – 10/5/2011	184
	NS14 – South Creek @ Richmond Road Bridge	Sydney Water	pH	10/1/1990 – 10/5/2011	377
	NS14 – South Creek @ Richmond Road Bridge	Sydney Water	Dissolved Oxygen	10/1/1990 – 10/5/2011	185
	NS04 – Lower South Creek @ Fitzroy Bridge	Sydney Water	Temperature	10/1/1990 – 8/6/2011	197
	NS04 – Lower South Creek @ Fitzroy Bridge	Sydney Water	pH	10/1/1990 – 8/6/2011	199
	NS04 – Lower South Creek @ Fitzroy Bridge	Sydney Water	Dissolved Oxygen	10/1/1990 – 8/6/2011	199
	NS04 – Lower South Creek @ Fitzroy Bridge	Sydney Water CMP	Dissolved Organic Carbon	2/11/2011 – 20/4/2012	6
	NS04 – Lower South Creek @ Fitzroy Bridge	Sydney Water CMP	Total Organic Carbon	2/11/2011 – 20/4/2012	6
	NS21 South Creek @ 8 th Avenue	Sydney Water	Temperature	10/1/1990 – 14/6/1995	110
	NS21 South Creek @ 8 th Avenue	Sydney Water	pH	10/1/1990 – 14/6/1995	112
	NS21 South Creek @ 8 th Avenue	Sydney Water	Dissolved Oxygen	10/1/1990 – 14/6/1995	111
	NS24 South Creek @ u/s St Marys WRP	Sydney Water	Temperature	19/5/1997 – 1/12/2009	183
	NS24 South Creek @ u/s St Marys WRP	Sydney Water	pH	19/5/1997 – 1/12/2009	183
	NS24 South Creek @ u/s St Marys WRP	Sydney Water	Dissolved Oxygen	19/5/1997 – 1/12/2009	157
	NS30 South Creek @ Great Western Highway	Sydney Water	Temperature	31/3/1992 – 19/11/1993	41
	NS30 South Creek @ Great Western Highway	Sydney Water	pH	31/3/1992 – 19/11/1993	43
	NS30 South Creek @ Great Western Highway	Sydney Water	Dissolved Oxygen	31/3/1992 – 19/11/1993	42
	NS35 South Creek @ Luddenham Road Bridge	Sydney Water	Temperature	10/1/1990 – 14/6/1995	100
	NS35 South Creek @ Luddenham Road Bridge	Sydney Water	pH	10/1/1990 – 14/6/1995	102
	NS35 South Creek @ Luddenham Road Bridge	Sydney Water	Dissolved Oxygen	10/1/1990 – 14/6/1995	101
	NS37 South Creek @ Erskine Park Road	Sydney Water	Temperature	15/9/1993 – 15/6/2001	31
	NS37 South Creek @ Erskine Park Road	Sydney Water	pH	15/9/1993 – 15/6/2001	186
	NS37 South Creek @ Erskine Park Road	Sydney Water	Dissolved Oxygen	15/9/1993 – 15/6/2001	31

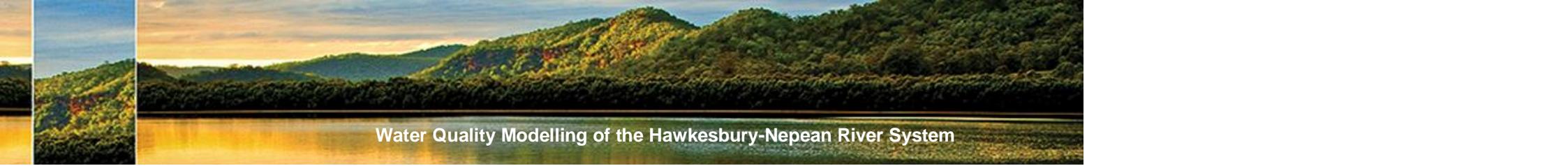
SINCLAIR KNIGHT MERZ



Water Quality Modelling of the Hawkesbury-Nepean River System

Region	Gauging location	Data Source	Data	Data period	Number of records
	NS45 South Creek @ Elizabeth Drive	Sydney Water	Temperature	10/1/1990 – 14/6/1995	100
	NS45 South Creek @ Elizabeth Drive	Sydney Water	pH	10/1/1990 – 14/6/1995	102
	NS45 South Creek @ Elizabeth Drive	Sydney Water	Dissolved Oxygen	10/1/1990 – 14/6/1995	101
	NS55 South Creek @ Bringelly Road	Sydney Water	Temperature	5/12/1989 – 18/5/1995	55
	NS55 South Creek @ Bringelly Road	Sydney Water	pH	5/12/1989 – 18/5/1995	55
	NS55 South Creek @ Bringelly Road	Sydney Water	Dissolved Oxygen	5/12/1989 – 18/5/1995	54
	NS62 South Creek @ Robens Crescent	Sydney Water	Temperature	10/6/1992 – 14/6/1995	36
	NS62 South Creek @ Robens Crescent	Sydney Water	pH	10/6/1992 – 14/6/1995	36
	NS62 South Creek @ Robens Crescent	Sydney Water	Dissolved Oxygen	10/6/1992 – 14/6/1995	35
	NS65 South Creek @ Hume Highway	Sydney Water	Temperature	29/6/1992 – 18/5/1995	14
	NS65 South Creek @ Hume Highway	Sydney Water	pH	29/6/1992 – 18/5/1995	14
	NS65 South Creek @ Hume Highway	Sydney Water	Dissolved Oxygen	29/6/1992 – 18/5/1995	14
Eastern Creek	Eastern Creek @ Garfield Road West	Blacktown City Council	Temperature	15/11/1991 – 1/6/1999	21
	Eastern Creek @ Garfield Road West	Blacktown City Council	pH	15/11/1991 – 1/6/1999	20
	Eastern Creek @ Garfield Road West	Blacktown City Council	Dissolved Oxygen	15/11/1991 – 1/6/1999	20
	Eastern Creek @ Eastern Road	Blacktown City Council	Temperature	4/3/1992 – 12/12/1995	13
	Eastern Creek @ Eastern Road	Blacktown City Council	pH	4/3/1992 – 12/12/1995	12
	Eastern Creek @ Eastern Road	Blacktown City Council	Dissolved Oxygen	4/3/1992 – 12/12/1995	12
	NS097 Eastern Creek @ Great Western Highway	Blacktown City Council / Sydney Water	Temperature	10/1/1990 – 1/6/1999	127
	NS097 Eastern Creek @ Great Western Highway	Blacktown City Council / Sydney Water	pH	10/1/1990 – 1/6/1999	128
	NS097 Eastern Creek @ Great Western Highway	Blacktown City Council / Sydney Water	Dissolved Oxygen	10/1/1990 – 1/6/1999	127
	Eastern Creek @ Grange Avenue	Blacktown City Council	Temperature	1/6/1996 – 1/6/1999	13
	Eastern Creek @ Grange Avenue	Blacktown City Council	pH	1/6/1996 – 1/6/1999	12
	Eastern Creek @ Grange Avenue	Blacktown City Council	Dissolved Oxygen	1/6/1996 – 1/6/1999	13
	Eastern Creek @ Bandon Road	Blacktown City Council	Temperature	1/12/1996 – 1/12/1998	9
	Eastern Creek @ Bandon Road	Blacktown City Council	pH	1/12/1996 – 1/3/1999	10

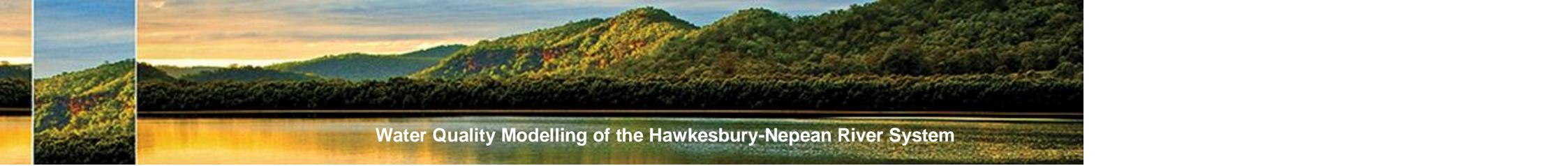
SINCLAIR KNIGHT MERZ



Water Quality Modelling of the Hawkesbury-Nepean River System

Region	Gauging location	Data Source	Data	Data period	Number of records
	Eastern Creek @ Bandon Road	Blacktown City Council	Dissolved Oxygen	1/12/1996 – 1/3/1999	10
	Eastern Creek @ unknown	Blacktown City Council	Temperature	19/8/2004 – 13/6/2007	30
	Eastern Creek @ unknown	Blacktown City Council	pH	19/8/2004 – 2/8/2006	30
	Eastern Creek @ unknown	Blacktown City Council	Dissolved Oxygen	24/8/2005 – 2/5/2007	18
	EA1 – Eastern Creek @ unknown	Blacktown City Council	Temperature	25/9/2008 – 2/10/2009	6
	EA1 – Eastern Creek @ unknown	Blacktown City Council	pH	25/9/2008 – 2/10/2009	6
	EA2 – Eastern Creek @ unknown	Blacktown City Council	Temperature	25/8/2008 – 4/8/2009	12
	EA2 – Eastern Creek @ unknown	Blacktown City Council	pH	25/8/2008 – 4/8/2009	12
	NS081 – Eastern Creek @ d/s Riverstone	Sydney Water	Temperature	17/8/1995 – 10/6/2008	279
	NS081 – Eastern Creek @ d/s Riverstone	Sydney Water	pH	17/8/1995 – 10/6/2008	235
	NS081 – Eastern Creek @ d/s Riverstone	Sydney Water	Dissolved Oxygen	17/1/1997 – 10/6/2008	215
	NS082 – Eastern Creek @ u/s Riverstone	Sydney Water	Temperature	17/8/1995 – 10/5/2011	311
	NS082 – Eastern Creek @ u/s Riverstone	Sydney Water	pH	17/8/1995 – 10/5/2011	263
	NS082 – Eastern Creek @ u/s Riverstone	Sydney Water	Dissolved Oxygen	17/1/1997 – 10/5/2011	247
	NS083 – Eastern Creek @ unknown	Sydney Water	Temperature	10/1/1990 – 21/6/2001	146
	NS083 – Eastern Creek @ unknown	Sydney Water	pH	10/1/1990 – 21/6/2001	208
	NS083 – Eastern Creek @ unknown	Sydney Water	Dissolved Oxygen	10/1/1990 – 21/6/2001	147
	NS085 Eastern Creek @ Douglas Road	Sydney Water	Temperature	16/3/1998 – 15/6/2001	33
	NS085 Eastern Creek @ Douglas Road	Sydney Water	pH	16/3/1998 – 15/6/2001	33
	NS085 Eastern Creek @ Douglas Road	Sydney Water	Dissolved Oxygen	16/3/1998 – 15/6/2001	33
	NS094 Eastern Creek @ u/s Breakfast Creek	Sydney Water	Temperature	16/3/2000 – 15/6/2001	33
	NS094 Eastern Creek @ u/s Breakfast Creek	Sydney Water	pH	16/3/2000 – 15/6/2001	194
	NS094 Eastern Creek @ u/s Breakfast Creek	Sydney Water	Dissolved Oxygen	16/3/2000 – 15/6/2001	33
	NS090 Breakfast Creek @ Falmouth	Sydney Water CMP	Dissolved Organic Carbon	15/11/2011 – 23/04/2012	6
	NS090 Breakfast Creek @ Falmouth	Sydney Water CMP	Total Organic Carbon	15/11/2011 – 23/04/2012	6
	NS087 Eastern Creek @ Quakers Hill Parkway	Sydney Water CMP	Dissolved Organic Carbon	15/11/2011 – 23/04/2012	6

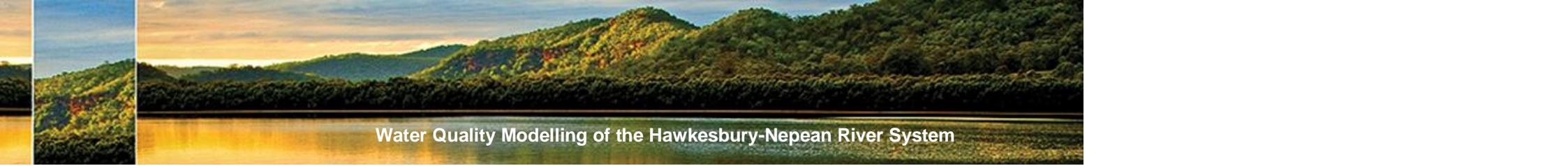
SINCLAIR KNIGHT MERZ



Water Quality Modelling of the Hawkesbury-Nepean River System

Region	Gauging location	Data Source	Data	Data period	Number of records
	NS087 Eastern Creek @ Quakers Hill Parkway	Sydney Water CMP	Total Organic Carbon	15/11/2011 – 23/04/2012	6
	NS082 Eastern Creek @ u/s Riverstone	Sydney Water CMP	Dissolved Organic Carbon	15/11/2011 – 23/04/2012	6
	NS082 Eastern Creek @ u/s Riverstone	Sydney Water CMP	Total Organic Carbon	15/11/2011 – 23/04/2012	6
Nepean River	E601 – Nepean River @ Inflow to Lake Nepean	SCA	Temperature	16/9/2009 – 14/2/2011	18
	E601 – Nepean River @ Inflow to Lake Nepean	SCA	pH	16/9/2009 – 14/2/2011	18
	E601 – Nepean River @ Inflow to Lake Nepean	SCA	Dissolved Oxygen	16/9/2009 – 14/2/2011	18
	E601 – Nepean River @ Inflow to Lake Nepean	SCA	Total Organic Carbon	16/9/2009 – 14/2/2011	17
	E601 – Nepean River @ Inflow to Lake Nepean	SCA	Dissolved Organic Carbon	16/9/2009 – 14/2/2011	17
	E697 – Nepean River @ McGuire's Crossing	SCA	Temperature	16/1/2007 – 8/2/2011	53
	E697 – Nepean River @ McGuire's Crossing	SCA	pH	16/1/2007 – 8/2/2011	53
	E697 – Nepean River @ McGuire's Crossing	SCA	Dissolved Oxygen	16/1/2007 – 8/2/2011	53
	E697 – Nepean River @ McGuire's Crossing	SCA	Total Organic Carbon	16/1/2007 – 8/2/2011	48
	E697 – Nepean River @ McGuire's Crossing	SCA	Dissolved Organic Carbon	16/1/2007 – 8/2/2011	51
	N44 – Nepean River @ Yarramundi	Sydney Water	Temperature	12/1/2007 – 24/2/2011	52
	N44 – Nepean River @ Yarramundi	Sydney Water	pH	12/1/2007 – 24/2/2011	52
	N44 – Nepean River @ Yarramundi	Sydney Water	Dissolved Oxygen	12/1/2007 – 24/2/2011	52
	N44 – Nepean River @ Yarramundi	Sydney Water CMP	Dissolved Organic Carbon	5/2/2007 – 17/4/2012	56
	N44 – Nepean River @ Yarramundi	Sydney Water CMP	Total Organic Carbon	1/11/2011 – 17/4/2012	9
	N57 – Nepean River @ Penrith Weir	Sydney Water	Temperature	12/1/2007 – 24/2/2011	52
	N57 – Nepean River @ Penrith Weir	Sydney Water	pH	12/1/2007 – 24/2/2011	51
	N57 – Nepean River @ Penrith Weir	Sydney Water	Dissolved Oxygen	12/1/2007 – 24/2/2011	52
	N57 – Nepean River @ Penrith Weir	Sydney Water CMP	Dissolved Organic Carbon	5/2/2007 – 17/4/2012	56
	N57 – Nepean River @ Penrith Weir	Sydney Water CMP	Total Organic Carbon	1/11/2011 – 17/4/2012	9
	N64 – Nepean River @ D/S Warra River	Sydney Water	Temperature	28/11/2007 – 22/2/2011	40
	N64 – Nepean River @ D/S Warra River	Sydney Water	pH	28/11/2007 – 22/2/2011	40
	N64 – Nepean River @ D/S Warra River	Sydney Water	Dissolved Oxygen	28/11/2007 – 22/2/2011	40

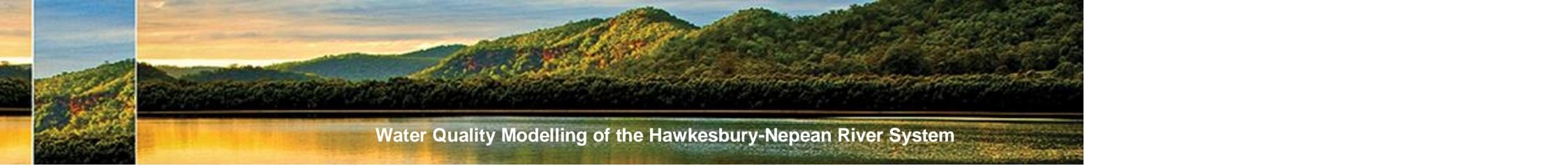
SINCLAIR KNIGHT MERZ



Water Quality Modelling of the Hawkesbury-Nepean River System

Region	Gauging location	Data Source	Data	Data period	Number of records
	N64 – Nepean River @ D/S Warra River	Sydney Water CMP	Dissolved Organic Carbon	28/11/2007 – 22/2/2011	39
	N67 – Nepean River @ Wallacia Bridge	Sydney Water	Temperature	12/1/2007 – 24/2/2011	55
	N67 – Nepean River @ Wallacia Bridge	Sydney Water	pH	12/1/2007 – 24/2/2011	53
	N67 – Nepean River @ Wallacia Bridge	Sydney Water	Dissolved Oxygen	12/1/2007 – 24/2/2011	55
	N67 – Nepean River @ Wallacia Bridge	Sydney Water CMP	Dissolved Organic Carbon	5/2/2007 – 16/4/2012	59
	N67 – Nepean River @ Wallacia Bridge	Sydney Water CMP	Total Organic Carbon	31/10/2011 – 16/4/2012	9
	N91 Nepean River @ Maldon Bridge	Sydney Water	Temperature	11/1/2011 – 16/4/2012	24
	N91 Nepean River @ Maldon Bridge	Sydney Water	pH	11/1/2011 – 16/4/2012	24
	N91 Nepean River @ Maldon Bridge	Sydney Water	Dissolved Oxygen	11/1/2011 – 16/4/2012	24
	N85 Nepean River @ Menangle Bridge	Sydney Water	Temperature	25/1/2011 – 16/4/2012	16
	N85 Nepean River @ Menangle Bridge	Sydney Water	pH	25/1/2011 – 16/4/2012	16
	N85 Nepean River @ Menangle Bridge	Sydney Water	Dissolved Oxygen	25/1/2011 – 16/4/2012	16
	N53 Nepean River @ Penrith Lakes	Sydney Water CMP	Dissolved Organic Carbon	1/11/2011 – 17/4/2012	9
	N53 Nepean River @ Penrith Lakes	Sydney Water CMP	Total Organic Carbon	1/11/2011 – 17/4/2012	9
	N48 Nepean River @ Smith Street	Sydney Water CMP	Dissolved Organic Carbon	1/11/2011 – 17/4/2012	9
	N48 Nepean River @ Smith Street	Sydney Water CMP	Total Organic Carbon	1/11/2011 – 17/4/2012	9
	N542 Boundary Creek @ u/s Penrith WRP	Sydney Water CMP	Dissolved Organic Carbon	16/11/2011	1
	N542 Boundary Creek @ u/s Penrith WRP	Sydney Water CMP	Total Organic Carbon	16/11/2011	1
	N542 Boundary Creek @ d/s Penrith WRP	Sydney Water CMP	Dissolved Organic Carbon	16/11/2011 – 27/4/2012	5
	N542 Boundary Creek @ d/s Penrith WRP	Sydney Water CMP	Total Organic Carbon	16/11/2011 – 27/4/2012	5
	N641 Warragamba River @ d/s Wallacia WRP	Sydney Water CMP	Dissolved Organic Carbon	16/11/2011 – 4/5/2012	5
	N641 Warragamba River @ d/s Wallacia WRP	Sydney Water CMP	Total Organic Carbon	16/11/2011 – 4/5/2012	5
	N75 Nepean River @ Sharpes Weir	Sydney Water CMP	Dissolved Organic Carbon	31/10/2011 – 16/4/2012	9
	N75 Nepean River @ Sharpes Weir	Sydney Water CMP	Total Organic Carbon	31/10/2011 – 16/4/2012	9
	N51 Nepean River @ Jackson Lane	Sydney Water CMP	Dissolved Organic Carbon	1/11/2011 – 17/4/2012	9
	N51 Nepean River @ Jackson Lane	Sydney Water CMP	Total Organic Carbon	1/11/2011 – 17/4/2012	9

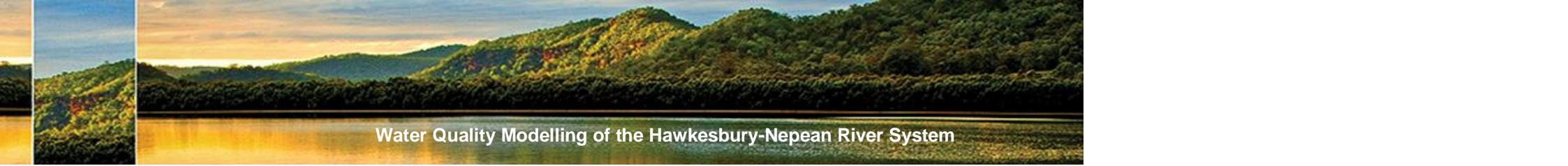
SINCLAIR KNIGHT MERZ



Water Quality Modelling of the Hawkesbury-Nepean River System

Region	Gauging location	Data Source	Data	Data period	Number of records
	N92 Nepean River @ Maldon Weir	Sydney Water CMP	Dissolved Organic Carbon	31/10/2011 – 16/4/2012	9
	N92 Nepean River @ Maldon Weir	Sydney Water CMP	Total Organic Carbon	31/10/2011 – 16/4/2012	9
Hawkesbury River	N14 – Hawkesbury River @ Wisemans Ferry	SCA / MHL	Temperature	12/1/2007 – 30/6/2011	32,279
	N14 – Hawkesbury River @ Wisemans Ferry	SCA	pH	12/1/2007 – 23/2/2011	52
	N14 – Hawkesbury River @ Wisemans Ferry	SCA	Dissolved Oxygen	12/1/2007 – 23/2/2011	52
	N14 – Hawkesbury River @ Wisemans Ferry	SCA	Dissolved Organic Carbon	5/2/2007 – 23/2/2011	51
	N21 – Hawkesbury River @ Lower Portland	SCA	Temperature	12/1/2007 – 23/2/2011	52
	N21 – Hawkesbury River @ Lower Portland	SCA	pH	12/1/2007 – 23/2/2011	52
	N21 – Hawkesbury River @ Lower Portland	SCA	Dissolved Oxygen	12/1/2007 – 23/2/2011	52
	N21 – Hawkesbury River @ Lower Portland	SCA	Dissolved Organic Carbon	5/2/2007 – 23/2/2011	51
	N35 – Hawkesbury River @ Windsor	Sydney Water	Temperature	12/1/2007 – 23/2/2011	52
	N35 – Hawkesbury River @ Windsor	Sydney Water	pH	12/1/2007 – 23/2/2011	52
	N35 – Hawkesbury River @ Windsor	Sydney Water	Dissolved Oxygen	12/1/2007 – 23/2/2011	52
	N35 – Hawkesbury River @ Windsor	Sydney Water CMP	Dissolved Organic Carbon	5/2/2007 – 17/4/2012	59
	N35 – Hawkesbury River @ Windsor	Sydney Water CMP	Total Organic Carbon	2/11/2011 – 17/4/2012	8
	N42 Hawkesbury River @ North Richmond	Sydney Water	Temperature	12/1/2007 – 24/2/2011	52
	N42 Hawkesbury River @ North Richmond	Sydney Water	pH	12/1/2007 – 24/2/2011	52
	N42 Hawkesbury River @ North Richmond	Sydney Water	Dissolved Oxygen	12/1/2007 – 24/2/2011	52
	N42 Hawkesbury River @ North Richmond	Sydney Water	Dissolved Organic Carbon	5/2/2007 – 24/2/2011	55
	N42 Hawkesbury River @ North Richmond	Sydney Water CMP	Total Organic Carbon	1/11/2011 – 17/4/2012	8
	N26 Hawkesbury River @ Sackville Ferry	MHL	Temperature	30/10/2009 – 30/6/2011	22,421
	N26 Hawkesbury River @ Sackville Ferry	Sydney Water	Dissolved Oxygen	13/6/1997 – 11/11/2002	38,012
	N26 Hawkesbury River @ Sackville Ferry	Sydney Water	pH	13/6/1997 – 7/6/2011	100,430
	N26 Hawkesbury River @ Sackville Ferry	Sydney Water CMP	Dissolved Organic Carbon	2/11/2011 – 17/4/2012	8
	N26 Hawkesbury River @ Sackville Ferry	Sydney Water CMP	Total Organic Carbon	2/11/2011 – 17/4/2012	8
	N04 Hawkesbury River @ Peats Ferry Bridge	Sydney Water	Temperature	16/2/2011 – 28/2/2012	12

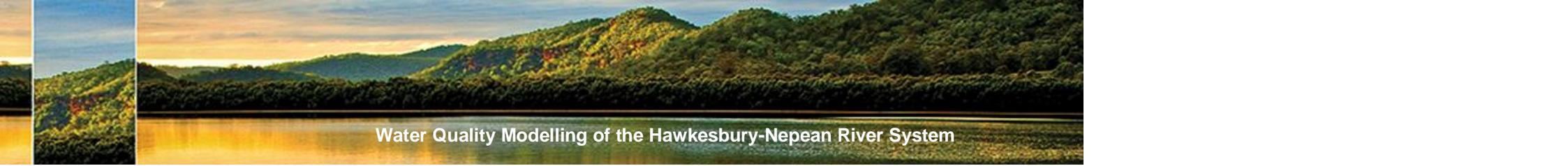
SINCLAIR KNIGHT MERZ



Water Quality Modelling of the Hawkesbury-Nepean River System

Region	Gauging location	Data Source	Data	Data period	Number of records
	N04 Hawkesbury River @ Peats Ferry Bridge	Sydney Water	pH	16/2/2011 – 28/2/2012	12
	N04 Hawkesbury River @ Peats Ferry Bridge	Sydney Water	Dissolved Oxygen	16/2/2011 – 28/2/2012	12
	N06 Hawkesbury River @ Marlowe Creek	Sydney Water	Temperature	16/2/2011 – 28/2/2012	12
	N06 Hawkesbury River @ Marlowe Creek	Sydney Water	pH	16/2/2011 – 28/2/2012	12
	N06 Hawkesbury River @ Marlowe Creek	Sydney Water	Dissolved Oxygen	16/2/2011 – 28/2/2012	12
	N18 Hawkesbury River @ Leets Vale	MHL	Temperature	22/6/2010 – 30/6/2011	32,179
	N18 Hawkesbury River @ Leets Vale	Sydney Water CMP	Dissolved Organic Carbon	2/11/2011 – 17/4/2012	8
	N18 Hawkesbury River @ Leets Vale	Sydney Water CMP	Total Organic Carbon	2/11/2011 – 17/4/2012	8
	NB13 Berowra Creek @ Calabash Point	Sydney Water CMP	Dissolved Organic Carbon	4/11/2011 – 17/4/2012	8
	NB13 Berowra Creek @ Calabash Point	Sydney Water CMP	Total Organic Carbon	4/11/2011 – 17/4/2012	8
	NB11 Berowra Creek @ Off Square Bay	Sydney Water CMP	Dissolved Organic Carbon	4/11/2011 – 17/4/2012	8
	NB11 Berowra Creek @ Off Square Bay	Sydney Water CMP	Total Organic Carbon	4/11/2011 – 17/4/2012	8
	N39 Hawkesbury River @ Freemans Reach	Sydney Water CMP	Dissolved Organic Carbon	2/11/2011 – 20/4/2012	9
	N39 Hawkesbury River @ Freemans Reach	Sydney Water CMP	Total Organic Carbon	2/11/2011 – 20/4/2012	9
	N3001 Hawkesbury River @ Off Cattai SRA	Sydney Water CMP	Dissolved Organic Carbon	2/11/2011 – 17/4/2012	8
	N3001 Hawkesbury River @ Off Cattai SRA	Sydney Water CMP	Total Organic Carbon	2/11/2011 – 17/4/2012	8
Cattai	NC6 – Cattai Creek @ d/s Castle Hill	Sydney Water	Dissolved Oxygen	15/8/2007 – 12/8/2010	38
	NC8 – Cattai Creek @ Bridge near WRP	Sydney Water	Temperature	26/1/1998 – 10/6/2008	142
	NC8 – Cattai Creek @ Bridge near WRP	Sydney Water	Dissolved Oxygen	26/1/2000 – 10/6/2008	121
	NC8 – Cattai Creek @ Bridge near WRP	Sydney Water	pH	17/3/1998 – 10/6/2008	129
	NC75 Cattai Creek @ d/s Castle Hill WRP	Sydney Water	Temperature	21/1/1998 – 10/6/2008	145
	NC75 Cattai Creek @ d/s Castle Hill WRP	Sydney Water	Dissolved Oxygen	21/2/2002 – 10/6/2008	85
	NC75 Cattai Creek @ d/s Castle Hill WRP	Sydney Water	pH	21/1/1998 – 10/6/2008	145
	NC5 Cattai Creek @ Annangrove	Sydney Water	Temperature	26/1/1998 – 12/8/2010	174
	NC5 Cattai Creek @ Annangrove	Sydney Water	pH	26/1/1998 – 12/8/2010	174
	NC5 Cattai Creek @ Annangrove	Sydney Water	Dissolved Oxygen	4/9/2000 – 12/8/2010	139

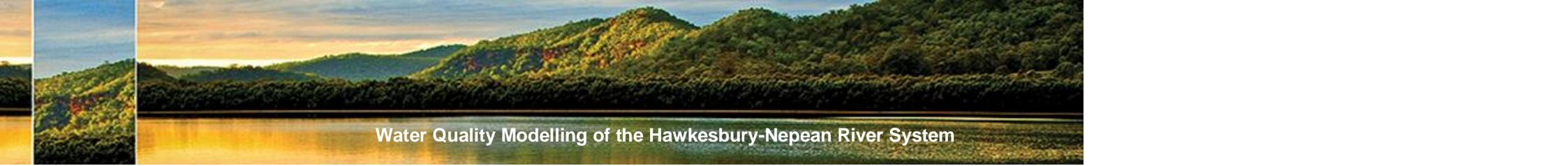
SINCLAIR KNIGHT MERZ



Water Quality Modelling of the Hawkesbury-Nepean River System

Region	Gauging location	Data Source	Data	Data period	Number of records
	NC2 Cattai Creek @ Cattai Road Bridge	Sydney Water	Temperature	8/2/1990 – 12/8/2010	303
	NC2 Cattai Creek @ Cattai Road Bridge	Sydney Water	pH	8/2/1990 – 12/8/2010	303
	NC2 Cattai Creek @ Cattai Road Bridge	Sydney Water	Dissolved Oxygen	4/9/2000 – 12/8/2010	146
	NC3 Cattai Creek @ Pitt Town	Sydney Water	Temperature	1/5/1990 – 12/8/2010	393
	NC3 Cattai Creek @ Pitt Town	Sydney Water	pH	1/5/1990 – 12/8/2010	794
	NC3 Cattai Creek @ Pitt Town	Sydney Water	Dissolved Oxygen	4/9/2000 – 12/8/2010	205
	A3 Cattai Creek @ unknown	The Hills Shire Council	Temperature	13/12/2005 – 27/5/2011	36
	A3 Cattai Creek @ unknown	The Hills Shire Council	pH	13/12/2005 – 4/11/2009	19
	A3 Cattai Creek @ unknown	The Hills Shire Council	Dissolved Oxygen	13/12/2005 – 27/5/2011	34
	I2 Cattai Creek @ unknown	The Hills Shire Council	Temperature	9/11/2005 – 27/5/2011	40
	I2 Cattai Creek @ unknown	The Hills Shire Council	pH	9/12/2005 – 4/11/2009	23
	I2 Cattai Creek @ unknown	The Hills Shire Council	Dissolved Oxygen	13/12/2005 – 27/5/2011	39
	K2 Cattai Creek @ unknown	The Hills Shire Council	Temperature	9/11/2005 – 27/5/2011	41
	K2 Cattai Creek @ unknown	The Hills Shire Council	pH	9/12/2005 – 4/11/2009	23
	K2 Cattai Creek @ unknown	The Hills Shire Council	Dissolved Oxygen	13/12/2005 – 27/5/2011	38
	NC11 Cattai Creek @ d/s Cattai Road	Sydney Water CMP	Dissolved Organic Carbon	2/11/2011 – 20/4/2012	9
	NC11 Cattai Creek @ d/s Cattai Road	Sydney Water CMP	Total Organic Carbon	2/11/2011 – 20/4/2012	9
Colo River	212407 Colo River @ Colo Junction	MHL	Temperature	7/11/2009 – 17/6/2011	56,291
	N2202 Colo River @ Putty Road Bridge	Sydney Water CMP	Dissolved Organic Carbon	2/11/2011 – 20/4/2012	9
	N2202 Colo River @ Putty Road Bridge	Sydney Water CMP	Total Organic Carbon	2/11/2011 – 20/4/2012	9
Warragamba	Warragamba Dam	SCA	Temperature	2/1/1990 – 4/7/2011	51,154
	Warragamba Dam	SCA	pH	2/1/1990 – 4/7/2011	50,589
	Warragamba Dam	SCA	Dissolved Oxygen	2/1/1990 – 4/7/2011	50,609
	Warragamba Dam	SCA	Dissolved Organic Carbon	2/1/1990 – 4/7/2011	2,794
	Warragamba Dam	SCA	Total Organic Carbon	2/1/1990 – 4/7/2011	2,573

SINCLAIR KNIGHT MERZ

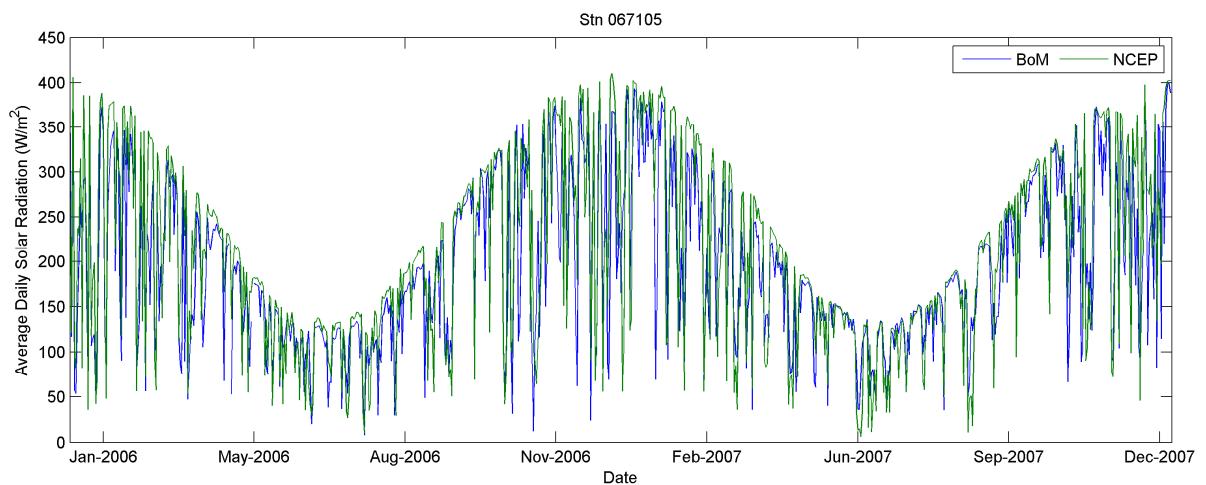


Water Quality Modelling of the Hawkesbury-Nepean River System

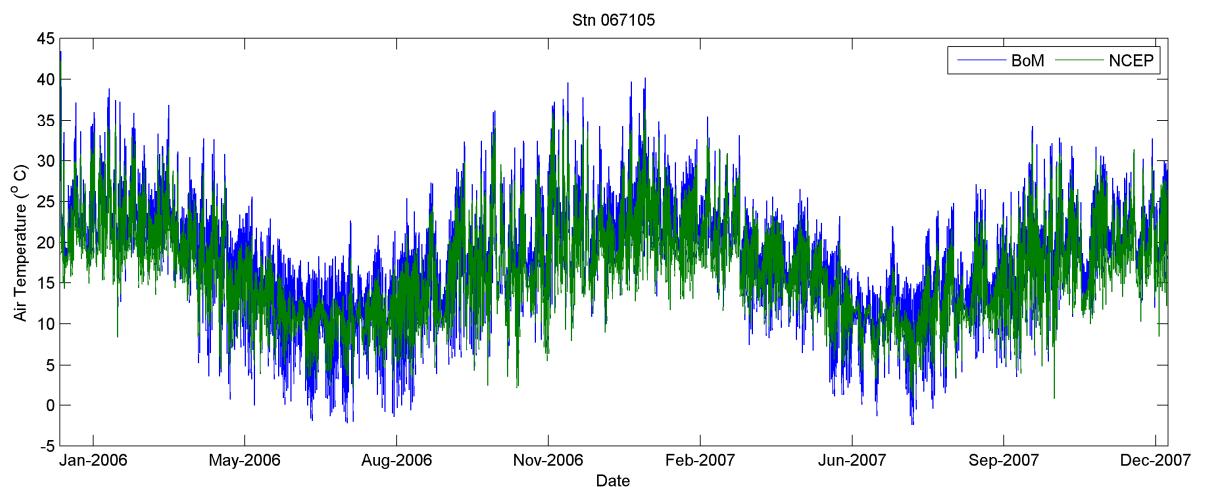
Region	Gauging location	Data Source	Data	Data period	Number of records
Pheasant's Nest	N92 Nepean River @ Maldon Weir	Sydney Water	Temperature	28/3/1985 – 8/2/2011	813
	N92 Nepean River @ Maldon Weir	Sydney Water	pH	1/8/1988 – 8/2/2011	509
	N92 Nepean River @ Maldon Weir	Sydney Water	Dissolved Oxygen	28/3/1985 – 8/2/2011	804
	N92 Nepean River @ Maldon Weir	Sydney Water	Dissolved Organic Carbon	26/7/2001 – 8/2/2011	118
	N92 Nepean River @ Maldon Weir	Sydney Water	Total Organic Carbon	26/7/2001 – 8/2/2011	61
Broughton Pass	HUC1 Broughton Pass Weir @ Wilton Road	Sydney Water	Temperature	2/1/2007 – 17/2/2011	136
	HUC1 Broughton Pass Weir @ Wilton Road	Sydney Water	pH	2/1/2007 – 17/2/2011	136
	HUC1 Broughton Pass Weir @ Wilton Road	Sydney Water	Dissolved Oxygen	2/1/2007 – 17/2/2011	136
	HUC1 Broughton Pass Weir @ Wilton Road	Sydney Water	Dissolved Organic Carbon	2/1/2007 – 17/2/2011	139
	HUC1 Broughton Pass Weir @ Wilton Road	Sydney Water	Total Organic Carbon	2/1/2007 – 17/2/2011	139

MHL – Manly Hydraulics Laboratory

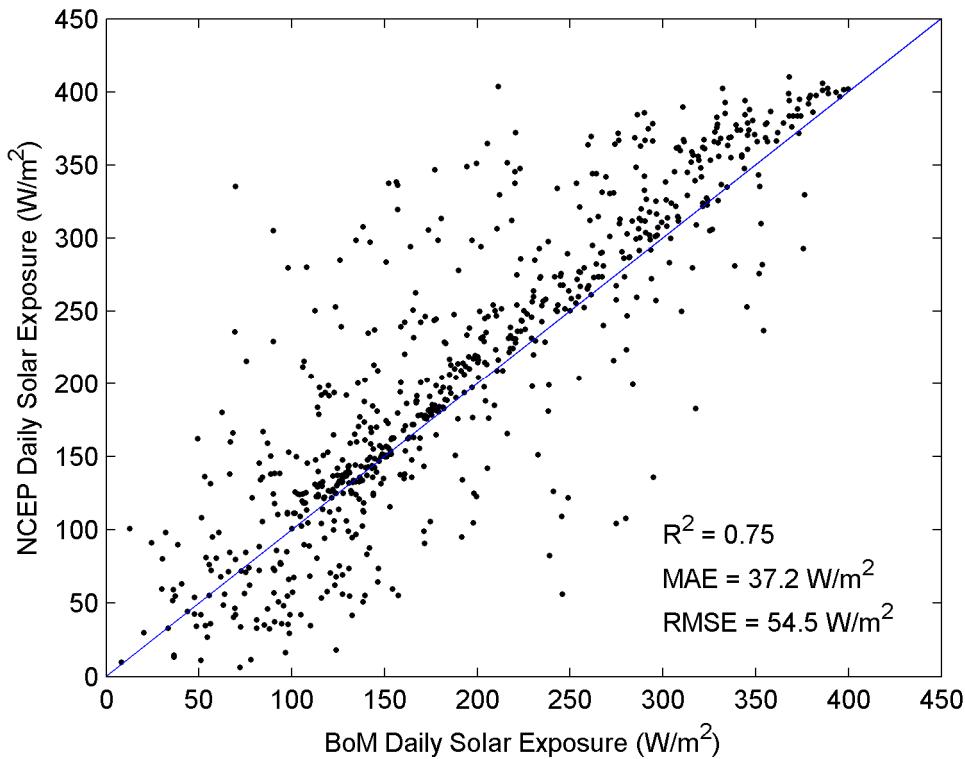
Appendix H Comparison of Meteorological Data



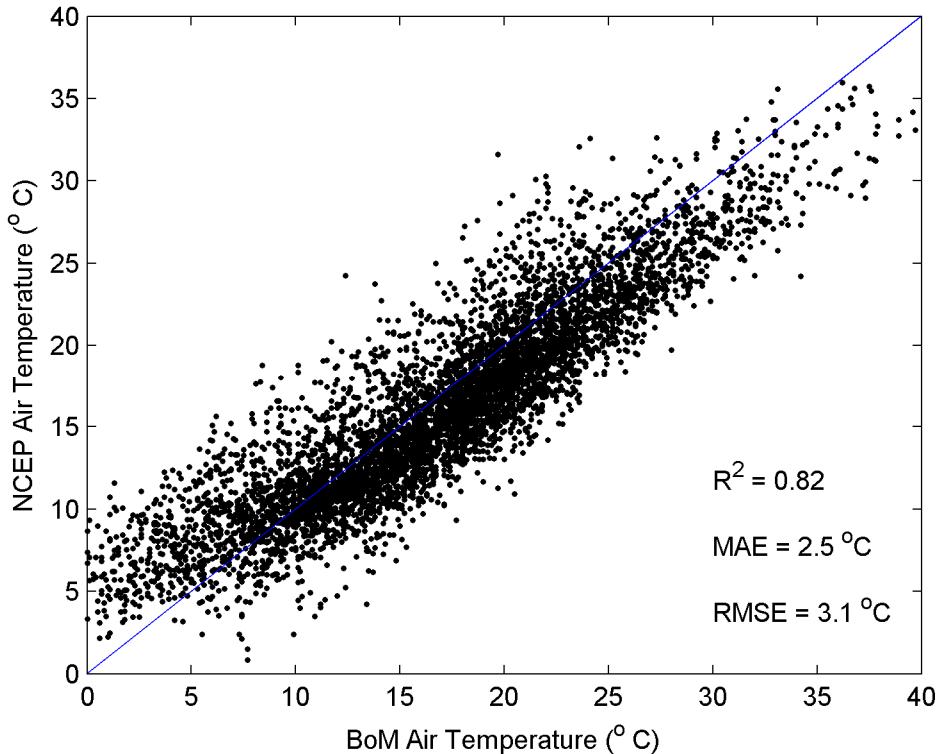
■ **Figure H-1 Timeseries of Average Daily Solar Radiation for Station 067105 (Richmond)**



■ **Figure H-2 Timeseries of Air Temperature for Station 067105 (Richmond)**



■ **Figure H-3 Scatter Plots of Average Daily Solar Exposure for Station 067105 (Richmond)**



■ **Figure H-4 Scatter Plots of Air Temperature for Station 067105 (Richmond)**

Appendix I Surface Heat Fluxes

Surface heat exchange in the TUFLOW FV model takes into account the effects of penetrative radiation (i.e. solar radiation), non-penetrative radiation (i.e. long-wave radiation), sensible heat transfer, and latent heat transfer. The equations adopted to compute these terms are described below.

A-1 Penetrative Radiation

Penetrative radiation consists of the light spectra with wavelength between 280 nm to approximately 1400 nm. The solar radiation reaching the water surface (in W/m²) penetrates the water column according to Beer's Law, as below.

$$I = I_o e^{-\eta z}$$

where I_o is the solar radiation reaching the water surface, η is a light extinction coefficient and z is the water depth. In effect, I_o and I are subdivided in different bands of the light spectrum, as each of these bands are absorbed at different rates in the water column. Four bands are assumed in the light spectrum:

- Ultra-Violet A (UVA): This consists of the light with wave length between 315 and 400 nm and accounts for 4.8% of the total incoming solar radiation. The light extinction coefficient for this band can be provided by the user. For the Hawkesbury-Nepean River System model η_{UVA} was set to 1.0 m⁻¹.
- Ultra-Violet B (UVB): This consists of the light with wave length between 280 and 315 nm and accounts for 0.2% of the total incoming solar radiation. The light extinction coefficient for this band can also be provided by the user. For the Hawkesbury-Nepean River System model η_{UVB} was set to 2.5 m⁻¹.
- Photosynthetic Active Radiation (PAR): This consists primarily of the visible light band (380 to 780 nm) and is the energy used by primary producers for photosynthesis and accounts for 52% of the total incoming solar radiation. The light extinction coefficient for this band can be provided by the user. For the Hawkesbury-Nepean River System model η_{PAR} was set to 0.25 m⁻¹.
- Near Infra-Red (NIR): This consists of the light with wave length larger than 380 nm and accounts for 43% of the total incoming solar radiation. The light extinction coefficient for this band can also be provided by the user. For the Hawkesbury-Nepean River System model η_{NIR} was set to 1.0 m⁻¹.

Taking the above into consideration, each band of the spectrum the penetrative heat flux is computed as:

$$I = 0.048 * I_o e^{-\eta_{UVA} z} + 0.002 * I_o e^{-\eta_{UVB} z} + 0.52 * I_o e^{-\eta_{PAR} z} + 0.33 * I_o e^{-\eta_{NIR} z}$$

The net penetrative radiation flux into the model is given by the difference between I in the top and bottom faces of the cell. I is computed with a downward sweep across the vertical cells of the domain. At the bed, 90% of the flux is lost to the sediments, and the rest is transferred with an upward sweep. Little radiation reaching the surface following the upward sweep is lost to the atmosphere.

In each cell the temperature increase ΔT associated with the penetrative radiation is calculated as:

$$\Delta T = \frac{(I_{up} - I_{dn}) * \Delta t}{\rho C_p} dz$$

where I_{up} is the total penetrative heat flux in the upper face of a model cell, I_{dn} is the total penetrative heat flux in the lower face of a model cell, Δt is the model time step, dz is the cell thickness, ρ is the water density in the cell, and C_p is the specific heat of water (4181.3 J/Kg/ $^{\circ}$ C).

A-2 Non-Penetrative Radiation

Non-penetrative radiation consists of radiation emitted by the atmosphere and the water itself. For the Hawkesbury Nepean River system, incoming non-penetrative longwave radiation is provided as an input. Longwave radiation emitted by the water is calculated assuming a Stephan-Boltzmann law.

$$I_W = \epsilon \sigma (T + 273.15)^4$$

where $\epsilon = 0.96$ is the water emissivity, σ is the Stephan Boltzmann constant (5.6697 J/m²/s/ $^{\circ}$ C⁴) and T is the preceding time step temperature. The net longwave radiation I_{LW} is computed as the difference between incoming, water-reflected, and water emitted terms:

$$I_{LW} = (1 - \alpha_{LW})I_{LW_o} - I_W$$

where α_{LW} is water long wave albedo coefficient (i.e. reflection), I_{LW_o} is the incoming long wave radiation.

A-3 Sensible and Latent Heat Transfer

Sensible and latent heat transfer also influence only the surface cell of the domain and are calculated using bulk aerodynamic formulae (i.e. TVA 1972, Fischer et al. 1979, Chapra 1998).

Specific heat transfer is given by:

$$H_S = C_s C_{pair} \rho_a U_{10} (T_A - T_S)$$

where C_s is the bulk aerodynamic sensible heat transfer coefficient (1.3×10^{-3}), ρ_a is the air density (1.2 kg/m³), C_{pair} is the specific heat of air (1005 J/kg/ $^{\circ}$ C), U_{10} is the wind velocity magnitude 10 m above the water surface, T_A is the air temperature and T_S is the water surface temperature.

Latent heat transfer is given by:

$$H_L = C_L \rho_a L_v U_{10} (E_s - E_A)$$

where C_L is the bulk aerodynamic latent heat transfer coefficient (1.3×10^{-3}), ρ_a is the air density (1005 g/m^3), L_v is the latent heat of vaporization (2.4433 J/kg), U_{10} is the wind velocity magnitude 10 m above the water surface, E_s is the specific humidity of the water surface and E_A is the specific humidity of the air. The specific humidity is calculated as a function of the vapour pressure (TVA 1972):

$$P_v = 100 * e^{2.3026\left(\frac{aT}{T+b}+c\right)}$$

where T is the temperature, $a= 7.5$, $b=237.3$, and $c = 0.7858$.

$$E_s = \frac{0.622P_v}{P_a}$$

where P_a is the air pressure at the water surface and P_v is the vapour pressure assuming the water surface temperature.

$$E_a = R_h \frac{0.622P_v}{P_a}$$

where R_h is the relative humidity of the air and P_v is the vapour pressure assuming the air temperature T_a . Both R_h and T_a are provide as model input.

A-4 Temperature and Mass Change

The temperature change associated with non-penetrative long wave radiation, sensible heat and latent heat are accounted for in each surface cell of the model domain as:

$$\Delta T = \frac{(I_{LW} + H_s + H_L) * \Delta t}{\rho C_p} dz$$

The evaporative mass change associated with the latent heat exchange is given by:

$$\Delta M = \frac{(H_L) * \Delta t}{L_v} dA$$

where dA is the of area of the top of the surface cell.

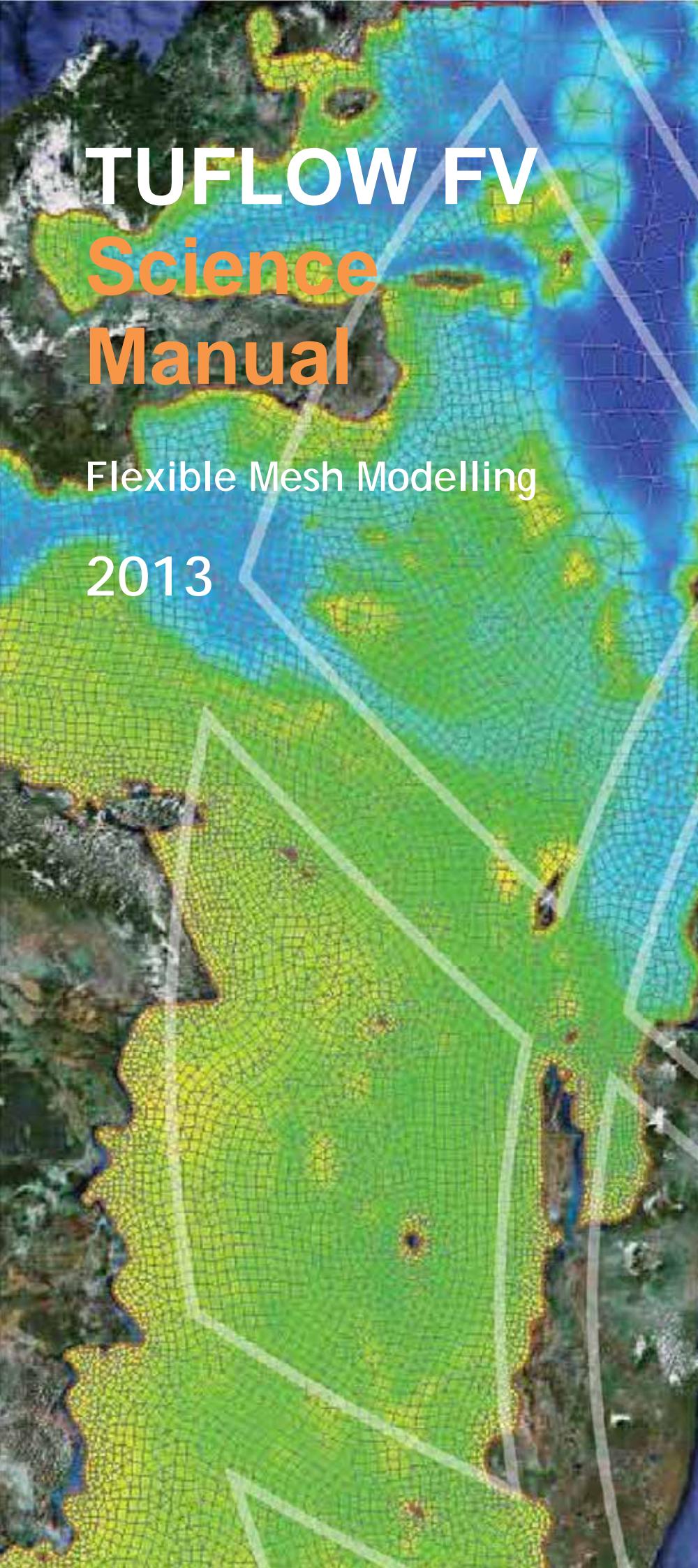
A-5 References

TVA (1972). Heat and Mass Transfer between a Water Surface and the Atmosphere. Water Resources Research Laboratory Report n. 14. Tennessee Valley Authority Report n. 0-6803.

Fischer, H.B., List, E.G., Koh, R.C.Y., Imberger, J., and Brooks, N.H. (1979). Mixing in Inland and Coastal Waters. Academic Press.

Chapra, S. C. (2008). Surface Water-Quality Modelling. Waveland Press. 2nd Edition.

Appendix J TUFLOW FV Science Manual



TUFLOW FV Science Manual

Flexible Mesh Modelling

2013

www.TUFLOW.com
www.TUFLOW.com/forum
wiki.TUFLOW.com
support@tuflow.com

CONTENTS

1	INTRODUCTION	1
2	NON-LINEAR SHALLOW WATER EQUATIONS (NLSWE)	3
3	SCALAR CONSERVATION EQUATIONS	5
4	NUMERICAL SCHEME	6
4.1	Discrete system	6
4.2	Spatial Order	6
4.3	Mode Splitting	8
4.4	Flux Terms	8
4.4.1	Viscous Fluxes	9
4.4.1.1	<i>Horizontal viscous fluxes</i>	9
4.4.1.2	<i>Vertical viscous fluxes</i>	9
4.4.2	Inviscid Fluxes	10
4.4.2.1	<i>Internal Mode</i>	10
4.4.2.2	<i>External Mode</i>	10
4.4.2.3	<i>Flux Correction</i>	11
4.4.2.4	<i>Scalar Inviscid Fluxes</i>	11
4.4.3	Total Flux	11
4.4.4	Flux Spatial Integration	11
4.5	Time integration	11
4.6	Wetting/Drying	12
4.7	Source terms	13
4.7.1	Bed slope	13
4.7.2	Coriolis	13
4.7.3	Wind Stress	13
4.7.4	Bed Friction	13
4.7.5	Surface Friction	14
4.7.6	Mean Sea Level and Baroclinic Pressure Gradients	15
4.7.7	Wave radiation stress	15
4.7.8	Scalar Decay	15
4.7.9	Scalar (Sediment) Settling	15
4.7.10	Other Sources/Sinks	16
4.8	Timestep Algorithm	17

1 Introduction

TUFLOW FV is a numerical hydrodynamic model for the two-dimensional (2D) and three-dimensional (3D) Non-Linear Shallow Water Equations (NLSWE). The model is suitable for solving a wide range of hydrodynamic systems ranging in scale from the open channels and floodplains, through estuaries to coasts and oceans.

The Finite-Volume (FV) numerical scheme employed by TUFLOW FV is capable of solving the NLSWE on both structured rectilinear grids and unstructured meshes comprised of triangular and quadrilateral elements. The flexible mesh allows for seamless boundary fitting along complex coastlines or open channels as well as accurately and efficiently representing complex bathymetries with a minimum number of computational elements. The flexible mesh capability is particularly efficient at resolving a range of scales in a single model without requiring multiple domain nesting.

Unstructured mesh geometries can be created using a suitable mesh generation tool. BMT staff generally use the SMS package (<http://www.aquaveo.com/sms>) for building meshes as well as undertaking a range of model pre-processing and post-processing tasks. Both Cartesian and Spherical mesh geometries can be used as the basis for TUFLOW FV simulations.

Three-dimensional simulations can be performed within TUFLOW FV using either sigma-coordinate or a hybrid z-coordinate vertical mesh. Three-dimensional simulations can optionally use a mode-splitting approach to efficiently solve the external (free-surface) mode in 2D at a timestep constrained by the surface wave speed while the internal 3D mode is updated less frequently.

Advection-Diffusion (AD) of multiple water-borne constituents can be solved within TUFLOW FV, either coupled with a hydrodynamic simulation, or alternatively in transport mode using a pre-calculated transport file. Simple constituent decay and settling can be accommodated in the AD solutions, or alternatively more complex sediment transport algorithms can be applied through the sediment transport module.

Baroclinic pressure-gradient terms can be optionally activated to allow the hydrodynamic solution to respond to temperature, salinity and sediment induced density gradients. Atmospheric heat exchange can also be calculated given standard meteorological parameter inputs by an integrated module.

TUFLOW FV has a variety of options for simulating horizontal turbulent mixing, including the Smagorinsky scheme. Simple parametric models for vertical mixing are incorporated within TUFLOW FV and for more complicated turbulence model algorithms an interface for linking with various external turbulence models has been implemented.

Both cohesive and non-cohesive sediment transport routines can be accessed through in-built TUFLOW FV modules which handle both bed and suspended load mechanisms. Dynamic morphology updating can be optionally activated.

TUFLOW FV provides a multitude of options for specifying modelboundary conditions, including:

- Various open boundary conditions
- Point source inflows

- Moving point source inflows
- Spatially and temporally varied forcing e.g. windfields, short-wave forcing

2 Non-Linear Shallow Water Equations (NLSWE)

TUFLOW FV solves the the NLSWE, including viscous flux terms and various source terms on a flexible mesh comprised of triangular and quadrilateral elements.

The NLSWE is a system of equations describing the conservation of fluid mass/volume and momentum in an incompressible fluid, under the hydrostatic pressure and Boussinesq assumptions. The standard form of the NLSWE, which relates the time-derivative of the conserved variables to flux-gradient and source terms, is given below.

$$\frac{\partial \mathbf{U}}{\partial t} + \nabla \cdot \mathbf{F}(\mathbf{U}) = \mathbf{S}(\mathbf{U}) \quad (1)$$

The finite-volume schemes are derived from the conservative integral form of the NLSWE, which are obtained by integrating the standard conservation equation over a control volume, Ω .

$$\int_{\Omega} \frac{\partial \mathbf{U}}{\partial t} d\Omega + \int_{\Omega} \nabla \cdot \mathbf{F}(\mathbf{U}) d\Omega = \int_{\Omega} \mathbf{S}(\mathbf{U}) d\Omega \quad (2)$$

Gauss' theorem is used to convert the flux-gradient volume integral into a boundary-integral:

$$\frac{\partial}{\partial t} \int_{\Omega} \mathbf{U} d\Omega + \oint_{\partial\Omega} (\mathbf{F} \cdot \mathbf{n}) ds = \int_{\Omega} \mathbf{S}(\mathbf{U}) d\Omega \quad (3)$$

where $\int_{\Omega} d\Omega$ represent volume integrals and $\oint_{\partial\Omega} ds$ represents a boundary integral and \mathbf{n} is the boundary unit-normal vector.

The NLSWE conserved variables are volume (depth),x-momentum and y-momentum:

$$\mathbf{U} = \begin{bmatrix} h \\ hu \\ hv \end{bmatrix} \quad (4)$$

where h is depth, u is x -velocity and v is y -velocity.

The x , y and z components of the inviscid flux (\mathbf{F}^I) and viscous flux (\mathbf{F}^V) terms in the NLSWE are given below.

$$\begin{aligned} \mathbf{F}_x^I &= \begin{bmatrix} hu \\ hu^2 + \frac{1}{2}gh^2 \\ huv \end{bmatrix}, \quad \mathbf{F}_x^V \approx \begin{bmatrix} 0 \\ -hK_v \frac{\partial u}{\partial x} \\ -hK_v \frac{\partial v}{\partial x} \end{bmatrix} \\ \mathbf{F}_y^I &= \begin{bmatrix} hv \\ huv \\ hv^2 + \frac{1}{2}gh^2 \end{bmatrix}, \quad \mathbf{F}_y^V \approx \begin{bmatrix} 0 \\ -hK_v \frac{\partial u}{\partial y} \\ -hK_v \frac{\partial v}{\partial y} \end{bmatrix} \\ \mathbf{F}_z^I &= \begin{bmatrix} hw \\ hwu \\ hwv \end{bmatrix}, \quad \mathbf{F}_z^V \approx \begin{bmatrix} 0 \\ -\nu_t \frac{\partial u}{\partial z} \\ -\nu_t \frac{\partial v}{\partial z} \end{bmatrix} \end{aligned} \quad (5)$$

where K_v and v_t are the horizontal and vertical eddy-viscosity terms.

Some of the various source terms to the NLSWE are provided below:

$$\mathbf{S} = \begin{bmatrix} 0 \\ gh \frac{\partial z_b}{\partial x} + fvh - \frac{h}{\rho_0} \frac{\partial p_a}{\partial x} - \frac{hg}{\rho_0} \int_z^\eta \frac{\partial \rho}{\partial x} dz - \frac{1}{\rho_0} \left(\frac{\partial s_{xx}}{\partial x} + \frac{\partial s_{xy}}{\partial y} \right) + \frac{\tau_{sx}}{\rho_0} - \frac{\tau_{bx}}{\rho_0} \\ gh \frac{\partial z_b}{\partial y} - fuh - \frac{h}{\rho_0} \frac{\partial p_a}{\partial y} - \frac{hg}{\rho_0} \int_z^\eta \frac{\partial \rho}{\partial y} dz - \frac{1}{\rho_0} \left(\frac{\partial s_{yx}}{\partial x} + \frac{\partial s_{yy}}{\partial y} \right) + \frac{\tau_{sy}}{\rho_0} - \frac{\tau_{by}}{\rho_0} \end{bmatrix} \quad (6)$$

where,

- $\frac{\partial z_b}{\partial x}, \frac{\partial z_b}{\partial y}$ are the x- and y-components of bed slope;
- f is the coriolis coefficient;
- ρ is the local fluid density, ρ_0 is the reference density and p_a is the mean sea level pressure;
- s_{ij} is the short-wave radiation stress tensor; and
- τ_s and τ_b are respectively the surface and bottom shear stress terms (where applicable).

Other source terms not included above include inflow/outflow to/from the water column.

3 Scalar Conservation Equations

Analogous conservation equations are solved for the transport of scalar constituents in the water column.

$$U = [hC] \quad (7)$$

where C is the constituent concentration. The flux components of the scalar conservation equation are:

$$\begin{aligned} F_x^I &= [huC], \quad F_x^V \approx \left[-h \left(D_{xx} \frac{\partial C}{\partial x} + D_{xy} \frac{\partial C}{\partial y} \right) \right] \\ F_y^I &= [hvC], \quad F_y^V \approx \left[-h \left(D_{yx} \frac{\partial C}{\partial x} + D_{yy} \frac{\partial C}{\partial y} \right) \right] \\ F_z^I &= [hwC], \quad F_z^V \approx \left[-hv'_t \frac{\partial C}{\partial z} \right] \end{aligned} \quad (8)$$

The source components may include scalar decay and settling:

$$S = [-K_d hC - w_s C] \quad (9)$$

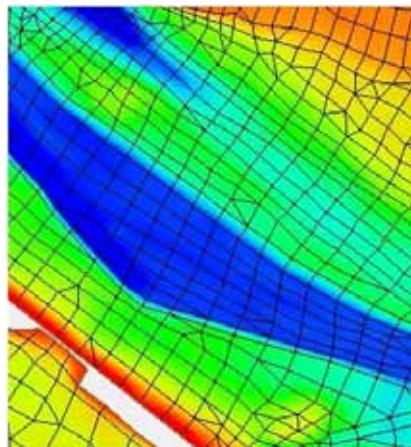
where K_d is a scalar decay-rate coefficient and w_s is a scalar settling velocity.

4 Numerical Scheme

The system of equations described above is solved using a Finite-Volume numerical scheme, as described below. Further details about Finite Volume methods for hyperbolic systems can be found in Leveque (2002).

4.1 Discrete system

The spatial domain is discretised using contiguous, non-overlapping triangular and quadrilateral cells (or elements).



A cell-centred spatial discretisation is adopted for all NLSWE conserved variables. The discrete form of the equations for cell i , with $k = 1, N_k$ cell-faces is:

$$\frac{\partial \mathbf{U}_i}{\partial t} = -\frac{1}{A_i} \sum_{k=1}^{N_k} (\mathbf{F}_k \cdot \mathbf{n}_k) L_k + \mathbf{S}_i \quad (10)$$

In this discrete equation \mathbf{U}_i represents the volume-average of the conserved variables in cell i , A_i is the cross-sectional (plan) area of the cell and \mathbf{S}_i is the volume-average source term/s. A first-order midpoint quadrature is used to evaluate the cell boundary flux integral, where \mathbf{n}_k is the boundary/face unit normal vector for face k and L_k is the corresponding face length. The discrete conserved variable field is assumed to be continuous within a cell but discontinuous at the cell-faces.

The finite-volume form of the conservation equation has delivered an Ordinary Differential Equation (ODE) from the original Partial Differential Equation (PDE) form of the conservation equation (Equation 1). This allows the solution of the conservation system of equations to be separated into a two stage algorithm:

- 1 the spatial integration of the discrete flux and source components (RHS of Equation 10)
- 2 the time integration of the discrete system of system of conservation equations

4.2 Spatial Order

The first-order form of the finite volume schemes assumes a piecewise constant \mathbf{U}_i within each model cell (Leveque, 2002). Finite-volume schemes with higher-order spatial accuracy can be derived by reconstructing a piecewise continuous $\mathbf{U}_i(x, y, z)$ within each model cell. For instance, a second-order

spatial scheme can be derived by re-construction of a piecewise linear $\mathbf{U}_i(x, y, z)$, while a third-order spatial scheme would require re-construction of a piecewise parabolic $\mathbf{U}_i(x, y, z)$. It should be noted that the discrete \mathbf{U}_i remains discontinuous at cell-faces even for schemes higher than first-order (Hubbard, 1999).

The higher spatial orders can significantly reduce numerical diffusion where the physical system being solved includes large spatial gradients relative to the discrete mesh size. Numerical diffusion can also be reduced through selection of a finer mesh resolution, however the higher spatial order schemes will generally achieve this outcome with less increase in computational overhead.

In general, the solution will only benefit from higher spatial order when the spatial gradients become sufficiently large relative to the mesh size. This can only be determined by testing for improvements in the higher-order solution relative to the first-order solution. If the first-order and high-order solutions are more or less identical for the particular model purpose, then it is generally appropriate to adopt the first-order accuracy. However, if the solutions are significantly different this suggests that first-order numerical diffusion is substantial relative to the physical fluxes that are being resolved in the model. In this case the higher-order solution is probably of a higher quality, though care must be exercised with the higher order solutions to ensure that spurious “overshoots” at the cell faces are avoided by the reconstruction procedure.

The Total Variation Diminishing (TVD) property (and hence stability) of the higher-order scheme solution is achieved using a choice of gradient limiter schemes. A variety of gradient limiters are available in TUFLOW FV and are listed in Table 1 in order from least to most “compressive”. The most “compressive” schemes will maximise the resolution of sharp gradients but may do so at the expense of additional computational overhead. The most compressive gradient limiter schemes also increase the risk of generating spurious “overshoots” within the solution.

Within TUFLOW FV horizontal and vertical reconstructions are performed separately. A first-order horizontal reconstruction can be combined with a second-order vertical reconstruction, and vice-versa.

Table 1 Overview of gradient limiter schemes applied in TUFLOW FV

	Horizontal gradient limiter scheme	Vertical gradient limiter scheme
Least Compressive		MINMOD Fringer et al. (2005)
↓	Limited Central Difference (LCD) Batten et al. (1996)	Maximum Central Fringer et al. (2005)
Most Compressive	Maximum Limited Gradient (MLG) Batten et al. (1996)	Superbee Fringer et al. (2005)

4.3 Mode Splitting

Efficient integration of the NLSWE is achieved through a mode splitting scheme, whereby different components of the governing equations are updated using an appropriate timestep selected by taking into account physical and numerical convergence and stability considerations (e.g. Shchepetkin & McWilliams, 2005).

A reduced set of equations comprising all terms other than the barotropic (or free-surface) pressure-gradients is initially partially solved. As part of this solution, an appropriate “internal mode” timestep is calculated that obeys both:

- Courant-Freidrich-Levy (CFL) constraints imposed by the advective current speeds
- Peclet number (Pe) constraints imposed by the diffusion terms

Prior to updating (or time-integrating) the solution an “external mode” loop is entered, in which a 2D depth-averaged reduction of the 3D NLSWE is solved multiple times, using a timestep that obeys the barotropic Courant-Freidrich-Levy (CFL) constraint imposed by the shallow water wave speed $\bar{u} \pm \sqrt{gh}$ (where \bar{u} is the depth-averaged current speed). The external mode loop is repeated until the cumulative timestep is approximately equal to the internal mode timestep.

The depth-averaged inviscid fluxes from the external mode solution are then used to correct the internal mode inviscid fluxes so that they now represent the total inviscid flux for the 3D solution. The corrected fluxes are used to update the full 3D solution.

A stability constraint imposed by the baroclinic internal wave speed is not explicitly calculated and in some instances may not be automatically met by the mode splitting scheme. This can be addressed by the user reducing the upper-limiting timestep, where oscillations in the pycnocline are seen to be generating numerical instabilities.

Viscous fluxes and both inviscid and viscous scalar transport fluxes are calculated only for the “internal mode” (outer) loop.

Mode splitting can be disabled for 2D simulations and this configuration can be more computationally efficient for fast, shallow flow scenarios where the “internal mode” and “external mode” timesteps are similarly restrictive.

Currently, 3D simulations are only supported with mode splitting enabled.

4.4 Flux Terms

A key step in the Finite-Volume numerical scheme is the calculation of numerical fluxes across cell boundaries:

- inviscid fluxes ($\mathbf{F}_x^I, \mathbf{F}_y^I, \mathbf{F}_z^I$) represent the directly resolved flux of mass and momentum between adjacent cells
- viscous fluxes ($\mathbf{F}_x^V, \mathbf{F}_y^V, \mathbf{F}_z^V$) represent the “mixing” of mass and momentum that is not directly resolved as advection within the numerical model

4.4.1 Viscous Fluxes

Viscous flux terms are calculated using the traditional gradient-diffusion model with a variety of options available for the calculation of eddy-viscosity and scalar diffusivity.

4.4.1.1 Horizontal viscous fluxes

The horizontal viscous fluxes ($\mathbf{F}_x^V, \mathbf{F}_y^V$) are calculated according to Equations 5 and 8. The horizontal eddy-viscosity can be specified directly or can be calculated from the Smagorinsky formulation below.

$$K_v = c_s^2 l_s^2 \sqrt{\left(\frac{\partial u}{\partial x}\right)^2 + \left(\frac{\partial v}{\partial y}\right)^2 + \frac{1}{2} \left(\frac{\partial u}{\partial y} + \frac{\partial v}{\partial x}\right)^2} \quad (11)$$

where c_s is the Smagorinsky coefficient and l_s is the Smagorinsky lengthscale which is related to the local mesh size.

The horizontal scalar-diffusivity tensor can also be specified directly (as an isotropic constant value) or can be calculated from a Smagorinsky formulation (Eq. 11) or from the “Elder” formulation below (Falconer et al., 2005). The Elder model calculates a non-isotropic diffusivity tensor that accounts for velocity dispersion processes not resolved in 2D depth-averaged models.

$$\begin{aligned} \mathbf{D}_{xx} &= (D_l u^2 + D_t v^2) h / u_* \\ \mathbf{D}_{yy} &= (D_l v^2 + D_t u^2) h / u_* \\ \mathbf{D}_{xy} = \mathbf{D}_{yx} &= (D_l - D_t) u v h / u_* \end{aligned} \quad (12)$$

and D_l, D_t are the Elder coefficients in the directions lateral to the local current and transverse to the local currents respectively and $u_* (= \sqrt{|\mathbf{t}_b|/\rho})$ is the friction velocity. The observed range of values for D_l, D_t derived from measurements are discussed in Fisher et al., 1979.

In 3D model simulations the Smagorinsky formulation is generally more applicable.

4.4.1.2 Vertical viscous fluxes

The vertical viscous fluxes \mathbf{F}_z^V are calculated according to Equations 5 and 8. An unconditionally stable semi-implicit scheme is adopted in the discretisation of \mathbf{F}_z^V in order to avoid these terms imposing restrictions on the model timestep.

The vertical eddy viscosity, v_t , can be directly specified or may be calculated from the simple parametric model formulation including Munk & Anderson (1948) stability function:

$$v_{t0} = \kappa u_* z \left(c_1 - c_2 \frac{z}{h} \right) \quad (13)$$

$$v_t = \sqrt{1 + 10 \cdot Ri} v_{t0} \quad (14)$$

where Ri is the gradient Richardson number defined as,

$$Ri = \frac{N^2}{(\partial u / \partial z)^2} \quad (15)$$

And N is the Brunt-Vaisala frequency (or buoyancy frequency)

$$N = \sqrt{-\frac{g}{\rho} \frac{\partial \rho}{\partial z}} \quad (16)$$

The scalar diffusivities, ν'_t , may also be directly specified or it may be calculated using the parametric model formulations below, which vary depending on scalar type:

Passive tracers:

$$\nu'_t = \nu_t$$

Temperature and salinity

$$\nu'_t = \begin{cases} \frac{1}{\sigma} \nu_t (1 + 3.33Ri)^{-1.5} & Ri > 0 \\ \frac{1}{\sigma} \nu_t & Ri \leq 0 \end{cases} \quad (17)$$

Sediment fractions

$$\nu'_t = \beta \nu_t$$

Where σ is the neutral turbulent Prandtl number and β is the sediment mixing coefficient.

4.4.2 Inviscid Fluxes

Inviscid fluxes ($\mathbf{F}_x^I, \mathbf{F}_y^I, \mathbf{F}_z^I$) represent the directly resolved flux of mass and momentum between adjacent cells.

Inviscid fluxes are calculated for each cell-face based upon the conserved variable state immediately on either side of the cell-face.

For the first-order spatial scheme these values are equivalent to the adjacent-cell-averages, whereas the higher-order schemes will have reconstructed the conserved variable state at the cell-faces from the cell-averages.

4.4.2.1 Internal Mode

The “internal mode” inviscid flux calculations solve the full 3D NLSWE, excluding the terms related to the free-surface pressure gradient. A centred scheme is used to evaluate the internal mode mass flux while an upwind scheme is used for the momentum flux terms. “Flux-like” source terms originating due to bed slope and from the baroclinic pressure gradients are included in the cell-face flux calculation rather than included in the volume-integrated source term in Equation 10 .

The stable internal mode timestep is dictated by internal advection CFL constraints in combination with viscous flux Peclet constraints. A stable internal mode timestep is selected prior to entering the external mode.

4.4.2.2 External Mode

The “external mode” inviscid flux calculations solve the 2D depth-averaged NLSWE. For 3D simulations, the external mode is initiated by calculating depth-averages of the 3D conserved variable fields. Viscous fluxes and baroclinic pressure gradients are also depth-integrated at the start of the external mode loop.

The 2D depth-averaged NLSWE are solved using Roe’s approximate Riemann solver (Roe, 1981). “Flux-like” source terms originating due to bed slope and from the depth-averaged baroclinic pressure gradients are included in the cell-face flux calculation rather than included in the volume-integrated source term in Equation 10 (refer Section 4.7).

The stable external mode timestep is dictated by the surface gravity wave CFL constraint in combination with the depth-averaged viscous flux Peclet constraints (Murillo et al., 2005). A stable external mode timestep is selected at each external mode sub-timestep. Within the external mode loop, multiple sub-timesteps are executed prior to returning to the outer “internal mode” loop.

4.4.2.3 Flux Correction

The “internal mode” inviscid fluxes are corrected using the depth-averaged “external mode” fluxes that have been integrated in time through the external mode loop.

When mode splitting is optionally disabled, the complete NLSWE (including free-surface pressure gradients) are solved directly using the same NLSWE flux scheme described for the External Mode calculation. This option is currently only available for 2D model simulations, and can be more computationally efficient than the mode split scheme for pure hydrodynamic simulations of relatively fast shallow flows.

4.4.2.4 Scalar Inviscid Fluxes

Scalar inviscid fluxes are calculated from the product of the “corrected” mass flux and the upwind cell-face concentration. Knowing the “corrected” horizontal inviscid fluxes the vertical inviscid fluxes are simply calculated from the continuity equation.

4.4.3 Total Flux

The total flux vector is simply the sum of the corrected inviscid and viscous flux components.

4.4.4 Flux Spatial Integration

The first term on the RHS of Equation 10 requires calculating the boundary-integral of the total flux vector normal component and is approximated using a simple midpoint quadrature rule.

The momentum flux terms are first converted to a momentum flux difference prior to the integration step. In the case of spherical coordinates the momentum and flux vectors are shifted from a face-centred to cell-centred basis by applying a “parallel transport” transformation. This accounts for rotation of the spherical coordinates vector basis during translation on the sphere (Rossmanith, 2004).

4.5 Time integration

Both internal mode and external mode temporal integration is performed with an explicit Euler scheme. Accordingly a stable time step must be bounded by the Courant-Friedrich-Levy (CFL) criterion for the wave propagation and advective terms and by the Peclet criterion for the diffusive terms (Murillo et al., 2005).

The external mode CFL criterion is given by:

$$\frac{|\mathbf{u} \cdot \mathbf{n} \pm \sqrt{gh}| \Delta t}{L^*} \leq 1 \quad (18)$$

where Δt is the integration timestep and L^* is a cell-size dependent length scale.

The internal mode CFL criterion is given by:

$$\frac{\max(|\mathbf{u} \cdot \mathbf{n}|, c_{baro}) \Delta t}{L^*} \leq 1 \quad (19)$$

where c_{baro} is the baroclinic (internal) wave speed.

The Peclet criterion is given by:

$$\frac{|\mathbf{D} \cdot \mathbf{n}| \Delta t}{L^*} \leq 1 \quad (20)$$

In the above stability criterion relationships the cell-size dependent length-scale L^* is calculated for each cell-face as:

$$L^* = \frac{\min(A_i A_j)}{L_k} \quad (21)$$

where A_i, A_j are the adjacent cell-areas and L_k is the face length.

A variable time step scheme is implemented to ensure that the CFL and Peclet criterion are satisfied at all points in the model with the largest possible time step. Outputs providing information relating to performance of the model with respect to the CFL criterion are provided to enable informed refinement of the model mesh in accordance with the constraints of computational time (refer TUFLOW FV user manual for details).

In stratified flows the baroclinic wave speed may impose a constraint on the stable internal mode timestep as shown in Eq. 19. However, the FV internal mode timestep is not automatically adjusted to satisfy the baroclinic wave speed limit. Additionally the mode splitting scheme stability may benefit from limiting the ratio between the internal and external mode timestep to around 10 or less.

Maximum and minimum timestep limits are specified by the user. The maximum limit should be used to limit the upper internal mode timestep. The minimum limit should be used to restrict the external mode timestep in the event of a model instability, as it is preferable to have the model violate the prescribed stability bounds than have the timestep decrease towards zero.

4.6 Wetting/Drying

In very shallow regions (~ 0.05 m depth), the momentum terms are dropped, in order to maintain stability as the NLSWE approach the zero-depth singularity. Mass conservation is maintained both locally and globally to the limit of numerical precision across the entire numerical domain, including wetting and drying fronts. A conservative mass re-distribution scheme is used to ensure that negative depths are avoided at numerically challenging wetting and drying fronts without recourse to adjusting the time step (Brufau et al., 2004; Murillo, 2006). Regions of the model domain that are effectively dry are readily dropped from the computations.

4.7 Source terms

4.7.1 Bed slope

Bed slope integral source terms are calculated using a face-centred “upwind flux correction” within the internal and external mode numerical flux solvers.

$$\int_{\Omega} -gh\nabla \mathbf{z}_b \partial\Omega \cong \sum_{k=1}^{N_k} \beta^*(\Delta z_b)_k L_k \quad (22)$$

That is the cell-face bed elevation jump (Δz_b) becomes a correction term $\beta^*(\Delta z_b)$ to the cell-face numerical flux terms. This numerical approach provides consistent upwinding between flux and bed-slope source terms. This is essential to obtaining the required numerical balance between these terms, at for instance the quiescent state equilibrium.

Further details are provided in the following references; Hubbard & Garcia-Navarro, 2000; Murillo, 2006.

4.7.2 Coriolis

Coriolis forces due to the earth’s rotation are calculated as cell-averaged source terms in the momentum equation. The coriolis coefficient f_c is calculated from:

$$f_c = 2\Omega_r \phi \quad (23)$$

where Ω_r is the angular frequency of the earth’s rotation (rad/s) and ϕ is the geographic latitude (radians).

For Cartesian coordinate system models the latitude is specified as a domain constant value. In spherical coordinate models the latitude is obtained locally from the y-coordinate value.

4.7.3 Wind Stress

The cell-averaged surface stress vector due to wind is calculated from

$$\boldsymbol{\tau}_{sw} = \rho_a c_{dw} \mathbf{u}_w |\mathbf{u}_w| \quad (24)$$

where the wind drag coefficient is calculated using the empirical formula of Wu (1980; 1982)

$$c_{dw} = \begin{cases} c_a & w_{10} < w_a \\ c_a + \frac{c_b - c_a}{w_b - w_a} (w_{10} - w_a) & w_a \leq w_{10} < w_b \\ c_b & w_{10} \geq w_b \end{cases} \quad (25)$$

With default parameters (w_a ; c_a ; w_b ; c_b) = (0.0; 0.8e-3; 50.0; 4.05e-03).

4.7.4 Bed Friction

Bed friction momentum sink terms are calculated using a quadratic drag law.

$$\boldsymbol{\tau}_{bf} = \rho c_{db} \mathbf{u} |\mathbf{u}| \quad (26)$$

where the bottom drag coefficient can be calculated using a roughness-length relationship:

$$c_{db} = \left(\frac{\kappa}{\ln(30.z'/k_s)} \right)^2 \quad (27)$$

The above relationship is based on the assumption of a rough-turbulent logarithmic velocity profile in the lowest model layer, where κ is von Karman's constant, k_s is the effective bed roughness length (equivalent Nikuradse roughness) and z' is the height of the bottom cell-centroid above the seabed.

Instead of specifying k_s a Manning's n roughness can be specified and is internally converted into an equivalent roughness length:

$$k_s = 15.h \exp\left(-\frac{\kappa h^{1/6}}{\sqrt{g}n}\right) \quad (28)$$

Bed roughness values (k_s : or Manning's n) may be specified globally or for “material” types as defined in the mesh geometry file.

The above bed friction formulations are generally applicable in both 2D (depth-averaged) and 3D configurations. In 2D situations the Manning's n formulation (Eqs. 27and 28) is equivalent to the following equation for the friction slope (Chow, 1959).

$$S_f = \frac{\tau_{bf}}{\rho gh} = \frac{n^2 \bar{u} |\bar{u}|}{h^{4/3}} \quad (29)$$

It should be noted that given the same bed-roughness parameters calculated bed friction energy losses are typically not exactly equivalent for 2D and 3D simulations except in the simplest fully-developed, uniform flow scenarios. This is because the 2D models “assume” a logarithmic velocity profile extending over full-depth, whereas 3D simulations resolve the vertical velocity profile,which may be non-logarithmic in complex flow situations.

Integrated bed friction source terms are calculated using a semi-implicit discretisation in order to maintain unconditional numerical stability of these terms in high-velocity or shallow flows (Brufau et al, 2004). Coupling of the internal/external modes is achieved by applying the internal mode (3D) bed friction as an explicit momentum sink/source term during external mode (2D) loop calculations.

4.7.5 Surface Friction

Surface friction (e.g. from ice or pontoon structures) can be applied using a quadratic drag law analogous to Equation 26.

Only a roughness length input (k_s) is supported for surface friction specification. It should be noted that the surface friction terms are calculated explicitly and therefore do not exhibit the same unconditional stability property as the bed friction terms. In some circumstances these terms may generate numerical instabilities in high-velocity or shallow flows, which can be treated with a timestep reduction.

Surface roughness values may be specified globally or for “material” types as defined in the mesh geometry file.

4.7.6 Mean Sea Level and Baroclinic Pressure Gradients

Mean Sea Level Pressure and Baroclinic pressure gradient source terms are calculated as a face-centred flux correction terms within the internal and external mode numerical flux solvers. That is the pressure gradient terms are treated in a similar manner to the bed slope source terms as described in Section 4.7.1, i.e.

$$\int_{\Omega} -(\nabla P) \partial \Omega \cong \sum_{k=1}^{N_k} \eta^* (\Delta P)_k L_k \quad (30)$$

where ∇P is the gradient of the combined atmospheric and baroclinic pressure fields and η^* is a face-centred flux correction due to the cell-face pressure jump ΔP . This is analogous to converting the cell-volume source term integral into a cell-boundary source term integral using Gauss' theorem.

4.7.7 Wave radiation stress

Wave fields are applied as spatially and temporally varying datasets on a 2D rectilinear/curvilinear grid. The wave field boundary condition data is specified in a netcdf file and applied to the TUFLOW FV model as described in the user manual.

Wave radiation stress gradients are calculated as cell-centred source terms:

$$\int_{\Omega} \left(\frac{\partial s_{xx}}{\partial x} + \frac{\partial s_{xy}}{\partial y} \right) \partial \Omega \quad (31)$$

or as face-centred momentum flux source terms.

The wave radiation stress gradients are currently distributed uniformly throughout the water column. More advanced options will be implemented in future release/s of the software.

4.7.8 Scalar Decay

Tracer constituents can be specified with a linear scalar decay property (Equation 9), where K_d is the constant linear decay coefficient. Scalar decay is discretised explicitly as a cell-centred integral source term.

Numerical stability of this term is not guaranteed for large K_d or for large model timesteps.

4.7.9 Scalar (Sediment) Settling

Tracer and sediment constituents can be specified with a settling velocity w_s (Equation 9).

Within the water column, the settling velocity contributes an additional (vertically downward) inviscid flux component. At the seabed the settling velocity contributes a sink from the water column and source into the bed. In the case of sediment fractions the mass transferred to the bed is subsequently tracked within the TUFLOW FV sediment module. The passive tracer constituent mass exiting the water column is no longer tracked.

4.7.10 Other Sources/Sinks

Inflows/outflows into/from model domain can be specified as boundary conditions to the model. These boundaries typically require specification of the volumetric flow rate (inflow = +ve, outflow = -ve) and associated scalar concentrations.

In the case of an outflow specification, either the internal domain concentration (at the extraction location) can be applied (this is the default) or alternatively the outflow concentration can be directly specified. The latter approach might be used to simulate evaporation from the water column, where there is no scalar mass loss corresponding to the volumetric loss, i.e. the outflow concentration for the scalar constituents is zero. Another option, where there is no volumetric source, is to directly specify the scalar mass fluxes.

The spatial definition of source/sink boundary conditions, includes the following options as described in the user manual:

- Global (spatially constant and variable) source/sinks
- Point source/sinks
- Moving point source/sinks

The vertical distribution of the source/sink terms can be specified as part of the boundary condition definition. A detailed description of the available source/sink boundary condition options is provided in the TUFLOW FV user manual.

The TUFLOW FV sediment module calculates the sediment settling/mixing parameters and bed-pickup sink/source terms required as inputs and boundary conditions to the suspended sediment advection/dispersion calculations. Additionally this module can calculate bed load transport and bed-elevation update in response to sediment transport gradients.

The TUFLOW FV atmospheric module calculates the transfer of mass/heat/momentun between the water column and the atmosphere.

4.8 Timestep Algorithm

The timestep algorithm within TUFLOW FV is summarised in the following flowchart.

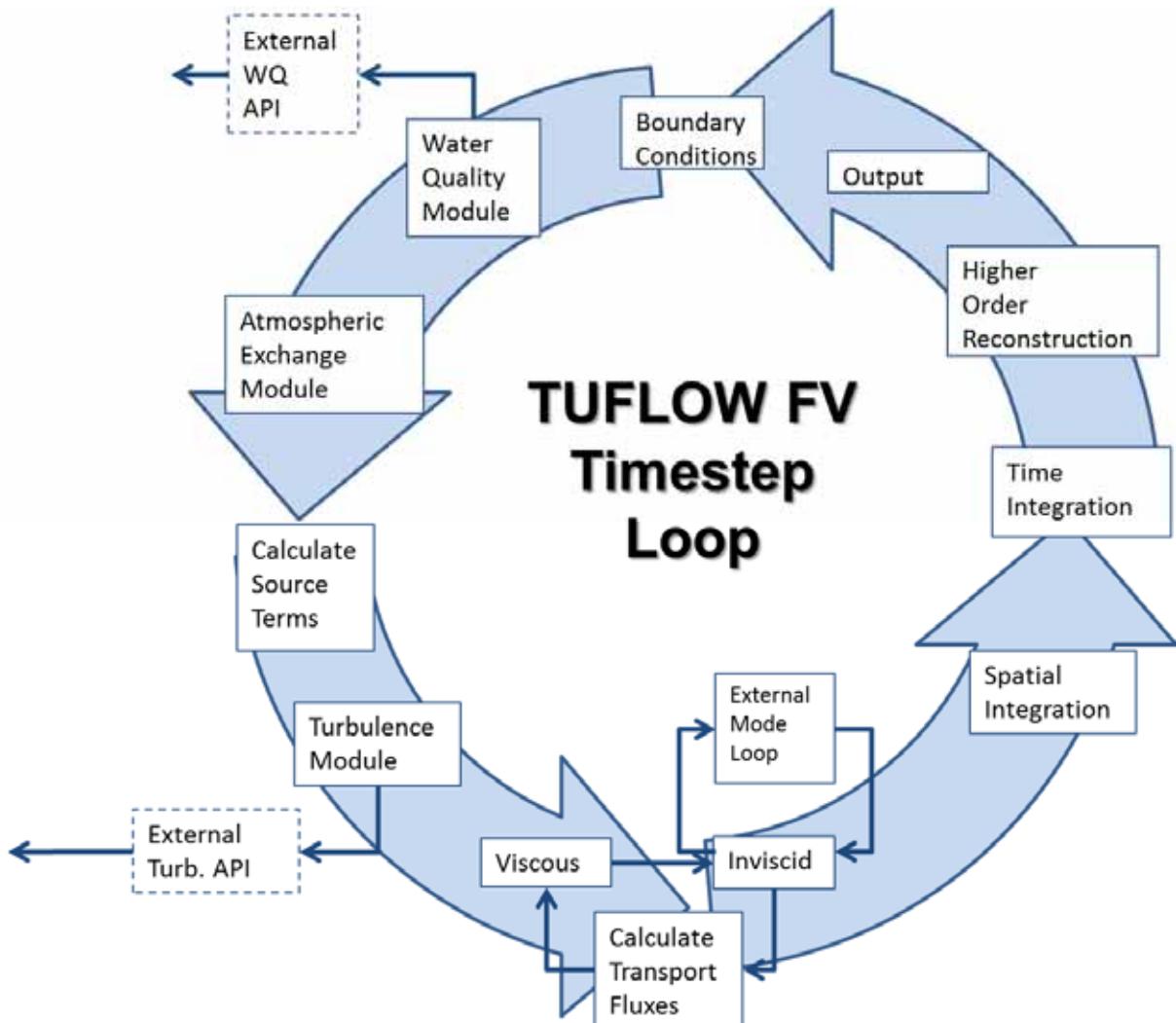


Figure 1 TUFLOW FV timestep loop illustration (further details outlined in Table 2)

Table 2 TUFLOW FV timestep algorithm

<ul style="list-style-type: none"> • Write output • Update Boundary Condition data • Do Water Quality calculations • Do Sediment Transport calculations • Do atmospheric exchange calculations • Reset source terms • Update cell-centred boundary conditions • Update structure flows • Calculate horizontal and vertical turbulent viscosities & diffusivities • Calculate density • Calculate cell-face pressure differences (due to MSLP and baroclinic gradients) • Calculate internal mode inviscid fluxes • Calculate viscous fluxes • Calculate cell-centred source terms • Determine internal mode timestep 	
<ul style="list-style-type: none"> • Enter external mode loop, initialising external mode variables 	
	<ul style="list-style-type: none"> • Calculate external inviscid flux • Determine external mode timestep • Integrate the external inviscid flux wrt time • Calculate total external mode • Spatially integrate external mode fluxes • Perform conservative mass redistribution • Perform time integration • Update external mode sub-timestep • Apply ghost-cell boundary conditions • Calculate primitive variables • Update nodal values • Calculate face-centred gradients • Higher order scheme reconstruction (if required) • Update cell-face values • Update wet/dry flags
<ul style="list-style-type: none"> • Exit external mode loop and perform internal mode flux corrections 	
<ul style="list-style-type: none"> • Calculate horizontal scalar inviscid fluxes • Calculate total horizontal fluxes • Spatially integrate horizontal fluxes • Calculate depth change (time integrate depth-averaged continuity equation) • Calculate vertical fluxes (inviscid and viscous) • Perform time integration • Update timestep • Apply ghost-cell boundary conditions • Calculate primitive variables • Update nodal values • Calculate face-centred gradients • Higher order scheme reconstruction (if required) • Update cell-face values • Update wet/dry flags • Check model bounds 	

5 References

- Batten, P., C. Lambert and D.M. Causon, 1996. Positively Conservative High-Resolution Convection Schemes for Unstructured Elements. International Journal for Numerical Methods in Engineering; 39, 1821-1838.
- Brufau, P., Garcia-Navarro, P. and Vazquez-Cendon, M.E., 2004. Zero mass error using unsteady wetting–drying conditions in shallow flows over dry irregular topography. International Journal for Numerical Methods in Fluids; 45, 1047-1082.
- Chow, V.T., 1959. Open Channel Hydraulics. MacGraw-Hill Book Company Incorporation: New York.
- Falconer, R.A., B. Lin and S.M. Kashefipour, 2005. Modelling water quality processes in estuaries; published in Computational Fluid Dynamics: Applications in Environmental Hydraulics. John Wiley & Sons.
- Fisher, H.B., E.J. List, R.C.Y. Koh, J. Imberger and N.H. Brooks, 1979. Mixing in Inland and Coastal Waterways. Academic Press.
- Fringer, O.B., S.W. Armfield and R.L. Street, 2005. Reducing numerical diffusion in interfacial gravity wave simulations. International Journal for Numerical Methods in Fluids; 49, 301-329.
- Hubbard, M.E., 1999. Multidimensional Slope Limiters for MUSCL-Type Finite Volume Schemes on Unstructured Grids. Journal of Computational Physics, 155, 54–74.
- Hubbard, M.E. and P. Garcia-Navarro, 2000. Flux Difference Splitting and the Balancing of Source Terms and Flux Gradients. Journal of Computational Physics; 165, 89–125.
- Leveque, R.J., 2002. Finite Volume Methods for Hyperbolic Problems. Cambridge University Press.
- Munk, W. H., and E. R. Anderson, 1948. Notes on the theory of the thermocline,. *Journal of Marine Research*, 3, 276-295.
- Murillo, J., J. Burguete, P. Brufau¶ and P. Garcia-Navarro, 2005. Coupling between shallow water and solute flow equations: analysis and management of source terms in 2D. International Journal for Numerical Methods in Fluids; 49, 267-299.
- Murillo, J., P. Garcia-Navarro, J. Burguete and P. Brufau, 2006. A conservative 2D model of inundation flow with solute transport over dry bed. International Journal for Numerical Methods in Fluids; 52, 1059–1092.
- Roe, P.L., Approximate Riemann solvers, parameter vectors and difference schemes. Journal of Computational Physics, 43, 357-372.
- Rossmanith, J.A. D.S. Bale, R.J. LeVeque, 2004. A wave propagation algorithm for hyperbolic systems on curved manifolds. Journal of Computational Physics; 199, 631-662.
- Shchepetkin, A. F. and J. C. McWilliams, 2005. The regional oceanic modeling system (ROMS): a split-explicit, free-surface, topography-following-coordinate oceanic model. Ocean Modelling 9 (4), 347-404.
- Wu, J., 1980. Wind-stress coefficients over sea surface and near neutral conditions – A revisit. Journal of Physical Oceanography, 10, 727-740.

- Wu, J., 1982. Wind-stress coefficients over sea surface from breeze to hurricane. Journal of Geophysical Research; 87, C12, 9704-9706.

Appendix K AED Aquatic Ecodynamics Model Overview

Oct 2013

Aquatic Ecodynamics (AED) Model Library

Science Manual

DRAFT v4 (Oct 2013)

M.R. Hipsey, L.C. Bruce & D.P. Hamilton



THE UNIVERSITY OF
WESTERN AUSTRALIA
Achieve International Excellence



Summary

This report outlines the Aquatic Ecodynamics (AED) modelling library - an open-source community-driven library of model components for simulation of “aquatic ecodynamics”. The model has been developed researchers at UWA to plug into the FABM framework, or alternatively the library components can also be called directly from other software applications. The model can therefore be used in a wide range of spatial contexts – including with 0D, 1D, 2D and 3D models that are able to simulate the aquatic environment.

In particular the AED library consists of numerous modules that are designed as individual model ‘components’ able to be configured in a way that facilitates custom aquatic ecosystem conceptualisations – either simple or complex. These may be relevant to specific water quality problems or aquatic ecosystem investigations. Users select water quality and ecosystem variables they wish to simulate and then are able to customize connections and dependencies with other modules, thereby constructing relevant interactions and feedbacks that may be occurring within an aquatic system. The code also allows for easy customisation at an algorithm level how model components operate (e.g. photosynthesis functions, sorption algorithms etc.). In general, model components consider the cycling of carbon, nitrogen and phosphorus, and other relevant components such as oxygen, and are able to simulate organisms including different functional groups of phytoplankton and zooplankton, and also organic matter. Modules to support simulation of water column and sediment geochemistry, including coupled kinetic-equilibria interactions, are also included.

This document summarises the mathematical basis for the balance equations and interactions between the modules. In addition a summary of parameter values for lake, river and estuary environments are also summarized from a range of sources.

Contents

SUMMARY	2
CONTENTS	3
<u>AQUATIC ECODYNAMICS (AED) MODEL APPROACH</u>	4
OVERVIEW	4
THE FRAMEWORK FOR AQUATIC BIOGEOCHEMICAL MODELS (FABM)	4
Available hydrodynamic driver platforms	6
Other candidate biogeochemical models	7
Further information on FABM	7
<u>AED MODULE DESCRIPTIONS</u>	8
OVERVIEW	8
MODULE CONCEPTUALIZATION	8
MODULE DESCRIPTIONS	10
General Notation	10
Light	10
Dissolved Oxygen	11
Carbon, Nitrogen, Phosphorus and Silica: aed_carbon, aed_nitrogen, aed_phosphorus, aed_silica, aed_organic_matter	12
Phytoplankton Dynamics – aed_phytoplankton	19
Zooplankton Dynamics – aed_zooplankton	24
Suspended Sediment & Turbidity : aed_tracer, aed_totals	25
Geochemical Dynamics : aed_geochemistry, aed_iron, aed_sulfur	25
Sediment Biogeochemistry – aed_sedflux, aed_seddiagenesis	25
Pathogens – aed_pathogens	25
PARAMETER SUMMARY	25
<u>CONFIGURING THE AED LIBRARY</u>	30
<u>REFERENCES</u>	32

Aquatic Ecodynamics (AED) Model Approach

Overview

This document outlines the **Aquatic Ecodynamics (AED) modelling library** - an open-source community-driven library of model components for simulation of “*aquatic ecodynamics*”, referring to water quality and general aquatic ecosystem dynamics. The model library has been primarily designed as a plugin to the FABM framework, described below, or alternatively the library objects and functions can also be called directly from other software applications.

Modern analyses of aquatic environments requires flexibility to join a range of coupled models of hydrodynamics/hydrology, biogeochemistry and aquatic ecology, however many model frameworks make this difficult due to rigid model structures. A major barrier identified is the simple practical aspect that there are lots of models and model approaches, but limited open-source codes and standards that bind the community or facilitate integration (Mooij et al., 2010; Trolle et al., 2012), and there has been limited comparisons of the most suitable types of models structures for different applications. There has also been *difficulty in linking between biogeochemical models of diverse aquatic systems* in real world complex landscapes. There is therefore a need for model systems that can cover a range of spatial dimensionality and system integration and frameworks that can use a diverse array of physical drivers (e.g., wetland/floodplain model, river model, lake model, estuary model) to couple with biogeochemical and/or ecological ‘components’ (e.g., see Figure 1).

The general philosophy of the AED library has been to create a software tool-kit that is easily customisable, fast to develop, accessible to non-developers, and contains a large range of options for different process parameterisations. In doing so, the aims is to create a widely-used code-base that evolves to include a diverse range of approaches to the simulation of a diverse range of aquatic applications. Through the FABM framework or custom model interfaces the library can be used to innovate a variety of model conceptualisations and link to numerous physical models.

In particular it has been used for numerous inland water applications, both lotic and lentic systems with numerous applications to lake, river and estuarine systems.

The Framework for Aquatic Biogeochemical Models (FABM)

The *Framework for Aquatic Biogeochemical Models* (FABM) is a relatively new code-base designed to facilitate the simulation of aquatic biogeochemical and ecological dynamics. It has been developed as an alternative to existing rigid water quality modelling approaches as much present-day software does not address the challenges faced in model coupling and a recognized need to develop improved standards and flexibility in model integration in concert with an active development community (Trolle et al., 2012). The basic framework has been developed by Dr. Jorn Bruggeman and colleagues under the EU7 project “Marine Ecosystem Evolution in a Changing Environment” (MEECE), and readers are referred to Bruggeman (2011) for further background.

FABM itself is not a water quality model, but rather it is a code framework (“API”) that facilitates integration of different biogeochemical/ecological model approaches and to enable coupling of these with a diverse array of physical (hydrodynamic) driver models. Therefore, its intention is not to be a

sophisticated “model of everything”, but users can configure it to be as simple or as complicated as desired. It supports numerous biogeochemical and ecological models from various developers with different approaches and varied applications.

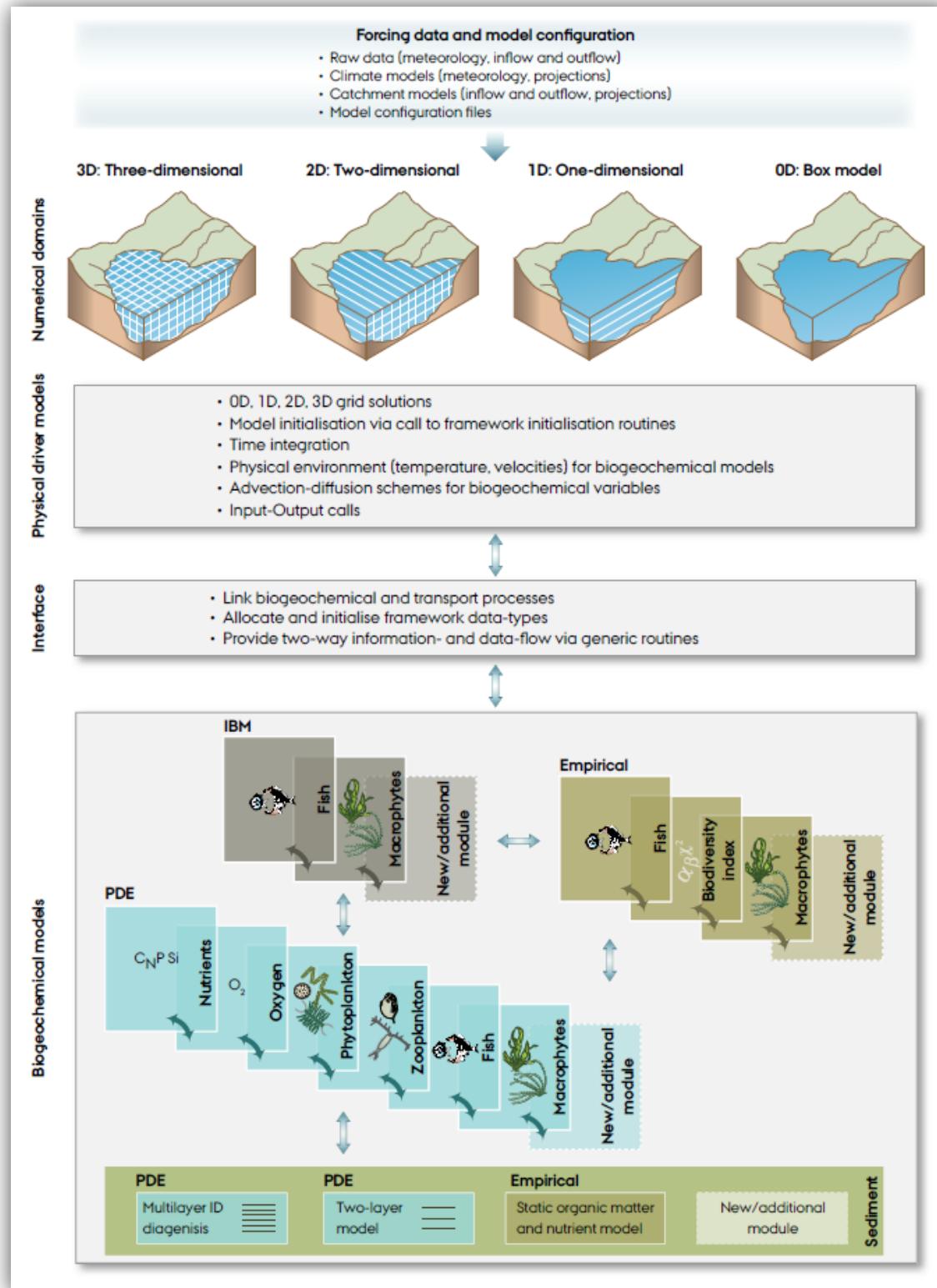


Figure 1: Schematic representation of coupling and biogeochemical modelling approach
(taken from Trolle et al., 2012).

Available hydrodynamic driver platforms

The underlying framework allows a flexible coupling interface to hydrodynamic models, and at its core it consists of a thin layer of code designed to manage communication and data exchange, through programming interfaces which a physical host (hydrodynamic model) and any number biogeochemical models pass information. It has been applied across numerous types of aquatic systems ranging from the global ocean via its coupling to MOM4 and GOTM, to estuaries and coasts via its coupling to the model GETM, and to lakes and reservoirs via its coupling to the 1D lake model GLM.

The model adopts a standard interface so that the code itself can be coupled with other forms of hydrodynamic models, or it can be run in isolation (0D) for hypothesis testing and ecological model prototyping. The advantage of the FABM approach over other platforms is its flexibility for coupling a diverse array of model approaches and its support for rigorous numerical solution schemes (e.g., Burchard *et al.*, 2005; Broekhuizen *et al.*, 2008) that are known to be important in achieving accurate solutions of complex biogeochemical model equation sets. Its code structure is also designed to be work well when used with parallel processors.

Users who can couple their hydrodynamic model with FABM - see instructions here: http://sourceforge.net/apps/mediawiki/fabm/index.php?title=Coupling_FABM_to_a_new_physical_model - can access the AED library in addition to numerous other models currently implemented as outlined next.

Table 1: Current physical driver models linked to FABM (also refer to <http://sourceforge.net/apps/mediawiki/fabm/index.php>).

Name	Dimensionality	Stratification	Comments
0D Driver	0D	-	Simple 'box' model for testing biogeochemical model operation
General Ocean Turbulence Model (GOTM)	1D	Library of range of simple and complex mixing approaches	Widely used library of vertical mixing algorithms http://www.gotm.net
General Estuarine Transport Model (GETM)	3D structured grid, with curvilinear option	Uses GOTM turbulence library	Open-source coastal/estuarine model http://www.getm.eu
Modular Ocean Model version 4 (MOM4)	3D		Widely used global ocean model http://www.gfdl.noaa.gov/fms
General Lake Model (GLM)	1D (vertical) – Lagrangian layered grid	Custom vertical mixing algorithms	Includes Ice cover Simple to use http://aed.see.uwa.edu.au/research/models/GLM/
TUFLOW-FV	3D (finite volume)	Several approaches available	Coupled model has been applied (Bruce <i>et al.</i> , 2013), but currently not available for general use.

Other candidate biogeochemical models

The AED modules described here that link to FABM are in addition to other common biogeochemical configurations such as the ‘Fasham’ model template (currently the most highly cited aquatic biogeochemical model approach; Arhonditsis *et al.* 2006), ERSEM, and ERGOM, as well as simple ‘NPZD’ model templates (e.g. Burchard *et al.* 2006). The range of ecosystem models that are implemented within the FABM framework are summarised briefly in Table 2, and since the focus of this document is the AED models, readers are referred to FABM documentation and associated references for details of the other models.

Table 2: Current coupled aquatic biogeochemical models included within the FABM framework.

Name	Description
pml/ carbonate	Carbonate chemistry
pml/ ersem	European Regional Seas Ecosystem Model
metu/ mnemiopsis	population model for Mnemiopsis
gotm/ npzd	Simple NPZD model (Burchard <i>et al.</i> , 2005), ported from GOTM
gotm/ fasham	Fasham <i>et al.</i> (1990) model with modifications by, ported from GOTM
iow/ ergom	Baltic Sea Research Institute ecosystem model
examples/ benthic	Example of a benthic predator
aed/ ...	<i>Aquatic Ecodynamics Library (focus of this report, described in the next section)</i>
	Oxygen Nitrogen Phosphorus Silica Organic Matter Phytoplankton Zooplankton Sediment Diagenesis Geochemistry Pathogens

Further information on FABM

For more information on the code structure and approach of FABM the reader is referred to Bruggerman *et al.* (2011).

FABM documentation, code and test cases are currently available from a Git repository at SourceForge: <http://sourceforge.net/apps/mediawiki/fabm/index.php>.

The contents of this repository can be obtained on UNIX/Linux/Mac OS X systems by executing:

```
git clone git://fabm.git.sourceforge.net/gitroot/fabm/fabm
```

AED Module Descriptions

Overview

The philosophy of the AED modules is that individual model ‘components’ can be configured in a way that facilitates custom aquatic ecosystem configurations. Users select modules they are wishing to simulate and then are able to customize connections with other modules. The modules exist within a hierarchy of dependencies, and connections must be set in the right order.

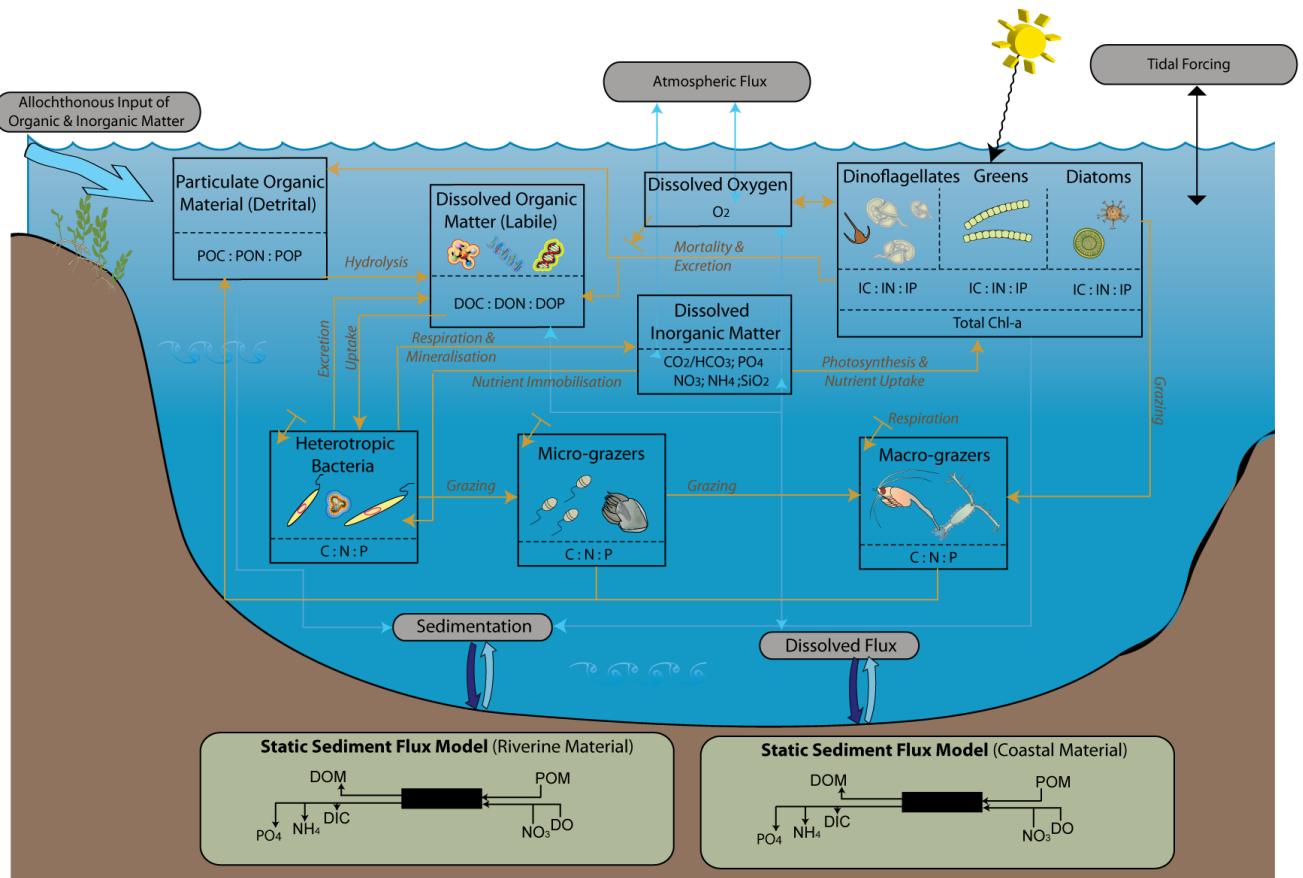
In general, model components consider the cycling of carbon, nitrogen and phosphorus, and other relevant components such as oxygen, and are able to simulate organisms including different functional groups of phytoplankton and zooplankton, and also organic matter. Much of the science basis and mathematical approach implemented in the AED modules is similar to similar models that have been used over the past two decades, and include many similarities to widely used approaches such as CAEDYM, CE-QUAL-W2, WASP and numerous others. The modules, however, are implemented within the FABM numerical framework and include numerous different process representations over these earlier studies, and are reported in detail below.

Module conceptualization

Whilst the AED modules are highly flexible and can be customised for user-defined biogeochemical and ecological configurations, they have generally been designed to simulate the interactions between nutrients, organic matter, phytoplankton and zooplankton. When coupled with the hydrodynamic driver, the modules allow for a comprehensive simulation of processes that govern the transport and fate of water quality attributes included suspended sediment, dissolved inorganic nutrients, organic matter (dissolved and particulate), phytoplankton and zooplankton, and relevant fluxes at the air-water and sediment-water interface. Given the flexible nature of model integration, multiple identical modules can be simulated allowing the user to further partition ecological components, for example, two organic matter modules can be enabled with unique parameters for each to reflect labile versus refractory material in a simulation. Similarly, multiple phytoplankton sub-modules can be configured allow for groups of functional types or groups of similar species to be configured. Other modules describing pathogens, and aqueous geochemistry may also be configured.

The modules together simulate the C, N, P, DO, and Si cycles including inorganic nutrient, organic matter, phytoplankton, and zooplankton. In a typical application (Figure 2) several phytoplankton groups (e.g., bacillariophytes / diatoms, D; chlorophytes or green algae, G; cyanobacteria or blue-green algae, B; etc.) would be simulated with zero or more zooplankton groups. Such a configuration would require around nine state variables are required to model the algal biomass (A_D , A_G , A_B) if the dynamically calculated internal nutrient stores of N (PHY_N_D , PHY_N_G , PHY_N_B) and P (PHY_P_D , PHY_P_G , PHY_P_B), and five dissolved inorganic nutrients (FRP, NO₃, NH₄, PIP, RSi), three dissolved (DOC, DON, DOP) and three particulate (POC, PON, POP) detrital organic matter groups, and dissolved oxygen (DO). With a two zooplankton groups configured this constitutes around 24 state variables, all of which are transported and subject to boundary forcing by the hydrodynamic driver.

A general summary of the key modules is included below and detailed equations and parameter descriptions and typical values used are presented in the following section.



Carbon & Nutrient Flux Pathways



Figure 2: AED module conceptual model of carbon and nutrient flux pathways and planktonic groups.

Module descriptions

In this section the detailed model mass balance and biogeochemical algorithms are described. These are not organized by AED modules, but rather based on the element or ecosystem component in line with the conceptual model.

Note that all balance equations in effect also have terms for advection, dispersion, turbulent mixing, and inflows and outflow boundary conditions, however these are highly specific to the particular hydrodynamic driver being used to run the AED or FABM-AED models. Due to potential differences between them, they are not included in the below expressions and the equations presented here solely focus on biogeochemical and ecological interactions. From a numerical perspective this is also consistent since AED processes are split from the numerical solution of the transport-reaction equations and solved sequentially after transport has taken place.

General Notation

N	= number of groups [integer]
a, om, z	= indices of various sub-groups of phytoplankton, organic matter and zooplankton [integer]
$\chi_{C:Y}^{group}$	= the stoichiometric ratio of “group” between C and element “ Y ” [mmol C/mmol Y]
$f_{process}^{var}$	= function that returns the mass flux of “ $process$ ” on “ var ” [mmol var/time]
$R_{process}^{var}$	= the rate of “ $process$ ” influencing the variable “ var ” [/time]
F_{max}^{var}	= the maximum benthic areal flux of variable “ var ” [mmol var/area/time]
p_{source}^{group}	= the preference of “ $group$ ” for “ $source$ ” [0-1]
$\Phi_{lim}^{group}(var)$	= dimensionless limitation or scaling function account for the effect of “ lim ” on “ $group$ ” [-]
k^{var}	= used to identify a generic fraction related to “ var ” [0-1]
Θ_{config}^{group}	= switch to configure selectable model component “ $config$ ” for a specific “ $group$ ” [0,1,2,...]
$c, \theta, \gamma \dots$	= coefficient [various units]

Light

Incident shortwave radiation is supplied by the hydrodynamic driver, where it is used for surface thermodynamics calculations, to FABM. For primary production, the shortwave (280-2800 nm) intensity at the surface is usually converted to the photosynthetically active component (PAR) based on the assumption that ~45% of the incident spectrum lies between 400-700 nm (eg. Jellison and Melack, 1993; Kirk, 1994). PAR penetrates into the water column according to the Beer-Lambert Law. The light extinction coefficient is able to be dynamically adjusted to account for variability in the concentrations of algal, inorganic and detrital particulates, and dissolved organic carbon levels based on user defined specific attenuation coefficients.

$$K_d = K_w + K_e SS + K_e DOC + K_e POC + \sum_a^{N_{PHY}} K_{e_a} PHY c_a$$

Dissolved Oxygen : aed_oxygen

DO dynamics account for atmospheric exchange, sediment oxygen demand, microbial use during organic matter mineralisation and nitrification, photosynthetic oxygen production and respiratory oxygen consumption, and respiration by other optional biotic components. Atmospheric exchange is based on the model of Wanninkhof (1992) and the flux equation of Riley and Skirrow (1974). A simple sediment oxygen demand flux is currently implemented that varies as a function of the overlying water temperature and dissolved oxygen levels. Microbial activity facilitates the breakdown of organic carbon (in particular, DOC) to CO₂, and a stoichiometrically equivalent amount of oxygen is removed. The process of nitrification also requires oxygen that is dependent on the stoichiometric factor for the ratio of oxygen to nitrogen and the half-saturation constant for the effect of oxygen limitation. Photosynthetic oxygen production and respiratory oxygen consumption is summed over the number of simulated phytoplankton groups.

Table 3: Mass balance and functions related to oxygen cycling.

<p><u>State variable mass balance equation:</u></p> $\frac{dO_2}{dt} = \pm f_{atm}^{O_2} - f_{sed}^{O_2} - \frac{f_{miner}^{DOC}}{\chi_{C:O_2}^{miner}} - \frac{f_{nitrif}}{\chi_{N:O_2}^{nitrif}} + \sum_a^{N_{PHY}} \left(\frac{f_{uptake}^{PHY-Ca}}{\chi_{C:O_2}^{PHY}} \right) - \sum_a^{N_{PHY}} \left(\frac{f_{resp}^{PHY-Ca}}{\chi_{C:O_2}^{PHY}} \right) - \sum_z^{N_{ZOO}} \left(\frac{f_{resp}^{ZOOz}}{\chi_{C:O_2}^{ZOO}} \right)$ <ul style="list-style-type: none"> = ± atmospheric O₂ exchange ± sediment O₂ demand <ul style="list-style-type: none"> - O₂ consumption by mineralisation of DOC (bacterial respiration) - O₂ consumption by nitrification + O₂ production by photosynthesis - O₂ consumption by phytoplankton respiration - O₂ consumption by zooplankton respiration 	
<p><u>Process parameterisations:</u></p> $f_{atm}^{O_2} = \begin{cases} \frac{c_{atm}^{O_2}([O_2]_{atm} - [O_2]_z)}{dz_s} & \text{if } z = z_s \\ 0 & \text{if } z \neq z_s \end{cases}$ <p style="text-align: right;">atmospheric oxygen exchange</p> $f_{sed}^{O_2} = F_{max}^{O_2} \frac{O_2}{K_{sed}^{O_2} + O_2} (\theta_{sed}^{O_2})^{T-20} \left(\frac{\widehat{A}_z}{dz_z} \right)$ <p style="text-align: right;">sediment oxygen demand (SOD)</p> <p>where $\widehat{A}_z = A_z^{ben}/A_z$ and dz_z is the thickness of the z^{th} layer/cell.</p>	
<p><u>Diagnostic & derived outputs:</u></p> <p>Oxygen saturation</p> <p><i>OXYPC</i> = ...</p>	

Carbon, Nitrogen, Phosphorus and Silica: aed_carbon, aed_nitrogen, aed_phosphorus, aed_silica, aed_organic_matter

Both the inorganic and organic, and dissolved and particulate forms of C, N and P are modelled explicitly along the degradation pathway of POM to DOM to dissolved inorganic matter (DIM). The decomposition and mineralisation process varies in response to temperature, and is additionally able to slow down under anaerobic conditions. The nitrogen cycle includes the additional processes of denitrification, nitrification and N₂ fixation (discussed in the phytoplankton section) that are not in the carbon and phosphorus cycles, though note N₂ levels are not tracked as a state variable. The phosphorus cycle also accounts for adsorption/desorption of PO₄ onto suspended solids (SS), and adopts the Langmuir isotherm model as implemented by Chao et al. (2010).

The silica cycle is simpler and includes the processes of biological uptake of dissolved Si (RSi) by diatoms into the internal Si (ISi) pool, dissolved sediment fluxes of RSi, diatom mortality directly into the RSi sediment pool, settling of ISi. This relatively simple representation assumes that diatom frustules rapidly mineralize.

Table 4: Mass balance and functions related to silica cycling.

<u>State variable mass balance equations:</u>	
$\frac{dRSi}{dt} = +f_{sed}^{RSi} - \sum_a^{N_{PHY}} f_{uptake}^{PHY-Si_a} + \sum_a^{N_{PHY}} f_{excr}^{PHY-Si_a}$	= ± sediment flux – uptake by phytoplankton groups – excretion by phytoplankton groups
<i>PHY_{Si}</i> is also included in the Si cycle and described in the phytoplankton module	
<u>Process parameterisations:</u>	
$f_{sed}^{O_2} = F_{max}^{O_2} \frac{O_2}{K_{sed}^{O_2} + O_2} \left(\theta_{sed}^{O_2} \right)^{T-20} \left(\frac{\widehat{A}_z}{dz_z} \right)$	sediment reactive Si flux
where $\widehat{A}_z = A_z^{ben} / A_z$ and dz_z is the thickness of the z^{th} layer/cell.	

Table 5: Mass balance and functions related to carbon cycling.

<u>State variable mass balance equations:</u>	
$\frac{dCH_4}{dt} = +f_{sed}^{CH_4} - f_{ox}^{CH_4}$	= ± sediment flux – oxidation to DIC
$\frac{dDIC}{dt} = f_{miner}^{DOC} + f_{sed}^{DIC} + \sum_a^{N_{PHY}} [f_{resp}^{PHY_{Ca}} - f_{uptake}^{PHY_{Ca}}] + \sum_z^{N_{ZOO}} f_{resp}^z$	= + respiration by bacteria during DOM breakdown ± sediment flux ± carbon fixation and respiration by phytoplankton groups + respiration by zooplankton groups
$\frac{dDOC}{dt} = f_{decom}^{POC} - f_{miner}^{DOC} + f_{sed}^{DOC} + \sum_a^{N_{PHY}} f_{excr}^{PHY_{Ca}} + \sum_z^{N_{ZOO}} f_{excr}^z$	= + decomposition from particulate detritus (POC) – mineralisation by bacteria ± sediment flux – excretion by phytoplankton groups – excretion by zooplankton groups
$\frac{dPOC}{dt} = -f_{decom}^{POC} - f_{sett}^{POC} + \sum_a^{N_{PHY}} f_{mort}^{PHY_{Ci}} + \sum_z^{N_{ZOO}} [(1 - k_{attm}^z) f_{attm}^z + (1 - k_{fsed}^z) f_{fecal}^z + f_{mort}^z]$	= – decomposition to DOC ± sedimentation + mortality from phytoplankton groups + messy feeding, faecal pellet release and mortality from zooplankton groups
<i>PHY_N</i> and <i>ZOO_N</i> are described in the phytoplankton and zooplankton sub-sections.	
<u>Process parameterisations:</u>	
$f_{sett}^{POC} = \frac{\omega_{POC}}{dz_z} [POC]$	sedimentation of particulate organic carbon
$f_{decom}^{POC} = R_{decom}^{POC} \frac{[O_2]}{K_{miner} + [O_2]} (\theta_{decom})^{T-20} [POC]$	hydrolysis/decomposition of POC
$f_{miner}^{DOC} = R_{miner}^{DOC} \frac{[O_2]}{K_{miner} + [O_2]} (\theta_{miner})^{T-20} [DOC]$	mineralisation of DOC
$f_{sed}^{DOC} = F_{max}^{DOC} \frac{K_{sed}^{DOC}}{K_{sed}^{DOC} + [DOC]} (\theta_{sed}^{DOC})^{T-20} \left(\frac{\widehat{A}_z}{dz_z} \right)$	DOC sediment flux
where $\widehat{A}_z = A_z^{ben}/A_z$ and dz_z is the thickness of the z^{th} layer/cell.	
<u>Diagnostic & derived outputs:</u>	
pH	$pH = -\log [H^+]$, where H^+ is determined based on the carbonate alkalinity (CA) and DIC concentrations.
Total Organic Carbon	

$$TOC = DOC + POC + \sum_a^{N_{PHY}} PHY_{Ca} + \sum_z^{N_{ZOO}} ZOO_z$$

note: if multiple POC/DOC pools are simulated then these can be included in TOC through the aed_totals routine.

Table 6: Mass balance and functions related to nitrogen cycling.

<u>State variable mass balance equations:</u>	
$\frac{dNH_4}{dt} = +f_{sed}^{NH_4} + f_{miner}^{DON} - f_{nitrif}^{NH_4} - \sum_a^{N_{PHY}} [p_{NH_4}^a \times f_{uptake}^{PHY-Na}]$	= ± sediment flux + mineralization from DON - nitrification - uptake from the phytoplankton community
$\frac{dNO_3}{dt} = -f_{sed}^{NO_3} + f_{nitrif}^{NH_4} - f_{denit}^{NO_3} - \sum_a^{N_{PHY}} [p_{NO_3}^a \times f_{uptake}^{PHY-Na}]$	= ± sediment flux + nitrification - denitrification - uptake from the phytoplankton community
$\frac{dDON}{dt} = +f_{decom}^{PON} + f_{sed}^{DON} - f_{miner}^{DON} + \sum_a^{N_{PHY}} f_{excr}^{PHY-Na} + \sum_z^{N_{ZOO}} \frac{f_{excr}^z}{\chi_{C:N}^z}$	= + decomposition from particulate detritus (POC) - mineralisation by bacteria ± sediment flux - excretion by phytoplankton groups - excretion by zooplankton groups
$\frac{dPON}{dt} = -f_{decom}^{PON} - f_{sett}^{PON} + \sum_i^{N_{PHY}} f_{mort}^{PHY-Na} + \sum_z^{N_{ZOO}} [(1 - k_{attm}^z) f_{attm}^z + (1 - k_{fsed}^z) f_{fecal}^z + f_{mort}^z] \frac{1}{\chi_{C:N}^z}$	= - decomposition to DOC ± sedimentation + mortality from phytoplankton groups + messy feeding, faecal pellet release and mortality from zooplankton groups
<i>PHY_N</i> and <i>ZOO_N</i> are described in the phytoplankton and zooplankton sub-sections.	
<u>Process parameterisations:</u>	
$f_{sed}^{NH_4} = F_{max}^{NH_4} \frac{K_{sed}^{NH_4}}{K_{sed}^{NH_4} + [O_2]} (\theta_{sed}^{NH_4})^{T-20} \left(\frac{\widehat{A}_z}{dz_z} \right)$	ammonium sediment flux
$f_{sed}^{NO_3} = F_{max}^{NO_3} \frac{[O_2]}{K_{sed}^{NO_3} + [O_2]} (\theta_{sed}^{NO_3})^{T-20} \left(\frac{\widehat{A}_z}{dz_z} \right)$	nitrate sediment flux
$f_{sed}^{DON} = F_{max}^{DON} \frac{K_{sed}^{DON}}{K_{sed}^{DON} + [DON]} (\theta_{sed}^{DON})^{T-20} \left(\frac{\widehat{A}_z}{dz_z} \right)$	DON sediment flux
$f_{sett}^{PON} = \frac{\omega_{PON}}{dz_z} [PON]$	sedimentation of particulate organic nitrogen
$f_{sett}^{PHY-Ni} = \frac{\omega_{PHY_i}}{dz_z} [PHY-Na]$	sedimentation of phytoplankton
$f_{decom}^{PON} = R_{decom}^{PON} \frac{[O_2]}{K_{miner} + [O_2]} (\theta_{decom})^{T-20} [PON]$	hydrolysis/decomposition of PON

$$f_{miner}^{DON} = R_{miner}^{DON} \frac{[O_2]}{K_{miner}+[O_2]} (\theta_{miner})^{T-20} [DON] \quad \text{mineralisation of DON}$$

$$f_{nitrif}^{NH_4} = R_{nitrif} \frac{[O_2]}{K_{nitrif}+[O_2]} (\theta_{nitrif})^{T-20} [NH_4] \quad \text{nitrification}$$

$$f_{denit}^{NO_3} = R_{denit} \frac{K_{denit}}{K_{denit}+[O_2]} (\theta_{denit})^{T-20} [NO_3] \quad \text{denitrification}$$

where $\widehat{A_z} = A_z^{ben}/A_z$ and dz_z is the thickness of the z^{th} layer/cell.

Diagnostic & derived outputs:

Total Nitrogen

$$TN = NO_3 + NH_4 + DON + PON + \sum_a^{N_{PHY}} PHY_{Na} + \sum_z^{N_{ZOO}} \frac{ZOO_z}{\chi_{C:N}^z}$$

Total Kjeldahl Nitrogen

$$TKN = NH_4 + DON + PON + \sum_a^{N_{PHY}} PHY_{Na} + \sum_z^{N_{ZOO}} \frac{ZOO_z}{\chi_{C:N}^z}$$

note: if multiple PON/DON pools are simulated then these can be included in TN through the aed_totals routine.

Table 7: Mass balance and functions related to phosphorus cycling.

<u>State variable mass balance equations:</u>	
$\frac{dPO_4}{dt} = +f_{sed}^{PO_4} + f_{miner}^{DON} \pm f_{ads}^{PO_4} - \sum_a^{N_{PHY}} [f_{uptake}^{PHY-Pa}]$	<ul style="list-style-type: none"> = ± sediment flux + mineralization from DOP ± adsorption/desorption - uptake from the phytoplankton community
$\frac{dPO_4^{ads}}{dt} = \pm f_{ads}^{PO_4} - f_{sett}^{PO_4^{atm}}$	<ul style="list-style-type: none"> = ± adsorption/desorption ± sedimentation
$\frac{dPOP}{dt} = -f_{decom}^{POP} - f_{sett}^{POP} + \sum_a^{N_{PHY}} f_{mort}^{PHY-Pa} + \sum_z^{N_{ZOO}} [(1 - k_{attm}^z) f_{attm}^z + (1 - k_{fsed}^z) f_{fecal}^z + f_{mort}^z] \frac{1}{\chi_{C:P}^z}$	<ul style="list-style-type: none"> = - decomposition to DOP ± sedimentation + mortality from phytoplankton groups + messy feeding, faecal pellet release and mortality from zooplankton groups
$\frac{dDOP}{dt} = f_{decom}^{POP} - f_{miner}^{DON} + f_{sed}^{DON} + \sum_a^{N_{PHY}} f_{excr}^{PHY-Pa} + \sum_z^{N_{ZOO}} 1/\chi_{C:P}^z f_{excr}^z$	<ul style="list-style-type: none"> = + decomposition from particulate detritus (POP) - mineralisation by bacteria ± sediment flux - excretion by phytoplankton groups - excretion by zooplankton groups
PHY _P and ZOO _P are described in the phytoplankton and zooplankton sub-sections.	
<u>Process parameterisations:</u>	
$f_{sed}^{PO_4} = F_{max}^{PO_4} \frac{K_{sed}^{PO_4}}{K_{sed}^{PO_4} + [O_2]} (\theta_{sed}^{PO_4})^{T-20} \left(\frac{\widehat{A}_z}{dz_z} \right)$	phosphate sediment flux
$f_{sed}^{DON} = F_{max}^{DON} \frac{K_{sed}^{DOP}}{K_{sed}^{DOP} + [DON]} (\theta_{sed}^{DON})^{T-20} \left(\frac{\widehat{A}_z}{dz_z} \right)$	dissolved organic phosphorus sediment flux
$f_{sett}^{POP} = \frac{\omega_{POP}}{dz_z} [POP]$	sedimentation of particulate organic phosphorus
$f_{sett}^{PHY-Pa} = \frac{\omega_{PHYa}}{dz_z} [PHY-Pa]$	sedimentation of phytoplankton
$f_{sett}^{PO_4^{atm}} = \frac{\omega_{SS}}{dz_z} [PO_4^{ads}]$	sedimentation of adsorbed phosphorus
$f_{ads}^{PO_4} = [\Phi_{ads}^{PO_4} ([TPO_4]^{t+1}, SS, pH) \times [TPO_4]^{t+1} - PO_4^{ads*}] \frac{1}{\Delta t}$	adsorption/desorption 'rate' of phosphorus

$$\Phi_{ads}^{PO_4}(TPO_4, SS, pH) = \frac{1}{2IP} \left[\left(TPO_4 + \frac{1}{c_{atm}^r} + c_{ads}^{max} \Phi_{ads}^{pH}(pH) SS \right) - \sqrt{\left(TPO_4 + \frac{1}{c_{atm}^r} + c_{ads}^{max} \Phi_{ads}^{pH}(pH) SS \right)^2 + \frac{4c_{atm}^{max} \Phi_{ads}^{pH}(pH)}{c_{atm}^r} SS} \right]$$

adsorbed fraction of total available inorganic phosphorus

where $\widehat{A}_z = A_z^{ben}/A_z$ and dz_z is the thickness of the z^{th} layer/cell.

Diagnostic & derived outputs:

Total Phosphorus

$$TP = PO_4 + PO_4^{ads} + DOP + POP + \sum_a^{N_{PHY}} PHY_{P_a} + \sum_z^{N_{ZOO}} \frac{ZOO_z}{\chi_{C:P}^z}$$

Total Inorganic Phosphate

$$TPO_4 = PO_4 + PO_4^{ads}$$

note: if multiple POP/DOP pools are simulated then these can be included in TN through the aed_totals routine.

Phytoplankton Dynamics – aed_phytoplankton

Each phytoplankton group configurable within the AED phytoplankton module is generic, and can include internal nitrogen, phosphorus and/or silica stores if desired. The algal biomass of each group, PHY_C , is simulated in units of carbon (mmol C m⁻³), and the group can be configured to have a constant C:N:P:Si ratio, or have dynamic uptake of N and P sources in response to changing water column condition and cellular physiology.

Balance equations for the phytoplankton related state variables are in Table 8.

Table 8: Mass balance and functions related to the phytoplankton model.

<u>State variable mass balance equations:</u>	
Carbon	$\frac{d(PHY_{C,a})}{dt} = +f_{uptake}^{PHY_{C,a}} - f_{excr}^{PHY_{C,a}} - f_{mort}^{PHY_{C,a}} - f_{resp}^{PHY_{C,a}} - f_{sett}^{PHY_{C,a}} - \sum_z^{N_{ZOO}} (f_{attn}^z \ p_a^z)$
Nitrogen	$\frac{d(PHY_{N,a})}{dt} = +f_{uptake}^{PHY_{N,a}} - f_{excr}^{PHY_{N,a}} - f_{mort}^{PHY_{N,a}} - f_{sett}^{PHY_{N,a}} - \sum_z^{N_{ZOO}} \left(f_{attn}^z \ p_a^z \ \frac{PHY_{N,a}}{PHY_{C,a}} \right)$
Phosphorus	$\frac{d(PHY_{P,a})}{dt} = +f_{uptake}^{PHY_{P,a}} - f_{excr}^{PHY_{P,a}} - f_{mort}^{PHY_{P,a}} - f_{sett}^{PHY_{P,a}} - \sum_z^{N_{ZOO}} \left(f_{attn}^z \ p_a^z \ \frac{PHY_{P,a}}{PHY_{C,a}} \right)$
Silica	$\frac{d(PHY_{Si,a})}{dt} = +f_{uptake}^{PHY_{Si,a}} - f_{excr}^{PHY_{Si,a}} - f_{sett}^{PHY_{Si,a}} - \sum_z^{N_{ZOO}} \left(f_{attn}^z \ p_a^z \ \frac{PHY_{Si,a}}{PHY_{C,a}} \right)$
= + uptake (C,N,P & Si)	
- excretion	
- mortality	
- vertical movement (settling or migration)	
- grazing	
<u>Diagnostic & derived outputs:</u>	
Chlorophyll-a	$TCHLA = \sum_a^{N_{PHY}} \left\{ \chi_{C:Chla}^{PHY_a} \ PHY_{C,a} \right\}$
Gross-primary production	$GPP = \sum_a^{N_{PHY}} \left\{ \chi_{C:Chla}^{PHY_a} \ PHY_{C,a} \right\}$

Process summary: Photosynthesis and nutrient uptake

For each phytoplankton group, the maximum potential growth rate at 20°C is multiplied by the minimum value of expressions for limitation by light, phosphorus, nitrogen and silica (when configured). While there may be some interaction between limiting factors, a minimum expression is likely to provide a realistic representation of growth limitation (Rhee and Gotham, 1981).

Therefore, photosynthesis is parameterized as the uptake of carbon, and depends on the temperature, light and nutrient dimensionless functions (adopted from Hipsey & Hamilton, 2008; Li *et al.*, 2013).

$$f_{\text{uptake}}^{\text{PHY}_{C_a}} = \underbrace{R_{\text{growth}}^{\text{PHY}_a}}_{\substack{\text{max growth} \\ \text{rate at } 20\text{C}}} \underbrace{(1 - k_{pr}^{\text{PHY}_a})}_{\text{photorespiratory loss}} \underbrace{\Phi_{\text{tem}}^{\text{PHY}_a}(T)}_{\text{temperature scaling}} \underbrace{\Phi_{\text{str}}^{\text{PHY}_a}(T)}_{\text{metabolic stress}} \dots \\ \dots \min \left\{ \underbrace{\Phi_{\text{light}}^{\text{PHY}_a}(I)}_{\text{light limitation}}, \underbrace{\Phi_N^{\text{PHY}_a}(NO_3, NH_4, \text{PHY}_{N_a})}_{\text{N limitation}}, \underbrace{\Phi_P^{\text{PHY}_a}(PO_4, \text{PHY}_{P_a})}_{\text{P limitation}}, \underbrace{\Phi_{Si}^{\text{PHY}_a}(RSi)}_{\text{Si limitation}} \right\} [\text{PHY}_{C_a}]$$

To allow for reduced growth at non-optimal temperatures, a temperature function is used where the maximum productivity occurs at a temperature T_{OPT} ; above this productivity decreases to zero at the maximum allowable temperature, T_{MAX} . Below the standard temperature, T_{STD} the productivity follows a simple Arrhenius scaling formulation. In order to fit a function with these restrictions the following conditions are assumed: at $T = T_{STD}$, $\Phi_{\text{tem}}(T) = 1$ and at $T = T_{OPT}$, $\frac{d\Phi_{\text{tem}}(T)}{dT} = 0$, and at $T = T_{MAX}$, $\Phi_{\text{tem}}(T) = 0$. This can be numerically solved using Newton's iterative method and can be specific for each phytoplankton group. The temperature function is calculated according to (Griffin *et al.* 2001):

$$\Phi_{\text{tem}}^{\text{PHY}_a}(T) = \vartheta_a^{T-20} - \vartheta_a^{k[T-c1_a]} + c0_a$$

where $c1_a$ and $c0_a$ are solved numerically given input values of: T_a^{std} , T_a^{opt} and T_a^{max} .

The level of light limitation on phytoplankton growth can be modelled as photoinhibition or non-photoinhibition. In the absence of significant photoinhibition, Webb *et al.* (1974) suggested a relationship for the fractional limitation of the maximum potential rate of carbon fixation for the case where light saturation behavior was absent (Talling, 1957), and the equations can be analytically integrated with respect to depth (Hipsey and Hamilton, 2008). For the case of photoinhibition, the light saturation value of maximum production (I_s) is used and the net level effect can be averaged over the cell by integrating over depth.

The `aed_phytoplankton` module contains several light functions, including those from a recent review by Baklouti *et al.* (2006). The user must select the sensitivity to light according to a photosynthesis-irradiance (P-I curve) formulation and each species must be set to be either non-photoinhibited or photoinhibited according to the options in Table 9.

Table 9: Selection of P-I functions available for selection for each species in aed_phytoplankton.

$\Phi_{light}^{PHY_a}(I) =$				
$1 - e^{\left(-\frac{I}{I_{K_a}}\right)}$	$\Theta_{Light}^{PHY_a} = 0$	Non-photoinhibited		Webb et al. (1974), with numerical integration over depth as in CAEDYM (Hipsey and Hamilton, 2008)
$\frac{\left(\frac{I}{I_{K_a}}\right)}{1 + \left(\frac{I}{I_{K_a}}\right)}$	$\Theta_{Light}^{PHY_a} = 1$	Non-photoinhibited		Monod (1950)
$\frac{I}{I_{S_a}} e^{\left(1 - \frac{I}{I_{S_a}}\right)}$	$\Theta_{Light}^{PHY_a} = 2$	Photoinhibited		Steele (1962)
$1 - e^{\left(-\frac{I}{I_{K_a}}\right)}$	$\Theta_{Light}^{PHY_a} = 3$	Non-photoinhibited		Webb et al. (1974)
$\tanh\left(\frac{I}{I_{K_a}}\right)$	$\Theta_{Light}^{PHY_a} = 4$	Non-photoinhibited		Jassby and Platt (1976)
$\frac{e^{\left(\frac{I}{I_{K_a}} + \epsilon\right)} - 1}{e^{\left(\frac{I}{I_{K_a}} + \epsilon\right)} + \epsilon}$	$\Theta_{Light}^{PHY_a} = 5$	Non-photoinhibited		Chalker (1980); $\epsilon \sim 0.5$
$\frac{(2 + A)\left(\frac{I}{I_{S_a}}\right)}{1 + A\left(\frac{I}{I_{S_a}}\right) + \left(\frac{I}{I_{S_a}}\right)^2}$	$\Theta_{Light}^{PHY_a} = 6$	Photoinhibited		Klepper et al. (1988); $A \sim 5$.

Limitation of the photosynthetic rate may be dampened according to nitrogen or phosphorus availability, and this is either approximated using a Monod expression of the static model is chosen, or based on the internal nutrient stoichiometry if the dynamic (Droop uptake) model is selected:

For advanced users, an optional metabolic scaling factor can be included to reduce the photosynthetic capacity of the simulated organisms, for example due to metabolic stress due to undertaking N₂ fixation:

$$\Phi_{str}^{PHY_a} = \underbrace{f_{NF}^{PHY_a} + [1 - f_{NF}^{PHY_a}] \Phi_N^{PHY_a}(NO_3, NH_4, PHY_{N_a})}_{N_2 \text{ fixation growth scaling}}$$

The above discussion relates to photosynthesis and carbon uptake by the phytoplankton community. In addition users must choose one of two options to model the P, N uptake dynamics for each algal group: a constant nutrient to carbon ratio, or dynamic intracellular stores. For the first model a simple Michaelis-Menten equation is used to model nutrient limitation with a half-saturation constant for the effect of external nutrient concentrations on the growth rate.

The internal phosphorus and nitrogen dynamics within the phytoplankton groups can be modelled using dynamic intracellular stores that are able to regulate growth based on the model of Droop (1974). This model allows for the phytoplankton to have dynamic nutrient uptake rates with variable internal nutrient concentrations bounded by user-defined minimum and maximum values (e.g., see Li *et al.*, 2013).

Table 10: N, P and Si phytoplankton uptake rate functions.

$f_{uptake}^{PHY_N_a}$				
$f_{uptake}^{PHY_Ca} / \chi_{C:N}^{PHY_a}$	$\Theta_{NO3\text{Uptake}}^{PHY_a} = 0,1$	Static uptake rate	-	
$R_{NO3\text{Uptake}}^{PHY_a} \Phi_{tem}^{PHY_a}(T) \left\{ \Phi_N^{PHY_a} \frac{\left(\frac{[PHY_N_a]}{[PHY_Ca]} - \chi_{NMIN}^{PHY_a} \right)}{(\chi_{NMAX}^{PHY_a} - \chi_{NMIN}^{PHY_a})} \right\} [PHY_N_a]$	$\Theta_{NO3\text{Uptake}}^{PHY_a} = 2$	Dynamic uptake rate	Hipsey and Hamilton (2008)	
$f_{uptake}^{PHY_P_a}$				
$f_{uptake}^{PHY_Ca} / \chi_{C:P}^{PHY_a}$	$\Theta_{PUptake}^{PHY_a} = 0,1$	Static uptake rate	-	
$R_{PUptake}^{PHY_a} \Phi_{tem}^{PHY_a}(T) \left\{ \Phi_P^{PHY_a} \frac{\left(\frac{[PHY_P_a]}{[PHY_Ca]} - \chi_{PMIN}^{PHY_a} \right)}{(\chi_{PMAX}^{PHY_a} - \chi_{PMIN}^{PHY_a})} \right\} [PHY_P_a]$	$\Theta_{PUptake}^{PHY_a} = 2$	Dynamic uptake rate	Hipsey and Hamilton (2008)	
$f_{uptake}^{PHY_Si_a}$				
$f_{uptake}^{PHY_Ca} / \chi_{C:Si}^{PHY_a}$		Static uptake rate	-	

The uptake of nitrogen must be partitioned into uptake of NO₃, NH₄ and potentially labile DON. In the present version, distinction between uptake of NO₃ and NH₄ is calculated automatically via a preference factor:

$$p_{NH4}^{PHY_a} = \frac{NO_3 \text{NH}_4}{(NH_4 + K_N^{PHY_a})(NO_3 + K_N^{PHY_a})} \frac{NH_4 K_N^{PHY_a}}{(NH_4 + NO_3)(NO_3 + K_N^{PHY_a})}$$

$$p_{NO3}^{PHY_a} = 1 - p_{NH4}^{PHY_a}$$

For diatom groups, silica processes are simulated that include uptake of dissolved silica. The silica limitation function for diatoms is similar to the constant cases for nitrogen and phosphorus which assumes a fixed C:Si ratio.

Process summary: Respiration, excretion and mortality

Metabolic loss of nutrients from mortality and excretion is proportional to the internal nitrogen to chla ratio multiplied by the loss rate and the fraction of excretion and mortality that returns to the detrital pool. Loss terms for respiration, natural mortality and excretion are modelled with a single 'respiration' rate coefficient. This loss rate is then divided into the pure respiratory fraction and losses due to mortality and excretion. The constant f_{DOM} is the fraction of mortality and excretion to the dissolved organic pool with the remainder into the particulate organic pool.

Nutrient losses through mortality and excretion for the internal nutrient model are similar to the simple model described above, except that dynamically calculated internal nutrient concentrations are used.

$$\hat{R} = R_{resp}^{PHY_a} \Phi_{sal}^{PHY_a}(S) (\vartheta_{resp}^{PHY_a})^{T-20}$$

$$f_{resp}^{PHY_Ca} = k_{fres}^{PHY_a} \hat{R} [PHY_{C_a}]$$

$$f_{excr}^{PHY_Ca} = (1 - k_{fres}^{PHY_a}) k_{fdom}^{PHY_a} \hat{R} [PHY_{C_a}]$$

$$f_{mort}^{PHY_Ca} = (1 - k_{fres}^{PHY_a}) (1 - k_{fdom}^{PHY_a}) \hat{R} [PHY_{C_a}]$$

$$f_{excr}^{PHY_Na} = k_{fdom}^{PHY_a} \hat{R} [PHY_{N_a}]$$

$$f_{mort}^{PHY_Na} = (1 - k_{fdom}^{PHY_a}) \hat{R} [PHY_{N_a}]$$

$$f_{excr}^{PHY_Pa} = k_{fdom}^{PHY_a} \hat{R} [PHY_{P_a}]$$

$$f_{mort}^{PHY_Pa} = (1 - k_{fdom}^{PHY_a}) \hat{R} [PHY_{P_a}]$$

$$f_{excr}^{PHY_{Si}a} = \hat{R} [PHY_{Si_a}]$$

The salinity effect on mortality is given by various quadratic formulations, depending on the groups sensitivity to salinity (Griffin et al 2001; Robson and Hamilton, 2004). An example of the use of various salinity limitation options is shown in Figure 3.

Table 11: Respiration multiplier as a function of salinity.

$\Phi_{sal}^{PHY_a}(S) =$			
1		$\Theta_{SalTol}^{PHY_a} = 0$	No salinity effect
$\begin{cases} 1 & \text{if } S < S_{opt}^{PHY_a} \\ 1 + \frac{(S_{bep}^{PHY_a} - 1) S^2}{(S_{max}^{PHY_a} - S_{opt}^{PHY_a})^2} - \frac{2(S_{bep}^{PHY_a} - 1) S_{opt}^{PHY_a} S}{(S_{max}^{PHY_a} - S_{opt}^{PHY_a})^2} + \frac{(S_{bep}^{PHY_a} - 1)(S_{opt}^{PHY_a})^2}{(S_{max}^{PHY_a} - S_{opt}^{PHY_a})^2} & \text{if } S > S_{opt}^{PHY_a} \end{cases}$	$\Theta_{SalTol}^{PHY_a} = 1$	Freshwater species	
$\begin{cases} 1 & \text{if } S < S_{opt}^{PHY_a} \\ \frac{(S_{bep}^{PHY_a} - 1) S^2}{(S_{opt}^{PHY_a})^2} - \frac{2(S_{bep}^{PHY_a} - 1) S}{(S_{opt}^{PHY_a})^2} & \text{if } S > S_{opt}^{PHY_a} \end{cases}$		$\Theta_{SalTol}^{PHY_a} = 2$	Marine species
$\begin{cases} 1 & \text{if } S < S_{opt}^{PHY_a} \\ S_{bep}^{PHY_a} + \frac{(S_{bep}^{PHY_a} - 1) S^2}{(S_{opt}^{PHY_a})^2} - \frac{2(S_{bep}^{PHY_a} - 1) S}{(S_{opt}^{PHY_a})^2} & \text{if } S > S_{opt}^{PHY_a} \end{cases}$		$\Theta_{SalTol}^{PHY_a} = 3$	Estuarine species

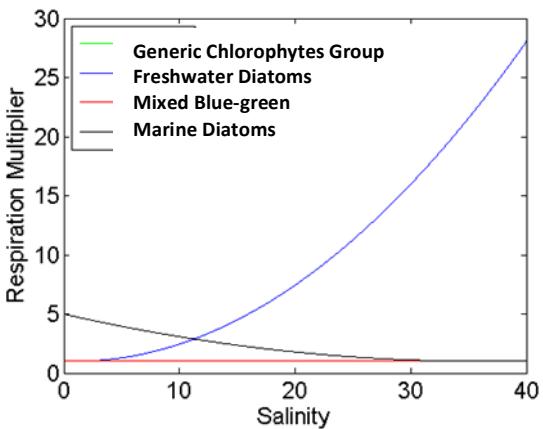


Figure 3: Example salinity response functions, $\Phi_{sal}^{PHY}(S)$, for four phytoplankton groups being simulated within a river-estuary model. This example demonstrates how fresh, estuarine and marine species can be incorporated together.

Zooplankton Dynamics – aed_zooplankton

Net zooplankton growth is calculated as a balance between food assimilation and losses from respiration, excretion, egestion, predation and mortality. Food assimilation is calculated as the product of the maximum potential rate of grazing, assimilation efficiency and temperature and food limitation functions. A constant internal nutrient ratio is assumed for simplicity, and since the various input and output fluxes have variable C:N:P ratios, the excretion of nutrients is dynamically adjusted each time-step to maintain this ratio at each time step.

Table 12: Zooplankton balance equations .

<u>State variable mass balance equations:</u>	
$\frac{d(ZOO_z)}{dt} = k_{attn}^z \times f_{attn}^z - f_{loss}^z - f_{mort}^z$	= + carbon and nutrient assimilation from grazing various ecosystem pools - carbon loss via respiration - excretion of DOM - faecal pellet production - mortality - predation by larger organisms
ZOO_N and ZOO_P are not dynamically solved but set at a constant ratio to zooplankton carbon.	
<u>Process parameterisations:</u>	
$f_{attn}^z = R_{grz}^{ZOO_P} \Phi_{tem}^z(T) [ZOO]$	zooplankton assimilation
$f_{loss}^z = R_{loss}^{ZOO_P} (\theta_{loss}^z)^{T-20} [ZOO]$	zooplankton loss
$f_{excr}^z = k_{excr}^z \times f_{loss}^z$	zooplankton excretion
$f_{fecal}^z = k_{fecal}^z \times f_{loss}^z$	zooplankton fecal pellets
$f_{mort}^z = R_{mort}^z \Phi_{sal}^z(S) \times (\theta_{loss}^z)^{T-20} [ZOO]$	zooplankton mortality

Suspended Sediment & Turbidity : aed_tracer, aed_totals

Modellers can use the aed_tracer to simulate a particulate tracer that can be set to also settle and decay. In addition to suspended sediment simulated in this way, the aed_totals module has an option to assign any number of FABM variables (including non-AED variables) to contribute to a turbidity, subject to a transformation coefficient.

Geochemical Dynamics : aed_geochemistry, aed_iron, aed_sulfur

The Oct 2013 release of AED with GLM v1.3.2 contains several geochemistry modules - documentation for these modules is pending.

Sediment Biogeochemistry – aed_sedflux, aed_seddiagenesis

The AED modules has aimed to provide flexibility in how users may want to simulate sediment-water interaction. This includes a simple flux equation, or a simple mass balance model maintains a mass balance of C, N, P, Si, DO and SS in both the water column and a single sediment layer. At this development stage only sufficient complexity is implemented in the sediments to maintain mass conservation. The sediment fluxes of dissolved inorganic and organic nutrients are based on empirical formulations that account for environmental sensitivities and require laboratory and field studies to establish parameter values. Resuspension of particulate nutrients is currently not configured, however note that the resuspension of inorganic sediments is performed through the TUFLOW-FV driver.

The Oct 2013 release of AED contains a more detailed sediment diagenesis model that includes vertical resolution - documentation for this module is pending.

Pathogens – aed_pathogens

The pathogen module is a reimplementation of Hipsey et al. (2008). Users are referred to this paper for details of simulatable variables, process parameterisations and parameter values.

Parameter summary

This section summarises the parameters introduced in the previous section with some comments and references to help those new to the model get started. Please note that the process of parameter estimation in aquatic ecosystem models is highly complex and this summary is by no means an exhaustive review of relevant parameter values, and applying these values may not lead to an acceptable validation.

Below Table 9 summarises sediment related parameters, Table 10 summarises biogeochemical parameters relevant to nutrient cycling, and Table 11 and 12 summarise phytoplankton and zooplankton parameters respectively.

Note that in collaboration with the Aquatic Ecological Modelling Network (AEMON), a more detailed database of species parameters is being developed which may be referred to search for specific parameters for a given species, or to see typical values for functional groups used in other modelling studies:

<https://sites.google.com/site/aquaticmodelling/>

Click on *Resources* and then follow the link to "*Parameter database*"

Table 13: Summary of sediment parameter descriptions, units and typical values.

Symbol	Description	Units	Default value	Comment
$F_{max}^{O_2}$	maximum flux of oxygen across the sediment water interface into the sediment	mmol O ₂ /m ² /d	48.0	Lake: 6 – 38 ^A River: 9.4 – 20.3 ^B Estuary: 48 ^C ; 79 ^D ; ~50 ^E
$K_{sed}^{O_2}$	half saturation constant for oxygen dependence of sediment oxygen flux	mmol O ₂ /m ³	150	Lake: 15.6 ^A Estuary: 150 ^C ; ~50 ^F
$\theta_{sed}^{O_2}$	temperature multiplier for temperature dependence of sediment oxygen flux	-	= θ_{sed} = 1.08	1.04 – 1.10 ^A
F_{max}^{RSi}	maximum flux of silica across the sediment water interface	mmol Si/m ² /d	4	Lake: 0.6 ^A Estuary: 4 – 40 ^E
K_{sed}^{RSi}	half saturation constant for oxygen dependence of sediment silica flux	mmol Si/m ³	150	estimated
θ_{sed}^{RSi}	temperature multiplier for temperature dependence of sediment silica flux	-	= θ_{sed} = 1.08	1.04 – 1.10 ^A
$F_{max}^{PO_4}$	maximum flux of phosphate across the sediment water interface	mmol P/m ² /d	0.2	Lake: 0.080 – 0.125 ^A River: 0.0 – 0.10 ^B Estuary: 0.3 – 4 ^E
$K_{sed}^{PO_4}$	half saturation constant for oxygen dependence of sediment phosphate flux	mmol O ₂ /m ³	20	Lake: 15.6 ^{A, J} Estuary: >200 ^F
$\theta_{sed}^{PO_4}$	temperature multiplier for temperature dependence of sediment phosphate flux	-	= θ_{sed} = 1.08	1.04 – 1.10 ^A
F_{max}^{DON}	maximum flux of dissolved organic phosphorus across the sediment water interface	mmol P/m ² /d	0.05	Lake: 0.03 ^A River: 0.05 – 0.10 ^B
K_{sed}^{DON}	half saturation constant for oxygen dependence of sediment dissolved organic phosphorus flux	mmol O ₂ /m ³	150	estimated
θ_{sed}^{DON}	temperature multiplier for temperature dependence of sediment dissolved organic phosphorus flux	-	= θ_{sed} = 1.08	1.04 – 1.10 ^A
$F_{max}^{NH_4}$	maximum flux of ammonium across the sediment water interface	mmol N/m ² /d	30.0	Lake: 1.35 – 6.42 ^A River: 4.3 – 12.8 ^B Estuary: 30 ^C ; 5 – 25 ^E
$K_{sed}^{NH_4}$	half saturation constant for oxygen dependence of sediment ammonium flux	mmol N/m ³	31.25	Lake: 1.56 – 15.6 ^A Estuary: 31.25 ^C
$\theta_{sed}^{NH_4}$	temperature multiplier for temperature dependence of sediment ammonium flux	-	1.08	1.04 – 1.10 ^A
$F_{max}^{NO_3}$	maximum flux of nitrate across the sediment water interface	mmol N/m ² /d	5.2	Lake: -21.4 – -7.14 ^A River: 4.3 – 12.8 ^B Estuary: 5.2 ^C ; -7.2 – 7.1 ^E
$K_{sed}^{NO_3}$	half saturation constant for oxygen dependence of sediment nitrate flux	mmol O ₂ /m ³	100.0	Lake: 2.14 – 15.6 ^A Estuary: 100 ^C
$\theta_{sed}^{NO_3}$	temperature multiplier for temperature dependence of sediment nitrate flux	-	= θ_{sed} = 1.08	1.04 – 1.10 ^A
F_{max}^{DON}	maximum flux of dissolved organic nitrogen across the sediment water interface	mmol N/m ² /d	5.2	Lake: 0.07 – 0.57 ^A River: 1.28 – 2.20 ^B
K_{sed}^{DON}	half saturation constant for oxygen dependence of sediment dissolved organic nitrogen flux	mmol N/m ³	100.0	estimated
θ_{sed}^{DON}	temperature multiplier for temperature dependence of sediment dissolved organic nitrogen flux	-	= θ_{sed} = 1.08	1.04 – 1.10 ^A

^A Converted from data on oligotrophic lakes (Romero et al. 2004) to eutrophic lakes (Gal et al. 2009), and justifications therein.

^B Based on Hipsey et al. (2010) ELCOM-CAEDYM model of the lower Murray River; estimated from field data from Justin Brookes.

^C Based on Bruce et al. (2013) FABM-AED application on the Yarra Estuary (Victoria); estimated from field data from Perran Cook.

^D Net flux measured during eddy correlation experiment in the Upper Swan Estuary (Kilmminster et al., 2011); varied in the range 20 – 150 mmol O₂/m²/d with a background concentration of 260 mmol O₂/m³, therefore $F_{max}^{O_2} \sim 50/(260/(260+150)) = 79$ mmol O₂/m²/d.

^E Based on benthic chamber studies showing an average net flux of 50 mmol O₂/m²/d the Upper Swan estuary (Smith et al 2007).

^F Based on Smith et al (2007) assessment of data from the Upper Swan estuary, limitation at low oxygen concentrations is not observed.

Table 14: Summary of water column biogeochemical parameter descriptions, units and typical values.

Symbol	Description	Units	Assigned value	Comment
$k_{atm}^O_2$	oxygen transfer coefficient	m/s	calculated	<i>Wanninkhof (1992)</i>
$[O_2]_{atm}$	atmospheric oxygen concentration	mmol O ₂ /m ³	calculated	<i>Riley and Skirrow (1975)</i>
$\chi_{C:O_2}^{miner, PHY}, \chi_{C:O_2}$	Stoichiometric conversion of C to O ₂	mmol C/mmol O ₂		12/32
$\chi_{N:O_2}^{nitrif}$	Stoichiometric conversion of N to O ₂	mmol N/mmol O ₂		14/32
R_{nitrif}	maximum rate of nitrification	/d	0.5	<i>Lake: 0.03 – 0.05^A; 0.037^G</i> <i>Estuary: 0.5^C</i>
K_{nitrif}	half saturation constant for oxygen dependence of nitrification rate	mmol O ₂ /m ³	78.1	<i>Lake: 62.5 – 93.7^A</i> <i>Estuary: 78.1^C</i>
θ_{nitrif}	temperature multiplier for temperature dependence of nitrification rate	-	1.08	<i>Lake: 1.08^A; 1.03^G</i> <i>Estuary: 1.08^C</i>
$R_{det PON}$	maximum rate of denitrification	/d	0.5	<i>Lake: 0.01 – 0.04^A</i> <i>Estuary: 0.5^C</i>
K_{denit}	half saturation constant for oxygen dependence of denitrification	mmol O ₂ /m ³	21.8	<i>Lake: 12.5 – 15.6^A</i> <i>Estuary: 21.8^C</i>
θ_{denit}	temperature multiplier for temperature dependence of denitrification	-	1.08	<i>Lake: 1.05^A</i> <i>Estuary: 1.08^C</i>
R_{decom}^{PON}	maximum rate of decomposition of particulate organic nitrogen	/d	0.5	<i>Lake: 0.005 – 0.01^A; 0.03^G</i> <i>Estuary: 0.5^C</i>
K_{decom}^{PON}	half saturation constant for oxygen dependence of mineralisation rate	mmol O ₂ /m ³	31.25	<i>Lake: 47 – 78^A</i> <i>Estuary: 31.25^C</i>
θ_{decom}^{PON}	temperature multiplier for temperature dependence of mineralisation rate	-	= $\theta_{OM} = 1.08$	<i>Lake: 1.08^A</i> <i>Estuary: 1.08^C</i>
R_{miner}^{DON}	maximum rate of mineralisation of dissolved organic nitrogen	/d	0.5	<i>Lake: 0.003 – 0.05^A</i> <i>Estuary: 0.001 – 0.028^H</i>
K_{decom}^{DON}	half saturation constant for oxygen dependence of mineralisation rate	mmol O ₂ /m ³	31.25	<i>Lake: 47 – 78^A</i>
θ_{miner}^{DON}	temperature multiplier for temperature dependence of mineralisation rate	-	= $\theta_{OM} = 1.08$	1.04 – 1.10 ^A
ω_{PON}	settling rate of particulate organic matter	m/d	= $\omega_{OM} = -1.0$	<i>Estuary: -1.0^C</i>
R_{decom}^{POC}	maximum rate of decomposition of particulate organic carbon	/d	0.5	<i>Lake: 0.01 – 0.07^A; 0.008^G</i>
K_{decom}^{POC}	half saturation constant for oxygen dependence of mineralisation rate	mmol O ₂ /m ³	31.25	<i>Lake: 47 – 78^A</i>
θ_{decom}^{POC}	temperature multiplier for temperature dependence of mineralisation rate	-	= $\theta_{OM} = 1.08$	1.04 – 1.10 ^A
R_{miner}^{DOC}	maximum rate of mineralisation of dissolved organic carbon	/d	0.5	<i>Lake: 0.003 – 0.05^A</i> <i>Estuary: 0.001 – 0.006^H</i>
K_{decom}^{DOC}	half saturation constant for oxygen dependence of mineralisation rate	mmol O ₂ /m ³	31.25	<i>Lake: 47 – 78^A</i>
θ_{miner}^{DOC}	temperature multiplier for temperature dependence of mineralisation rate	-	= $\theta_{OM} = 1.08$	1.04 – 1.10 ^A
ω_{POC}	settling rate of particulate organic matter	m/day	= $\omega_{OM} = -1.0$	
R_{decom}^{POP}	maximum rate of decomposition of particulate organic phosphorus	/d	0.5	<i>Lake: 0.01 – 0.03^A; 0.099^G</i>
K_{decom}^{POP}	half saturation constant for oxygen dependence of mineralisation rate	mmol O ₂ /m ³	31.25	<i>Lake: 47 – 78^A</i>
θ_{decom}^{POP}	temperature multiplier for temperature dependence of mineralisation rate	-	= $\theta_{OM} = 1.08$	1.04 – 1.10 ^A
R_{miner}^{DON}	maximum rate of mineralisation of dissolved organic phosphorus	/d	0.5	<i>Lake: 0.01 – 0.05^A</i>

K_{decom}^{DON}	half saturation constant for oxygen dependence of mineralisation rate	mmol O ₂ /m ³	31.25	Lake: 47 – 78 ^A
θ_{miner}^{DON}	temperature multiplier for temperature dependence of mineralisation rate	-	= θ_{OM} = 1.08	1.04 – 1.10 ^A
ω_{POP}	settling rate of particulate organic matter	m/d	= ω_{OM} = -1.0	
$\Phi_{ads}^{pH}(pH)$	Function characterizing pH effect on	-	calculated	-0.0088(pH) ² + 0.0347(pH) + 0.9768 ^I
c_{ads}^r	ratio of adsorption and desorption rate coefficients	l/mg		Lake: 0.7 ^J
c_{ads}^{max}	maximum adsorption capacity of SS	mmol P/mg SS		Lake: 0.00016 ^J

- ^A Converted from data on oligotrophic lakes (Romero et al. 2004) to eutrophic lakes (Gal et al. 2009), and justifications therein.
- ^C Based on Bruce et al. (2013) FABM-AED application on the Yarra Estuary (Victoria); estimated from field data from Perran Cook.
- ^G Based on Schladow & Hamilton (1997) for Prospect Reservoir.
- ^H Based on incubations by Petrone et al. (2009) for Swan Estuary (Western Australia).
- ^I Based on regression of data from Salmon et al. (submitted) based on data review from 6 papers
- ^J Based on model of Chao et al. (2010).

Table 15: Summary of phytoplankton parameter descriptions, units and example values for typical species.

parameter	description	units	Diatom	Greens	Blue-greens	Reference
R_{growth}^{PHY}	phytoplankton growth rate at 20C	/d	3.0	0.9	1.0	Various
I_K	light % saturation constant for algal limitation	$\mu\text{E m}^{-2} \text{s}^{-1}$	60	80	130	Romero et al. (2004)
I_S	saturating light intensity	$\mu\text{E m}^{-2} \text{s}^{-1}$	150	150	150	Schladow & Hamilton (1997)
θ_{growth}^{PHY}	Arrhenius temperature scaling for growth	-	1.06	1.06	1.06	Kruger and Ellof (1978), Coles and Jones (2000), Schladow & Hamilton (1997)
T_{std}	standard temperature	C	20	20	20	Griffin et al. (2001)
T_{opt}	optimum temperature	C	25	27	28	Griffin et al. (2001)
T_{max}	maximum temperature	C	32	33	35	Griffin et al. (2001)
R_{resp}^{PHY}	phytoplankton respiration rate at 20C	/d	0.085	0.085	0.085	Schladow & Hamilton (1997)
k_{fres}^{PHY}	fraction of metabolic loss that is respiration	-	0.25	0.25	0.25	Gal et al. 2009
k_{fdom}^{PHY}	fraction of metabolic loss that is DOM	-	0.2	0.2	0.2	Gal et al. 2009
θ_{resp}^{PHY}	Arrhenius temperature scaling for respiration	-	1.12	1.05	1.05	Gal et al. 2009
K_N	half-saturation concentration of nitrogen	mmol N /m ³	3.5	2.7	1.0	Gal et al. 2009
$R_{NO_2\text{NO}_3}^{PHY}$	maximum nitrogen uptake rate	mmol N /m ³ /d				
χ_{NMIN}^{PHY}	minimum internal nitrogen concentration	mmol N / mmol C				
χ_{NMAX}^{PHY}	maximum internal nitrogen concentration	mmol N / mmol C				
K_P	half-saturation concentration of phosphorus	mmol P /m ³	0.15	0.07	0.05	Gal et al. 2009
$R_{NO_2\text{PO}_4}^{PHY}$	maximum phosphorus uptake rate	mmol P /m ³ /d				
χ_{PMIN}^{PHY}	minimum internal phosphorus concentration	mmol P / mmol C				
χ_{PMAX}^{PHY}	maximum internal phosphorus concentration	mmol P / mmol C				
K_{Si}	half-saturation concentration of silica	mmol Si /m ³	2.5	-	-	Romero et al. 2004
$\chi_{C:Si}^{PHY}$	internal silicate concentration	mmol Si / mmol C		-	-	
ω_{PHY}	phytoplankton sedimentation rate	m/d	-0.86	-0.01	-0.02	Gal et al. 2009; Romero et al. 2004
MORE...						

Table 16: Summary of zooplankton parameter descriptions, units and typical values.

parameter	description	units	Example parameter value
ε_{min}^z	Minimum zooplankton concentration	mmol C/m ³	0.1
R_{grz}^z	Zooplankton grazing rate	/day	1.5
k_{attm}^z	Assimilation efficiency for zooplankton grazing	-	0.9
K_{grz}^z	Half saturation constant for zooplankton grazing	-	40
θ_{grz}^z	Temperature multiplier for zooplankton grazing	-	1.08
T_{std}^z	Standard temperature for zooplankton grazing	°C	20.0
T_{opt}^z	Optimum temperature for zooplankton grazing	°C	22.0
T_{max}^z	Maximum temperature for zooplankton grazing	°C	30.0
p_z^z	Preference factor of zooplankton grazing on phytoplankton	-	0.7
$p_{PHY_a}^z$	Preference factor of zooplankton grazing on zooplankton	-	0.0
p_{POM}^z	Preference factor of zooplankton grazing on particulate organic matter	-	0.3
p_b^z	Preference factor of zooplankton grazing on bacteria	-	0.0
ε_{grz}^z	Concentration of prey at which grazing by zooplankton is limited	mmol C/m ³	10.0
R_{loss}^z	Respiration rate coefficient	/day	0.1
R_{mort}^z	Mortality rate coefficient	/day	0.01
k_{fecal}^z	Fecal pellet fraction of loss rate	-	0.2
k_{excr}^z	Excretion fraction of loss rate	-	0.7
k_{fsed}^z	Fraction of fecal pellets that sink directly to sediments (hard fraction)	-	0.15
θ_{loss}^z	Temperature multiplier for zooplankton loss	-	1.08
$\chi_{C:N}^z$	Ratio of internal nitrogen to carbon	mmol N / mmol C	0.2
$\chi_{C:P}^z$	Ratio of internal phosphorus to carbon	mmol P / mmol C	0.01
θ_{sal}^z	Type of salinity limitation function		1
S_{max}^z	Maximum or optimal salinity	psu	0.0
S_{min}^z	Minimum salinity	psu	35.0
S_{int}^z	Salinity intercept, for S=0	-	10.0
θ_{oxy}^z	Simulate oxygen limitation		1
ε_{oxy}^z	Minimum concentration of dissolved oxygen at which zooplankton can survive	mmol O ₂ /m ³	0.05

Configuring the AED library

All the possible state variables that can be simulated by the AED modules are listed in Table 17. Each of the variables listed below can also be specified as an output via the NetCDF output. They are generally available as a suffix to the module name, `aed_module_varname`, for example, to view oxygen search for the `aed_oxygen_oxy`. The keywords for most of the simulated variables are also used to specify the inflow boundary conditions in relevant inflow files (depending on the hydrodynamic driver).

Although there are numerous state variables in total, many are not compulsory and depend on the modules selected and how the interactions between modules are configured. This configuration is done via options outlined in the `fabm.nml` file (or `aed.nml` if FABM is not being used). An example of a AED module setup and the necessary interactions that can be configured is shown in Figure 4. For example, setting the target for excretion would be done by setting the variable:

```
n_excretion_target_variable = "aed_organic_matter_don"
```

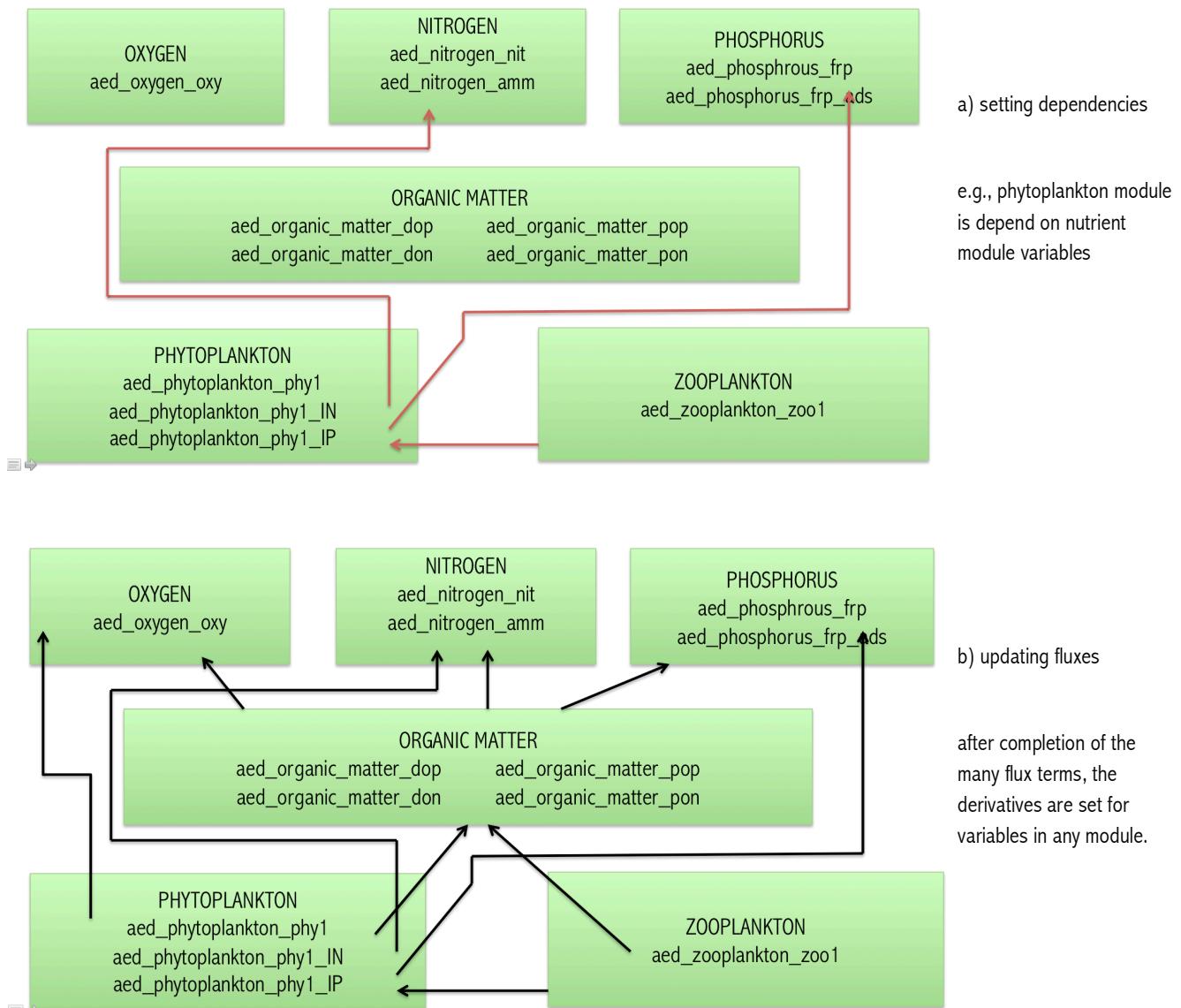


Figure 4: Example of linkages that need to be set in a AED simulation, outlining a) dependencies for a phytoplankton and zooplankton that must be configured, and b) linkages that are updated during operation of the model system.

Table 17: Current coupled aquatic biogeochemical models included within the FABM framework.

Symbol	Name	Units	AED module
General			
t	time	days	
dz	layer height	m	
A	layer/cell area	m^2	
Environmental dependencies			
T	Temperature	$^\circ\text{C}$	
S	Salinity	ppt	
I_{PAR}	Photosynthetically active radiation (PAR: 400-700nm)	W/m^2	
Oxygen			
O_2	concentration of dissolved oxygen	$\text{mmol O}/\text{m}^3$	aed_oxygen
Silica			
RSi	reactive silica (SiO_2) concentration	$\text{mmol Si}/\text{m}^3$	aed_silica
Nitrogen			
NH_4	concentration of ammonium	$\text{mmol N}/\text{m}^3$	aed_nitrogen
NO_3	concentration of nitrate	$\text{mmol N}/\text{m}^3$	aed_nitrogen
Phosphorus			
PO_4	concentration of filterable reactive phosphorus (PO_4)	$\text{mmol P}/\text{m}^3$	aed_phosphorus
PO_4^{ads}	concentration of adsorbed phosphate	$\text{mmol P}/\text{m}^3$	aed_phosphorus
Carbon			
CH_4	concentration of methane	$\text{mmol C}/\text{m}^3$	aed_carbon
DIC	concentration of dissolved inorganic carbon	$\text{mmol C}/\text{m}^3$	aed_carbon
pH	pH	-	aed_carbon
Organic Matter (DOM & POM)			
POC	concentration of particulate organic carbon	$\text{mmol C}/\text{m}^3$	aed_organic_matter
DOC	concentration of dissolved organic carbon	$\text{mmol C}/\text{m}^3$	aed_organic_matter
PON	concentration of particulate organic nitrogen	$\text{mmol N}/\text{m}^3$	aed_organic_matter
DON	concentration of dissolved organic nitrogen	$\text{mmol N}/\text{m}^3$	aed_organic_matter
POP	concentration of particulate organic phosphorus	$\text{mmol P}/\text{m}^3$	aed_organic_matter
DOP	concentration of dissolved organic phosphorus	$\text{mmol P}/\text{m}^3$	aed_organic_matter
Phytoplankton			
N_{PHY}	number of simulated phytoplankton groups	-	aed_phytoplankton
PHY_C	concentration of phytoplankton carbon	$\text{mmol C}/\text{m}^3$	aed_phytoplankton
PHY_N	concentration of phytoplankton nitrogen	$\text{mmol N}/\text{m}^3$	aed_phytoplankton
PHY_P	concentration of phytoplankton phosphorus	$\text{mmol P}/\text{m}^3$	aed_phytoplankton
PHY_{Si}	concentration of phytoplankton silica	$\text{mmol Si}/\text{m}^3$	aed_phytoplankton
Zooplankton			
N_{zoo}	number of simulated zooplankton groups	-	aed_zooplankton
ZOO	concentration of zooplankton carbon	$\text{mmol C}/\text{m}^3$	aed_zooplankton
Totals			
TN	Total nitrogen	$\text{mmol N}/\text{m}^3$	aed_totals
TP	Total phosphorus	$\text{mmol P}/\text{m}^3$	aed_totals
TSS	Total suspended solids	$\text{mg SS}/\text{m}^3$	aed_totals
$Turbidity$	Turbidity	NTU	aed_totals

In summary, currently the modules support the following process descriptions and features, and they are presented here **in order of hierarchical dependence**, which is important in setting the order of module configuration in the `fabm.nml` control file:

aed_oxygen:

- Surface/bottom exchange
- Photosynthesis / respiration
- OM mineralisation

aed_silica

- benthic flux
- phyto uptake

aed_phosphorus

- benthic flux of PO_4
- phytoplankton uptake
- organic matter mineralisation
- adsorption to inorganic particles

aed_nitrogen

- benthic flux of NO_3 and NH_4
- phytoplankton uptake
- denitrification/nitrification
- organic matter mineralisation

aed_organic_matter

- POM and DOM for C, N, and P
- Decomposition and hydrolysis of detrital material, and mineralisation
- Benthic flux of dissolved organic material
- phytoplankton production through excretion, exudation and mortality
- Multiple “pools” can be configured (eg. labile/refractory), by simulating multiple instances.

aed_chla:

- generic bulk phytoplankton module for simulating growth of chl-a

aed_phytoplankton:

- Multiple groups, support flexible setting of interactions and configuration (eg. N uptake of NH_4 , NO_3 , DON, N_2 possible)
- Uses a “parameter library file”, `aed_phyto_pars.nml`, which stores many pre-configured parameter sets that users can choose from.
- Includes numerous options for temperature, salinity, light, & nutrient environmental dependencies
- Variable IN:IP (droop) or fixed N:P (static) allowed

aed_zooplankton:

- Multiple groups can be configures to represent species/functional groups or size classes within species/functional groups.
- Physiological parameters set by user in name list: `aed_zoop_pars.nml`.
- Choice of food set in name list from phytoplankton, bacteria and particulate organic matter

aed_pathogens:

- Multiple groups can be configures to represent species/functional groups
- Processes for mortality and inactivation depending on environmental conditions, and optional growth term also included.
- Physiological parameters set by user in name list `aed_pathogen_pars.nml`.

References

- Ambrose, R.B. Jr., Wool, T.A., Conolly, J.P., and Scahnz, R.W.. 1988. A Hydrodynamic and Water Quality Model: Model Theory, Users Manual, and Programmers manual: WASP4 Environmental Research Laboratory, US EPA, EPA 600/3-87/039, Athens, GA.
- Arhonditsis, G.B., Adams-Vanharn, B.A., Nielsen, L., Stow, C.A., and Reckhow, K.H., 2006. Evaluation of the current state of mechanistic aquatic biogeochemical modeling: citation analysis and future perspectives. *Environ. Sci. Technol.*, **40**, 6547-6554.
- Bruce, L.C., Hipsey, M.R. and Cook, P.M., 2011. Quantification of sediment and water processing of nitrogen in a periodically anoxic urban estuary using a 3D hydrodynamic-biogeochemical model. *MODSIM*.
- Bruce LC, Hamilton DP, Imberger J, Gal G, Gophen M, Zohary T, Hambright KD, 2006. A numerical simulation of the role of zooplankton in C, N and P cycling in Lake Kinneret, Israel. *Ecol. Model.* **193**:412-436.
- Broekhuizen, N., Rickard, G. J., Bruggeman, J. & Meister, A. 2008. An improved and generalized second order, unconditionally positive, mass conserving integration scheme for biochemical systems. *Applied Numerical Mathematics* 58:319–40.
- Bruggeman, J. 2011. D2.14 Users guide and report for models in the MEECE library – Framework for Aquatic Biogeochemical Models (FABM). Report for the EC FP7 MEECE project 212085. 57pp.
- Burchard H et al. 2005. Application of modified Patankar schemes to stiff biogeochemical models, *Ocean Dyn*, **55**: 326-37
- Burchard, H., Bolding, K., Kuhn, W., Meister, A., Neumann, T. & Umlauf, L. 2006. Description of a flexible and extendable physical- biogeochemical model system for the water column. *Journal of Marine Systems* 61: 180-211.
- Chao, X., Jia, Y., Shields, F.D., Wang, S.S.Y., and Cooper, C.M., 2010. Three-dimensional numerical simulation of water quality and sediment-associated processes with application to a Mississippi Delta lake. *Journal of Environmental Management* **91**: 1456 – 1466.
- Chalker, B.E., 1980. Modelling light saturation curves for photosynthesis: an exponential function. *Journal of Theoretical Biology* 84, 205–215.
- Coles, J.F. and R.C. Jones. 2000. Effect of temperature on photosynthesis-light response and growth of four phytoplankton species isolated from a tidal freshwater river. *J. Phycology*, **36**: 7-16.
- Droop, M.R. 1974. The nutrient status of algal cells in continuous culture. *J. Mar. Biol. Assoc. UK*, **54**: 825–855.
- Fasham, M.J.R., Ducklow, H.W. & Mckelvie, S.M., 1990. A nitrogen-based model of plankton dynamics in the oceanic mixed layer. *J Mar Res* 48: 591-639
- Gal, G., Hipsey, M.R., Paparov, A., Makler, V. and Zohary, T., 2009. Implementation of ecological modeling as an effective management and investigation tool: Lake Kinneret as a case study. *Ecol. Model.*, **220**: 1697-1718.
- Griffin, S.L., Herzerfeld, M., Hamilton, D.P., 2001. Modelling the impact of zooplankton grazing on phytoplankton biomass during a dinoflagellate bloom in the Swan River Estuary, Western Australia. *Ecological Engineering*, **16**: 373-394.
- Hipsey, M.R., Salmon, S.U., Aldrige, K.T. and Brookes, J.D., 2010. Impact of hydro-climatological change and flow regulation on physical and biogeochemical dynamics of the Lower River Murray, Australia. *8th International Symposium on Ecohydraulics (ISE2010)*, September, 2010, Korea.
- Hipsey, M.R., and Hamilton, D.P., 2008. The Computational Aquatic Ecosystem Dynamics Model (CAEDYM): v3 Science Manual. Centre for Water Research Technical Report, Perth, Australia.
- Jassby, A.D., Platt, T., 1976. Mathematical formulation of the relationship between photosynthesis and light for phytoplankton. *Limnology and Oceanography* 21 (4), 540–547.
- Jellison, R. & Melack, J.M. 1993. Meromixis and vertical diffusivities in hypersaline Mono Lake, California. *Limnol. Oceanogr.* **38**: 1008–1019.
- Kilminster et al., 2011. Unpublished data.
- Kirk, J.T.O .1994. Light and Photosynthesis in Aquatic Ecosystems. Cambridge University Press.
- Klepper, O., Peters, J.C.H., Van de Kamer, J.P.G., Eilers, P., 1988. The calculation of primary production in an estuary. A model that incorporates the dynamic response of algae, vertical mixing and basin morphology. In: Marani, A. (Ed.), Advances in Environmental Modelling. Elsevier, pp. 373–394.
- Kromkamp, J. & Walsby, A.E. 1990. A computer model of buoyancy and vertical migration in cyanobacteria. *J. Plankton Res.* **12**: 191–183.
- Kruger, G.H.J. and J.N. Eloff. 1977. The influence of light intensity on the growth of different *Microcystis* isolates. *J. Limnol. Soc. Sth Africa*. **3**: 21-25.

- Monod (1950). Monod, J., 1950. La technique de culture continue. théorie et applications. *Annales de L Institut Pasteur* 79, 390–410.
- Mooij, W.M., Trolle, D., Jeppesen, E., Arhonditsis, G., Belolipetsky, P.V., Chitamwebwa, D.B.R., Degermendzhy, A.G., DeAngelis, D.L., De Senerpont Domis, L.N., Downing, A.S., Elliott, A.E., Fragoso Jr, C.R., Gaedke, U., Genova, S.N., Gulati, R.D., Håkanson, L., Hamilton, D.P., Hipsey, M.R., Hoen, J., Hülsmann, S., Los, F.J., Makler-Pick, V., Petzoldt, T., Prokopkin, I.G., Rinke, K., Schep, S.A., Tominaga, K., Van Dam, A.A., Van Nes, E.H., Wells, S.A., Janse, J.H., 2010. Challenges and opportunities for integrating lake ecosystem modelling approaches, *Aquatic Ecology*, **44**: 633–667.
- Petrone K.C. Richards, J.S. and Grierson, P.F., 2009. Bioavailability and composition of dissolved organic carbon and nitrogen in a near coastal catchment of south-western Australia. *Biogeochemistry*, **92**: 27–40.
- Romero, J.R., Antenucci, J.P., & Imberger, J. 2004. One- and Three- Dimensional biogeochemical Simulations of Two Differing Reservoirs. *Ecol. Model.*.
- Riley, J.P. & Skirrow, G.. 1974. Chemical Oceanography Academic Press, London.
- Robarts, R.D. and T. Zohary. 1987. Temperature effects on photosynthetic capacity, respiration and growth rates of bloom forming cyanobacteria. *N.Z. J Mar. Freshwater Res.* **21**: 391-399.
- Schladow, S.G. & Hamilton, D.P. 1997 Water quality in lakes and reservoirs. Part II Model calibration, sensitivity analysis and application. *Ecol. Model.* **96**: 111–123.
- Rhee, G.Y. & Gotham, E.J. 1981 The effect of environmental factors on phytoplankton growth: temperature and the interactions of temperature with nutrient limitation. *Limnol. Oceanogr.* **26**, pp. 635–648.
- Smith, C.S., Haese, R.R. and Evans, S. 2010. Oxygen demand and nutrient release from sediments in the upper Swan River estuary. Geoscience Australia Record, 2010/28. Commonwealth Government, Canberra.
- Smith, C.S., Murray, E.J., Hepplewhite, C. and Haese, R.R. (2007. Sediment water interactions in the Swan River estuary: Findings and management implications from benthic nutrient flux surveys, 2000-2006. Geoscience Australia Record 2007/13.
- Steele, J.H., 1962. Environmental control of photosynthesis in the sea. *Limnology and Oceanography* 7, 137–150.
- Spillman, C.M., Hamilton, D.P., Hipsey, M.R. and Imberger, J., 2008. A spatially resolved model of seasonal variations in phytoplankton and clam (*Tapes philippinarum*) biomass in Barbamarco Lagoon, Italy, *Estuarine, Coastal and Shelf Science*, **79**: 187-203.
- Spillman, C.M., Imberger, J., Hamilton, D.P., Hipsey, M.R. and Romero, J.R., 2007. Modelling the effects of Po River discharge, internal nutrient cycling and hydrodynamics on biogeochemistry of the Northern Adriatic Sea. *Journal of Marine Systems*, **68**: 127-200.
- Talling, J. F. 1957. The phytoplankton population as a compound photosynthetic system. *New Phytol.* **56**: 133-149
- Trolle, D., Hamilton, D.P., Hipsey, M.R., Bolding, K., Bruggeman, J., Mooij, W. M., Janse, J. H., Nielsen, A., Jeppesen, E., Elliott, J. E., Makler-Pick, V., Petzoldt, T., Rinke, K., Flindt, M. R., Arhonditsis, G.B., Gal, G., Bjerring, R., Tominaga, K., Hoen, J., Downing, A. S., Marques, D. M., Fragoso Jr, C. R., Søndergaard, M. and Hanson, P.C. 2012. A community-based framework for aquatic ecosystem models. *Hydrobiologia*, 683(1): 25-34.
- Wanninkhof, R.. 1992. Relationship between windspeed and gas exchange over the ocean. *J. Geophys. Res. (Oceans)* **97**(C5): 7373–7382.
- Webb, W.L., Newton, M., & Starr, D. 1974. Carbon dioxide exchange of *Alnus rubra*: a mathematical model. *Oecologia* **17**: 281–291.

Appendix L Final Calibration Parameters

- **Table L-1 Summary of Oxygen Parameter Descriptions, Units and Values**

Parameter	Description	Units	Value
oxy_initial	Initial concentration of dissolved oxygen	mmol O/m ³	225
Ksed_oxy	Half saturation constant for oxygen dependence of sediment oxygen flux	mmol O/m ³	25
theta_sed_oxy	Temperature multiplier for temperature dependence of sediment oxygen flux	-	1.08

- **Table L-2 Summary of Silica Parameter Descriptions, Units and Values**

Parameter	Description	Units	Value
rsi_initial	Initial reactive silica (SiO ₂) concentration	mmol Si/m ³	12.5
Ksed_rsi	Half saturation constant for oxygen dependence of sediment silica flux	mmol Si/m ³	25
theta_sed_rsi	Temperature multiplier for temperature dependence of sediment silica flux	-	1.08

- **Table L-3 Summary of Nitrogen Parameter Descriptions, Units and Values**

Parameter	Description	Units	Value
amm_initial	Initial concentration of ammonium	mmol N/m ³	12.5
nit_initial	Initial concentration of nitrate	mmol N/m ³	27.6
Rnitrif	Maximum rate of nitrification	/day	0.3
Rdenit	Maximum rate of denitrification	/day	1.25
Knitrif	Half saturation constant for oxygen dependence of nitrification rate	mmol O/m ³	78.1
Kdenit	Half saturation constant for oxygen dependence of denitrification rate	mmol O/m ³	5
Ksed_amm	Half saturation constant for oxygen dependence of sediment ammonium flux	mmol N/m ³	25
Ksed_nit	Half saturation constant for oxygen dependence of sediment nitrate flux	mmol N/m ³	25
theta_nitrif	Temperature multiplier for temperature dependence of nitrification rate	-	1.08
theta_denit	Temperature multiplier for temperature dependence of denitrification rate	-	1.08
theta_sed_amm	Temperature multiplier for temperature dependence of sediment ammonium flux	-	1.08
theta_sed_nit	Temperature multiplier for temperature dependence of sediment nitrate flux	-	1.08

Water Quality Modelling of the Hawkesbury-Nepean River System

■ Table L-4 Summary of Phosphorus Parameter Descriptions, Units and Values

Parameter	Description	Units	Value
frp_initial	Initial concentration of filterable reactive phosphorus (PO4)	mmol P/m ³	0.25
Ksed_frp	Temperature multiplier for temperature dependence of sediment phosphate flux	mmol P/m ³	30
theta_sed_frp	Temperature multiplier for temperature dependence of sediment phosphate flux	-	1.08
Kadsratio	Ratio of adsorption and desorption rate coefficients	-	0.0217
Qmax	Equilibrium adsorption concentration	mmol P/m ³ per mg/L SS	0.825
w_po4ads	Settling velocity of adsorbed phosphorus	m/d	-1.2

■ Table L-5 Summary of Organic Matter Parameter Descriptions, Units and Values

Parameter	Description	Units	Value
pon_initial	Initial concentration of particulate organic nitrogen	mmol N/m ³	70
don_initial	Initial concentration of dissolved organic nitrogen	mmol N/m ³	50
w_pon	Settling rate of particulate organic nitrogen	m/day	-0.25
Rpon_miner	Maximum rate of mineralisation of particulate organic nitrogen	/d	0.2
Rdon_miner	Maximum rate of mineralisation of dissolved organic nitrogen	/d	0.01
Kpon_miner	Half saturation constant for oxygen dependence of mineralisation rate	mmol O/m ³	31.25
Kdon_miner	Half saturation constant for oxygen dependence of mineralisation rate	mmol O/m ³	31.25
Ksed_don	Half saturation constant for oxygen dependence of sediment dissolved organic nitrogen flux	mmol N/m ³	4.5
theta_pon_miner	Temperature multiplier for temperature dependence of mineralisation rate	-	1.08
theta_don_miner	Temperature multiplier for temperature dependence of mineralisation rate	-	1.08
theta_sed_don	Temperature multiplier for temperature dependence of sediment dissolved organic nitrogen flux	-	1.08
pop_initial	Initial concentration of particulate organic phosphorus	mmol P/m ³	10
dop_initial	Initial concentration of dissolved organic phosphorus	mmol P/m ³	10
w_pop	Settling rate of particulate organic phosphorus	m/day	-0.25
Rpop_miner	Maximum rate of mineralisation of particulate organic phosphorus	/d	0.01



Water Quality Modelling of the Hawkesbury-Nepean River System

Parameter	Description	Units	Value
Rdop_miner	Maximum rate of mineralisation of dissolved organic phosphorus	/d	0.012
Kpop_miner	Half saturation constant for oxygen dependence of mineralisation rate	mmol O/m ³	31.25
Kdop_miner	Half saturation constant for oxygen dependence of mineralisation rate	mmol O/m ³	31.25
Ksed_dop	Half saturation constant for oxygen dependence of sediment dissolved organic phosphorus flux	mmol P/m ³	40.5
theta_pop_miner	Temperature multiplier for temperature dependence of mineralisation rate	-	1.08
theta_dop_miner	Temperature multiplier for temperature dependence of mineralisation rate	-	1.08
theta_sed_dop	Temperature multiplier for temperature dependence of sediment dissolved organic phosphorus flux	-	1.08
poc_initial	Initial concentration of particulate organic carbon	mmol C/m ³	80
doc_initial	Initial concentration of dissolved organic carbon	mmol C/m ³	700
w_poc	Settling rate of particulate organic matter	m/day	-0.05
Rpoc_miner	Maximum rate of mineralisation of particulate organic carbon	/d	0.001
Rdoc_miner	Maximum rate of mineralisation of dissolved organic carbon	/d	0.001
Kpoc_miner	Half saturation constant for oxygen dependence of mineralisation rate	mmol O/m ³	31.25
Kdoc_miner	Half saturation constant for oxygen dependence of mineralisation rate	mmol O/m ³	31.25
Ksed_doc	Half saturation constant for oxygen dependence of sediment dissolved organic carbon flux	mmol C/m ³	4.5
theta_poc_miner	Temperature multiplier for temperature dependence of mineralisation rate	-	1.08
theta_doc_miner	Temperature multiplier for temperature dependence of mineralisation rate	-	1.08
theta_sed_doc	Temperature multiplier for temperature dependence of sediment dissolved organic carbon flux	-	1.08
KeDOM	Light extinction coefficient for dissolved organic matter	mmol ⁻¹ m ³ m ⁻¹	0.0005
KePOM	Light extinction coefficient for particulate organic matter	mmol ⁻¹ m ³ m ⁻¹	0.001



Water Quality Modelling of the Hawkesbury-Nepean River System

■ **Table L-6 Summary of Sediment Flux Parameter Descriptions, Units and Values**

Parameter	Description	Units	Value										
			D/S Spencer - Webbs Ck	Webbs Ck - Sackville	Sackville - South Ck	Macdonald River - Colo Ck	South Ck	South Ck - Penrith Weir	Penrith Weir - Wallacia	Mangrove Ck - Mangroves	Eastern Ck	Wallacia Weir - Camden Weir	Penrith Weir U/S and D/S
Fsed_oxy	Maximum flux of oxygen across the sediment water interface into the sediment	mmol O/m ² /d	-5	-5	-5	-5	-5	-5	-5	-5	-5	-5	-5
Fsed_rsi	Maximum flux of silica across the sediment water interface into the sediment	mmol si/m ² /d	0	0	0	0	0	0	0	0	0	0	0
Fsed_amm	Maximum flux of ammonium across the sediment water interface into the sediment	mmol N/m ² /d	0.7	0.7	1.9	0.7	1.9	-0.23	0	0.7	1.9	0.7	0.7
Fsed_nit	Maximum flux of nitrate across the sediment water interface into the sediment	mmol N/m ² /d	-0.2	-0.2	-0.305	-0.2	-0.305	-3.28	-0.4	-0.2	-0.305	-0.2	-0.2
Fsed_frp	Maximum flux of phosphate across the sediment water interface into the sediment	mmol P/m ² /d	-0.004	0.015	0.14	0.015	1	0	0	0	0.5	0	0
Fsed_pon	Maximum flux of particulate organic nitrogen across the sediment water interface into the sediment	mmol N/m ² /d	0	0	0	0	0	0	0	0	0	0	0
Fsed_don	Maximum flux of dissolved organic nitrogen across the sediment water interface into the sediment	mmol N/m ² /d	2	3	2	3	2	-3.051	1.5	3	2	3	3

SINCLAIR KNIGHT MERZ



Water Quality Modelling of the Hawkesbury-Nepean River System

Parameter	Description	Units	Value										
			D/S Spencer - Webbs Ck	Webbs Ck - Sackville	Sackville - South Ck	Macdonald River - Colo Ck	South Ck	South Ck - Penrith Weir	Penrith Weir - Wallacia	Mangrove Ck - Mangroves	Eastern Ck	Wallacia Weir - Camden Weir	Penrith Weir U/S and D/S
Fsed_pop	Maximum flux of particulate organic phosphorus across the sediment water interface into the sediment	mmol P/m ² /d	0	0	0	0	0	0	-0.1	0	0	0	0
Fsed_dop	Maximum flux of dissolved organic phosphorus across the sediment water interface into the sediment	mmol P/m ² /d	0	0.024	-0.005	0.024	-0.005	-0.063	-0.1	0	-0.005	0	0
Fsed_poc	Maximum flux of particulate organic carbon across the sediment water interface into the sediment	mmol C/m ² /d	-0.08	-0.08	-0.08	-0.08	-0.08	-0.08	-0.08	-0.08	-0.08	-0.08	-0.08
Fsed_doc	Maximum flux of dissolved organic carbon across the sediment water interface into the sediment	mmol C/m ² /d	0	0	0	0	0	0	0	0	0	0	0



Water Quality Modelling of the Hawkesbury-Nepean River System

▪ **Table L-7 Summary of Phyto Parameter Descriptions, Units and Values**

Parameter	Description	Units	Value			
p_name	Name of phytoplankton group	-	Green	Blue-green	Freshwater diatom	Marine water-diatom
p_initial	Initial concentration of phytoplankton	mmol C/m ³	10	10	10	10
p0	Minimum concentration of phytoplankton	mmol C/m ³	0.2	0.2	0.2	0.2
w_p	Sedimentation rate	m/d	0	0	-0.2	-0.2
Ycc	Carbon to chlorophyll ratio	mg C/mg chla	50	40	50	50
R_growth	Phyto max growth rate @20C	/d	1.8	1.2	3.3	3.3
theta_growth	Arrhenius temperature scaling for growth function	-	1.06	1.06	1.05	1.05
T_std	Standard temperature	deg C	18	23	12	12
T_opt	Optimum temperature	deg C	23	28	16	16
T_max	Maximum temperature	deg C	35	38	23	23
I_K	Half saturation constant for light limitation of growth	μE/m ² /s	180	150	200	200
I_S	Saturating light intensity	μE/m ² /s	100	120	100	100
KePHY	Specific attenuation coefficient	(mmol C m ⁻³) ⁻¹ m ⁻¹	0.00408	0.0051	0.0048	0.0048
f_pr	Fraction of primary production lost to exudation	-	0.025	0.025	0.025	0.025
R_resp	Phytoplankton respiration/metabolic loss rate @ 20	(degC)	0.02	0.02	0.03	0.0375
theta_resp	Arrhenius temperature scaling factor for respiration	-	1.04	1.04	1.09	1.09
k_fres	Fraction of metabolic loss that is true respiration	-	0.7	0.7	0.7	0.7
k_fdom	Fraction of metabolic loss that is DOM	-	0.3	0.3	0.3	0.3
S_bep	Salinity limitation value at maximum salinity S_maxsp	-	1	5	1	5
S_maxsp	Maximum salinity	g/kg	36	16	36	40

SINCLAIR KNIGHT MERZ



Water Quality Modelling of the Hawkesbury-Nepean River System

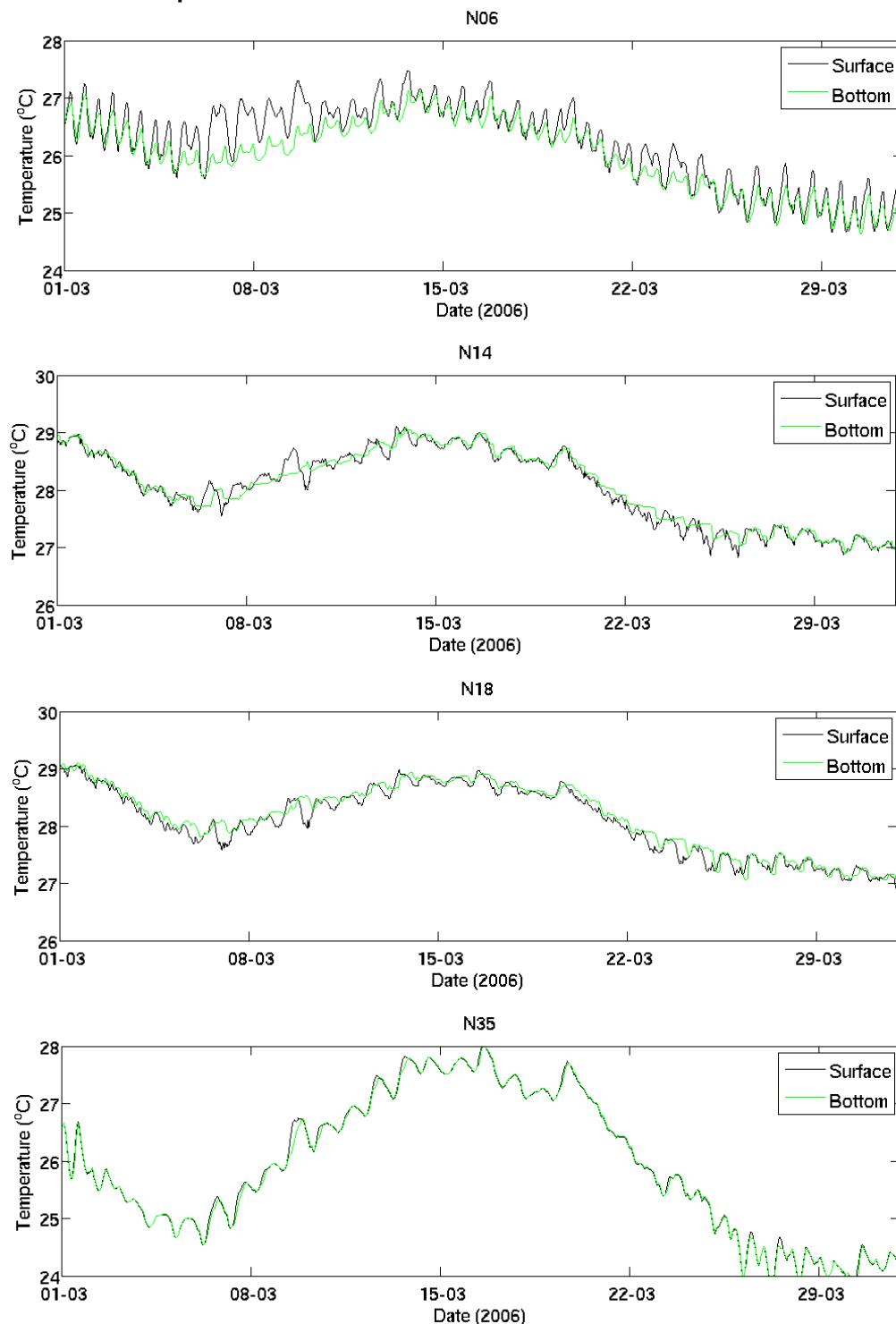
Parameter	Description	Units	Value			
S_opt	Optimal salinity	g/kg	1	1	1	33
N_o	Nitrogen concentration below which uptake is 0	mmol N/m ³	0.071	0.071	0.071	0.071
K_N	Half-saturation concentration of nitrogen	mmol N/m ³	1.786	2.143	2.5	1.6
X_ncon	Constant internal nitrogen concentration	mmol N/ mmol C	0.151	0.151	0.151	0.137
R_nuptake	Maximum nitrogen uptake rate	mmol N/m ³ /d	0.069	0.032	0.257	0.206
k_nfix	Growth rate reduction under maximum nitrogen fixation	/d	0.7	0.7	0.7	0.7
R_nfix	Nitrogen fixation rate	mmol N/mmol C/day	0.0006	0.00075	0.0006	0.0006
P_0	Phosphorus concentration below which uptake is 0	mmol P/m ³	0.0645	0.0645	0.0645	0.0645
K_P	Half-saturation concentration of phosphorus	mmol P/m ³	0.3226	0.1935	0.1935	0.1935
X_pcon	Constant internal phosphorus concentration	mmol P/ mmol C	0.0094	0.0094	0.0039	0.0039
R_puptake	Maximum phosphorus uptake rate	mmol P/m ³ /d	0.0031	0.0019	0.0015	0.0023
Si_0	Silica concentration below which uptake is 0	mmol Si/m ³	0	0	0	0
K_Si	Half-saturation concentration of silica	mmol Si /m ³	8	8	15.7143	3.9
X_sicon	Constant internal silica concentration	mmol Si/mmol C	0.0171	0.0214	0.1029	0.1096

■ **Table L-8 Summary of Pathogen Parameter Descriptions, Units and Values**

Parameter	Description	Value			Units
		Crypto	Ecoli	Totalcoli	
p_name	See Appendix N Hipsey et al. publication	Crypto	Ecoli	Totalcoli	See Appendix N Hipsey et al. publication
coef_mort_kd20		0.03	0.48	0.34	
coef_mort_theta		1.08	1.08	1.11	
coef_mort_c_SM		0.00	2e-10	2e-7	
coef_mort_alpha		0.0	6.1	4.2	
coef_mort_beta		0.0	0.25	0.25	
coef_mort_c_PHM		0.0	50.0	50.0	
coef_mort_K_PHM		0.0	6.0	6.0	
coef_mort_delta_M		0.0	4.0	4.0	
coef_mort_fdoc		0.0	0.5	0.5	
coef_light_kb_vis		0.000	0.097	0.097	
coef_light_kb_uva		0.00	1.16	1.16	
coef_light_kb_uvب		0.00	36.4	36.4	
coef_light_cSb_vis		0.0067	0.0067	0.0067	
coef_light_cSb_uva		0.0067	0.0067	0.0067	
coef_light_cSb_uvب		0.0067	0.0067	0.0067	
coef_light_kDOB_vis		0.5	0.5	0.5	
coef_light_kDOB_uva		0.5	0.5	0.5	
coef_light_kDOB_uvب		0.5	0.5	0.5	
coef_light_cpHb_vis		10.0	10.0	10.0	
coef_light_cpHb_uva		10.0	10.0	10.0	
coef_light_cpHb_uvب		10.0	10.0	10.0	
coef_light_KpHb_vis		5.0	5.0	5.0	
coef_light_KpHb_uva		5.0	5.0	5.0	
coef_light_KpHb_uvب		5.0	5.0	5.0	
coef_light_delb_vis		3.0	3.0	3.0	
coef_light_delb_uva		3.0	3.0	3.0	
coef_light_delb_uvب		3.0	3.0	3.0	
coef_pred_kp20		0.0	0.2	0.2	
coef_pred_theta_P		1.00	1.04	1.04	
coef_sett_fa		0.0	0.94	0.81	
coef_sett_w_path		0.0	0.0	0.0	

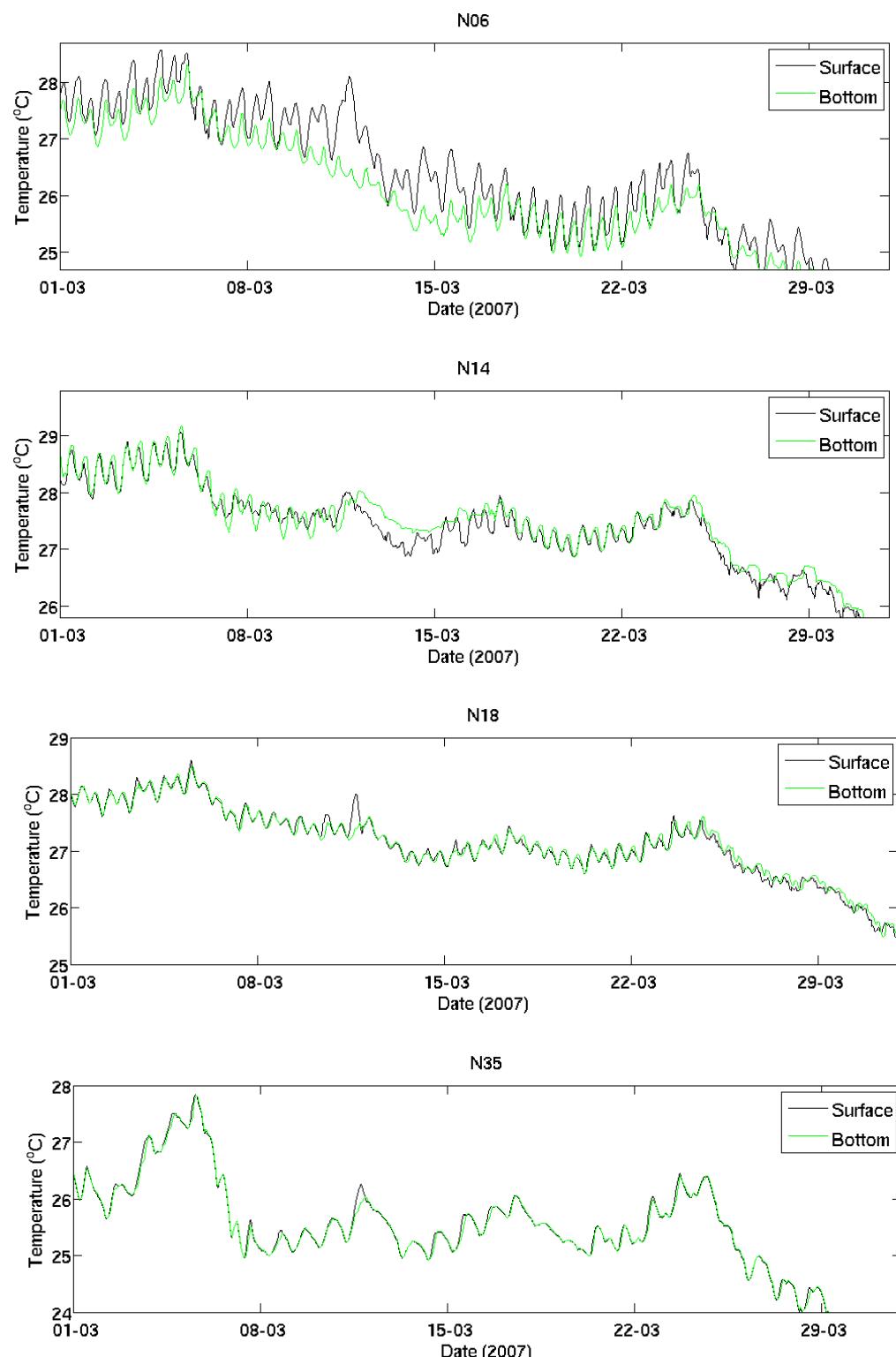
Appendix M Diurnal Fluctuations

M-1 Diurnal Temperature Fluctuations



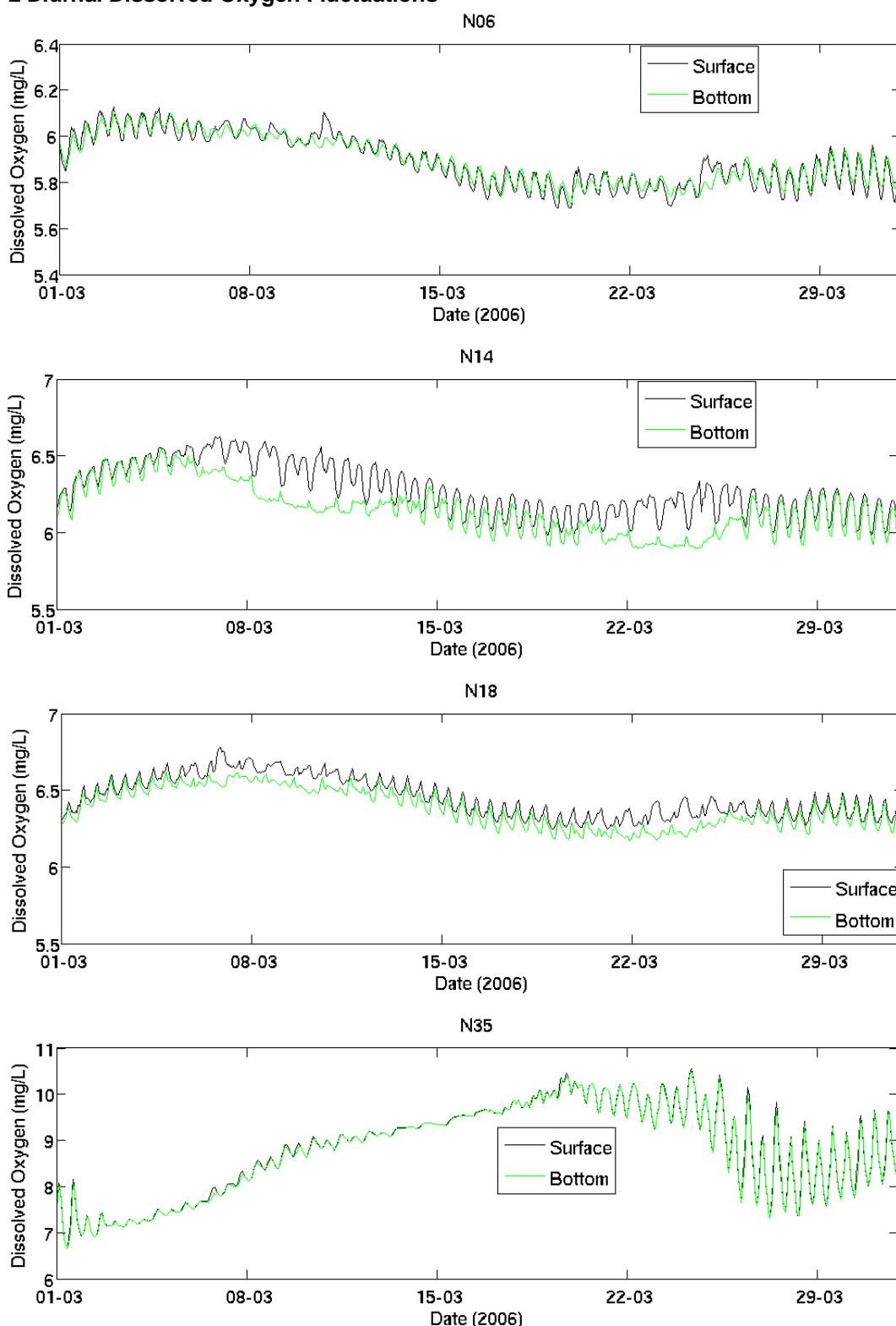
- **Figure B- 1 Daily Fluctuations of Temperature at Sites N06, N14, N18, and N35 – March 2006.**

Water Quality Modelling of the Hawkesbury-Nepean River System



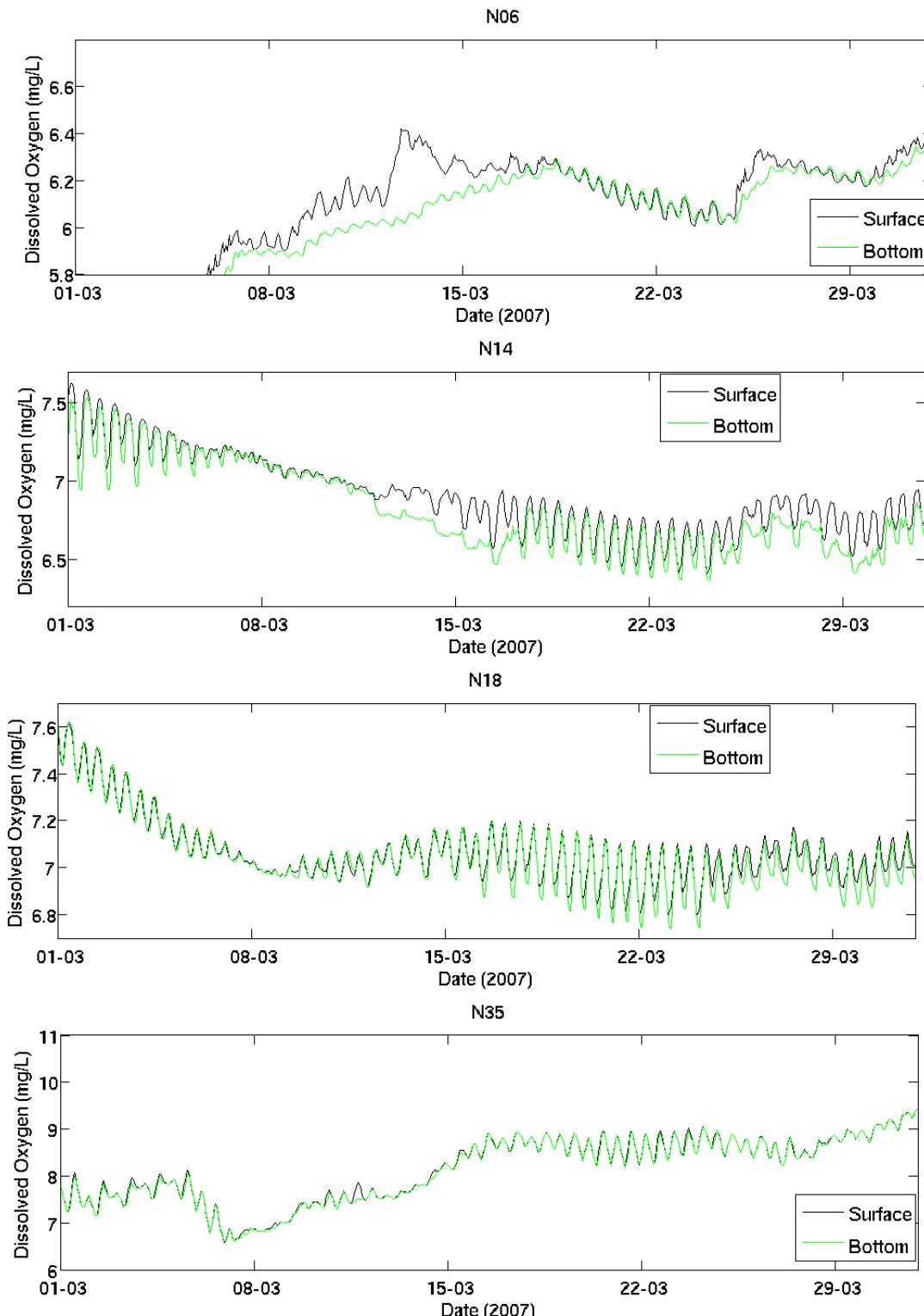
■ **Figure B- 2 Daily Fluctuations of Temperature at Sites N06, N14, N18, and N35 – March 2007**

M-2 Diurnal Dissolved Oxygen Fluctuations



- **Figure B- 3 Daily Fluctuations of Dissolved Oxygen at Sites N06, N14, N18, and N35 – March 2006**

Water Quality Modelling of the Hawkesbury-Nepean River System



- **Figure B- 4 Daily Fluctuations of Dissolved Oxygen at Sites N06, N14, N18, and N35 – March 2007**

Appendix N Bacterial Model Publication

A generic, process-based model of microbial pollution in aquatic systems

Matthew R. Hipsey,¹ Jason P. Antenucci,¹ and Justin D. Brookes^{2,3}

Received 31 July 2007; revised 16 January 2008; accepted 12 March 2008; published 17 July 2008.

[1] Based on a comprehensive synthesis of data available within the literature, a new process-based model of microbial pollution is presented, which is applicable for surface and coastal waters. The model is based on a generic set of parameterisations that describe the dynamics of most protozoan, bacterial and viral organisms of interest, including pathogens and microbial indicator organisms. The parameterisations dynamically account for the effects of temperature, salinity, pH, dissolved oxygen, sunlight, nutrients and turbidity on the growth and mortality of enteric organisms. Parameters for a range of organisms are also presented which are based on collation of literature data. The model has been implemented within an aquatic ecology model, Computational Aquatic Ecosystem Dynamics Model (CAEDYM), which can couple to multidimensional hydrodynamic models. Without adjustment of the literature derived parameter values, a 3-D implementation is validated against observed data from three freshwater systems that differ in their climatic zone, trophic status and operation. The simulations highlight the spatial and temporal variability that may be encountered by operators. Additionally, large differences in the fate and distribution of different species originate from variable rates of growth, mortality and sedimentation and it is emphasized that the use of surrogates for quantifying risk is problematic. The model can be used to help design targeted monitoring programs, explore differences between species, and to support real-time decision-making. Areas where insufficient understanding and data exist are discussed.

Citation: Hipsey, M. R., J. P. Antenucci, and J. D. Brookes (2008), A generic, process-based model of microbial pollution in aquatic systems, *Water Resour. Res.*, 44, W07408, doi:10.1029/2007WR006395.

1. Introduction

[2] Understanding and managing microbial pollution of surface waters is one of the foremost challenges presently facing the water industry. Generally, water management authorities routinely monitor concentrations of bacterial and viral organisms as indicators for actual pathogenic contamination. Certain bacterial and viral indicators may also be used as surrogates or models of pathogen behavior, for example in treatment processes or in natural environments. The indicator organisms themselves are mostly harmless, but due to the relative ease and cost of their measurement, they are monitored rather than direct measurement of the pathogen(s) of concern.

[3] Pathogens of concern vary between systems depending on the nature of the catchment and the intended use of the water. Because of their longevity and resistance to chemical disinfectants, the (oo)cysts of the protozoan organisms *Cryptosporidium* spp. and *Giardia* spp. are a typical concern in water bodies used for drinking water. In poorly

treated and recreational waters, other problem organisms include bacteria such as *Salmonella* spp., *Shigella* spp., *Vibrio* spp., *Clostridium* spp. and *Staphylococcus aureus* and numerous human enteric viruses such as those from the genera *Enterovirus*, *Hepatovirus*, *Rotavirus* and *Norovirus* [Fong and Lipp, 2006].

[4] The most widely used indicator organisms are the enteric coliform bacteria, which are gram-negative bacilli that belong to the family *Enterobacteriaceae* (e.g., *Klebsiella* spp., *Enterobacter* spp., *Citrobacter* spp., *Escherichia coli*). Specific coliform measurements include total coliforms, faecal coliforms, and in particular *E. coli*. The latter two are the most common since they are abundant in the faeces of humans and other warm blooded animals, and are hence thought to be a reliable indicator of faecal pollution. Total coliforms are used less frequently since they include organisms from soil and cold-blooded animals. Except for certain strains of pathogenic *E. coli* (e.g., O157), coliform bacteria are not a threat to human health, but their high abundance means that they are easy to detect, thereby alerting water authorities to pollution events that may contain other problem organisms. Other routinely used indicator bacteria include the gram-positive cocci, Enterococci and faecal streptococci, and spores of the gram-positive bacilli *Clostridium perfringens*. Viral indicators most commonly measured include the F-specific RNA (F⁺ RNA) bacteriophages (e.g., strains MS2 and F2) and somatic coliphages (e.g., strains T₂, T₇ and φX174).

¹Centre for Water Research, The University of Western Australia, Crawley, Western Australia, Australia.

²School of Earth and Environmental Sciences, The University of Adelaide, Adelaide, South Australia, Australia.

³CRC for Water Quality and Treatment, Salisbury, South Australia, Australia.

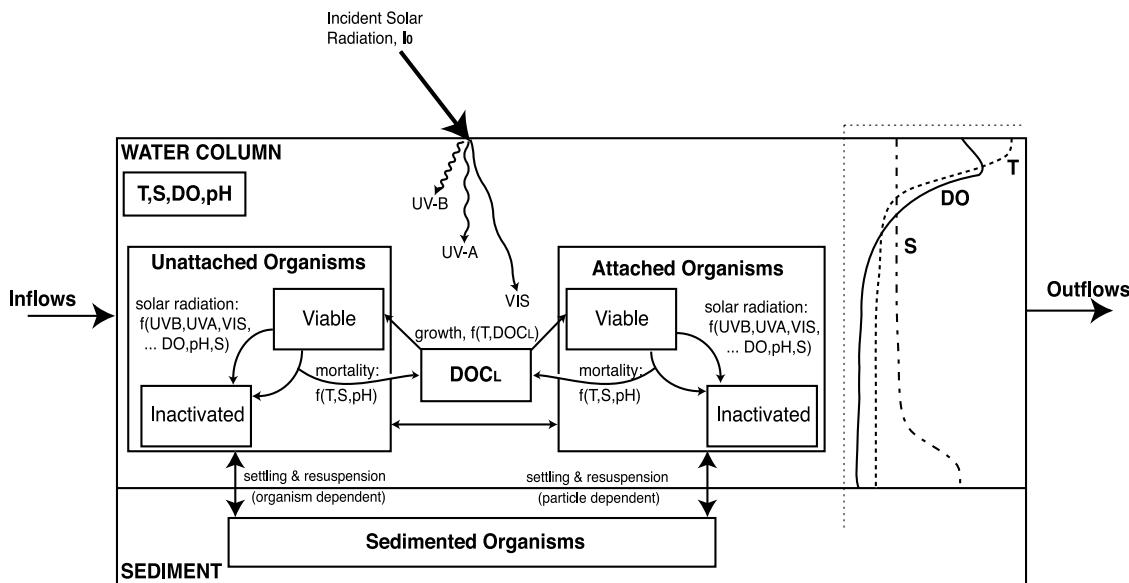


Figure 1. Schematic representation of processes simulated by the model.

[5] Although there are several decades of literature on the dynamics of enteric organisms in surface and coastal waters (for a review see Brookes *et al.* [2004], and Sinton [2005], respectively), most investigations that have aimed to quantify the kinetics of these organisms under different environmental conditions have focused on coliforms and *E. coli* in particular. Nonetheless, sufficient evidence exists to conclude that the various organism classes can exhibit markedly different behavior from one another once exposed to a range of environmental pressures, and consequently much debate exists on the reliability of “bioindicators” of pathogen exposure risk.

[6] The use of numerical models to augment existing monitoring and risk-management activities is becoming increasingly widespread since they are able to highlight dominant processes controlling organism dynamics, and can be used to fill knowledge gaps and test management scenarios. Such models have also been used to support real-time decision making by forecasting pathogen concentrations [e.g., Romero *et al.*, 2006]. There have been several models used to simulate different components of microbial pollution reported in the literature that range in sophistication and that are relevant for different surface water environments, including freshwater lakes and reservoirs [Auer and Niehaus, 1993; Walker and Stedinger, 1999; Jin *et al.*, 2003; Hipsey *et al.*, 2004, 2005], streams and rivers [Wilkinson *et al.*, 1995; Medema and Schijven, 2001], and estuaries and coastal lagoons [Salomon and Pommepuy, 1990; Steets and Holden, 2003; McCorquodale *et al.*, 2004]. However, it remains difficult for practitioners within the water industry to confidently implement these models, since they tend to be system or organism specific.

[7] From a modeling perspective, the dominant processes affecting organism fate and distribution are similar for most species; that is, all are subject to advection and mixing, mortality, sedimentation, etc., and so it is appealing to build a generic model for microbial pollutants. This requires that the parameterizations are based upon actual process descriptions with different responses of simulated species or groups achieved through appropriate modification of the kinetic

coefficients that account for their sensitivity to environmental parameters (e.g., temperature, salinity, light). The development of a common architecture for models of microbial pollution is attractive as it has the potential to encourage a nonsite specific standard parameter set for each species of interest, thereby allowing more confident model implementation and use by industry practitioners for a range of environments.

[8] In light of the above, the aims of this analysis are threefold. First, based on review of the available literature, a new model structure is presented that advances existing models and is generic for protozoan, bacterial and viral organisms. Second, collation of numerous literature data sources is presented to provide the current best estimates of parameter values and to highlight the key areas where data and knowledge gaps exist. Third, the model is applied to three different surface water systems without calibration and the performance evaluated against measured data sets.

2. Literature Review and Model Development

[9] Enteric organisms are susceptible to numerous stresses once they enter the aquatic environment and leave the warm, nutritious habitat within their mammalian hosts. These include biotic stresses from the autochthonous biota that may graze and compete for resources, and they may also be exposed to potentially harmful microbial exudates or infection. Abiotic pressures include inactivation by sunlight, and exposure to undesirable temperatures, salinities and pH. Numerous reviews on these factors are available, specific to fresh waters [Brookes *et al.*, 2004], and seawater [Sinton, 2005; Fayer and Trout, 2005; Gerba, 2005]. Should conditions be suitable, growth and multiplication may also occur (although this is less relevant to organisms such as the cyst forming protozoa, or the enteric viruses) and factors such as the scarcity of assimilable nutrients may become important.

[10] As the basis for the model presented herein, a general conceptual picture of the dynamics of pathogens and indicator organisms is presented (Figure 1). The model has been implemented as an optional module within the

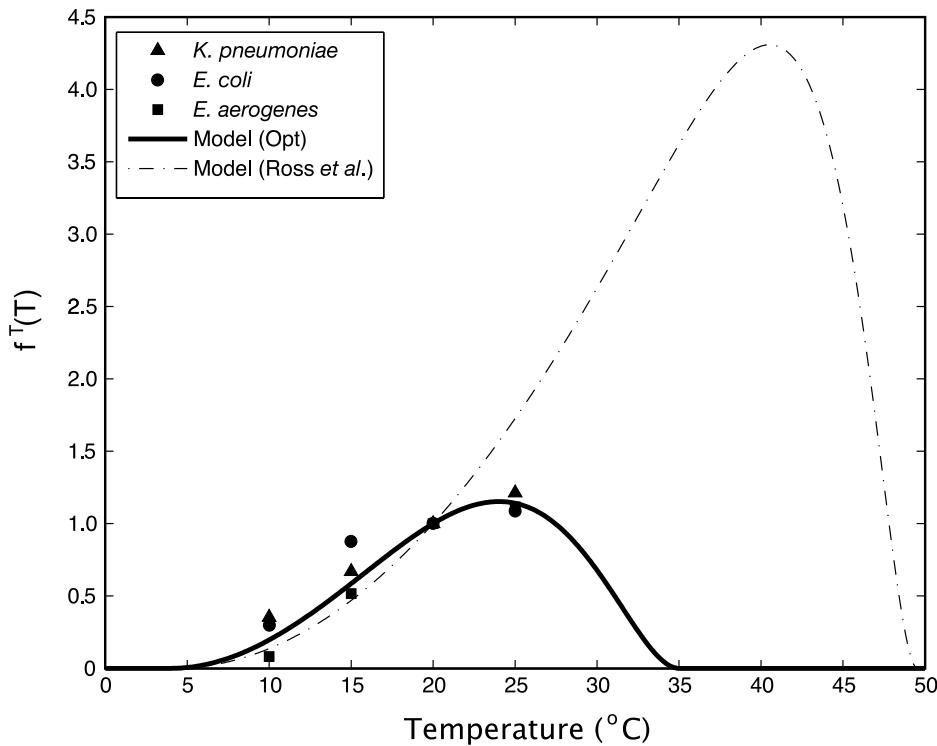


Figure 2. Coliform growth response as a function of temperature showing data from various species presented by Camper *et al.* [1991] and the present model (equation (2)) using parameters from Ross *et al.* [2003] and optimum parameters (Table 1) to fit the Camper *et al.* data.

larger Computational Aquatic Ecosystem Dynamics Model (CAEDYM), a freeware code that includes comprehensive descriptions of the light climate, phytoplankton and zooplankton dynamics, nutrient cycles (C, N, P, Si), dissolved oxygen (DO), pH and suspended sediment (SS) dynamics [Hipsey *et al.*, 2006b]. CAEDYM is a generic water quality model capable of dynamic coupling to range of hydrodynamic drivers, including 1, 2 and 3-D models of lakes and reservoirs [Romero *et al.*, 2004; Bruce *et al.*, 2006], rivers and estuaries [Chan *et al.*, 2002; Robson and Hamilton, 2004], and the coastal ocean [Spillman *et al.*, 2007; Hillmer and Imberger, 2007].

2.1. Growth

[11] The question of enteric organism population growth within natural aquatic systems has received little attention within the literature. Generally it is thought that in most coastal or surface water environments there are insufficient nutrients for enteric organisms to multiply, in addition to the numerous other environmental pressures. However, in wastewater treatment systems where nutrients are abundant, regrowth is frequently observed [Parhad and Rao, 1974; Liu, 2002], and it is therefore not surprising that nutrient pollution of natural waters has been seen to motivate growth of enteric organisms. Chamberlin and Mitchell [1978] observed a temperature dependent relationship between the percentage of a nutrient rich synthetic sewage medium mixed with seawater and the observed decay rate of coliform bacteria. Similarly, while experimenting on the influence of increased sewage nutrient concentrations on the die-off of a range of enteric organisms, Evison [1988] found that growth could be stimulated for certain organisms with as little as 2.5–25% sewage in both fresh and saline waters.

In their study, the growth response was only seen in the pathogenic bacteria, and not in *E. coli*. In a tropical coastal environment, Lopez-Torres *et al.* [1988] observed the coliforms *E. coli* and *Klebsiella pneumoniae* surviving and actively respiring in waters impacted by nutrient rich effluent. Aquatic sediments have also been identified as a region that can support growth of enteric bacteria due to heightened nutrient levels [Gerba and McLeod, 1976; Hood and Ness, 1982; LaLiberte and Grimes, 1982; Marino and Gannon, 1991; Davies *et al.*, 1995].

[12] Furthermore, there is mounting evidence to support the concept of growth of enteric bacteria within oligotrophic systems, both fresh and saline. As early as four decades ago, Hendricks and Morrison [1967] found a range of indicator and pathogenic enteric bacteria could grow and multiply in a low-nutrient, low-temperature environment characteristic of a cold mountain stream, and like Gerba and McLeod [1976] and Davies *et al.* [1995], they found that other processes such as competition and predation suppressed the biomass. More recently, Korhonen and Martikainen [1991], Camper *et al.* [1991], Ashbolt *et al.* [1995], Fujioka *et al.* [1999], Solo-Gabriele *et al.* [2000], Desmarais *et al.* [2002], and Byappanahalli *et al.* [2003] have demonstrated the ability of faecal indicator bacteria to grow in low-nutrient environmental waters, often in the absence of any recent faecal contamination.

[13] It is likely that growth is a complicating factor in many of the survival experiments reported within the literature and is responsible for some of the variability seen in laboratory and field determinations of decay rates. Under certain circumstances growth should therefore be resolved dynamically within a model, however, a model accounting

for growth in natural systems remains elusive, even for the well-studied coliform bacteria. A simple model for growth in a drinking water distribution system by *Dukan et al.* [1996] makes use of a maximum growth rate that is mediated by temperature and nutrient limitation functions, similar to those that may be used for simulating autochthonous organisms:

$$k_g = \mu_{MAX} f^T(T) f^{LIM}(N) \quad (1)$$

where k_g is the growth rate (day^{-1}), μ_{MAX} is the maximum growth rate at 20°C under no nutrient limitation, $f^T(T)$ is a function that mediates growth response to temperature, T , and $f^{LIM}(N)$ is the nutrient limitation function with N defined as the limiting substrate required for growth. The temperature function has not been well characterized, but it is known that temperature plays an important role and it has been noted that temperatures must exceed $15\text{--}18^\circ\text{C}$ before growth effects are noticeable [*Chamberlin and Mitchell*, 1978; *Ashbolt et al.*, 1995; *Dukan et al.*, 1996; *LeChevalier et al.*, 1996]. *Dukan et al.* [1996] used a simple exponential function of temperature dependence in their model of coliform growth in a drinking water system, although the function included no limitation at high temperatures. Within the food microbiology literature, *Salter et al.* [2000] and *Ross et al.* [2003] presented a more general expression for the temperature dependence of bacterial growth, which takes the form:

$$f^T(T) = \{c_{T_1}(T - T_{\min})(1 - \exp[c_{T_1}(T - T_{\max})])\}^2 \quad (2)$$

where c_T , T_{\min} and T_{\max} are species specific constants controlling the exact shape of the function. The function is specified to be 0 below T_{\min} and above T_{\max} and defined to be 1 at 20°C . A similar shaped function was presented by *Zanoni et al.* [1993] for enterococci. However, these functions were found to perform poorly against observations by *Camper et al.* [1991] and *Byappanahalli et al.* [2003] who measured growth rates of environmental strains of coliforms (Figure 2). On the basis of the *Camper et al.* [1991] observations, alternate parameter values for equation (2) were estimated using numerical techniques (Table 1). The optimal function however indicates no growth at a maximum temperature of 35°C which seems unreasonable given their affinity for warm-blooded animals and suggests an environmentally adapted strain (discussed below); more experimental data on growth response to temperature is required to extend this formulation above 30°C .

[14] In the simplest approximation, the nutrient limitation function assumes the common Michaelis-Menten form:

$$f^{LIM}(N) = \frac{N}{K_N + N} \quad (3)$$

where K_N is the half-saturation constant controlling the sensitivity to the substrate concentration. Although nitrogen and phosphorus and other macronutrients may become limiting, carbon has been identified as the predominant nutrient in oligotrophic systems that is required to stimulate growth [*Camper et al.*, 1991; *LeChevalier et al.*, 1996; *LeChevalier*, 2003; *van der Kooij*, 2003; *Bouteleux et al.*, 2005], or at least as a proxy for the availability of sufficient organic substrate including all the necessary elements for

growth. Of particular importance is the assimilable organic carbon fraction, which can be measured using the Assimilable Organic Carbon (AOC) or Biodegradable Dissolved Organic Carbon (BDOC) methods [*van der Kooij*, 2003]. In freshwaters, the assimilable fraction of a typical DOC measurement is $0.1\text{--}0.2 \text{ mg C L}^{-1}$ using the BDOC method, and $0.005\text{--}0.05 \text{ mg C L}^{-1}$ using the AOC method, although the fractions will vary depending on the predominant carbon sources for the site of interest (for example, autochthonous DOC generation through primary production generally has a higher labile component than allochthonous sources). Recently, *Bouteleux et al.* [2005] highlighted that the carbon source is significant in determining the growth rate of *E. coli*. Estimates of the maximum growth rate and half-saturation constant for *E. coli* and faecal coliforms (Table 1) are based on experiments by *Camper et al.* [1991], where growth was measured over a range of assimilable carbon concentrations at constant temperature. Depending on the species, maximum growth rates were $0.1\text{--}0.4 \text{ h}^{-1}$ and half-saturation constants were $0.05\text{--}0.24 \text{ mg C L}^{-1}$, and *Camper et al.* [1991] also highlight that strains within species show considerable differences. Qualitatively, the values reported here compare favorably with observations from *Dukan et al.* [1996], *LeChevalier et al.* [1996] and *Bouteleux et al.* [2005] who report that $0.1\text{--}0.3 \text{ mg L}^{-1}$ of assimilable organic carbon is required before coliform growth occurs.

[15] Combining equations (1)–(3), the growth equation is:

$$k_g = \mu_{MAX} \{c_{T_1}(T - T_{\min})(1 - \exp[c_{T_2}(T - T_{\max})])\}^2 \cdot \left(\frac{DOC_L}{K_{DOC_L} + DOC_L} \right) \quad (4)$$

where the assimilable carbon concentration is denoted DOC_L to distinguish from AOC.

[16] More advanced forms of the nutrient limitation function may be required for more specific applications. It is well established that organisms coming directly from enriched sources (e.g., wastewater discharges) tend to exhibit a shoulder in their decay curve; that is, a lag is often seen between their introduction and the log linear section of the die-off curve, the so-called maintenance and decay phases respectively [*Orlob*, 1956; *Mancini*, 1978; *Crane and Moore*, 1986; *Darakas*, 2002]. It has been shown experimentally by various authors that previous growth history can influence future performance in a nutrient depleted environment since bacteria are capable of accumulating a luxury store of nutrients [*Ghoul et al.*, 1990; *Gauthier et al.*, 1991]. This is an important dynamic to consider in risk assessments since the origin of the microbial pollution will influence its persistence once it has entered an aquatic system. For example, organisms from a raw sewage ocean outfall may enter the coastal environment enriched with nutrients and display the associated broad shoulder (and even growth) before first order decay is observed, whereas organisms washed in from a surrounding agricultural catchment may have been existing on minimal nutrients for some time before entering the water column and unable to maintain a significant level of growth. If a model is to capture this dynamic it must account for variability in internal nutrient stores and the nutrient limi-

Table 1. Summary of Parameters Required for the Model, With Typical Values Presented for 7 Organism Types^a

Parameter Description	Symbol	Units	Cryptosporidium oocysts (Cr)	Total Coliforms (TC)	Faecal Coliforms (FC)	<i>E. coli</i> (EC)	Enterococci (En)	F ⁺ RNA Phages (FP)	Values		Reference/Remarks
									Growth	Somatic Coliphages (SC)	
Potential growth rate at 20C	μ_{MAX}	day ⁻¹	NA	NI	2.4–3.6	2.4	NI	NI	NI	NI	Estimated from Camper et al. [1991]
Minimum temperature	T_{min}	°C	NA	NI	4	4	NI	NI	NI	NI	Estimated net growth rates
Maximum temperature	T_{max}	°C	NA	NI	35	35; 49.5	NI	NI	NI	NI	Estimated from Camper et al. [1991]
Growth temperature function shape parameter 1	c_{T1}	-	NA	NI	0.008	0.008; 0.279	NI	NI	NI	NI	data (Figure 2); Higher values for EC from Ross et al. [2003] in food studies.
Growth temperature function shape parameter 2	c_{T2}	-	NA	NI	0.1	0.1; 0.26	NI	NI	NI	NI	EC values from Camper et al. [1991]
Half-saturation constant for growth dependence on DOCL	K_{DOC_L}	mg DOC _L L ⁻¹	NA	NI	0.05–0.24	0.05–0.15	NI	NI	NI	NI	<u>data</u> , range highlights different response from environmental and clinical strains; FC values based on range of Camper et al. [1991] data for <i>K. pneumoniae</i> , <i>E. coli</i> and <i>Enterobacter</i> spp.
Mortality rate in <i>freshwater</i> at 20C	k_{d20}	day ⁻¹	0.03–0.08	0.34	0.71	0.48	0.45	0.34	0.16	0.16	Cr: Calculated from Walker and Stedinger [1999] expression, and King et al. [2005] data TC, FC, EC, En, FP, SC; Figure 3
Mortality temperature multiplier in <i>freshwater</i>	ϑ_M	-	1.14	1.11	1.06	1.11	1.04	1.10	1.01	1.01	Cr: Johnson et al. [1997] based on two measurements. Data scaled to 20°C assuming 1.14 multiplier. TC, FC, EC, En, FP, SC;
Mortality rate in <i>seawater</i> at 20C	k_{d20}	day ⁻¹	0.01	1.04	1.66	1.09	0.28	0.30	1.08	1.08	Figure 4: Note: not required model parameters, but may be used in place of salinity dependence expression for seawater only applications
Mortality temperature multiplier in <i>seawater</i>	ϑ_M	-	NI	1.05	1.10	1.09	1.06	1.02	1.05	1.05	Cr: Salinity has been implicated but insufficient data exists to characterize these parameters TC, FC, EC, En, FP, SC; Figure 5
Salinity effect on mortality	c_{S_M}	day ⁻¹ psu ⁻¹	NI	2e-7	2e-3	2e-10	0.0	0.0	1e-8	1e-8	Roughly estimated from Pommepuy et al. [1992] <i>Salmonella</i> data assuming 10% OM is labile for growth.
Parameter controlling salinity dependence	α	-	NI	4.2	1.8	6.1	0.0	0.0	5.0	5.0	EC, FC; Figure 6 SC; Rossi and Aragno [1999] reported no sensitivity to pH between 5–9
Parameter controlling effect of DOC on salinity induced mortality	β	-	NI	0.05–0.3	NI	NI	NI	NI	NI	0	Cr, TC, En, FP;
pH effect on mortality	c_{PH_M}	-	NI	NI	50	50	NI	NI	NI	0	insufficient information available
Parameter controlling pH dependence K_{PH_M}	-	NI	NI	6	6	NI	NI	NI	0	0	

Table 1. (continued)

Parameter Description	Symbol	Units	Cryptosporidium oocysts (Cr)	Total Coliforms (TC)	Faecal Coliforms (FC)	<i>E. coli</i> (EC)	Enterococci (En)	F ⁺ RNA Phages (FP)	Values		Reference/Remarks
									NI	0	
Parameter controlling pH dependence	δ	-	NI	NI	NI	NI	NI	NI	NI	0	Cr: Calculated from Figure 6 in King et al. [2008]
Inactivation effect of UV-B radiation	k_{UVB}	$m^2 MJ^{-1}$	33.7	NI	36.4	NI	NI	NI	21.1	54.7	Cr: Calculated from Figure 6 in King et al. [2008] FC, En, FP, SC: Calculated from data in Figure 5 of Sinton et al. [2002]
Salinity enhancement of UV-B radiation	$c_{S_{UVB}}$	$m^2 MJ^{-1} psu^{-1}$	NI	NI	0.0066	0.0067	0.0023	0.0033	0.0044	0.0044	FC, EC, En, FP, SC: Calculated from data in Table 4 of Sinton et al. [2002]
Half-saturation constant for the oxygen dependence of UV-B radiation	$K_{DO_{UVB}}$	mg DO L ⁻¹	NI	NI	2.0	0.5	0.1	0.05	NI	NI	FC: Estimated from Curtis et al. [1992a, 1992b] data EC, En, FP: estimated from Davies-Colley et al. [1999] data
pH enhancement of UV-B radiation	cPH_{UVB}	-	NI	NI	NI	NI	10.0	NI	NI	NI	EC: Estimated from Davies-Colley et al. [1999] data
Half-saturation constant for the pH dependence of UV-B radiation	$K_{PH_{UVB}}$	-	NI	NI	NI	NI	4.5	NI	NI	NI	EC: Estimated from Davies-Colley et al. [1999] data
Parameter controlling sensitivity of pH dependence of UV-B radiation	δ_{UVB}	-	NI	NI	NI	NI	3.0	NI	NI	NI	EC: Estimated from Davies-Colley et al. [1999] data
Inactivation effect of UV-A radiation	k_{UVA}	$m^2 MJ^{-1}$	2.3	NI	1.16	NI	16.9	0.73	6.7	Cr: Calculated from Figure 6 in King et al. [2008]	
Salinity enhancement of UV-A radiation	$c_{S_{UVA}}$	$m^2 MJ^{-1} psu^{-1}$	NI	NI	0.0066	0.0067	0.0023	0.0033	0.0044	0.0044	FC, EC, En, FP, SC: Calculated from data in Figure 5 of Sinton et al. [2002]
Half-saturation constant for the oxygen dependence of UV-A radiation	$K_{DO_{UVA}}$	mg DO L ⁻¹	NI	NI	2.0	0.5	0.1	0.05	NI	NI	FC: Calculated from data in Figure 5 of Sinton et al. [2002]
pH enhancement of UV-A radiation	cPH_{UVA}	-	NI	NI	NI	NI	10.0	NI	NI	NI	FC: Estimated from Curtis et al. [1992a, 1992b] data EC, En, FP: Estimated from Davies-Colley et al. [1999] data
Half-saturation constant for the pH dependence of UV-A radiation	$K_{PH_{UVA}}$	-	NI	NI	NI	NI	4.5	NI	NI	NI	EC: Estimated from Davies-Colley et al. [1999] data
Parameter controlling sensitivity of pH dependence of UV-A radiation	δ_{UVA}	-	NI	NI	NI	NI	3.0	NI	NI	NI	EC: Estimated from Davies-Colley et al. [1999] data
Inactivation effect of VIS radiation	k_{VIS}	$m^2 MJ^{-1}$	0.0	NI	0.097	NI	0.882	0.250	0.128	Cr: Calculated from Figure 6 in King et al. [2008]	
Salinity enhancement of VIS radiation	$c_{S_{VIS}}$	$m^2 MJ^{-1} psu^{-1}$	NI	NI	0.0066	0.0067	0.0023	0.0033	0.0044	0.0044	FC, EC, En, FP, SC: Calculated from data in Figure 5 of Sinton et al. [2002]
Half-saturation constant for the oxygen dependence of VIS radiation	$K_{DO_{VIS}}$	mg DO L ⁻¹	NI	NI	2.0	0.5	0.1	0.05	NI	NI	FC: Calculated from data in Figure 5 of Sinton et al. [2002]
pH enhancement of VIS radiation	cPH_{VIS}	-	NI	NI	NI	NI	10.0	NI	NI	NI	FC: Estimated from Curtis et al. [1992a, 1992b] data EC, En, FP: Estimated from Davies-Colley et al. [1999] data
Half-saturation constant for the pH dependence of VIS radiation	$K_{PH_{VIS}}$	-	NI	NI	NI	NI	4.5	NI	NI	NI	EC: Estimated from Davies-Colley et al. [1999] data
Parameter controlling sensitivity of pH dependence of VIS radiation	δ_{VIS}	-	NI	NI	NI	NI	3.0	NI	NI	NI	EC: estimated from Davies-Colley et al. [1999] data
Predation rate at 20°C	$k_{p_{20}}$	day ⁻¹	NI	NI	NI	NI	Predation	NI	NI	NI	NI
Temperature multiplier for predation rate	ϑ_P	-	NI	NI	NI	NI	NI	NI	NI	NI	NI

Table 1. (continued)

Parameter Description	Symbol	Units	Cryptosporidium oocysts (Cr)	Total Coliforms (TC)	Faecal Coliforms (FC)	<i>E. coli</i> (EC)	Enterococci (En)	F ⁺ RNA Phages (FP)	Values		Reference/Remarks
									Somatic Coliphages (SC)	Values	
Minimum concentration before enhanced predation		NI	NI	NI	NI	NI	NI	NI	NI	NI	
Predation rate dependence on prey concentration		NI	NI	NI	NI	NI	NI	NI	NI	NI	
Settling velocity of free organisms at 20°C	V_c	m day ⁻¹	0.025–0.035	0.0	0.0	0.0	0.0	0.0	0.0	0.0	Cr. Medema <i>et al.</i> [1998]; Dai and Boll [2006] TC, FC, EC, En, FP, SC: Settling of unattached organisms assumed to be negligible
Attached fraction	$f_{A_{water}}$	-	0.0	0.8	0.8–1.0	0.8–1.0	NI	0.5–1.0	0.5–1.0	0.5–1.0	Cr. Hipsey <i>et al.</i> [2004]; Dai and Boll [2003, 2006] all suggest oocysts exist in isolation TC, FC, EC: Hipsey <i>et al.</i> [2006a], Auer and Niehaus [1993] RP, DP; Rossi and Aragno [1999], Gerba and Schaitberger [1975], Payment <i>et al.</i> [1998]
Sediment attached fraction	$f_{A_{sed}}$	-	0.0	0.8	0.8–1.0	0.8–1.0	Resuspension	NI	0.5–1.0	0.5–1.0	Assumed to be similar to the water column
Resuspension rate of free organisms	α_C	orgs m ⁻² s ⁻¹	10 ⁴	NI	NI	NI	NI	NI	NI	NI	Cr. Estimated by Hipsey <i>et al.</i> [2004]
Critical shear stress of free organisms	τ_{c_c}	N m ⁻²	0.005	NI	NI	NI	NI	NI	NI	NI	Cr. Estimated by Hipsey <i>et al.</i> [2004]

^aNA = Not Applicable; NI = No Information available.

tation on growth should depend on the internal rather than the external (water column) nutrient concentration. Such a model must define uptake and excretion/mortality functions that are not in tandem with the growth and decline of the actual number of organisms, however a model of this nature is beyond the scope of the present study and is left for a separate analysis.

2.2. Natural Mortality

[17] Natural mortality, or the “dark-death rate”, k_d , is an important process influencing protozoan, bacterial and viral dynamics in surface and coastal waters. Across the literature there is a large amount of variation in the values assigned to the mortality rate, even for identical organisms [Chamberlin and Mitchell, 1978; Kapuscinski and Mitchell, 1980; Bitton et al., 1983; Crane and Moore, 1986; Auer and Niehaus, 1993; Mayo, 1995], which is not surprising considering the large range of environmental conditions that are covered by these studies. The predominant factors known to influence mortality include temperature, salinity, and pH, each discussed in more detail below. Other factors that have been studied include previous growth history [Munro et al., 1987; Gauthier et al., 1992], the nutritional status of the medium [Carlucci and Pramer, 1960b; Chamberlin and Mitchell, 1978; Lessard and Sieburth, 1983; Evison, 1988], the competitiveness of the autochthonous bacterial population [McCambridge and McMeekin, 1981; Flint, 1987; Medema et al., 1997; Gordon and Toze, 2003; Ottosson and Stenstrom, 2003], hydrostatic pressure and dissolved oxygen. With the exception of the last two, most of these factors are less relevant to mortality and relate to growth, as addressed previously. Dissolved oxygen concentrations can vary significantly within surface water and coastal water environments, although there has been little direct examination of the effect of oxygen on the mortality response from enteric organisms. The available studies indicate that oxygen sensitivity is weak [Pearson et al., 1987; Mayo, 1995; Curtis et al., 1992b], and it is thought to be more significant mediating the effect of sunlight-induced inactivation (addressed below).

[18] Various authors have attempted to develop models that disaggregate k_d to dynamically account for variability in temperature, salinity and pH [Klock, 1971; Chamberlin and Mitchell, 1978; Mancini, 1978; Mayo, 1995; McCorquodale et al., 2004], although they are mostly empirical or statistical and difficult to apply outside of the system for which they were developed. Such models have also only been applied to prediction of coliform dynamics and there is little available for other organisms. Here we attempt to develop a process-based description of these influences by taking a staged approach in developing the necessary parameterizations; this involves negating competing effects and estimating the individual components of $k_d = k_d(T, S, pH)$.

2.2.1. Temperature

[19] Metabolic processes increase as temperatures rise and the relationship between population decay and temperature in natural waters has been intensively studied for enteric protozoa [Naik *et al.*, 1982; deRegnier *et al.*, 1989; Robertson *et al.*, 1992; Medema *et al.*, 1997; Fayer *et al.*, 1998; Walker and Stedinger, 1999; King *et al.*, 2005], bacteria [Carlucci and Pramer, 1960a; Klock, 1971; Vasconcelos and Swartz, 1976; Mancini, 1978; Gould and Munro, 1981; Lantrip, 1983; Flint, 1987; Evison, 1988; Rhodes and Kator,

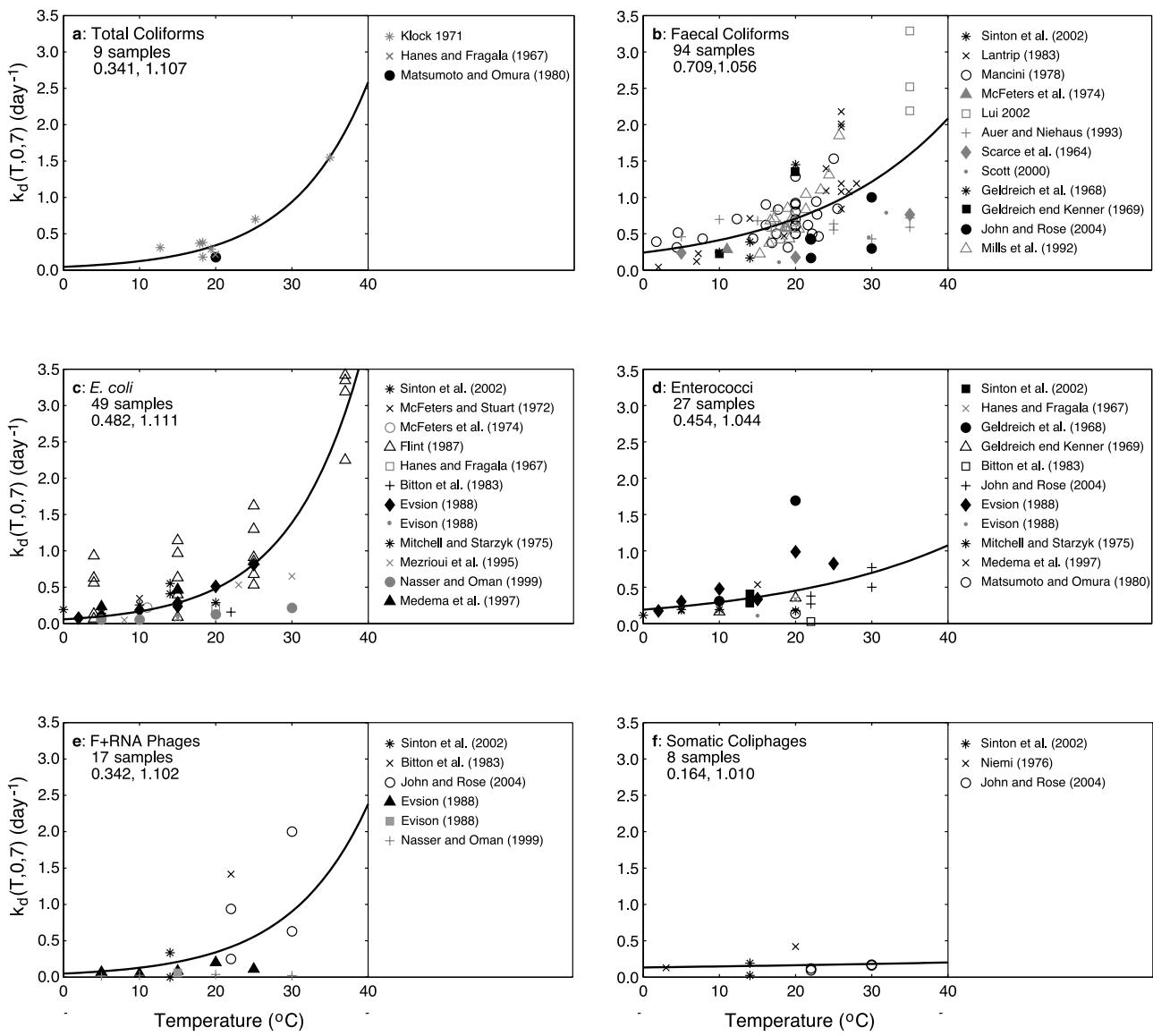


Figure 3. Variation of published natural mortality (“dark death”) rates as a function of temperature for 6 different organism groups. Only investigations from waters with salinity <3‰ and pH values between 6–8 were included. Data points collected from studies in a relatively nutrient rich medium are shown in gray and points collected from studies conducted within a nutrient poor medium are colored black. The solid line indicates the optimum fit to the data for equation (5) based on a least squares regression with all data and model parameters $k_{d_{20}}$ and ϑ_M are included.

1988; Mills et al., 1992; Solic and Krstulovic, 1992; Mezrioui et al., 1995; Sarikaya and Saatchi, 1995; Howell et al., 1996; Nasser and Oman, 1999; Craig et al., 2004] and viruses and phages [Niemi, 1976; O’Brien and Newman, 1977; McDaniels et al., 1983; Evison, 1988; Nasser and Oman, 1999; Rossi and Aragno, 1999]. As with many biological processes, the most convenient form for the loss rate, when salinity and pH are held constant, is the Arrhenius expression:

$$k_d(T) = k_{d_{20}} \vartheta_M^{T-20} \quad (5)$$

where T is temperature ($^{\circ}\text{C}$), $k_{d_{20}} = k_d(20)$ is the observed dark death rate at 20°C in fresh water and ϑ_M controls the sensitivity of k_d to temperature change.

[20] Collation of available data from the fresh water literature for the most commonly used microbial indicator organisms, (total coliforms, faecal coliforms, *E. coli*, enterococci/faecal streptococci, F^+ RNA phages and somatic coliphages), are shown in Figure 3. Data included in this plot were measured at salinities below 3‰ and pH values between 6 and 8 to negate any variability caused by salinity toxicity and either excessive acidity or alkalinity (each discussed separately below). Data points that were sourced from a nutrient enriched medium are separated to highlight that they tend to exhibit lower mortality (45 of 66 gray points fall below the average line). Enrichment status was a qualitative indicator based on the medium the researchers used to measure the die-off, with wastewater effluent being considered enriched and others considered not to be

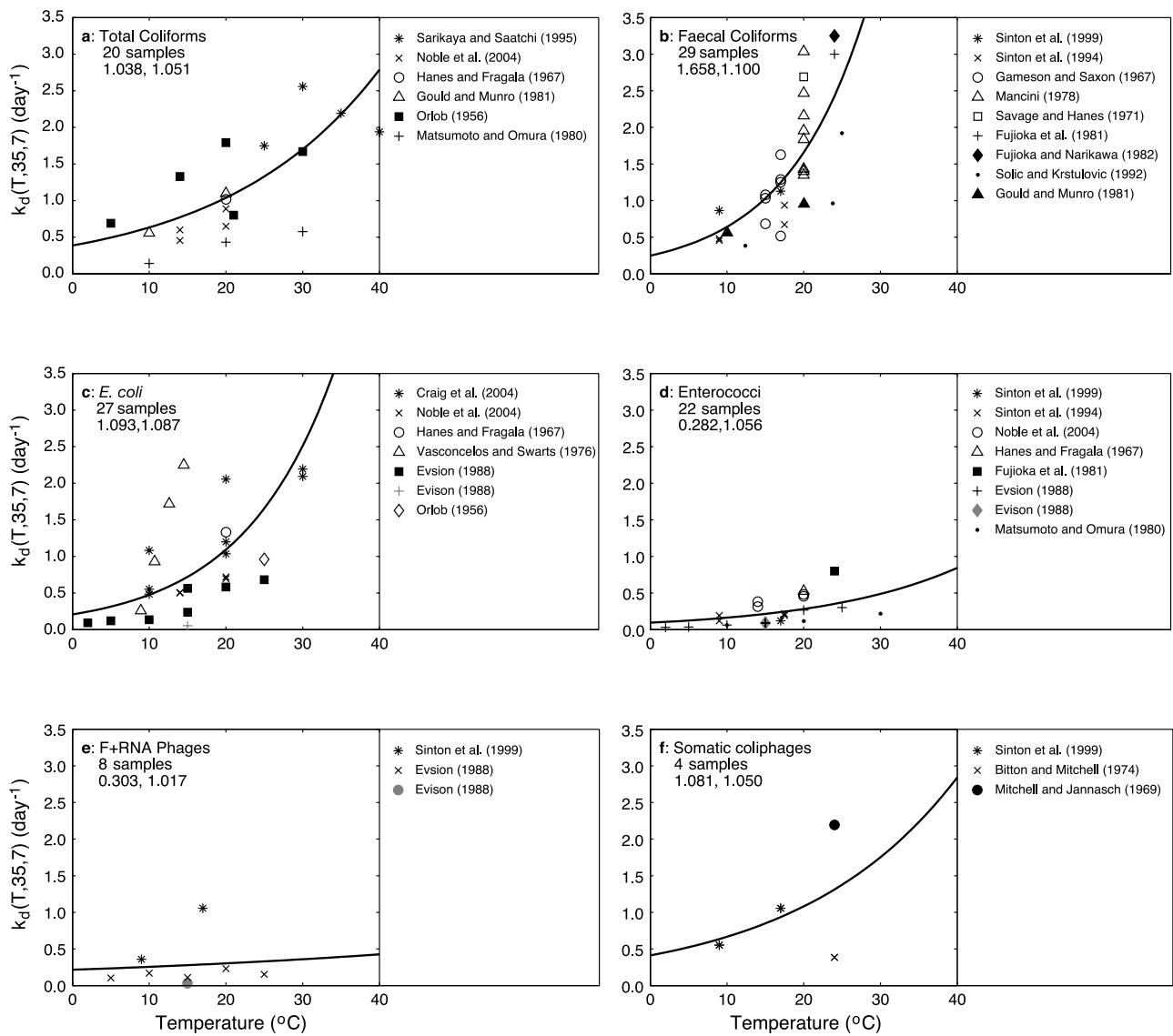


Figure 4. Variation of published natural mortality (“dark death”) rates as a function of temperature for 6 different organism groups. Only investigations from waters with salinity $>30\%$ and pH values between 6–8 were included. Data points collected from studies in a relatively nutrient rich medium are shown in gray and points collected from studies conducted within a nutrient poor medium are colored black. The solid line indicates the optimum fit to the data for equation (5) based on a least squares regression with all data and model parameters k_{d20} and ϑ_M are shown.

enriched. It is theorized that this trend is seen because the results of these studies are more indicative of net die-off rather than actual mortality and the measurements are complicated by a significant growth component.

[21] For each organism group shown in Figure 3, the parameters that produced the optimum least squares fit for equation (5) are summarized in Table 1. The data suggests similarity between coliforms, with temperature multipliers, ϑ_M , of 1.06–1.11. Enterococci show a lower sensitivity to temperature than the coliform bacteria ($\vartheta_M = 1.04$), which has been documented previously by *Noble et al.* [2004] and *Sinton et al.* [1994, 1999]. F⁺ RNA phages show similar mortality rates and temperature sensitivity as the coliform bacteria ($\vartheta_M = 1.10$), but the somatic coliphages exhibited lower mortality rates that vary little as a function of temperature ($\vartheta_M = 1.01$).

[22] A similar analysis was performed for seawater samples by selecting only studies where salinity was recorded to have been between 30–35 % and pH was between 6 and 8 (Figure 4; best fit parameters in Table 1). The comparison indicates that values of ϑ_M are comparable for both fresh and seawater, but the magnitude of the mortality rate is higher for all but enterococci, which show a notable decrease in mortality in seawater.

2.2. Salinity

[23] Where salinity within the simulation domain varies significantly, such as an estuarine setting or a large ocean outfall, the effect of salinity must be parameterized since it is known to have a considerable effect mediating the mortality rate for many organisms [Carlucci and Pramer, 1960b; Hanes and Fragala, 1967; Mancini, 1978; Anderson et al., 1979; Evison, 1988; Solic and Krstulovic, 1992;

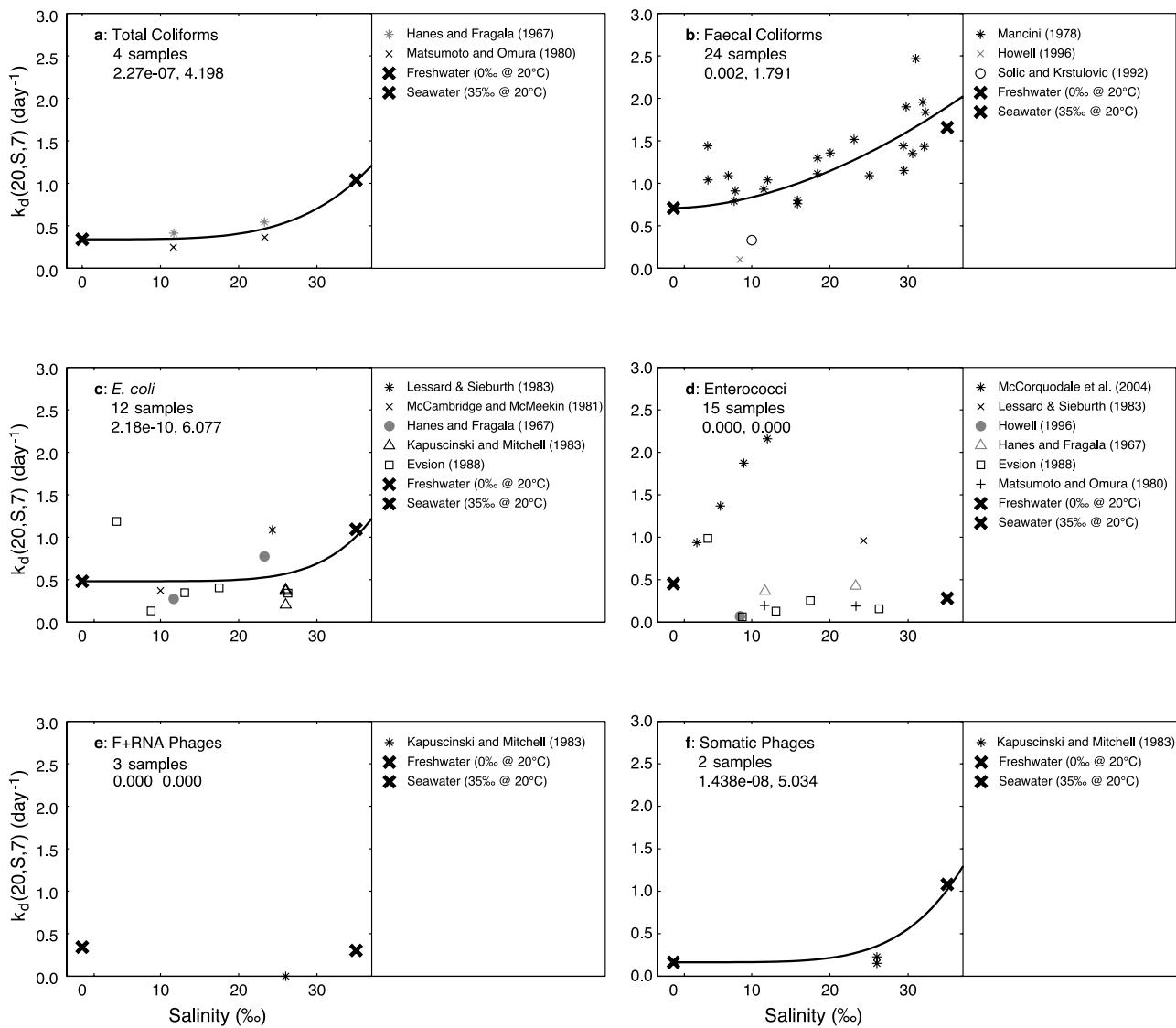


Figure 5. Variation of published natural mortality (“dark death”) rates as a function of salinity for 6 different organism groups. Only investigations from waters with a temperature of 20°C and pH values between 6–8 were included; to increase the number of samples included in the analysis, measurements made between 15 and 25°C were included but the measured mortality values were scaled to their 20°C value using the value of ϑ_M listed in Table 1. Data points collected from studies in a relatively nutrient rich medium are shown in gray and points collected from studies conducted within a nutrient poor medium are colored black. The solid line indicates the optimum fit to the data for equation (6) based on a least squares regression with all data and the model parameters c_{s_M} and κ as shown (Note regression line for d and e indicate no trend was identified).

[Kaspar and Tamplin, 1993; Johnson et al., 1997; Sinton et al., 2002]. Although here only bacteria and phages are examined due to insufficient data for other organisms classes, Johnson et al. [1997] observed salinity effects on *Giardia* spp. cysts suggesting the above function may still apply but further experimentation is needed.

[24] To extract a suitable salinity function, a subset of available data that had a constant temperature (20°C) and was within a neutral pH range (6–8) was collated. To increase the number of samples included in the analysis, measurements made between 15 and 25°C were included but the measured mortality values were scaled to their 20°C value using the value of ϑ_M listed in Table 1. The 20°C

mortality rate, k_{d20} , was plotted against salinity (Figure 5), and a simple power law dependence was estimated based on least squares regression analysis:

$$k_d(20, S, 7) = k_{d20} + \frac{c_{s_M} S^\kappa}{35} \quad (6)$$

where S is salinity (‰), c_s is a constant controlling the effect of salinity on the mortality rate ($\text{d}^{-1} \text{‰}^{-1}$), k_{d20} is the fresh water mortality rate at 20°C (d^{-1}) and κ is a parameter controlling the sensitivity of k_d to salinity.

[25] Generally the variability in the data is large, but the analysis suggests that the effect of salinity is most notable in the coliforms. Enterococci and the F⁺ RNA phages showed

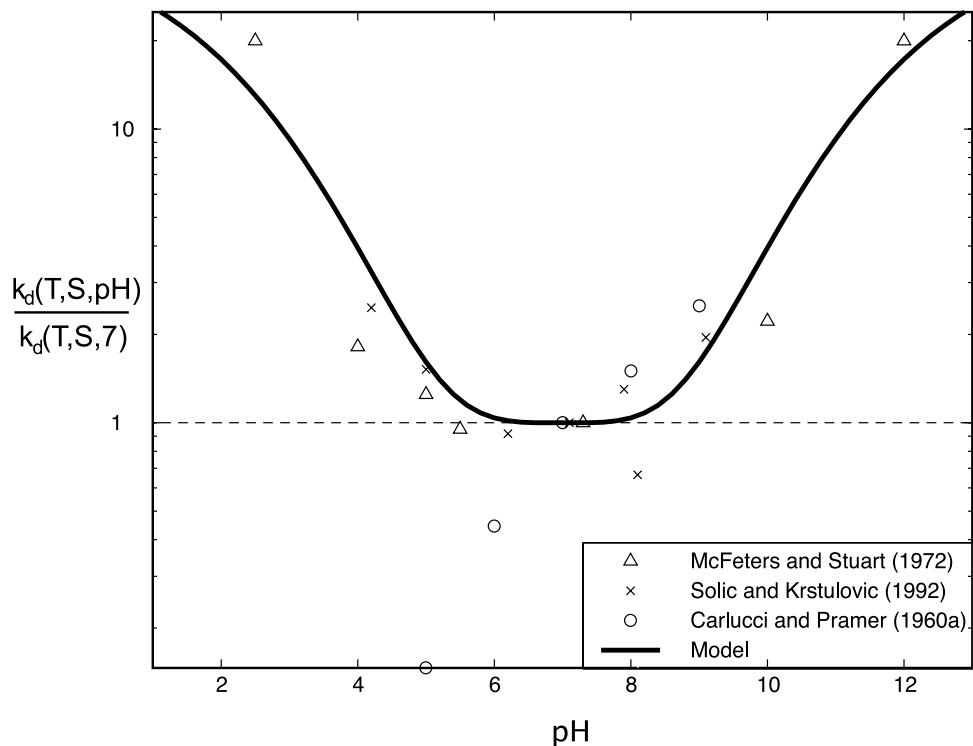


Figure 6. Variation of coliform mortality rate as a function of pH, showing data from different authors and the model (equation (8)). Model parameters are listed in Table 1.

no discernable sensitivity across the range 0–35 %, although only limited data were available within the salinity range. However, this pattern is supported by *Matsumoto and Omura* [1980] and *Evison* [1988].

[26] It is known from laboratory studies that bacterial cells can protect themselves from high salinities by synthesizing osmoregulators. The effect of this has been seen in the field during the investigation of *Pommepuy et al.* [1992] where it was observed that the sensitivity to salinity for coliforms was dependent on the external DOM concentration. Molecular analyses outlined by *Rozen and Belkin* [2005] suggest that this sensitivity varies depending on the internal nutrient status of the cells, such that those with a luxury store can afford to spend more resources osmoregulating. By exploiting the nutrient limitation function defined previously (equation (3)), the following parameterization is proposed:

$$k_d(20, S, 7) = k_{d0} + \frac{c_{S_M} S^\kappa}{35} [1 - f^{LIM}(DOC_L)]^\beta \quad (7)$$

where β is an empirically determined constant that controls the sensitivity of salinity to nutrient limitation. Currently insufficient data exists to test this parameterization in detail, however, based on a qualitative analysis of the data presented by *Pommepuy et al.* [1992], it is estimated that a β value of between 0.05 and 0.3 would be relevant depending on the limitation status.

2.2.3. pH

[27] The effect of pH on survival of coliforms has been documented both within the wastewater literature [*Klock*, 1971; *Parhad and Rao*, 1974; *Mayo*, 1995], and also in fresh [McFeters and Stuart, 1972] and saline [Carlucci and

Pramer, 1960b; *Ayres*, 1977; *Solic and Krstulovic*, 1992] surface water environments. Little to no data exists for other organisms of interest. From the range of coliform studies, there is some doubt as to the optimum pH for organisms (i.e., the pH at which the decay rate is least); *Carlucci and Pramer* found it to be 5, *McFeters and Stuart* found it to be 5.5, *Solic and Krstulovic* found it to be 2, and *Ayres* found it to be above 7. Nonetheless, most authors found mortality rates significantly increase outside of the “neutral” range. On the alkaline side, which is of most interest to practitioners in coastal and eutrophic freshwaters, the end of this range is around 9–10.

[28] Insufficient data exists within the literature to develop plots for pH as done for temperature and salinity. Instead, the relative change in k_d with pH, by normalizing with k_d at pH 7, was calculated based on the dark experiments by *McFeters and Stuart* [1972: fresh water at 10°C], *Solic and Krstulovic* [1992: sea water at ~20°C] and *Carlucci and Pramer* [1960b: sea water at 20°C] (Figure 6). The collated data set clearly indicates a gradual increase in mortality beyond a range of 6–8, and then a substantial increase outside the range 4–10. The data were fit to a sigmoidal “dose-response” toxicity function of the form (Figure 6):

$$\frac{k_d(T, S, pH)}{k_d(T, S, 7)} = 1 + c_{PH_M} \left[\frac{(pH^*)^{\delta_M}}{K_{PH_M}^{\delta_M} + (pH^*)^{\delta_M}} \right] \quad (8)$$

where c_{PH_M} is the maximum effect pH toxicity can have on the mortality rate, K_{PH_M} and δ_M mediate the sensitivity of mortality to change in pH, and $pH^* = |pH - 7|$ is the magnitude of the pH departure from neutrality (assumed to be

7.0). The optimum values for this function for the coliform dataset (Table 1) were determined using a nonlinear fitting procedure.

2.2.4. Combined

[29] Combining equations (5)–(8), gives a complete expression for natural mortality as a function of temperature, salinity and pH:

$$k_d(T, S, pH) = \left[k_{d20} + \frac{c_{S_M} S^\alpha}{35} [1 - f^{LIM}(DO_C)]^\beta \right] \cdot \left[1 + c_{PH_M} \left[\frac{(pH^*)^\delta}{K_{PH_M}^\delta + (pH^*)^\delta} \right] \right] \vartheta^{T-20} \quad (9)$$

[30] For the majority of applications, much of the complexity in equation (9) can be simplified depending on the dominant processes controlling the microbial response.

2.3. Sunlight Inactivation

[31] Sunlight exposure is an important inactivation mechanism for all forms of pathogens and microbial indicators in both fresh and saline waters [Gameson and Saxon, 1967; Mancini, 1978; Fujioka et al., 1981; Gould and Munro, 1981; McCambridge and McMeekin, 1981; Kapuscinski and Mitchell, 1980; Evison, 1988; Rhodes and Kator, 1990; Curtis et al., 1992a; Solic and Krstulovic, 1992; Auer and Niehaus, 1993; Davies-Colley et al., 1994; Sinton et al., 1994, 1999, 2002; Sarikaya and Saatchi, 1995; Johnson et al., 1997; Burkhardt et al., 2000; Noble et al., 2004; King et al., 2008]. In waters of high clarity, it has long been regarded as the most dominant inactivation mechanism. The dynamics of solar inactivation varies significantly between species, so it is necessary to account for the different processes contributing to the solar inactivation response if a generic model framework is to be developed. Despite a sophisticated understanding of these processes, to date no model has been presented in the literature that resolves these dynamics.

[32] The majority of the energy in the solar radiation incident at the Earth's surface is from 300–1000 nm, encompassing the UV-B, UV-A and visible bandwidths. Organisms are susceptible to different wavelengths as described by an organism-specific “action spectrum”. The most potent bactericidal region within the action spectra is the UV bandwidths, and in particular from 250–280 nm (UV-C) as this wavelength coincides with the characteristic length scale of the DNA molecule and directly causes damage that hinders DNA replication. Ozone in the atmosphere prevents UV-C reaching the Earth's surface, and so only UV-B, UV-A and visible regions are active within aquatic systems. Although UV-B (280–320 nm) is not as potent as UV-C wavelengths, it has significant potential to inactivate organisms by directly damaging DNA [Harm, 1980], and has been reported to inactivate all forms of enteric organisms, including *Cryptosporidium* oocysts [King et al., 2008], coliforms [Sinton et al., 1999], and viruses and phages [Murray and Jackson, 1993; Davies-Colley et al., 1999].

[33] As wavelengths increase into the UV-A region (320–400 nm), the direct inactivation effect weakens, although for some organisms it weakens less than would be predicted by the organism's action spectrum. This is because of indirect inactivation effects caused by photo-

oxidation, whereby sunlight excites sensitizer compounds that ultimately react with oxygen and oxidize organic molecules [Webb and Brown, 1979]. Sensitizers originate either within the cell and cause oxidative damage to DNA, or they can originate from outside the cell and damage the cell membrane. The latter are known to adsorb a wide range of wavelengths and their effects can be seen within the visible spectrum [Arana et al., 1992; Davies-Colley et al., 1999].

[34] At least for bacteria, most sunlight-induced inactivation is caused by photo-oxidative effects [Curtis et al., 1992b; Sinton, 2005], primarily because of the high attenuation of the short UV wavelengths. This method of inactivation is dependent on sufficient dissolved oxygen within the system [Webb and Lorenz, 1970; Webb and Brown, 1979; Curtis et al., 1992a, 1992b; Davies-Colley et al., 1999; Khaengraeng and Reed, 2005]. It is also well documented that the lethal effect of sunlight is enhanced at higher salinities for a range of organisms [Dutka, 1984; Evison, 1988; Davies and Evison, 1991; Solic and Krstulovic, 1992; Sinton et al., 2002]. It has been suggested that the increased sensitivity to osmotic stress in sunlight is due to photo-oxidative effects exciting exogenous sensitizers that cause membrane damage [Moss and Smith, 1981]. For similar reasons, pH sensitivity increases when bacteria are also exposed to sunlight [Curtis et al., 1992a, 1992b; Davies-Colley et al., 1999].

[35] In developing a model for inactivation due to exposure to sunlight, there are several factors that must be included. First, inactivation efficiencies vary with wavelength, and this pattern varies between organisms, so it is necessary to partition the incoming solar spectrum into discrete regions. Second, each of the discrete bandwidth regions is attenuated differently within the water column, and the attenuation varies with the presence of dissolved organic matter and suspended material. Third, the model must consider the effect of variable oxygen and pH values on the efficiency of light inactivation, in particular for the UV-A and visible bandwidths. Finally, it is necessary to include the effect of salinity on the inactivation efficiency of solar radiation.

[36] Here, a new generic model for inactivation due to sunlight exposure, k_l , is developed. It takes the form:

$$k_l = \sum_{b=1}^{N_B} [\varphi(k_b + c_{S_b} S) I_b f_b^{LIM}(DO) f_b^{LIM}(pH)] \quad (10)$$

where N_B is the number of discrete solar bandwidths to be modeled, b is the bandwidth class $\{1, 2, \dots, N_B\}$, k_b is the freshwater inactivation rate coefficient for exposure to the b^{th} class ($\text{m}^2 \text{ MJ}^{-1}$), c_s is a coefficient that enhances the lethal effect of light under saline conditions ($\text{m}^2 \text{ MJ}^{-1} \text{‰}^{-1}$), I_b is the intensity of the b^{th} bandwidth class (W m^{-2}), φ is a constant to convert units from seconds to days and J to MJ ($=8.64 \times 10^{-2}$), $f_b(DO)$ is an oxygen dependence function for light inactivation coefficient (–), and $f_b(pH)$ is a pH dependence function for the light inactivation coefficient (–).

[37] Equation (10) assumes population decay through light exposure is purely exponential, and does not account for the sometimes observed “shoulder” and “recovery” phases of the decay curve [Harm, 1980; Sinton et al., 1994]. Parameterizing these effects in a multidimensional model is difficult since mixing of computational cells that have

experienced different light histories would require each cell to be treated as a unique cohort and this would become unmanageable for simulations with large computational domains.

[38] Light in each bandwidth region, b , is characterized by a unique extinction coefficient, η_b , which governs how incident light is attenuated within the water column according to the Beer-Lambert Law:

$$I_b = f_b I_0 e^{-\eta_b z} \quad (11)$$

where f_b is the fraction of incident light intensity in bandwidth b (–), I_0 is the incident shortwave light intensity at the water's surface (Wm^{-2}), z is the depth below the surface (m). In a numerical simulation, equation (11) must be integrated over the depth of the computational cell, Δz , to provide the depth-averaged irradiance, denoted \bar{I} . For bandwidth b , this is defined as [Morowitz, 1950]:

$$\bar{I}_b = f_b I_0 \left(\frac{1 - e^{-\eta_b \Delta z}}{-\eta_b \Delta z} \right). \quad (12)$$

[39] The attenuation coefficients are known to be dependent on dissolved organic matter (DOM) and suspended particulate matter, and are therefore site specific. In CAE-DYM, they are calculated dynamically using constants that linearly relate the effect of DOM and particulate matter to the extinction value. The incoming bandwidth fractions, f_b , are dependent on atmospheric conditions that can vary during the day, but for the purposes of this investigation they are assumed to be constants.

[40] If oxygen levels within the simulated environment are not likely to be depleted, then the function $f_b(DO)$ can safely be disregarded, but for applications where large variations or depletion of oxygen are seen (e.g., stratified reservoirs), it is necessary to parameterise the function $f_b(DO)$ for simulation of the photo-oxidative component. Here, Monod kinetics are assumed, as this was able to capture much of the variability seen in the *Curtis et al.* [1992b] and *Davies-Colley et al.* [1999] data:

$$f_b^{LIM}(DO) = \frac{DO}{K_{DO_b} + DO} \quad (13)$$

where K_{DO_b} controls the sensitivity of the bandwidth b to DO . For pH, a function of the following form is used:

$$f_b^{LIM}(pH) = 1 + c_{PH_b} \frac{(pH^*)^{\delta_b}}{(K_{PH_b})^{\delta_b} + (pH^*)^{\delta_b}} \quad (14)$$

where δ_b is a coefficient that describes the effect of a large pH excursion on the light inactivation constant, and K_{PH_b} is a constant that mediates the sensitivity of light inactivation to pH change. Estimates for the value of K_{DO} are presented in Table 1, although there is insufficient data to be able to resolve this for each bandwidth. For bandwidths that act purely in a direct manner (i.e., no photo-oxidative component), then the sensitivity to DO and pH can be removed in the model by setting K_{DO_b} , K_{PH_b} and c_{PH_b} to zero.

[41] By combining equations (10)–(14), the complete expression for inactivation due to exposure to solar radiation becomes:

$$k_l(I_0, z, \eta, S, DO, pH) = \sum_{b=1}^{N_B} \left[\varphi(k_b + c_{S_b} S) f_b I_0 \cdot \left(\frac{1 - e^{-\eta_b \Delta z}}{-\eta_b \Delta z} \right) \left(\frac{DO}{K_{DO_b} + DO} \right) \cdot \left(1 + c_{PH_b} \frac{(pH^*)^{\delta_b}}{K_{PH_b}^{\delta_b} + (pH^*)^{\delta_b}} \right) \right] \quad (15)$$

which is applicable over any number of bandwidths. For most applications, and based on the available data, it is suggested the discrete bandwidths be limited to visible, UV-A and UV-B. Parameter value estimates for these bandwidths are based upon data presented by *Curtis et al.* [1992b], *Davies-Colley et al.* [1999], and *Sinton et al.* [2002] for a range of microbial indicator organisms and from *King et al.* [2008] for *Cryptosporidium* spp. oocysts (Table 1). Although there are numerous other authors who have examined the response of organisms to sunlight, only these studies measured the effect of the discrete bandwidths by filtering the incident shortwave, in addition to controlling the DO and pH levels; insufficient data of this detail is available for other organisms. Note that equation (15) could be applied using a single bandwidth, but care should be taken since the optimum parameters will then become highly site dependent according to differences in water clarity and light attenuation between systems.

[42] The parameter values highlight the findings of these studies; the most potent wavelengths for coliforms are within the UV-B spectrum (70% inactivation due to UV-B, 13% for UV-A and 17% for visible), Enterococci are most sensitive to UV-A (9% inactivation due to UV-B, 51% due to UV-A and 40% due to visible light), the F⁺ RNA phages are susceptible across the entire spectrum (44% inactivation due to UV-B, 9% due to UV-A and 47% due to visible light) and the somatic coliphages are most susceptible to the short UV wavelengths (51% inactivation due to UV-B, 38% due to UV-A and 11% due to visible light). For *Cryptosporidium* oocysts, the most potent wavelength is UV-B, with minor sensitivity to UV-A and negligible sensitivity to visible light. These results therefore highlight that models that employ a single bandwidth parameterisation are potentially losing a dynamic that will be important in differentiating the behavior of different organisms.

2.4. Predation and Grazing

[43] The consumption and/or inactivation of enteric organisms by autochthonous microbiota holds important implications for their fate and transport. There are numerous reports on the significance of predation (by bacteria), grazing (by larger eukaryotic organisms such as protozoa) or infection (by phages). *Enzinger and Cooper* [1976], *Roper and Marshall* [1978], *McCambridge and McMeekin* [1980a, 1980b, 1981], *Anderson et al.* [1983], *Rhodes and Kator* [1988], *Barcina et al.* [1991], *Iribarri et al.* [1994a, 1994b], *Hartke et al.* [2002], and *Menon et al.* [1996, 2003] all report high levels of loss of faecal bacteria in the presence of natural microbiota relative to filtered or sterilized controls. *Yates et al.* [1990] reported a similar trend for viruses.

[44] *Barcina et al.* [1997] summarized many of these studies and concluded that grazing by protozoa (particularly flagellates) was significantly more important than predation or infection, and suggested that grazing pressures in natural waters may in fact be the most important control on survival of allochthonous bacterial populations. For protozoan pathogens, *Stott et al.* [2001] investigated *Cryptosporidium* oocyst grazing by ciliated protozoa and documented significant consumption rates, however they were exposed to high prey densities that would be unlikely in surface waters. *Fayer et al.* [2000] examined the ingestion of oocysts by zooplankton and noted oocyst accumulation within the digestive tracts of rotifer species. Oocysts were also found to be aggregated together when excreted, however it was uncertain whether they were rendered inactive. Little is reported for phages and viruses.

[45] Numerical prediction of grazing rates in environmental waters is complicated, particularly since the grazing pressure is a result of numerous (and often unidentified) species of bacteriovores [*Hartke et al.*, 2002]. The autochthonous grazers vary significantly between different aquatic environments and predation rates also vary depending on the prey organism [*Gonzalez et al.*, 1990]. Further, their population dynamics also vary depending on the trophic status and temperature of the system. Grazing is therefore a very site-specific process and difficult to simply parameterise. It is beyond the scope of this model to explicitly simulate the higher biology, and for the purposes of this study a simple loss expression that relates the predation pressure to the temperature of the water is adopted, which is modified to include an optional nonlinear term:

$$k_p(T) = \vartheta_P^{T-20} [k_{p20} + \max(0, \varepsilon(C - C_{\min}))] \quad (16)$$

where k_{p20} is the minimum rate due to predation at 20°C (d^{-1}), ϑ_P accounts for the sensitivity of predation to temperature and C is the organism concentration. The second term on the RHS enhances the base predation rate, k_{p20} , when above the threshold C_{\min} , according to the rate ε , and accounts for potentially higher densities of grazers as prey concentrations increase. Such dynamics have been observed in numerous of the above studies.

2.5. Sedimentation and Association With Particles

[46] Enteric organisms may exist in isolation or be associated with either organic or inorganic suspended particles. Depending on the surface properties of the organism and the nature of the suspended material within the system, the attached fraction can vary considerably. The protozoa *Cryptosporidium* spp. are generally thought to exist in isolation as free-floating oocysts within environmental systems as indicated by laboratory and field experiments [*Drozd and Schwartzbrod*, 1996; *Considine et al.*, 2001; *Dai and Boll*, 2003; *Hipsey et al.*, 2004] although significant sedimentation rates have been observed [*Medema et al.*, 1998] under some circumstances. On the other hand it is well established that bacteria can associate with particulates; *Weiss* [1951] and *Pommepuy et al.* [1992] found considerable attachment of faecal bacteria in a turbid estuarine environment, *Auer and Niehaus* [1993] found with sediment traps that bacteria within a freshwater lake were all attached to particles, and *Hipsey et al.* [2006a] reported high association rates (80–100%) of total coliforms and *E. coli* based

on measurements within a drinking water reservoir. Similar high association rates have been reported for bacteria in seawater [*Sinton*, 2005]. Viruses and phages are also known to strongly associate with particulate matter [see *Bitton*, 1975; *Murray and Laband*, 1979; *Gerba*, 2005] and this is known to be sensitive to electrical conductivity, pH and other factors such as the amount of humic acids [*Rossi and Aragno*, 1999].

[47] Attachment to particles is important since attached organisms undergo a concomitant increase in sedimentation, which is particularly important if clays and silts dominate the composition of the suspended material. *Brookes et al.* [2005] observed that association with particles, and therefore differential sedimentation rates, was the primary factor responsible for creating significantly different attenuation signatures between microbial indicator organisms and pathogens during an inflow event in a cool drinking water reservoir. Although the model need not simulate aggregation dynamically, provision should be made to adjust the fraction of organisms that are associated with particles. Generally it is also appropriate to simulate several discrete classes of particles corresponding to those seen in the field. A sedimentation function can therefore be written as:

$$k_s(T, S, SS) = (1 - f_a) \frac{V_c}{\Delta z} + f_a \sum_{s=1}^{N_S} \left[\frac{V_s}{\Delta z} \left(\frac{A_s}{\sum_p^{N_S} A_p} \right) \right] \quad (17)$$

where f_a is the attached fraction, V_s is the settling velocity of each particle size group, V_c is the settling velocity of the unattached organisms, Δz is the vertical dimension of the computational cell (m), and the surface area available for attachment is defined for each group, A_s , by assuming spherical particles:

$$A_s = n_s \tilde{A}_s = \frac{6SS_s}{\rho_s d_s} \quad (18)$$

where \tilde{A}_s is the surface area of an individual particle ($\text{m}^2 \text{ m}^{-3}$) within size class s , n is the number of particles, SS_s is concentration of group s (g m^{-3}), d_s is the particle diameter (m) and ρ_s is the particle density (g m^{-3}). Here it is assumed bacteria are attached on a surface area basis, and the model does not account for preferred attachment surfaces, although this is likely in reality. Adding a preference factor for certain particle classes could facilitate this but currently there is insufficient data to justify such increased complexity. For coliforms, it has been observed that the attached fraction can increase in proportion to the concentration of suspended material [*Pommepuy et al.*, 1992], presumably due to the increased area available for attachment. In such a case, the attached fraction could be parameterised accordingly, for example, $f_a = a(\sum_s^{N_S} A_s)^b$ where a and b are empirically determined, or by using a dynamic aggregation model [*Hipsey et al.*, 2004]. Here a constant value is assumed for simplicity and since it has been observed that the attached fraction varies little where the variation in SS concentration is small [*Hipsey et al.*, 2006a].

[48] The settling velocity of each particle group is calculated from the particle size and density according to Stoke's Law:

$$V_s(T, S) = \frac{gd_s^2[\rho_s - \rho_w(T, S)]}{18\mu(T)} \quad (19)$$

where g is acceleration due to gravity (m s^{-2}), μ is the dynamic viscosity of water ($\text{g m}^{-1} \text{s}^{-1}$) which varies as a function of temperature, and ρ_w is the density of water (g m^{-3}) calculated as a function of temperature and salinity.

2.6. Sediment Survival and Resuspension

[49] The role of sediment in accumulating enteric organisms is well documented and it is not uncommon for concentrations of bacteria and phages to be 1–3 orders of magnitude higher than the overlying water [Van Donsel and Geldreich, 1971; Goyal *et al.*, 1978; Hood and Ness, 1982; Shirais *et al.*, 1987; Struck, 1998]. High concentrations are seen in sediments since they act as sink for deposited organisms, the absence of sunlight, and also because of prolonged survival times (and potentially growth), due to the relatively high nutrient availability [Gerba and Mcleod, 1976; Craig *et al.*, 2004; Davies *et al.*, 1995; Howell *et al.*, 1996; Gerba and Schaibenger, 1975]. Resuspension through shear induced by tidal currents, internal waves and wind-wave action may potentially contribute high concentrations of viable organisms back into the water column.

[50] It is therefore necessary to separately model the store of sediment microorganisms in systems where their resuspension would significantly increase risk, which has been reported in lakes [Whitman and Nevers, 2003], rivers, estuaries [Pommepuy *et al.*, 1992] and coastal areas [Palmer, 1988]. The organisms within this store operate similarly to those in the water column in terms of growth and mortality, although it may be necessary to use sediment specific parameters for these processes.

[51] Resuspension of sediment particles into the overlying water column is parameterised within CAEDYM based on the shear stress experienced at the sediment-water interface, such that no resuspension occurs below a critical shear stress value, and above this a linear response is assumed:

$$f_s^{RES} = \alpha_s \frac{(\tau - \tau_{cs})}{\tau_{ref}} \frac{1}{\Delta z_{bot}} \quad (20)$$

where τ is the shear stress (N m^{-2}), τ_c is the critical shear stress (N m^{-2}) and α_s is the resuspension rate constant for sediment group s ($\text{g m}^{-2} \text{s}^{-1}$). The shear stress at the sediment surface is estimated by adding stresses due to steady currents (as predicted by the hydrodynamic model) and wave-induced oscillatory currents [Beach and Sternberg, 1992]. The critical shear stress can be estimated from particle grain size and density as related by the Sheild's curve.

[52] Resuspension of organisms is calculated from the particulate resuspension rates and the concentration of organisms in the sediment, C_{SED} (orgs m^{-3}), weighted equally among particles of different sizes on a surface area basis:

$$C_r(\tau, SS_{SED}, C_{SED}) = \underbrace{\alpha_c \frac{(\tau - \tau_{cs})}{\tau_{ref}} \frac{1}{\Delta z_{bot}}}_{\text{non-attached organisms}} + \sum_{s=1}^{Ns} \underbrace{\left[f_s^{RES}(\tau) \frac{C_{SED}}{SS_{SED}s} \left(\frac{A_s}{\sum_p^{Ns} A_p} \right) \right]}_{\text{attached organisms}} \quad (21)$$

where C_r is the resuspension loss ($\text{orgs m}^{-3} \text{s}^{-1}$), α_c is the resuspension rate constant for nonattached organisms ($\text{orgs m}^{-2} \text{s}^{-1}$), SS_{SED} is the concentration of sediment in the “active” sediment layer, i.e., the top few centimeters associated with sedimentation and resuspension (g m^{-3}).

2.7. Model Synthesis and Implementation

[53] Synthesis of the above expressions for growth, mortality, predation, sedimentation and resuspension with expressions for advection and mixing result in an overall conservation expression for each organism type, C (orgs m^{-3}). In the water column:

$$\underbrace{\frac{dC}{dt}}_{\text{unsteady}} + \underbrace{\frac{\partial}{\partial x_j} (CU_j)}_{\text{advection}} = \underbrace{\frac{\partial}{\partial x_j} \left(\kappa_j \frac{\partial C}{\partial x_j} \right)}_{\text{turbulent diffusion}} + \underbrace{C_{in} - C_{out}}_{\text{inflows/outflows}} + \underbrace{C_r(\tau, SS_{SED}, C_{SED})}_{\text{resuspension from sediment}} + \left[\underbrace{k_g(T, S, DOC_L)}_{\text{growth}} - \underbrace{k_d(T, S, pH)}_{\text{mortality}} - \underbrace{k_l(I_o, S, DO, pH)}_{\text{sunlight}} - \underbrace{k_s(T, S, SS)}_{\text{sedimentation}} - \underbrace{k_p(T)}_{\text{predation}} \right] C \quad (22)$$

where t is time, x_j is the distance in the j -th dimension (m), U_j is the velocity in the j -th dimension (m s^{-1}), κ_j is the eddy-diffusivity and C_{in} and C_{out} are the inflow and outflow fluxes respectively ($\text{orgs m}^{-3} \text{s}^{-1}$). Organism concentrations in the sediment are calculated similarly but ignore the effects of advection and mixing leaving:

$$\underbrace{\frac{dC_{SED}}{dt}}_{\text{unsteady}} = \underbrace{k_s(T, S, SS)}_{\text{sedimentation from bottom water}} - \underbrace{C_r(\tau, SS_{SED}, C_{SED})}_{\text{resuspension to bottom water}} + \left[\underbrace{k_g(T, S, DOC_L)}_{\text{growth}} - \underbrace{k_d(T, S, pH)}_{\text{mortality}} - \underbrace{k_p(T)}_{\text{predation}} \right] C_{SED}. \quad (23)$$

[54] For this analysis, the above expressions are numerically solved as part of a coupled three-dimensional (3-D) model of hydrodynamics and water quality; the Estuary, Lake and Coastal Ocean Model (ELCOM) is used as the hydrodynamic driver and simulates the advection, mixing and inflow and outflow terms listed above, in addition to simulating the waterbody temperature, salinity and velocity dynamics [Hodges *et al.*, 2000; Laval *et al.*, 2003]. The growth, mortality, predation, sedimentation and resuspension functions for the water column and sediment were implemented separately within CAEDYM, similar to Hipsey *et al.* [2004]. In addition to simulating the microbial dynamics, CAEDYM provides the necessary information for the above functions, including light (UV-B, UV-A and visible bandwidths), pH, and DO, DOC and SS concentrations. These variables are calculated dynamically and are important in shaping the microbial responses, however, discussion on how they are modeled is beyond the scope of this paper and readers are referred to the CAEDYM documentation for a detailed account [Hipsey *et al.*, 2006b].

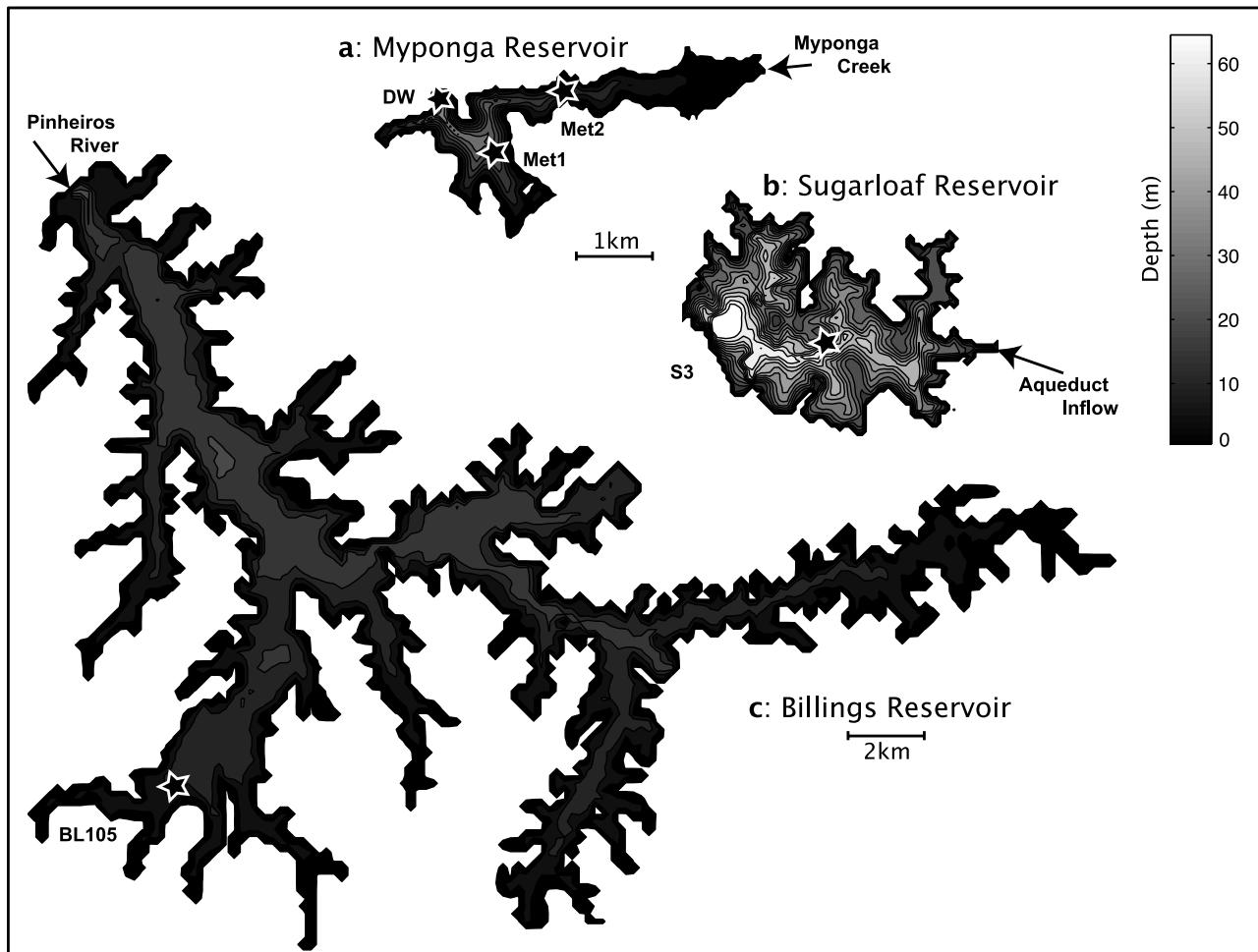


Figure 7. Bathymetric maps of (a) Myponga Reservoir (South Australia), (b) Sugarloaf Reservoir (Victoria, Australia) and (c) Billings Reservoir (Sao Paulo, Brazil), indicating the sampling locations (*). Note the horizontal scale difference for Billings Reservoir.

[55] When validating model against observed data, care must be taken to ensure the comparison is appropriate. Most assays for the enumeration of enteric organism concentrations generally count culturable cells. However, most routine assays for the protozoan pathogens, *Cryptosporidium* spp. and *Giardia* spp., count both infective and inactivated organisms, and so must include both of these classes in the numerical model [Hipsey et al., 2004] if the results are to be compared to field data. Note also for bacteria that there is much discussion in the literature about cells existing in a viable but not culturable (VBNC) state, which is an important consideration when developing risk management strategies as data obtained using traditional methodologies may under predict organism persistence [Karunasagar and Karunasagar, 2005].

[56] A further consideration that is rarely accounted for is the role of different strains of a particular organism type that may make interpretation of results difficult. For example, Power et al. [2005] have shown that certain *E. coli* strains are able to bloom in oligotrophic waters when temperatures exceed 18°C. The identified strains were encapsulated and unique from those of faecal origins. Similarly, Camper et al. [1991] found that environmental isolates of coliforms had a greater growth rate in surface waters than clinical isolates. This is a further complication from a modeling perspective

since for each organism group, as measured in the field, there are potentially multiple strains of the same organism with different environmental sensitivities and, as a result, growing and decaying at different rates. Barnes and Gordon [2004] examined the significance of this by implementing a simple multistrain model of *E. coli* growth, decay and dilution for a lake that included two hypothetical strains. The study highlighted that different growth and death rates between strains can significantly impact the dynamics of the overall organism group. Such a multistrain model can be implemented with the framework presented here by defining any organism group as the sum of any number of strains, $C = \sum_i C_i$ and solving equations (22)–(23) for each strain.

3. Model Validation

[57] To demonstrate use of the model across a range of environments, various configurations are compared against data sets from three different inland waters (Figure 7) that vary in their size, operation, trophic status, and exposure to enteric organisms (Table 2).

3.1. Myponga Reservoir: Riverine Pulse

[58] Myponga Reservoir is a small storage located south of Adelaide, South Australia, with a maximum depth of

Table 2. Overview of the Three Validation Sites Summarizing the key Physical and Chemical Parameters

	Myponga Reservoir	Sugarloaf Reservoir	Billings Reservoir
<i>Description:</i>			
<i>Location</i>	Adelaide, Australia	Melbourne, Australia	Sao Paulo, Brazil
<i>Volume (GL)</i>	26	96	1200
<i>Max Depth, m</i>	40	70	23
<i>Surface Area, km²</i>	2.8	4.4	127
<i>Typical Peak Inflow, m³ s⁻¹</i>	10	15	300
<i>Parameters:</i>			
<i>DO, mg O₂ L⁻¹</i>	8–10	8–10	0–10
<i>pH</i>	6–7	6–7	8–9
<i>TOC, mg C L⁻¹</i>	10–20	2–5	15–25
$\alpha_{DOC_L} (-)$	0.01	0.01	0.05
η_{VIS} , m ⁻¹	1.1	0.6	1.0
η_{UVA} , m ⁻¹	5.8	5.0	5.8
η_{UVB} , m ⁻¹	10.0	10.0	10.0

40 m. It is fed by a 124 km² catchment that is predominantly cleared for pasture that is used to support dairy and beef cattle. It experiences a relatively dry and strongly seasonal climate, and inflows to the reservoir are largely event based. These events seed the reservoir with considerable loads of pathogenic and indicator organisms and can travel from the inflow to the dam wall within 2 d [Hipsey *et al.*, 2004]. In 2003, a comprehensive field experiment was conducted to examine the attenuation of the enteric organisms through the reservoir. Details of the experiment and results have been described previously [Hipsey *et al.*, 2004; Brookes *et al.*, 2005]; here data from this experiment is used to validate the model for *E. coli*, enterococci and somatic bacteriophages.

[59] The model was configured to account for the effects of growth, sunlight inactivation, natural mortality and sedimentation. Inactivation dependencies on salinity and pH were not included since neither varied considerably. Although not reported in the earlier studies, comprehensive measurements of total DOC were also made during the experimental period [L. Linden, unpublished data], with samples taken coincident with the microbiological constituents. On the basis of local evidence from Withers and Drikas [1998], 1% of the total DOC was assumed to be sufficiently labile for uptake by the simulated bacteria (i.e., DOC_L). The simulations also included two size classes of suspended inorganic particles for organisms to attach to, the results of which were previously validated against data from an in situ particle profiler during the same event [Hipsey *et al.*, 2004]. Kinetic parameters used were taken directly from Table 1, without adjustment. The predation rate for all groups was estimated to be 0.2 d⁻¹, and the growth of phages and the resuspension of all organisms was disabled.

[60] The flood event (9.8 m³ s⁻¹ peak relative to <1.0 m³ s⁻¹ background flow rate) created a distinct intrusion of riverine water that was significantly more dense and turbid than the ambient reservoir water. The pulse traveled along the reservoir thalweg toward the dam wall, and was progressively attenuated due to entrainment of reservoir water and sedimentation of the large particles. The model accurately captured the attenuation of the three simulated microbiological constituents within the riverine pulse as it progressed through the reservoir (Figure 8). The inflow peak of 22,700 colony forming units (cfu)/100 mL was reduced to approximately 5000 cfu/100 mL by Met2, and ultimately to 1100 cfu/100 mL by the dam wall; 5% of the

inflow value. The enterococci data showed a similar attenuation rate, although the model and observed concentrations at the dam wall are approximately 10% of the inflow peak. This is in agreement with the frequently reported observation that enterococci are more persistent than coliform bacteria. Although, the standard deviation between the measured samples is relatively small, the low temporal resolution of concentrations measured during the steep increase in the inflow hydrograph is reflected in the forcing boundary conditions of the simulation, and is thought to be responsible for much of the discrepancy.

3.2. Sugarloaf Reservoir: Pumped Inflow

[61] Sugarloaf Reservoir is a moderately sized storage supplying Melbourne, Australia. It has a maximum depth of approximately 75 m and only a minor natural catchment. Most water enters the reservoir through a large pumped inflow that is operated for considerable periods and sources water from a nearby aqueduct that drains agricultural land. Although the residence time of the reservoir is of the order of months, it has been observed that inflowing water can reach the off-take within several days. The inflow tends to create a “steady state” intrusion characterized by distinct gradients in temperature, turbidity and coliform concentrations, as measured during a 5-d intensive experimental campaign [Hipsey *et al.*, 2006a]. Forcing meteorological and inflow data, and application and discussion of the model ELCOM during the experimental period is presented by Hipsey *et al.* [2005].

[62] During the experiment, total coliform and *E. coli* concentrations were measured at three depths (surface, mid, and bottom) at various locations between the inflow and dam wall each day over the experimental period, in addition to other physico-chemical parameters required by the model. The microbial model was configured identical to the Myponga Reservoir simulation except total coliforms and *E. coli* were simulated, and particle sizes were based directly on the Hipsey *et al.* [2006a] LISST measurements.

[63] During the simulated period, the inflowing water was generally cooler than the ambient water temperature, although during days 236–237 the inflow water was warm and briefly formed an interflow. The inflowing water pulse is seen clearly in the concentrations of total coliforms. The initial concentration peak of 13,000 cfu/100 mL is seen at concentrations of 3000 cfu/100 mL at the middle of the reservoir, approximately 1.5 km from the inflow. The inflow

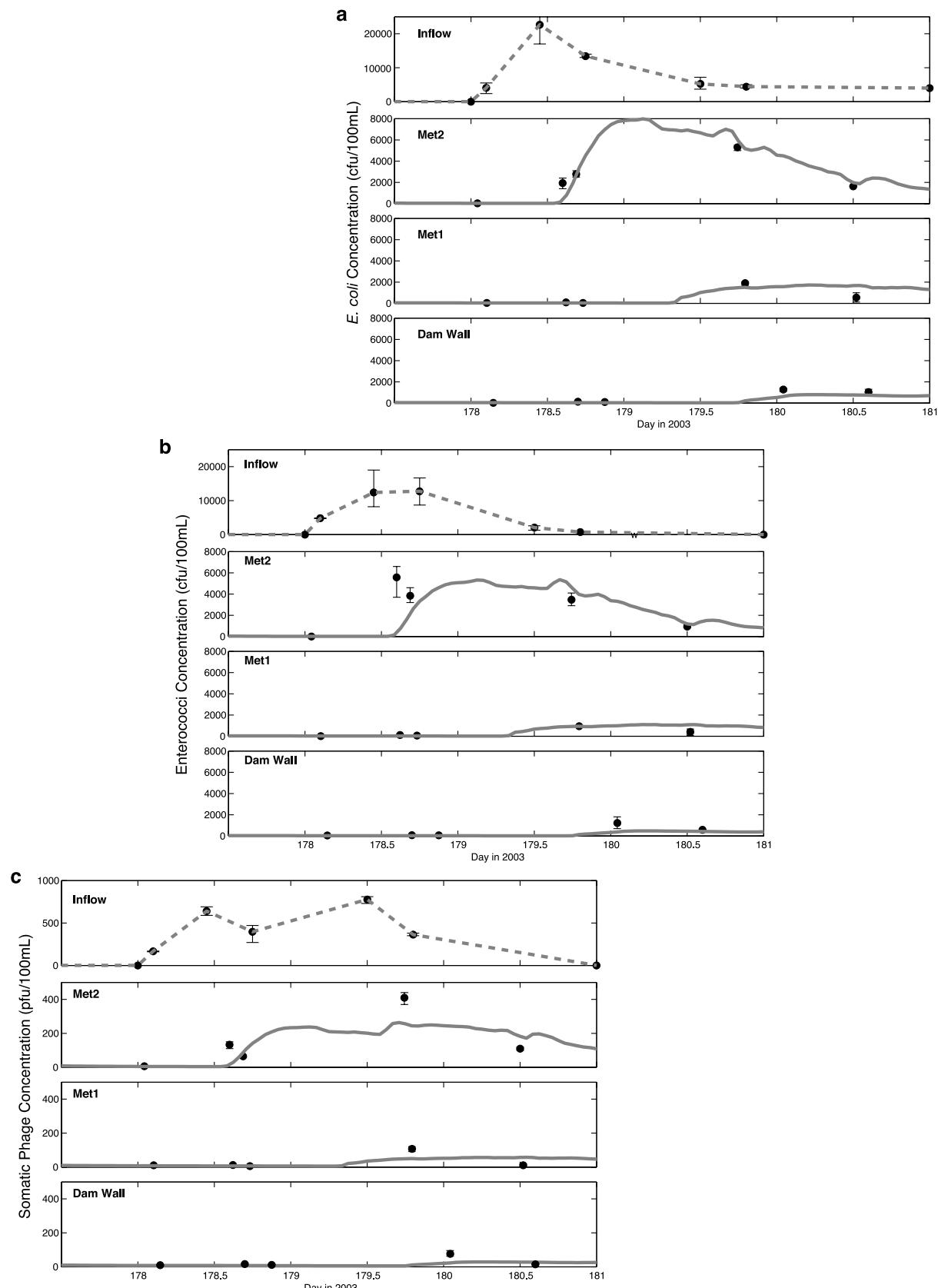


Figure 8. Comparison of modeled (ELCD) and observed (Field) data from Myponga Reservoir for three organism types. Results are shown at the inflow (dashed-line indicates the interpolated boundary condition used to force the model), and 2.5 m above the bottom at Met2, Met1 and dam wall sampling locations, for (a) *E. coli*, (b) enterococci and (c) somatic coliphages. Error bars on the observed data indicate the observed maximum and minimum of three replicates.

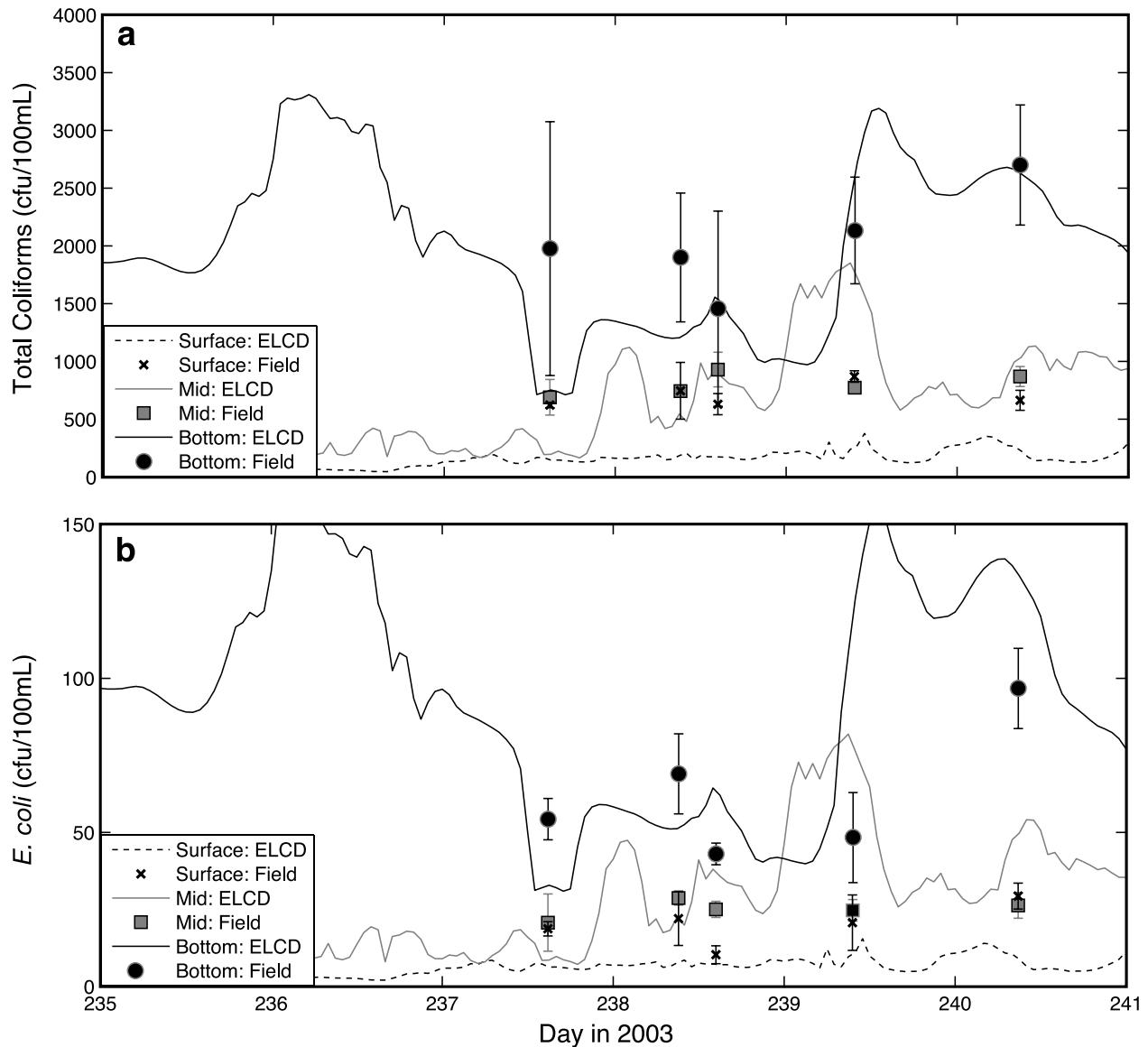


Figure 9. Comparison of modeled (ELCD) and observed (Field) coliform data for Sugarloaf Reservoir at location S3. Results are shown at surface, middle, and bottom depths, for (a) Total Coliforms, and (b) *E. coli*. Error bars on the observed data indicate the standard deviation of 5 collected samples.

water was only faintly observed at the dam wall (not presented here) due to high outflow rates entraining large volumes of water. The model predictions successfully capture the observed variability in the bottom and middepth total coliform and *E. coli* concentrations (Figure 9). The surface concentrations were consistently underestimated, suggesting that the predicted rates of light inactivation may have been too high. However, similar concentrations were seen in the mid and surface regions of the most distant sampling location, which was far from the influence of the inflowing coliforms. This suggests a “native” coliform population creating a low background concentration, as has been reported by Power *et al.* [2005] and Camper *et al.* [1991].

3.3. Billings Reservoir: Tropical, Eutrophic System

[64] Billings Reservoir is a large drinking water storage located near Sao Paulo, Brazil, with a maximum depth of 23 m. In addition to numerous point and diffuse inflows along its perimeter, it periodically receives large flows that

are pumped from the Pinheiros River, and are heavily contaminated with organic matter and faecal organisms. Because of limited data availability, the aim of simulating Billings Reservoir was not to reproduce the dynamics of a specific event as done in the previous two examples, but to simulate the broad seasonal trends in coliform concentrations and to investigate the dominant processes that create these trends. Faecal coliform concentrations were measured within the reservoir at the offtake site (BL105) at a weekly fortnightly sampling interval. High variability in the 2002 data was observed, showing concentrations between 0 and 5000 cfu/100 mL.

[65] A detailed 3D hydrodynamic-biogeochemical model of the reservoir has been setup previously using ELCOM-CAE-DYM [Antenucci *et al.*, 2005], and the phytoplankton, nutrient cycles (C, N, and P) and oxygen dynamics were validated against available monitoring data collected during 2002 at 2–3 locations within the reservoir. The simulations were forced by

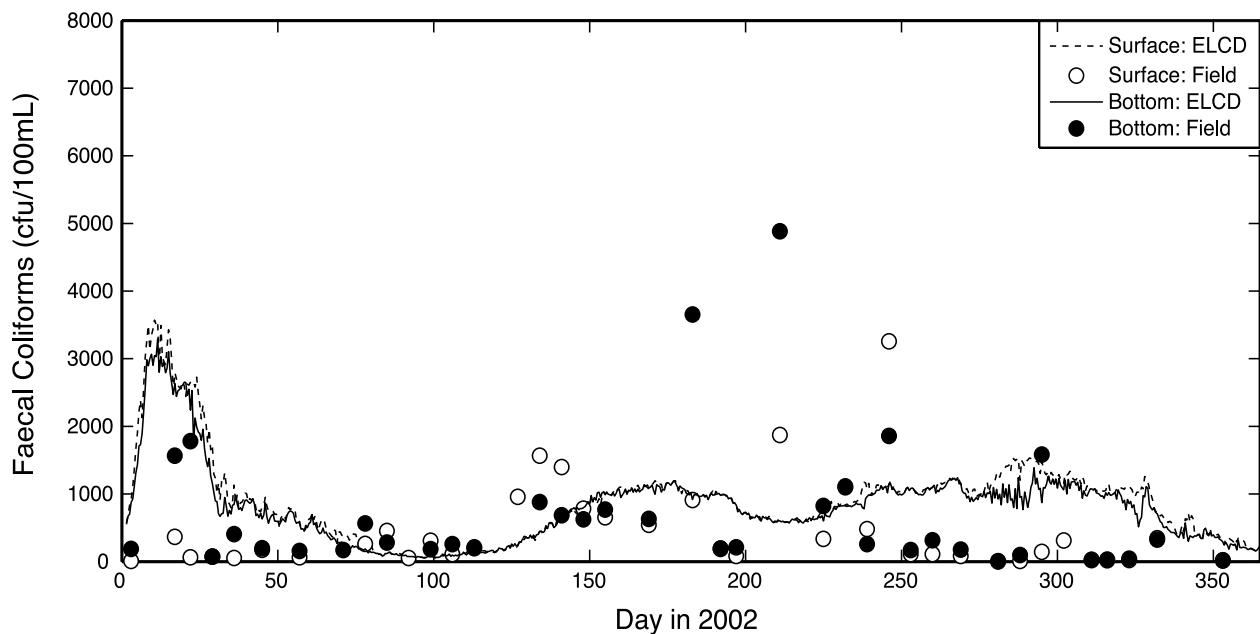


Figure 10. Comparison of modeled (ELCD) and observed (Field) faecal coliform data for Billings Reservoir at location BL105. Results are shown at surface and bottom depths.

known concentrations and flows at the Pinheiros River input, and by a runoff-load model that is based on empirical correlations of nutrient and coliform concentrations as a function of flow rate for each of the 15 subcatchments.

[66] During this analysis, simulations conducted with a traditional coliform model (accounting for sedimentation, natural mortality and sunlight inactivation) highlighted that it was not possible to predict concentrations of the magnitude of those observed at BL105. This was despite the high inflow loads, and use of tempered mortality rates (e.g., reduced by 50%), since the inflow coliform load was able to be entirely attenuated over 12 km of reservoir. Furthermore, application of the present model using a similar configuration as the previous examples, except using faecal coliform specific parameter values and a higher predation rate of 0.4 d^{-1} , was unable to predict any nonzero concentrations at BL105 even with the maximum growth rate set to 2.4 d^{-1} . A second, “environmental”, *E. coli* isolate was therefore included within the simulation, and it was configured to have a higher maximum growth rate of 3.0 d^{-1} . Although higher, this is still within the range measured by Camper *et al.* [1991]; other parameters were set to those in Table 1, except for the nonlinear predation term, which was adjusted to maintain observed coliform levels.

[67] Surface and bottom data and simulation results from the location BL105 (Figure 10) show the model is able to reproduce the observed trends to a reasonable degree, particularly when the high variability in the field data and uncertainty in the growth and predation rates are considered. The magnitude and seasonality are comparable with the observed data and the model captures the period where no coliforms were measured in either the surface or bottom locations during February to April.

4. Discussion

[68] This study aimed to bring together a large body of literature on enteric organism biology and numerical pre-

diction into a complete description and model of microbial behavior. The model is intended for use by scientists and engineers interested in quantifying risk caused by microbial pollutants, to help in the design and implementation of monitoring programs, and also for testing the effects of proposed engineering interventions and catchment management remediation scenarios. Although numerous modeling studies have been presented within the literature, the present analysis significantly advances previous studies in several areas. First, inclusion of the growth term allows for simulation of organisms in warm, nutrient rich environments, where typical die-off models tend to over-predict loss rates. The growth term allows for simulation of potential regrowth effects as has been reported in environmental waters by Korhonen and Martikainen [1991], Camper *et al.* [1991], Ashbolt *et al.* [1995], Fujioka *et al.* [1999], Solo-Gabriele *et al.* [2000], Desmarais *et al.* [2002] and Byappanahalli *et al.* [2003] and includes nutrient and temperature limitation functions. Second, the natural mortality term has been extended to independently account for the effects of salinity and pH, in addition to temperature. The salinity-mediated mortality has also been adapted to account for the nutrient status of the medium to simulate the importance of nutrient starvation on the ability of an organism to survive under osmotic stress. Third, a new model for sunlight-mediated mortality is presented that dynamically accounts for mortality induced by visible, UV-A and UV-B bandwidths. This additionally has capacity to simulate the photo-oxidative and photo-biological mechanisms of inactivation through included sensitivities to dissolved oxygen and pH. Fourth, the model allows for organisms to be split between free and attached pools, and sediment organisms may become resuspended in response to high shear stress events at the water-sediment interface caused by high velocities or wind-wave action. Fifth, the enteric organism module has been implemented within the bio-geochemical model CAEDYM, which gives it dynamic access to concentrations of dis-

solved oxygen, organic carbon, and suspended solids, in addition to pH, shear stress and light climate information.

[69] Although the model introduces numerous parameters, some of which remain poorly characterized, the advantage of the present approach is that the parameterisations are sufficiently process-oriented such that the parameters and model can be more easily ported between systems. For many applications, a critical evaluation of the dominant processes controlling variability will generally highlight that the model described here in its entirety is unnecessarily complex. For example, application of the model in a cool, oligotrophic freshwater system could safely justify negating the effects of oxygen, salinity and pH since these are unlikely to play a dynamic role.

[70] A multifaceted approach to set parameter values for such complex models should include identification of universal values across systems from the literature (as we have attempted to do for the core parameters that govern growth, mortality and sunlight inactivation, Table 1); determination of site-specific parameter values from field and/or laboratory measurements (for example, predation rates or size of suspended particles); and cross-system validation of the parameter set, since increased confidence in model parameters results if they can be “fixed” over a range of water bodies [Romero et al., 2004]. Use of this combined approach avoids reliance on calibration to achieve accurate predictions, as has been exemplified by application of the model to the three systems presented here to a high level of success, without relying on parameter estimation.

[71] Looking specifically at *E. coli*, which was studied in each of the three locations, interrogation of each of the kinetic terms in equation (22) highlights the large variability seen between process values (Figure 11). Importantly, it is clear that in different systems, different processes ultimately control the observed microorganism concentrations, and this is reflected in the sensitivity of the simulations to the different terms (Table 3). The dominant processes controlling organism fate also vary depending on the spatial and temporal scale of interest, as is highlighted by the choice of validation data sets presented here. In Myponga Reservoir, the major pathogen risk is from large flood events that enter and dissipate quickly, and the dominant mechanisms controlling concentrations were mixing, sedimentation and natural mortality. Sedimentation was important as most of the attached organisms quickly settle with the large particles once they enter the reservoir. Sunlight inactivation was mostly negligible due to the high color and light absorption rates. In Sugarloaf Reservoir, the long-term, relatively constant seeding of organisms from the pumped inflow are gradually attenuated by sunlight inactivation, natural mortality and predation. Growth is less than in Myponga Reservoir due to the lower available organic carbon concentrations, and sedimentation is also much lower. In Billings’s Reservoir, event-based inflow loading from the Pinherios River is also important, but due to the warm temperatures and high concentrations of assimilable nutrients, growth is an order of magnitude higher than in the previous examples. Near the off-take site (BL105) it is in fact the balance between growth and the combined effect of mortality, predation and solar inactivation that controls the coliform concentrations. Interestingly, Billings Reservoir is the most shallow of the three examples and has the

largest absolute magnitude solar inactivation, yet relative to the other sites, losses due to solar inactivation are of secondary importance. This simulation also exemplifies the seasonal variability in growth, mortality and predation, mainly due to the lower temperatures experienced during the middle of the year.

[72] Despite the large body of literature on enteric organism fate and transport and the relative accuracy of the predictions presented here, the study has additionally served to highlight the numerous areas where insufficient information still exists. Analysis of Table 1 indicates that all the processes covered by the model have some or all of their parameters that are poorly defined, even for the most commonly used organism groups. In general, the natural mortality rate is the best quantified process, particularly for the coliforms, however, more information is required for oocyst and phage response to salinity and pH. Sunlight inactivation parameters for the organisms presented in Table 1 are fairly well established from the Sinton et al. [2002], Davies-Colley et al. [1999] and King et al. [2008] studies, however further investigation is required to quantify the oxygen and pH sensitivity of each discrete bandwidth class for most organisms.

[73] The areas that are in the most urgent need of attention are the parameters (and parameterizations) of both growth and predation. Evidence of growth of coliforms and enterococci in environmental waters is substantial, however, only the Camper et al. [1991] study is sufficiently quantitative for estimation of the growth rate and nutrient and temperature sensitivities as required by the model. Similarly for predation, substantial evidence of grazing and/or predation of enteric organisms exists, but it is difficult to convert the results of these studies into a form relevant to a model of this nature. Furthermore, little is known on the spatial and temporal variability in predation pressures in different aquatic environments.

[74] The uncertainty in the growth and predation predictions will vary in importance depending on the nature of the aquatic system being simulated. Growth is maximal between 20 and 30°C, and nutrients also tend to be more abundant in more productive systems, and predation is enhanced as the productivity of the system is increased. Therefore in temperate and cool waters, these terms will be of secondary importance relative to natural mortality and sedimentation (e.g., Figures 11a and 11b), but for simulation of enteric organisms in tropical and subtropical waters, and particularly those with a high trophic status, growth and predation are of primary importance (e.g., Figure 11c), and there is a need for further research into these areas. For these reasons, this study has been unable to suitably validate every algorithm across different types of aquatic systems, but instead has aimed to lay a foundation and provide a context for future experimental work.

[75] Ultimately, it is envisaged that the database of parameters (Table 1) be extended beyond the organisms selected for this study to include the numerous others of interest to the water industry. In particular, the majority of studies to date have focused on the indicator organisms (coliforms, enterococci and phages), with less quantification of actual pathogens. Notable exceptions include *Giardia lamblia* cysts, *Salmonella* spp., *Clostridium perfringens*, *Vibrio* spp., and the numerous enteric viruses of concern

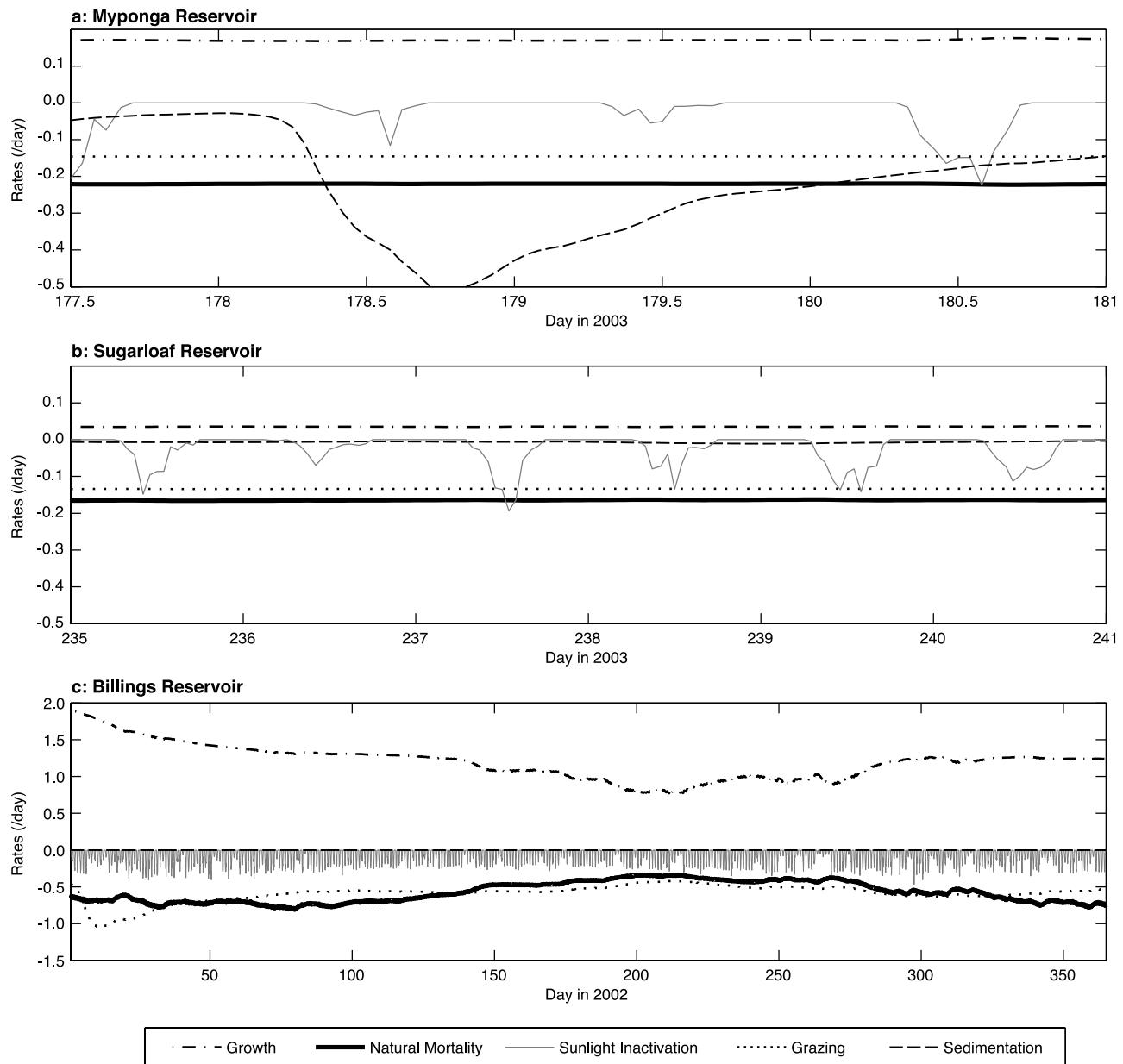


Figure 11. Simulated rates affecting *E. coli* dynamics in each of the three validation reservoirs, highlighting the large variability in dynamical behavior seen between systems for the same organism. Rates were calculated in each wet cell within the computational domain and then integrated across the entire domain to give the basin average value. Note the different scales on both *x* and *y* axes.

(e.g., *Enterovirus*, *Hepatovirus*, *Rotavirus* and *Norovirus*). Currently limited data exists for these organisms, but there is little information on mortality and sunlight inactivation, and less for growth and predation. It is hoped that this investigation will encourage further experimentation for these organisms with the aim of improving estimates of parameter values and process sensitivities. The advantage of a common nomenclature and approach being adopted by the research community (encompassing microbiologists, engineers, modelers and public health professionals) and the water industry is increased penetration and application of results, and heightened transferability of results and data.

[76] There is much discussion within the literature about the most suitable indicators of faecal pollution. Enterococci

and faecal streptococci are generally recommended as being more suitable than the widely used coliform indicators due to their lower mortality rates [e.g., *Hanes and Fragala*, 1967; *Mitchell and Starzyk*, 1975; *Noble et al.*, 2004, Figure 3] and predation losses [*Gonzalez et al.*, 1990; *Iribarri et al.*, 1994a, 1994b]. *Clostridium perfringens* has also been recommended [*Payment and Franco*, 1993; *Medema et al.*, 1997; *Brookes et al.*, 2005], particularly as a surrogate for the protozoan pathogens since it is also spore forming and persists for longer than the traditional bacterial indicators. Phages are typically used as model organisms for the enteric viruses, but there are several reports where they have performed poorly [*Stetler*, 1984; *Havelaar et al.*, 1993]. The model presented herein has the potential to

Table 3. Summary of Sensitivity Analysis Results^a

Description	Myponga Reservoir	Sugarloaf Reservoir	Billings Reservoir
Natural mortality (k_d) -20%	0.5266	0.1455	0.1238
Natural mortality (k_d) +20%	-0.4723	-0.2104	-0.1908
Growth (k_g) -20%	-0.0873	-0.0490	-0.3879
Growth (k_g) +20%	0.1169	0.0712	0.4098
Predation (k_p) -20%	0.3571	0.2095	0.4812
Predation (k_p) +20%	-0.3303	-0.2701	-0.5301
Sedimentation (k_s) -20%	0.4034	0.2661	0.1876
Sedimentation (k_s) +20%	-0.3721	-0.9309	-0.2981
Sunlight inactivation (k_l) -20%	0.1372	0.1321	0.1109
Sunlight inactivation (k_l) +20%	-0.0083	-0.0452	-0.0749

^aSensitivity was calculated using $(\Delta C/\bar{C})/(\Delta p/p_{vd})$ integrated over each of the relevant time series at the site presented for each case study. ΔC is the change in the simulated variable (*E. coli*), and \bar{C} is the reference value (defined as the mean), Δp is the change in value of the relevant parameter, and p_{vd} is its validation reference value (as calculated from parameters in Table 2).

improve our understanding of the differences between the routinely sampled microbial indicator organisms and the pathogens that ultimately present a public health risk. Analysis of Figure 11 highlights that even the same species can behave quite differently across a range of systems and over different timescales, making it difficult to specify a single “best” indicator. A different approach however would be to simulate both the indicator and pathogen organisms, and use the model to “correct” the risk implied by observed indicator organism concentrations.

[77] **Acknowledgments.** Much of the analysis and field data presented in this paper was made possible through a grant from the American Water Works Association Research Foundation (AwwaRF), under project 2752 “Hydrodynamic distribution of pathogens in lakes and reservoirs” managed by Michael Burch at the Australian CRC for Water Quality and Treatment, to whom we are grateful. Data from Billings Reservoir in Brazil was provided courtesy of Companhia de Tecnologia de Saneamento Ambiental (CETESB). We also acknowledge the constructive comments by the reviewers who have helped to improve the quality of this paper.

References

- Anderson, I. C., M. W. Rhodes, and H. I. Kator (1979), Sublethal stress in *Escherichia coli*: A function of salinity, *Appl. Environ. Microbiol.*, **38**, 1147–1152.
- Anderson, I. C., M. W. Rhodes, and H. I. Kator (1983), Seasonal variation in survival of *Escherichia coli* exposed in situ in membrane diffusion chambers containing filtered and non-filtered water, *Appl. Environ. Microbiol.*, **45**, 1877–1883.
- Antenucci, J. P., M. Whiteley, B. Devkota, M. R. Hipsey, and J. Imberger (2005), *Mathematical Model for the Upper and Middle Tiete River Basin in the Metropolitan Sao Paulo Area*, Centre for Water Res., Univ. of Western Australia, Perth, WA, Australia.
- Arana, I., A. Muela, J. Iribarri, L. Egea, and I. Barcina (1992), Role of hydrogen peroxide in loss of culturability mediated by visible light in *Escherichia coli* in a freshwater ecosystem, *Appl. Environ. Microbiol.*, **58**, 3903–3907.
- Ashbolt, N., M. R. Dorsch, P. T. Cox, and B. Banens (1995), Blooming *E. coli*, what do they mean?, in *Coliforms and E. coli: Problem or Solution?*, edited by D. Kay and C. Fricker, pp. 78–85, The R. Soc. of Chem., Cambridge, U.K.
- Auer, M. T., and S. L. Niehaus (1993), Modeling fecal coliform bacteria: 1. Field and laboratory determination of loss kinetics, *Water Res.*, **27**, 693–701.
- Ayres, P. A. (1977), Coliphages in the marine environment, in *Aquatic Microbiology*, edited by F. A. Skinner and J. M. Shewman, pp. 275–298, Elsevier, New York.
- Barcina, I., J. M. Gonzalez, J. Iribarri, and L. Egea (1991), Role of protozoa in the regulation of enteric bacteria populations in seawater, *Mar. Microb. Food Webs*, **5**, 179–187.
- Barcina, I., P. Lebaron, and J. Vives-Rego (1997), Survival of allochthonous bacteria in aquatic systems: A biological approach, *FEMS Microbiol. Ecol.*, **23**, 1–9.
- Barnes, B., and D. M. Gordon (2004), Coliform dynamics and the implications for source tracking, *Environ. Microbiol.*, **6**, 501–509.
- Beach, R. A., and R. W. Sternberg (1992), Suspended sediment transport in the surf zone: Response to incident wave and longshore current interaction, *Mar. Geol.*, **108**, 275–294.
- Bitton, G. (1975), Absorption of viruses onto surfaces in soil and water, *Water Res.*, **9**, 473–484.
- Bitton, G., S. R. Farrah, R. H. Ruskin, J. Butner, and Y. J. Chou (1983), Survival of pathogenic and indicator organisms in ground water, *Groundwater*, **21**, 405–410.
- Bouteleux, C., S. Saby, D. Tozza, J. Cavard, V. Lahoussine, P. Hartemann, and L. Mathieu (2005), *Escherichia coli* behavior in the presence of organic matter released by algae exposed to water treatment chemicals, *Appl. Environ. Microbiol.*, **71**, 734–740.
- Brookes, J. D., J. P. Antenucci, M. R. Hipsey, M. D. Burch, N. Ashbolt, and C. M. Ferguson (2004), Fate and transport of pathogens in lakes and reservoirs, *Environ. Int.*, **30**, 741–759.
- Brookes, J. D., M. R. Hipsey, M. D. Burch, R. H. Regel, L. Linden, C. Ferguson, and J. P. Antenucci (2005), Relative value of surrogate indicators for detecting pathogens in lakes and reservoirs, *Environ. Sci. Technol.*, **39**, 8614–8621.
- Bruce, L. C., D. P. Hamilton, J. Imberger, G. Gal, M. Gophen, and T. Zohary (2006), A numerical simulation of the role of zooplankton in C, N and P cycling in Lake Kinneret, Israel, *Ecol. Modell.*, **193**, 412–436.
- Burkhardt, W., K. R. Calci, W. D. Watkins, S. R. Rippey, and S. J. Chirtel (2000), Inactivation of indicator microorganisms estuarine waters, *Water Res.*, **34**, 2207–2214.
- Byappanahalli, M. N., D. A. Shively, M. B. Nevers, M. J. Sadowsky, and R. L. Whitman (2003), Growth and survival of *Escherichia coli* and enterococci populations in the macro-alga *Cladophora* (Chlorophyta), *FEMS Microbiol. Ecol.*, **46**, 203–211.
- Camper, A. K., G. A. McFeters, W. G. Characklis, and W. L. Jones (1991), Growth kinetics of coliform bacteria under conditions relevant to drinking water distribution systems, *Appl. Environ. Microbiol.*, **57**, 2233–2239.
- Carlucci, A. F., and D. Pramer (1960a), An evaluation of factors affecting the survival of *Escherichia coli* in sea water. part II: Salinity, pH and nutrients, *Appl. Microbiol.*, **8**, 247–250.
- Carlucci, A. F., and D. Pramer (1960b), An evaluation of factors affecting the survival of *Escherichia coli* in sea water. part I: Experimental procedures, *Appl. Microbiol.*, **8**, 243–246.
- Chamberlin, C. E., and R. Mitchell (1978), A decay model for enteric bacteria in natural waters, in *Water Pollution Microbiology*, edited by R. Mitchell, pp. 325–348, Wiley-Interscience, New York.
- Chan, T. U., D. P. Hamilton, B. J. Robson, B. R. Hodges, and C. Dallimore (2002), Impacts of hydrological changes on phytoplankton succession in the Swan River, Western Australia, *Estuaries*, **25**, 1406–1415.
- Considine, R. F., C. J. Drummond, and D. R. Dixon (2001), Force of interaction between a biocolloid and an inorganic oxide: Complexity of surface deformation, roughness and brushlike behavior, *Langmuir*, **17**, 6325–6335.
- Craig, D. L., H. J. Fallowfield, and N. J. Cromar (2004), Use of microcosms to determine persistence of *Escherichia coli* in recreational coastal water and sediment and validation with in situ measurements, *J. Appl. Microbiol.*, **96**, 922–930.

- Crane, S. R., and J. A. Moore (1986), Modeling enteric bacterial die-off: A review, *Water Air Soil Pollut.*, **27**, 411–439.
- Curtis, T. P., D. D. Mara, and S. A. Silva (1992a), Influence of pH, oxygen and humic substances on ability of sunlight to damage fecal coliforms in waste stabilization pond water, *Appl. Environ. Microbiol.*, **58**, 1335–1343.
- Curtis, T. P., D. D. Mara, and S. A. Silva (1992b), The effect of sunlight on faecal coliforms in ponds: Implications for research and design, *Water Sci. Technol.*, **26**, 1729–1738.
- Dai, X., and J. Boll (2003), Evaluation of attachment of *Cryptosporidium parvum* and *Giardia lamblia* to soil particles, *J. Environ. Qual.*, **32**, 296–304.
- Dai, X., and J. Boll (2006), Settling velocity of *Cryptosporidium parvum* and *Giardia lamblia*, *Water Res.*, **40**, 1321–1325.
- Darakas, E. (2002), *E. coli* kinetics - Effect of temperature on the maintenance and respectively the decay phase, *Environ. Monit. Assess.*, **78**, 101–110.
- Davies, C. M., and L. M. Evison (1991), Sunlight and the survival of enteric bacteria in natural waters, *J. Appl. Bacteriol.*, **70**, 265–274.
- Davies, C. M., J. A. H. Long, M. Donald, and N. J. Ashbolt (1995), Survival of fecal microorganisms in marine and freshwater sediments, *Appl. Environ. Microbiol.*, **61**, 1888–1896.
- Davies-Colley, R. J., R. G. Bell, and A. M. Donnison (1994), Sunlight inactivation of enterococci and fecal coliforms in sewage effluent diluted in seawater, *Appl. Environ. Microbiol.*, **60**, 2049–2058.
- Davies-Colley, R. J., A. M. Donnison, D. J. Speed, C. M. Ross, and J. W. Nagels (1999), Inactivation of faecal indicator micro-organisms in waste stabilization ponds: Interactions of environmental factors with sunlight, *Water Res.*, **33**, 1220–1230.
- deRegnier, D. P., L. Cole, D. G. Schupp, and S. L. Erlandsen (1989), Viability of *Giardia* cysts suspended in lake, river and tap water, *Appl. Environ. Microbiol.*, **55**, 1223–1229.
- Desmarais, T. R., H. M. Solo-Gabriele, and C. J. Palmer (2002), Influence of soil and fecal indicator organisms in a tidally influenced subtropical environment, *Appl. Environ. Microbiol.*, **68**, 1165–1172.
- Drozd, C., and J. Schwartzbrod (1996), Hydrophobic and electrostatic cell surface properties of *Cryptosporidium parvum*, *Appl. Environ. Microbiol.*, **62**, 1227–1232.
- Dukan, S., Y. Levi, P. Piriou, F. Guyon, and P. Villon (1996), Dynamic modelling of bacterial growth in drinking water networks, *Water Res.*, **30**, 1991–2002.
- Dutka, B. J. (1984), Sensitivity of *Legionella pneumophila* to sunlight in fresh and marine waters, *Appl. Environ. Microbiol.*, **48**, 970–974.
- Enzinger, R. M., and R. C. Cooper (1976), Role of bacteria and protozoa in the removal of *Escherichia coli* from estuarine waters, *Appl. Environ. Microbiol.*, **31**, 758–763.
- Evison, L. M. (1988), Comparative studies on the survival of indicator organisms and pathogens in fresh and sea water, *Water Sci. Technol.*, **20**, 309–315.
- Fayer, R., and J. M. Trout (2005), Zoonotic protists in the marine environment, in *Oceans and Health: Pathogens in the Marine Environment*, edited by S. Belkin and R. R. Colwell, pp. 143–164, Springer, New York.
- Fayer, R., J. M. Trout, and M. C. Jenkins (1998), Infectivity of *Cryptosporidium parvum* oocysts in water at environmental temperatures, *J. Parasitol.*, **84**, 1165–1169.
- Fayer, R., J. M. Trout, E. Walsh, and R. Cole (2000), Rotifers ingest oocysts of *Cryptosporidium parvum*, *Eukaryotic Microbiol.*, **47**, 161–163.
- Flint, K. P. (1987), The long-term survival of *Escherichia coli* in river water, *J. Appl. Bacteriol.*, **63**, 261–270.
- Fong, T., and E. K. Lipp (2006), Enteric viruses of humans and animals in aquatic environments: Health risks, detection, and potential water quality assessment tools, *Microbiol. Mol. Biol. Rev.*, **69**, 357–371.
- Fujioka, R. S., and O. T. Narikawa (1982), Effect of sunlight on enumeration of indicator bacteria under field conditions, *Appl. Environ. Microbiol.*, **44**, 395–401.
- Fujioka, R. S., H. H. Hashimoto, E. B. Siwak, and R. H. F. Young (1981), Effect of sunlight on survival of indicator bacteria in seawater, *Appl. Environ. Microbiol.*, **41**, 690–696.
- Fujioka, R. S., C. Sian-Denton, M. Borja, J. Castro, and K. Morphew (1999), Soil: The environmental source of *Escherichia coli* and enterococci in Guam's streams, *J. Appl. Microbiol.*, **85**, 83–89.
- Gameson, A. L. H., and J. R. Saxon (1967), Field studies on effect of daylight on mortality of coliform bacteria, *Water Res.*, **1**, 279–295.
- Gauthier, M. J., G. N. Flatau, D. Le Rudulier, R. L. Clement, and M. P. Combarro (1991), Intracellular accumulation of potassium and glutamate specifically enhances survival of *Escherichia coli* in seawater, *Appl. Environ. Microbiol.*, **57**, 272–276.
- Gauthier, M. J., G. N. Flatau, R. L. Clement, and P. M. Munro (1992), Sensitivity of *Escherichia coli* cells to seawater closely depends on their growth stage, *J. Appl. Bacteriol.*, **73**, 257–262.
- Geldreich, E. E., and B. A. Kenner (1969), Concepts of fecal streptococci in stream pollution, *J. Water Pollut. Control Fed.*, **41**, 336–352.
- Geldreich, E. E., E. C. Best, B. A. Kenner, and D. J. Van Doesel (1968), The bacteriological aspects of stormwater pollution, *J. Water Pollut. Control Fed.*, **40**, 1861–1872.
- Gerba, C. P. (2005), Survival of viruses in the marine environment, in *Oceans and Health: Pathogens in the Marine Environment*, edited by S. Belkin and R. R. Colwell, pp. 133–142, Springer, New York.
- Gerba, C. P., and J. S. McLeod (1976), Effect of sediments on the survival of *Escherichia coli* in marine waters, *Appl. Environ. Microbiol.*, **32**, 114–120.
- Gerba, C. P., and G. E. Schaiberg (1975), Effect of particulates on virus survival in seawater, *J. Water Pollut. Control Fed.*, **47**, 93–103.
- Ghoul, M., T. Bernard, and M. Cormier (1990), Evidence that *Escherichia coli* accumulates Glycine Betaine from marine sediments, *Appl. Environ. Microbiol.*, **56**, 551–554.
- Gonzalez, J. M., J. Iribarri, L. Egea, and I. Barcina (1990), Differential rates of digestion of bacteria by freshwater and marine phagotrophic protozoa, *Appl. Environ. Microbiol.*, **56**, 1851–1857.
- Gordon, C., and S. Toze (2003), Influence of groundwater characteristics on the survival of enteric viruses, *J. Appl. Microbiol.*, **95**, 536–544.
- Gould, D. J., and D. Munro (1981), Relevance of microbial mortality to outfall design, in *Coastal Discharges*, edited, pp. 45–50, Thomas Telford Ltd., London.
- Goyal, S. M., C. P. Gerba, and J. L. Melnick (1978), Prevalence of human enteric viruses in coastal canal communities, *J. Water Pollut. Control Fed.*, **50**, 2247–2256.
- Hanes, N. B., and R. Fragala (1967), Effect of seawater concentration on survival of indicator bacteria, *J. Water Pollut. Control Fed.*, **39**, 97–104.
- Harm, W. (1980), *Biological Effects of Ultraviolet Radiation*, 216 pp., Cambridge Univ. Press, London.
- Hartke, A., S. Lemarinier, V. Pichereau, and Y. Auffray (2002), Survival of *Enterococcus faecalis* in seawater microcosms is limited in the presence of bacterivorous zooflagellates, *Curr. Microbiol.*, **44**, 329–335.
- Havelaar, A. H., M. van Olphen, and Y. C. Drost (1993), F-specific RNA bacteriophages are adequate model organisms for enteric viruses in fresh water, *Appl. Environ. Microbiol.*, **59**, 2956–2962.
- Hendricks, C. W., and S. M. Morrison (1967), Multiplication and growth of selected enteric bacteria in clear mountain stream water, *Water Res.*, **1**, 567–576.
- Hillmer, I., and J. Imberger (2007), Influence of advection on time and space scales of ecological variables in a coastal equilibrium flow, *Cont. Shelf Res.*, **27**, 134–153.
- Hipsey, M. R., J. P. Antenucci, J. D. Brookes, M. D. Burch, R. H. Regel, and L. Linden (2004), A three dimensional model of *Cryptosporidium* dynamics in lakes and reservoirs: A new tool for risk management, *Intl. J. River Basin Manage.*, **2**, 181–197.
- Hipsey, M. R., J. D. Brookes, J. P. Antenucci, M. D. Burch, R. H. Regel, C. Davies, N. J. Ashbolt, and C. Ferguson (2005), *Hydrodynamic Distribution of Pathogens in Lakes and Reservoirs*, Awwa Res. Found., Colorado.
- Hipsey, M. R., J. D. Brookes, R. H. Regel, J. P. Antenucci, and M. D. Burch (2006a), In situ evidence for the association of total coliforms and *Escherichia coli* with suspended inorganic particles in an Australian reservoir, *Water Air Soil Pollut.*, **170**, 191–209.
- Hipsey, M. R., J. R. Romero, J. P. Antenucci, and D. P. Hamilton (2006b), The computational aquatic ecosystem dynamics model (CAEDYM): v3.2 Science Manual, edited, Report by Centre for Water Res., Univ. of Western Australia, Perth, Australia.
- Hodges, B. R., J. Imberger, A. Saggio, and K. B. Winters (2000), Modeling basin-scale internal waves in a stratified lake, *Limnol. Oceanogr.*, **45**, 1603–1620.
- Hood, M. A., and G. E. Ness (1982), Survival of *Vibrio cholerae* and *Escherichia coli* in estuarine waters and sediments, *Appl. Environ. Microbiol.*, **43**, 578–584.
- Howell, J. M., M. S. Coyne, and P. L. Cornelius (1996), Effect of sediment particle size and temperature on fecal bacteria mortality rates and the fecal coliform/fecal streptococci ratio, *J. Environ. Qual.*, **25**, 1216–1220.
- Iribarri, J., B. Ayo, I. Artolozaga, I. Barcina, and L. Egea (1994a), Grazing on allochthonous vs autochthonous bacteria in river water, *Lett. Appl. Microbiol.*, **18**, 12–14.
- Iribarri, J., I. Azua, A. Labirua-Iturburu, I. Artolozaga, and I. Barcina (1994b), Differential elimination of enteric bacteria populations in seawater, *J. Appl. Bacteriol.*, **77**, 476–483.

- Jin, G., A. J. Englande, and A. Liu (2003), A preliminary study on coastal water quality monitoring and modeling, *J. Environ. Sci. Health, A38*, 493–509.
- John, D. E., and J. B. Rose (2004), Survival of fecal indicator bacteria, bacteriophage and protozoa in Florida's surface and ground waters: Potential implications for aquifer storage and recovery, edited, Report by Univ. of Florida, Fla.
- Johnson, D. C., C. E. Enriquez, I. L. Pepper, T. L. Davis, C. P. Gerba, and J. B. Rose (1997), Survival of *Giardia*, *Cryptosporidium*, poliovirus and *Salmonella* in marine waters, *Water Sci. Technol.*, 35, 261–268.
- Kapuscinski, R. B., and R. Mitchell (1980), Process controlling virus inactivation in coastal waters, *Water Res.*, 17, 363–371.
- Kaspar, C. W., and M. L. Tamplin (1993), Effects of temperature and salinity on the survival of *Vibrio vulnificus* in seawater and shellfish, *Appl. Environ. Microbiol.*, 59, 2425–2429.
- Karunasagar, I., and Karunasagar, I. (2005), Retention of pathogenicity in viable but non-culturable pathogens, in *Oceans and Health: Pathogens in the Marine Environment*, edited by S. Belkin and R. R. Colwell, pp. 69–92, Springer, New York.
- Khaengraeng, R., and R. H. Reed (2005), Oxygen and photoinactivation of *Escherichia coli* in UVA and sunlight, *J. Appl. Microbiol.*, 99, 39–50.
- King, B. J., A. R. Keegan, P. T. Monis, and C. P. Saint (2005), Environmental temperature controls *Cryptosporidium* oocyst metabolic rate and associated retention of infectivity, *Appl. Environ. Microbiol.*, 71, 3848–3857.
- King, B. J., D. Hoefel, D. P. Damiñato, S. Fanok, and P. T. Monis (2008), Solar UV reduces *Cryptosporidium parvum* oocyst infectivity in environmental waters, *J. Appl. Microbiol.*, 104, 1311–1323.
- Klock, J. W. (1971), Survival of coliform bacteria in wastewater treatment lagoons, *J. Water Pollut. Control Fed.*, 43, 2071–2083.
- Korhonen, L. K., and P. J. Martikainen (1991), Survival of *Escherichia coli* and *Campylobacter jejuni* in untreated and filtered lake water, *J. Appl. Microbiol.*, 71, 379–382.
- LaLiberte, P., and D. J. Grimes (1982), Survival of *Escherichia coli* in lake bottom sediment, *Appl. Environ. Microbiol.*, 43, 623–628.
- Lantrip, B. M. (1983), *The Decay of Enteric Bacteria in an Estuary*, John Hopkins Univ., Baltimore, Md.
- Laval, B. E., J. Imberger, B. R. Hodges, and R. Stocker (2003), Modeling circulation in lakes: Spatial and temporal variations, *Limnol. Oceanogr.*, 48, 983–994.
- LeChevalier, M. W. (2003), Conditions favouring coliform and HPC bacterial growth in drinking-water and on contact water surfaces, in *Heterotrophic Plate Counts and Drinking-Water Safety*, edited by J. Bartram et al., pp. 177–197, IWA Publishing, London, U.K.
- LeChevalier, M. W., N. J. Welch, and D. B. Smith (1996), Full-scale studies of factors related to coliform regrowth in drinking water, *Appl. Environ. Microbiol.*, 62, 2201–2211.
- Lessard, E. J., and J. M. Sieburth (1983), Survival of natural sewage populations of enteric bacteria in diffusion and batch chambers in the marine environment, *Appl. Environ. Microbiol.*, 45, 950–959.
- Liu, S. (2002), Fecal coliform decay and regrowth kinetics in an anaerobic dairy wastewater environment, M.Sc. thesis, 75 pp., Louisiana State Univ., La.
- Lopez-Torres, A. J., L. Prieto, and T. C. Hazen (1988), Comparison of the in situ survival and activity of *Klebsiella pneumoniae* and *Escherichia coli* in tropical marine environments, *Microbiol. Ecol.*, 15, 41–57.
- Mancini, J. L. (1978), Numerical estimates of coliform mortality rates under various conditions, *J. Water Pollut. Control Fed.*, 50, 2477–2484.
- Marino, R. P., and J. J. Gannon (1991), Survival of faecal coliforms and faecal streptococci in storm drain sediment, *Water Res.*, 25, 1089–1098.
- Matsumoto, J., and T. Omura (1980), Some factors affecting the survival of fecal indicator bacteria in seawater, *Tech. Rep.*, 45, 169–185.
- Mayo, A. W. (1995), Modeling coliform mortality in waste stabilization ponds, *J. Environ. Eng.*, 121, 140–152.
- McCambridge, J., and T. A. McMeekin (1980), Effect of temperature on activity of predators of *Salmonella typhimurium* and *Escherichia coli* in estuarine waters, *Aust. J. Mar. Freshwater Res.*, 31, 851–855.
- McCambridge, J., and T. A. McMeekin (1980), Relative effects of bacterial and protozoan predators on survival of *Escherichia coli* in estuarine water samples, *Appl. Environ. Microbiol.*, 40, 907–911.
- McCambridge, J., and T. A. McMeekin (1981), Effect of solar radiation and predaceous microorganisms on survival of fecal and other bacteria, *Appl. Environ. Microbiol.*, 41, 1083–1087.
- McCorquodale, J. A., I. Georgiou, S. Carnelos, and A. J. Englande (2004), Modeling coliforms in storm water plumes, *J. Environ. Eng. Sci.*, 3, 419–431.
- McDaniels, A. E., K. W. Cochran, J. J. Gannon, and G. W. Williams (1983), Rotavirus and reovirus stability in microorganism-free distilled and wastewater, *Water Res.*, 17, 1349–1353.
- McFeters, G. A., and D. G. Stuart (1972), Survival of coliform bacteria in natural waters: Field and laboratory studies with membrane-filter chambers, *Appl. Microbiol.*, 24, 805–811.
- McFeters, G. A., G. K. Bissonnette, J. J. Jezeski, C. A. Thomson, and D. G. Stuart (1974), Comparative survival of indicator bacteria and enteric pathogens in well water, *Appl. Microbiol.*, 27, 805–811.
- Medema, G. J., and J. F. Schijven (2001), Modelling the sewage discharge and dispersion of *Cryptosporidium* and *Giardia* in surface water, *Water Res.*, 35, 4307–4316.
- Medema, G. J., M. Bahar, and F. M. Schets (1997), Survival of *Cryptosporidium parvum*, *Escherichia coli*, Faecal Enterococci and *Clostridium perfringens* in river water: Influence of temperature and autochthonous microorganisms, *Water Sci. Technol.*, 35, 249–252.
- Medema, G. J., F. M. Schets, P. F. M. Teunis, and A. H. Havelaar (1998), Sedimentation of free and attached *Cryptosporidium* oocysts and *Giardia* cysts in water, *Appl. Environ. Microbiol.*, 64, 4460–4466.
- Menon, P., S. Becquevert, G. Billen, and P. Servais (1996), Kinetics of flagellate grazing in the presence of two types of bacterial prey, *Microbiol. Ecol.*, 31, 89–101.
- Menon, P., G. Billen, and P. Servais (2003), Mortality rates of autochthonous and fecal bacteria in natural aquatic ecosystems, *Water Res.*, 37, 4151–4158.
- Mezrioui, N., K. Oufdou, and B. Baleux (1995), Dynamics of non-O1 *Vibrio cholerae* and faecal coliforms in experimental stabilization ponds in the arid region of Marrakesh, Morocco, and the effect of pH, temperature, and sunlight on their experimental survival, *Can. J. Microbiol.*, 41, 489–498.
- Mills, S. W., G. P. Alabaster, D. D. Mara, H. W. Pearson, and W. N. Thitai (1992), Efficiency of faecal bacteria removal in waste stabilization ponds in Kenya, *Water Sci. Technol.*, 26, 1739–1748.
- Mitchell, R., and H. W. Jannagh (1969), Processes controlling virus inactivation in seawater, *Environ. Sci. Technol.*, 3, 941–943.
- Mitchell, D. O., and M. J. Starzyk (1975), Survival of *Salmonella* and other indicator microorganisms, *Can. J. Microbiol.*, 21, 1420–1421.
- Morowitz, H. J. (1950), Absorption effects in volume irradiation of micro-organisms, *Science*, 111, 229–230.
- Moss, S. H., and K. C. Smith (1981), Membrane damage can be a significant factor in the inactivation of *Escherichia coli* by near ultraviolet radiation, *Photochem. Photobiol.*, 33, 541–543.
- Munro, P. M., F. Laumond, and M. J. Gauthier (1987), A previous growth of enteric bacteria on salted medium increased their survival in seawater, *Lett. Appl. Microbiol.*, 4, 121–124.
- Murray, A. G., and G. A. Jackson (1993), Viral dynamics II: A model of the interaction of ultraviolet light and mixing processes on virus survival in seawater, *Mar. Ecol. Prog. Ser.*, 102, 105–114.
- Murray, J. P., and S. J. Laband (1979), Degradation of poliovirus by adsorption on inorganic surfaces, *Appl. Environ. Microbiol.*, 37, 480–486.
- Naik, S. R., A. Aggarwal, G. L. Sharma, and V. K. Vinayak (1982), Effect of salinity, pH, and temperature on the survival of cysts of *Giardia lamblia*, *Indian J. Parasitol.*, 6, 231–232.
- Nasser, A. M., and S. D. Oman (1999), Quantitative assessment of the inactivation of pathogenic and indicator viruses in natural water sources, *Water Res.*, 33, 1748–1772.
- Niemi, M. (1976), Survival of *Escherichia coli* phage T7 in different water types, *Water Res.*, 10, 751–755.
- Noble, R. T., I. M. Lee, and K. C. Schiff (2004), Inactivation of indicator micro-organisms from various sources of faecal contamination in seawater and freshwater, *J. Appl. Microbiol.*, 96, 464–472.
- O'Brien, R. T., and J. S. Newman (1977), Inactivation of polioviruses and coxsackieviruses in surface water, *Appl. Environ. Microbiol.*, 33, 334–346.
- Orlob, G. T. (1956), Viability of sewage bacteria in seawater, *Sew. Indust. Wastes*, 28, 1147–1167.
- Ottosson, J., and T. A. Stenstrom (2003), Growth and reduction of micro-organisms in sediments collected from a graywater treatment system, *Lett. Appl. Microbiol.*, 36, 168–172.
- Palmer, M. (1988), Bacterial loadings from resuspended sediments in recreational beaches, *Can. J. Civ. Eng.*, 15, 450–455.
- Parhad, N. M., and N. U. Rao (1974), Effect of pH on survival of *Escherichia coli*, *J. Water Pollut. Control Fed.*, 46, 980–986.
- Payment, P., and E. Franco (1993), *Clostridium perfringens* and somatic coliphages as indicators of the efficiency of drinking water treatment for viruses and protozoan cysts, *Appl. Environ. Microbiol.*, 59, 2418–2424.
- Payment, P., E. Morin, and M. Trudel (1988), Coliphages and enteric viruses in the particulate phase of river water, *Can. J. Microbiol.*, 34, 907–910.

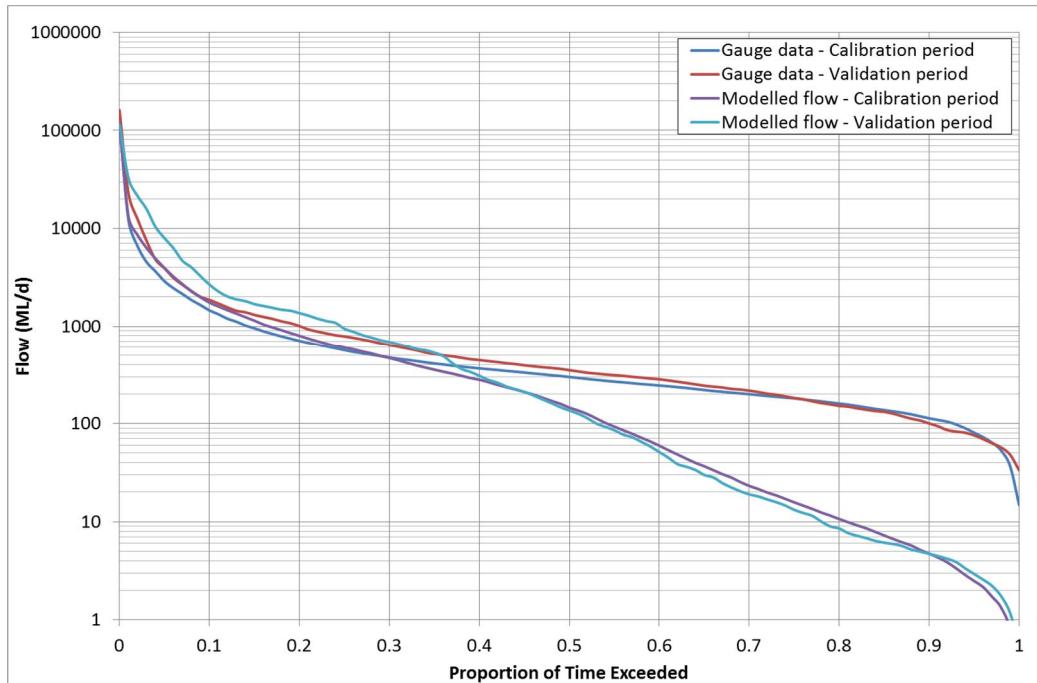
- Pearson, H. W., D. D. Mara, S. W. Mills, and D. J. Smallman (1987), Physico-chemical parameters influencing faecal bacterial survival in waste stabilization ponds, *Water Sci. Technol.*, **18**, 145–152.
- Pommepuy, M., J. F. Guillaud, E. Dupray, A. Derrien, F. LeGuyader, and M. Cormier (1992), Enteric bacteria survival factors, *Water Sci. Technol.*, **25**, 93–103.
- Power, M. L., J. Littlefield-Wyer, D. M. Gordon, D. A. Veal, and M. B. Slade (2005), Phenotypic and genotypic characterization of encapsulated *Escherichia coli* isolated from blooms in two Australian lakes, *Environ. Microbiol.*, **7**, 631–640.
- Rhodes, M. W., and H. I. Kator (1988), Survival of *Escherichia coli* and *Salmonella* spp. in estuarine environments, *Appl. Environ. Microbiol.*, **54**, 2902–2907.
- Rhodes, M. W., and H. I. Kator (1990), Effects of sunlight and autochthonous microbiota on *Escherichia coli* survival in an estuarine environment, *Curr. Microbiol.*, **21**, 65–73.
- Robertson, L. J., A. T. Campbell, and H. V. Smith (1992), Survival of *Cryptosporidium parvum* oocysts under various environmental pressures, *Appl. Environ. Microbiol.*, **58**, 3494–3500.
- Robson, B. J., and D. P. Hamilton (2004), Three-dimensional modelling of a *Microcystis* bloom event in the Swan River estuary, Western Australia, *Ecol. Modell.*, **174**, 203–222.
- Romero, J. R., J. P. Antenucci, and J. Imberger (2004), One- and three-dimensional biogeochemical simulations of two differing reservoirs, *Ecol. Modell.*, **174**, 143–160.
- Romero, J. R., J. Imberger, J. P. Antenucci, and C. J. Dallimore (2006), ARMS (Aquatic Real-time Management System): An automated decision support system for lakes, estuaries and coastal zones, Proceedings of the 2nd Intl. Symp. Mangt. Engin. Informatics (MEI), Orlando, Florida.
- Roper, M. M., and K. C. Marshall (1978), Biological control agents of sewage bacteria in marine habitats, *Aust. J. Mar. Freshwater Res.*, **29**, 335–343.
- Rossi, P., and M. Aragno (1999), Analysis of bacteriophage inactivation and its attenuation by adsorption onto colloidal particles by batch agitation techniques, *Can. J. Microbiol.*, **45**, 9–17.
- Ross, T., D. A. Ratkowsky, T. A. Mellefont, and T. A. McMeekin (2003), Modelling the effects of temperature, water activity, pH and lactic acid concentration on the growth rate of *Escherichia coli*, *Intl. J. Food Microbiol.*, **82**, 33–43.
- Rozen, Y., and S. Belkin (2005), Survival of enteric bacteria in seawater: Molecular aspects, in *Oceans and Health: Pathogens in the Marine Environment*, edited by S. Belkin and R. R. Colwell, pp. 93–108, Springer, New York.
- Salomon, J. C., and M. Pommepuy (1990), Mathematical model of bacterial contamination of the Morlaix Estuary (France), *Water Res.*, **24**, 983–994.
- Salter, M. A., D. A. Ratkowsky, T. Ross, and T. A. McMeekin (2000), Modelling the combined temperature and salt (NaCl) limits for growth of a pathogenic *Escherichia coli* strain using nonlinear logistic regression, *Intl. J. Food Microbiol.*, **61**, 159–167.
- Sarikaya, H. Z., and A. M. Saatchi (1995), Bacterial die-away rates in Red Sea waters, *Water Sci. Technol.*, **32**, 45–52.
- Savage, H. P., and N. B. Hanes (1971), Toxicity of seawater to coliform bacteria, *J. Water Pollut. Control Fed.*, **43**, 855–861.
- Scarse, L. E., S. H. Rubenstein, and S. Megregian (1964), Survival of indicator bacteria in receiving waters under various conditions, paper presented at 7th Conference on Great Lakes Research, Great Lakes Res. Inst., Ann Arbor, Mich.
- Scott, D. M. (2000), *Fecal Coliform Decay in an Anaerobic Dairy Wastewater Environment*, Louisiana State Univ., La.
- Shiraish, M. P., A. C. Rex, G. W. Pettibone, K. Keay, P. McManus, M. A. Rex, J. Ebersole, and E. Gallagher (1987), Distribution of indicator bacteria and *Vibrio parahaemolyticus* in sewage-polluted intertidal sediments, *Appl. Environ. Microbiol.*, **53**, 1756–1761.
- Sinton, L. W. (2005), Biotic and abiotic effects, in *Oceans and Health: Pathogens in the Marine Environment*, edited by S. Belkin and R. R. Colwell, pp. 69–92, Springer, New York.
- Sinton, L. W., R. J. Davies-Colley, and R. G. Bell (1994), Inactivation of enterococci and fecal coliforms from sewage and meatworks effluent in seawater chambers, *Appl. Environ. Microbiol.*, **60**, 2040–2048.
- Sinton, L. W., R. K. Finlay, and P. A. Lynch (1999), Sunlight inactivation of fecal bacteriophages and bacteria in sewage-polluted seawater, *Appl. Environ. Microbiol.*, **65**, 3605–3613.
- Sinton, L. W., C. H. Hall, P. A. Lynch, and R. J. Davies-Colley (2002), Sunlight inactivation of fecal indicator bacteria and bacteriophages from waste stabilization pond effluent in fresh and saline waters, *Appl. Environ. Microbiol.*, **68**, 1122–1131.
- Solic, M., and N. Krstulovic (1992), Separate and combined effects of solar radiation, temperature, salinity and pH on the survival of faecal coliforms in seawater, *Mar. Pollut. Bull.*, **24**, 411–416.
- Solo-Gabriele, H. M., M. A. Wolfert, T. R. Desmarais, and C. J. Palmer (2000), Sources of *Escherichia coli* in a coastal subtropical environment, *Appl. Environ. Microbiol.*, **66**, 230–237.
- Spillman, C. M., J. Imberger, D. P. Hamilton, M. R. Hipsey, and J. R. Romero (2007), Modelling the effects of Po River discharge, internal nutrient cycling and hydrodynamics on biogeochemistry of the Northern Adriatic Sea, *J. Mar. Syst.*, **68**, 167–200.
- Steets, B. M., and P. A. Holden (2003), A mechanistic model of runoff-associated fecal coliform fate and transport through a coastal lagoon, *Water Res.*, **37**, 589–608.
- Stetler, R. E. (1984), Coliphages as indicators of enteroviruses, *Appl. Environ. Microbiol.*, **48**, 668–676.
- Stott, R., E. May, E. Matsushita, and A. Warren (2001), Protozoan predation as a mechanism for the removal of *Cryptosporidium* oocysts from wastewaters in constructed wetlands, *Water Sci. Technol.*, **44**, 191–198.
- Struck, P. H. (1998), The relationship between sediment fecal coliform levels in a Puget Sound estuary, *J. Environ. Health*, **50**, 403–407.
- van der Kooij, D. (2003), Managing regrowth in drinking-water distribution systems, in *Heterotrophic Plate Counts and Drinking-Water Safety*, edited by J. Bartram et al., pp. 199–232, IWA Publishing, London, U.K.
- Van Donsel, D. J., and E. E. Geldreich (1971), Relationship of salmonellae to fecal coliforms in bottom sediments, *Water Res.*, **5**, 1079–1087.
- Vasconcelos, G. J., and R. G. Swartz (1976), Survival of bacteria in seawater using a diffusion chamber apparatus in situ, *Appl. Environ. Microbiol.*, **31**, 913–920.
- Walker, F. R., and J. R. Stedinger (1999), Fate and transport model of *Cryptosporidium*, *J. Environ. Eng.*, **125**, 325–333.
- Webb, R. B., and M. S. Brown (1979), Action spectra for oxygen-dependent and independent activation of *Escherichia coli* WP2s from 254 to 460 nm, *Photochem. Photobiol.*, **29**, 407–409.
- Webb, R. B., and J. R. Lorenz (1970), Oxygen dependence and repair of lethal effects of near ultraviolet and visible light, *Photochem. Photobiol.*, **12**, 383–389.
- Weiss, C. M. (1951), Adsorption of *Escherichia coli* on river and estuarine silts, *Sew. Indust. Wastes*, **23**, 227–237.
- Whitman, R. L., and M. B. Nevers (2003), Foreshore sand as a source of *Escherichia coli* in nearshore water of a Lake Michigan beach, *Appl. Environ. Microbiol.*, **69**, 5555–5562.
- Wilkinson, J., A. Jenkins, M. Wyer, and D. Kay (1995), Modelling faecal coliform dynamics in streams and rivers, *Water Res.*, **29**, 847–855.
- Withers, N., and M. Drikas (1998), Bacterial regrowth potential: Quantitative measure by acetate carbon equivalents, *Water*, **25**, 19–23.
- Yates, M. V., L. D. Stetzenbach, C. P. Gerba, and N. A. Sinclair (1990), The effect of indigenous bacteria on virus survival in ground water, *J. Environ. Sci. Health*, **A25**, 81–100.
- Zanoni, B., C. Garzaroni, S. Anselmi, and G. Rondinini (1993), Modeling the growth of *Enterococcus faecium* in bologna sausage, *Appl. Environ. Microbiol.*, **59**, 3411–3417.

J. P. Antenucci and M. R. Hipsey, Centre for Water Research, The University of Western Australia, 35 Stirling Highway, Crawley, WA 6009, Australia. (hipsey@cwr.uwa.edu.au)

J. D. Brookes, School of Earth and Environmental Sciences, The University of Adelaide, North Terrace, Adelaide, SA 5005, Australia.

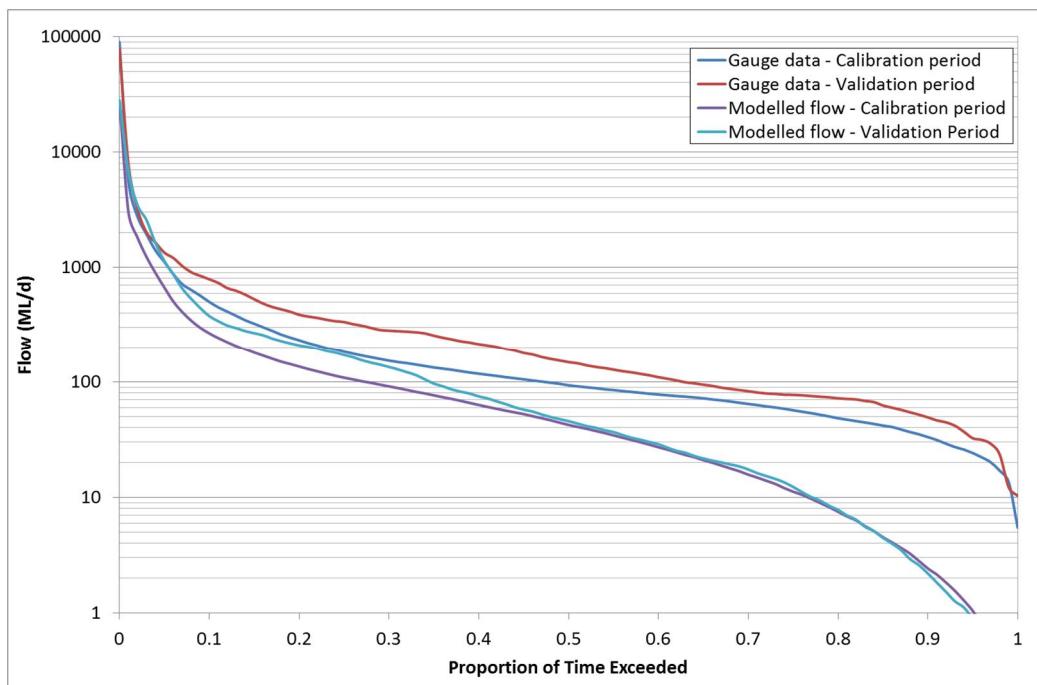
Addendum 1 Flow Duration Curves

Calibration flow duration curves for each of the catchments are provided in **Figure AD1 1 to Figure AD1 7**. Following this, the response provided to the Environmental Flows River Health Outcome Group (EFRHOG) Technical Working Group (TWG) is appended.

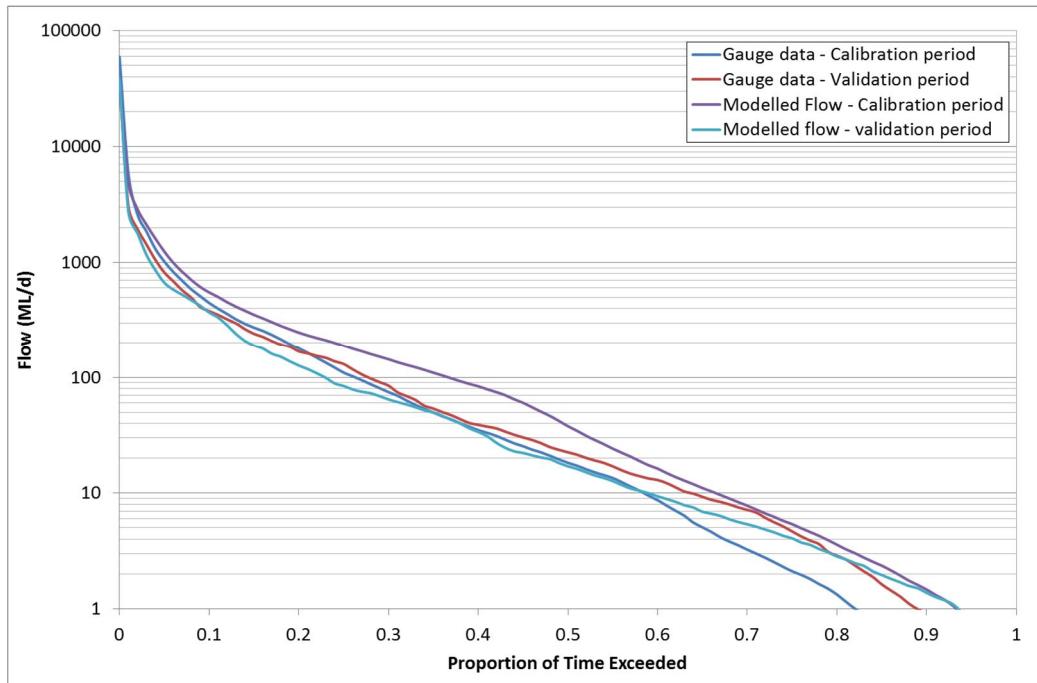


- **Figure AD1 1 Colo River (no. 212290) calibration flow duration curve**

Water Quality Modelling of the Hawkesbury-Nepean River System

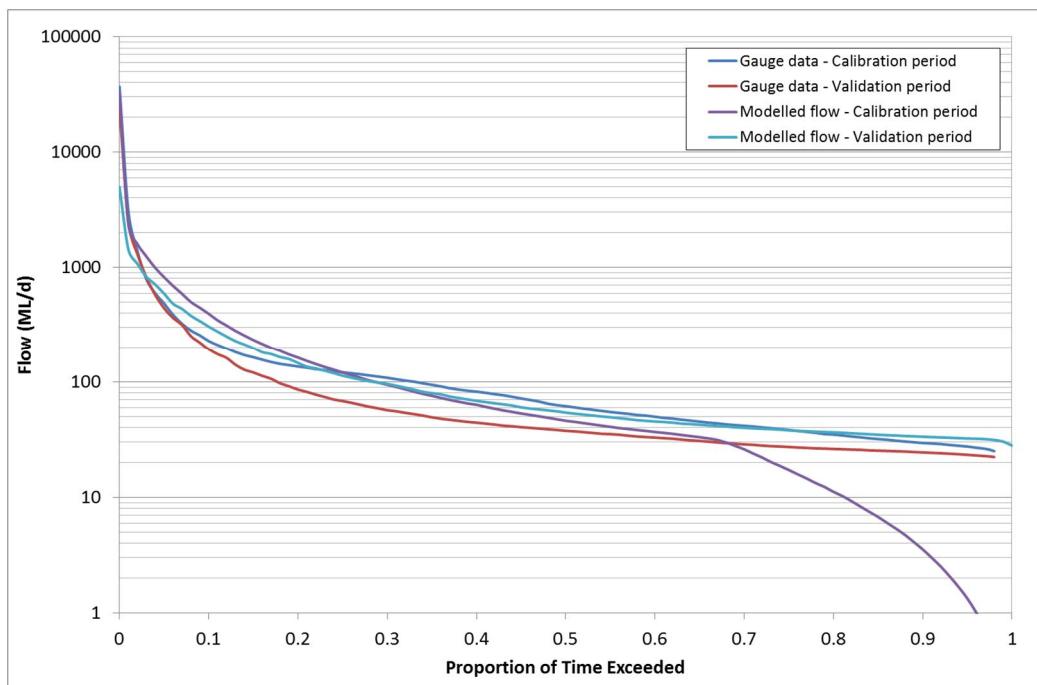


■ **Figure AD1 2 Grose River (no. 212291) calibration flow duration curve**

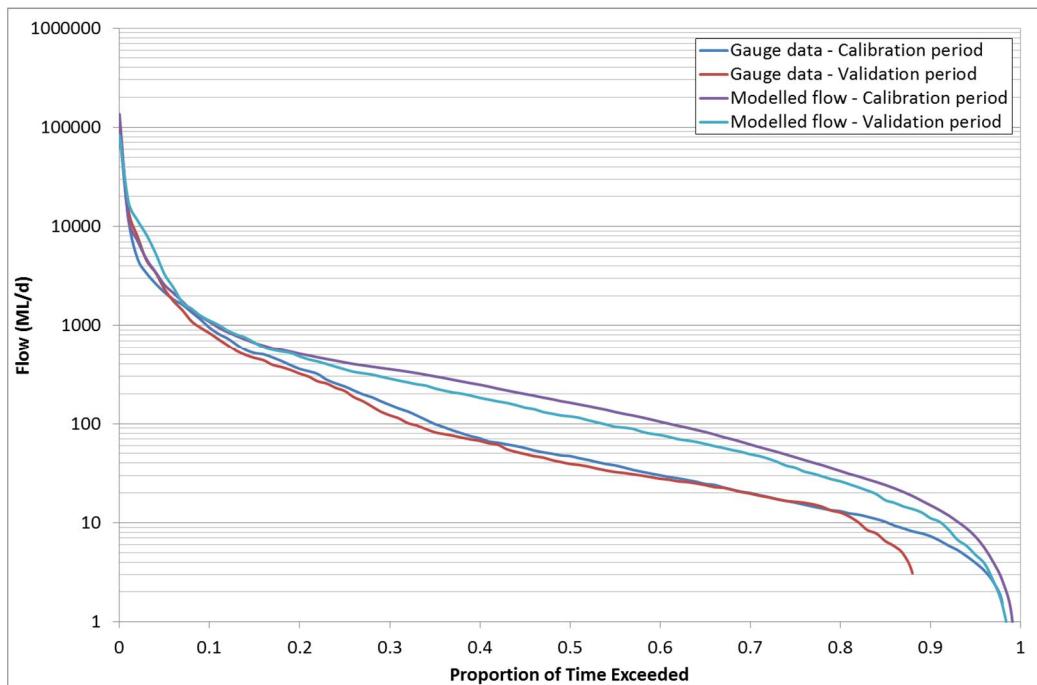


■ **Figure AD1 3 MacDonald River (no. 212228) calibration flow duration curve**

Water Quality Modelling of the Hawkesbury-Nepean River System

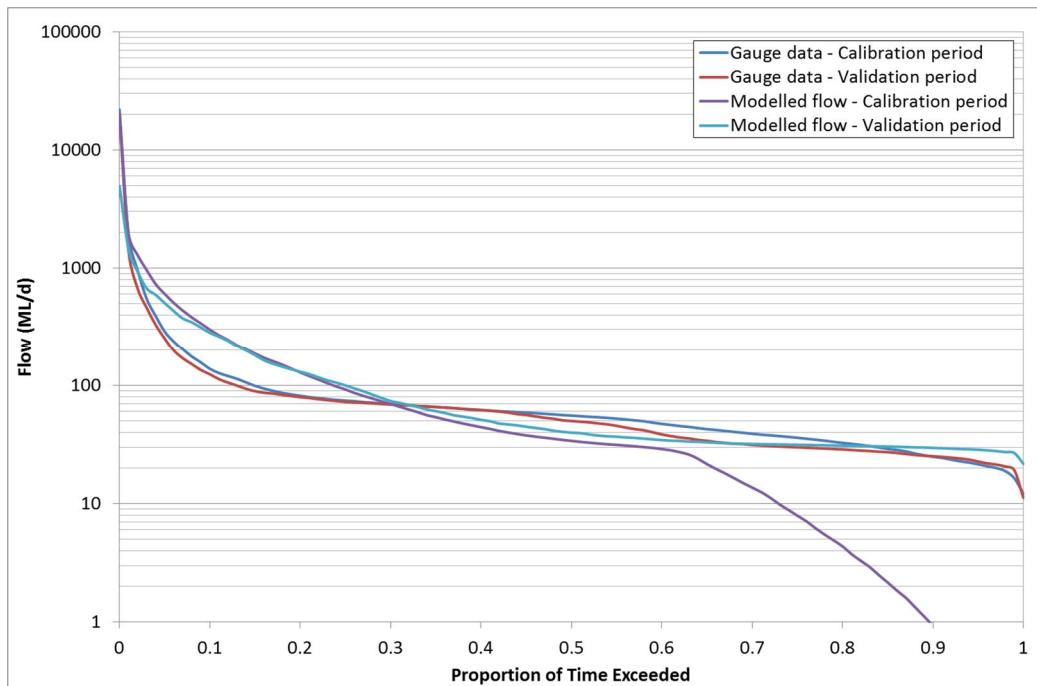


■ **Figure AD1 4 South Creek (no. 212297) calibration flow duration curve**

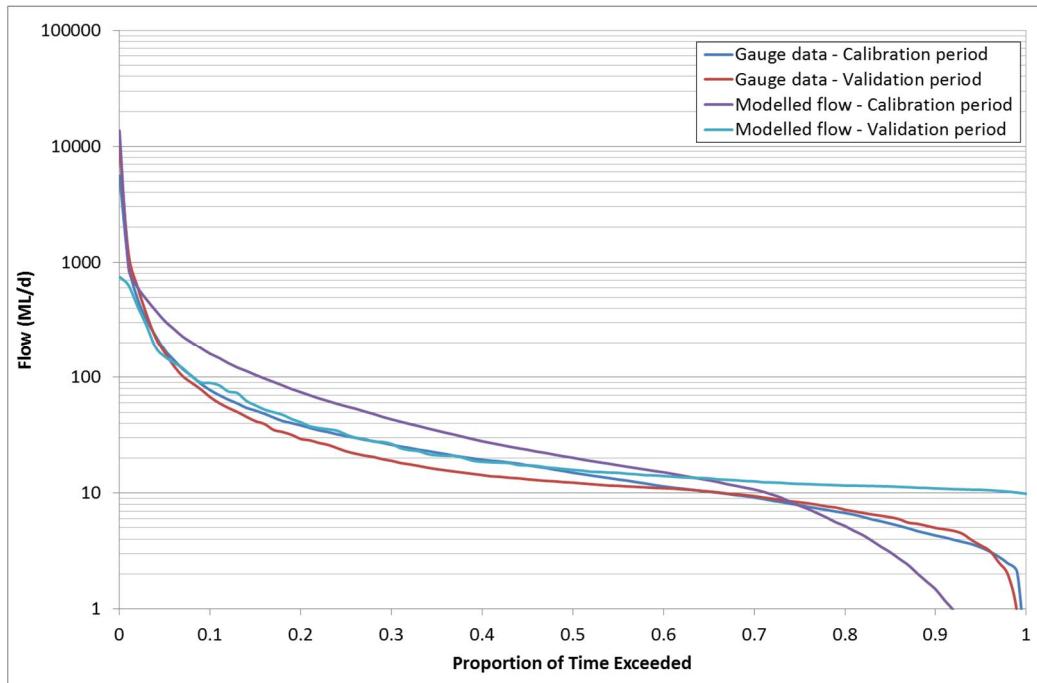


■ **Figure AD1 5 Mt Hunter Weir (no. 212213) calibration flow duration curve**

Water Quality Modelling of the Hawkesbury-Nepean River System



■ **Figure AD1 6 Eastern Creek (no. 212296) calibration flow duration curve**



■ **Figure AD1 7 Cattai Creek (no. 212295) calibration flow duration curve**

Response to EFRHOG TWG model calibration questions

The Environmental Flows River Health Outcome Group (EFRHOG) Technical Working Group (TWG) has raised concerns over the quality of the Hawkesbury Nepean River and South Creek model calibration. These concerns are hindering the use of the model output in the environmental flows decisions. This memo seeks to address these concerns and respond to questions raised at the modellers forum.

Context

The calibration of the Hawkesbury Nepean River and South Creek model was accepted by Sydney Water and the CSIRO (independent peer reviewer) in August 2013. The CSIRO reviewed the model twice which is beyond industry practise in terms of peer review frequency. The contractors, SKM in partnership with BMT WBM and eWater Ltd, then commenced running the scenarios which were complete by the end of November 2013.

Following acceptance of the model calibration, Sydney Water:

- provided copies of the calibration report to our agency stakeholders (September 2013)
- held an interagency briefing with key internal and external stakeholders which included a general overview of the scenarios, timeframes, model output and analysis (September 2013)
- chaired a detailed modellers discussion forum for relevant agencies to ask technical questions directly to our modelling contractors (October 2013).

The intent was to promote an open transparent process and understanding of the model.

The modellers forum was attended by modellers and technical staff from the Office of Environment and Heritage, NSW Office of Water, Sydney Catchment Authority and Sydney Water. The Working Notes from this forum are provided as an attachment to this memo.

During the modellers forum, agency stakeholders raised two main concerns that required clarification:

1. Source model was only calibrated for high flows and as such the low flows are under represented
2. South Creek water quality is under predicted and this has impacted water quality results downstream of the South Creek inflow, particularly chlorophyll a levels.

A response to these questions has been provided by SKM and are included in the below 'Analysis' section (Questions 1 and 2).

A further concern raised by the Environmental Flows River Health Outcome Group (EFRHOG) Technical Working Group (TWG) is that the model does not appear to perform well when compared to measured data. A response to this is also provided in the below 'Analysis' section (Question 3).

Analysis

Question 1: The Source model was only calibrated for high flows and as such the low flows are under represented

The eWater Source model was calibrated and validated to observed flow data across the full range of recorded flows. Data was used from eleven streamflow gauging sites which cover approximately three-quarters of the overall study area. Flow duration curves for some key catchments, (Colo, Grose and MacDonald rivers), are provided in Attachment 1. These show a good fit for high and low flows.

The calibration process involved both comparison to flow duration curves and comparison of the shape, peaks and timing of the hydrograph time series. Both manual and automated calibration of rainfall runoff parameters was used. During automated calibration the optimisation algorithm was tuned to optimise to the Nash Sutcliffe Coefficient of Efficiency (CoE) and/or the shape of the flow duration curve. There was considerable attention paid to fitting to low flows, particularly the slope of the baseflow recessions, which were largely calibrated manually. Once the baseflow recessions were calibrated, the lower zone parameters were normally fixed and then the later stages of automated calibration focussed on the upper zone and in-stream routing parameters of the Sacramento models.

In the South Creek catchment the same process was adopted but the data for extractions was limited and in the absence of such data the IQQM crop model, as provided by the NSW Office of Water, was used. These are unrestricted demands and are consistent with the low level of enforcement of regulations at the time. The flow duration curve for South Creek is shown in Attachment 1. This shows a good fit for the validation period over the full range of flows and for 70% of the time during the calibration period.

Question 2: South Creek water quality is under predicted and this has impacted water quality results downstream of the South Creek inflow, particularly chlorophyll a levels

The modelled concentrations of total nitrogen in South Creek are a good match to observed concentrations in both high and low flows (Attachment 2). For phosphorus, the match is good in low flows however is slightly underestimated during event (high) flows. More data collected during events would be needed to improve this prediction.

Water quality downstream of South Creek is influenced by a number of factors of which South Creek is only one. It is not appropriate to infer that South Creek water quality alone controls the water quality downstream.

Plots showing the calibration (2006) and validation (2007) of chlorophyll a are presented in Attachment 3.

The site located on the Hawkesbury River immediately downstream of the South Creek inflow (N35 - Hawkesbury River at Wilberforce) shows a very good chlorophyll a calibration. The next site downstream is N3001 (Hawkesbury River off Cattai Creek National Park downstream of Cattai Creek inflow). There was no data available for this site for the 2006 and 2007 calibration and validation period to compare, however the plot has a similar shape and magnitude to N35 upstream. The next site downstream is N26 (Hawkesbury River at Sackville). N26 is located 26 km downstream of the South Creek confluence. For most of the 2006 calibration period, the model predictions are correct with the exception of the last few months which were low. For the 2007 validation period, there were only five data points to compare and the model picks up on three of these.

The furthermost downstream sites are at Leetsvale and Wisemans Ferry (N18 and N14 respectively). The model represents chlorophyll a at these sites accurately.

Overall, with the exception of a few months in 2006, the model is representing chlorophyll a downstream of the South Creek inflow very well.

Question 3: The model does not appear to perform well when compared to measured data

Hawkesbury Nepean River and South Creek model is NOT a predictive model, so the model output cannot be compared with observed data ie the model is not predicting what the output should be. Hindcast modelling has been used to calibrate and validate the model. Data AND the climate sequence from 2006-07 were used for this process. It is only data from this 2006-07 period that can be compared with the corresponding model output.

The model is a scenario based model that produces relative output. This enables the comparison between scenarios to understand relative differences and evaluate different options on the same basis. It is not appropriate to compare the modelled output with absolute values. The reasons for this are:

- the modelled output is based on the 1985-1994 climate sequence but using 2011 wastewater treatment options. There is no physical data possible to match both these time periods, and analyses that attempt to compare model output with observations cannot, by definition, produce valid outcomes
- the sequence and intensity of rainfall and dry spells will influence water quality, so it is not appropriate to, for example, compare a dry year in the 1985-94 period with a recent dry year and expect to get the same results.

SKM has offered to meet with the Warragamba Environmental Flows Project Director and Program Manager to help them to better understand the model and further discuss any concerns they may have. Please contact Merran Griffith (merran.griffith@sydneywater.com.au) if you would like to proceed with this meeting.

Prepared by:

Merran Griffith, Principal Advisor Waterway Health
17 February 2014

1. Endorsed by:

Peter Tate, Analytics Strategist

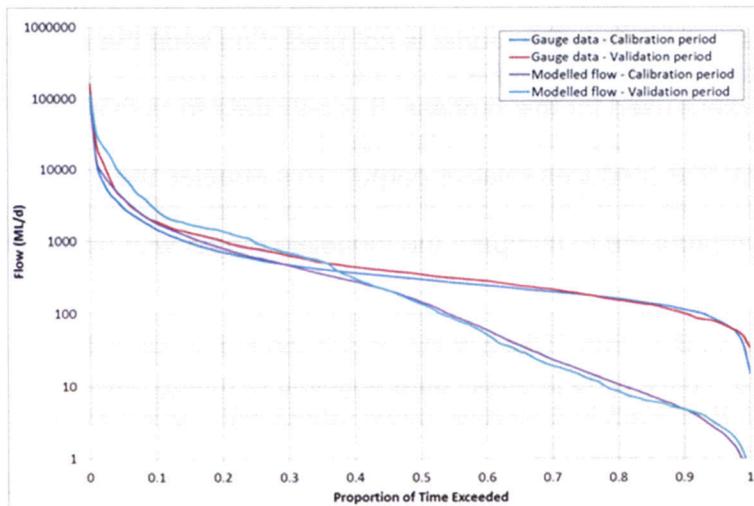
2. Endorsed by:

Peter Cox, Health Environment and Asset Science Manager

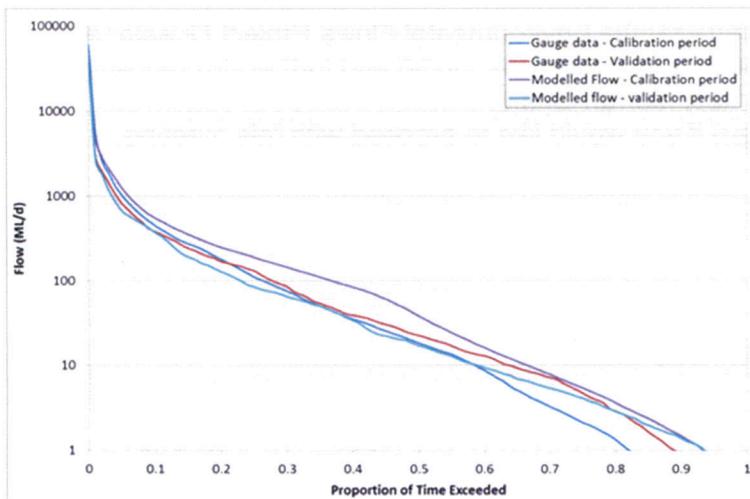
3. Endorsed by:

Greg Allen, Manager Corporate Strategy

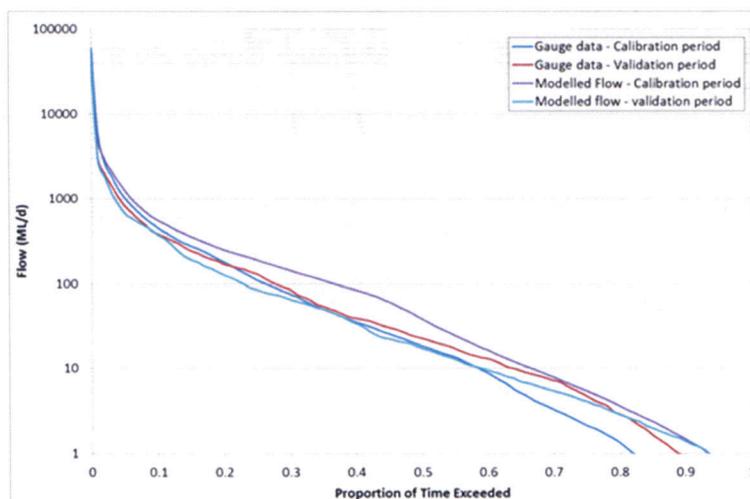
Attachment 1 Flow duration curves for key catchment inflows



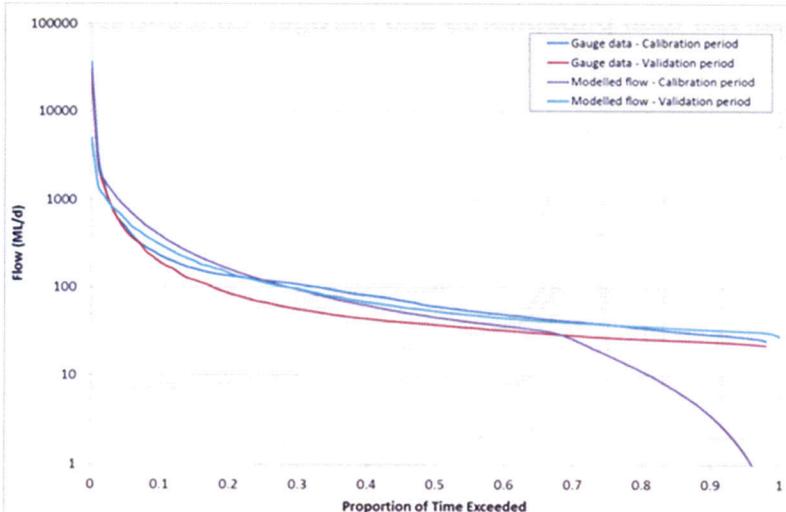
Colo River (station 212290)



MacDonald River (station 212228)

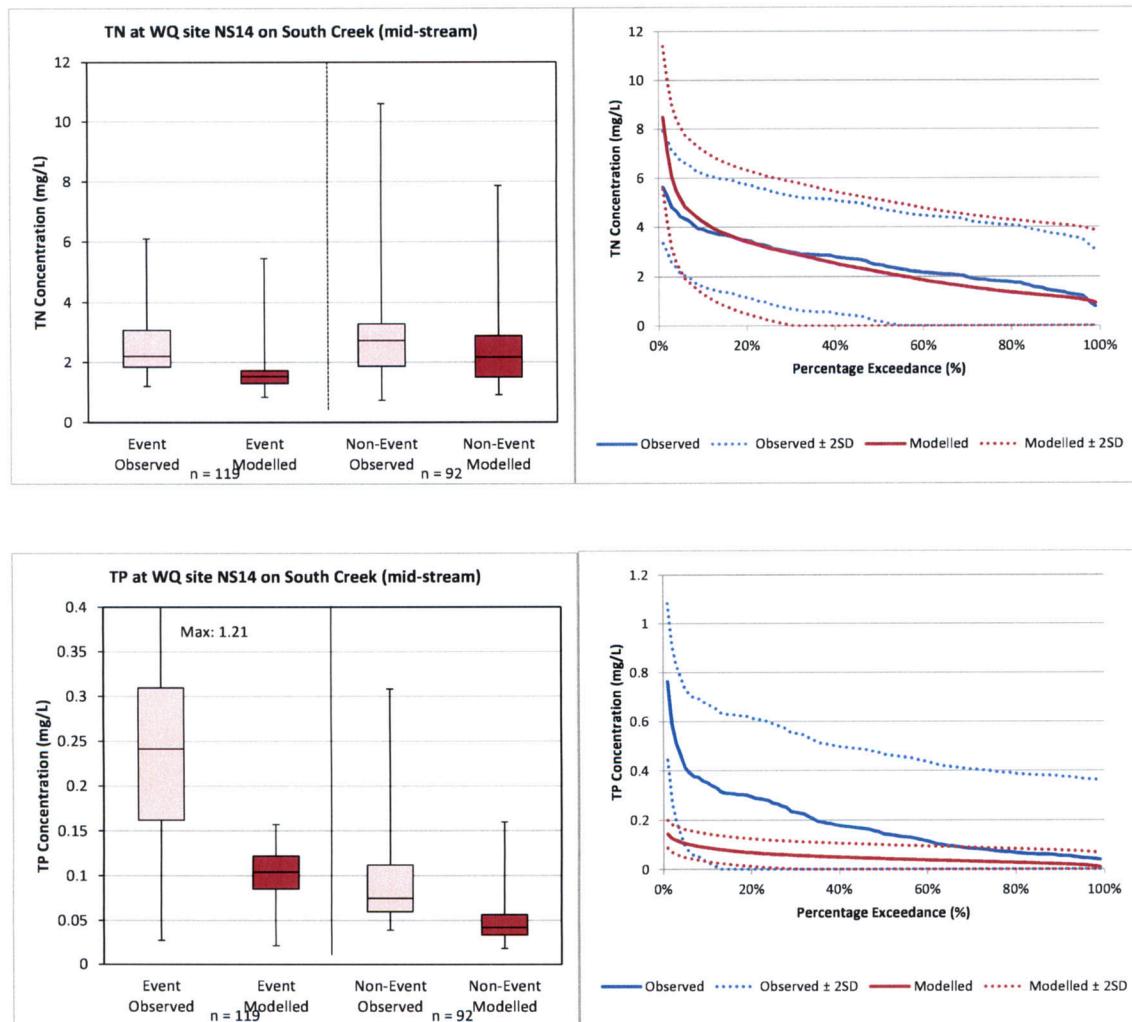


Grose River (station 212291)



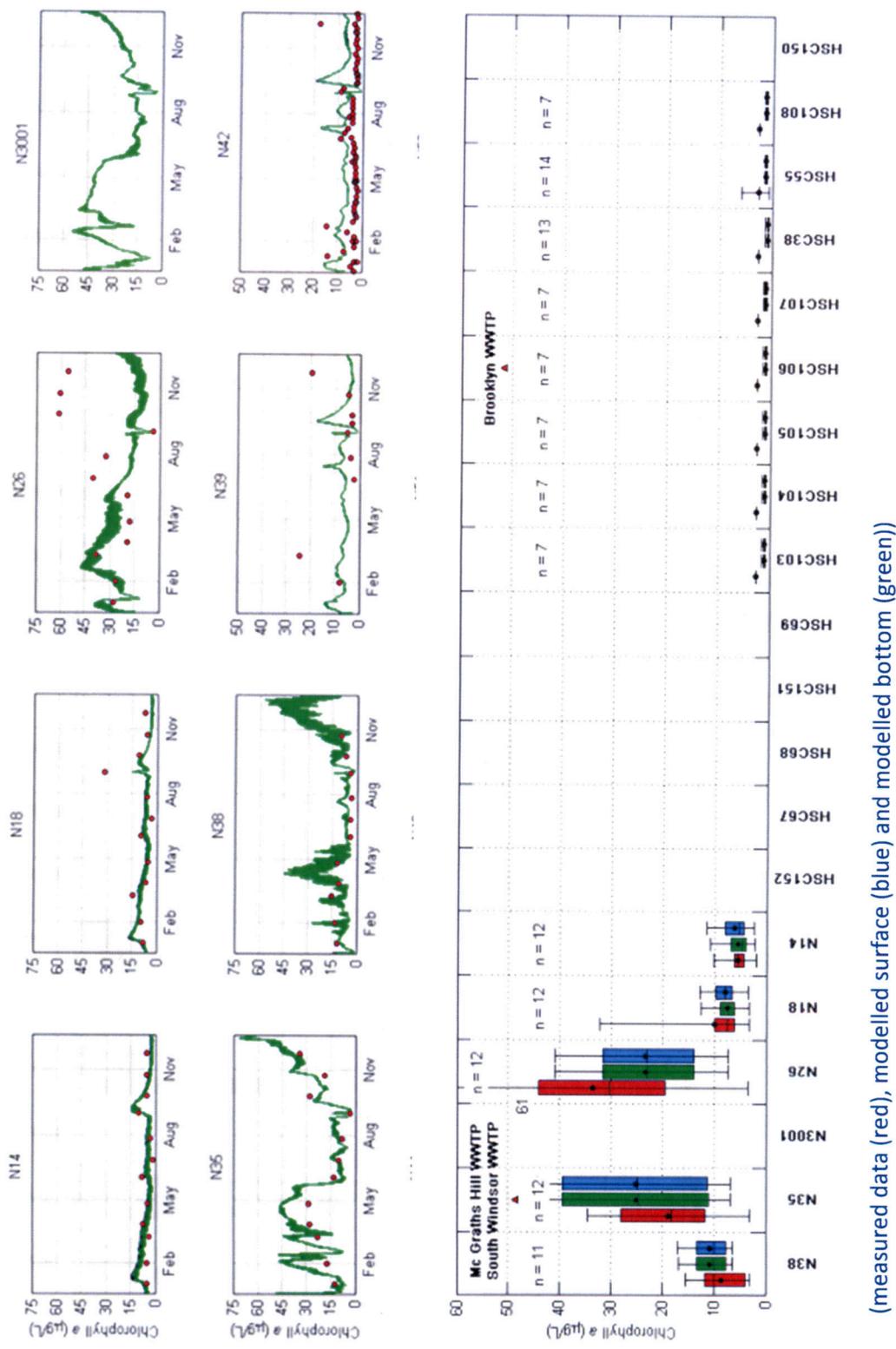
South Creek (station 212297)

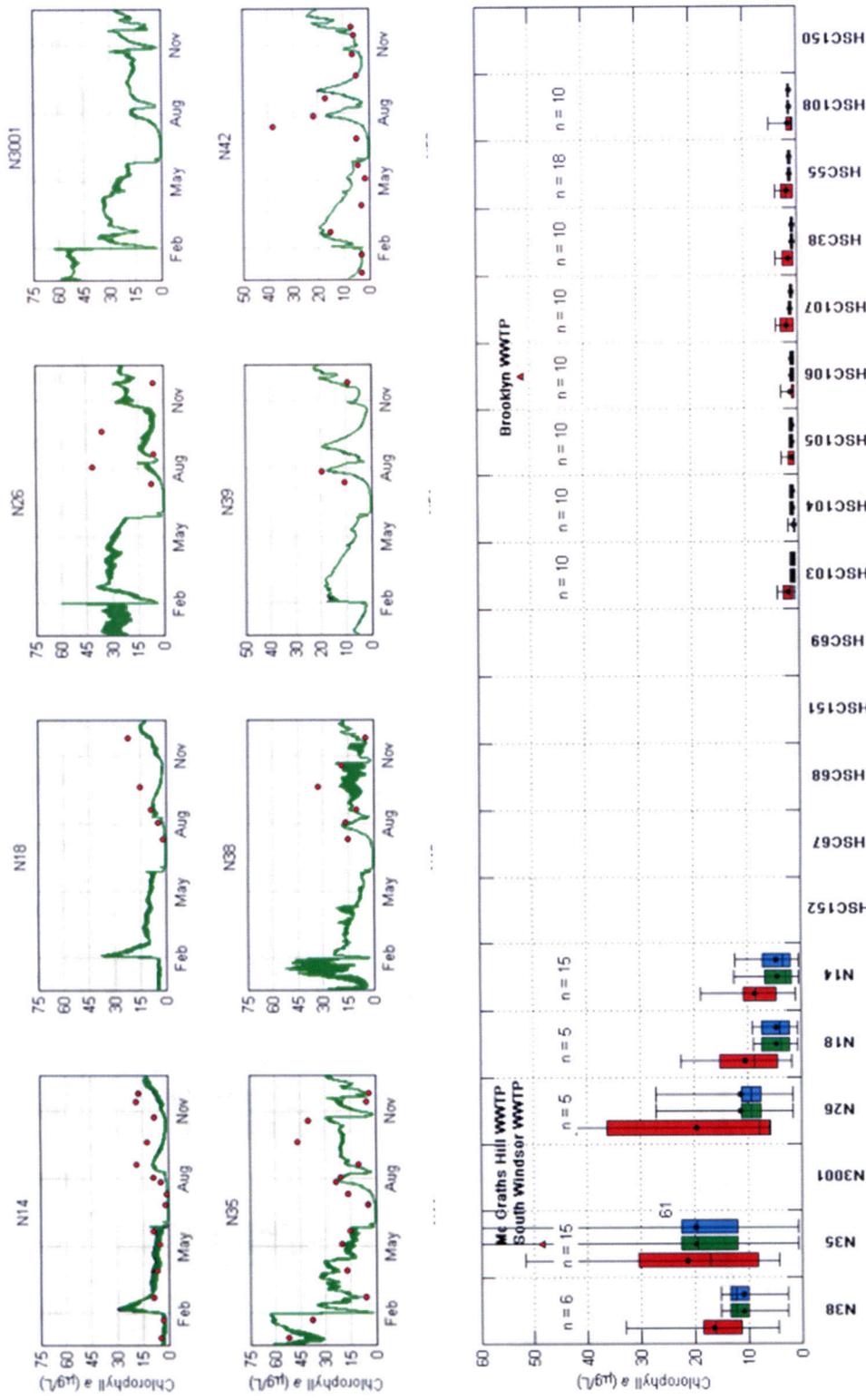
Attachment 2 Modelled and observed total phosphorus and nitrogen concentrations at South Creek (NS14)



Attachment 3 Calibration and validation plots for chlorophyll a in the Hawkesbury River

2006: Calibration





(measured data (red), modelled surface (blue) and modelled bottom (green))

Working Notes

Hawkesbury Nepean Modelling Modellers forum

Purpose of the meeting:

- Inform Sydney Water stakeholders of the Modelling Project
- Explain how the models work, their calibration, verification and limitations
- Answer questions from stakeholders on model performance
- Outline how model will be used in assessment of scenarios

Date: Wednesday 23 October 2013

Time: 0900 – 1300

Location: Room 4.07 and 4.08, Sydney Water Head Office

Present:

Sydney Water	Peter Tate (Technical Reviewer)
Sydney Water	Merran Griffith (Project Manager)
Sydney Water	Michael Blackmore (Manager, WWTPs)
Sydney Water	Heidi Muras Senior Policy and Project Officer
Sydney Water	Jonathan Dixon Senior Data Analyst
Sydney Water	Wang Yue-cong, Strategic Data and Modelling Analyst
SKM	Steve Linforth (Project Director)
SKM	Dr Phillip Jordan SOURCE modeller
BMT-WBM	Dr Michael Barry TUFLOW AED modeller
BMT-WBM	Dr Ian Teakle TUFLOW developer
UWA	Dr Matt Hipsey AED Water Quality Modeller
Yorb	Nick Marsh, Macrophytes and Hawkeye developer
OEH	John Floyd, Modeller
OEH	Anthony Pik, Technical Policy Advisor
OEH	Martin Krogh, Project Team Leader (Monitoring)
SCA	Mahes Maheswaran, Manager, Strategic Supply Planning
NOW	Hemantha Perera, Water Modeller
NOW	Richard Beecham, A/Director, Water Analysis an Modelling

Apologies

SCA	Jason Martin, Modeller
NOW	Helen Keenan, Senior Natural Resource Officer

1. Introduction

- Merran Griffith opened proceedings with a short presentation which is attached. It covered the following areas:
 - Welcome
 - How today will be run
 - Overview of the modelling project
 - Purpose of the model
 - Overview of the model suite setup to compare scenarios
 - What is being modelled and what is not being modelled

2. Source Model

- Phillip Jordan gave a 30 minute presentation on the Source model and incorporated answers to the prepared questions in his presentation which is attached. It covered the following topics:
 - Catchment Node Link Network
 - Definition of Functional Units
 - Climate Forcing in Source Model
 - Point Inflows into the Model
 - Extractions from the Model
 - IQQM extractions
 - Flow Duration Curves
 - Flow Calibration
 - Phosphorus Export from South Creek
- There were a series of questions and requests for information from the workshop participants. These centred around the questions issued before the meeting including:
 - Inclusion of flow duration curves into the calibration report for the gauge sites
 - The mass balance stats for observed and simulated flows at calibration gauging sites.
 - Separate flow duration curves for the 1985-1994 simulation at all gauge sites
 - Comparison between gauged and modelled flows for the calibration and verification years (flow duration curves, hydrographs, scatter plots at Penrith, Camden and Wallacia). These were not used to calibrate SOURCE as they were in the TUFLOW domain
 - Mt Hunter rating curve which is in the SMEC report
 - Request for inclusion of a catchment isohyetal map and other map types to allow further assessment of rainfall depth estimation method

Total P estimation in South Creek was discussed. It was suggested that the model was under estimating nutrient concentrations in this area (NS14) by an order of magnitude which could lead to underestimates of algae production downstream. A review of downstream concentrations showed that whilst concentrations modelled were lower than measured during events this was not an order of magnitude lower and during non-events modelled and measured concentrations were similar. This was most likely due to the dominating influence of WWTP flows outside of events.

3. TUFLOW

- Michael Barry and Ian Teakle gave a short presentation on TUFLOW which is attached. The presentation covered the following areas
 - Overview

- Finite Volume Scheme
- Model Geometry
- Timestep Algorithm
- Sediment Transport Module
- Interface description
- Application to Hawkesbury Nepean
- Overview
- Modules
- Scheme Details
- Calibration
- Seasonality of Macrophyte Drag
- Grid Resolution
- Bathymetry
- The presentation largely answered most of the questions which had been tabled earlier
 - Seasonality of macrophyte drag appears to be real phenomena. It is clear that water levels in the Freemans reach area can vary from year to year with no change in flow rates.
 - The applicability of Smagorinsky was discussed and the model response to salt recovery gives the model developers confidence that mixing processes are well represented. In the upstream end of the river model the main transport process is advection and the model is not sensitive to the dispersion model coefficients
 - The discretisation of the model was discussed acknowledging in the upper reaches the model is only a few cells wide. This was as a result of focussing on the models main function as a water quality model which needed to be run in a practical time period. The target period being one year of hydrodynamic simulation in one day of HPC computing time (which was achieved). It was noted that if more detail was needed in an area subsequently then a more detailed model could be developed for this area, with the results of this study used as boundary conditions.

4. Water Quality (AED (formerly known as FABM))

- Matt Hipsey gave a short presentation taking the workshop through the fundamentals of the water quality module. this talk covered the following areas
 - Overview
 - FABM-AED use in Australia
 - Technical Details
 - Approach to setup
 - A comment on uncertainty and validation approach
 - Holistic Approach for complex models
 - On-going research for addressing these challenges

Michael Barry followed this with specific detail as applied to the Hawkesbury Nepean system

- Overview
- Modules
- Processes
- Inputs
- Outputs

- Calibration
- Dissolved Oxygen
- FRP/TP
- NOx/TKN
- Algae

This session was followed by a range of questions and comments from the workshop participants. Key questions included:

- Was light limitation included in the model? To which the answer was yes
- There were questions on the sensitivity of algae to salinity and it was agreed that Blue Greens were not as sensitive to salinity as represented in the diagram

5. Macrophyte Model

- Nick Marsh gave a brief overview of the development of the *Egeria densa* model which is attached. It covered the main considerations as follows:
 - Assemblage structure controlled by many factors
 - Boundary conditions
 - Conceptual model
 - Basic approach
 - Available calibration data
 - Hydraulic decay
 - Temperature
 - Nutrient limitation
 - Example output

6. General Discussion, Questions and Meeting Close

- There was a wide ranging discussion on each of the models and their development
- Mahes Maheswaran noted that the model was substantive improvement on the earlier generation models known as SalmonQ. He had a range of comments on nutrient generation rates in the South Creek catchment and the impact of light limitation and coloured water discharging from South Creek. He did not agree with the use of 2 standard deviations when plotting cumulative statistics.
- There were a number of comments around using future scenario runs to test the model sensitivity to the issues raised in the workshop

For further information about the Catchment and Environmental Modelling of the Hawkesbury-Nepean River and South Creek Project, please contact:

Merran Griffith
Sydney Water Project Manager
Phone: 02 8849 5732
Email: merran.griffith@sydneywater.com.au

For further information regarding SKM's role in the project please contact:

Steven Linforth
SKM Project Manager
Phone: 02 9928 2216
Email: slinforth@globalskm.com